ERIODICAL

960

1960

WOODS HOLE
OCEANOGRAPHIC INSTITUTION

COLLECTED REPRINTS

1960

LIBRARY
NOV 28 1961
FISH & WILDLIFE SERVICE

JULY, 1961

PERIODICAL

Woods Hole
Oceanogr.
Institution

Collected
Reprints

1960

LIBRARY
BUREAU OF COMMERCIAL FISHERIES
U. S. FISH AND WILDLIFE SERVICE
P. O. BOX 3830
HONOLULU 12, HAWAII

WOODS HOLE
OCEANOGRAPHIC INSTITUTION

COLLECTED REPRINTS

1960

JULY, 1961

This volume contains contributions from the Woods Hole Oceanographic Institution which were published in 1960; also the Annual Report of the Director for the year 1960.

TABLE OF CONTENTS

Contribution No.

BACKUS, RICHARD H.
Notes on Western North Atlantic Sharks, No. 2 1076

BARAKAT, RICHARD and ROBERT BARAKAT
Optical Studies of the Diffraction of Water Waves by Circular and Thin Elliptic Cylinders 1074

BARNES, H. and MARGARET BARNES
The Effect of Temperature on the Oxygen Uptake and Rate of Development of the Egg-Masses of Two Common Cirripedes, *Balanus balanoides* (L.) and *Pollicipes polymerus* J. B. Sowerby 1075

BLUMER, MAX
Pigments of a Fossil Echinoderm 1112

BOWEN, VAUGHAN T. and THOMAS T. SUGIHARA
Strontium-90 in the 'Mixed Layer' of the Atlantic Ocean 1095

BRYAN, KIRK
The Instability of a Two-Layered System Enclosed between Horizontal, Coaxially Rotating Plates 1077

BRYAN, KIRK and ELIZABETH SCHROEDER
Seasonal Heat Storage in the North Atlantic Ocean 1107

BUDINGER, THOMAS F.
Iceberg Detection by Radar 1093

BUMPUS, DEAN F.
Sources of Water Contributed to the Bay of Fundy by Surface Circulation 1086

BUNKER, ANDREW F.
Heat and Water-Vapor Fluxes in Air Flowing Southward over the Western North Atlantic Ocean 1031

CLARKE, GEORGE L. and LLOYD R. BRESLAU
Studies of Luminescent Flashing in Phosphorescent Bay, Puerto Rico, and in the Gulf of Naples Using a Portable Bathyphotometer 1090

CONOVER, ROBERT J.
The Feeding Behavior and Respiration of Some Marine Planktonic Crustacea 1115

CURL, HERBERT, JR.
Primary Production Measurements in the North Coastal Waters of South America 1102

DAY, C. GODFREY
Bottom Water Temperature on Browns Ledge off Southern Massachusetts 1089

DOW, WILLARD
A Telemetering Hydrophone 1130

FALLER, ALAN J.
Further Examples of Stationary Planetary Flow Patterns in Bounded Basins . 1069

Contribution No.

FEJER, ANDREW A. and RICHARD H. BACKUS
Porpoises and the Bow-Riding of Ships Under Way 1070

FRAENKEL, G.
Lethal High Temperatures for Three Marine Invertebrates: *Limulus polyphemus*, *Littorina littorea* and *Pagurus longicarpus* 1087

GRICE, GEORGE D.
Copepods of the Genus *Oithona* from the Gulf of Mexico 1116

HANKS, JAMES E.
A Method for Preparing the Marine Polychaete, *Pectinaria gouldi* (Verrill) for Histological Study 1080

HERSEY, J. B.
Acoustically Monitored Bottom Coring 1052

HULBURT, E. M., J. J. A. McLAUGHLIN and P. A. ZAHL
Katodinium dorsalisulcum, a New Species of Unarmored Dinophyceae 803

HULBURT, E. M., J. H. RYTHER and R. R. L. GUILLARD
The Phytoplankton of the Sargasso Sea off Bermuda 1068

KANWISHER, JOHN
pCO_2 in Sea Water and its Effect on the Movement of CO_2 in Nature 1103

KETCHUM, BOSTWICK H.
Oceanographic Research Required in Support of Radioactive Waste Disposal . . 1111

KETCHUM, BOSTWICK H., RALPH F. VACCARO and NATHANIEL CORWIN
The Annual Cycle of Phosphorus and Nitrogen in New England Coastal Waters 1007

LACKEY, JAMES B.
Calkinsia aureus gen. et sp. nov.; a New Marine Euglenid 1009

LEWIN, JOYCE C. and RALPH A. LEWIN
Auxotrophy and Heterotrophy in Marine Littoral Diatoms 1062

MALKUS, JOANNE S.
Recent Developments in Studies of Penetrative Convection and an Application to Hurricane Cumulonimbus Towers 1044

MALKUS, J. S. and H. RIEHL
On the Dynamics and Energy Transformations in Steady-State Hurricanes 1034

MALKUS, JOANNE S. and CLAUDE RONNE
Cloud Distributions over the Tropical Oceans in Relation to Large-Scale Flow Patterns 1051

MARSHALL, SHEINA M. and A. P. ORR
Some Uses of Antibiotics in Physiological Experiments in Sea Water 1005

MATHER, FRANK J., III
Recaptures of Tuna, Marlin and Sailfish Tagged in the Western North Atlantic 1092

MATHER, FRANK J., III and HOWARD A. SCHUCK
Growth of Bluefin Tuna of the Western North Atlantic 836

MATTHIESSEN, GEORGE C.
Observations on the Ecology of the Soft Clam, *Mya arenaria*, in a Salt Pond . . 1056

Contribution No.

McLACHLAN, JACK
The Culture of *Dunaliella tertiolecta* Butcher - a Euryhaline Organism 1097

MENZEL, D. W. and J. H. RYTHER
The Annual Cycle of Primary Production in the Sargasso Sea off Bermuda 1042

METCALF, WILLIAM G.
A Note on Water Movement in the Greenland-Norwegian Sea 1101

MILLER, ROBERT L. and JOHN M. ZEIGLER
A Study of the Relation between Dynamics and Sediment Pattern in the Zone of Shoaling Wave, Breaker, and Foreshore 1124

MORDY, W. A.
Differences in Coalescence Tendencies in Computed Condensation Cloud Droplet Spectra 1079

MOULTON, JAMES M.
Swimming Sounds and the Schooling of Fishes 1126

REDFIELD, ALFRED C.
The Influence of the Continental Shelf on the Tides of the Atlantic Coast of the United States 1000

REDFIELD, ALFRED C.
The Distribution of Phosphorus in the Deep Oceans of the World 1134

RICHARDS, FRANCIS A.
Dissolved Silicate and Related Properties of Some Western North Atlantic and Caribbean Waters 990

RICHARDS, FRANCIS A.
Some Chemical and Hydrographic Observations along the North Coast of South America — 1. Cabo Tres Puntas to Curaçao, Including the Cariaco Trench and the Gulf of Cariaco 1100

RICHARDSON, WILLIAM S. and CHARLES J. HUBBARD
The Contouring Temperature Recorder 1046

ROBINSON, ALLAN R.
The General Thermal Circulation in Equatorial Regions 1065

RYTHER, JOHN H.
Organic Production by Plankton Algae and its Environmental Control 1049

RYTHER, J. H. and E. M. HULBURT
On Winter Mixing and the Vertical Distribution of Phytoplankton 1088

RYTHER, JOHN H. and DAVID W. MENZEL
The Seasonal and Geographical Range of Primary Production in the Western Sargasso Sea 1067

SANDERS, HOWARD L.
Benthic Studies in Buzzards Bay. III. The Structure of the Soft-Bottom Community 1033

Contribution No.

SCHEVILL, WILLIAM E. and RICHARD H. BACKUS
Daily Patrol of a *Megaptera* 1040

SOULE, FLOYD M. and P. A. MORRILL
Physical Oceanography of the Grand Banks Region and the Labrador Sea in 1959 1091

SOULE, FLOYD M. and R. M. MORSE
Physical Oceanography of the Grand Banks Region and the Labrador Sea in 1958 1018

SPIEGEL, E. A. and G. VERONIS
On the Boussinesq Approximation for a Compressible Fluid 1081

STEELE, J. H. and C. S. YENTSCH
The Vertical Distribution of Chlorophyll 1078

STOMMEL, HENRY
Wind-Drift near the Equator 1084

STOMMEL, HENRY and A. B. ARONS
On the Abyssal Circulation of the World Ocean. I. Stationary Planetary Flow Patterns on a Sphere 1023

STOMMEL, HENRY and A. B. ARONS
On the Abyssal Circulation of the World Ocean. II. An Idealized Model of the Circulation Pattern and Amplitude in Oceanic Basins 1055

STROSS, RAYMOND G.
Growth Response of *Chlamydomonas* and *Haematococcus* to the Volatile Fatty Acids 1106

TURNER, HARRY J., JR. and JAMES E. HANKS
Experimental Stimulation of Gametogenesis in *Hydroides dianthus* and *Pecten irradians* during the winter 1099

TUTTLE, SHERWOOD D.
Evolution of the New Hampshire Shore Line 991

VACCARO, RALPH F. and JOHN H. RYTHER
Marine Phytoplankton and the Distribution of Nitrite in the Sea 1096

VERONIS, G.
An Approximate Theoretical Analysis of the Equatorial Undercurrent 1082

VON ARX, WILLIAM S.
The Line of Zero Set 1125

WEXLER, RAYMOND and RUTH WEXLER
Cold Clouds over Tropical Oceans 1083

WHITNEY, G. G., JR.
Procedure for and Comments on Ice Point Tests of Deep Sea Reversing Thermometers 1064

Contribution No.

WIESER, WOLFGANG
Benthic Studies in Buzzards Bay. II. The Meiofauna 1054

WIESER, WOLFGANG and JOHN KANWISHER
Vorschlag zum Anlegen einer "Stoffwechselkartei" für marine Tiergemeinschaften 1053

WIESER, WOLFGANG and JOHN KANWISHER
Growth and Metabolism in a Marine Nematode, *Enoplus communis* Bastian 1059

WOODCOCK, A. H.
The Origin of Trade-Wind Orographic Shower Rains 1094

YENTSCH, CHARLES S.
The Influence of Phytoplankton Pigments on the Colour of Sea Water 1058

ZEIGLER, J. M., W. S. HOFFMEISTER, GRAHAM GIESE and HERMAN TASHA
Discovery of Eocene Sediments in Subsurface of Cape Cod, Massachusetts 1128

ZEIGLER, JOHN M., G. G. WHITNEY, JR. and CARLYLE R. HAYES
Woods Hole Rapid Sediment Analyzer 1073

THE WOODS HOLE OCEANOGRAPHIC INSTITUTION

Report for the Year 1960

LIST OF CONTRIBUTIONS

The following contributions are not included in this volume:

DAY, C. GODFREY
Oceanographic Observations, 1959, East Coast of the United States 1104

FUGLISTER, F. C.
Atlantic Ocean Atlas of Temperature and Salinity Profiles and Data from the International Geophysical Year of 1957–1958 1108

KETCHUM, BOSTWICK H.
Marine Pollution Problems in the North Atlantic Area 1035

Contribution No. 803

Katodinium dorsalisulcum, a New Species of Unarmored Dinophyceae*

EDWARD M. HULBURT, J. J. A. McLAUGHLIN and P. A. ZAHL

*Woods Hole Oceanographic Institution, Woods Hole, Mass. and Haskins Laboratories,
New York, N. Y.*

SYNOPSIS. A new species of naked Dinophyceae is described and the culture medium for its continued growth defined. The species is distinctive in having a posteriorly placed girdle, characteristic of the genus *Katodinium* (Fott, 1957), and in possessing a counterclockwise loop of the sulcus about the apex.

KATODINIUM dorsalisulcum n.sp., was isolated from an outdoor marine aquarium on the island of Bimini in the British West Indies. It was obtained from sediment on the bottom of the aquarium rather than from the overlying water (replenished in turn by nearby tidal water). From the samples containing the brown-green sediment, cyst-like bodies were picked up with a micropipette and transferred to sea water media enriched as previously described(12,15). The free-swimming cells that erupted from the cysts were washed by 18 serial passages through sterile media and axenic cultures established. Subcultures derived by isolating single cells have been maintained through 8 transfers at monthly intervals in an artificial enriched sea water medium (Table I). For convenience the medium is given in full; certain components have been detailed elsewhere(12,13). This isolation medium differs from previous ones mainly in having yeast autolysate, adenylic acid, and monoethyl phosphate in combination with excess chelation of trace elements. During these morphological studies, we noticed that the flagellates liberate an extraordinary amount of carbohydrate mucus into the medium, so much so that cultures become semi-solid. This is being studied.

Since the clones were established by single-cell isolation, the illustrations show the great morphological variation that existed in the progeny of a single cell. Figs. 1 to 6 show the change from an epicone that is wider than the hypocone to one that is not so wide as the hypocone. These figures illustrate the gradation from a globular to an elongate form, from a type with the greatest width in the midsection to a type with a posterior maximum width. Extremes of size, of shape, and of symmetry and asymmetry are exemplified by Figs. 7, 8 and 9. All of these features exhibit great variation from specimen to specimen. But the sulcus, though its course may veer, passes always to the left of the apex and then across the dorsal surface (Fig. 7), and the girdle, its position clearly rather variable, is always posterior to the middle of the cell.

The marked displacement of the girdle ends of *Katodinium dorsalisulcum* is similar to that of the species of *Gyrodinium*. On the average, however, the girdle seems not quite near enough the cell middle to allow the new species to fall within the genus *Gyrodinium*. Thus *Katodinium* Fott (1957) appears to be the genus fitting for the new species. *Katodinium*, which is synonymous with *Massartia* Conrad(5), is the appropriate category for all naked Dinophyceae with definitely posterior girdles and no torsion of the sulci.

Fott places 24 species in *Katodinium*. In addition to those he lists there are three more and one variety in Conrad & Kufferath(6) under the name *Massartia*. These four could now be renamed:

Katodinium galeata (Conrad) *comb. nov.*

Katodinium rotundatum (Lohman) var. *conradi* (Kufferath) *comb. nov.*

Katodinium thiophila (Conrad) *comb. nov.*

Katodinium uncinata (Kufferath) *comb. nov.*

None of the 28 species in the genus has a well-defined portion of the sulcus that crosses left of the apex to

TABLE I. Enriched artificial marine medium for *Katodinium dorsalisulcum*.

Amounts for 100 ml. of final medium			
NaCl	2.6 g.	Monoethyl phosphate	0.001 g.
KCl	0.06 g.	Adenylic acid (yeast)	0.001 g.
$MgSO_4 \cdot 7H_2O$	0.6 g.	†Vitamin mix	0.05 ml.
Ca (as Cl^-)	0.02 g.	B_{12}	0.01 μg.
Fe	0.05 mg.	Nitrilotriacetic acid	0.01 g.
*"P II" metal mix	1.0 ml.	Na_2S	0.01 mg.
		Yeast autolysate	0.05 mg.
Na_2CO_3	0.005 mg.	‡Tris	0.1 g.
$NaNO_3$	0.003 g.	pH 7.4-8.0	

* 1.0 ml. = Na_2 Versenate (ethylenediamine tetraacetate), 1.0 mg.; Fe, 0.01 mg.; B, 0.2 mg.; Mn, 0.04 mg.; Zn, 0.005 mg.; Co, 0.001 mg. (adjusted to pH 7.5 with conc. NaOH).

† 1.0 ml. = thiamine · HCl, 0.2 mg.; biotin, 0.5 μg.; B_{12}, 0.05 μg.; folic acid, 0.0025 mg.; folinic acid, 0.2 μg.; *p*-aminobenzoic acid, 0.01 mg.; nicotinic acid, 0.1 mg.; thymine, 0.8 mg.; choline H_2 citrate, 0.5 mg.; inositol, 1.0 mg.; putrescine · 2HCl, 0.04 mg.; riboflavin, 0.005 mg.; pyridoxamine · 2HCl, 0.02 mg.; pyridoxine · 2HCl, 0.04 mg.; orotic acid, 0.02 mg.; Ca pantothenate, 0.1 mg.

‡ Tris = tris(hydroxymethyl)aminomethane.

---

* Contribution No. 803 from the Woods Hole Oceanographic Institution. The junior authors are indebted to the director of the Lerner Marine Laboratory for facilities made available to us on Bimini, B.W.I., and support under Public Health Service Grant B-1198.

Copyright 1960 by the Society of Protozoologists
Reprinted from THE JOURNAL OF PROTOZOOLOGY.
J. PROTOZOOL. 7(4), 323-326 (1960).

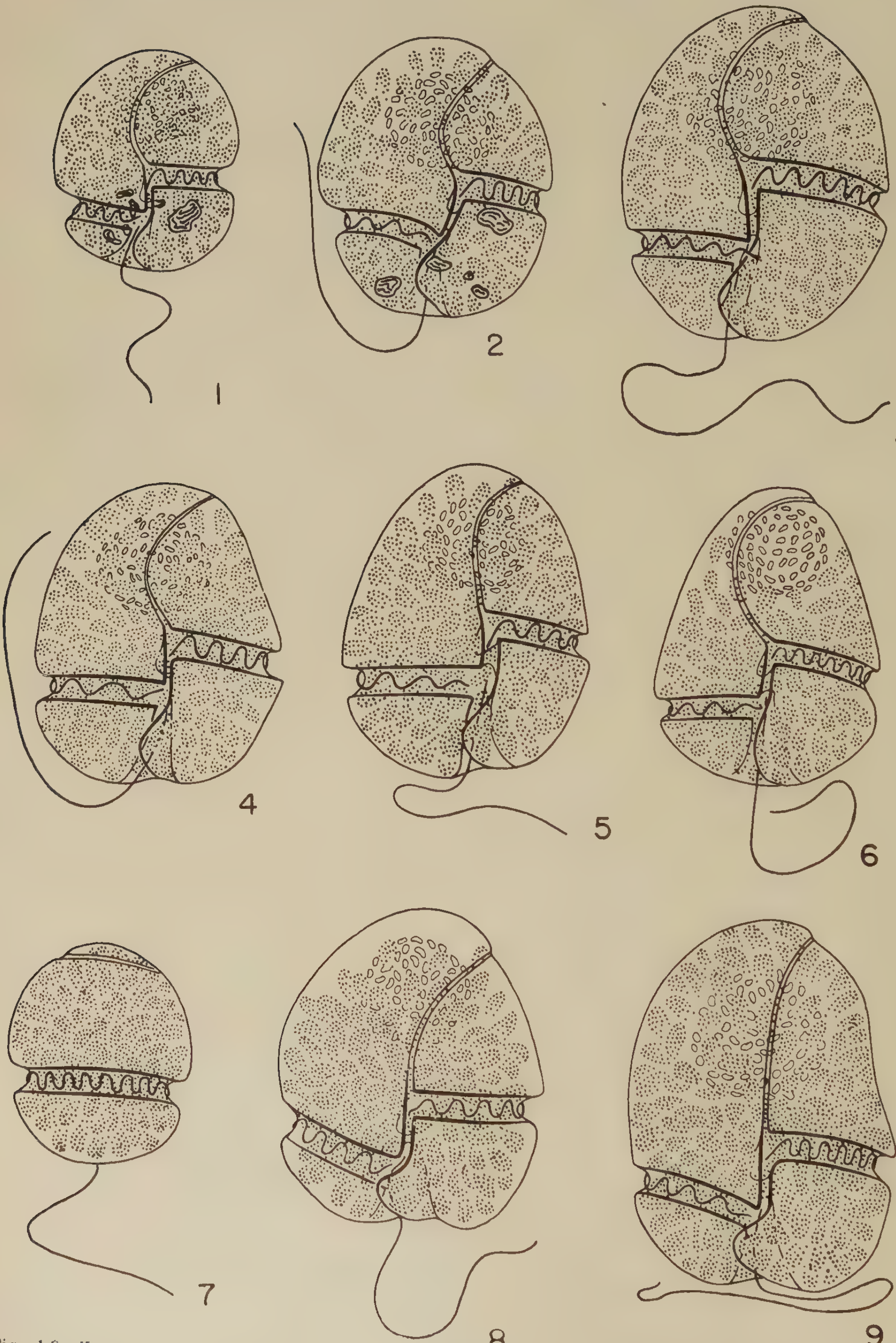

Figs. 1-9. *Katodinium dorsalisulcum* n. sp.

Figs. 1-6 and 8 and 9, ventral views; Fig. 7, dorsal view.

the dorsal side, although the sulcus veers to the left side to form a well-developed loop in *Katodinium hyperxanthoides* (Harris) Fott(8). *Katodinium dorsalisulcum* has many chromatophores per cell, whereas the photosynthetic species have only a few chromatophores per cell. With a possible exception in *Katodinium musei* (Danysz) Fott, most species of the genus lack chromatophores; only about one-fifth possess them. Most do not have markedly displaced girdle ends, and most, 22 of the 28, are smaller than *K. dorsalisulcum*(14).

K. dorsalisulcum is rather exceptional in the course of the sulcus to the left of the apex. However, in *Gyrodinium pavillardi* Biecheler(1) the sulcus makes an ample and almost complete counter-clockwise loop to the left of the apex, delimiting a greater portion of the epicone than in *K. dorsalisulcum*. In *Gymnodinium cruciatum* Massart(11,5), the sulcus goes to the left of the apex and then to the right across the dorsal surface very much as in *K. dorsalisulcum,* though a smaller portion of the apex is delimited. A still smaller, apical portion is set apart by a similar, reverse loop of the sulcus in *Gyrodinium viridescens* Kofoid and Swezy and *Torodinium robustum* Kofoid and Swezy(10). These 5 species appear to be the only ones described at present in which the sulcus makes a well-defined, clearly visible counter-clockwise loop around the apex, and they are in contrast to a much larger number of dinophycean species which have clockwise apical loops.

Perhaps the comparative rarity of the counterclockwise apical loop has been overemphasized, because with silver staining Chatton & Hovasse(4) and Biecheler(1,2) found the counterclockwise loop in 7 other species. But the loop was often difficult to see on the living organism. One species, *Katodinium asymmetricum* (Massart) Fott, has been studied by several investigators(11,3,2,9) but only Biecheler, after experience in detecting the apical loop, was able to see a continuation of the sulcus to the left of the apex and on to the dorsal surface in the living organism.

Although *K. dorsalisulcum* is quite like *Gymnodinium cruciatum* in epiconal sulcus, it is very different in other ways. There is some resemblance of *K. dorsalisulcum* to *Gyrodinium aureolum* Hulburt(9). The two species possess a roughly similar outline, many brown chromatophores, the same degree of displacement of the girdle ends, a very moderate amount of dorsi-ventral flattening, and like size. The new species differs in the course of the sulcus, the posterior position of the girdle, and the tendency of the hypocone to be wider than the epicone. It is even less like other species of Dinophyceae and seems therefore to be well separated from all described members of its class.

The body is essentially ellipsoidal, somewhat compressed dorsi-ventrally, with a tendency for the maximum width to be posterior to the middle of the body. The epicone in ventral or dorsal view is hemispherical to somewhat conical, asymmetric, longer than the hypocone, either wider or less wide than the hypocone, 0.6-0.7 of the body length, the right contour markedly convex, the left contour moderately convex to occasionally straight or even concave, the apex often eccentrically indented. The hypocone is wider than long, sub-hemispherical to truncate-pyramidal, with sloping, usually convex, though rarely straight sides, with the antapex rounded or indented or slightly lobed. The girdle is wide, moderately deep, displaced 0.15 to 0.20 of the body length, the left limb at the middle of the cell or a little posterior, the right limb always well posterior. The sulcus extends as a shallow, narrow groove from the left end of the girdle to the apex either in a rightwardly then leftwardly curving arc or in an initially straight then leftwardly curving course, passing well to the left of the apex and crossing the dorsal surface to the right margin in a slightly posteriorly sloping direction; the sulcus is deep but usually narrow in the intercingular region, widening abruptly on the hypocone to form a large excavation, which is covered over by a rightwardly projecting lobe of the left margin. The anterior flagellar chamber is a short, posteriorly directed pocket; the posterior flagellar chamber is the anterior extension of the sulcal excavation, reaching just beyond the anterior margin of the right girdle limb. The anterior flagellum is thick, completely encircling the body; the posterior flagellum is thinner, body length, arising far anteriorly in the hypoconal excavation.

The chromatophores are numerous, yellow-brown, indistinct, heterogeneously arranged. The nucleus lies completely within the epicone, is spherical, its structure composed of short, unoriented elements. Dark red bodies of various sizes are present at times. The cell is surrounded by a widish, hyaline pellicle occasionally.

Length 23-37 μ, width 18-28 μ.

Corpore elliptico, paulum dorsali-ventraliter compresso, epicono longiore quam hypocono, hemispherico vel paulum conico, margine dextro convexiore quam margine sinistro, latere sinistro apicis saepe paululum cavato; hypocono sub-hemispherico vel truncato-pyramidali; cingulo in posteriore parte corporis posito, extremitatibus cinguli longitudinis corporis transpositis; sulco trans latus sinistrum apicis et ad marginem dextrum dorsaliter extendente. Chromatophoris multis, luteo-fuscis; nucleo intro epiconum posito. Longitudo 23-27 μ, latitudo 18 μ. In insula Bimini, British West Indies.

REFERENCES

1. Biecheler, B., 1934. Sur le réseau argentophile et la morphologie de quelques Péridiniens nus. *Compt. rend. soc. biol.* **115**, 1039-42.

2.——— 1952. Recherche sur les Péridiniens. *Bull. Biol. France Belgique, Suppl.* **36**, 1-149.

3. Carter, N. 1937. New or interesting algae from brackish water. *Arch. Protistenk.* **90**, 1-68.

4. Chatton, E. & Hovasse, R. 1934. L'existence d'un réseau argentophile chez les *Polykrikos* et les precisions qu'il a la morphologie péridinienne. *Compt. rend. soc. biol.* **115**, 1036-9.

5. Conrad, W. 1926. Recherches sur les Flagellates de nos eaux saumâtres. 1^e Partie: Dinoflagellates. *Arch. Protistenk.* **55**, 63-100.

6. Conrad, W. & Kufferath, H. 1954. Recherches sur les eaus saumâtres des environs de Lilloo. *Mém. Inst. Roy. Sci. Nat. Belq.* **127**, 1-346.

7. Fott, B. 1957. Taxonomie drobnohledné flory nasich vod. *Preslia* **29**, 278-319.

8. Harris, T. M. 1939. A contribution to the knowledge of the British freshwater Dinoflagellata. *Proc. Lin. Soc. London* **152**, 4-33.

9. Hulburt, E. M. 1957. The taxonomy of unarmored Dinophyceae of shallow embayments on Cape Cod, Massachusetts. *Biol. Bull.* **112**, 196-219.

10. Kofoid, C. A. & Swezy, O. 1921. The free living unarmored Dinoflagellata. *Mem. Univ. Calif.* **5**, 1-562.

11. Massart, J. 1920. Recherche sur les organismes inférieurs. VIII. Sur la motilité des Flagellates. *Bull. Cl. Sci., Acad. Roy. Belg. Sér.* 5, **6**, 116-41.

12. McLaughlin, J. J. A. & Zahl, P. A. 1957. Studies in marine biology. II. *In vitro* culture of Zooxanthellae. *Proc. Soc. Exptl. Biol. Med.* **95**, 115-20.

13. Provasoli, L., McLaughlin, J. J. A., & Droop, M. R. 1957. The development of artificial media for marine algae. *Arch. Mikrobiol.* **25**, 392-428.

14. Thompson, R. H. 1947. Fresh-water dinoflagellates of Maryland. *Chesapeake Biol. Lab. Publ. No.* **67**, 1-28.

15. Zahl, P. A., & McLaughlin, J. J. A. 1957. Isolation and cultivation of Zooxanthellae. *Nature* **180**, 199-200.

Contribution No. 836

UNITED STATES DEPARTMENT OF THE INTERIOR • Fred A. Seaton, *Secretary*
FISH AND WILDLIFE SERVICE • Arnie J. Suomela, *Commissioner*
BUREAU OF COMMERCIAL FISHERIES • Donald L. McKernan, *Director*

GROWTH OF BLUEFIN TUNA OF THE WESTERN NORTH ATLANTIC

BY FRANK J. MATHER III AND HOWARD A. SCHUCK

March 3, 1849

FISHERY BULLETIN 179
From the Fishery Bulletin of the Fish and Wildlife Service
VOLUME 61

[Contribution No. 836, Woods Hole Oceanographic Institution]

UNITED STATES GOVERNMENT PRINTING OFFICE • WASHINGTON : 1960

CONTENTS

	Page
Introduction	39
Readings of annuli	39
Analysis of length frequencies	42
Age determination	44
Growth of young bluefin tuna	47
Estimated annual growth of bluefin tuna through 10 years	48
Conclusions	49
Literature cited	51

ABSTRACT

Growth of bluefin tuna *Thunnus thynnus* (Linnaeus) based on specimens captured mostly in the Cape Cod and Long Island areas was studied by counting annuli on scales and vertebrae and by analyzing length-frequency data. Similar results obtained by these two methods support their validity for ages 0–4. Older ages were determined by counting annuli only, but tag returns and weight-frequency data afford some corroboration for ages 5–7. Growth is believed to be extremely rapid during the first summer and about four-fifths of an inch per month in the first winter. During the next 3½ years, bluefin tuna grow at a rate of about 1¼ inches per month in summer and about one-third of an inch per month in winter, or about 7 inches per year. Tables of estimated sizes for each month of the first 5 years of life, and at midsummer through the age of 10 years, are presented. The growth rate appears to decline gradually to about 4 inches per year in this range. Only slight differences were found between the sizes and growth rates of fish of the same age taken in different years.

GROWTH OF BLUEFIN TUNA OF THE WESTERN NORTH ATLANTIC

By Frank J. Mather III and Howard A. Schuck

Information on the growth of bluefin tuna (*Thunnus thynnus*) of the western North Atlantic Ocean is incomplete, and limited to the smaller sizes for which age-with-length studies are published (Westman and Gilbert, 1941; Westman and Neville, 1942). Only fragmentary data are available on specimens longer than 46 inches. As a result of the growing interest in bluefin tuna by sport and commercial fishermen, we began a cooperative project, in 1950, to accumulate material for an age-determination study of the bluefin throughout its entire size range. The present paper is an account of our interpretation of this naterial to date.

In the preparation of this paper, we received valuable advice from Dr. Lionel A. Walford of the U.S. Bureau of Commercial Fisheries, and Dr. Henry B. Bigelow and Dr. William C. Schroeder, both of the Woods Hole Oceanographic Institution and Harvard University. Dr. James R. Westman of Rutgers University made available to us his extensive data on bluefin tuna. Other material was collected and measurements were obtained through the kindness of several Cape Cod commercial fishermen, notably Capts. John Vetorino, Adam Rupkus, Mike Goulart, and Nathaniel Wixon of Barnstable; also John A. Worthington of North Truro, Joseph Francis and Stuart Joseph of Provincetown, as well as through the cooperation of many sport fishermen and charter boat captains. Many of the length measurements were made by Frank Riley of the U.S. Bureau of Commercial Fisheries at Provincetown, Mass. Several other people contributed length measurements as noted in the frequency tables. Assistance in obtaining and processing data and in preparing this paper was received from members of the U.S. Bureau of Commercial Fisheries at Woods Hole, including Donald M. Allen who worked 4 years on this study, also from several members of the Woods Hole Oceanographic Institution. Their assistance is gratefully acknowledged.

READINGS OF ANNULI

As in other species of fishes, including several other tunas, annuli are formed on the scales, and also on the centra of the vertebrae (Sella, 1929; Aikawa and Kato, 1938; Westman and Gilbert, 1941; Westman and Neville, 1942; Partlo, 1955). Because these annuli are not consistently distinct in either of these two structures, and for other reasons which will be explained later in the text, we examined both. In the beginning we assumed that the annuli which we counted were formed once each year and therefore indicated the age in years. For verification of this assumption we depend on the internal evidence furnished by our material, including consistency of the age determinations with analysis of length-frequency data.

Most of our data are from fish caught in the vicinity of Cape Cod in pound nets or by hook and line. We took scales or vertebrae (or both) from as many specimens as time and opportunity permitted. There was rarely any difficulty in obtaining scales from fishermen's catches. This was less true for vertebrae, for frequently we were permitted to take them only from the tail, which is usually cut off in dressing the fish. Owing to unfavorable working conditions, it was not always possible to measure the fish from which the tails were cut. In such cases, we estimated the length from a regression of fork length against caudal spread [1] or, if the weight of the fish could be obtained, from a length-weight curve based on 778 specimens from 34 to 270 centimeters long.

We prepared celluloid impressions of the scales (Arnold, 1951), and studied them with the aid of a magnifying projector. Figure 1 shows the annuli, zones of crowding, or discontinuity of the circuli, which research workers consider to be formed annually. We also counted the rings on the centra of the vertebrae (fig. 2). These rings were marked

---

[1] Regression formula with a correlation coefficient of 0.997 computed from 55 specimens, 29 to 270 centimeters long, where X is fork length, Y is caudal pread—$\text{Log } X = 0.7271 + 0.8642 \text{ Log } Y$.

Note.—Frank J. Mather III, Woods Hole Oceanographic Institution, Voods Hole, Mass.; Howard A. Schuck, Alaskan Air Command, Anchorage, laska, formerly fishery biologist, U.S. Bureau of Commercial Fisheries, Voods Hole, Mass.

This project was supported in part by grants from the National Science oundation.

Approved for publication March 11, 1960. Fishery Bulletin 179.

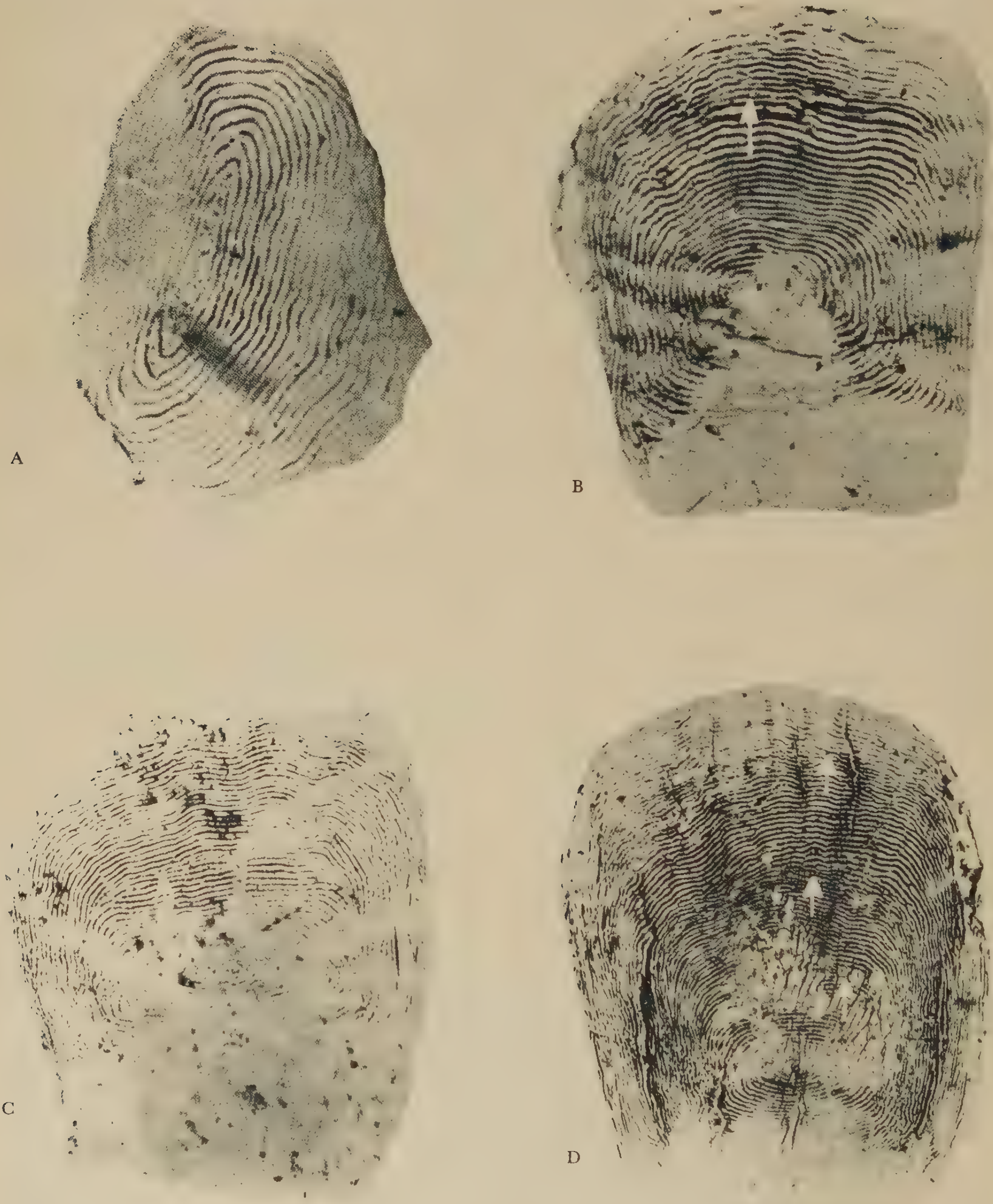

FIGURE 1.—Projected impressions of scales of bluefin tuna. Arrows indicate annuli. A. Scale from fish 34 cm. long taken off Martha's Vineyard, September 1952; no annulus. B. Scale from fish 60 cm. long taken off Martha's Vineyard, July 1950; 1 annulus. C. Scale from fish 80 cm. long taken off Martha's Vineyard, August 1952; 2 annuli. D. Scale from fish 104 cm. long taken off Cape Cod, October 1950; 3 annuli.

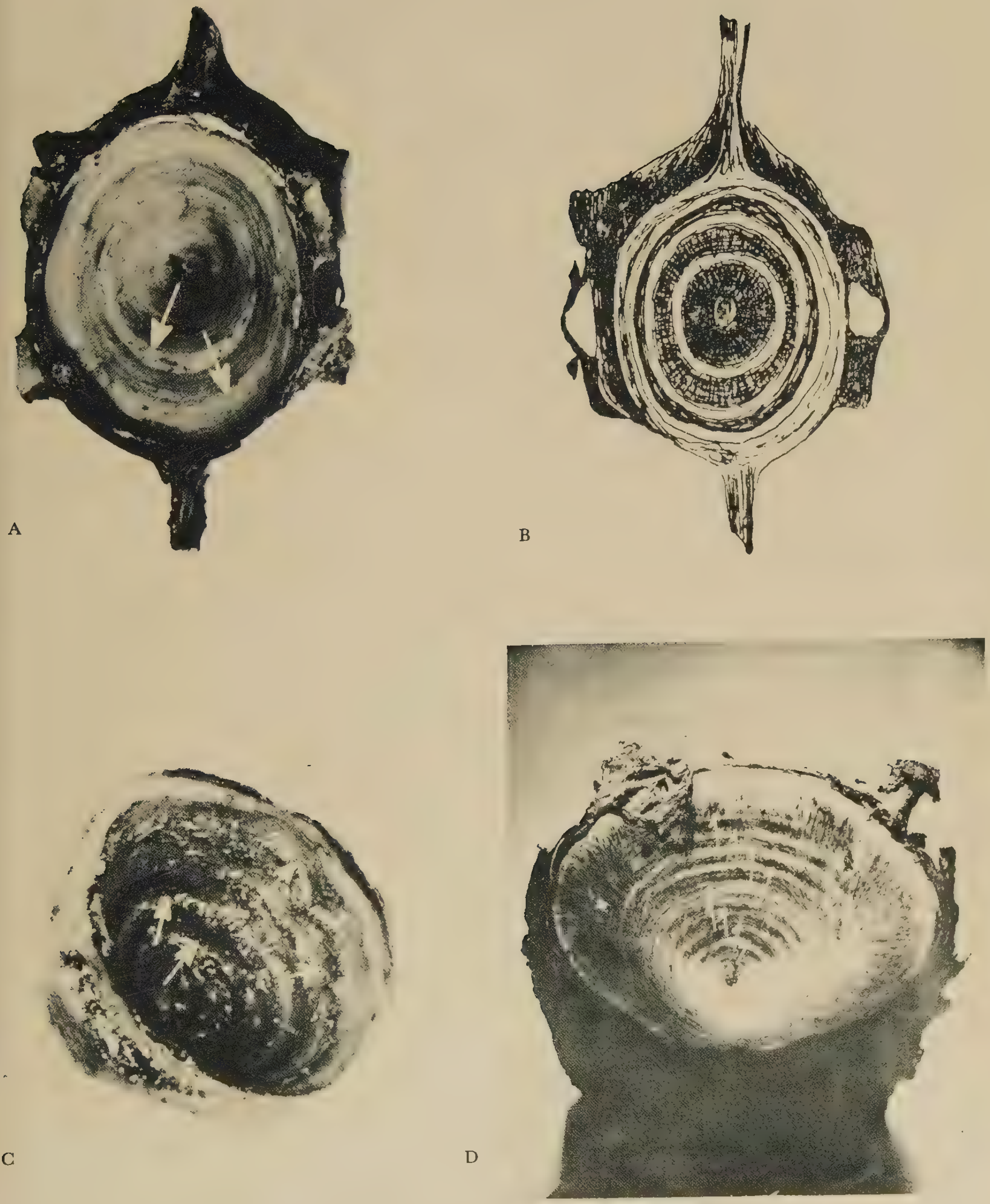

igure 2.—Centra of vertebrae of bluefin tuna. Arrows indicate annuli. A. Vertebra from fish 77.5 cm. long taken off Martha's Vineyard, August 1951; 2 annuli. B. Drawing of stained vertebra from a fish 104 cm. long, taken off Cape Cod, October 1950; 3 annuli. Scale in figure 1 D is from the same fish. (Reproduced from Galtsoff (1952) by permission of the author and publishers.) C. Stained vertebra of fish 110 centimeters long taken off Cape Cod, October 1950; 4 annuli. D. Vertebra of giant tuna taken off Cape Cod; about 11 annuli. Annuli beyond the 9th or 10th are usually small and indistinct and disappear soon after dissection. (A, C, and D, unretouched.)

Table 1.—*Fork lengths (in cm.) of bluefin tuna taken in the vicinity of Cape Cod, for each number of annuli*

[Numbers in parentheses estimated from regression of length on caudal spread or on weight]

0	1	2	3	4	5	6	7	8	9	10	11	12	13	14
34.2	51.5	71.0	84.0	107.2	(120.3)	(144.4)	155.8	162.9	179.0	182.0	223.4	207.5	236.6	247.0
35.3	52.1	71.0	84.7	107.7	(124.5)	(145.0)	156.7	170.8	179.4	184.5	225.6	229.0	237.0	248.0
(37.5)	52.2	73.0	85.3	108.0	(126.0)	(151.5)	(157.6)	174.8	183.0	190.4		234.0	240.0	(249.0)
37.8	53.3	74.0	85.7	108.6	126.2	153.0	(161.7)	176.5	185.2	218.0		241.5	240.6	
41.2	53.8	74.0	85.7	110.0	(127.1)	(153.2)	(164.4)	176.6	193.6	221.5		244.3	244.0	
42.2	55.4	74.0	85.9	110.0	(129.0)	(153.7)	(165.8)	177.8	(196.6)	224.0		245.7	248.0	
	56.0	74.5	85.9	112.1	130.0	154.0	(169.0)	182.0					257.0	
	56.1	74.7	86.1	(113.7)	(130.4)	(156.0)								
	58.2	74.8	87.1	114.1	130.8	158.2								
	58.8	74.9	87.4	114.5	(131.3)	(158.7)								
	59.0	75.0	87.8	114.6	132.0	(166.0)								
	59.7	75.0	88.2	115.0	(132.0)	(170.9)								
	60.0	75.6	88.4	115.0	(132.0)									
		75.7	88.7	116.1	(133.0)									
		75.7	89.0	116.6	(133.5)									
		76.3	89.0	117.5	(134.0)									
		76.7	89.7	(118.3)	135.0									
		76.9	90.2	118.5	135.0									
		77.1	90.8	(118.6)	(135.5)									
		77.5	91.1	(119.0)	(137.2)									
		77.5	91.6	119.6	(137.4)									
		77.6	92.1	120.0	140.0									
		(77.9)	92.9	122.0	140.0									
		78.2	95.0	(122.8)	(140.0)									
		78.5	(98.0)	(123.0)	142.2									
		79.1	103.3	124.4	146.0									
		79.5	104.4	124.5	(150.2)									
		80.0	104.8	125.6	(157.0)									
		(80.8)		129.0	(160.3)									
		(81.8)		(130.2)										
		81.9		(130.4)										
				(130.7)										
				(132.1)										

by depressions in the surface and also by variations in color, which were accentuated when the vertebrae were soaked in water, or when they were stained (Galtsoff, 1952). We examined the vertebrae either with the naked eye or with the aid of a wide-field binocular microscope. We believe that these annuli on scales and vertebrae are probably formed during winter or early spring.

Scales were legible for most fish weighing 50 pounds or less, but rarely for larger ones. As scales could be more readily collected than vertebrae, we used scales for most of our age determinations of small fish, resorting to vertebrae for larger specimens. The material from each specimen was usually examined independently, and often also by our colleague Donald Allen. When readings differed, material was reexamined. If the difference between extremes remained greater than 2, the specimen was discarded. For differences of 2 or less, the average value or the unit closest to it was used. Actually, there were few disagreements in readings for fish up to 50 or 60 pounds. Legible scales and vertebrae were found for 28 fish and counts of annuli on scales agreed with those on the vertebrae. Readings for fish of 70 to 270 pounds often differed by 1 year; those for larger fish sometimes differed by 2 years or more. Lengths (table 1) are from annuli counted from scales or vertebrae, or both; length-frequency distributions (fig. 3) are for each year of age; average length (table 2) is for each year.

Table 2.—*Average fork length of bluefin tuna taken in the vicinity of Cape Cod, for each year of age from readings of annuli on scales and vertebrae*

Age in years	Length in cm.	Number of specimens
0	38.0	6
1	55.9	13
2	76.5	31
3	90.5	28
4	118.8	34
5	135.0	29
6	155.4	12
7	161.6	7
8	174.4	7
9	186.1	6
10	203.4	6
11	224.5	2
12	233.7	6
13	243.3	7
14	248.0	3

ANALYSIS OF LENGTH FREQUENCIES

Another method of estimating age and growth is by following the seasonal progression of dominant size groups. This is especially useful for species that spawn over a fairly short season and grow rapidly. Evidently the bluefin tuna meets these conditions, as even casual observers notice the regularity with which catches of small tuna can be ranked in size categories by eye. Moore (1952) and Postel (1954) analyzed size frequencies to determine the ages of yellowfin tuna in the Pacific and the tropical eastern Atlantic, respectively. Aikawa and Kato (1938) used the ame method in conjunction with counts of ertebral rings in studying the growth of western 'acific tunas, as did Partlo (1955) for northeastern 'acific albacore. Westman and Gilbert (1941) nd Westman and Neville (1942) used the method ı conjunction with scale studies for bluefin tuna ıken off Long Island, N.Y.

We have based our size-frequency study on ngths rather than on weights, as we believe ıat, for fish of a given age, lengths are subject) smaller and more regular variations. Because 'e lack sufficient data on the large sizes, we have not attempted to analyze lengths greater than 56.5 inches.

From various sources, we have compiled length measurements of 4,990 bluefin tuna less than 56.5 inches long. With the exception of the 1941 sample which was measured on Long Island by Westman and Neville (1942), and several fish less than 20 inches long which were from more southerly waters, most of these were taken in the New England area from 1950 to 1957. With the exception of a few specimens less than 20 inches long, the fish were caught from late June to mid-October. We have followed the method of Westman and Neville in measuring the fish to the nearest inch with a tape from the snout to the fork of the tail, following the curvature of the body. Where we used calipers for determining length, we estimated the "curved" measurement from a conversion factor.[2] The measurements for fish more than 20 inches long, for all localities and years combined, are listed by half monthly periods in table 3. The data for smaller fish were gathered from more diverse localities and extend over a greater portion of the year, hence are listed in more detail in table 4.

ABLE 3.—*Length frequencies of bluefin tuna from 20.5 to 56.5 inches long taken off Long Island [1] in 1941 and off New England [2] in 1950–57 from late June to mid-October*

Length in inches	Number of tuna							Age in years
	July		August		September		October	
	[3] 1–15	16–31	1–16	17–31	1–15	16–30	1–18	
	7							I
	9	31	4	1				
	5	33	13	9	4	1		
		25	17	31	42	4		
		4	12	10	58	7	2	
		1	1	1	26	14		
	1	2		1		3		
		5	3		1	2		
	23	24	10	3				II
	60	68	88	5	3	1		
	57	114	122	41	1	1	2	
	25	64	65	97	3	7	3	
	10	28	22	72	3	15	8	
	9	1	6	17	9	15	15	
				4	6	5	9	
	30	27	7	3				
	69	50	44	13	4	5	4	
	87	120	119	46	8	6	6	III
	53	100	178	153	24	6	8	
	14	56	141	253	40	26	22	
	1	20	96	203	94	29	26	
		7	31	112	76	28	18	
	1	8						
		2	9	33	52	23	10	
	13	10	4					
	19	15	11	11	16	14	5	
					4	2	3	
	28	17	18	23	8			IV
	37	14	11	57	9	4	6	
	58	11	8	23	8	2	11	
	29	8	7	6	15	6	13	
	24	3	4		9	4	21	
	5	3	6		5	1	9	
		1						
	5	1		4	1		7	
	5	2	2	1			7	
	2			2		2	2	
	5	2				2	1	
	1	3				1	6	
	2	2		4		2	6	
	3			5	1	3	1	

Westman and Neville's (1942) sample consisting of 1,129 fish, was meas- ed at Freeport, L.I., (N.Y.).

A few fish caught off Nova Scotia, Long Island (N.Y.), and New Jersey ɜ included. Most of this sample was taken in the vicinity of Cape Cod, ıt many of the fish were from the offshore waters, mostly in the vicinity Georges Bank. Frank Riley measured 1,891 fish at Provincetown (Mass.) 1953–54. We are indebted to Lewis R. Day of the Fisheries Board of ınada for measuring 5 fish in Nova Scotia in 1950, Jean McClean Wight of est Hartford (Conn.) for measuring 5 fish in Nova Scotia in 1954, Capt. ıarles A. Mayo, Jr., of Provincetown (Mass.) for measuring 57 fish there 1956, and Dr. Robert H. Gibbs, Jr., recently of the Woods Hole Oceano- ıphic Institution, for measuring 69 fish in the Cape Cod area in 1956 and 57. The remainder of the sample was measured by the authors and Donald . Allen.

Includes 102 fish measured June 28–30, 1953.

551440 O—60——2

TABLE 4.—*Lengths of bluefin tuna less than 20 inches long, with dates and localities of capture and sources*

Date	Length in inches	Number of fish	Locality	Source
June 9, 1953	1.8	1	Miami area, Fla	Rivas (1954).
July 14, 1953	11.7	1	do	Do.
July 17, 1953	12.3	1	do	Do.
July 19, 1953	10.3	1	do	Do.
July 16–23, 1954	12.0	1	Atlantic City, N.J.	William Upperman.[1]
July 19–26, 1954	9.0	1	do	Do.
July 23, 1953	11.4	1	Miami area, Fla	Rivas (1954).
July 23, 1957	7.7	1	do	Al Pflueger.[2]
July 24, 1953	11.8	1	do	Rivas (1954).
Do	12.9	1	do	Do.
July 25, 1954	12.7	1	do	Al Pflueger.[1]
July 26, 1953	11.9	1	do	Rivas (1954).
July 29, 1953	12.2	3	do	Do.
Do	13.5	1	do	Do.
July 30, 1953	11.2	1	do	Do.
July 31, 1953	11.7	1	do	Do.
July 31, 1954	12.0	2	do	Al Pflueger.[2]
Aug. 10, 1953	12.4	1	do	Rivas (1954).
Aug. 12, 1954	13.0	1	Brielle, N.J	Mrs. K. R. Mayer.[3]
Aug. 23, 1940	14.2	1	do	Manasquan Marlin and Tuna Club.
Aug. 25, 1953	9.0	1	do	Mrs. K. R. Mayer.[3]
Aug. 29, 1938	12.7	1	do	C. W. Hoffman.[1]
Aug. 29, 1952	15.5	1	Off Martha's Vineyard, Mass.	R/V *Bear*, R. Wolf.[2]
Sept. 2, 1939	12.5	1	Brielle, N.J	Westman and Gilbert (1941).
Sept. 1–7, 1953	12.7	4	Gulf of Mexico, (29°03′ N, 88°54′ W).	U.S. National Museum.[4]
Do	13.8	1	do	Do.[4]

See footnotes at end of table.

---

[2] A straight line fitted by inspection to a plot of straight (caliper) length against curved (tape) length, based on measurements for 185 individuals 37 to 257 cm. long, indicated that straight length was 0.958 of curved length.

Table 4.—*Lengths of bluefin tuna less than 20 inches long, with dates and localities of capture and sources*—Continued

Date	Length in inches	Number of fish	Locality	Source
Sept. 5, 1953	16.0	2	Brielle, N.J	Mrs. K. R. Mayer.[3]
Do	16.5	1	do	Do.[3]
Sept. 5, 1957	12.0	1	Ocean City, Md	F. J. Mather.
Sept. 6, 1952	15.6	1	Off Martha's Vineyard, Mass.	Do.
Sept. 7, 1957	12.0	1	Ocean City, Md	M. L. Dennis.
Do	13.0	1	do	Do.
Sept. 12, 1952	15.0	1	Off Long Island, N.Y.	Rivas (1954).
Sept. 12, 1953	9.8	1	Brielle, N.J	Mrs. K. R. Mayer.[3]
Do	11.0	1	do	Do.[3]
Do	14.0	3	do	Do.[3]
Sept. 14, 1957	13.2	20	Ocean City, Md	M. L. Dennis.
Sept. 15, 1953	18.0	1	Brielle, N.J	Mrs. K. R. Mayer.[3]
Sept. 17, 1952	14.1	1	Off Martha's Vineyard, Mass.	R/V *Caryn*, F. J. Mather.
Sept. 18, 1952	16.9	1	do	Do.
Sept. 20, 1957	14.0	1	Ocean City, Md	M. L. Dennis.
Sept. 21, 1954	13.9	1	Off the Carolinas, (33°10′ N, 77°25′ W).	U.S. Fish and Wildlife, Brunswick, Ga.
Sept. 21, 1957	31.0	3	Ocean City, Md	M. L. Dennis.
Do	14.0	1	do	Do.
Sept. 22, 1957	14.0	1	do	Do.
Do	15.0	1	do	Do.
Sept. 23-24, 1953	17.4	1	Off Martha's Vineyard, Mass.	M/V *Albatross III*, J. Taylor.[2]
Sept. 24, 1957	13.0	1	Ocean City, Md	M. L. Dennis.
Do	14.0	10	do	Do.
Do	15.0	6	do	Do.
Oct. 11, 1953	15.0	1	Brielle, N.J	Mrs. K. R. Mayer.[3]
Oct. 13, 1952	14.5	1	Cape Hatteras, N.C.	F. J. Mather.
Oct. 18, 1953	17.0	4	Brielle, N.J	Mrs. K. R. Mayer.[3]
Nov. 10, 1953	15.6	1	Miami area, Fla	Rivas (1954).
Nov. 12, 1952	17.7	1	do	Do.
Nov. 16, 1952	16.6	1	do	Do.
Nov. 27, 1952	17.6	1	do	Do.
Jan. 5, 1951	18.3	1	do	Do.
Jan. 27, 1959	18.8	3	Off Cape Hatteras, N.C.	M/V *Albatross III*. R. Brigham and L. Lawday.[3]

[1] Measurements were checked with ruler on photographic prints.

[2] Specimens were made available to us by kindness of the individuals listed.

[3] Measurements taken by charter boat captains who tagged the tuna, and collected for us by Mrs. Mayer.

[4] Measurements were made by Isaac Ginsburg and transmitted to us by Dr. L. P. Schultz.

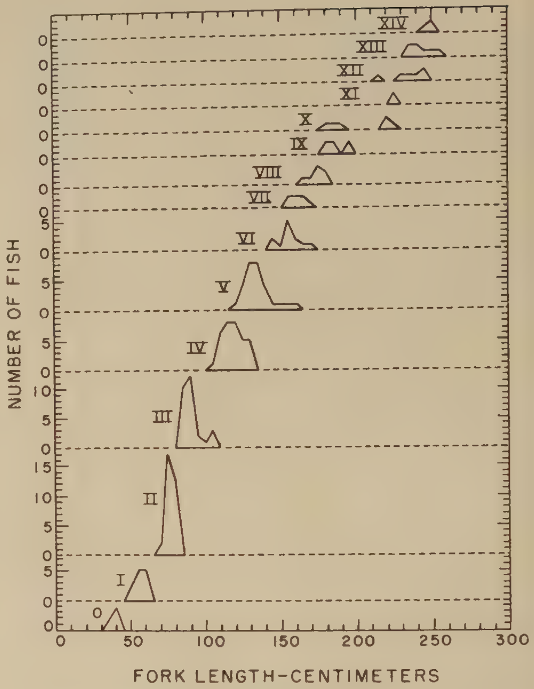

Figure 3.—Frequency distribution by 5-centimeter groups of lengths of bluefin tuna for counts of annuli.

The length frequencies for all localities combined between late June and mid-October are shown graphically for each half monthly period by years in figures 4–10, and for all years combined, by half monthly periods in figure 11. The number of fish in any given size group and period varies considerably from year to year, due to nonuniform sampling and availability, and to variations in the numerical strength of year classes. The general pattern of size groupings is consistent, however, with maximum and minimum numbers occurring around the same lengths year after year. It seems obvious that these groupings represent different ages. We have arbitrarily designated with vertical lines the points which we believe best separate the various age groups. Usually there seems to be little question as to where these lines should be drawn. If doubtful we based our judgment on a comparative study of data for the entire series of years. In a few such cases, we assigned some of the fish at a low point to one age and the rest to the other. Corresponding broken lines separate the data in table 3.

AGE DETERMINATION

The question arises as to whether or not the fish forming the first modal group appearing in our length frequency study are young of the year. In figure 12, we have compared the lengths of fish in each age group as determined by counts of annuli with the lengths of those in corresponding age groups as determined by length frequencies. On examining this figure, we find the assumption that fish in the first modal group are young of the

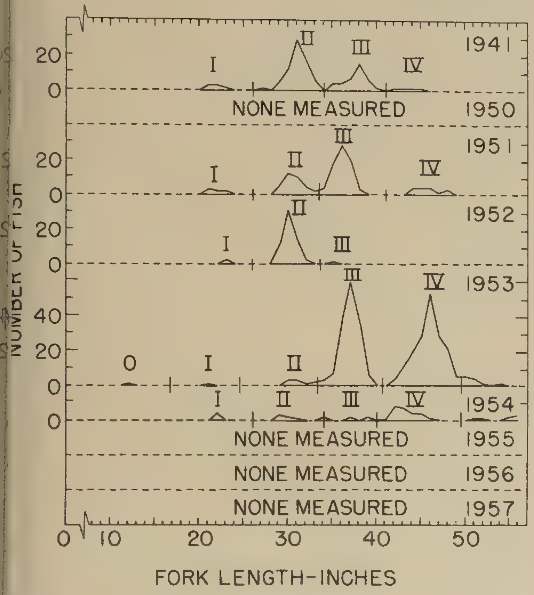

Figure 4.—Frequency distribution by 1-inch groups of lengths of bluefin tuna taken July 1–15, by years. The 1953 sample includes 102 fish measured June 28–30.

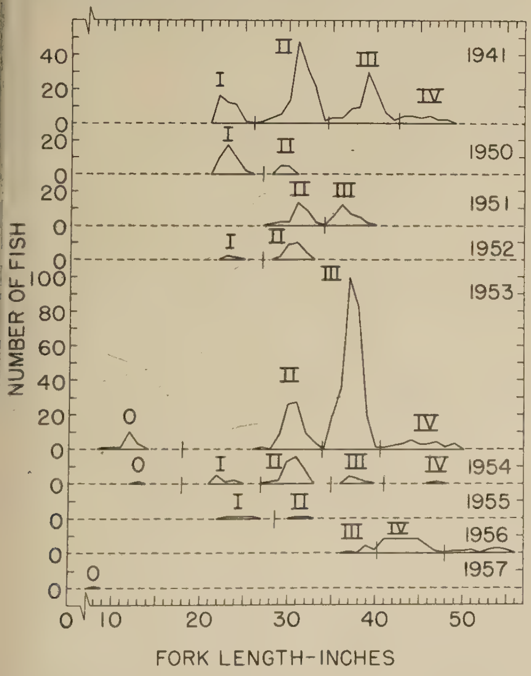

Figure 5.—Frequency distribution by 1-inch groups of lengths of bluefin tuna taken July 16–31, by years.

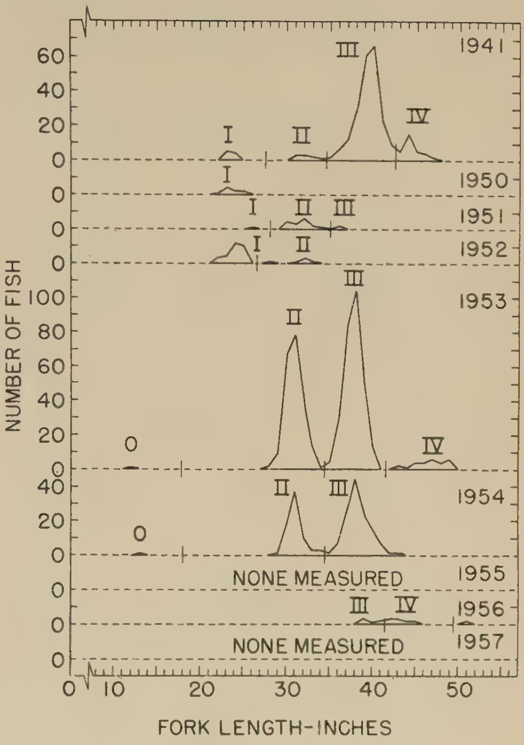

Figure 6.—Frequency distribution by 1-inch groups of lengths of bluefin tuna taken August 1–16, by years.

year is supported by the fact that no annuli are found on scales and vertebrae of fish of this size. Moreover, it is in accord with the conclusions of Sella (1929) and others studying the European bluefin tuna, which were officially accepted by the International Council for Exploration of the Sea in 1932 at Malaga (Conseil International pour l'Exploration de la Mer, 1933), and with those reached by Westman and Gilbert (1941), Westman and Neville (1942), and by Rivas (1954), for bluefin taken off New York and Miami, Fla. It is supported by our failure in all our observations, inquiries, and searching of literature and records, to find any evidence that a smaller size group exists. We conclude therefor that tuna in the second size group (corresponding to fish with 1 annulus) are 1 year old; in the third size group (2 annuli) are 2 years old; and so on through 4

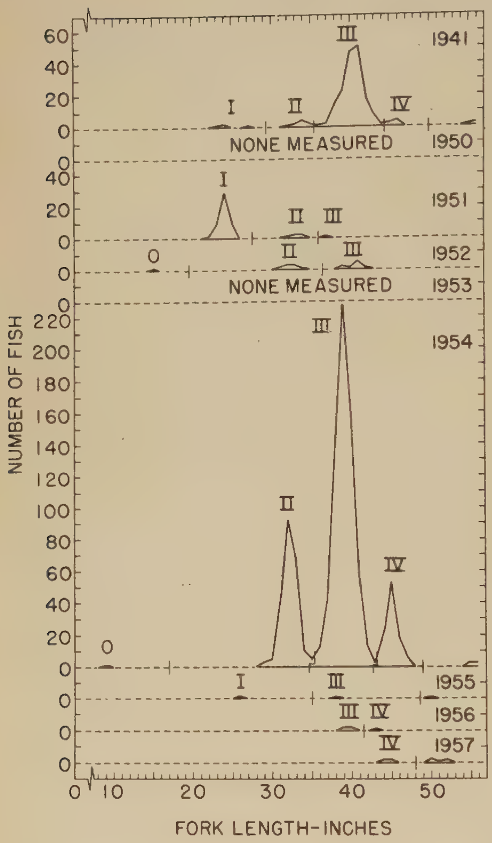

Figure 7.—Frequency distribution by 1-inch groups of lengths of bluefin tuna taken August 17–31, by years.

years. Although length data on older ages are not sufficient for analysis, we believe that counts of annuli are useful for estimating the age of older fish despite the decreasing reliability of readings with increasing age.

We find also that the analysis of length-frequency curves is consistent with age determinations by counts of annuli on scales and vertebrae. Such discrepancies as exist probably result from the fact that the samples for age readings were smaller and less uniformly distributed through the seasons than were those taken for length measurements. For example, most of our samples for counts of annuli of 3-year-olds were collected in early summer or fall rather than in midsummer. Even so, correspondence in conclusions reached from the two kinds of data is close.

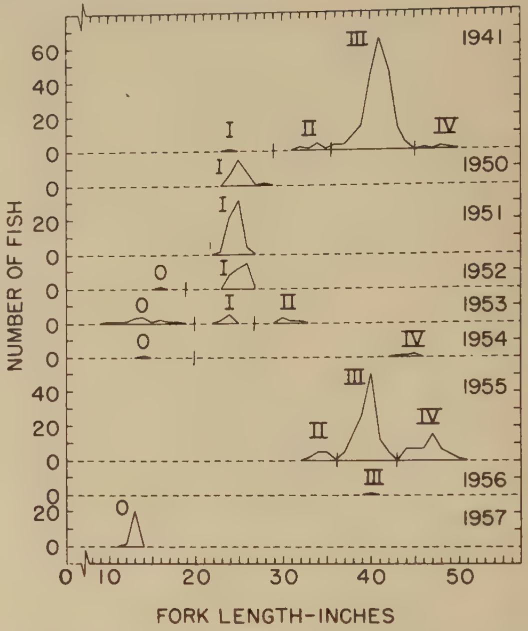

Figure 8.—Frequency distribution by 1-inch groups of lengths of bluefin tuna taken September 1–15, by years.

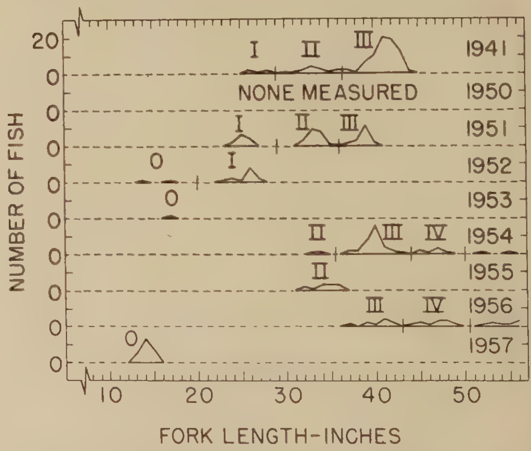

Figure 9.—Frequency distribution by 1-inch groups of lengths of bluefin tuna taken September 16-30, by years.

Weight frequencies of landings of medium-sized bluefin tuna in Cape Cod Bay and Nova Scotia in the years 1948–51 (fig. 13) show a tendency for modal weights to coincide with sizes determined by counts of annuli for ages 5–7. Most clear cut cases are the 5-year-olds in Cape Cod Bay and 6-year-olds in Nova Scotia in 1948,

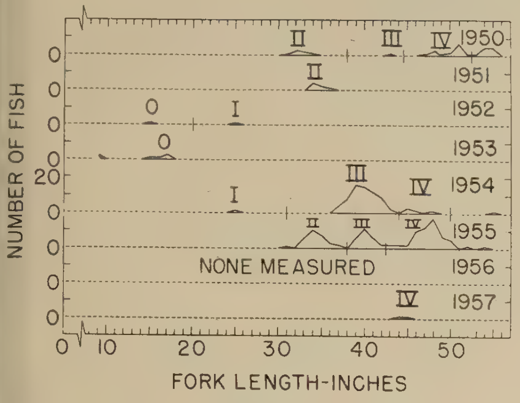

FIGURE 10.—Frequency distribution by 1-inch groups of lengths of bluefin tuna taken October 1–18, by years.

and the 6-year-olds in Nova Scotia in 1949. Split modes show a preponderance of 7-year-olds in both areas in 1950, suggesting the progression of the year class of 1943 through the Cape Cod Bay fishery 1948–50 and the Nova Scotia fishery 1949–50.

Two successful tagging experiments with bluefin tuna yielded approximate data on their actual growth. One fish, tagged off Cape Cod, Mass., July 27, 1954, was recaptured by French fishermen in the Bay of Biscay August 16, 1959. When tagged, the fish measured 72.5 cm., and its weight when recaptured was reported as approximately 65–70 kilograms (143–154 pounds equivalent to about 150–154 cm.). These sizes are near the lower limits for ages 2 and 7, respectively, from table 1. The other was tagged August 11, 1957, off Chatham, Mass., and recaptured August 30, 1959, off Gloucester, Mass. Its weight when tagged was estimated as 65 pounds (equivalent to about 114 cm.) by an experienced fisherman, and it weighed 130 pounds (equivalent to about 150 cm.) when recaptured. These lengths are in good agreement with those listed in table 1 for ages 4 and 6, respectively. Hence the results of these experiments are in reasonable agreement with our age determinations by counts of annuli.

GROWTH OF YOUNG BLUEFIN TUNA

As length measurements are several times as numerous as counts of annuli, and permit us to trace growth during each summer as well as from year to year, we shall base our discussion of growth of young tuna on length frequency analysis.

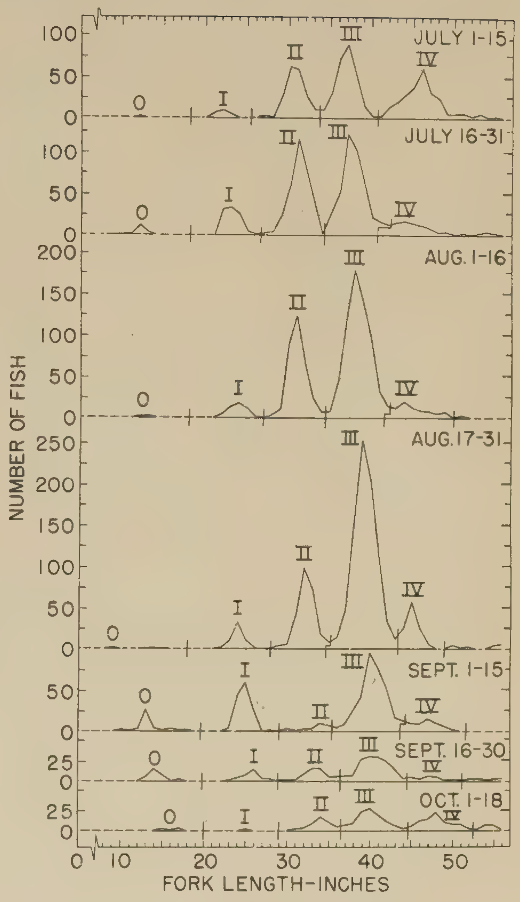

FIGURE 11.—Frequency distribution by 1-inch groups of lengths of bluefin tuna taken in 1941 off Long Island and in 1950–57, mostly off New England, by periods. Three very small tuna taken off New Jersey in 1938–40 are also included.

Table 5 lists the average lengths of the fish in each age group of fish more than 20 inches long, as demarcated by vertical lines in figures 4–11. It identifies year classes and also shows average lengths for all years combined. We plotted these lengths by periods in figure 14 and fitted curves to them empirically, taking into account the number of measurements represented by each point, except in 2 or 3 where the preponderant samples were not, in our opinion, composed of average-sized fish.

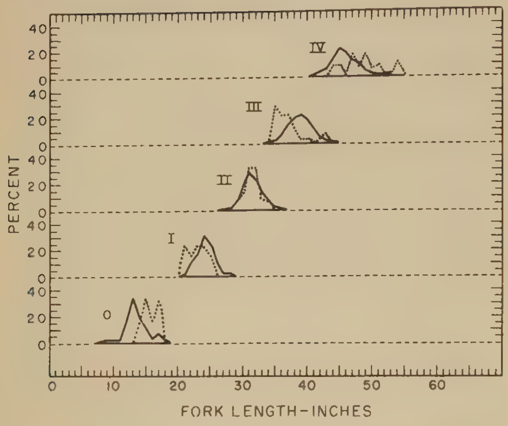

Figure 12.—Frequency distribution by 1-inch groups of lengths of bluefin tuna for age groups 0–IV as determined by length frequencies (solid lines) and by counts of annuli (dotted lines).

The fish less than 20 inches long listed in table 4 obviously form a distinct age group. Figure 15 shows the averages of these measurements with a curve drawn by inspection to fit the points and also to fit in with the curve for 1-year-olds from figure 14. Although our unpublished studies of the distribution of the bluefin tuna indicate that all these fish belong to one population, samples from different areas have been designated by different symbols. Figure 16 shows a curve of estimated growth of bluefin tuna for the first 4½ years of life, and table 6 lists the average sizes at the middle of each month, as indicated by this curve.

Figure 16 indicates extremely rapid initial growth and distinct seasonal variations in growth rate. Bluefin tuna spawn during an undefined period in spring (Rivas, 1954; Bullis and Mather, 1956). Assuming, as we did in drawing figure 16, that hatching occurs in mid-May, the young may grow at a rate of nearly 6 inches per month to reach a size of 8½ inches by July 1. In the ensuing discussion, however, we shall consider July 1 as the date of birth and shall refer to the period July 1–October 16 as "summer" and the remainder of the year as "winter." The growth rate diminishes rapidly during the first summer, but the average rate is estimated at 2 inches per month. The rate continues to decrease during most of the first winter, averaging about four-fifths of an inch per month. For the remainder of the period studied, ages 1–4, the growth rate does not change greatly with age, averaging about 1½ inches per month in summer and about one-third of an inch per month in winter.

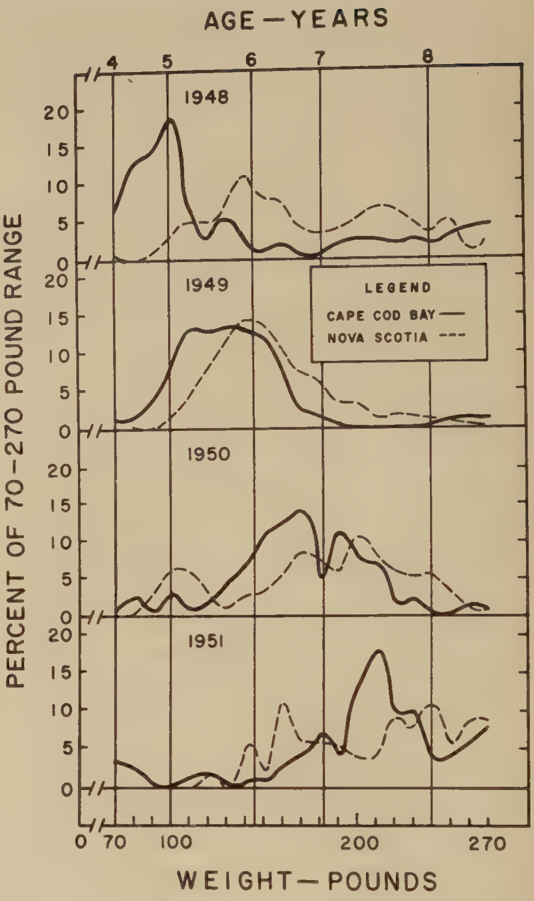

Figure 13.—Weight frequencies by 10-pound groups of bluefin tuna from 70 to 270 pounds, taken in Cape Cod Bay and off Nova Scotia in 1948–51, by years.

ESTIMATED ANNUAL GROWTH OF BLUEFIN TUNA THROUGH 10 YEARS

The average sizes at each age, determined by length frequency analysis for ages 0–4, and by counts of annuli for older ages, are plotted in figure 17. The curve shown was derived graphically, starting from the point for 3-year-olds, from the

Walford (1946) transformation of our data. As we found it possible to read only a small percentage of the material available for ages beyond 10 years, we have drawn the curve to that point only. Average sizes at mid-summer for bluefin tuna of ages 0–10 as indicated by this curve are listed in table 7.

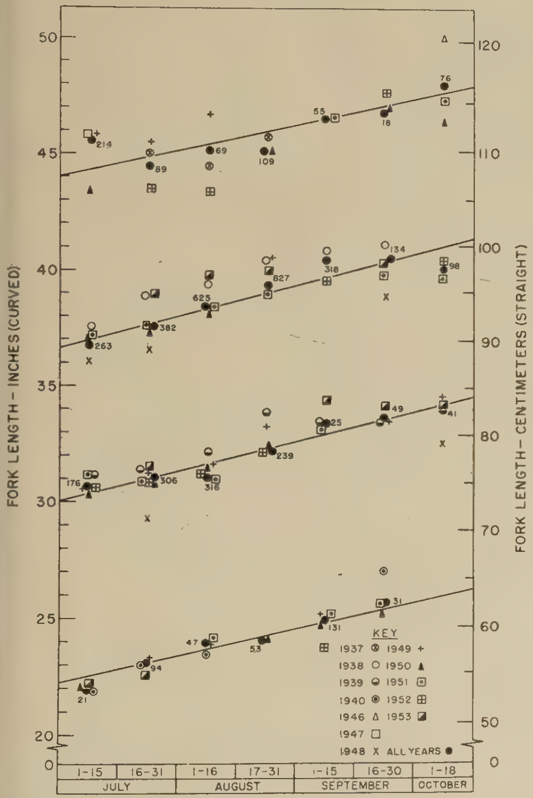

Figure 14.—Average lengths of bluefin tuna by age groups as indicated in figures 4 to 11. Curves were fitted empirically. The numbers of fish in the samples for all years combined are indicated. Samples consisting of less than 5 fish were not shown.

CONCLUSIONS

Our results through the fifth summer of life for bluefin tuna taken off New England are substantially in agreement with those of Westman and Neville (1942) for fish taken off Long Island. Our study of the growth of these young tunas, however, was based on a much larger sample, and the sampling was spread over several years rather than 1 year. Differences in growth between year classes were found to be slight and the results of the analysis of the composite sample are believed to approximate the average encountered in nature. Although it was not possible to fully verify the readings of annuli for older fish by the analysis of size frequencies, and difficulties in reading the annuli increased with their number, we have extended our determinations to considerably older ages than has previously been done for western Atlantic bluefin tuna.

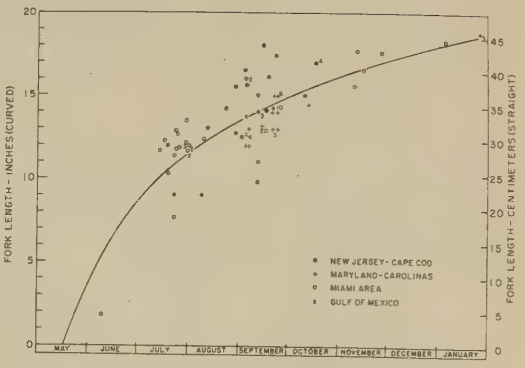

Figure 15.—Lengths of bluefin tuna less than 20 inches long (young of the year), from table 4. The curve of estimated growth was fitted by inspection.

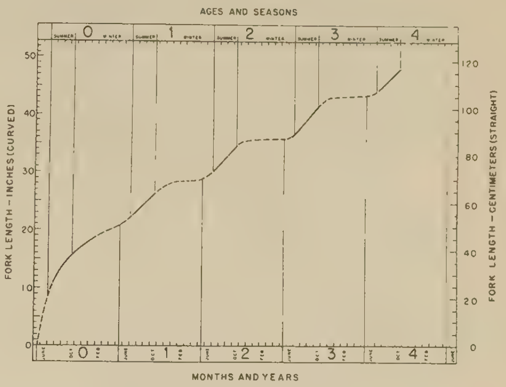

Figure 16.—Estimated growth of young bluefin tuna. Broken lines indicate estimated lengths in periods for which data are lacking. The upper scale shows ages and seasons as assumed in the text, and the lower scale shows ages assuming that hatching occurs at mid-May.

TABLE 5.—*Average lengths of bluefin tuna, in each age group as indicated in figures 4 to 11, listed by ages, years of measurement, and year classes*

Age in years	Year of measurement	Average lengths of fish in inches (numbers of fish in parentheses)							Year class
		July		August		September		October	
		1–15	16–31	1–16	17–31	1–15	16–30	1–18	
I	1941	21.8(7)	22.9(40)	23.4(9)	24.5(4)	24.0(1)	27.0(5)	------	1940.
	1950	------	23.1(39)	23.6(9)	------	25.2(29)	------	------	1949.
	1951	21.9(7)	------	26.0(1)	24.0(48)	24.6(59)	25.1(12)	------	1950.
	1952	23.0(2)	23.3(3)	24.0(28)	------	25.2(35)	25.6(14)	25.0(1)	1951.
	1953	21.0(1)	------	------	------	23.7(7)	------	------	1952.
	1954	22.0(4)	22.6(8)	------	------	------	------	25.0(1)	1953.
	1955	------	24.5(4)	------	26.0(1)	------	------	------	1954.
	All years	21.9(21)	23.1(94)	23.9(47)	24.1(53)	24.8(131)	25.6(31)	25.0(2)	All years.
II	1941	31.1(71)	31.3(126)	32.1(9)	33.8(9)	33.5(8)	33.3(14)	------	1939.
	1950	------	29.2(10)	------	------	------	------	32.5(7)	1948.
	1951	30.5(33)	31.2(29)	31.6(16)	33.2(5)	------	33.4(21)	34.6(7)	1949.
	1952	30.2(57)	30.7(25)	31.4(6)	32.3(9)	------	------	------	1950.
	1953	31.2(9)	30.7(75)	30.9(214)	------	31.1(5)	------	------	1951.
	1954	30.8(7)	30.6(39)	31.2(71)	32.2(216)	------	33.5(2)	------	1952.
	1955	------	31.5(2)	------	------	34.4(13)	34.2(12)	34.2(29)	1953.
	All years	30.6(176)	30.9(306)	31.0(316)	32.2(239)	33.3(25)	33.6(49)	33.9(41)	All years.
III	1941	37.5(37)	38.9(78)	39.3(208)	40.4(163)	40.8(202)	41.1(72)	------	1938.
	1950	------	------	------	------	------	------	43.0(1)	1947.
	1951	36.0(72)	36.5(30)	36.0(2)	37.0(1)	------	38.8(17)	------	1948.
	1952	35.0(1)	------	------	40.5(9)	------	------	------	1949.
	1953	36.9(147)	37.2(259)	37.8(285)	------	------	------	------	1950.
	1954	37.2(5)	37.6(8)	38.4(126)	39.0(648)	------	39.8(34)	39.8(65)	1951.
	1955	------	------	------	38.0(1)	39.6(113)	------	40.4(27)	1952.
	1956	------	39.0(7)	39.8(6)	40.0(5)	40.0(1)	40.3(10)	------	1953.
	All years	36.7(263)	37.5(382)	38.4(625)	39.3(827)	40.4(318)	40.5(134)	40.1(98)	All years.
IV	1941	43.5(4)	45.0(19)	44.4(30)	45.7(6)	47.9(4)	------	------	1937.
	1950	------	------	------	------	------	------	50.0(15)	1946.
	1951	45.8(16)	------	------	------	------	------	------	1947.
	1953	45.8(169)	45.5(24)	46.7(27)	------	------	------	48.0(1)	1949.
	1954	43.3(25)	47.0(1)	------	45.1(99)	44.3(4)	47.0(8)	46.3(6)	1950.
	1955	------	------	------	------	46.6(48)	------	47.4(55)	1951.
	1956	------	43.5(45)	43.4(10)	------	------	47.7(11)	------	1952.
	1957	------	------	------	44.5(4)	------	------	44.5(2)	1953.
	All years	45.5(214)	44.4(89)	45.1(69)	45.1(109)	46.5(55)	46.8(18)	48.0(76)	All years.

TABLE 6.—*Estimated sizes of young bluefin tuna at the middle of each month derived from figure 16*

Month	Fork length in inches curved measurement					Fork length in centimeters straight measurement					Weight in pounds				
	Age in years					Age in years					Age in years				
	0	I	II	III	IV	0	I	II	III	IV	0	I	II	III	IV
May	0	21.0	28.7	35.8	43.5	0	51.1	69.9	87.1	106.0	0	6.2	15.5	31.2	51.0
June	6.5	21.7	29.5	36.2	43.7	15.8	52.8	71.8	88.1	106.7	0.2	6.8	17.0	32.0	52.0
July	10.3	22.7	30.6	37.3	44.5	25.1	55.3	74.5	90.9	108.5	0.6	7.8	19.0	34.0	55.0
August	12.6	23.9	32.0	38.6	45.7	30.6	58.2	77.6	94.0	111.3	1.1	9.4	22.0	36.5	60.5
September	14.3	25.0	33.2	40.0	46.9	34.8	60.9	80.9	97.4	114.1	1.9	10.0	24.4	42.0	65.0
October	15.3	26.1	34.5	41.4	48.0	37.2	63.5	84.0	100.8	117.0	2.1	11.5	26.5	46.0	68.0
November	16.7	27.2	35.3	42.6	------	40.6	66.2	85.9	103.9	------	2.9	13.5	29.0	49.0	------
December	17.6	27.8	35.4	43.0	------	42.9	67.7	86.2	104.8	------	3.5	14.2	30.0	49.5	------
January	18.4	28.2	35.5	43.1	------	44.8	68.6	86.4	105.0	------	4.1	14.6	30.4	50.0	------
February	19.1	28.3	35.6	43.2	------	46.5	68.9	86.6	105.1	------	4.6	14.9	30.6	50.2	------
March	19.7	28.4	35.7	43.3	------	48.0	69.1	86.9	105.3	------	5.0	15.1	30.8	50.4	------
April	20.2	28.5	35.8	43.4	------	49.1	69.4	87.1	105.7	------	5.4	15.3	31.0	50.7	------

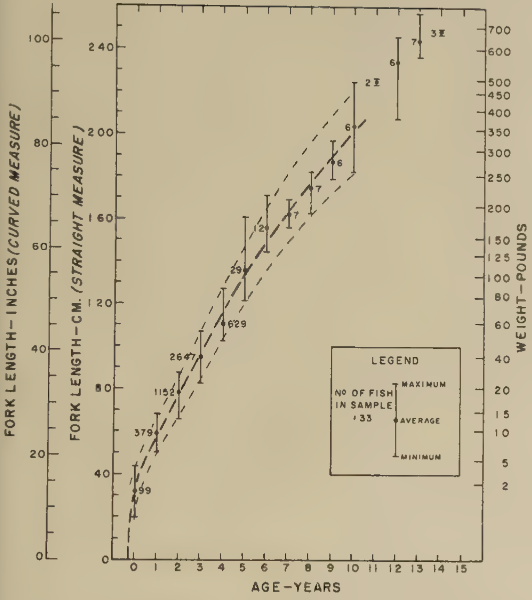

Figure 17.—Estimated growth curve for bluefin tuna (heavy broken line), with points derived from length frequencies for ages 0–IV years and from counts of annuli for older ages. Lighter broken lines, fitted by inspection, show estimated limits of variation.

Table 7.—*Estimated sizes of bluefin tuna during the summer for ages 0–10 years*

From figure 17

Age in years	Length				Weight in pounds	
	Centimeters (straight)		Inches (curved)			
	Average	Range	Average	Range	Average	Range
0	32	22–43	13.0	9–18	1.5	0.6–3.5
I	57	50–66	23.5	20–27	8.5	5–13
II	77	66–88	31.5	27–36	22.0	14–30
III	95	83–109	39.0	34–45	40	25–50
IV	114	102–127	47.0	42–52	69	45–90
V	133	122–148	55.0	50–61	100	80–140
VI	149	134–165	61.5	55–68	140	105–190
VII	163	148–182	67.0	61–75	185	140–250
VIII	177	161–197	73.0	66–81	240	180–320
IX	190	172–210	78.0	71–86	290	220–395
X	201	182–221	82.5	75–91	340	255–455

Our growth data for fish up to 10 years of age are in good agreement with those of Sella (1929) for Mediterranean bluefin tuna. Our few readings for older ages indicated somewhat larger sizes for western Atlantic fish for the respective ages. Sella's work was based on a larger sample than ours, and he used special instruments which we did not have. Therefore this apparent difference may result from less complete sampling and less precise reading of annuli for the western Atlantic bluefin, rather than to an actual difference in the growth of the larger fish from the respective areas.

LITERATURE CITED

Aikawa, Hiroaki, and M. Kato.
1938. Age determination of fish (Preliminary Rept. 1). Bull. Japanese Society Scientific Fisheries, vol. 7, No. 1, pp. 79–88. Translation from the Japanese by W. G. Van Campen in U.S. Department of the Interior, Fish and Wildlife Service, Special Scientific Report—Fisheries No. 21.

Arnold, Edgar L., Jr.
*1951. An impression method for preparing fish scales for age and growth analysis. U.S. Department of the Interior, Fish and Wildlife Service, Progressive Fish Culturist, vol. 13, pp. 11–16.

Bullis, Harvey R., Jr., and F. J. Mather, III.
1956. Tunas of the genus *Thunnus* of the northern Caribbean. American Museum Novitates, No. 1765, pp. 1–12.

Conseil International pour l'Exploration de la Mer.
1933. Conference d'experts pour l'examen des méthodes scientifiques et techniques à appliquer à l'étude des poissons de la famille des thonidés. Conseil International pour l'Exploration de la Mer, Rapports et Procès-Verbaux, vol. 84, pp. 91–103.

Galtsoff, Paul S.
1952. Staining of growth rings in the vertebrae of tuna (*Thunnus thynnus*). Copeia, No. 2, pp. 103–105.

Moore, Harvey L.
1951. Estimation of age and growth of yellowfin tuna (*Neothunnus macropterus*) in Hawaiian waters by size frequencies. U.S. Department of the Interior, Fish and Wildlife Service, Fishery Bulletin, No. 65, vol. 52, pp. 133–149.

Partlo, J. M.
1955. Distribution, age and growth of eastern Pacific albacore (*Thunnus alalunga* Gmelin). Journal of the Fisheries Research Board of Canada, vol. 12, pp. 35–60.

Postel, E.
1954. La croissance du thon á nageoires jaunes *Neothunnus albacora* (Lowe) dans l'Atlantique tropical. Bulletin de la Société Zoologique de France, vol. 79, No. 2–3, pp. 85–90.

Rivas, Luis Rene.
1954. A preliminary report on the spawning of the western North Atlantic bluefin tuna (*Thunnus thynnus*) in the Straits of Florida. Bulletin of Marine Science of the Gulf and Caribbean, vol. 4, pp. 302–322.

Sella, Massimo.
1929. Migrazioni e habitat del tonno (*Thunnus thynnus* L.) studiati col metodo degli ami, con osservazioni su l'accrescimento, sul regime delle tonnare ecc. R. Comitato Talassografico Italiano.

SELLA, MASSIMO.
Mem. 156, pp. 3–24. Translation in U.S. Department of the Interior, Fish and Wildlife Service, Special Scientific Report—Fisheries No. 76.

WALFORD, LIONEL A.
1946. A new graphic method of describing the growth of animals. Biological Bulletin, vol. 90, pp. 141–147.

WESTMAN, J. R., and P. W. GILBERT.
1941. Notes on age determination and growth of the Atlantic bluefin tuna, *Thunnus thynnus* (Linnaeus). Copeia, No. 2, pp. 70–72.

WESTMAN, JAMES R., and W. C. NEVILLE.
1942. The tuna fishery of Long Island, New York. Board of Supervisors, Nassau County, Long Island, N.Y., pp. 1–31.

○

Library of Congress catalog card for the series, Fishery Bulletin of the Fish and Wildlife Service:

U. S. *Fish and Wildlife Service.*
Fishery bulletin. v. 1–
Washington, U. S. Govt. Print. Off., 1881–19
v. in illus., maps (part fold.) 23–28 cm.

Some vols. issued in the congressional series as Senate or House documents.

Bulletins composing v. 47– also numbered 1–
Title varies: v. 1–49, Bulletin.
Vols. 1–49 issued by Bureau of Fisheries (called Fish Commission, v. 1–23)

1. Fisheries—U. S. 2. Fish-culture—U. S. I. Title.
SH11.A25 639.206173 9—35239*

Library of Congress [59r55b1]

Contribution No. 990

DISSOLVED SILICATE AND RELATED PROPERTIES OF SOME WESTERN NORTH ATLANTIC AND CARIBBEAN WATERS[1]

BY

FRANCIS A. RICHARDS

Woods Hole Oceanographic Institution

> "*As marine plants are the ultimate source of food for much of the animal life in the sea, the role played by silicon is of fundamental importance*".
>
> T. G. Thompson and R. J. Robinson, 1932

ABSTRACT

Dissolved silicate, phosphate, nitrate, and oxygen as well as salinity and temperature were observed in several regions around the Antilles Arc and in the Woods Hole-Bermuda area. It is shown that silicate is generally in low concentration in surface waters, where its ratio to phosphate, nitrate and oxygen consumption is variable. At intermediate depths, silicate, phosphate and nitrate regeneration and oxygen consumption (AOU) proceed in the ratios, by atoms, of Δ AOU: Δ Si: Δ N: Δ P $= 270:16:16:1$. In some of the water masses, silicate, nitrate and phosphate occur in these same ratios but are in excess of the amount of regeneration expected from the amount of oxygen consumption. However, silicate is clearly and linearly related to biological processes. In other water masses, notably in deep water of the North Atlantic, the Puerto Rico Trench and the eastern Caribbean Sea, and in anaerobic water of the Cariaco Trench, there are higher concentrations of silicate than would be expected from the amounts of phosphate present. These may originate from *in situ* re-solution of skeletal remains of diatoms or from re-solution of bottom deposits followed by upward diffusion.

Introduction. The wide variability of silicate in the ocean should make it a valuable characteristic for tracing water masses, and its biological involvement in the sea is of special interest. Although silicate is used in relatively large quantities by only a few groups of organisms, principally diatoms, these occur in large numbers and are important primary producers of organic matter. This special relationship between silicate, the diatoms, and organic production sets silicon apart from nitrogen and phosphorus, which are used by all organisms. Some of the silicate which diatoms fix concurrently with

---

[1] Contribution No. 990 from the Woods Hole Oceanographic Institution.

REPRINT FROM JOURNAL OF MARINE RESEARCH, VOLUME 17, 1958

their organic matter is redissolved in the water column upon their death and thus re-enters the ecological cycle. The balance eventually becomes incorporated in bottom sediments, there to become a part of the geological record and to represent a phase in the geochemical migration of silicon. This paper relates the distribution of silicate in several oceanic areas to the biological cycle through nitrogen, phosphorus and dissolved oxygen and to hydrography through its distribution and temperature-salinity correlations.

Studies of seasonal variations in silicate have demonstrated a close relationship between diatom growth and depletion of silicate from the water, and conversely, between regeneration of silicate and a decrease in the diatom population (Rabin, 1905a, b, 1910, 1914; Brandt, 1920; Atkins, 1923a, b, 1926a, b, 1928, 1930; Thompson and Johnson, 1930; *et al.*). Studies of silicate and its distribution have been made by Clowes (1938), by Graham and Moberg (1944), and by others. The data of Atkins (1928, 1953, *inter alia*), Cooper (1933, *et seq.*), and others of the laboratory of the Marine Biological Association at Plymouth, England, show seasonal variations in silicate and phosphate which are more or less parallel; Cooper's paper on factors affecting the distribution of silicate shows (1952: fig. 1) an approximately linear relationship between phosphate and silicate between about 25 and 600 m at a station in the Bay of Biscay.

It has been stated that silicate in the ocean increases continuously with depth (Sverdrup, *et al.*, 1942; Graham and Moberg, 1944), but some of the DISCOVERY data (Discovery Committee, 1941: Sts. 1162–1184) show silicate maxima at slightly less than 1000 m in the equatorial and South Atlantic. This type of vertical distribution was the rule in a series of stations occupied by ATLANTIS in the equatorial Atlantic in 1952. The maxima were clearly associated with the phosphate maxima and oxygen minima. These observations made it clear that some features of the silicate distribution resulted from closely correlated biological phenomena.

Observations. Silicate was determined in samples from the eastern Venezuelan Basin and the Cariaco Trench in the Caribbean Sea; the Atlantic region east of the Windward Islands from Tobago to Martinique; the Puerto Rico Trench-Anegada Passage region (Table I); and the area between Woods Hole and Bermuda. Observations between Woods Hole and Bermuda were made on R/V BEAR Cruise 185, May 12 to 16, 1958 and R/V CRAWFORD Cruise 19,

TABLE I. Stations in the Antilles Arc Region

Date	*Station Number*	*North Lat.*	*West Long.*	*Bottom Depth (m)*	*Depths at which eq. (1) is Satisfied*
Venezuelan Basin					
1955					
12. II	5272	13°30′	65°24′	3860	Phosphates not available
14. II	5273	14 14	63 25	1464	Phosphates not available
6. III	5282	13 09	62 15	2885	192–482; 867
7. III	5283	14 13	62 55	1483 ?	195–781
9. III	5284	16 03	66 02	4301	267–806
Anegada-Jungfern Passages					
12. III	5285	17°54′	65°51.5′	1955	188–1038; 1623–1818 (d.s.)
14–15. III	5286	17 53	65 20	3820	266–1030; 1850–3440 (d.s.)
15. III	5287	17 54.5	64 16	1975	279–854
Puerto Rico Trench Region					
17. III	5288	18°52′	63°05′	5880	455–2898
19. III	5289	19 56	62 50	6050	406–1461
20–21. III	5290	19 54	64 32	7260	385–2395
22. III	5291	19 52	66 35	7690	352–1964
East of the Windwards					
19. II	5274	14°80′	60°42′	1089	140–488
21. II	5275	13 54	59 47	717	147–495
22. II	5276	13 25	58 19	2880	197–2750 (d.s.)
23. II	5277	13 50	56 53	4812	189–2387
24. II	5278	12 36	58 34	1851	195–1744 (d.s.)
26. II	5279	12 41	59 40	1020	181–561
Cariaco Trench Region					
1957					
1. XI	5596	10°52′	66°00′	185	54–161
1. XI	5597	10 06	66 05	260	200–230 (not in Trench)
2. XI	5597 A	10 48	65 52	252	150–245
2. XI	5598	10 44	65 54	412	200
4. XI	5599	10 19	65 32	58	none
4. XI	5600	10 28	65 43	554	200 only
4. XI	5601	10 37	65 32	722	none sampled
5. XI	5602	10 52	65 33	845	197, 342
6. XI	5603	11 15	65 07	784	174–498 (not in Trench)
6. XI	5604	10 54	65 08	58	none
6. XI	5605	10 38	65 08	933	228 only
8. XI	5606	10 32	64 40	1343	186 only
8. XI	5607	10 32	64 41	1337	196 only

d.s. = deepest sample.

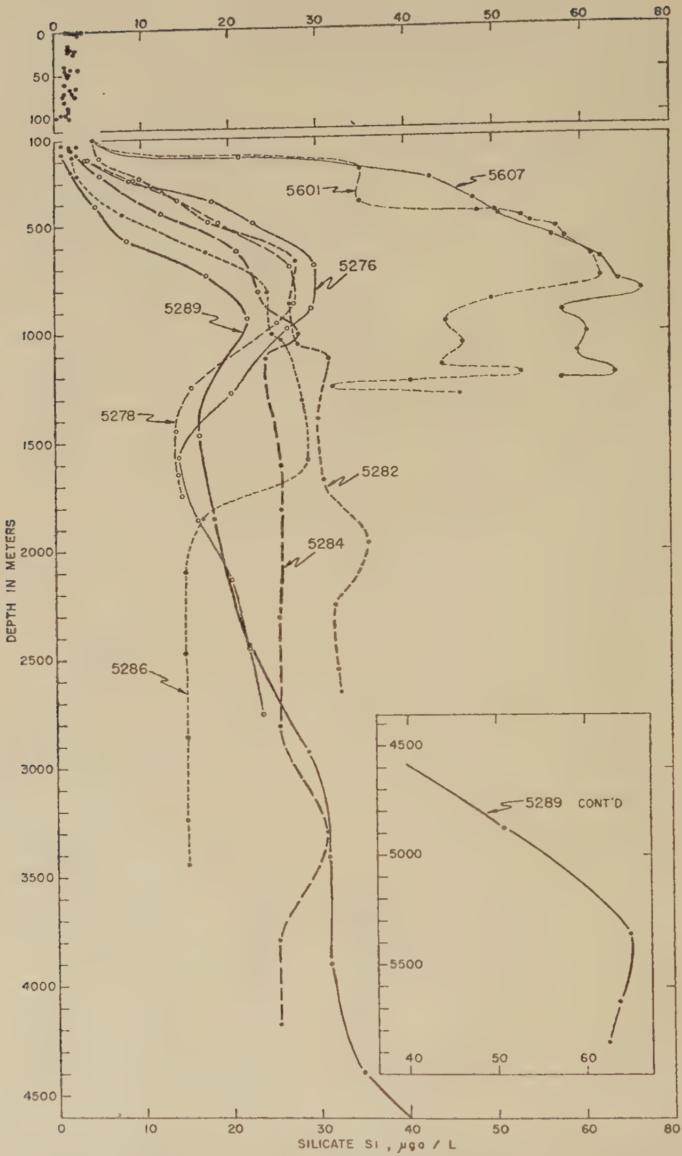

Figure 1. Silicate concentrations *vs* depth at representative stations in the Antilles Arc region. Sts. 5601 and 5607 in the Cariaco Trench; 5282 and 5284, Venezuelan Basin; 5276, 5278, Atlantic Ocean east of the Windwards; 5289, Puerto Rico Trench; 5286, Anegada-Jungfern Passage region. Open circles correspond to those in Figs. 3 and 4.

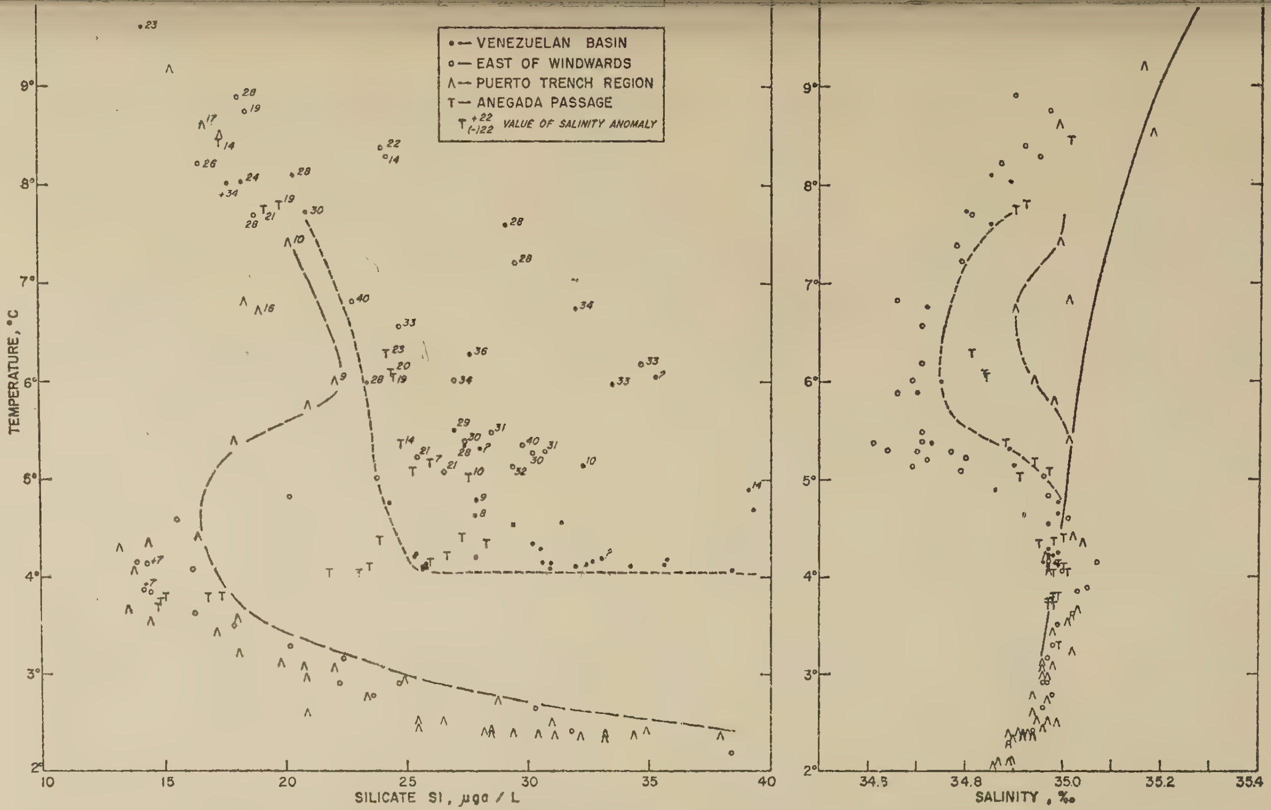

Figure 2. Temperature-silicate and temperature-salinity correlations. The solid curve is Iselin's (1936) correlation for western Sargasso Sea waters. Numbers on the temperature-silicate diagram are salinity anomalies and are negative unless otherwise indicated. Points having no numbers have salinity anomalies less than ± 5. Question marks indicate no salinity values are available. The short dashes envelope the samples from the Venezuelan Basin on the T/Si diagram, and those from the Puerto Rico Trench and from east of the Windwards on the T/S diagram. The long dashes envelope the samples from the Puerto Rico Trench on both diagrams. All samples from between Woods Hole and Bermuda having more than 20 μg-at silicate-Si/l (Crawford Cruise 19) come from depths greater than 2500 m.

July 7 to 19, 1958; locations of the stations on these two cruise are shown by Ketchum, *et al.* (1958: fig. 1). Temperature, salinity dissolved oxygen, inorganic phosphate, total phosphorus, and silicat were observed. Nitrate data are also available for the Woods Hole-Bermuda samples, and sulfides were determined for the Cariac Trench samples.

Analytical Methods. Impetus has recently been given to the stud of silicates by the introduction of the new sensitive and reproducibl analytical methods of Armstrong (1951) and Mullin and Riley (1955) Samples from the Antilles Arc regions were analyzed by Armstrong' method directly after collection; color comparisons were made wit the photoelectric colorimeter described by Ford (1950), using a re (Corning No. 2404) filter.

The remaining samples, including those from the Cariaco Trench were analyzed using Armstrong's system of internal standards combined with Mullin and Riley's reagents and procedures; a Beckma Model DU Spectrophotometer was used for color comparison i these determinations (one cm cells, 812 mμ). These samples, immediately frozen in polyethylene bottles, were so kept until abou 12 hours prior to analysis, when they were thawed and allowed t come to room temperature. Experience in this laboratory has show this to be a satisfactory procedure for phosphates, nitrates, and nitrites (Ketchum, *et al.*, 1958) as well as for silicates.

Depth Distribution. Plots of silicate against depth at representativ stations in the area studied (Fig. 1) often show distinct silicate maxima at intermediate depths (800 to 1200 m), decreases at greate depths to secondary minima (1400 to 1800 m), and increasing concentrations with depth below 1800 m. Exceptions to this rule ar found in the Venezuelan Basin, where the high concentrations observed at 800 to 1200 m are maintained into water of greater dept than 1200 m. The silicate concentrations in the Cariaco Trenc (Sts. 5601, 5607) are much higher than those at other location sampled, but maxima occur at about 800 m. The high silicate concentrations observed in the Venezuelan Basin between 1100 an 2600 m are in striking contrast to concentrations in waters of simila depth in western North Atlantic water masses. The differences obvious on both depth-silicate and temperature-silicate diagram (Fig. 2), may prove useful in indicating the isolation of the deepe Caribbean water.

Hydrography. In the region of the Antilles Arc, the Atlantic currents generally flow westward and northwestward. In the northern part of the region (represented by the Puerto Rico Trench stations, Fig. 2), the "salt half" of the North Equatorial Current (Montgomery, 1938) carries water through the island passages into the northern part of the Venezuelan Basin. This "North Atlantic" water is close to Iselin's (1936: figs. 25 and 53) western Sargasso Sea water in its temperature-salinity characteristics, though a trifle fresher in part of the temperature range (Fig. 2). The deepest of this water which can enter the Caribbean does so through the Jungfern Passage, which, according to Frasetto and Northrop (1957), has a controlling sill depth of 1072 fathoms (1961 m).

In the southern part of the region (represented by the stations east of the Windward Islands), the fresh tongue of the North Atlantic Equatorial Current (between 5 and something above 10° C; 400 to 1000 m) contains admixtures of Antarctic Intermediate water which are significantly fresher than western Sargasso Sea water. The deepest sill along the Windwards, which according to Sverdrup, *et al.* (1942) is between Dominica and Martinique, has a depth of less than 1500 m.

The Cariaco Trench is an isolated basin to the south of the Venezuelan Basin. Its sill has a maximum depth of about 150 m, and below this depth the basin is so poorly ventilated that it has become anaerobic and contains sulfides from about 400 m to the bottom at about 1400 m (Richards and Vaccaro, 1956).

Silicate-Temperature-Salinity Relationships. The water masses of the Antilles Arc region have been characterized by plotting silicate and salinity, respectively, against temperature (Fig. 2). These diagrams are useful, at temperatures below 7° C, in distinguishing water of four areas: (a) The eastern Venezuelan Basin; (b) The Atlantic Ocean east of the southern islands of the Antilles Arc, *i. e.*, the Windward Islands from Martinique to Tobago; (c) The Atlantic Ocean north of the Antilles in the region of the Puerto Rico Trench; and (d) The region of the Anegada and Jungfern Passages between Puerto Rico and the Virgin Islands.

The waters of these areas colder than 10° C have been compared with Iselin's (1936: figs. 25 and 53) temperature-salinity diagrams for the western Sargasso Sea, and salinity anomalies have been computed. Where these have a value greater than ± 5, they have been entered on the temperature-silicate diagram (Fig. 2).

Significant negative salinity anomalies, indicating admixture of Antarctic Intermediate water, are accompanied by correspondingly high silicates. Water of this type is found in the 6 to 7° C range east of the Windwards, at the Anegada-Jungfern Passage stations, and in the Venezuelan Basin. It extends down to 5° C east of the Windwards, but the 5 to 6° C water in the Anegada-Jungfern Passage region and in the Venezuelan Basin tends to be somewhat more saline, the latter being more like the Antarctic Intermediate water than the former.

At temperatures colder than 5° C there are no significant salinity anomalies in the Antilles Arc region, *i. e.*, all of the water masses have about the same temperature-salinity correlations. It is in the 4 to 5° C range that silicate concentrations are distinctive and clearly distinguish the silicate-rich Caribbean waters from the silicate-poor Atlantic waters, with the Anegada-Jungfern Passage samples being of an intermediate character. Water colder than 4° C is absent from the Caribbean, but such waters have similar silicate and salinity characteristics in both of the Atlantic regions concerned. The still colder water in the depths of the Puerto Rico Trench continues to increase in silicate to the greatest depths sampled.

Biochemical Relationships. The requirement of diatoms for large quantities of silicate, the marked correspondence between diatom outbursts and silicate depletion, and the preponderance of diatoms among photosynthetic marine plants lead one to inquire into the possibility of relating the distribution of silicate in the ocean to biological phenomena. Redfield (1934), Fleming (1940), Cooper (1938), Gilson (1937) and others have demonstrated statistical correlations among inorganic phosphate, nitrate, carbon dioxide, and dissolved oxygen in the water and the composition of marine organisms (see Richards and Vaccaro, 1956, for a review). In the regions studied, the concentration of silicate is also shown to be linearly related to the regeneration of phosphate and nitrate and to oxygen consumption in much of the water column. On the other hand, there are, in addition, hydrographic sources of silicate, not demonstrably related to biological fixation and regeneration, which account for significant proportions of silicate, particularly in shallow and very deep waters.

Silicate-Phosphate Relationships. Plots of silicate as a function of inorganic phosphate (Fig. 3) show that, at the intermediate depths

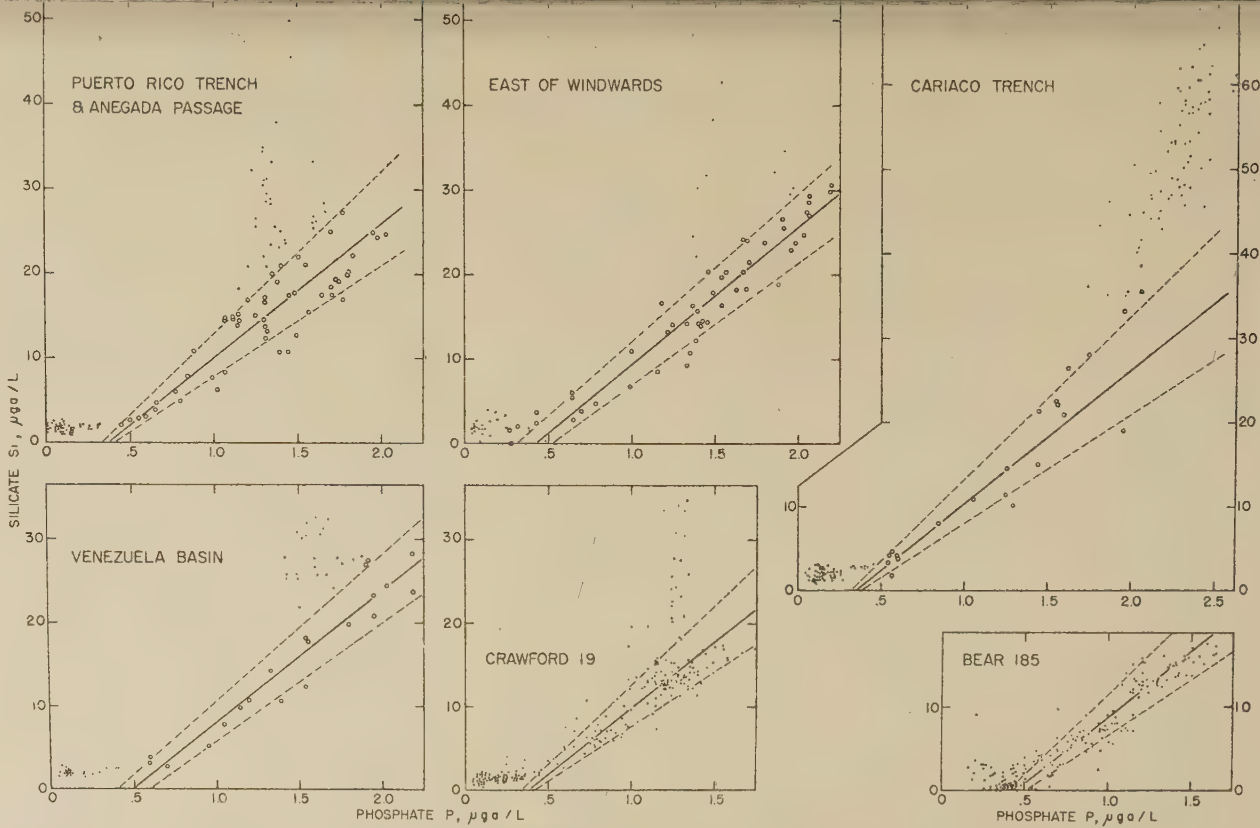

Figure 3. Silicate-phosphate relationships. The regression lines (solid) have slopes of $\Delta Si : \Delta P = 16:1$, by atoms. The broken envelope lines include all points along the regression lines with allowances for ± 9 % analytical errors in phosphate and ± 10 % in silicate. Open circles represent samples in which eq. (1) is assumed to be satisfied (see text).

listed in Table I and shown by open circles in Figs. 3 and 4, there is a high degree of correlation between the two variables. At these depths, the ratio of change in phosphate and silicate has a nearly constant value, of approximately `16 atoms of silicate to one of phosphate, *i. e.*,

$$\Delta \text{Si} = \text{I} + 16 \times \Delta \text{P}. \tag{1}$$

In this equation, both silicate-silicon and phosphate-phorsphorus concentrations are expressed in microgram atoms per liter. The value of the intercept, I, may vary from station to station and from location to location, but it is not zero, emphasizing that the constancy of ratio applies only to the rate of change in concentrations, Δ Si/Δ P.

The above relationship holds neither in surface layers, which are low in both phosphate and silicate, nor in many of the deep water samples, in which there are very high concentrations of silicate and high ratios of Δ Si/Δ P.

In the Cariaco Trench (Richards and Vaccaro, 1956), eq. (1) is satisfied only in a thin layer just above the anerobic zone. The depths at which (1) is satisfied within an analytical range of ± 9 $^0/_0$ for phosphate and ± 10 $^0/_0$ for silicate, holding I constant, at the stations near the Antilles Arc, are shown in Table I and are indicated by open circles in Figs. 1, 3 and 4.

Silicate-Oxygen Relationships. Redfield (1934, 1942) has demonstrated relationships between the consumption of oxygen from sea water (the AOU, apparent oxygen utilization, being the difference between the observed oxygen concentration and the concentration which would be in equilibrium with the normal atmosphere at the *in situ* temperature and salinity), the regeneration of inorganic phosphate and nitrate, and the composition of plankton organisms. In view of the direct relationship which generally holds between phosphate and nitrate and in view of the similar relationship between silicate and phosphate, a close relationship between silicate and oxygen consumption would be expected, and is found. However, plots of silicate as a function of AOU (Fig. 4) indicate that in many samples which satisfy (1) (indicated by open circles) there are large departures from any simple linear relationship between silicate and AOU. These are samples containing appreciable quantities of pre-

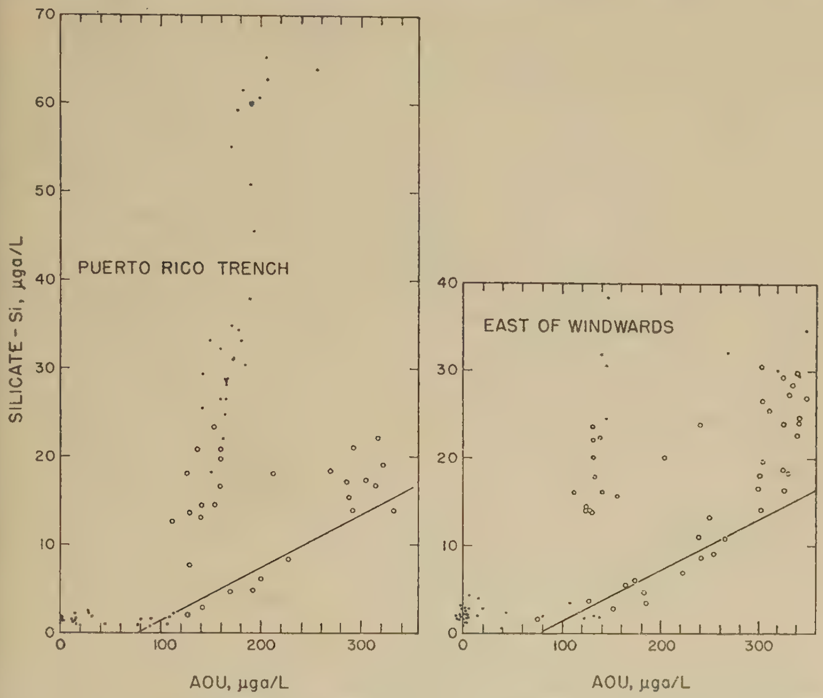

Figure 4. Silicate *vs* oxygen consumption (AOU) at stations in the Puerto Rico Trench and the Atlantic Ocean east of the Windward Islands. Open circles correspond to those in Figs. 1 and 3.

formed[2] phosphate and preformed silicate which are present in the ratio of approximately 16 atoms of silicon to one atom of phosphorus.

The plots of silicate against oxygen consumption indicate the presence, in upper waters, of a layer of variable thickness in which there is a low and relatively uniform concentration of silicate but in which AOU values vary from nil to 80 or more µg-at/l.

Silicate-Nitrate Relationships. A fairly good positive correlation exists between nitrate and silicate concentrations observed between

---

[2] Oxygen consumption is linearly related to the amount of phosphate (and nitrate) regenerated on the decomposition of marine organisms. However, there may be an additional amount of inorganic phosphate (and nitrate), which was in the surface water at the time it became saturated with oxygen and sank beneath the surface with its burden of organic matter. This phosphate (and nitrate) is referred to by Redfield (1942) as "preformed".

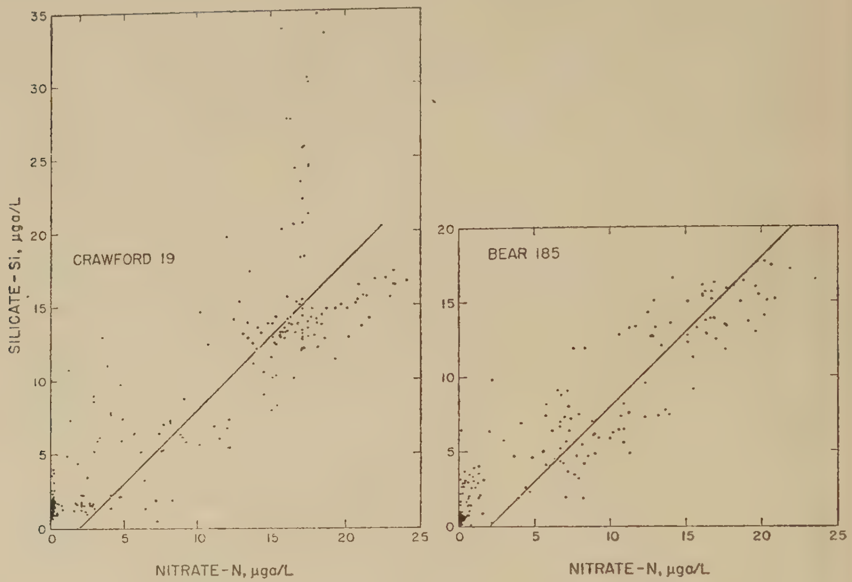

Figure 5. Silicate *vs* nitrate at stations between Woods Hole and Bermuda.

Woods Hole and Bermuda in May and July 1958 (Bear Cruise 185 and Crawford Cruise 19; see fig. 5), except in near-surface waters generally in both May and July and in the deep samples taken near Bermuda in July. Though there is much scatter in these data, the ratio of change in silicate-silicon to nitrate-nitrogen is close to one for one, by atoms. In deep waters near Bermuda in July (not sampled in May), the Si/N ratio of 1/1 is greatly exceeded.

The near-surface samples from this region show different situations prevailing during the two periods. The surface waters all have excess quantities of phosphate, as shown by Ketchum, *et al.* (1958), but concentrations of both silicate and nitrate are so low that one or the other or both may limit the further growth of planktonic organisms. The May samples show low nitrates (< 2 µg-atN/l) accompanied by up to 4 µg-at/l of silicate-silicon. However, in July, many of the low concentrations of silicate (< 2 µg-at/l) were accompanied by up to 3 and, in a few cases, by over 5 µg-at/l of nitrate-nitrogen. This suggests that, in May, low concentrations of nitrate were more probably limiting the growth of phytoplankton than low concentrations of silicate, while the opposite situation prevailed in July.

Discussion. The distributions of silicate and other variables in the waters studied indicate that silicate may be directly related to biological regeneration in some of the strata and to hydrographic factors in others. Direct relationships between silicate and the biologically conditioned concentrations of phosphate, nitrate and dissolved oxygen are generally found in an intermediate layer whereas different ratios between these variables are found in surface and deep waters, in water colder than about 5° C in the Venezuelan Basin, and in the anaerobic strata of the Cariaco Trench.

The ratios AOU: Δ C: Δ N: Δ P = 270:106:16:1 in sea water have been established by previous workers (Redfield, 1934; Gilson, 1937; Fleming, 1940; Cooper, 1938; see Richards and Vaccaro, 1956). In the geographical areas and water masses described in this paper, we can now add: Δ Si:Δ P = 16:1, and Δ N:Δ Si = 1:1. These relationships hold in more samples than does the ratio Δ AOU:Si = 16.9:1, which indicates that the values 16:16:1 for Δ N:Δ Si:Δ P are valid in samples which contain preformed phosphate and nitrate; *i. e.*, there are larger concentrations of phosphate, nitrate, and silicate than would be expected from the amount of oxygen consumption.

Near-surface waters contain silicates in low concentrations which vary from place to place and from time to time, and the ratios of silicate to nitrate and to phosphate are also variable in these waters. Between Woods Hole and Bermuda, where all three of these variables have been studied, there is evidence (Ketchum, *et al.*, 1958) that inorganic phosphate was always present in sufficiently high concentrations that growth of planktonic organisms was not limited. On the other hand, either silicate or nitrate might have been limiting, for there is a suggestion in the data that first one and then the other may be exhausted while nonlimiting concentrations of the other are still present.

In many of the waters studied, particularly the deeper samples, there are additional increments to the concentration of silicate, independent not only of the amount of oxygen consumption but also of the amounts of phosphate (and nitrate) regenerated. It appears that (1) silica re-solution may continue in deeper water after the regneration of phosphate (and nitrate) has gone to completion in shallower strata, or (2) there may be re-solution of silica from bottom sediments with subsequent upward diffusion. These high silicate concentrations were observed in:

a. The Venezuelan Basin and Anegada Passage, where, between 4 and 5° C, they may arise from *in situ* re-solution of siliceous organic remains;

b. The Cariaco Trench, a special locus of isolated water in which there has been extensive accumulation of silicate from re-solution of siliceous materials; and

c. Deep Atlantic water; some of the increment in the deeper part of the Puerto Rico Trench may also be of local, *in situ* origin.

The high silicate concentrations in the deep water of the Venezuelan Basin constitute the most strikingly different water-mass characteristic which has been observed to distinguish Caribbean and western North Atlantic water. However, Caribbean water is also more than 0.5 ml/l poorer in oxygen and somewhat richer in phosphate than the Atlantic water directly to the north. These are the kinds of chemical differences which distinguish the stagnant or very poorly renewed deep water of the Cariaco Trench and which one would expect to find in any stagnant or poorly flushed marine basin. For these reasons, it seems that, contrary to Sverdrup, *et al.* (1942: 640), the renewal of the deep water of the Venezuelan Basin must be a relatively slow, not a relatively rapid, process. Worthington's (1955) observations have pointed toward these same conclusions, which the silicate observations tend to corroborate.

Acknowledgements. On this occasion it is a great pleasure to express appreciation and thanks to Professor Thomas G. Thompson, who first interested the author in chemical oceanography and then taught and directed him in his first studies and research in the subject. One could not wish for a better friend, wiser mentor, or more illustrious example.

This work was supported in part by Contract Nonr-2196(00) NR 083–004 with the Office of Naval Research and by grants from the National Science Foundation. Observations between Woods Hole and Bermuda were partially supported by Contract AT (30–1)–1918 with the U.S. Atomic Energy Commission. Special thanks are due Mr. R. F. Vaccaro and Mr. L. A. E. Doe, both of whom accompanied the author on one of the Caribbean cruises, Dr. J. M. Zeigler, Mr. N. Corwin and Mr. James Wright for their co-operation, and Dr. B. H. Ketchum, Mr. Vaccaro and Mr. Corwin, who kindly made their manuscript available for reference.

REFERENCES

Armstrong, F. A. J.

1951. The determination of silicate in sea water. J. Mar. biol. Ass. U.K., *30*: 149–160.

Atkins, W. R. G.

1923a. The phosphate content of fresh and salt waters in its relationship to the growth of the algal plankton. J. Mar. biol. Ass. U.K., *13*: 119–150.

1923b. The silica content of some natural waters and of culture media. J. Mar. biol. Ass. U.K., *13*: 151–159.

1926a. Seasonal changes in the silica content of natural waters in relation to the phytoplankton. J. Mar. biol. Ass. U.K., *14*: 89–99.

1926b. The phosphate content of sea water in relation to the growth of the algal population. J. Mar. biol. ass. U.K., *14*: 447–467.

1928. Seasonal variation in the phosphate and silicate content of sea water in relation to the phytoplankton crop. Part V. November 1927 to April 1929, compared with earlier years from 1928. J. Mar. biol. Ass. U.K., *16*: 821–852.

1930. Seasonal variations in the phosphate and silicate content of sea-water in relation to the phytoplankton crop. Part V. November 1927 to April 1929 compared with earlier years from 1923. J. Mar. biol. Ass. U.K., *16*: 821–852.

1953. Seasonal variations in the phosphate and silicate content of sea water. Part VI. 1948 compared with the 1923–25 period. J. Mar. biol. Ass. U.K., *31*: 489–492.

Brandt, K.

1920. Über den Stoffwechsel im Meere. Wiss. Meeresuntersuch., (Kiel N.F.) *18*: 185–430.

Clowes, A. J.

1938. Phosphate and silicate in the southern ocean. Discovery Rep., *19*: 1–120.

Cooper, L. H. N.

1933. Chemical constituents of biological importance in the English Channel, November 1930 to January 1932. Part I. Phosphate, silicate, nitrate, nitrite, ammonia. J. Mar. biol. Ass. U.K., *18*: 677–728.

1938. Redefinition of the anomaly of the nitrate-phosphate ratio. J. Mar. biol. Ass. U.K., *23*: 179.

1952. Factors affecting the distribution of silicate in the North Atlantic Ocean and the formation of North Atlantic deep water. J. Mar. biol. Ass. U.K., *30*: 511–526.

Discovery Committee

1941. Station List, 1931–1933. Discovery Rep., *21*: 1–226.

Fleming, R. H.

1940. The composition of plankton and units for reporting populations and production. Proc. 6th Pacif. Sci. Congr., Calif. 1939, *3*: 535–540.

Ford, W. L.

1950. Seagoing photoelectric colorimeter. Anal. Chem., *22*: 1431–1435.

Frassetto, Roberto and John Northrop

1957. Virgin Islands bathymetric survey. Deep-Sea Res., *4*: 138–146.

Gilson, H. C.

1937. The nitrogen cycle. Sci. Rep. John Murray Exped., 1933–34, *2* (8): 21–81.

Graham, H. W. and E. G. Moberg

1944. Chemical results of the last cruise of the Carnegie. Publ. Carneg. Instn., No. 562; vii + 58 pp.

Iselin, C. O'D.

1936. A study of the circulation of the western North Atlantic. Pap. phys. Oceanogr. Meteorol., *4* (4); 101 pp.

Ketchum, B. H., R. F. Vaccaro and N. Corwin

1958. The annual cycle of phosphorus and nitrogen in New England coastal waters. J. Mar. Res., *17*: 282–301.

Montgomery, R. B.

1938. Circulation in upper layers of southern North Atlantic deduced with use of isentropic analysis. Pap. phys. Oceanogr. Meteorol., *6* (2): 55 pp.

Mullin, J. B. and J. P. Riley

1955. The colorimetric determination of silicate with special reference to sea and natural waters. Anal. Chim. Acta, *12*: 162–176.

Rabin, E.

1905a. Quantitative Bestimmung der im Meerwasser Gelösten Kieselsäure. Wiss. Meeresuntersuch., (Kiel, N.F.) *8*: 99–101.

1905b. Weitere Mitteilungen über quantitative Bestimmung von Stickstoffverbindungen und von gelöster Kieselsäure im Meerwasser. Wiss. Meeresuntersuch., (Kiel N.F.) *8*: 279–287.

1910. Dritte Mitteilung über quantitative Bestimmungen von Stickstoffverbindungen und von gelöster Kieselsäure im Meerwasser. Wiss. Meeresuntersuch., (Kiel N.F.) *11*: 303–319.

1914. Vierte Mitteilung über quantitative Bestimmungen von Stickstoffverbindungen im Meerwasser und Boden sowie von gelöster Kieselsäure im Meerwasser. Wiss. Meeresuntersuch., (Kiel N.F.) *16*: 207–229.

Redfield, A. C.

1934. On the proportions of organic derivatives in sea water and their relation to the composition of plankton, *in*: James Johnstone Memorial Vol., Univ. Press, Liverpool; pp. 176–192.

1942. The processes determining the concentrations of oxygen, phosphate, and other organic derivatives within the depths of the Atlantic Ocean. Pap. phys. Oceanogr. Meteorol., *9* (2); 22 pp.

Richards, F. A. and R. F. Vaccaro

1956. The Cariaco Trench, an anaerobic basin in the Caribbean Sea. Deep-Sea Res., *2*: 182–199.

Sverdrup, H. U., M. W. Johnson and R. H. Fleming

1942. The Oceans. Prentice-Hall, Inc., New York. x + 1087 pp.

THOMPSON, T. G. AND M. W. JOHNSON

1930. The sea water at the Puget Sound Biological Station from September 1928 to September 1929. Publ. Puget Sd. Mar. (biol.) Sta., *7*: 345–368.

THOMPSON, T. G. AND R. J. ROBINSON

1932. Chemistry of the sea. Bull. nat. Res. Coun. Wash., No. 85, Chap. 5: 95–203.

WORTHINGTON, L. V.

1955. A new theory of Caribbean bottom-water formation. Deep-Sea Res., *3*: 82–87.

Contribution No. 991

BULLETIN OF THE GEOLOGICAL SOCIETY OF AMERICA
VOL. 71, PP. 1211–1222, 1 FIG. AUGUST 1960

EVOLUTION OF THE NEW HAMPSHIRE SHORE LINE

BY SHERWOOD D. TUTTLE

ABSTRACT

The encroaching sea came against glacially eroded bedrock and several types of glacial and glaciomarine deposits in New Hampshire. Wave action, concentrating on till headlands and rock promontories, has built a variety of beach types. Detritus has been drifted locally in both directions along the shore, and the longshore drifting has no over-all pattern. The beach trends are not parallel to the general shore-line trend, and the writer suggests that individual beaches are oriented normal to the largest storm waves that reach the area. Following deglaciation, the land has risen isostatically and the seal level eustatically. Evidence indicates that a postglacial sequence of relative submergence, emergence, and submergence has occurred. Classical geomorphic shore-line classifications do not fit every part of the area, and it is therefore best described geographically and in terms of its evolution.

CONTENTS

TEXT

Page
ıtroduction 1211
cknowledgments 1211
eneral geology of the area 1213
Iappable units along the shore 1213
nalyses of beach sands 1217
each drifting 1217
/ave erosion 1218
each alignment 1218
rowned forests 1219
lassification of the shore line 1220
eographic description of the shore line 1220
volution of the shore line 1220
ummary 1221
eferences cited 1221

ILLUSTRATION

Figure Page
1. Map of New Hampshire shore line 1212

TABLES

Table Page
1. Types and characteristics of beaches along the New Hampshire coast from north to south 1214
2. Summary of analyses of beach sands, New Hampshire shore line 1218
3. Beach orientation along the New Hampshire shore line 1219

INTRODUCTION

The New Hampshire shore line, only 13 iiles long, lies on the western edge of the Gulf f Maine; the coast extends from the State ne at Salisbury Beach in Massachusetts to ıe mouth of the Piscataqua River and Portsıouth Harbor, ending at Kittery, Main Fig. 1). In this paper the term shore line is sed in the broader sense to include both the each areas and the coast.

Fenneman (1938) included the coastal area f New Hampshire in the seaboard lowland ection of the New England province. He ıggested that the segment of the coast beween Portland, Maine, and Cape Ann, Massaıusetts, is simple in outline because it parallels the structural trends of the bedrock. He stated that a postglacial rise of sea level brought into being a narrow coastal plain 5–10 miles wide. The constructional nature of the plain was the result of deposition of glaciofluvial material and clay that produced an area of low relief.

ACKNOWLEDGMENTS

This study was part of a larger investigation of the glacial and postglacial features of the coastal area of New Hampshire (Tuttle, 1952; 1952, Ph.D. Thesis, Harvard Univ.). The area studied extended from the New Hampshire edge of Portsmouth Harbor southward to the bridge across the mouth of Hampton Harbor. Chute's map of the shore line north of Cape Ann, Massachusetts, extends approximately

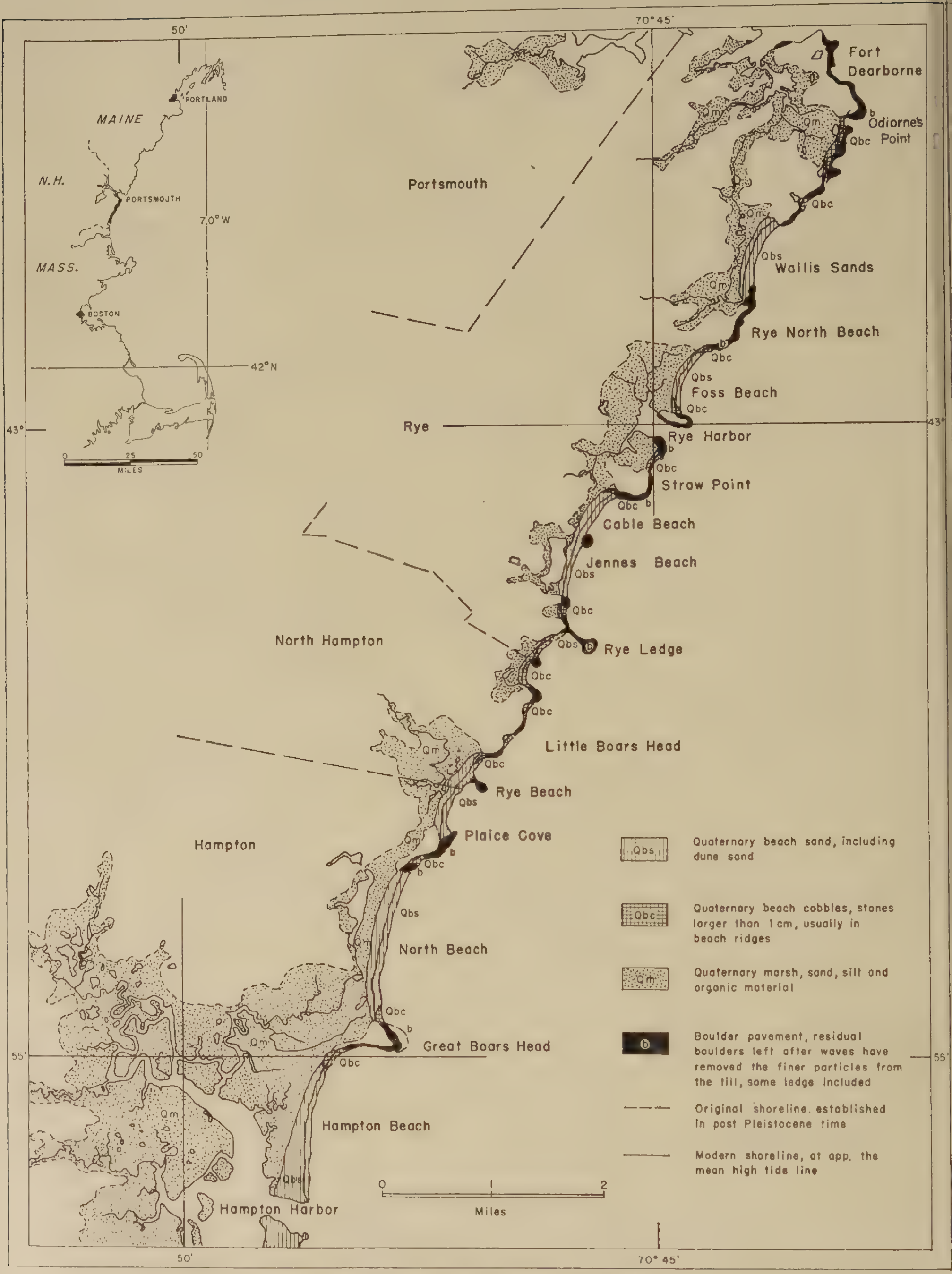
50'
70°45'
MAINE
PORTLAND
N.H.
PORTSMOUTH
70°W
MASS.
BOSTON
42°N
43°
0 25 50
MILES
Portsmouth
Fort Dearborne
Odiorne's Point
Qm
Qbc
b
Wallis Sands
Qbs
Rye North Beach
Foss Beach
Rye
Rye Harbor
Straw Point
Cable Beach
Jenness Beach
North Hampton
Rye Ledge
Little Boars Head
Rye Beach
Plaice Cove
Hampton
North Beach
Great Boars Head
55'
Hampton Beach
Hampton Harbor
0 1 2
Miles
Qbs Quaternary beach sand, including dune sand
Qbc Quaternary beach cobbles, stones larger than 1 cm, usually in beach ridges
Qm Quaternary marsh, sand, silt and organic material
b Boulder pavement, residual boulders left after waves have removed the finer particles from the till, some ledge included
Original shoreline established in post Pleistocene time
Modern shoreline, at app. the mean high tide line

FIGURE 1.—MAP OF NEW HAMPSHIRE SHORE LINE.

to Hampton Beach (Chute and Nichols, 1941). The field study of the beaches was done mainly during the summer of 1951. Financial assistance was granted from the Shaler Memorial Fund and the Robert W. Sayles Fund of Harvard University, and subsistence was received under the provisions of Public Law 346.

The late Henry Stetson encouraged the au-

hor in the study of the shore line and discussed he problems with him. The Beach Studies Group of the Woods Hole Oceanographic nstitution, working under ONR-Geography Branch, Contract No. Nor-1254(00) (NR-388-018), assisted in the preparation of the manuscript. Dr. John Zeigler of Woods Hole has critically and helpfully read the manuscript.

General Geology of the Area

On the New Hampshire coast waves modify bedrock outcrops, glacial till deposited as ground moraine and drumlins, stratified drift, and postglacial deposits of clay and sand.

Most of the bedrock is metasedimentary rocks of pre-Devonian age (Freedman, 1950; Billings, 1955) and consists of closely jointed quartzites, slates, schists, gneissic complexes, and a few mafic dikes. Although the rocks are reasonably resistant to decomposition, most of them break easily into small, wedge-shaped pieces.

The glacial deposits are unweathered and scarcely eroded. They are shown on the Glacial Map of North America (Flint, 1948) as being Wisconsin in age and are probably Cary substage (MacClintock, 1953; Flint, 1953).

The till, which is sandy with a large volume of small stones, is similar to that described elsewhere in New England (Jahns, 1951; Mather, Goldthwait, and Theismeyer, 1942; L. Goldthwait, 1948). The pebbles are of two types: small, angular, tablet-shaped fragments of the local metasedimentary rocks and larger, rounded cobbles of hard, phaneritic rocks, massive quartz, and gneisses. Varying amounts of sand, silt, and clay make up the finer components of the till.

The stratified drift is composed of sand and gravel with varying amounts of silt and clay.

The postglacial clay and sand is a blanket deposit ranging from 2 to 15 feet thick which occurs within the first 50 feet above present-day sea level and lies on top of bedrock, till, and stratified drift (Chapman, 1950). These deposits are probably the equivalent of the "Leta Clay" (Katz, 1913) of southwestern Maine.

Mappable Units along the Shore

The erosional and depositional features of the shore line include boulder pavements, marsh deposits, beach cobbles, beach and dune sands, and ledges. The boulder pavements are residual accumulations of large, loose stones similar in size and lithology to the erratics and harder stones in the till but containing few large pieces of the local bedrock. The boulders average a foot in diameter and appear little modified in shape by wave action. They are typical examples of soled and rounded glacial boulders derived from resistant rock types (von Engeln, 1930). Johnson and Reed (1910) described similar boulder pavements, or "lost drumlins," at Nantucket Beach in Massachusetts.

The marsh deposits consist of accumulations of poorly sorted sand and silt with intermixed organic matter. The beach cobbles, or shingle, are stones larger than 1 cm in diameter, usually similar in lithology to the pebbles in the till. These stones, whether of glacial origin or derived from the nearby bedrock, are rounded, smoothed, and polished. The sand is made up of quartz grains, mica flakes, feldspar grains, and little chips and fragments of slates, schists, quartzites, and phyllites.

Analysis of the interrelations of wave refraction, erosion, and longshore drifting on materials of known character and distribution produces an explanation for the origin of a shore line. The types, characteristics, and locations of the individual beaches of the New Hampshire coast can be seen by comparing Table 1 with Figure 1.

FT. DEARBORNE-ODIORNE'S POINT: The irregular points and bays along this northern part of the coast were formed by the submergence of glacially scoured bedrock. Subsequent wave action on the brittle, jointed rocks and a thin mantling of till produced large quantities of shingle in numerous small beaches. Little beach drifting could have occurred here, because the many rocky points prevent lateral movement.

In the middle and at the south end of this stretch of shore, little baymouth bars have shut off small coves, forming lakes that are, in part, rock-rimmed. Just south of Odiorne's Point, shingle berm ridges have closed off the shallow estuary—now a marsh, almost filled in—behind the rocky headland. The marsh and the beach ridge connect what was formerly an island to the mainland. Next to the marsh are several small beach deltas where waves have washed stones over the tops of the shingle ridges.

Many small, steplike indentations of the water line occur where the shore line crosses massive ledges. The longer sides of these notches trend northeast and the shorter north-

Table 1.—Types and Characteristics of Beaches Along the New Hampshire Coast, from North to South

	Length in miles	Type of beach	Feature on north	Feature on south	Direction of beach drift	Beach material
Ordiorne's Point beaches		Tombolos, baymouth bars, and pocket beaches	Ledges	Till and ledge island	. .	Shingle
Wallis Sands	0.8	Baymouth bar	Till and ledge island	Till and ledge point	North and south	Sand
Foss Beach	0.7	Tombolo	Till and ledge point	Till and ledge island	North and south	Shingle with some sand in the center
Rye Harbor Spit	0.3	Spit	. .	Till island	North	Shingle
Cable and Jennes beaches	1.3	Tombolo	Till island	Till and ledge point	North and south	Shingle and sand
Bass Beach	0.2	Baymouth bar	Till and ledge point	Till and ledge point	North and south	Shingle
Rye Beach	1.0	Tombolo	Till and ledge point	Till island	North and south	Shingle and sand
North Beach (Hampton)	1.8	Tombolo	Till island	Till island (drumlin)	North and south	Sand with some shingle
Hampton Beach	1.6	Baymouth bar	Till island (drumlin)	(Salisbury Beach, Plum Island, and Castle Island)	South	Sand with some shingle

st. The longer segments are controlled by bedding-plane cleavage, which strikes north- t here.

WALLIS SANDS: This beach, almost a mile g, is a slightly curved baymouth bar con- cting the rocky headland of Rye North ach on the south with a bedrock hill on the rth. The bar cuts off a large irregular bay ich is nearly filled with marsh deposits. the middle and highest parts of the bar is a e of stable sand dunes, approximately 500 t long.

Analysis of samples from the beach showed at sand at the north end is slightly finer an at the south end, which suggests northward ach drifting. However, in 1951 the outlet for e lagoon and marsh was located at the south d but had been closed by sand that locally d been drifted southward. Apparently—over period of time—beach drifting at Wallis nds has changed direction in an irregular anner.

An area of boulder pavement lying off the rtheast end of the rocky point at the south d of Wallis Sands suggests that till covered e bedrock at one time. Waves have eroded e till mass, leaving the boulders and building e finer fragments into beaches.

RYE NORTH BEACH: This bedrock area, partly antled by till, lies between Wallis Sands on e North and Foss Beach on the south. A ulder pavement nearly 600 feet wide and a w, wave-cut cliff lie around the southeast rner of the point. Large cobbles and one all pocket of shingle are all that remain of e till cover, which was once more extensive re.

FOSS BEACH: This is a slightly curved tombolo nnecting the rocky point of Rye North ach with the small hill of till and bedrock the south where Rye Harbor State Park is cated. The till mass was once an island but s been joined to the mainland by the accumu- tion of marsh deposits behind the beach. xcept for the boat anchorage of Rye Harbor hich is protected by jetties and has been epened by dredging), the large lagoon behind oss Beach is nearly filled in.

Apparently the sand and shingle of Foss each came from the boulder pavements at oth ends, and the heavier shingle was heaped gher in the middle and along the crest. The ingle reaches down to the low-tide level at oth ends of the beach and laps up on the atches of boulder pavement. At the south d the patches of boulder pavement are much more extensive, indicating greater removal of till there. Smaller amounts of sand and shingle came from the eroded front of the Rye North Beach till mass. The shingle is somewhat finer toward the north end, and analyses of sand samples, which show no difference in grain size along the beach, suggest that sorting is better toward the south end (Table 2).

In the summer of 1951 a blanket of sand could be seen on the middle of the beach, lying against the seaward side of the shingle beach ridge. This was probably a recent and temporary accumulation brought by the gentle summer waves which moved nothing larger than particles of sand size.

The growth of the Foss Beach tombolo was mainly the result of waves striking the offshore ledges and till masses and being refracted inward, thus eroding them rapidly and transporting the debris backward and sideways. However, as suggested by Lewis (1931) and others, the highest beach ridges are built by the largest waves that can reach the shore line. The high ridge in the center of Foss Beach and along the crest, formed of the larger shingle, was probably built by unrefracted waves striking the center of the beach. These waves, possessing more energy, would be able to pile pebbles higher than refracted waves at either end.

RYE HARBOR STATE PARK: This narrow point of bedrock and till is flanked by boulder pavement, indicative of the once greater extent of the till cover. The point projects seaward because of the original position of the till mass rather than because of differential resistance to erosion.

RYE HARBOR SPIT: Enclosing the south end of the Rye Harbor marsh is a cobble spit built northward from Straw Point. This feature is the highest and largest storm beach along the New Hampshire shore line; the crest at about its midpoint rises more than 30 feet above the low-tide line. Shingle probably came from both ends, since extensive flats of boulder pavement occur both north and south of the spit. The seaward end of the Straw Point hill has apparently been cut back 50–100 feet, leaving a wide apron of large boulders. This spit may have been formed as a tombolo that once connected a small patch of till to Straw Point. All that is now left of the till mass is the boulder pavement. In a pocket at the north end of the spit is a small beach of coarse sand. Analysis of a sample from it showed that the median grain size was much larger than that of samples from any of the other beaches.

STRAW POINT: This low till mass, half a mile long and a third of a mile wide, was probably once an island. It is now joined to the mainland by a marsh and by Cable and Jennes beaches. Wave erosion has produced a low sea cliff in the till and a boulder pavement—widest along its south side—across the seaward end of Straw Point.

CABLE AND JENNES BEACHES: The next large beach to the south, nearly a mile and a half long and slightly curved, is called Cable Beach on its northern end and Jennes Beach to the south (Photo 2). Technically, the beach could be called a tombolo, but the term baymouth bar is preferable since Jennes Beach cuts off the Eel Pond lagoon. With its natural outlet now obliterated by beach drifting and highway building, Eel Pond is now drained by a culvert.

The size of the cobbles in the shingle ridges decreases from both ends, becoming finer toward the center. Cable and Jennes beaches, however, differ from Foss Beach in that the shingle ridges are located at the ends and diminish in volume toward the center. Pebbles and other debris have been swept backward from the till masses at each end, but because this beach is long, the shingle has not yet moved into the center. This description is of the summer beach; in winter it probably has much less sand. Analyses of sand from points along the beach show no change in median diameter but indicate better sorting at the north end (Table 2).

Another factor here is the "lost till mound" that is represented by the boulder pavement in front of the beach. This obstacle causes waves to break and refract, preventing them from building a high storm ridge. A part of this former till mound sticks up through the middle of the beach, separating it into two bars. Cable and Jennes beaches give no morphological indication of any significant direction of beach drifting. They appear to have been formed mainly from material from both ends.

RYE HEADLANDS AND LITTLE BOARS HEAD: Between the Rye Beach Club and the end of Little Boars Head the village of Rye Beach is built on a ledge and till promontory. Along this shore are several small pocket beaches, such as Bass Beach, which have been built between rocky points and in several cases cut off small, marshy lagoon areas. These are baymouth bars on a miniature scale. Johnson took photographs here about 40 years ago and described these features as "small but remarkably fine cobblestone pocket beaches," (1925, p. 430, Fig. 205; *see* 1919, p. 78, Pl. IX). No noticeab changes have taken place on this part of th shore since Johnson's photograph was taken.

Little Boars Head is a low drumlin at th south end of an irregular till mass. The seawar edge of the hill is skirted by a wide bould pavement, indicating extensive wave erosio This washing away of the till produced th large volume of shingle and cobbles that a now piled in the beach ridges.

RYE BEACH:[1] Rye Beach, a tombolo, connec Little Boars Head to a till mass at Plaice Cov Marsh deposits have accumulated behind th beach and joined it to the mainland. A stor ridge of shingle lies at its north end, but mo of the beach is made up of sand. A stretch ridge about 200 feet long at the south end Rye Beach is topped by stable sand dunes. I the middle of the beach an outlet channel fro the lagoon has been blocked by sand. As see from the air, the channel, which is at least 7 feet wide, has a distinct S-shaped cours because the mouth has been displaced abou 300 feet northward by beach drifting. Th artificial outlet at the north end of the lagoo probably prevents the lagoon water fro using the partially blocked outlet in the cent of the beach, except when runoff is excessive.

Analysis of the sand shows a slight decreas in grain size northward along the beach an poorer sorting on the north end than on th middle and southern parts. At the south end Rye Beach an extensive boulder pavement li at the northeast corner of Plaice Cove, and i front of Rye Beach is a small patch of bould pavement, similar to those found on the Cab and Jennes beaches. Behind the beach tw small till hills are surrounded by Little Riv swamp deposits. Rye Beach is probably multiple tombolo which first connected th little till mass represented by the bould pavement and then was moved backward as th till hill disappeared. The boulder paveme still breaks up the large waves and sets u conflicting patterns of beach drifting.

PLAICE COVE HEADLAND: This mass of till bordered by a low cliff and boulder pavemen with numerous large erratics which are visib offshore at low tide. A patch of shingle li against the south end of this point, and the

---

[1] The designation Rye Beach for this tombolo fo lows local usage. Neither the sheets of the Army Ma Service nor the U. S. Geological Survey quadrangl give a name for this beach. The village of Ry Beach is not at the same place as the tombo referred to here.

bbles are stones that have been eroded from
e till and carried back along the south side
the headland to be piled up at the north end
North Beach.

NORTH BEACH: This tombolo, roughly 2 miles
ng, connects the Plaice Cove headland to
eat Boars Head drumlin. The storm ridge
ng the entire length of this beach is made
shingle with an apron of sand spread out in
nt of it. Analyses of the sand from several
ints along the beach show no change in
rting or in grain size. No obstructions occur
front of this beach, and direct wave action
d longshore drifting have functioned to
oduce a smooth beach with a high shingle
ge in its center. The concrete seawall pro-
cting the base of the shingle storm ridge
events severe storms from washing cobbles
er the top of the beach and down onto the
ghway built at the foot of the backshore.

GREAT BOARS HEAD: This conspicuous land-
ark is an eroded drumlin. The writer assumes
at Great Boars Head once had a typical
umlin shape; it has been reduced to about
lf of its original length by wave action on its
award side (the lee or distal end). Hitchcock
878) told of the many hundreds of feet of
aterial removed from the drumlin during the
me between the settlement of the New
ampshire coastal area and the middle of the
th century, roughly 200 years. The wide
ulder pavements on both sides of the hill
dicate that at least 100 feet of erosion has
ken place on either flank. The wave-cut
iff of Great Boars Head is more than 40
et high and is the only feature of such
ajor size on the New Hampshire shore.
espite sea walls and revetments, the cliff is
ill retreating. Pebbles and sand produced by
e erosion of the hill have been carried by
each drifting both up and down the shore line
build North Beach and Hampton Beach.

HAMPTON BEACH: Hampton Beach and its
uthward continuation, Seabrook and Salis-
ury beaches, are all part of a much larger
each system. Chute (Chute and Nichols,
41, p. 18) pointed out that all the beaches
etween Boars Head and the tip of Cape Ann
e geologically similar throughout and neither
se nor gain sand from areas to the north and
uth.

The nature and arrangement of the materials
n Hampton Beach, shingle on the north end
nd sand to the south, indicate that much of
e material came by longshore drifting from
e erosion of Boars Head. Analyses of samples show that the material now collecting outside the jetties, which keep Hampton Harbor open, is larger in grain size and slightly better sorted than the sand on the main part of the beach. Examination of maps and photographs suggests that beach drifting in the vicinity of the mouth of Hampton Harbor goes both north and south and that much material is collecting alongside both jetties. A few small sand dunes are now forming inland of the high-tide line in the area where the beaches have grown seaward.

A U.S. Army Corps of Engineers report (1953) dealing with beach erosion control at Hampton Beach suggests a moderate southward drift of material on the beach as well as an offshore source. Detailed measurements show that the loss of material from the beach, foreshore and offshore out to a depth of 18 feet, exceeds the rate of supply. During 1955 about 700,000 cubic yards of fill was pumped from Hampton Harbor and added to the beach along about 6000 feet of its length. This doubled the width of the public beach in front of massive sea walls.

Analyses of Beach Sands

Samples of sand, collected from all the beaches and analyzed in the laboratory, were taken from the top inch of material on the beach about midway between the high- and low-tide lines. Comparison of samples (Table 2) is based on the median diameter and the coefficients of sorting and skewness following Trask (*in* Krumbein and Pettijohn, 1938). The procedures of Schalk (1938) served as a model for this study. These values do not vary greatly from each other and do not indicate any over-all trends in grain size or sorting. Their random irregularity indicates that each beach operates independently in terms of source material and direction of sediment movement.

Beach Drifting

A study of the shapes of the wave-built features, the locations and migrations of outlet streams, and decreases in grain size indicates no apparent dominant and prevailing direction of longshore drifting. The decreasing volume of beach sand and the decreasing size and length of beaches northward from the mouth of the Merrimac River at Newburyport, about 6 miles south of the mouth of Hampton Harbor, suggest the simple picture of a source of material at the river mouth and its deposition in decreasing amounts northward. However, a comparison of the median diameters of the sand grains and the sorting coefficients of the few samples analyzed does not substantiate this generalization.

TABLE 2.—SUMMARY OF ANALYSES OF BEACH SANDS, NEW HAMPSHIRE SHORE LINE

Samples were taken from the top inch of beach material midway between high- and low-tide levels.

	Median diameter in mm	Coefficient of sorting	Log of skewness
North end, Wallis Sands	0.17	1.19	−0.01
South end, Wallis Sands	0.27	1.46	−0.05
North end, Foss Beach	0.19	1.25	0.03
South end, Foss Beach	0.18	1.28	0.03
South of jetty, Rye Harbor	1.80	1.36	−0.04
North end, Cable Beach	0.18	1.24	0.03
Middle, between Cable and Jennes beaches	0.17	1.02	0.01
South end, Jennes Beach	0.18	1.31	−0.05
North end, Rye Beach	0.24	1.44	−0.04
Middle, Rye Beach	0.33	1.19	−0.03
Plaice Cove, south end, Rye Beach	0.35	1.21	−0.08
North end, North Beach	0.22	1.18	0.04
Middle, North Beach	0.20	1.18	−0.04
North end, Hampton Beach	0.20	1.25	0.0
South end, Hampton Beach	0.20	1.18	0.01
North of north jetty, Hampton Harbor	0.38	1.17	−0.02

A possible explanation for the decrease in size and number of beaches northward may be the lessening volume of glacial drift and an increasing amount of bedrock. Chute (Chute and Nichols, 1941, p. 19) suggested that many reversals of shore drift occurred between Boars Head and Cape Ann and that neither direction was dominant.

Although no single major direction of beach drifting can be identified on the New Hampshire shore line, dozens of local examples exist where either northward or southward drift is dominant. Many beaches appear to have been built by both northward and southward drift. Under the influence of the variable New England weather, the amount and direction of beach drifting surely changes irregularly. The alternation and variation in drift can be seen in the variety and different sizes of beach types described above.

WAVE EROSION

Along the New Hampshire shore line wave erosion is subordinate to wave deposition. Where the waves strike against outcrops solid bedrock, very little evidence of wav erosion can be seen, except on the less resista trap dikes where deep narrow notches hav been eroded. Sea cliffs have been cut in the u consolidated glacial deposits. At Boars Hea Little Boars Head, Straw Point, and at Ry Harbor State Park wave action has produce steep slopes with evidence of landslidin slopewash, and undercutting. The presence boulder pavements in many places in front drumlins and elsewhere suggests considerab wave erosion of till in the past.

BEACH ALIGNMENT

Examination of maps and charts of the sho lines of northern Massachusetts, New Ham shire, and southwestern Main shows that t long axes of the beaches are not parallel to t major trends of the coast line. In the Ne Hampshire area the direction of the shore lin measured from the north side of Hampt Harbor to the northeast end of the bedro point at Fort Dearborne, is about N. 30° The approximate alignment of all the beach except Rye Beach is closer to a north-sou line than the trend of the coast line. The alig ment directions are shown in detail in Table

These beaches are arranged en echelon (Fi 1). This is well shown by the way Hampt

TABLE 3.—BEACH ORIENTATION ALONG THE NEW HAMPSHIRE SHORE LINE

	Direction of beach trend	Deviation from approximate shore line trend
Wallis Sands	N. 20° E.	10° W.
Foss Beach	N. 15° E.	15° W.
Cable and Jennes Beaches	N. 20° E.	10° W.
Rye Beach	N. 35° E.	5° E.
North Beach	N. 10° E.	20° W.
Hampton Beach	N. 5° E.	25° W.

Beach on the south butts against Boars Head approximately 3000 feet west of the seaward end of the drumlin. The south end of North Beach touches Boars Head about 1200 feet back from the end. The north end of North Beach joins the south side of the Plaice Cove till mass about 1200 feet inland from the seaward end. Rye Beach meets the north side of the point scarcely any distance back from its end. Most of the beaches curve seaward at their ends where they join headlands and curve seaward convexly in a cuspate form wherever ledges or boulder pavements occur off the beach.

The foregoing observations can best be explained in terms of Lewis's Dominant Breaker Hypothesis (1931; 1938). Lewis observed that many freestanding shingle beaches in England did not align themselves parallel to the general trends of the coast line but rather were formed at right angles to the direction of the largest waves that reach the coast. Lewis analyzed over-all beach construction as a two-step process. Whete detritus of many sizes is available, the ordinary waves will cause longshore drifting within the surf zone, extending spits and bars lengthwise. During storms the large waves will pile shingle in ridges along the back of the beach. Thus, with the passage of time, a ridge or berm complex accumulates to form the backbone of a beach. Since the beaches that Lewis studied all faced the direction of the largest waves to reach that coast, he concluded that this factor controlled the orientation of beaches and their over-all direction of elongation. Wherever promontories, islands, or shoals create a partial lee and cause wave shadows, smaller beaches still face the direction of longest fetch.

When waves are considerably refracted, they do not have so much energy as unrefracted waves. Thus large storm waves coming straight in against a beach will build higher storm ridges than at the ends of a beach or along the sides of a promontory. The orientation of the New Hampshire beaches and the locations of their highest berm ridges indicate that the largest storm waves come against this coast line more or less from the east and that they are not generally perpendicular to the major trend of the shore line, which is N.30°E.

The numerous points and ledges that project essentially perpendicular to the trend of the shore line might act as large groins. On beaches with groins, deposition occurs, and the beaches widen on one side of the groins. If the prevailing direction of drift on the New Hampshire shore line were southward, deposition would take place on the north sides of the peninsula groins. In this case, the shore-line trend is approximately N.30°E., and the beaches would trend more nearly north-south. Table 3 shows that individual beaches along the New Hampshire coast line fit this theoretical case. However, this does not seem to be the explanation for the beach orientation; large-scale southward movement of detritus does not occur for two reasons: (1) the till cover, which could serve as a source of beach sand and shingle, is very thin and patchy along the north part of the shore line; (2) the tidal Piscataqua River carries very little sediment into the sea because the deep inland bays serve as settling basins for material brought seqward by the Piscataqua's several tributaries.

These echelon beaches are not found on great open coasts, such as those along the seaward edge of Cape Cod, but occur only where numerous points and islands cause wave refraction. Charts and maps of the shore line of New England show countless examples of beaches that face the direction of longest fetch. Along the coast line of New Hampshire, which has few deep esturaries or long promontories, waves coming from any direction between northeast and southeast by south can reach the beaches. Thus the dominantly north-south allignment of the New Hampshire beaches suggest that the major storm waves that constructed them came from the east.

DROWNED FORESTS

J. W. Goldthwait (1925, p. 70; Goldthwait *et al.*, 1951, p. 60) reported the occurrence of rotting black stumps exposed only at neap tides at the northern end of Jennes Beach, to the south of Straw Point in Rye, and at Odiorne's Point in the northeast corner of

Rye. The stumps were not visible during the summer of 1951. The "drowned forests" suggest either compaction of marsh deposits under the weight of shoreward migrating beaches or a eustatic rise in sea level. Since Marmer (1951) suggested on the basis of tide-gauge records that the New England coast is being drowned at a rate of 0.02 feet per year, the drowning probably records a eustatic rise.

Classification of the Shore line

According to Johnson's (1919) widely used system of classification the shore line of New Hampshire is one of submergence in middle youth. Such a shore line has an irregular trace with numerous promontories, inlets, and islands formed when a landscape maturely dissected is partially covered by an encroaching sea. This is especially applicable if one considers the entire coastal area of New Hampshire with the drowned valley of the Piscataqua River and its tributaries. Drowning is not so obvious between Fort Dearborne and Hampton Harbor because the intervening area was not so deeply dissected by preglacial or glacial erosion.

Johnson (1925, p. 146–149) described the shore line of central New England as having characteristics of submergence in the north and emergence in the south. Elsewhere Johnson (1925, p. 486–487) pictured the large, almost continuous beaches between Boars Head and the south end of Plum Island, Massachusetts, as an offshore bar, indicative of a young shore lime of emergence.

These apparent contradictions illustrate the principal shortcomings of Johnson's classification. In Johnson's first case—that of the shore line north of Portland, Maine—the relief of the land and of the sea floor close to the land was great enough so that whatever the final change in sea level was, the irregular shore line, indicative of submergence, was not changed. Here also, Johnson used the presence of elevated marine deposits to suggest secondary emergence. In the case of the offshore bar in the vicinity of the New Hampshire-Massachusetts line, the relief of the land and the offshore sea floor was slight. Thus, even with submergence, the waves, which had to break far out from the shore line because of the shallowing water, built an offshore bar, a feature more typical of an emerging shore line.

In an attempt to provide a classification of shore line that would cope with these inconsistencies, Shepard (1937; 1948) proposed using two divisions of criteria for classifying a shore line: (1) shore lines whose configuration is primarily due to nonmarine agents and (2) shore lines whose configuration is mainly the result of marine agents. In general, the shore line of New Hampshire, according to Shepard's classification, fits into the second category, specifically a coast shaped by marine deposition, straightened by the building of bars across estuaries, and characterized by offshore bars and longshore spits.

In terms of Shepard's first division, the configuration of the New Hampshire shore line is due to drowned river valleys and partially submerged drumlins and other glacial hills and has been modified since by wave deposition. If one considers the history and sequence of events of a shore line, a different difficulty arises in using Shepard's classification rather than Johnson's because with Shepard's one may use several unrelated criteria. Shepard accepts this (1937, p. 605): "There is no reason . . . why two classes should not be used for the same coast, as, for example, a ria coast with offshore bars."

Some geomorphologists have made classifications of shore lines on the basis of topographic maps or charts alone; others used combinations of field data and map information. However, difficulties arise in trying to relate the morphologic shapes and locations of beach features to an interpretation of the history of the shore area.

The author's opinion, based on the experience of the present study, is that shore lines must be described in terms of the present, and beyond this geographical description, the Quaternary history must be worked out, showing how the present shore-line configuration evolved.

Geographic Description of the Shore Line

The New Hampshire shore line, an area of low relief, is fairly straight and has two large estuaries—Great Bay, deep and complex with a dendritic pattern, and Hampton Harbor, shallow and simple in shape. Northward along the shore, beaches are fewer and smaller, and many ledges occur. Rocky headlands, drumlins, and till hills joined together by baymouth bars and tombolos form a series of points connected by slightly arched stretches of beach. Small lagoons and marshes lie behind the shore (Fig. 1).

Evolution of the Shore Line

Some information is available to suggest the development of the shore features under discussion. Following deposition of ground moraine drumlins, and stratified drift, glaciers stagnated and melted away (Tuttle, 1952; 1952, Ph.D. thesis, Harvard Univ.). Presumably during postglacial time the relationships between isostatic and eustatic change were as follows: Both the land and sea level were rising; eustatic rise of sea level was essentially synchronous with the deglaciation and caused submergence. Isostatic rebound followed; when it was at a maximum, it overcame eustatic rise, and the coastal area emerged. With the slowing down of isostatic rebound, eustatic rise again caused submergence.

The postglacial marine clays record several indications of the fluctuations of sea level. Their present elevation of at least 50 feet above sea level in the coastal area indicates that submergence has occurred. Clay flats in the valley of Little River in North Hampton appear to be graded to a wave-cut notch on the south side of the Little Boars Head drumlin. This suggests a former higher stand of the sea.

Throughout the coastal area of New Hampshire, the smooth, flat clay plains have been cut by small tributary valleys. They are 40–50 feet deep and steep-sided. The bottoms are drowned and filled with water and marsh deposits. These streams appear to have been graded to a base level perhaps 20–30 feet lower than present sea level; this suggests emergence. Katz (1913) described similar topography on the "Leda Clays" in southwestern Maine.

At the present time eustatic rise of sea level along the New England coast is about 0.01–0.02 feet per year (Marmer, 1951, p. 58; Thorarinsson, 1940). (It was probably this rise that drowned the forests along the New Hampshire shore.) Isostatic rebound, never of great magnitude here, is slowing down (Gutenberg, 1941). Thus, at present, sea level is rising and has probably come up from the level indicated by the drowned gullies. Before that, sea level probably receded from a level at least 50 feet higher while clays were being deposited over the glacial deposits.

This combination of submergence, emergence, and submergence of the land finally brought the sea against an area of low relief, allowing salt water to penetrate many miles up the major drainages and to form an irregular line along the shore zone over the deposits of till, stratified drift, and clay. Some of the till hills stood as islands in the shallow seas. Wave action, which concentrated on the headlands, eroded the soft glacial deposits and spread them as connecting links across the mouths of shallow bays. Whenever a ledge was uncovered, it caused a halt in the recession of the headland, and the protruding ledge refracted the waves against its flanks, dissipating their energy. Boulder pavements remain where hills of glacial till were destroyed and the fine material was worked into beaches. Shallow bays, cut off by growing bars, filled with silt and peat up to high-tide level.

The erosion of the glacial debris and the construction of the beaches has probably occurred since the Postglacial Optimum, and the level of the sea has risen very slowly during the last several thousand years.

SUMMARY

During deglaciation and since then, the sea oscillated above and below its present level. The major configuration of the shore line resulted from the sea encroaching on modified glacial topography. Wave action rapidly chewed into the soft glacial deposits and transported the sand and pebbles laterally along the shore line, forming bars, spits, and tombolos. The boulders in the till, too large to be moved by the waves, were left behind as boulder pavements. Beach drifting occurred both north and south. The minor curves and positions of the beaches are the results of wave refraction. The slightly oblique orientation of the beaches from the shore-line trend is due to the fact that they face the direction from which the greatest storm waves approach. Beach development has smoothed out the shore line, in a geographic sense, by bridging the bays and connecting the islands.

REFERENCES CITED

Billings, M. P., 1955, Geological map of New Hampshire: Concord, N. H., N. H. State Plan. and Devel. Comm., Harvard Univ., and U. S. Geol. Survey

Chapman, D. H., 1950, Clays of New Hampshire, Mineral Resource Survey, Part 12: Concord, N. H., N. H. State Plan. and Devel. Comm., 27 p.

Chute, N. E., and Nichols, R. L., 1941, The geology of the coast of northeastern Massachusetts: Mass. Dept. Public Works-U. S. Geol. Survey Cooperative Geology Proj. Bull. 7, 48 p.

von Engeln, O. D., 1930, Type form of faceted and striated glacial pebbles: Am. Jour. Sci., v 19, p. 9–16

Fenneman, N. M., 1938, Physiography of eastern United States: New York, McGraw-Hill Book Co., 714 p.

Flint, R. F., *Chairman*, 1948, Glacial map of North America: Geol. Soc. America Special Paper 60

Flint, R. F., 1953, Probable Wisconsin substages and late Wisconsin events in northeastern United States and southeastern Canada: Geol. Soc. America Bull., v. 64, p. 897–920

Freedman, Jacob, 1950, Stratigraphy and structure of the Mt. Pawtuckaway quadrangle, southeastern New Hampshire: Geol. Soc. America Bull., v. 61, p. 449–491

Goldthwait, J. W., 1925, The geology of New Hampshire: Concord, N. H., N. H. Acad. Sci. Handb. 1, 86 p.

Goldthwait, J. W., Goldthwait, Lawrence, and Goldthwait, R. P., 1951, The geology of New Hampshire, Part 1, Surficial geology: Concord, N. H., N. H. State Plan. and Devel. Comm., 81 p.

Goldthwait, Lawrence, 1948, Glacial till in New Hampshire, Mineral Resource Survey, Part 10: Concord, N. H., N. H. State Plan. and Devel. Comm., 11 p.

Gutenberg, Beno, 1941, Changes in sea level, postglacial uplift and mobility of the earth's interior: Geol. Soc. America Bull., v. 52, p. 721–772

Hitchcock, C. H., 1878, The geology of New Hampshire: Concord, N. H., 2061 p. (3 volumes)

Jahns, R. H., 1951, Surficial geology of the Mt. Toby quadrangle, Massachusetts: U. S. Geol. Survey Quadrangle map

Johnson, D. W., 1919, Shore processes and shoreline development: New York, John Wiley & Co., 584 p.

—— 1925, The New England-Acadian shoreline: New York, John Wiley & Co., 591 p.

Johnson, D. W., and Reed, W. G., 1910, The form of Nantasket Beach: Jour. Geology, v. 18, p. 162–189

Katz, F. J., 1913, Clays in the Portland region, Maine: U. S. Geol. Survey Bull. 530i, p. 202–206

Krumbein, W. C., and Pettijohn, F. J., 1938, Manual of sedimentary petrography: New York, Appleton-Century-Crofts, 549 p.

Lewis, W. V., 1931, The effects of wave incidence on the configuration of a shingle beach: Royal Geog. Soc. Jour., v. 78, p. 128–148

—— 1938, The evolution of shoreline curves: Geologists Assoc. Proc., v. 49, p. 107–127

MacClintock, Paul, 1953, Leaching of Wisconsin glacial gravels in eastern North America: Geol. Soc. America Bull., v. 65, p. 369–384

Marmer, H. A., 1951, Tidal datum planes: U. S. Dept. Commerce, Coast and Geod. Survey Special Pub. 135, 142 p.

Mather, K. F., Goldthwait, R. P., and Thiesmeyer, L. R., 1942, Pleistocene geology of western Cape Cod: Geol. Soc. America Bull., v. 53, p. 1127–1174

Schalk, M. A., 1938, A textural study of the outer beach on Cape Cod, Massachusetts: Jour. Sed. Petrology, v. 8, p. 41–54

Shepard, F. P., 1937, Revised classification of marine shorelines: Jour. Geology, v. 45, p. 602–624

—— 1948, Submarine geology: New York, Harper and Bros., 338 p.

Thorarinsson, Sigurdur, 1940, Present glacier shrinkage and eustatic changes of sea level: Geog. Annaler, v. 22, p. 131–159

Tuttle, S. D., 1952, Kame terraces and kame plains in southeastern New Hampshire (Abstract): Geol. Soc. America Bull., v. 63, p. 1307

U. S. Army, Corp. of Engineers, 1953, Beach erosion control report on cooperative study of Hampton Beach, New Hampshire: Boston, Mass., Office of the Div. Eng., New England Div., 27 p.

DEPT. OF GEOLOGY, STATE UNIVERSITY OF IOWA, IOWA CITY, IOWA

MANUSCRIPT RECEIVED BY THE SECRETARY OF THE SOCIETY, SEPTEMBER 4, 1958

WOODS HOLE OCEANOGRAPHIC INSTITUTION CONTRIBUTION 991

Contribution No. 1000

REPRINT FROM JOURNAL OF MARINE RESEARCH, VOLUME 17, 1958

THE INFLUENCE OF THE CONTINENTAL SHELF ON THE TIDES OF THE ATLANTIC COAST OF THE UNITED STATES

By

ALFRED C. REDFIELD

Woods Hole Oceanographic Institution[1]

ABSTRACT

Examination is made of the hypothesis that the tide along the eastern coast of the United States results from a co-oscillation of water over the Continental Shelf engendered by motion at the continental slope, the barrier against which the oceanic tidal wave is reflected. Using methods which are effective in analyzing tides in embayments, the range of tide and the time of high water over the continental slope have been estimated from data on the tide at the coast and from the topography of the off-lying shelf. Estimates indicate that the time of high water and the mean range of tide along the continental slope are much more uniform than those at corresponding positions along the coastline, as consideration of the velocity of waves in deep and shallow water demands. Estimated mean ranges along the 1000 m contour agree closely with those observed at oceanic islands in the Northwest Atlantic. The estimated velocities of tidal motion across the Shelf agree roughly with the velocities of tidal currents measured from anchored vessels. It is concluded that the variation in local characteristics of the tide along this coast may be explained by the influence of the topography of the Continental Shelf upon tidal motion. The general application of these results is discussed.

INTRODUCTION

Present knowledge of tidal movement in oceanic basins is based almost exclusively on observations made along the coasts. It is only at oceanic islands that the ocean tide has been observed unaffected by the disturbing influence of continental boundaries. Consequently charts of cotidal lines of the oceans, such as those prepared by Whewell (1833), Harris (1904), Sterneck (1920) and Dietrich (1944), assume of necessity that the timing of the ocean tide is related to the time of high water at the coast. It has been recognized, of course, that shallow water distorts tidal behavior. Whewall wrote in 1836: "... the velocity of the tide-wave ... is very much less near the shore than it is in the open ocean: perhaps we may even consider the velocity of the tide-wave in littoral regions as a quantity of a different order, and governed by different laws from its velocity in the open ocean ...". Since then the special laws which relate the tide at the coast to the tide of the deep ocean do not seem to have received the attention they deserve.

---

[1] Contribution No. 1000 from the Woods Hole Oceanographic Institution.

The author's interest in tidal phenomena began during a visit to Friday Harbor at Professor Thompson's invitation in 1948, and his first publication on the subject contains a consideration of the tides in that region. The present paper is contributed in grateful recognition of the stimulus received from Professor Thompson at that time.

The influence of embayments on tidal behavior is well understood, at least in situations of simple topography. In narrow embayments the tide may be considered to be a co-oscillation engendered by the oscillation in the "outer sea". This co-oscillation approaches a standing wave in form (Doodson and Warburg, 1941). The influence of reflection at the head of an embayment is such that it augments the amplitude of the tide to a degree which depends on the relation of the time required for the wave to traverse the length of the bay to the period of the wave. Amplification is maximal when this time is $^1/_4$ period. The effect of friction is to delay the time of high water relative to that in the "outer sea" (Redfield, 1950). Fleming (1938), who has employed these principles in examining the tides in the Gulf of Panama, has extended his examination out to the continental slope so as to draw some conclusions about the effect of the Shelf's profile on the velocities of the tidal currents developed.

In the present paper the hypothesis is presented that along the eastern coast of the United States the tide on the Continental Shelf may be treated as a co-oscillation strictly analogous to that occurring in embayments. This co-oscillation is engendered by the ocean tide at the continental slope, which forms the effective barrier to the oceanic oscillation. The tidal wave on the Shelf is delayed in crossing the shallow water and is augmented by reflection at the coast so as to produce the varied elevations and tidal intervals observed along its length.

When the profile of the continental margin is considered, it is evident that the principal barrier to the oceanic oscillation must be the continental slope, since at this region the depth decreases abruptly from about 3,000 to 100 m. Tidal motion over the Continental Shelf must have negligible influence on the oceanic oscillation because of the relatively small volume of water involved. However, the ocean tide will give rise to a wave moving across the Continental Shelf which is reflected at the coast. The properties of the tide observed at the coast are derived from the oceanic oscillation after modification by the character of the co-oscillation across the shallow water of the Shelf. See Fig. 1.

By analogy with tides in embayments, it may be expected that the tide at the coast will be amplified by reflection to a degree increasing with the width of the Shelf up to the point where the time required for a wave to cross it equals $^1/_4$ period and that the time of high water will be delayed. If the oceanic wave front is nearly parallel to the continental slope and if the shelf is of variable width, it may be expected, because of the higher velocity of waves in deep water, that high water will occur more nearly simultaneously at the slope than along the shore. For the same reason, the gradients in elevation should be smaller at the slope than along the coast.

Cotidal charts of the Atlantic indicate that the eastern coast of the United States lies in a broad area in which the M_2 component, which dominates the Atlantic tide, occurs at about 12 hours after the moon's transit at Greenwich. Harris (1900) proposed that the semidiurnal tide along this coast was due to a standing oscillation of ocean water across a nodal line extending northeastward from the Windward Islands. The American coast forms a barrier, almost at right angles to the assumed direction of motion, against which this wave is reflected.

Along the coast the range of tide decreases progressively from nearly seven feet in Georgia to about half that value at Cape Hatteras, north of which the tidal range increases to about four and one-half feet at New York. The time of high water varies in a parallel way. The width of the Continental Shelf between Georgia and New York varies in a manner similar to the tidal characteristics.

Concepts which are effective in the analysis of tides in embayments have been used to deduce the properties of the tidal wave across the Continental Shelf from data obtained at the coast and from the topography of the Shelf. The agreement of the times of high water estimated for positions along the continental slope and of the amplitudes at these positions and at oceanic islands provides a criterion of the applicability of the procedures employed and of the validity of the hypothesis on which they are based. The outcome explains the variation in tidal behavior observed along the coast.

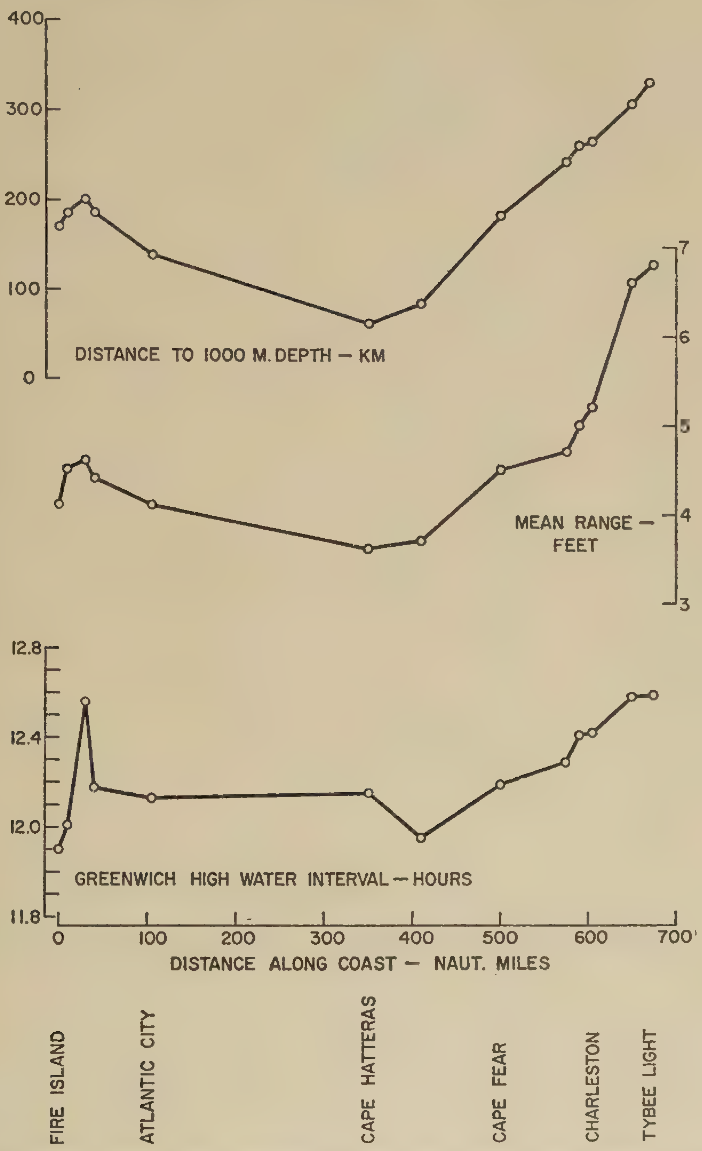

Figure 1. Mean range of tide, Greenwich High Water Interval, and distance to 1,000 m contour for selected outlying stations along the eastern coast of the United States.

Data. Data for the high water interval and mean range of tide recorded in Tide Tables Atlantic Ocean (U.S. Coast and Geodetic Survey, 1951) have been selected for 13 outlying positions. See Table I. The high water intervals for Cape Hatteras and Cape Lookout are revised figures supplied by the Coast and Geodetic Survey. Positions close to the mouths of larger bays have been eliminated because they appear to be influenced by tidal exchanges with the bay, resulting in delayed high water intervals and, usually, in relatively small ranges. The data for Sandy Hook, which are included, are suspect for this reason. East of Fire Island, New York, the tides at outlying positions appear to be greatly modified by the tidal exchange with Long Island Sound and the Gulf of Maine, while south of Svannah, Georgia the tidal ranges diminish progressively, presumably as a result of tidal motion through the Straits of Florida.

TABLE I.

Station	*Lat. N*	*Long. W*	*Mean Range (feet)*	*Greenwich High Water Interval (hrs)*	*Distance from Shore to 1,000 m Depth (km)*
Fire Island Breakwater	40°37′	73°18′	4.1	11.90	170
Long Beach	40°35′	73°39′	4.5	12.01	185
Sandy Hook	40°28′	74°01′	4.6	12.56	200
Sea Bright	40°22′	73°58′	4.4	12.18	185
Atlantic City	39°21′	74°25′	4.1	12.13	139
Cape Hatteras	35°14′	75°31′	3.6	12.15	62
Cape Lookout	34°37′	76°32′	3.7	11.95	85
Cape Fear	33°51′	77°58′	4.5	12.19	185
Cape Romain	33°01′	79°21′	4.7	12.29	245
Bull Bay, Jack Creek Entrance	32°56′	79°35′	5.0	12.41	263
Charleston Entrance, North Jetty	32°44′	79°48′	5.2	12.42	267
Hilton Head	32°14′	80°40′	6.6	12.58	310
Tybee Light, Savannah River	32°02′	80°51′	6.8	12.59	334

Elevations are expressed as mean range of tide in feet, assumed to equal approximately twice the amplitude of the M_2 component.

Times are expressed in hours as the high water intervals relative to the moon's transit at Greenwich.

For each of six positions between Fire Island Inlet and Tybee Light (Savannah, Ga.), the contour of the sea bottom was determined along the shortest line to the 1,000 fathom contour, using U.S. Coast and Geodetic Survey Charts 1000 and 1001.

Estimation of the Mean Range of Tide at the Continental Slope. If it is assumed that the tide on the Continental Shelf is a free co-oscillation driven by the ocean tide and reflected at the coast, the method of Sterneck (1915) may be employed to estimate, by successive application of approximate difference equations, the maximum elevation of the sea surface at increasing distances from the coast. This method was used successfully by Sterneck and by Defant (1919) in analyzing the tides in a number of landlocked seas. The procedure is described by Proudman (1953: 233). It is assumed in this application of Sterneck's method that the motion is along the shortest path between the coastal point and the 1,000 m contour and is modified only by the distribution of depth along that path. The motion along such a path is thus considered to be like that in a narrow gulf of unit width.

The method disregards friction, and it is implied in its application that components of motion at right angles to the path are negligible. The latter assumption cannot be justified rigorously since it is evident from the rotatory character of tidal currents observed at lightships that such components of motion are present.

Application of the method enables one to estimate the ratio η/η_0 at any distance from the coast and thus to obtain the maximum elevation, η, at that distance if the elevation at the coast, η_0, is known. The 1,000 m contour is used to define the position of the continental slope, and values of η found there are taken to indicate the mean range of the oceanic tidal wave at the slope.

Sterneck's method was applied to determine the relative elevation, η/η_0, at successive intervals of 10 km from the shore. The result of the calculation for Atlantic City is shown in Fig. 2. Note that over the continental slope, or beyond, the maximum elevations change very little with distance, which shows that the arbitrary depth of 1,000 m used to define the position of reflection of the oceanic wave might be varied considerably without changing significantly the estimate of the range of the oceanic tide. The maximum elevation at the 1,000 m contour is 0.66 that at the coast. Since the mean range at Atlantic City is 4.1 feet, the mean range at the 1,000 m contour off Atlantic City is estimated to be 2.71 feet.

Table II shows results of similar calculations for the six selected positions. The mean range at the 1,000 m contour is estimated to increase from 2.71 feet at Fire Island to 3.36 feet at Cape Hatteras and then to decrease to 2.79 feet at Tybee Light. This is an extreme difference of 0.65 feet as compared to 3.2 feet for the tidal ranges along the coast. The measured mean range of tide in nearby oceanic islands, Sable Island, Bermuda, Eleuthera, San Salvador, *et al.* is given as 2.6 feet, which is close to the ranges estimated for the 1,000 m contour off Atlantic City and Savannah.

The first criterion, that the oceanic oscillation has almost uniform elevations over great distances, is thus confirmed by the computation. Actually, the results show that the effect of the bottom topography

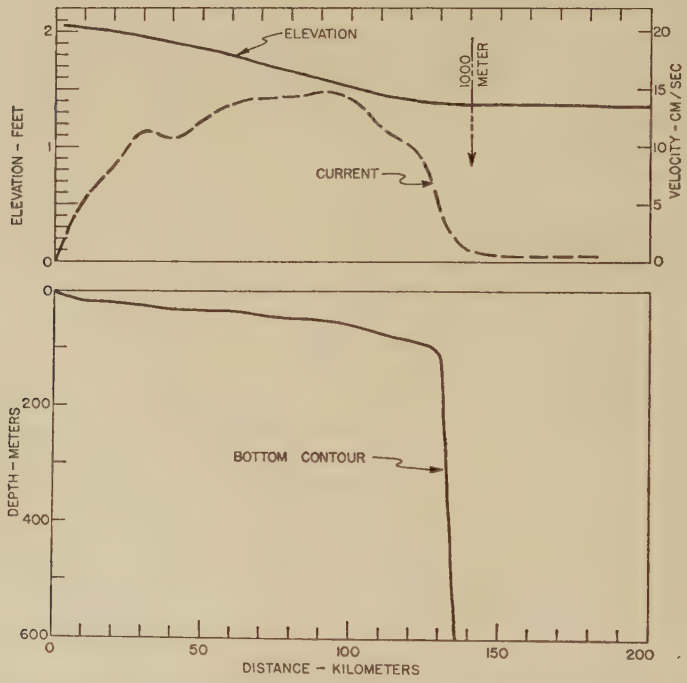

Figure 2. Profile of the Continental Shelf off Atlantic City and the distribution of estimated elevations at high water and maximum velocities of onshore and offshore tidal currents across this Shelf.

TABLE II. ESTIMATES OF THE MEAN RANGE OF TIDE AT THE 1,000 M CONTOUR

Station	*Bearing of Section-True*	*Mean Range at Coast (feet)*	η/η_0 *at 1,000 m Contour*	*Mean Range at 1,000 m Contour (feet)*
Fire Island	133°	4.1	0.66	2.71
Atlantic City	132°	4.1	0.66	2.71
Cape Hatteras	112°	3.6	0.93	3.36
Cape Lookout	120°	3.7	0.89	3.28
Cape Romain	118°	4.7	0.64	3.00
Tybee Light	105°	6.8	0.41	2.79

is *more* than enough to account for differences in the tidal range at the coast, since the greatest elevations of the oceanic tide are estimated to be off the capes of North Carolina, where the coastal range is in fact least.

Estimation of the Time of High Water at the Continental Slope. To account for the differences in high water intervals along the coast by the proposed hypothesis, it is necessary to introduce the assumption that the tidal wave is damped as it crosses the Continental Shelf. Otherwise high water would occur simultaneously, both along the coast and at the continental slope.

For a wave undergoing reflection and damping in a channel of uniform width, it may be deduced that

$$\eta/\eta_0 = {}^1/_2\,(\cosh\ 2\mu x + \cos 2kx), \tag{1}$$

where η/η_0 is the ratio of the elevation at high water at the position at which η is measured relative to that at the barrier from which the wave is reflected, kx is the phase difference due to the position at which η is measured relative to the barrier, k is 360°, and μ is a damping coefficient defined so that the attenuation per period is $e^{-\mu}$ (Redfield, 1950). Using this relation, the phase difference between the tidal wave at the 1,000 m contour and the adjacent coast may be estimated for any chosen value of the damping coefficient μ from the values of η/η_0 obtained by the Sterneck method and given in Table II.

Under similar conditions, the time of high water at any distance from the reflecting barrier is given by

$$\sigma t_H = \tan^{-1}\,(-\tan\ kx\ \tanh\ \mu x), \tag{2}$$

where σt_H is the time angle of high water at a point where the phase difference is kx. Having obtained the value of kx at the 1,000 m contour by eq. (1), the time of high water there relative to the time at the coast may be obtained, assuming the same value for the damping coefficient, μ, in both steps of the calculation. For example, at Atlantic City η/η_0 is found to be 0.66 at the 1,000 m contour. Assuming $\mu = 1.0$, kx is found to be $-50°$, using eq. (1). Applying this value of kx to eq. (2), σt_H is found to be $-9.2°$, or -0.32 hours. The Greenwich High Water Interval for the tide at Atlantic City is 12.13 hours; consequently it is 11.81 hours at the continental slope.

Lacking information on the damping coefficient to be applied over the Continental Shelf, values characteristic of large embayments have been employed. It has been found that a damping coefficient of $\mu = 1.0$ satisfies the conditions in Long Island Sound and the Bay of Fundy; 1.5 to 2.0 in the Straits of Juan de Fuca and Georgia (Redfield, 1950). Results of estimations using $\mu = 0.5$, 1.0, 2.0 are presented in Table III.

Estimates obtained with $\mu = 0.5$ are the most satisfactory. The extreme differences in Greenwich High Water Interval at the 1,000 m contour are found to be 0.43 hours, or 0.22 hours if the early time at Fire Island Inlet is left out of account. This compares with a difference of 0.69 hours at the corresponding coastal positions. Moreover the trend is progressive, high water occurring earliest at the northeastern part of the slope, latest toward the southwest. Using $\mu = 1.0$, the spread of times is slightly less, 0.38 hours, but high water is estimated to occur latest in the middle section of the coast, which appears to be unreasonable. A damping coefficient of 2.0 gives results which are quite unsatisfactory. The spread in values at 1,000 m is nearly as great as that at the coast, and high

TABLE III. ESTIMATES OF GREENWICH HIGH WATER INTERVAL AT THE 1,000 M CONTOUR

Station	$\mu = 0.5$	$\mu = 1.0$	$\mu = 2.0$
Fire Island	11.75	11.58	11.14
Atlantic City	11.98	11.81	11.37
Cape Hatteras	12.13	12.10	12.04
Cape Lookout	11.95	11.87	11.77
Cape Romain	12.13	11.96	11.49
Tybee Light	12.18	11.69	—

water occurs distinctly later off the North Carolina capes than to the north or south. No solution can be obtained for Tybee Light, since the theory does not provide for such reduced values of η/η_0 as are estimated by the Sterneck method.

Although the assumption of the value of the damping coefficient is quite arbitrary, it may be concluded that, by choosing a reasonable value for this coefficient, the second criterion of the hypothesis may be confirmed; namely, that the oceanic oscillation attains maximum elevations almost simultaneously over great distances along the continental slope. The topography of the slope is consequently such as to account for the variation in both tidal range and time of high water along the eastern coast of the United States.

Cotidal Lines of Continental Shelf. The mean range of tide and the high water interval may be estimated for any point on the Continental Shelf by precisely the same procedure as that employed for the 1,000 m contour. Such estimates were made for points where the sections cross the 50, 100 and 400 m contours. The resulting values, together with those for the 1,000 m contour and for the coastal points of observation, have been combined in Figs. 3 and 4 in order to construct cotidal charts for mean range and time of high water on the Continental Shelf.

The approximate character of these charts is recognized. However, they serve to give a co-ordinated picture of the estimated results and probably show in a general way the character of the tidal motion. The ocean tide appears to approach the coast at right angles to the trend of the continental slope from a direction of 110°. South of Cape Hatteras, where the coast line falls away toward the west, the crest of high water appears to cross the Shelf obliquely and becomes progressively delayed in reaching the coast. The widening Shelf leads to substantial increase in tidal ranges along this part of the coast.

Tidal Currents on the Continental Shelf. The hypothesis under examination considers that the tidal motion across the Shelf is rectilinear and perpendicular to the 1,000 m contour. It thus ignores any components of motion parallel to the coast. In contrast, observations from lightships and other anchored vessels show that the tidal currents are rotary except near the entrances to the larger bays (Haight, 1942). The current roses are so oriented, however, that at about three hours before high water, when maximal flow

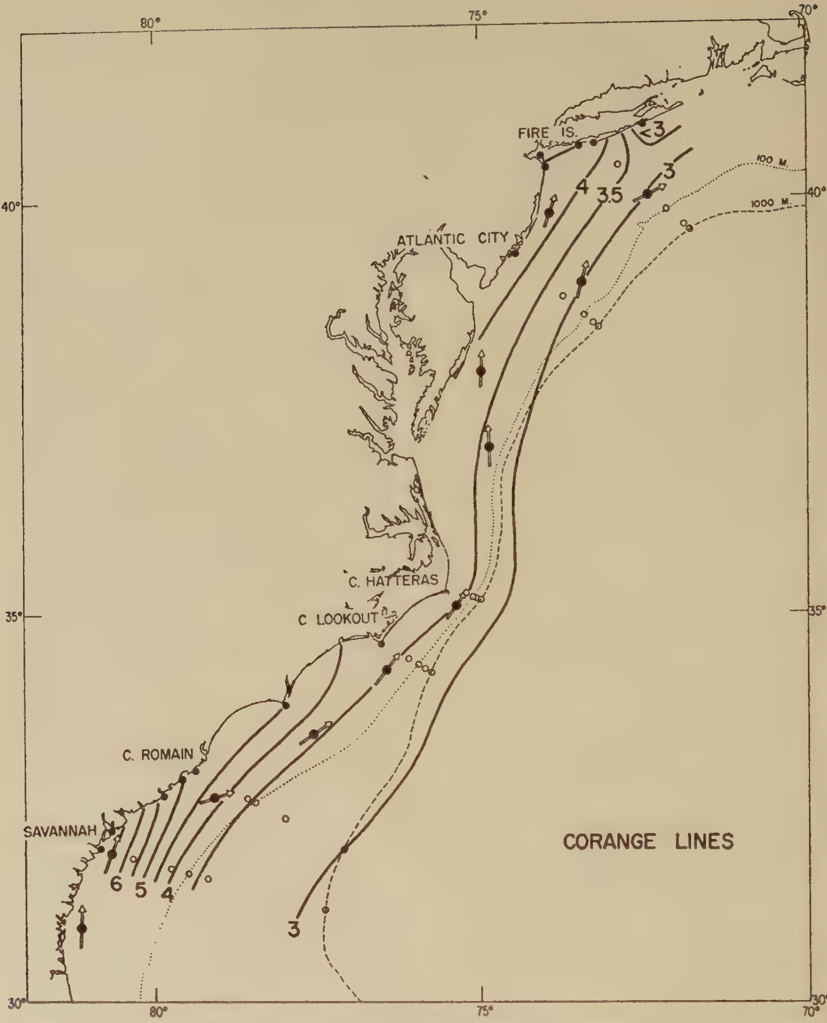
80°
75°
70°
40°
35°
30°
FIRE IS.
ATLANTIC CITY
C. HATTERAS
C LOOKOUT
C. ROMAIN
SAVANNAH
<3
4
3.5
3
6
5
4
3
100 M.
1000 M.
CORANGE LINES

Figure 3. Estimated mean range of tide, in feet, on the Continental Shelf off the eastern coast of the United States. Arrows show the direction of observed currents at high water.

onto the Shelf is expected, the direction of flow is approximately normal to the coast. At high water, when the change in elevation is zero, the currents flow northeasterly, parallel to the shore line.

These relations are illustrated in Figs. 3 and 4, in which arrows indicate the direction of motion observed at anchored vessels. In Fig. 4 the direction of current when the shoreward component of

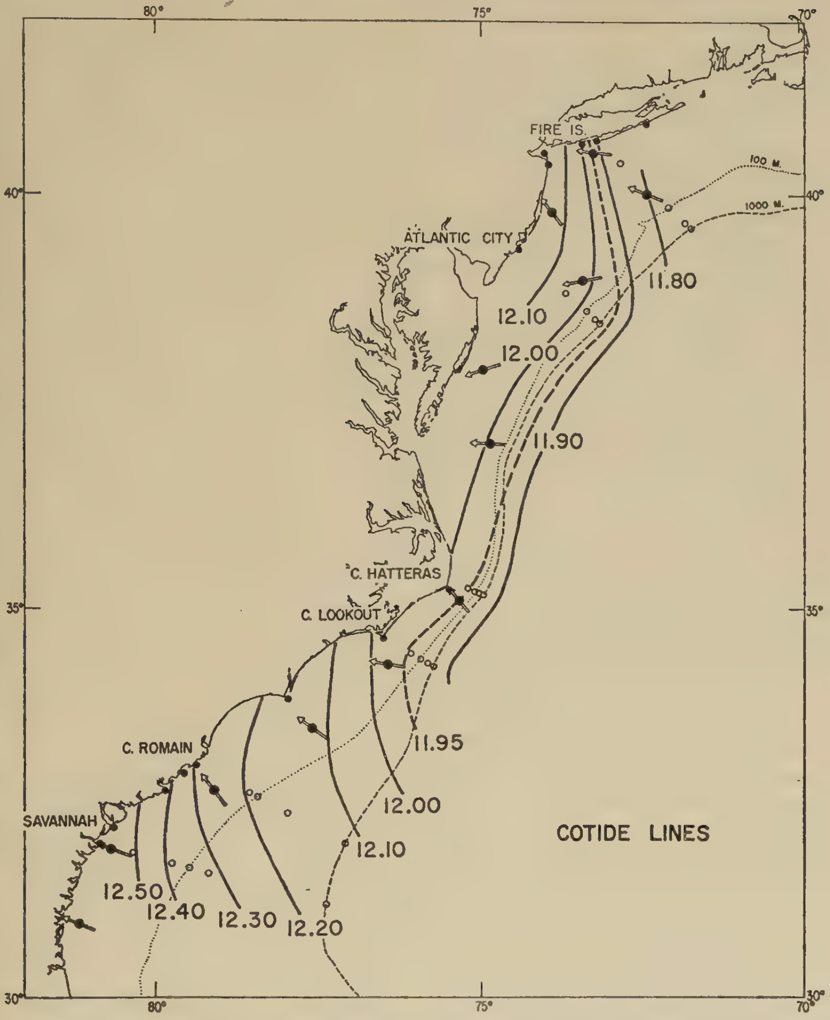
80°
75°
70°
40°
35°
30°
FIRE IS.
ATLANTIC CITY
C. HATTERAS
C. LOOKOUT
C. ROMAIN
SAVANNAH
100 M.
1000 M.
11.80
12.10
12.00
11.90
11.95
12.00
12.10
12.20
12.30
12.40
12.50
COTIDE LINES

Figure 4. Estimated time of high water, in hours after the moon's transit at Greenwich, on the Continental Shelf of the United States, made on the assumption that the damping coefficient, μ, is 0.5. Arrows show the direction of observed currents three hours before high water.

flow is maximal, approximately three hours before high water, is shown superimposed on the cotidal lines. In Fig. 3 the direction of flow at high water is shown superimposed on contours indicating the relative elevation of the sea surface at that time.

The assumption that components of motion parallel to the coast may be ignored is justified to a certain extent by the fact that these components are small at the time of maximal flow on and off the Shelf and that they reach their maximum strength only at high and low water, when on- and off-shore flow is zero. Moreover, the change in volume caused by such components flowing out of a section on one side will be compensated by flow into the section from the other.

The latter assumption is not exact, however, because it is observed that the coastwise currents at the time of high and low water are much stronger south of Cape Lookout than north of that point. Such a distribution of coastwise components may be expected to augment the elevations on the coast at high water in the neighborhood of Cape Hatteras and Cape Lookout, in a degree not considered by the theory. Such augmentation in turn would lead to exaggerated estimates of the tidal range at the 1,000 m contour and thus may account for the higher values estimated for these positions.

The method employed to calculate elevations of the sea surface across the Shelf yields also estimates of the maximum velocity of flow associated with tidal motion. The distribution of velocity obtained along the Atlantic City section is shown in Fig. 2. Using similar data for the several sections, Fig. 5 has been prepared to show the estimated maximum transverse velocities along the Shelf between Fire Island and Savannah.

As shown in Fig. 5, beyond the 1,000 m contour the tidal velocities are less than 2 cm/sec. The currents increase markedly at about the 100 m contour and attain greatest velocities in most regions a short distance inside this contour. These relations are similar to those estimated by Fleming (1938) for the Gulf of Panama. The highest velocities occur off Savannah relatively near the coast because of the local bottom topography. This section and that off Cape Romain show also some influence of the relatively shoal water over the Blake Plateau in accelerating the oceanic tidal movement. Between the 1,000 and 100 m contours the current increases from 2.5 to 5 cm/sec as the Continental Shelf is approached.

The estimated velocities may be compared with direct measurements of surface tidal currents made with current poles from anchored vessels. See Table IV. The mean hourly velocities and directions of such tidal currents, from which the nontidal current has been eliminated, are given by Haight (1942). The maximum flood and ebb velocities have been averaged to give the values for mea-

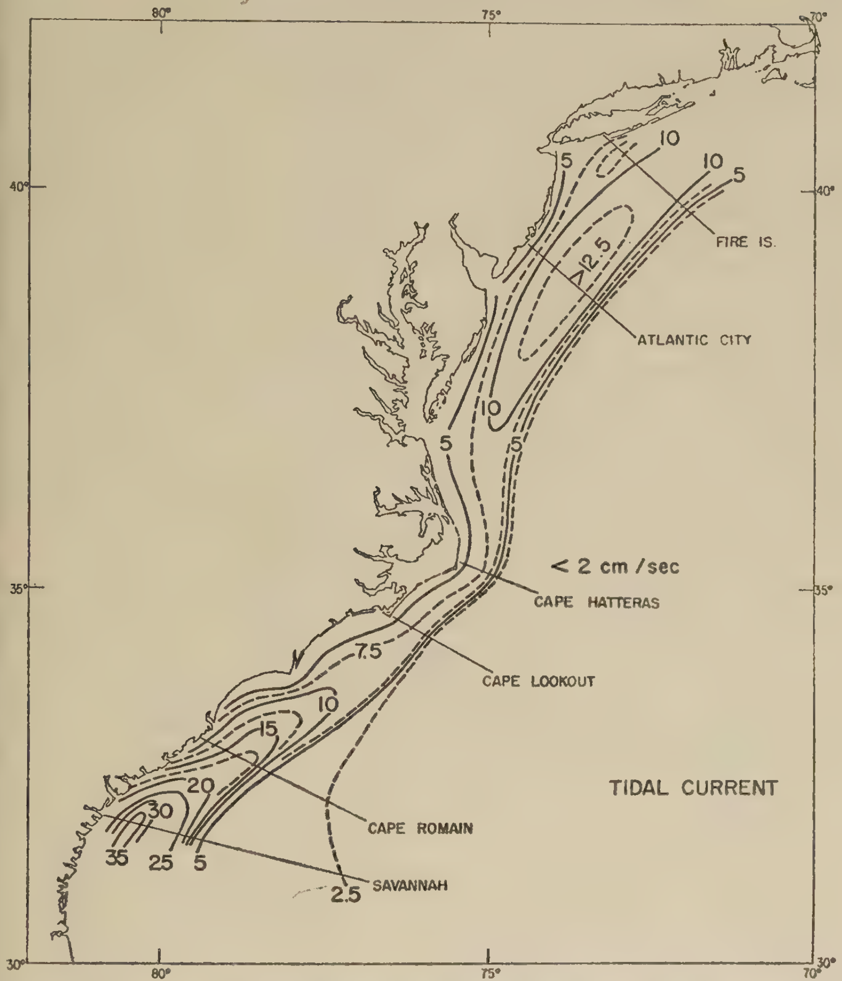
80°
75°
70°
40°
35°
30°
5
10
10
5
FIRE IS.
12.5
ATLANTIC CITY
10
5
5
< 2 cm /sec
CAPE HATTERAS
7.5
CAPE LOOKOUT
10
15
20
30
35
25
5
CAPE ROMAIN
SAVANNAH
2.5
TIDAL CURRENT

Figure 5. Estimated maximum onshore and offshore tidal current, in centimeters per second, on the Continental Shelf off the eastern coast of the United States.

sured currents listed in Table IV. No correction has been made for the departure in direction from a path normal to the coast. Such correction would decrease the values up to 20 $^0/_0$. The estimated currents at the position of the vessels are taken from Fig. 5 and are given to the nearest 2.5 cm/sec.

Comparison of the measured currents with those estimated shows general agreement in order of magnitude and in indicating much stronger currents off the coasts of Georgia and South Carolina than to the northward. The estimates for Cape Lookout Shoals and Frying Pan Shoals Lightship are substantially too high while those from positions north of Cape Hatteras are generally too low. Where measurements have been made at two or three different periods at the same position, the agreement between successive periods is not better than that between the estimate and the nearest measurement. It seems probable that lack of agreement is due to inadequacies in measurement quite as much as to faults in the estimations, and it may be concluded that the estimated currents have some validity, if not great precision, when applied to tides of the Continental Shelf.

TABLE IV. Onshore and Offshore Tidal Currents Measured from Anchored Vessels (Haight, 1942: table 5) compared with Estimated Currents shown in Fig. 5

Vessel	*Lat. N*	*Long. W*	*Date*	*Tidal Current (cm/sec)* *Measured*	*Estimated*
Fire Island l.s.	40°28′	73°11′	1938–39	7.2	7.5
u.s.s. Cardinal	40°16′	73°15′	1919	5.9	7.5
u.s.s. Finch	40°04′	72°43′	1919	6.4	10.0
u.s.s. Falcon	39°04′	72°25′	1919	3.1	12.5
Winter Quarter Shoal l.s.	37°55′	74°56′	1912–13	5.0	10.0
			1918–20	3.6	
u.s.s. Brant	37°05′	74°51′	1919	9.3	10.0
Diamond Shoal l.s.	35°05′	75°19′	1921	1.8	7.5
Cape Lookout Shoals l.s.	34°20′	76°25′	1912	21.0	7.5
			1918–19	9.0	
Frying Pan Shoals l.s.	33°34′	77°48′	1912	23.5	10.0
			1918–21	16.0	
u.s.s. Long Island	32°42′	79°06′	1919	15.0	17.5
Charleston l.s.	32°41′	79°44′	1912	21.6	15.0
			1915–16	16.2	
			1921	15.7	
Martin's Industry l.s.	32°06′	80°28′	1912	26.7	25.0
			1916	22.9	
Savannah l.s.	31°57′	80°40′	1912	21.1	25.0
			1916	15.7	

DISCUSSION

The correlation between the tidal range on the Atlantic coast of the United States and the width of the Continental Shelf and the demonstration that variations in amplitude and time of high water along the coast may be explained by the influence of the Shelf's configuration suggest that similar relations may exist more widely.

Examination of the amplitude of the M_2 component along the coasts of the world oceans, shown for example by Dietrich (1944: tafel 3), indicates that semidiurnal tides of exceptional amplitude occur in areas with unusually broad continental shelves. Examples are the southeast coast of South America and the northwest coasts of Europe and Australia. Conversely, long stretches of coasts having relatively narrow shelves have semidiurnal tides of small amplitude. Examples are the west coasts of Africa and South America and the east coast of Asia. However, when the amplitude of the M_2 component at a large number of coastal positions throughout the world is compared with the width of the off-lying continental coast, say, to the 1,000 m contour, no satisfactory correlation is obtained. The greatest amplitude of the M_2 tide occurring at any width of shelf does increase with the width at a rate of about one foot per 20 nautical miles. However, at any one width, amplitudes of any value less than the maximum may occur. It is only when the width of the shelf is greater than 150 nautical miles that the smaller amplitudes are not to be found. It is evident that factors other than the width of the shelf influence the amplitude of the tide at the coast.

Among such factors may be listed: the amplitude of the ocean tide itself; the angle of approach of the oceanic wave; the actual profile of the bottom across the shelf, which may be relatively deep or shallow within the limits on the shelf; the influence of local embayments in the coast line; and the period of the tidal component in question. Understanding of the relation of the tide, as observed along the coast, to the oscillation of the off-lying deep water consequently requires a detailed examination of these factors as they apply to any region in question. The coast under consideration in the present paper is particularly favorable for such studies because the ocean tide occurs so nearly simultaneously along its length that tidal movement on the Shelf may be dealt with as a transverse oscillation. The system of motion in other regions is no doubt much more complicated, but it is hoped that the application of principles similar to those employed in the present case may be effective in clarifying the relation of the coastal tide to that of the ocean basins.

REFERENCES

Defant, Albert

1919. Untersuchungen über die Gezeitenerscheinungen in Mittel- und Randmeeren, in Buchten und Kanälen. Denkschr. Akad. Wiss. Wien, *96*: 57–174.

Dietrich, G.

1944. Die Schwingunsysteme der halb- und eintatigen Tiden in den Ozeanen. Veroff. Inst. Meeresk. Univ. Berl., n.f.A., geogr.-naturwis., *4*: 1–68.

Doodson, A. T. and H. D. Warburg

1941. Admiralty Manual of Tides. London. 270 pp.

Fleming, R. H.

1938. Tides and tidal currents in the Gulf of Panama. J. Mar. Res., *1*: 192–206.

Haight, F. J.

1942. Coastal currents along the Atlantic coast of the United States. Spec. Publ. U.S. Cst. geod. Surv., No. 230; 73 pp.

Harris, R. A.

1900. Manual of tides. Part IV A. Outlines of tidal theory. Rep. U.S. Cst. geod. Surv., App. No. 7: 537–699.

1904. Manual of tides. Part IV B. Cotidal lines for the world. Rep. U.S. Cst. geod. Surv., App. No. 5: 313–400.

Proudman, Joseph

1953. Dynamical oceanography. Methuen, London; Wiley, New York. 409 pp.

Redfield, A. C.

1950. The analysis of tidal phenomena in narrow embayments. Pap. phys. Oceanogr. Meteorol., *11* (4): 1–36.

Sterneck, R. V.

1915. Hydrodynamische Theorie der halbtägigen Gezeiten des Mittelmeeres. S.B. Akad. Wiss. Wien, Math.-Naturwiss., Abt. II a, *124*: 905–979.

1920. Die Gezeiten der Ozeane. S.B. Akad. Wiss. Wien, Math.-naturwiss., Abt. II a, *129*: 131–150.

U.S. Coast and Geodetic Survey

1951. Tide Tables East Coast North and South America for the Year 1952. Ser. No. 742. Washington, D.C. 174 pp.

Whewell, William

1833. Essay towards a first approximation to a map of cotidal lines. Philos. Trans., 1833: 147–236.

1836. On the results of an extensive series of tidal observations. Philos. Trans., 1836 (II): 289–342.

Contribution No. 1005

SOME USES OF ANTIBIOTICS IN PHYSIOLOGICAL EXPERIMENTS IN SEA WATER[1]

BY

S. M. MARSHALL AND A. P. ORR

Marine Station, Millport, Scotland
and *Woods Hole Oceanographic Institution*

ABSTRACT

The oxygen content of sea water can be kept constant by use of antibiotics for periods up to more than a fortnight. With living animals present, the bacteriostatic effect probably lasts for a shorter time. Chloromycetin was the most effective antibiotic used; streptomycin was also satisfactory. However, some samples of chloromycetin may prove harmful to marine animals; it sometimes inhibited the feeding of copepods. A combination of chloromycetin and streptomycin proved suitable for controlling bacterial action in measurements of phosphorus excretion. Since we do not know the original bacterial content of the sea water used, the results are bound to vary from one experiment to another, but in general the use of antibiotics can extend the scope and accuracy of physiological work.

In the open sea bacteria are generally found attached to solid particles. Although in open sea water a large number of free bacteria is not usually found, the situation changes whenever the water is brought into the laboratory, for bacteria then develop rapidly on the surface of the container (Waksman and Renn, 1936; ZoBell and Anderson, 1936). Their multiplication may lead to considerable changes in the constituents of the water, *e. g.*, the oxygen and dissolved phosphate.

Antibiotics have been used in sea water to control bacterial growth in experiments varying from the culture of phytoplankton organisms (Fish, 1950; Spencer, 1952) to the preservation of fish (Tarr, *et al.*, 1950). Cviić (1953) worked on the effect of antibiotics on particular species of marine bacteria. Oppenheimer (1955) found that the use of suitable antibiotics prevented bacterial growth on the surface of pelagic fish eggs and he thus increased the percentage hatch of both cod and sardine eggs. Walne (1958) observed increased production of spat by *Ostrea edulis* in the presence of penicillin, and

---

[1] Contribution No. 1005 from the Woods Hole Oceanographic Institution.

REPRINT FROM JOURNAL OF MARINE RESEARCH, VOLUME 17, 1958

Harris (1957), finding that terramycin decreased the uptake of ^{32}P by *Gammarus*, concluded that it had killed the bacteria on which *Gammarus* had fed.

In the following account the influence of a number of common antibiotics on the respiration, feeding and excretion of marine copepods is reported. The antibiotics used are listed in Table I.

TABLE I. ANTIBIOTICS EMPLOYED

Antibiotic	*Salt*	*Strength (units)*	*Source*
Penicillin	Benzylpenicillin, crystalline potassium salt	10,000/ 50–60 mg tablet	Burroughs Wellcome, Ltd.
Chloromycetin	Chloramphenicol B.P.	Pure	Parke Davis, Ltd.
Streptomycin	Dihydrostreptomycin sulphate B.P.	5 mega/g	Glaxo, Ltd.
Polymixin	Polymixin B sulphate B.P.C.	6000/mg	Burroughs Wellcome, Ltd.
Tetracycline	Tetracyn hydrochloride	Pure	Pfizer, Ltd.
Bacitracin	—	70/mg	Pfizer, Ltd.

Oxygen consumption. When natural sea water is incubated in the laboratory, an initial lag period is followed first by a rapid decline and then by a more gradual decline in oxygen content (Rakestraw, 1947). In measurements of the respiration of marine animals lasting for more than a few hours, allowance has to be made for this. In order to obtain sufficient reduction in oxygen content with small animals in short-term experiments, the volume of water per individual has to be small, and this may affect metabolism. The difficulty can be overcome by using antibiotics to keep the bacterial population low and thus increase the duration of the experiment.

Sea water was filtered through a membrane filter of average pore diameter $< 1\ \mu$ to remove most of the living and particulate matter which might affect oxygen consumption. To these filtered samples the different antibiotics were added in concentrations of 50 mg/l. Filled bottles were kept in the dark at 10° C, and at intervals the water was analysed for oxygen by the Winkler method. Controls without antibiotics were also used. Results are shown in Fig. 1.

Chloromycetin was the most effective antibiotic since, with 50 mg/l, the oxygen remained constant for 11 to 21 days; at a lower concentration of 10 mg/l it was reliable for periods of only 5 to 7 days. Streptomycin was tested several times; it maintained a constant oxygen in the water for 3 to 7 days. Tetracycline was tested twice; in one case there was actually a slight increase in oxygen and the antibiotic effect lasted for 6 days; in the second, it lasted 3 to 4 days. A tetracycline solution turns pink on exposure to light. With bacitracin there was a steep fall in oxygen after three days, this being more marked than in the control. Unfortunately, penicillin cannot be used since it reacts with iodine liberated in the Winkler method.

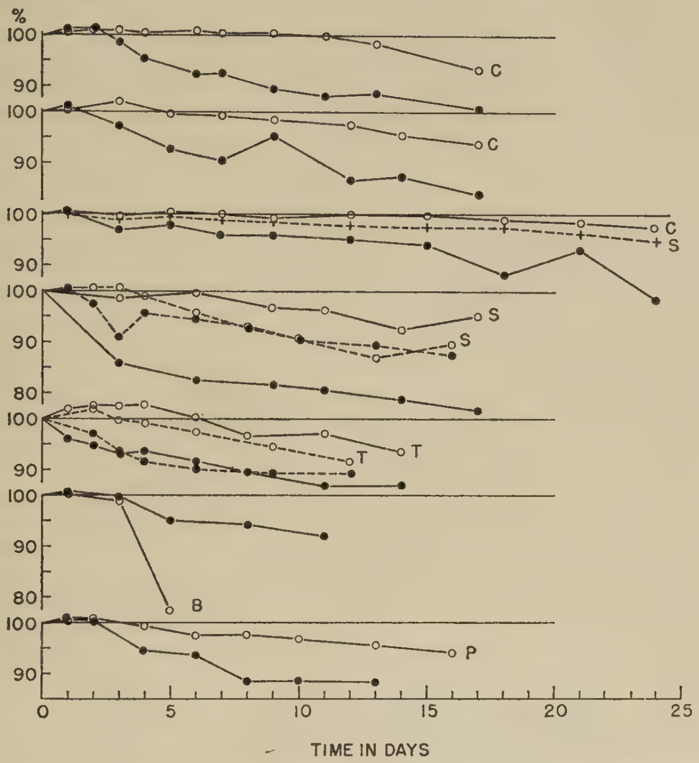

Figure 1. Oxygen consumption in samples of sea water with and without antibiotics added. Oxygen expressed in percent of initial value. Open circles, with antibiotic; solid circles, without antibiotic (controls). C, Chloromycetin; S, Streptomycin; T, Tetracycline; B, Bacitracin; P, Polymixin. All 50 mg/l except C in the second graph from the top, which had 10 mg/l.

To test whether or not antibiotics affected the respiration of experimental animals, the oxygen consumption of two sets of female *Calanus finmarchicus* was compared, one without addition of antibiotics and one with chloromycetin and streptomycin added (50 mg/l of each). Each set consisted of ten bottles, each containing 5 *Calanus*; there were three controls with no *Calanus*. The respiration in those bottles with antibiotics was 0.383 μl/*Calanus*/h (range 0.29–0.52) and in those without, 0.341 (range 0.17–0.46). There is therefore no significant effect.

Feeding. Although antibiotics are helpful in controlling bacterial growth when culturing marine animals, some antibiotics may inhibit feeding or have other harmful effects. According to Dr. R. H. Millar (personal communication), chloromycetin may kill oyster larvae. Experiments on feeding were made with *Calanus* as test animal.

One *Calanus* was put into each of a number of small dishes which usually contained 15 ml sea water to which the antibiotic (50 mg/l) and diatoms had been added. There were usually 10 experimental *Calanus* and 20 controls. After about 24 hours the copepods were removed and the amount of food eaten was measured by counting the number of faecal pellets produced. In different experiments the number varied with the concentration of diatoms and with the species used. There is great individual variation, and in any experiment there were usually one or two *Calanus* which did not feed at all.

With penicillin, feeding was always good. Chloromycetin usually depressed feeding markedly as did the mixture of chloromycetin and streptomycin. Streptomycin by itself had little or no effect. The other antibiotics tested were only slightly depressing. It is interesting that the streptomycin and chloromycetin mixture used at Millport had much less of a tendency to depress feeding than that used at Woods Hole, which presumably came from a different source.

Chloromycetin proved so useful in experiments on oxygen control that further feeding experiments were performed with the concentration reduced from 50 to 25 and 10 mg/l. In the first experiment the *Calanus* fed unexpectedly well at all strengths, but in the second there was a rise in faecal pellet production with decreasing strength of antibiotic.

Experiments were also carried out to find if solutions of chloromycetin lose their harmful effect on keeping. As before, the copepods did not feed well, but there was no apparent change in feeding in solutions one day and nine days old.

Excretion. In a series of experiments on phosphorus excretion by marine copepods, cultures of diatoms and flagellates labelled with ^{32}P were used as food. An attempt was then made to estimate the excretion by measuring either the decrease in ^{32}P in the copepod itself or the gain in ^{32}P by the water in which the copepod had been kept. The first method is less suitable since it is less accurate and involves the exposure of the copepod in a small drop of water for several minutes, which may injure it. The figures of loss from the copepod and gain by the water should have been the same, but in only one set of experiments did they agree fairly well, for about 12 days. In most cases the loss from the copepod was much above the gain by the water.

Since it is probable that bacteria on the walls of the container take up phosphorus, two series of experiments were carried out with antibiotics (chloromycetin and streptomycin, 50 mg/l of each) added to the water. In these the measurements of loss from the body and gain by the water were much closer. In the first experiment, with six individuals, measurements were made on alternate days, and the ratio of gain of P in the water to loss from the copepod body varied from 85 to 112 $^0/_0$, averaging 96.4 $^0/_0$. In the second (14 individuals), the interval between measurements was increased to three days, and in this case the ratio varied from 80 to 111 $^0/_0$, with an average of 99 $^0/_0$. The antibiotics therefore make it possible to get a fairly accurate estimate of phosphorus excretion without any harm to the animal. Penicillin or a combination of penicillin and streptomycin would probably be more suitable since neither affects feeding.

We should like to thank the Director and Staff of the Woods Hole Oceanographic Institution for their hospitality. We are also grateful to Dr. R. Cruickshank, Professor of Bacteriology, University of Edinburgh, for his help and to Messrs. Burroughs Wellcome & Co. and Messrs. Pfizer, Ltd. for samples of antibiotics.

REFERENCES

Cvičć, Vlaho

1953. The bactericidal and bacteriostatic action of antibiotics on marine bacteria. Acta Adriat., *5* (7): 1–30.

Fish, G. R.

1950. A method of obtaining bacteria-free cultures of a marine flagellate and *Enteromorpha intestinalis*, using penicillin. Acta Hort. gothoburg, *18*: 81–89.

Harris, Eugene

1957. Radiophosphorus metabolism in zooplankton and microorganisms. Canad. J. Zool., *35*: 769–782.

Oppenheimer, C. H.

1955. The effect of marine bacteria on the development and hatching of pelagic fish egos and the control of such bacteria by antibiotics. Copeia, 1955: 43–49.

Rakestraw, N. W.

1947. Oxygen consumption in sea water over long periods. J. mar. Res., *6*: 259–263.

Spencer, C. P.

1952. On the use of antibiotics for isolating bacteria-free cultures of marine phytoplankton organisms. J. Mar. biol. Ass. U.K., *31*: 97–106.

Tarr, H. L. A., B. A. Southcott and A. M. Bissett

1950. Effect of several antibiotics and food preservatives in retarding bacterial spoilage of fish. Progr. Rep. Fish. Res. Bd. Canada, No. 83: 35–38.

Waksman, S. A. and C. E. Renn

1936. Decomposition of organic matter in seawater by bacteria. III. Factors influencing the rate of decomposition. Biol. Bull. Woods Hole, *70*: 472–483.

Walne, P. R.

1958. The importance of bacteria in laboratory experiments on rearing the larvae of *Ostrea edulis* (L.). J. Mar. biol. Ass. U.K., *37*: 415–425.

ZoBell, C. E. and D. Q. Anderson

1936. Observations on the multiplication of bacteria in different volumes of stored sea water and the influence of oxygen tension and solid surfaces. Biol. Bull. Woods Hole, *71*: 324–342.

Contribution No. 1007

REPRINT FROM JOURNAL OF MARINE RESEARCH, VOLUME 17, 1958

THE ANNUAL CYCLE OF PHOSPHORUS AND NITROGEN IN NEW ENGLAND COASTAL WATERS

BY

BOSTWICK H. KETCHUM, RALPH F. VACCARO
AND NATHANIEL CORWIN

Woods Hole Oceanographic Institution[1]

ABSTRACT

Distributions of phosphorus and nitrogen in New England coastal waters at various times of year are described. In surface waters the nitrate-nitrogen content is sometimes completely exhausted, even though small concentrations (0.2–0.5μg-at/l) of phosphorus are always available. The ratio of concentrations by atoms, N:P, varies in surface waters from maximum values of about 10:1 to values approaching zero as the nitrate is exhausted. However, the ratio of change, ΔN:ΔP, is approximately 15:1 except during summer months when it decreases. During summer, vertical mixing supplies nitrogen and phosphorus to the euphotic zone at higher ratios than the ratios of concentration in the euphotic zone. In deep offshore waters the N:P ratio is about 12.5:1, and no significant seasonal variation in either the phosphorus or nitrate concentration at the oxygen minimum-nutrient maximum layer could be detected.

INTRODUCTION

Phosphorus and nitrogen concentrations in surface waters of the sea decrease as a result of utilization by phytoplankton but are replenished by decomposition of organic matter *in situ* and by mixing, which brings supplies back to the surface from richer, deeper waters. The concentration of these two elements change in a correlated way. Harvey (1926) commented upon the remarkable fact that during the spring outburst of phytoplankton in the English Channel both nitrogen and phosphorus were reduced simultaneously to negligible concentrations. Redfield (1934) showed that this observation of Harvey's was generally applicable to various oceanic bodies of water and that the ratio of change of concentration was similar in all of the waters studied. When the phosphorus concentration values are corrected for salt error, as suggested by Cooper (1938), these elements vary in a ratio of 15 atoms of nitrogen to one of phosphorus. As shown by Redfield (1934) and Fleming (1940), the ratio in which the elements vary in sea water is closely comparable to the concentration found within living marine organisms.

---

[1] Contribution No. 1007 from the Woods Hole Oceanographic Institution. This investigation was supported in part by Contract AT (30-1)-1918, with the U.S. Atomic Energy Commission and in part by grants from the National Science Foundation.

When the ratio of concentrations in a single sample of water is calculated, it is frequently found that this has a different value from the 15:1 ratio of change. Cooper (1937, 1938) termed the difference between the 15:1 ratio and the observed ratio the anomaly of the N:P ratio; and he pointed out also that this anomaly is greatest in confined seas such as the Mediterranean. Phifer and Thompson (1937) showed that this ratio had a mean annual value in San Juan Channel of 12.7 but that it varied throughout the year from 11.9 to 13.6. Even more extreme values for the N:P ratio were found by Riley and Conover (1956) in Long Island Sound. There, on a seasonal cycle, the ratio varied from nearly zero to 8:1. The extremely low values reflect the fact that phytoplankton were able to remove practically all of the nitrogen from the water even though there was a small residual concentration of phosphorus (about 0.5 μg-at/l).

Over the last two years, during investigations in coastal waters off New England at stations shown in Fig. 1, concentrations of nitrogen and phosphorus have been measured on each cruise. Even in these exposed coastal waters the ratio of concentrations in surface waters is low, and, as in Long Island Sound, values fluctuate from near zero in the summertime to 5–10 in midwinter. In spite of these low ratios of *concentration*, the ratio of *change* of nitrogen and phosphorus in the surface waters corresponds closely to a ratio of 15:1, excepting changes in surface waters in summertime.

METHODS

The cruises which have been made to the area indicated in Fig. 1 are listed in Table I. Aliquots of samples taken from various depths were frozen immediately in 500 ml plastic bottles at a temperature of about −15° C. Duplicate analyses of fresh samples at sea and of frozen samples have confirmed the fact that frozen samples give satisfactory results for inorganic phosphorus, nitrate, nitrite and

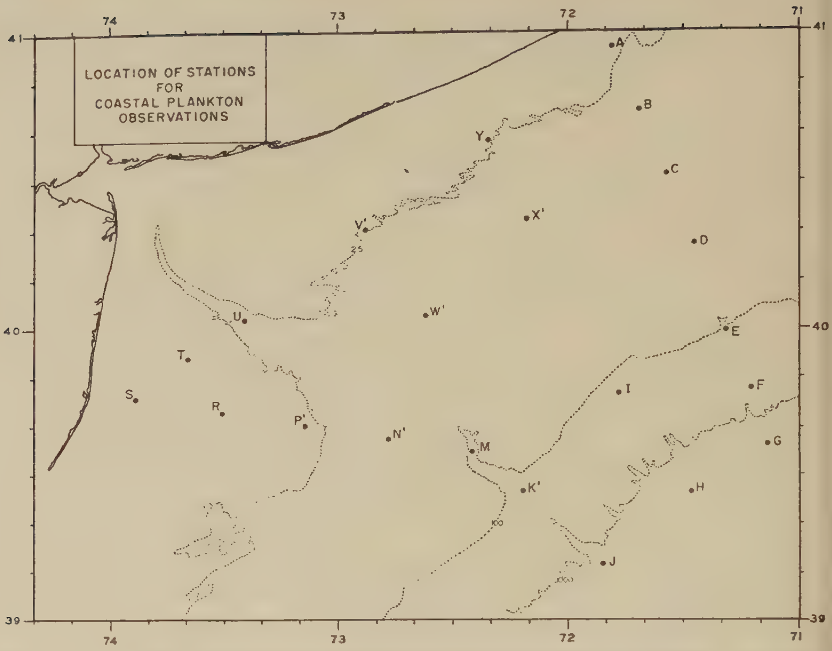

Figure 1. Location of stations occupied during coastal cruises, September 1956–1958.

ammonia nitrogen and silicate analyses for periods of at least a month of frozen storage.

The method for inorganic phosphorus determination has been described by Wattenberg (1937), Robinson and Thompson (1948), and Wooster and Rakestraw (1951). The color developed was measured in a photoelectric colorimeter (Ford, 1950), using a red light filter (Corning 2408) and absorption cells of 29 and 8 cm light path for concentrations of less than 1.0 and more than 1.0 μg-at P/l, respectively. The reproducibility of the method was discussed by Ketchum, *et al.* (1955), who have given analytical variations of $\pm 7\ ^0/_0$ for the low concentrations in the 29 cm tube and of $\pm 9\ ^0/_0$ for the higher concentrations in the 8 cm tube. Total phosphorus was determined by the method described by Harvey (1948) as modified by Ketchum, *et al.* (1955).

The nitrate concentration was determined by hydrazine reduction according to the method of Mullin and Riley (1955). The nitrite produced was reacted with alpha napthylamine, and the concen-

TABLE I. DATES OF CRUISES MADE TO THE NEW ENGLAND COASTAL WATERS

Vessel and Cruise No.	*Date*
ATLANTIS, 227	10–15 September 1956
CRAWFORD, 8	28 November–3 December 1956
BEAR, 159	13–17 February 1957
BEAR, 162	21–25 March 1957
BEAR, 165	29 April–3 May 1957
CRAWFORD, 13	10–20 July 1957
BEAR, 174	16–20 September 1957
BEAR, 179	18–23 November 1957
BEAR, 181	21–27 January 1958
BEAR, 183	6–10 March 1958
BEAR, 185	12–16 May 1958
CRAWFORD, 19	7–19 July 1958
BEAR, 195	5–8 September 1958

TABLE II. REPRODUCIBILITY OF THE DETERMINATION OF NITRATE-NITROGEN BASED ON STANDARDIZATION DATA. ANALYSES WERE MADE IN A BECKMAN DU SPECTROPHOTOMETER AT A WAVELENGTH OF 524 $m\mu$

Concentration Range (μg-at/l)	*Cell Length (cm)*	*No. of Standards*	*Calibration Factor*	*Standard (units)*	*Deviation (%)*
0– 3.75	10	25	5.85	.75	12.9
1.0–50	1	67	53.2	7.38	13.9

tration was then determined in a Beckman DU Spectrophotometer using a wavelength of 520 $m\mu$. The result will be referred to in this paper as nitrate-nitrogen, but both nitrate and nitrite-nitrogen are included in the analysis. The concentration of nitrite-nitrogen, which has also been determined for these samples, is generally less than 10 % of the nitrate plus nitrite-nitrogen.

The reproducibility of the method has been evaluated by comparing standard solutions at various concentrations. Standards were prepared by adding known amounts of nitrate to nitrate-free sea water and, after correcting for reagent blank and for the quantity of nitrate-nitrogen in the sea water used, the factor relating optical density of the photometer with concentration was calculated for each sample. For low concentrations ($< 4\ \mu$g-at/l) a 10 cm cell has been used; the ratio of concentration to optical density is $5.85 \pm .75$, or a variability of about 13 % (see Table II). For samples containing more nitrogen than this, a one centimeter cell was used; an average factor of 53.2± 7.38 was found for these concentrations, indicating a variability of about 14 %.

Total nitrogen is the sum of the concentrations of nitrate and nitrite-nitrogen, ammonia nitrogen and amine-amide nitrogen. Ammonia nitrogen has been determined by the method of Riley (1953). Amine-amide nitrogen has been determined by micro-Kjeldahl digestion according to Pregl (1946) followed by distillation of the ammonia according to Riley (1953).

THE ANNUAL CYCLE IN SURFACE WATERS

Variations in the nitrogen and phosphorus concentrations and in the N:P ratio for surface waters in Sections A-G-J (see Fig. 1) are shown in Figs. 2, 3 and 4. Five of the 13 cruises have been selected as representing adequately the seasonal variations. The density structure for the same five cruises is presented in Fig. 5 for comparison. In July and September, when the density stratification is greatest, the concentration of both nutrients in the surface layers is small, the lowest values being observed during the September cruises. In waters below 100 m at these times there is considerable parallelism not only between the distribution of the two nutrients but between each of these and the distribution of density. Thus, for example, there is always present just off the Continental Shelf, at St. E, a high concentration of nutrients in the same area; this shows as an upward bulge in the density contours. In contrast, lower values are found at Sts. G and H where comparable density contours are at greater depths than at St. E.

By November the density stratification has decreased markedly and surface concentrations of nitrogen and phosphorus have increased. Over the Continental Shelf, the increases in waters of less than 50 m are accompanied by decreases in waters below 50 m, indicating that much of the observed change may be due to mixing of the water column rather than to regeneration of nutrients *in situ*. Beyond the edge of the Continental Shelf, however, the nitrogen and phosphorus content has increased below 100 m of depth, indicating that mixing here has extended to greater depths.

In January, waters over the Shelf are vertically homogeneous in density, and the nutrient concentrations, though much less than those found in the deeper offshore waters, have reached maximum values for the year. By May, stratification in the water column has been intensified, both by freshening of the inshore water (at St. A) and by warming of the surface layers. The surface nitrate values at this time are almost all less than 1 μg-at/l and the surface phosphorus concentrations less than 0.5 μg-at/l—conditions which represent closely the concentrations observed in July and September.

The ratio of N:P (in atoms) in the surface waters, shown in Fig. 4, is consistently below 5 in July, September and November, with minimum values of zero in some of the September observations indicating complete exhaustion of the nitrate. By January the ratio of concentration has increased to values generally above 5 in surface waters over the Continental Shelf and commonly above 10 at the offshore stations. By May, when the growth of plants has again depleted the supply of nutrients, the ratio of concentration in surface waters is again less than 5.

The fact that the growth of plants in surface waters over the Shelf reduces the N:P ratio implies that plants are assimilating these elements in a higher ratio than the ratio of concentration which is presented to them. In regard to the constancy of the ratio of change, Redfield (1934) commented that "it appears to mean that the relative quantities of nitrate and phosphate occurring in the oceans of the world are just those that are required for the composition of the animals and plants which live in the sea". In the case of the coastal waters of New England, these elements are presented to the population in quite a different ratio from the *normal* 15:1 ratio. It is pertinent to inquire, therefore, whether these coastal populations have become adapted to these low ratios and utilize these elements in a ratio comparable to the ratio of concentration in the water.

An evaluation of the ratio by which biological populations modify the concentrations of phosphorus and nitrogen can be obtained from our data. This is done by plotting one against the other so that the slope of the line joining the high and low concentrations represents the ratio of *change* rather than that of concentration which has been discussed so far. This has been done for all of the 10-m water samples obtained on the 13 cruises at stations of intermediate depth over the Continental Shelf (B, C and D). The results are shown in Fig. 6. The slope of the envelope which encloses the majority of the points corresponds to the *normal* ratio of *change* of 15 atoms of nitrogen to one of phosphorus. The shaded area

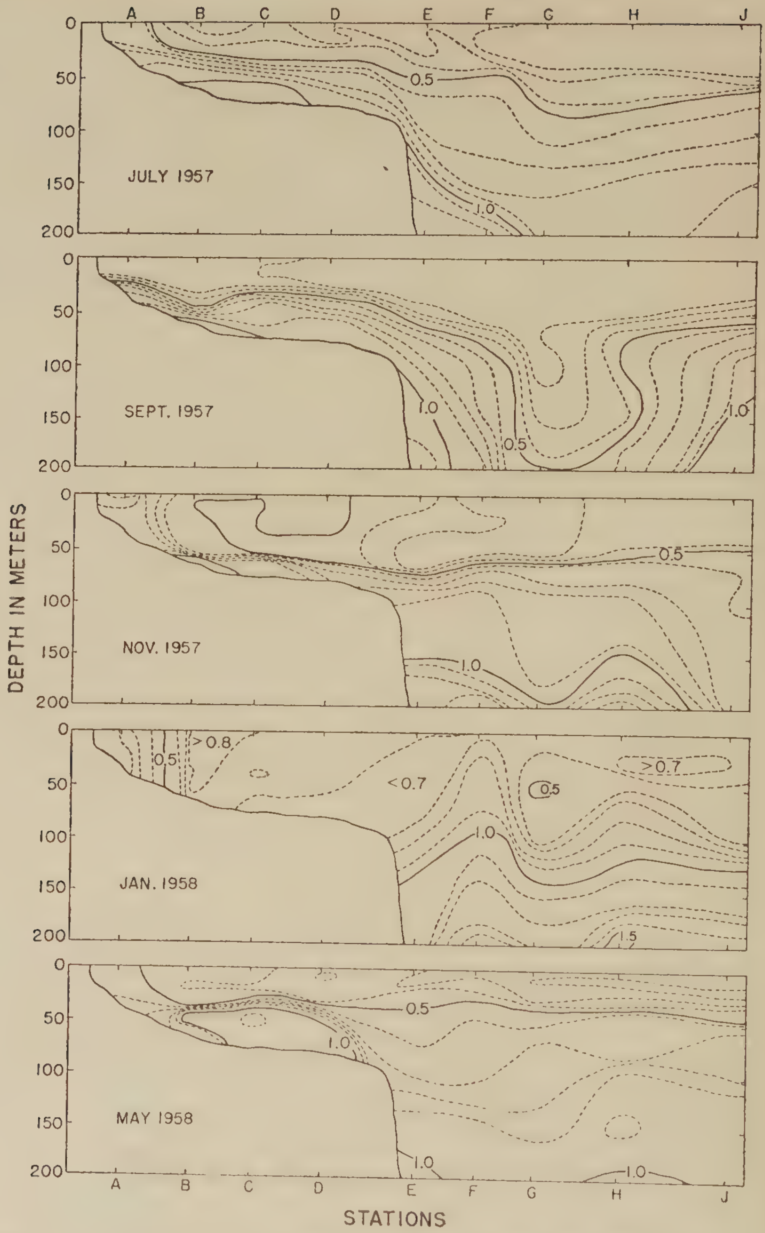

Figure 2. Distribution of inorganic phosphorus (Vertical exaggeration 400:1).

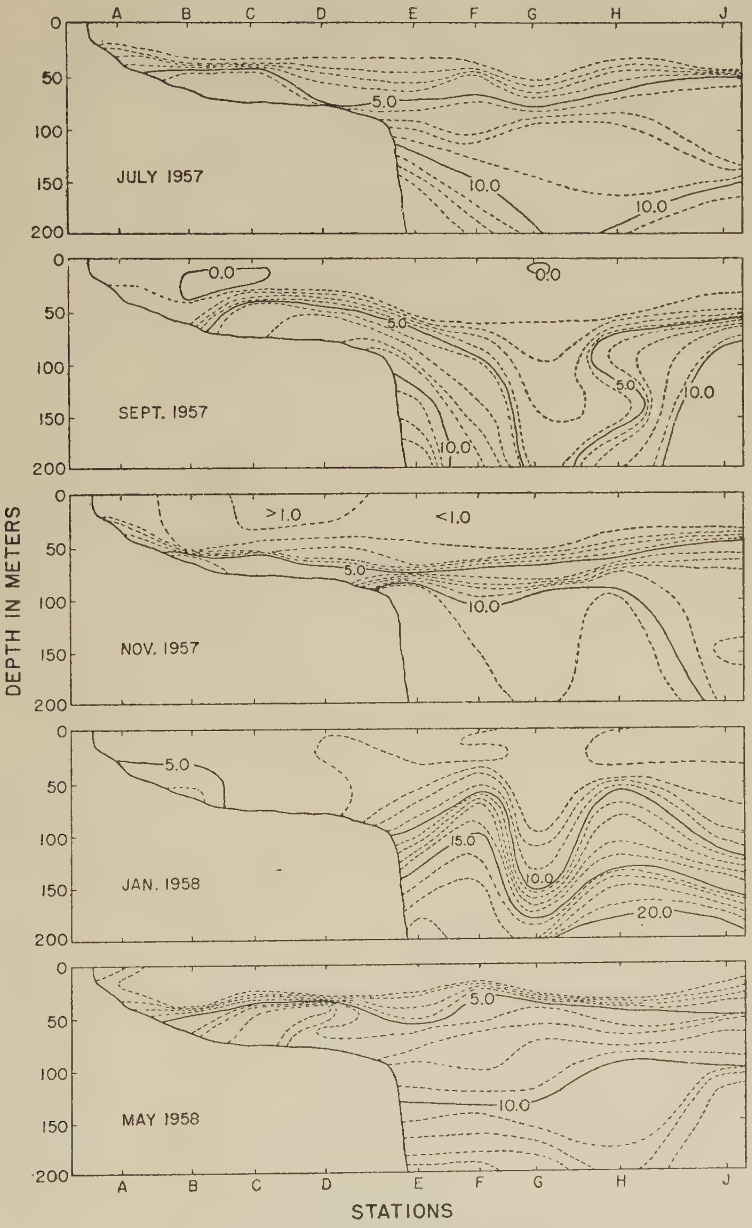

Figure 3. Distribution of nitrate-nitrogen.

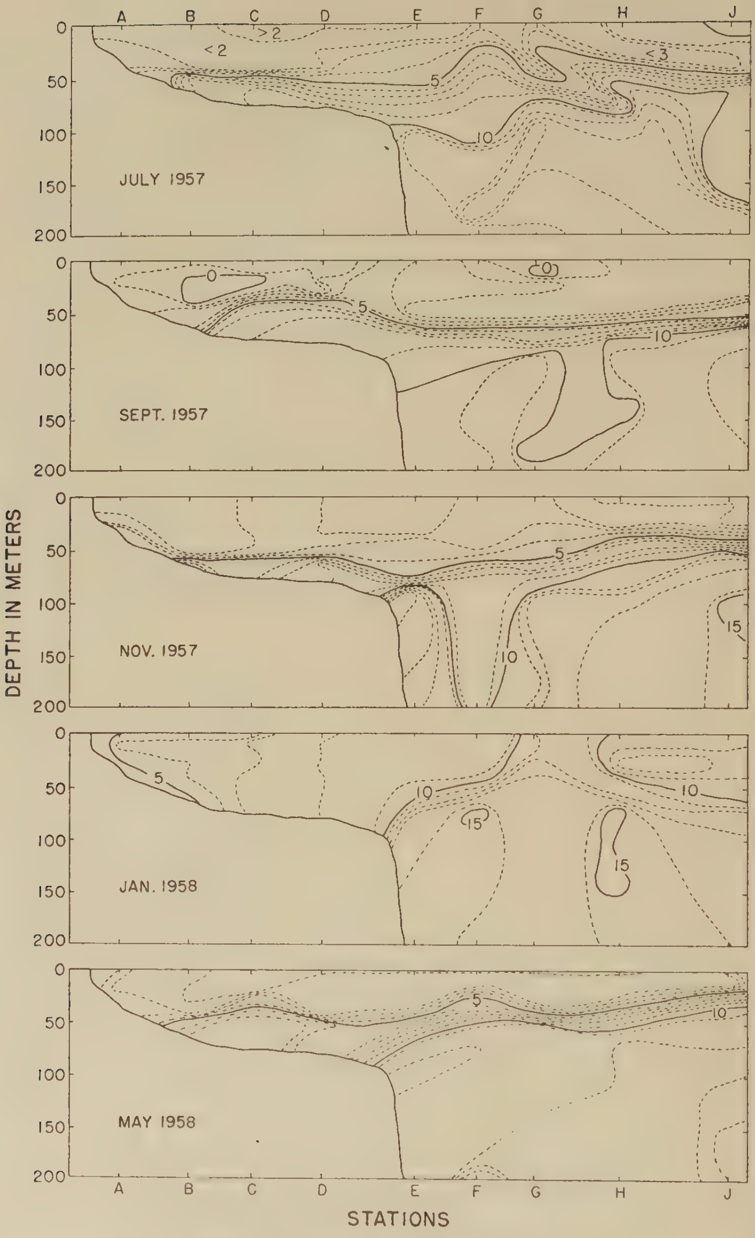

Figure 4. Distribution of N:P ratios.

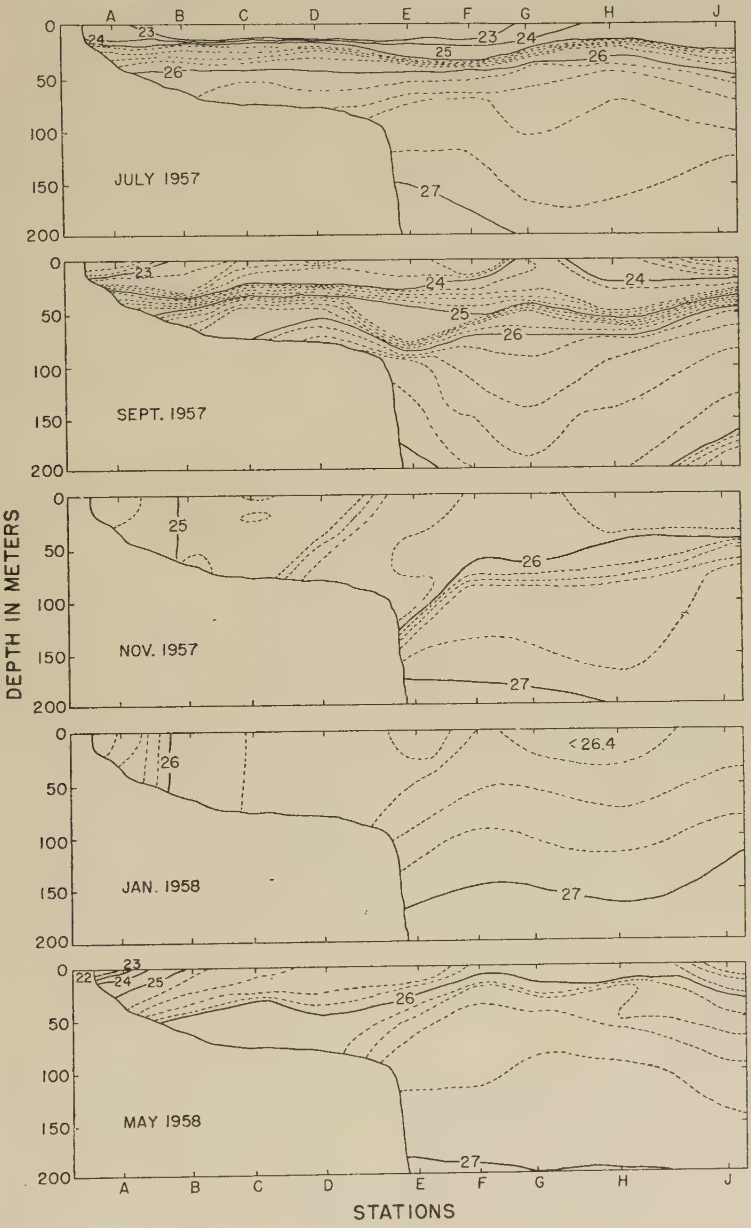

Figure 5. Distribution of density (σ_t).

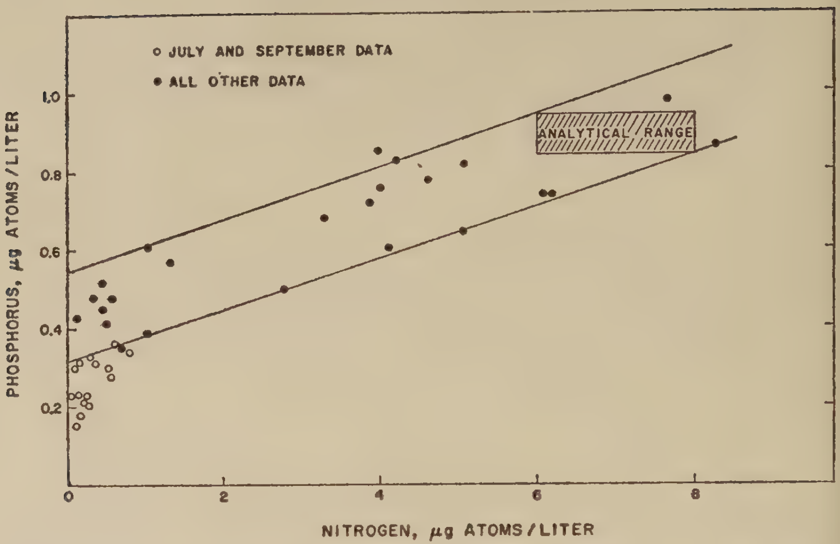

Figure 6. Ratio of change, $\Delta N{:}\Delta P$, for the 10 m samples at Sts. B, C, D. The slope of the envelope corresponds to $\Delta N{:}\Delta P = 15{:}1$.

labeled *analytical range* corresponds to a variation of ±0.05 μg-at P/l and ±1.0 μg-at N/l. All of the observations made in July and September (open circles) suggest a lower ratio of *change* during these months, when concentrations, especially of nitrate, are extremely low. Throughout most of the year, therefore, the biological populations in this part of the ocean, where they are exposed to an abnormally low N:P ratio, are assimilating (and regenerating) nitrogen and phosphorus in the *normal* ratio of 15:1. In the period July to September, however, when nitrogen concentrations are less than 1 μg-at/l, the populations are able to assimilate relatively little nitrogen while still reducing the phosphorus concentration. This may imply accomodation to the abnormal ratios at these low concentrations.

The intercept of the envelope noted above corresponds to excess phosphorus concentrations lying between 0.32 and 0.55 μg-at/l. Of course this excess is reflected in the low N:P ratios of concentration, becoming increasingly important as their concentrations are diminished.

It should be pointed out that neither vertical nor horizontal mixing processes in this area can account for a ratio of change of 15:1

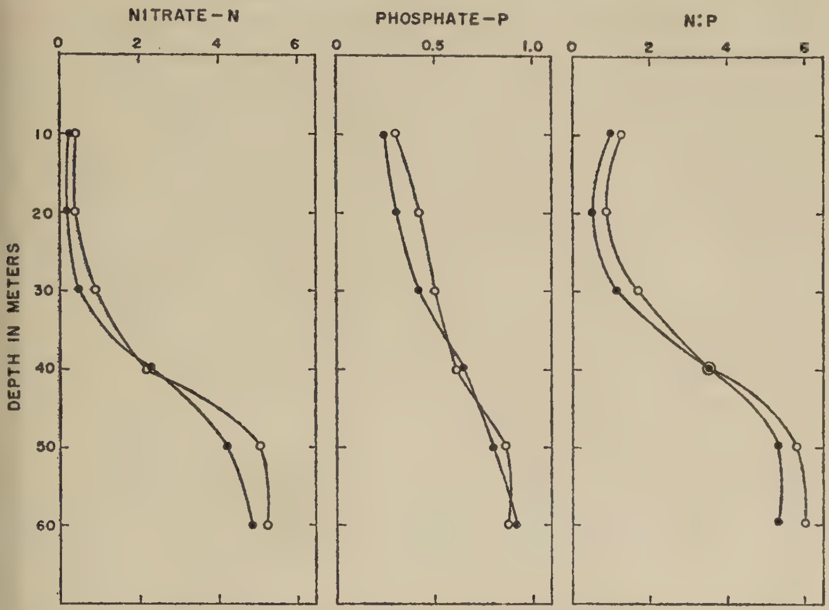

Figure 7. Average vertical distribution of nitrogen, phosphorus and the N:P ratio at stations of intermediate depth (B, C, D); open circles, September; solid circles, July.

for these two elements. However, it was suggested by Mr. John Steele that mixing must supply, in large part, the phosphorus and nitrogen required by the populations while the concentrations in surface waters are low. The ratio in which these two elements would be supplied by mixing is considerably higher than the ratio of their concentrations in the surface waters. The vertical distributions of nitrogen, phosphorus, and of the N:P ratio at Sts. B, C, and D are

TABLE III. Gradients of Nitrogen and Phosphorus in July and September at Sts. B, C, and D. Mean Concentration in μg-at/l.

	Nitrate-N			*Phosphorus*			
	Surface	*Deep*	*Difference*	*Surface*	*Deep*	*Difference*	*ΔN:ΔP*
September 1956	.23	3.78	3.55	.35	.93	.58	6.1
July 1957	.63	6.07	5.44	.35	.86	.51	10.7
September 1957	.13	5.56	5.43	.21	.86	.65	8.4
July 1958	.46	4.11	3.65	.44	.91	.47	7.8
September 1958	.48	3.96	3.48	.40	.74	.34	10.2

shown in Fig. 7. The data have been averaged at each depth for three September cruises and for two July cruises.

Vertical mixing will bring these elements to the surface waters at rates proportional to the gradient of concentrations. For each cruise this gradient has been evaluated by comparing averages of the 10, 20 and 30 m observations with those taken at 50 and 60 m. The results are given in Table III. The differences listed are the gradients over a depth of 20 m, and the ratio at which nitrogen and phosphorus will be delivered to the surface waters by mixing is given by the ratio of these gradients. They range from 6.1 to 10.7, all much higher than the ratio of concentration in the surface waters. Thus, while populations in the surface waters are living in a medium with an abnormally low N:P ratio, the conditions are not as abnormal as would be suggested by the observed ratio of concentrations. The fact that mixing, at these times, does not increase the ratio of concentration in the surface waters suggests that the populations assimilate these elements as rapidly as they become available.

Another source of supply of nitrogen and phosphorus is the decomposition of organic materials *in situ*. In Table IV the ratio of total nitrogen to total phosphorus is compared with the inorganic ratio observed in the 10 m samples for stations of intermediate depth on various cruises. Some of the cruises have been omitted because ammonia and amine-amide nitrogen, necessary to derive the total, were not determined. The ratio of concentration of total N:total P is considerably higher than the ratio of the inorganic concentrations. Decomposition of the organically combined nitrogen and phosphorus would thus supply the populations with high

TABLE IV. AVERAGE INORGANIC AND TOTAL N:P RATIOS (BY ATOMS) FOR 10-M WATER SAMPLES AT STATIONS OF INTERMEDIATE DEPTHS ON THE CONTINENTAL SHELF

Cruise Date	*Inorganic*	*Total*
September 1956	1.21	16.3
November-December 1956	4.55	25.9
February 1957	5.78	15.9
July 1957	2.41	30.2
September 1957	1.55	23.1
November 1957	1.81	21.0
January 1958	7.08	14.9

ratios of these elements. Presumably all of the organic phosphorus compounds are ultimately decomposed, since the concentration of organic phosphorus is negligible in deep waters (Ketchum, *et al.*, 1955). The deep waters, however, contain considerable amounts of combined nitrogen, as indicated by Krogh (1934) and by von Brand and Rakestraw (1941), and storage in the laboratory does not appreciably decrease the concentration. This suggests that some of the organic nitrogen in sea water is not readily decomposed, but it is not known how much of the organic nitrogen is available for metabolism of the populations.

VARIATIONS IN DEEP WATER

At Sts. G, H and J (Fig. 1), samples were taken to depths of 2000 m. In deep waters, of course, photosynthesis is not possible because of the lack of light. However, decomposition of organic material sinking from surface layers at these stations might be expected to give seasonal changes in the concentrations of nitrogen and phosphorus.

In order to permit comparison of the results, concentrations of nitrogen and phosphorus at depths greater than 100 m have been plotted against density (σ_t). This was done for the cruises which were made between February 1957 and May 1958 inclusive, with one exception[2]. Thus results from three stations were available, and for each cruise an average curve relating nitrogen and phosphorus to density was constructed. These average curves were then traced on a single graph, and the envelope in Fig. 8 describes the range of concentrations observed at various times of year.

Throughout most of the water column the range of variation in the nitrogen and phosphorus concentrations is no more than would be expected from analytical variation. The values of the maximum concentration for each cruise are presented in Table V. The average concentration of nitrate-nitrogen at the maximum was 20.7 μg-at/l, with a standard deviation of ±1.97. This corresponds to a variation of approximately 10 $^0/_0$, which would be expected for this analysis. The average phosphorus concentration was 1.65 μg-at/l, with a standard deviation of 0.11, or about 7 $^0/_0$. This variation is also to be expected from analytical errors.

---

[2] Results of BEAR cruise 165 made in April and May 1957 are not included in this treatment. In the nitrate analysis, calibration of the one centimeter cell gave anomalously low color development, and results calculated with the factor from this calibration are all considerably lower than any for the other cruises. We believe that, for some reason, reduction by the hydrazine in the high concentrations was incomplete for this set; however, the calibration and the concentrations for the more dilute samples measured in the 10 cm cells were apparently satisfactory and have been used in the previous section.

The N:P ratios vary from 11.2 to 14.6 at the maximum concentration of these elements, with a mean value of 12.5. Even for the deep waters immediately off the Continental Shelf in this region, therefore, there is an excess of phosphorus over nitrogen, producing a low N:P ratio.

For all depths at the deep stations, the concentration of phosphorus has been plotted as a function of the concentration of nitrogen. All of the results for each cruise can be enclosed in an envelope with a

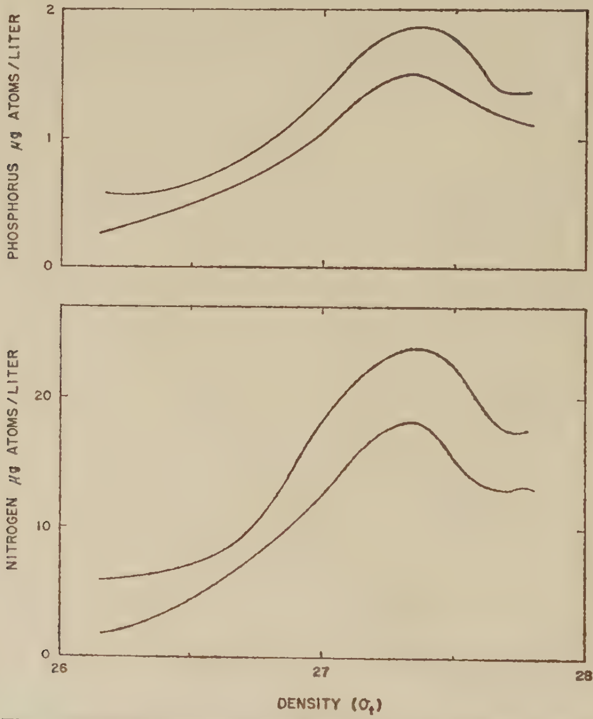

Figure 8. The relationship between phosphorus and nitrogen and the density of the water at depths greater than 100 m. The envelope describes the maximum range of concentrations observed at various times of year.

TABLE V. MAXIMUM CONCENTRATIONS OF INORGANIC PHOSPHORUS AND NITRATE-NITROGEN IN μG-AT/l AT STS. G, H AND J

Date	*Phosphorus*	*Nitrogen*	*N:P (atoms)*
February 1957	1.86	20.8	11.2
March 1957	1.72	19.8	11.5
July 1957	1.63	20.0	12.3
September 1957	1.64	18.2	11.1
November 1957	1.52	18.8	12.4
January 1958	1.54	22.5	14.6
March 1958	1.67	24.2	14.5
May 1958	1.62	21.4	13.2
Mean	1.65	20.7	12.5
Standard deviation	0.11	1.97	—

slope of 15 atoms of nitrogen to 1 of phosphorus, provided it is assumed that the waters contain excess phosphorus, *i. e.*, the median line of the envelope intercepts the ordinate at a phosphorus concentration greater than zero. However, the width of the envelope exceeds the standard deviation of the method of analysis. The excess phosphorus determined by extrapolation and the ranges of variation are presented in Table VI. The mean value for excess phosphorus for the deep stations is 0.22 μg-at/l, somewhat less than that found

TABLE VI. RELATIONSHIP BETWEEN NITROGEN AND PHOSPHORUS IN μG-AT/l AT STS. G, H, J. THE EXCESS PHOSPHORUS IS THE INTERCEPT OF THE MEDIAN LINE OF AN ENVELOPE ENCLOSING ALL POINTS, HAVING A SLOPE OF $\Delta N:\Delta P = 15:1$. THE RANGE IS THE DISTANCE FROM THE MEDIAN LINE TO THE BOUNDARIES OF THE ENVELOPE

Cruise	*Exess P*	*Envelope Range*	
		P	*N*
September 1956	0.31	±0.30	±4.5
November 1956	0	±0.25	±3.8
February 1957	0.25	±0.25	±3.8
March 1957	0.25	±0.25	±3.8
July 1957	0.35	±0.35	±5.25
September 1957	0.25	±0.25	±3.8
November 1957	0.25	±0.25	±3.8
January 1958	0.13	±0.22	±3.3
March 1958	0.22	±0.28	±4.2
May 1958	0.26	±0.25	±3.8

for the shallow inshore waters, which ranged from 0.32 to 0.55. Variations in the data, as defined by the distance between the envelope and median line, are generally two or three times the standard analytical deviation, even at the highest concentrations observed (*c. f.* Table V). This excess variation, suggesting inhomogeneity in the water masses, is as yet unexplained. These differences are apparently not accompanied by related variations in either temperature or salinity of the water, which would have been apparent in the plots as a function of density (Fig. 8). They thus demonstrate an inhomogeneity which would have escaped detection by the usual oceanographic techniques.

DISCUSSION

In his original paper on the proportions of organic derivatives in sea water, Redfield (1934) speculated that biological processes might determine these proportions. He has recently (1958) presented a discussion of the ways in which this could be accomplished. It is also possible, of course, that the sea, when it originated in eons past, had concentrations of the essential nutrients in the same proportions as the sea today. The fact that marine organisms, and indeed all living matter, contain in their protoplasm nitrogen and phosphorus in approximately the same ratio as they are found in the deep sea would then be attributed to the adaptive ability of the biological system. Ketchum (1939) showed that, for a given concentration of phosphate, the marine diatom *Nitzschia closterium* (*Phaeodactylum tricornutum*) absorbs constant proportions of phosphorus and nitrogen from the water, regardless of the ratio of their concentration. As the concentration of phosphorus in the medium was increased, the ratio of assimilation ((ΔN:ΔP) decreased. No variation was apparent with nitrogen concentrations at constant phosphorus except when the nitrogen content was less than 1 μg-at/l, which produced low values for the ratio of assimilation. Ketchum (1939a) showed that, when either nitrogen or phosphorus was exhausted from the water, the plants continued to grow and divide but developed a deficiency in the internal concentration of the exhausted element. The maximum nitrogen deficiency in *Chlorella pyrenoidosa* produced an internal N:P ratio of 2.35 (by atoms) and the maximum phosphorus deficiency produced a ratio of 31.2.

Our observations on surface coastal waters confirm these conclusions. In spite of the anomalously low N:P ratio, plants apparently assimilate these nutrients in the *normal* ratio of 15:1 until extremely low concentrations are reached. At such times the cells can apparently assimilate relatively little nitrogen while still depleting the phosphorus which is present in excess. It would clearly be desirable to have analyses of photyplankton collected in September, when the low ratio of assimilation is inferred to have taken place over a period of about three months. Harris and Riley (1956) did make such analyses of phytoplankton growing in Long Island Sound, where the ratio of concentrations is comparable to that found in our coastal waters. Their average value for the N:P ratio in phytoplankton was 16.7:1, suggesting that the plants generally maintained a high ratio of composition in spite of the low ratio of concentration in the waters in which they had grown. However, their lowest value, 13.1:1 by atoms, was obtained in August, approximately four months after the nearly complete removal of nitrogen from the water, as shown by Riley and Conover (1956).

The nearly complete assimilation of nitrate-nitrogen from the surface waters suggests that it may be an important nutrient limitation to the growth of phytoplankton. Phosphorus is always present in some excess in these waters, hence it may not be limiting, although its concentration does fall below the value of 0.55 μg-at/l, frequently quoted as limiting the rate of phytoplankton growth (Ketchum, 1939). The nutrient concentrations in surface waters did not change appreciably from July to September. Ryther and Yentsch (1958) have shown, however, that phytoplankton production continues during this period, but at a low rate. This production must be supported by nutrients supplied through turbulent mixing or by regeneration *in situ.* Both of these processes require more rigorous evaluation.

Our observations emphasize the dangers inherent in an interpretation of the nutritional status of plankton populations from observations of only one nutrient element. It is probable that a more complete understanding of phytoplankton periodicity will require observations not only of nitrogen and phosphorus but of other nutrients as well.

REFERENCES

Cooper, L. H. N.

1937. On the ratio of nitrogen to phosphorus in the sea. J. Mar. biol. Ass. U.K., *22*: 177–182.

1938. Redefinition of the anomaly of the nitrate-phosphate ratio. J. Mar. biol. Ass. U.K., *23*: 179.

Fleming, R. H.

1940. The composition of plankton and units for reporting populations and production. Proc. 6th Pacif. Sci. Congr., Calif. 1939, *3*: 535–540.

Ford, W. L.

1950. Seagoing photoelectric colorimeter. Anal. Chem., *22*: 1431–1435.

Harris, Eugene and G. A. Riley

1956. Oceanography of Long Island Sound. VIII. Chemical composition of the plankton. Bull. Bingham oceanogr. Coll., *15*: 315–323.

Harvey, H. W.

1926. Nitrate in the sea. J. Mar. biol. Ass. U.K., *14*: 71–88.

1948. The estimation of phosphate and of total phosphorus in sea waters. J. Mar. biol. Ass. U.K., *27*: 337–359.

Ketchum, B. H.

1939. The absorption of phosphate and nitrate by illuminated cultures of *Nitzschia closterium*. Amer. J. Bot., *26* (6): 399–407.

1939a. The development and restoration of deficiencies in the phosphorus and nitrogen composition of unicellular plants. J. cell. comp. Physiol., *13* (3): 373–381.

Ketchum, B. H., N. Corwin, and D. J. Keen

1955. The significance of organic phosphorus determinations in ocean waters. Deep-Sea Res., *2*: 172–181.

Krogh, August

1934. Conditions of life in the ocean. Ecol. Monogr., *4*: 421–429.

Mullin, J. B. and J. P. Riley

1955. The spectrophotometric determination of nitrate in natural waters, with particular reference to sea water. Anal. Chim. Acta, *12* (5): 464–480.

Phifer, L. D. and T. G. Thompson

1937. Seasonal variations in the surface waters of San Juan Channel during the five year period January 1931–December 30, 1935. J. Mar. Res., *1*: 34–59.

Pregl, F.

1946. Quantitative organic microanalysis. 4th Engl. Ed. Revised and edited by J. Grant. The Blakiston Co., Philadelphia. 238 pp.

Redfield, A. C.

1934. On the proportion of organic derivatives in sea water and their relation to the composition of plankton. James Johnstone Memorial Vol., Univ. of Liverpool, pp. 176–192.

1958. The biological control of chemical factors in the environment. Amer. Sci., *46*: 205–221.

RILEY, G. A. AND S. A. M. CONOVER
1956. Oceanography of Long Island Sound, 1952–1954. III. Chemical Oceanography. Bull. Bingham oceanogr. Coll., *15*: 47–61.

RILEY, J. P.
1953. The spectrophotometric determination of amnonia in natural waters, with particular reference to sea water. Anal. Chim. Acta, *9* (6): 575–589.

RYTHER, J. H. AND C. S. YENTSCH
1958. Primary production of continental shelf waters off New York. Limnol. Oceanogr., *3*: 327–335.

ROBINSON, R. J. AND T. G. THOMPSON
1948. The determination of phosphates in sea water. J. Mar. Res., 7 (1): 33–41.

VON BRAND, THEODOR, AND N. W. RAKESTRAW
1941. The determination of dissolved organic nitrogen in sea water. J. Mar. Res., *4* (1): 76–80.

WATTENBERG, HERMANN
1937. Critical review of the methods used for determining nutrient salts and related constituents in salt water. I. Methoden zur Bestimmung von Phosphat, Silikat, Nitrat und Ammoniak im Seewasser. Rapp. Cons. Explor. Mer, *103*: 1–26.

WOOSTER, W. S. AND N. W. RAKESTRAW
1951. The estimation of dissolved phosphate in sea water. J. Mar. Res., *10* (1): 91–100.

Contribution No. 1009

CALKINSIA AUREUS GEN. ET SP. NOV:, A NEW MARINE EUGLENID

JAMES B. LACKEY
University of Florida, Gainesville

Most of the marine members of the Euglenophyceae are colorless—species of the genera *Anisonema, Dinema, Peranema* and others. On the whole it seems probable there are more marine than fresh water species of these colorless genera. *Eutreptia* is a chlorophyll-containing genus of the high seas; there are several species of *Euglena* encountered in brackish water (Pringsheim, 1953). Finally, there are several genera whose affinities, because of insufficient investigation, are regarded as somewhat uncertain (Hollande, 1952).

None of the marine forms thus far described have any color except that due to chlorophyll. *Trachelomonas* and *Strombomonas* (fresh water forms) frequently have shells (tests) of varying brown shades, generally said to be due to iron, within which the organism lives.

OCCURRENCE

In September, 1958, the mud-water interface of core samples taken from the Eel Pond at Woods Hole, Massachusetts, contained small numbers, about three per drop, of the beautiful golden brown organism described here. Three cores were taken with a Phleger sampler within a radius of about eight feet. Each core brought up about six inches of mud, and a twelve inch column of water from a depth of about fourteen feet. The black mud was certainly anaerobic, and it seems probable that the interface was nearly anaerobic as is judged from the organisms, mostly ciliates and flagellates which occurred there. Most of the water column was decanted, and centrifuged. It yielded very few organisms; none of the yellow flagellate. Centrifuged surface water samples likewise showed none of this particular organism. It was not found in the mud, from perhaps two or three millimeters deep to several centimeters, but apparently it is confined to the interface region. This may account for no previous record of such a striking form from the well-investigated waters around Woods Hole.

It was not found in similar core samples, however, from both sand and mud bottoms in nearby Buzzards Bay. These samples showed an almost complete cover of copepod pellets, largely lacking in the Eel Pond cores, and a large colorless euglenid population, perhaps 100–300 per drop. There was less evidence of anaerobism at the interface as indicated by the kinds of organisms indicated. The new flagellate evidently is a facultative anaerobe. If slides containing the cells are put aside for 24 hours in a moist chamber, the organisms tend to occur the next day in the center of the slide. In view of the known pollution of the Eel Pond the flagellate is probably sapropelic for there is no evidence that it ingests food.

Calkinsia aureus gen. et sp. nov.

DESCRIPTION

Organism elongately oval, narrowly oval in cross section, enclosed in rigid pellicle, metaboly not possible; body proper 40–50 μ long; pellicle

Reprinted from TRANSACTIONS OF THE AMERICAN MICROSCOPICAL SOCIETY
Vol. LXXIX (1): 105–107. January, 1960

rolled inward along ventral margin, deep at anterior end, diminishing toward caudal spine; mouth area beneath ventral anterior margin of pellicle, opening into a short gullet-reservoir. No contractile vacuole observed. Flagella two, subequal, emerging from reservoir floor, of equal diameter, neither one tapering as in *Anisonema* or *Peranema*, the shorter carried back, 25–30 µ long, anterior 80 µ or longer, may be

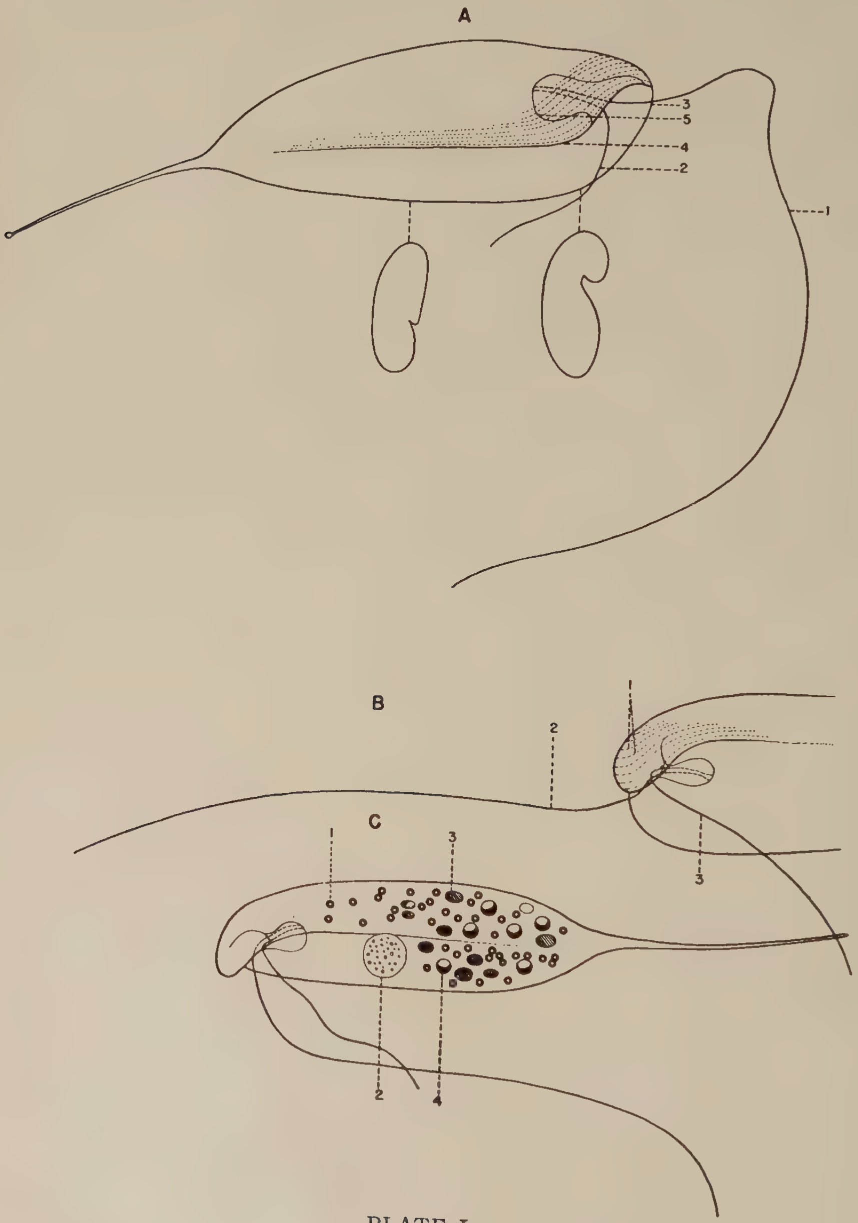

PLATE I

suddenly retractile, then thrust sideways at an angle of 45 degrees or greater, to change direction of progression. It may be used to pull, by looping. When the organism is still, this flagellum is vibratile along its distal quarters, appearing to have a probing function. Forward movement slow, deliberate.

Nucleus large, in right median plane, granular, no visible endosome; no visible blepharoplasts or staborgan in living organism; paramylum present as small discs 4–8 μ in diameter; sometimes black refringent granules like sulfur droplets in *Beggiatoa* are present; color clear, translucent, golden; no chromatophores; color in pellicle or cytoplasm with no variation in intensity noted; pellicle faintly striated, longitudinally except around ventral margin, where it becomes spiral; stigma absent; division and encystment not seen; nutrition saprozoic; anaerobic or microaerophyllic.

Genus named for Gary N. Calkins who taught protozoology at the marine Biological Laboratory for many years, and the species for its color.

Classification

The affinities of the organism are somewhat obscure. However, it could fall better in Hollandes' family Petalomonidae (according to Hall (1953) the order Euglenida, suborder Petalomonadoidina) than either the Peranemidae, which are metabolic, or the Anisonemidae which are not metabolic but contain some sort of rod apparatus. In addition its flagellation is a bar to inclusion in the last two families. In the Peranemidae, the anterior flagellum is heavy and tapers somewhat, whereas in this organism the anterior flagellum is tenuous. In the Anisonemidae, the posterior flagellum is thick, and is the longer. This organism is not compressed in the same fashion as *Petalomonas*, but its flagellar insertion is quite like that of *Tropidoscyphus*.

Literature Cited

Pringsheim, E. G. 1953. "Salzwasser–Euglenien". Arch. Mikrobiol., 18: 149–164.

Hollande, A. 1952. *In:* Traite de Zoologie. Tome 1. Fascieule premier. pp. 238-282. Masson et Cie. Paris.

Hall, R. P. 1953. "Protozoology". pp. 160–168 Prentice-Hall, Inc. New York.

EXPLANATION OF PLATE I

Diagrammatic Sketches to Show the Morphology of
Calkinsia aureus, n.g., n.s.

A. 1. The long probing or anterior flagellum.
  2. The short trailing flagellum.
  3. Rounded edge of pellicle, dorsal side.
  4. Ventral fold of pellicle, which extends back to form a groove as indicated in the two cross sections.
  5. Base of the reservoir, a sac whose mouth opening is anterior, between the dorsal and ventral pellicle folds.

B. 1. Pellicular striations.
  2. Anterior flagellum.
  3. Posterior flagellum.

C. 1. Black refringent bodies, possibly oil or sulfur.
  2. Nucleus.
  3. Paramylum.
  4. Reserve materials

Contribution No. 1018

PHYSICAL OCEANOGRAPHY OF THE GRAND BANKS REGION AND THE LABRADOR SEA IN 1958[1]

By Floyd M. Soule and R. M. Morse
(U. S. Coast Guard)

The oceanographic vessel of the International Ice Patrol in 1958 was again the 180-foot tender class *USCGC Evergreen*. The arrangement of labratory and deck facilities and equipment have been described in earlier bulletins of this series. There are no major changes for the 1958 season.

During the 1958 season the *Evergreen* made three dynamic topographic surveys in the Grand Banks region. Of these the first covered the waters over and immediately seaward of the southern and eastern slopes of the Grand Banks from just westward of the Tail of the Banks northward to the latitude of Flemish Cap. This survey included 88 stations which were occupied between the morning of 3 April and the afternoon of 15 April. The work of collection of data began at the southwestern end of the area and progressed northward with no major interruption.

The second survey covered the waters over and immediately seaward of the northeastern slope of the Grand Banks from Flemish Cap northwestward and included an occupation of the Bonavista triangle. On this survey 80 stations were occupied between the early morning of 27 April and the morning of 5 May. Except for about an hour on the afternoon of 27 April, during which the ship was working through an ice string, there were no major interruptions. The work of collection of data began at the Bonavista triangle and progressed southeastward toward Flemish Cap.

The area covered by the third survey was similar to that covered by the first survey with the extension of section W (a north-south section at 50°15′W.) southward across the Atlantic Current. It was expedient to occupy this section from south to north and then continue with the network survey working northward toward Flemish Cap. The southernmost position necessary to completely cross the Atlantic Current was estimated as 38° N. To insure against missing part of it, from a possible deviation of the current from its expected position, observations were begun at 37°30′N. On this southward extension of section W stations were spaced

---

[1] To be reprinted as Contribution No. 1018 in the Collected Reprints of the Woods Hole Oceanographic Institution.

[Extract from U.S. Coast Guard Bulletin No. 44, pages 29–99. Reprinted as Contribution No. 1018 in Collected Reprints of the Woods Hole Oceanographic Institution.]

30 miles apart and the observations extended to a depth of about 3,000 meters instead of the usual 1,500 meters and were supplemented by bathythermograph casts every half hour on the runs between stations. The addition of this section was a contribution to United States participation in the International Geophysical Year. The section was occupied between the morning of 23 May and the night of 25 May. The ensuing network survey was completed on the morning of 5 June. There were no interruptions or unusual delays during this period. On this survey 95 stations were occupied, the first 15 of these being along section W.

A postseason cruise had been planned to include an occupation of the Bonavista triangle and the section across the Labrador Sea from South Wolf Island, Labrador, to Cape Farewell, Greenland. Normally, ice conditions would have made it inadvisable to approach Cape Farewell before mid-July. This year, however, all available information indicated that ice deterioration was about two weeks ahead of a normal season. Accordingly, the *Evergreen* departed Boston for the postseason cruise on the unusually early date of 23 June. The Bonavista triangle, including 30 stations, was occupied between the morning of 27 June and the early morning of 30 June. The Labrador Sea section, including 24 stations, was occupied between the morning of 1 July and the morning of 6 July. There were delays occasioned by heavy weather as follows: 16 hours on 4 July prior to station 6882, 5½ hours on 5 July following station 6883, and 5 hours on 5 July prior to station 6885. Of the last 5-hour delay only about 2 hours was on account of weather, the remaining 3 hours being to coordinate the approach to Cape Farewell with the best chance of good visibility. The final station was occupied just outside a coastal belt of sea ice 7½ miles off Cape Farewell.

The oceanographic work was under the supervision of Oceanographer Floyd M. Soule who was assisted by Lt. R. M. Morse. Other assistants in the observational work were Elwood C. Gray, aerographer's mate first class; William G. Carpenter, yeoman third class; R. J. Messier, seaman (during the first survey); D. C. Bailey, aerographer's mate first class (during the first and second surveys); Herbert A. Ashmore, aerographer's mate third class (during the first and second surveys); Herbert J. Spiegel, aerographer's mate third class (during the second and third surveys and the postseason cruise); Richard C. Norris, aerographer's mate first class (during the third survey and postseason cruise); and O. W. Warf, Jr., radarman third class (during the third survey and postseason cruise). Temperature and salinity observations were made at each of the 317 stations. At the 24 stations forming the section across the Labrador Sea the observations extended from the surface to as near bottom as was practicable. At the 10 stations forming the southern end of section W on the third survey the observations extended to 3,000 meters. At the remaining stations the observations were limited to the upper 1,500 meters. The intended depths of observation, in meters, were 0, 25, 50, 75, 100, 150, 200, 300, 400, 600, 800, 1,000, and thence by 500-meters intervals, except for the extra southerly extension of section W during the third survey where the depths of observation in the second 1,000 meters were 1,200, 1,400, 1,600 and 2,000 meters.

Temperatures were measured with protected deep sea reversing thermometers, mostly of Richter & Wiese manufacture but with some manufactured by Negretti & Zambra, G. M. Manufacturing Co. and Kahl Scientific Inst. Corp. Depths of observation are based on unprotected reversing thermometers made by Richter & Wiese and by Kahl. As in other years, a program of intercomparison of protected thermometers was carried out in the field measurements. The thermometers were used in pairs and one of each pair was shifted periodically so that the same thermometer was eventually paired with a number of other thermometers. From a total of 2,201 intercomparisons, the probable difference between the corrected readings of a pair of protected thermometers was 0.010° C. Of these comparisons, 280 involved thermometers having a range of +3° to +13° with a probable difference of 0.006°, 1,268 comparisons were between thermometers of range —2° to +8° and gave a probable difference of 0.009°, and 653 comparisons were between thermometers having a range of —2° to +20° or greater and gave a probable difference of 0.013°. As most of the observed temperatures listed in the Table of Oceanographic Data are the means of the corrected readings of a pair of thermometers and since many of the thermometers used had recent laboratory comparisons with thermometers tested by the National Bureau of Standards, it is considered that the tabulated observed temperatures are good to 0.01°C.

Salinities were measured with a Wenner salinity bridge. During the winter of 1957–58 an examination of a section extending eastward from the Grand Banks at about latitude 45° N., occupied by *Discovery II* on 16–18 April 1957 indicated a probable discrepancy of about 0.04°/₀₀ between salinities as determined by *Discovery II* and as determined on the Evergreen during a survey of the area which included a nearby section occupied 12–13 April 1957. It was learned that *Discovery's* salinities were in essential agreement with those determined by the Woods Hole Oceanographic Institution. A series of check measurements was therefore made to determine if the calibration curve for the Coast Guard's Wenner bridge were in error.

Three composite carboys of seawater were prepared by the Woods Hole Oceanographic Institution and designated numbers 1, 5, and 7. Another carboy of actual seawater collected from the surface at about 50° N., 49° W., about 7½ months earlier (25 July, 1957) was made available by the Coast Guard Oceanographic Unit. This carboy, designated C–1–58, was a polyethylene plastic container. The other carboys were glass and had been filled with water stored for varying periods in glass containers. None of the carboys had special seals until the beginning of the measurements, when C–1–58 was placed under an oil seal.

The WHOI laboratory ran 20 titrations on carboy 1, 14 titrations on carboy 5, 9 titrations on carboy 7 and 10 titrations on carboy C–1–58. The carboys were also measured on the WHOI bridge and on the CGOU bridge. Mean values determined were as follows:

Carboy	*Titration*	*WHOI bridge*	*CGOU bridge*
1	35.04_9	35.06_5	35.03_4
5	35.50_1	35.53_2	35.49_6
7	34.18_6	34.21_8	34.19_1
C–1–58	34.45_7	34.47_6	34.44_8

Whence the following differences were obtained:

Carboy	*Titration-WHOI bridge*	*Titration-CGOU bridge*	*WHOI bridge CGOU bridge*
1	-0.01_6	$+0.01_5$	$+0.03_1$
5	-0.03_1	$+0.00_5$	$+0.03_6$
7	-0.03_2	-0.00_5	$+0.02_7$
C–1–58	-0.01_9	$+0.00_1$	$+0.03_1$
	aver.	$+0.00_6$	$+0.03_1$

Since both the CGOU bridge (model 4) and the WHOI bridge (Bradshaw and Schleicher) were Wenner bridges they were both more precise than titration, which is reflected in the smaller variation in the difference between the two bridges than between either bridge and titration. However, neither makes direct measurements of salinity and each determines the electrical resistivity of a sample of unknown salinity in terms of that of a sample of known salinity, and hence depends upon a standardization. In the case of the CGOU bridge this is accomplished by the construction of a calibration curve on the basis of a number of samples of actual seawater having a range of salinity and measured on the bridge and by titration against Copenhagen standard water. In the case of the WHOI bridge the standardization is accomplished by using the Copenhagen standard water as a conductivity standard, assuming its conductivity is the same as the conductivity of a sample of actual seawater whose chlorine content is the same as the stated chlorine of the Copenhagen standard water.

The calibration curve of the CGOU bridge used in the above measurements was determined prior to the beginning of the 1957 season. In view of the foregoing, the same curve, with a constant adjustment of $0.006^{\circ}/_{\circ\circ}$, to accommodate the above difference between titration and bridge measurements, was used in 1958. In spite of this, however, there still appears to be a discrepancy between the *Evergreen* salinities and those determined by the Woods Hole Oceanographic Institution if one may judge by comparing the potential temperature-salinity relationship of the deeper samples beneath the Atlantic Current south of the Grand Banks in May 1958, with that found by WHOI in the deep water west of Bermuda. Aside from this unsolved question of perhaps $0.04^{\circ}/_{\circ\circ}$ discrepancy in the absolute values of salinity, we may state that the precision of the observed salinities listed in the Table of Oceanographic Data is $\pm\ 0.005^{\circ}/_{\circ\circ}$ although the accuracy is only that of silver nitrate titration.

In the field measurements the bridge was standardized with water from an oilsealed carboy of actual sea water. At least twice during each salinity run, Copenhagen standard water of the batch P23 was measured as an unknown. At the end of each survey these measurements were used to determine whether a correction to the salinities for the survey was required. The corrections thus indicated were as follows: first survey $-\ 0.00_2{}^{\circ}/_{\circ\circ}$; second survey $-\ 0.00_1{}^{\circ}/_{\circ\circ}$; third survey $+0.00_3\ {}^{\circ}/_{\circ\circ}$; postseason cruise $-\ 0.00_6{}^{\circ}/_{\circ\circ}$. The corrections for the season's surveys were negligible and for these no corrections were applied to the values tabulated. The correction of $-\ 0.00_6{}^{\circ}/_{\circ\circ}$ has been applied to the salinities for the postseason cruise.

Figures 19 through 22 show, in chronological order, the dynamic topography found during the three surveys made during the season and during the occupation of the Bonavista triangle on the postseason cruise. Figure 23 shows the monthly mean barometric pressure at seal level in the North Atlantic for the months of January, February, and March 1958 in comparison with the normal[2] barometric pressure distribution for these months. It will be seen that throughout this protracted period the Azores high, which usually controls the North Atlantic area, was very weak and displaced toward the southeast and that the atmospheric circulation was dominated by a vigorous low in the vicinity of Newfoundland. The resulting easterly winds experienced along the Laborador coast, and to a lesser extent the Newfoundland east coast, were expected to have a pronounced effect on the currents in the Grand Banks region.

The abnormal wind pattern ended just prior to the beginning

---

[2] Normals are from U.S. Weather Bureau Technical Paper No. 21. Normal Weather Charts for the Northern Hemisphere, Washington Oct 1952.

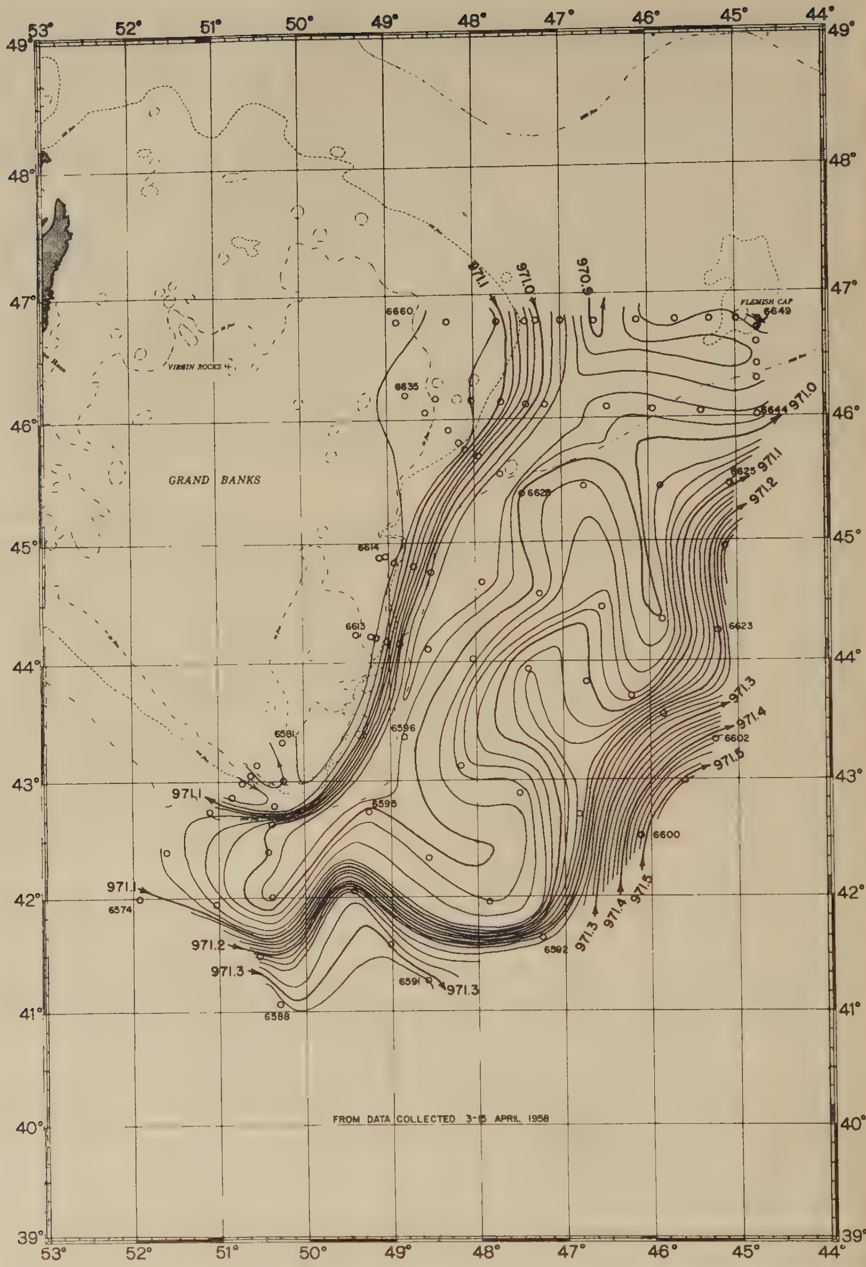
53°
52°
51°
50°
49°
48°
47°
46°
45°
44°
49°
48°
47°
46°
45°
44°
43°
42°
41°
40°
39°
GRAND BANKS
VIRGIN ROCKS
FLEMISH CAP
6649
6660
6635
6644
6625
6629
6614
6613
6623
6581
6596
6602
6595
6600
6574
6592
6591
6588
971.1
971.0
970.9
971.0
971.1
971.2
971.3
971.4
971.5
971.1
971.1
971.2
971.3
971.3
971.3
971.4
971.5
FROM DATA COLLECTED 3-15 APRIL 1958

FIGURE 19.—Dynamic topography of the sea surface relative to the 1000-decibar surface from data collected 3-15 April 1958. Oceanographic station positions are indicated and the station numbers given at turning points.

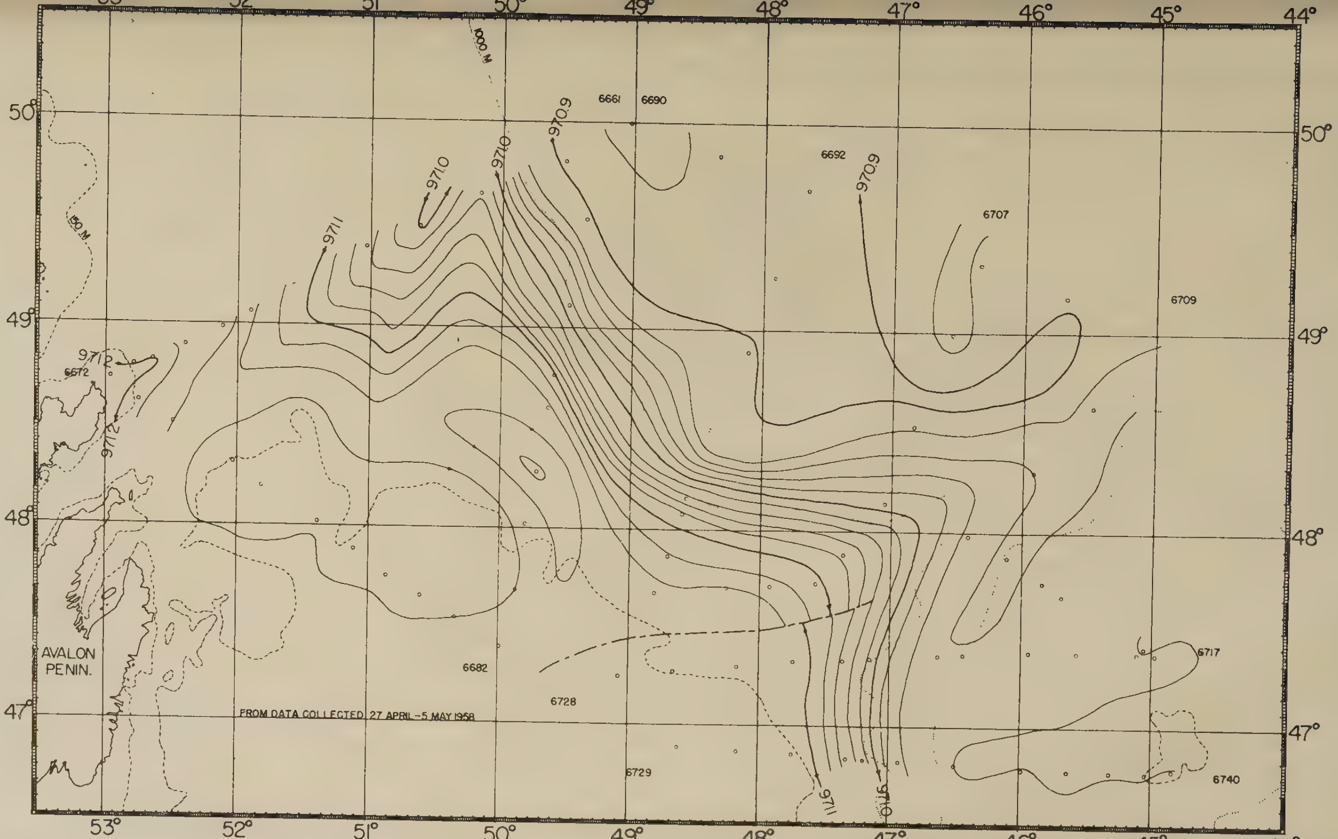
50°
49°
48°
47°
53°
52°
51°
50°
49°
48°
47°
46°
45°
44°
1000 M
150 M
6661
6690
970.9
971.0
971.0
971.1
971.2
971.2
6672
6692
970.9
6707
6709
6717
6740
6682
6728
6729
971.1
971.0
AVALON PENIN.
FROM DATA COLLECTED 27 APRIL–5 MAY 1958

FIGURE 20.—Dynamic topography of the sea surface relative to the 1000-decibar surface from data collected 27 April-5 May 1958. Oceanographic station positions are indicated and the station numbers given at turning points.

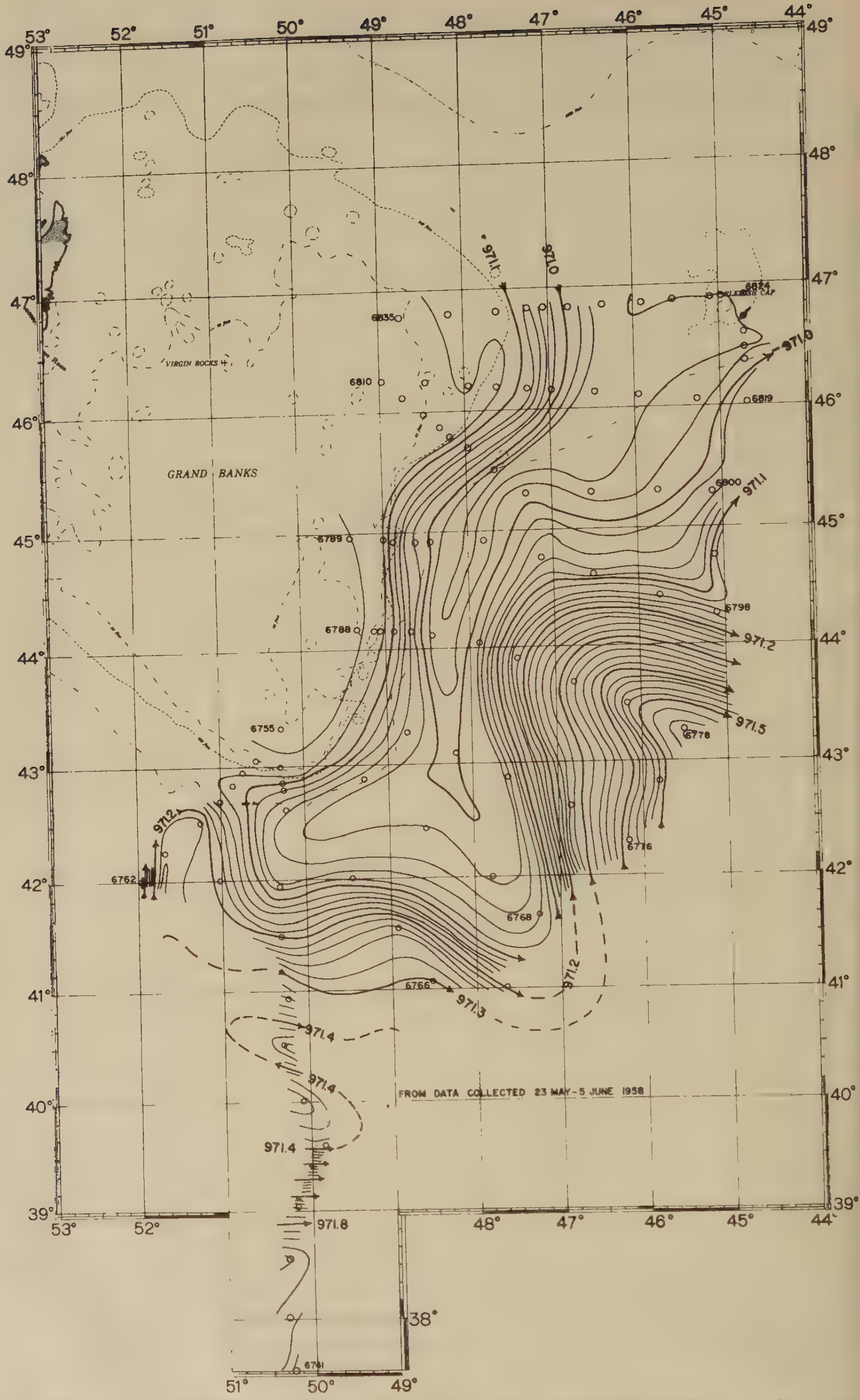
GRAND BANKS
VIRGIN ROCKS
FLEMISH CAP
FROM DATA COLLECTED 23 MAY-5 JUNE 1958
971.0
971.1
971.2
971.3
971.4
971.5
971.6
971.8
6824
6835
6810
6819
6800
6789
6788
6798
6755
6778
6776
6762
6768
6766
6741
53°
52°
51°
50°
49°
48°
47°
46°
45°
44°
43°
42°
41°
40°
39°
38°

FIGURE 21.—Dynamic topography of the sea surface relative to the 1000-decibar surface from data collected 23 May-5 June 1958. Oceanographic station positions are indicated and the station numbers given at turning points.

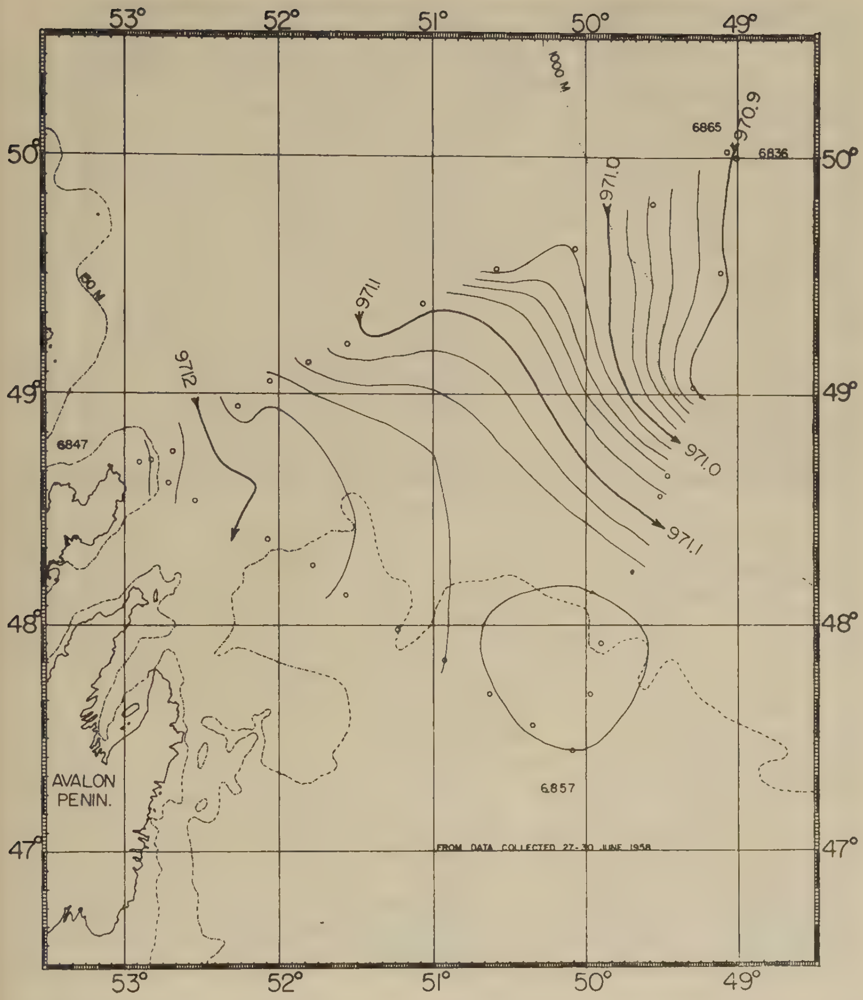
53°
52°
51°
50°
49°
50°
49°
48°
47°
1000 M
6865
970.9
6836
971.0
971.1
971.2
6847
971.0
971.1
6857
AVALON
PENIN.
FROM DATA COLLECTED 27-30 JUNE 1958

FIGURE 22.—Dynamic topography of the sea surface relative to the 1000-decibar surface from data collected 27-30 June 1958. Oceanographic station positions are indicated and the station numbers given at turning points.

of the 1958 survey work. During the first survey the warm water found in the surveyed area was not as warm as usual but it was found over a greater geographical extent than usual. The coldest water of the Labrador Current was about a degree warmer than usual but cold water extended to greater depths than usual. Salinities at intermediate depths down to at least 1,000 meters were fresher than usual. Yet the resulting density distribution produced a Labrador Current which, as seen from figure 19, was rather broad at the northern end of the surveyed area and narrowed with increasing velocity toward the Tail of the Banks.

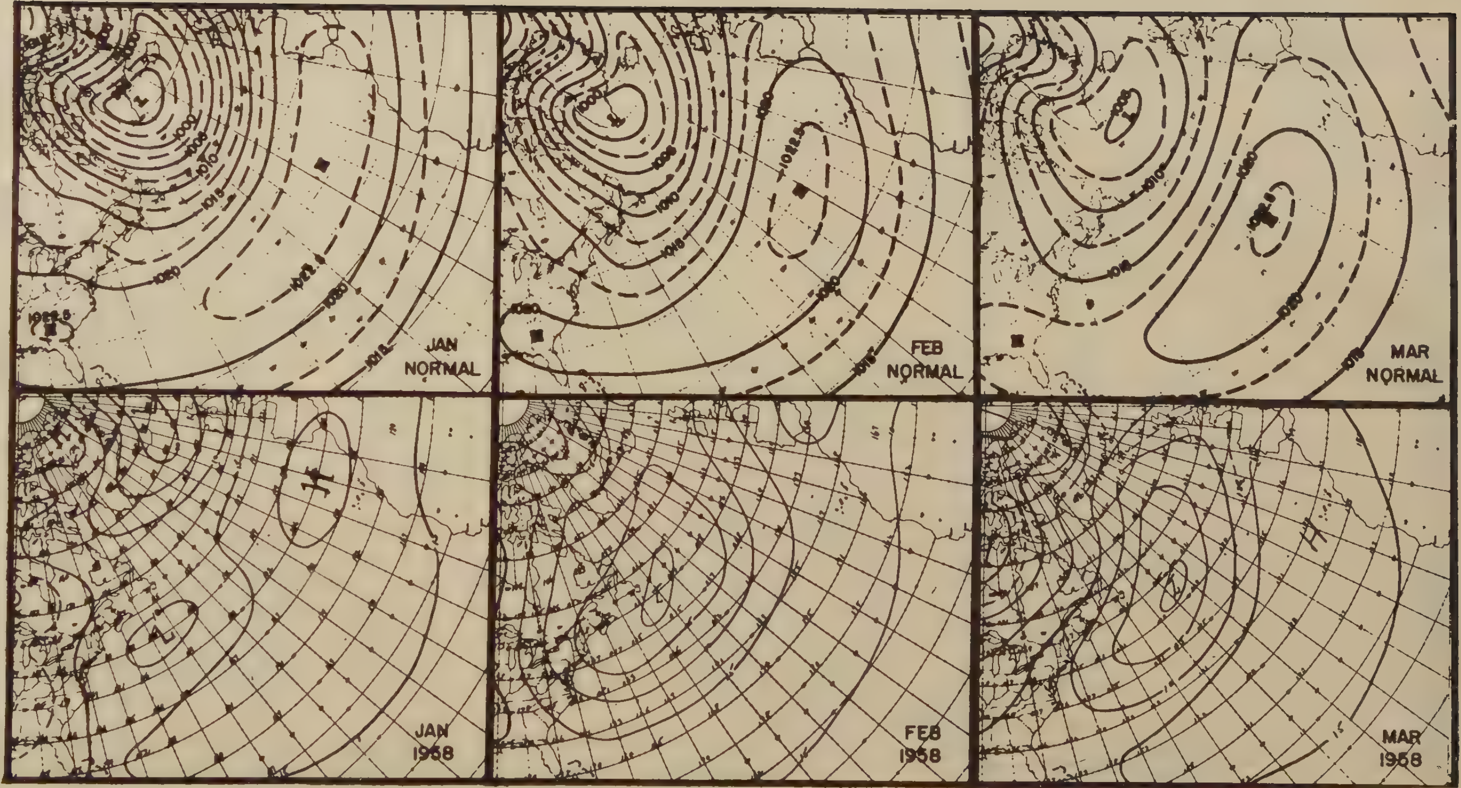
JAN
NORMAL
FEB
NORMAL
MAR
NORMAL
JAN
1958
FEB
1958
MAR
1958
1000
1005
1010
1015
1020
1022.5
H
L

FIGURE 23.—The monthly mean barometric pressure distribution in the North Atlantic during January, February and March, 1958, compared with the normal distribution.

During the second survey (fig. 20) it was again observed that the minimum temperature of the Labrador Current was warmer than usual and that the salinity of the intermediate water down to 1,000 meters was fresher than usual. The use of the Helland-Hansen and Nansen method of arriving at the dynamic heights of stations where the depth of water is less than that of the reference surface involves some uncertaintiy depending upon the construction of a vertical section of anomaly of specific volume for the extrapolated values of the anomaly along the bottom from the shallow station to the depth of the reference surface. The shallow ends of such sections are cross checked by providing two or more approaches to guard against gross errors in the construction of the anomaly sections and to produce a consistent network survey. In the construction of figure 20 such cross checks showed an irreconcilable discrepancy of about 32 dynamic millimeters between the two southernmost sections and the area to the northwestward. The figure has been drawn with the discontinuity indicated by a dashed line and it has been assumed that an adjustment between two steady states occurred in the approximately 3-day interval between the occupation of the southern sections and the stations to the northwest of them. The current pattern is similar on each side of the discontinuity but the shallow water velocities are different.

It would appear from figure 20 that an exceptionally large part of the surface circulation of the Labrador Current in the Bonavista triangle was following the eastern branch. An analysis of the volume transports past the three sides of the triangle, however, indicates that 90 percent of the current was following the eastern branch. This is only slightly more than the seasonal normal of 88.3 percent. The seasonal normals, however, are based on data which include only one occupation at a seasonal date earlier than that of the second survey of 1958, and are consequently less reliable than they are for somewhat later seasonal dates. In the eastern part of the surveyed area figure 20 indicates that the eastern branch of the Labrador Current suffered but little loss from water recurving northward north of Flemish Cap.

The dynamic topography found during the third survey is shown in figure 21. As in other current charts of the Grand Banks region, a reference surface of 1,000 decibars has been used in this figure to permit the presentation of the extra-southerly section and the rest of the survey in a single chart. It is realized that this reference surface is too shallow to give accurate values of current velocity in the vicinity of the southern section but an inspection of the data indicates the current pattern is similar when the topography is referred to the 2,000-decibar surface although use of the deeper reference surface gives higher velocities.

The southern edge of the eastward flowing current was found at about 38°30′N. A reversal of direction was observed between 40° N. and 40°30′N. This appears to be associated with a meander to the northwestward and is identified with the current pattern found between 42° N. and 42°30′N. between 51° W. and 52 W. It is interesting to note that the highest dynamic height found in the Atlantic Current in the eastern part of the surveyed area (station 6778 in the vicinity of 43°15′N., 45°30′W.) is found in the middle of the swiftest band of current between stations 6744 and 6745 on the southern section. Compared with the first survey, the Labrador Current lost the high velocities found earlier near the Tail of the Banks but its temperature minimum remained decidedly warmer than normal, the coldest temperature observed being −1.00°, found in the northernmost section.

The dynamic topography shown in figure 22 is that found during the postseason cruise occupation of the Bonavista triangle. Compared with the similar area of figure 20, there was a northward and seaward shift of the current pattern. There is usually a seasonal decrease in the proportion of the Labrador Current following the eastern branch. This decrease was somewhat greater than normal in 1958. It dropped from 90 percent during the second survey (compared with a seasonal normal of 88.3 percent) to 82½ percent at the time of the postseason cruise (compared with a seasonal normal of 84½ percent). The minimum observed temperatures along the three sides of the triangle were close to normal during the postseason cruise although the coldest temperature occured along the northwestern side instead of the southwestern side where it usually is found.

The first and third surveys took place in the region of the Grand Banks from which sufficient data are available to permit a comparison of the temperature-salinity characteristics of the water masses found there in 1958 with the mean T-S characteristics for earlier years. Labrador Current water and Atlantic Current water are water masses found in this region and these parent water masses usually mix in a sufficiently constant proportion to produce a mixed water which may be regarded as a virtual water mass. Figure 24 shows the relationships found in 1958 as solid line curves. The broken lines represent the 11-year means for the period 1948–58.

Of the three the mixed water is least definite and some stations are found where the mixing is atypical and data from these stations are excluded in determining the T-S relationship of the

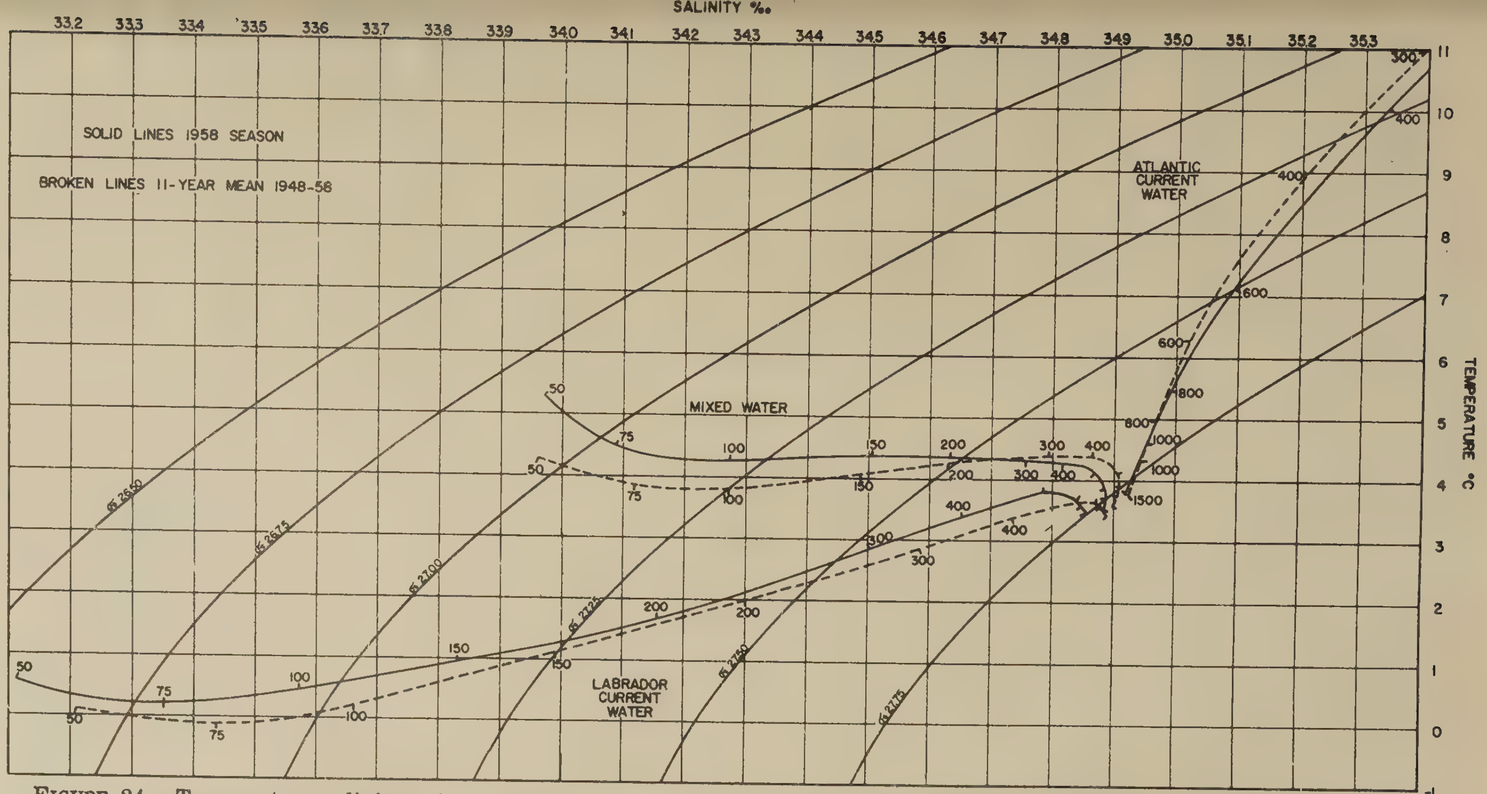

FIGURE 24.—Temperature-salinity relationships for Labrador Current water, Atlantic Current water and mixed water found in the Grand Banks region. Solid lines show conditions found during 1958 and broken lines represent the 11-year means for the period 1948-58. An approximate depth scale in meters is given.

mixed water. In 1958 there were a number of such stations showing atypical mixing, especially during the third survey. By far the greatest number of these stations showed mixtures intermediate between typical mixed water and Atlantic Current water. The curve for the 11-year mean for the Atlantic Current water is not accurately representative since in most years the surveys do not include sections which completely cross this current. All of the surveys do result in a complete and representative sampling of the Labrador Current and consequently fluctuations found in this water mass are considered to be the best indicator of changes taking place in the Ice Patrol area.

Figure 24 shows lighter than average water present in 1958 at each level and for each water mass. In the Atlantic Current water above about 1,000 meters the effect of higher than average salinities was outweighed by the higher temperatures. In the mixed water the lower densities were largely the result of higher temperatures in the upper 200 meters (with about average salinities) while below 200 meters colder temperatures could not balance the lower than average salinities. In the Labrador Current water the salinities were below average at all levels and the temperatures were above average except at the 150, 200 and 300-meters levels where the temperatures were colder than average.

Figure 25 shows the departures from average of the temperatures and salinities in the Labrador Current water and their approximate contributions to the departures from average density.

Starting with the abnormal onshore wind system and considering that this moved surface and near surface water in to the beach forcing a downward and seaward circulation along the bottom at least to the depth of the shelf (ca 200 meters), this would set up temporary instabilities the erasure of which, through the resulting mixing, would tend to wipe out the temperature minimum of the Labrador Current (50 to 100 meters) and lower the temperature of the water at levels immediately beneath the normal minimum. Such an hypothesis would explain the shape of the curves in figure 25 down to about 300 meters, and except for the small inversion in the salinity anomaly curve between 300 and 400 meters, might satisfy the deeper part of the salinity anomaly curve if further downward movement resulted from the mixing near the upper part of the continental slope. It does not, however, offer a clear explanation of the pronounced positive temperature anomaly at 600 meters.

The temperature maximum of the Labrador Current occurs at a depth of about 600 meters and is a part of the warm water tongue, which in a vertical section across the Labrador Current characteristically extends downward toward the beach at inter-

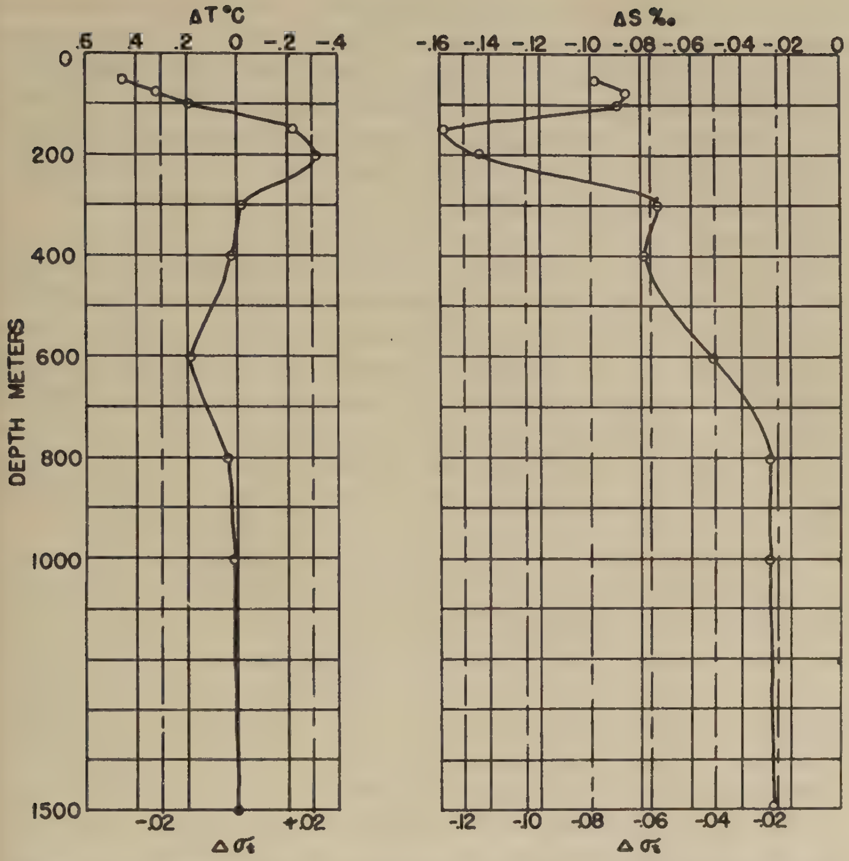

FIGURE 25.—Departures of temperature and salinity of the Labrador Current in 1958 from the 11-year means 1948-58. Dashed vertical lines indicate the approximate effect on density.

mediate depths, and is considered to be the combined result of cabbeling and isentropic movement along the offshore margins of the Labrador Current. It would appear from the results summarized in figure 25 that these processes of formation of the warm intermediate water were also stimulated by the onshore winds.

Past bulletins have given the position of the cold wall for each survey of the area southeastward of the Grand Banks in terms of the area between the cold wall and the following rhumb lines: the 45th parallel from the cold wall to 45° N. 49°W.; the 49th meridian from 45° N. to 43° N.; a line from 43°N. 49 W. through 42°N. 47°W. extended to the cold wall. Using the same criterion as in the past for the location of the cold wall (the horizontal projection of the line along which a temperature of 6 corresponds to a salinity of 34.95°/$_{\circ\circ}$), the area between the cold wall and the rhumb lines was 7.75×10^4 square km during the first survey and 8.31×10^4 square km during the third survey. These areas are presumed to represent the net effect of the Labrador Current tending to enlarge the area, and of the Atlantic Current tending to reduce the area. The volume transport of the Labrador Current passing section U (about 45°N.) was 5.50×10^6 cubic m/sec at the time of the first survey and was 4.29 at the time of the third survey.

In the general picture of the surface circulation of the North Atlantic a meridional section from the southern end of the Grand Banks to the central part of the North Atlantic eddy would cross the eastward flowing Atlantic Current, the westward flowing Labrador Current and branches of these. In the diagram shown in figure 26 an important part of the Atlantic Current crosses the section as A. Some of A recurves toward Bermuda as B, some recurves northwestward as D and some continues to the eastward as C without again crossing the section. D again recurves to the eastward and is joined by a part G of the Atlantic Current which recurves northwestward before reaching the longitude of the section. G may be considered to include a small amount of water from the United States and Canadian shelves and G and D together make up E. The Labrador Current F crossing the section to the westward recurves and recrosses the section to the eastward, now, with small amounts of G and D, as mixed water paralleling and on the northern side of E. E and C, then, represent the net contribution of the Atlantic Current to the eastward of the Grand Banks region.

There are geographical shifts in this pattern so that a section at a fixed longitude may cross different relative parts of the pattern at different times. Ships of the International Ice Patrol have occupied this section on three occasions. In 1938 the *General*

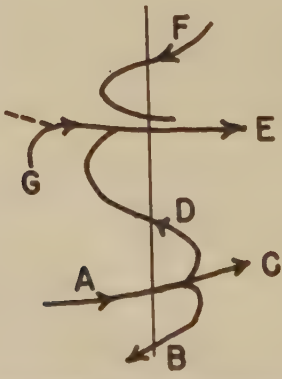

FIGURE 26.—Schematic diagram of currents crossing the meridian of 50°15′W south of the Grand Banks.

Greene ran the section at about the time the *Altair* and *Armauer Hansen* were conducting their work in the vicinity of the Azores in connection with the International Survey of the Gulf Stream Area. In 1950 the *Evergreen* occupied the section at about the time of the multiship Operation Cabot to the westward of the Grand Banks. In 1958 the *Evergreen* occupied the section as a part of the activity of the International Geophysical Year. Figures 27, 28, and 29 show, respectively, the temperature, salinity and velocity distribution found in 1958. In figure 29 the velocities are referred to the 2,000-decibar surface.

The dynamic topography of the sea surface relative to the 1,000-decibar surface is shown in figure 21. As mentioned earlier, the 1,000-decibar surface gives a fair representation of the current pattern in the vicinity of this section but the velocities are greater than indicated by this relative topography. Current directions shown in figure 21 are in good agreement with those derived from GEK current fixes obtained about every 10 miles along this section. In figure 27 the greater part of the section is dependant upon the observations from reversing thermometers at the stations. In the upper 200 meters, however, these observations were supplemented by bathythermograph casts made about every 5 miles between stations from station 6741 to station 6752. The most pronounced cold wall was found near station 6749 with the greater part of the Atlantic Current and its branches being found south of this station. However, at station 6750 the water below about 400 meters was Atlantic Current water. Southward of station 6749 the inclination of the isotherms is a good indication of the direction of flow across the section and the components E, D, A, and B of figure 26 are apparent. Except for the water above the Grand Banks, the thermal structure of the Labrador Current F and the eastward moving mixed water is more complex and the circulation picture is better shown by the velocity section (fig. 29).

The salinity distribution (fig. 28) shows a pattern similar to that presented by the temperature distribution. The deeper observations of salinity have been plotted against potential temperature in figure 30. Here the individual observations are given and are identified with the last two digits of the station numbers of their origin, station 6741 being the southernmost and 6750 being the northernmost of this series. From this small number of observations there is no clear cut grading of salinity for a corresponding potential temperature along the section. There is apparent, however, the difference of about 0.04°/₀₀ in salinity between the observations of the *Evergreen* and those of the

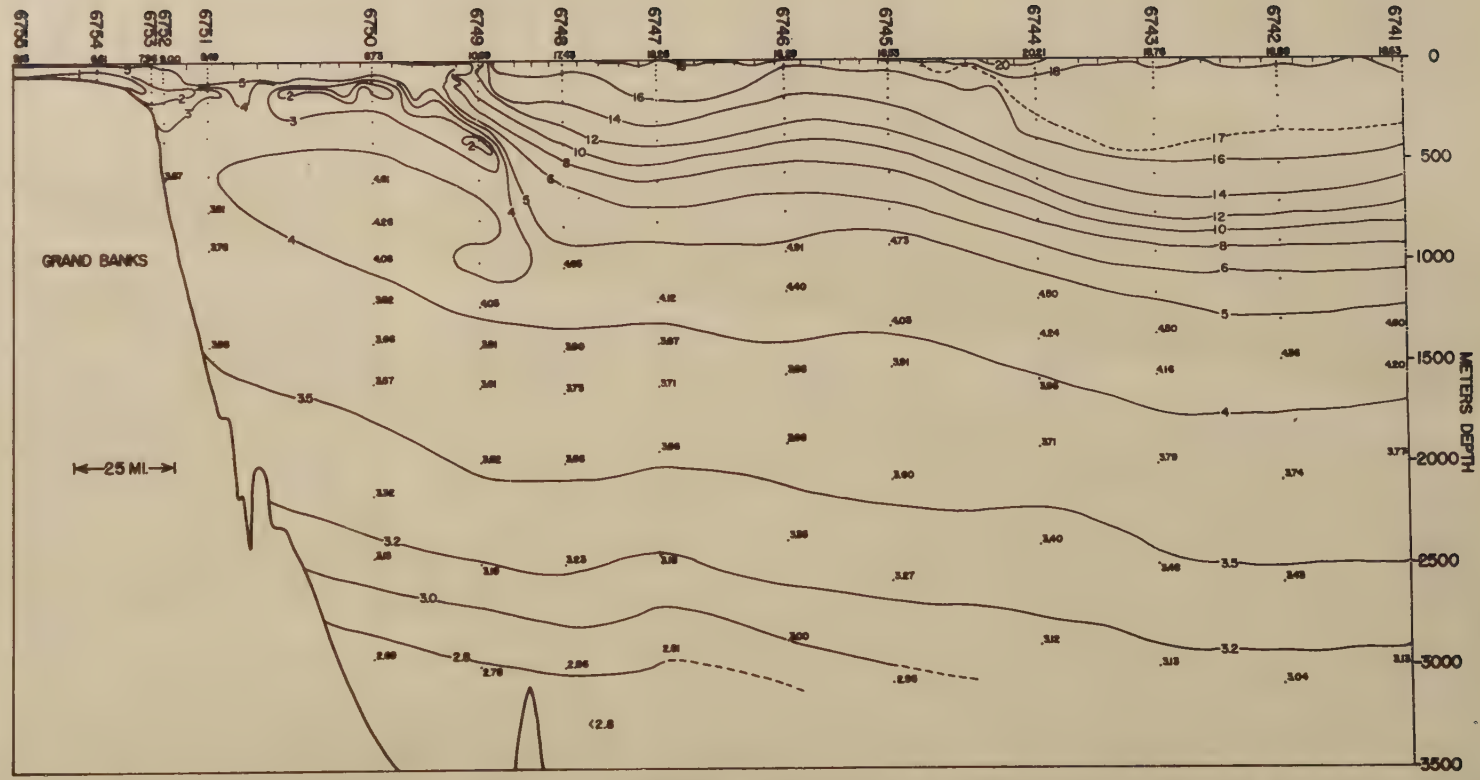

FIGURE 27.—Temperature distribution along meridional section at 50°15′W from data collected 23-26 May 1958.

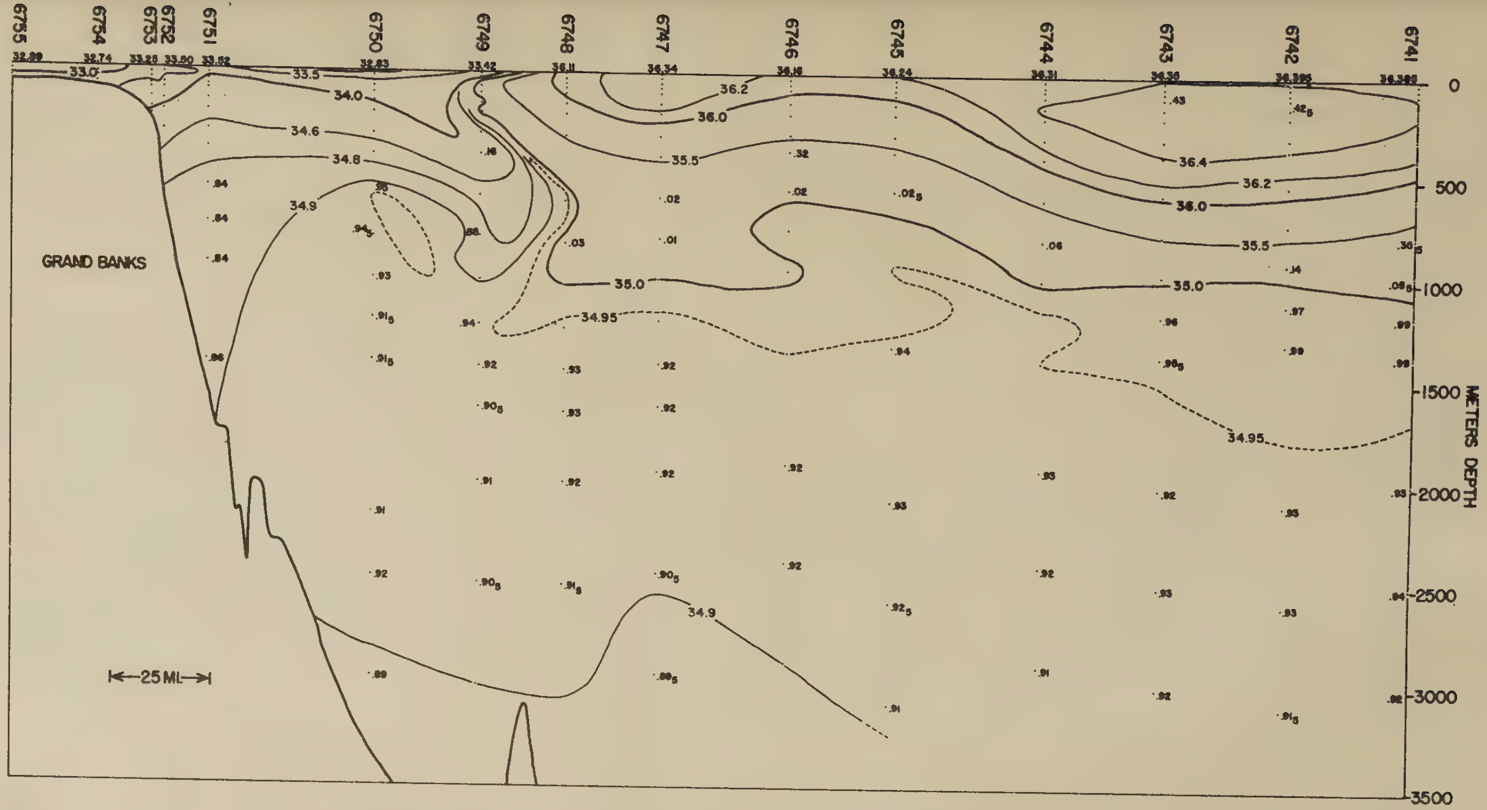

FIGURE 28.—Salinity distribution along meridional section at 50°15′W from data collected 23-26 May 1958.

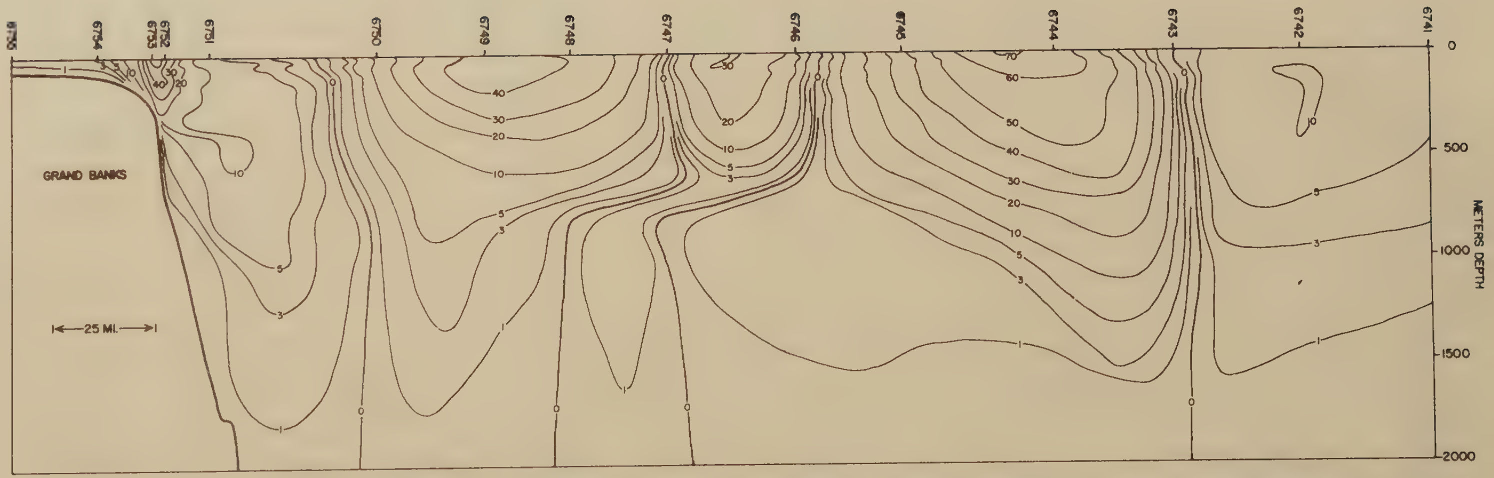

FIGURE 29.—Velocity distribution along meridional section at 50°15′W from data collected 23-26 May 1958. Velocities are referred to the 2000-decibar surface.

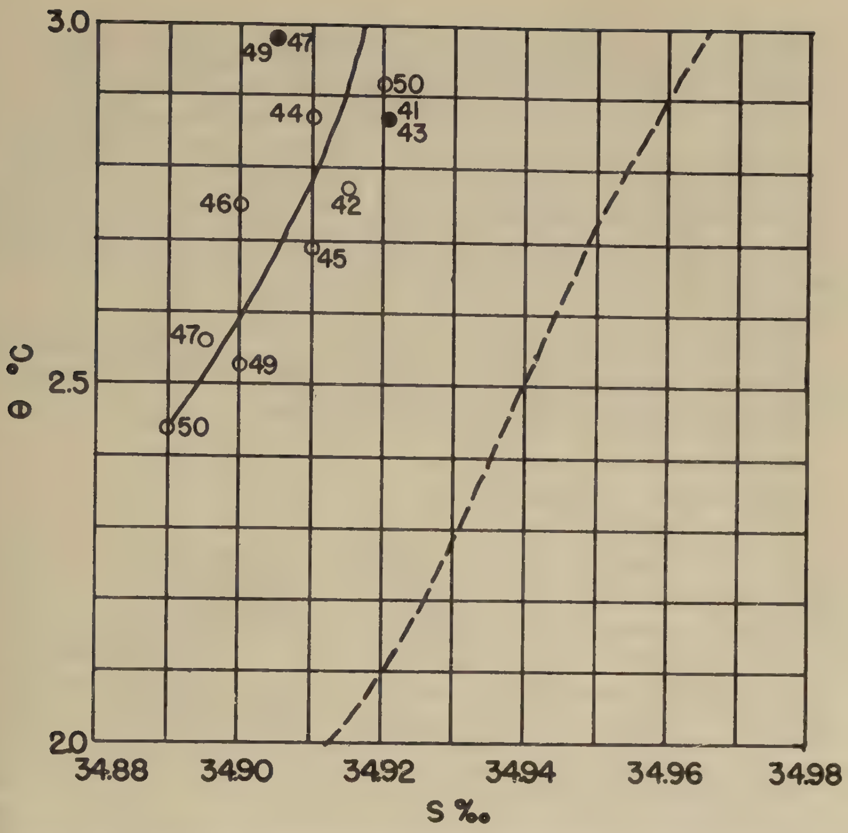

FIGURE 30.—Potential temperature-salinity relationship found beneath the Atlantic Current south of the Grand Banks 23-26 May 1958 (solid line) compared with the relationship reported by the Woods Hole Oceanographic Institution for the deep water west of Bermuda (broken line). Last two digits of station number identify location of observation.

Woods Hole Oceanographic Institution, as mentioned in the discussion of methods of measurement.

An inspection of figure 29 will show the components indicated in figure 26. The southernmost easterly flowing current is A in figure 26. This was computed to have a volume transport (expressed in millions of cubic meters per second) of 48.6. South of this is the westerly return toward Bermuda, B. The section did not completely cross B. By computation the part that is on the section is 7.6 and it is estimated that another 2.2 lies south of the section for an estimated total B of 9.8. Northward of A a westerly flowing band represents the part of A which recurves to the northwestward as D. By computation this amounted to 5.6. By subtraction of D and B from A the southerly contribution to the eastward, C, was 33.2. The northernmost band of current, flowing westward, is the Labrador Current, F. Some uncertainty arises in this part of the section where the motionless surface is probably inclined. With 1,000 decibars as the reference surface F was 3.3, but with reference to the 2,000-decibar surface F was computed as 6.7. To conform to the rest of the section the latter figure is used here. Just south of F the easterly band of current was made up of the returning F plus E, whence by difference E was 13.2, and the two contributions of Atlantic Current to the eastward of the section were E (13.2) and C (33.2) for a total of 46.4.

For the occupations of 1938 and 1950 not all of the individual components shown in figure 26 can be derived. For comparison, however, the following recapitulation is given.

	1938	1950	1958
A+F+E−D...	(computed)......58.6		
A..............	....	(56.4) computed plus 3.5 estimated). 59.9	(computed).........48.6
D..............	(by planimeter).. 0.1	(computed)..........18.5	(computed).......... 5.6
E+F..........	....	(computed)..........31.4	(computed).........19.9
F..............	(computed)...... 2.8	(computed).......... 2.0	(computed).......... 6.7
E..............	....	(by difference).......29.4	(by difference)......13.2
B..............	(computed)......21.7	(completely south of section).	(7.6 computed plus 2.2 estimated). 9.8
C..............	....	....	(by difference)......33.2
G..............	....	(by difference).......10.9	(by difference)...... 7.6
E+C..........	(by difference)....24.1	......................*55.0	(by difference)......46.4
C+B..........	....	(by difference).......41.4	(by difference)......43.0
E+C+B.......	(by difference)...45.8	(by difference).......70.8	(by difference)......56.2

* Applying mean B for 1938 and 1958 to E+C+B for 1950.

The foregoing shows considerable variation in volume transport for the different years. A most significant value is that of E+C, the combined contribution of the Atlantic Current to the eastward of the Grand Banks. The figure of 55.0 for the 1950 occupation, derived by difference using the mean of the value of B for 1938 and 1958 is highly questionable and is shown only to point out what is also apparent from the other 1950 values, that the volume transport in 1950 was exceptionally large. The tabulation also seems to indicate that 1938 was a year in which the volume transport to the eastward of the Grand Banks was small and the return toward Bermuda was large.[3]

In 1958, the volume transport to the eastward was intermediate between the 1938 low and the 1950 high values. The heat transport of component E was 159.4 million °m^3/sec with a mean temperature of 12.1° and the heat transport of component C was 447.0 with a mean temperature of 13.5°. The consequent combined contribution to the eastward of the Grand Banks, then,

---

[3] As 1938 was the year in which *Altair* and *Armauer* Hansen conducted their intensive survey work in the vicinity of the Azores and as these observations were heavily weighted by Sverdrup, Johnson, and Fleming in their transport balance of the North Atlantic; (The Oceans, Prentice-Hall, New York 1942, fig. 187 page 684) it seems that the transports shown in that figure for the North Atlantic Current are somewhat too small. In the same figure the value of 6 million m^3/sec for the Labrador Current is too large to be representative, 4 being more nearly an average value.

(E+C) was 606.4 with a mean temperature of 13.1°. In arriving at the heat transport figures the same procedures of estimates and differences used in deriving the volume transports above were followed.

Certain sections across the Labrador Current have been repeatedly occupied in connection with the routine current surveys of the Grand Banks region and on the postseason cruises. The velocity and temperature distribution in these vertical sections has been studied in some detail and over the years the accumulated data have permitted the development of tentative seasonal variation relationships for some of the sections for a part of the year. The locations of the sections occupied in 1958 and subjected to detailed analysis are as follows: Sections NW, SW and SE are the northwestern, southwestern and southeastern sides of the Bonavista triangle which is defined by its corners located at 50° N., 49° W., 47°20′N., 50° W., and just off Cape Bonavista, Newfoundland. Section H is roughly parallel to the southeastern side of the Bonavista triangle and extends north-northeasterly from about 47°10′N., 49°15′W. Section G extends northeasterly from about 47°10′N., 48°40′W. Section F_2 is an east-west section between the Grand Banks and Flemish Cap along the parallel of 47°15′N. Section F is similar to F_2 but about 30 miles farther south. Section T extends southeasterly from about 46°20′N., 49°00′W. Section U extends easterly from the Grand Banks at about 45°N. Section W extends southerly from the Grand Banks along the meridian of 50°15′W. The South Wolf Island section extends northeasterly from South Wolf Island, Labrador and is a part of the section across the Labrador Sea from South Wolf Island to Cape Farewell, Greenland.

Tentative seasonal normal relationships for the West Greenland Current off Cape Farewell were published in bulletin 35 of this series. The seasonal normal relationships for the Labrador Current which have been developed previously were published as follows:

Sections T, U and W........................bulletin No. 36 (season of 1950)
Sections NW, SW and SE..............bulletin No. 39 (season of 1953)
Sections F and G...............................bulletin No. 42 (season of 1956)

Insufficient data are at hand for the development of seasonal normals for sections H and F_2. Shown herewith in figure 31 are the tentative seasonal normal relationships for the South Wolf Island section.

In 1958 there were 19 occupations of such sections across the Labrador Current. The results are summarized below in table 1. In this table, as well as in the text, the volume transport is given in millions of cubic meters per second, the mean temperature and

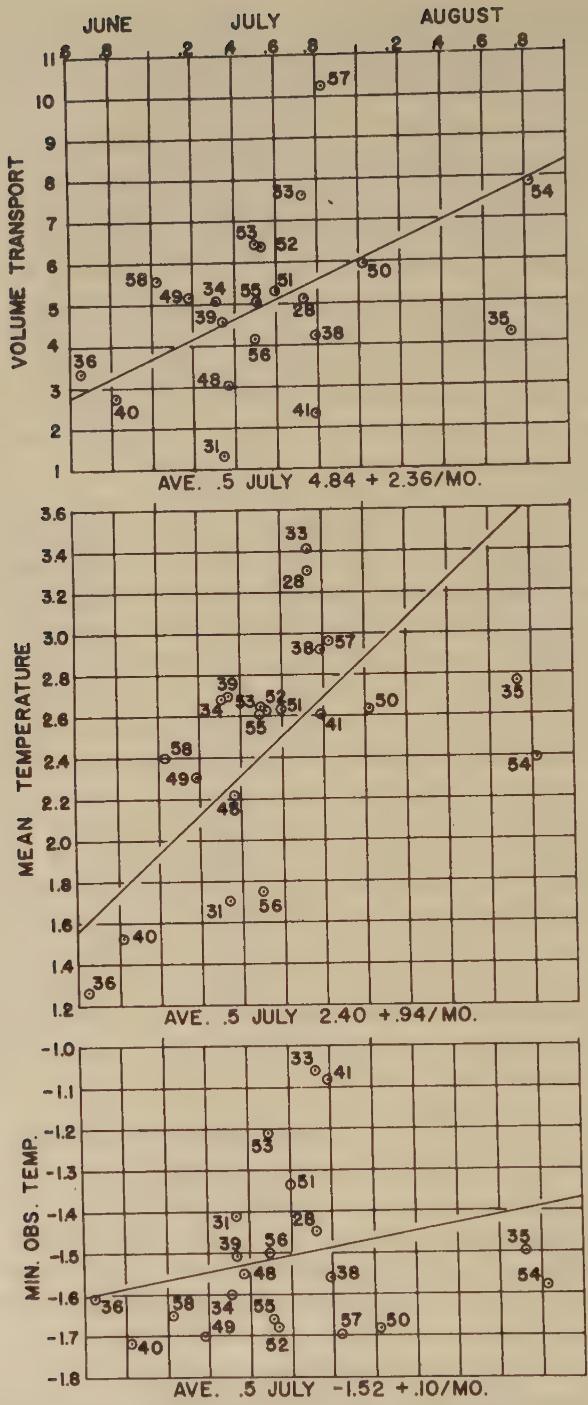

FIGURE 31.—Tentative normal seasonal change in volume transport, mean temperature and minimum observed temperature of the Labrador Current off South Wolf Island, Labrador.

Table 1.—Summary of Velocity Sections Across the Labrador Current Occupied in 1958

Section	Volume Transport			Mean Temperature			Minimum Observed Temperature			Heat Transport		
	1958	Normal	Anomaly	1958	Normal	Anomaly	1958	Normal	Anomaly	1958	Normal	Anomaly
First survey:												
F	5.14	2.73	+2.41	2.19	1.56	+0.63	−0.53	−1.26	+0.73	11.25	4.26	+6.99
T	4.66	3.33	+1.33	2.13	1.95	+0.18	−0.39	−1.40	+1.01	9.92	6.49	+3.43
U	5.50	5.31	+0.19	1.63	1.51	+0.12	−0.30	−1.23	+0.93	8.96	8.02	+0.94
W	4.56	4.24	+0.32	2.82	2.04	+0.78	−0.05	−0.51	+0.46	12.84	8.65	+4.19
Second survey:												
NW	4.23	3.09	+1.14	1.37	0.81	+0.56	−1.57	−1.79	+0.22	5.81	2.50	+3.31
SW	0.54	0.30	+0.24	−0.55	−0.98	+0.43	−1.48	−1.62	+0.14	−0.30	−0.29	−0.01
SE	4.84	2.82	+2.02	1.28	1.29	−0.01	−1.09	−1.46	+0.37	6.21	3.64	+2.57
H	4.85			1.63			−0.73			7.90		
G	4.73	3.61	+1.12	1.45	1.58	−0.13	−0.74	−1.22	+0.48	6.87	5.70	+1.17
F2	2.86			1.84			−0.67			5.27		
F	3.12	2.88	+0.24	2.00	1.73	+0.27	−0.65	−1.28	+0.63	6.24	4.98	+1.26
Third Survey:												
F	3.38	3.12	+0.26	2.61	2.01	+0.60	−1.00	−1.33	+0.33	8.84	6.27	+2.57
T	2.67	2.64	+0.03	1.84	1.73	+0.11	−0.79	−1.56	+0.77	4.92	4.57	+0.35
U	4.29	3.72	+0.57	2.32	2.40	−0.08	−0.55	−1.25	+0.70	9.96	8.93	+1.03
W	3.34	4.13	−0.79	3.95	3.15	+0.80	0.51	−0.39	−0.90	13.17	13.01	−0.16
Post Season:												
NW	4.47	3.86	+0.61	0.73	1.30	−0.57	−1.72	−1.65	−0.07	3.26	5.02	−1.76
SW	0.98	0.56	+0.42	0.80	−0.14	+0.94	−1.62	−1.64	+0.02	0.77	−0.08	+0.85
SE	4.61	3.22	+1.39	2.10	1.85	+0.25	−1.66	−1.56	−0.10	9.68	5.96	+3.72
S. Wolf Is.	5.57	3.73	+1.84	2.40	1.96	+0.44	−1.65	−1.57	−0.08	13.36	7.31	−6.05

minimum observed temperature are given in °C. and the heat transport is given in millions of cubic meter °C. per second. For purposes of comparison the observed value is followed by the seasonal normal where available and the anomaly from the seasonal normal.

Figure 32 is a schematic diagram representing the circulation deduced from the volume transports found during the different surveys and listed in table 1. In the first survey the volume transport and mean temperature were above normal in amounts progressively smaller from section F through section U with longer positive anomalies for both at section W. As noted earlier, the temperature minimum of the Labrador Current was decidedly warmer than usual. The positive anamalies of both volume and mean temperature are reflected in the considerable positive anomalies in heat transport throughout the first survey.

In the second survey the volume transport at the Bonavista triangle is clearly above normal. The mean temperature, however, was somewhat inconsistent with the result that the positive anomaly in the heat transport was contributed to by both volume and mean temperature of the water entering the triangle and largely the result of the volume of the water leaving the triangle. In figure 32 rounded mean values of volume transport have been used for the triangle both for the second survey and for the postseason cruise, assuming that there was no net transport vertically across the reference surface of 1,000 decibars. Farther

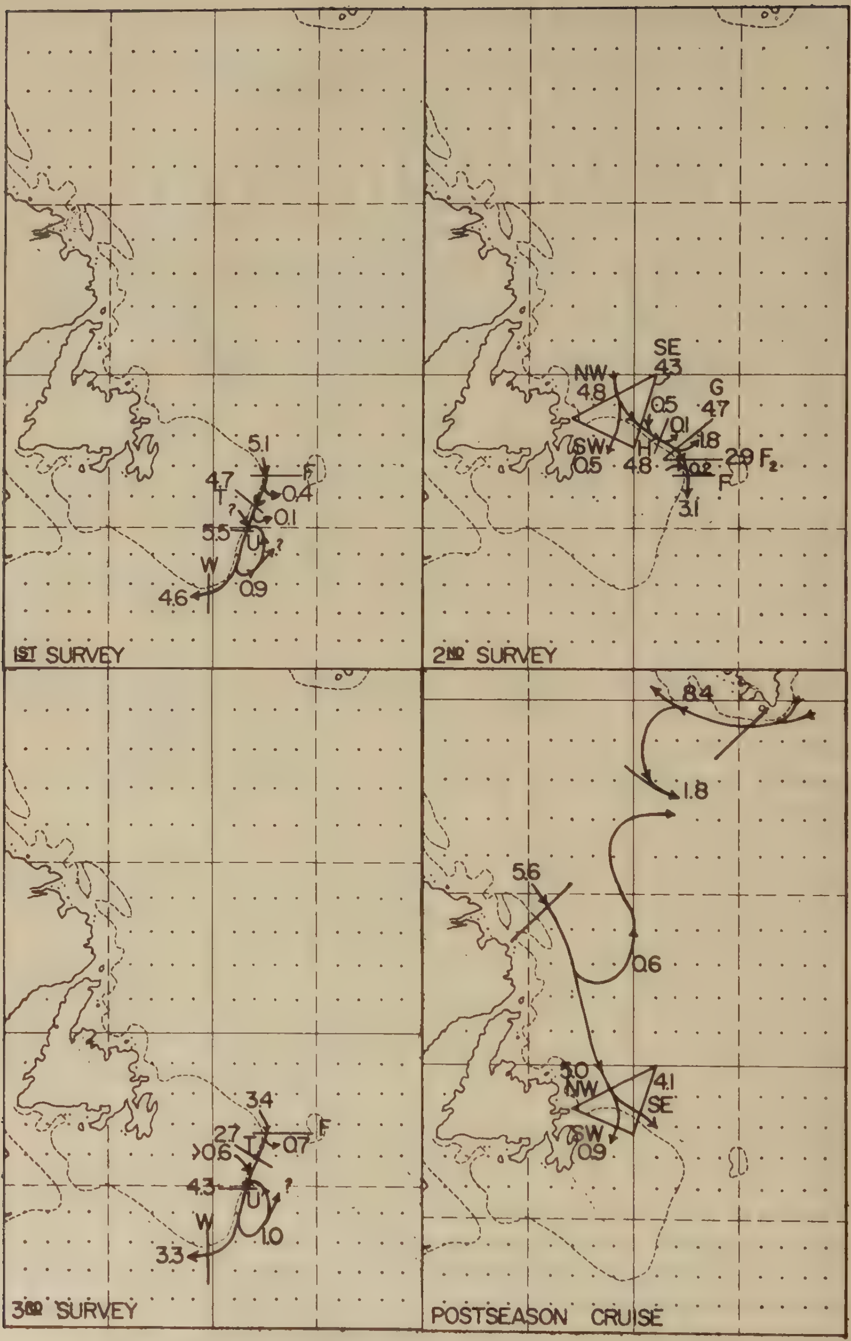
1ST SURVEY
5.1
F
4.7
T
0.4
C
0.1
5.5
U
W
0.9
4.6
2ND SURVEY
SE
4.3
NW
4.8
G
0.5
4.7
0.1
1.8
SW
H
0.5
4.8
0.2
2.9 F2
F
3.1
3RD SURVEY
3.4
F
2.7
T
0.7
>0.6
4.3
U
W
1.0
3.3
POSTSEASON CRUISE
8.4
1.8
5.6
0.6
3.0
NW
4.1
SE
SW
0.9

FIGURE 32.—Schematic representation of circulation deducted from sections occupied in 1958. Numerals indicate volume transport in units of $m^3 \times 10^6$/sec.

south at section F, while the volume transport and mean temperature were still above normal, they were much less so than in the first survey. The coldest water, however, continued to have a positive anomaly only slightly less than in the first survey.

In the third survey section F continued to have about the same positive anomaly of volume transport as in the second survey, but the additional water making up the seasonal increase in volume was of warmer water, increasing the anomaly of mean temperature to +0.6. The minimum temperature dropped to more nearly the seasonal normal.

The postseason occupation of the Bonavista triangle again showed a large positive anomaly in volume transport but less than during the occupation of the second survey. Minimum temperatures were about normal, but the mean temperatures were decidedly abnormal. The northwestern section was below normal in mean temperature, largely because the water below about 400 meters in the offshore end of the section where the water is relatively warm (about 3.5°) was motionless. The other two sections were above normal in mean temperature, resulting in a computed excess of heat leaving the triangle over that entering of about 7.2×10^6 m^3°C/sec. It will be noted that in each occupation of the triangle the computed volume transport leaving the triangle (SW + SE) exceed that entering the triangle (NW) by about 1.1×10^6.

The section off South Wolf Island, Labrador, occupied immediately following the Bonavista triangle on the postseason cruise, again showed a warmer minimum observed temperature than that found at the triangle. The volume transport of the Labrador Current here was well above normal as was the volume of the West Greenland Current off Cape Farewell. The mean temperature of the Labrador Current off South Wolf Island also was above normal by almost a half degree. In consequence the heat transport was almost twice the normal value.

Figures 33, 34, and 35 show, respectively, the dynamic topography of the sea surface in the vicinity of the section across the Labrador Sea, and the temperature and salinity distribution along that section. The West Greenland Current past this section was computed to have a volume transport of 8.36, a mean temperature of 4.48 and a heat transport of 37.40. On the assumption of this current being made up of an East Greenland Current component of constant mean temperature of 3.2 and an Irminger Current of constant mean temperature of 5.5, these components were computed to have had volume transports of 3.73 and 4.63 as compared with their respective seasonal normals of 2.45 and 2.41. The heat transport found (37.40) is 16.3 greater than the seasonal normal of 21.1.

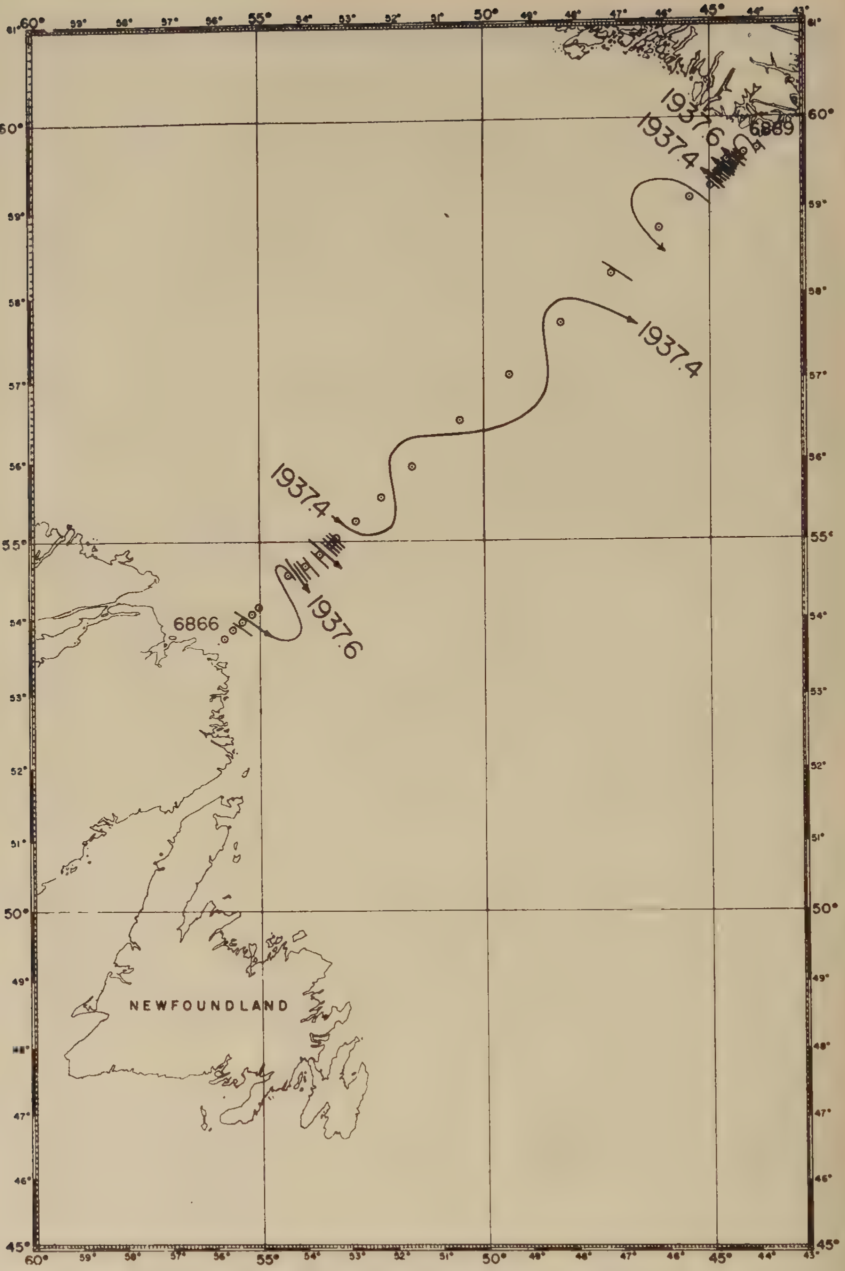
1937.6
1937.4
6869
1937.4
1937.4
1937.6
6866
NEWFOUNDLAND
60°
55°
50°
45°

FIGURE 33.—Dynamic topography of the sea surface relative to the 2000-decibar surface from data collected 1-6 July 1958. Oceanographic station positions are indicated by circles.

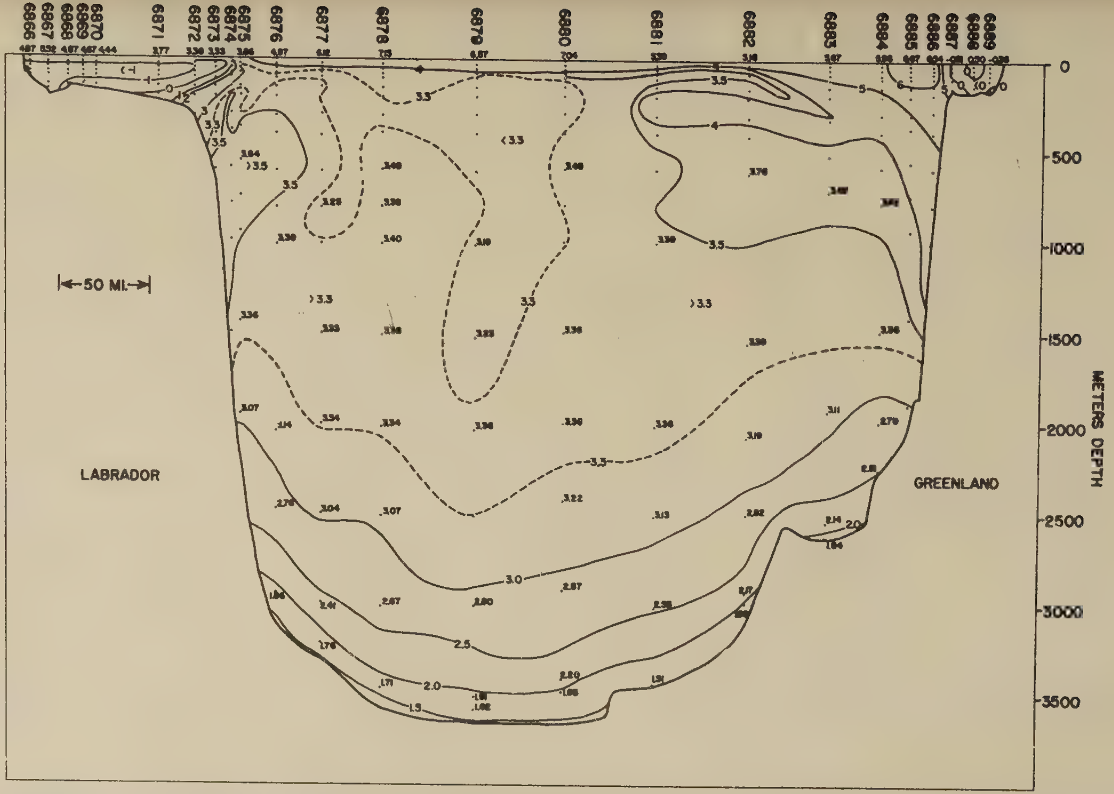

FIGURE 34.—Temperature distribution along section between South Wolf Island, Labrador and Cape Farewell, Greenland 1-6 July 1958.

Thus, on the basis of temperature, the abnormally high volume transport of the West Greenland Current was being contributed to more by the Irminger Current than by the East Greenland Current; although the salinity maximum in the West Greenland Current, as shown by figure 35, was about $0.06^{\circ}/_{\circ\circ}$ fresher than found in the occupations prior to 1949. The vigorous circulation in the Labrador Sea indicated by the positive anomalies in volume transport of the West Greenland Current off Cape Farewell and of the Labrador Current off South Wolf Island points to the greater amounts of warm West Greenland Current crossing to the American side as the reason for the higher than normal mean temperature of the Labrador Current off South Wolf Island. This is not consistant with the results obtained for the post-season occupation of the Bonavista triangle and casts further doubt on the triangle results. The previously mentioned disagreement between inflowing and outflowing heat combined with the foregoing indicate that the source of the discrepancy was section NW of the triangle.

In figure 34 the frigid part of the Labrador Current over the shelf is recognizable as is the West Greenland Current with its cold inshore and warm offshore components. On the Labrador side the tongue of maximum temperature which characteristically inclines downward toward the beach at intermediate depths on the offshore side of the Labrador Current is interrupted and colder water was found between the warm upper layers and the tongue (defined by the 3.5° isotherm in fig. 34) during this occupation of the section. In the central part of the section is to be seen the temperature minimum of the intermediate water and the corresponding temperature maximum below it. The warm water in the upper 1,000 meters between stations 6881 and 6883 is associated with the return southeastward of some of the West Greenland Current.

The fresher water over the Labrador and Greenland shelves, associated with the colder parts of the Labrador and West Greenland Currents, is evident in figure 35. The salinity maximum core of the Irminger Current component of the West Greenland Current is shown by the isohaline enclosing water of greater than $34.95^{\circ}/_{\circ\circ}$. The deep salinity maximum layer between 2,000 and 3,000 meters was slightly fresher than usual and while thus not as well defined by the $34.90^{\circ}/_{\circ\circ}$ isohaline it can be traced by inspection of the numerals showing the individual observations.

The analysis of the intermediate water and the deep water of this section as described in bulletin 42 of this series was continued for the 1958 occupation with the following average values of temperature and salinity resulting:

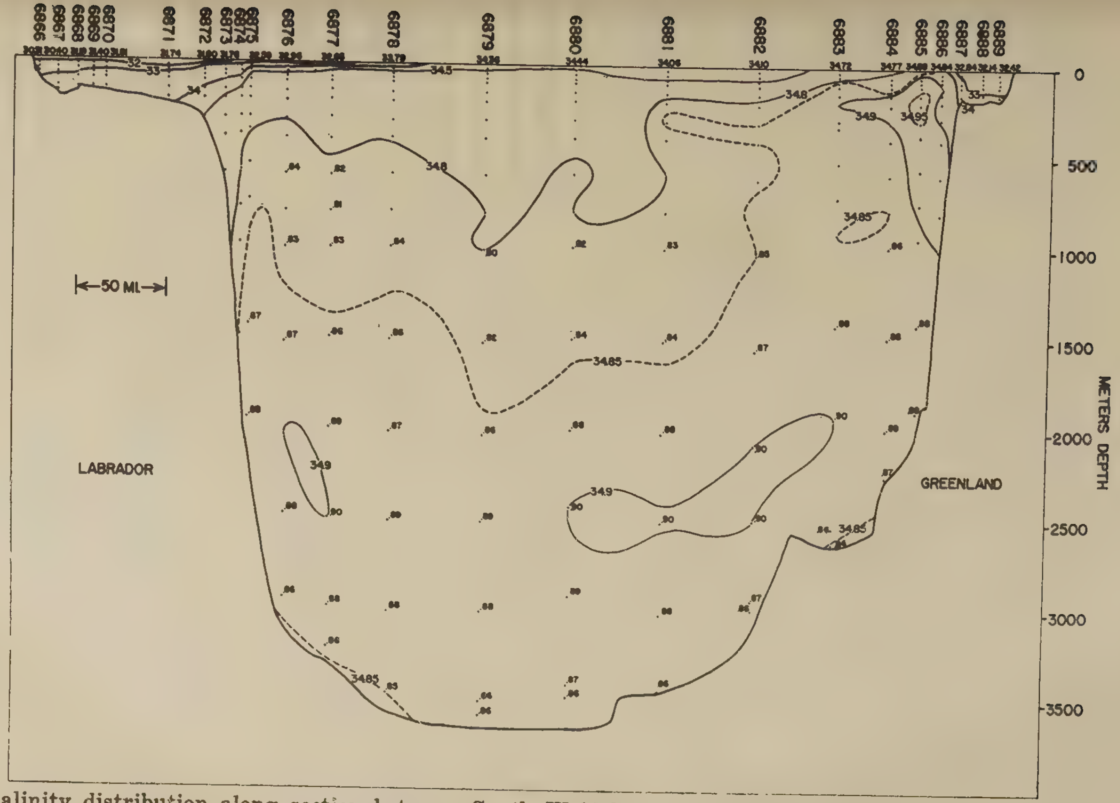

FIGURE 35.—Salinity distribution along section between South Wolf Island, Labrador and Cape Farewell, Greenland 1-6 July 1958.

	Temperature	*Salinity*
Intermediate water (stations 6877–6881)	3.35	34.82_2
2,000 meters	3.23	34.88_8
2.500 meters	2.95	34.89_1
3,000 meters	2.41	34.87_6
3,500 meters	1.82	34.85_7

In each case (except at 2,500 meters where the temperature was the same) the temperature was slightly higher and the salinity slightly lower than the corresponding values for 1957. The average increase in temperature was 0.06° and the average decrease in salinity was 0.006°/₀₀ thus each contributing about equally to the average decrease in σ_t of 0.01.

An inspection of the isentropic surfaces intersecting the section indicated that for this occupation the most nearly motionless level was probably between 1,500 and 2,000 meters and closer to the latter than the former. A reference surface of 2,000 decibars was used, therefore, in the construction of figure 33 and in studying the volume and heat transports across the section. The net volume transport across the section, beach to beach, above this reference surface was computed to be 1.00×10^6 m^3/sec. in a northwesterly direction. As the volume transport of West Greenland Current exceeded that of the Labrador Current by 2.8, a value of 1.8 has therefore been assigned to that part of the West Greenland Current which recurves and recrosses the section to the southeastward as indicated in figure 32. The net volume transport across the section below the 2,000-decibar surface was also computed and it also was directed northwesterly with a computed magnitude of about 1 million cubic meters per second. (3.1 by one computation, 1.2 by another method and 0.9 by difference of the 11.46 flowing northwesterly between station 6879 and Greenland and the 10.53 flowing southeasterly between station 6879 and Labrador.)

In the past the net volume transport across the section above the reference surface has been computed to be directed northwesterly in some years and southeasterly in others. Following is a summary for the post war years:

	Reference surface decibars	Net volume transport m^3×10^6/sec	Direction
1948	1,500	1.2	SE
1949	1,500	1.8	SE
1950	1,500	1.3	NW
1951	1,500	0.8	SE
1952	1,500	0.8	NW
1953	2,500	1.8	SE
1954	1,500	1.5	NW
1955	1,500	1.2	NW
1956	1,500	2.5	NW
1957	2,000	1.4	SE
1958	2,000	1.0	NW

In considering the meaning of the net transport in the past a net southeasterly flow has been taken to mean the excess of contributions into Baffin Bay through the northern openings (Smith Sound, Lancaster Sound, Jones Sound), over the amounts which sank below the reference surface in the Labrador Sea to exit to the Atlantic below the reference surface. When the net transport was northwesterly the balance was again presumed to be accomplished by sinking past the reference surface between the section and Davis Strait with a resulting net outflow below the reference surface. While it is realized that the cumulative errors of the second depth integral which are involved in the transport computation make the computed net transport below the reference surface of doubtful accuracy, if the northwesterly direction is significant it requires some revision in our thinking regarding the movement of the deep water of the Labrador Sea.

The tendency of the deeper isentropic surfaces in the Labrador Sea to parallel the bottom, resulting in an inclination upward toward Davis Strait ridge provides the possibility for water to change depth with the performance of a minimum of work. Thus it seems probable that the transfer of water across Davis Strait ridge is not always from north to south and that the oxygen-poor water in the deeper waters of Baffin Bay are kept from complete depletion of oxygen not only by water sinking from high levels within Baffin Bay itself but also by water crossing the threshold of Davis Strait from the south. Similar considerations suggest that the contributions of the Labrador Sea to the deep and bottom water of the North Atlantic may not be an annual cycle but may involve irregular periods with no contributions in one or more succeeding winters. The system cannot be clearly defined until such time as more extensive and repeated observations are available from both the Labrador Sea and Baffin Bay.

SUMMARY

1. Three dynamic topographic charts resulting from as many surveys of the Grand Banks region made in 1958 have been presented.

2. The Effects of the abnormal amount of onshore winds along the Labrador coast in the first 3 months of 1958 is altering the thermo-haline structure of the Labrador Current have been discussed.

3. The temperature-salinity characteristics of the three water masses found in the Grand Banks in 1958 have been compared with mean values 1948–58.

4. An extra southerly extension of a section southward from the Grand Banks completely crossing the Atlantic Current and

occupied during the third survey has been discussed with reference to the volume and heat transport of that current and compared with similar occupations of the section in 1938 and 1950.

5. The volume and heat transports, and the mean and minimum observed temperatures have been presented in a detailed examination of the Labrador Current for 19 sections occupied in 1958 and the departures from normal noted.

6. Tentative seasonal normal relationships for the Labrador Current off South Wolf Island, Labrador have been presented for the summer months.

7. The exceptionally vigorous circulation in the Labrador Sea found in 1958 has been presented by means of an examination of velocity and temperature sections across the Labrador Current off South Wolf Island and the West Greenland Current off Cape Farewell, Greenland.

8. Net volume transport across the section from South Wolf Island, Labrador to Cape Farewell, Greenland from surface to bottom has been computed and the northwesterly transport at all levels has been discussed.

TABLE OF OCEANOGRAPHIC DATA

The data collected in 1958 are tabulated below. The individual station headings give the station number, date, geographical position, depth of water and dynamic height of the sea surface used in the construction of the dynamic topographic charts shown in figures 19, 20, 21, 22, and 33. The depths of water are rough approximations being the uncorrected sonic soundings based on a sounding velocity of 800 fathoms per second and containing an additional mechanical speed error of about 1/60. Where the depths of scaled values are enclosed in parentheses, the data are based on extrapolated vertical distribution curves of temperature or salinity or both. Astrisks appearing before observed temperatures indicate that these temperatures were determined from the depth of reversal and the corrected reading of an unprotected thermometer. The symbol σ_t signifies 1,000 (density–1) at atmospheric pressure and temperature t.

STATIONS OCCUPIED IN 1958

Station 6573; 3 April; 41°56′ N., 51°02′ W.; depth 3,475 m.; dynamic height 971.056.

Observed values			Scaled values			
Depth, meters	Temperature, ° C.	Salinity, °/₀₀	Depth, meters	Temperature, ° C.	Salinity, °/₀₀	σ t
0.......	5.49	33.64	0......	5.49	33.64	26.56
25......	4.30	33.64	25.....	4.30	33.64	26.70
50......	7.19	34.22	50.....	7.19	34.22	26.80
76......	3.80	33.93	75.....	3.90	33.94	26.97
101.....	0.84	33.74	100....	0.85	33.74	27.06
151.....	2.83	34.16	150....	2.80	34.15	27.25
202.....	4.53		200....	4.50	34.44	27.31
303.....	4.41	34.60	300....	4.45	34.59	27.43
407.....	5.34	34.93	400....	5.30	34.93	27.60
608.....	4.74	34.885	600....	4.75	34.89	27.63
808.....	4.39	34.955	800....	4.45	34.95	27.72
1,009...	4.00	34.92	1,000..	4.00	34.92	27.75
1,511...	3.61	34.91				

Station 6574; 3 April 41°59′ N., 51°56′ W.; depth 4,024 m.; dynamic height 971.108.

0.......	6.81	34.71	0......	6.81	34.71	26.24
24......	6.40	33.76	25.....	6.40	33.76	26.55
48......	6.78	33.90	50.....	7.00	34.00	26.65
73......	10.88	35.07	75.....	10.85	35.08	26.88
97......	10.50	35.10	100....	10.35	35.09	26.98
145.....	8.16	34.62	150....	8.15	34.63	26.98
193.....	8.28	34.91	200....	8.15	34.90	27.19
290.....	5.38	34.68	300....	5.30	34.68	27.40
398.....	5.02	34.79	400....	5.00	34.79	27.53
598.....	4.82	34.945	600....	4.80	34.94	27.66
799.....	4.13	34.89	800....	4.15	34.89	27.70
996.....	3.86	34.885	1,000..	3.85	34.89	27.73
1,483...	3.72	34.915				

Station 6575; 3–4 April; 42°23′ N., 51°36′ W.; depth 3,109 m.; dynamic height 971.078.

0.......	7.74	33.99	0......	7.74	33.99	26.53
25......	8.15	34.21	25.....	8.15	34.21	26.65
50......	10.69	34.92	50.....	10.69	34.92	26.79
74......	11.10	35.04	75.....	11.10	35.05	26.82
99......	10.96	35.18	100....	10.90	35.18	26.95
148.....	8.65	34.91	150....	8.65	34.91	27.12
198.....	8.45	34.92	200....	8.45	34.92	27.16
297.....	6.29	34.90	300....	6.25	34.90	27.46
401.....	5.10	34.865	400....	5.10	34.87	27.58
598.....	4.73	34.935	600....	4.75	34.93	27.66
793.....	4.20	34.92	800....	4.20	34.92	27.73
990.....	3.99	34.92	1,000..	4.00	34.92	27.75
1,484...	3.67	34.91				

Station 6576; 4 April; 42°44′ N., 51°06′ W.; depth 2,103 m.; dynamic height 971.064.

0.......	6.18	33.84	0.......	6.18	33.84	26.64
25......	4.19	33.74	25......	4.19	33.74	26.79
50......	0.52	33.50	50......	0.52	33.50	26.89
75......	0.77	33.60	75......	0.77	33.60	26.96
100.....	0.37	33 66	100.....	0.37	33.66	27.03
150.....	0.44	33.72	150.....	0.44	33.72	27.07
201.....	1.44	34.09	200.....	1.40	34.08	27.30
301.....	2.14	34 26	300.....	2.15	34.26	27.39
369.....	3.29	34.60	400.....	3.55	34.66	27.58
550.....	4.42	34.80	600.....	4.30	34.81	27.63
728.....	3.90	34.835	800.....	3.85	34.85	27.70
911.....	3.81	34.86	1,000...	3.75	34.86	27.72
1,369...	3.56	34.85				

Station 6577; 4 April; 42°51′ N., 50°50′ W.; depth 1,079 m.; dynamic height 971.142.

Observed values			Scaled values			
Depth, meters	Temperature, ° C.	Salinity, °/₀₀	Depth, meters	Temperature, ° C.	Salinity, °/₀₀	σ t
0......	0.30	33.25	0.......	0.30	33.25	26.70
25......	0.49	33.30	25......	0.49	33.30	26.72
50......	0.61	33.33	50......	0.61	33.33	26.74
74......	0.13	33.36	75......	0.15	33.36	26.79
99......	0.07	33.38	100.....	0.05	33.38	26.82
148.....	0.18	33.40	150.....	0.20	33.40	26.83
197.....	0.12	33.54	200.....	0.10	33.55	26.95
296.....	0.88	33.94	300.....	0.90	33.96	27.24
300.....	......	33.97	400.....	2.25	34.34	27.44
474.....	3.08	34.55	600.....	3.75	34.77	27.65
655.....	3.82	34.83	800.....	3.80	34.84	27.70
863.....	3.81	34.84	(1,000)..	3.80	34.85	27.71

Station 6578; 4 April; 42°59′ N., 50°43′ W.; depth 622 m.; dynamic height 971.149.

0.......	0.35	33.19	0.......	0.35	33.19	26.65
25......	0.13	33.21	25......	0.13	33.21	26.68
49......	0.11	33.24	50......	0.10	33.24	26.71
74......	0.07	33.25	75......	0.05	33.25	26.72
99......	0.12	33.27	100.....	0.10	33.27	26.73
147.....	0.05	33.30	150.....	0.05	33.30	26.75
196.....	0.00	33.35	200.....	0.00	33.37	26.81
295.....	0.68	33.84	300.....	0.75	33.86	27.17
343.....	1.21	34.09	400.....	1.95	34.34	27.47
542.....	3.65	34.77	(600)...	3.85	34.84	27.69

Station 6579; 4 April; 43°03′ N., 50°37′ W.; depth 170 m.; dynamic height 971.128.

0.......	0.53	33.23	0......	0.53	33.23	26.67
26......	0.16	33.24	25.....	0.15	33.24	26.70
51......	0.17	33.24	50.....	0.15	33.24	26.70
77......	0.21	33.26	75.....	0.20	33.26	26.71
103.....	0.17	33.28	100....	0.15	33.28	26.73
154.....	0.20	33.32	150....	0.20	33.32	26.76

Station 6580; 4 April; 43°08.5′ N., 50°33′ W.; depth 93 m.; dynamic height 971.110.

0.......	1.07	33.36	0......	1.07	33.36	26.74
26......	0.39	33.38	25.....	0.40	33.38	26.80
52......	0.41	33.385	50.....	0.40	33.39	26.81
78......	0.55	33.44	75.....	0.55	33.43	26.83

Station 6581; 4 April; 43°20′ N., 50°16′ W.; depth 68 m.; dynamic height 971.126.

0.......	2.25	33.14	0......	2.25	33.14	26.49
25......	1.66	33.185	25.....	1.66	33.185	26.57
50......	1.66	33.19	50.....	1.66	33.19	26.57

Station 6582; 4 April; 43°00′ N., 50°15′ W.; depth 86 m.; dynamic height 971.120.

0.......	1.31	33.10	0......	1.31	33.10	26.52
25......	0.48	33.14	25.....	0,48	33.14	26.60
50......	0.62	33.28	50.....	0.62	33.28	26.71
75......	0.60	33.39	75.....	0.60	33.39	26.79

TABLE OF OCEANOGRAPHIC DATA—Continued

STATIONS OCCUPIED IN 1958—Continued

Station 6583; 4 April; 42°47′ N., 50°21′ W.; depth 320 m.; dynamic height 971.135.

Observed values			Scaled values			
Depth, meters	Temperature, ° C.	Salinity, ‰	Depth, meters	Temperature, ° C.	Salinity, ‰	σ t
0	0.02	33.12	0	0.02	33.12	26.61
24	−0.05	33.13	25	−0.05	33.13	26.62
48	−0.05	33.135	50	−0.05	33.14	26.63
72	−0.02	33.16	75	0.00	33.16	26.64
96	0.04	33.16	100	0.05	33.16	26.64
144	0.10	33.23	150	0.15	33.27	26.72
191	0.62	33.71	200	0.75	33.78	27.10
287	1.98	34.27	(300)	2.15	34.31	27.43

Station 6584; 4 April; 42°37.5′ N., 50°22′ W.; depth 1,509 m.; dynamic height 971.003.

Observed values			Scaled values			
Depth, meters	Temperature, ° C.	Salinity, ‰	Depth, meters	Temperature, ° C.	Salinity, ‰	σ t
0	5.03	33.54	0	5.03	33.54	26.54
25	6.25	33.92	25	6.25	33.92	26.69
51	5.48	34.19	50	5.50	34.18	26.98
76	3.38	34.09	75	3.65	34.09	27.12
102	4.38	34.30	100	4.35	34.29	27.20
152	4.44	34.43	150	4.45	34.43	27.30
203	3.45	34.42	200	3.45	34.42	27.40
305	4.29	34.75	300	4.25	34.73	27.56
402	4.39	34.82	400	4.40	34.82	27.62
602	3.96	34.845	600	4.00	34.85	27.69
			800	3.70	34.85	27.72
1,001	3.61	34.855	1,000	3.60	34.85	27.73
1,426	3.53	34.855				

Station 6585; 4–5 April; 42°23′ N., 50°26′ W.; depth 2,650 m.; dynamic height 971.001.

Observed values			Scaled values			
Depth, meters	Temperature, ° C.	Salinity, ‰	Depth, meters	Temperature, ° C.	Salinity, ‰	σ t
0	6.82	33.68	0	6.82	33.68	26.43
24	5.57	33.70	25	5.50	33.70	26.61
48	3.25	33.84	50	3.25	33.85	26.96
72	3.50	34.10	75	3.50	34.12	27.16
96	3.25	34.21	100	3.30	34.24	27.27
144	4.73	34.55	150	4.85	34.57	27.38
193	5.24	34.68	200	5.20	24.69	27.42
289	4.57	34.74	300	4.50	34.74	27.54
363	4.02	34.74	400	4.10	34.77	27.62
545	4.53	34.93	600	4.55	34.94	27.70
728	4.31	34.95	800	4.30	34.95	27.73
916	4.09	34.935	1,000	4.10	34.93	27.74
1,395	3.60	34.92				

Station 6586; 5 April; 42° 00′ N., 50°22′ W.; depth 3,383 m.; dynamic height 970.974.

Observed values			Scaled values			
Depth, meters	Temperature, ° C.	Salinity, ‰	Depth, meters	Temperature, ° C.	Salinity, ‰	σ t
0	5.90	33.60	0	5.90	33.60	26.48
26	5.32	33.70	25	5.35	33.70	26.63
51	3.31	33.93	50	3.40	33.91	27.00
76	2.86	34.12	75	2.85	34.11	27.21
101	3.53	34.34	100	3.50	34.33	27.32
151	3.55	34.47	150	3.55	34.47	27.43
202	3.34	34.56	200	3.35	34.51	27.48
303	4.89	34.88	300	4.90	34.87	27.61
418	5.19	34.99	400	5.20	34.98	27.65
625	4.21	34.915	600	4.30	34.92	27.71
829	4.15	34.93	800	4.15	34.93	27.73
1,036	3.86	34.915	1,000	3.90	34.92	27.76
1,555	3.55	34.905				

Station 6587; 5 April; 41°29′ N., 50°32′ W.; depth 3,558 m.; dynamic height 971.223.

Observed values			Scaled values			
Depth, meters	Temperature, ° C.	Salinity, ‰	Depth, meters	Temperature, ° C.	Salinity, ‰	σ t
0	14.27	35.76	0	14.27	35.76	26.73
22	14.28	35.75	25	14.25	35.74	26.72
44	13.53	34.62	50	13.40	35.59	26,78
66	13.22	35.55	75	13.20	35.56	26.80
88	13.31	35.57	100	13.40	35.59	26.78
132	13.56	35.64	150	13.35	35.58	26.79
176	12.89	35.49	200	12.40	35.40	26.84
264	10.36	35.18	(300)	9.00	35.03	27.16
			(400)	6.30	34.70	27.30
			(600)	4.70	34.75	27.53
			(800)	4.15	34.87	27.69
			(1,000)	3.85	34.91	27.75

Station 6588; 5 April; 41°04′ N., 50°18′ W.; depth 3,676 m.; dynamic height 971.327.

Observed values			Scaled values			
Depth, meters	Temperature, ° C.	Salinity, ‰	Depth, meters	Temperature, ° C.	Salinity, ‰	σ t
0	15.30	35.99	0	15.30	35.99	26.68
25	15.35	35.98	25	15.35	35.98	26.66
50	15.31	35.98	50	15.31	35.98	27.67
75	15.27	35.99	75	15.27	35.99	26.69
100	15.27	35.99	100	15.27	35.99	26.69
150	15.27	35.99	150	15.27	35.99	26.69
200	15.24	35.98	200	15.24	35.98	26.69
300	14.05	35.99	300	14.05	35.99	26.96
371	......	35.38	400	10.30	35.28	27.13
553	7.55	35.05	600	6.90	35.02	27.47
733	5.37	34.975	800	4.95	34.98	27.68
926	4.61	34.96	1,000	4.50	34.96	27.72
1,426	3.88	34.925				

Station 6589; 5–6 April; 42°03′ N., 49°26′ W.; depth 3,329 m.; dynamic height 971.260.

Observed values			Scaled values			
Depth, meters	Temperature, ° C.	Salinity, ‰	Depth, meters	Temperature, ° C.	Salinity, ‰	σ t
0	14.41	35.84	0	14.41	35.84	26.77
22	14.39	35.835	25	14.40	35.83	26.76
45	14.40	35.83	50	14.40	35.83	26.76
67	14.42	35.83	75	14.40	35.83	26.76
89	14.44	35.835	100	14.40	35.83	26.76
133	14.42	35.835	150	14.40	35.83	26.76
178	14.36	35.82	200	13.90	35.73	26.78
267	11.91	35.41	300	11.15	35 31	27.01
391	9.31	35.14	400	9.15	35.12	27.21
588	5.97	34.97	600	5.85	34.97	27.57
789	4.80	34.97	800	4.75	34.97	27.70
994	4.36	34.96	1,000	4.35	34.96	27.74
1,519	3.62	34.91				

Station 6590; 6 April; 41°34′ N., 49°01′ W.; depth 3,658 m.; dynamic height 971.296.

Observed values			Scaled values			
Depth, meters	Temperature, ° C.	Salinity, ‰	Depth, meters	Temperature, ° C.	Salinity, ‰	σ t
0	14.51	35.85	0	14.51	35.85	26.75
20	14.49	35.85	25	14.50	35.84	26.74
41	14.52	35.84	50	14.50	35.84	26.74
62	14.51	35.84	75	14.50	35.84	26.74
83	14.50	35.84	100	14.50	35.85	26.75
124	14.47	35.85	150	14.25	35.80	26.77
165	14.13	35.78	200	13.95	35.73	26.77
248	13.69	35.65	300	12.05	35.47	26.97
287	12.29	35.50	400	10.05	35.26	27.16
425	9.56	35.22	600	6.25	34.95	27.50
560	6.89	35.00	800	4.55	34.90	27.67
713	4.85	34.88	1,000	4.35	34.94	27.72
1,119	4.19	34.96				

TABLE OF OCEANOGRAPHIC DATA—Continued

STATIONS OCCUPIED IN 1958—Continued

Station 6591; 6 April; 41°16′ N., 48°34′ W.; depth 3,475 m.; dynamic height 971.320.

Observed values			Scaled values			
Depth, meters	Temperature, ° C.	Salinity, ‰	Depth, meters	Temperature, ° C.	Salinity, ‰	σt
0	14.71	35.79	0	14.71	35.79	26.66
23	14.73	35.79	25	14.75	35.79	26.65
46	14.89	35.84	50	14.95	35.87	26.67
69	15.04	35.96	75	15.05	35.96	26.72
92	15.00	35.95	100	14.95	35.95	26.74
138	14.91	35.95	150	14.80	35.92	26.74
184	14.25	....	200	14.10	35.72	26.74
276	13.49	35.54	300	12.90	35.49	26.81
390	10.47	35.28	400	10.25	35.25	27.12
581	6.11	34.93	600	5.90	34.93	27.53
770	4.99	34.96	800	4.90	34.96	27.68
971	4.55	34.96	1,000	4.50	34.96	27.72
1,488	3.76	34.915				

Station 6592; 6 April; 41°37′ N., 47°16′ W.; depth 4,289 m.; dynamic height 971.228.

Observed values			Scaled values			
Depth, meters	Temperature, ° C.	Salinity, ‰	Depth, meters	Temperature, ° C.	Salinity, ‰	σt
0	14.29	35.80	0	14.29	35.80	26.76
26	14.25	35.80	25	14.25	35.80	26.77
51	14.23	35.78	50	14.25	35.78	26.76
77	14.17	35.77	75	14.15	35.77	26.77
103	14.15	35.77	100	14.15	35.77	26.77
153	13.74	35.69	150	13.80	35.70	26.79
205	13.09	35.54	200	13.20	35.55	26.80
308	10.71	35.30	300	10.95	35.32	27.06
408	7.68	35.00	400	7.90	35.02	27.33
611	5.33	34.95	600	5.40	34.95	27.61
814	4.53	34.92	800	4.60	34.92	27.68
1,018	4.05	34.905	1,000	4.05	34.91	27.73
1,531	3.68	34.91				

Station 6593; 6 April; 41°57′ N., 47°52′ W.; depth 3,830 m.; dynamic height 971.021.

Observed values			Scaled values			
Depth, meters	Temperature, ° C.	Salinity, ‰	Depth, meters	Temperature, ° C.	Salinity, ‰	σt
0	6.38	33.77	0	6.38	33.77	26.56
26	6.38	33.76	25	6.40	33.76	26.55
53	6.19	33.75	50	6.25	33.75	26.56
79	4.50	33.95	75	4.70	33.91	26.87
105	5.66	34.41	100	5.50	34.32	27.10
157	5.21	34.63	150	5.25	34.61	27.36
210	5.29	34.72	200	5.25	34.70	27.43
315	5.50	34.92	300	5.50	34.90	27.56
526	....	34.97	400	5.40	34.96	27.62
638	4.80	34.995	600	4.90	34.99	27.70
835	4.23	34.95	800	4.35	34.96	27.74
1,048	3.80	34.91	1,000	3.85	34.92	27.76
1,587	3.47	34.89				

Station 6594; 7 April; 42°20′ N., 48°34′ W.; depth 3,383 m.; dynamic height 971.013.

Observed values			Scaled values			
Depth, meters	Temperature, ° C.	Salinity, ‰	Depth, meters	Temperature, ° C.	Salinity, ‰	σt
0	6.32	33.73	0	6.32	33.73	26.53
24	6.34	33.72	25	6.35	33.72	26.52
48	8.70	34.76	50	8.65	34.68	26.94
71	7.99	34.72	75	7.80	34.71	27.10
95	7.06	34.60	100	6.80	34.58	27.13
144	5.34	34.52	150	5.30	34.52	27.28
191	5.15	34.62	200	5.15	34.64	27.39
286	5.18	34.84	300	5.20	34.86	27.56
392	5.09	34.93	400	5.10	34.93	27.62
588	4.84	34.99	600	4.80	34.99	27.71
784	4.09	34.915	800	4.05	34.91	27.73
984	3.80	34.90	1,000	3.80	34.90	27.75
1,494	3.51	34.89				

Station 6595; 7 April 42°43.5′ N., 49°15′ W.; depth 2,469 m.; dynamic height 971.011.

Observed values			Scaled values			
Depth, meters	Temperature, ° C.	Salinity, ‰	Depth, meters	Temperature, ° C.	Salinity, ‰	σt
0	6.51	33.78	0	6.51	33.78	26.54
25	6.47	33.78	25	6.47	33.78	26.55
51	6.42	33.78	50	6.40	33.78	26.56
76	4.77	34.10	75	4.80	34.09	27.00
102	5.63	34.46	100	5.60	34.43	27.17
152	5.72	34.64	150	5.75	34.63	27.31
204	5.48	34.75	200	5.50	34.74	27.43
306	5.74	34.96	300	5.75	34.95	27.56
420	5.04	34.96	400	5.15	34.96	27.65
623	4.43	34.95	600	4.50	34.95	27.71
823	3.98	34.91	800	4.05	34.92	27.74
1,032	3.66	34.89	1,000	3.70	34.89	27.75
1,557	3.43	34.87				

Station 6596; 7 April; 43°22′ N., 48°50′ W.; depth 1,920 m.; dynamic height 970.988.

Observed values			Scaled values			
Depth, meters	Temperature, ° C.	Salinity, ‰	Depth, meters	Temperature, ° C.	Salinity, ‰	σt
0	5.97	33.96	0	5.97	33.96	26.76
25	5.45	33.95	25	5.45	33.95	26.82
49	5.19	33.94	50	5.20	33.94	26.84
74	5.19	34.11	75	5.20	34.12	26.98
99	6.75	34.66	100	6.75	34.66	27.21
148	3.34	34.33	150	3.35	34.33	27.33
197	3.94	34.58	200	3.95	34.58	27.47
296	3.81	34.70	300	3.85	34.70	27.58
408	4.29	34.82	400	4.30	34.81	27.63
604	4.13	34.90	600	4.15	34.90	27.71
794	3.88	34.89	800	3.90	34.89	27.73
995	3.73	34.90	1,000	3.75	34.90	27.75
1,501	3.48	34.885				

Station 6597; 7 April; 43°07′ N., 48°11′ W.; depth 3,017 m.; dynamic height 971.051.

Observed values			Scaled values			
Depth, meters	Temperature, ° C.	Salinity, ‰	Depth, meters	Temperature, ° C.	Salinity, ‰	σt
0	8.18	34.06	0	8.18	34.06	26.53
25	7.66	34.06	25	7.66	34.06	26.61
50	7.55	34.16	50	7.55	34.16	26.70
74	7.90	34.45	75	7.90	34.45	26.88
99	7.56	34.58	100	7.55	34.58	27.03
149	7.67	34.78	150	7.65	34.78	27.17
198	7.04	34.82	200	7.05	34.82	27.29
297	5.92	34.85	300	5.90	34.85	27.47
380	5.28	34.90	400	5.25	34.91	27.60
565	5.08	35.01	600	4.95	35.00	27.70
748	4.33	34.95	800	4.20	34.94	27.74
941	3.99	34.92	1,000	3.95	34.92	27.75
1,432	3.60	34.905				

Station 6598; 7 April; 42°53′ N., 47°30′ W.; depth 3,695 m.; dynamic height 971.027.

Observed values			Scaled values			
Depth, meters	Temperature, ° C.	Salinity, ‰	Depth, meters	Temperature, ° C.	Salinity, ‰	σt
0	6.68	33.72	0	6.68	33.72	26.48
24	8.04	34.24	25	8.04	34.24	26.69
49	5.44	34.08	50	5.45	34.08	26.91
74	5.46	34.26	75	5.45	34.26	27.06
98	6.76	34.64	100	6.75	34.64	27.19
147	5.99	34.64	150	6.00	34.64	27.29
197	6.70	34.84	200	6.70	34.84	27.35
295	5.73	34.86	300	5.70	34.86	27.50
385	5.00	34.88	400	4.95	34.88	27.60
572	4.60	34.92	600	4.60	34.93	27.68
757	4.79	35.02	800	4.70	35.01	27.74
952	4.23	34.95	1,000	4.15	34.94	27.74
1,449	3.58	34.90				

TABLE OF OCEANOGRAPHIC DATA—Continued

STATIONS OCCUPIED IN 1958—Continued

Observed values			Scaled values			
Depth, meters	Temperature, °C.	Salinity, ‰	Depth, meters	Temperature, °C.	Salinity, ‰	σt
Station 6599; 8 April; 42°41.5′ N., 46°50′ W.; depth 5,035 m.; dynamic height 971.144.						
0	7.00	33.58	0	7.00	33.58	26.32
25	6.30	33.62	25	6.30	33.62	26.45
50	6.56	33.78	50	6.56	33.78	26.54
75	5.00	33.82	75	5.00	33.82	26.77
100	4.33	33.75	100	4.33	33.75	26.78
150	4.57	33.79	150	4.57	33.79	26.78
201	5.65	34.00	200	5.65	34.00	26.83
301	4.88	34.42	300	4.90	34.41	27.24
351	4.98	34.86	400	5.00	34.90	27.62
521	4.91	34.95	600	4.65	34.94	27.69
686	4.41	34.92	800	4.20	34.92	27.73
873	4.12	34.92	1,000	3.95	34.91	27.74
1,364	3.57	34.88				
Station 6600; 8 April; 42°30.5′ N., 46°06′ W.; depth 4,115 m.; dynamic height 971.484.						
0	15.79	36.12	0	15.79	36.12	26.68
24	15.79	36.11	25	15.80	36.11	26.67
49	15.81	36.115	50	15.80	36.11	26.67
73	15.82	36.12	75	15.80	36.12	26.67
98	15.79	36.11	100	15.80	36.11	26.67
145	15.78	36.11	150	15.75	36.11	26.68
194	15.76	36.11	200	15.75	36.11	26.68
292	14.43	35.86	300	14.35	35.85	26.78
417	13.42	35.74	400	13.55	35.76	26.89
614	9.81	35.25	600	10.05	35.27	27.17
803	6.63	35.06	800	6.70	35.06	27.53
1,009	4.96	34.96	1,000	5.00	34.96	27.67
1,528	3.95	34.925				
Station 6601; 8 April; 42°59′ N., 45°36′ W.; depth 4,676 m.; dynamic height 971.520.						
0	15.62	36.11	0	15.62	36.11	26.70
26	15.72	36.11	25	15.70	36.10	26.69
51	15.73	36.10	50	15.70	36.10	26.68
77	15.76	36.11	75	15.75	36.11	26.68
102	15.77	36.10	100	15.75	36.10	26.67
153	15.76	36.11	150	15.75	36.11	26.68
204	15.76	36.11	200	15.75	36.11	26.68
306	15.75	36.09	300	15.75	36.10	26.67
383	14.56	35.94	400	14.20	35.90	26.85
562	11.34	35.44	600	10.60	35.35	27.14
738	7.82	35.10	800	6.90	35.06	27.50
928	5.63	35.00	1,000	5.20	34.98	27.65
1,409	4.03	34.93				
Station 6602; 8 April; 43°20′ N., 45°15′ W.; depth 4,709 m.; dynamic height 971.428.						
0	15.71	36.05	0	15.71	36.05	26.64
27	15.69	36.06	25	15.70	36.06	26.65
53	15.66	36.06	50	15.65	36.06	26.66
80	15.68	36.045	75	15.65	36.05	26.65
106	15.69	36.05	100	15.70	36.05	26.64
160	15.66	36.045	150	15.65	36.05	26.65
214	15.04	35.90	200	15.20	35.94	26.67
320	14 38	35.93	300	14.55	35.93	26.80
325	14 40	35.95	400	12.40	35.56	26.96
476	10.62	35.18	600	8.55	35.16	27.33
620	8.24	35.16	800	6.10	35.05	27.60
778	6.32	35.06	1,000	4.75	34.99	27.71
1,175	4.19	34.95				

Observed values			Scaled values			
Depth, meters	Temperature, °C.	Salinity, ‰	Depth, meters	Tem- Salin- ture, °C.	σt ity, ‰	σt
Station 6603; 8–9 April; 43°33′ N., 45°51′ W.; depth 4,663 m.; dynamic height 971.246.						
0	14.58	35.89	0	14.58	35.89	26.77
27	14.58	35.885	25	14.60	35.89	26.76
53	14.57	35.895	50	14.60	35.89	26.76
80	14.58	35.88	75	14.60	35.88	26.75
106	14.54	35.875	100	14.55	35.88	26.76
160	13.37	35.63	150	13.55	35.67	26.82
213	12.81	35.58	200	12.95	35.59	26.87
319	10.24	35.285	300	11.30	35.41	27.06
344	10.78	35.355	400	8.45	35.06	27.27
494	6.04	34.65	600	4.95	34.79	27.53
632	4.80	34.825	800	4.50	34.91	27.68
794	4.50	34.915	1,000	4.20	34.91	27.72
1,204	3.92	34.91				
Station 6604; 9 April; 43°42.5′ N., 46°13′ W.; depth 3,998 m.; dynamic height 971.061.						
0	6.86	33.62	0	6.86	33.62	26.37
27	6.35	33.66	25	6.35	33.66	26.47
54	6.36	33.78	50	6.35	33.75	26.54
81	7.19	34.30	75	7.00	34.21	26.82
107	5.12	34.20	100	5.65	34.22	27.00
162	4.56	34.36	150	4.60	34.31	27.20
216	4.61	34.52	200	4.60	34.48	27.32
323	4.14	34.64	300	4.20	34.61	27.48
412	4.77	34.84	400	4.70	34.82	27.59
612	4.60	34.935	600	4.60	34.93	27.68
809	4.19	34.93	800	4.20	34.93	27.73
1,019	3.89	34.91	1,000	3.90	34.91	27.75
1,556	3.61	34.905				
Station 6605; 9 April; 43°50′ N., 46°44′ W.; depth 3,566 m.; dynamic height 971.108.						
0	12.36	35.38	0	12.36	35.38	26.83
27	12.36	35.37	25	12.35	35.37	26.83
53	12.36	35.37	50	12.35	35.37	26.83
80	12.38	35.38	75	12.40	35.38	26.83
107	12.40	35.39	100	12.40	35.39	26.83
161	12.22	35.39	150	12.30	35.39	26.85
214	10.99	35.36	200	11.40	35.37	27.01
321	7.25	35.25	300	7.90	35.24	27.50
424	6.66	35.06	400	6.85	35.13	27.56
635	4.93	....	600	5.15	34.98	27.66
848	4.04	34.89	800	4.25	34.90	27.70
1,062	3.58	34.86	1,000	3.65	34.87	27.74
1,599	3.47	34.885				
Station 6606; 9 April 43°56′ N., 47°24′ W.; depth 4,207 m.; dynamic height 971.139.						
0	12.26	35.36	0	12.26	35.36	26.84
25	12.24	36.36	25	12.24	35.36	26.84
50	12.21	35.36	50	12.21	35.36	26.85
76	12.24	35.36	75	12.25	35.36	26.84
101	12.24	35.36	100	12.20	35.36	26.85
150	12.26	35.365	150	12.25	35.37	26.85
200	11.43	35.32	200	11.45	35.32	26.96
301	8.15	35.00	300	8.20	35.00	27.26
417	5.29	34.79	400	5.50	34.80	27.48
622	4.21	34.84	600	4.30	34.84	27.65
825	3.86	34.86	800	3.90	34.86	27.71
1,034	3.86	34.895	1,000	3.85	34.89	27.63
1,566	3.50	34.88				

TABLE OF OCEANOGRAPHIC DATA—Continued

STATIONS OCCUPIED IN 1958—Continued

Station 6607; 9 April; 44°02′ N., 48°02′ W.; depth 3,932 m.; dynamic height 971.013.

Observed values			Scaled values			
Depth, meters	Temperature, ° C.	Salinity, ‰	Depth, meters	Temperature, ° C.	Salinity, ‰	σ t
0	8.33	34.09	0	8.33	34.09	26.53
26	7.80	34.08	25	7.80	34.08	26.60
53	9.11	34.65	50	9.05	34.63	26.84
79	7.80	34.65	75	8.00	34.65	27.02
105	7.33	34.73	100	7.40	34.72	27.16
157	6.95	34.78	150	7.00	34.78	27.26
210	4.19	34.53	200	4.65	34.57	27.40
315	4.68	34.79	300	4.65	34.76	27.55
352	4.53	34.82	400	4.50	34.85	27.63
527	4.33	34.89	600	4.30	34.90	27.69
700	4.09	34.905	800	3.90	34.90	27.74
884	3.70	34.89	1,000	3.65	34.88	27.74
1,359	3.43	34.86				

Station 6608; 9 April; 44°07′ N., 48°33′ W.; depth 3,475 m.; dynamic height 970.970.

Observed values			Scaled values			
Depth, meters	Temperature, ° C.	Salinity, ‰	Depth, meters	Temperature, ° C.	Salinity, ‰	σ t
0	4.93	33.95	0	4.93	33.95	26.87
23	4.72	33.94	25	4.70	33.94	26.89
45	4.41	33.91	50	4.15	33.89	26.90
68	2.64	33.78	75	1.90	33.78	27.02
91	0.98	33.80	100	1.55	33.91	27.15
137	4.89	34.55	150	5.25	34.66	27.40
182	5.71	34.78	200	5.55	34.80	27.47
273	4.67	34.80	300	4.45	34.84	27.63
292	4.47	34.87	400	4.30	34.88	27.68
472	4.22	34.895	600	4.05	34.90	27.72
677	3.95	34.90	800	3.85	34.89	27.73
869	3.82	34.88	(1,000)	3.75	34.87	27.73
1,386	3.45	34.81				

Station 6609; 10 April; 44°10′ N., 48°53′ W.; depth 1,650 m.; dynamic height 971.008.

Observed values			Scaled values			
Depth, meters	Temperature, ° C.	Salinity, ‰	Depth, meters	Temperature, ° C.	Salinity, ‰	σ t
0	0.32	33.00	0	0.32	33.00	26.50
24	0.29	33.01	25	0.35	33.01	26.51
49	2.33	33.76	50	2.35	33.77	26.98
73	1.46	33.93	75	1.45	33.94	27.18
98	1.56	34.05	100	1.60	34.06	27.27
145	1.92	34.20	150	1.95	34.21	27.37
194	2.16	34.32	200	2.20	34.33	27.44
292	3.01	34.56	300	3.05	34.57	27.56
297	3.05	34.56	400	3.85	34.71	27.59
431	3.96	34.74	600	4.00	34.83	27.67
557	4.03	34.82	800	3.75	34.84	27.70
714	3.78	34.835	1,000	3.60	34.84	27.72
1,136	3.51	34.84				

Station 6610; 10 April; 44°11.5′ N., 49°03′ W.; depth 622 m.; dynamic height 971.116.

Observed values			Scaled values			
Depth, meters	Temperature, ° C.	Salinity, ‰	Depth, meters	Temperature, ° C.	Salinity, ‰	σ t
0	0.37	32.96	0	0.37	32.96	26.46
19	0.36	32.99	25	0.35	33.00	26.50
39	0.31	33.01	50	0.00	33.11	26.60
58	−0.26	33.21	75	0.05	33.43	26.86
77	0.10	33.46	100	0.30	33.58	26.96
115	0.39	33.65	150	0.45	33.78	27.11
154	0.51	33.80	200	1.15	33.98	27.23
231	1.53	34.10	300	1.65	34.21	27.39
263	1.50	34.14	400	2.30	34.39	27.48
411	2.40	34.41	(600)	3.20	34.61	27.58

Station 6611; 10 April; 44°12.5′ N., 49°09′ W.; depth 169 m.; dynamic height 971.140.

Observed values			Scaled values			
Depth, meters	Temperature, ° C.	Salinity, ‰	Depth, meters	Temperature, ° C.	Salinity, ‰	σ t
0	0.45	32.98	0	0.45	32.98	26.48
24	0.40	32.99	25	0.40	32.99	26.49
48	−0.07	33.16	50	−0.10	33.16	26.64
71	−0.11	33.20	75	−0.10	33.22	26.69
95	−0.02	33.43	100	0.00	33.47	26.90
143	0.53	33.76	150	0.65	33.79	27.11

Station 6612; 10 April; 44°13′ N., 49°12′ W.; depth 91 m.; dynamic height 971.148.

Observed values			Scaled values			
Depth, meters	Temperature, ° C.	Salinity, ‰	Depth, meters	Temperature, ° C.	Salinity, ‰	σ t
0	0.46	32.94	0	0.46	32.94	26.44
24	0.46	32.94	25	0.45	32.94	26.45
49	0.14	33.02	50	0.10	33.02	26.53
73	−0.01	33.11	75	0.00	33.11	26.60

Station 6613; 10 April; 44°14′ N., 49°23′ W.; depth 54 m.; dynamic height 971.147.

Observed values			Scaled values			
Depth, meters	Temperature, ° C.	Salinity, ‰	Depth, meters	Temperature, ° C.	Salinity, ‰	σ t
0	0.60	32.94	0	0.60	32.94	26.44
24	0.56	32.94	25	0.55	32.94	26.44
47	0.57	32.94	50	0.55	32.94	26.44

Station 6614; 10 April; 44°53′ N., 49°06′ W.: depth 73 m.; dynamic height 971. 153.

Observed values			Scaled values			
Depth, meters	Temperature, ° C.	Salinity, ‰	Depth, meters	Temperature, ° C.	Salinity, ‰	σ t
0	0.85	32.84	0	0.85	32.84	26.35
25	0.66	32.84	25	0.66	32.84	26.36
50	0.29	32.93	50	0.29	32.93	26.45

Station 6615; 10 April; 44°53.5′ N., 49°02′ W.; depth 89 m.; dynamic height 971.150.

Observed values			Scaled values			
Depth, meters	Temperature, ° C.	Salinity, ‰	Depth, meters	Temperature, ° C.	Salinity, ‰	σ t
0	0.84	32.85	0	0.84	32.85	26.36
25	0.62	32.87	25	0.62	32.87	26.38
50	0.11	33.00	50	0.11	33.00	26.52
75	0.04	33.04	75	0.04	33.04	26.55

Station 6616; 10 April; 44°50.5′ N., 48°56′ W.; depth 640 m.; dynamic height 971.147.

Observed values			Scaled values			
Depth, meters	Temperature, ° C.	Salinity, ‰	Depth, meters	Temperature, ° C.	Salinity, ‰	σ t
0	0.89	32.84	0	0.89	32.84	26.34
25	0.88	32.86	25	0.88	32.86	26.36
49	−0.16	33.15	50	−0.15	33.15	26.64
74	−0.24	33.21	75	−0.25	33.21	26.70
99	−0.30	33.25	100	−0.30	33.25	26.72
148	−0.24	33.31	150	−0.25	33.32	26.78
197	0.18	33.52	200	0.20	33.53	26.93
296	1.60	34.18	300	1.65	34.20	27.38
387	2.27	34.39	400	2.35	34.41	27.49
592	3.15	34.64	600	3.15	34.65	27.61

TABLE OF OCEANOGRAPHIC DATA—Continued

STATIONS OCCUPIED IN 1958—Continued

Station 6617; 10 April; 44°48.5′ N., 48°42′ W.; depth 1,829 m.; dynamic height 971.073.

Observed values			Scaled values			
Depth, meters	Temperature, °C.	Salinity, ‰	Depth, meters	Temperature, °C.	Salinity, ‰	σt
0	0.72	32.89	0	0.72	32.89	26.38
25	0.38	32.97	25	0.38	32.97	26.47
50	−0.13	33.34	50	−0.13	33.34	26.79
76	0.16	33.50	75	0.15	33.50	26.91
101	0.25	33.60	100	0.25	33.60	26.99
151	0.33	33.67	150	0.35	33.66	27.03
201	0.95	33.94	200	0.95	33.93	27.20
302	1.75	34.26	300	1.75	34.25	27.41
			(400)	2.35	34.46	27.53
			(600)	3.10	34.70	27.66
			(800)	3.35	34.81	27.72
			(1,000)	3.40	34.85	27.75

Station 6618; 10 April; 44°45.5′ N., 48°30′ W.; depth 1.646 m.; dynamic height 970.980.

Observed values			Scaled values			
Depth, meters	Temperature, °C.	Salinity, ‰	Depth, meters	Temperature, °C.	Salinity, ‰	σt
0	0.55	33.04	0	0.55	33.04	26.52
25	0.54	33.08	25	0.54	33.08	26.55
49	1.02	33.62	50	1.05	33.64	26.97
73	0.93	33.90	75	0.95	33.92	27.20
97	1.79	34.04	100	1.85	34.05	27.24
147	2.22	34.24	150	2.25	34.25	27.37
196	2.85	34.46	200	2.90	34.47	27.50
293	3.95	34.72	300	4.00	34.73	27.59
364	4.10	34.79	400	4.10	34.80	27.64
550	3.93	34.845	600	3.85	34.85	27.70
740	3.65	34.86	800	3.60	34.85	27.73
935	3.51	34.845	1,000	3.50	34.85	27.74
1,439	3.42	34,865				

Station 6619; 11 April; 44°40′ N., 47°55′ W.; depth 3,557 m.; dynamic height 970.947.

Observed values			Scaled values			
Depth, meters	Temperature, °C.	Salinity, ‰	Depth, meters	Temperature, °C.	Salinity, ‰	σt
0	6.22	33.94	0	6.22	33.94	26.71
26	6.21	33.945	25	6.20	33.94	26.71
52	5.82	33.90	50	5.85	33.90	26.73
78	4.26	34.28	75	4.30	34.23	27.16
104	4.51	34.51	100	4.50	34.48	27.34
156	4.69	34.72	150	4.70	34.71	27.50
208	4.70	34.82	200	4.70	34.81	27.58
312	4.27	34.85	300	4.30	34.85	27.66
411	4.36	34.90	400	4.35	34.90	27.69
616	3.93	34.885	600	3.95	34.89	27.72
823	3.59	34.86	800	3.60	34.86	27.74
1,033	3.60	34.89	1,000	3.60	34.89	27.76
1,565	3.47	34.90				

Station 6620; 11 April; 44°34′ N., 47°15′ W.; depth 4,023 m.; dynamic height 971.008.

Observed values			Scaled values			
Depth, meters	Temperature, °C.	Salinity, ‰	Depth, meters	Temperature, °C.	Salinity, ‰	σt
0	5.81	33.85	0	5.81	33.85	26.69
22	5.82	33.84	25	5.80	33.84	26.68
43	5.80	33.85	50	5.70	33.87	26.73
65	5.48	33.96	75	5.50	34.11	26.93
86	5.59	34.25	100	5.20	34.28	27.10
129	4.36	34.32	150	4.35	34.39	27.28
172	4.40	34.47	200	4.45	34.56	27.41
258	4.57	34.72	300	4.60	34.80	27.58
333	4.61	34.84	400	4.45	34.87	27.66
513	4.20	34.89	600	4.05	34.88	27.70
701	3.87	34.85	800	3.70	34.85	27.72
890	3.58	34.85	1,000	3.55	34.85	27.73
1,385	3.45	34.87				

Station 6621; 11 April; 44°28′ N., 46°32′ W.; depth 3,932 m.; dynamic height 971.076.

Observed values			Scaled values			
Depth, meters	Temperature, °C.	Salinity, ‰	Depth, meters	Temperature, °C.	Salinity, ‰	σt
0	8.34	34.22	0	8.34	34.22	26.63
25	8.32	34.22	25	8.32	34.22	26.63
50	8.42	34.26	50	8.42	34.26	26.65
75	8.53	34.38	75	8.53	34.38	26.73
100	9.20	34.78	100	9.20	34.78	26.93
151	8.82	34.91	150	8.80	34.91	27.10
201	7.97	34.89	200	8.00	34.89	27.21
301	6.41	34.905	300	6.40	34.90	27.44
358	6.03	34.95	400	5.70	34.95	27.57
533	4.82	34.93	600	4.50	34.92	27.69
706	4.04	34.88	800	3 90	34.89	27.73
895	3.76	34.89	1,000	3.70	34.89	27.75
1,388	3.49	34.88				

Station 6622; 11 April; 44°21.5′ N., 45°50′ W.; depth 4,006 m.; dynamic height 971.005.

Observed values			Scaled values			
Depth, meters	Temperature, °C.	Salinity, ‰	Depth, meters	Temperature, °C.	Salinity, ‰	σt
0	7.80	34.10	0	7.80	34.10	26.62
27	7.34	34.05	25	7.40	34.05	26.64
53	6.58	34.03	50	6.65	34.03	26.72
80	5.79	34.15	75	5.95	34.13	26.89
106	4.30	34.21	100	4.40	34.19	27.12
160	5.00	34.58	150	4.90	34.52	27.33
214	4.76	34.67	200	4.80	34.64	27.43
320	4.96	34.86	300	4.95	34.84	27.57
429	4.36	34.85	400	4.50	34.85	27.63
639	3.85	34.86	600	3.90	34.86	27.71
849	3.66	34.87	800	3.70	34.87	27.74
1,063	3.65	34.88	1,000	3.65	34.88	27.74
1,599	3.49	34.895				

Station 6623; 11 April; 44°15.5′ N., 45°12′ W.; depth 4,572 m.; dynamic height 971.191.

Observed values			Scaled values			
Depth, meters	Temperature, °C.	Salinity, ‰	Depth, meters	Temperature, °C.	Salinity, ‰	σt
0	15.10	35.95	0	15.40	35.95	26.70
27	15.11	35.95	25	15.10	35.95	26.70
52	15.08	35.95	50	15.10	35.95	26.70
79	14.04	35.70	75	14.20	35.74	26.73
105	13.56	35.59	100	13.65	35.60	26.74
158	12.96	35.59	150	13.05	35.59	26.85
210	10.50	35.16	200	10.85	35.27	27.03
315	7.83	34.92	300	8.15	34.94	27.22
432	6.18	34.83	400	6.50	34.84	27.38
642	5.27	34.96	600	5.45	34.94	27.59
850	4.59	34.955	800	4.75	34.96	27.69
1,064	4.01	34.915	1,000	4.20	34.93	27.73
1,598	3.59	34.89				

Station 6624; 11 April; 44°57′ N., 45°08′ W.; depth 4,390 m.; dynamic height 971.290.

Observed values			Scaled values			
Depth, meters	Temperature, °C.	Salinity, ‰	Depth, meters	Temperature, °C.	Salinity, ‰	σt
0	14.21	35.88	0	14.21	35.88	26.83
26	14.27	35.88	25	14.25	35.88	26.83
51	14.26	35.88	50	14.25	35.88	26.83
77	14.26	35.89	75	14.25	35.88	26.83
102	14.27	35.88	100	14.25	35.88	26.83
154	13.76	35.78	150	13.80	35.79	26.85
205	13.51	35.73	200	13.55	35.74	26.87
307	12.47	35.58	300	12.55	35.59	26.95
381	11.09	35.40	400	10.60	35.34	27.13
578	6.16	34.895	600	6.05	34.90	27.49
782	5.18	34.98	800	5.10	34.98	27.66
986	4.42	34.93	1,000	4.40	34.93	27.70
1,513	3.68	34.89				

TABLE OF OCEANOGRAPHIC DATA—Continued

STATIONS OCCUPIED IN 1958—Continued

Station 6625; 12 April; 45°28′ N., 45°04′ W.; depth 4,134 m.; dynamic height 971.084.

Observed values			Scaled values			
Depth, meters	Temperature, °C.	Salinity, ‰	Depth, meters	Temperature, °C.	Salinity, ‰	σt
0	9.10	34.50	0	9.10	34.50	26.73
26	9.44	34.52	25	9.40	34.52	26.70
51	9.38	34.65	50	9.35	34.64	26.80
76	10.41	34.98	75	10.40	34.98	26.88
101	9.97	34.94	100	10.00	34.94	26.92
152	7.45	34.67	150	7.50	34.67	27.11
203	7.53	34.79	200	7.55	34.79	27.19
304	5.63	34.74	300	5.70	34.74	27.40
416	5.73	34.96	400	5.75	34.93	27.55
621	4.49	34.90	600	4.55	34.90	27.67
825	4.17	34.91	800	4.20	34.91	27.72
1,033	3.92	34.90	1,000	3.95	34.90	27.73
1,558	3.48	34.87				

Station 6626; 12 April 45°27′ N., 45°51′ W.; depth 3,466 m.; dynamic height 971.020.

Observed values			Scaled values			
Depth, meters	Temperature, °C.	Salinity, ‰	Depth, meters	Temperature, °C.	Salinity, ‰	σt
0	8.45	34.36	0	8.45	34.36	26.72
24	8.46	34.37	25	8.45	34.37	26.73
49	8.47	34.37	50	8.45	34.37	26.73
73	7.81	34.37	75	7.70	34.36	26.84
98	4.94	34.11	100	4.95	34.12	27.01
147	6.72	34.74	150	6.70	34.73	27.26
196	4.98	34.60	200	5.00	34.60	27.38
294	5.31	34.86	300	5.30	34.86	27.55
379	4.70	34.85	400	4.60	34.85	27.62
566	4.06	34.875	600	4.05	34.88	27.70
760	4.06	34.91	800	4.00	34.91	27.74
956	3.73	34.89	1,000	3.70	34.89	27.75
1,454	3.43	34.88				

Station 6627; 12 April; 45°27′ N., 46°43′ W.; depth 3.017 m.; dynamic height 971.027.

Observed values			Scaled values			
Depth, meters	Temperature, °C.	Salinity, ‰	Depth, meters	Temperature, °C.	Salinity, ‰	σt
0	9.55	34.71	0	9.55	34.71	26.82
25	9.54	34.71	25	9.54	34.71	26.82
50	9.53	34.71	50	9.53	34.71	26.82
74	9.54	34.71	75	9.55	34.71	26.82
99	9.47	34.70	100	9.45	34.70	26.83
149	7.58	34.80	150	7.60	34.80	27.20
198	6.57	34.78	200	6.50	34.78	27.33
297	4.37	34.74	300	4.35	34.74	27.56
397	4.47	34.85	400	4.45	34.85	27.63
590	4.31	34.915	600	4.30	34.91	27.70
779	4.02	34.915	800	4.00	34.91	27.74
977	3.75	34.90	1,000	3.75	34.90	27.75
1,477	3.48	34.88				

Station 6628; 12 April; 45°24′ N., 47°26′ W.; depth 2,743 m.; dynamic height 971.004.

Observed values			Scaled values			
Depth, meters	Temperature, °C.	Salinity, ‰	Depth, meters	Temperature, °C.	Salinity, ‰	σt
0	8.75	34.42	0	8.75	34.42	26.73
25	8.48	34.46	25	8.48	34.46	26.79
50	8.56	34.49	50	8.56	34.49	26.81
75	8.25	34.58	75	8.25	34.58	26.92
100	7.22	34.70	100	7.22	34.70	27.17
150	7.07	34.83	150	7.07	34.83	27.29
199	6.27	34.87	200	6.25	34.87	27.44
299	5.16	34.86	300	5.15	34.86	27.57
403	4.13	34.80	400	4.15	34.80	27.63
602	3.82	34.83	600	3.75	34.83	27.69
798	3.97	34.90	800	3.95	34.90	27.73
999	3.46	34.84	1,000	3.45	34.84	27.73
1,500	3.39	34.875				

Station 6629; 12 April; 45°34′ N., 47°43′ W.; depth 1,463 m.; dynamic height 970.947.

Observed values			Scaled values			
Depth, meters	Temperature, °C.	Salinity, ‰	Depth, meters	Temperature, °C.	Salinity, ‰	σt
0	2.70	33.62	0	2.70	33.62	26.83
25	3.22	33.76	25	3.22	33.76	26.89
50	3.52	34.00	50	3.52	34.00	27.06
75	1.86	33.96	75	1.86	33.96	27.17
99	2.94	34.28	100	3.00	34.29	27.34
149	4.50	34.70	150	4.50	34.70	27.51
199	4.28	34.72	200	4.25	34.72	27.56
298	4.09	34.80	300	4.10	34.80	27.64
372	4.09	34.83	400	4.05	34.84	27.67
559	3.82	34.85	600	3.75	34.85	27.71
746	3.60	34.84	800	3.60	34.84	27.72
940	3.52	34.83	1,000	3.50	34.83	27.72
1,337	3.42	34.83				

Station 6630; 12 April; 45°42.5′ N., 47°58′ W.; depth 622 m.; dynamic height 971.026.

Observed values			Scaled values			
Depth, meters	Temperature, °C.	Salinity, ‰	Depth, meters	Temperature, °C.	Salinity, ‰	σt
0	1.14	32.76	0	1.14	32.76	26.26
25	0.23	33.66	25	0.23	33.66	27.04
49	0.86	33.93	50	0.90	33.93	27.21
74	0.99	34.04	75	1.00	34.04	27.29
99	1.12	34.11	100	1.15	34.11	27.34
148	1.29	34.13	150	1.30	34.13	27.34
197	1.51	34.21	200	1.50	34.21	27.40
296	1.62	34.24	300	1.65	34.24	27.41
394	2.20	34.38	400	2.25	34.39	27.48
587	3.86	34.74	(600)	3.95	34.76	27.62

Station 6631; 12 April; 45°46′ N., 48°06′ W.; depth 169 m.; dynamic height 971.120.

Observed values			Scaled values			
Depth, meters	Temperature, °C.	Salinity, ‰	Depth, meters	Temperature, °C.	Salinity, ‰	σt
0	0.95	32.76	0	0.95	32.76	26.27
24	0.30	32.83	25	0.30	32.83	26.36
48	−0.09	32.97	50	−0.10	32.99	26.51
73	−0.32	33.24	75	−0.30	33.26	26.73
97	−0.04	33.40	100	−0.05	33.40	26.84
145	0.01	33.42	150	0.00	33.42	26.86

Station 6632; 13 April; 45°49′ N., 48°10′ W.; depth 108 m.; dynamic height 971.131.

Observed values			Scaled values			
Depth, meters	Temperature, °C.	Salinity, ‰	Depth, meters	Temperature, °C.	Salinity, ‰	σt
0	0.81	32.75	0	0.81	32.75	26.28
24	0.51	32.74	25	0.50	32.74	26.28
48	0.27	32.90	50	0.25	32.92	26.44
73	−0.39	33.16	75	−0.40	33.16	26.66
2	−0.39	33.165	(100)	∓0.40	33.17	26.67

Station 6633; 13 April; 45°55′ N., 48°18′ W.; depth 89 m.; dynamic height 971.132.

Observed values			Scaled values			
Depth, meters	Temperature, °C.	Salinity, ‰	Depth, meters	Temperature, °C.	Salinity, ‰	σt
0	0.87	32.73	0	0.87	32.73	26.25
25	0.84	33.74	25	0.84	32.74	26.27
51	0.29	32.90	50	.30	32.90	26.42
76	−0.33	33.16	75	−0.30	33.15	26.64

TABLE OF OCEANOGRAPHIC DATA—Continued

STATIONS OCCUPIED IN 1958—Continued

Station 6634; 13 April; 46°03.5′ N., 48°34′ W.; depth 73 m.; dynamic height 971.134.

Observed values			Scaled values			
Depth, meters	Temperature, °C.	Salinity, ‰	Depth, meters	Temperature, °C.	Salinity, ‰	σt
0.......	1.40	32.79	0......	1.40	32.79	26.27
24......	1.39	32.80	25.....	1.40	32.80	26.28
48......	1.19	32.82	50.....	1.15	32.84	26.33
62......	0.04	33.10	[75]....	−0.25	33.15	26.64

Station 6635; 13 April; 46°12′ N., 48°47′ W.; depth 73 m.; dynamic height 971.135.

Observed values			Scaled values			
Depth, meters	Temperature, °C.	Salinity, ‰	Depth, meters	Temperature, °C.	Salinity, ‰	σt
0.......	1.30	32.78	0......	1.30	32.78	26.27
23......	1.36	32.78	25.....	1.35	32.78	26.26
47......	1.37	32.77	50.....	1.35	32.77	26.25
61......	1.28	32.78	[75]....	1.15	32.79	26.29

Sta. 6636; 13 April; 46°10.5′ N., 48°26′ W.; depth 89 m.; dynamic height 971.134.

Observed values			Scaled values			
Depth, meters	Temperature, °C.	Salinity, ‰	Depth, meters	Temperature, °C.	Salinity, ‰	σt
0.......	1.32	32.79	0......	1.22	32.79	26.28
24......	1.20	32.75	25.....	1.20	32.75	26.26
49......	1.07	32.76	50.....	1.05	32.77	26.28
73......	−0.26	33.28	(75)....	−0.35	33.31	26.77

Station 6637; 13 April; 46°09.5′ N., 48°00′ W.; depth 115 m.; dynamic height 971.119.

Observed values			Scaled values			
Depth, meters	Temperature, °C.	Salinity, ‰	Depth, meters	Temperature, °C.	Salinity, ‰	σt
0.......	1.03	32.74	0......	1.03	32.74	26.26
27......	0.99	32.76	25.....	1.00	32.75	26.26
54......	0.07	32.90	50.....	0.20	32.87	26.40
81......	−0.30	33.20	75.....	−0.25	33.14	26.64
108.....	−0.31	33.34	100....	−0.30	33.30	26.76

Station 6638; 13 April; 46°08.5′ N., 47°42′ W.; depth 169 m.; dynamic height 971.098.

Observed values			Scaled values			
Depth, meters	Temperature, °C.	Salinity, ‰	Depth, meters	Temperature, °C.	Salinity, ‰	σt
0.......	0.41	32.96	0......	0.41	33.96	26.46
26......	0.32	32.95	25.....	0.35	32.95	26.46
52......	−0.02	33.10	50.....	0.00	33.08	26.58
78......	−0.21	33.32	75.....	−0.20	33.28	26.75
104.....	0.07	33.56	100....	0.05	33.52	26.94
155.....	0.45	33.77	150....	0.45	33.75	27.09

Station 6639; 13 April; 46°07′ N., 47°24′ W.; depth 631 m.; dynamic height 971.037.

Observed values			Scaled values			
Depth, meters	Temperature, °C.	Salinity, ‰	Depth, meters	Temperature, °C.	Salinity, ‰	σt
0.......	0.27	32.92	0......	0.27	32.92	26.44
26......	0.15	32.96	25.....	0.20	32.95	26.46
51......	−0.04	33.41	50.....	−0.05	33.40	26.84
77......	0.46	33.68	75.....	0.40	33.66	27.03
103.....	0.78	33.87	100....	0.75	33.85	27.16
153.....	1.33	34.14	150....	1.30	34.13	27.34
205.....	1.76	34.26	200....	1.70	34.25	27.41
308.....	2.42	34.44	300....	2.35	34.43	27.50
408.....	3.22	34.58	400....	3.15	34.57	27.55
605.....	4.02	34.81	600....	4.00	34.80	27.65

Station 6640; 13 April; 46°07′ N., 47°10′ W.; depth 1,463 m.; dynamic height 970.973.

Observed values			Scaled values			
Depth, meters	Temperature, °C.	Salinity, ‰	Depth, meters	Temperature, °C.	Salinity, ‰	σt
0.......	0.78	33.34	0......	0.78	33.34	26.74
25......	0.76	33.36	25.....	0.76	33.36	26.76
50......	1.01	33.62	50.....	1.01	33.62	26.96
75......	1.69	34.05	75.....	1.69	34.05	27.25
100.....	2.54	34.26	100....	2.54	34.26	27.36
150.....	2.46	34.36	150....	2.46	34.36	27.44
200.....	2.75	34.50	200....	2.75	34.50	27.53
300.....	3.43	34.65	300....	3.43	34.65	27.58
397.....	3.95	34.75	400....	3.95	34.75	27.61
593.....	3.97	34.835	600....	3.95	34.84	27.68
787.....	3.61	34.84	800....	3.60	34.84	27.72
987.....	3.52	34.84	1,000..	3.50	34.84	27.73
1,391...	3.46	34.85				

Station 6641; 13 April; 46°05.5′ N., 46°35′ W.; depth 732 m.; dynamic height 970.971.

Observed values			Scaled values			
Depth, meters	Temperature, °C.	Salinity, ‰	Depth, meters	Temperature, °C.	Salinity, ‰	σt
0.......	5.93	33.98	0......	5.93	33.98	26.78
21......	5.91	33.99	25.....	5.90	33.99	26.79
42......	5.91	34.01	50.....	5.90	34.02	26.81
64......	5.88	34.06	75.....	5.50	34.10	26.92
85......	4.98	34.15	100....	4.15	34.20	27.16
128.....	2.66	34.29	150....	3.45	34.44	27.41
170.....	4.31	34.62	200....	4.60	34.73	27.52
255.....	4.84	34.87	300....	4.50	34.86	27.64
241.....	4.82	34.84	(400)...	3.95	34.84	27.68
361.....	3.92	34.84	(600)...	4.00	34.87	27.71

Station 6642; 13–14 April; 46°04.5′ N., 45°55′ W.; depth 1,893 m.; dynamic height 970.972.

Observed values			Scaled values			
Depth, meters	Temperature, °C.	Salinity, ‰	Depth, meters	Temperature, °C.	Salinity, ‰	σt
0.......	5.98	34.04	0......	5.98	34.04	26.81
23......	5.87	34.06	25.....	5.85	34.06	26.85
44......	5.71	34.08	50.....	5.65	34.08	26.89
67......	5.48	34.08	75.....	4.90	34.07	26.97
88......	3.75	34.06	100....	3.70	34.10	27.12
133.....	3.63	34.32	150....	4.00	34 44	27 36
178.....	4.34	34.62	200....	4.35	34.70	27.53
266.....	4.34	34.80	300....	4.25	34.80	27.62
331.....	4.21	34.80	400....	4.30	34.84	27.65
503.....	4.38	34.91	600....	4.25	34.91	27.71
680.....	4.02	34.905	800....	3.80	34.89	27.74
867.....	3.69	....	1,000..	3.60	34.87	27.75
1,365...	3.38	34.86				

Station 6643; 14 April; 46°03′ N., 45°23′ W.; depth 4,407 m.; dynamic height 970.961.

Observed values			Scaled values			
Depth, meters	Temperature, °C.	Salinity, ‰	Depth, meters	Temperature, °C.	Salinity, ‰	σt
0.......	8.09	34.36	0......	8.09	34.36	26.78
27......	7.92	34.36	25.....	7.95	34.36	26.80
52......	7.04	34.26	50.....	7.15	34.26	26.84
79......	6.26	34.36	75.....	6.40	34.34	27.00
105.....	5.91	34.56	100....	5.95	34.52	27.20
158.....	5.84	34.74	150....	5.85	34.73	27.37
210.....	3.93	34.66	200....	4.20	34.67	27.53
315.....	3.89	34.78	300....	3.90	34.76	27.63
376.....	3.96	34.84	400....	3.95	34.84	27.68
565.....	3.65	34.85	600....	3.60	34.85	27.73
756.....	3.46	34.85	800....	3.45	34.85	27.74
951.....	3.40	34.85	1,000..	3.40	34.85	27.75
1,450...	3.38	34.86				

TABLE OF OCEANOGRAPHIC DATA—Continued

STATIONS OCCUPIED IN 1958—Continued

Station 6644; 14 April; 46°01.5′ N., 44°45′ W.; depth 3,581 m.; dynamic height 970.963.

Observed values			Scaled values			
Depth, meters	Temperature, ° C.	Salinity, ‰	Depth, meters	Temperature, ° C.	Salinity, ‰	σ_t
0	8.36	34.53	0	8.36	34.53	26.87
26	8.36	34.53	25	8.35	34.53	26.87
51	4.36	34.11	50	4.35	34.11	27.06
77	4.47	34.21	75	4.45	34.20	27.12
102	5.70	34.46	100	5.55	34.43	27.17
154	6.22	34.80	150	6.20	34.80	27.39
206	3.72	34.58	200	3.85	34.60	27.50
306	4.00	34.77	300	4.00	34.76	27.62
375	4.00	34.80	400	4.00	34.81	27.66
563	3.82	34.85	600	3.75	34.85	27.71
751	3.58	34.85	800	3.55	34.85	27.73
961	3.49	....	1,000	3.50	34.86	27.75
1,527	3.36	34.87				

Station 6645; 14 April; 46°19.5′ N., 44°45′ W.; depth 2,459 m.; dynamic height 970.932.

Observed values			Scaled values			
Depth, meters	Temperature, ° C.	Salinity, ‰	Depth, meters	Temperature, ° C.	Salinity, ‰	σ_t
0	4.71	33.98	0	4.71	33.98	26.92
26	4.67	33.99	25	4.70	33.99	26.93
52	3.74	34.04	50	3.80	34.03	27.05
78	3.69	34.15	75	3.70	34.13	27.14
104	3.67	34.33	100	3.70	34.30	27.28
156	3.40	34.63	150	3.40	34.60	27.55
208	4.03	34.74	200	4.00	34.73	27.59
312	4.01	34.82	300	4.00	34.82	27.67
412	3.87	34.83	400	3.90	34.83	27.68
612	3.60	34.835	600	3.60	34.83	27.71
809	3.46	34.845	800	3.50	34.84	27.73
1,012	3.39	34.86	1,000	3.40	34.86	27.76
1,523	3.39	34.86				

Station 6646; 14 April; 46°26′ N., 45°45′ W.; depth 622 m.; dynamic height 970.924.

Observed values			Scaled values			
Depth, meters	Temperature, ° C.	Salinity, ‰	Depth, meters	Temperature, ° C.	Salinity, ‰	σ_t
0	4.67	33.95	0	4.67	33.95	26.90
24	4.61	33.97	25	4.60	33.97	26.93
49	4.54	34.17	50	4.55	34.17	27.09
73	3.55	34.21	75	3.55	34.22	27.23
98	3.69	34.44	100	3.70	34.45	27.40
146	3.88	34.70	150	3.90	34.71	27.59
195	3.88	34.77	200	3.85	34.77	27.64
293	3.85	34.78	300	3.85	34.78	27.64
405	3.81	34.81	400	3.85	34.81	27.67
597	3.68	34.82	600	3.70	34.82	27.70

Station 6647; 14 April; 46°36′ N., 44°44′ W.; depth 220 m.; dynamic height 970.930.

Observed values			Scaled values			
Depth, meters	Temperature, ° C.	Salinity, ‰	Depth, meters	Temperature, ° C.	Salinity, ‰	σ_t
0	4.65	33.96	0	4.65	33.96	26.91
25	4.62	33.97	25	4.62	33.97	26.92
50	4.33	34.00	50	4.33	34.00	26.97
75	3.95	34.18	75	3.95	34.18	27.16
100	3.38	34.34	100	3.38	34.34	27.34
151	3.80	34.68	150	3.80	34.68	27.57
201	3.77	34.76	200	3.80	34.76	27.64

Station 6648; 14 April; 46°42.5′ N., 44°44′ W.; depth 169 m.; dynamic height 970.947.

Observed values			Scaled values			
Depth, meters	Temperature, ° C.	Salinity, ‰	Depth, meters	Temperature, ° C.	Salinity, ‰	σ_t
0	4.74	33.98	0	4.74	33.98	26.91
25	4.70	33.99	25	4.70	33.99	26.93
51	4.49	34.05	50	4.50	34.05	27.00
76	4.15	34.11	75	4.15	34.10	27.08
102	3.94	34.20	100	3.95	34.19	27.17
153	3.68	34.42	150	3.70	34.40	27.36

Station 6649; 14 April; 46°47′ N., 44°44′ W.; depth 137 m.; dynamic height 970.946.

Observed values			Scaled values			
Depth, meters	Temperature, ° C.	Salinity, ‰	Depth, meters	Temperature, ° C.	Salinity, ‰	σ_t
0	4.73	33.98	0	4.73	33.98	26.92
23	4.72	33.99	25	4.70	33.99	26.93
47	4.52	34.02	50	4.50	34.03	26.98
70	4.31	34.07	75	4.25	34.08	27.05
94	4.10	34.12	100	4.00	34.15	27.13
117	3.79	34.28	[150]	3.75	34.42	27.37

Station 6650; 14 April; 46°47′ N., 44°58′ W.; depth 169 m.; dynamic height 970.938.

Observed values			Scaled values			
Depth, meters	Temperature, ° C.	Salinity, ‰	Depth, meters	Temperature, ° C.	Salinity, ‰	σ_t
0	4.63	34.00	0	4.63	34.00	26.94
25	4.62	34.02	25	4.62	34.02	26.96
50	4.57	34.10	50	4.57	34.10	27.03
75	3.94	34.18	75	3.94	34.18	27.16
100	3.67	34.21	100	3.67	34.21	27.21
150	3.80	34.35	150	3.80	34.35	27.31

Station 6651; 14 April; 46°47′ N., 45°16′ W.; depth 220 m.; dynamic height 970.929.

Observed values			Scaled values			
Depth, meters	Temperature, ° C.	Salinity, ‰	Depth, meters	Temperature, ° C.	Salinity, ‰	σ_t
0	5.41	34.08	0	5.41	34.08	26.92
25	5.49	34.09	25	5.49	34.09	26.91
50	5.34	34.10	50	5.34	34.10	26.94
74	3.65	34.18	75	3.65	34.18	27.19
99	3.64	34.32	100	3.65	34.33	27.31
149	3.85	34.58	150	3.85	34.58	27.48
198	3.82	34.68	200	3.85	34.68	27.56

Station 6652; 14 April; 46°47′ N., 45°41′ W.; depth 276 m.; dynamic height 970.950.

Observed values			Scaled values			
Depth, meters	Temperature, ° C.	Salinity, ‰	Depth, meters	Temperature, ° C.	Salinity, ‰	σ_t
0	7.84	34.31	0	7.84	34.31	26.78
24	7.74	34.30	25	7.75	34.30	26.78
49	6.97	34.21	50	6.95	34.21	26.83
73	5.33	34.12	75	5.25	34.12	26.97
98	4.58	34.36	100	4.60	34.38	27.25
146	6.17	34.82	150	6.05	34.81	27.42
195	4.08	34.59	200	4.00	34.60	27.49
244	3.78	34.75	[300]	4.05	34.87	27.70

TABLE OF OCEANOGRAPHIC DATA—Continued

STATIONS OCCUPIED IN 1958—Continued

Station 6653; 14 April; 46°47′ N., 46°08′ W.; depth 320 m.; dynamic height 970.835.

Observed values			Scaled values			
Depth, meters	Temperature, ° C.	Salinity, ‰	Depth, meters	Temperature, ° C.	Salinity, ‰	σ t
0	5.15	34.00	0	5.15	34.00	26.89
25	5.14	34.01	25	5.14	34.01	26.90
50	5.10	34.06	50	5.10	34.06	26.94
75	5.06	34.10	75	5.06	34.10	26.98
100	4.07	34.34	100	4.07	34.34	27.28
150	4.53	34.66	150	4.53	34.66	27.48
199	3.93	34.67	200	3.95	34.67	27.55
299	4.11	34.87	300	4.10	34.87	27.70

Station 6654; 15 April; 46°47′ N., 46°36′ W.; depth 622 m.; dynamic height 970.887.

Observed values			Scaled values			
Depth, meters	Temperature, ° C.	Salinity, ‰	Depth, meters	Temperature, ° C.	Salinity, ‰	σ t
0	3.39	33.72	0	3.39	33.72	26.85
24	2.34	34.17	25	2.35	34.17	27.30
48	2.66	34.43	50	2.70	34.44	27.48
71	3.28	34.58	75	3.45	34.61	27.55
95	3.90	34.72	100	3.90	34.72	27.60
143	4.00	34.74	150	4.00	34.74	27.60
190	4.03	34.77	200	4.05	34.78	27.62
285	4.08	34.80	300	4.10	34.81	27.65
383	4.27	34.89	400	4.25	34.89	27.69
578	3.84	34.87	(600)	3.80	34.87	27.73

Station 6655; 15 April; 46°47′ N., 47°00′ W.; depth 1,143 m.; dynamic height 970.974.

Observed values			Scaled values			
Depth, meters	Temperature, ° C.	Salinity, ‰	Depth, meters	Temperature, ° C.	Salinity, ‰	σ t
0	0.89	33.48	0	0.89	33.48	26.85
23	0.81	33.49	25	0.80	33.49	26.86
45	0.71	33.57	50	0.75	33.59	26.95
68	0.96	33.70	75	1.00	33.77	27.08
90	1.03	33.99	100	1.15	34.04	27.28
135	1.76	34.21	150	2.00	34.28	27.41
181	2.46	34.41	200	2.65	34.46	27.51
271	3.19	34.62	300	3.50	34.67	27.60
334	3.73	34.73	400	3.90	34.79	27.65
510	4.00	34.845	600	3.90	34.84	27.69
693	3.80	34.82	800	3.65	34.82	27.70
939	3.55	34.84	(1,000)	3.55	34.85	27.73

Station 6656; 15 April; 46°47′ N., 47°17′ W.; depth 622 m.; dynamic height 971.010.

Observed values			Scaled values			
Depth, meters	Temperature, ° C.	Salinity, ‰	Depth, meters	Temperature, ° C.	Salinity, ‰	σ t
0	0.38	32.98	0	0.38	32.98	26.48
24	0.46	33.47	25	0.45	33.47	26.87
48	0.51	33.57	50	0.55	33.58	26.95
72	0.83	33.84	75	0.85	33.85	27.15
97	0.94	33.94	100	0.95	33.95	27.22
145	1.46	34.13	150	1.50	34.15	27.35
193	1.96	34.32	200	2.00	34.34	27.46
290	2.92	34.53	300	3.00	34.55	27.55
403	3.80	34.705	400	3.80	34.70	27.59
600	4.05	34.82	600	4.05	34.82	27.66

Station 6657; 15 April; 46°47′ N., 47°24′ W.; depth 320 m.; dynamic height 971.049.

Observed values			Scaled values			
Depth, meters	Temperature, ° C.	Salinity, ‰	Depth, meters	Temperature, ° C.	Salinity, ‰	σ t
0	0.21	32.75	0	0.21	32.75	26.30
25	0.05	32.98	25	0.05	32.98	26.50
50	−0.05	33.14	50	−0.05	33.14	26.63
75	0.11	33.51	75	0.11	33.51	26.92
100	0.31	33.70	100	0.31	33.70	27.06
150	1.43	34.14	150	1.43	34.14	27.35
200	1.86	34.30	200	1.86	34.30	27.44
300	2.57	34.48	300	2.57	34.48	27.53

Station 6658; 15 April; 46°47′ N., 47°44′ W.; depth 169 m.; dynamic height 971.120.

Observed values			Scaled values			
Depth, meters	Temperature, ° C.	Salinity, ‰	Depth, meters	Temperature, ° C.	Salinity, ‰	σ t
0	0.57	32.72	0	0.57	32.72	26.26
25	0.17	32.79	25	0.17	32.79	26.34
50	−0.14	32.90	50	−0.14	32.90	26.44
75	−0.53	33.03	75	−0.53	33.03	26.56
100	−0.34	33.17	100	−0.34	33.17	26.66
150	0.01	33.48	150	0.01	33.48	26.90

Station 6659; 15 April; 46°47′ N., 48°17′ W.; depth 112 m.; dynamic height 971.130.

Observed values			Scaled values			
Depth, meters	Temperature, ° C.	Salinity, ‰	Depth, meters	Temperature, ° C.	Salinity, ‰	σ t
0	1.29	32.70	0	1.29	32.70	26.20
26	0.91	32.71	25	0.95	32.71	26.23
52	0.76	32.72	50	0.80	32.72	26.25
78	−0.41	33.07	75	−0.35	33.03	26.55
104	−0.33	33.24	100	−0.35	33.22	26.70

Station 6660; 15 April; 46°47′ N., 48°52′ W.; depth 80 m.; dynamic height 971.133.

Observed values			Scaled values			
Depth, meters	Temperature, ° C.	Salinity, ‰	Depth, meters	Temperature, ° C.	Salinity, ‰	σ t
0	1.74	32.72	0	1.74	32.72	26.19
25	1.29	32.71	25	1.29	32.71	26.21
50	1.17	32.74	50	1.17	32.74	26.25
70	0.30	32.92	(75)	0.05	32.96	26.48

Station 6661; 27 April; 49°59.5′ N., 49°01′ W.; depth 2,158 m.; dynamic height 970.868.

Observed values			Scaled values			
Depth, meters	Temperature, ° C.	Salinity, ‰	Depth, meters	Temperature, ° C.	Salinity, ‰	σ t
0	2.28	34.34	0	2.28	34.34	27.44
23	2.34	34.33	25	2.35	34.33	27.42
45	2.33	34.34	50	2.35	34.34	27.43
68	2.25	34.36	75	2.25	34.40	27.49
90	2.46	34.48	100	2.55	34.53	27.57
135	3.06	34.67	150	3.20	34.70	27.65
181	3.44	34.75	200	3.50	34.77	27.68
271	3.70	34.81	300	3.75	34.82	27.69
358	3.73	34.82	400	3.75	34.83	27.69
539	3.71	34.85	600	3.65	34.85	27.72
722	3.54	34.855	800	3.50	34.85	27.74
922	3.45	34.85	1,000	3.40	34.86	27.76
1,401	3.30	34.89				

TABLE OF OCEANOGRAPHIC DATA—Continued

STATIONS OCCUPIED IN 1958—Continued

Station 6662; 27 April; 49°49′ N., 49°31′ W.; depth 1,701 m.; dynamic height 970.894.

Observed values			Scaled values			
Depth, meters	Temperature, ° C.	Salinity, °/₀₀	Depth, meters	Temperature, ° C.	Salinity, °/₀₀	σ t
0	1.66	34.08	0	1.66	34.08	27.28
21	1.67	34.09	25	1.70	34.09	27.28
40	1.69	34.09	50	1.65	34.12	27.32
61	1.64	34.18	75	1.65	34.20	27.38
81	1.70	34.22	100	2.05	34.34	27.46
122	2.58	34.53	150	2.75	34.59	27.60
162	2.85	34.61	200	3.20	34.69	27.64
243	3.59	34.75	300	3.65	34.76	27.65
300	......	34.76	400	3.65	34.79	27.67
457	3.68	34.81	600	3.70	34.85	27.72
618	3.70	34.85	800	3.55	34.86	27.74
800	3.52	34.865	1,000	3.45	34.87	27.76
1,304	3.38	34.865				

Station 6663; 27 April; 49°38′ N., 50°03′ W.; depth 612 m.; dynamic height 971.038.

Observed values			Scaled values			
Depth, meters	Temperature, ° C.	Salinity, °/₀₀	Depth, meters	Temperature, ° C.	Salinity, °/₀₀	σ t
0	0.14	32.89	0	0.14	32.89	26.41
27	0.11	32.97	25	0.10	32.96	26.48
53	0.20	33.06	50	0.20	33.04	26.54
80	0.01	33.13	75	0.05	33.11	26.60
106	0.59	33.68	100	0.45	33.52	26.91
160	0.79	33.94	150	0.75	33.89	27.19
212	1.53	34.24	200	1.30	34.18	27.38
318	2.72	34.515	300	2.55	34.48	27.53
376	3.09	34.59	400	3.20	34.62	27.59
575	3.85	34.85	(600)	3.85	34.86	27.71

Station 6664; 27 April; 49°29.5′ N., 50°37′ W.; depth 338 m.; dynamic height 970.996.

Observed values			Scaled values			
Depth, meters	Temperature, ° C.	Salinity, °/₀₀	Depth, meters	Temperature, ° C.	Salinity, °/₀₀	σ t
0	0.41	33.01	0	0.41	33.01	26.51
25	0.39	33.04	25	0.39	33.04	26.53
50	−0.02	33.21	50	−0.02	33.21	26.69
75	0.08	33.46	75	0.08	33.46	26.88
100	0.30	33.78	100	0.30	33.78	27.12
150	0.84	34.00	150	0.84	34.00	27.27
200	1.52	34.23	200	1.52	34.23	27.41
300	3.25	34.64	300	3.25	34.64	27.59

Station 6665; 27 April; 49°23′ N., 51°02′ W.; depth 348 m.; dynamic height 971.047.

Observed values			Scaled values			
Depth, meters	Temperature, ° C.	Salinity, °/₀₀	Depth, meters	Temperature, ° C.	Salinity, °/₀₀	σ t
0	−0.71	32.47	0	−0.71	32.47	26.12
24	−0.34	32.72	25	−0.35	32.74	26.32
47	−0.02	33.10	50	0.00	33.12	26.61
71	−0.02	33.22	75	0.00	33.22	26.69
94	−0.20	33.27	100	−0.20	33.31	26.77
141	−0.09	33.69	150	0.00	33.74	27.11
188	0.81	33.95	200	1.00	34.00	27.26
282	2.14	34.37	(300)	2.35	34.45	27.52

Station 6666; 27 April; 49°11.5′ N., 51°34′ W.; depth 320 m.; dynamic height 971.118.

Observed values			Scaled values			
Depth, meters	Temperature, ° C.	Salinity, °/₀₀	Depth, meters	Temperature, ° C.	Salinity, °/₀₀	σ t
0	−1.21	32.17	0	−1.21	32.17	25.89
24	−1.26	32.18	25	−1.25	32.19	25.90
49	−1.57	32.65	50	−1.55	32.66	26.29
73	−1.53	32.80	75	−1.50	32.80	26.41
97	−1.36	32.90	100	−1.35	32.92	26.50
146	−0.04	33.40	150	0.00	33.43	26.86
195	0.60	33.68	200	0.65	33.71	27.05
292	2.00	34.335	(300)	2.15	34.38	27.48

Station 6667; 27 April; 49°03.5′ N., 51°54′ W.; depth 307 m.; dynamic height 971.143.

Observed values			Scaled values			
Depth, meters	Temperature, ° C.	Salinity, °/₀₀	Depth, meters	Temperature, ° C.	Salinity, °/₀₀	σ t
0	−1.07	32.23	0	−1.07	32.23	25.93
24	−1.09	32.24	25	−1.10	32.24	25.94
48	−1.57	32.66	50	−1.55	32.67	26.30
73	−1.48	32.78	75	−1.45	32.78	26.39
97	−1.32	32.87	100	−1.30	32.88	26.46
145	−0.95	33.06	150	−0.95	33.08	26.61
194	−0.38	33.38	200	−0.35	33.42	26.87
286	1.00	34.02	(300)	1.25	34.09	27.32

Station 6668; 27 April; 48°59′ N., 52°07′ W.; depth 302 m.; dynamic height 971.171.

Observed values			Scaled values			
Depth, meters	Temperature, ° C.	Salinity, °/₀₀	Depth, meters	Temperature, ° C.	Salinity, °/₀₀	σ t
0	−1.06	32.31	0	−1.06	32.31	26.00
22	−1.06	32.32	25	−1.10	32.34	26.03
44	−1.47	32.48	50	−1.50	32.51	26.17
66	−1.55	32.61	75	−1.55	32.66	26.29
88	−1.48	32.74	100	−1.45	32.77	26.38
132	−1.29	32.85	150	−1.05	32.95	26.52
177	−0.57	33.17	200	−0.30	33.30	26.76
256	0.36	33.58	(300)	0.85	33.79	27.10

Station 6669; 27 April; 48°54′ N., 52°24′ W.; depth 357 m.; dynamic height 971.173.

Observed values			Scaled values			
Depth, meters	Temperature, ° C.	Salinity, °/₀₀	Depth, meters	Temperature, ° C.	Salinity, °/₀₀	σ t
0	−0.48	32.28	0	−0.48	32.28	25.95
23	−0.83	32.29	25	−0.85	32.29	25.97
47	−0.16	32.31	50	−0.20	32.34	26.00
70	−0.92	32.66	75	−1.00	32.69	26.30
94	−1.33	32.77	100	−1.30	32.78	26.38
141	−1.10	32.88	150	−1.05	32.90	26.47
187	−0.83	33.02	200	−0.70	33.13	26.65
281	0.90	33.92	(300)	1.15	34.06	27.30

Station 6670; 28 April; 48°49.5′ N., 52°39′ W.; depth 220 m.; dynamic height 971.200.

Observed values			Scaled values			
Depth, meters	Temperature, ° C.	Salinity, °/₀₀	Depth, meters	Temperature, ° C.	Salinity, °/₀₀	σ t
0	0.00	32.11	0	0.00	32.11	25.80
25	0.00	32.11	25	0.00	32.11	25.80
50	−1.47	32.54	50	−1.47	32.54	26.20
76	−1.33	32.65	75	−1.35	32.65	26.28
101	−1.36	32.74	100	−1.35	32.74	26.35
151	−1.26	32.82	150	−1.25	32.82	26.42
202	−1.19	32.93	200	−1.20	32.93	26.50

Station 6671; 28 April; 48°47′ N., 52°47′ W.; depth 146 m.; dynamic height 971.196.

Observed values			Scaled values			
Depth, meters	Temperature, ° C.	Salinity, °/₀₀	Depth, meters	Temperature, ° C.	Salinity, °/₀₀	σ t
0	−0.56	32.09	0	−0.56	32.09	25.80
24	−0.55	32.09	25	−0.55	32.09	25.80
49	−1.43	32.50	50	−1.40	32.51	26.17
73	−1.25	32.67	75	−1.25	32.67	26.30
98	−1.31	32.73	100	−1.35	32.73	26.34
122	−1.32	32.74	[150]	−1.30	32.75	26.36

STATIONS OCCUPIED IN 1958—Continued

Station 6672; 28 April; 48°44′ N., 52°58′ W.; depth 101 m.; dynamic height 971.212.

Observed values			Scaled values			
Depth, meters	Temperature, °C.	Salinity, ‰	Depth, meters	Temperature, °C.	Salinity, ‰	σt
0	−0.52	32.07	0	−0.52	32.07	25.79
27	−0.52	32.06	25	−0.50	32.06	25.78
53	−1.25	32.34	50	−1.20	32.31	26.00
80	−1.34	32.48	75	−1.35	32.46	26.13
			(100)	−1.35	32.55	26.20

Station 6673; 28 April; 48°37′ N., 52°43′ W.; depth 252 m.; dynamic height 971.184.

Observed values			Scaled values			
Depth, meters	Temperature, °C.	Salinity, ‰	Depth, meters	Temperature, °C.	Salinity, ‰	σt
0	−0.27	32.56	0	−0.27	32.56	26.17
24	−0.37	32.57	25	−0.35	32.57	26.18
48	−1.07	32.58	50	−1.10	32.58	26.22
72	−1.45	32.72	75	−1.45	32.72	26.34
96	−1.48	32.74	100	−1.50	32.74	26.36
144	−1.28	32.81	150	−1.25	32.85	26.44
192	−0.20	33.32	(200)	0.00	33.42	26.86

Station 6674; 28 April; 49°31′ N., 52°29′ W.; depth 223 m.; dynamic height 971.161.

Observed values			Scaled values			
Depth, meters	Temperature, °C.	Salinity, ‰	Depth, meters	Temperature, °C.	Salinity, ‰	σt
0	0.05	32.62	0	0.05	32.62	26.21
25	0.02	32.64	25	0.02	32.64	26.23
50	−0.55	32.71	50	−0.55	32.71	26.30
75	−0.90	32.84	75	−0.90	32.84	26.42
100	−0.79	32.96	100	−0.79	32.96	26.51
150	−0.45	33.18	150	−0.45	33.18	26.68
200	0.18	33.46	200	0.18	33.46	26.88

Station 6675; 28 April; 48°19′ N., 52°02′ W.; depth 187 m.; dynamic height 971.179.

Observed values			Scaled values			
Depth, meters	Temperature, °C.	Salinity, ‰	Depth, meters	Temperature, °C.	Salinity, ‰	σt
0	0.20	32.51	0	0.20	32.51	26.11
23	0.15	32.53	25	0.15	32.53	26.13
46	0.09	32.52	50	−0.05	32.53	26.14
69	−0.91	32.68	75	−1.00	32.72	26.33
92	−1.15	32.83	100	−1.15	32.85	26.44
138	−0.94	32.94	150	−0.70	33.04	26.58
161	−0.51	33.16	[200]	0.25	33.36	26.79

Station 6676; 28 April; 48°12′ N., 51°48′ W.; depth 190 m.; dynamic height 971.176.

Observed values			Scaled values			
Depth, meters	Temperature, °C.	Salinity, ‰	Depth, meters	Temperature, °C.	Salinity, ‰	σt
0	0.20	32.46	0	0.20	32.46	26.07
24	0.17	32.49	25	0.15	32.49	26.09
48	−0.11	32.48	50	−0.20	32.48	26.11
72	−1.07	32.79	75	−1.05	32.82	26.41
96	−1.15	32.90	100	−1.15	32.91	26.48
143	−0.69	33.03	150	−0.60	33.09	26.60
172	−0.31	33.27	[200]	0.05	33.44	26.87

Station 6677; 28 April; 48°01.5′ N., 51°23′ W.; depth 183 m.; dynamic height 971.163.

Observed values			Scaled values			
Depth, meters	Temperature, °C.	Salinity, ‰	Depth, meters	Temperature, °C.	Salinity, ‰	σt
0	0.53	32.50	0	0.53	32.50	26.08
25	0.32	32.54	25	0.32	32.54	26.13
49	−0.40	32.65	50	−0.45	32.66	26.26
74	−1.05	32.79	75	−1.05	32.80	26.40
98	−0.87	32.92	100	−0.85	32.93	26.49
147	−0.52	33.27	150	−0.50	33.29	26.76
172	−0.50	33.38	[200]	−0.45	33.47	26.92

Station 6678; 28 April; 47°53′ N., 51°06′ W.; depth 161 m.; dynamic height 971.168.

Observed values			Scaled values			
Depth, meters	Temperature, °C.	Salinity, ‰	Depth, meters	Temperature, °C.	Salinity, ‰	σt
0	0.52	32.48	0	0.52	32.48	26.07
25	0.39	32.47	25	0.39	32.47	26.07
50	0.10	32.49	50	0.10	32.49	26.09
74	−1.16	32.75	75	−1.15	32.75	26.36
99	−1.02	32.89	100	−1.00	32.89	26.46
144	−0.54	33.30	(150)	−0.50	33.36	26.82

Station 6679; 28 April; 47°45′ N., 50°51′ W.; depth 117 m.; dynamic height 971.162.

Observed values			Scaled values			
Depth, meters	Temperature, °C.	Salinity, ‰	Depth, meters	Temperature, °C.	Salinity, ‰	σt
0	0.97	32.52	0	0.97	32.52	26.08
25	0.86	32.52	25	0.86	32.52	26.08
51	0.78	32.53	50	0.80	32.53	26.10
76	0.33	32.80	75	0.35	32.78	26.32
102	−0.31	33.21	100	−0.25	33.18	26.67

Station 6680; 28 April; 47°39′ N., 50°36′ W.; depth 119 m.; dynamic height 971.165.

Observed values			Scaled values			
Depth, meters	Temperature, °C.	Salinity, ‰	Depth, meters	Temperature, °C.	Salinity, ‰	σt
0	1.46	32.62	0	1.46	32.62	26.13
25	1.41	32.62	25	1.41	32.62	26.13
50	1.31	32.63	50	1.31	32.63	26.15
76	0.73	32.68	75	0.75	32.68	26.22
101	−0.22	33.03	100	−0.20	33.02	26.54

Station 6681; 28 April; 47°32.5′ N., 50°19′ W.; depth 119 m.; dynamic height 971.160.

Observed values			Scaled values			
Depth, meters	Temperature, °C.	Salinity, ‰	Depth, meters	Temperature, °C.	Salinity, ‰	σt
0	1.66	32.68	0	1.66	32.68	26.16
26	1.62	32.66	25	1.65	32.66	26.14
52	1.49	32.68	50	1.50	32.67	26.16
78	0.92	32.83	75	1.00	32.81	26.32
104	−0.18	33.16	100	0.05	33.10	26.59

Station 6682; 28 April; 47°23.5′ N., 49°59′ W.; depth 82 m.; dynamic height 971.151.

Observed values			Scaled values			
Depth, meters	Temperature, °C.	Salinity, ‰	Depth, meters	Temperature, °C.	Salinity, ‰	σt
0	1.93	32.75	0	1.93	32.75	26.20
25	1.93	32.77	25	1.93	32.77	26.22
50	1.78	32.74	50	1.78	32.74	26.20
70	0.41	32.91	(75)	0.10	32.98	26.50

Station 6683; 29 April; 47°41′ N., 49°52′ W.; depth 116 m.; dynamic height 971.160.

Observed values			Scaled values			
Depth, meters	Temperature, °C.	Salinity, ‰	Depth, meters	Temperature, °C.	Salinity, ‰	σt
0	1.18	32.62	0	1.18	32.62	26.15
26	1.19	32.62	25	1.20	32.62	26.15
52	1.09	32.62	50	1.10	32.62	26.15
78	0.00	32.75	75	0.10	32.73	26.30
104	−0.32	33.17	100	−0.30	33.12	26.62

TABLE OF OCEANOGRAPHIC DATA—Continued

STATIONS OCCUPIED IN 1958—Continued

Station 6684; 29 April; 48°01.5′ N., 49°48′ W.; depth 169 m.; dynamic height 971.157.

Observed values			Scaled values			
Depth, meters	Temperature, ° C.	Salinity, ‰	Depth, meters	Temperature, ° C.	Salinity, ‰	σ t
0.......	0.27	32.66	0......	0.27	33.66	26.23
24......	0.26	32.67	25.....	0.25	32.67	26.24
48......	0.25	32.66	50.....	0.20	32.67	26.24
72......	−0.90	32.86	75.....	0.90	32.88	26.45
96......	−0.59	32.99	100....	−0 55	33.00	26.54
144.....	−0.34	33.26	(150)...	−0.30	33.29	26.75

Station 6685; 29 April; 48°17′ N., 49°43′ W.; depth 220 m.; dynamic height 971.116.

Observed values			Scaled values			
Depth, meters	Temperature, ° C.	Salinity, ‰	Depth, meters	Temperature, ° C.	Salinity, ‰	σ t
0.......	−0.11	32.74	0......	−0.11	32.74	26.31
25......	−0.84	32.83	25.....	−0.84	32.83	26.41
50......	−0.56	33.10	50.....	−0.56	33.10	26.61
75......	−0.23	33.26	75.....	−0.23	33.26	26.73
100.....	0.05	33.41	100....	0.05	33.41	26.85
149.....	0.46	33.63	150....	0.45	33.63	26.99
199.....	0.48	33.64	200....	0.50	33.64	27.00

Station 6686; 29 April; 48°36′ N., 49°38′ W.; depth 603 m.; dynamic height 971.146.

Observed values			Scaled values			
Depth, meters	Temperature, ° C.	Salinity, ‰	Depth, meters	Temperature, ° C.	Salinity, ‰	σ t
0.......	−0.31	32.54	0......	−0.31	32.54	26.16
25......	−1.09	32.64	25.....	−1.09	32.64	26.27
50......	−0.63	32.82	50.....	−0.63	32.82	26.40
75......	−0.76	32.98	75.....	−0.76	32.98	26.53
101.....	−0.64	33.07	100....	−0.65	33.06	26.59
151.....	0.00	33.36	150....	0.00	33.35	26.80
201.....	0.60	33.79	200....	0.55	33.77	27.11
302.....	0.85	34.04	300....	0.85	34.03	27.29
370.....	1.91	34.32	400....	2.25	34.43	27.51
564.....	3.75	34.825	(600)...	3.90	34.83	27.68

Station 6687; 29 April; 48°46′ N., 49°35′ W.; depth 1,225 m.; dynamic height 971.101.

Observed values			Scaled values			
Depth, meters	Temperature, ° C.	Salinity, ‰	Depth, meters	Temperature, ° C.	Salinity, ‰	σ t
0.......	−0.17	32.52	0......	−0.17	32.52	26.14
22......	−0.60	32.68	25.....	−0.60	32.69	26.28
44......	−0.48	32.86	50.....	−0.55	32.89	26.44
67......	−0.73	32.98	75.....	−0.70	33.01	26.56
89......	−0.61	33.08	100....	−0.45	33.14	26.65
133.....	0.08	33.41	150....	0.25	33.53	26.93
177.....	0.59	33.74	200....	0.80	33.88	27.17
266.....	1.51	34.25	300....	1.90	34.38	27.50
355.....	2.81	34.54	400....	3.20	34.63	27.59
543.....	3.76	34.79	600....	3.80	34.82	27.69
739.....	3.83	34.85	800....	3.75	34.85	27.71
947.....	3.52	32.85	1,000..	3.50	34.85	27.74

Station 6688; 29 April; 49°06.5′ N., 49°28′ W.; depth 1,417 m.; dynamic height 970.988.

Observed values			Scaled values			
Depth, meters	Temperature, ° C.	Salinity, ‰	Depth, meters	Temperature, ° C.	Salinity, ‰	σ t
0.......	0.80	33.18	0......	0.80	33.18	26.62
21......	0.51	33.40	25.....	0.50	33.40	26.81
42......	0.45	33.41	50.....	0.30	33.44	26.85
63......	−0.04	33.52	75.....	0.10	33.64	27.02
84......	0.20	33.77	100....	0.45	33.87	27.19
125.....	0.93	34.01	150....	1.25	34.15	27.37
167.....	1.50	34.26	200....	1.85	34.37	27.50
251.....	2.57	34.52	300....	3.00	34.62	27.61
224.....	1.97	34.45	400....	3.90	34.77	27.64
332.....	3.51	34.68	600....	3.95	34.85	27.69
436.....	3.99	34.81	800....	3.70	34.85	27.72
584.....	3.98	34.845	(1,000)	3.55	34.85	27.73
923.....	3.59	34.85				

Station 6689; 29 April; 49°32′ N., 49°21′ W.; depth 1,464 m.; dynamic height 970.908.

Observed values			Scaled values			
Depth, meters	Temperature, ° C.	Salinity, ‰	Depth, meters	Temperature, ° C.	Salinity, ‰	σ t
0.......	1.72	34.00	0......	1.72	34.00	27.21
27......	1.50	34.01	25.....	1.50	34.01	27.24
52......	1.38	34.05	50.....	1.40	34.04	27.27
79......	1.55	34.15	75.....	1.50	34.11	27.32
105.....	2.28	34.46	100....	2.10	34.39	27.49
158.....	2.83	34.59	150....	2.75	34.58	27.59
210.....	3.13	34.64	200....	3.10	34.63	27.60
315.....	3.67	34.76	300....	3.60	34.75	27.65
405.....	3.75	34.79	400....	3.75	34.79	27.66
605.....	3.78	34.85	600....	3.75	34.85	27.71
804.....	3.59	34.845	800....	3.60	34.85	27.73
1,007...	3.46	34.855	1,000..	3.45	34.85	27.74
1,414...	3.36	34.865				

Station 6690; 29 April; 50°00.5′ N., 49°00′ W.; depth 1,884 m.; dynamic height 970.877.

Observed values			Scaled values			
Depth, meters	Temperature, ° C.	Salinity, ‰	Depth, meters	Temperature, ° C.	Salinity, ‰	σ t
0.......	2.52	34.30	0......	2.52	34.30	27.39
26......	2.34	34.32	25.....	2.35	34.32	27.42
52......	2.33	34.32	50.....	2.35	34.32	27.42
79......	2.34	34.38	75.....	2.35	34.37	27.46
105.....	2.38	34.45	100....	2.40	34.43	27.50
157.....	3.36	34.72	150....	3.30	34.67	27.62
209.....	3.56	34.77	200....	3.55	34.76	27.66
314.....	3.73	34.81	300....	3.70	34.81	27.69
419.....	3.80	34.835	400....	3.80	34.83	27.69
625.....	3.59	34.84	600....	3.65	34.84	27.71
828.....	3.47	34.85	800....	3.50	34.85	27.74
1,036...	3.39	34.865	1,000..	3.40	34.86	27.76
1,559...	3.27	34.88				

Station 6691; 30 April; 49°51′ N., 48°20′ W.; depth 2,743 m.; dynamic height 970.886.

Observed values			Scaled values			
Depth, meters	Temperature, ° C.	Salinity, ‰	Depth, meters	Temperature, ° C.	Salinity, ‰	σ t
0.......	3.27	34.39	0......	3.27	34.39	27.39
25......	3.13	34.38	25.....	3.13	34.38	27.40
50......	3.05	34.38	50.....	3.05	34.38	27.40
75......	2.86	34.39	75.....	2.86	34.39	27.43
100.....	2.75	34.45	100....	2.75	34.45	27.49
150.....	3.23	34.67	150....	3.23	34.67	27.62
199.....	3.47	34.74	200....	3.50	34.74	27.65
299.....	3.72	34.79	300....	3.75	34.79	27.66
401.....	3.80	34.82	400....	3.80	34.82	27.69
598.....	3.71	34.85	600....	3.70	34.85	27.72
791.....	3.53	34.84	800....	3.55	34.84	27.72
991.....	3.41	34.85	1,000...	3.40	34.85	27.75
1,497...	3.29	34.885				

TABLE OF OCEANOGRAPHIC DATA—Continued

STATIONS OCCUPIED IN 1958—Continued

Station 6692; 30 April; 49°41′ N., 47°40.5′ W.; depth 2,705 m.; dynamic height 970.894.

Observed values			Scaled values			
Depth, meters	Temperature, ° C.	Salinity, ‰	Depth, meters	Temperature, ° C.	Salinity, ‰	σt
0	4.85	34.42	0	4.85	34.42	27.26
25	4.52	34.39	25	4.52	34.39	27.27
50	4.12	34.37	50	4.12	34.37	27.29
75	3.29	34.36	75	3.29	34.36	27.37
100	3.28	34.55	100	3.28	34.55	27.52
150	3.42	34.67	150	3.42	34.67	27.60
199	4.00	34.78	200	4.00	34.78	27.63
299	3.87	34.81	300	3.90	34.81	27.67
398	3.87	34.82	400	3.85	34.82	27.68
596	3.63	34.85	600	3.65	34.85	27.72
794	3.50	34.85	800	3.50	34.85	27.74
995	3.44	34.85	1,000	3.45	34.85	27.74
1,501	3.35	34.875				

Station 6693; 30 April; 49°15.5′ N., 47°54′ W.; depth 2,432 M.; dynamic height 970.890.

Depth, meters	Temperature, ° C.	Salinity, ‰	Depth, meters	Temperature, ° C.	Salinity, ‰	σt
0	3.29	34.26	0	3.29	34.26	27.29
25	3.28	34.33	25	3.28	34.33	27.34
49	3.14	34.32	50	3.15	34.32	27.35
74	3.05	34.34	75	3.05	34.34	27.37
98	2.99	34.44	100	3.00	34.45	27.47
147	3.33	34.66	150	3.35	34.67	27.61
196	3.58	34.74	200	3.50	34.75	27.66
294	3.74	34.80	300	3.75	34.80	27.67
385	3.75	34.80	400	3.75	34.80	27.67
575	3.67	34.84	600	3.65	34.84	27.71
763	3.48	34.85	800	3.45	34.85	27.74
959	3.42	34.86	1,000	3.40	34.86	27.76
1.456	3.32	34.875				

Station 6694; 30 April; 48°53.5′ N., 48°06′ W.; depth 2,377 m.; dynamic height 970.902.

Depth, meters	Temperature, ° C.	Salinity, ‰	Depth, meters	Temperature, ° C.	Salinity, ‰	σt
0	3.53	34.28	0	3.53	34.28	27.28
23	3.22	34.30	25	3.20	34.30	27.33
46	3.16	34.29	50	3.15	34.29	27.32
69	3.15	34.30	75	3.15	34.30	27.33
91	3.21	34.35	100	3.25	34.40	27.40
137	3.28	34.61	150	3.30	34.63	27.58
182	3.31	34.66	200	3.35	34.68	27.61
273	3.57	34.75	300	3.65	34.77	27.66
326	3.69	34.78	400	3.75	34.82	27.69
494	3.77	34.84	600	3.70	34.84	27.71
665	3.63	34.84	800	3.50	34.84	27.73
858	3.50	34.85	1,000	3.45	34.85	27.74
1,386	3.35	34.87				

Station 6695; 30 April; 48°30′ N., 48°23′ W.; depth 1,847 m.; dynamic height 970.908.

Depth, meters	Temperature, ° C.	Salinity, ‰	Depth, meters	Temperature, ° C.	Salinity, ‰	σt
0	2.22	33.85	0	2.22	33.85	27.05
24	1.77	33.80	25	1.80	33.80	27.04
48	2.09	34.07	50	2.10	34.09	27.25
73	2.06	34.31	75	2.05	34.33	27.45
97	2.49	34.49	100	2.50	34.50	27.55
145	2.93	34.62	150	3.00	34.63	27.61
193	3.44	34.70	200	3.50	34.70	27.62
290	3.67	34.76	300	3.70	34.77	27.66
399	3.80	34.81	400	3.80	34.81	27.68
597	3.73	34.84	600	3.75	34.84	27.70
794	3.55	34.84	800	3.55	34.84	27.72
994	3.45	34.85	1,000	3.45	34.85	27.74
1,500	3.33	34,875				

Station 6696; 30 April; 48°09.5′ N., 48°34′ W.; depth 1,847 m.; dynamic height 970.908.

Depth, meters	Temperature, ° C.	Salinity, ‰	Depth, meters	Temperature, ° C.	Salinity, ‰	σt
0	0.58	32.93	0	0.58	32.93	26.43
25	−0.01	32.95	25	−0.01	32.95	26.48
50	0.07	33.02	50	0.07	33.02	26.53
75	−0.18	33.39	75	−0.18	33.39	26.84
100	0.31	33.57	100	0.31	33.57	26.96
150	0.70	33.85	150	0.70	33.85	27.16
200	1.39	34.18	200	1.39	34.18	27.38
300	2.66	34.47	300	2.66	34.47	27.51
401	3.52	34.70	400	3 50	34.70	27.62
600	3.92	34.83	600	3.90	34.83	27.68

Station 6697; 30 April; 48°05′ N., 48°36′ W.; depth 326 m.; dynamic height 971.084.

Depth, meters	Temperature, ° C.	Salinity, ‰	Depth, meters	Temperature, ° C.	Salinity, ‰	σt
0	0.99	32.96	0	0.99	32.96	26.43
24	0.43	32.95	25	0.45	32.95	26.46
48	0.23	32.94	50	0.20	32.94	26.46
72	−0.17	33.01	75	−0.20	33.05	26.56
96	−0.10	33.41	100	−0.05	33.47	26.90
144	0.56	33.81	150	0.60	33.84	27.15
193	0.95	34.09	200	1.00	34.11	27.35
289	1.90	34.30	(300)	2.00	34.32	27.45

Station 6698; 30 April; 47°52′ N., 48°42′ W.; depth 224 m.; dynamic height 971.122.

Depth, meters	Temperature, ° C.	Salinity, ‰	Depth, meters	Temperature, ° C.	Salinity, ‰	σt
0	0.28	32.76	0	0.28	32.76	26.31
25	0.02	32.78	25	0.02	32.78	26.34
50	0.44	32.88	50	0.44	32.88	26.40
75	−0.73	33.01	75	−0.73	33.01	26.56
100	−0.40	33.20	100	−0.40	33.20	26 70
149	0.28	33.54	150	0.30	33.55	26.94
199	0.74	33.90	200	0.75	33.91	27.21

Station 6699; 1 May; 47°40.5′ N., 48°48′ W.; depth 169 m.; dynamic height 971.147.

Depth, meters	Temperature, ° C.	Salinity, ‰	Depth, meters	Temperature, ° C.	Salinity, ‰	σt
0	1.07	32.66	0	1.07	32.66	26.19
23	0.88	32.66	25	0.85	32.66	26.20
46	0.36	32.70	50	0.25	32.72	26.28
69	−0.45	32.85	75	−0.55	32.89	26.44
92	−0.68	33.02	100	−0.65	33.08	26.61
138	−0.21	33.36	(150)	−0.05	33.44	26.87

Station 6700; 1 May; 47°42′ N., 48°15′ N.; depth 223 m.; dynamic height 971.141.

Depth, meters	Temperature, ° C.	Salinity, ‰	Depth, meters	Temperature, ° C.	Salinity, ‰	σt
0	1.14	32.66	0	1.14	32.66	26.18
23	1.01	32.67	25	0.95	32.67	26.20
47	−0.02	32.72	50	−0.15	32.74	26.32
70	−0.65	32.96	75	−0.60	33.00	26.54
93	−0.49	33.12	100	−0.40	33.16	26.66
140	−0.06	33.42	150	0.00	33.46	26.89
186	0.23	33.59	(200)	0.30	33.62	27.00

TABLE OF OCEANOGRAPHIC DATA—Continued

STATIONS OCCUPIED IN 1958—Continued

Station 6701; 1 May; 47°43′ N., 47°55′ W.; depth 265 m.; dynamic height 971.133.

Observed values			Scaled values			
Depth, meters	Temperature, ° C.	Salinity, ‰	Depth, meters	Temperature, ° C.	Salinity, ‰	σ_t
0	0.74	32.88	0	0.74	32.88	26.38
24	0.52	32.92	25	0.50	32.92	26.42
48	0.50	32.93	50	0.50	32.93	26.43
71	0.05	32.96	75	−0.10	32.96	26.48
95	−0.74	32.98	100	−0.70	33.00	26.55
143	−0.03	33.37	150	0.10	33.43	26.86
190	0.58	33.70	200	0.65	33.75	27.08
238	0.79	33.93	[300]	1.40	34.26	27.45

Station 6702; 1 May; 47°44′ N., 47°34′ W.; depth 307 m.; dynamic height 971.105.

Observed values			Scaled values			
Depth, meters	Temperature, ° C.	Salinity, ‰	Depth, meters	Temperature, ° C.	Salinity, ‰	σ_t
0	0.54	32.79	0	0.54	32.79	26.32
26	0.40	32.85	25	0.40	32.85	26.38
51	−0.16	32.89	50	−0.15	32.88	26.43
77	−0.66	33.01	75	−0.65	32.99	26.54
102	−0.27	33.27	100	−0.30	33.25	26.72
154	0.38	33.69	150	0.35	33.67	27.04
205	0.62	33.93	200	0.60	33.90	27.20
289	1.96	34.29	(300)	2.15	34.32	27.44

Station 6703; 1 May; 47°53′ N., 47°22′ W.; depth 369 m.; dynamic height 971.078.

Observed values			Scaled values			
Depth, meters	Temperature, ° C.	Salinity, ‰	Depth, meters	Temperature, ° C.	Salinity, ‰	σ_t
0	0.56	32.86	0	0.56	32.86	26.37
25	0.37	32.95	25	0.37	32.95	26.46
49	0.32	32.98	50	0.35	32.98	26.48
74	0.53	33.06	75	0.55	33.06	26.53
99	−0.27	33.26	100	−0.25	33.27	26.74
148	0.56	33.83	150	0.60	33.84	27.15
197	1.25	34.14	200	1.25	34.15	27.37
296	2.57	34.47	300	2.60	34.48	27.52
350	2.97	34.56	[400]	3.20	34.62	27.59

Station 6704; 1 May; 48°08′ N., 47°03′ W.; depth 1,024 m.; dynamic height 970.991.

Observed values			Scaled values			
Depth, meters	Temperature, ° C.	Salinity, ‰	Depth, meters	Temperature, ° C.	Salinity, ‰	σ_t
0	0.99	33.06	0	0.99	33.06	26.51
23	0.69	33.09	25	0.65	33.09	26.55
45	0.15	33.26	50	0.15	33.35	26.78
68	0.21	33.66	75	0.35	33.73	27.08
91	0.60	33.88	100	0.75	33.93	27.22
136	1.29	34.12	150	1.55	34.19	27.37
181	2.10	34.34	200	2.35	34.41	27.49
272	3.16	34.61	300	3.35	34.65	27.59
354	3.63	34.71	400	3.70	34.74	27.63
538	3.80	34.81	600	3.80	34.83	27.69
725	3.73	34.85	800	3.65	34.85	27.72
886	3.56	34.845	(1,000)	3.50	34.84	27.73

Station 6705; 1 May; 48°31.5′ N., 46°50′ W.; depth 2,523 m.; dynamic height 970.919.

Observed values			Scaled values			
Depth, meters	Temperature, ° C.	Salinity, ‰	Depth, meters	Temperature, ° C.	Salinity, ‰	σ_t
0	1.57	33.43	0	1.57	33.43	26.77
22	1.18	33.78	25	1.15	33.80	27.09
45	0.98	34.07	50	1.00	34.08	27.32
67	1.35	34.13	75	1.50	34.16	27.36
90	1.80	34.27	100	2.00	34.33	27.45
135	2.63	34.48	150	2.80	34.51	27.53
179	2.95	34.56	200	3.10	34.59	27.57
269	3.66	34.74	300	3.65	34.75	27.64
318	3.56	34.75	400	3.80	34.81	27.68
482	3.82	34.83	600	3.80	34.85	27.71
649	3.77	34.85	800	3.55	34.85	27.73
830	3.51	34.85	1,000	3.45	34.85	27.74
1.313	3.37	34.86				

Station 6706; 1 May; 48°59.5′ N., 46°32′ W.; depth 2,862 m.; dynamic height 970.925.

Observed values			Scaled values			
Depth, meters	Temperature, ° C.	Salinity, ‰	Depth, meters	Temperature, ° C.	Salinity, ‰	σ_t
0	5.24	34.40	0	5.24	34.40	27.19
23	5.23	34.40	25	5.20	34.40	27.20
45	4.91	34.39	50	4.90	34.39	27.22
70	4.75	34.38	75	4.65	34.37	27.24
93	4.19	34.34	100	4.00	34.36	27.30
139	3.30	34.54	150	3.30	34.51	27.49
186	3.27	34.61	200	3.30	34.63	27.58
279	3.71	34.75	300	3.80	34.77	27.65
387	4.02	34.83	400	4.00	34.83	27.67
582	3.72	34.84	600	3.70	34.84	27.71
779	3.55	34.845	800	3.55	34.85	27.73
981	3.44	34.85	1,000	3.45	34.85	27.74
1,498	3.35	34.86				

Station 6707; 1 May; 49°19.5′ N., 46°20′ W.; depth 3,127 m.; dynamic height 970.916.

Observed values			Scaled values			
Depth, meters	Temperature, ° C.	Salinity, ‰	Depth, meters	Temperature, ° C.	Salinity, ‰	σ_t
0	5.63	34.42	0	5.63	34.42	27.16
27	5.62	34.43	25	5.60	34.43	27.17
53	5.55	34.44	50	5.55	34.44	27.18
80	5.04	34.42	75	5.15	34.42	27.22
106	4.23	34.44	100	4.35	34.43	27.31
160	4.32	34.74	150	4.30	34.71	27.55
231	4.34	34.81	200	4.35	34.79	27.60
320	4.03	34.83	300	4.10	34.83	27.66
431	3.87	34.84	400	3.90	34.84	27.69
643	3.66	34.865	600	3.70	34.86	27.73
854	3.49	34.85	800	3.55	34.85	27.73
1,068	3.41	34.855	1,000	3.45	34.85	27.74
1,604	3.36	34.875				

Station 6708; 2 May; 49°10′ N., 45°41′ W.; depth 2,926 m.; dynamic height 970.902.

Observed values			Scaled values			
Depth, meters	Temperature, ° C.	Salinity, ‰	Depth, meters	Temperature, ° C.	Salinity, ‰	σ_t
0	4.15	34.29	0	4.15	34.29	27.22
24	4.15	34.30	25	4.15	34.30	27.23
49	3.82	34.30	50	3.80	34.30	27.27
73	3.40	34.29	75	3.40	34.29	27.30
98	3.32	34.48	100	3.35	34.49	27.46
145	3.53	34.65	150	3.55	34.66	27.58
194	3.51	34.69	200	3.50	34.69	27.61
292	3.69	34.76	300	3.70	34.76	27.65
378	3.81	34.805	400	3.80	34.81	27.68
569	3.76	34.845	600	3.75	34.85	27.71
761	3.54	34.86	800	3.50	34.86	27.75
958	3.43	....	1,000	3.45	34.86	27.75
1,464	3.35	34.865				

TABLE OF OCEANOGRAPHIC DATA—Continued

STATIONS OCCUPIED IN 1958—Continued

Station 6709; 2 May; 49°00′ N., 44°59′ W.; depth 1,737 m.; dynamic height 970.913.

Observed values			Scaled values			
Depth, meters	Temperature, ° C.	Salinity, °/₀₀	Depth, meters	Temperature, ° C.	Salinity, °/₀₀	σ t
0	3.25	34.05	0	3.25	34.05	27.12
24	2.94	34.08	25	2.90	34.08	27.18
47	2.25	34.09	50	2.25	34.11	27.26
71	2.20	34.32	75	2.20	34.34	27.45
95	2.27	34.40	100	2.30	34.41	27.50
142	2.77	34.53	150	2.85	34.54	27.55
189	3.10	34.61	200	3.15	34.63	27.59
284	3.79	34.74	300	3.85	34.76	27.63
414	3.91	34.82	400	3.90	34.81	27.67
617	3.70	34.83	600	3.75	34.83	27.69
816	3.48	34.84	800	3.50	34.84	27.73
1,022	3.38	34.86	1,000	3.40	34.86	27.76
1,537	3.32	34.87				

Station 6710; 2 May; 48°37.5′ N., 45°28′ W.; depth 1,188 m.; dynamic height 970.933.

Observed values			Scaled values			
Depth, meters	Temperature, ° C.	Salinity, °/₀₀	Depth, meters	Temperature, ° C.	Salinity, °/₀₀	σ t
0	2.34	33.74	0	2.34	33.74	26.95
24	3.33	33.95	25	3.30	33.96	27.05
48	2.76	34.08	50	2.75	34.09	27.20
73	2.91	34.30	75	2.90	34.31	27.37
97	2.87	34.35	100	2.90	34.36	27.41
145	3.24	34.53	150	3.30	34.54	27.51
193	3.49	34.62	200	3.55	34.63	27.55
290	3.99	34.78	300	4.00	34.78	27.63
375	3.81	34.77	400	3.80	34.78	27.65
564	3.84	34.84	600	3.80	34.84	27.70
754	3.58	34.85	800	3.55	34.85	27.73
957	3.46	34.84	(1,000)	3.45	34.84	27.73

Station 6711; 2 May; 48°18′ N., 45°55′ W.; depth 1,188 m.; dynamic height 970.940.

Observed values			Scaled values			
Depth, meters	Temperature, ° C.	Salinity, °/₀₀	Depth, meters	Temperature, ° C.	Salinity, °/₀₀	σ t
0	2.32	33.58	0	2.32	33.58	26.83
26	2.30	33.68	25	2.30	33.67	26.91
51	2.51	34.12	50	2.50	34.11	27.24
77	1.29	34.12	75	1.35	34.12	27.34
102	1.67	34.24	100	1.60	34.23	27.40
153	2.55	34.48	150	2.50	34.46	27.52
204	2.89	34.58	200	2.90	34.57	27.58
306	3.61	34.73	300	3.60	34.72	27.63
396	3.95	34.785	400	3.95	34.79	27.64
597	3 78	34.85	600	3.80	34.85	27.71
801	3.71	34.84	800	3.70	34.84	27.71
1,015	3 53	34.84	1,000	3.55	34.84	27.72

Station 6712; 2 May; 47°58.5′ N., 46°24′ W.; depth 1,216 m.; dynamic height 970.956.

Observed values			Scaled values			
Depth, meters	Temperature, ° C.	Salinity, °/₀₀	Depth, meters	Temperature, ° C.	Salinity, °/₀₀	σ t
0	1.47	33.22	0	1.47	33.22	26.61
26	1.67	33.70	25	1.65	33.68	26.96
51	2.00	34.04	50	2.00	34.02	27.21
77	1.16	34.10	75	1.20	34.10	27.33
102	1.56	34.24	100	1.50	34.22	27.41
154	2 45	34.44	150	2.40	34.42	27.50
206	2.98	34.56	200	2.95	34.54	27.54
308	3.45	34.67	300	3.45	34.66	27.59
358	3.47	34.70	400	3.55	34.73	27.63
559	3.95	34.83	600	3.95	34.84	27.68
775	3.73	34.84	800	3.70	34.84	27.71
1,006	3.46	34.83	1,000	3.50	34.83	27.72

Station 6713; 2 May; 47°52′ N., 46°08′ W.; depth 1,051 m.; dynamic height 970.932.

Observed values			Scaled values			
Depth, meters	Temperature, ° C.	Salinity, °/₀₀	Depth, meters	Temperature, ° C.	Salinity, °/₀₀	σ t
0	2.90	33.77	0	2.90	33.77	26.94
27	2.73	33.78	25	2.75	33.78	26.95
53	1.78	33.91	50	1.80	33.88	27.10
80	2.00	34.15	75	1.90	34.10	27.28
106	2.83	34.37	100	2.70	34.32	27.39
160	3.54	34.64	150	3.40	34.60	27.55
212	4.04	34.76	200	3.95	34.74	27.60
318	4.02	34.81	300	4.00	34.81	27.65
400	3.84	34.81	400	3 80	34.81	27.68
600	3.60	34.83	600	3.60	34.83	27.71
802	3.51	34.84	800	3.55	34.84	27.72
1,005	3.41	34.85	1,000	3.45	34.85	27.74

Station 6714; 2 May; 47°44.5′ N., 45°50′ W.; depth 414 m.; dynamic height 970.948.

Observed values			Scaled values			
Depth, meters	Temperature, ° C.	Salinity, °/₀₀	Depth, meters	Temperature, ° C.	Salinity, °/₀₀	σ t
0	4.24	33.73	0	4.24	33.73	26.77
25	4.21	33.73	25	4.21	33.73	26.78
51	5.36	34.04	50	5.35	34.04	26.89
76	2.87	33.90	75	2.95	33.90	27.03
102	2.34	34.18	100	2.35	34.15	27.28
152	4.05	34.66	150	4.00	34.64	27.52
203	4.05	34.76	200	4.00	34.75	27.61
305	3 93	34.82	300	3.95	34.82	27.67
406	3.84	34.82	400	38.5	34.82	27.68

Station 6715; 3 May; 47°40.5′ N., 45°41′ W.; depth 317 m.; dynamic height 970.955.

Observed values			Scaled values			
Depth, meters	Temperature, ° C.	Salinity, °/₀₀	Depth, meters	Temperature, ° C.	Salinity, °/₀₀	σ t
0	5.60	34.00	0	5.60	34.00	26.83
24	5.59	34.00	25	5.60	34.00	26.83
48	5.47	34.01	50	5.45	34.01	26.86
73	5.20	34.06	75	5.15	34.06	26.94
97	4.56	34 19	100	4.50	34.21	27.13
145	3.76	34.52	150	3.75	34.55	27.47
193	3.85	....	200	3.85	34.79	27.65
290	3.78	34.29	300	3.80	34.79	27.66

Station 6716; 3 May; 47°25′ N., 45°03′ W.; depth 216 m.; dynamic height 970.965.

Observed values			Scaled values			
Depth, meters	Temperature, ° C.	Salinity, °/₀₀	Depth, meters	Temperature, ° C.	Salinity, °/₀₀	σ t
0	5.81	34.04	0	5.81	34.04	26.84
25	5.72	34.04	25	5.72	34.04	26.85
50	5.44	34.04	50	5.44	34.04	26.88
76	5.30	34.07	75	5.30	34.07	26.93
101	4.26	34.20	100	4.30	34.19	27.13
151	4.02	34.51	150	4.05	34.50	27.40
201	3.80	34.63	200	3.80	34.63	27.53

Station 6717; 3 May; 47°23′ N., 44°58′ W.; depth 190 m.; dynamic height 970.956.

Observed values			Scaled values			
Depth, meters	Temperature, ° C.	Salinity, °/₀₀	Depth, meters	Temperature, ° C.	Salinity, °/₀₀	σ t
0	5.93	34.06	0	5.93	34.06	26.84
25	5.93	34.07	25	5.93	34.07	26.85
51	5.51	34.06	50	5.55	34.06	26.89
76	4.85	34.13	75	4.85	34.12	27.02
101	3.81	34.28	100	3.80	34.27	27.25
152	3.93	34.55	150	3.95	34.54	27.44
			[200]	3.85	34.72	27.60

TABLE OF OCEANOGRAPHIC DATA—Continued

STATIONS OCCUPIED IN 1958—Continued

Station 6718; 3 May; 47°23′ N., 45°06′ W.; depth 220 m.; dynamic height 970.953.

Observed values			Scaled values			
Depth, meters	Temperature, ° C.	Salinity, ‰	Depth, meters	Temperature, ° C.	Salinity, ‰	σ_t
0	5.91	34.05	0	5.91	34.05	26.83
25	5.66	34.06	25	5.66	34.06	26.88
50	5.46	34.09	50	5.46	34.09	26.92
76	4.24	34.15	75	4.25	34.15	27.10
101	3.69	34.24	100	3.70	34.24	27.23
152	3.90	34.53	150	3.90	34.52	27.44
202	3.78	34.64	200	3.80	34.63	27.53

Station 6719; 3 May; 47°23.5′ N., 45°34′ W.; depth 274 m.; dynamic height 970.956.

Observed values			Scaled values			
Depth, meters	Temperature, ° C.	Salinity, ‰	Depth, meters	Temperature, ° C.	Salinity, ‰	σ_t
0	5.60	33.98	0	5.60	33.98	26.82
25	5.60	33.99	25	5.60	33.99	26.82
51	5.59	34.05	50	5.60	34.05	26.87
76	4.97	34.04	75	4.95	34.04	26.94
101	4.20	34.26	100	4.20	34.24	27.18
152	4.09	34.64	150	4.05	34.63	27.50
202	4.26	34.78	200	4.25	34.78	27.60
253	4.12	34.78	[300]	3.95	34.78	27.63

Station 6720; 3 May; 47°23.5′ N., 45°56′ W.; depth 320 m.; dynamic height 970.953.

Observed values			Scaled values			
Depth, meters	Temperature, ° C.	Salinity, ‰	Depth, meters	Temperature, ° C.	Salinity, ‰	σ_t
0	5.72	34.00	0	5.72	34.00	26.82
25	5.70	34.01	25	5.70	34.01	26.83
50	5.59	34.05	50	5.59	34.05	26.87
75	5.29	34.06	75	5.29	34.06	26.92
100	4.20	34.27	100	4.20	34.27	27.21
150	3.90	34.60	150	3.90	34.60	27.50
200	3.92	34.72	200	3.92	34.72	27.59
300	3.82	34.80	300	3.82	34.80	27.67

Station 6721; 3 May; 47°22.5′ N., 46°25′ W.; depth 626 m.; dynamic height 970.948.

Observed values			Scaled values			
Depth, meters	Temperature, ° C.	Salinity, ‰	Depth, meters	Temperature, ° C.	Salinity, ‰	σ_t
0	3.97	33.60	0	3.97	33.60	26.70
24	3.83	33.60	25	3.85	33.60	26.71
48	3.59	33.90	50	3.60	33.94	27.00
72	4.10	34.26	75	4.10	34.27	27.22
96	3.40	34.36	100	3.40	34.37	27.37
144	3.70	34.55	150	3.80	34.57	27.49
193	4.40	34.76	200	4.40	34.77	27.58
289	4.33	34.84	300	4.30	34.84	27.65
364	4.10	34.84	400	4.05	34.84	27.67
557	3.91	34.86	(600)	3.90	34.86	27.71

Station 6722; 3 May; 47°22′ N., 46°37′ W.; depth 1,170 m.; dynamic height 970.943.

Observed values			Scaled values			
Depth, meters	Temperature, ° C.	Salinity, ‰	Depth, meters	Temperature, ° C.	Salinity, ‰	σ_t
0	3.01	33.48	0	3.01	33.48	26.69
26	2.63	33.48	25	2.65	33.48	26.72
52	2.14	33.82	50	2.15	33.79	27.01
78	2.45	34.14	75	2.40	34.11	27.25
103	2.60	34.28	100	2.60	34.26	27.35
156	3.38	34.57	150	3.20	34.53	27.51
208	4.07	34.75	200	4.00	34.73	27.59
311	4.05	34.81	300	4.05	34.81	27.65
387	4.08	34.83	400	4.05	34.83	27.66
590	3.66	34.845	600	3.65	34.85	27.72
800	3.53	34.85	800	3.55	34.85	27.73
1,017	3.42	34.85	1,000	3.45	34.85	27.74

Station 6723; 2 May; 47°21′ N., 47°09′ W.; depth 914 m.; dynamic height 971.015.

Observed values			Scaled values			
Depth, meters	Temperature, ° C.	Salinity, ‰	Depth, meters	Temperature, ° C.	Salinity, ‰	σ_t
0	1.63	33.04	0	1.63	33.04	26.45
26	0.93	33.13	25	1.00	33.22	26.64
52	−0.21	33.34	50	−0.20	33.32	26.78
78	0.54	33.67	75	0.50	33.63	26.99
104	0.60	33.86	100	0.60	33.84	27.15
155	1.20	34.10	150	1.15	34.08	27.31
206	1.93	34.30	200	1.80	34.28	27.43
310	3.15	34.60	300	3.05	34.57	27.56
416	3.90	34.76	400	3.85	34.74	27.61
622	3.94	34.84	600	3.95	34.83	27.67
826	3.70	34.85	800	3.75	34.85	27.71

Station 6724; 3 May; 47°20.5′ N., 47°21′ W.; depth 329 m.; dynamic height 971.054.

Observed values			Scaled values			
Depth, meters	Temperature, ° C.	Salinity, ‰	Depth, meters	Temperature, ° C.	Salinity, ‰	σ_t
0	1.34	32.92	0	1.34	32.92	26.37
25	1.37	32.92	25	1.37	32.92	26.37
49	0.68	33.04	50	0.65	33.04	26.51
74	0.13	33.23	75	0.10	33.24	26.71
99	−0.13	33.54	100	−0.20	33.55	26.97
148	0.65	33.87	150	0.70	33.88	27.18
197	1.27	34.12	200	1.30	34.13	27.34
296	2.33	34.39	300	2.35	34.39	27.47

Station 6725; 3 May; 47°20′ N., 47°44′ W.; depth 224 m.; dynamic height 971.116.

Observed values			Scaled values			
Depth, meters	Temperature, ° C.	Salinity, ‰	Depth, meters	Temperature, ° C.	Salinity, ‰	σ_t
0	1.22	32.64	0	1.22	32.64	26.16
23	1.12	32.68	25	1.10	32.68	26.20
47	0.57	32.72	50	0.40	32.73	26.28
70	−0.67	32.88	75	−0.65	32.91	26.47
94	−0.49	33.06	100	−0.45	33.10	26.61
141	−0.17	33.38	150	−0.10	33.44	26.87
188	0.31	33.64	(200)	0.40	33.69	27.05

Station 6726; 3 May; 47°18.5′ N., 48°09′ W.; depth 168 m.; dynamic height 971.111.

Observed values			Scaled values			
Depth, meters	Temperature, ° C.	Salinity, ‰	Depth, meters	Temperature, ° C.	Salinity, ‰	σ_t
0	1.90	32.64	0	1.90	32.64	26.12
26	1.66	32.68	25	1.70	32.68	26.16
52	−0.03	32.80	50	0.10	32.79	26.35
78	−0.65	33.03	75	−0.60	33.01	26.55
105	−0.26	33.24	100	−0.30	33.21	26.70
156	−0.24	33.41	150	−0.25	33.39	26.84

Station 6727; 4 May; 47°17′ N., 48°39′ W.; depth 128 m.; dynamic height 971.111.

Observed values			Scaled values			
Depth, meters	Temperature, ° C.	Salinity, ‰	Depth, meters	Temperature, ° C.	Salinity, ‰	σ_t
0	1.35	32.60	0	1.35	32.60	26.13
25	0.95	32.68	25	0.95	32.68	26.21
50	0.00	32.76	50	0.00	32.76	26.32
76	−0.65	32.96	75	−0.65	32.95	26.50
101	−0.38	33.20	100	−0.35	33.20	26.69
116	−0.31	33.26				

STATIONS OCCUPIED IN 1958—Continued

Observed values			Scaled values			
Depth, meters	Temperature, ° C.	Salinity, °/₀₀	Depth, meters	Temperature, ° C.	Salinity, °/₀₀	σ t
Station 6728; 4 May; 47°15′ N., 49°04′ W.; depth 95 m.; dynamic height 971.113.						
0	1.55	32.62	0	1.55	32.62	26.12
22	1.18	32.65	25	1.10	32.65	26.18
48	0.80	32.70	50	0.75	32.70	26.23
72	−0.47	33.04	75	−0.55	33.06	26.58
Station 6729; 4 May; 46°53.5′ N., 48°37′ W.; depth 101 m.; dynamic height 971.118.						
0	2.04	32.65	0	2.04	32.65	26.12
26	2.05	32.70	25	2.05	32.70	26.15
51	1.20	32.70	50	1.25	32.70	26.20
77	−0.44	32.93	75	−0.40	32.91	26.46
92	−0.37	33.08	(100)	−0.30	33.14	26.64
Station 6730; 4 May; 46°52.5′ N., 48°09′ W.; depth 117 m.; dynamic height 971.116.						
0	2.09	32.58	0	2.09	32.58	26.05
25	1.90	32.64	25	1.90	32.64	26.12
50	1.50	32.68	50	1.50	32.68	26.17
76	−0.21	33.08	75	−0.20	33.05	26.56
101	−0.33	33.29	100	−0.35	33.28	26.75
Station 6731; 4 May; 46°51.5′ N., 47°44′ W.; depth 169 m.; dynamic height 971.115.						
0	1.41	32.66	0	1.41	32.66	26.16
25	1.21	32.66	25	1.21	32.66	26.18
50	0.29	32.74	50	0.29	32.74	26.29
75	−0.65	32.94	75	−0.65	32.94	26.50
100	−0.58	33.08	100	−0.58	33.08	26.60
150	−0.17	33.38	150	−0.17	33.38	26.83
Station 6732; 4 May; 46°50.5′ N., 47°19′ W.; depth 320 m.; dynamic height 971.054.						
0	1.32	32.76	0	1.32	32.76	26.25
25	1.04	32.76	25	1.04	32.76	26.27
51	0.70	33.12	50	0.70	33.11	26.56
76	−0.28	33.32	75	−0.30	33.31	26.77
101	0.29	33.62	100	0.25	33.60	26.99
152	0.74	33.93	150	0.70	33.91	27.21
203	1.49	34.21	200	1.40	34.19	27.39
304	3.06	34.59	300	3.00	34.57	27.57
Station 6733; 4 May; 46°50′ N., 47°11′ W.; depth 629 m.; dynamic height 971.030.						
0	1.40	32.96	0	1.40	32.96	26.40
25	0.26	33.04	25	0.26	33.04	26.54
51	0.32	33.26	50	0.35	33.24	26.69
77	0.31	33.57	75	0.30	33.55	26.94
103	0.42	33.77	100	0.40	33.75	27.10
153	0.50	33.94	150	0.50	33.93	27.23
205	1.78	34.27	200	1.65	34.25	27.42
308	3.31	34.64	300	3.20	34.60	27.57
409	3.95	34.75	400	3.95	34.74	27.60
608	3.96	34.84	600	3.95	34.84	27.68

Observed values			Scaled values			
Depth, meters	Temperature, ° C.	Salinity, °/₀₀	Depth, meters	Temperature, ° C.	Salinity, °/₀₀	σ t
Station 6734; 4 May; 46°49.5′ N., 46°54′ W.; depth 1,225 m.; dynamic height 970.961.						
0	2.38	33.35	0	2.38	33.35	26.64
25	2.26	33.46	25	2.26	33.46	26.75
50	1.99	33.75	50	1.99	33.75	26.99
75	2.62	34.06	75	2.62	34.06	27.19
100	2.59	34.25	100	2.59	34.25	27.34
150	2.44	34.39	150	2.44	34.39	27.46
199	3.68	34.64	200	3.70	34.64	27.55
299	4.06	34.78	300	4.05	34.78	27.62
414	3.99	34.81	400	4.00	34.80	27.65
617	3.72	34.84	600	3.75	34.84	27.70
817	3.52	34.84	800	3.55	34.84	27.72
1,031	3.41	34.845	1,000	3.45	34.84	27.73
Station 6735; 4 May; 46°48.5′ N., 46°29′ W.; depth 614 m.; dynamic height 970.960.						
0	6.36	34.00	0	6.36	34.00	26.74
25	6.36	34.00	25	6.36	34.00	26.74
50	6.09	34.06	50	6.09	34.06	26.82
75	4.90	34.28	75	4.90	34.28	27.13
100	5.82	34.64	100	5.82	34.64	27.31
150	5.56	34.77	150	5.56	34.77	27.44
201	4.52	34.73	200	4.50	34.73	27.53
301	3.87	34.77	300	3.85	34.77	27.64
403	3.86	34.80	400	3.80	34.80	27.67
597	3.56	34.83	600	3.55	34.83	27.71
Station 6736; 4–5 May; 46°47.5′ N., 45°58′ W.; depth 320 m.; dynamic height 970.959.						
0	5.75	33.93	0	5.75	33.93	26.76
22	5.77	33.95	25	5.80	33.95	26.77
46	5.87	34.08	50	5.80	34.09	26.88
68	5.23	34.11	75	4.95	34.12	27.01
91	4.46	34.17	100	4.45	34.23	27.14
136	4.32	34.60	150	4.25	34.63	27.48
182	4.09	34.69	200	4.10	34.72	27.58
273	4.30	34.83	(300)	4.30	34.85	27.66
Station 6737; 5 May; 46°47′ N., 45°38′ W.; depth 258 m.; dynamic height 970.977.						
0	5.62	33.89	0	5.62	33.89	26.75
24	5.59	33.89	25	5.60	33.89	26.75
47	4.98	33.92	50	4.90	33.92	26.86
71	4.64	33.96	75	4.50	33.97	26.94
94	3.70	34.03	100	3.70	34.04	27.07
142	4.31	34.17	150	4.25	34.25	27.18
189	3.85	34.70	200	3.85	34.71	27.59
236	3.86	34.73	[300}	3.85	34.79	27.65
Station 6738; 5 May; 46°47′ N., 45°18′ W.; depth 223 m.; dynamic height 970.961.						
0	5.33	33.89	0	5.33	33.89	26.78
25	5.34	33.89	25	5.34	33.89	26.78
50	4.43	33.90	50	4.43	33 90	26.88
76	4.00	33.91	75	3.85	33.92	26.96
101	3.14	34.06	100	3.15	34.06	27.14
151	3.63	34.50	150	3.65	34.49	27.44
202	3.79	34.68	200	3.75	34.67	27.57

TABLE OF OCEANOGRAPHIC DATA—Continued

STATIONS OCCUPIED IN 1958—Continued

Station 6739; 5 May; 46°46.5′ N., 45°01′ W.; depth 172 m.; dynamic height 970.963.

Observed values			Scaled values			
Depth, meters	Temperature, ° C.	Salinity, °/oo	Depth, meters	Temperature, ° C.	Salinity, °/oo	σ t
0	5.59	33.88	0	5.59	33.88	26.74
24	5.58	33.87	25	5.55	33.87	26.74
48	4.92	33.88	50	4.90	33.88	26.82
72	4.80	33.98	75	4.75	33.99	26.92
96	4.23	34.12	100	4.15	34.15	27.12
144	3.69	34.55	(150)	3.70	34.60	27.52

Station 6740; 5 May; 46°47.5′ N., 44°50′ W.; depth 143 m.; dynamic height 970.953.

Observed values			Scaled values			
Depth, meters	Temperature, ° C.	Salinity, °/oo	Depth, meters	Temperature, ° C.	Salinity, °/oo	σ t
0	5.36	33.90	0	5.36	33.90	26.79
24	4.95	33.89	25	4.90	33.89	26.83
49	4.16	33.91	50	4.15	33.91	26.92
73	4.14	34.17	75	4.10	34.18	27.14
97	3.91	34.27	100	3.90	34.28	27.24
131	3.90	34.32	[150]	3.90	34.34	27.29

Station 6741; 23 May; 37°30′ N., 50°16′ W.; depth 5,395 m.; dynamic height 971.819.

Observed values			Scaled values			
Depth, meters	Temperature, ° C.	Salinity, °/oo	Depth, meters	Temperature, ° C.	Salinity, °/oo	σ t
0	18.63	36.385	0	18.63	36.385	26.19
24	18.15	36.38	25	18.15	36.38	26.31
49	18.12	36.38	50	18.10	36.38	26.32
73	18.08	36.395	75	18.05	36.395	26.35
97	17.80	36.40	100	17.80	36.40	26.41
146	17.61	36.40	150	17.60	36.40	26.46
194	17.56	36.40	200	17.55	36.40	26.47
291	17.25	36.345	300	17.20	36.33	26.50
387	16.65	36.22	400	16.50	36.19	26.56
580	14.09	35.745	600	13.80	35.70	26.79
771	11.04	35.355	800	10.50	35.30	27.12
962	7.24	35.055	1,000	6.65	35.03	27.51
1,159	5.30	34.99	1,500	4.30	34.97	27.75
1,357	4.60	34.99	2,000	3.75	34.93	27.77
1,557	4.20	....	2,500	3.50	34.94	27.81
1,984	3.77	34.93	3,000	3.15	34.92	27.83
2,491	3.50	34.94				
3,001	3.13	34.92				

Station 6742; 23 May; 38°01′ N., 50°18′ W.; depth 5,395 m.; dynamic height 971.851.

Observed values			Scaled values			
Depth, meters	Temperature, ° C.	Salinity, °/oo	Depth, meters	Temperature, ° C.	Salinity, °/oo	σ t
0	18.88	36.395	0	18.88	36.395	26.14
24	18.13	36.40	25	18.15	36.40	26.32
49	17.90	36.40	50	17.90	36.40	26.39
73	17.88	36.40	75	17.80	36.40	26.40
98	17.89	36.40	100	17.85	36.40	26.40
146	17.69	36.425	150	17.65	36.42	26.46
194	17.58	36.40	200	17.55	36.40	26.47
292	17.49	36.40	300	17.50	36.40	26.48
347	17.48	36.40	400	17.10	36.33	26.52
529	15.83	36.10	600	15.00	35.96	26.73
716	13.34	35.685	800	11.25	35.44	27.09
910	8.57	35.14	1,000	6.75	35.00	27.47
1,103	5.56	34.97	1,500	4.35	34.98	27.75
1,300	4.92	34.99	2,000	3.80	34.93	27.77
1,500	4.36	....	2.500	3.50	34.93	27.80
2,094	3.74	34.93	3,000	3.15	34.92	27.83
2,595	3.43	34.93				
3,096	3.04	34.915				

Station 6743; 23 May; 38°32.5′ N., 50°18′ W.; depth 5,395 m.; dynamic height 971.881.

Observed values			Scaled values			
Depth, meters	Temperature, ° C.	Salinity, °/oo	Depth, meters	Temperature, ° C.	Salinity, °/oo	σ t
0	18.76	36.35	0	18.76	36.35	26.13
26	18.04	36.415	25	18.05	36.41	26.36
52	18.00	36.43	50	18.00	36.43	26.38
78	17.92	36.43	75	17.90	36.43	26.41
103	17.80	36.43	100	17.80	36.43	26.43
154	17.66	36.42	150	17.70	36.42	26.45
206	17.61	36.405	200	17.60	36.40	26.46
309	17.57	36.41	300	17.60	36.41	26.47
382	17.53	36.40	400	17.45	36.39	26.49
576	15.72	36.04	600	15.30	35.98	26.67
770	12.12	35.505	800	11.55	35.42	27.02
967	7.40	35.04	1,000	6.70	35.00	27.48
1,166	5.15	34.96	1,500	4.30	34.95	27.73
1,369	4.50	34.95	2,000	3,80	34.92	27.77
1,574	4.16	....	2,500	3.50	34.93	27.80
2,012	3.79	34.92	3,000	3.15	34.92	27.83
2,508	3.48	34.93				
3,007	3.13	34.92				

Station 6744; 23–24 May; 39°01.5′ N., 50°11′ W.; depth 5,350 m.; dynamic height 971.756.

Observed values			Scaled values			
Depth, meters	Temperature, ° C.	Salinity, °/oo	Depth, meters	Temperature, ° C.	Salinity, °/oo	σ t
0	20.21	36.31	0	20.21	36.31	25.73
25	20.08	36.32	25	20.08	36.32	25.76
51	18.74	36.265	50	18.80	36.27	26.06
77	18.13	36.29	75	18.20	36.29	26.22
103	17.69	36.31	100	17.70	36.31	26.37
153	17.73	36.435	150	17.70	36.43	26.45
205	17.47	36.38	200	17.50	36.38	26.47
308	16.84	36.27	300	16.90	36.28	26.54
405	15.94	36.08	400	16.00	36.09	26.60
604	12.72	35.59	600	12.80	35.59	26.91
801	8.17	35.06	800	8.20	35.06	27.31
995	5.59	35.01	1,000	5.55	35.01	27.64
1,194	4.50	34.94	1,500	4.10	34.95	27.76
1,392	4.24	34.95	2,000	3.65	34.93	27.78
1,591	3.96	....	2,500	3.35	34.92	27.81
1,927	3.71	34.93	(3,000)	3.10	34.91	27.83
2,409	3.40	34.92				
2,899	3.12	34.91				

Station 6745; 24 May 39°39.5′ N., 49°50′ W.; depth 5,395 m.; dynamic height 971.384.

Observed values			Scaled values			
Depth, meters	Temperature, ° C.	Salinity, °/oo	Depth, meters	Temperature, ° C.	Salinity, °/oo	σ t
0	18.53	36.24	0	18.53	36.24	26.11
25	16.26	36.08	25	16.26	36.08	26.53
49	16.11	36.08	50	16.10	36.08	26.57
74	15.86	36.08	75	15.85	36.08	26.63
98	15.72	36.06	100	15.70	36.05	26.64
147	14.79	35.85	150	14.75	35.84	26.69
197	14.27	35.76	200	14.25	35.76	26.74
295	13.32	35.65	300	13.25	35.64	26.85
375	11.71	35.43	400	11.10	35.36	27.06
561	7.80	35.025	600	7.30	35.02	27.41
745	5.78	34.99	800	5.35	34.98	27.63
928	4.73	34.95	1,000	4.65	34.96	27.71
1,175	4.48	34.97	1,500	3.95	34.94	27.76
1,326	4.03	34.94	2,000	3.65	34.93	27.78
1,530	3.91	....	2,500	3.30	34.925	27.82
2,085	3.60	34.93	3,000	3.00	34.91	27.84
2,583	3.27	34.925				
3,081	2.95	34.91				

TABLE OF OCEANOGRAPHIC DATA—Continued

STATIONS OCCUPIED IN 1958—Continued

Station 6746; 24 May; 40°00′ N., 50°06′ W.; depth 5,376 m.; dynamic height 971.331.

Observed values			Scaled values			
Depth, meters	Temperature, ° C.	Salinity, ‰	Depth, meters	Temperature, ° C.	Salinity, ‰	σ_t
0	18.29	36.16	0	18.29	36.16	26.11
24	16.42	36.05	25	16.40	36.05	26.48
49	15.81	36.05	50	15.80	36.05	26.62
73	15.57	36.05	75	15.55	36.05	26.67
97	15.56	35.99	100	15.30	35.99	26.68
145	14.74	35.87	150	14.65	35.85	26.72
194	13.90	35.70	200	13.80	35.69	26.78
291	12.68	35.56	300	12.45	35.53	26.93
375	10.74	35.32	400	10.15	35.26	27.15
566	7.12	35.02	600	6.65	35.01	27.50
758	5.31	34.98	800	5.15	34.98	27.66
953	4.91	35.01	1,000	4.85	35.00	27.71
1,153	4.40	34.98	1,500	3,90	34.94	27.77
1,356	4.03	34.95	2,000	3.60	34.92	27.79
1,561	3.86	....	2,500	3.25	34.92	27.82
1,907	3.66	34.92	(3,000)	2.90	34.90	27.84
2,387	3.35	34.92				
2,876	3.00	34.90				

Station 6747; 24 May; 40°30.5′ N., 50°18′ W.; depth 3,640 m.; dynamic height 971.460.

Observed values			Scaled values			
Depth, meters	Temperature, ° C.	Salinity, ‰	Depth, meters	Temperature, ° C.	Salinity, ‰	σ_t
0	18.25	36.34	0	18.25	36.34	26.25
25	17.56	36.35	25	17.56	36.35	26.43
50	17.49	36.35	50	17.49	36.35	26.45
76	17.47	36.36	75	17.45	36.36	26.46
101	17.44	36.36	100	17.45	36.36	26.46
151	17.09	36.34	150	17.10	36.34	26.53
201	15.87	36.10	200	15.90	36.10	26.63
302	14.59	35.86	300	14.65	35.87	26.74
403	12.51	35.56	400	12.55	35.57	26.94
604	7.91	35.02	600	8.00	35.02	27.31
803	5.42	35.01	800	5.45	35.01	27.65
1,003	4.69	35.00	1,000	4.70	35.00	27.73
1,208	4.12	34.94	1,500	3.80	34.92	27.77
1,416	3.87	34.92	2,000	3.50	34.91	27.79
1,624	3.71	34.92	2,500	3.15	34.90	27.81
1,948	3.56	34.92	(3,000)	2.75	34.895	27.85
2,444	3.18	34.905				
2,946	2.81	34.895				

Station 6748; 24–25 May; 40°54′ N., 50°14′ W.; depth 4,262 m.; dynamic height 971.344.

Observed values			Scaled values			
Depth, meters	Temperature, ° C.	Salinity, ‰	Depth, meters	Temperature, ° C.	Salinity, ‰	σ_t
0	17.43	36.11	0	17.43	36.11	26.28
25	16.33	36.14	25	16.33	36.14	26.56
51	16.29	36.14	50	16.30	36.14	26.57
76	15.92	36.10	75	15.90	36.10	26.63
102	15.66	36.05	100	15.70	36.05	26.64
152	14.75	35.86	150	14.80	35.87	26.70
202	14.04	35.72	200	14.10	35.73	26.74
304	12.67	35.57	300	12.75	35.58	26.91
420	9.72	35.20	400	10.40	35.25	27.10
627	5.96	34.92	600	6.25	34.93	27.48
831	5.27	35.03	800	5.35	35.02	27.67
1,034	4.65	35.00	1,000	4.75	35.01	27.73
1,242	4.10	34.94	1,500	3.85	34.93	27.76
1,449	3.90	34.93	2,000	3.55	34.92	27.79
1,658	3.73	34.93	2,500	3.25	34.915	27.81
2,001	3.56	34.92	(3,000)	2.85	34.91	27.85
2,502	3.23	34.915				
3,004	2.86	....				

Station 6749; 25 May; 41°27′ N., 50°19′ W.; depth 4,023 m.; dynamic height 971.198.

Observed values			Scaled values			
Depth, meters	Temperature, ° C.	Salinity, ‰	Depth, meters	Temperature, ° C.	Salinity, ‰	σ_t
0	10.69	33.42	0	10.69	33.42	25.62
24	9.76	34.24	25	9.75	34.28	26.45
49	13.32	35.34	50	13.30	35.34	26.61
73	11.74	35.15	75	11.70	35.14	26.77
97	11.29	35.07	100	11.25	35.06	26.80
146	10.65	34.97	150	10.60	34.97	26.84
195	9.94	35.04	200	9.85	35.03	27.02
292	6.60	34.59	300	6.25	34.55	27.18
398	1.74	34.16	400	1.75	34.16	27.34
596	3.66	34.72	600	3.70	34.73	27.62
795	4.18	34.88	800	4.15	34.88	27.69
994	3.71	34.86	1,000	3.90	34.88	27.72
1,027	4.04	34.90	1,500	3.75	34.915	27.76
1,228	4.05	34.94	2,000	3.50	34.91	27.79
1,430	3.81	34.92	2,500	3.20	34.905	27.81
1,631	3.61	34.905	3,000	2.80	34.90	27.84
1,994	3.52	34.91				
2,495	3.19	34.905				
3,000	2.78	34.90				

Station 6750; 25 May; 41°53.5′ N., 50°19′ W.; depth 3,329 m.; dynamic height 971.062.

Observed values			Scaled values			
Depth, meters	Temperature, ° C.	Salinity, ‰	Depth, meters	Temperature, ° C.	Salinity, ‰	σ_t
0	8.73	32.83	0	8.73	32.83	25.48
25	6.25	33.30	25	6.25	33.30	26.20
50	5.35	33.52	50	5.35	33.52	26.49
75	4.66	33.66	75	4.66	33.66	26.68
99	2.45	33.76	100	2.45	33.76	26.96
149	1.67	34.06	150	1.65	34.07	27.28
199	2.95	34.30	200	2.95	34.30	27.35
298	3.06	34.53	300	3.05	34.53	27.52
402	3.62	34.72	400	3.60	34.71	27.62
602	4.61	34.95	600	4.60	34.95	27.70
802	4.26	34.945	800	4.25	34.945	27.74
1,002	4.06	34.93	1,000	4.05	34.945	27.74
1,204	3.82	34.915	1,500	3.65	34.915	27.77
1,404	3.66	34.915	2,000	3.40	34.91	27.80
1,607	3.57	....	2,500	3.10	34 92	27.84
2,158	3.32	34.91	(3,000)	2.65	34.89	27.85
2,465	3.13	34.92				
2,985	2.69	34.89				

Station 6751; 25 May; 42°54′ N., 50°14′ W.; depth 1,554 m.; dynamic height 971.040.

Observed values			Scaled values			
Depth, meters	Temperature, ° C.	Salinity, ‰	Depth, meters	Temperature, ° C.	Salinity, ‰	σ_t
0	8.49	33.52	0	8.49	33.52	26.06
25	7.60	33.82	25	7.60	33.82	26.42
49	7.87	34.16	50	7.85	34.16	26.66
74	6.42	34.17	75	6.30	34.17	26.88
98	5.02	34.13	100	4.95	34.13	27.01
147	2.44	34.16	150	2.45	34.17	27.29
196	3.94	34.46	200	3.95	34.48	27.40
294	3.61	34.67	300	3.60	34.67	27.59
375	3.81	34.74	400	3.85	34.76	27.63
560	3.96	34.84	600	3.95	34.84	27.68
745	3.81	34.84	800	3.80	34.84	27.70
935	3.78	34.84	1,000	3.80	34.84	27.70
1,418	3.58	34.86	(1,500)	3.55	34.86	27.74

TABLE OF OCEANOGRAPHIC DATA—Continued

STATIONS OCCUPIED IN 1958—Continued

Observed values			Scaled values			
Depth, meters	Temperature, ° C.	Salinity, °/₀₀	Depth, meters	Temperature, ° C.	Salinity, °/₀₀	σ t
Station 6752; 25 May; 42°44.5′ N., 50°15′ W.; depth 590 m.; dynamic height 971.075.						
0.......	9.0	33.50	0......	9.0	33.50	25.97
25......	6.49	33.92	25.....	6.49	33.92	26.66
50......	1.54	33.50	50.....	1.54	33.50	26.83
75......	1.50	33.52	75.....	1.50	33.52	26.85
100.....	4.71	33.99	100....	4.71	33.99	26.93
150.....	1.15	33.90	150....	1.15	33.90	27.17
199.....	2.09	34.10	200....	2.10	34.10	27.26
299.....	2.75	34.46	300....	2.75	34.46	27.50
396.....	3.37	34.60	400....	3.40	34.60	27.55
586.....	3.87	34.80	600....	3.90	34.80	27.66
Station 6753; 25 May; 42°48′ N., 50°15′ W.; depth 238 m.; dynamic height 971.105.						
0.......	7.96	33.25	0......	7.96	33.25	25.93
25......	3.28	33.19	25.....	3.28	33.19	26.44
49......	1.70	33.44	50.....	1.70	33.44	26.77
74......	2.70	33.58	75.....	2.70	33.58	26.80
98......	2.06	33.60	100....	2.00	33.60	26.88
147.....	1.09	33.73	150....	1.10	33.74	27.04
196.....	1.31	33.85	200....	1.50	33.94	27.18
221.....	2.66	34.42				
Station 6754; 25 May; 42°46.5′ N., 50°17′ W.; depth 90 m.; dynamic height 971.137.						
0.......	6.61	32.74	0......	6.61	32.74	25.72
26......	2.63	32.86	25.....	2.90	32.86	26.21
52......	0.97	33.05	50.....	1.05	33.04	26.50
78......	0.51	33.18	75.....	0.55	33.17	26.62
Station 6755; 26 May; 43°17.5′ N., 50°16′ W.; depth 66 m.; dynamic height 971.147.						
0.......	9.16	32.89	0......	9.16	32.89	25.46
26......	4.58	32.86	25.....	4.90	32.86	26.01
52......	1.25	33.02	50.....	1.45	33.00	26.44
Station 6756; 26 May; 43°02′ N., 50°36′ W.; depth 91 m.; dynamic height 971.134.						
0.......	6.93	32.79	0......	6.93	32.79	25.72
25......	3.29	32.88	25.....	3.29	32.88	26.19
51......	1.01	33.03	50.....	1.10	33.02	26.47
76......	0.30	33.33	75.....	0.30	33.31	26.75
Station 6757; 25 May; 42°56′ N., 50°45′ W.; depth 168 m.; dynamic height 971.127.						
0.......	9.52	32.80	0......	9.52	32.80	25.34
25......	6.82	33.44	25.....	6.82	33.44	26.24
50......	6.55	33.86	50.....	6.55	33.86	26.60
75......	4.83	34.00	75.....	4.83	34.00	26.92
99......	7.24	34.39	100....	7.20	34.39	26.93
149.....	4.54	34.24	150....	4.50	34.24	27.15

Observed values			Scaled values			
Depth, meters	Temperature, ° C.	Salinity, °/₀₀	Depth, meters	Temperature, ° C.	Salinity, °/₀₀	σ t
Station 6758; 26 May; 42°49.5′ N., 50°53′ W.; depth 622 m.; dynamic height 971.104.						
0.......	10.50	33.07	0......	10.50	33.07	25.38
25......	6.95	33.53	25.....	6.95	33.53	26.29
50......	3.24	33.42	50.....	3.24	33.42	26.63
75......	2.92	33.52	75.....	2.92	33.52	26.73
100.....	4.05	33.98	100....	4.05	33.98	26.99
150.....	3.71	34.13	150....	3.71	34.13	27.14
200.....	3.52	34.22	200....	3.52	34.22	27.24
300.....	3.30	34.44	300....	3.30	34.44	27.43
405.....	3.13	34.57	400....	3.15	34.56	27.54
598.....	3.84	34.80	600....	3.85	34.80	27.66
Station 6759; 26 May; 42°41.5′ N., 50°01′ W.; depth 1,518 m.; dynamic height 971.129.						
0.......	13.21	33.83	0......	13.21	33.83	25.46
25......	12.13	34.84	25.....	12.13	34.84	26.46
50......	12.17	35.22	50.....	12.17	35.22	26.75
75......	12.00	35.28	75.....	12.00	35.28	26.83
99......	12.02	35.31	100....	12.00	35.31	26.85
149.....	9.94	35.01	150....	9.85	35.00	27.00
199.....	7.20	34.64	200....	7.20	34.64	27.13
298.....	6.45	34.84	300....	6.40	34.84	27.39
397.....	5.48	34.88	400....	5.45	34.88	27.54
593.....	4.20	34.82	600....	4.20	34.82	27.65
787.....	4.05	34.86	800....	4.05	34.86	27.69
986.....	3.81	34.87	1,000..	3.80	34.87	27.73
1,487...	3.54	34.875				
Station 6760; 26 May; 42°30′ N., 51°15′ W.; depth 2,195 m.; dynamic height 971.225.						
0.......	17.36	36.08	0......	17.36	36.08	26.27
25......	15.99	35.98	25.....	15 89	35.98	26.52
50......	15.78	36.07	50.....	15.78	36.07	26.64
75......	15.12	35.94	75.....	15.12	35.94	26.69
99......	14.71	35.84	100....	14.65	35.84	26.71
149.....	13.40	35.62	150....	13.40	35.62	26.81
199.....	12.96	35.58	200....	12.90	35.58	26.88
298.....	10.03	35.22	300....	9.95	35.21	27.15
387.....	7.92	35.02	400....	7.70	35.01	27.35
588.....	5.62	34.98	600....	5.50	34.98	27.62
793.....	4.43	34.905	800....	4.45	34.91	27.69
993.....	4.51	34.975	1,000..	4.50	34.97	27.73
1,496...	3.72	34.91	(1,500).	3.70	34.91	27.76
Station 6761; 26 May; 42°14.5′ N., 51°41′ W.; depth 3,109 m.; dynamic height 971.238.						
0.......	17.71	36.06	0......	17.71	36.06	26.17
25......	15.64	35.94	25.....	15.64	35.94	26.56
51......	15.16	35.94	50.....	15.15	35.94	26.69
76......	14.55	35.83	75.....	14.55	35.84	26.73
102.....	13.83	35.69	100....	13.85	35.70	26.78
152.....	13.47	35.64	150....	13.45	35.64	26.81
203.....	13.19	35.62	200....	13.20	35.62	26.85
305.....	10.86	35.34	300....	11.00	35.35	27.07
376.....	8.84	35.11	400....	8.25	35.06	27.30
568.....	5.70	34.96	600....	5.50	34.96	27.60
761.....	4.79	34.97	800....	4.70	34.97	27.71
954.....	4.33	34.96	1,000..	4.30	34.96	27.74
1,444...	3.79	34.93				

TABLE OF OCEANOGRAPHIC DATA—Continued

STATIONS OCCUPIED IN 1958—Continued

Station 6762; 26 May; 41°59.5′ N., 51°59′ W.; depth 3,749 m.; dynamic height 971.045.

Observed values			Scaled values			
Depth, meters	Temperature, ° C.	Salinity, ‰	Depth, meters	Temperature, ° C.	Salinity, ‰	σ t
0	15.23	34.03	0	15.23	34.03	25.19
27	7.91	34.44	25	8.45	34.42	26.77
53	6.25	34.40	50	6.45	34.41	27.05
80	1.98	34.02	75	2.65	34.06	27.19
106	3.46	34.29	100	3.10	34.23	27.28
160	3.60	34.38	150	3.60	34.37	27.35
213	3.31	34.40	200	3.40	34.40	27.39
319	2.55	34.34	300	2.65	34.35	27.42
405	4.40	34.76	400	4.35	34.75	27.57
604	4.57	34.905	600	4.55	34.90	27.67
800	4.53	34.93	800	4.55	34.93	27.69
1,007	4.60	34.97	1,000	4.60	34.97	27.72
1,533	3.70	34.92	1,500	3.75	34.92	27.77

Station 6763; 27 May; 42°00′ N., 51°02′ W.; depth 3,200 m.; dynamic height 971.190.

Observed values			Scaled values			
Depth, meters	Temperature, ° C.	Salinity, ‰	Depth, meters	Temperature, ° C.	Salinity, ‰	σ t
0	16.95	35.93	0	16.95	35.93	26.25
25	16.03	36.03	25	16.03	36.03	26.55
50	14.45	35.78	50	14.45	35.78	26.71
74	13.94	35.70	75	13.95	35.70	26.75
99	13.76	35.68	100	13.75	35.68	26.78
149	13.40	35.64	150	13.40	35.64	26.82
198	12.97	35.58	100	12.90	35.57	26.88
297	9.48	35.16	300	9.40	35.15	27.19
418	6.62	34.98	400	6.95	35.00	27.45
623	3.88	34.76	600	4.00	34.78	27.63
826	3.90	34.845	800	3.90	34.84	27.69
1,034	3.70	34.86	1,000	3.75	34.86	27.72
1,552	3.52	34.88	1,500	3.55	34.88	27.75

Station 6764; 27 May; 42°00′ N., 49°27′ W.; depth 3,292 m.; dynamic height 971.065.

Observed values			Scaled values			
Depth, meters	Temperature, ° C.	Salinity, ‰	Depth, meters	Temperature, ° C.	Salinity, ‰	σ t
0	12.42	33.26	0	12.42	33.26	25.17
25	9.77	34.40	25	9.77	34.40	26.54
51	9.10	34.35	50	9.10	34.35	26.61
76	5.91	34.06	75	5.95	34.06	26.84
102	8.20	34.64	100	8.15	34.64	26.99
152	3.99	34.18	150	4.15	34.19	27.15
203	2.30	34.18	200	2.30	34.18	27.31
305	4.84	34.76	300	4.80	34.74	27.51
388	4.21	34.79	400	4.20	34.79	27.62
579	3.97	34.84	600	3.95	34.84	27.68
769	3.78	34.86	800	3.80	34.87	27.73
970	4.06	34.93	1,000	4.05	34.93	27.74
1,484	3.68	34.92				

Station 6765; 27 May; 41°32′ N., 48°56′ W.; depth 3,109 m.; dynamic height 971.252.

Observed values			Scaled values			
Depth, meters	Temperature, ° C.	Salinity, ‰	Depth, meters	Temperature, ° C.	Salinity, ‰	σ t
0	18.24	36.17	0	18.24	36.17	26.12
25	15.99	36.04	25	15.99	36.04	26.56
50	15.60	36.02	50	15.60	36.02	26.63
75	15.35	36.01	75	15.35	36.01	26.69
101	15.18	35.98	100	15.20	35.98	26.70
151	14.24	35.77	150	14.25	35.77	26.75
201	13.43	34.64	200	13.45	35.64	26.81
302	10.61	35.30	300	10.65	35.31	27.10
404	8.15	35.05	400	8.45	35.06	27.30
603	5.09	34.89	600	5.10	34.89	27.59
800	4.49	34.92	800	4.50	34.92	27.69
1,002	4.15	34.915	1,000	4.15	34.915	27.72
1,511	3.52	34.88				

Station 6766; 27 May; 41°04′ N., 48°31′ W.; depth 3,383 m.; dynamic height 971.302.

Observed values			Scaled values			
Depth, meters	Temperature, ° C.	Salinity, ‰	Depth, meters	Temperature, ° C.	Salinity, ‰	σ t
0	18.14	36.11	0	18.14	36.11	26.10
23	15.81	36.04	25	15.75	36.04	26.62
46	15.49	36.02	50	15.45	36.01	26.67
68	15.22	35.99	75	15.20	35.99	26.70
91	15.24	36.00	100	15.10	35.97	26.72
137	14.15	35.76	150	13.80	35.69	26.78
182	13.21	35.55	200	13.20	35.55	26.80
274	13.16	35.58	300	12.90	35.56	26.87
326	12.37	35.52	400	9 40	35.18	27.21
485	5.84	34.81	600	3.55	34.61	27.54
640	3.32	34.60	800	3.95	34.78	27.63
817	4.00	34.79	1,000	3.85	34.82	27.68
1,287	3.70	34.87				

Station 6767; 27 May; 41°00.5′ N., 47°39′ W.; depth 3,365 m.; dynamic height 971.197.

Observed values			Scaled values			
Depth, meters	Temperature, ° C.	Salinity, ‰	Depth, meters	Temperature, ° C.	Salinity, ‰	σ t
0	17.96	36.10	0	17.96	36.10	26.14
27	15.35	35.79	25	15.55	35.80	26.48
53	14.33	35.74	50	14.45	35.74	26.68
80	13.88	35 69	75	13.95	35.70	26.75
107	13.65	35.66	100	13.70	35.67	26.79
161	13.40	35.64	150	13.45	35.64	26.81
214	11.70	35.34	200	12.35	35.43	26.87
321	3.87	34.22	300	5.35	34.43	27.20
344	6.00	34.60	400	5.00	34.61	27.39
503	3.37	34.63	600	4.15	34.79	27.62
654	4.39	34.875	800	4.40	34.94	27.71
825	4.38	34.94	1,000	4.20	34.93	27.73
1,263	3.83	34.895				

Station 6768; 28 May; 41°39.5′ N., 47°15′ W.; depth 4,097 m.; dynamic height 971.050.

Observed values			Scaled values			
Depth, meters	Temperature, ° C.	Salinity, ‰	Depth, meters	Temperature, ° C.	Salinity, ‰	σ t
0	13.39	33.29	0	13.39	33.29	25.00
22	8.27	33.38	25	7.75	33.39	26.06
45	4.67	33.53	50	4.40	33.57	26.64
67	3.78	33.80	75	3.55	33.85	26.93
89	3.13	33.94	100	2.95	33.99	27.10
134	2.78	34.19	150	3.20	34.31	27.34
179	3.99	34.51	200	4.05	34.55	27.44
268	4.30	34.68	300	4.50	34.74	27.54
406	5.35	34.955	400	5.30	34.95	27.62
605	4.73	34.97	600	4.75	34.97	27.70
804	4.41	34.97	800	4.45	34.97	27.74
1,011	3.99	34.925	1,000	4.00	34.93	27.75
1,535	3.63	34.91				

Station 6769; 28 May; 42°00′ N., 47°48′ W.; depth 3,667 m.; dynamic height 971.011.

Observed values			Scaled values			
Depth, meters	Temperature, ° C.	Salinity, ‰	Depth, meters	Temperature, ° C.	Salinity, ‰	σ t
0	12.97	33.44	0	12.97	33.44	25.21
25	6.25	33.45	25	6.25	33.45	26.32
50	3.13	33.69	50	3.13	33.69	26.85
75	3.44	33.98	75	3.44	33.98	27.05
100	3.95	34.19	100	3.95	34.19	27.17
150	3.59	34.36	150	3.59	34.36	27.34
199	4.59	34.67	200	4.60	34.67	27.48
299	5.17	34.91	300	5.15	34.91	27.61
412	4.90	34.94	400	4.95	34.94	27.65
616	4.25	34.93	600	4.30	34.93	27.71
818	4.03	34.93	800	4.05	34.93	27.74
1,025	3.75	34.91	1,000	3.75	34.91	27.76
1,545	3.50	34.90				

STATIONS OCCUPIED IN 1958—Continued

Station 6770; 28 May; 42°25′ N., 48°34′ W.; depth 3,246 m.; dynamic height 971.022.

Observed values			Scaled values			
Depth, meters	Temperature, ° C.	Salinity, ‰	Depth, meters	Temperature, ° C.	Salinity, ‰	σ t
0	12.92	33.44	0	12.92	33.44	25.22
25	6.89	33.56	25	6.89	33.56	26.32
50	5.39	34.10	50	5.39	34.10	26.94
75	4.86	34.15	75	4.86	34.15	27.04
100	4.78	34.24	100	4.78	34.24	27.12
150	4.70	34.42	150	4.70	34.42	27.27
200	5.03	34.63	200	5.03	34.63	27.40
300	4.15	34.70	300	4.15	34.70	27.55
402	4.97	34.93	400	4.95	34.93	27.64
598	4.40	34.95	600	4.40	34.95	27.72
791	3.95	34.92	800	3.95	34.92	27.75
993	3.41	34.86	1,000	3.40	34.86	27.76
1,505	3.36	34.87				

Station 6771; 28 May; 42°52′ N., 49°18′ W.; depth 1,643 m.; dynamic height 971.023.

Observed values			Scaled values			
Depth, meters	Temperature, ° C.	Salinity, ‰	Depth, meters	Temperature, ° C.	Salinity, ‰	σ t
0	11.80	33.08	0	11.80	33.08	25.16
25	9.22	33.54	25	9.22	33.54	25.96
49	7.20	33.81	50	7.05	33.81	26.50
74	3.66	33.99	75	3.60	34.00	27.05
98	3.26	34.16	100	3.25	34.17	27.22
148	3.63	34.44	150	3.65	34.45	27.40
197	3.79	34.58	200	3.80	34.58	27.49
295	4.55	34.82	300	4.55	34.82	27.61
403	4.37	34.86	400	4.40	34.86	27.65
601	3.82	34.86	600	3.85	34.86	27.71
796	3.58	34.85	800	3.60	34.85	27.73
997	3.47	34.84	1,000	3.45	34.84	27.73
1,503	3.43	34.87				

Station 6772; 28 May; 43°17′ N., 48°46′ W.; depth 1,866 m.; dynamic height 971.039.

Observed values			Scaled values			
Depth, meters	Temperature, ° C.	Salinity, ‰	Depth, meters	Temperature, ° C.	Salinity, ‰	σ t
0	8.80	32.59	0	8.80	32.59	25.29
25	1.78	32.76	25	1.78	32.76	26.22
49	0.11	33.18	50	0.10	33.23	26.70
74	5.19	34.16	75	5.20	34.17	27.02
99	5.88	34.46	100	5.90	34.46	27.16
148	4.97	34.49	150	4.90	34.49	27.30
197	4.60	34.57	200	4.60	34.57	27.40
296	4.88	34.79	300	4.85	34.79	27.54
400	4.62	34.88	400	4.60	34.88	27.64
599	4.16	34.88	600	4.15	34.88	27.69
796	3.59	34.84	800	3.60	34.84	27.72
996	3.49	34.85	1,000	3.50	34.85	27.74
1,500	3.39	34.865				

Station 6773; 29 May; 43°05.5′ N., 48°12′ W.; depth 3,017 m.; dynamic height 970.999.

Observed values			Scaled values			
Depth, meters	Temperature, ° C.	Salinity, ‰	Depth, meters	Temperature, ° C.	Salinity, ‰	σ t
0	14.20	33.44	0	14.20	33.44	24.96
25	7.10	33.62	25	7.10	33.62	26.34
50	6 27	34.27	50	6.27	34.27	26.96
75	6.96	34.61	75	6.96	34.61	27.14
100	5.99	34.59	100	5.99	34.59	27.25
150	4 03	34.50	150	4.03	34.50	27.40
200	4.75	34.73	200	4.75	34.73	27.51
300	4.23	34.79	300	4.23	34.79	27.62
393	4.25	34.84	400	4.25	34.84	27.65
590	3.95	34.87	600	3.95	34.87	27.71
788	3.63	34.86	800	3.65	34.86	27.73
990	3.54	34.87	1,000	3.55	34.87	27.75
1,505	3.37	34.875				

Station 6774; 29 May; 42°52′ N., 47°36′ W.; depth 3,658 m.; dynamic height 971.023.

Observed values			Scaled values			
Depth, meters	Temperature, ° C.	Salinity, ‰	Depth, meters	Temperature, ° C.	Salinity, ‰	σ t
0	14.06	33.25	0	14.06	33.25	24.84
25	4.53	33.51	25	4.53	33.51	26.57
50	4.33	33.89	50	4.33	33.89	26.88
75	6.02	34.42	75	6.02	34.42	27.11
100	5.50	34.47	100	5.50	34.47	27.22
150	6.25	34.74	150	6.25	34.74	27.33
200	5.83	34.77	200	5.83	34.77	27.41
300	5.13	34.84	300	5.13	34.84	27.55
408	5.40	34.99	400	5.40	34.98	27.63
609	4.68	34.98	600	4.70	34.98	27.71
808	4.15	34.94	800	4.15	34.94	27.74
1,011	3.91	34.92	1,000	3.90	34.92	27.76
1,520	3.51	34.90				

Station 6775; 29 May; 42°36.5′ N., 46°52′ W.; depth 4,024 m.; dynamic height 971.274.

Observed values			Scaled values			
Depth, meters	Temperature, ° C.	Salinity, ‰	Depth, meters	Temperature, ° C.	Salinity, ‰	σ t
0	16.83	35.65	0	16.83	35.65	26.07
22	16.01	36.06	25	16.00	36.07	26.59
43	15.89	36.07	50	15.85	36.07	26.63
65	15.70	36.05	75	15.50	36.01	26.66
87	15.22	35.97	100	15.00	35.93	26.70
129	14.59	35.84	150	14.35	35.79	26.74
172	13.96	35.72	200	12.90	35.55	26.86
259	10.74	35.16	300	10.15	35.14	27.05
417	8.82	35.12	400	9.05	35.12	27.22
621	4.00	34.70	600	4.30	34.73	27.56
822	5.00	34.99	800	4.95	34.97	27.68
1,029	4.19	34.93	1,000	4.30	34.94	27.72
1,548	3.66	34.905				

Station 6776; 29 May; 42°17.5′ N., 46°10′ W.; depth 4,755 m.; dynamic height 971.423.

Observed values			Scaled values			
Depth, meters	Temperature, ° C.	Salinity, ‰	Depth, meters	Temperature, ° C.	Salinity, ‰	σ t
0	18.93	36.31	0	18.93	36.28	26.04
25	17.37	36.30	25	17.37	36.30	26.44
50	16.87	36.25	50	16.87	36.25	26.52
75	16.65	36.25	75	16.65	36.25	26.57
101	16.14	36.14	100	16.15	36.14	26.60
150	15.57	36.04	150	15.57	36.04	26.66
200	15.17	35.96	200	15.17	35.96	26.69
301	13.49	35.64	300	13.50	35.64	26.80
361	12.66	35.57	400	12.00	35.48	26.98
543	8.72	35.105	600	7.30	34.99	27.39
726	5.12	34.85	800	5.10	34.90	27.60
918	5.09	34.99	1,000	4.70	34.98	27.71
1,416	3.92	34.92				

Station 6777; 29 May; 42°49′ N., 45°48′ W.; depth 4,727 m.; dynamic height 971.479.

Observed values			Scaled values			
Depth, meters	Temperature, ° C.	Salinity, ‰	Depth, meters	Temperature, ° C.	Salinity, ‰	σ t
0	18.85	36.28	0	18.85	36.28	26.06
25	17.11	36.30	25	17.11	36.30	26.50
51	16.54	36.18	50	16.55	36.18	26.55
76	16.2[illegible]	36.16	75	16.30	36.16	26.59
102	16.11	36.15	100	16.15	36.15	26.61
152	15.84	36.09	150	15.90	36.09	26.62
202	14.90	35.90	200	14.90	35.91	26.71
304	13.40	35.60	300	13.45	35.61	26.79
397	12.99	35.65	400	12.95	35.65	26.92
592	9.26	35.185	600	9.15	35.17	27.25
785	5.73	34.90	800	5.60	34.90	27.54
984	4.92	34.94	1,000	4.90	34.94	27.66
1,489	4.04	34.935				

TABLE OF OCEANOGRAPHIC DATA—Continued

STATIONS OCCUPIED IN 1958—Continued

Observed values			Scaled values			
Depth, meters	Temperature, ° C.	Salinity, ‰	Depth, meters	Temperature, ° C.	Salinity, ‰	σ_t
Station 6778; 29 May; 43°15.5′ N., 45°31′ W.; depth 4,709 m.; dynamic height 971.558.						
0	18.82	36.34	0	18.82	36.34	26.11
23	17.06	36.21	25	17.00	36.21	26.46
47	16.67	36.23	50	16.60	36.23	26.57
71	16.14	36.14	75	16.15	36.14	26.60
95	16.08	36.16	100	16.05	36.15	26.64
142	15.84	36.11	150	15.85	36.11	26.65
189	15.80	36.11	200	15.80	36.11	26.67
284	15.61	36.08	300	15.45	36.05	26.70
370	14.64	35.90	400	14.30	35.84	26.79
561	11.89	35.50	600	11.00	35.40	27.11
757	7.47	35.03	800	6.85	35.03	27.48
959	5.71	35.03	1,000	5.55	35.02	27.65
1,484	3.89	34.90				
Station 6779; 30 May; 43°30′ N., 46°10′ W.; depth 4,572 m.; dynamic height 971.484.						
0	19.06	36.34	0	19.06	36.34	26.05
24	18.24	36.36	25	18.20	36.36	26.28
49	17.52	36.38	50	17.50	36.38	26.47
73	17.27	36.34	75	17.25	36.34	26.50
98	17.04	36.32	100	17.00	36.32	26.55
147	16.04	36.14	150	16.00	36.13	26.63
196	15.79	36.11	200	15.75	36.10	26.67
294	14.65	35.87	300	14.60	35.86	26.74
405	13.31	35.715	400	13.30	35.73	26.91
605	8.67	35.13	600	8.80	35.14	27.28
805	6.00	35.02	800	6.05	35.02	27.58
1,010	4.77	34.975	1,000	4.80	34.98	27.70
1,525	3.85	34.93				
Station 6780; 30 May; 43°41′ N., 46°47′ W.; depth 4,271 m.; dyanmic height 971.338.						
0	18.15	35.77	0	18.15	35.77	25.84
24	16.61	36.17	25	16.55	36.17	26.54
49	16.01	36.08	50	16.00	36.07	26.59
73	15.54	36.02	75	15.55	36.02	26.65
97	15.46	36.03	100	15.45	36.03	26.68
146	14.82	35.90	150	14.75	35.89	26.72
195	13.83	35.70	200	13.75	35.69	26.79
292	12.70	35.54	300	12.55	35.52	26.90
393	10.38	35.28	400	10.20	35.27	27.15
597	6.48	34.94	600	6.40	34.94	27.47
779	5.60	35.04	800	5.50	35.04	27.66
980	4.72	35.02	1,000	4.65	35.01	27.75
1,497	3.75	34.91				
Station 6781; 30 May; 43°55′ N., 47°27′ W.; depth 4,097 m.; dynamic height 971.178.						
0	11.97	33.03	0	11.97	33.03	25.09
24	13.83	35.39	25	13.85	35.44	26.58
48	14.37	35.78	50	14.35	35.78	26.73
71	13.69	35.65	75	13.60	35.64	26.78
95	13.13	35.57	100	12.55	35.54	26.92
142	7.98	34.56	150	7.75	34.53	26.96
190	7.26	34.49	200	7.20	34.50	27.02
285	6.91	34.70	300	6.90	34.73	27.24
416	7.11	35.02	400	7.10	35.01	27.43
621	5.35	35.01	600	5.45	35.01	27.65
825	4.65	34.98	800	4.75	34.98	27.70
1,033	4.12	34.94	1,000	4.20	34.94	27.74
1,556	3.53	34.89				

Observed values			Scaled values			
Depth, meters	Temperature, ° C.	Salinity, ‰	Depth, meters	Temperature, ° C.	Salinity, ‰	σ_t
Station 6782; 30 May; 44°02.5′ N., 47°54′ W.; depth 3,749 m.; dyanmic height 971.024.						
0	14.48	33.55	0	14.48	33.55	24.99
23	7.64	33.42	25	7.50	33.42	26.13
46	6.58	33.81	50	6.40	33.83	26.60
69	5.20	33.91	75	4.60	33.93	26.89
92	3.34	33.97	100	3.30	34.02	27.10
138	3.25	34.34	150	3.45	34.43	27.40
184	4.27	34.64	200	4.30	34.67	27.52
276	4.31	34.77	300	4 40	34.80	27.60
368	4.63	34.88	400	4.60	34.89	27.65
556	4.20	34.91	600	4.15	34.91	27.72
746	3.85	34.89	800	3.80	34.88	27.73
939	3.62	34.875	1,000	3.60	34.88	27.75
1,436	3.47	34.885				
Station 6783; 30 May; 44°06.5′ N., 48°26′ W.; depth 2,926 m.; dynamic height 970.971.						
0	8.97	32.72	0	8.97	32.72	25.36
25	5.69	33.75	25	5.69	33.75	26.63
51	2.84	33.80	50	2.85	33.80	26.96
76	2.62	34.04	75	2.60	34.02	27.16
102	2.56	34.23	100	2.55	34.21	27.32
151	3.17	34.48	150	3.15	34.47	27.47
202	3.63	34.64	200	3.60	34.64	27.56
304	4.04	34.80	300	4.05	34.80	27.64
410	4.02	34.83	400	4.00	34.83	27.67
612	3.68	34.84	600	3.70	34.84	27.71
814	3.55	34.855	800	3.55	34.85	27.73
1,018	3.45	34.85	1,000	3.45	34.85	27.74
1,534	3.39	34.86				
Station 6784; 30 May; 44°08.5′ N., 48°43′ W.; depth 1,646 m.; dynamic height 971.042.						
0	5.99	32.30	0	5.99	32.30	25.44
24	1.80	32.83	25	1.65	32.84	26.29
49	−0.15	33.27	50	−0.15	33.28	26.75
73	0.17	33.48	75	0.20	33.49	26.90
97	0.43	33.72	100	0.45	33.74	27.08
145	1.10	33.95	150	1.20	33.98	27.43
194	2.09	34.28	200	2.20	34.32	27.44
291	4.03	34.74	300	4.00	34.74	27.60
400	3.78	34.73	400	3.80	34.73	27.61
595	4.00	34.835	600	4.00	34.83	27.67
786	3.64	34.84	800	3.65	34.84	27.71
983	3.52	34.845	1,000	3.50	34.84	27.72
1,476	3.47	34.84				
Station 6785; 30 May; 44°09.5′ N., 48°55′ W.; depth 622 m.; dynamic height 971.103.						
0	7.87	32.60	0	7.87	32.60	25.44
25	0.01	32.89	25	0.01	32.89	26.42
51	−0.34	33.10	50	−0.35	33.09	26.59
76	−0.14	33.31	75	−0.15	33.30	26.76
102	0.32	33.64	100	0.30	33.63	27.00
152	0.49	33.78	150	0.50	33.77	27.11
204	0.61	33.88	200	0.60	33.87	27.18
306	1.30	34.13	300	1.20	34.11	27.34
394	3.07	34.55	400	3.15	34.57	27.55
589	3.92	34.84	(600)	3.95	34.84	27.68

TABLE OF OCEANOGRAPHIC DATA—Continued

STATIONS OCCUPIED IN 1958—Continued

Observed values			Scaled values			
Depth, meters	Temperature, ° C.	Salinity, ‰	Depth meters	Temperature, ° C.	Salinity, ‰	σ t
Station 6786; 30–31 May; 44°09.5′ N., 49°04′ W.; depth 188 m.; dynamic height 971.139.						
0	8.72	32.68	0	8.72	32.68	25.37
25	1.52	32.71	25	1.52	32.71	26.19
49	0.74	33.10	50	0.75	33.10	26.55
74	0.75	33.15	75	0.75	33.16	26.60
99	−0.01	33.36	100	0.00	33.36	26.80
148	0.28	33.50	150	0.30	33.50	26.90
Station 6787; 31 May; 44°09′ N., 49°10′ W.; depth 86 m.; dynamic height 971.135.						
0	8.90	32.68	0	8.90	32.68	25.34
25	1.95	32.81	25	1.95	32.81	26.25
49	1.20	33.10	50	1.15	33.10	26.53
74	0.14	33.24	75	0.10	33.24	26.71
Station 6788; 31 May; 44°10′ N., 49°21′ W.; depth 55 m.; dynamic height 971.143.						
0	9.63	32.69	0	9.63	32.69	25.23
20	3.82	32.73	25	2.80	32.75	26.14
46	1.24	32.88	...	1.10	32.90	26.37
Station 6789; 31 May; 44°58′ N., 49°24′ W.; depth 68 m.; dynamic height 971.140.						
0	8.65	32.67	0	8.65	32.67	25.37
25	3.11	32.69	25	3.11	32.69	26.05
51	0.31	33.00	50	0.35	32.98	26.48
Station 6790; 31 May; 44°56.5′ N., 49°01′ W.; depth 91 m.; dynamic height 971.138.						
0	5.97	32.52	0	5.97	32.52	25.62
25	2.92	32.58	25	2.92	32.58	25.99
51	−0.43	32.96	50	−0.35	32.94	26.48
76	−0.55	....	(75)	−0.55	33.07	26.59
Station 6791; 31 May; 44°55′ N., 48°52′ W.; depth 640 m.; dynamic height 971.080.						
0	5.35	32.46	0	5.35	32.46	25.65
25	−0.50	32.84	25	−0.50	32.84	26.41
49	−0.23	33.07	50	−0.20	33.08	26.59
74	−0.26	33.23	75	−0.25	33.24	26.72
98	0.00	33.44	100	0.00	33.45	26.88
147	0.44	33.78	150	0.45	33.79	27.12
196	0.87	33.98	200	0.90	34.00	27.27
294	2.13	34.37	300	2.20	34.39	27.49
382	3.15	34.61	400	3.30	34.64	27.59
584	3.95	34.81	(600)	3.95	34.82	27.67
Station 6792; 31 May; 44°55′ N., 48°38′ W.; depth 1,536 m.; dynamic height 971.007.						
0	7.26	32.48	0	7.26	32.48	25.42
24	5.14	33.52	25	5.10	33.53	26.52
49	4.43	33.68	50	4.40	33.69	26.73
73	3.09	33.88	75	3.00	33.89	27.02
97	1.79	34.01	100	1.90	34.02	27.22
145	4.66	34.58	150	4.65	34.59	27.41
194	3.87	34.60	200	3.85	34.60	27.50
291	3.81	34.71	300	3.85	34.72	27.60
175	4.32	34.61	400	4.00	34.82	27.67
352	4.00	34.78	600	3.80	34.84	27.70
537	3.86	34.845	800	3.65	34.84	27.71
728	3.65	34.84	1,000	3.50	34.85	27.74
1,031	3.48	34.85				
Station 6793; 31 May; 44°55′ N., 48°27′ W.; depth 2,103 m.; dynamic height 971.002.						
0	8.23	32.83	0	8.23	32.83	25.56
26	3.04	33.06	25	3.25	33.04	26.32
52	0.96	33.64	50	1.00	33.60	26.94
78	5.22	34.43	75	4.55	34.32	27.21
104	5.39	34.54	100	5.40	34.53	27.27
155	5.25	34.67	150	5.25	34.66	27.40
207	5.45	34.82	200	5.45	34.80	27.48
311	5.02	34.89	300	5.10	34.89	27.59
410	4.53	34.88	400	4.60	34.88	27.64
614	4.10	34.89	600	4.15	34.89	27.70
818	3.78	34.88	800	3.80	34.88	27.73
1,024	3.62	34.87	1,000	3.65	34.87	27.74
1,537	3.43	34.88				
Station 6794; 31 May; 44°55.5′ N., 47°50′ W.; depth 3,155 m.; dynamic height 970.966.						
0	9.19	32.94	0	9.19	32.94	25.50
26	3.90	33.32	25	4.10	33.29	26.43
52	3.43	34.00	50	3.45	33.95	27.02
78	2.70	34.13	75	2.80	34.12	27.23
104	1.99	34.22	100	2.05	34.21	27.36
155	2.56	34.40	150	2.50	34.39	27.46
206	2.72	34.50	200	2.70	34.49	27.52
310	4.00	34.80	300	3.90	34.78	27.64
400	3.98	34.84	400	4.00	34.84	27.68
602	3.75	34.86	600	3.75	34.86	27.72
805	3.60	....	800	3.60	34.86	27.74
1,009	3.44	34.855	1,000	3.45	34.86	27.75
1,524	3.39	34.87				
Station 6795; 31 May; 44°45.5′ N., 47°09′ W.; depth 3,749 m.; dynamic height 971.054.						
0	14.56	33.70	0	14.56	33.70	25.09
26	10.65	33.78	25	10.80	33.77	25.88
51	7.04	33.98	50	7.05	33.96	26.61
77	7.54	34.51	75	7.50	34.48	26.95
103	7.66	34.72	100	7.65	34.71	27.12
153	1.75	34.14	150	1.80	34.15	27.33
205	1.75	34.26	200	1.75	34.24	27.40
308	6.00	34.97	300	5.80	34.94	27.55
414	4.44	34.84	400	4.60	34.85	27.62
619	4.21	34.90	600	4.25	34.90	27.70
823	3.79	34.88	800	3.85	34.88	27.72
1,032	3.63	34.875	1,000	3.65	34.88	27.74
1,557	3.44	34.88				

TABLE OF OCEANOGRAPHIC DATA—Continued

STATIONS OCCUPIED IN 1958—Continued

Station 6796; 1 June; 44°36.5′ N., 46°31′ W.; depth 3,731 m.; dynamic height 971.068.

Observed values			Scaled values			
Depth, meters	Temperature, °C.	Salinity, °/₀₀	Depth, meters	Temperature, °C.	Salinity, °/₀₀	σt
0	14.60	33.52	0	14.60	33.52	24.94
26	6.93	33.59	25	7.20	33.59	26.30
51	3.65	33.68	50	3.65	33.67	26.79
77	6.72	34.37	75	6.45	34.34	26.99
102	7.40	34.59	100	7.40	34.59	27.06
152	6.26	34.58	150	6.35	34.58	27.19
203	4.98	34.50	200	5.00	34.50	27.30
305	6.22	34.95	300	6.20	34.95	27.51
404	5.24	34.91	400	5.25	34.91	27.60
607	4.98	35.00	600	5.00	35.00	27.70
811	4.30	34.95	800	4.35	34.95	27.73
1,015	3.92	34.92	1,000	3.95	34.92	27.75
1,531	3.57	34.90				

Station 6797; 1 June; 44°26′ N., 45°45′ W.; depth 3,823 m.; dynamic height 971.140.

Observed values			Scaled values			
Depth, meters	Temperature, °C.	Salinity, °/₀₀	Depth, meters	Temperature, °C.	Salinity, °/₀₀	σt
0	10.63	33.40	0	10.63	33.40	25.61
26	7.71	33.50	25	7.70	33.49	26.15
52	9.17	34.49	50	9.15	34.42	26.66
78	8.88	34.70	75	8.90	34.69	26.91
104	8.96	34.77	100	8.95	34.76	26.96
155	8.26	34.70	150	8.30	34.70	27.01
208	9.99	35.24	200	9.85	35.20	27.15
312	5.51	34.60	300	5.85	34.66	27.32
416	5.70	34.88	400	5.70	34.85	27.49
621	5.25	35.01	600	5.35	35.01	27.66
824	4.18	34.91	800	4.30	34.92	27.71
1,033	3.76	34.885	1,000	3.80	34.89	27.74
1,559	3.53	34.885				

Station 6798; 1 June; 44°16′ N., 45°06′ W.; depth 4,353 m.; dynamic height 971.142.

Observed values			Scaled values			
Depth, meters	Temperature, °C.	Salinity, °/₀₀	Depth, meters	Temperature, °C.	Salinity, °/₀₀	σt
0	11.33	33.32	0	11.33	33.32	25.44
26	9.27	33.64	25	9.25	33.62	26.02
51	10.78	34.54	50	10.75	34.53	26.47
77	7.93	34.52	75	8.10	34.53	26.91
102	7.35	34.41	100	7.40	34.42	26.93
153	6.72	34.43	150	6.75	34.43	27.02
204	5.63	34.47	200	5.65	34.46	27.19
306	5.42	34.68	300	5.45	34.66	27.37
396	5.54	34.84	400	5.55	34.84	27.50
595	4.75	34.90	600	4.70	34.90	27.65
795	4.10	34.89	800	4.10	34.89	27.71
997	3.85	34.89	1,000	3.85	34.89	27.73
1,510	3.50	34.88				

Station 6799; 1 June; 44°45′ N., 45°06′ W.; depth 4,024 m.; dynamic height 971.113.

Observed values			Scaled values			
Depth, meters	Temperature, °C.	Salinity, °/₀₀	Depth, meters	Temperature, °C.	Salinity, °/₀₀	σt
0	13.53	33.69	0	13.53	33.69	25.29
26	9.85	33.95	25	9.95	33.94	26.15
51	8.44	34.16	50	8.45	34.15	26.56
77	9.47	34.77	75	9.45	34.77	26.89
102	8.05	34.60	100	8.20	34.61	26.96
153	6.49	34.52	150	6.55	34.52	27.12
204	5.61	34.54	200	5.65	34.53	27.24
306	6.82	34.96	300	6.80	34.95	27.43
400	5.90	34.96	400	5.90	34.96	27.56
604	4.75	34.95	600	4.80	34.95	27.68
811	4.21	34.885	800	4.25	34.89	27.69
1,022	3.70	34.88	1,000	3.75	34.88	27.73
1,560	3.49	34.89				

Station 6800; 1 June; 45°17.5′ N., 45°08′ W.; depth 4,024 m.; dynamic height 971.031.

Observed values			Scaled values			
Depth, meters	Temperature, °C.	Salinity, °/₀₀	Depth, meters	Temperature, °C.	Salinity, °/₀₀	σt
0	12.97	33.85	0	12.97	33.85	25.52
22	9.77	33.98	25	9.50	33.98	26.26
43	8.20	33.95	50	8.15	34.07	26.54
65	7.96	34.45	75	7.05	34.43	26.98
87	6.17	34.38	100	5.70	34.40	27.14
130	5.19	34.50	150	5.10	34.57	27.35
173	5.02	34.64	200	4.90	34.69	27.46
260	4.73	34.75	300	4.60	34.78	27.56
380	4.40	34.82	400	4.35	34.83	27.63
583	4.15	34.88	600	4.10	34.88	27.70
795	3.59	34.84	800	3.60	34.84	27.72
1,004	3.48	34.86	1,000	3.50	34.86	27.75
1,545	3.40	34.87				

Station 6801; 1 June; 45°18.5′ N., 45°45′ W.; depth 3,567 m.; dynamic height 970.983.

Observed values			Scaled values			
Depth, meters	Temperature, °C.	Salinity, °/₀₀	Depth, meters	Temperature, °C.	Salinity, °/₀₀	σt
0	11.65	33.78	0	11.65	33.78	25.73
26	7.14	33.82	25	7.30	33.82	26.47
51	5.81	34.06	50	5.85	34.06	26.85
77	4.80	....	75	4.85	34.12	27.02
102	4.32	34.28	100	4.35	34.27	27.19
152	3.80	34.54	150	3.80	34.53	27.45
203	4.19	34.71	200	4.20	34.70	27.55
305	4.13	34.80	300	4.15	34.80	27.63
362	4.06	34.82	400	4.00	34.83	27.67
558	3.78	34.85	600	3.75	34.85	27.71
764	3.59	34.845	800	3.60	34.85	27.73
970	3.53	34.87	1.000	3.55	34.87	27.75
1,509	3.38	34.87				

Station 6802; 2 June; 45°18.5′ N., 46°32′ W.; depth 3,227 m.; dynamic height 970.964.

Observed values			Scaled values			
Depth, meters	Temperature, °C.	Salinity, °/₀₀	Depth, meters	Temperature, °C.	Salinity, °/₀₀	σt
0	11.13	33.64	0	11.13	33.64	25.71
26	5.85	33.92	25	6.05	33.92	26.72
51	5.10	34.00	50	5.15	34.00	26.89
77	3.96	34.20	75	3.95	34.18	27.16
103	4.85	34.42	100	4.80	34.40	27.24
153	3.52	34.56	150	3.55	34.55	27.49
204	4.41	34.79	200	4.40	34.78	27.58
307	4.02	34.81	300	4.05	34.81	27.65
381	4.02	34.84	400	4.00	34.84	27.68
578	3.75	34.85	600	3.75	34.85	27.71
780	3.64	34.86	800	3.65	34.86	27.73
987	3.46	34.86	1,000	3.45	34.86	27.75
1,528	3.34	34.88				

Station 6803; 2 June; 45°18.5′ N., 47°19′ W.; depth 2,926 m.; dynamic height 970.933.

Observed values			Scaled values			
Depth, meters	Temperature, °C.	Salinity, °/₀₀	Depth, meters	Temperature, °C.	Salinity, °/₀₀	σt
0	7.53	33.06	0	7.53	33.06	25.84
23	3.96	32.99	25	3.75	33.03	26.26
47	2.19	33.61	50	2.20	33.65	26.90
70	2.52	33.83	75	2.25	33.83	27.03
93	1.18	33.82	100	1.30	33.87	27.14
140	2.63	34.24	150	2.85	34.32	27.38
186	3.53	34.55	200	3.65	34.60	27.52
279	3.91	34.74	300	3.90	34.76	27.63
400	3.95	34.82	400	3.95	34.82	27.67
598	4.09	34.895	600	4.10	34.89	27.71
796	3.78	34.885	800	3.80	34.88	27.73
1,000	3.48	34.865	1,000	3.50	34.87	27.76
1,521	3.40	34.88				

TABLE OF OCEANOGRAPHIC DATA—Continued

STATIONS OCCUPIED IN 1958—Continued

Station 6804; 2 June; 45°30.5′ N., 47°41′ W.; depth 1,518 m.; dynamic height 970.982.

Observed values			Scaled values			
Depth, meters	Temperature, ° C.	Salinity, ‰	Depth, meters	Temperature, ° C.	Salinity, ‰	σ_t
0	6.91	32.91	0	6.91	33.91	25.80
23	5.58	33.12	25	5.30	33.18	26.22
47	2.64	33.81	50	2.45	33.83	27.01
70	1.24	33.96	75	1.35	34.00	27.24
93	1.88	34.15	100	1.85	34.17	27.34
139	1.70	34.27	150	1.80	34.30	27.45
186	2.33	34.41	200	2.55	34.46	27.52
279	3.61	34.69	300	3.75	34.73	27.61
404	4.11	34.84	400	4.10	34.84	27.67
607	3.85	34.855	600	3.85	34.85	27.70
811	3.61	34.85	800	3.65	34.85	27.72
1,014	3.55	34.865	1,000	3.55	34.86	27.74
1,473	3.41	34.87				

Station 6805; 2 June; 45°41.5′ N., 48°00′ W.; depth 640 m.; dynamic height 971.077.

Observed values			Scaled values			
Depth, meters	Temperature, ° C.	Salinity, ‰	Depth, meters	Temperature, ° C.	Salinity, ‰	σ_t
0	5.43	....	0	5.43	32.59	25.74
25	−0.03	32.79	25	−0.03	32.79	26.35
50	−0.70	32.98	50	−0.70	32.98	26.53
75	−0.33	33.24	75	−0.33	33.24	26.72
99	−0.05	33.42	100	−0.05	33.42	26.86
149	0.28	33.60	150	0.30	33.60	26.98
199	0.66	33.90	200	0.70	33.91	27.21
298	3.30	34.62	300	3.30	34.62	27.58
378	3.56	34.70	400	3.65	34.72	27.62
570	3.95	34.83	(600)	4.00	34.84	27.68

Station 6806; 2 June; 45°48′ N., 48°11′ W.; depth 169 m.; dynamic height 971.129.

Observed values			Scaled values			
Depth, meters	Temperature, ° C.	Salinity, ‰	Depth, meters	Temperature, ° C.	Salinity, ‰	σ_t
0	5.41	32.47	0	5.41	32.47	25.65
25	2.41	32.60	25	2.41	32.60	26.05
50	0.12	32.77	50	0.12	32.77	26.33
75	−0.79	32.92	75	−0.79	32.92	26.48
101	−0.57	33.06	100	−0.60	33.05	26.58
151	−0.20	33.32	150	−0.20	33.31	26.77

Station 6807; 2 June; 45°52.5′ N., 48°19′ W.; depth 110 m.; dynamic height 971.123.

Observed values			Scaled values			
Depth, meters	Temperature, ° C.	Salinity, ‰	Depth, meters	Temperature, ° C.	Salinity, ‰	σ_t
0	5.35	32.43	0	5.35	32.43	25.63
25	4.42	32.51	25	4.42	32.51	25.78
50	−0.15	32.93	50	−0.15	32.93	26.47
75	0.12	33.09	75	0.12	33.09	26.58
100	−0.30	33.22	100	−0.30	33.22	26.70

Station 6808; 2 June; 45°59′ N., 48°29′ W.; depth 97 m.; dynamic height 971.122.

Observed values			Scaled values			
Depth, meters	Temperature, ° C.	Salinity, ‰	Depth, meters	Temperature, ° C.	Salinity, ‰	σ_t
0	7.31	32.56	0	7.31	32.56	25.48
26	2.95	32.62	25	3.10	32.62	26.00
51	0.94	32.76	50	1.00	32.75	26.26
77	−0.32	33.19	75	−0.25	33.16	26.65

Station 6809; 2 June; 46°07.5′ N., 48°44′ W.; depth 77 m.; dynamic height 971.121.

Observed values			Scaled values			
Depth, meters	Temperature, ° C.	Salinity, ‰	Depth, meters	Temperature, ° C.	Salinity, ‰	σ_t
0	7.14	32.57	0	7.14	32.57	25.52
26	3.21	32.65	25	3.35	32.65	26.00
52	0.89	32.77	50	1.10	32.75	26.26
67	0.07	33.08	(75)	−0.25	33.20	26.69

Station 6810; 2 June; 46°16.5′ N., 48°59′ W.; depth 68 m.; dynamic height 971.125.

Observed values			Scaled values			
Depth, meters	Temperature, ° C.	Salinity, ‰	Depth, meters	Temperature, ° C.	Salinity, ‰	σ_t
0	7.31	32.59	0	7.31	32.59	25.51
26	3.64	32.64	25	3.80	32.64	25.96
53	1.98	32.76	50	2.10	32.74	26.18

Station 6811; 2 June; 46°15′ N., 48°27′ W.; depth 89 m.; dynamic height 971.121.

Observed values			Scaled values			
Depth, meters	Temperature, ° C.	Salinity, ‰	Depth, meters	Temperature, ° C.	Salinity, ‰	σ_t
0	6.98	32.57	0	6.98	32.57	25.54
25	3.02	32.64	25	3.02	32.64	26.03
51	1.62	32.72	50	1.70	32.71	26.18
76	−0.18	33.11	75	−0.15	33.09	26.59

Station 6812; 2–3 June; 46°13′ N., 47°57′ W.; depth 115 m.; dynamic height 971.118.

Observed values			Scaled values			
Depth, meters	Temperature, ° C.	Salinity, ‰	Depth, meters	Temperature, ° C.	Salinity, ‰	σ_t
0	7.02	32.55	0	7.02	32.55	25.51
25	2.92	32.62	25	2.92	32.62	26.02
51	0.30	32.80	50	0.35	32.79	26.33
76	−0.33	33.06	75	−0.30	33.05	26.56
102	−0.35	33.28	100	−0.35	33.26	26.73

Station 6813; 3 June; 46°12′ N., 47°38′ W.; depth 169 m.; dynamic height 971.121.

Observed values			Scaled values			
Depth, meters	Temperature, ° C.	Salinity, ‰	Depth, meters	Temperature, ° C.	Salinity, ‰	σ_t
0	6.01	32.51	0	6.01	32.51	25.61
25	2.09	32.59	25	2.09	32.59	26.06
50	−0.08	32.82	50	−0.08	32.82	26.37
75	−0.63	32.96	75	−0.63	32.96	26.51
100	−0.57	33.08	100	−0.57	33.08	26.60
150	0.02	33.46	150	0.02	33.46	26.89

Station 6814; 3 June; 46°11′ N., 47°16′ W.; depth 622 m.; dynamic height 971.091.

Observed values			Scaled values			
Depth, meters	Temperature, ° C.	Salinity, ‰	Depth, meters	Temperature, ° C.	Salinity, ‰	σ_t
0	5.08	32.36	0	5.08	32.36	25.60
26	1.21	32.59	25	1.35	32.58	26.11
51	−0.49	32.86	50	−0.40	32.84	26.41
77	−0.70	32.99	75	−0.70	32.97	26.52
103	−0.39	33.24	100	−0.45	33.20	26.70
153	0.40	33.80	150	0.35	33.77	27.12
205	1.36	34.15	200	1.25	34.12	27.35
308	2.68	34.50	300	2.60	34.47	27.52
378	3.51	34.71	400	3.60	34.73	27.63
575	3.81	34.80	(600)	3.85	34.81	27.67

TABLE OF OCEANOGRAPHIC DATA—Continued

STATIONS OCCUPIED IN 1958—Continued

Station 6815; 3 June; 46°10′ N., 46°58′ W.; depth 1,463 m.; dynamic height 971.021.

Observed values			Scaled values			
Depth, meters	Temperature, ° C.	Salinity, ‰	Depth, meters	Temperature, ° C.	Salinity, ‰	σt
0	5.42	32.30	0	5.42	32.30	25.51
25	1.94	32.84	25	1.94	32.84	26.27
49	0.33	33.16	50	0.30	33.18	26.65
74	0.18	33.52	75	0.20	33.53	26.93
98	0.34	33.77	100	0.40	33.80	27.14
147	1.35	34.17	150	1.40	34.18	27.38
196	1.95	34.32	200	2.00	34.33	27.45
294	3.14	34.63	300	3.20	34.64	27.60
386	3.75	34.76	400	3.80	34.77	27.65
581	3.90	34.84	600	3.90	34.84	27.69
779	3.68	34.845	800	3.65	34.85	27.72
980	3.56	34.85	1,000	3.55	34.85	27.73
1,390	3.45	34.86				

Station 6816; 3 June; 46°08′ N., 46°28′ W.; depth 1,097 m.; dynamic height 970.947.

Observed values			Scaled values			
Depth, meters	Temperature, ° C.	Salinity, ‰	Depth, meters	Temperature, ° C.	Salinity, ‰	σt
0	9.75	33.51	0	9.75	33.51	25.85
24	5.94	33.89	25	5.90	33.90	26.72
48	4.76	34.04	50	4.50	34.05	27.00
72	2.93	34.19	75	2.95	34.21	27.28
96	3.75	34.44	100	3.85	33.49	27.41
144	4.71	34.72	150	4.70	34.73	27.51
193	4.59	34.80	200	4.55	34.80	27.59
289	4.12	34.81	300	4.10	34.81	27.65
365	4.18	34.86	400	4.15	34.86	27.68
558	3.76	34.865	600	3.70	34.86	27.73
743	3.61	34.855	800	3.60	34.85	27.73
943	3.50	34.85	1,000	3.50	34.85	27.74

Station 6817; 3 June; 46°06.5′ N., 45°57′ W.; depth 1,829 m.; dynamic height 970.956.

Observed values			Scaled values			
Depth, meters	Temperature, ° C.	Salinity, ‰	Depth, meters	Temperature, ° C.	Salinity, ‰	σt
0	11.95	33.90	0	11.95	33.90	25.76
26	6.15	33.94	25	6.35	33.94	26.69
52	5.56	34.02	50	5.60	34.01	26.84
78	3.39	34.26	75	3.45	34.23	27.24
103	3.42	34.43	100	3.40	34.42	27.41
154	3.70	34.63	150	3.70	34.62	27.54
206	3.93	34.76	200	3.95	34.75	27.61
309	3.86	34.80	300	3.85	34.80	27.66
400	3.79	34.81	400	3.80	34.81	27.68
602	3.64	34.83	600	3.65	34.83	27.70
805	3.60	34.84	800	3.60	34.84	27.72
1,010	3.51	34.85	1,000	3.50	34.85	27.74
1,529	3.39	34.87				

Station 6818; 3 June; 46°04′ N., 45°17′ W.; depth 2,743 m.; dynamic height 970.976.

Observed values			Scaled values			
Depth, meters	Temperature, ° C.	Salinity, ‰	Depth, meters	Temperature, ° C.	Salinity, ‰	σt
0	12.17	33.57	0	12.17	33.57	25.46
25	5.50	33.69	25	5.50	33.69	26.60
49	4.45	33.84	50	4.40	33.85	26.85
74	4.14	34.24	75	4.15	34.25	27.20
98	4.41	34.44	100	4.40	34.45	27.33
147	4.62	34.63	150	4.60	34.63	27.44
196	4.01	34.67	200	4.00	34.67	27.55
294	3.89	34.78	300	3.90	34.78	27.64
387	3.83	34.80	400	3.85	34.80	27.66
581	3.79	34.845	600	3.75	34.85	27.71
774	3.57	34.85	800	3.55	34.85	27.73
971	3.46	34.85	1,000	3.45	34.85	27.74
1,465	3.36	34.87				

Station 6819; 3 June; 46°02.5′ N., 44°41′ W.; depth 3,658 m.; dynamic height 971.050.

Observed values			Scaled values			
Depth, meters	Temperature, ° C.	Salinity, ‰	Depth, meters	Temperature, ° C.	Salinity, ‰	σt
0	13.78	33.91	0	13.78	33.91	25.41
25	9.91	33.96	25	9.91	33.96	26.18
50	8.66	34.09	50	8.66	34.09	26.48
75	7.73	34.50	75	7.73	34.50	26.94
100	6.26	34.39	100	6.26	34.39	27.06
150	5.94	34.56	150	5.94	34.56	27.23
199	5.02	34.62	200	5.00	34.62	27.40
299	4.85	34.80	300	4.85	34.80	27.55
397	4.73	34.88	400	4.75	34.88	27.62
593	3.97	34.86	600	3.95	34.86	27.70
788	3.64	34.86	800	3.65	34.86	27.73
988	3.66	34.895	1,000	3.65	34.89	27.75
1,492	3.38	34.88				

Station 6820; 4 June; 46°23′ N., 44°42′ W.; depth 1,829 m.; dynamic height 970.980.

Observed values			Scaled values			
Depth, meters	Temperature, ° C.	Salinity, ‰	Depth, meters	Temperature, ° C.	Salinity, ‰	σt
0	13.35	33.85	0	13.35	33.85	25.45
25	7.84	33.98	25	7.84	33.98	26.51
50	5.42	33.92	50	5.42	33.92	26.79
75	5.05	34.28	75	5.05	34.28	27.12
100	4.00	34.35	100	4.00	34.35	27.29
150	5.38	34.73	150	5.38	34.73	27.44
200	5.00	34.79	200	5.00	34.79	27.53
300	4.18	34.82	300	4.18	34.82	27.65
387	4.06	34.84	400	4.05	34.84	27.67
583	3.87	34.865	600	3.85	34.86	27.71
782	3.61	34.855	800	3.60	34.86	27.74
982	3.50	34.86	1,000	3.50	34.86	27.75
1,487	3.42	34.875				

Station 6821; 4 June; 46°29′ N., 44°42′ W.; depth 612 m.; dynamic height 970.957.

Observed values			Scaled values			
Depth, meters	Temperature, ° C.	Salinity, ‰	Depth, meters	Temperature, ° C.	Salinity, ‰	σt
0	11.74	33.77	0	11.74	33.77	25.70
25	5.78	33.75	25	5.78	33.75	26.61
49	5.67	34.16	50	5.65	34.17	26.96
74	5.42	34.38	75	5.40	34.39	27.15
98	4.50	34.44	100	4.50	34.45	27.32
147	4.42	34.63	150	4.35	34.63	27.47
196	3.45	34.66	200	3.45	34.66	27.59
294	3.89	34.78	300	3.90	34.79	27.65
394	3.91	34.84	400	3.90	34.84	27.69
593	3.67	34.85	600	3.65	34.85	27.72

Station 6822; 4 June; 46°37′ N., 44°42′ W.; depth 229 m.; dynamic height 970.956.

Observed values			Scaled values			
Depth, meters	Temperature, ° C.	Salinity, ‰	Depth, meters	Temperature, ° C.	Salinity, ‰	σt
0	12.18	33.79	0	12.18	33.79	25.64
26	5.84	33.81	25	6.10	33.81	26.63
52	4.42	33.98	50	4.55	33.96	26.92
78	3.33	34.20	75	3.35	34.18	27.21
103	3.36	34.30	100	3.35	34.28	27.29
154	3.71	34.62	150	3.70	34.60	27.52
206	3.76	34.71	200	3.75	34.70	27.59

TABLE OF OCEANOGRAPHIC DATA—Continued

STATIONS OCCUPIED IN 1958—Continued

Station 6823; 4 June; 46°44′ N., 44°42′ W.; depth 169 m.; dynamic height 970.067.

Observed values			Scaled values			
Depth, meters	Temperature, ° C.	Salinity, ‰	Depth, meters	Temperature, ° C.	Salinity, ‰	σt
0.......	10.50	33.58	0......	10.50	33.58	25.77
25......	5.16	33.85	25.....	5.16	33.85	26.77
50......	5.22	34.04	50.....	5.22	34.04	26.91
75......	4.34	33.99	75.....	4.34	33.99	26.96
101.....	3.43	34.10	100....	3.45	34.09	27.13
151.....	3.63	34.52	150....	3.65	34.51	27.45

Station 6824; 4 June; 46°54.5′ N., 44°42′ W.; depth 150 m.; dynamic height 970.965.

Observed values			Scaled values			
Depth, meters	Temperature, ° C.	Salinity, ‰	Depth, meters	Temperature, ° C.	Salinity, ‰	σt
0.......	10.44	33.71	0......	10.44	33.71	25.89
24......	6.74	33.98	25.....	6.65	33.98	26.68
49......	5.44	34.01	50.....	5.40	34.01	26.87
73......	4.73	34.04	75.....	4.65	34.05	26.98
97......	3.89	34.24	100....	3.85	34.25	27.23
136.....	3.63	34.37	(150)...	3.60	34.41	27.38

Station 6825; 4 June; 46°54.5′ N., 44°59′ W.; depth 201 m.; dynamic height 970.958.

Observed values			Scaled values			
Depth, meters	Temperature, ° C.	Salinity, ‰	Depth, meters	Temperature, ° C.	Salinity, ‰	σt
0.......	10.81	33.94	0......	10.81	33.94	26.00
25......	6.38	33.97	25.....	6.38	33.97	26.71
50......	5.46	34.03	50.....	5.46	34.03	26.87
75......	4.30	34.05	75.....	4.30	34.05	27.02
101.....	3.63	34.13	100....	3.65	34.12	27.15
151.....	3.61	34.55	150....	3.60	34.54	27.48
191.....	3.67	34.63	(200)...	3.70	34.64	27.55

Station 6826; 4 June; 46°54′ N., 45°06′ W.; depth 226 m.; dynamic height 970.963.

Observed values			Scaled values			
Depth, meters	Temperature, ° C.	Salinity, ‰	Depth, meters	Temperature, ° C.	Salinity, ‰	σt
0.......	11.16	33.90	0......	11.16	33.90	25.91
24......	8.45	33.94	25.....	8.35	33.94	26.41
48......	5.70	34.00	50.....	5.50	34.00	26.84
71......	4.47	34.03	75.....	4.20	34.04	27.02
95......	3.38	34.15	100....	3.35	34.18	27.21
142.....	3.21	34.44	150....	3.25	34.49	27.47
190.....	3.76	34.70	200....	3.80	34.75	27.63

Station 6827; 4 June; 46°53′ N., 45°32′ W.; depth 284 m.; dynamic height 970.960.

Observed values			Scaled values			
Depth, meters	Temperature, ° C.	Salinity, ‰	Depth, meters	Temperature, ° C.	Salinity, ‰	σt
0.......	11.67	33.89	0......	11.67	33.89	25.81
25......	6.70	33.92	25.....	6.70	33.92	26.63
50......	5.11	33.95	50.....	5.11	33.95	26.85
75......	4.21	34.07	75.....	4.21	34.07	27.05
100.....	3.34	34.19	100....	3.34	34.19	27.22
149.....	3.62	34.53	150....	3.65	34.54	27.47
199.....	3.81	34.70	200....	3.80	34.70	27.59
269.....	3.87	34.76	300....	3.85	34.78	27.64

Station 6828; 4 June; 46°52.5′ N., 45°54′ W.; depth 320 m.; dynamic height 970.972.

Observed values			Scaled values			
Depth, meters	Temperature, ° C.	Salinity, ‰	Depth, meters	Temperature, ° C.	Salinity, ‰	σt
0.......	11.07	33.91	0......	11.07	33.91	25.93
25......	8.10	33.89	25.....	8.10	33.89	26.40
50......	5.89	33.91	50.....	5.89	33.91	26.73
75......	4.54	33.98	75.....	4.54	33.98	26.94
100.....	3.31	34.10	100....	3.31	34.10	27.16
150.....	3.70	34.54	150....	3.70	34.54	27.47
199.....	3.93	34.71	200....	3.95	34.71	27.58
299.....	3.90	34.80	300....	3.90	34.80	27.66

Station 6829; 4 June; 46°51.5′ N., 46°22′ W.; depth 620 m.; dynamic height 970.946.

Observed values			Scaled values			
Depth, meters	Temperature, ° C.	Salinity, ‰	Depth, meters	Temperature, ° C.	Salinity, ‰	σt
0.......	10.96	....	0......	10.96	33.91	25.96
25......	5.97	33.91	25.....	5.97	33.91	26.72
50......	5.09	33.94	50.....	5.09	33.94	26.85
75......	3.56	34.11	75.....	3.56	34.11	27.15
100.....	3.37	34.32	100....	3.37	34.32	27.33
150.....	3.93	34.63	150....	3.93	34.63	27.52
200.....	3.90	34.72	200....	3.90	34.72	27.60
300.....	3.88	34.80	300....	3.88	34.80	27.66
398.....	3.71	34.82	400....	3.70	34.82	27.70
597.....	3.53	34.85	600....	3.55	34.85	27.73

Station 6830; 4 June; 46°50.5′ N., 46°45′ W.; depth 1,207 m.; dynamic height 970.993.

Observed values			Scaled values			
Depth, meters	Temperature, ° C.	Salinity, ‰	Depth, meters	Temperature, ° C.	Salinity, ‰	σt
0.......	8.57	82.99	0......	8.57	32.99	25.64
24......	3.47	33.38	25.....	3.40	33.39	26.58
48......	1.87	33.76	50.....	1.75	33.76	27.02
73......	0.72	33.86	75.....	0.75	33.88	27.18
97......	2.40	34.13	100....	2.40	34.14	27.27
145.....	1.46	34.20	150....	1.45	34.21	27.40
193.....	2.02	34.36	200....	2.10	34.38	27.48
290.....	3.32	34.64	300....	3.40	34.66	27.60
388.....	3.78	34.77	400....	3.80	34.78	27.65
583.....	3.87	34.83	600....	3.85	34.83	27.68
780.....	3.66	34.84	800....	3.65	34.84	27.71
980.....	3.51	34.84	1,000..	3.50	34.84	27.73
1,132...	3.41	34.85				

Station 6831; 4 June; 46°50.5′ N., 47°04′ W.; depth 713 m.; dynamic height 971.033.

Observed values			Scaled values			
Depth, meters	Temperature, ° C.	Salinity, ‰	Depth, meters	Temperature, ° C.	Salinity, ‰	σt
0.......	4.86	32.36	0......	5.86	32.36	25.51
25......	2.00	32.93	25.....	2.00	32.93	26.34
49......	0.09	33.17	50.....	0.10	33.18	26.66
74......	−0.11	33.49	75.....	−0.10	33.50	26.92
98......	0.36	33.68	100....	0.40	33.70	27.06
147.....	0.82	33.98	150....	0.85	34.00	27.27
196.....	1.59	34.23	200....	1.65	34.25	27.42
294.....	3.03	34.59	300....	3.10	34.60	27.58
390.....	3.76	34.76	400....	3.80	34.77	27.65
587.....	3.90	34.84	600....	3.90	34.84	27.69

TABLE OF OCEANOGRAPHIC DATA—Continued

STATIONS OCCUPIED IN 1958—Continued

Observed values			Scaled values			
Depth, meters	Temperature, ° C.	Salinity, ‰	Depth, meters	Temperature, ° C.	Salinity, ‰	σ t
Station 6832; 4 June; 46°50′ N., 47°15′ W.; depth 326 m.; dynamic height 971.072.						
0.......	5.88	32.46	0......	5.88	32.46	25.59
26......	1.29	32.60	25.....	1.45	32.59	26.11
52......	−1.00	32.85	50.....	−1.00	32.83	26.41
78......	−0.76	33.06	75.....	−0.80	33.04	26.58
103.....	−0.34	33.28	100....	−0.40	33.25	26.74
154.....	0.48	33.68	150....	0.40	33.65	27.02
206.....	2.01	34.32	200....	1.80	34.26	27.42
309.....	3.56	34.72	300....	3.50	34.70	27.62
Station 6833; 4 June; 46°49.5′ N., 47°36′ W.; depth 169 m.; dynamic height 971.117.						
0.......	6.82	32.53	0......	6.82	32.53	25.52
25......	2.87	32.60	25.....	2.87	32.60	26.01
51......	0.33	32.81	50.....	0.20	32.80	26.35
76......	−0.50	33.00	75.....	−0.50	32.99	26.53
101.....	−0.39	33.20	100....	−0.40	33.19	26.69
152.....	−0.08	33.48	150....	−0.10	33.47	26.90
Station 6834; 5 June; 46°48.5′ N., 48°11′ W.; depth 112 m.; dynamic height 971.116.						
0.......	6.83	32.53	0......	6.83	32.53	25.52
25......	2.88	32.58	25.....	2.88	32.58	25.99
50......	0.51	32.78	50.....	0.51	32.78	26.31
76......	−0.50	33.08	75.....	−0.50	33.07	26.59
101.....	−0.30	33.29	100....	−0.30	33.28	26.75
Station 6835; 5 June; 46°47′ N., 48°45′ W.; depth 89 m.; dynamic height 971.124.						
0.......	6.86	32.58	0......	6.86	32.58	25.56
25......	5.02	32.59	25.....	5.02	32.59	25.79
50......	1.56	32.74	50.....	1.56	32.74	26.22
75.....	−0.27	33.10	75.....	−0.27	33.10	26.60
Station 6836; 27 June; 49°59.5′ N., 49°00′ W.; depth 1,920 m.; dynamic height 970.907.						
0.......	6.33	33.20	0......	6.33	33.20	26.12
25......	6.23	34.35	25.....	6.23	34.35	27.03
49......	3.07	34.365	50.....	3.05	34.36	27.39
74......	2.86	34.455	75.....	2.85	34.46	27.49
99......	2.36	34.46	100....	2.35	34.46	27.53
148.....	2.66	34.575	150....	2.70	34.58	27.59
197.....	3.01	34.65	200....	3.00	34.65	27.63
296.....	3.31	34.735	300....	3.30	34.74	27.67
382.....	3.47	34.79	400....	3.45	34.78	27.68
575.....	3.47	34.81	600....	3.45	34.80	27.70
768.....	3.51	34.85	800....	3.50	34.85	27.74
963.....	3.51	34.85	800....	3.50	34.85	27.74
963.....	3.41	34.85	1,000..	3.40	34.84	27.74
1,458...	3.35	34.88				
Station 6837; 27 June; 49°48′ N., 49°34′ W.; depth 1,408 m.; dynamic height 970.958.						
0.......	4.29	32.41	0......	4.29	32.41	25.73
24......	0.26	32.98	25.....	0.20	33.00	26.51
47......	−0.05	33.63	50.....	−0.05	33.66	27.05
71......	0.51	33.89	75.....	0.60	33.90	27.20
95......	0.94	34.08	100....	1.05	34.10	27.34
142.....	1.69	34.30	150....	1.80	34.32	27.47
189.....	2.45	34.49	200....	2.55	34.52	27.57
284.....	3.21	34.71	300....	3.30	34.72	27.66
352.....	3.55	34.77	400....	3.55	34.78	27.67
531.....	3.47	34.81	600....	3.50	34.82	27.72
712.....	3.52	34.845	800....	3.50	34.84	27.73
900.....	3.46	34.85	1,000..	3.45	34.85	27.75
1,239...	3.37	34.865				
Station 6838; 27 June; 49°36.5′ N., 50°04′ W.; depth 622 m.; dynamic height 971.023.						
0.......	5.53	32.70	0......	5.53	32.69	25.80
25......	3.50	32.82	25.....	3.50	32.81	26.12
49......	−0.70	33.17	50.....	−0.70	33.18	26.69
74......	−0.53	33.47	75.....	−0.50	33.47	26.92
99......	−0.06	33.72	100....	−0.05	33.73	27.10
148.....	0.70	33.97	150....	0.75	33.98	27.27
197.....	1.61	34.26	200....	1.65	34.28	27.44
296.....	2.73	34.56	300....	2.75	34.56	27.58
397.....	3.48	34.71	400....	3.50	34.71	27.63
599.....	3.59	34.83	600....	3.60	34.82	27.71
Station 6839; 27 June; 49°31.5′ N., 50°35′ W.; depth 338 m.; dynamic height 971.016.						
0.......	5.67	32.64	0......	5.67	32.64	25.75
25......	4.23	32.81	25.....	4.23	32.80	26.04
50......	−0.20	33.29	50.....	−0.20	33.28	26.75
74......	−0.56	33.54	75.....	−0.55	33.54	26.97
99......	−0.09	33.70	100....	−0.05	33.71	27.09
149.....	0.83	34.02	150....	0.85	34.02	27.29
198.....	1.53	34.24	200....	1.60	34.25	27.42
297.....	3.43	34.72	300....	3.50	34.72	27.64
Station 6840; 27 June; 49°22.5′ N., 51°04′ W.; depth 336 m.; dynamic height 971.099.						
0.......	5.12	32.00	0......	5.12	32.00	25.31
24......	1.94	32.34	25.....	1.75	32.35	25.90
49......	−1.66	32.72	50.....	−1.65	32.72	26.35
74......	−1.40	32.85	75.....	−1.40	32.85	26.44
99......	−1.03	33.06	100....	−1.00	33.07	26.61
147.....	−0.46	33.50	150....	−0.40	32.52	26.96
196.....	0.62	33.90	200....	0.70	33.93	27.22
295.....	2.25	34.45	300....	2.30	34.48	27.55
Station 6841; 27 June; 49°12.5′ N., 51°33′ W.; depth 315 m.; dynamic height 971.112.						
0.......	5.50	31.78	0......	5.50	31.78	25.09
27......	5.36	31.81	25.....	5.40	31.80	25.12
52......	−1.41	32.69	50.....	−1.35	32.62	26.26
79......	......	33.04	75.....	−1.15	33.00	26.56
105.....	−0.70	33.32	100....	−0.80	33.27	26.76
158.....	0.27	33.67	150....	0.10	33.62	27.01
210.....	1.06	34.05	200....	0.90	33.98	27.25
315.....	2.32	34.46	300....	2.15	34.40	27.50

TABLE OF OCEANOGRAPHIC DATA—Continued

STATIONS OCCUPIED IN 1958—Continued

Observed values			Scaled values			
Depth, meters	Temperature, ° C.	Salinity, °/₀₀	Depth, meters	Temperature, ° C.	Salinity, °/₀₀	σt
Station 6842; 28 June; 49°08′ N., 51°49′ W.; depth 294 m.; dynamic height 971.137.						
0.......	6.14	31.55	0......	6.14	31.54	24.82
25.......	0.01	32.30	25.....	0.01	32.29	25.94
51.......	−1.69	32.64	50.....	−1.70	32.63	26.27
76.......	−1.70	32.72	75.....	−1.70	32.72	26.35
101.....	−1.62	32.79	100....	−1.60	32.78	26.39
152.....	−1.00	33.23	150....	−1.05	33.20	26.72
202.....	0.17	33.76	200....	0.05	33.73	27.10
268.....	1.54	34.24	[300]...	2.10	34.39	27.49
Station 6843; 28 June; 49°03′ N., 52°03′ W.; depth 278 m.; dynamic height 971.174.						
0.......	6.15	31.56	0......	6.15	31.56	24.85
23.......	4.68	31.79	25.....	4.20	31.86	25.30
47.......	−1.62	32.61	50.....	−1.65	32.61	26.26
70.......	−1.69	32.68	75.....	−1.70	32.68	26.31
94.......	−1.72	32.73	100....	−1.70	32.74	26.36
140.....	−1.44	32.85	150....	−1.35	32.92	26.50
188.....	−0.87	33.33	200....	−0.60	33.50	26.94
257.....	1.13	34.17	[300]...	1.95	34.39	27.51
Station 6844; 28 June; 48°56.5′ N., 52°16′ W.; depth 357 m.; dynamic height 971.172.						
0.......	5.98	31.66	0......	5.98	31.65	24.94
24.......	0.50	32.27	25.....	0.30	32.29	25.93
49.......	−1.56	32.68	50.....	−1.55	32.69	26.31
74.......	−1.57	32.75	75.....	−1.55	32.74	26.36
99.......	−1.55	32.79	100....	−1.55	32.78	26.39
147.....	−1.17	32.92	150....	−1.15	32.93	26.50
196.....	−0.63	33.24	200....	−0.55	33.28	26.76
295.....	1.74	34.29	(300)...	1.85	34.31	27.45
Station 6845; 28 June; 48°45.5′ N., 52°42′ W.; depth 180 m.; dynamic height 971.236.						
0.......	6.35	31.50	0......	6.35	31.50	24.77
22.......	5.64	31.69	25.....	4.70	31.82	25.21
44.......	−1.22	32.52	50.....	−1.45	32.56	26.21
66.......	−1.53	32.65	75.....	−1.55	32.68	26.30
88.......	−1.53	32.73	100....	−1.55	32.76	26.37
131.....	−1.54	32.83	150....	−1.40	32.90	26.48
175.....	−1.07	33.00				
Station 6846; 28 June; 48°43′ N., 52°49′ W.; depth 119 m.; dynamic height 971,244.						
0.......	6.35	31.39	0......	6.35	31.38	24.67
25.......	4.03	31.68	25.....	4.03	31.67	25.17
51.......	−1.04	32.48	50.....	−0.80	32.45	26.10
76.......	−1.47	32.62	75.....	−1.45	32.62	26.26
102.....	−1.63	32.70	100....	−1.60	32.69	26.32
Station 6847; 28 June; 48°42.5′ N., 52°54′ W.; depth 113 m.; dynamic height 971.251.						
0.......	6.55	31.28	0......	6.55	31.28	24.58
26.......	4.51	31.57	25.....	4.65	31.56	25.02
52.......	−0.92	32.48	50.....	−0.85	32.39	26.06
78.......	−1.30	32.58	75.....	−1.30	32.57	26.22
104.....	−1.46	32.65	100....	−1.45	32.64	26.28

Observed values			Scaled values			
Depth, meters	Temperature, ° C.	Salinity, °/₀₀	Depth, meters	Temperature, ° C.	Salinity, °/₀₀	σ t
Station 6848; 28 June; 48°37′ N., 52°43′ W.; depth 278 m.; dynamic height 971.233.						
0.......	6.86	31.69	0......	6.86	31.69	24.86
25.......	5.68	31.78	25.....	5.68	31.78	25.07
50.......	−1.41	32.61	50.....	−1.41	32.61	26.25
75.......	−1.62	32.69	75.....	−1.62	32.68	26.31
100.....	−1.60	32.76	100....	−1.60	32.76	26.38
149.....	−1.33	32.87	150....	−1.30	32.87	26.46
199.....	−0.56	33.26	200....	−0.55	33.27	26.75
249.....	0.68	33.85	300....	2.00	34.23	27.37
Station 6849; 28 June; 48°32.5′ N., 52°32′ W.; depth 230 m.; dynamic height 971.220.						
0.......	6.71	31.82	0......	6.71	31.82	24.97
25.......	6.03	31.84	25.....	6.03	31.84	25.08
50.......	−1.44	32.62	50.....	−1.44	32.62	26.26
75.......	−1.58	32.71	75.....	−1.58	32.70	26.33
100.....	−1.51	32.78	100....	−1.51	32.78	26.39
149.....	−1.21	32.97	150....	−1.20	32.97	26.54
199.....	−0.19	33.41	200....	−0.15	33.42	26.87
Station 6850; 28 June; 48°22.5′ N., 52°05′ W.; depth 201 m.; dynamic height 971.198.						
0.......	6.53	31.80	0......	6.53	31.80	24.99
25.......	4.95	31.86	25.....	4.94	31.85	25.21
49.......	−1.46	32.62	50.....	−1.45	32.62	26.26
74.......	−1.59	32.72	75.....	−1.60	32.72	26.35
99.......	−1.41	32.80	100....	−1.40	32.80	26.41
148.....	−0.79	33.08	150....	−0.75	33.09	26.61
183.....	−0.28	33.39	(200)...	−0.05	33.53	26.94
Station 6851; 28 June; 48°15.5 N., 51°47′ W.; depth 198 m.; dynamic height 971.189.						
0.......	6.71	31.90	0......	6.71	31.90	25.04
25.......	6.05	31.92	25.....	6.05	31.92	25.14
49.......	−1.11	32.62	50.....	−1.20	32.62	26 26
74.......	−1.43	32.76	75.....	−1.40	32.76	26.37
98.......	−0.98	32.88	100....	−0.95	32.89	26.46
148.....	−0.62	33.20	150....	−0.60	33.22	26.71
182.....	0.24	33.62	[200]...	0.50	33.82	27.15
Station 6852; 28 June; 48°08′ N., 51°34′ W.; depth 192 m.; dynamic height 971.180.						
0.......	6.48	32.16	0......	6.48	32.16	25.27
25.......	5.94	32.22	25.....	5.94	32.21	25.38
49.......	−0.14	32.62	50.....	−0.35	32.62	26.22
74.......	−1.41	32.77	75.....	−1.40	32.77	26.38
98.......	−1.11	32.89	100....	−1.05	32.90	26.47
147.....	−0.52	33.18	150....	−0.50	33.19	26.69
172.....	−0.49	33.30	200....	−0.45	33.42	26.88

TABLE OF OCEANOGRAPHIC DATA—Continued

STATIONS OCCUPIED IN 1958—Continued

Observed values			Scaled values			
Depth, meters	Temperature, ° C.	Salinity, °/₀₀	Depth, meters	Temperature, ° C.	Salinity, °/₀₀	σ t
Station 6853; 28 June; 47°58.5′ N., 51°14′ W.; depth 176 m.; dynamic height 971.172.						
0	5.59	32.04	0	5.59	32.04	25.30
25	5.11	32.12	25	5.11	32.12	25.41
49	−0.83	32.68	50	−0.85	32.69	26.29
74	−1.19	32.83	75	−1.20	32.84	26.43
99	−0.60	33.02	100	−0.60	33.02	26.55
148	−0.47	33.26	150	−0.45	33.27	26.75
Station 6854; 28 June; 47°50.5′ N.; 50°56′ W.; depth 119 m.; dynamic height 971.164.						
0	6.50	32.37	0	6.50	32.26	25.43
23	5.88	32.38	25	5.50	32.38	25.57
46	1.32	32.66	50	0.80	32.69	26.22
68	−0.05	32.82	75	−0.20	32.88	26.42
91	−0.44	33.06	100	−0.40	33.13	26.64
114	−0.41	33.19				
Station 6855; 28 June; 47°41.5′ N., 50°38′ W.; depth 121 m.; dynamic height 971.163.						
0	6.73	32.39	0	6.73	32.38	25.42
25	6.31	32.40	25	6.31	32.39	25.48
50	0.51	32.73	50	0.51	32.73	26.27
75	−0.43	32.90	75	−0.43	32.89	26.44
100	−0.33	33.19	100	−0.33	33.18	26.67
Station 6856; 29 June; 47°33.5′ N., 50°21′ W.; depth 110 m.; dynamic height 971.167.						
0	6.89	32.39	0	6.89	32.38	25.39
26	6.35	32.41	25	4.45	32.40	25.70
52	2.23	32.62	50	2.70	32.57	26.01
77	0.20	32.99	75	0.30	32.95	26.46
98	0.04	33.04	100	0.05	33.04	26.55
Station 6857; 29 June; 47°26.5′ N., 50°06′ W.; depth 77 m.; dynamic height 971.164.						
0	6.84	32.40	0	6.84	32.40	25.42
26	6.40	32.45	25	6.45	32.44	25.79
52	0.99	32.68	50	1.50	32.65	26.14
73	−0.21	33.08	75	−0.25	33.10	26.60
Station 6858; 29 June; 47°41.5′ N., 49°58′ W.; depth 113 m.; dynamic height 971.165.						
0	6.38	32.33	0	6.38	32.33	25.42
25	6.02	32.38	25	6.02	32.38	25.51
51	0.63	32.70	50	0.70	32.68	26.22
76	−0.20	32.97	75	−0.20	32.94	26.48
102	−0.32	33.16	100	−0.30	33.14	26.64
Station 6859; 29 June; 47°54.5′ N., 49°54′ W.; depth 169 m.; dynamic height 971.168.						
0	6.15	32.18	0	6.15	32.18	25.33
25	5.54	32.26	25	5.54	32.26	25.46
50	−0.94	32.72	50	−0.94	32.72	26.33
75	−0.57	32.90	75	−0.57	32.90	26.45
101	−0.57	33.02	100	−0.55	33.02	26.55
151	−0.23	33.34	150	−0.25	33.33	26.79
Station 6860; 29 June; 48°13.5′ N., 49°42′ W.; depth 218 m.; dynamic height 971.153.						
0	5.82	31.89	0	5.82	31.89	25.14
25	4.46	31.98	25	4.46	31.97	25.35
50	−1.66	32.68	50	−1.66	32.68	26.31
76	−1.60	32.76	75	−1.60	32.75	26.37
101	−1.28	32.88	100	−1.30	32.86	26.45
151	−0.76	33.25	150	−0.75	33.23	26.73
202	0.35	33.73	200	0.35	33.71	27.07
Station 6861; 29 June; 48°33′ N., 49°31′ W.; depth 640 m.; dynamic height 971.090.						
0	5.80	32.10	0	5.80	32.10	25.31
25	2.69	32.50	25	2.69	32.49	25.92
50	−1.19	32.84	50	−1.19	32.83	26.42
74	−0.95	33.09	75	−0.95	33.09	26.62
99	−0.86	33.34	100	−0.85	33.34	26.82
149	0.34	33.80	150	0.35	33.81	27.15
198	0.98	34.08	200	1.00	34.08	27.32
297	2.27	34.45	300	2.35	34.45	27.52
397	3.14	34.64	400	3.15	34.64	27.60
604	3.70	34.79	600	3.70	34.78	27.66
Station 6862; 29 June; 49°38.5′ N., 49°28′ W.; depth 1,097 m.; dynamic height 971.066.						
0	6.04	32.15	0	6.04	32.15	25.32
25	3.94	32.21	25	3.94	32.20	25.59
49	0.81	33.07	50	0.70	33.07	26.54
74	−0.29	33.27	75	−0.30	33.26	26.73
99	−0.35	33.53	100	−0.35	33.53	26.95
148	0.41	33.90	150	0.45	33.90	27.21
197	1.26	34.17	200	1.25	34.18	27.39
296	2.45	34.50	300	2.50	34.51	27.56
364	3.04	34.64	400	3.25	34.68	27.62
556	3.70	34.81	600	3.70	34.81	27.69
754	3.67	34.845	800	3.65	34.84	27.71
960	3.42	34.87	(1,000).	3.40	34.86	27.76
Station 6863; 29 June; 49°01.5′ N., 49°17′ W.; depth 1,692 m.; dynamic height 970.902.						
0	6.78	33.30	0	6.78	33.30	26.13
25	5.12	33.64	25	5.12	33.64	26.61
49	2.71	34.37	50	2.70	34.38	27.43
74	2.68	34.53	75	2.70	34.53	27.55
98	2.97	34.63	100	3.00	34.63	27.61
148	3.55	34.76	150	3.55	34.75	27.65
197	3.66	34.79	200	3.65	34.78	27.66
295	3.70	34.81	300	3.70	34.81	27.69
382	3.64	34.82	400	3.60	34.82	27.71
576	3.50	34.825	600	3.50	34.82	27.72
772	3.48	34.85	800	3.50	34.85	27.74
972	3.42	34.86	1,000	3.40	34.85	27.75
1,483	3.32	34.88				

TABLE OF OCEANOGRAPHIC DATA—Continued

STATIONS OCCUPIED IN 1958—Continued

Station 6864; 29 June; 49°30.5′ N., 49°07′ W.; depth 1,701 m.; dynamic height 970.909.

Observed values			Scaled values			
Depth, meters	Temperature, °C.	Salinity, ‰	Depth, meters	Temperature, °C.	Salinity, ‰	σ_t
0	6.58	32.98	0	6.58	32.98	25.91
25	5.12	34.17	25	5.12	34.17	27.02
49	3.10	34.40	50	3.05	34.40	27.42
74	2.68	34.44	75	2.70	34.44	27.48
98	3.14	34.57	100	3.15	34.57	27.55
147	3.69	34.71	150	3.70	34.70	27.60
196	3.66	34.73	200	3.65	34.73	27.62
294	3.56	34.78	300	3.55	34.78	27.67
393	3.47	34.79	400	3.50	34.78	27.68
592	3.52	34.825	600	3.50	34.82	27.72
794	3.49	34.85	800	3.50	34.84	27.73
998	3.41	34.85	1,000	3.40	34.84	27.74
1,518	3.33	34.87				

Station 6865; 30 June; 50°01.5′ N., 49°05′ W.; depth 1,820 m.; dynamic height 970.900.

Observed values			Scaled values			
Depth, meters	Temperature, °C.	Salinity, ‰	Depth, meters	Temperature, °C.	Salinity, ‰	σ_t
0	4.54	32.37	0	4.54	32.36	25.66
25	1.24	33.18	25	1.24	33.17	26.58
50	2.43	34.44	50	2.43	34.43	27.50
75	2.80	34.59	75	2.80	34.59	27.59
99	3.12	34.66	100	3.10	34.66	27.63
149	3.25	34.72	150	3.25	34.71	27.65
199	3.39	34.76	200	3.40	34.75	27.67
298	3.52	34.80	300	3.50	34.80	27.70
408	3.44	34.80	400	3.45	34.80	27.70
612	3.52	34.84	600	3.50	34.83	27.72
815	3.39	34.85	800	3.400	34.84	27.74
1,022	3.37	34.85	1,000	3.40	34.84	27.74
1,544	3.33	34.87				

Station 6866; 1 July; 53°43′ N., 55°48′ W.; depth 113 m.; dynamic height 1937.653.

Observed values			Scaled values			
Depth, meters	Temperature, °C.	Salinity, ‰	Depth, meters	Temperature, °C.	Salinity, ‰	σ_t
0	4.87	30.51	0	4.87	30.51	24.16
25	−0.72	32.46	25	−0.72	32.45	26.10
50	−1.55	32.74	50	−1.55	32.74	26.36
74	−1.62	32.83	75	−1.60	32.83	26.43
99	−1.61	32.99	100	−1.60	33.00	26.57

Station 6867; 1 July; 53°50′ N., 55°36′ W.; depth 187 m.; dynamic height 1937.652.

Observed values			Scaled values			
Depth, meters	Temperature, °C.	Salinity, ‰	Depth, meters	Temperature, °C.	Salinity, ‰	σ_t
0	5.52	30.40	0	5.52	30.40	24.00
24	0.29	32.24	25	0.15	32.29	25.93
49	−1.62	32.81	50	−1.60	32.81	26.42
73	−1.62	32.92	75	−1.60	32.93	26.51
97	−1.60	33.03	100	−1.60	33 05	26.61
146	−1.45	33.25	150	−1.45	33.28	26.79
170	−1.31	33.38	(200)	−1.05	33.54	26.99

Station 6868; 1 July; 53°58′ N., 55°23′ W.; depth 169 m.; dynamic height 1937.626.

Observed values			Scaled values			
Depth, meters	Temperature, °C.	Salinity, ‰	Depth, meters	Temperature, °C.	Salinity, ‰	σ_t
0	4 87	31.19	0	4.87	31.19	24.70
25	0.75	32.23	25	0.75	32.22	25.85
50	−1.65	32.81	50	−1.65	32.80	26.41
75	−1.60	33.00	75	−1.60	32.99	26.56
100	−1.43	33.24	100	−1.43	33.24	26.76
150	−0.76	33.62	150	−0.76	33.61	27.04

Station 6869; 1 July; 54°03.5′ N., 55°11′ W.; depth 163 m.; dynamic height 1937.615.

Observed values			Scaled values			
Depth, meters	Temperature, °C.	Salinity, ‰	Depth, meters	Temperature, °C.	Salinity, ‰	σ_t
0	4.67	31.40	0	4.67	31.40	24.89
25	1.98	32.14	25	1.98	32.14	25.70
51	−1.48	32.95	50	−1.45	32.91	26.49
76	−1.45	33.20	75	−1.45	33.18	26.71
101	−1.34	33.38	100	−1.35	33.37	26.86
147	−0.43	33.76	(150)	−0.35	33.77	27.15

Station 6870; 1 July; 54°08.5′ N., 55°04′ W.; depth 169 m.; dynamic height 1937.607.

Observed values			Scaled values			
Depth, meters	Temperature, °C.	Salinity, ‰	Depth, meters	Temperature, °C.	Salinity, ‰	σ_t
0	4.44	31.82	0	4.44	31.81	25.22
25	1.67	32.17	25	1.67	32.16	25.74
50	−1.48	32.98	50	−1.48	32.98	26.55
75	−1.50	33.19	75	−1.50	33.185	26.72
100	−1.38	33.36	100	−1.38	33.36	26.85
150	−0.11	33.84	150	−0.11	33.83	27.18

Station 6871; 1 July; 54°38′ N., 54°23′ W.; depth 223 m.; dynamic height 1937.626.

Observed values			Scaled values			
Depth, meters	Temperature, °C.	Salinity, ‰	Depth, meters	Temperature, °C.	Salinity, ‰	σ_t
0	3.77	31.74	0	3.77	31.74	25.24
25	2.61	31.82	25	2.61	31.82	25.40
50	−1.52	32.82	50	−1.52	32.82	26.43
75	−1.47	33.14	75	−1.47	33.13	26.67
100	−1.33	33.31	100	−1.33	33.31	26.81
149	−0.69	33.66	150	−0.70	33.66	27.08
199	0.30	33.92	200	0.35	33.92	27.24

Station 6872; 1–2 July; 54°46′ N., 53°55′ W.; depth 325 m.; dynamic height 1937.542.

Observed values			Scaled values			
Depth, meters	Temperature, °C.	Salinity, ‰	Depth, meters	Temperature, °C.	Salinity, ‰	σ_t
0	3.39	31.60	0	3.39	31.59	25.16
25	−1.27	32.96	25	−1.27	32.96	26.53
51	−1.00	33.42	50	−1.00	33.41	26.89
75	−0.90	33.59	75	−0.90	33.58	27.02
101	−0.40	33.78	100	−0.45	33.76	27.15
151	0.84	34.06	150	0.80	34.05	27.31
202	2.49	34.41	200	2.45	34.39	27.46
303	2.84	34.51	300	2.85	34.50	27.52

Station 6873; 2 July; 54°52.5′ N., 53°39′ W.; depth 636 m.; dynamic height 1937.512.

Observed values			Scaled values			
Depth, meters	Temperature, °C.	Salinity, ‰	Depth, meters	Temperature, °C.	Salinity, ‰	σ_t
0	3.33	31.77	0	3.33	31.76	25.29
25	−0.60	33.07	25	−0.60	33.06	26.58
50	−0.92	33.46	50	−0.92	33.46	26.93
75	0.05	33.73	75	0.05	33.72	27.10
101	0.94	34.06	100	0.90	34.02	27.29
150	2.50	34.39	150	2.50	34.38	27.45
200	2.98	34.52	200	3.00	34.51	27.52
301	3.35	34.66	300	3.35	34.65	27.59
403	3.33	34.68	400	3.35	34.68	27.61
601	3.62	34.78	600	3.60	34.77	27.67

TABLE OF OCEANOGRAPHIC DATA—Continued

STATIONS OCCUPIED IN 1958—Continued

Station 6874; 2 July; 54°58.5′ N., 53°28′ W.; depth 1,609 m.; dynamic height 1937.457.

Observed values			Scaled values			
Depth, meters	Temperature, °C.	Salinity, ‰	Depth, meters	Temperature, °C.	Salinity, ‰	σ_t
0	3.47	32.27	0	3.47	32.27	25.68
24	0.22	33.60	25	0.25	33.63	27.01
49	1.07	34.00	50	1.10	34.00	27.26
73	1.38	34.17	75	1.45	34.18	27.37
98	2.04	34.33	100	2.10	34.33	27.44
147	3.12	34.56	150	3.15	34.57	27.55
195	3.54	34.68	200	3.55	34.68	27.59
293	3.34	34.70	300	3.35	34.69	27.62
388	3.43	34.73	400	3.45	34.72	27.64
586	3.77	34.80	600	3.75	34.79	27.66
785	3.75	34.825	800	3.75	34.82	27.69
986	3.57	34.84	1,000	3.55	34.83	27.71
1,496	3.43	34.86	1,500	3.45	34.85	27.74

Station 6875; 2 July; 55°02′ N., 53°21′ W.; depth 2,140 m.; dynamic height 1937.406.

Observed values			Scaled values			
Depth, meters	Temperature, °C.	Salinity, ‰	Depth, meters	Temperature, °C.	Salinity, ‰	σ_t
0	3.86	32.59	0	3.86	32.59	25.91
24	3.95	33.57	25	3.95	33.60	26.70
49	3.01	34.38	50	3.00	34.42	27.45
73	2.94	34.60	75	2.95	34.60	27.59
97	3.26	34.66	100	3.25	34.66	27.61
145	3.16	34.68	150	3.15	34.68	27.63
194	3.35	34.72	200	3.35	34.71	27.65
291	3.30	34.73	300	3.35	34.73	27.65
363	3.71	34.79	400	3.75	34.81	27.68
551	3.84	34.84	600	3.80	34.84	27.70
743	3.55	34.83	800	3.55	34.82	27.71
938	3.54	34.85	1,000	3.50	34.85	27.74
1,432	3.36	34.875	1,500	3.35	34.87	27.77
1,941	3.07	34.89	(2,000)	3.00	34.88	27.81

Station 6876; 2 July; 55°14.5′ N., 52°54′ W.; depth 3,091 m.; dynamic height 1937.394.

Observed values			Scaled values			
Depth, meters	Temperature, °C.	Salinity, ‰	Depth, meters	Temperature, °C.	Salinity, ‰	σ_t
0	4.97	32.96	0	4.97	32.96	26.09
26	4.56	33.96	25	4.55	33.90	26.87
51	3.82	34.40	50	3.80	34.37	27.33
77	3.36	34.62	75	3.40	34.61	27.56
102	3.10	34.66	100	3.10	34.65	27.62
153	3.37	34.73	150	3.40	34.72	27.65
204	3.32	34.74	200	3.35	34.74	27.66
306	3.54	34.79	300	3.55	34.78	27.67
404	3.70	34.82	400	3.70	34.82	27.70
606	3.68	34.84	600	3.70	34.84	27.71
809	3.43	34.84	800	3.45	34.83	27.72
1,011	3.39	34.84	1,000	3.40	34.83	27.73
1,525	3.36	34.87	1,500	3.35	34.86	27.76
2,040	3.14	34.90	2,000	3.15	34.89	27.80
2,469	2.76	34.88	2,500	2.75	34.88	27.83
2,934	1.86	34.86	(3,000)	1.65	34.86	27.91

Station 6877; 2 July; 55°31′ N., 52°21′ W.; depth 3,292 m.; dynamic height 1937.395.

Observed values			Scaled values			
Depth, meters	Temperature, °C.	Salinity, ‰	Depth, meters	Temperature, °C.	Salinity, ‰	σ_t
0	6.12	32.66	0	6.12	32.65	25.72
24	5.96	34.21	25	5.90	34.22	26.97
49	3.42	34.57	50	3.40	34.56	27.52
74	3.17	34.64	75	3.15	34.64	27.60
99	3.17	34.68	100	3.15	34.67	27.63
148	3.35	34.72	150	3.35	34.72	27.65
197	3.26	34.74	200	3.25	34.73	27.66
296	3.31	34.75	300	3.30	34.75	27.67
412	3.39	34.79	400	3.40	34.78	27.69
610	3.45	34.82	600	3.45	34.82	27.72
808	3.25	34.81	800	3.25	34.81	27.73
1,005	3.31	34.84	1,000	3.30	34.83	27.74
1,499	3.33	34.86	1,500	3.35	34.86	27.76
1,994	3.34	34.89	2,000	3.35	34.88	27.77
2,492	3.04	34.905	2,500	3.05	34.90	27.82
2,982	2.41	34.885	3,000	2.35	34.88	27.86
3,208	1.76	34.86				

Station 6878; 2 July; 55°55′ N., 51°40′ W.; depth 3,566 m.; dynamic height 1937.411.

Observed values			Scaled values			
Depth, meters	Temperature, °C.	Salinity, ‰	Depth, meters	Temperature, °C.	Salinity, ‰	σ_t
0	7.13	33.80	0	7.13	33.79	25.69
25	6.91	34.10	25	6.91	34.10	26.74
51	3.66	34.54	50	3.70	34.52	27.46
77	3.59	34.65	75	3.60	34.64	27.56
102	3.49	34.68	100	3.50	34.67	27.60
152	3.33	34.71	150	3.35	34.70	27.63
203	3.34	34.73	200	3.35	34.72	27.65
305	3.12	34.73	300	3.10	34.73	27.68
400	3.48	34.79	400	3.50	34.79	27.69
600	3.49	34.84	600	3.50	34.83	27.72
801	3.38	34.82	800	3.40	34.82	27.73
1,002	3.40	34.85	1,000	3.40	34.84	27.74
1,508	3.38	34.865	1,500	3.40	34.86	27.76
2,015	3.34	34.875	2,000	3.35	34.87	27.77
2,506	3.07	34.90	2,500	3.10	34.89	27.81
3,007	2.67	34.89	3,000	2.70	34.88	27.83
3,459	1.71	34.86	(3,500)	1.55	34.85	27.91

Station 6879; 3 July; 56°29.5′ N., 50°30′ W.; depth 3,658 m.; dynamic height 1937.396.

Observed values			Scaled values			
Depth, meters	Temperature, °C.	Salinity, ‰	Depth, meters	Temperature, °C.	Salinity, ‰	σ_t
0	6.57	34.36	0	6.57	34.36	26.99
25	6.21	34.46	25	6.21	34.46	27.12
51	4.63	34.68	50	4.65	34.66	27.47
76	3.62	34.71	75	3.65	34.71	27.61
102	3.03	34.72	100	3.05	34.72	27.68
152	3.11	34.75	150	3.10	34.74	27.69
202	3.13	34.75	200	3.10	34.75	27.70
304	3.12	34.75	300	3.10	34.74	27.69
406	3.14	34.75	400	3.15	34.74	27.68
609	3.19	34.76	600	3.20	34.76	27.70
811	3.40	34.805	800	3.40	34.80	27.71
1,014	3.19	34.80	1,000	3.20	34.80	27.73
1,523	3.23	34.83	1,500	3.25	34.82	27.74
2,032	3.36	34.86	2,000	3.35	34.86	27.76
2,510	3.29	34.90	2,500	3.30	34.89	27.79
3,009	2.90	34.89	3,000	2.90	34.88	27.82
3,509	1.91	34.865	3,500	1.95	34.86	27.89
(3,609)	1.62	34.86				

TABLE OF OCEANOGRAPHIC DATA—Continued

STATIONS OCCUPIED IN 1958—Continued

Station 6880; 3 July; 57°02.5′ N., 49°24′ W.; depth 3,658 m.; dynamic height 1937.382.

Observed values			Scaled values			
Depth, meters	Temperature, ° C.	Salinity, ‰	Depth, meters	Temperature, ° C.	Salinity, ‰	σ t
0	7.04	34.45	0	7.04	34.44	26.99
25	6.25	34.57	25	6.25	34.56	27.20
49	4.59	34.64	50	4.55	34.64	27.46
74	3.83	34.68	75	3.80	34.67	27.57
98	3.33	34.70	100	3.30	34.70	27.64
147	3.23	34.73	150	3.20	34.73	27.67
196	3.07	34.72	200	3.05	34.72	27.68
294	3.22	34.76	300	3.25	34.76	27.69
400	3.32	34.78	400	3.35	34.78	27.69
599	3.45	34.82	600	3.45	34.82	27.72
799	3.31	34.81	800	3.30	34.80	27.72
998	3.29	34.825	1,000	3.30	34.82	27.72
1,499	3.36	34.85	1,500	3.35	34.84	27.74
1,999	3.38	34.89	2,000	3.40	34.88	27.77
2,424	3.22	34.90	2,500	3.20	34.90	27.81
2,919	2.87	34.90	3,000	2.80	34.89	27.83
3,411	2.20	34.88	(3,500)	1.95	34.86	27.89
(3,508)	1.93	34.87				

Station 6881; 3 July; 57°36.5′ N., 48°14′ W.; depth 3,438 m.; dynamic height 1937.410.

Observed values			Scaled values			
Depth, meters	Temperature, ° C.	Salinity, ‰	Depth, meters	Temperature, ° C.	Salinity, ‰	σ t
0	5.39	34.07	0	5.39	34.06	26.91
25	4.02	34.07	25	4.02	34.06	27.07
51	3.99	34.38	50	4.00	34.36	27.30
76	3.47	34.52	75	3.50	34.51	27.47
102	3.44	34.64	100	3.45	34.62	27.56
152	3.89	34.78	150	3.85	34.77	27.64
203	4.13	34.84	200	4.15	34.83	27.65
305	4.15	34.87	300	4.15	34.86	27.68
402	3.79	34.84	400	3.80	34.83	27.69
602	3.43	34.80	600	3.45	34.80	27.70
803	3.50	34.84	800	3.50	34.83	27.72
1,004	3.39	34.835	1,000	3.40	34.83	27.73
1,509	3.36	34.84	1,500	3.35	34.84	27.84
2,015	3.38	34.89	2,000	3.40	34.88	27.77
2,509	3.13	34.905	2,500	3.15	34.90	27.81
3,015	2.53	34.88	3,000	2.55	34.88	27.85
3,450	1.51	34.86				

Station 6882; 4 July; 58°11.5′ N., 47°05′ W.; depth 3,109 m.; dynamic height 1937.381.

Observed values			Scaled values			
Depth, meters	Temperature, ° C.	Salinity, ‰	Depth, meters	Temperature, ° C.	Salinity, ‰	σ t
0	5.18	34.10	0	5.18	34.10	26.96
26	5.18	34.10	25	5.20	34.09	26.95
52	3.63	34.37	50	3.75	34.34	27.31
78	3.07	34.55	75	3.10	34.51	27.51
104	3.59	34.70	100	3.55	34.67	27.59
155	3.87	34.79	150	3.85	34.77	27.64
208	4.02	34.82	200	4.00	34.81	27.66
312	4.07	34.86	300	4.05	34.85	27.68
413	3.86	34.86	400	3.90	34.85	27.70
620	3.76	34.85	600	3.75	34.84	27.70
827	3.60	34.86	800	3.60	34.86	27.74
1,034	3.48	34.86	1,000	3.50	34.85	27.74
1,553	3.39	34.875	1,500	3.40	34.87	27.77
2,073	3.19	34.91	2,000	3.25	34.90	27.88
2,495	2.82	34.90	2,500	2.80	34.90	27.84
2,935	2.17	34.88	(3,000)	1.95	34.86	27.89
2,988	1.98	34.87				

Station 6883; 5 July; 58°41′ N., 46°01′ W.; depth 2,633 m.; dynamic height 1937.352.

Observed values			Scaled values			
Depth, meters	Temperature, ° C.	Salinity, ‰	Depth, meters	Temperature, ° C.	Salinity, ‰	σ t
0	5.67	34.73	0	5.67	34.72	27.40
24	5.68	34.73	25	5.70	34.73	27.39
49	5.65	34.73	50	5.60	34.72	27.41
73	5.31	34.89	75	5.30	34.88	27.56
97	5.08	34.89	100	5.05	34.89	27.60
145	4.94	34.89	150	4.90	34.89	27.62
194	4.49	34.90	200	4.45	34.90	27.68
291	3.98	34.86	300	4.00	34.86	27.70
324	4.10	34.88	400	4.05	34.87	27.70
520	3.91	34.87	600	3.80	34.86	27.72
716	3.69	34.86	800	3.60	34.86	27.74
912	3.48	34.855	1,000	3.45	34.86	27.75
1,418	3.39	34.88	1,500	3.35	34.88	27.77
1,924	3.11	34.90	2,000	3.05	34.90	27.82
2,534	2.14	34,865	2,500	2.25	34.87	27.87
2,624	1.84	34.85				

Station 6884; 5 July; 58°59.5′ N., 45°18′ W.; depth 2,268 m.; dynamic height 1937.355.

Observed values			Scaled values			
Depth, meters	Temperature, ° C.	Salinity, ‰	Depth, meters	Temperature, ° C.	Salinity, ‰	σ t
0	5.98	34.77	0	5.98	34.77	27.40
25	5.96	34.82	25	5.96	34.82	27.44
50	5.96	34.83	50	5.96	34.82	27.44
74	5.92	....	75	5.90	34.82	27.45
99	5.81	34.81	100	5.80	34.80	27.44
149	5.06	34.92	150	5.05	34.92	27.63
198	4.78	34.93	200	4.75	34.92	27.66
297	4.36	34.90	300	4.35	34.90	27.69
392	4.04	34.86	400	4.05	34.86	27.69
589	3.84	34.86	600	3.85	34.86	27.71
785	3.52	34.85	800	3.50	34.85	27.74
982	3.49	34.865	1,000	3.50	34.86	27.75
1,482	3.36	34.89	1,500	3.35	34.88	27.77
1,982	2.79	34.89	2,000	2.80	34.89	27.83
2,243	2.51	34.88				

Station 6885; 5–6 July; 59°13′ N., 45°00′ W.; depth 2,030 m.; dynamic height 1937.372.

Observed values			Scaled values			
Depth, meters	Temperature, ° C.	Salinity, ‰	Depth, meters	Temperature, ° C.	Salinity, ‰	σ t
0	6.67	34.90	0	6.67	34.89	27.40
25	6.65	34.90	25	6.65	34.90	27.41
49	6.63	34..92	50	6.65	34.92	27.43
74	6.62	34.93	75	6.60	34.92	27.43
98	6.44	34.94	100	6.45	34.93	27.45
147	5.63	34.99	150	5.60	34.98	27.60
196	5.31	34.98	200	5.30	34.98	27.64
294	4.99	34.96	300	5.00	34.95	27.66
370	4.75	34.94	400	4.70	34.93	27.67
557	4.39	34.92	600	4.30	34.92	27.71
746	4.04	34.92	800	3.95	34.90	27.73
935	3.82	34.89	1,000	3.80	34.88	27.73
1,410	3.48	34.885	1,500	3.40	34.88	27.77
1,887	2.95	34.90	(2,000)	2.75	34.89	27.84

TABLE OF OCEANOGRAPHIC DATA—Continued

STATIONS OCCUPIED IN 1958—Continued

Station 6886; 6 July; 59°23′ N., 44°50′ W.; depth 1,170 m. to 914 m.; dynamic height 1937.462.

Observed values			Scaled values			
Depth, meters	Temperature, ° C.	Salinity, °/₀₀	Depth, meters	Temperature, ° C.	Salinity, °/₀₀	σ t
0	6.54	34.85	0	6.54	34.84	27.37
23	6.53	34.87	25	6.55	34.86	27.39
46	6.58	34.88	50	6.60	34.88	27.40
70	6.59	34.88	75	6.60	34.88	27.40
93	6.55	34.92	100	6.50	34.92	27.45
139	5.81	34.88	150	5.60	34.87	27.52
185	5.18	34.86	200	5.20	34.85	27.55
278	5.18	34.90	300	5.20	34.90	27.59
398	5.19	34.95	400	5.20	34.94	27.62
596	4.76	34.92	600	4.75	34.92	27.66
794	4.61	34.92	800	4.60	34.91	27.67
998	4.33	34.91	1,000	4.35	34.90	27.69

Station 6887; 6 July; 59°32′ N., 44°39′ W.; depth 165 m.; dynamic height 1937.595.

Observed values			Scaled values			
Depth, meters	Temperature, ° C.	Salinity, °/₀₀	Depth, meters	Temperature, ° C.	Salinity, °/₀₀	σ t
0	−0.51	32.85	0	−0.51	32.84	26.41
24	−0.56	32.85	25	−0.55	32.85	26.42
48	−0.28	33.11	50	−0.25	33.10	26.60
73	−0.09	33.13	75	−0.05	33.15	26.64
97	0.78	33.50	100	0.85	33.52	26.89
145	1.26	33.64	(150)	1.30	33.64	26.95

Station 6888; 6 July; 59°36′ N., 44°17′ W.; depth 170 m.; dynamic height 1937.676.

Observed values			Scaled values			
Depth, meters	Temperature, ° C.	Salinity, °/₀₀	Depth, meters	Temperature, ° C.	Salinity, °/₀₀	σ t
0	0.50	32.14	0	0.50	32.14	25.80
22	0.28	32.13	25	0.25	32.13	25.80
45	0.08	32.28	50	0.10	32.29	25.94
67	0.19	32.38	75	0.15	32.42	26.04
89	0.07	32.50	100	0.00	32.62	26.21
134	−0.23	33.10	(150)	−0.30	33.28	26.75

Station 6889; 6 July; 59°38′ N., 43°59′ W.; depth 165 m.; dynamic height 1937.653.

Observed values			Scaled values			
Depth, meters	Temperature, ° C.	Salinity, °/₀₀	Depth, meters	Temperature, ° C.	Salinity, °/₀₀	σ t
0	−0.36	32.43	0	−0.36	32.42	26.07
25	−0.40	32.52	25	−0.40	32.52	26.15
50	−0.36	32.55	50	−0.36	32.54	26.16
75	−0.32	32.62	75	−0.32	32.61	26.21
100	−0.36	32.25	100	−0.36	32.64	26.24
148	0.34	33.33	150	0.40	33.36	26.78

☆ U.S. GOVERNMENT PRINTING OFFICE : 1960 O—551760

Contribution No. 1023

Deep-Sea Research, 1960, Vol. 6, pp. 140 to 154. Pergamon Press Ltd., London. Printed in Great Britain

On the abyssal circulation of the world ocean—I. Stationary planetary flow patterns on a sphere

HENRY STOMMEL and A. B. ARONS

(*Received* 20 *February* 1959)

Abstract—A treatment of stationary planetary flow patterns driven by source-sink distributions in a cylindrical tank (Stommel *et al.*, 1958) is extended to predict flow patterns which might be expected under similar circumstances on a rotating sphere. Flow patterns are sketched for various source-sink distributions and meridional and zonal boundary conditions.

(1) INTRODUCTION

IN a previous paper (STOMMEL *et al.*, 1958) we defined a regime of flow specified by the following elements : (a) the flow in the whole layer is steady and geostrophic except and only (b) at the western boundary where a narrow, intense boundary current is permitted to depart markedly from geostrophy, and (c) the system, which would otherwise be at rest, is driven by a distribution of sources and sinks of fluid (this might include driving agents, such as wind, which can be expressed in terms of source and sink distributions).

Such regimes can occur in a homogeneous layer of fluid (a) of uniform or varying depth on a rotating sphere (b) of uniform or varying depth on a beta plane (c) of radially non-uniform depth on a rotating plane, i.e., in a cylindrical rotating tank with a level bottom. Predictions of patterns of flow deduced from the defined regime have been verified experimentally in the cylindrical rotating tank. It is our purpose here to set forth some theoretical results with respect to circulation patterns which may be deduced for similar flows on a rotating sphere. Where these circulation patterns can be related to existing geometry and boundary conditions in the actual ocean, they might be taken as highly abstracted and idealized models of abyssal ocean circulation. Such models are, of course, highly speculative, since we do not have clear cut confirmation of the existence of the flows described, but we have been encouraged by the success of the rotating tank results to put forth a number of spherical models in order to stimulate further speculation.

In applying this model to the abyssal layer of the ocean, we visualize a distributed sink as involving a transfer of fluid *upward* through the main thermocline, and a concentrated source as a supply of sinking, cold fluid generated in a small area at high latitude.

Our justification for assuming, in these simple models, that there is a general upward flow of water — of several centimetres per day — at mid-depths, is the theory of the oceanic thermocline developed by ROBINSON and STOMMEL (1959). This theory treats each ocean basin as a separate entity. We will show in Part II of this report how a series of such basins can be, in principle, connected together to form a model of the abyssal circulation of the world ocean.

(2) THE FORMULATION OF THE EQUATIONS FOR A HOMOGENEOUS OCEAN

Consider a globe of radius a, rotating with angular velocity ω, covered with a layer of homogeneous water of depth h. Let u be southward component of velocity, and v be eastward component of velocity at a point in co-latitude ϑ and longitude ϕ. (Fig. 1.). Assuming hydrostatic pressure in the vertical, small motions, and absence of an external disturbing force, the linearized dynamical equations are*

$$\frac{\partial u}{\partial t} - 2\omega v \cos\vartheta = -\frac{g}{a}\frac{\partial \zeta}{\partial \vartheta}$$

$$\frac{\partial v}{\partial t} + 2\omega u \cos\vartheta = \frac{-g}{a \sin\vartheta}\frac{\partial \zeta}{\partial \phi}$$

where ζ is the displacement of the free surface.

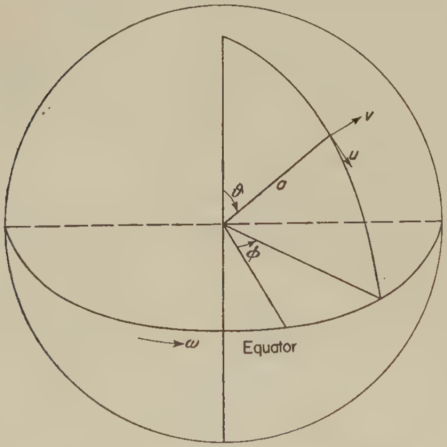

Fig. 1. Notation for co-ordinates and velocities.

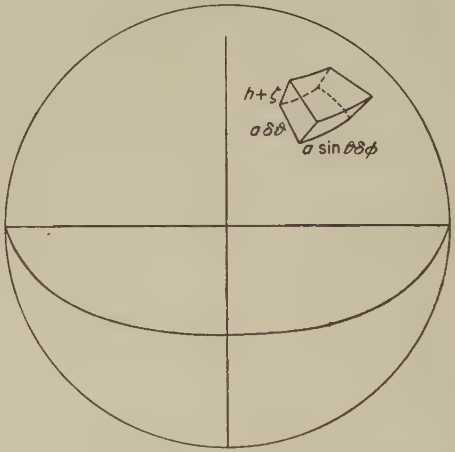

Fig. 2. Element of fluid for formulation of continuity equation.

We must now obtain a suitable form of the continuity equation. Consider a column of water shown in Fig. 2. Neglecting the quantity ζ compared to h, the rate of flow of water out of the column through the vertical walls is

$$\frac{\partial}{\partial \vartheta}(hua \sin\vartheta)\, \delta\phi\, \delta\vartheta + \frac{\partial}{\partial \phi}(hva)\, \delta\phi\, \delta\vartheta$$

At the top of the column, which is of area $a^2 \sin\vartheta\, \delta\phi\, \delta\vartheta$, the free surface is rising at the rate $\partial\zeta/\partial t$, and also there is passage of water through the free surface (positive upward) of $Q(\vartheta, \phi)$ per unit area. (We avoid GOLDSBROUGH's notation $P(\vartheta, \phi)$ because it suggests the word precipitation, of which it is indeed negative, and also looks like Legendre polynomials). We shall call Q the sink function ; it represents a distributed sink.

The total flux upward is therefore $\left(Q + \frac{\partial \zeta}{\partial t}\right) a^2 \sin\vartheta\, \delta\vartheta\, \delta\phi$. Hence the continuity equation is

---

*We set up the same equations as GOLDSBROUGH (1933).

$$\frac{\partial}{\partial \vartheta}(hu \sin \vartheta) + \frac{\partial}{\partial \phi}(hv) + \left(Q + \frac{\partial \zeta}{\partial t}\right) a \sin \vartheta = 0 \tag{1.2}$$

Let us now consider a steady circulation in a layer of uniform depth. In this case h is constant, and $\frac{\partial u}{\partial t} = \frac{\partial v}{\partial t} = \frac{\partial \zeta}{\partial t} = 0$. The solution of (1) and (2) is then

$$u = - \operatorname{cotan} \vartheta \,.\, \frac{Qa}{h} \tag{1.3}$$

$$\frac{\partial v}{\partial \phi} = - \tan \vartheta \,.\, \frac{a}{h} \cdot \frac{\partial (\cos^2 \vartheta \,.\, Q)}{\partial (\cos \vartheta)} \tag{1.4}$$

$$\frac{\partial \zeta}{\partial \phi} = 2\omega \frac{a^2}{gh} \cos^2 \vartheta \,.\, Q \tag{1.5}$$

An alternate form of (4) :

$$\frac{\partial v}{\partial \phi} = \frac{a}{h} \frac{1}{\cos \vartheta} \frac{\partial}{\partial \vartheta} (Q \cos^2 \vartheta)$$

$$= \frac{a}{h} \left[\cos \vartheta \frac{\partial Q}{\partial \vartheta} - 2 \sin \vartheta \,.\, Q \right] \tag{1.6}$$

(3) EVAPORATION — PRECIPITATION HEMISPHERES WITHOUT MERIDIONAL BOUNDARIES

Consider the globe with no boundaries (coasts). The sink function $Q(\vartheta, \phi)$ is taken as

$$Q = Q_0 \sin \phi \sin \vartheta \tag{2.1}$$

This form of source-sink distribution corresponds to dividing the sphere into a western hemisphere ($\pi \leqslant \phi < 2\pi$) in which Q is negative (precipitation, source) and an eastern hemisphere ($0 \leqslant \phi < \pi$) in which Q is positive (evaporation, sink).

The expressions for u, v, ζ are as follows :

$$u = \frac{Q_0 a}{h} \sin \phi \cos \vartheta \tag{2.2}$$

$$\frac{\partial v}{\partial \phi} = \frac{Q_0 a}{h} [3 \cos^2 \vartheta - 2] \sin \phi \tag{2.3}$$

$$\frac{\partial \zeta}{\partial \phi} = \frac{2\omega a^2 Q_0}{gh} \cos^2 \vartheta \sin \vartheta \sin \phi \tag{2.4}$$

or when integrated

$$u = \frac{Q_0 a}{h} \sin \phi \cos \vartheta \tag{2.5}$$

$$v = \frac{Q_0 a}{h} [2 - 3 \cos^2 \vartheta] \cos \phi + \frac{g}{2\omega a \cos \vartheta} \frac{dG}{d\vartheta} \tag{2.6}$$

$$\zeta = - \frac{2\omega a^2 Q_0}{gh} \cos^2 \vartheta \sin \vartheta \cos \phi + G(\vartheta) \tag{2.7}$$

where $G(\vartheta)$ is an arbitrary function physically associated with an arbitrary zonal flow superposable as an initial condition in the general solution.

The distribution of the sink-function and contours of disturbed height ζ, or simply isobars, are shown in Fig. 3, for $G(\vartheta) = 0$.

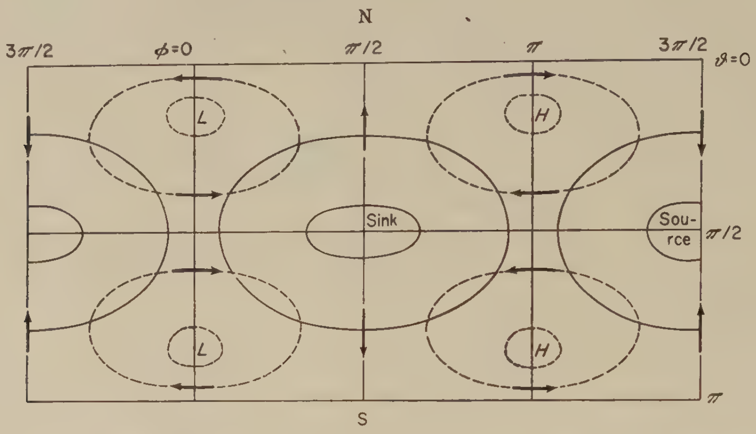

Fig. 3. Circulation pattern for $Q = Q_0 \sin \phi \sin \vartheta$ with no meridional boundaries.

Four self-contained circulation cells exist, separated by the meridian $\phi = 0$, π and by the equator $\vartheta = \pi/2$. The flow is equatorward in the source hemisphere, poleward in the sink hemisphere. The geostrophic planetary flow field is divergent because the Coriolis parameter $2\omega \cos \vartheta$ is a function of latitude. Although all flow is parallel to the isobars, the transport between isobars must vary with latitude. The fields of motion which we derive by the method of GOLDSBROUGH are precisely those whose planetary-geostrophic convergence matches the distributed sink function everywhere.

If we choose the 'step' distribution corresponding to $Q = + Q_0$ on the sink hemisphere $(0 \leqslant \phi < \pi)$ and $Q = - Q_0$ on the source hemisphere $(\pi \leqslant \phi < 2\pi)$, the solutions of (1.5) and (1.6) are

$$\begin{aligned} \zeta &= \frac{2\omega a^2 Q_0}{gh} \cos^2 \vartheta \,.\, \phi + G_1(\vartheta), \qquad (0 \leqslant \phi < \pi) \\ &= -\frac{2\omega a^2 Q_0}{gh} \cos^2 \vartheta \,.\, \phi + G_2(\vartheta), \qquad (\pi \leqslant \phi < 2\pi) \end{aligned} \tag{2.8}$$

$$\begin{aligned} v &= -\frac{2Q_0\, a}{h} \sin \vartheta \,.\, \phi + \frac{g}{2\omega a \cos \vartheta} \frac{dG_1}{d\vartheta}, \qquad (0 \leqslant \phi < \pi) \\ &= \frac{2Q_0\, a}{h} \sin \vartheta \,.\, \phi + \frac{g}{2\omega a \cos \vartheta} \frac{dG_2}{d\vartheta}, \qquad (\pi \leqslant \phi < 2\pi) \end{aligned} \tag{2.9}$$

where G_1 and G_2 must be selected so as to provide continuity of ζ at the boundary between the two hemispheres.

A simple, symmetrical flow pattern analogous to that of Fig. 3 is obtained if we take G_1 and G_2 such as to make $\zeta = 0$ around the great circle meridian $\phi = \frac{\pi}{2}, \frac{3\pi}{2}$.

The result is :

$$\zeta = \frac{2\omega a^2 Q_0}{gh} \cos^2 \vartheta \,.\left(\phi - \frac{\pi}{2}\right), \qquad (0 \leqslant \phi < \pi)$$

$$= \frac{2\omega a^2 Q_0}{gh} \cos^2 \vartheta \,.\left(\frac{3\pi}{2} - \phi\right), \qquad (\pi \leqslant \phi < 2\pi) \tag{2.10}$$

$$v = \frac{2Q_0 a}{h} \sin \vartheta \,.\left(\frac{\pi}{2} - \phi\right), \qquad (0 \leqslant \phi < \pi)$$

$$= \frac{2Q_0 a}{h} \sin \vartheta \,.\left(\phi - \frac{3\pi}{2}\right), \qquad (\pi \leqslant \phi < 2\pi) \tag{2.11}$$

and u is given by (1.3) with appropriate substitution of $\pm Q_0$ for Q. The circulation pattern is sketched in Fig. 4. There is a singularity at the poles where the velocity u is infinite. Since these conditions are contradictory with the original requirement that the motions be small, we can expect that a higher order dynamical system will be required to explain the detailed configuration at the poles themselves. This points up some of the difficulties which actually could occur in applying the GOLDSBROUGH method to a simple experimental or geophysical system. These difficulties can be avoided, of course, if we are able to use certain simple forms of sink function such

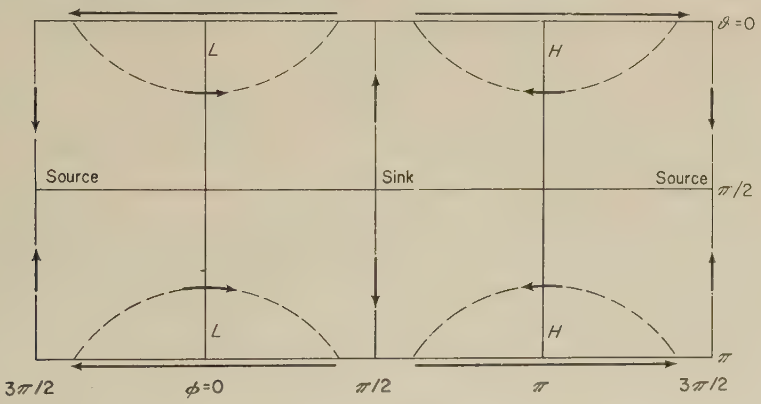

Fig. 4. Circulation pattern for $Q = +Q_0$, $(0 \leqslant \phi < \pi)$, and $Q = -Q_0$, $(\pi \leqslant \phi < 2\pi)$, with no meridional boundaries.

as that employed in Fig. 3. To indicate in Fig. 4 the need for an additional higher order regime at the poles, we resort to a simple symbolic device: We close the isobars in a narrow boundary region at the poles as shown in Fig. 4, so that we do not represent a mathematical discontinuity in pressure, and we draw a heavy arrow at the top to indicate the direction of the singular flow over the poles in this region. The arrows over the lows and highs are both in the same direction, the projection makes them look different. On the sphere, looking at the North Pole, the picture looks something like that shown in Fig. 5.

For simplicity of expression, let us call this little intense stream, the ‘ polar jet,’ or ‘ polar pinch.’

The polar jet, perhaps surprisingly at first glance, flows from the sink hemisphere to the source hemisphere.

The transport of water in the polar jet must be

$$\frac{gh}{2\omega}(\zeta_{\max} - \zeta_{\min}) \tag{2.12}$$

From equation (2.8) we find

$$\zeta_{\max} - \zeta_{\min} = \frac{2\omega a^2}{gh}\pi Q_0 \tag{2.13}$$

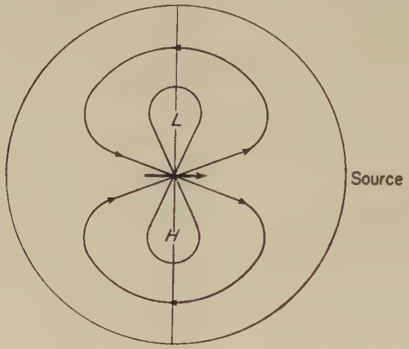

Fig. 5. Circulation pattern of Fig. 4 as seen looking down on the North Pole.

Thus the transport of both the polar jets into the source hemisphere is

$$2\pi a^2 Q_0 \tag{2.14}$$

The total integrated source flowing into the source hemisphere is

$$2\pi a^2 Q_0.$$

Therefore, in the steady state there must be a relatively massive flow, $4\pi a^2 Q_0$, flowing geostrophically from the source hemisphere into the sink hemisphere across the great circle — meridian — bounding the two hemispheres. We may verify this by the following direct calculation: From (2.11) we have for the total zonal flux, F, of material out of the source hemisphere along the great circle meridian $\phi = 0, \pi$:

$$F = 2\pi a\, Q_0 \sin\vartheta.$$

The total zonal flow out of the source hemisphere is then

$$\int_0^\pi 2\pi a^2 Q_0 \sin\vartheta\, d\vartheta = 4\pi a^2 Q_0,$$

in agreement with the value calculated above from the sum of the transport in the polar jet and the distributed source.

(It might be noted that a somewhat different flow pattern with similar polar jet and zonal transports is obtained if one selects G_1 and G_2 in (2.8) in such a way as to make $\zeta = 0$ along the great circle meridian $\phi = 0, \pi$).

(3) BASINS BOUNDED BY MERIDIANS

We now proceed to discuss the case where an ocean basin is bounded by meridians ϕ_1 and ϕ_2 extending all the way to the poles. Here we develop the pressure pattern from the eastern boundary ϕ_2 where, of course, there can be no zonal transport, so we take $\phi = \phi_2$ as an isobar : $\zeta = 0$. As before, we require geostrophic flow in the interior, but we shall now satisfy continuity requirements by allowing departure from geostrophy in a western boundary current. Our justification for the treatment carried out below rests on the success with which the same method predicts and describes similar flow patterns in a rotating cylindrical tank (STOMMEL *et al.*, 1958).

As an initial illustration we take a uniformly distributed sink Q_0 over the entire surface and balance this by a concentrated source S_0 at the pole, considering the basin north of the equator for simplicity (Fig. 6). Since the surface area of the sector is $a^2(\phi_2 - \phi_1)$, we take the concentrated source at the north pole as $S_0 = Q_0 a^2 (\phi_2 - \phi_1)$. The geostrophic velocities and surface isobars are given by :

$$u = -\frac{Q_0 a}{h} \cot \vartheta$$

$$v = \frac{2 Q_0 a}{h} \sin \vartheta \, . \, (\phi_2 - \phi)$$

$$\zeta = \frac{2 \omega a^2 Q_0}{g h} \cos^2 \vartheta \, . \, (\phi - \phi_2) \tag{3.1}$$

The pattern of the isobars is shown in Fig. 6. (There is a singularity at the pole similar to that encountered in Section 2).

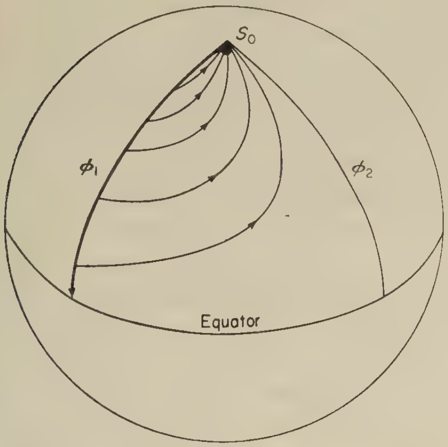

Fig. 6. Circulation pattern in meridionally bounded ocean with concentrated source S_0 at North Pole and a uniformly distributed sink Q_0, such that $S_0 = Q_0 a^2 (\phi_2 - \phi_1)$.

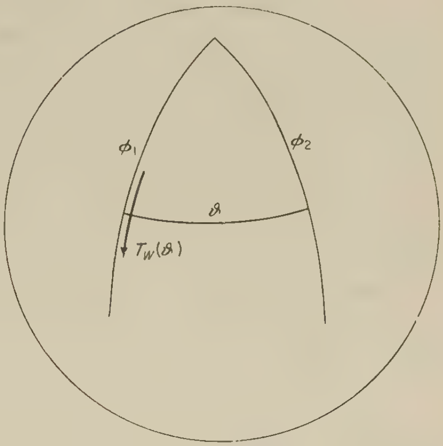

Fig. 7. Notation for evaluating strength of western boundary current $T_W(\vartheta)$ by consideration of continuity of mass flow in a sector.

This flow does not satisfy boundary conditions at $\phi = \phi_1$, and, following the procedure used by (STOMMEL, *et al.*, 1958) we introduce symbolicaly a western boundary current $T_W(\vartheta)$ shown positive southward by the heavy arrow in Fig. 7.

Consider a section of the ocean (Fig. 7) bounded by ϕ_1, ϕ_2, and ϑ. The total outward flux of mass from portions of the basin so bounded consists of four parts :

1. The western boundary current $T_W(\vartheta)$.

2. The flux integrated over the surface area of the basin

$$= \int_{0}^{\vartheta}\int_{\phi_1}^{\phi_2} Q\, a^2 \sin\vartheta \,.\, d\vartheta\, d\phi.$$

3. The flux across ϑ in the interior of the ocean, away from the western boundary current

$$\int_{\phi_1}^{\phi_2} ahu \sin\vartheta\, d\phi.$$

4. The flux $-S_0$ from any concentrated source present in the section.

In the stationary state these must add up to zero, hence

$$T_W(\vartheta) = -\int_{\phi_1}^{\phi_2} ahu \sin\vartheta\, d\phi - \int_{0}^{\vartheta}\int_{\phi_1}^{\phi_2} Qa^2 \sin\vartheta\, d\vartheta\, d\phi + S_0 \tag{3.2}$$

Evaluating equation 3.2 in the light of 3.1, we obtain for case of Fig. 6 :

$$\begin{aligned} T_W &= 2Q_0\, a^2 (\phi_2 - \phi_1) \cos\vartheta \qquad (3.3)\\ &= 2S_0 \cos\vartheta. \end{aligned}$$

Thus in the neighbourhood of the pole the transport in the western boundary current, $T_W(0) = 2Q_0\, a^2 (\phi_2 - \phi_1) = 2S_0$, is *twice* the transport associated with the concentrated source alone, and, as in the cylindrical case developed by STOMMEL *et al.* (1958) a large volume of water is continually being *recirculated* in such a steady-state system.

Equation (3.3) however, reveals a very interesting difference between the spherical and the cylindrical geometries. Where, in the cylindrical basin, the western boundary current does not vary with radial position and, flows undiminished all the way to the outer rim of the tank, the current in the spherical geometry diminishes as it flows to lower latitudes (Fig. 6), dropping to zero at the equator. (Of course, if we assumed a concentrated source S_0 at the pole *larger* than the internal distributed sink flux $Q_0\, a^2 (\phi_2 - \phi_1)$, the excess would flow across the equator to feed the sector on the other side).

The internal consistency of equations (3.1) and (3.3) is readily checked by evaluating the total zonal transport at $\phi = \phi_1$ and showing it to be equal to the initial total western boundary current $T_W(0)$, i.e.

$$\int_{0}^{\pi/2} hau\,(\phi_1)\, d\vartheta = 2Q_0\, a^2 (\phi_2 - \phi_1)$$

A somewhat different pattern of western boundary currents arises if we alter the situation in Fig. 6 only by transferring the concentrated source from the pole to the southwest corner of the sector at the equator (i.e. this could stem from a western boundary current crossing the equator from the southern side). We still assume that the source strength S_0 just balances the distributed sink $Q_0\, a^2 (\phi_2 - \phi_1)$.

If we now evaluate $T_W(\vartheta)$ from equation (3.2), remembering that there is no longer a concentrated source within the section being considered in Fig. 7, we obtain :

$$T_W(\vartheta) = Q_0\, a^2 (\phi_2 - \phi_1)(1 - 2\cos\vartheta) \tag{3.4}$$

The interior flow pattern is still defined by (3.1) exactly as it was in Fig. 6, but the nature of the western boundary current is very different and is sketched in Fig. 8.

A current of recirculated water equal to the source strength starts at the pole and flows toward the source just as in the cylindrical case (STOMMEL *et al.*, 1958), but in the spherical geometry this current gradually diminishes to zero at $\vartheta = 60°$ (30° north latitude). A northward current of equal strength starts at the equatorial source and also diminishes to zero at 30° north latitude. (This feature is completely absent in the corresponding cylindrical situation). The zonal transport out of these two currents feeds exactly the same interior flow pattern as in Fig. 6.

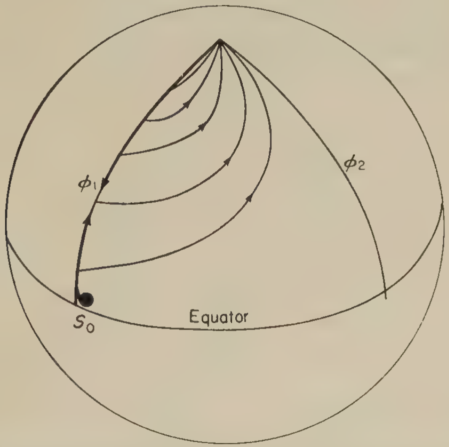

Fig. 8. Circulation pattern in meridionally bounded ocean with concentrated source S_0 (fed by western boundary current from below the equator) and a uniformly distributed sink Q_0 such that $S_0 = Q_0 a^2 (\phi_2 - \phi_1)$.

In the second paper of this series, we shall repreatedly make use of the above results in order to sketch idealized patterns of boundary currents and interior circulation in various basins of the world ocean.

(4) FURTHER ILLUSTRATIONS OF CIRCULATIONS IN MERIDIONALLY BOUNDED BASINS

Applying the analytical method outlined in Section 3, we now state the results obtained for a few other basically interesting cases of source-sink distributions.

(a) A simple form of the function Q which avoids singular flows at the poles is

$$Q = Q_0 \sin^n \vartheta \cos \vartheta, \qquad n \geqslant 1 \tag{4.1}$$

Thus the half of the basin north of the equator is a sink while the southern half is an equal source. S_0 is taken as zero.

The isobars are given by the disturbed height

$$\zeta = \frac{2\omega a^2 Q_0}{gh} \sin^n \vartheta \cos^3 \vartheta \, . \, (\phi - \phi_2) \tag{4.2}$$

and the western boundary current transport by

$$T_W(\vartheta) = Q_0 a^2 \frac{\sin^n \vartheta}{n+2} [(n+3) \cos^2 \vartheta - 1] \, . \, (\phi_2 - \phi_1). \tag{4.3}$$

The interior isobars and nature of the western boundary current are sketched for the case $n = 0$ in Fig. 9. The north and southbound boundary currents fall to zero at $\vartheta = 54{\cdot}7°$. Here the flow has a singularity at the poles. The singularity is eliminated when $n \geqslant 1$. For larger values of n the flow is essentially similar to that sketched in Fig. 9 with isobars somewhat more concentrated in mid-latitudes.

(b) It is interesting to examine the effect of a sloping bottom, taking $h = h_0 \sin\vartheta$. Here we must go back to the continuity equation in the form of (1.2). For a uniformly distributed sink $Q = Q_0$ and a concentrated source in the south, we obtain :

$$u = -\frac{Q_0\, a}{h_0}\cos\vartheta$$

$$v = \frac{Q_0\, a\,(\phi - \phi_2)}{h_0}(1 - 3\sin^2\vartheta)$$

$$\zeta = \frac{Q_0\, a^2\, \omega}{g h_0}(\phi - \phi_2)\cos\vartheta\,\sin^2\vartheta$$

$$T_W(\vartheta) = Q_0\, a^2\,(\phi_2 - \phi_1)\left[\cos\vartheta\,(1 + \sin^2\vartheta) - 1\right] \tag{4.4}$$

The isobars and western boundary transport are sketched in Fig. 10. Comparing with Fig. 6, we see that the effect of the sloping bottom is to cause the isobars to intersect the ϕ_1 meridian at different latitudes instead of requiring a common intersection at the pole as in the case of uniform depth. It should also be noted that the southward flowing boundary current first increases in intensity and then decreases instead of showing a monotonic decrease.

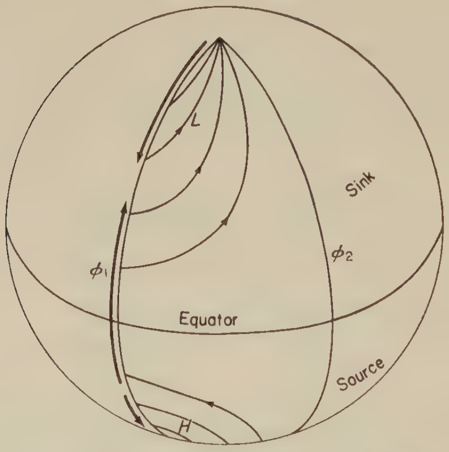

Fig. 9. Circulation pattern for $Q = Q_0 \cos\vartheta$ with no concentrated sources. Note boundary current crossing equator.

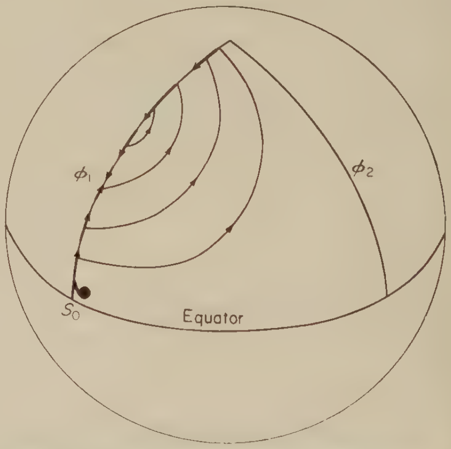

Fig. 10. Circulation pattern in meridionally bounded ocean with sloping bottom. $h = h_0 \sin\vartheta$. Concentrated southern source and uniformly distributed sink.

(c) In any source-sink distribution in which Q becomes zero along a latitude circle, the interior geostrophic flow does not cross this latitude circle, and the circulation in a basin is divided up into separate cells. As an illustration we take

$$Q = -\,Q_0 \cos 2\vartheta \tag{4.5}$$

giving a distributed source in latitudes higher than 45° and a distributed sink in the belt between the 45° latitude circles. Since the source flux is smaller than the sink flux, we balance the flux by introducing concentrated sources $S_0 = \frac{1}{3} Q_0 a^2 (\phi_2 - \phi_1)$ at each pole. In this case we obtain for a basin of uniform depth :

$$u = \frac{Q_0 a}{h} \cdot \frac{2\cos^3\vartheta - \cos\vartheta}{\sin\vartheta}$$

$$v = \frac{2Q_0 a}{h} (\phi - \phi_2) \sin 3\vartheta$$

$$\zeta = -\frac{2Q_0 a^2 \omega}{gh} (\phi - \phi_2) \cos 2\vartheta \cos^2\vartheta$$

$$T_W(\vartheta) = \frac{Q_0 a^2}{3} (\phi_2 - \phi_1) \cos\vartheta (3 - 4\cos^2\vartheta) \tag{4.6}$$

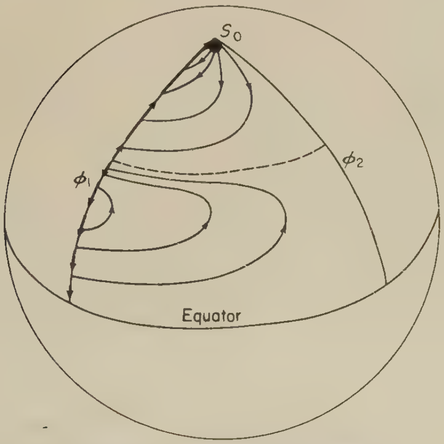

Fig. 11. Circulation pattern divided into separate cells when $Q = 0$ along a latitude circle. $S_0 = \frac{1}{3} Q_0 a^2 (\phi_2 - \phi_1)$; $Q = - Q_0 \cos 2\vartheta$.

The isobars and western boundary transports are sketched in Fig. 11, showing the cells into which the circulation is divided.

(5) BASINS BOUNDED BY MERIDIANS ϕ_1, ϕ_2 AND A NORTHERN LATITUDE ϑ, (FIG. 12)

For any distribution of Q, the expressions for u, v and ζ are the same as before, except now it will, in general, be necessary to add a boundary layer at both $\vartheta = \vartheta_1$ and $\phi = \phi_1$. The expression for $T_W(\vartheta)$ must be changed because there is no loss from the sink defined north of ϑ_1 ;
thus

$$T_W(\vartheta) = - \int_{\phi_1}^{\phi_2} ahu \sin\vartheta \, d\phi - \int_{\phi_1}^{\phi_2} \int_{\vartheta_1}^{\vartheta} Q a^2 \sin\vartheta \, d\vartheta \, d\phi \tag{5.1}$$

As an example, we may choose $Q = Q_0$, a constant. Hence

$$T_W(\vartheta) = Q_0 a^2 (\phi_2 - \phi_1)(2\cos\vartheta - \cos\vartheta_1) \tag{5.2}$$

The critical latitudes, where the western current reverses direction, are at

$$\vartheta = \cos^{-1}\left(\tfrac{1}{2}\cos\vartheta_1\right) \tag{5.3}$$

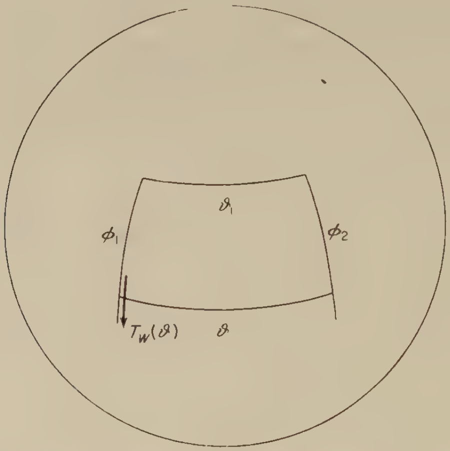

Fig. 12. Notation for sector with rigid boundary at co-latitude ϑ_1.

In the limiting case where the latitude of the northern boundary approaches the pole ($\vartheta_1 \to 0$) the latitude of reversal of the western boundary current is about ($\vartheta = 60°$) 30° N lat.

In some actual applications an additional point source S_0 should be added in the basins, near the poles, to supply the material lost by the distributed sink. In this case we must add S_0 to the equation on the right hand member.

(6) COMPLETELY CLOSED BASIN BOUNDED BY MERIDIANS ϕ_1, ϕ_2 AND LATITUDE CIRCLES ϑ_1, ϑ_2 (FIG. 13)

Again, we take a distributed sink function $Q = Q_0$. The quantities u, $\zeta, T_W(\vartheta)$ are the same as in the case of Section 5, but, of course, for a steady state there must be a source of water somewhere. We place it at the point ϕ_1, ϑ_2. Its intensity must be equal to that of the distributed sink over the whole ocean area.

$$S_0 = \int_{\phi_1}^{\phi_2}\int_{\vartheta_1}^{\vartheta_2} Qa^2 \sin\vartheta \, d\vartheta \, d\phi = Q_0 \, a^2 (\phi_2 - \phi_1)(\cos\vartheta_1 - \cos\vartheta_2) \tag{6.1}$$

The isobar pattern is given by

$$\zeta = \frac{2Q_0 \, a^2 \, \omega}{gh} (\phi_2 - \phi) \cos^2\vartheta \tag{6.2}$$

the pressure pattern being developed from the eastern boundary with zero zonal transport at $\phi = \phi_2$ as before.

In Fig. 13 the isobar pattern according to (6.2) is drawn. It is seen that boundary currents must be drawn at all except the eastern boundary. The western boundary current flows northward from the source, and across the equator, and is met in middle northern latitudes by a southward flowing western boundary current. For example, if we take the latitude of the northern boundary of the ocean 70°N, the latitude of the reversal of the western boundary current is 18·5°N ($\vartheta = 81{\cdot}5°$) from equation (5.3).

If, in the configuration shown in Fig. 13 we now put another point source S_1, at the north-western corner of the basin, and assert that there is a distributed sink whose intensity integrated over the entire area of the ocean is equal to the sum of the two point sources : $S_0 + S_1$, we get a variety of circulation patterns, depending on the relative strengths of sources S_0 and S_1. If they are equal, the flow is in two separate gyres with no flow across the equator (Fig. 14). If the sources are not equal there is a flow across the equator in the western boundary current (there is never transequatorial flow in the interior) from the basin with the larger source, the pattern then looking more like that shown in Fig. 13. The only difference in these patterns, as we vary the relative strength of S_0 and S_1 is in the latitude of reversal of the western boundary current.

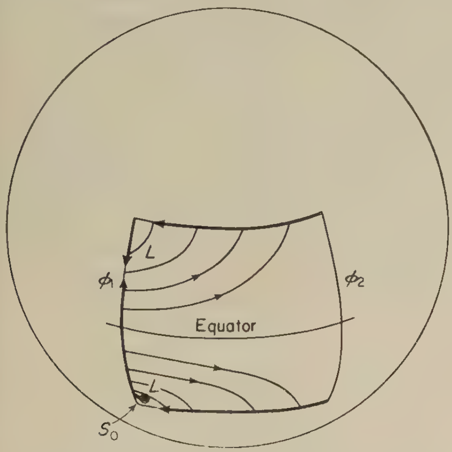

Fig. 13. Circulation pattern in sector bounded by meridians and latitude circles. Boundary currents will be present along north and south boundaries as well as along the western boundary. Single concentrated source.

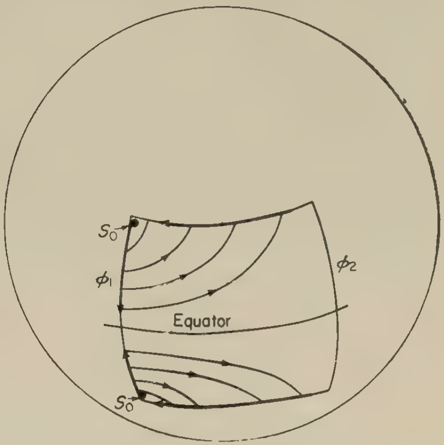

Fig. 14. Circulation pattern in sector of Fig. 13 with equal concentrated sources in each hemisphere.

(7) SOME COMMENTS ON THE VARIOUS BOUNDARY LAYERS

The various boundary layers introduced in the preceding examples can be avoided, formally, by proper choice of the sink function Q. Thus, all boundary currents on latitude circles can be avoided by choosing Q so that it approaches zero at the boundary. Similarly, western boundary currents can be avoided if we restrict $Q(\vartheta, \phi)$ to forms which satisfy the integral relation

$$\int_{\phi_1}^{\phi_2} Q(\vartheta, \phi)\, d\phi = 0$$

where ϕ_2 and ϕ_1 are the longitudes of the meridional boundaries of the basin. In effect, these are the restrictions which GOLDSBROUGH imposes in his investigation. Such restrictions are, however, quite artificial from a physical point of view. Most simple physical regimes in experiments, such as those in the rotating circular basin with parabolic depth law (STOMMEL *et al.*, 1958) as well as geophysical or oceanographic situations, are certainly not bound to conform to such artificial restrictions. Thus, there is a need to take a rather broad view in choosing models with various forms of Q, and this evidently requires introduction of appropriate boundary layers.

(8) PARTIAL BARRIERS

What will the regime of flow look like when there are meridional barriers which end abruptly at some latitude far from any other coast? Let us return to the simple configuration originally drawn in Fig. 7, but now we put a long barrier along the longitude ϕ' $(\phi_1 < \phi' < \phi_2)$ extending from the pole to colatitude ϑ' but not beyond it (Fig. 5).

We can make use of the same kind of reasoning we used before to construct interior solutions in the open ocean portion. However it is clear that we can now have two western boundary currents along ϕ_1 and ϕ', with transports T_W and T_W'. If upon calculation of the transport T_W' along the partial barrier ϕ' it is found that $T_W' \neq 0$ at $\vartheta = \vartheta'$, then clearly the only resort is a zonal current (Z in Fig. 16) to connect the western boundary current on the barrier ϕ' to that on the barrier ϕ_1. In this way continuity can be preserved. To see how this alters the picture of the circulation we can compare Figs. 8 and 16. The former shows the pattern of circulation for a basin, bounded by two meridians and the equator, filled by a source S_0 at the equator, and emptied by a uniformly distributed sink over the whole oceanic area. In Fig. 16 a meridional barrier ϕ' has been added part way down from the pole, and the mass flux into the eastern basin occurs partly as a zonal current toward the east. The fact that this zonal current can indeed ' round the corner ' to join the western boundary current has been demonstrated in rotating tank experiments by A. J. FALLER (private communication). Both north and south of the zonal current there is an interior meridional component of flow which must join properly to the zonal current.

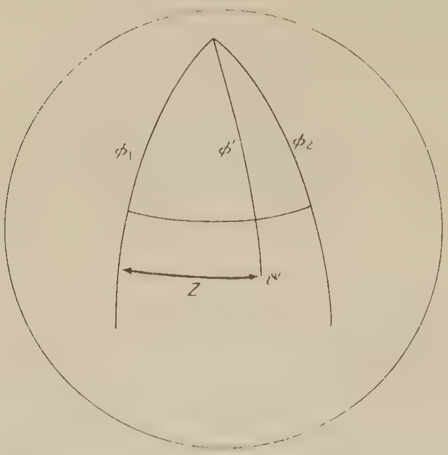

Fig. 15. Meridionally bounded sector (ϕ_1, ϕ_2) with partial meridional barrier extending from pole to longitude ϕ'.

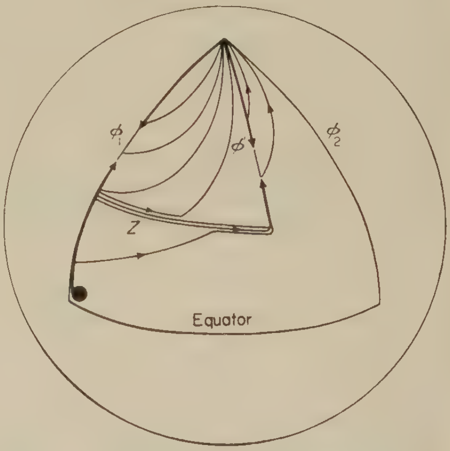

Fig. 16. Circulation pattern in sector with partial meridional barrier. Western boundary currents along ϕ_1 and ϕ' are connected by zonal flow Z.

Therefore the zonal current is not strictly speaking a continuous current ; water is added from the south and thrown off to the north along its length, as the drawing of the isobars indicates.

Woods Hole Oceanographic Institution
Woods Hole, Mass.

Contribution No. 1023 *Woods Hole Oceanographic Institution. Part of this work was done while one of us* (*A.B.A.*) *was the recipient of a Fellowship of the John Simon Guggenheim Memorial Foundation.*

REFERENCES

GOLDSBROUGH G. R. (1933) Ocean currents produced by evaporation and precipitation. *Proc. Roy. Soc.* **A141**, 512-517.

ROBINSON A. and STOMMEL HENRY (1959) The oceanic thermocline and the associated thermohaline circulation. *Tellus* **11**, (3). In press.

STOMMEL HENRY, ARONS A. B. and FALLER A. J. (1958) Some examples of stationary planetary flow patterns in bounded basins. *Tellus* **10**, (2), 179-187.

Printed in Great Britain by The Salisbury Press Ltd., Publicity House, Wilton Road, Salisbury, Wilts. (20254)

Contribution No. 1031

HEAT AND WATER-VAPOR FLUXES IN AIR FLOWING SOUTHWARD OVER THE WESTERN NORTH ATLANTIC OCEAN[1]

Andrew F. Bunker

Woods Hole Oceanographic Institution

(Original manuscript received 15 April 1959; revised manuscript received 18 September 1959)

ABSTRACT

Turbulent transports of sensible heat and water vapor have been measured from an airplane within southerly-flowing air masses over the western North Atlantic Ocean. It is found that the lower levels of these air masses are unstable and warmed by the transport of heat from the water below, while the higher levels are stable and warmed by diffusion from the subsidence-inversion air aloft. Average values of the upward flux of sensible heat were found to be 2.1 mcal cm^{-2} sec^{-1} in the middle latitudes and 0.1 mcal cm^{-2} sec^{-1} in the tropics. The downward heat flux was 0.3 mcal cm^{-2} sec^{-1} in the region above the potential temperature minimum formed between the warm air aloft and the water-warmed air below. The flux of latent heat of condensation in the form of water vapor was found to be less than the flux of sensible heat from the ocean in the middle latitudes within 300 km of the east coast and about one order of magnitude greater than the sensible flux farther offshore and in the tropics. The observations are discussed in relation to various theories of heat transport and the process by which the atmosphere accumulates heat from the earth's surface.

1. Introduction

The low-level air masses flowing southeastward over the ocean from the polar regions and the trade-wind air flowing southwestward in the tropics have been selected for study as prime examples of relatively cool dry air masses important in the heat-accumulating phase of the atmospheric-heat cycle. As these subsiding diverging air masses flow over the warmer water, sensible and latent heat is transported by turbulent convection into the unstable lower layers. Some of this heat is retained in the subcloud layer, while part of it is transported to higher levels by cumulus-cloud-convection processes. By the time the air masses begin to converge and to ascend in the mid-latitude storms, the equatorial belt, or heated regions of the continents, they are warmer and moister. Part of the water is condensed, releasing the latent heat of condensation, but that which is not condensed in the lifting process is carried throughout the troposphere and indirectly modifies the potential-temperature distribution through the radiative balance. Only the accumulation of heat from the earth's surface is studied in the present paper. The following phase of the heat cycle has been studied by Riehl and Malkus (1958) in their work on the release of energy and the heat balance in the equatorial trough.

To date, the heat and water-vapor flow has been deduced indirectly from accumulations of heat and water vapor, precipitation, estimates of radiational losses, and empirical formulae by Jacobs (1942, 1943, 1951), Riehl *et al.* (1951), Budyko (1956), London (1957), and others. While these methods are invaluable in the determination of the net heating on a global scale, they supply no information about the details of processes operating within the air mass or the magnitude or directions of the heat flows at different heights.

Direct observations of the vertical heat and water-vapor flux are now possible through the development of a system of measuring vertical velocities of the turbulent air from an airplane. This method has been described by Bunker (1955) and Lettau and Davidson (1957). When a record of airplane accelerations, airspeeds, altitudes, dry- and wet-bulb temperatures is reduced, a time series of the values of the turbulent vertical velocities of the air, temperature deviations, and water-vapor deviations is obtained. Values of the flows of sensible and latent heat may be found by averaging the products of the velocities with the temperature and water-vapor deviations.

Flux data of this type have been obtained in selected air masses chosen on the basis of certain characteristics—namely, low-level instability, subsidence, and southerly motion over the western North Atlantic Ocean. One hundred and twenty-five observations have been made at altitudes ranging from 8 m to 2100 m and in latitudes from 9N to 43N. Some of the earlier observations were made from a U. S. Navy PBY-6A (Catalina) aircraft while the remainder were made from a Navy R4D (DC-3, or Dakota).

2. Methods of observation and reduction of data

The methods of obtaining and reducing the data to values of heat flux have been described in *Exploring*

---

[1] Contribution No. 1031 from the Woods Hole Oceanographic Institution. This research was conducted under a contract with Office of Naval Research.

the Atmosphere's First Mile, edited by Lettau and Davidson, 1957. In this work, the vertical-velocity equation is derived as

$$w_i = a\Delta n/\rho V - b\Delta V/\rho V^2 - V\Delta\alpha_{att} + \sum_{0}^{t_i} \Delta n\Delta t + w_0. \quad (1)$$

The equation gives the vertical velocity w_i at the instant t_i in terms of the following: Δn, the vertical acceleration; ΔV, the deviations of the airspeed from the mean; $\Delta\alpha_{att}$, the deviation of the altitude of the airplane from the mean; and w_0, the airplane vertical velocity at the beginning of the run. One fifth-second averages of the observations were used in (1) to obtain a time series of w_i. Most of the runs lasted 2 min, although some of the earliest runs lasted only 30 sec.

The turbulent flow of sensible heat through a horizontal surface at the height, z_0, may be defined as

$$H \equiv c_p\overline{\rho w'T'} \quad (2)$$

when $\overline{\rho w'} = 0$. Here, w' is the vertical component of a gust velocity, and T' is the temperature deviation from the mean at z_0. In the present study, series have been obtained of observed values of w_i, the vertical velocities of the gusts measured according to equation (1), and T_i, the air temperatures, measured with a thermopile mounted on the airplane. The values in a given series were not obtained at a constant height, z_0, but at varying heights, $z_0 + \Delta z_i$, depending upon the altitude of the airplane. Under these conditions, the heat flux is redefined by the following form of the heat-flux expression:

$$c_p\overline{\rho w'T'} = c_p\overline{[\rho_i+f_\rho(\Delta z_i)][w_i-at-\bar{w}_i-f_w(\Delta z_i)] \times[T_i-bt-\bar{T}_i-f_T(\Delta z_i)]}. \quad (3)$$

Here, $f_\rho(\Delta z_i)$, $f_w(\Delta z_i)$, and $f_T(\Delta z_i)$ represent corrections to the observed values of ρ_i, w_i, and T_i obtained at $z_0 + \Delta z_i$ to make the values applicable to the reference height, z_0. The terms at and bt are the products of the slopes of the lines of regression of w_i and T_i against time. These terms are required since any short series of observations made in the atmosphere always will have a trend due to fluctuations with a period longer than the duration of the observations.

Equation (3) could be used for the computations of the heat flux in the atmosphere, but it will be shown now that a much simplified expression can be found that introduces errors of less than 2 per cent. First, it is necessary to show that the altitude of the airplane varies only a small amount during a two-minute observing flight. Root-mean-square altitude deviations were computed for several flights as a measure of the variation. The most extreme altitude variation observed during the entire program yielded an rms value of 16 m. Other values obtained in very rough, unstable air off the east coast were less than one-half of this value—*i.e.*, around 4 to 8 m. In the more stable air of the trade winds, the rms height values dropped to 1 or 2 m.

Using these figures, the results of neglecting the correction terms can be investigated. Considering first $f_\rho(\Delta z_i)$ a displacement, Δz_i, of 10 m in an atmosphere with an adiabatic lapse rate gives a temperature change of 0.1C and a value for $f_\rho(\Delta z_i)$ of 0.0004 kg m^{-3}. As this value is less than $\frac{1}{10}$ of a per cent of the density of the air in the regions studied, it can be neglected safely.

A single vertical-velocity measurement, w_i, is an average over the area of 360 m^2 which is the area swept out by an airplane wing in $\frac{1}{5}$ second. This area defines the horizontal dimensions of the gusts measured, and it may be assumed that the gust has comparable vertical dimensions. For the small vertical displacements that the airplane undergoes during its flight, the value of the gust at the reference level z_0 is included in the measured average. From the values of rms vertical velocities entered in table 1, it is seen that the vertical velocities vary slightly with height; hence, the value of $f_w(\Delta z_i)$ will be very small. Although the magnitude of $f_w(\Delta z_i)$ is very small, it cannot be dropped without first investigating the correlations that arise between it, T_i, and $f_T(\Delta z_i)$.

To evaluate the magnitude of the error in a heat flux determination resulting from correlations between the velocity and temperature, corrections and the gust velocities, densities, and temperature deviations, the following computation has been made. A gust has been assumed varying sinusoidally with a velocity amplitude of 100 cm sec^{-1} and a temperature amplitude of 0.3C in phase with the velocity and with a period of 4 sec. An atmosphere with an adiabatic temperature lapse rate and with an increase of rms vertical velocity of 20 cm sec^{-1} per 100 m is assumed. The height variation of the airplane was computed from the known characteristic response of the airplane, assuming no change in attitude and no horizontal component of the gust. It is found that the altitude reaches a maximum at 2.7 sec with an amplitude of 76 cm. The values of w_i, T_i, and ρ_i that would be observed from the airplane flying this path through the assumed gust were computed. The heat flux was computed by using this series of values and compared with the heat flux, $c_p\overline{\rho w'T'}$ being computed from the originally assumed values. The difference between the two computations was found to be less than one per cent. The flux was recomputed by using the average value of the density rather than the instantaneous observed value, ρ_i. The heat flux computed in this manner differed from the original flux, $c_p\rho\overline{w'T'}$, by only 1.2 per cent. From these computations, it is concluded that an error of only one or two per cent is introduced by neglecting corrective terms and using

TABLE 1. Airplane observations of temperature, humidity, turbulence, and fluxes.

Case I

17 December 1953, 1600 to 1620 EST, Region 1, 42.5N–68.5W, winds 325°, 7.8 m sec^{-1}, overcast, snow showers.

Height m	Pot. temp. K	Mix. ratio g kg^{-1}	σ_w cm sec^{-1}	σ_T C	$c_p\rho\overline{w'T'}$ mcal cm^{-2} sec^{-1}	$\rho\overline{w'q'}$ μg cm^{-2} sec^{-1}	$L\rho\overline{w'q'}$ mcal cm^{-2} sec^{-1}
0	283	8	—	—	—	—	—
140	267.7	1.2	93	0.39	6.0	—	—
280	267.1	1.2	96	0.21	4.5	0.5	0.3
560	267.0	1.2	131	0.33	6.0	2.0	1.2

Case II

23 December 1953, 1300 to 1325 EST, 42.5N–68.5W, Region 1, winds 284° 13.9 m sec^{-1}, 7/10 sky coverage by cumulus clouds.

0	282	7	—	—	—	—	—
50	277.4	—	54	0.21	0.3	—	—
150	277.6	—	68	0.15	0.9	—	—
290	278.1	—	82	0.18	1.5	—	—
580	277.3	—	87	0.18	0.3	—	—
840	278.1	—	39	0.30	−1.2	—	—
1620	287.5	—	12	0.09	0.0	—	—

Case III

5 January 1954, 1205 to 1230 EST, Region 1, over water north of Provincetown, Mass., winds 267° 6.3 m sec^{-1}, cirrus overcast.

0	278	5	—	—	—	—	—
15	272.5	2.9	44	0.27	−2.1	—	—
45	272.5	2.9	50	0.21	1.5	—	—
95	272.8	3.1	39	0.15	0.6	—	—
150	272.9	3.0	53	0.18	1.2	0.1	0.07
305	272.9	3.1	33	0.24	−0.9	0.4	0.3
440	274.0	2.2	15	0.12	0.0	0.1	0.04
610	280.8	2.9	16	0.30	0.0	—	—
915	284.5	3.0	12	0.33	0.3	—	—

Case IV

7 January 1954, 1300 to 1320 EST, Region 1, 42.5N–68.5W, winds 309° 6.5 m sec^{-1}, cumulus overcast.

0	281	7	—	—	—	—	—
55	275.5	—	69	0.15	1.5	—	—
140	275.5	—	79	0.30	4.8	—	—
270	275.5	—	58	0.15	0.6	—	—
550	275.7	—	98	0.18	3.0	—	—
740	276.0	—	46	0.15	−1.2	—	—

Case V

29 January 1954, 1445 to 1530 EST, Region 1, 42.5N–68.5W, winds 307° 6.9 sec^{-1}, 2/10 sky coverage by cumulus.

0	278	5	—	—	—	—	—
85	265.8	1.5	92	0.42	5.7	—	—
185	266.0	1.5	108	0.63	10.5	0.1	0.1
340	266.4	1.4	121	0.24	6.6	0.7	0.4
630	266.3	1.4	44	0.39	2.7	−0.4	−0.2
875	269.8	0.2	18	0.30	−0.9	—	—
1140	271.5	0.2	16	0.15	0.3	—	—

TABLE 1—*Continued.*

Case VI

24 February 1954, 1420 to 1520 EST, Region 2, Weather Ship 'H' 36N–70W, winds 285° 8.2 m sec^{-1}, 8/10 sky coverage by cumulus clouds.

Height m	Pot. temp. K	Mix. ratio g kg^{-1}	σ_w cm sec^{-1}	σ_T C	$c_p\rho\overline{w'T'}$ mcal cm^{-2} sec^{-1}	$\rho\overline{w'q'}$ μg cm^{-2} sec^{-1}	$L\rho\overline{w'q'}$ mcal cm^{-2} sec^{-1}
0	289	12	—	—	—	—	—
30	288.3	5.2	52	0.30	2.7	—	—
60	288.1	5.0	64	0.27	2.4	—	—
180	288.5	4.8	57	0.12	1.2	—	—
330	288.3	4.8	57	0.09	0.3	—	—
610	288.2	4.5	93	0.27	0.3	—	—
915	289.4	4.8	40	0.24	−0.3	—	—
1220	289.5	3.8	35	0.45	0.6	—	—
1585	293.3	2.2	22	0.33	−1.8	—	—
2135	298.7	2.0	14	0.54	1.2	—	—

Case VII

14 January 1955, 1455 to 1535 EST, Region 1, 41.1N–71.5W 20mi. SE of Block Island, winds 340° 20.5 m sec^{-1}, clear.

0	279	6	—	—	—	—	—
60	273.3	1.2	74	0.55	2.6	—	—
150	273.0	1.2	133	0.12	0.2	10.8	6.5
305	272.5	1.0	96	0.12	−0.3	1.5	0.9
610	273.0	0.9	45	0.08	−0.3	0.0	0.0
915	273.5	0.9	89	0.26	−0.3	—	—
1220	275.0	1.0	19	0.11	−0.4	—	—
1220	279.0	1.0	44	0.30	−0.9	—	—

Case VIII

18 January 1955, Regions 1 and 2, Rhode Island to Bermuda, winds 307° 11.7 m sec^{-1}.

Series 1: 100 km offshore, 1305 to 1320 EST, 4/10 sky cover by cumulus clouds.

0	276	6	—	—	—	—	—
150	270.2	1.9	94	0.08	1.1	—	—
335	270.4	1.7	121	0.07	1.7	—	—
520	270.5	1.6	86	0.05	0.1	—	—

Series 2: 270 km offshore, 1350 to 1400 EST, complete stratocumulus overcast.

0	283	8	—	—	—	—	—
150	274.1	—	135	0.19	3.9	—	—
305	274.5	—	107	0.08	1.1	—	—

Series 3: 530 km offshore, 1455 to 1505 EST, 10/10 overcast.

0	290	12	—	—	—	—	—
120	282.5	5.9	177	0.18	1.3	—	—
460	282.0	6.0	174	0.10	2.1	—	—

Series 4: 800 km offshore, 1550 to 1610 EST, breaks in overcast.

0	289	11	—	—	—	—	—
120	286.7	6.6	138	0.11	2.1	—	—
305	286.2	6.0	134	0.10	2.0	15.0	9.0
550	286.2	5.5	122	0.09	1.1	15.0	9.0

Series 5: 1000 km offshore, 100 km NW Bermuda, 1650 to 1710 EST, 6/10 cumulus.

0	289	12	—	—	—	—	—
90	288.0	6.0	138	0.13	2.4	—	—
305	288.4	4.9	151	0.08	1.1	19.0	11.5
550	288.5	5.6	129	0.07	0.8	6.6	4.0

TABLE 1—*Continued.*

Case IX

20 January 1955, 1030 to 1055 AST, Region 2, 32.5N–65.0W NW of Bermuda, winds 320° 22.0 m sec⁻¹, 8/10 sky coverage by cumulus and cumulonimbus.

Height m	Pot. temp. K	Mix. ratio g kg⁻¹	σ_w cm sec⁻¹	σ_T C	$c_p\rho\overline{w'T'}$ mcal cm⁻² sec⁻¹	$\rho\overline{w'q'}$ μg cm⁻² sec⁻¹	$L\rho\overline{w'q'}$ mcal cm⁻² sec⁻¹
0	292	13	—	—	—	—	—
60	290.3	—	98	0.15	1.1	—	—
150	289.8	—	87	0.08	0.6	—	—
305	290.8	—	111	0.10	1.3	—	—
610	291.4	—	65	0.09	0.6	—	—

Case X

22 January 1955, 1310 EST, Region 1, 39N–69W, wind 270° 6.0 m sec⁻¹, 8/10 sky coverage by post cold-frontal cumulus clouds.

0	286	10	—	—	—	—	—
100	278.8	—	61	0.11	−0.4	—	—
300	280.0	—	—	—	—	—	—

Case XI

7 December 1955, Bermuda to Rhode Island, winds 360° 1 m sec⁻¹, 4/10 sky coverage by cumulus clouds.
Series 1: 1200 to 1220 EST, Region 2, 600 km offshore.

0	292	13	—	—	—	—	—
15	284.6	—	67	0.18	2.1	—	—
60	284.4	—	98	0.15	2.8	—	—
140	284.7	—	96	0.10	1.8	—	—
325	284.8	—	102	0.10	1.5	—	—
565	284.7	—	92	0.08	0.5	—	—

Series 2: 1310 to 1330 EST, Region 1, 300 km offshore.

0	290	13	—	—	—	—	—
15	278.1	—	54	0.14	1.1	—	—
60	278.2	—	71	0.10	1.0	—	—
150	278.3	—	89	0.08	1.1	—	—
300	277.6	—	78	0.06	0.4	—	—
600		—	55	0.09	−0.1	—	—

Series 3: 1430 to 1450 EST, Region 1, 100 km offshore.

0	283	8	—	—	—	—	—
60	273.0	—	78	0.10	1.2	—	—
150	272.9	—	77	0.08	0.5	—	—
300	272.8	—	72	0.06	0.4	—	—
600	273.4	—	58	0.05	0.2	—	—

Case XII

9 March 1956, 1215 to 1310 EST, Region 1, 39.5N–70.5W, winds 275° 6.8 m sec⁻¹, 6/10 sky coverage by cumulus clouds.

0	280	7	—	—	—	—	—
60	275.0	2.8	86	0.17	1.9	(5.6)	(3.4)
200	275.1	2.7	105	0.14	0.5	—	—
305	275.3	2.7	92	0.10	1.0	—	—
610	274.9	2.7	85	0.07	0.8	—	—
940	277.6	1.7	45	0.30	−0.7	—	—

TABLE 1—*Continued.*

Case XIII

11 August 1956, Region 3, 19N–66W, 550 km ahead of hurricane Betsy.

Series 1: 1135 to 1225 AST, wind 058° 8.7 m sec⁻¹, 3/10 sky coverage by cumulus.

Height m	Pot. temp. K	Mix. ratio g kg⁻¹	σ_w cm sec⁻¹	σ_T C	$c_p\rho\overline{w'T'}$ mcal cm⁻² sec⁻¹	$\rho\overline{w'q'}$ μg cm⁻² sec⁻¹	$L\rho\overline{w'q'}$ mcal cm⁻² sec⁻¹
0	300	24	—	—	—	—	—
8	299.0	18.4	26	0.12	0.5	—	—
15	299.0	18.3	29	0.10	0.2	—	—
30	299.1	18.0	53	0.10	0.3	—	—
60	299.1	18.1	43	0.08	−0.1	—	—
150	299.5	17.9	40	0.07	0.2	1.5	0.9
305	299.4	17.5	48	0.12	0.4	5.1	3.2
610	299.8	16.3	33	0.20	0.2	5.6	3.3
1005	301.1	13.3	36	0.21	−0.5	2.3	1.2

Series 2: 1335 to 1410 AST, wind 060° 9.0 sec⁻¹, 3/10 sky cover by cumulus.

0	300	24	—	—	—	—	—
15	299.4	18.1	29	0.07	0.2	—	—
30	299.4	18.1	37	0.06	0.2	—	—
60	299.5	18.3	48	0.08	−0.3	—	—
150	299.6	18.0	50	0.05	0.2	5.8	3.4
305	299.6	17.4	52	0.14	0.4	3.2	1.9
610	299.9	16.2	37	0.34	−0.1	5.6	3.3

Case XIV

15 August 1956, 1030 to 1130 AST, Region 2, 19N–66W, wind 080° 8.5 m sec⁻¹, 3/10 sky coverage by small cumulus clouds.

0	300	24	—	—	—	—	—
15	299.7	20.4	27	0.11	0.3	—	—
30	299.6	19.9	28	0.08	0.1	—	—
60	299.7	19.9	40	0.08	0.1	—	—
150	300.0	19.5	33	0.07	0.0	1.0	0.6
305	299.6	18.9	39	0.08	−0.1	1.6	0.9
490	299.9	18.3	25	0.21	−0.3	1.8	1.0

Case XV

16 August 1956, 0735 to 0830 AST, Region 3, 19N–66W, wind 035° 5.2 m sec⁻¹, showery, 6/10 sky coverage cumulus and cumulonimbus.

0	300	24	—	—	—	—	—
30	299.0	18.9	30	0.07	0.2	—	—
60	299.1	18.9	44	0.06	0.1	—	—
150	299.8	18.6	44	0.04	0.2	0.7	0.4
305	299.8	17.8	26	0.05	0.0	0.9	0.5
470	299.7	17.6	20	0.08	−0.1	−0.1	−0.1

Case XVI

20 August 1956, 1725 to 1810 AST, Region 4, 13N–59W, wind 080° 4.8 m sec⁻¹, 4/10 sky coverage by cumulus clouds.

0	300	24	—	—	—	—	—
15	299.9	18.8	29	0.05	0.1	—	—
30	299.9	18.0	29	0.04	0.0	—	—
60	300.0	18.0	28	0.03	0.0	—	—
150	299.9	18.0	44	0.05	−0.1	—	—
305	299.7	17.3	50	0.04	−0.1	1.7	1.0
610	300.3	16.2	26	0.15	0.0	3.1	1.8

TABLE 1—*Continued.*

Case XVII

21 August 1956, 1445 to 1520 AST, Region 4, 12N–57W, wind 080° 6.8 m sec^{-1}, 7/10 sky coverage by cumulus and cumulonimbus in weak disturbance in easterlies.

Height m	Pot. temp. K	Mix. ratio g kg^{-1}	σ_w cm sec^{-1}	σ_T C	$\overline{c_p\rho w'T'}$ mcal cm^{-2} sec^{-1}	$\overline{\rho w'q'}$ μg cm^{-2} sec^{-1}	$\overline{L\rho w'q'}$ mcal cm^{-2} sec^{-1}
0	300	24	—	—	—	—	—
15	298.9	18.8	29	0.08	0.0	—	—
30	299.0	18.4	29	0.05	0.1	—	—
60	298.9	18.4	41	0.06	0.2	—	—
150	299.4	17.8	42	0.08	−0.2	−3.8	−2.3
305	299.4	17.7	31	0.05	−0.2	—	—
455	299.8	17.2	20	0.06	−0.1	2.5	1.5

Case XVIII

24 August 1956, 1110 to 1155 AST, Region 4, 11.5N–59.5W, wind 0.80° 7.2 m sec^{-1}, 4/10 sky coverage by cumulus clouds.

0	300	24	—	—	—	—	—
15	300.1	18.0	26	0.05	0.1	—	—
30	300.1	18.0	32	0.05	0.1	—	—
60	300.1	18.0	39	0.06	0.0	—	—
150	300.3	17.4	45	0.05	−0.4	1.5	0.9
305	300.2	16.6	45	0.10	−0.1	4.3	2.5
575	300.1	16.0	42	0.20	−0.2	5.7	3.3

Case XIX

15 November 1957, 1248 to 1258 AST, Region 4, 9N–58W, wind 080° 8.0 m sec^{-1}, 4/10 sky coverage by cumulus clouds.

0	301	25	—	—	—	—	—
60	299.8	18.7	33	0.22	0.4	—	—
150	300.2	18.6	28	0.10	−0.3	0.9	0.5

Case XX

22 February 1958, 1440 to 1455 AST, Region 3, 19N–64W, wind 040° 9.8 m sec^{-1}, 5/10 sky coverage by cumulus clouds.

0	297	20	—	—	—	—	—
30	295.7	13.5	70	0.06	0.4	—	—
150	296.0	13.0	97	0.08	−1.9	12.1	7.3
300	295.8	12.7	73	0.05	−0.2	−8.2	−4.9

Case XXI

24 February 1958, 1102 to 1150 AST, Region 4, 11N–60W, wind 050° 5.0 m sec^{-1}, 8/10 sky coverage by cumulonimbus and cumulus clouds.

0	299	22	—	—	—	—	—
30	297.8	17.0	38	0.06	0.1	—	—
125	298.0	15.9	56	0.09	−0.6	0.7	0.4
320	298.3	16.3	41	0.09	−0.2	0.3	0.2
555	298.3	15.7	52	0.09	−0.7	3.0	1.8
800	299.2	13.5	59	0.08	0.1	1.4	0.8
1120	301.9	11.2	46	0.06	−0.1	−1.8	−1.1

Case XXII

25 February 1958, 0946 to 1115 AST, Region 4, 11N–60W, wind 070° 8.0 m sec^{-1}, 5/10 sky coverage by cumulus clouds.

0	299	22	—	—	—	—	—
30	297.9	16.9	68	0.07	−0.6	—	—
165	298.0	16.7	50	0.06	−0.1	1.7	1.0
470	298.4	15.5	55	0.13	−1.4	4.4	2.6
900[1]	299.8	12.4	37	0.22	−0.1	0.5	0.3
900	299.8	14.9	50	0.09	−1.0	4.2	2.5
960[2]	300.2	13.6	136	—	—	25.0	15.0
1200[3]	300.5	11.3	71	0.13	−2.2	−4.8	−2.9

[1] Flight under an overhanging section of cumulus cloud.
[2] Flight through a cumulus cloud.
[3] Flight between the tops of two small cumulus clouds.

the average value of the density of air. Hence, the sensible heat flux may be expressed by the following equation:

$$\overline{c_p\rho w'T'} \approx c_p\bar{\rho}\overline{(w_i - at - \bar{w}_i)(T_i - bt - \bar{T}_i)}. \quad (4)$$

A form better suited for computation is obtained by multiplying, averaging, and simplifying with the identity $\overline{atT_i} = \overline{btw_i} = ab\overline{t^2}$. We get the following equation which has been used in all computations:

$$\overline{c_p\rho w'T'} \approx c_p\bar{\rho}(\overline{w_iT_i} - \bar{w}_i\bar{T}_i - ab\overline{t^2}). \quad (5)$$

Similar equations are used for computation of σ_w, σ_T, and $\overline{\rho w'q'}$.

The probable error of flux determinations cannot be established for all conditions, since the error depends on the range of sizes of the gusts producing the transport. If the gust sizes are all within the size range of 20 m to 6 km, the airplane and the instruments would respond completely and the necessary data would be recorded with good accuracy. The errors present would be small and caused by airplane deformation, reading, and calibrating errors. Probable errors under these circumstances would be about 5 per cent for the heat flux. Whenever a significant portion of the total transport is carried by gusts smaller than 20 m or larger than 6 km, the determined values will be too small. From studies made by Panofsky and McCormick (1954) of the spectra of turbulence at 100 m at the Brookhaven tower, it is concluded that very little transport is accomplished by gusts smaller than 20 m. Gusts larger than 6 km may transport significant amounts of heat and water vapor, but little is known about transport in this spectral region. As a check upon transport by large gusts and the over-all accuracy of the airplane measurements, the average of a series of heat-flux determinations made over Long Island was compared with the total heat accumulated in the air mass as it moved across the island. The agreement was within 4 per cent, indicating good accuracy of the method and that transport by gusts outside the 20 m-to-6 km range was small in this case. It cannot be said, however, that transport by gusts outside the specified size range will be small in all cases.

Comparisons of the heat fluxes measured from the airplane with fluxes measured from ground-based instruments at O'Neill, Nebraska (Lettau and Davidson, 1957) showed that the airborne instruments gave values 60 per cent too small. Heat fluxes measured over the Gulf of Maine also were only one-third of the fluxes computed from observations of the initial and final temperature soundings along air trajectories. It was concluded that the mass of the thermopile housing increased the effective lag of the thermopile and seriously decreased the measured amplitude of the temperature variations. Consequently, a correction factor of three has been applied to the data of the first six cases. No other corrections have been applied to any data in this paper. A new thermopile and housing were constructed which were less massive, better-ventilated, and utilized smaller thermocouple wire. This thermopile has a response time of about 0.2 sec at aircraft speeds.

Mixing-ratio values used in the computation of water-vapor flows were determined from wet- and dry-bulb thermistors exposed to the free air stream in a venturi housing. The thermistors, No. 31D4 of Victory Engineering Corporation, have a thermal response time of about one second when mounted in the housing and ventilated at airplane speeds. Since this response time is greater than the response time of the velocity-measurement system, individual mixing-ratio values were matched for multiplication with the average velocity for the preceeding five fifth-second intervals. Values were read from the record every second giving 120 values per run. For sub-freezing temperatures, a lithium-chloride strip was used to measure humidities and similarly matched with velocities averaged over one second.

The contribution of the high-frequency end of the transport spectrum is lost by the slow response of the thermal elements. Comparisons were made between the fluctuations in mixing ratio as measured by the thermistors and as measured by a University-of-Texas-model refractometer. The refractometer measurements, made under the direction of R. M. Cunningham of Geophysical Research Directorate while a C-130 was flying off the wing tip of the R4D in the trade-wind region, confirmed the suspicion that the fluctuations of mixing ratio were too fast to be recorded reliably by the thermistors at the 30-m level. At the 150-m level, the fluctuations have a predominant wave length in the 100- to 500-m range. The thermistors can respond satisfactorily to fluctuations of this scale when flown through these regions at 60 m sec^{-1}. Hence, only those water-vapor flux measurements made above the 150-m level have been included in this report.

3. Presentation of data

The reduced data for the 22 cases studied have been collected in table 1. For each case, the date, time, location, wind, and cloudiness are given in the heading. The winds were observed from drift-sight readings or rawin reports and represent averages through the layer studied. Potential temperatures and mixing ratios at zero height are values for the air in immediate contact with the water as determined from ship reports of the water temperature.

4. Turbulent vertical velocities

The root-mean-square vertical velocities, σ_w, are presented in table 1 as a measure of the air mass's degree of turbulence and kinematic ability to transport properties vertically. Inspection of the values listed shows considerable variation from day to day and region to region. A variation which is noted in nearly every case is an increase in intensity upward through the lowest levels, a broad maximum in the lower half of the ground layer, and a decrease in the upper half of the ground layer and the inversion or cloud layer. In cases of greater instability, the maximum velocities are displaced higher toward the top of the ground layer. When the horizontal turbulent velocities, which were measured but not listed in table 1, are combined with the vertical velocities to form an rms total turbulent velocity vector, the height variation transforms into a distribution with a maximum at the lowest levels and a gradual diminution of intensity up into the cloud layer.

These distributions are interpreted to be the result of both the production of turbulence near a surface and the damping of the vertical component of the gust near a surface and in the stable air aloft. The upward displacement of the maximum vertical velocities in the unstable case results from the buoyancy acceleration of warm air parcels. Another source of turbulence is the buoyancy associated with the condensation of water vapor in cumulus clouds. This type of motion originates near the condensation level of the air mass. The vertical velocities first increase to a maximum of several m sec^{-1} and then decrease rapidly whenever a stable layer is penetrated. If all three sources of turbulence are equally effective in a given air mass, the resulting distribution of turbulence will be very complex. However, many cases in table 1 represent a predominance of one or two sources of turbulent energy. Case XI is an excellent example of pure convective turbulence, since the water was warmer than the air and the wind was only about 1 m sec^{-1}. Many observations taken in Region 1 represent a combination of mechanical and convective turbulence. In the trade-wind region where the air-sea temperature difference is slight, only mechanical and condensation-convective turbulence is important in producing the observed vertical-velocity profile. Here the moderate values of the turbulence observed in the sub-cloud layer are the consequence of the absence of convection, the moderate winds, and the inability of the turbulence of the cumulus clouds to penetrate the air beneath them.

No theory has been developed to treat the interrelation of the different types of turbulence, but the uncomplicated situation of heating from below in the

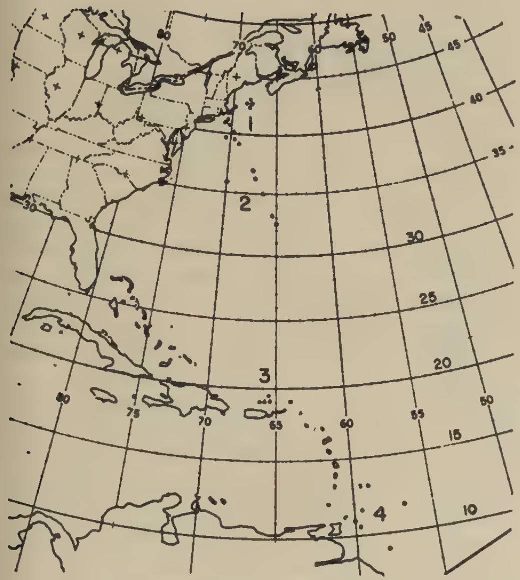

FIG. 1. Map of western North Atlantic Ocean. Dots represent location of observations. Figures identify regions mentioned in text.

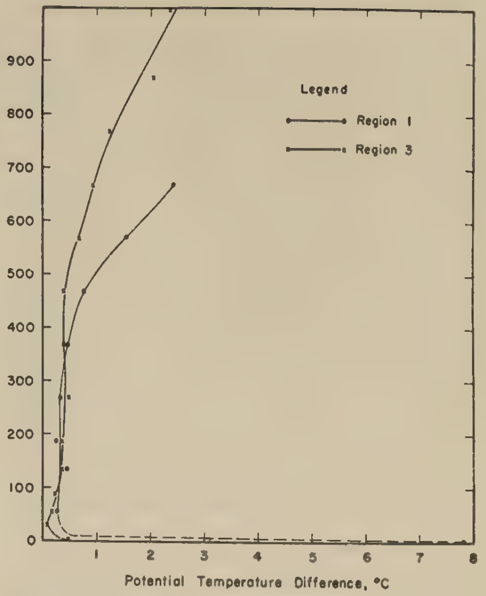

FIG. 2. Potential-temperature difference-height diagram. Average temperature differences of table 2 for Regions 1 and 3 are plotted to show potential-temperature minimum.

absence of a mean wind has been studied by Malkus (1954). His theory determines the heat transport through a fluid contained between a heated horizontal surface and an upper cooled parallel surface. The transport is given in terms of the smallest eddy size representing the stability restrictions on the fluid motion.

The mean total turbulent velocities may be predicted from the theory and compared with the observations of case XI. Malkus' equation gives $\overline{V\cdot V} = \frac{1}{9}(K/h)^2\lambda$ where $\lambda \equiv \alpha g\beta_0 h^4/K\nu$. Here, h is the height of the layer of unstable air considered; K is the thermometric conductivity of air; α is the coefficient of thermal expansion of air; β_0 is the mean negative temperature gradient between the sea surface and the height, h; ν is the kinematic viscosity of air; and g is the acceleration of gravity. The space average of the squared turbulent velocities $\overline{V\cdot V}$ is thus a function of the gradient, the dimensions of the layer, and the molecular properties of air. In case XI, the air-sea temperature difference was about 10C, the wind only about 1 m sec^{-1}, the height of the unstable air about 300 m, and the total rms turbulent velocities were found to reach a maximum of 180 cm sec^{-1}. When the dimensions of the system and the temperature difference are entered in the equation, an upper limit to rms total velocity of 520 cm sec^{-1} is found. The agreement between the two values is fair enough to encourage further exploration of the theory. The small observed velocities may be explained by the stable air aloft which is capable of damping the turbulent gusts which enter from below, while the theory was developed on the basis of a solid lid at the upper boundary.

5. Sensible heat flux

Convergence of heat flux. An upward flux of sensible heat was observed in all but two cases in the lowest layers of unstable air above the warmer water. In these two cases (X and XXII), observations were not made low enough to be in the unstable layer, and, hence, downward fluxes were observed. In sixteen cases, the direction of the heat flux reversed with height so that at the upper stable levels the flux was directed downward. In the remaining four cases, the soundings were terminated at 550 m to 610 m for operational reasons. A convergence of sensible heat into the ground layer is produced by the decrease to zero of the upward flux and the increase in downward flux with height. Thus, the air in this layer is heated both by the heat transported upward from the water and by the heat transported downward from the warm air of the subsidence inversion. In the middle latitudes, a greater proportion of the heat expended in warming the air is derived from the ocean. In the lower latitudes, a greater proportion of sensible heat is derived from the warm air aloft.

Persistence of potential temperature minimum. A cold subsiding continental air mass has a stable lapse rate before it begins moving southward over the warm land or the ocean. Over the ocean, the lowest layer is heated rapidly, thus producing a potential-temperature curve with a minimum at some relatively low level. If the convergence of heat into the air mass is equal at all levels, then the temperature profile will retain the minimum at a low level as the air mass travels southward. To determine whether this occurs in the air masses under study, averages of the potential temperatures in several height ranges were found for four different geographical regions. The four regions, shown in fig. 1 (*i.e.*, (1) offshore New England, (2) Bermuda, (3) Puerto Rico trade-wind region, and (4) Trinidad trade-wind region), represent different downstream positions or durations over the ocean. In table 2, the average differences in potential temperature from the minimum temperature of an individual sounding are tabulated. No averages are given whenever one or more of the cases used had no values available in a given height range. Sea temperatures are given since they represent the temperature of the air in contact with the water. The shape of the temperature profile from the ocean surface to the lowest level given in the table is not known, but it can be inferred from other studies in micrometeorology to be strongly super-adiabatic in the lowest meter and less unstable at higher levels. Fig. 2 has been drafted to show this feature graphically. The table shows that the air in the level from 20 m to roughly 300 m has a lower potential temperature than the air in contact with the water below or the air above it in all four regions, indicating that the diffusion processes in combination with radiative processes operate in such a manner as to produce equal convergence in each layer.

TABLE 2. Average potential-temperature differences.

Height range in meters	Region 1	Region 2	Region 3	Region 4
0 (sea temp)	7.8	3.30	0.48	1.30
20 to 40	—	—	0.10	—
40 to 70	0.26	—	0.19	0.16
70 to 110	—	0.15	0.22	0.35
110 to 160	0.44	0.20	0.38	0.49
160 to 220	0.24	0.44	0.39	0.38
220 to 320	0.32	0.52	0.48	0.39
320 to 420	0.46	0.71	0.36	0.55
420 to 520	0.72	0.69	0.36	0.71
520 to 620	1.54	0.92	0.67	0.80
620 to 720	2.40	1.12	0.92	1.27
720 to 820	—	—	1.22	1.46
820 to 1020	—	—	2.04	2.44
1020 to 1220	—	—	2.38	3.48
1220 to 1620	—	—	4.80	5.05

Fluxes interpreted by theories of heat transport. The several physical processes operating in a moving air mass heated both from below and above interact strongly and cannot be described completely by any existing theory. No attempt will be made here to review the vast field of transport theory but rather to discuss a few works that help interpret the fluxes observed in the present study.

The theory of heat diffusion developed by Taylor (1915) and Schmidt (1921) states that heat will be transported by turbulence down a potential-temperature gradient with a magnitude proportional to the gradient and a diffusion parameter. Table 1 shows that the majority of the fluxes conform to this theory in so far as the direction is concerned. As the theory cannot specify the diffusion factor for a given air mass, no magnitudes can be computed.

In many layers, it is noted that the flux is upward although the diffusion theory states that the flux should be downward. These observations are in agreement with the convective-turbulence theory of Priestley and Swinbank (1947). This theory states that the heat-diffusion equation is incomplete without a term depending upon the buoyancy of the individual parcels of air. The effect of this term is to allow an upward transport of heat through a stable atmosphere. This buoyancy effect attains importance under certain conditions of heating, turbulence, and parcel size which allow the parcel to receive and maintain an excess temperature for a sufficiently long time. Priestley (1954) extended this notion by developing equations which gave the heat flux in terms of the observed temperature fluctuations. Bunker (1956) has shown that these equations give values that are in good agreement with observed fluxes, using the observations contained in the present case VIII.

The theory of thermal turbulence developed by Malkus (1954) has been found capable of predicting the heat flux in case XI with order-of-magnitude accuracy. This theory gives a heat flux of 0.4 mcal cm^{-2} sec^{-1} while the observed fluxes averaged 1.1 mcal cm^{-2} sec^{-1} and ranged from 0.4 to 2.8 mcal cm^{-2} sec^{-1}. The theory also predicts rms temperature deviations of 0.05C, while the observed fluctuations ranged from 0.05C to 0.18C.

Regional variations. Averages were found for the upward flux by averaging all of the values at or below 60 m. If no observation was made at 60 m, the 150-m observation was used provided the air was still unstable at 150 m. The average downward fluxes were formed similarly from all of the observations taken in the stable layer above the level at which the flux changes sign. Excluded from this average are the two cloud flights of case XXII. The averages are entered in table 3 together with latent-heat-flux averages.

The most significant regional variation is noticed in the upward flux of sensible heat. The decrease from 2.3 mcal cm^{-2} sec^{-1} in Region 1 to 0.1 mcal cm^{-2} sec^{-1} in Region 4 is associated with the decrease of air-sea temperature differences from Region 1 to 4. This decrease directly affects the transport by decreasing

TABLE 3. Regional averages of sensible- and latent-heat fluxes.

	mcal cm⁻² sec⁻¹		
Region	Upward sensible-heat flux	Downward sensible-heat flux	Latent-heat flux
1	2.30	0.39	1.08
2	2.00	0.08	8.38
3	0.17	0.46	1.54
4	0.10	0.32	1.17

the temperature gradient and indirectly affects it by decreasing the convective turbulence. The variation of the downward flux of heat is rather slight and suggests a compensating relation between gradient and turbulence. The ratio of the upward to the downward flux of sensible heat shows that in the first two regions the air is being warmed primarily by the heat derived from the ocean. In the tropical regions, nearly three times as much heat is diffused downward from the inversion air as is diffused upward from the sea surface.

A comparison has been made between the regional averages of upward heat flux and the averages determined by others in either the same region or meteorologically comparable regions. The values to be compared are presented in table 4 in calories cm^{-2} day^{-1}. The averages given by Jacobs (1943) were computed from a vast number of ship reports of surface winds, air temperatures, humidities, and sea temperatures by use of empirical formulae relating these quantities to heat and water-vapor flow. The winter-season averages are entered in table 4 for Regions 1 and 2 since all of the present measurements were made in the winter time. For Regions 3 and 4, Jacobs' (1951) annual averages are used for comparison. Annual values computed by Budyko (1956) are presented in the next column. These were computed from ship reports by use of empirical formulae. The next three columns present values obtained not in Regions 1, 2, or 3, but in regions that are meteorologically similar. The values under the headings Manabe (1957, 1958) and Miyazahi (1949) were determined over the Japan Sea, which is similar to Regions 1 and 2. The fluxes of Riehl *et al.* (1951) were found from empirical formulae over the sea between San Francisco and Hawaii, an area which is similar to Region 3. The measurements of Manabe were made during January and February, 1955. Fluxes of sensible heat were obtained by an integral method which used radiosonde observations around the Sea to determine the amount of heat taken up by the air. The flux determined by Miyazahi was computed from empirical formulae and represents a five-year wintertime average.

TABLE 4. Comparisons of average sensible-heat fluxes.

		cal cm⁻² day⁻¹				
Author:	Bunker	Jacobs	Budyko	Manabe	Miyazahi	Riehl
Method:	$c_p\rho\overline{w'T'}$	Em. For.	Em. For.	Integral	Em. For.	Em. For.
Region						
1	199	120W	82	555	180	—
2	182	70 to 260W	87	555	180	—
3	15	0	27	—	—	8 to 16
4	9	−5	3	—	—	—

Comparing the averages of Region 1, it is seen that the turbulence method gives a higher value than do the empirical formulae. Much of the difference comes from the fact that the averages of Jacobs and Budyko include winds from all directions. A fair agreement occurs between the values of Region 1 and 2 and those obtained over the Japan Sea. The value obtained by the turbulence method falls between the high value obtained by Manabe using the integral method and the low value obtained by Miyazahi using the empirical-formulae method. The downward flux of heat should be added to the upward flux to obtain a value to be compared to the total sensible-heat flux found by Manabe. The total flux obtained, 232 cal cm^{-2} day^{-1}, is still smaller than 555 cal cm^{-2} day^{-1} but not too small to be explained as the result of differences due to local variations or errors intrinsic in the methods of determination.

In the trade-wind region, excellent agreement is reached between the turbulence-method values and the values of Riehl determined in a comparable region of the Pacific Ocean trade winds. Riehl's observations were obtained from weather ships stationed between San Francisco, California and Hawaii during July through October, 1945. These observations are more reliable than the observations taken by commercial ships elsewhere. The values of Jacobs and Budyko disagree, but their average agrees well with the values of Riehl and Bunker. In Region 4, the magnitudes of the flux are small, and Jacobs indicates a flux of heat into the ocean.

6. Latent-heat fluxes

Regional variations. The latent-heat fluxes observed in the ground layer have been averaged and included in table 3. No values observed in the cloud layer are included in the average, as these fluxes would be unrepresentative of the turbulent flux from the sea surface since the upward flux in the cloud layer is strongly organized by the cumulus clouds into preferred cloudy areas. The increase of latent-heat flux from Region 1 to Region 2 is the result of the increased gradient caused by the warming of the air and the consequent increase in the ability of the air to retain water vapor. In Region 1, the saturation mixing ratio of the air varies from 2 to 5 g kg^{-1}, while in Region 2 the saturation mixing ratio is 10 to 15 g kg^{-1}. As the turbulence is about the same in the two regions, the air's ability to hold water vapor accounts for the difference in gradient and flux. The flux is much lower in Regions 3 and 4. Here, the low value must be attributed to the decrease in the magnitude of the turbulence, since the gradient of the moisture is nearly the same as in Region 2. Inspection of table 1 shows that the rms vertical velocities in the trade winds are one half or a third of the intensity in Region 2. In spite of the decreased latent-heat flux in the trades, it is about one order of magnitude larger than the sensible-heat flux.

TABLE 5. Regional averages of the latent-heat flux.

	cal cm^{-2} day^{-1}				
Author:	Bunker	Jacobs	Budyko	Manabe	Riehl
Method:	$c_p\rho\,\overline{w'T'}$	Em. For.	Em. For.	Integral	Em. For.
Region					
1	94	120? W	230	340	—
2	720	480 to 600W	330	340	—
3	132	200	275	—	250
4	100	<200	165	—	—

Table 5 has been compiled to compare the fluxes with those observed by Jacobs, Budyko, Manabe, and Riehl. With the exception of the average for Region 2, the turbulence method gives lower values than the other methods.

Local variations. Inspection of the water-vapor fluxes fails to show any systematic variation with height in the ground layer, but it shows a large range of fluxes from -8 to 19 μg cm^{-2} sec^{-1}. The possibility of this wide range resulting from instrumental difficulties or failures was eliminated by checking records, calibrations, and data reductions. About ten per cent of the observations show a flux opposed to the mean gradient of the mixing ratio. In these cases, the net flux for the particular flight was found to be dominated by the presence of one or more very dry or moist updrafts or downdrafts of relatively long duration indicating a sampling that was too small. Had the runs been 12 or 18 km long instead of 6 km, the range would have been decreased and the negative fluxes possibly eliminated.

Large dominating gusts appear to be associated with active cumulus or cumulonimbus clouds. Case VIII yielded the largest fluxes, and many active cumuli were building up and dissipating in the area. The value of -4 μg cm^{-2} sec^{-1} was observed in case XVII at 150 m in the presence of cumulonimbus associated with a disturbance in the easterlies. The negative flux of case XX was observed in a modifying polar air mass that had penetrated into the trade-wind area.

The effect of cumulus clouds upon the flux of sensible heat and water vapor in both the cloud air and air surrounding the clouds was studied on 25 February 1958, case XXII. In addition to the regular flux measurements, three special flights were made through and near clouds. The first was made under the overhanging of a cumulus tilted by the shear of the wind, the second was through a cumulus cloud, and the last was between the tops of two small clouds. The first run gave an upward water-vapor flux that was much smaller than the flux obtained at the same level but far from the cloud. The records of vertical velocities and water vapor show that as the airplane passed under the overhang it penetrated a dry air parcel for 30 sec (2 km) which was ascending. When this negative flux is averaged with a positive flux observed in the remainder of the run (4 km), a small positive flux results. The cloud penetration yielded a large water-vapor flux as was expected. The flight between the cloud tops gave a rather large negative flux. Here again, the flux was dominated by a single intense gust. Further investigation of the association with clouds will have to be made before these gusts are understood and their origin established.

Comparison of fluxes with evaporation determined by formula. The empirical evaporation formula,

$$E = k(e_s - e_a)W_a,$$

was developed and used by Jacobs (1942) and others to compute the evaporation E, in mm day^{-1}, from the saturation water-vapor pressure above the ocean surface e_s, in mb, from the water-vapor pressure at anemometer level, e_a, and the wind speed, W_a, in m sec^{-1}. The value of the evaporation factor, k, was computed from the balance of energy received and lost by an air mass and was found to lie between 0.07 and 0.19. Jacobs has adopted $k = 0.14$ and computed values of evaporation for the North Atlantic and Pacific Oceans. The value 0.086 was found by Wüst from the METEOR observations to apply to the NE trade-wind region. Sverdrup (1951) gives a complete discussion of these values and the problems of evaporation measurement.

A comparison of the results of the formula method with the airplane fluctuation method was carried out in August 1956 in the trade-wind region north of Puerto Rico. Surface meteorological and oceanographical observations were made from the R/V CRAWFORD on three days when water-vapor-flux measurements were made from a PBY-6A flying overhead. The airplane technique gave evaporations 25 per cent smaller than the formula method when 0.086 was used for the value of k.

7. Heat and water-vapor accumulation

The process of the heat and water-vapor accumulation in the air masses studied undergoes several distinct phases which now may be summarized. Before a polar continental air mass reaches the ocean, its lowest layers are well mixed by mechanical and dry-

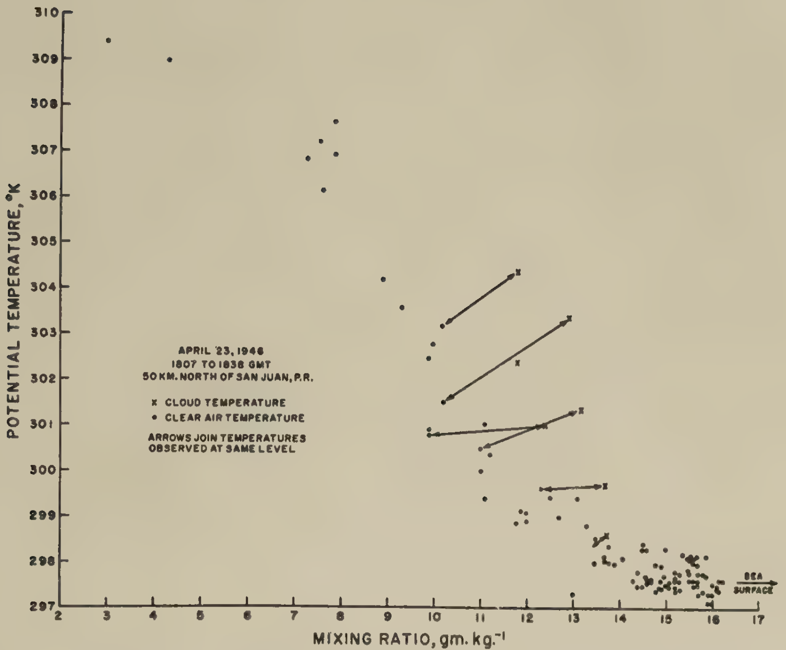

Fig. 3. Potential temperature-mixing ratio diagram of clear air and air within cumulonimbus cloud. The lines connect values inside and outside of the cloud at the same altitude.

convective turbulence. Heat is being transported upward in the mixed layer and downward in the smooth subsidence-inversion layer. Very small amounts of water vapor may be diffused upward from the ground. When the air mass moves out over the ocean, the sensible heat-flux pattern remains the same but an upward flow of water vapor is initiated or greatly accelerated. An approximate daily heat budget for winter-time polar air in this state at 45N may be made using average values of radiational loss and gain by London (1957). He finds a cooling of about 0.8C per day in the lowest kilometer. A flow of 2.1 mcal cm^{-2} sec^{-1} upward and 0.4 mcal cm^{-2} sec^{-1} downward into the layer gives a warming of 8.8C per day. Therefore, a net warming of 8.0C per day results from the summation of solar radiation, long-wave radiation exchange, and the turbulent transport of sensible heat. Neglected in this estimate is any warming due to air subsiding into the layer, any heating due to the condensation of water vapor, or loss of heat by transport to higher levels.

Dry-convective and mechanical turbulence continues as the diffusing agent until the turbulent ground layer air approaches saturation. At this stage, the buoyancy produced by the condensation of water vapor becomes an important factor in the acceleration of diffusion of heat and water vapor into the smooth air of the inversion layer. The change from mechanical and dry-convective turbulence to mechanical, dry- and moist-convective turbulence produces a change in the distribution of intensity of turbulence in the ground layer as well as in the inversion layer. In the ground layer, the turbulence increases moderately and the level of maximum intensity may rise. In the inversion air, the turbulence is increased one or two orders of magnitude locally where the cumulus clouds build up and a general moderate increase of turbulence occurs in the inter-cloud space. By this more rapid process, the atmosphere is heated and moistened to heights of many kilometers. The continuation of the cumulus activity creates a new cloud layer above the ground layer in the subsidence-inversion air. This layer is more moist and less stable than the subsidence layer.

If rain falls from the clouds building up in this layer, the heating of the air mass is hastened since the released heat will not all be consumed in the later evaporation of cloud drops. One example of heating through cumulonimbus activity is presented in fig. 3. The points on this potential temperature-mixing ratio diagram were computed from airplane psychrograph records obtained by Wyman and Woodcock in the Puerto Rico region in 1946 and reported by Bunker *et al.* (1949). The points observed inside the cloud are potentially warmer and drier than the air in the surface layer and warmer and more moist than the air which surrounds them. As this cloud mixes with the environmental air, a net warming and moistening of the cloud-layer air will result.

In the low latitudes, dry-convective turbulence ceases to be of importance in transporting heat and water vapor, since the air-sea temperature difference may drop to less than 1C. Hence, only mechanical turbulence produced at the air-sea interface and condensation convection in the cloud layer maintain the mixing process. Turbulence in the ground layer is moderate, while vertical velocities in the cumulus clouds may reach several meters per second. With the decrease in turbulence in the ground layer and the decrease in temperature gradient, the sensible heat flux drops sharply. The water-vapor flux decreases but not as markedly since the vapor gradient remains large. Using London's computations of radiational losses from the troposphere, it is estimated that the lowest levels of the atmosphere in Region 3 will lose about 60 cal cm^{-2} day^{-1}. Since this is more than the observed flow of sensible heat both from the sea and from the upper air into the layer, it is concluded that the condensation of water vapor makes up for the radiational loss. The daily heat budget for the trade winds in Region 3 is 17 cal cm^{-2} upward sensible heat, 34 cal cm^{-2} downward sensible-heat flow, 154 cal cm^{-2} upward latent-heat flow, and a loss of 60 cal cm^{-2} by radiation. A net amount of about 400 cal cm^{-2} is accumulated in a trade-wind air column during a three-day passage through the region.

The magnitude of the heat accumulated during an outburst of polar air may be estimated by summing the average values observed in the first three regions and subtracting the estimated radiation losses. If it is assumed that an air mass spends one day in each of the first three regions, 1176 cal cm^{-2} will be added to the air, and from London's work it is estimated that 120 cal cm^{-2} will be lost from the lowest levels of the atmosphere during the movement to 20N. Thus, more than 1000 cal cm^{-2} would be accumulated by the air column. Since polar air masses reach the tropics rather infrequently, their annual transport into these regions is slight. Their energies are more likely to contribute to the middle-latitude cyclones, since these air masses are usually deflected easterly or westerly before they reach the tropics. As an exporter of water vapor and sensible heat to the equatorial regions, the trade-wind system is much more important because of its greater geographical extent and constancy of flow.

REFERENCES

Budyko, M. I., 1956: Teplovoi balans zemnoi poverkhnosti. *Gidromèteorologicheskoe izdatel'stvo*, Leningrad, 255 pp. (U. S. Wea. Bur. translation, 1958: Heat balance of the earth's surface. PB131692 259 pp.)

Bunker, A. F., 1955: Turbulence and shearing stresses measured over the North Atlantic Ocean by an airplane-acceleration technique. *J. Meteor.*, **12**, 445–455.

——, 1956: Measurements of counter-gradient heat flows in the atmosphere. *Aust. J. Phys.*, **9**, 133–143.

Bunker, A. F., B. Haurwitz, J. S. Malkus, and H. Stommel, 1949: Vertical distribution of temperature and humidity over the Caribbean Sea. *Pap. Phys. Oceanogr. and Meteor.*, **11**, 1–82.

Jacobs, W. C., 1942: On the energy exchange between sea and atmosphere. *J. Mar. Res.*, **5**, 37–66.

——, 1943: Sources of atmospheric heat and moisture over the North Pacific and North Atlantic Oceans. *Ann. N. Y. Acad. Sci.*, **44**, 19–40.

——, 1951: Large-scale aspects of energy transformations over the ocean, in *Compendium Meteor.* Boston, Amer. meteor. Soc., 1057–1070.

Lettau, H. H., and B. Davidson, 1957: *Exploring the atmosphere's first mile*, Vol. 1. London, Pergamon Press, 376 pp.

London, J., 1957: *A study of the atmospheric heat balance.* Unpubl. rep. to Air Force, AFCRC–TR–57–287. Astia no. 117227.

Malkus, W. V. R., 1954: The heat transport and spectrum of thermal turbulence. *Proc. r. Soc.* A, **225**, 196–212.

Manabe, S., 1957: On the modification of airmass over the Japan Sea when the outburst of cold air predominates. *J. meteor. Soc. Jap.* Sec. II, **35**, 311–326.

——, 1958: On the estimation of energy exchange between the Japan Sea and the atmosphere during winter based upon the energy budget of both the atmosphere and the sea. *J. Meteor. Soc. Jap.* Sec. II, **36**, 123–133.

Miyazaki, M., 1949: The incoming and outgoing heat at the sea surface along the Tsushima warm current. *Ocean. Mag.* Tokyo, **1**, 103–111.

Panofsky, H. A., and R. A. McCormick, 1954: Properties of spectra of atmospheric turbulence at 100 metres. *Quart. J. r. Meteor. Soc.*, **80**, 546–564.

Priestley, C. H. B., and W. C. Swinbank, 1947: Vertical transport of heat by turbulence in the atmosphere. *Proc. r. Soc.* A, **189**, 543–561.

Priestley, C. H. B., 1954: Vertical heat transfer from impressed temperature fluctuations. *Aust. J. Phys.*, **7**, 202–209.

Riehl, H., T. C. Yeh, J. S. Malkus, and N. E. LaSeur, 1951: The north-east trade of the Pacific Ocean. *Quart. J. r. Meteor. Soc.*, **77**, 598–626.

Riehl, H., and J. S. Malkus, 1958: On the heat balance in the equatorial trough zone. *Geophysica*, **6**, 503–537.

Schmidt, W., 1921: Wird die Atmosphäre durch Konvection von der Erdoberfläche hererwärmt? *Meteor. Z.*, **38**, 262–268.

Sverdrup, H. U., 1951: Evaporation from the oceans, in *Compendium Meteor.* Boston, Am. meteor. Soc., 1071–1081.

Taylor, G. I., 1915: Eddy motion in the atmosphere. *Phil. trans. r. Soc.* A, **215**, 1–26.

Contribution No. 1033

Made in United States of America
Reprinted from Limnology and Oceanography
Vol. 5, No. 2, April, 1960
pp. 138–153

BENTHIC STUDIES IN BUZZARDS BAY
III. THE STRUCTURE OF THE SOFT-BOTTOM COMMUNITY

by Howard L. Sanders

BENTHIC STUDIES IN BUZZARDS BAY
III. THE STRUCTURE OF THE SOFT-BOTTOM COMMUNITY[1]

Howard L. Sanders

Woods Hole Oceanographic Institution, Woods Hole, Mass.

ABSTRACT

A series of 24 samples was taken at periodic intervals at a single locality in Buzzards Bay from February 1956 to January 1958. With the exception of 4 samples which departed markedly from the others in regard to sediment composition, very high indices of faunal affinity were obtained within the series. The silt-clay fraction of the sediment in the 20 samples with high faunal indices varied from 78–91%, and when the contained species were ranked by abundance, the commoner species achieved approximately the same rank from sample to sample. Thus, 8 or 9 species are a constant part of the biological environment of this association, and there is an approximately constant numerical proportionality among them. Seventy-nine species were obtained from the 20 samples of typical sediment composition. However, 11 species comprised almost 95% of the total fauna by number while the lamellibranch *Nucula proxima* (58.86%) and the polychaete *Nephthys incisa* (17.21%) were commonest. Ten species make up 95% of the total biomass. Thus the community, both numerically and by biomass, is characterized by pronounced dominance of few species. The niches of the 9 most common species, representing 93.5% of the community by number, were categorized by method of feeding, kind of food and spatial distribution. Considering only these few factors, it was possible to demonstrate certain differences in niche preference. The relationship of animal numbers to animal weight revealed the expected pyramid of numbers with very few organisms in the largest weight categories and numerous individuals in the smaller weight groups. However, when the biomass within each weight category was determined, the expected inverted pyramid did not result. Numbers are considered more valid than biomass in quantitative benthic studies, since only 0.15% of the fauna constitute 55.17% of the entire weight. The presence or absence of a rare, randomly distributed large animal may alter the biomass of an individual sample by two orders of magnitude.

INTRODUCTION

This paper, the third in a series dealing with the benthic fauna of Buzzards Bay, Massachusetts, is concerned primarily with the community of animals present in the finer sediments. The term "community" is used in this study to mean a group of species that show a high degree of association by tending to reoccur together.

I am indebted to Dr. Wolfgang Wieser for numerous discussions regarding this study and for making available to me some of his unpublished data concerning the meiofauna.

METHODS

From the initial survey (Sanders 1958), Buzzards Bay station R (41° 30′ N 70° 31′ W) was selected as being characteristic of the *Nephthys incisa-Nucula proxima* community, the fauna typically present in the softer sediments. While most of the sediment at this locality is composed largely of silts and clays, subsequent samplings did reveal patchiness. At approximately monthly intervals from February 1, 1956 to March 3, 1957, paired quantitative samples were taken at this station, which is situated in about 19 m of water, using a modification of the Forster anchor dredge. For the following 10-month period (April 1957 to January 1958) single samples were collected at appreciably longer intervals of time.

A small aliquot of the sediment from each sample was retained and analysed for particle-size composition. The sands were divided into various size categories using a graded series of sieves while the silts and clay fractions were determined by the pipetting method (Soil Survey Staff 1951). The results of the mechanical analyses are given in Table 1.

---

[1] Contribution No. 1033 from the Woods Hole Oceanographic Institution. This research was supported by National Science Foundation Grant G-4812.

TABLE 1. *The particle size analysis by per cent weight of the 24 samples from station R in Buzzards Bay*

Sample	Date	Gravel		Sand					Silt					Clay	
		(8.0–4.0 mm)	(3.9–2.0 mm)	(1.9–1.0 mm)	(0.9–0.5 mm)	(0.49–0.25 mm)	(0.24–0.125 mm)	(0.124–0.062 mm)	(61–31µ)	(30–16µ)	(15.8 µ)	(7–4 µ)	(3–2 µ)	(<2µ)	0/0< 50µ
1RA	2/1/56		0.6	0.2	0.1	0.3	1.4	3.3	24.4	21.1	10.1	12.0	8.1	18.4	85.8
1RB	2/1/56		0.6	0.4	0.8	1.3	2.1	3.2	26.7	16.0	13.4	11.4	7.4	16.7	82.5
2RA	3/13/56			0.1	0.5	2.0	3.2	3.8	34.9	25.4	5.3	7.4	0.4	17.0	78.5
2RB	3/13/56			0.1	0.5	1.4	1.7	3.3	29.3	17.6	11.7	11.7	11.7	11.0	83.0
3RA	4/27/56			0.2	1.3	3.4	5.3	4.6	23.7	12.5	13.8	8.1	10.6	6.5	67.1
4RA	6/6/56				0.6	1.5	1.6	2.6	24.7	15.9	14.8	13.2	5.4	19.7	85.3
4RB	6/6/56		1.2	1.4	5.7	13.6	10.1	3.8	18.5	12.1	7.8	6.3	7.8	11.7	57.9
6RA	7/12/56	1.8	5.5	5.7	15.8	26.2	15.7	0.4	8.9	3.9	3.6	3.9	3.3	5.3	25.9
6RB	7/12/56				0.1	0.4	1.1	1.8	18.4	15.4	7.7	19.9	14.1	21.1	90.3
7RA	8/14/56			0.1	0.1	0.3	1.0	2.9	32.1	17.5	12.7	12.2	11.6	9.5	84.7
7RB	8/14/56			0.1	0.2	0.5	0.8	2.2	28.0	15.9	23.3	10.1	9.0	9.9	86.7
8RA	9/6/56			0.1	0.3	0.5	1.2	2.7	31.8	14.7	13.9	13.1	7.3	14.4	84.4
8RB	9/6/56		0.6	0.2	0.4	1.0	3.4	3.8	29.1	16.4	12.9	10.7	7.6	13.9	80.7
9RA	10/4/56		0.2	0.9	5.4	16.8	16.1	6.4	15.1	8.7	7.4	4.8	5.2	13.0	49.1
9RB	10/4/56		0.2	1.3	0.4	3.8	4.1	4.0	20.1	15.9	11.8	9.4	8.1	20.9	79.4
10RA	11/5/56			0.2	0.3	0.4	1.0	2.2	23.6	16.4	14.6	15.5	4.6	21.2	87.9
10RB	11/5/56			0.2	0.2	0.5	1.1	2.3	25.8	16.5	15.5	12.7	9.6	15.6	86.9
11RA	12/19/56		1.3	0.2	0.1	0.2	1.3	4.7	29.6	10.6	17.3	11.8	8.4	14.5	82.1
11RB	12/19/56			0.1	0.1	0.2	1.7	5.5	17.5	17.1	14.5	12.8	9.8	20.7	86.5
12RA	3/6/57			0.1	0.2	0.5	1.2	2.2	26.9	17.4	12.8	13.1	7.1	18.5	86.7
12RB	3/6/57		0.3	0.1	0.1	0.4	1.1	2.7	21.5	19.4	4.5	21.8	8.3	19.8	88.0
14R	6/20/57	0.1	0.2	0.4	1.0	2.2	3.7	5.3	25.4	14.9	12.7	9.7	0.2	24.2	78.4
15R	9/12/57			0.1	0.1	0.6	1.7	3.5	27.2	17.9	11.6	7.6	9.6	20.1	84.8
17R	1/30/58		0.3	0.2	0.4	1.2	1.8	3.0	25.0	14.7	12.2	11.0	7.9	22.3	84.6

The volume of the remainder of the sample was measured and the contents were passed through a screen with 0.2 mm mesh openings. The writer has demonstrated in previous studies using a series of graded screens, that very large fractions of the smaller sized species and most of the younger stages of the larger forms are not retained by the larger meshed screens. Obviously the loss of such faunal components would seriously compromise the validity of the results, and the use of a very fine seive is essential to this study.

The sediment

The predominant sediment components at this station are the silts and clays (see Table 1). Hereafter the term "% silt-clay" is used to mean the part of the sediment that is less than 50µ. This fraction is listed in the column at the extreme right in Table 1. Such a procedure was adopted in order to make the present investigation comparable with earlier studies (Sanders 1956, 1958). In most cases this silt-clay fraction makes up from 78 to 91% of the samples. If an undisturbed core is taken, the sediment can be clearly divided into two parts; a lower consolidated gray silty zone and a brown unconsolidated flocculent layer which comprises the top two or three centimeters of the substratum. The upper layer, as observed from core samples, is readily moved even by the slightest disturbance. Apparently this flocculent layer sloshes continuously back and forth over the consolidated sediment. The layer is appreciably thicker in such an environment than on coarser sediments and its accumulation here is most probably the result of the much reduced bottom currents characteristic of areas of deposition.

It is reasonable to suppose that the organic content of the flocculent layer should be appreciably higher than that of the underlying sediment since the "rain" of detritus from the water column as well as broken fragments of seaweed are being incorporated continuously into it. When samples from the two zones were placed in an oven at 500°C for 24 hours, 7.4% of the flocculent sample was burned as compared

TABLE 2. *Showing the actual number of various species in each of the R station samples*

Species	1RA	1RB	2RA	2RB	3RA	3RB	4RA	4RB	6RA	6RB	7RA	7RB	8RA	8RB	9RA	9RB	10RA	10RB	11RA	11RB	12RA	12RB	14R	15R	17R
Polychaeta:																									
Nephthys incisa	143	53	13	45	13	77	36	17	9	325	171	550	223	23	64	45	187	154	19	105	242	129	129	36	61
Ninoe nigripes	17	8	11	25	5	77	12	32	60	22	23	94	70	5	108	12	84	47	2	19	76	60	34	13	37
Lumbrinereis tenuis	93	24	2	25	3	15	2	10	15	15	16	32	8	—	4	3	10	18	2	10	11	5	2	4	8
Lumbrinereis fragilis						4		1														1			2
Arabella iricolor		1				5	1	2	5	1			2		1	1	1	2		1	4	3		1	1
Drilonereis longa		1		1		6			1												1	1			
Diopatra cuprea						1			2			2			3						1				
Harmothoe extenuata										1															
Pholoe minuta	1					6		1							3	3									
Syllis cornuta		1				7		1					1		2			1							
Phyllodoce arenae																									1
Paranaitis speciosa								1																	
Nereis grayei									1															1	
Glycera americana						4		1	1				1				2				5	17		1	2
Dorvillea caeca	57				22	14				1		1	9				3	4		14					
Scolopos acuta						1																			
Scalibregma inflatum						6															2		1		
Aricidea jeffreysii	12	4	4	5		36		2					1		2		1	1			10	2		2	1
Paraonis gracilis						1	1	1		1	1	4	1	2		2	2	4	1	1	1		1		1
Tharyx sp.	57		4	15	1	14	1	2	2		1	2			1	3	2			3	2	1	1	2	34
? *Spio filicornis*	63	1	4	5	1	7	1			2		2	5			2	7			3	1		1	3	
Capitellid	14	2	1			4			1	2						1	2					2		2	2
Spiochaetopterus oculatus																				1	1	2	2	1	1
Flabelligera affinis								1	4	1					1					1					1
Maldanopsis elongata	1		1							1	1		2	1	4	3	4	1			3	3			1
Praxillella praetermissa					1																				
Melinna cristata	2	4	1	1		1	1			1		1	1	1	3		3	2							
Ampharete arctica						4		1		20		2			1										1
? *Nicolea* sp.					1																				
Asabellides oculata																						1			
Polycirrus sp.				2		10				1															
Pectinaria gouldii	5	1		2		1		1				1			1		1	1							
Exogone sp.									1			1													
Oligochaeta:						1											2				1			5	

Turbellaria:																									
Anaperus sp.																				2				5
Flatworm b.															1			1							1
Nemertinea:																									
Tubolonus pellucidus		2	1	2		1	2									1				1				2	8
Micrura leidyi	6	1					1				1													1	1
Sipunculoidea:																									
Phascolon strombi				5				1															1		
Phascolosoma verrilli	1				1				4	1															
Enteropneusta:																									
Dolichoglossus Kowalevskii	1	3	2		1	2																			1
Tunicata:																									
Bostrichobranchus pilularis				5		6										1	3	2	2	6	3	1	14		
Anthozoa:																									
Cerianthus americana	4	1							1							2						1		1	1
Edwardsia sp.								1				1	1			1						1		1	1
Mollusca:																									
Nucula proxima	1940	1180	82	422	9	274	116	1	3	256	241	1170	743	40	3	184	504	290	8	105	560	280	592	551	295
Nucula delphinodonta	4	4		1			1	1	1	10		9	1		2		2					2	1	1	1
Yoldia limatula		17	1	5		2	1			4	1	6		1				1					1	1	
Macoma tenta		8	1	3		2		1		1						1	1	2					2		2
Callocardia morrhuana	73	49	3	43	4	19	5	21	2	31	29	128	8	2	1	3	18	12	2	10	36	19	22	1	11
Mulinia lateralis	3	2		3		1										1			1						
Astarte subaequilatera	2										1	3						1				1	1		1
Astarte undata								2								1									
Arca pextata	2					1						2					1				1				
Cerastoderma pinnulatum	1		1																		1	1			
Pandora gouldiana																					1				1
Commensal clam								5															3		
Cylichna orzya	138	117	17	63	2	36	2			29	14	35	5		1	5	28	29	1	2	38	25	13	16	71
Retusa caniculata	17	11	4	13		5	2			12	2	11	1		1	1	6	10	1	1	10	9	4	1	4
Acteon punctostriatus	3	2		3		1									1			1							
Turbonilla a	13	34	1	10	1	11	3	4		3		2	4			8	17	12	1	7	7	8	6	4	5
Turbonilla b	1								4						26						1	1			
Crepidula plana	1		1																		1	1			
Anachis avara															1										

TABLE 2. *Continued*

Species	1RA	1RB	2RA	2RB	3RA	3RB	4RA	4RB	6RA	6RB	7RA	7RB	8RA	8RB	9RA	9RB	10RA	10RB	11RA	11RB	12RA	12RB	14R	15R	17R
Mitrella lunata		1								3					3										1
Nassarius triviattatus	1	3		7					4	2	5	11	3	1	3		1			1		2	3	5	
Eupleura caudata			1	2				1		1							1					1		1	
Bela turricola	2	2		1								1					1					1			
Natica pusilla				1				1										3							
Polynices triseriata		1		1		1							1								1				
Gastropod a												1													
Crustacea:																									
Hutchinsoniella macracantha	2			2	23	3	——75——				15	1	—68—		— 25 —		— 58 —		1	28	— 68 —			10	2
Ampelisca spinipes	3	5		1		168	1	17	2		2	9			32	4	13	10	1	2			1	1	1
Ampelisca macrocephala						36										1				1					
Byblis serrata						9		2																	
Leptocheirus pinguis								34	84						3						1		4		
Unciola irrorata	18	1			9			7	1						17	2		1		2	15	1	1		17
Corophium acherusicum	1								1			1				1	1		1		1	2		1	
Corophium insidiosum									1										1						
Corophium tuberculatum															2										
Siphonoecetes smithianus						1																			
Lysianopsis alba	1																								
Stenothoe cypris	1																								
Batea secunda					2													1							
Hyperia galba	1																								
Aeginella longicornis									1																1
Amphipod A								2	1								1								
Edotea triloba	1							1			1	1				1	7	2		3	1	4	2		14
Oxyurostylis smithi	1	2		1		1						1											1	3	
Diastylis sp.	1	1		1		1										1		1					2	1	
Eudorella emarginata	1																								
Petalosarsia declivus	1																								
Pagurus annulipes									1			1													
Libinia sp.	1																								
Pinnixia cylindrica									1															1	
Pycnogonida:																									
Anoplodactylus lentus												1									1				1
Ophiuroidea:																				1					

to 6.0% for the consolidated sediment sample. It would seem then that the amount of organic matter present in the two layers is not appreciably different and therefore the food resources for the deposit-feeders are approximately as abundant in one zone as in the other.

However, there may be a qualitative difference in the organic matter of the two zones. Some very preliminary measurements of free small chain sugars in the sediment seem highly suggestive. Detectable quantities of these substances were found only in the uppermost two centimeters. Such sugars should serve as a ready food source for the deposit-feeders. The organic matter in the consolidated sediments, being separated from the sources of detritus both in time and space, may be refractory or "fossil" in nature and thus less utilizable as a food source.

The distribution of the animals in the sediment column further supports such a conjecture, although anaerobic conditions deeper in the sediment may largely determine the pattern. A series of cores was split approximately at the interface between the two sediment zones. It should be emphasized that there was considerable contamination of one zone by the other. Yet nearly 75% of the animals were present in the upper zone and the remaining animals were limited to the top 2 cm of the consolidated layer. In another series of cores, none of the approximately one hundred specimens were found below a depth of 6 cm.

Faunal homogeneity

The numerical distribution of the fauna in the 24 samples comprising this series is shown in Table 2.

It is obviously necessary in a community study to demonstrate that the species components of the included samples show faunal similarity. To measure such affinities a matrix method, the "trellis diagram," was adopted. The percentage composition of the various species in each sample is determined. The samples are then arranged linearly at right angles along the ordinate and abcissa and all possible pairs are compared regarding their faunal content. The resultant value, the "index of affinity," is a measure of the percentage of the fauna common to a pair of samples and it is obtained by summing the smaller percentages of those species present in both samples. The table is then rearranged so that the samples with the highest values are brought into closer proximity. In this way the samples that are most ecologically alike are grouped together. The resulting diagram is shown in Figure 1.

It is immediately evident from this figure that samples 9RA, 6RA, 4RB and 3RA have low indices of affinity; that is, these 4 samples have a markedly different faunal composition from the other 20. Inspection of Table 1 suggests a possible reason for this difference. These same 4 samples agree in having much lower percentages of silt-clay. Whereas the sediments of the 20 samples with high indices of affinity range from 78.4 to 90.3% silt-clay, with a mean of 84.3%, the silt-clay percentages of the 4 samples in question are as follows: 3RA, 67.1; 4RB, 57.9; 9RA, 49.1; 6RA, 25.9. Another sample, 3RB, was omitted from consideration when it became evident that a part of sample 3PB from the sand bottom community series was accidentally included with it.

An average index of affinity value for all possible sample pairs (276) is 56.6. If the four aberrant samples are excluded, the value of the remaining paired combinations (190) becomes 69.3. In order to determine the significance of this number, a comparison with other values, either given in the literature or calculated from other studies, is summarized in Table 3.

From Wieser's (1960) investigation of the meiofauna of Buzzards Bay, the average correlation coefficient is given for all samples and for the four samples collected at station R with a homogenous sediment composition. Correlation values were calculated for the macrofaunal survey of Buzzards Bay (Sanders 1958) and indices are given for all stations included in the survey, those stations carrying a fauna largely characteristic of the *Ampelisca* spp. com-

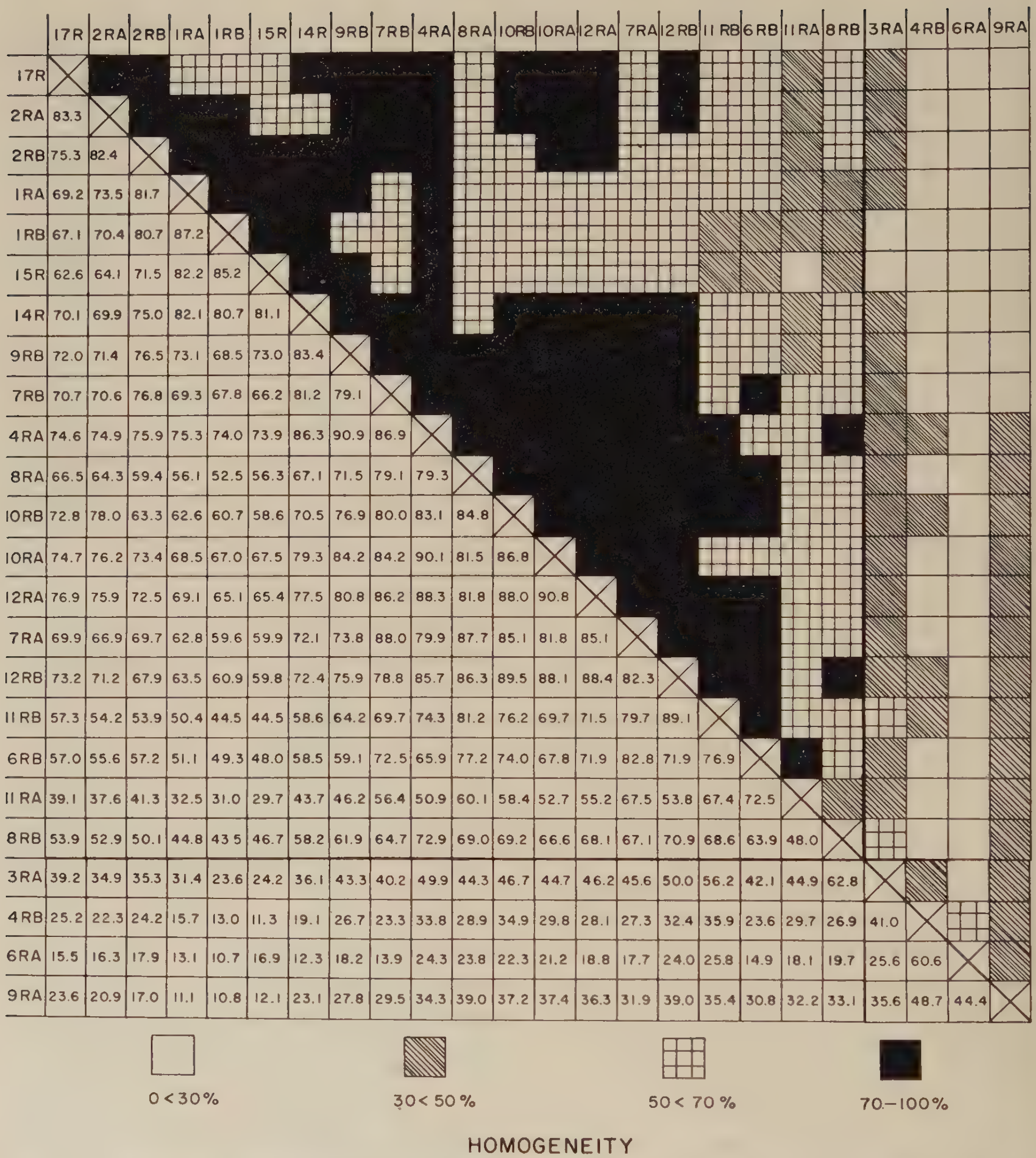

	17R	2RA	2RB	1RA	1RB	15R	14R	9RB	7RB	4RA	8RA	10RB	10RA	12RA	7RA	12RB	11RB	6RB	11RA	8RB	3RA	4RB	6RA	9RA
17R	☒																							
2RA	83.3	☒																						
2RB	75.3	82.4	☒																					
1RA	69.2	73.5	81.7	☒																				
1RB	67.1	70.4	80.7	87.2	☒																			
15R	62.6	64.1	71.5	82.2	85.2	☒																		
14R	70.1	69.9	75.0	82.1	80.7	81.1	☒																	
9RB	72.0	71.4	76.5	73.1	68.5	73.0	83.4	☒																
7RB	70.7	70.6	76.8	69.3	67.8	66.2	81.2	79.1	☒															
4RA	74.6	74.9	75.9	75.3	74.0	73.9	86.3	90.9	86.9	☒														
8RA	66.5	64.3	59.4	56.1	52.5	56.3	67.1	71.5	79.1	79.3	☒													
10RB	72.8	78.0	63.3	62.6	60.7	58.6	70.5	76.9	80.0	83.1	84.8	☒												
10RA	74.7	76.2	73.4	68.5	67.0	67.5	79.3	84.2	84.2	90.1	81.5	86.8	☒											
12RA	76.9	75.9	72.5	69.1	65.1	65.4	77.5	80.8	86.2	88.3	81.8	88.0	90.8	☒										
7RA	69.9	66.9	69.7	62.8	59.6	59.9	72.1	73.8	88.0	79.9	87.7	85.1	81.8	85.1	☒									
12RB	73.2	71.2	67.9	63.5	60.9	59.8	72.4	75.9	78.8	85.7	86.3	89.5	88.1	88.4	82.3	☒								
11RB	57.3	54.2	53.9	50.4	44.5	44.5	58.6	64.2	69.7	74.3	81.2	76.2	69.7	71.5	79.7	89.1	☒							
6RB	57.0	55.6	57.2	51.1	49.3	48.0	58.5	59.1	72.5	65.9	77.2	74.0	67.8	71.9	82.8	71.9	76.9	☒						
11RA	39.1	37.6	41.3	32.5	31.0	29.7	43.7	46.2	56.4	50.9	60.1	58.4	52.7	55.2	67.5	53.8	67.4	72.5	☒					
8RB	53.9	52.9	50.1	44.8	43.5	46.7	58.2	61.9	64.7	72.9	69.0	69.2	66.6	68.1	67.1	70.9	68.6	63.9	48.0	☒				
3RA	39.2	34.9	35.3	31.4	23.6	24.2	36.1	43.3	40.2	49.9	44.3	46.7	44.7	46.2	45.6	50.0	56.2	42.1	44.9	62.8	☒			
4RB	25.2	22.3	24.2	15.7	13.0	11.3	19.1	26.7	23.3	33.8	28.9	34.9	29.8	28.1	27.3	32.4	35.9	23.6	29.7	26.9	41.0	☒		
6RA	15.5	16.3	17.9	13.1	10.7	16.9	12.3	18.2	13.9	24.3	23.8	22.3	21.2	18.8	17.7	24.0	25.8	14.9	18.1	19.7	25.6	60.6	☒	
9RA	23.6	20.9	17.0	11.1	10.8	12.1	23.1	27.8	29.5	34.3	39.0	37.2	37.4	36.3	31.9	39.0	35.4	30.8	32.2	33.1	35.6	48.7	44.4	☒

☐ 0<30%
▨ 30<50%
⊞ 50<70%
■ 70–100%

HOMOGENEITY

FIG. 1. A comparison of the average faunal index of affinity at station R with indices from other studies.

munity, and the stations predominantly with faunal elements present in the *Nephthys incisa-Nucula proxima* community. Renkonnen (1944) used the trellis diagram for a study of beetles inhabiting the supralittoral zone of a lake in southwest Finland. From his analysis he recognized 5 communities; the average correlation values within each of his communities are also given in Table 3. Finally Macfadyen (1954) used the same technique, together with other methods of analysis, in his investigation of the invertebrate fauna of Jan Mayen Island (East Greenland). Measuring the affinites among the Collembola species, he found two associations and the average correlation value within each association is included.

Table 3 reveals that the present study gives by far the highest index of affinity. This value was obtained despite the fact

TABLE 3. *A comparison of the average faunal index of affinity at station R with indices from other studies*

	Index of Affinity
Macrofauna at station R (all samples)	56.6
Macrofauna at station R less 5 samples of aberrant sediment composition	69.3
Meiofauna of Buzzards Bay (Wieser 1960)	27.2
Meiofauna of R samples with similar sediment composition (*op. cit.*)	55.7
Macrofauna of Buzzards Bay (Sanders 1958)	21.4
Ampelisca spp. community (Sanders 1958)	31.2
Nephthys incisa–Nucula proxima community (Sanders 1958)	37.2
Beetle fauna from lake shore in SW Finland (Renkonnen 1944)	
Total of 40 stations	24.3
Community 1 (1 station)	—
Community 2 (4 stations)	54.2
Community 3 (23 stations)	33.5
Community 4 (15 stations)	34.2
Community 5 (16 stations)	36.9
Collembola of Jan Mayen Island (Macfadyen 1954)	
Association 1 (11 species)	24.7
Association 2 (9 species)	24.6

that, in contrast to the other studies, the samples were taken at all seasons of the year. Because recruitment is not synchronous in the dominant species, the numerical proportionality should be constantly altering and one should expect a lowered index of affinity. Therefore, it seems valid to conclude that the fauna at station R represents a very stable and homogenous assemblage except in the aberrant sediments. However, it should be mentioned that station R was selected because it was thought to be faunally homogeneous.

There are certain weaknesses inherent in this method of analysis. No discrimination is made against ubiquitous species (see Macfayden 1954). Furthermore, the method is not quantitative and unless care is taken gross errors may be introduced. For example, species A at a station X carrying a sparse fauna may comprise 80% of the population while at another station, Y, with a more numerous fauna the same species may constitute only 2% of the population. It is conceivable, however, that species A may be numerically more common at Station Y. Yet by the method of analysis used, species A is the dominant species at station X and it will be assumed that the environmental conditions will be more favorable at a station (X) where the species is dominant than at a station where it is not (Y).

Neither of these criticisms seem particularly pertinent to the present study, however. In Buzzards Bay there appears to be no species that is both ubiquitous and very common (see Tables 3 and 4, Sanders 1958). Concerning the second point, if the samples with aberrant sediments are omitted (3RA, 4RB, 6RA and 9 RA), all the remaining samples are of a single sediment type.

The community

Since the association of animals appears to possess the features of a community as the term was defined earlier in this paper, it would be of interest to attempt to determine the species structure of such a natural assemblage.

The data presented in Table 4 show the evidence of dominance by a few species. In fact, the two most common forms, the lamellibranch *Nucula proxima* and the polychaete *Nephthys incisa* make up respectively about 59% and 17% by number of the community. Together the two species comprise more than 76% of the fauna. Ninety-five per cent of the assemblage is formed by only 11 of the 79 species present. If the community is evaluated on the basis of biomass rather than number the same pronounced dominance by a few species is evident. Only 13 species make up 95% of the biomass. The per cent composition by weight of these species are shown in Table 4. Only some of the numerically more abundant species contribute significantly to the biomass (*Nephthys*, *Nucula*, *Callocardia* and *Ninoe*) while certain numerically rare forms such as the tunicate *Bostrichobranchus pilularis*, the nemertean *Micrura leidyi*, and the polychaetes *Arabella iricolor* and *Lumbrinereis fragilis*, because of their large individual size, represent major biomass components of the fauna.

Such a pattern could result from the bias of a few unusually large samples. To test such a possibility, each sample was ranked

TABLE 4. *The structure of the* Nephthys incisa–Nucula proxima *community at station R. The species present in the 20 samples characterized by "typical" sediment composition (78–91% silt-clay) are listed according to their numerical abundance. The totals given (column 2) are the sum of the numbers of individuals of the given species in the 20 samples. Columns 3, 4, 5, 6 and 7 list respectively the cumulative per cent by number, the per cent composition by number, the dry weights, the per cent composition by weight and feeding type.*

Rank by no.	Species	No.	Cumulative % by no.	% of fauna by no.	Dry wt. (g.)	% by wt.	Rank by wt.	Feeding Type[1]
1	*Nucula proxima*	9195	58.86	58.86	2.9694	13.98	4	SDF
2	*Nephthys incisa*	2689	76.07	17.21	6.1489	28.95	1	NSDF
3	*Ninoe nigripes*	671	80.37	4.30	0.3791	1.78	8	NSDF
4	*Cylichna orzya*	647	84.51	4.14	0.0782			?
5	*Callocardia morrhuana*	525	87.87	3.36	3.1803	14.97	3	SF
6	*Hutchinsoniella macracantha*	307	89.84	1.97	0.0583			NSDF
7	*Lumbrinereis tenuis*	286	91.67	1.83	0.0620			NSDF
8	*Turbonilla* a	145	92.60	0.93	0.0053			?
9	?*Spio filicornis*	135	93.46	0.86	0.0186			SDF
10	*Retusa caniculata*	120	94.23	0.77	0.0440			?C
11	*Dorvillea caeca*	103	94.89	0.66	0.0099			?C
12	*Tharyx* sp.	89	95.46	0.57	0.0100			SDF
13	*Unciola irrorata*	58	95.83	0.37	0.0286			SDF
14	*Ampelisca spinipes*	54	96.18	0.35	0.0324			SF
15	*Nassarius triviattatus*	45	96.47	0.29	0.1726	0.81	9	NSDF
16	*Bostrichobranchus pilularis*	40	96.73	0.26	4.9878	23.49	2	SF
17	*Yoldia limatula*	39	96.98	0.25	0.1084	0.51	13	SDF
18	*Nucula delphinodonta*	37	97.22	0.24	0.0060			SDF
19	*Edotea triloba*	37	97.46	0.24	0.0381			S
20	*Paraonis gracilis*	31	97.66	0.20	0.0032			SDF
21	*Melinna cristata*	25	97.82	0.16	0.0461			SDF
22	Capitellid	24	97.97	0.15	0.0007			NSDF
23	*Ampharete arctica*	24	98.12	0.15	0.0154			SDF
24	*Macoma tenta*	22	98.26	0.14	0.0094			SDF
25	*Arabella iricolor*	19	98.36	0.12	0.8000	3.77	6	?C
26	*Tubolonus pellucidus*	19	98.50	0.12	0.0019			?C
27	*Maldanopsis elongata*	17	98.61	0.11	0.0488			NSDF
28	*Mulinia lateralis*	12	98.69	0.08	0.0059			SF
29	*Pectinaria gouldii*	11	98.76	0.07	0.0185			NSDF
30	*Micrura leidyi*	11	98.83	0.07	1.0263	4.83	5	C
31	*Oxyurostylis smithi*	9	98.89	0.06	0.0071			
32	*Cerianthus americana*	9	98.95	0.06	0.1578	0.74	10	
33	*Corophium acherusicum*	9	99.01	0.06	0.0049			
34	*Diastylis* sp.	8	99.06	0.05	0.0063			
35	*Acteon punctostriatus*	8	99.11	0.05	0.0004			
36	*Dolichoglossus kowalevskii*	8	99.16	0.05	0.0124			
37	*Spiochaetopterus oculatus*	8	99.21	0.05	0.0063			
38	*Bela turricola*	8	99.26	0.05	0.0053			
39	*Astarte subaequilatera*	8	99.31	0.05	0.0029			
40	*Eupleura caudata*	7	99.35	0.04	0.0069			
41	*Leptocheirus pinguis*	6	99.39	0.04	0.0213			
42	*Phascolon strombi*	6	99.43	0.04	0.0352			
43	*Anaperus* sp.	6	99.47	0.04	0.0004			
44	Oligochaeta	6	99.51	0.04	0.0002			
45	*Arca pextata*	6	99.55	0.04	0.0027			
46	*Mitrella lunata*	5	99.58	0.03	0.0033			
47	*Edwardsia* sp.	5	99.61	0.03	0.0500			
48	*Diopatra cuprea*	4	99.64	0.03	0.0468			
49	*Flabelligera affinis*	4	99.67	0.03	0.1403	0.66	11	
50	*Natica pusilla*	4	99.70	0.03	0.0017			
51	*Cerastoderma pinnulatum*	4	99.73	0.03	0.1382	0.65	12	
52	*Lumbrinereis fragilis*	3	99.75	0.02	0.3954	1.86	7	NSDF
53	*Glycera americana*	3	99.77	0.02	0.0480			
54	*Pholoe minuta*	3	99.79	0.02	0.0012			

TABLE 4. *Continued*

Rank by no.	Species	No.	Cumulative % by no.	% of fauna by no.	Dry wt. (g.)	% by wt.	Rank by wt.	Feeding type[1]
55	Flatworm b	3	99.81	0.02	0.0008			
56	*Anoplodactylus lentus*	3	99.83	0.02	0.0008			
57	*Polynices triseriata*	3	99.85	0.02	0.0047			
58	*Syllis cornuta*	2	99.86	0.01	0.0009			
59	*Polycirrus* sp.	2	99.87	0.01	0.0033			
60	*Phascolosoma verrilli*	2	99.88	0.01	0.0007			
61	*Ampelisca macrocephala*	2	99.89	0.01	0.0160			
62	*Turbonilla* b	2	99.90	0.01	0.0001			
63	*Pandora gouldiana*	2	99.91	0.01	0.0062			
64	*Crepidula plana*	2	99.92	0.01	0.0021			
65	*Batea secunda*	1						
66	*Astarte undata*	1	99.93	0.01				
67	*Nereis grayei*	1						
68	*Harmothoe extenuata*	1	99.94	0.01				
69	*Phyllodoce arenae*	1						
70	?*Nicolea* sp.	1	99.95	0.01				
71	*Asabellides oculata*	1						
72	*Corophium insidiosum*	1	99.96	0.01				
73	*Eudorella emarginata*	1			0.0150			
74	*Petalosarsia emarginata*	1	99.97	0.01				
75	*Pagurus annulipes*	1						
76	*Libinia* sp.	1	99.98	0.01				
77	*Pinnixia cylindrica*	1						
78	Ophiuroid	1	99.99	0.01				
79	Gastropod a	1						
	Total	15,622			21.2374			
	Number/m^2	8,985						
	Biomass/m^2				12.1858			

[1] SDF = Selective deposit-feeder
NSDF = Non-selective deposit-feeder
SF = Suspension-feeder
C = Carnivore
S = Scavenger

separately (Fager 1957), thus giving equal weight to each of the samples. Table 5 lists the frequency of a given species appearing as one of the 10 most abundant species (maximum frequency = 20); and the quantitative importance of the species. This latter factor is determined by ranking the species from 1 to 10 by abundance within each sample. A rank of 1 is given a value of 10 points; a rank of 2 equals 9 points; 3 is equivalent to 8 points,....., and a rank of 10 equals one point. Thus if a species is ranked first in all 20 samples, it will have 200 points, the highest possible score.

The results in Table 5 verify the findings given in Table 4. *Nucula proxima,* with almost the maximum possible points, is the most abundant species in 18 samples and is second most common in the remaining two giving a score of 198. *Nephthys incisa,* ranking first in two, second in 13 and third in 5 samples has the very high score of 177. Other species with high scores are the polychaete, *Ninoe nigripes* (132); the gastropod, *Cylichna orzya* (177); the lamellibranch, *Callocardia morrhuana* (109); the crustacean, *Hutchinsoniella macracantha* (83); and the polychaete, *Lumbrinereis tenuis* (62). Each of the above species is present in at least 80% and is one of the 10 most common species in 65–100% of the samples. Two other gastropods, *Turbonilla* a and *Retusa caniculata,* with somewhat lower scores (38 and 30) are present in 18 and 19 of the samples respectively. The analysis demonstrates, therefore, that these 9 species represent a very significant and constant part of the biological environment of this community. It follows that some knowledge of the niches of these species

TABLE 5. *Faunal frequency evaluation of the 20 samples with homogeneous sediment composition*

Species	1	2	3	4	5	6	7	8	9	10	Frequency	Frequency as one of ten most common species	Biological index value
Nucula proxima	18	2									20	20	198
Nephthys incisa	2	13	5								20	20	177
Ninoe nigripes			6	9	3				1	1	20	20	132
Cylichna orzya		4	2	4	2	2	3	1			19	18	117
Callocardia morrhuana			4	3	4	4	1	2	1		20	19	109
Hutchinsoniella macracantha		1	3	2	4	1	1	1			17	13	83
Lumbrinereis tenuis				1	1	5	2	3	3	1	19	16	62
Turbonilla a				1	1	1	2	2	2	2	18	11	38
Retusa caniculata							1	6	3	2	19	12	30
?*Spio filicornis*					1	2			1	2	16	6	20
Dorvillea capeca					2		2				11	4	20
Nassarius triviattatus						1	1	2		2	13	6	17
Ampelisca spinipes							1	1	4		14	6	15
Bostrichobranchus pilularis					1	1			1		10	3	13
Paraonis gracilis					1	1				1	15	3	12
Tharyx sp.							2	1		1	12	4	12
Unciola irrorata						1	1		1		9	3	11
Yoldia limatula							1	1		1	11	3	8
Edotea triloba							1			1	11	2	5
Ampharete arctica						1					2	1	5

would help in understanding the community structure.

The *Nephthys incisa-Nucula proxima* community can be considered to belong to the category defined by Elton (1946) as "animal communities in which species live on comparatively few basic sources of food." Besides aquatic benthic deposit-and suspension-feeders, he includes log-dwelling herbivores, soil animals, zooplankton, driftline animals and blood-sucking ectoparasites in this category. In the *Nephthys incisa-Nucula proxima* community a minimum of 87.5% of the animals by number are deposit-feeders, obtaining their food from detritus either on or in the sediment. The other primary feeding type, the suspension-feeder, is present in much smaller numbers (4.3%) as might be expected from the nature of the sediment (see Sanders 1958).

Nucula proxima, the overwhelming dominant member of the community, normally lies just below the surface of the sediment feeding on the sediment immediately beneath it by long appendages derived from the palp. The inner surfaces of these structures are grooved and lined with ciliated epithelium (Drew 1899; Yonge 1939). Only the fine particles are moved along the groove to the palps where they are passed again by cilia to the mouth. *Nucula* then is a selective deposit-feeder.

The genus to which the other very abundant species, *Nephthys incisa,* belongs is considered to be carnivorous (Blegvad 1914; Smith 1932; Mare 1942; Holme 1949; Savilov 1957; Longhurst 1958). Yet in an earlier study in Long Island Sound (Sanders 1956) the writer has shown that the gut contents of those individuals examined were filled with sediments and there was no evidence of animal remains, indicating that the animal was primarily a deposit-feeder. Turpaeva (1957) also regards members of this genus as deposit-feeders.

These conclusions were further verified in the present study. Generally the gut contents were of two sorts. They either consisted of fine silt particles indicating the animal was ingesting the sediment from the lower gray consolidated zone or of large detrital particles, a few sand grains, intact diatoms including such benthic forms as *Gyrosigma* and various naviculoids as well as empty diatom frustules of both pelagic and benthic forms. Apparenly this actively burrowing form swallows the medium through which it moves indiscriminately ingesting sediment from both zones of the habitat. This does not imply that *Nephthys* *incisa* cannot and would not act as a carnivore under certain circumstances. However in the community under discussion it represents such a significant fraction of the fauna both in regard to number and biomass (see Table 4) that it would not be feasible for the animal to be primarily predaceous and, indeed, the contents of the gut would certainly not support any such idea.

Third in abundance in this association is another polychaete, *Ninoe nigripes,* belonging to the family Lumbrinereidae. Being an errant polychaete with well developed jaws, and because other lumbrinereids are considered to be predators, this form too should be carnivorous. However, as in the case of *Nephthys,* stomach analysis revealed that the species is a non-selective deposit-feeder but unlike *Nephthys* the gray silty sediments were absent from the gut. The evidence therefore indicates that *Ninoe* feeds almost exclusively from the brown flocculent zone since the gut contents usually reveal large pieces of detritus, diatom frustules, benthic diatoms and few sand grains. Furthermore, *Ninoe* differs from *Nephthys* in being sedentary. It constructs a simple slime tube and the slow movement of the flocculent layer replenishes the source of its food.

The minute opistobranch gastropod, *Cylichna orzya,* is numerically the fourth most common species. In contrast to the previously mentioned forms, this animal is found only at the surface of the sediment. Because of its small size, the gut contents could not be satisfactorily analyzed.

The lamellibranch, *Callocardia morrhuana,* fifth in rank by number and third in rank by weight, is a representative of the other major primary consumer group, the suspension-feeders. It draws in its food by means of the inhalant siphon from the suspended matter in the overlying water column.

The sixth ranking species, surprisingly, is the remarkably primitive and supposedly very rare crustacean, *Hutchinsoniella macracantha.* The limb movements of this animal are metachronal and, as the space between two consecutive appendages enlarge, a suction chamber is formed from the interlimb space. The deposited material that is temporarily stirred up by the action of the large terminal spines on the inner ramus of the limb is sucked into this space. Subsequently, this material is squeezed into the mid-ventral food groove, where it is passed forward by spine-like processes at the base of the thoracic and maxillary limbs. The material in the food groove, gut, and in the fecal pellets was shown to be composed of detritus, diatom frustules, and sand grains. It is therefore a non-selective deposit-feeder eating in the flocculent non-consolidated sediment. A detailed study of the functional morphology of *Hutchinsoniella* is at present being undertaken by the writer.

The 6 species just discussed represent almost 90% of the entire macrofaunal assemblage. As they differ in spatial distribution, in their diet and methods of obtaining it, the niches of these animals are clearly different.

Another polychaete, *Lumbrinereis tenuis,* is ranked seventh in abundance in this community. Members of the genus *Lumbrinereis* (=*Lumbriconereis*) are classified as carnivores (Smith 1932, Savilov 1957, Longhurst 1958). The few gut contents of the species examined contained detritus. Like *Ninoe* the animal is sedentary and ensheathes itself in a slime tube. Furthermore, it feeds in the same manner and on the same sort of food as *Ninoe.* The few factors evaluated show no difference in the niches of these two lumbrinereid polychaetes.

The small pyramidellid gastropod designated as *Turbonilla* a, the eighth most common species, presents an enigma. All pyramidellids are ectoparasites (Fretter and Graham 1949); each species has a specific host, a sessile organism that protrudes part of its body to feed. All known hosts are either polychaetes and coelenterates that feed by tentacles or molluscs which are with a single exception epifaunal. In the former cases the pyramidellid pierces the tentacles or body wall with a stylet at the tip of a long eversible proboscis and sucks in the blood or body fluids; in the latter situation it is the mantle that is pierced. There is, however, one report where the siphon of a lamellibranch was parasitized (Medcof 1948). As indicated in an earlier paper (Sanders 1958) it is difficult to accept this specific pyramidellid as being an ectoparasite since in slightly coarser sediments (50–70% silt-clay) it may comprise 25–50% of the fauna. Furthermore, there seem to be no suitable hosts among the species living in the same habitat, when abundance, size and mode of life are considered. The lamellibranch *Callocardia* might provide a possible exception; however the great majority of these clams are of the same small size as their possible parasite, a highly unlikely relationship. It is tentatively suggested that, in this environment, *Turbonilla* a is a deposit-feeder, using its buccal pump to draw in the flocculent superficial sediment.

The small spionid polychaete, ?*Spio filicornis,* the ninth most abundant member of the community, utilizes still another mode of feeding. Two large tentacles on the head protrude above the substratum and move over the surface of the surrounding sediment. A ciliated groove situated along the length of the tentacle draws in and carries fine superficial particles to the mouth. The animal therefore is a selective deposit-feeder exploiting only the finer deposited material at the very surface of the sediment.

The remaining 6.5% of the fauna consists of 70 species, none of which make an appreciable numerical contribution to the community. Some members of this group use the same methods of feeding as the common species. However, the significant finding in this study is that definite niche differences can be demonstrated for those few species that make up the vast majority of the fauna.

This study also demonstrates the danger of assuming a carnivorous feeding habit, particularly in the case of polychaetes, from morphology or by feeding experiments in the laboratory. Because of this, two other predatory polychaetes, *Arabella iricolor* and *Lumbrinereis fragilis* were examined to provide data on their food. While both species are of little importance numerically, they are relatively large animals and rank fifth and seventh respectively in regard to biomass (see Table 4). The gut contents of the two specimens of *Arabella* were empty while the single representative of *Lumbrinereis fragilis* contained detritus, numerous centric diatoms and sand grains.

Evidence has now been presented which indicates that biological interaction, or perhaps a better expression would be biological accommodation, plays an important part in the structure of the animal assemblage at station R. It should not be inferred that such a community therefore represents a sharply circumscribed group of species, each with identical distribution patterns. On the contrary, frequently both the sediment ranges of the species and the sediment composition where the maximal numbers are found vary significantly (see Sanders 1958). In fact, the species components of the benthic fauna in Buzzards Bay constitute a continuum varying with the gradual change in sediment composition. Implicit in such distribution patterns is the effect of physical factors. However, as demonstrated in the present study, at a given point (station R) on the sediment spectrum the species structure of the association is similar even when the sampling is done at various times of the year. The interpretation made is that accommodations among the species, biological effects, play a major role in determining the structure of a community. Thus the faunal proportions will vary at different locations on the sediment spectrum in Buzzards Bay and at any point on the spectrum the community structure will be determined by both physical and biological factors. Obviously the gradients of physical factors other than sediment composition play a role. For example, the lamellibranch, *Macoma tenta,* appears to be much more abundant in the same type of sediment in slightly shallower environments. Because of the greater abundance of *Macoma,* it would be interesting to observe what modifications have occurred in the structure of the community at such a location in contrast to that found at station R.

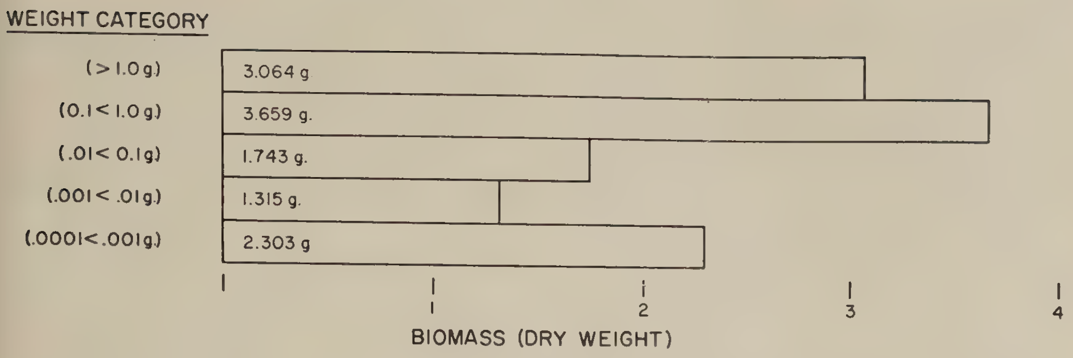

FIG. 2. The relationship of numbers (left) to weight (right) for the benthic community at station R.

For further comments on the subject of biological versus physical regulation see Jones (1950), Hedgpeth (1954) and Longhurst (1958).

Animal numbers and animal weight

Another aspect of the structure of an animal community is the relationship of numbers to weight. It is a common assumption that the smaller the animals the more abundant they will be. Therefore, if the individuals are grouped by number into size or weight categories, a pyramid can be constructed with the smallest size or weight category forming the base and the largest category the apex of the pyramid. Conversely, if the total weight rather than the number is calculated for each of the categories, an inverted pyramid results, with the largest biomass present in the largest size category and the smallest biomass in the smallest size group. However, there is little field evidence in support of this.

The present data lend themselves to the comparison of numbers to weight (Fig. 2). Only the data from the 20 samples with high indices of faunal affinity (*i.e.*, those with similar sediment composition) were used. The intervals chosen were logarithmic rather than arithmetic, thus each category is an order of magnitude larger than the preceding category. Those animals weighing less than 0.0001 g are only partially sampled by a screen with 0.2 mm mesh and therefore those smaller than 0.0001 g are not included in Figure 2. Thus the analysis has validity only for those organisms weighing 0.0001 g or more. Within the range from 0.0001 to more than 1.0 g, there is a constant decrease in numbers from one interval to another (see Fig. 2) which is in agreement with the accepted concept. The average increase in number of individuals is × 8.5 as one moves from one category to that containing the next smallest animals. A single category, the interval 0.0001–0.001 g, includes 69.4% of the fauna by number.

When the same treatment is applied to total weight or biomass within each of the categories, no trend is evident (see Fig. 3) and the expected inverted pyramid does not materialize. Despite the fact that this situation differs from the theoretical, one should be cautious about generalizing from the results. Obviously the biomass histogram describes the structure of this particular community and to a considerable degree, the form of the histogram reflects the nature of the dominant species. The larger than expected biomass value in the 0.0001 <0.001 g interval is undoubtedly due to concentrations of adult *Nucula* and juvenile *Nephthys*. Possibly different kinds of animal communities can be described by characteristic biomass histograms and it may prove feasible to use such histograms as another tool in describing communities.

The present analysis brings out the uncertainty of our knowledge of the feeding habits of many benthic invertebrates and, therefore, a precise definition of number and weight relationships from the trophic aspect cannot be attempted at this time. It

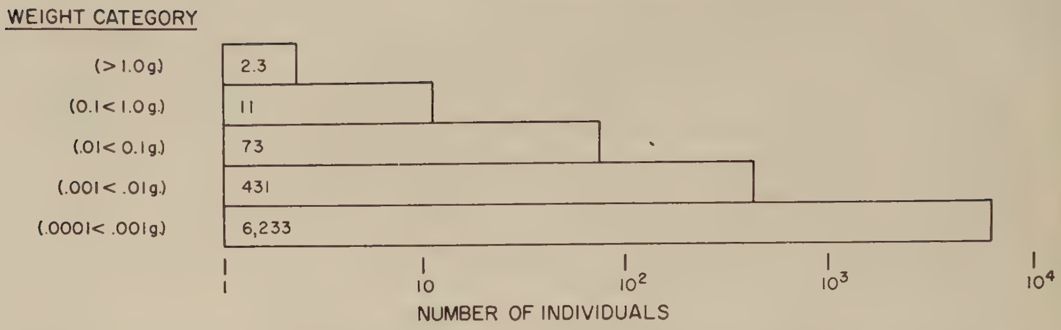

Fig. 3. The relationship of weight categories (left) to biomass (right) for the benthic community at station R.

can be stated, however, that true carnivores make up, at most, about 8% of the fauna by number. The actual percentage is probably much lower.

Finally, some mention should be made of the meiofauna, such as nematodes, kinorhynchs, ostracods and benthic copepods and the contribution it makes to the histograms of numbers and weights at station R. The 4 samples from R station that showed the typical sediment composition in Wieser's study (1960) are considered.

There are about 930,000 meiofaunal animals per m^2, which indicates that they are about a hundred times more numerous than the macrofauna. However, their biomass of 0.3662 g/m^2 is only 1/33 the weight of the macrofauna. The most overwhelmingly abundant group is the nematodes, which comprise 97.66% of the meiofauna by number.

Because it is very difficult to obtain individual weights for such small animals, average weights were used. Therefore the weight ranges within each group cannot be determined and, as a result, it is impossible to assign the proper fraction of each group to its correct weight category.

Wieser found that the average weight of a nematode is $0.00028\mu g$, a kinorhynch, $0.003\mu g$, a benthic copepod, $0.0017\mu g$, and an ostracod, $0.018\mu g$. Thus there is little overlap between the macro- and the meiofauna. Obviously, since the meiofauna consists overwhelmingly of nematodes and the average weight of these animals is appreciably less than the other groups, much of the meiofaunal biomass must be present in the smaller weight categories. Therefore, like the macrofauna, it would seem highly unlikely that a biomass pyramid of the meiofauna at station R would approximate the theoretical inverted form.

In the light of what has been shown regarding animal weights and numbers, it may be convenient here to consider the relative validity of numbers and weights in quantitative faunal studies. Generally speaking, the larger animals are less abundant than smaller animals. Only 13.3 specimens in the largest two categories (see Fig. 2), representing less than 0.15% of the fauna by number, constitute 55.17% of the entire biomass. Since the latter figure represents the average percentage of 20 samples, the effect of these animals on the biomass of individual samples would be much more extreme. It would seem that the presence or absence of the rare, randomly distributed large animals effectively determines the biomass of a sample (see also Sanders 1956). Unless this component is separately assayed, comparative biomass values become relatively meaningless. Because of this difficulty, the writer feels that animal numbers are the more valid measurement providing, of course, that a standard screen with small enough apertures is used so that an adequate number of animals is captured.

REFERENCES

Blegvad, H. 1914. Food and conditions of nourishment among the communities of invertebrate animals found on or in the sea bottom in Danish waters. Rep. Danish biol. Sta., **22**: 41–78.

Drew, G. A. 1899. Some observations on the habits, anatomy and embryology of members of the Prosobranchia. Anat. Anz., **15**: 493–519.

Elton, C. 1946. Competition and the structure of ecological communities. J. Anim. Ecol., **15**: 54–68.

Fager, E. W. 1957. Determination and analysis of recurrent groups. Ecol., **38**: 586–595.

Fretter, V., and A. Graham. 1949. The structure and mode of life of the Pyramidellidae, parasitic opistobranchs. J. Mar. Biol. Ass. U. K., **28**: 493–532.

Hedgpeth, J. W. 1954. Bottom communities of the Gulf of Mexico. U. S. Fish and Wildlife Service, Fishery Bull., 89, **55**: 203–214.

Holme, N. A. 1949. The fauna of the sand and mud banks near the mouth of the Exe. J. Mar. Biol. Ass. U. K., **28**: 189–237.

Jones, N. S. 1950. Marine bottom communities. Biol. Rev., **25**: 283–313.

Longhurst, A. R. 1958. An ecological survey of the west African marine benthos. Colonial Office. Fish. Publ., **11**: 1–102.

Macfadyen, A. 1954. The invertebrate fauna of Jan Mayen Island (East Greenland). J. Anim. Ecol., **23**: 261–297.

Mare, M. F. 1942. A study of a marine benthic community with special reference to the microorganisms. J. Mar. Biol. Ass. U. K., **25**: 517–554.

Medcof, J. C. 1948. A snail commensal with the soft-shell clam. J. Fish. Res. Bd. Can., **7**: 219–220.

Renkonnen, O. 1944. Die Carabiden- und Staphylinidenbestaende eines Seeufers in SW-Finnland. Ann. Entom. Fenn., **10**: 33–104.

Sanders, H. L. 1956. Oceanography of Long Island Sound, 1952–1954. X. Biology of marine bottom communities. Bull. Bingham Oceanogr. Coll., **15**: 345–414.

———. 1958. Benthic studies in Buzzards Bay. I. Animal-sediment relationships. Limn. & Oceanogr. **3**: 245–258.

Savilov, A. I. 1957. Biologic aspect of the bottom-fauna of the northern Okhotsk Sea. Trudy Inst. Okeanol., **20**: 88–170. (*In Russian.*)

Smith, J. E. 1932. The shell gravel deposits and infauna of the Eddystone grounds. J. Mar. Biol. Ass. U. K., **18**: 243–278.

Soil Survey Staff. 1951. Soil Survey Manual, U. S. Dept. Agr. Handbook No. **18**: 1–503.

Turpaeva, E. P. 1957. Food relationships between the dominant species of marine bottom biocenoses. Trudy Inst. Okeanol., **20**: 171–185. (*In Russian.*)

Wieser, W. 1960. Benthic studies in Buzzards Bay. II. The meiofauna. Limn. & Oceanogr., **5**: 121–137.

Yonge, C. M. 1939. The protobranchiate Mollusca; a functional interpretation of their structure and evolution. Phil. Trans. B, **230**: 79–147.

Contribution No. 1034

Särtryck ur Tellus nr 1, 1960

On the Dynamics and Energy Transformations in Steady-State Hurricanes

By J. S. MALKUS, Woods Hole Oceanographic Institution[1],
and H. RIEHL, The University of Chicago.

(Manuscript received May 5, 1959)

Abstract.

A dynamic model of the inflow layer in a steady mature hurricane is evolved, relating wind speed, pressure gradient, surface shearing stress, mass flow, and convergence. The low-level air trajectories are assumed to be logarithmic spirals. With this hypothesis, properties such as maximum wind and central pressure are determined through choice of a parameter depending on the inflow angle: a moderate hurricane arises with inflow angles of about 20°, while 25° gives an intense or extreme storm.

Most of this study treats the moderate storm. In order to maintain its core pressure gradients, an oceanic source of sensible and latent heat is required. As a result, latent heat release in the inner hurricane area occurs at higher heat content (warmer moist adiabats) than mean tropical subcloud air. The heat transfer from the ocean and the release of latent heat in the core determine the pressure gradient along the trajectory, and this prescribes the particular trajectory selected by the air among an infinite number available from the logarithmic spiral family.

This selection principle is evolved using recent work on "relative stability" of finite amplitude thermal circulations. Of an infinite number of dynamically possible spirals, the one is realized which maximizes the rate of kinetic energy production under the thermodynamic constraints, here formulated in terms of the relation between heat release and pressure gradient.

Finally, rainfall, efficiency of work done by the storm, and kinetic energy budgets are examined in an attempt to understand the difference between the hurricane—a rare phenomenon—and the common sub-hurricane tropical storm.

1. Introduction

The tropical hurricane is a thermally driven circulation whose primary energy source is release of latent heat of condensation. This heating acts to establish the pressure gradients which produce and maintain hurricane winds. Radar photographs, since the early 1940's, have demonstrated abundantly that latent heat is not released uniformly through the rain area, but that it is concentrated in spiral convective bands of narrow width and especially in a central ring surrounding the eye (MAYNARD 1945, WEXLER 1947). In this paper the low-level air along an inward spiralling convective band will be followed from the outskirts to the eye. The purpose is to begin a study of the mechanisms by which energy release along such a path is utilized to maintain the pressure field of a mature storm in steady state.

Large pressure gradients are required to sustain a narrow ring of hurricane winds, with order of 30 mb in 60 km. The central pressure of a hurricane of moderate strength must be about 960 mb, 4—5 per cent below mean sea level pressure. Available evidence suggests that this substantial reduction is brought about by tropospheric heating, and that an undisturbed top may be assumed within the limits of interest in this investigation. As demonstrated by HAURWITZ (1935), pressures in hurricanes are very nearly hydrostatic and, given a fixed top, lateral pressure gradients are produced by density variations within the troposphere. Such variations may result from release of latent heat in the precipitation area and from dry-adiabatic sinking in the eye.

---

[1] Contribution No. 1034 from the Woods Hole Oceanographic Institution.

Formerly it was held that an outward slope of the eye wall with height could explain the low pressures in the inner convective ring around the eye. According to MALKUS (1958), the slope of the cumulonimbi forming the eye wall is governed by the factors generally determining the slant of such clouds. From consideration of cloud dynamics and angular momentum constraints, an eye wall is prevented from slanting more than 45°—60° from the vertical. Since the height of the cumulonimbi is 10—14 km, this means that, in a storm with eye radius of 20—30 km, the eye slope can at most account for rain area pressures to distances of 30—40 km from the center. Extensive photography of eye walls by the National Hurricane Research Project of the U.S. Weather Bureau and various radar studies have demonstrated that such large slopes are rarely, if ever, realized; these data suggest that, more likely, the eye wall is nearly perpendicular.

Hence, the contribution of dry-adiabatic sinking to lateral density gradients in the rain area may be neglected. It is assumed that the whole density gradient is derived from latent heat release; further that the cloud towers are nearly vertical to about 9—10 km altitude. In the high troposphere the mass ascending in the cumulonimbi converges vertically and spreads laterally covering large horizontal areas. Although the winds turn with height in this layer, often sharply, we assume as a first approximation that the air above the vertical portion of a cumulonimbus has the same properties as would have been obtained from continued vertical ascent to the top of the convective layer. Thus the surface pressure at any point may be computed hydrostatically from the ascent path of the surface air to the high troposphere.

The warmest possible ascent of normal tropical air lies along the moist adiabat with equivalent potential temperature (Θ_E) of about 350° A. If the top of the circulation is taken at 150 mb at standard height for the Caribbean area in summer, the lowest surface pressure obtained through this ascent will be about 1,000 mb from the hydrostatic equation (RIEHL 1954). This is a threshold value, and it is interesting to note that many tropical storms reach equilibrium at this central pressure. The total heat content of normal tropical air, raised undilute (without entrainment) to the level of zero buoyancy, is insufficient to generate pressures substantially below 1,000 mb. It follows that a local heat source must exist within hurricanes to permit increases of Θ_E of the surface air above 350° A. The existence of such a heat source has been inferred by BYERS (1944) and demonstrated to exist from surface observations (RIEHL 1954).

It also follows that variations in the rate of import, condensation and export of normal tropical air will not lead to variations in surface pressure because the ascent path, and therewith the density of the vertical column, is entirely determined by the Θ_E of the rising air. A storm will not deepen if simply more water is condensed at $\Theta_E = 350°$ A in the core; it can do so only if there is an additional heat source so that condensation will occur at Θ_E greater than 350° A.*

As first step, the surface pressure was computed from a series of moist adiabats with the foregoing model, namely that vertical ascent can be assumed to the level of zero buoyancy. The undisturbed top was taken as 100 mb and a mean tropical atmosphere (JORDAN 1957) was used for the layer between the 100 mb and the pressure at zero buoyancy. For moist adiabatic ascents between $\Theta_E = 350°$ A and 365° A, surface pressure (p_s) and Θ_E are related linearly. One obtains

$$-\delta p_s = 2.5\ \delta\Theta_E \qquad (1)$$

Following this relation, the sea level pressure will drop about 12.5 mb for an increase of 5° A in Θ_E. Suppose that the oceanic heat source begins to become effective at $p_s = 1{,}000$ mb with $\Theta_E = 350°$ A. Then, if the increment in Θ_E is 15° A, the central pressure will be 962.5 mb at $\Theta_E = 365°$ A. This rise in Θ_E corresponds to an increase of the heat content of the surface air of 3—4 cal/gm which must be absorbed from the ocean if ascent at 365° A is to occur. The question is whether in reality such a heat exchange can be realized. In the following a dynamical model will be developed for the inflow layer which will permit computation of the pressure drop required for a steady-state vortex. Then, from estimates of heat exchange between sea and air, it will be determined whether this pressure decrease is consistent with equation (1).

---

* It should be noted, however, that in cases when mid-tropospheric air not derived from the surface enters the rain area (SIMPSON and RIEHL 1958) with characteristic Θ_E of only 330°—340° A, an increased rate of surface mass inflow at 350° A will act to maintain the heat content of a storm's interior. The constraint upon hurricane growth and maintenance arising from such lateral "ventilation" will be considered in subsequent publications.

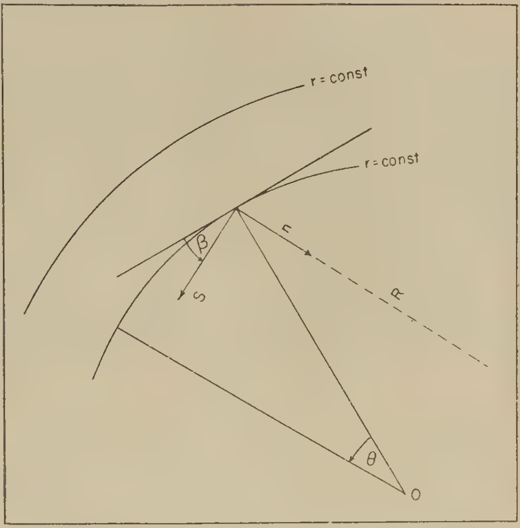

Fig. 1. Coordinate system used for hurricane models. Origin at O. *r* and ϑ form a standard cylindrical system. The direction *s* is chosen along the trajectories, positive downstream, with *n* the normal coordinate. β is the inflow or "crossing" angle formed between *s* and circles of constant radius. *R* is the radius of curvature of the trajectories.

2. A Dynamic Model of the Low-Level Rain Area

The inflow into a hurricane is confined mainly to low levels. Subcloud air is accelerated inward along spiral-shaped trajectories; acceleration results from excess work done by pressure gradient forces over frictional retardation. We shall consider the dynamics of the inflow layer in a natural coordinate framework, found useful in studies of other types of thermal circulations (RIEHL ET AL., 1951; MALKUS, 1956; RIEHL and FULTZ, 1957). This coordinate system, superposed on cylindrical coordinates is illustrated in Fig. 1, where *s* is distance along the trajectory, *n* is the normal coordinate and *z* the vertical coordinate, directed to form a right-handed system. The crossing angle between trajectory and circles of equal radius *r* from the storm center o is denoted by β; the radius of curvature of the trajectories is *R*. The tangential and normal equations of motion to be used are as follows:

$$\frac{dv}{dt} \cong v\frac{\partial v}{\partial s} = -\frac{1}{\varrho}\frac{\partial p}{\partial s} + \frac{1}{\varrho}\frac{\partial \tau_{sz}}{\partial z} = -\frac{1}{\varrho}\frac{\partial p}{\partial r}\sin\beta + \frac{1}{\varrho}\frac{\partial \tau_{sz}}{\partial z} \tag{2}$$

$$\frac{v^2}{R} + fv = -\frac{1}{\varrho}\frac{\partial p}{\partial n} = \frac{1}{\varrho}\frac{\partial p}{\partial r}\cos\beta \tag{3}$$

Here *t* is time, *r* the radial coordinate (positive outward), *v* velocity, *p* pressure, ϱ density, *f* the Coriolis parameter and τ_{sz} the shearing stress component transferring *s*-momentum along the vertical.

Assumptions introduced so far are as follows:

1) The storm is in steady state, either stationary or very slowly moving.

2) The pressure field is radially nearly symmetrical, i.e. $\frac{\partial p}{r\partial\vartheta} \ll \frac{\partial p}{\partial r}$. Since all other quantities may vary from one trajectory to the next, and thence with azimuth angle, this choice does not restrict the applicability of the model to symmetrical circulations.

3) The vertical transport of *s*-momentum by the mean motion, $w\frac{\partial v}{\partial z}$ (*w* is the vertical velocity component) is small compared to $v\frac{\partial v}{\partial s}$. This assumption is valid because the vertical motion is zero at the ground and $\frac{\partial v}{\partial z}$ is small throughout the inflow layer except quite close to the ground. Vertical momentum transport by convective-scale elements is included in the shearing stress term.

4) Lateral turbulent transport of *s*-momentum is neglected compared to vertical transport with the hypothesis that momentum from the air inside the hurricane is abstracted by the ocean and not diffused laterally outward by small-scale eddies. This assumption is probably weak if single trajectories or only small segments of a storm are considered, but due to the difficulty of prescribing the vertical eddy transport accurately, is not critical at present.

5) The wind direction is nearly constant with height through the inflow layer so that the shearing stress term $\frac{\partial \tau_{nz}}{\partial z}$ may be omitted.

We shall now substitute $\frac{r}{\cos \beta}$ for R, the radius of trajectory curvature in (3). This is exact for the logarithmic spiral where $\cos \beta =$ constant and nearly true when the inflow angle varies slowly along the trajectory. When $\beta \approx 20°$ or less, R differs from r by only about 6 % for any trajectory. Let equation (2) be multiplied by $\cos \beta$ and equation (3) by $\sin \beta$. The pressure gradient force is then eliminated by combining these equations and we have, after dividing again by $\cos \beta$,

$$\frac{v^2}{r} \sin \beta + fv \tan \beta - v \frac{\partial v}{\partial s} = - \frac{1}{\varrho} \frac{\partial \tau_{sz}}{\partial z} \tag{4}$$

Upon averaging vertically through the inflow layer of height δz, we have

$$\tilde{\varrho} \delta z \left[\frac{\tilde{v}^2}{r} \sin \beta + f \tilde{v} \tan \beta - \tilde{v} \frac{\partial \tilde{v}}{\partial s} \right] = \\ = \tau_{so} = K_F \varrho_0 {v_0}^2, \tag{5}$$

using the commonly assumed dependence of τ_{so} upon the square of the surface wind. The symbol ~ denotes vertical averaging, K_F is an empirically determined coefficient, and the subscript zero denotes surface properties. We shall neglect the slight difference between ϱ_0 and $\tilde{\varrho}$, also between $\tilde{v}$ and v_0, since the vertical shear above anemometer level generally is considered to be very weak in the interior of hurricanes, especially over water. The important assumption in going from the right side of equation (4) to that of equation (5) is that the shearing stress vanishes at the top of the inflow layer in accord with the hypothesis that $\frac{\partial v}{\partial z}$ is very weak above the ground layer. In the remainder of this section only quantities averaged through the inflow layer will be consisidered and the symbol ~ will again be omitted for convenience.

Dividing out a v and utilizing the definition that $\frac{\partial v}{\partial s} = - \frac{\partial v}{\partial r} \sin \beta$, we derive the following first-order differential equation for the velocity v along any trajectory as a function of radial distance r from the storm center,

$$\frac{dv}{dr} + v \left[\frac{1}{r} - \frac{K_F}{\sin \beta \, \delta z} \right] = - \frac{f}{\cos \beta} \tag{6}$$

Since it will prove more convenient to set boundary conditions on v_ϑ, the tangential velocity component, we may obtain an equation for it by using the fact that $v = \frac{v_\vartheta}{\cos \beta}$, namely

$$\frac{dv_\vartheta}{dr} + v_\vartheta \left[\frac{1}{r} + C(r) \right] = -f \tag{7}$$

where $C(r) = \frac{-K_F}{\sin \beta \delta z}$.

It should be noted that equation (7) specifies the dependence of v upon r for a single trajectory; it may be integrated separately for one or more trajectories within a single storm or for the mean trajectories of several storms. Whichever is done, the difference between trajectories is determined by the parameter $C(r)$. Equation (7) may be integrated analytically if $C(r)$ is a constant or varies in some simple manner with the radius. Numerical integration may be undertaken if it should prove desirable to treat a complex dependence of C upon r.

The results of PALMÉN and RIEHL (1957) suggest that although K_F and ∂z may each vary by a factor of two under hurricane conditions (increasing inward) their ratio is constant within 20 %. We chose $K_F / \partial z = 1.36 \times 10^{-8}$ cm^{-1} for the following analysis, which permits K_F to vary from 1.1 to 3.0×10^{-3} for a range of the depth of the inflow layer from 750 m to 2.2 km.

We shall make the simplest possible choice of β for our trajectory calculations, namely $\beta = \beta_L =$ constant for the outer rain area, $r >$ 100 km, and decreasing from there linearly to zero at $r = 25$ km, the assumed radius of the eye wall. The solution to (7) is thus an infinite family of simple logarithmic spirals (modified slightly in the interior) each differing from the others by means of a different inflow angle β.

Integrating equation (7) when $C(r)=$ constant,

$$v_\vartheta r = \frac{f}{C^2}(1-Cr) + C_1 e^{-Cr} \qquad (8)$$

An outer boundary condition must be applied to evaluate the constant of integration C_1. This will be done by choosing an outer radius r_0 where the relative vorticity vanishes, that is $\frac{dv_\vartheta}{dr}+\frac{v_\vartheta}{r}=0$. Since $v_r=v_\vartheta \tan\beta$, v_r also satisfies this relation at r_0, which thus separates the region of inner horizontal convergence from outer horizontal divergence. Choice of r_0 is arbitrary, but the computed structure of the storm core is not sensitive to this choice as long as $r_0 \geq 500$ km. For moderate hurricanes such as Carrie (September 15, 1957) and Daisy (August 27, 1958), data from the National Hurricane Research Project of the U.S. Weather Bureau suggest that $r_0 \cong 500$ km is satisfactory. For bigger storms, such as some Pacific typhoons, r_0 might be 800—1000 km.

When the outer boundary condition is applied, $C_1=\frac{-f}{C^2}e^{Cr_0}$ and

$$v_\vartheta r = \frac{f}{C^2}\left[1 - Cr - e^{C(r_0-r)}\right]. \qquad (9)$$

For the inner rain area, namely $r_E < r < r_1$ where r_1 is 100 km and r_E, the eye boundary, is 25 km, we choose

$$\sin\beta = \sin\beta_L \frac{r-r_E}{r_1-r_E}.$$

Equation (7) may be solved exactly under this assumption, matching v at $r_1=100$ km. However, near the core Coriolis forces are negligible compared to centrifugal, leaving only the homogeneous part of the equation. This yields a simple solution for the inner rain area.

$$v_\vartheta r = C_2[r-r_E]^{-(r_1-r_E)C} \qquad (10)$$

where C_2 is obtained by matching v_ϑ at 100 km with the results of (9).

We now calculate two model hurricane trajectories at latitude 20°, a moderate and an intense one, with $r_0=500$ km in both cases. The only difference between them lies in the choice of $\sin\beta_L$, which for the moderate trajectory is 0.342 ($\beta_L=20°$); and for the intense hurricane $\sin\beta_L=0.423$ ($\beta_L=25°$). The other parameters such as ϱ, f, $\frac{K_F}{\delta z}$, r_1, and r_E are the same for both cases, with values as noted. Tangential speed as a function of radius in the two situations is given in Table 1.

Table 1. Tangential Wind Speeds in Moderate and Intense Model Hurricane Trajectories.

A. Moderate		B. Intense
r (km)	$\beta_L=20°$; $C=-4.0\times10^{-8}$ cm^{-1} v_ϑ (m/sec)	$\beta_L=25°$; $C=-3.2\times10^{-8}$ cm^{-1} v_ϑ (m/sec)
800	3.4	5.8
700	6.9	9.4
600	9.9	12.5
500	12.4	15.6
400	15.0	19.0
300	18.1	23.3
200	23.3	30.7
100	37.2	50.7
50	53.8	78.2
30	55.4	87.5

The results of this table can be regarded as applying to single trajectories within a storm or storms, or to a mean trajectory; in the latter case v_ϑ represents the azimuth-averaged tangential wind speed for an entire hurricane. Highest wind speed is about 112 knots for case A which will be called "moderate storm". In case B, 175 knots are attained. This range of maximum wind is realistic, as is also the distribution of v_ϑ with radius. Between 500 and 200 km distance from the center the wind profile may be represented by the relation $v_\vartheta r^x=$ constant, where $x=0.6$ to 0.7, in agreement with the findings of HUGHES (1952) for a mean typhoon. Further calculations for the moderate storm are made in the next section.

3. The Moderate Storm

In Table 2 surface pressure, mass flow, divergence, and frictional stresses are presented for the moderate case.

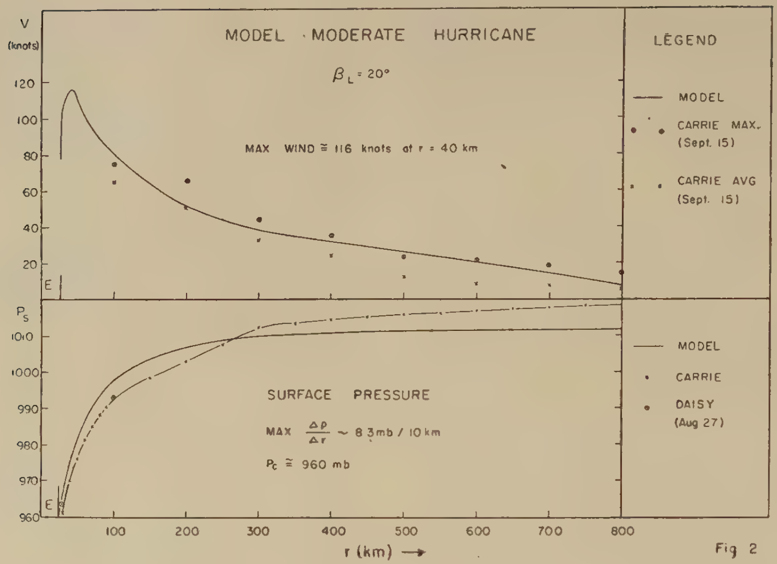

Fig. 2. Wind profile (above) and surface pressure profile (below) for model moderate storm (see Table 2). Observations from actual hurricanes (Carrie, 1957, and Daisy, 1958) were provided by courtesy of the National Hurricane Project of the U. S. Weather Bureau. In the upper graph, circles represent the peak windspeed at each radius in Carrie, while the *x*'s denote the radial average. In the lower graph the Carrie pressure profile is the x-ed line, while the two circles are values from Daisy.

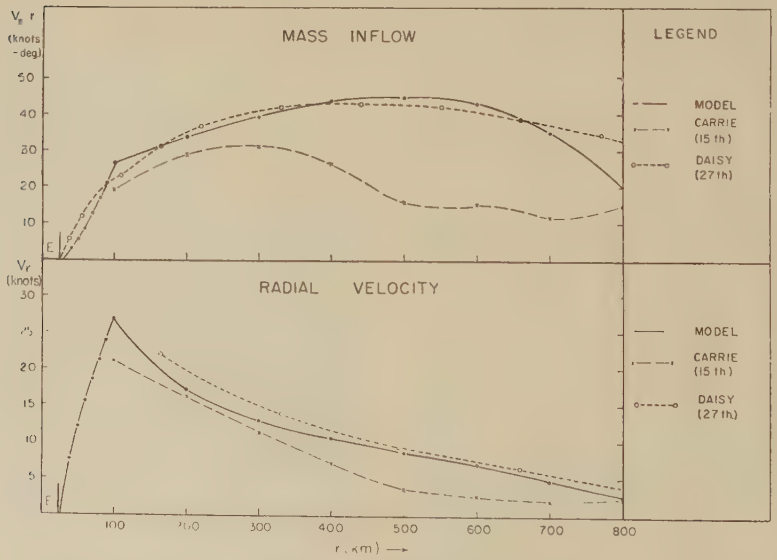

Fig. 3. Mass inflow (above) and radial velocity (below) profiles for model moderate hurricane of Table 2. Dashed curves were calculated from ship observations.

Table 2. Moderate Model Hurricane.

r km	v_ϑ m/sec	v_r m/sec	β degrees	$v_r r \cdot 10^{-9}$ c.g.s.	div. 10^5 cm^{-1}	w cm/sec	v m/sec	τ_0 dynes/cm^2	p_s mb
800	3.4	1.2	20	9.6	1	—1.1	3.6	0.18	1011.8
700	6.9	2.5	20	17.55	0.6	—0.66	7.3	0.71	1011.7
600	9.9	3.6	20	21.6	0.2	—0.22	10.5	1.65	1011.5
500	12.4	4.5	20	22.5	—0.1	+0.11	13.2	2.61	1011.2
400	15.0	5.5	20	22.0	—0.65	+0.72	16	3.84	1010.5
300	18.1	6.6	20	19.8	—1.1	+1.2	19.2	5.53	1009.5
200	23.3	8.5	20	17.0	—2.3	+2.5	24.8	9.23	1007.2
100	37.2	13.5	20	13.5	—29.6	+32.6	39.6	23.5	997.7
90	40.0	11.9	17.3	10.7	—25.3	+27.9	42.0	26.5	996.0
80	42.7	10.7	14.6	8.6	—26.5	+29.7	44.2	29.3	993.8
70	46.0	9.4	11.8	6.6	—28.4	+31.3	47.2	33.4	991.0
60	49.6	7.9	9.2	4.7	—30.7	+33.8	50.3	38.0	987.35
50	53.8	6.1	6.5	3.05	—33.6	+37.0	54.0	43.8	982.4
40	57.7	3.9	3.6	1.6	—33.4	+36.7	57.9	50.2	975.35
30	55.4	1.3	1.3	0.39	—25.5	+28.0	55.4	46.0	966.0
26	39.4	0.2	0.25	0.05			39.4	23.3	962.85

For the purposes of the vertical motion and shearing stress calculations of this table, the depth of the inflow layer ∂z has been chosen as 1.1 km, thus K_F in equation (5) becomes 1.5×10^{-3}. The product $v_r r$ is proportional to the ageostrophic mass inflow; v_r is calculated from $v_\vartheta \tan \beta$. The horizontal velocity divergence is $\frac{1}{r}\frac{\partial}{\partial r}(v_r \cdot r)$, yielding the mean vertical motion w at 1.1 km from mass continuity. Irregular values of divergence and vertical motion occur at $r = 100$ km through rapid reduction in mass flow arising from the assumption that the inflow angle β begins to decrease at that radius. This minor difficulty apart, it is seen that all strong convergence is concentrated in the core. An average ascent rate of about 30 cm/sec or 1 km/hr is required at the top of the inflow layer.* The surface pressure p_s was calculated from evaluating gradients over short radial intervals (10 km in core) from equation (3) and integrating graphically, with a boundary pressure of 1,011.8 mb at $r = 800$ km.

The features of Table 2 are realistic and consistent with presently available observations. Figs. 2—4 show some comparisons. Fig. 2 contains wind and pressure profiles of Table 2 together with those of two medium strength hurricanes obtained by the National Hurricane Research Project; both storms were encountered between 25°—30° N. Fig. 3 compares mass inflow and radial velocity distributions for these same storms with those calculated in Table 2. Fig. 4 shows good agreement between

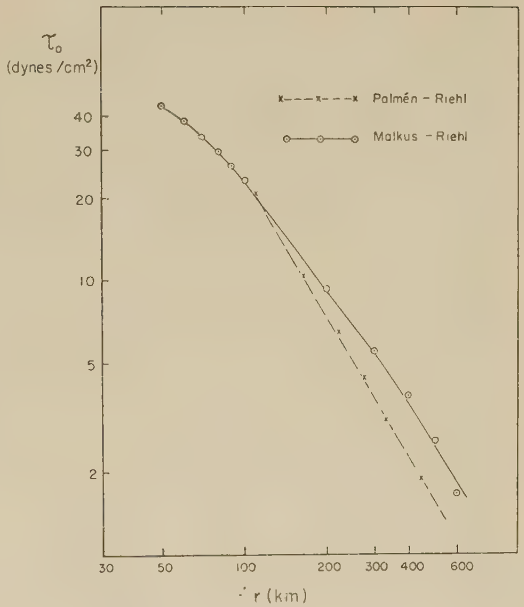

Fig. 4. Surface shearing stress (dynes/cm²) versus radius (km). Solid curve from model moderate storm; dashed curve from momentum budgets calculated by Palmén and Riehl (1957) for mean hurricane data.

---

*We do not regard this as a gradual layer ascent of this magnitude, but rather envisage that about 5 %—10 % of the inner area is covered with updrafts of 3—6 m/sec at this level, since recent evidence suggests that the net convergence is achieved largely by restricted ascent in a few undilute cumulonimbus towers.

the shearing stresses as a function of radius calculated in Table 2 with those obtained by Palmén and Riehl (1957) from momentum budget requirements established from mean hurricane data.

4. Pressure Field and Oceanic Heat Source

As just demonstrated, pressures and pressure gradients of the moderate hurricane are similar to those observed in storms of moderate intensity such as Carrie (1957). Outward of $r = 90$ km where $p_s \sim 996$ mb, the pressure field may be maintained by a mixture of the air with the characteristics of the average tropical atmosphere and varying amounts of subcloud air that has ascended in cumulus towers. The admixture of low-level air must increase inward so that at $r = 90$ km the vertical temperature distribution becomes entirely controlled by the moist-adiabatic ascent. Inward of $r \sim 30$ km or $p_s \sim 966$ mb, a sloping eye wall may be called upon to compute the excessive pressure drop often encountered just inside the eye boundary. Neither of these solutions can account for the pressure drop of approximately 30 mb between $r = 90$ km and $r = 30$ km. This pressure drop must be related to adiabatic ascent at increasing values of Θ_E; from equation (1) Θ_E of the ascending air must rise from 350° to 362.5° A along the trajectory while the surface pressure decreases from 996 to 966 mb. Such an increase in Θ_E can only be obtained through a local heat source, namely transfer of sensible and latent heat from ocean to atmosphere as proposed by Byers (1944) and discussed by Riehl (1954).

It is the objective of this section to calculate the necessary heat exchange between sea and air and to inquire whether the ocean can supply the required heat in the available time which, from Table 5, is less than three hours.

Sensible heat transfer: In the outskirts of a hurricane the temperature of the inflowing air drops slowly due to adiabatic expansion during (horizontal) motion toward lower pressure. It is one of the remarkable observations in hurricanes that this drop ceases at pressures of 990—1,000 mb and that thereafter isothermal expansion takes place. Presumably, the temperature difference between sea and air attains a value large enough for the oceanic heat supply to take place at a sufficient rate to keep the temperature difference constant. In the last part of this paper, it will be shown that this corresponds to a maximum rate of conversion of the sensible heat gained to kinetic energy. For the present we shall merely utilize the fact of isothermal expansion. The first law of thermodynamics then becomes

$$dh_s = -\alpha A^* dp \tag{11}$$

where dh_s is the sensible heat gained from the ocean, α specific volume and A^* the heat equivalent of mechanical work. Radiation may be neglected as a very small term. With use of the gas equation

$$dh_s = -RTd(\ln p) \tag{12}$$

where R, the gas constant for air, is expressed in heat units. Integrating over a portion of the trajectory of the surface air,

$$(h_s - h_{s0})/T = R\,(\ln p_0 - \ln p), \tag{13}$$

where the subscript zero denotes properties at the starting point. Given $T \sim 300°$ A, heat increments $h_s - h_{s0}$ can be readily computed; for steps of 20 km radial distance they have the values shown below.

Table 3. Sensible Heat Source at Ocean Surface

Radial distance (km)	70—90	50—70	30—50	30—90
$h_s - h_{s0}$ (cal/gm)	.11	.17	.37	.65

Total and latent heat transfer: The equivalent potential temperature is defined by

$$\ln \Theta_E = \ln \Theta + Lq/c_pT \tag{14}$$

where Θ is potential temperature, L latent heat of condensation, q specific humidity and c_p specific heat at constant pressure. Since the temperature is constant

$$d(\ln \Theta_E) = d(\ln \Theta) + Ldq/c_pT. \tag{15}$$

Equation (12) may also have been written

$$dh_s = c_pT/\Theta\, d\Theta \sim c_p d\,\Theta \tag{16}$$

near the ground. Since dh and $d\Theta_E$ are known, equation (15) may be solved for dq. This yields the latent heat addition to the air. The

Table 5. Thermodynamic Properties of Inflow Layer.

r km	P_s mb	Θ_E °A	Θ °A	T °C	q gm/kg	rh %	LCL m	Δs km	Δt min
90	996	350	299.4	26.0	18.5	84	400		
70	991	352.1	299.9	26.0	19.1	86	300	79.7	30
50	982.4	355.7	300.5	26.0	20.1	90	200	125.4	42
30	966	362.5	301.8	26.0	21.8	97	80	294.0	88

Δs denotes distance along each trajectory leg, from 90 to 70 km etc.
Δt is time needed to traverse each leg.
CL is the lifting condensation level, or cloud base height.

following table shows sensible, latent and total heat increments.

Table 4. Oceanic Heat Source for Moderate Hurricanes

Radial distance (km)	70—90	50—70	30—50	30—90
Sensible heat increment (cal/g)	.11	.17	.37	.65
Latent heat increment (cal/g)	.32	.56	1.01	1.89
Total heat increment (cal/g)	.43	.73	1.38	2.54

Lagrangian exchange coefficients: One should expect that, following a particle, the heat transfer from the ocean will be governed only by the differences in temperature and vapor pressure between sea and air and wind speed. The subscript P will denote calculations performed with respect to the moving particle. Denoting sensible and latent heat transfer by Q_{SP} and Q_{eP}, we may postulate that

$$Q_{SP} = K_{SP} V (T_w - T_a), \tag{17}$$

$$Q_{eP} = K_{eP} V (e_w - e_a). \tag{18}$$

Here the subscripts 'w' and 'a' denote properties of the water surface and of the air, e is vapor pressure, and K_{SP} and K_{eP} are coefficients of turbulent exchange. Now $\int Q_{SP} dt = h_s - h_{s0}$; $\int Q_{eP} dt = h_e - h_{e0}$, where h_e denotes latent heat content. Integrating equations (17) and (18) from t_0 to t during which time interval the particle moves the distance D along the trajectory

$$(h_s - h_{so})/D(T_w - T_a) = K_{SP}, \tag{19}$$

$$(h_e - h_{eo})/D(e_w - e_a) = K_{eP}. \tag{20}$$

The ocean temperature will be taken as 28° C, typical for the West Atlantic hurricane area, and T_w—T_a will be assumed as 2° C. With this assumption, based on observations, and with equation (14) all properties of the inflowing air are given, including relative humidity and height of the cloud base. They are summarized in Table 5.

From equations (19) and (20) and from Table 5 the following values are obtained for K_{SP} and K_{eP}.

Table 6. Lagrangian Coefficients of Turbulent Exchange.

Radial distance (km)	70—90	50—70	30—50
K_{SP} (10^{-9} cal/gm cm deg)	6.9	6.8	6.3
K_{eP} (10^{-9} cal/gm cm mb)	4.5	5.4	5.1

It is seen that the coefficients are constant within computational limits, hence that the air trajectory, computed purely from dynamic considerations, is consistent with the independent constraints of equations (17) and (18). The trajectory takes a course such that physically impossible demands are not placed on the thermodynamic interaction between sea and air.

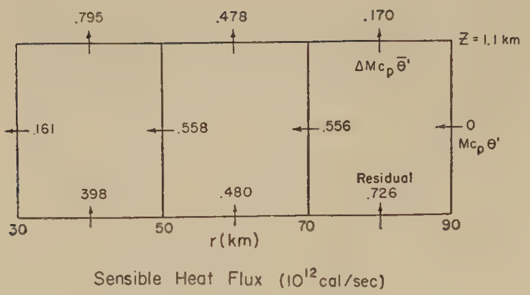

Fig. 5. Sensible heat budget for moderate storm. Heat fluxes (10^{12} cal/sec) into and out of inflow layer by boxes with $\Delta r = 20$ km. Lateral fluxes have been calculated as shown with $\Theta' = \Theta - 299.4$; for vertical fluxes it has been assumed that vertical mass flux leaves with mean Θ' of interval, $\bar{\Theta}'$. Input from ocean calculated as residual. Mass flow from dynamic model, Table 2.

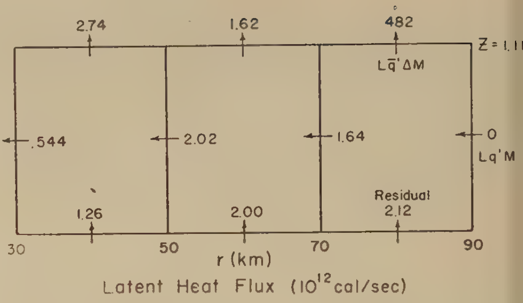

Fig. 6. Latent heat budget for moderate storm. Heat fluxes (10^{12} cal/sec) into and out of inflow layer by boxes with $\Delta r = 20$ km. Lateral fluxes have been calculated with $q' = q - 18.5$ gm/kg; for vertical fluxes it has been assumed that vertical mass flux leaves with mean q' of the interval, $\bar{q}'$. Input from ocean calculated as residual. Mass flow from dynamic model, Table 2.

In the following still another approach will be taken to investigate whether the rates of heat transfer from the sea are reasonable.

Heat energy budget for the inflow layer: Up to now, the calculations have followed a particle on its path. Now heat flux and energy exchange between sea and air will be examined spatially. The purpose in doing this lies in the desire to compare the heat flux per cm² of ocean surface as determined here and as estimated previously from turbulence theory and airplane measurements. For this purpose it will at first be necessary to compute a heat budget. This requires the assumption that the radial distribution of various properties following the trajectory in Tables 2 and 5 may be taken as valid for means around concentric cylinders. Further, a top must be assigned to the inflow layer; it will be taken as 1.1 km, corresponding to a pressure interval of 100 mb as in Table 2.

Differentiating equation (16) with respect to time, multiplying with the density ϱ and integrating over the volume V,

$$\int \varrho \frac{dh}{dt} dV = c_p \int \varrho \frac{d\Theta}{dt} dV \tag{21}$$

The heat source $\int \varrho \frac{dh}{dt} dV = Q_S$, now referred to space in contrast to Q_{SP} in equation (17). Because of the steady state $\frac{d\Theta}{dt} = \mathbf{v} \cdot \nabla \Theta$ where $\mathbf{v}$ is the three-dimensional velocity vector and ∇ the three-dimensional gradient operator.

Then

$$c_p \int \varrho \frac{d\Theta}{dt} dV = c_p \int \varrho \mathbf{v} \cdot \nabla \Theta dV =$$
$$= c_p \int (\nabla \cdot \varrho \mathbf{v} \Theta - \Theta \nabla \cdot \varrho \mathbf{v})\ dV.$$

The second term is zero from mass continuity. Applying Stokes' theorem

$$Q_S = c_p \int \varrho c_n \Theta d\sigma = c_p \sum_\sigma M_\sigma \Theta \tag{22}$$

where σ is the surface bounding the volume V and c_n is the velocity component normal to this surface, positive outward. On the right side of the expression, actually used for calculation, M_σ is the mass flux in gm/sec through each face σ of the box considered.

The latent heat flow may be determined from

$$d/dt\,(Lq) = \mathbf{v} \cdot \nabla (Lq). \tag{23}$$

After transformations corresponding to those just shown for sensible heat, the oceanic latent heat source (Q_e), also referred to space, is

$$Q_e = \int Lq \varrho c_n d\sigma = \sum_\sigma Lq M_\sigma \tag{24}$$

The total heat source is therefore

$$Q_S + Q_e = \int (Lq + c_p \Theta) \varrho c_n d\sigma =$$
$$= \sum_\sigma (Lq + c_p \Theta) M_\sigma \tag{25}$$

Radial and vertical fluxes of sensible and latent heat may be computed from the data in Tables 2 and 5. These fluxes, and the heat sources required for balance are shown in Tables 7 and 8 and Figs. 5—6. These diagrams were derived as follows: The mass flux through each vertical face (at $r=90$, 70, 50, and 30 km) was obtained from $M=v_r r\ 2\ \pi\ \frac{dp}{g}$, where $v_r r$ was taken from Table 2. The mass flux through the top face, $\triangle M$, is the difference between the horizontal fluxes through successive vertical faces. Mass leaving through the top of each box was assumed to go out with the mean property of the air in the box. Heat sources were calculated as residuals to meet continuity. Over the area within the core the source is 5.38×10^{12} cal/sec latent heat of water vapor, and 1.60×10^{12} cal/sec sensible heat, a total of 6.98×10^{12} cal/sec. This corresponds to a heat increment of 2.50 cal/gm, within computational error of the result of Table 4.

Table 7. Sensible Heat Flux.

r km	Θ' °A	M gm/sec 10^{-12}	$\triangle M$ gm/sec 10^{-12}	$Mc_p\Theta'$ cal/sec 10^{-12}	$c_p\overline{\Theta'}$ cal/sec gm	$\triangle Mc_p\overline{\Theta'}$ cal/sec 10^{-12}
90	0	7.40		0		
			2.8		.060	.170
70	0.5	4.65		.556		
			2.5		.191	.478
50	1.1	2.15		.558		
			1.9		.418	.795
30	2.4	0.28		.161		

Θ' denotes Θ—299.4 and the bar indicates area averaging.

Table 8. Latent Heat Flux.

r km	q' gm/kg	Lq' cal/gm	$Lq'M$ 10^{-12} cal/sec	$L\overline{q'}$ cal/gm	$\triangle ML\overline{q'}$ 10^{-12} cal/sec
90	0	0	0		
				.172	.482
70	0.6	.353	1.64		
				.647	1.62
50	1.6	.941	2.02		
				1.44	2.74
30	3.3	1.94	0.544		

q' denotes q — $18.5^0/_{00}$ and the bar indicates area averaging.

From turbulence theory (cf. JACOBS 1942) the following formulae have been determined for latent and sensible heat exchange between sea and air

$$Q_S/A = K_S\,(T_w - T_a)\,v, \tag{26}$$

$$Q_e/A = K_e L\,(q_w - q_a)\,v. \tag{27}$$

Here Q_S and Q_e are the fluxes in cal/sec computed from equations (22) and (24) respectively; A is the area in cm² of ocean surface; $T_w - T_a$ the difference in °C between deck level and sea surface temperature; q_w—q_a the difference in gm/gm between the saturation specific humidity at the temperature of the sea surface and the actual specific humidity at deck level, and v is the wind speed in cm/sec. K_S and K_e are coefficients of turbulent exchange analogous to those of equations (17) and (18). But, as already stressed, the meaning of these equations is quite different because they refer to the heat flow per unit area of ocean surface. RIEHL ET AL. (1951) have used the following constants for calculation of heat exchange in the trades, based on MONTGOMERY (1948): $K_S=4.16 \times 10^{-7}$, $K_e=1.71 \times 10^{-6}$. Recent direct flux measurements by BUNKER (1959) under normal and disturbed trade conditions have confirmed these values within about 25 %. When we solve equations (26) and (27) for the constants and use the results of Figs. 5—6 and Tables 7—8, we obtain for the hurricane the constants shown in Table 9.

Table 9.

r km	T_w–T_a °C	q_w—q_a gm/kg	$\bar{v}$ Area-Ave m/sec	A 10^{-12} cm²	K_S 10^7	K_e 10^6	Q_S/Q_e %
90—70	2	5.2	44	100	8.6	1.64	34
70—50	2	4.6	50	76	6.3	1.95	24
50—30	2	3.5	56	50	7.1	2.19	32
Area Ave					7.4	1.92	30

The most interesting result of Table 9 lies in the fact that the coefficients of turbulent exchange differ very little from those for the trades. No special demand is created during transition from trade wind speeds of about 7 mps to hurricane velocities for an increase of the transport efficiency of the energy spectrum near the ground. No impossible or difficult restriction is made when it is postulated that lowering of surface pressures in hurricanes arises mainly through an 'extra' oceanic heat source in a storm's interior.

The actual transports, of course, are very large in the hurricane compared to the trades. Sensible heat pickup is 720 cal/cm²/day, an increase by a factor of 50 over the trades (RIEHL ET AL. 1951); latent heat pickup is 2,420 cal/cm²/day, higher by a factor of 12—13. The difference arises largely through the high wind speed. The fact that the inflowing air is observed to cool by about 2° C before onset of active heating from the ocean, accounts for the larger rise in sensible heat pickup. While $q_w - q_a$ remains about constant, $T_w - T_a$ increases from a mean of about 0.5° C in the trades over the western parts of the ocean during summer to 2° C or more inside hurricanes.

In trade-wind disturbances it has also been noted that Q_S and Q_e are higher than in the undisturbed trades, and that the increase in Q_S is percentually larger (GARSTANG 1958). However, the increase of $T_w - T_a$ in this type of situation must be related to evaporation of falling rain and thunderstorm downdrafts rather than to adiabatic expansion during horizontal motion toward lower pressure. These mechanisms for lowering the air temperature need not be discounted in hurricane circulations, especially in the outskirts at pressures above 1,000 mb. As calculated by RIEHL and MALKUS (1958), re-cycling of air at upper levels to the surface by means of cumulonimbus downdrafts makes an important contribution to the heat budget of the equatorial trough zone, especially to the pickup of sensible heat from the ground. For this region the ratio Q_S/Q_e was found to be 0.4, compared to estimates of 0.05—0.1 for the trades at large, and compared to 0.3 for the hurricane from Tables 4 and 9.

5. Thermal constraints, relative stability, and conditions for extreme storms

The solutions to the dynamic equations for the hurricane inflow layer contain a parameter $C = \frac{-K_F}{\sin\beta\delta z}$, variations in which give rise to an infinite family of logarithmic spiral trajectories for each choice of boundary condition r_0. We saw from Table 1 that when $r_0 = 500$ km, a choice of $C = -4.0 \times 10^{-8}$ cm^{-1} gave a moderate storm with maximum wind of 110 knots, while a choice of $C = -3.2 \times 10^{-8}$ cm^{-1} gave an intense storm with maximum wind of 175 knots.

It is the purpose of this section to suggest that the thermal constraints which, in nature, operate upon the system in addition to the dynamic ones impose a choice between, or a limit upon, the range of dynamically possible trajectories so that most or even all of these may be prevented from occurring in a real situation. We shall show that the thermal constraints operate through the surface pressure gradient along s in the storm core and that the realizable $\frac{\partial p}{\partial s}$ is restricted by the possible heat transfer at the air-sea boundary and by the thermodynamics of the condensation heat release in the vertical.

In Section 4, the pressure reduction following a parcel along an inflow trajectory was related to the sensible heat transfer from the ocean using the first law of thermodynamics (equation 11) in the form that obtains if heat is added at constant temperature. As mentioned, this implies maximum production of kinetic energy through the sensible heat source. When equation (11) is differentiated with respect to time,

$$J\frac{dh_s}{dt} = -\frac{1}{\varrho}\frac{dp}{dt}, \tag{28}$$

where J is the mechanical equivalent of heat. For particles moving horizontally toward the center

$$\frac{1}{\varrho}\frac{dp}{dt} = \frac{v}{\varrho}\frac{\partial p}{\partial s} \tag{29}$$

The well-known kinetic energy equation is obtained by multiplying equation (2) by v,

$$v\frac{dv}{\delta t} = -\frac{v}{\varrho}\frac{\partial p}{\partial s} + \frac{v}{\varrho}\frac{\partial \tau_{sz}}{\partial z} \tag{30}$$

The term $\frac{-v}{\varrho}\frac{\partial p}{\delta s}$ is the production of kinetic energy by pressure forces, and it is now apparent that kinetic energy is produced from the oceanic heat source at a maximum rate during isothermal and horizontal motion.

From equations (17), (28) and (29) the pressure gradient force may be related explicitly to boundary heat transfers,

$$J\frac{dh_s}{dt} = JQ_{SP} = JK_{SP}(T_w - T_a)\,v = -\frac{v}{\varrho}\frac{\partial p}{\partial s},$$

so that

$$-\frac{1}{\varrho}\frac{\partial p}{\partial s} = JK_{SP}\,(T_w - T_a) \qquad (31)$$

The pressure gradient along the trajectory is thus limited by the input rate of sensible heat from sea to air.

A second thermal constraint must be met by the system. Since hydrostatic equilibrium prevails, pressures exerted by and on subcloud air particles must be consistent with the density of the air column above them. If the lapse rate is essentially wet adiabatic, equation (1) relates the surface pressure to the equivalent potential temperature Θ_E of the vertical column. This places a simultaneous constraint upon the total, latent plus sensible, heat addition.

From equation (1)

$$\frac{\partial p}{\partial s} = -\varkappa\frac{\partial \Theta_E}{\partial s} \qquad (32)$$

where $\varkappa = 2.5$ mb/° A.
Furthermore,

$$\frac{d\Theta_E}{dt} = v\frac{\partial \Theta_E}{\partial s} \cong \frac{Q_{SP} + Q_{eP}}{c_p} \qquad (33)$$

Combining (32) and (33) and substituting from (18), we have

$$-\frac{1}{\varrho}\frac{\partial p}{\partial s} = \frac{\varkappa}{v}\frac{1}{\varrho c_p}(Q_{SP} + Q_{eP}) = \frac{\varkappa}{\varrho c_p}[K_{SP}(T_w - T_a) + K_{eP}\,(e_w - e_a)]$$

To be consistent with (31)

$$K_{SP}\,(T_w - T_a) = \frac{\varkappa}{p c_p}\,[K_{SP}\,(T_w - T_a) + K_{eP}\,(e_w - e_a)] \qquad (34)$$

and a relation between sensible and latent heat pick-up is prescribed. With the data of Section 4, $Q_{SP} = {}^1/_3\, Q_{eP}$ from equation (34) for the moderate storm.

Maximum kinetic energy production and relative stability criterion. As shown, the core surface pressure gradient is restricted by thermal processes, sea-air transfer on a turbulent-convective scale and condensation heating on a convective cloud scale. These operate to limit the realizable values of C and thus impose a restriction upon the selection of actual trajectory. The upper limit may be calculated, based on a thermal circulation theory by W. MALKUS and VERONIS (1958). They showed that when several solutions to the equations of motion are possible, that one is selected which maximizes, under the thermodynamic constraints, the kinetic energy production, or strictly, potential energy release minus frictional dissipation of kinetic energy. The theory takes the form of a "relative stability" criterion. It is rigorous if production and dissipation terms, and constraints, can be stated formally in the kinetic energy equation.

If equation (30) is integrated vertically through the inflow layer with the assumptions and methods applied to equation (4)

$$\frac{dK}{dt} = \frac{1}{2}\frac{dv^2}{dt} = -\frac{v}{\varrho}\frac{\partial p}{\partial s} - \frac{K_F}{\delta z}v^3, \qquad (35)$$

where K is kinetic energy per unit mass. Following Malkus and Veronis, we shall substitute the dynamic solution for v as a function of C (equation 9) into (35) and maximize dK/dt as a function of C. The weakness of the approach relative to that of Malkus and Veronis is that we are as yet unable to formulate the constraints rigorously. All dissipation of kinetic energy is incorporated into friction at the boundary in terms of an empirical coefficient K_F. The pressure production term we believe to be limited by boundary transfers and cloud scale releases; clearly these may depend upon the dynamics in a manner as yet unknown. Nevertheless, the results are of interest and point the direction for further investigation.

The maximization of dK/dt as a function of C in equation (35) will be carried out at $r = r_1 = 100$ km, where the core pressure gradients maintain and where the angle β is still assumed constant at β_L. Selection of β at this radius (together with r_0) completely

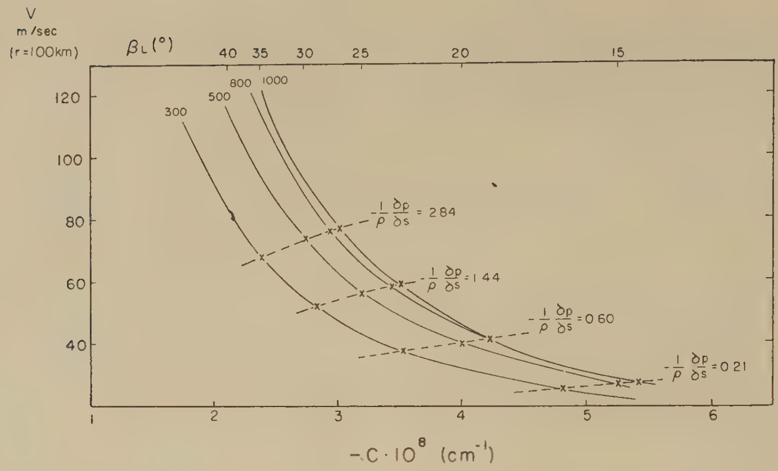

Fig. 7. Graph showing results of trajectory selection by relative stability criterion. Calculation made at $r = 100$ km. Solid lines show relationship between v in m/sec (ordinate) as function of —$C(r)$ (abscissa) when r_0 is chosen as labelled at the left of each solid curve. For a single choice of r_0 these dynamic solutions permit an infinity of v's at 100 km depending on choice of C. The x's show how the relative stability (maximum kinetic energy production) criterion selects only one of these when the core pressure gradient—$\frac{1}{\varrho}\,\partial p/\partial s$ is prescribed. Fixing—$\frac{1}{\varrho}\,\partial p/\partial s$ chooses from each curve only one possible solution, indicated by intersection of dashed and solid lines.

determines the dynamic solution. When $-\frac{1}{\varrho}\frac{\partial p}{\partial s}$ from equation (31) is substituted into (35), the latter equation has the form

$$dK/dt = A\ v_1 - B\,v_1^3$$

where $v = v_1$ at r_1, $A = -\frac{1}{\varrho}\frac{\partial p}{\partial s} = JK_{SP}\ (T_w - T_a)$ and $B = K_F/\delta z$. dK/dt is an implicit function of C through equation (9). Differentiating with respect to v_1 and equating the derivative to zero, we find the value of v_1 which maximizes dK/dt, namely

$$d/dv_1\ (dK/dt) = A - 3Bv_1^2 = 0,$$

and

$$v_{1m} = \sqrt{\frac{A}{3B}} = \sqrt{\frac{JK_{SP}\,(T_w - T_a)}{3K_F/\delta z}} \qquad (36)$$

where v_{1m} is the value of v_1 which maximizes dK/dt. Substitution from equation (9) for v in terms of C permits solution for the maximum constant C_m when $K_{SP}\ (T_w - T_a)$ and the other parameters are prescribed. In general, this leads to a transcendental equation in C_m which had to be solved numerically. The procedure will be illustrated for the case when $r_0 \geq 800$ km so that the exponential term in equation (9) is negligible, with the approximation that $v \sim v_\vartheta$ which for kinetic energy considerations is very nearly true. Then equation (9) becomes

$$v_{1m} = \frac{f}{C_m^2 r_1}\,[1 - C_m r_1]. \qquad (37)$$

Combining (36) and (37)

$$C_m^2 r_1 \sqrt{\frac{JK_{SP}\,(T_w - T_a)}{3K_F/\delta z}} + fC_m r_1 - f = 0 \qquad (38)$$

If we substitute the values of $JK_{SP}\ (T_w - T_a$ calculated from Table 3 for the moderate storm, and also the values of the other parameters assumed for the model, $C_m = -4.35 \times 10^{-8}$ cm^{-1} and $\beta = 18°\ 10'$. Using the exac equation (9), $C_m = -4.0 \times 10^{-8}$ cm^{-1} o $\beta = 20°$ for $r_0 = 500$ km.

Fig. 7 shows the result of the calculation The solid lines denote v as *a* function of C a 100 km for different values of r_0. The x's o these curves were arrived at by the relativ stability criterion using the exact equation (9 and various values of $JK_{SP}\,(T_w - T_a)$. These are entered in terms of $-\frac{1}{\varrho}\frac{\partial p}{\partial s}$ (by 31) in the figure, with dashed lines interpolated to show what points would be chosen on dynamic curves intermediate between those actually drawn. We see that for the intense storm ($r_0 = 500$ km; $C = -3.2 \times 10^{-8}$) $-\frac{1}{\varrho}\frac{\partial p}{\partial s}$ in the core must be about 1.44 cm/sec² or 2.4 times that of the moderate storm, which means that the product $JK_{SP}(T_w - T_a)$ must be 2.4 times greater as well as the sum of $Q_{SP} + Q_{eP}$. We do not yet know whether there is an upper limit upon $T_w - T_a$ and $e_w - e_a$, which for example might be imposed by the dewpoint of the inflowing air.

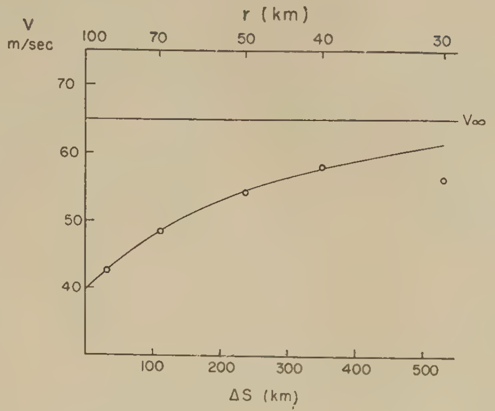

A Moderate

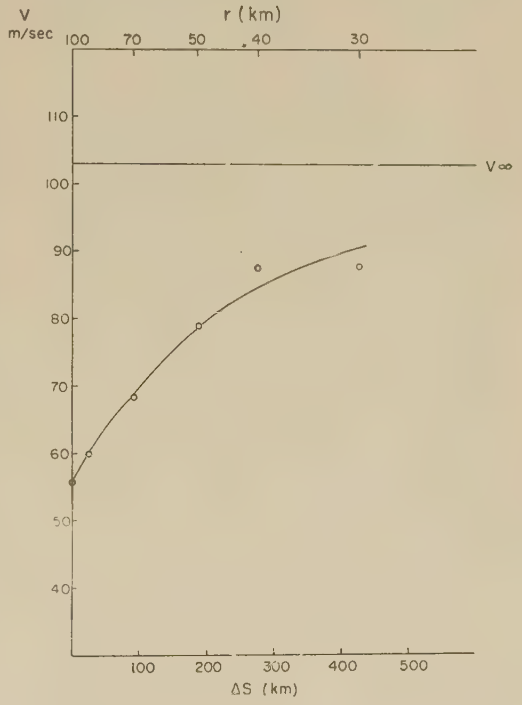

B Intense

Fig. 8. Core velocity (m/sec) as function of r and Δs (distance along trajectory from $r = 100$ km); A for moderate storm, B for intense storm. Solid curves show profile from solution to equation (39) representing maximum kinetic energy production, with $-\frac{1}{\varrho}\,\partial p/\partial s$ chosen as prescribed by Fig. 7. Points are values from dynamic model via equations (9—10).

The criterion of maximum rate of kinetic energy production within the thermal constraints of the system would determine, if we could formulate the latter rigorously, the selection between dynamically possible trajectories. Actually we have said only how the heat must be transferred and released to realize these and must look further into the controls upon convective and turbulent scale processes and their interaction with large-scale dynamics. However, once $\frac{1}{\varrho}\frac{\partial p}{\partial s}$ (core) and r_0 determine β, a relatively simple method for estimating the strongest wind within the core is available from formulation and integration of equation (35) with respect to s, namely

$$\frac{1}{2}\frac{dv^2}{ds} + \frac{K_F}{\delta z}v^2 = -\frac{1}{\varrho}\frac{\partial p}{\partial s} = K_{SP}(T_w - T_a) \quad (39)$$

when dv/dt is written $v\,dv/ds$ and a v is divided out. The solution is

$$v^2 = v_0^2 e^{-\frac{2K_F s}{\delta z}} + \frac{K_{SP}(T_w - T_a)\,\delta z}{K_F}\left(1 - e^{-\frac{2K_F s}{\delta z}}\right) \quad (40)$$

with $v = v_0$ at $s = 0$, which is to be the value of v at $r = 100$ km. Fig. 8 gives the results for the moderate and intense storms. The comparison with the v's (points in Fig. 8) calculated from equation (10) is, as expected from Table 6, excellent except in the inmost regions, showing that the arbitrary linear decrease in sin β with radius in the core is a fair approximation to maximum kinetic energy production

Table 10. Comparison of Moderate, Intense, and Extreme Hurricane.

Storm	β_L (deg)	r_0 (km)	$v_{\max}$ (m/sec)	$\left(-\frac{1}{\varrho}\frac{\partial p}{\partial s}\right)$ core (cm/sec^2)	Ratio core press. grad. to moderate storm	P_c (mb)	Θ_E(max) (°A)
A. Moderate	20	500	60	0.6	1.0	966	362.5
B. Intense	25	500	90	1.44	2.4	910	385
C. Extreme......	25	800	105	2.0	3.4	882	396

at first, but decreases the inflow angle too rapidly near the eye wall.

Equation (40) shows that as s becomes large, the velocity asymptotically approaches a limiting value, called v_∞ in Fig. 8, namely

$$v_\infty = \sqrt{\frac{K_{SP}(T_w - T_a)\,\delta z}{K_F}} \tag{41}$$

which is determined by heat transfer (or core pressure gradient along s) and the ratio of depth of inflow layer to surface friction coefficient only. For the moderate storm, v_∞ has the value 66.5 m/sec and for the intense storm it is 106 m/sec. For the normal range of inflow angles considered, the maximum wind attained just outside the eye wall is about 90 % of v_∞. Therefore if we know the velocity and inflow angle (radial average) at r = 100 km, we can read from Fig. 7 the core value of $-\frac{1}{\varrho}\frac{\partial p}{\partial s} = JK_{SP}(T_w - T_a)$ and estimate the maximum windspeed from the relation

$$v_{\max} = 0.9\sqrt{\frac{K_{SP}(T_w - T_a)\,\delta z}{K_F}} \tag{42}$$

Conditions for extreme storms. We may now inquire into conditions for an extreme storm with maximum winds on the order of 200 knots and central pressures below 900 mb. From equation (42) a core pressure gradient of 2.0 cm/sec^2 (3.4 times that of the moderate storm) produces a maximum wind of about 105 m/sec or 210 knots. Using Fig. 7, such a storm will be obtained with $\beta_L = 25°$, r_0 = 800 km. A dynamic calculation was carried out for this storm, in the same manner as for the previous two. At latitude 20°, a hurricane for which this trajectory is a mean would need a central pressure of 882 mb, about as low as any hurricane or typhoon pressure on record. The requirements of moderate, intense, and extreme storm are compared in Table 10.

To maintain hydrostatically the extreme pressure of 882 mb, the required Θ_E is 396° A from equation (1). Although pressures above 100 mb must be somewhat disturbed by such a deep storm and ascents of this heat content, this would not occur unless $\Theta_E \geq$ 395° A. Ascent with this very high heat content is possible if subcloud air is heated isothermally at T = 28.2° C and the specific humidity is 27 gm/kg (cloud base ~ 100 m). If the sea surface temperature is about 30° C, the same air-sea temperature and vapor pressure differences are obtained as used in Section 4 for the moderate storm. Thus to achieve an extreme storm in the framework of this model, transfer coefficients enhanced by a factor of 3—4 appear to be necessary. This deduction is based on the premises used in deriving equations (31) and (42) and is sensitive to the modelling assumption of a nearly vertical eye wall. Using the eye calculations of MALKUS (1958), we find that a wall cloud slope of about 45° could, under certain conditions, give surface pressures in the inmost rain area in the vicinity of 900 mb, and presumably extreme winds, without appreciably increased transfer coefficients. To date, no such extreme wall cloud slopes have been obtained from the observation sample worked up by the National Hurricane Research Project, which do not, however, include any storms with winds in the neighborhood of 200 knots.

We thus postulate two simultaneous thermal constraints which restrict the solution to the dynamics of the hurricane inflow. The first is set by the air-sea boundary and the sensible heat transfer, the second by the boundary latent heat transfer and the ability of the at-

Table 11. Precipitation and Efficiency of Hurricane Circulations.

Storm	$\overline{R}$ Rainfall 90—30 km cm/day	$\overline{H}$ Latent Heat Release joules/sec 10^{12}	$\overline{GF}$ Ground friction joules/sec 10^{12}	Efficiency $\overline{GF}/\overline{H}$ %	$\overline{PW}$ Pressure-Work joules/sec 10^{12}	Production $\overline{PW}$—$\overline{GF}$ joules/sec 10^{12}
A. Moderate	48	272	3.7	1.4	6.6	2.9
B. Intense	78	443	11.7	2.6	22.8	11.1
C. Extreme......	94.5	535	17.6	3.3	36.2	18.6

— denotes area average between $r = 90$ km and $r = 30$ km.

mosphere to convert the latent to sensible heat by moist adiabatic ascent. During deepening of a storm to moderate intensity our results suggest that the latter restriction is usually the binding one, in that super-normal transfer rates per property difference and wind speed are not required. During deepening to the extreme strength, the model suggests that boundary constraints may become predominant, although lack of critical observational tests of its postulates for these cases leaves this point still open.

In conclusion of this section, we see that higher average inflow angles, or more exactly lower (numerical) values of C, permit more intense storms due to reduction of trajectory distance and thereby of frictional dissipation of kinetic energy. The larger the inflow angle, the closer the velocity profile approaches that of the constant angular momentum vortex which, without friction, would arise from any inflow angle. Very high angles are prevented in real situations due to thermodynamic restrictions on the realizable pressure gradients. When the trajectory distance is reduced, the air cannot pick up and release by condensation enough extra heat energy to achieve the required gradient of Θ_E and thus of surface pressure. In each hurricane situation there is a balance whereby the trajectory adjusts its angle so that just enough heat is supplied and released to maintain the pressure gradients that the resulting dynamic fields require.

6. Rainfall and Kinetic Energy

It is desirable to determine whether the models evolved permit precipitation in the amounts commonly observed in hurricanes, and what the efficiency of the latent heat release must be in this type of thermal engine. We may estimate the area-averaged precipitation in the cores of storms A, B and C, following the method of RIEHL and BYERS (1958). The method consists in determining the difference in moisture import between $r = 90$ km and $r = 30$ km and assuming that this amount of vapor is lifted and condensed; the storm outflow is hypothesized to occur high enough so that 75 % of the converging vapor is precipitated and only 25 % or less is exported in the upper outflow. With these assumptions Table 11 is obtained.

Since the amount of additional water vapor evaporated from the sea surface in this interval is less than 10 % of the difference in horizontal transport, this increment is within the uncertainty of the percentage exported and is, in this calculation, ignored. The maximum possible rainfall is thus nearly 1.5 times that shown in the Table. The small ratio of water vapor increment to transport and release emphasizes the point that it is not the total amount or rate of condensation which is important to storm maintenance, but the heat content or Θ_E at which the release occurs that affects the surface pressure (eq. 1). Thus curiously enough, the oceanic source of water vapor, apparently so vital for the very existence of the storm, makes a negligible contribution to its water budget. Similar comments hold for the oceanic source of sensible heat. In fact, Table 4 showed that the total added heat energy from the ocean is on the order (for the moderate storm) of 2.5 cal/gm, while the average normal heat content (latent plus sensible) of tropical air is about 80 cal/gm.

Determination of the radial velocity from dynamic calculation gives the mass flow as a function of radius for any chosen depth of the inflow layer. The latter is assumed here to extend over a pressure depth of 100 mb, a low estimate. In actual cases, some inflow has been observed to occur as high as the middle troposphere. Mixing ratios are obtained from the data of Section 4. The first column of Table 11 shows a rainfall of 48 cm/day inside the 90-km radius for the moderate storm, which agrees favorably with the average of 33.7 cm/day in the inner 1°-latitude (111 km) radius quoted by RIEHL (1954), where the same inflow depth was used, and with the order of magnitude of precipitation observed in hurricanes. The second column in the table labelled "Latent Heat Release" is computed directly from the amount of precipitation.

We may inquire about the relative magnitude of the latent heat release compared to the frictional kinetic energy dissipation in the core to estimate the storm's "efficiency" as defined by RIEHL and BYERS, DEFANT (1958), and others.

The dissipation of kinetic energy by ground friction ($\overline{GF}$) may be obtained from the expression

$$\overline{GF} = -K_F \varrho_0 \overline{v_0^3} A,$$

where $A = 2.26 \times 10^{14}$ cm^2 is the area between $r = 90$ km and $r = 30$ km, and $\overline{v_0^3}$ is the area average of the cube of the wind speed. Alternately, $\overline{GF}$ may be computed from equation (35) by multiplying $\overline{v_0^3}$ therein by the mass in the core. The results for $\overline{GF}$ and the efficiency of the circulation defined here as $\overline{GF}/\overline{H}$ are shown in Table 11. It is interesting to note that the more intense storms require a more efficient release of latent heat, due to the increase of $\overline{GF}$ with the cube of v, while the moisture convergence increases approximately as v.

The last two columns in Table 11 give the area-averaged pressure work, and the difference between kinetic energy production and dissipation by ground friction for the inflow layer. These columns were obtained from equation (35) taking area-averages of v and v^3 and multiplying by the mass. It is seen that the production rate is roughly twice the dissipation rate forall three storms. Since steady-state hurricanes are considered, the dissipation of kinetic energy by internal friction ($\overline{IF}$) may at least equal the boundary dissipation. Normally the wind speed is much higher in the inflow layer at $r = 90$ km than in the high-tropospheric outflow layer, so that kinetic energy is imported from the outer regions of a hurricane toward the core. This implies that internal may exceed the boundary dissipation. Thus our definition of efficiency in Table 11 may not correspond to the more rigorous one of DEFANT (1958) which takes the ratio of the irreversible part of the work done to the heat release. We do not know how much kinetic energy export by eddies, if any, should be subtracted from the pressure work term and thus cannot prescribe the sum $\overline{GF} + \overline{IF}$ with certainty. The upper limit efficiency ($\overline{PW}/\overline{H}$), however, is about twice the percentages shown in Table 11. A more complete kinetic energy budget for the moderate storm is computed in the following.

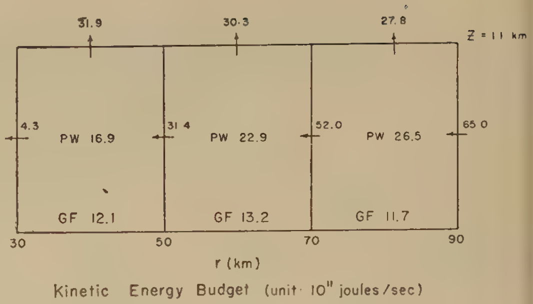

Fig. 9. Kinetic energy budget of inflow layer for moderate storm computed by same radial intervals as Figs. 5 and 6. Unit 10^{11} joules/sec. The term PW denotes work done by pressure forces, GF dissipation of kinetic energy by ground friction. The terms with arrows indicate lateral and vertical transports.

The kinetic energy budget for the core region of the moderate storm is shown in Fig. 9, broken down into the same intervals as the heat and moisture budget was in Section 4. The horizontal imports and exports through vertical walls were calculated by multiplying the kinetic energy per unit mass, $v^2/2$, with the radial mass flow. Similarly, the flux through the top of the layer was determined by multiplying the area average of $v^2/2$ for each increment of 20 km in radius with the vertical mass flow for each of the three areas. The boundary dissipation GF was calculated as residual; total GF coincides with that of Table 11. This agreement supports the calculations of Table 11 materially, because an arbitrary coefficient K_F need not be assumed for Fig. 9.

It is seen that the pressure work PW exceeds GF in each interval but by decreasing amounts as the center is approached. Total production for the whole area is 66.3 units, almost the same as the import through the outer boundary. Thus a major fraction of the kinetic energy of a hurricane is produced outside its core (cf. also PALMÉN and RIEHL 1957).

It would, however, be misleading to deduce that the core is maintained chiefly by importation of kinetic energy produced in the outskirts. To illustrate this, the budget of Fig. 9 may be recomputed equating $GF=PW$ in the intervals 90—70 km and 70—50 km. Given the requirement that the vertical export be at the value of $\overline{v^2}$, we have a wind speed of only 34 m/sec at $r = 50$ km, and a minimal strength hurricane with a maximum wind of 42 m/sec at $r = 70$ km. Further, as shown by RIEHL and GENTRY (1958), non-hurricane tropical storms may possess total kinetic energies comparable to that of small hurricanes, with maximum winds at a great distance (about 150 n.mi.) from the center. What these storms apparently do not possess is the core production necessary to accelerate the small amount of mass penetrating to the center to high speeds. Therefore, an essential ingredient determining the difference between tropical storm and hurricane appears to be the core production which in turn depends on the extra oceanic heat source and the release of the latent heat at high Θ_E.

The kinetic energy transported through the top of the inflow layer in Fig. 9 will in small measure be exported by the outflow; the latter may also move slightly toward higher pressure above the huricane core. However, the bulk of the kinetic energy is likely to be dissipated by internal friction over the depth of the troposphere.

7. Concluding Remarks

Some aspects of the model proposed here have been subjected to observational test, using data from flights of the National Hurricane Research Project. In particular, it was desired to learn how closely realized was the hierarchy of wet adiabatic ascents postulated to maintain surface pressure gradients. Hydrostatic calculations were undertaken for the rather complete set of flights into hurricane DAISY (1958); while temperatures 1—3° colder than wet adiabatic ascent of surface air were common in the mid-tropospheric levels of the core, the high levels of the storm were found to be filled with air of the required Θ_E. Since the hydrostatic calculations demonstrated that about 75 % of the surface pressure lowering is achieved by warming above 500 mb, the mid-tropospheric low temperatures have a negligibly small effect on the mass distribution. These temperature deficiencies suggest, however, that the moist adiabatic ascent does not take place by means of uniform and gradual ascent of the whole mass in the hurricane but, that as postulated by RIEHL and MALKUS (1958) for the equatorial trough zone, it is largely concentrated in regions of rapidly ascending buoyant hot towers. This subject is being developed further in current studies, which also include heat, mass and energy budgets for observed hurricanes to be used in comparison with the present results.

Acknowledgements

The writers gratefully acknowledge the support and cooperation by the National Hurricane Research Project of the United States Weather Bureau and its staff at every stage of the present work. Without the body of knowledge and trained personnel developed by this group, attempts to test analyses such as the present one with observations would be impossible. The former Director of the Project, Mr. R. H. Simpson, has generously contributed his support and extensive experience in hurricane studies throughout the investigation.

This research was supported by contracts of the Office of Naval Research and the United States Weather Bureau with the Woods Hole Oceanographic Institution and the University of Chicago.

REFERENCES

BYERS, H. R., 1944: General Meteorology. *McGraw-Hill Book Co.*, New York. 2nd Ed. p. 645.

BUNKER, A. F., 1959: Latent and sensible heat flows in air flowing southward over the Western North Atlantic. *Unpublished manuscript submitted to J. Meteor.* Contribution No. 1031 from the Woods Hole Oceanographic Institution.

DEFANT, A., and F., 1958: Physikalische Dynamik der Atmosphare. *Akademische Verlagsgesellschaft M. B. H.*, Frankfurt Am Main. P. 527.

GARSTANG, M., 1958: Some meteorological aspects of the low-latitude tropical Western Atlantic. Results of *Crawford* cruise No. 15. Unpublished manuscript. Woods Hole Oceanographic Institution. Ref. No. 58—42.

HAURWITZ, B., 1935: The height of tropical cyclones and of the 'eye' of the storm. *Mon. Wea. Rev.*, Wash., **63**, pp. 45—49.

HUGHES, L. A., 1952: On the low-level wind structure of tropical storms. *J. Meteor.*, **9**, pp. 422—428.

JACOBS, W. C., 1942: On the energy exchange between sea and atmosphere. *J. Mar. Res.*, **5**, pp. 37—66.

JORDAN, C. L., 1957: A mean atmosphere for the West Indies area. *National Hurricane Research Project, Rep. No.* **6**, Washington, D. C., p. 17.

MALKUS, J. S., 1956: On the maintenance of the trade winds. *Tellus*, **8**, pp. 335—350.

— 1958: On the structure and maintenance of the mature hurricane eye. *J. Meteor.*, **15**, pp. 337—349.

MALKUS, W. V. R., and VERONIS, G., 1958: Finite Amplitude Cellular Convection. *J. Fluid Mech.*, **4**, p. 2.

MAYNARD, R. H., 1945: Radar and weather. *J. Meteor.*, **2**, pp. 214—226.

MONTGOMERY, R. B., 1948: Vertical eddy flux of heat in the atmosphere. *J. Meteor.*, **5**, pp. 265—274.

PALMÉN, E., and RIEHL, H., 1957: Budget of angular momentum and energy in tropical cyclones. *J. Meteor.*, **14**, pp. 150—159.

RIEHL, H., 1954: Tropical Meteorology. *McGraw-Hill Book Co.* New York. p. 392.

RIEHL, H., and BYERS, H. R., 1958: Flood rains in the Bocono Basin, Venezuela. *Rep. prepared for R. J. Tipton Assoc. Engineers. On file Univ. of Chicago*, p. 57.

RIEHL, H., and FULTZ, D., 1957: Jet streams and long waves in a steady rotating dishpan experiment: Structure of Circulation. *Q. J. Roy. Met. Soc.*, **83**, pp. 215—231.

RIEHL, H., and GENTRY, R. C., 1958: Analysis of tropical storm Frieda, 1957. A preliminary report. *National Hurricane Research Project, Rep. No.* **17**, Washington, D. C., p. 16.

RIEHL, H., YEH, T. C., MALKUS, J. S., and LA SEUR, N. E., 1951: The Northeast trade of the Pacific Ocean. *Q. J. Roy. Met. Soc.*, **77**, pp. 598—626.

SIMPSON, R. H., and RIEHL, H., 1958: Mid-tropospheric ventilation as a constraint on hurricane development and maintenance. Proc. Technical Conf. on Hurricanes, *Am. Met. Soc.*, D41—10.

WEXLER, H., 1947: Structure of hurricanes as determined by radar. *Am. N. Y. Acad. Sci.*, **48**, pp. 821—844.

PRINTED IN SWEDEN
ESSELTE, STHLM 60

Contribution No. 1040

Made in United States of America
Reprinted from Journal of Mammalogy
Vol. 41, No. 2, May 20, 1960
pp. 279–281

DAILY PATROL OF A *MEGAPTERA*

The long-distance migrations of whales have commanded some attention, though by no means enough. One hears less, however, of the smaller-scale circulations of cetaceans. A paper by Caldwell (Jour. Mamm., 36: 304–305, 1955) reports sighting the same *Tursiops truncatus* three times at intervals of 84 and 55 days in an area of about 0.12 square sea mile.

We have to report the daily patrolling of a somewhat larger beat by a single humpback whale, *Megaptera novaeangliae,* which repeatedly traversed an area of about 20 square sea miles (4x5).

Over ten days (29 October through 7 November 1958) we observed a large *Megaptera,* recognized as the same one, in about the same near-shore area, and on six of these days at about the same time of day. This was near Fletchers Neck, which is about 10 sea miles southwest of Cape Elizabeth, near Portland, Maine.

Megaptera novaeangliae is a species in which minor individual variations are often sufficiently conspicuous and distinctive to enable even a shipboard observer to recognize individual whales out of small groups. Of the four *Megaptera* that we saw during these days, our subject was readily distinguishable by its larger size, by the shape of the dorsal fin or hump (especially variable in this species), and by the distinctive color pattern of the underside of the flukes (markedly unlike any of the others with it). The characteristic serrated trailing edge of the flukes was conspicuous; the dorsal fin was often seen to wobble in the wind, or as waves slapped it. Both sides of the flippers were white, as usual in the western North Atlantic. The rest of the whale's upper surface was a very dark gray, nearly black, with lighter scratches and grayer patches. This animal was about 14 m. long with 4.5-m. fluke span (estimated by comparison with our 12-m. boat). We observed and photographed it from the boat and from the air; it was not at all shy and often came near the boat, frequently surfacing within 5 m. It breached occasionally, but luckily at some-

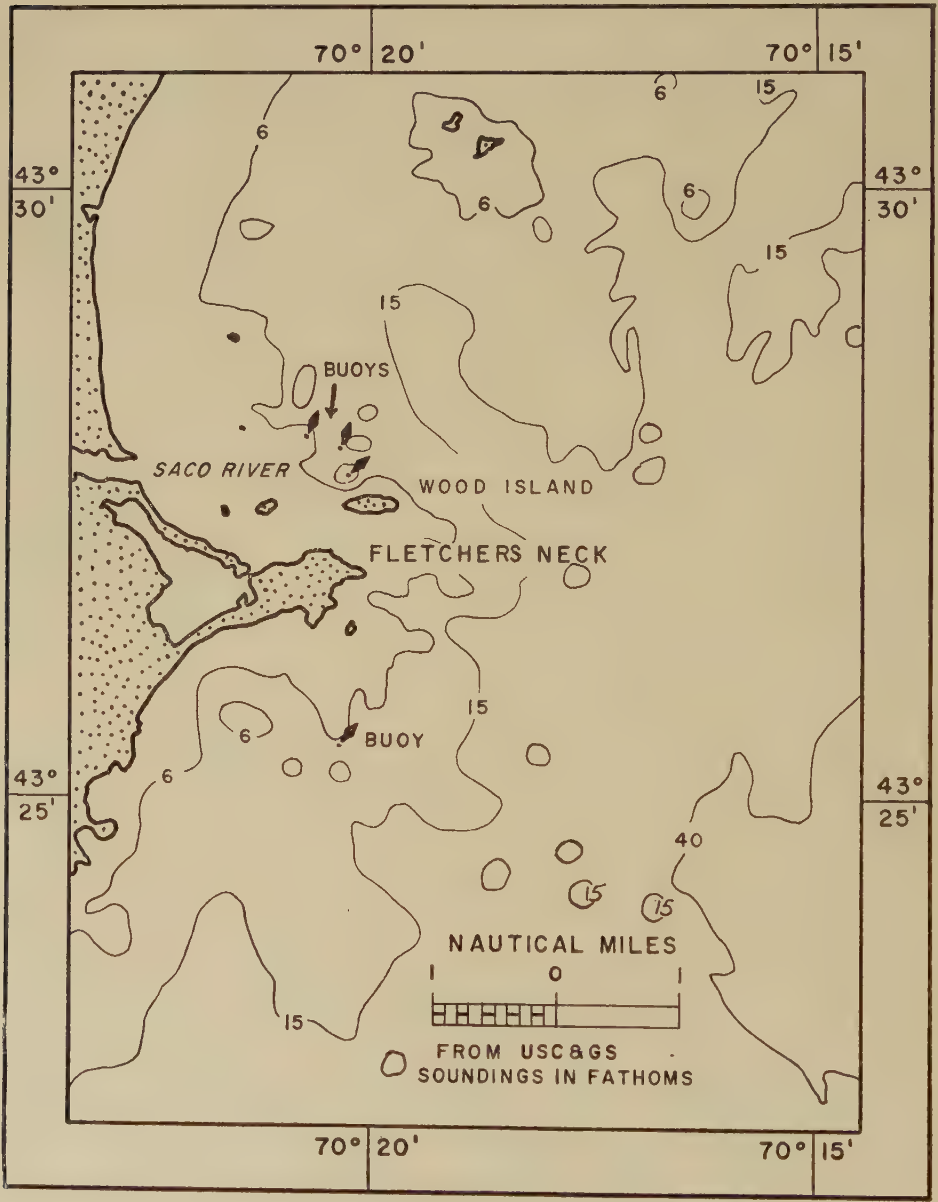
70° 20'
70° 15'
43° 30'
43° 25'
6
15
40
BUOYS
SACO RIVER
WOOD ISLAND
FLETCHERS NECK
BUOY
NAUTICAL MILES
1 0 1
FROM USC&GS
SOUNDINGS IN FATHOMS

FIG. 1.—Chart of the area frequented by a humpback whale.

what greater distances. It also lobtailed briefly and spectacularly three times, and sometimes raised its head well out of water. It was by itself almost all the time we saw it. The long dives (after fluking) were usually not longer than 3 minutes. Several times the flukes were noted to be at "hard dive" just before disappearing. The whale's breath was very fetid, as we have now and again noticed with this species. We supposed, but without direct evidence, that it was feeding; its track was very erratic in detail while making good a general northwesterly course.

Unfortunately the water was turbid, so that even from the air it was usually not easy to spot the whale more than about a fathom under water. Robert G. Weeks watched a pair of these *Megaptera* from the air on 30 October: one fluked and went down out of sight; the other passed the diving point, turned down through 90° and hung head down with flukes awash and the white belly showing; the position or activity of the flipper was not noted, because of the turbidity of the water.

The earliest we ever saw our whale was 0930, but usually the first contact was near 1300 to 1400. We ordinarily met it about 4 sea miles southeasterly of Fletchers Neck, in about 15 to 40 fathoms; it then continued to the northwestward until the water depth decreased to about 6 fathoms or a little less, when it would turn back to sea, sometimes skirting the reefs a while first (Fig. 1). On two occasions it came in to the buoy south of Fletchers Neck and then turned right and coasted along near the 8-fathom line until it was near Wood Island, when it turned back offshore, to the southeast. Another time it continued on around to the north of Wood Island, past the entrance buoys for Saco River. We never traced it much later than 1600, since the early darkness obliged us to head for our harbor nearly 10 miles away as soon after 1530 as possible. Our small vessel was weatherbound on four days, but on two of these we managed to spot our whale from Fletchers Neck as it came in between us and the offing of Wood Island, right on schedule.

Of these ten days, we saw the *Megaptera* on seven; on two of the unproductive days we were weatherbound, and on the other we found no sign of *Megaptera* in the area, only a 60-foot *Balaenoptera physalus* (finback); this was the only day we saw one of these. On six of the *Megaptera* days, we found the whale in about the same place in the early afternoon; on the other we had it from 0930 to about 1100. To sum up, the same whale swam through the same area at the same time on 29 and 30 October and on 2, 4, 6 and 7 November. We were struck by the persistence of this routine and its consistency with the clock. Had the whale kept a constant relation to the tides which one might suppose would influence its prey, it would be easier to explain; but had this been the case, by 7 November the whale should have been about seven hours later than on 29 October. We regret that we were not able to outstay the whale in this vicinity.

During January 1954 the senior author noted that *Tursiops truncatus* (bottle-nosed porpoise) followed a tidal routine at St. Augustine, Florida. At low water slack, the bay teemed with porpoises; as the tide rose, they went up the rivers and creeks with it, so that at high water slack scarcely a porpoise was left in the bay, but by low tide they had come back and occupied the bay again. This routine was independent of the clock and was presumably largely a response to the tidal movement of prey. We do not know whether our Fletchers Neck *Megaptera* was feeding but, whatever it was doing, it evidently followed the sun and not the moon.—WILLIAM E. SCHEVILL AND RICHARD H. BACKUS, *Woods Hole Oceanographic Institution, Woods Hole, Massachusetts.* *Received 1 May 1959.*

[Contribution 1040 from the Woods Hole Oceanographic Institution.]

Contribution No. 1042

Deep-Sea Research, 1960, Vol. 6, pp. 351 to 367. Pergamon Press Ltd., London. Printed in Great Britain

The annual cycle of primary production in the Sargasso Sea off Bermuda

D. W. MENZEL and J. H. RYTHER

(*Received* 22 *June*, 1959)

Abstract—Gross and net primary production have been measured at bi-weekly intervals for 18 months in the North-western Sargasso Sea 15 miles SE. of Bermuda in 1500 fm of water. Ancillary data include temperature, salinity, phosphate, nitrite, nitrate, disolved oxygen, plant pigments, light penetration and incident radiation.

A seasonal cycle of production was observed with high levels in the winter and early spring, low levels in the later spring, summer and early fall. Gross production ranged from 0·13 to 2·00, averaging 0·44 g carbon assimilated/m^2/day or 160 g C/m^2/year. Net production ranged from 0·05 to 0·83 and averaged 0·20 g C/m^2/day or 72 g C/m^2/year.

Production was closely dependent upon vertical mixing, high levels occurring when the water was isothermal and mixed to or near the depth of the permanent thermocline (400 m), low levels being associated with the presence of a seasonal thermocline in the upper 100 m. Nutrient concentrations were extremely low (maxima of 1·8 μgAN/L and 0·16 μg AP/L as inorganic compounds in the upper 100 m) and showed little seasonal variability. Mixing and enrichment from the permanent thermocline is negligible, production being largely dependent upon the rapid re-cycling of nutrients within the upper 400 m.

The environmental factors controlling production which make this region differ from temperate or boreal waters, and which permit high production throughout the winter are: (1) low nutrient concentrations, (2) clear water, (3) relatively high incident radiation in winter, (4) a shallow winter mixed layer and (5) a rapid re-cycling of nutrients, possibly due to higher temperatures.

INTRODUCTION

IN THE fall of 1957 a study was initiated of the plankton biology and the related chemistry and hydrography at a single, fixed position in the North-western Sargasso Sea. This programme has been carried out from the Bermuda Biological Station, employing that Institution's research vessel *Panulirus*. The oceanographic station (referred to henceforth as Station ' S ') is located 15 miles SE. of Bermuda (32°N, 65°W) in 1500 fm of water where conditions appear to be typical of the North-western Sargasso Sea; there have been no indications of island effects since the programme was started. The same position has been occupied since 1954 for the purpose of making routine standard hydrographic observations under a joint arrangement with the Woods Hole Oceanographic Institution. The biological programme may be considered as an adjunct to the continuing hydrographic studies.

The location of a truly oceanic station just 15 miles from land presents obvious advantages and unique features, since it may be occupied at frequent intervals throughout the year with a minimum expenditure of time and funds. Thus the study of annual cycles, seasonal and yearly variations, etc., of various oceanographic phenomena, never before possible, may be routinely undertaken. The present report will describe one aspect of the current programme, the seasonal cycle of primary production, as followed over a period of 18 months.

The annual rate of primary production in the open ocean has been a warmly debated subject in recent years. This has resulted primarily from the large discrepancy between the values reported for the Sargasso Sea by RILEY *et al.* (1949) and STEEMANN NIELSEN (1952). There have been various conflicting explanations for this lack of agreement (STEEMANN NIELSEN, 1952, 1954; RILEY, 1953; RYTHER, 1954, 1956a, 1956b) which have done little more than confuse the issue. More recently RILEY (1957) has attempted to resolve the problem by making new estimates for the same region by means independent of either of the earlier investigations. The three separate studies are summarized in Table 1 showing the methods employed and the results obtained in each case.

Table 1. *Summary of data for average daily gross primary production in the Sargasso Sea,* 1949–1957

Reference	*Method*	gC/m²/*day*
RILEY *et al.* (1949)	(oxygen change, light and dark bottles)	0·46
STEEMANN NEILSEN (1952)	C^{14}	0·05
RILEY (1957)	*in situ* 0_2 changes	0·27

RILEY's latest figures were based upon *in situ* oxygen changes in the upper 300 m of water as estimated from physical oceanographic calculations of oxygen production and consumption. The present authors offer no criticism of this method, which has many advantages over the available experimental techniques. However, his oxygen data were obtained from four *Atlantis* cruises between 1932 and 1949, while his mixing coefficients were based on bathythermograph records taken in 1950-1952 by Weather Ship personnel at Station E. Hence, the resulting values of primary production can be no more than rough approximations. Furthermore, though data were obtained for more different times of the year than previously available, giving indications of considerable variability, no true picture of the seasonal cycle could yet be obtained.

It was obviously worthwhile, therefore, to undertake the study of primary oceanic production at the semi-tropical latitude of Bermuda on a seasonal and year-to-year basis. The objectives of this study were (1) to establish the annual rate of primary production, (2) to determine whether or not there is a well defined seasonal cycle similar to that observed in temperate and northern waters, (3) to study variations from year to year in the magnitude of production and characteristics of the annual cycle and (4) to study the chemical and physical factors which control and limit production in these waters.

METHODS

In the 18 month period between November, 1957 and April, 1959 Station S was occupied on more than 55 occasions for an average of better than three times per month. Although all operations were not carried out each time the station was occupied, a total of 34 complete hydrographic stations and 48 productivity measurements (each usually by two independent methods) were completed.

At each hydrographic station, measurements were made to an indicated depth of 2600 m of temperature, salinity, inorganic phosphorus, total phosphorus, nitrite, nitrate, silicate, and dissolved oxygen*. Two- to four-litre water samples were collected from five depths to 100 m for the analysis of plankton pigments by the method of RICHARDS with THOMPSON (1952) as modified by CREITZ and RICHARDS (1955). These samples were collected in two-litre, non-metallic samplers of the type described by VAN DORN (1956). In addition, a transparent and opaque 150 ml glass stoppered bottle was filled from each of these samples. To these bottles were added approximately 20 μ curies of $CO_3^{=}$. This was prepared essentially as described by STEEMANN NIELSEN (1952). For the first part of the study (November, 1957–April, 1958) the bottles were fastened to the hydrographic wire and lowered to the depths from which the samples were taken (usually 0, 10, 25, 50 and 100 m), where they were held for half the daylight portion of a day (i.e. noon to sunset). After April, the samples were collected from the respective depths to which 100 per cent, 50 per cent, 25 per cent, 10 per cent and 1 per cent of the surface light penetrated. The samples were then dispensed into bottles and C^{14} added as before, and the bottles were placed in a box cooled with running surface water and covered with a series of Kodak Wratten neutral density filters which transmitted the same fraction of the incident radiation as that to which the contained organisms had been exposed *in situ*. The samples were held in the filter box for 24 hrs. After exposure (by both the above mentioned methods) the contents of the bottles were filtered through HA millipore filters (pore size 0·5 μ), the filters were rinsed with 10 ml of 0·001 N HCl in a 3 per cent NaCl solution, dried in a desiccator for at least 24 hrs, and counted in a gas flow Geiger counter. The activity of the filtered material from the dark bottles was subtracted from that of the corresponding transparent bottles, and the net activity was used to calculate productivity by the method described by STEEMANN NIELSEN (1952) but with no correction for respiration. The resulting value is interpreted as net daily production (RYTHER, 1956b; STEEMANN NIELSEN and HANSEN, 1959).

The light penetration of the water was determined for each station with a Secchi disc and the extinction coefficient per metre was calculated according to the formula of POOLE and ATKINS (1929). This was checked periodically with a submarine photometer. Total incident radiation was recorded on shore in Bermuda with an Eppley 10 junction pyrheliometer. From the chlorophyll *a* concentration at the depths of penetration of 100 per cent, 50 per cent, 25 per cent, 10 per cent and 1 per cent of the surface light and the total daily incident radiation, daily gross production at each of these depths, was calculated by the method of RYTHER and YENTSCH (1957). Since pyrheliometer records were not available for the entire period, radiation values for this study were estimated from KIMBALL's (1928) tables.

The daily rates of net (C^{14} method) and gross (chlorophyll-light method) production for each of the five above mentioned depths was then plotted on graph paper as a function of depth and the areas of the two resulting curves were measured with a planimeter giving daily net and gross production beneath a square metre of surface. A sample graph showing these plots is given in Fig. 1.

---

*Salinity (Knudson method) and total phosphorus (Harvey method as modified by KETCHUM *et al.*, 1955) were determined at the Woods Hole Oceanographic Institution. All other analyses were completed by the senior author at the Bermuda Biological Station by the following methods : phosphate (MURPHY and RILEY, 1958), nitrite and nitrate (MULLIN and RILEY, 1955a), silicate (MULLIN and RILEY, 1955b) and oxygen (WINKLER method).

The accuracy of the 'chlorophyll-light' method in estimating gross primary production in continental shelf waters has been studied and is discussed by RYTHER and YENTSCH (1958). The method has not been similarly evaluated for the semi-tropical Sargasso Sea, and there appears to be no satisfactory way of doing so. It is based upon the following assumptions : (1) a constant assimilation number (photosynthesis per unit of chlorophyll at optimal light intensity), and (2) a constant and predictable relationship between photosynthesis at optimal light intensity and at any other naturally occurring intensity. The latter relationship which is used in the formulation of the method has, in fact, been found not to describe accurately the photosynthesis-light intensity curve of the Sargasso Sea plankton, in that it fails to account for light adaptation by the organisms (RYTHER and MENZEL, in press). On this account alone the resulting values are probably somewhat too low.

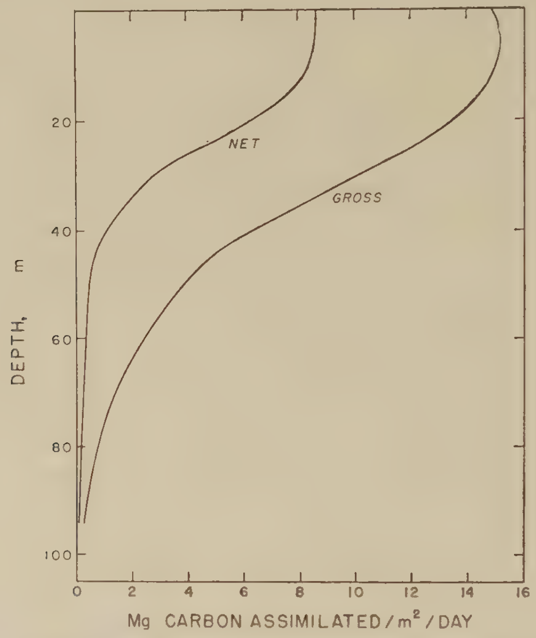

FIG. 1. Daily net and gross photosynthesis on January 30, 1959.

The assimilation number cannot be checked without an independent method of measuring total photosynthesis. C^{14} uptake (net photosynthesis) does not bear a constant relationship to total photosynthesis and hence cannot be used for this purpose. In relatively rich coastal waters the 'light and dark bottle' oxygen method may be used, but it is too insensitive for the oligotrophic Sargasso Sea. Therefore the assimilation number must be assumed to be the same as that of the continental shelf plankton. This assumption is partly justified by the fact that Sargasso Sea phytoplankton populations are qualitatively and quantitatively similar to those of the off-shore continental shelf waters.

HYDROGRAPHY

The Sargasso Sea may be thought of as a lens of homogeneous water characterized by a salinity of almost exactly 36·50‰ and a temperature within a few tenths of a degree of 18 °C. This lens tapers upward from a thickness of almost 500 m in the central Sargasso Sea to become nearly extinguished at its boundaries. In the vicinity of Bermuda it extends to a depth of some 400 m. Below this lens lies the permanent thermocline. Above it a seasonal thermocline extends to a depth of 100-150 m. At the latitudes of Bermuda and above, the seasonal thermocline may be destroyed in winter, the 18° water extending all the way to the surface. South of Bermuda, with less surface cooling, the upper thermocline persists throughout the year and merges more gradually with the 18° water below.

Two publications have recently appeared concerning this interesting ' 18° water.' The first by SCHROEDER *et al.* (1959) describes the remarkable climatic stability of this layer which, though seasonally in contact with the surface, has apparently retained its T-S characteristics for at least the 85 years for which records are available. The second, by WORTHINGTON (1959) is concerned with the geographical distribution of this water mass and, particularly, its seasonal formation at the surface at and North, of the latitude of Bermuda and its subsequent intrusion southward beneath the permanently stratified surface waters. Despite the mysterious retention of its temperature and salinity characteristics, the seasonal changes of the oxygen concentration of this water indicate that it is annually renewed, and this applies as well to the 18° water south of Bermuda where the surface waters never approach this temperature.

We are concerned here principally with hydrographic features around Bermuda and their relationship to primary production. Since our interests centre around the upper few hundred metres, the 18° water and its seasonal cycle of stabilization and overturn are especially pertinent. The paper by SCHROEDER *et al.* is based upon the hydrographic observations at Station S since 1954; hence we need not reproduce the record prior to 1957 here. However, their published data stop with June, 1958, and thus include only half the period in which we are interested. Therefore the temperature and salinity records to a depth of 900 m are presented here for the period November, 1957 through April, 1959 (Fig. 2).

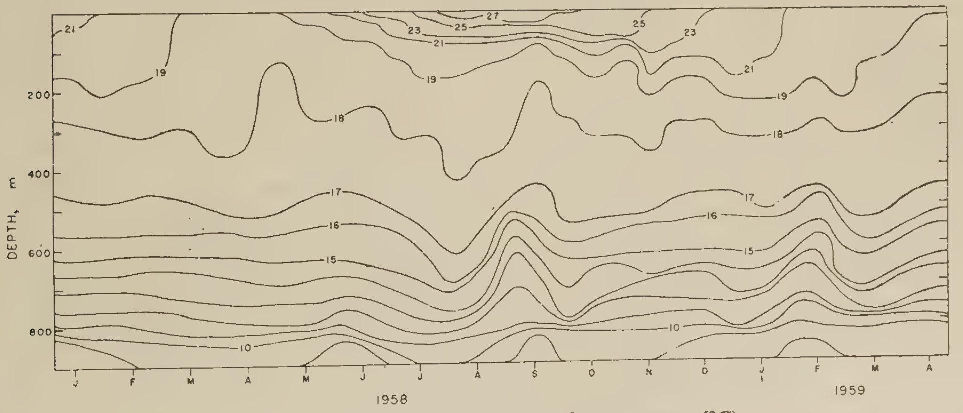

FIG. 2. The seasonal depth profile of temperature (°C).

The temperature record shows that the water was isothermal within a few tenths of 18° from the surface to almost 400 m from mid-February to mid-April, 1958. By April, the seasonal thermocline formed and was strongly developed throughout the summer and early fall, extending some 50-100 m in depth. By mid-September, surface mixing and cooling became apparent, the mixed surface layer increasing in depth to about 200 m as the surface temperature dropped from 23° in November, to 19° in February, 1959. However, the surface water never cooled to 18° in 1959 and hence the water column did not become mixed to the depth of the permanent thermocline, as in 1958. The greater cooling and mixing in the early spring of 1958 may have been related to abnormally low air temperatures that year (Table 2). An examination of the thermal structure of the upper water since 1954 (Schroeder *et al.* 1959) reveals that 18° surface temperatures occur sporadically and probably not too frequently at the latitude of Bermuda. This hydrographic feature is believed to play an important part in the seasonal cycle of primary production and will be discussed later.

Table 2. Mean monthly air temperature at St. Georges, Bermuda, January–March

Month	1958	1959	*Mean* 1954–1959
January	64·0	64·0	64·3
February	61·6	65·0	64·0
March	63·8	66·5	66·7

As described above, the 18° water is further characterized by a salinity of 36·50‰ and water of nearly this salinity thus occurs over most of the upper 400 m. However, at the very surface during that part of the year when the seasonal thermocline is present, the salinity is irregular and less predictable, but consistently lower than 36·50‰. This relatively fresher layer may be as much as 100 m in depth and at times (i.e. July and October, 1958) the surface salinity may drop to as low as 36·00‰ (Fig. 3). It is not inconceivable that this freshening may result from rainfall, for a total of 10-20 inches would dilute 100 m of water to the extent observed. W. H. Sutcliffe (personal communication) has found a rather close inverse correlation between rainfall and the mean salinity of the upper 100 m. The mean annual rainfall

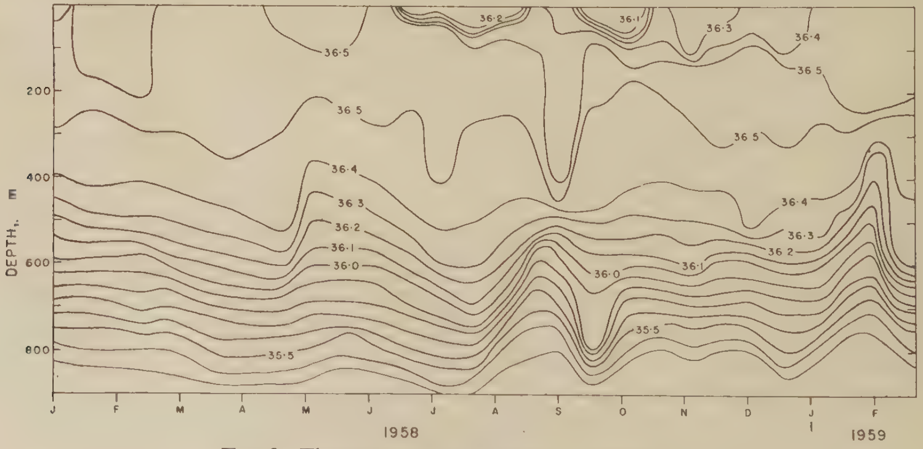

Fig. 3. The seasonal depth profile of salinity (‰).

at Bermuda is approximately 60 inches, and 5-10 inches per month is not uncommon. This does not take evaporation into consideration, which might be expected to exceed precipitation in the summer months, though ISELIN (1936) suggests that the higher summer humidity may actually retard the process. However, the explanation is almost incompatable with the observed constancy of the salinity of the 18° water. It is difficult to imagine this water warming and freshening simultaneously at the surface, but how or why it should return to exactly the same salinity when it cools to 18° is inconceivable.

The only other possible explanation for this freshwater surface layer is that it represents an intrusion of another water mass, presumably from the Gulf Stream. This has been seriously suggested but also presents difficulties. For one thing, there are no changes in other properties (temperature, chemical nutrients, etc.) accompanying the occurrences of low salinity surface water which one might expect with a different water mass. Furthermore, this phenomenon appears to be so widespread over much of the Western Sargasso Sea and such a regular feature throughout most of the late summer (ISELIN, 1936; FUGLISTER, 1947; SCHROEDER *et al.* 1959) that it is difficult to conceive of eddies or outflows of Gulf Stream water of such magnitude, persistence and regularity. Intriguing as this problem is, it need not concern us here, for the low salinity surface water appears to have no direct effect on the plankton biology of the region beyond contributing to the stability of the surface layer.

NUTRIENT CHEMISTRY

The seasonal cycle of the plant nutrients which have been studied (phosphate, nitrite, nitrate and silicate) may be treated rather briefly. Their concentrations in the euphotic zone, and even in the mixed layer in winter, are low and do not show the seasonal variations found in temperate and northern waters. The indications are that (1) the supply of these nutrients to the euphotic zone is severely limited and (2) they are utilized by the phytoplankton almost as quickly as they are made available. Consequently their concentrations at any one time give only a very rough picture of their availability and rates of utilization by the plants.

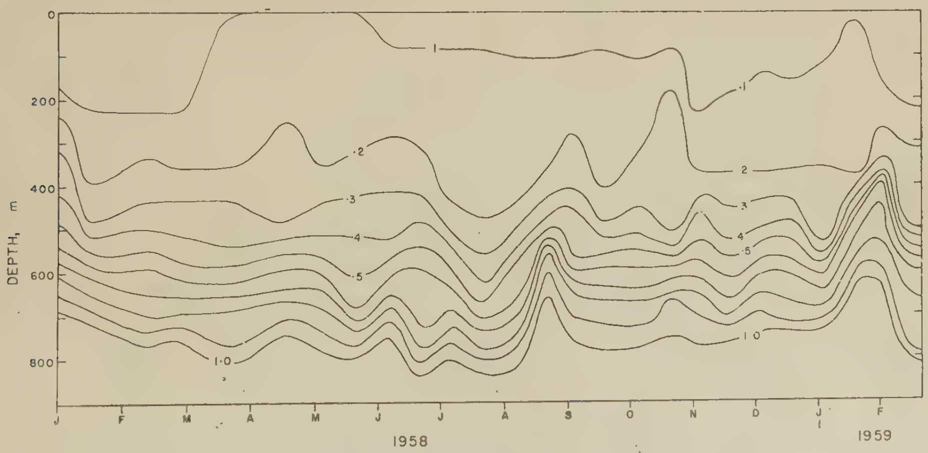

FIG. 4. The seasonal depth profile of a phosphate-phosphorus (μg A/L).

Figs. 4-6 show the seasonal distribution of phosphate, nitrite plus nitrate and silicate respectively in the upper 900 m. Silicate analyses were not begun until August, 1958. Phosphate values range from 0·02 to 0·16 μg AP/L, nitrites and nitrates from undetectable amounts to 1·8 μg AN/L, silicates from 0·3 to 1·8 μg ASi/L in the upper 100 m respectively. In the case of the nitrogen and phosphorus compounds, the minimum surface values occurred in summer and when the water was stratified, the maxima in the winter and early spring when the greatest vertical mixing occurred. Silicate showed little evidence of a seasonal cycle in these surface waters.

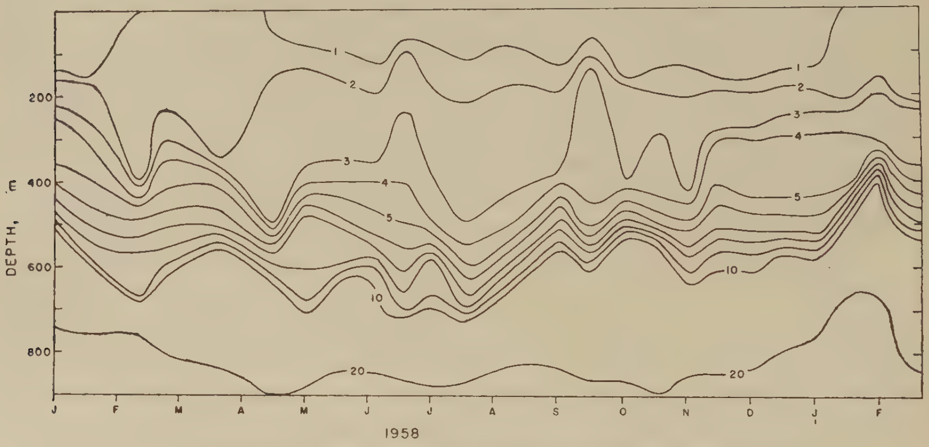

FIG. 5. The seasonal depth profile of nitrite and nitrate-nitrogen (μg A/L).

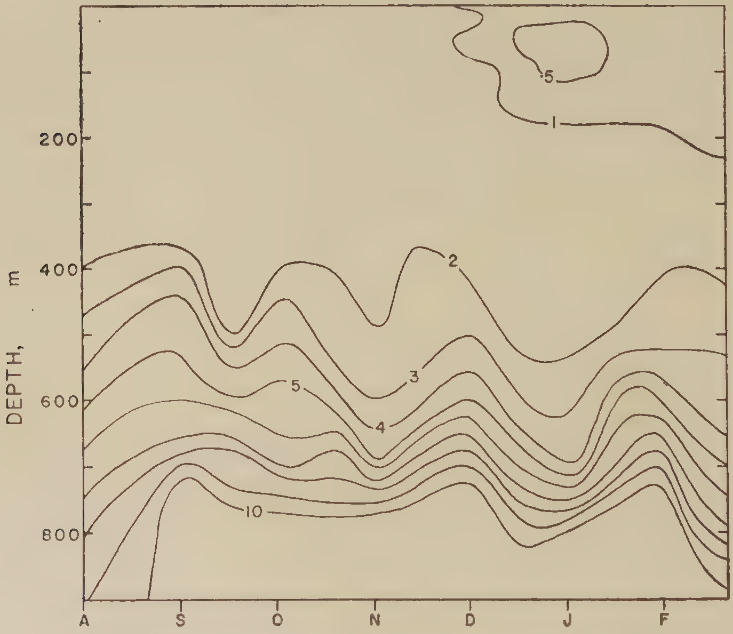

FIG. 6. The seasonal depth profile of silicate-silicon (μg A/L).

The variations in the nitrogen and phosphorus compounds are obviously correlated with and controlled by the hydrographic cycle described in the previous section. This is a familiar relationship in oceanography resulting from the fact that these materials are utilized nearly to exhaustion in the summer, removed from the euphotic zone through sinking of the phytoplankton, and thereby rendered unavailable for plant growth until winter and spring mixing returns them to the surface. Further discussion of the subject will be deferred until it is considered together with the phytoplankton and its rate of primary production in the final section. However, one important feature may be brought out here. The constancy of the 18° water with respect to its temperature and salinity was emphasized in the preceeding section. The same is very nearly true of its inorganic nitrogen and phosphorus concentrations (2-3 μg AN/L and 0·10–0·15 μg AP/L respectively) despite the fact that they are non-conservative properties. Within and below the permanent thermocline, the concentrations of these elements increase rapidly. The relative constancy of all of these properties is indicative of minor upward transport of nutrients from the region of the permanent thermocline and below. As far as concerns the phytoplankton and the factors which contribute to its growth, the Sargasso Sea may be considered an oligotrophic basin roughly 400 m deep almost out of contact with the rest of the ocean.

PHYTOPLANKTON STANDING CROPS

Fig. 7 shows the seasonal profile of chlorophyll *a* concentrations to a depth of 100 m, roughly contoured in the following categories: $<$ 0·10, 0·10–0·25, 0·26–0·50 and 0·51–1·00 mg/m^3. The striking contrast between winter, homogeneous and summer, stratified distribution, is at once obvious. Beginning in the late fall of 1957, we see what appears to be the remnants of a fall flowering in the deeper water. This is followed by moderately high levels (0·35–0·50 mg/m^3) evenly distributed with depth and remarkably constant in concentration which persists throughout the winter and early spring. By early April a spring flowering of short duration appeared, lasting for about one month in the surface but then sinking and remaining in the lower half of the euphotic zone for another month. Peak chlorophyll concentrations in this ‘ bloom ’ were about 1·00 mg/m^3. There followed the summer period with thermal stratification of the surface waters and extremely low surface chlorophyll (0·1 mg/m^3) increasing with depth to about 0·5 mg/m^3 at 100 m. As soon as surface cooling and mixing started in September, 1958, the surface chlorophyll picked up slightly and a short-lived, minor flowering occurred in November when the pigments again returned to a constant depth distribution to 100 m. In the early winter of 1958-1959, the pigments were somewhat lower than in 1957-1958, but returned to about the same level by mid-January. A striking difference in the second year was the ‘spring’ flowering which began in mid-January and lasted until early in March, two and a half months earlier than in 1958, slightly lower in magnitude (maximum of 0·75 mg/m^3 on February 26), and lasting for about twice as long. By the end of March, the phytoplankton were again vertically stratified to 100 m, repeating but two months in advance of the 1958 cycle.

On June 6 and December 18, 1958, chlorophyll measurements were made to 400 m. These data, together with temperatures and inorganic phosphorus values are shown in Fig. 8. On both dates the surface waters were thermally stratified, throughout

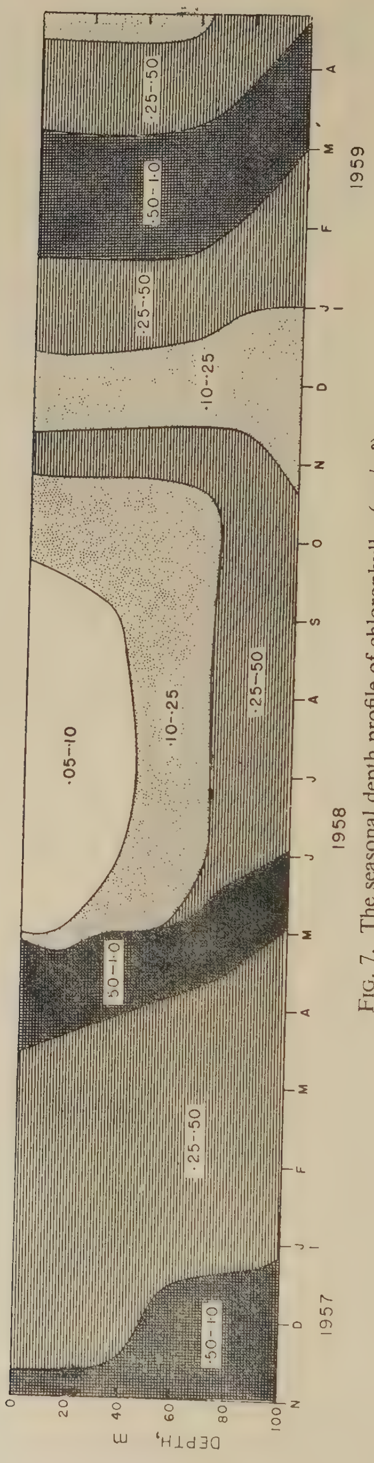

FIG. 7. The seasonal depth profile of chlorophyll *a* (mg/m³).

the upper 100 m in June and from 50-100 m in December. In each case the surface chlorophyll values were low but then increased to maxima at or near 100 m. The nutrients were also low at the surface and began to increase with depth at about 100 m. This is shown by the phosphate distribution and is also true of nitrate, which increased from 0·29 and 0·23 μg AN/L at 50 m to 1·3 μg AN/L at 150 m on the two dates.

Chlorophyll maxima at or near the lower limit of the euphotic zone appear to be a common distributional pattern whenever surface waters are thermally stratified (see Fig. 7). J. H. STEELE and C. S. YENTSCH (unpublished data) have recently considered the causes of this intermediate chlorophyll peak. It appears to be composed of the same organisms which inhabit the surface waters and does not represent a distinct population. It therefore probably results from the sinking of organisms from the surface layers. Assuming no differential grazing in the upper 150 m, the only thing which could cause the organisms to accumulate at a depth below that at which optimum photosynthesis occurs (i.e. 25–50 m) would be a change in their sinking rate. STEELE and YENTSCH postulated that nutrient deficient phytoplankton sinking from the surface layers might reduce their sinking rate when they encounter the relatively rich water at the base of the euphotic zone. They substantiated this theory experimentally by showing that the settling rate of nutrient starved diatoms was significantly reduced if the cultures were enriched.

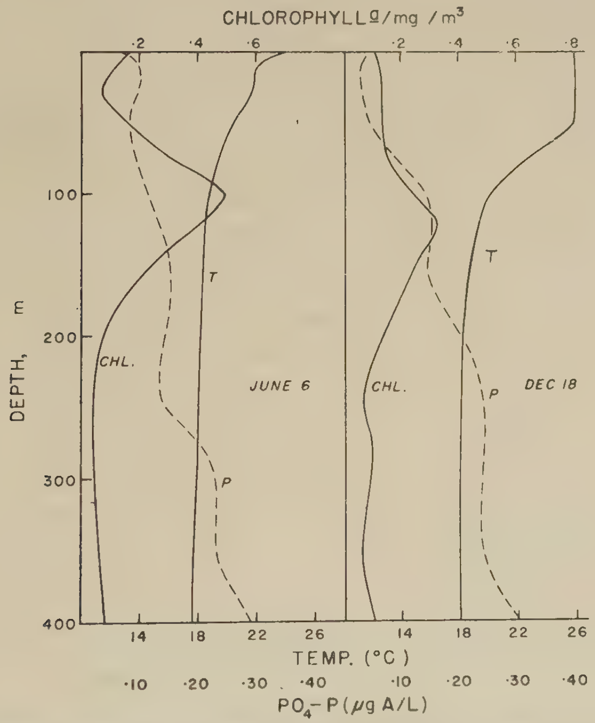

FIG. 8. The vertical distribution of chlorophyll *a* (Chl), temperature (T) and phosphate-phosphorus (P) on June 6 and December 18, 1958.

This seems to be a logical explanation for the summer chlorophyll distribution which we have observed. However, phytoplankton counts, which are not yet completed, will be necessary to confirm the fact that the phytoplankton at 100 m, are not, in fact, a separate community, or that the chlorophyll peak at that depth is not simply a matter of ' shade adaptation ' in which the chlorophyll per cell is much higher than at the surface. The latter is probably true to some extent, but it seems unlikely that it alone could account for the observed differences in pigment concentrations.

It is noteworthy that some chlorophyll was found all the way to 400 m, though the concentration decreased rapidly from the 100–150 m peak to extremely low concentrations in the deeper waters. We have investigated the problem of whether the chlorophyll at the aphotic depths below 100 m is ' active ' in the sense of being capable of carrying out photosynthesis. C^{14} uptake of samples from 0 to 400 m was measured at 1500 ft candles for 24 hrs in a water-cooled, artificially-illuminated incubator. The results, corrected for dark C^{14} uptake, showed no carbon assimilation in any of the samples from below 100 m (Table 3). This may have resulted from light inhibition of the deep, ' shade adapted ' plankton when exposed to the experimental intensity of 1500 ft candles (see RYTHER and MENZEL, in press). Note, for example, that photosynthesis at this constant light intensity decreased with increasing depth of the sample between 0 and 100 m despite the fact that the chlorophyll increased with depth to that level. However, the absorption spectra of pigment extracts from depths below 100 m are quite different from that of plants in the euphotic zone, and it therefore seems likely that the equations of RICHARDS with THOMPSON (1952) are not applicable under such conditions.

Table 3. *Photosynthesis* (C^{14} *uptake*) *for* 24 *hrs at* 1500 *ft candles of water from different depths at Station S on December* 18, 1958

Depth in metres	mg *carbon assimilated per* m^3 *per* 24 hr
0	3·05
17	2·10
34	2·20
60	2·90
120	0·47
150	0·00
200	0·00
250	0·00
300	0·00
350	0·00
400	0·00

PRIMARY PRODUCTION

The values for gross and net primary production in grams carbon assimilated per m^2 per day are shown in Fig. 9. The net production (C^{14} uptake) data for the first four months are rather unreliable for various technical reasons, most important of which being the use of C^{14} solution of insufficiently high activity. Thereafter the data are believed to be accurate within the limits of the methods.

Gross production, based partially on the chlorophyll content of the water, naturally followed closely the chlorophyll distribution. Net production values, with one exception, were consistently lower, ranging from about 10 per cent to 90 per cent and averaging about 50 per cent of gross production (omitting the first four months). The closest agreement between the two methods occurred at the termination of the spring flowering and throughout the summer of 1958. Beginning in December, 1957, and throughout the early spring of 1958, including the early flowering of that year, a rather constant discrepancy of about 50 per cent between the methods persisted. For the most part, the irregularities in the seasonal cycle of one set of values is closely paralleled by those of the other.

Gross production was relatively high and constant throughout the early winter of 1958, began to increase slowly and irregularly by mid-January, 1959, culminating in a peak of 2·0 g C/m²/day on April 15. Following this maximum, gross production decreased rapidly for the next two weeks, reaching its low, summer level (0.1–0.2 g C/m²/day) by May 1.

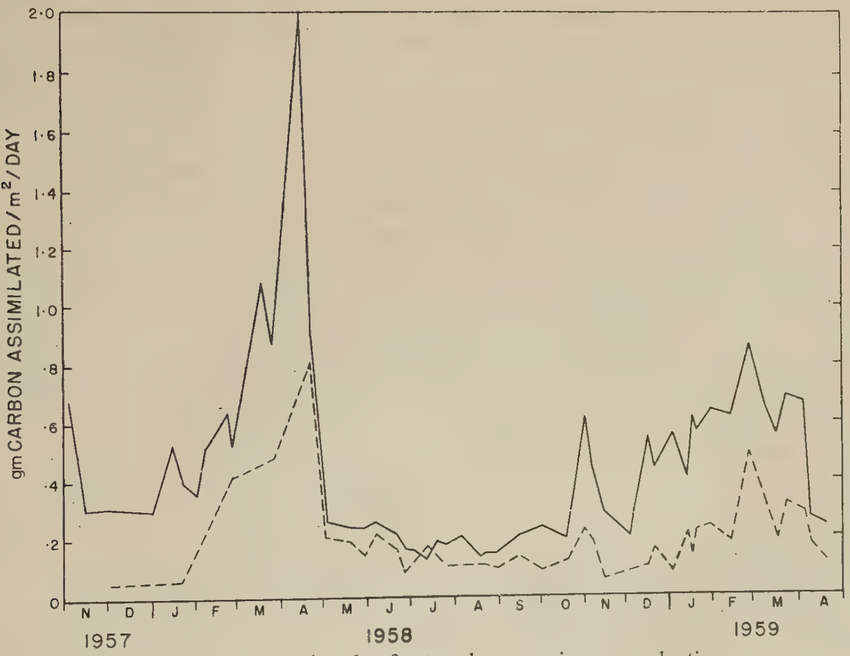

FIG. 9. The annual cycle of net and gross primary production.

In the early part of November there was a brief increase in production which, probably by coincidence, occurred at the same time and attained the same magnitude (0·6 g C/m²/day) as in the fall of 1957. Production then decreased, returning to 0·2 g C/m²/day in December, following which the same gradual and irregular build-up occurred throughout the winter as in 1957-1958, but this time beginning a month sooner and reaching a lower maximum (0·86 g C/m²/day) on February 26. Rather than the sudden drop-off observed in late April, 1958, the decline in the spring of 1959 was also gradual and more irregular. In contrast to the brief flowering of relatively high magnitude in the spring of 1958, the 1959 bloom was more moderate but spread over a much longer period.

Unfortunately, no measurement of net production was made at the peak of the 1958 flowering. Four days later on April 19, when gross production had dropped to 1·5 g C/m^2/day, net production was only 0·8, or about half of gross production. Two days, after that, however, and thereafter for several months, the two measurements were in close proximity. The discrepancy on April 19 may have been due to an error of measurement, but the values for March 25 show the same feature, which indicates that net production was only about half of gross production during the build-up of the spring flowering, between 75 per cent and 90 per cent of gross production during the decline of the bloom and the summer period of minimum production. This same trend was observed when production was measured by these methods in the continental shelf waters off New York (RYTHER and YENTSCH, 1958). It may represent some systematic error in either of the methods under conditions of high productivity. One would ordinarily expect that the ratio net/gross production might be highest during periods of most rapid growth of the algae. This is not necessarily so, however. A review by RABINOWITCH (1951) of several investigations shows that respiration is markedly stimulated by the products of photosynthesis. It follows that starved plants respire less, have a greater P/R ratio, and hence a closer relationship between gross and net production than healthy growing cells, which must metabolize at a greater rate to convert their first product of photosynthesis into new cellular materials. Thus the observed relationships between net and gross production are not incompatable with the evidence of plant physiology, though this is clearly an area in which further experimental work is needed.

The annual rate of production obviously depends upon the choice of time within the twelve-month period. For 1958 (January-December) gross and net production were respectively 160 and 72 g C/m^2. Daily gross production ranged from 0·13 to 2·00 with an annual mean of 0·44 g C/m^2/day, which agrees more closely with the much maligned values of RILEY *et al.* (1949) than with any of the more recent estimates. Net production ranged from 0·05 to 0·83 and averaged 0·20 g C/m^2/day. The minimum (observed in November) is identical to that reported by STEEMANN NIELSEN for the Sargasso Sea (Table 1) in June. Our June values ranged from 0·09 to 0·17 g C/m^2/day, not appreciably different from STEEMANN NIELSEN's, though his values are increased by a respiratory factor to make them equivalent to gross production.

Most of the year's production occurred during the winter build-up and the spring flowering, if indeed the two can be separated. In the four-month period between January 1 and April 30, 1958, gross production was 92 g C/m^2, almost 60 per cent of the year's total. If we consider the equivalent period of the following year to extend from December 1, 1958 through mid-April, 1959, gross production amounted to 76 g C/m^2/year, or 82 per cent of the previous year's value for the similar period. It appears likely, therefore that annual production does not vary greatly from one year to the next, as if the total amount of organic matter which may be produced is more or less fixed in some way, perhaps by the available nutrients. On the other hand, the way in which this potential is expended over the year is highly variable and probably dependent upon local and transient meteorological and hydrographic features which will be discussed in the following, final section.

THE ENVIRONMENTAL CONTROL OF PRIMARY PRODUCTION

It was stated earlier that, as far as the phytoplankton were concerned, the Sargasso

Sea could be considered as a basin 400–500 m deep, its bottom the discontinuity between the 18° water and the permanent thermocline. This obviously is not entirely true, for sinking and downward transport to 1000 m or more by the migratory zooplankton must result in some loss of organic matter from the surface layers. The nutrients bound in this material must be replenished in some way to the upper water if the fertility of the area is not to be progressively diminished. Yet the constancy of the temperature and salinity of the surface layer is a convincing argument against the occurrence of any large-scale mixing between the thermocline and the overlying waters. It follows, then, that the nutrient elements must complete almost their entire biochemical cycle of assimilation and regeneration within the upper 400 m. It also follows that production must be severely limited by the relatively low concentrations of nutrients in this layer.

Within the upper 400 m, the highest concentration of nitrite plus nitrate nitrogen and phosphate phosphorus are about 1200 mg atoms and 60 mg atoms/m^2 respectively. If all of these nutrients were incorporated into phytoplankton of normal elementary composition, the resulting crop would be equivalent to some 75–100 grams carbon/m^2, which is roughly the value obtained for net annual production. If the nutrient regenerative processes were slow, one might expect that the levels of inorganic nitrogen and phosphorus would decline at a rate inversely proportioned to primary production. REDFIELD *et al.* (1937), STEELE (1956) and others were able to estimate production rates by the disappearance of phosphorus from the surface waters of temperate latitudes. However, no such simple relationship exists in the Sargasso Sea. The dissolved nutrients in the 400 m water column vary only slightly and in an irregular and unpredictable way. For example, during the winter and spring flowering of 1958 there was a net production of 46 g C/m^2 between January 1 and May 1. This is equivalent to a utilization of 570 mg AN and 38 mg AP/m^2, half the amount present. Yet within that period there was a loss of only 250 mg A/m^2 of nitrogen and a *gain* of 35 mg A/m^2 of phosphorus. Clearly the regenerative processes occur so rapidly in these semi-tropical waters that the concentrations of inorganic nutrients present at any time are almost without significance.

It may, of course, be argued that these irregularities in the upper 400 m merely reflect exchanges with the deeper, thermocline waters. Unfortunately the limitations of the analytical methods result in absolute errors which are much greater in deeper waters, where concentrations are higher, and probably obscure the relatively small losses and gains which would be necessary to balance the changes in the surface waters. A further complication is the vertical displacement of properties in the thermocline region by as much as 100 m from one set of observations to the next (Figs. 2–6) which SCHROEDER *et al.* (1959) have attributed to short-period internal waves. Because of these, the homogeneous layer should technically be considered with respect to a density discontinuity rather than a fixed depth, but in view of the limitations of the analytical methods the need for such a refinement is hardly indicated.

There is, however, a gross seasonal cycle of nutrients in the upper 400 m which illustrates at least qualitatively the environmental control of production. For example, in the winter and early spring, when water is mixed to depths as great as 400 m, the nutrients reach their highest values at the surface (1–2 μg AN/L, 0·1–0·2 μg AP/L) and their lowest values at the depths 100–400 m. The euphotic zone remains almost constant throughout the year at about 100 m. In winter, the phytoplankton is evenly distributed from 0–400 m and the entire population, though limited by light, is able to grow. When thermal stratification of the surface waters first begins to develop, the plants are maintained in the euphotic zone at relatively high nutrient concentrations, giving rise to a vigorous but short-lived flowering. A typical example of this is the maximum of production on April 15, 1958 of 2·0 g C/m^2/day, which approaches the highest recorded values for primary production anywhere (RYTHER, in press). Since growth at this rate would require an average daily consumption of 0·25 μg A/L of nitrogen and 0·02 μg A/L of phosphorus within the 100 m euphotic zone, it is obvious that nutrient exhaustion must quickly terminate this flowering. The bulk of the spring bloom then sinks and accumulates at 100–150 m (Figs. 7 and 8) and the organisms or their decomposition products remain there until mixing returns them to the surface the following winter. The low level of summer production is undoubtedly dependent upon the rapid partial re-cycling of nutrients *in situ* in the euphotic zone, perhaps augmented by occasional mixing below 100 m during summer storms.

There is nothing unique or even unusual in the general nature of this cycle. What distinguished the Northern Sargasso Sea from more temperate regions are the following characteristics : (1) a relatively shallow winter mixed layer, (2) greater solar radiation in winter, (3) clear water, (4) low level of nutrients in the mixed layer and (5) the rapid re-cycling of nutrients, possibly due to higher temperatures. As a result of this combination of factors, the levels of maximum and minimum production in these semi-tropical waters are less extreme but the annual rate is as high as or higher than that of temperate and northern waters (see, for example, RYTHER and YENTSCH, 1958).

As we have shown, the degree of winter mixing is variable and apparently dependent upon winter air temperatures and perhaps winds. This effects the timing and nature of the seasonal cycle of production, but does not appear to influence the overall annual rate as long as the water becomes mixed to a depth significantly below the euphotic zone. By oceanographic criteria, a separation between semi-tropical conditions must exist very near the latitude of Bermuda. A short distance to the South, surface temperatures never fall below 20° and winter mixing probably never extends below 100–150 m. Under these conditions it is likely that primary production proceeds at a low rather steady rate throughout the year, comparable to summer conditions in Bermuda. The results of this study cannot therefore be taken as ‘ typical ’ of the Sargasso Sea or the open ocean in general, since probably neither is as uniform as is generally implied.

Woods Hole Oceanographic Institution, Woods Hole Massachusetts.

Contribution No. 254 *from Bermuda Biological Station*

**Contribution No.* 254 *from the Bermuda Biological Station and Contribution No.* 1042 *from the Woods Hole Oceanographic Institution under Contract AT* (30-1)-2078 *with the U.S. Atomic Energy Commission with partial support of NSF Research Grant* G-3234.

REFERENCES

CREITZ G. I. and RICHARDS F. A. (1955) The estimation and characterization of plankton populations by pigment analyses, III. A note on the use of ‘ millipore ’ membrane filters in the estimation of plankton pigments. *J. Mar. Res.* **14**, 211-216.

FUGLISTER F. C. (1947) The hydrography of the North-western Sargasso Sea. Unpublished manuscript.

ISELIN C. O'D. (1936) A study of the circulation of the Western North Atlantic. *Pap. Phys. Oceanogr. and Meteorol.* **4**, 1-101.

KETCHUM B. H., CORWIN N. and KEEN D. J. (1955) The significance of organic phosphorus determinations in ocean waters. *Deep-Sea Res.* **2**, 172-181.

MULLIN J. B. and RILEY J. P. (1955a) The colorometric determination of silicate with special reference to sea and natural waters. *Analyt. Chim. Acta.* **12**, 162-175.

MULLIN J. B. and RILEY J. P. (1955b) The spectrophotometric determination of nitrate in natural waters, with special reference to sea water. *Ibid.* **12**, 464-480.

MURPHY J. and RILEY J. P. (1958) A single solution method for the determination of soluble phosphate in sea water. *J. Mar. Biol. Assoc. U.K.* **37**, 9-14.

POOLE H. H. and ATKINS W. R. G. (1929) Photo-electric measurements of submarine illumination throughout the year. *Ibid.* **16**, 297-324.

RABINOWITCH E. I. (1951) *Photosynthesis and related processes.* Vol. 1. Intersciences Publ., New York.

REDFIELD A. C., SMITH H. P. and KETCHUM B. H. (1937) The cycle of organic phosphorus in the Gulf of Marine. *Biol. Bull.* **73**, 421-443.

RICHARDS F. A. with THOMPSON T. G. (1952) The estimation and characterization of plankton populations by pigment analyses, II. A spectrophotometric method for the estimation of plankton pigments. *J. Mar. Res.* **11**, 156-172.

RILEY G. A. (1953) Letter to the editor. *J. du Cons. Internat. Explor. Mer.* **19**, 85-89.

RILEY G. A. (1957) Phytoplankton of the north central Sargasso Sea. *Limnol. and Oceanogr.* **2**, 252-270.

RILEY, G. A., STOMMEL H. and BUMPUS D. F. (1949) Quantitative ecology of the plankton of the Western North Atlantic. *Bull. Bing. Oceanogr. Coll.* **12**, 1-169.

RYTHER J. H. (1954) The ratio of photosynthesis to respiration in marine plankton algae and its effect upon the measurement of productivity. *Deep-Sea Res.* **2**, 134-139.

RYTHER J. H. (1956a) Interrelation between photosynthesis and respiration in the marine flagellate, *Dunaliella euchlora*. *Nature, Lond.* **178**, 861-862.

RYTHER J. H. (1956b) The measurement of primary production. *Limnol. and Oceanogr.* **1**, 72-84.

RYTHER J. H. (1959) The potential productivity of the Sea. *Science.* **130**, 602-608.

RYTHER J. H. and YENTSCH C. S. (1957) The estimation of phytoplankton production in the ocean from chlorophyll and light data. *Limnol. and Oceanogr.* **2**, 281-286.

RYTHER J. H. and YENTSCH C. S. (1958) Primary production of Continental Shelf waters off New York. *Ibid.* **3**, 327-335.

RYTHER J. H. and MENZEL D. W. (in press) Light adaptation by marine photoplankton. *Ibid.*

SCHROEDER E., STOMMEL H., MENZEL D. and SUTCLIFFE W. Jr. (1959) Climatic stability of 18° water at Bermuda. *J. Geophys. Res.* **64**, 363-366.

STEELE J. H. (1956) Plant production on the Fladen Ground. *J. Mar. Biol. Assoc. U.K.* **35**, 1-33.

STEEMANN NIELSEN E. (1952) The use of radioactive carbon (C^{14}) for measuring organic production in the sea. *J. du Cons. Internat. Explor. Mer.* **18**, 117-140.

STEEMANN NIELSEN E. (1954) On organic production in the oceans. *Ibid.* **19**, 309-328.

STEEMANN NIELSEN E. and HANSEN V. Kr. (1959) Measurements with the C^{14}-technique of the respiration rates in natural populations of phytoplankton. *Deep-Sea Res.* **5**, 222-233.

VAN DORN W. G. (1956) Large volume water sampler. *Trans. Amer. Geophys. Union* **37**, 682-684.

WORTHINGTON L. V. (1959) The 18° water in the Sargasso Sea. *Deep-Sea Res.* **5**, 297-305.

Printed in Great Britain by The Salisbury Press Ltd., Publicity House, Wilton Road, Salisbury, Wilts. (22856)

Contribution No. 1044

RECENT DEVELOPMENTS IN STUDIES OF PENETRATIVE CONVECTION AND AN APPLICATION TO HURRICANE CUMULONIMBUS TOWERS*†

JOANNE S. MALKUS
Woods Hole Oceanographic Institution

Abstract—Recent observational and theoretical work on cumulus convection is summarized and a promising model of individual elements evolved by Levine[5] is described, extended, and tested in a hurricane context.

The model treats an isolated bubble-like element whose internal circulation resembles that of a vortex ring, turning inside out as it rises and exchanging a constant fraction of its mass with the surroundings on each cycle. The equations for Hill's vortex are used to describe the internal circulation and a well-known type equation for the rate of rise W derived where the acceleration is the difference between buoyancy and drag forces, which are to be evaluated including mixing and state changes as the equation is integrated numerically in a series of height steps.

Levine's framework permits derivation of an explicit relationship between element size and fractional entrainment rate with height, clarifying the concept of "protected cores" in penetrative convection. The model is applied to individual cumulonimbus towers in hurricane Daisy (1958) for which the National Hurricane Project has provided plentiful data. Photographic measurements are used to test the results of the computation. The range of validity and applicability of the model to real convection clouds is considered.

INTRODUCTION

CUMULUS convection studies during the past ten years have focused attention upon the dilution of the clouds by mixing, or entrainment of environment air. Most cumuli exhibit temperatures and liquid water contents considerably lower than those of the classical or undiluted parcel, and due to buoyancy exhaustion by mixing with drier air terminate well below the level at which the moist adiabat from cloud base recrosses the environment sounding. Nevertheless, occasional penetrative towers are observed to levels approaching or even exceeding the tropopause. Empirically, these penetrative towers have been found to require a large horizontal dimension and the idea of a critical diameter has been proposed (Malkus and Ronne[8]). It has been inferred, however, largely from results of the "bubble theory" (Malkus and Scorer[9]) that towers cease to rise when their buoyancy is exhausted; thus penetrative towers would have to be undiluted or very nearly so, and their ascent curve would represent a virtual temperature versus height relation very little different from that of the adiabatic parcel. The prediction that ascent ceases when buoyancy goes to zero appears to be in contradiction with observations by Vonnegut and Moore[17], Koldovsky[4] and others apparently showing

---

* Contribution No. 1044 from the Woods Hole Oceanographic Institution.

† This research has been supported under Contract No. Cwb 9509 with the National Hurricane Research Project of the U.S. Weather Bureau and under Grant No. 7368 from the National Science Foundation.

significant overshooting of cumulonimbus towers into the stratosphere, almost without doubt against negative buoyancy. As will be shown presently, this question of overshooting, its magnitudes and circumstances, is an important one to resolve and has implications concerning synoptic and larger-scale circulations in the tropics, as well as for precipitation physics.

One of the important questions now faced in convection dynamics is, what are the conditions necessary for penetrative cumulonimbus development? A model has been recently developed (Levine[5]), which for the first time evolves a theoretical framework in which this subject may be approached quantitatively; the present paper develops this model further in a hurricane context. First, however, it is desirable to summarize briefly our existing observational knowledge.

Classical parcel dynamics predicts penetrative towers whenever conditional instability prevails through a deep layer of the troposphere, presumably the more likely the greater the "positive area". In the tropics, lapse rates steeper than wet adiabatic are the rule, and in the old days it was believed that tropical convection would occur in a random fashion, with isolated cumulonimbi here, there, and everywhere. Actually, nothing could be farther from the truth. In fact, pioneer workers in the tropics discovered an inverse relation between instability and the occurrence of cumulonimbi! In an early paper Riehl[11] says "Increasing steepness of the lapse rate beyond the moist adiabatic, however, except for the layer near the ground, was not indicative of higher probability of thunderstorm development. The atmosphere pays the price of increased stability for replenishment of its moisture. Air with a nearly dry adiabatic lapse rate is likely to be very dry. Conversely, superior air has the steepest lapse rates. Thus, if other conditions are favorable, the fact that the lapse rate exceeds the moist adiabatic only slightly need not be considered as an obstacle to thunderstorm formation."

A recent low-latitude cloud survey in the Pacific using combined photographic and synoptic analyses (Riehl, Gray, Malkus, and Ronne[12]) dealt the death blow to the classical concept of tropical convection, and in so doing clarified observationally some of the conditions for runaway cumulonimbus development. Cumulonimbus clouds were extremely rare; most of the tropical oceans were dominated most of the time by stunted trade cumuli with maximum tops at the level of the trade-wind inversion. *Cumulonimbi and significant precipitation were confined entirely to synoptic disturbances and within these developed in not a random but highly organized fashion, generally in rows parallel to the low-layer wind.*

In all cases where such clouds were found, the lapse rate was generally very close to moist adiabatic and far less unstable than that prevailing under normal trade-wind conditions. In fact, the most unstable lapse rates were found under suppressed conditions, with few or small stunted cumuli, when an upper cold low was superposed upon a lower ridge and vertical stretching of columns was brought about due to diverging descent in the troposphere! In the context of the present work on hurricane cumulonimbus, it is illuminating to compare the temperature lapse rates in the inner rain area (about 30 km from storm center) of Hurricane Daisy, 1958, where cumulonimbi were rampant with the mean West Indies sounding (Jordan[3]) which, when it prevails, gives rise to trade cumulus convection only.

Table 1 brings out the startling result that in the best cumulonimbus factory known, the hurricane, the static stability is 25 per cent higher than average conditions over the tropical oceans, wherein no penetrative developments occur, and that furthermore the mean lapse rate over the main body of the troposphere averages barely wet adiabatic in the hurricane, while it exceeds it by 10 per cent in mean tropical!

Table 1. *Lapse Rates and Stability in Hurricane Daisy* (*Inner Rain Area*) *compared with Mean Tropical Layer 900–200 mb*

	$-\frac{dT}{dz}$ (°C/km)	$\frac{1}{\theta}\frac{d\theta}{dz} \times 10^7$ (cm^{-1})	Per cent of wet adiabatic lapse rate (%)
Mean Tropical	6.6	1.2	110
Daisy	6.0	1.5	100

Nor does moisture distribution provide the whole key to the difference in convection. A previous cumulonimbus study (Malkus and Ronne[8]) showed that spectacular cumulonimbi can grow even in the face of a relatively dry atmosphere above 3 km. The Pacific work confirmed this and suggested that the presence and degree of synoptic-scale convergence was the critical factor. All cumulonimbi were observed in areas where low-level inflow (and presumably upper outflow) could be inferred qualitatively from the synoptic charts with a high degree of certainty—most in so-called "tropical disturbances", easterly waves, equatorial vortices, hurricanes, etc.

The fact that on many occasions when cumulonimbus were found, stunted trade cumuli were simultaneously observed, and the stunted clouds always had smaller diameters than the tall ones, suggested that the convergence produces penetrative development by permitting large diameter elements to form. We hypothesized that large towers could achieve great heights with less dilution than the smaller ones, but no theory existed for relating degree of dilution to element size. Such a framework has been developed by the recent work of Levine. This paper will consider his model further and emphasize the matter of element size in particular.

The hurricane context for this investigation has been chosen for several reasons, the most obvious being that documentation for cumulonimbus towers reaching the tropopause and considerable supplementary information for Hurricane Daisy, 1958, exists by the courtesy of the National Hurricane Research Project. This is, thus, an excellent "proving ground" for Levine's model, and the testing of the adequacy of the present development of cumulus dynamics.

Actually, however, an even more significant reason for the choice is that penetrative cumulonimbus towers have been proposed (Malkus[7]) as the key mechanism in carrying out hurricane heat and mass flows and thereby as an essential link in the storm energetics, pressure gradient and wind maintenance. To develop and test this hurricane model further, it is necessary to relate theoretically the heights, sizes, draughts and buoyancies in cumulonimbi under hurricane conditions, and to see whether the predictions agree with the micro- and macro-scale observations made by the hurricane project aircraft; for example, if "hot towers" are required to have higher excess temperatures over greater distances than can be found by the proper statistical sampling from the aircraft records, either the hurricane model or the cloud model or both are inadequate. If, on the other hand, the requirements of the cloud model are easily met by the hurricane observations, then a long step has been accomplished in cumulus dynamics, hurricane dynamics and in understanding the vital interaction between these two scales of motion in the atmosphere.

BACKGROUND AND IMPLICATIONS OF LEVINE'S MODEL

The two most promising models of individual convection elements since the collapse of the classical parcel theory have been the so-called "entrainment" and "bubble" models, whose merits and defects have been discussed elsewhere (see, for example, Malkus and Witt[10]). The latter appeared most suitable for cloud towers, but its major shortcoming was that it assumed no dilution of the bubble cap at all; caps shed their protuberances into a wake and continued rising until they had eroded away altogether. All loss of vertical momentum was thought to take place by means of a form drag (Malkus and Scorer[9]). This was in direct contradiction to the entrainment model, which

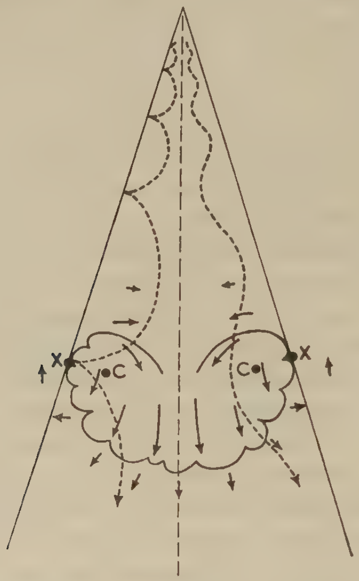

Fig. 1—(After Scorer and Ronne[15].) The field of motion around and in a laboratory (mud slurry) bubble. The arrows show the velocity of the particles not taking the turbulent mixing into account. The particles inside the bubble are moving faster than those outside and are moving into and mixing with the fluid in the path of the bubble. The bubble is turned inside out several times, each time being represented by a step in the paths of two typical particles shown. The particle on the left appears close to the front and passes round to the rim where it becomes temporarily stationary. The particle on the right remains inside the bubble circulating round the core of the vortex ring (*C*). The ring grows in proportion to the size of the bubble and the motion would appear to be circulating round the core to an observer moving with the bubble. To a stationary observer it appears to be circulating round the ring *X* on the rim of the bubble. The time for a cycle is defined as the time for half the mass in the element to pass between *X* and the dashed center line, or for all the mass to pass between the *X*'s.

hypothesized that the major reduction of vertical momentum relative to that of the non-interacting parcel arises from buoyancy reduction by dilution; observations (Malkus[6]) supported the latter viewpoint, although other features of the bubble theory proved useful in interpreting time-lapse cloud photographs.

Laboratory experiments undertaken at the Imperial College (Scorer and Ronne[15]; Woodward[19]) resolved some of these difficulties, and suggested how a bubble model which included entrainment or dilution could be evolved. The experimental bubbles, which were mud "slurries" released into a resting unstratified mass of water, exhibited vortex ring circulations which expanded along a cone (Fig. 1) as they advanced, the expansion resulting from incorporation of external fluid, about 60 per cent from ahead and 40 per cent from the sides. If an internal cycle is defined as the time required for the entire mass within the element to pass between the *X*s in Fig. 1 (this is the same as the time required for a hypothetical "average" particle to make the complete circuit of the vortex ring), expansion along a cone implies a fractional mass dilution per cycle which is a constant. Although bubbles released into an unstratified fluid expanded rather than "eroding" or shedding mass into a wake as the experimenters might have wished, release of similar bubbles into a stably stratified tank produced erosion; it was possible by adjusting the stratification to achieve a balance between mass shed by erosion and that incorporated from the surroundings so that the elements progressed with nearly constant mass flux in their circulation, as is apparently quite frequently the case with cumulus towers.

The physical basis of Levine's model is best described in the framework of these experiments. We are thus treating individual active convection elements, whose rate of rise and internal motions we wish to describe analytically. Application of the results to real cumuli must thus be undertaken with some caution, and are best made when dealing with clouds formed by a succession of intermittent discrete elements, as tropical oceanic clouds frequently are. The case of a columnar, relatively steady updraught or plume is not explicitly approached here and since convective clouds frequently exhibit this form, particularly when a relatively constant source of heat or moist air is available (as for example, in certain mountainous regions), we may profitably inquire later to what degree the equations derived are restricted by the particular choice of model. In Levine's (*loc. cit.*) own words, the general background of his treatment and its relation to cumulus convection is briefly as follows: "The physical picture of the visible cumulus cloud may be described as a relatively large diffuse mass of liquid water droplets slowly mixing with the environment and evaporating. The portion of the cloud in which no strong updraughts are occurring may be considered to be inactive. The inactive portion may be cooler than the environment and therefore negatively buoyant with respect to the clear environment. The inactive portion of the cloud may not have acquired an appreciable downward velocity with respect to the clear environment on account of the upward drag by a rapid succession of bubbles passing through.

"The existence of bubble-like entities has been inferred from observation of time lapse motion pictures. The inactive mass of the cloud at lower levels is characterized by fuzzy boundaries, but the towers which shoot up from the fuzzy mass appear sharply defined. The cauliflower-like appearance of cumulus cloud tops has led to the inference that these bubbles have nearly spherical tops. The towers are considered to be bubbles which have escaped the protective environment of the fuzzy mass.

'The bubble is considered to be protected from the cooling effects of evaporation while immersed in the inactive cloud. When the bubble penetrates the inactive cloud top, it appears as a bulge or tower which rapidly loses its buoyancy in the clear air and gradually evaporates completely or becomes part of the inactive cloud mass. The cloud base may be considered the principal source of bubbles. Turbulent motions in the sub-cloud layer may cause isolated bubbles of relatively warm air to start upwards through the inactive cloud mass."

In his analytic treatment, he postulates that the active cumulus convection elements (either within a body of inactive cloud matter or rising alone as towers) may be envisaged as spherical, with internal circulation describable by the equations for Hill's vortex; the elements dilute as they rise by exchanging a fixed fraction K of their total mass with the surroundings on each half-cycle, an approximate balance being maintained between influx and efflux (the latter assumption is not essential to the model).

With relatively few additional simplifying assumptions, the following equation is derived for the rate of rise W of the element, namely

$$\frac{dW}{dt} = g\frac{(\theta - \theta_0)}{\theta_0} - \frac{3}{8}\left(\frac{3}{2}K + C_D\right)\frac{W^2}{a} \tag{1}$$

where t is time, g is the acceleration of gravity, θ is the virtual potential temperature of the element, θ_0—that of the surroundings, K—the fraction of mass exchanged per half cycle, C_D—the form drag coefficient, and a—the radius. This equation is to be integrated numerically in a series of height steps along with another equation for the buoyancy term $g(\theta - \theta_0)/\theta_0$, evaluated including the effects of the exchange coefficient K, the condensation of liquid water, etc., when an environment sounding is given.

The form of the differential equation (1), giving the substantial time rate of change of W as the difference between buoyancy and drag forces, is not dependent upon the particular modelling adopted by Levine and is clearly not necessarily restricted in application to the type of element he described. In fact, an equation similar in form, namely with drag term proportional directly to W^2 and inversely to horizontal dimension, was employed and tested earlier by measurements* from time-lapse films by Malkus and Scorer.[9] The new feature of the formulation in (1) is the division of the coefficient of W^2/a in the drag term into "mixing drag" and "form drag" to be considered jointly, although the physically most important effect of the mixing is in the reduction of the buoyancy below wet adiabatic, included here but ignored in previous "bubble theory" developments. The specific model of Levine's using the Hill's vortex equations gives rise to the actual numbers in the drag term in eq. (1) and relates the internal circulation within the element to its rate of rise. The vortex equations show that the maximum "updraught" within the element is 2.5 times W, while the maximum downdraughts at its edges are $-$ 0.5 W, in exact correspondence with the Imperial College experiments.

The drag term, which we see is inversely proportional to radius a, warrants considerable discussion. Although K and C_D must be assumed arbitrarily, their possible ranges are, within the range of validity of this model, rather small. The form drag coefficient C_D would be 9/8 for a solid sphere, but this is probably too high for a miscible element, with some of the impinging mass moving into rather than around it. Since

---

* It is to be noted that the measurements by Malkus and Scorer cited above tested only the form of the differential equation and not the magnitudes of the coefficients therein.

$K = 1$ corresponds to a complete exchange of mass with environment on each half cycle, the bubble concept has no meaning for K many times larger than this, while the lower limit $K = 0$ corresponds to the undiluted element. Although later we shall see that comparison of calculations from the theory with observations will permit a rough assessment of these constants, neither this nor even their small range is the main virtue of this manner of formulating the entrainment process. The point is that while K is envisaged as more or less constant for elements of all sizes, the fractional entrainment rate with height defined by Stommel[16] may be shown thereby to be inversely dependent upon element dimension and we thus are able to show quantitatively how penetration of towers depends on size and derive theoretically the "critical" dimension under given environmental conditions.

The relation between Stommel's entrainment rate with height $1/M\,\mathrm{d}M/\mathrm{d}z$ and Levine's exchange coefficient K may be derived readily as follows:

Stommel considered a rising jet incorporating extra mass flux at the rate $1/M\,\mathrm{d}M/\mathrm{d}z$. In his first concept, all entrained mass was retained in the jet. As far as dilution and calculations from soundings are concerned, the unrealism of this is irrelevant, although later modifications of the entrainment model allowed for outflow or shedding of cloud air also.

Levine considered both influx and efflux from his bubbles, namely $\mathrm{d}M/\mathrm{d}t_+$ and $\mathrm{d}M/\mathrm{d}t_-$ respectively. His important assumption was to assume these proportional to the mass flux within the bubble, namely $3/8\,\pi\varrho Wa^2$, where the latter is the expression for the downward mass flux at the element edges in bubble coordinates, which for continuity must equal the upward flux in the central updraught portion.

Therefore, he postulates

$$\left(\frac{\mathrm{d}M}{\mathrm{d}t}\right)_- = \frac{3}{8}K_1\pi\varrho Wa^2$$

and

$$\left(\frac{\mathrm{d}M}{\mathrm{d}t}\right)_+ = \frac{3}{8}K_2\pi\varrho_0 Wa^2$$

where K_1 is the fraction of downward flux transferred out to the environment and K_2 is the fraction of upward flux transferred in from the environment.

To compare with Stommel's model we are interested in K_2 and since

$$\frac{\mathrm{d}M}{\mathrm{d}t} = W\frac{\mathrm{d}M}{\mathrm{d}z} \text{ and } M = \frac{4}{3}\pi\varrho a^3$$

Therefore

$$\frac{1}{M}\frac{\mathrm{d}M}{\mathrm{d}z} = \frac{9}{32}\frac{K_2}{a} = \frac{1}{1.78}\frac{K_2}{D} \times 10^{-5} \tag{2}$$

where D is element diameter in km. In all cases studied so far we have assumed $K_1 = K_2 = K$.

The time for a cycle is thus the number of seconds required for the total mass to pass through the central plane in the updraught, or M divided by the mass flux in the updraught, namely

$$\frac{\frac{4}{3}\pi\varrho a^3}{\frac{3}{8}\pi\varrho Wa^2} = \frac{32}{9}\frac{a}{W} = T_{\text{cycle}} \tag{3}$$

The relationship between entrainment rate and element size of eq. (2) is plotted on a semi-logarithmic graph in Fig. 2 for different values of K. The curve for $K = 0.5$ is emphasized, since the observations discussed by Levine and those later in this paper suggest that this value is roughly correct for large cumulus towers. However, it will be noted that variations of K within the possible range make minor difference in entrainment

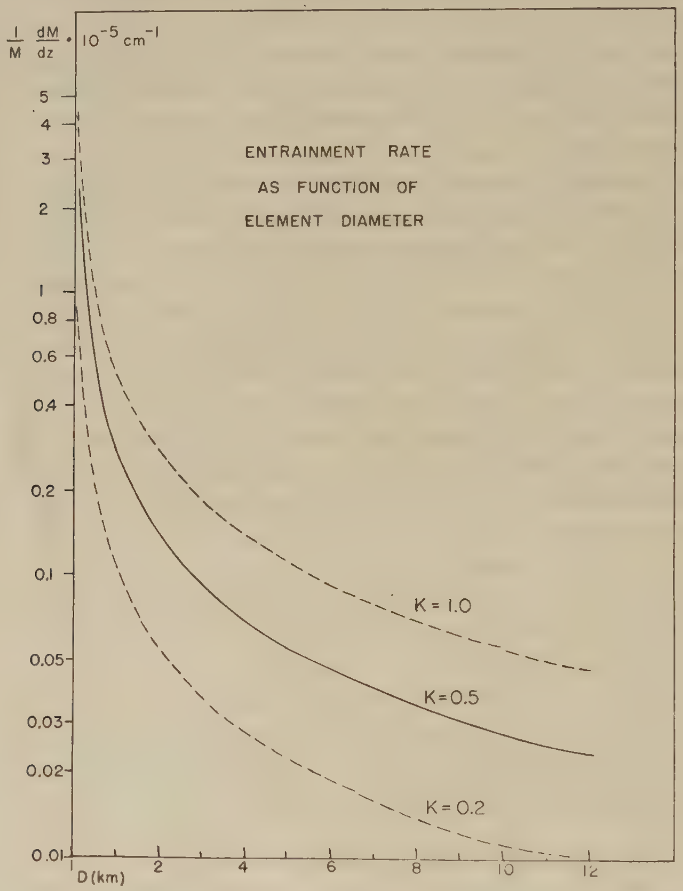

Fig. 2—Graph of entrainment rate $1/M\, dM/dz$ (as defined by Stommel[16]) as a function of element diameter. Curves calculated from eq. (2). Note that abscissa varies by three orders of magnitude for cloud sizes 100 m–10 km. Entrainment rates $\leqslant 0.1 \times 10^{-5}$ cm^{-1} lead to insignificant dilution of clouds under saturated conditions, while entrainment rates $\leqslant 0.05 \times 10^{-5}$ lead to insignificant dilution even under fairly dry conditions.

or dilution rate compared to the effects of element size, observable ranges in which $1/M\, dM/dz$ change by three orders of magnitude.

When $K = 0.5$, the element exchanges a mass equal to its own in one cycle, or just less than two diameters ascent. Since it thus displaces about twice its own mass, one half of which moves through the element rather than around it (this acceleration of outside mass is regarded as the origin of form drag), a C_D of about $1/2 \times 9/8$ or 0.563

is consistent with $K = 0.5$. Thus this combination was used throughout the calculations to follow. We plan additional tests of the sensitivity of the results to the choice of parameters.

Figure 2 shows that for bubbles 500 m across (trade cumulus size) the entrainment rates are of the order $0.5 - 1.0 \times 10^{-5}$ cm ^{1}, or in the range measured by Stommel[16] and Malkus[8] in trade cumuli, while for elements 5 km across (thunderstorm size) the entrainment rate is $0.05 - 0.1 \times 10^{-5}$ cm^{-1} comparable to that determined by Byers and Hull[2] for cumulonimbi. The theoretical result is borne out by the Imperial College experiments, which showed that all bubbles expanded along a similar cone, with the same aperture angle. It is also borne out by meteorological experience; we finally gain real insight into the qualitative idea of "protected cores". Cores of large towers are protected from dilution because the element rises through a great vertical distance before turning inside out and exposing its interior to exchange with the dry environment. The idea of "critical dimension" is confirmed: to achieve a given penetration, the element must retain buoyancy all or almost all the way; the point at which buoyancy is exhausted is prescribed by size under given external conditions. That the problem of penetrative cumulonimbus reduces almost entirely to one of element size is demonstrated even more cogently in the following sections.

AN APPLICATION OF THE MODEL TO HURRICANE CUMULONIMBUS TOWERS

A spectacular and well documented case of extraordinary cumulonimbus development occurred in the inner rain area and eye wall of Hurricane Daisy on 27 August 1958. The tallest towers were found by radar measurements* to have achieved heights of not less than 60,000 ft, almost certainly above the tropopause. Aircraft temperature, humidity and photographic observations generously furnished by the National Hurricane Research Project of the U.S. Weather Bureau provide sufficient information for a quantitative test of the cumulonimbus model.

The calculations undertaken here for the environment conditions of the inner rain area of Hurricane Daisy were identical in procedure to those carried out for the Anegada and Wake Island cases described by Levine, and involved step-wise numerical integration of eq. (1). The environment temperature sounding used is shown on a tephigram in Fig. 3, along with mean tropical (after Jordan[3]) and a moist adiabat (dashed) allowing 1°C excess virtual temperature at cloud base. Below 238 mb, the hurricane sounding was reconstructed from the N.H.R.P. aircraft measurements. Above that, it was extrapolated upward in a manner consistent with hydrostatic requirements, although the exact height of the tropopause in the hurricane core is unknown. The height of 98 mb (16.8 km = 55,000 ft) shown in Fig. 3 is probably an upper limit, however, since radiosondes in the storm outskirts showed it at 14.8 km. Nor is the lapse rate in the tropopause layer known, and three possibilities have been considered, although the most stable is the most probable, if stratospheric temperatures are to return to mean tropical in a reasonable interval.

Comparing the tropospheric portion of this Daisy sounding with those for Anegada and Wake Island used for the penetrative tower calculations by Levine, we immediately see that the maximum available buoyancy (maximum parcel temperature excess ~ 3°C) is far less than in his cases, and yet in Daisy cumulonimbi reached beyond the tropopause, while they failed to do so by 2–4 km in the situations he studied. Wherein lies the difference? The only freedom of input parameters we are allowed, besides element sizes, are C_D, K, buoyancy and vertical motion at cloud base, and degree of saturation of the environment: spatial variations from 60–100 per cent relative humidity seem to be common aloft even in hurricane cores.

---

* Reported verbally to the author by Dr. C. L. Jordan of Florida State University.

The procedure was to divide the sounding, as shown in Fig. 3, into five intervals of approximately linear vertical variation of the difference between moist adiabatic and environment temperature, and integrate Levine's equations stepwise over these intervals under various combinations of initial and environment conditions. This procedure clearly involves smoothing of the sounding in addition to that already employed by constructing it from only three levels of aircraft measurement. Thus, any irregularities or fluctuations in rate of rise of elements are bound to be lost. Our purpose here is, however, only to predict relations between heights achieved, element size, buoyancy and rate of rise. These are to be tested, where possible, by observation and we are not presently interested in the details of the ascent. That the overall environment lapse rates of Fig. 3 are realistic for hurricane conditions, however, we are reassured by comparison with the mean hurricane rain area radiosondes of Schacht[14] and the few hurricane rain area dropsondes which are available and on file at the National Hurricane Research Project headquarters. The element diameter was chosen at cloud base and allowed to expand with decreasing pressure so that the mass inside remained constant. Table 2 gives the ratio of the diameter in each interval to that in the lowest, namely 960 mb (cloud base) to 600 mb.

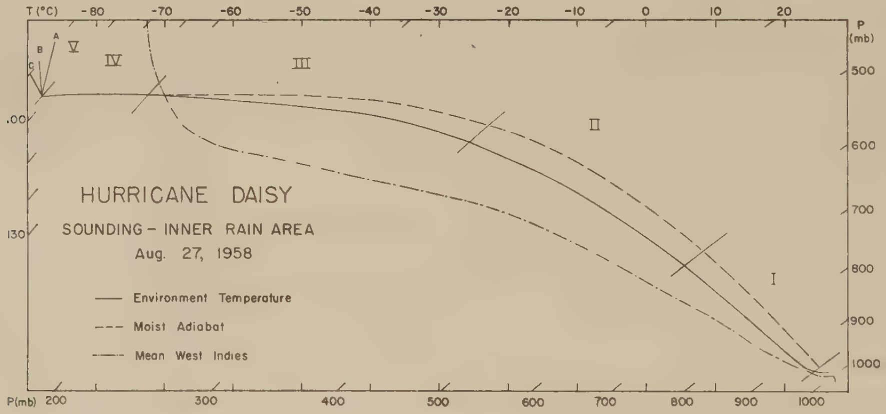

Fig. 3—Tephigram showing sounding constructed for Daisy inner rain area ($r \sim 30$ km) 27 August 1958, using N.H.R.P. aircraft data and hydrostatic considerations. Dashed curve is moist adiabat rising with $\Delta\theta = 1$°C at cloud base; dash-dotted curve is the mean West Indies sounding for August (after Jordan[3]). The lapse rate in the stratosphere was unknown, so A, B, and C were considered. Roman numerals indicate the regions, used for computation, where the difference between the temperature along the adiabat and that along the sounding changed linearly with height. The eye wall sounding ($r \sim 10$ km) was warmer throughout but the stability structure, which is the feature relevant for the cloud calculation, apparently was quite similar, and appears to vary little under hurricane conditions.

Table 2. *Tower Diameter at Upper Levels Relative to that in Lowest Interval*

	Height interval (m)	Pressure interval (mb)	Ratio of diameters (to interval I)
I	210–4210	960–600	1
II	4210–9610	600–300	1.2
III	9610–15,210	300–130	1.4
IV	15,210–16,810	130–98	1.7
V	16,810–17,310	98–90	1.7

Table 3. *Cloud Towers in Hurricane Daisy—Inner Rain Area*, 27 *August* 1958

Saturated Environment

$C_D = 0.563$ $K = 0.5$ Cloud base 210 m θ_E (Ave. Subcloud) 359°A

Element radius (960–600 mb)	Top height	Rise rate W_{max}	Rise rate Level	Rise rate at tropopause	$\Delta\theta$ at 4.2 km	Zero $\Delta\theta$ Level	Zero $\Delta\theta$ θ_E	Overshoot $\Delta\theta$	Overshoot Δz	θ_E Cld. base
(km)	(km)	(m/sec)	(km)	(m/sec)	(°C)	(km)	(°A)	(°C)	(m)	(°A)
0.125	7.8	2.2	1.2	—	0.44	7.8	354.3	0	0	361.5
0.25	10.2	3.8	1.2–4.2	—	0.90	9.7	356.4	− 0.35	500	361.5
0.50	11.1	7.0	5.0	—	1.53	10.5	358	− 0.40	600	361.5
1.0	13.3	11.4	5.4	—	2.10	11.7	359	− 0.80	1600	361.5
2.0	15.6	17.1	8.0	—	2.50	13.0	360	− 1.10	2600	361.5
3.0	17.1	21.2	9.6	8.9	2.65	13.7	360.5	− 8.5	3400	361.5
3.0*	17.3	23.0	9.6	12.2	3.07	14.2	361	− 12.5	3100	362

* $\Delta\theta_b$ for this element = 1.5°C; all remaining had $\Delta\theta_b$ = 1°C.

Table 4. *Cloud Towers in Hurricane Daisy—Inner Rain Area*, 27 *August* 1958

Environment relative humidity 70% above 4.2 km

$C_D = 0.563$ $K = 0.5$ Cloud base 210 m θ_E (Ave. subcloud) 359°A

Element radius (960–600 mb)	Top height	Reduction of top height cf. Sat. env.	Zero $\Delta\theta$ Level	Zero $\Delta\theta$ θ_E	Reduction Zero $\Delta\theta$ Level	Reduction Zero $\Delta\theta$ θ_E	Overshoot $\Delta\theta$	Overshoot Δz	Change in overshoot
(km)	(km)	(km)	(km)	(°A)	(km)	(°A)	(°C)	(m)	(m)
0.125	4.5	3.3	4.4	353.3	3.4	1.0	− 0.25	100	+ 100
0.25	5.1	5.1	4.8	353.6	4.9	2.8	− 0.30	300	− 200
0.50	7.0	4.1	6.5	354.1	4.0	3.9	− 0.30	500	− 100
1.0	11.5	1.8	10.1	357.5	1.6	1.5	− 0.75	1400	− 200
2.0	14.4	1.2	12.1	359.4	0.9	0.6	− 1.10	2300	− 300
3.0	17.0	0.1	13.0	360	0.7	0.5	− 4.2	4000	+ 600

$\Delta\theta_b$ = 1°C for all elements.

The examples calculated, conditions and results are summarized in Tables 3 and 4 and Figs. 4–7. The choice of parameters and initial and environmental conditions may be commented on as follows: (1) The constants C_D and K were taken to be 0.563 and 0.5 respectively throughout the calculation. Halving them or doubling them both gave rise to results in obvious and qualitative disagreement with observations, the former

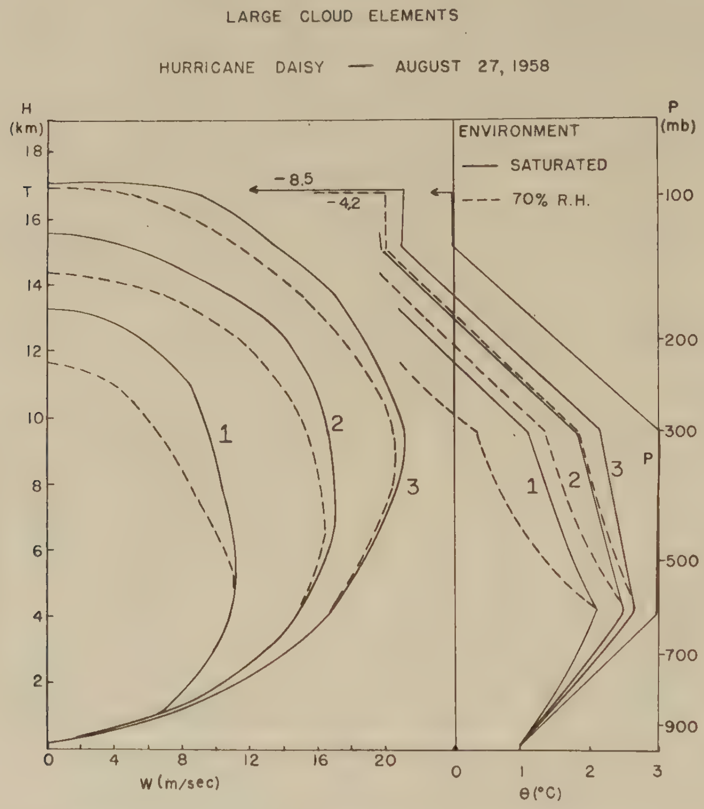

Fig. 4—Vertical ascent rates (W) and virtual potential temperature anomalies ($\Delta\theta$, proportional to buoyancy) as a function of height (H) and pressure (p) for small cloud elements, under conditions of Hurricane Daisy, 27 August 1958. The numbers written by each curve are element radii a in the lowest interval I (960–600 mb). Thus the curve labelled 1 shows 2 km diameter elements at their outset, which grow to be 3.4 km in diameter at the tropopause, etc. The $\Delta\theta$ curve labelled P stands for the undiluted parcel ascent with $\Delta\theta = 1°C$ at cloud base (960 mb). Dashed alterations to each curve above 4.2 km shows effect of reduction of outside relative humidity to 70 per cent.

permitting clouds of 2 km diameter (960–600 mb) to penetrate the tropopause and the latter permitting no clouds of diameter less than 10 km to reach the tropopause. Preliminary photogrammetric measurements from the aircraft nose camera films show that the clouds reaching 50,000 ft or thereabouts had diameters in the neighborhood of 7 km. Thus the dilution and drag parameters have been restricted within a factor of about two: further comparison of photographic and temperature measurements with these calculations may set closer limits. (2) The calculation was arbitrarily terminated at that level where the ascent rate W was first reduced to zero and this level was defined (Tables 3 and 4) as the "top height" of the tower. Since, almost without exception, the elements exhibited a negative virtual potential temperature anomaly relative to the environment sounding (negative buoyancy) at that level, had the calculation been continued thereafter they would have descended and perhaps oscillated subsequently.

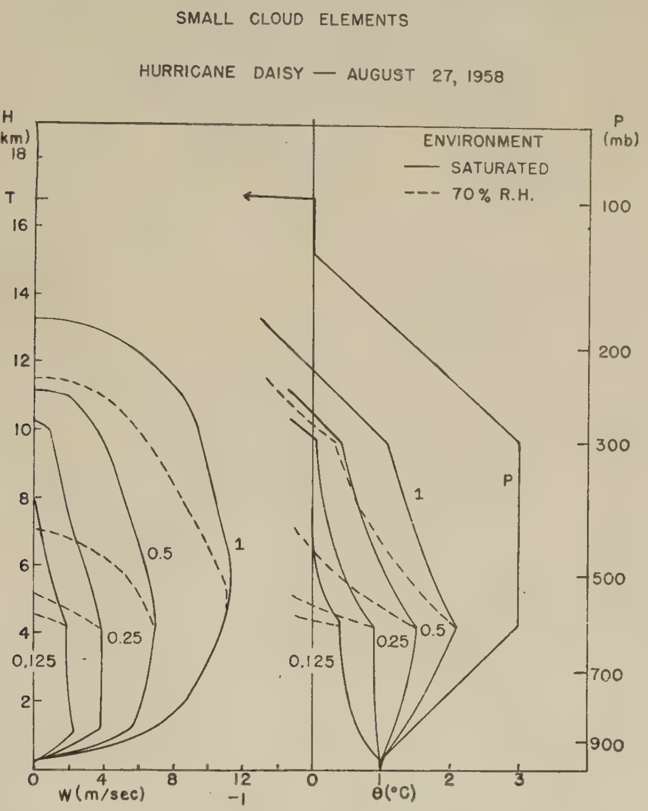
SMALL CLOUD ELEMENTS

HURRICANE DAISY — AUGUST 27, 1958

Fig. 5—Graph similar to Fig. 4 for large cloud elements. Only the 3 km radius element overshoots the tropopause (with diameter 10.1 km at that level). The extreme negative values of $\Delta\theta$ could not be plotted in the stratospheric portion but are indicated by the − 8.5 (degrees) for the saturated and − 4.2 (degrees) for the unsaturated case. Note the much weaker effect of the drier environment on the large elements.

Although there is some doubt about the applicability of the bubble-like vortex mode beyond the point where W first goes to zero, the form of the differential equation (1) is probably still valid and tests can be made to determine the period and amplitude of such oscillation, if present. It should be pointed out here that we have not attempted so far to describe the growth of a whole cumulonimbus cloud, which may be achieved by an intermittent succession of such pulsating towers, but are merely trying to obtain a relation between size and maximum height penetrated of each individual element which becomes visible as a single tower on emerging from the cloud body. (3) For all calculations shown W_b (W at cloud base) was zero. Other test calculations showed that varying the cloud base value of W within $\pm$ 2 m/sec had little or no effect on cumulus development and the elements had "forgotten" their initial W within a few kilometers, resembling exactly the similar cases where $W_b = 0$. The choice of $\Delta\theta_b$ (proportional to buoyancy at cloud base), however, was more critical. For all calculations except the last in Table 3, $\Delta\theta_b$ was chosen as 1°C, in agreement with numerous observations that virtual temperature excess within the bases of tropical clouds is in this neighborhood; $\Delta\theta_b = 1.5$°C was considered to be an upper limit. We shall see that large towers have no difficulty in reaching the tropopause if $\Delta\theta_b \gg 1$°C, while overshooting is little enhanced if it is larger. (4) Two environmental moisture distributions have been considered so far, namely that of Table 3 which presents elements rising in saturated surroundings and that of Table 4 where the only alteration has been to reduce the environment relative humidity to 70 per cent at and above 600 mb (4.2 km).

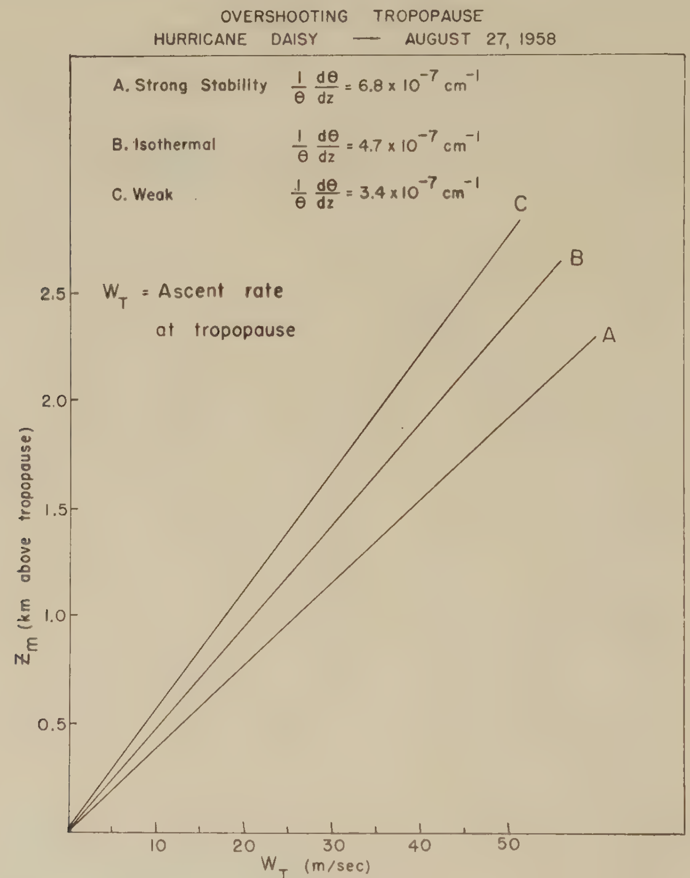

Fig. 6—Amount of tropopause overshooting (Z_m) as a function of rise rate at tropopause (W_T) for the different stratospheric stabilities shown in Fig. 3. Regardless of wide variations in the latter, ~ 20 m/sec per km overshoot is required.

The calculation (see especially Figs. 4 and 5) shows clearly that reducing the humidity of the cloud environment is disastrously inhibiting to the small cloud elements and increasingly less effective as element size becomes larger, obviously because the large elements rise so much farther on each internal cycle and thus are far less dilute at their upper levels. The column labelled "Zero $\Delta\theta$" in Tables 3 and 4 gives the level of zero buoyancy of each element and the equivalent potential temperature, θ_E (proportional to total energy), at that level. The amount of dilution is readily seen by comparing this value of θ_E with that at cloud base level, given in the last column of Table 3 (it was 361.5°A for all elements in Table 4). The large elements penetrate the layer between 200–100 mb with relatively little dilution and with total energy content comparable to or exceeding that of average sub-cloud air.

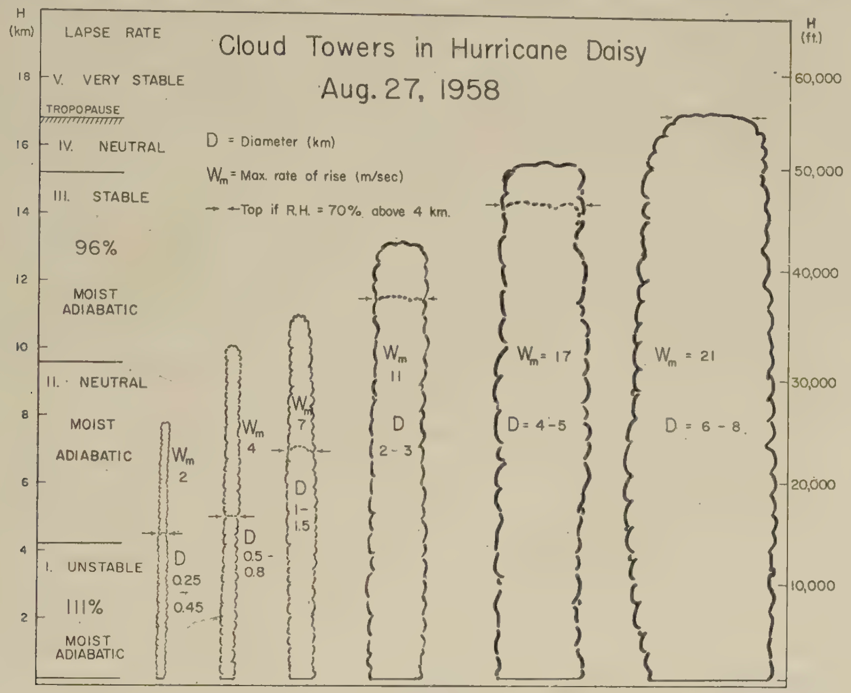
H (km)
LAPSE RATE
Cloud Towers in Hurricane Daisy
Aug. 27, 1958
H (ft.)
18
V. VERY STABLE
TROPOPAUSE
16
IV. NEUTRAL
D = Diameter (km)
W_m = Max. rate of rise (m/sec)
Top if R.H. = 70% above 4 km.
14
III. STABLE
96%
12
MOIST ADIABATIC
10
II. NEUTRAL
8
MOIST ADIABATIC
6
4
I. UNSTABLE
111%
2
MOIST ADIABATIC
W_m 2
D 0.25 - 0.45
W_m 4
D 0.5 - 0.8
W_m 7
D 1 - 1.5
W_m 11
D 2 - 3
W_m = 17
D = 4 - 5
W_m = 21
D = 6 - 8
60,000
50,000
40,000
30,000
20,000
10,000

Fig. 7—Schematic presentation of cloud penetration as function of horizontal dimension in core of Hurricane Daisy, 27 August 1958. W_m stands for maximum rise rate in m/sec. D is diameter in km, range being due to expansion with height. Arrows and dashed tops show reduction resulting from decreasing environment relative humidity from saturation to 70 per cent above 4.2 km. The lapse rate in the various layers is indicated at the extreme left.

The calculation further illustrates that for a given element size, reduction in environment humidity is most effective at low levels and increasingly less inhibitory the higher up it sets in, being totally negligible above 300 mb. The reason is clearly that the difference in mixing ratio between saturation and lower relative humidities is extremely large in low levels and becomes vanishingly small aloft as the saturation mixing ratio diminishes. Entrainment of drier air is thus only severely restrictive to penetrative cloud growth in the low troposphere; elements which survive this portion may easily continue growing to great heights. We plan further calculations to test the effect of greater humidity reduction at still lower levels: the selectivity toward large elements may be expected to be still more pronounced.

Overshooting the Tropopause

Consideration of the terms on the right in eq. (1) shows that in the tropopause layer (interval V, Fig. 3, 98–90 mb) all terms may be neglected compared to the buoyancy, which is very large and negative. Furthermore, all elements large enough to penetrate this layer dilute so slowly that their ascent curve may be regarded as adiabatic, and thus eq. (1) may be integrated directly. Figure 6 shows the results, giving the amount of penetration into the stratosphere as a function of W_T, the ascent rate at the tropopause. Considerable variation in the static stability of the layer is seen to affect the penetration very little, and thus it is not serious that we are unable to specify the lapse rate there. For cloud towers to reach 17.3 km ($\sim$ 57,000 ft), the highest of any of those computed here, ascent rates W_T at the tropopause must be in the vicinity of 10 m/sec, which implies a maximum ascent rate (at 9.6 km) of about 21 m/sec. This conclusion is relatively independent of any of the particular assumptions of this model, and has been worked out earlier by Vonnegut and Moore[17] who also showed that for every km penetration into the stratosphere, a W_T of 20 m/sec is required. As they so cogently argue further, the very existence of radar echoes above the tropopause demonstrates rather conclusively that ascent rates of these magnitudes are present.

As pointed out earlier, since in the model the maximum updraft is 2.5 times the ascent rate of the element, we are implying that updraughts of 50 m/sec existed in the eye wall of Hurricane Daisy (the only portion of the storm where radar echoes penetrated well above 50,000 ft or into the stratosphere). Since this figure is even on the high side for middle latitude thunderstorms (Byers and Braham[1]), it might be regarded by some as preposterous. To dismiss it as such, however, would imply either, (a) the tropopause was lifted to 18 km in Daisy's core, or, (b) the radar evidence is totally wrong. Fortunately some reports from reconnaissance pilots* indirectly confirm these figures. On one occasion in the eye wall of Typhoon Ophelia (15 January 1958) a B-50 rose at 22 m/sec while diving with full power; the pilot estimated the draught speed as 40–50 m/sec. On another occasion in an eye wall a reconnaissance plane descended at this rate, while endeavoring to climb. Clearly with high flying aircraft now available an attempt to determine the exact amount of tropopause overshooting should be made, as it is a simple and infallible way of ascertaining whether vertical velocities of this magnitude do, in fact, exist and under what conditions.

We note that, in contrast with earlier bubble concepts (Malkus and Scorer[9]), this model permits an element to overshoot its level of zero buoyancy. Towers are found still rising with negative $\Delta\theta$ (virtual potential temperature anomaly relative to environment) up to $-12.5°$C, in an extreme case of a 3 km radius element penetrating the stratosphere (last element, Table 3). All the large elements, however (Fig. 5), showed considerable overshooting, while decreasing the element size (Fig. 4) or drying the environment (dashed lines, Figs. 4–5) reduced it. Some observational evidence exists (Wexler and Malkus[18]) of overshooting, particularly in rather large cumuli in disturbed (unusually moist) situations.

---

* Verbal reports to Mr. R. C. Gentry, Director of the National Hurricane Research Project.

COMPARISON WITH OBSERVATIONS

Among the many possible types of observational tests to which the foregoing calculations might be subjected, only one has been completed to date, namely a test of the size versus height penetrated relationship using the N.H.R.P. aircraft nose camera motion picture photographs. The results of this test are shown in Fig. 8. The solid curve is plotted from the first two columns of Table 3, giving the top height versus radius (diameter shown in Fig. 8, values at cloud base) when the environment is saturated; the dashed curve gives the relationship when the environment relative humidity is reduced to 70 per cent above 4.2 km. The X's show diameter (corrected to cloud base) versus height attained for nine towers measured from the upper level ($\sim$ 37,000 ft) aircraft nose camera film for 27 August 1958. Only those towers were chosen which showed rounded tops and were apparently just terminating their active rise period when sighted. The measurements were made by a method described elsewhere in detail by Ronne[13]. The base of the largest clouds generally could not be seen and their tops relative to flight level were measured; although this may be in error by 20 per cent (despite knowledge of camera tilt) the absolute heights are thereby correct within about 3000 ft or 1 km.

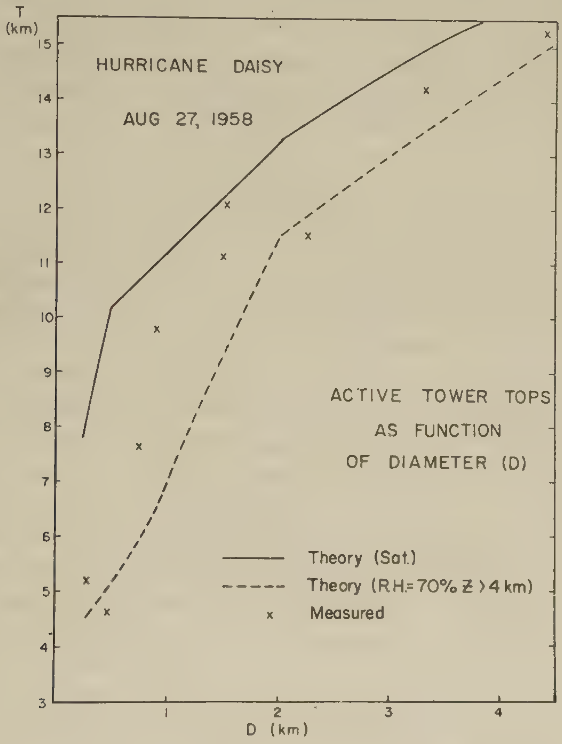

Fig. 8—Comparison of theory and measurement on relation between tower diameter and maximum height penetrated. Solid theoretical curve constructed from first two columns of Table 3; dashed curve constructed from first two columns of Table 4. Measured values (crosses) obtained from aircraft nose camera films as described in text and by Ronne[13].

Smaller clouds with visible bases were measured in total thickness as well as relative to flight level, and 1 km accuracy in top height is applicable also to them. Clearly the variations in environment humidity, assumption in the theory of constant mass (expanding diameter according to Table 2) and difficulty in determining whether a given tower had truly reached its maximum level are far more serious shortcomings than this uncertainty in measurement. The real significance of the results in Fig. 8 is the general correlation between height and horizontal size, which is both real and a valid test of the basic idea of the model. It is possible also to see in the distribution of crosses in Fig. 8 a break from strong to weaker upward slope between $D = 1$–2 km similar to both calculated curves. Naturally we plan many other tests of this model in hurricane and other contexts; it is hoped also to use the N.H.R.P. aircraft temperature records to investigate whether a relationship is obtained between amplitude and diameter of virtual temperature anomalies.

CONCLUSIONS

The first conclusion is that there seems to be no difficulty in getting penetrative towers to the tropopause in Hurricane Daisy with reasonable sizes, buoyancies, and entrainment rates. The draught speeds for even small penetration into the tropopause layer are high, but the model calculation gives these for towers in the size range photographed; furthermore, indirect radar and pilot evidence supports the suggestion that updraughts 40–50 m/sec may occur in at least some hurricane eye walls. All towers with initial (960–600 mb) diameters from 4–6 km reached 200 mb or higher (even with environment humidity below saturation) with a heat energy content θ_E equal to or larger than that of the subcloud layer. These were thus so nearly undiluted that the "undiluted hot tower" concept need not be rejected. It therefore appears that a confirmatory link has been added to the evidence that penetrative cumulonimbi play a significant role in maintaining the mass and heat budgets of the storm, and pump air of the required warmth to great heights.

Another important conclusion, however, is that the "hot" towers need not, in fact cannot, be very hot since the classical parcel, which gives approximately the upper limit of buoyancy, has a maximum $\Delta\theta$ of 3°C, if it began with $\Delta\theta_b$ of 1°C. The extreme element computed here (last in Table 3) with $\Delta\theta_b$ of 1.5°C just barely reached a maximum $\Delta\theta$ of 3.07°C, while most element virtual temperature anomalies are less than 2.5°C higher than the surroundings. Negative anomalies due to overshooting do not exceed 1°C except in the stratosphere.

Therefore it is not disappointing, as was first thought, but absolutely inevitable that no regions of very pronounced temperature excess were found on the N.H.R.P. aircraft temperature records. Since the surroundings of the clouds were near saturation, cooling by evaporation in downdraughts can lead to cold regions only 2–3°C in amplitude and thus total temperature variations locally should not exceed 5°C and are probably less.

As Riehl* pointed out, this also explains the relative lack of turbulence in hurricane rain areas, since evaporation to maintain strong downdraughts in the near vicinity of updraughts is inhibited by the high humidity. Quite a different situation was found by Levine in the Anegada and Wake Island towers which rose through a much less stable and drier environment. Here parcel buoyancies up to 6–10°C were found and hot towers having maximum $\Delta\theta$'s of 5–6°C predicted. Clearly these are the situations where intense turbulence in the vicinity of cumulonimbi should be forecast, since evaporation could give rise to violent downdraughts in close vicinity to the updraughts with possibly disastrous consequences to aircraft.

---

* Personal conversation.

Finally, we must consider, although we cannot draw conclusions, the question of "ventilation" and the mid-tropospheric temperature "minimum" (reduction several degrees below wet adiabatic). It appears that a mid-tropospheric temperature minimum is not inhibitory, but on the contrary necessary to penetrative development, since we must have a less stable than wet adiabatic layer of some depth above cloud base. Ventilation by drier air from outside can, however, be severely inhibitory to all but the largest elements and perhaps even to these, if build-ups of smaller predecessors are required to pave the way for them. These matters form the subject of further studies under hurricane conditions and other situations in the tropics.

The most important result of this work, if valid, is the dominant role played by element size. It appears that the clue to cumulonimbus production lies in the association between convergence and large cloud dimension. What this relation is quantitatively, and wherein lies its physical foundation is the biggest question now faced in convection dynamics and probably in tropical meteorology as a whole.

ACKNOWLEDGMENTS

This work has been carried out under contract with the National Hurricane Project of the U.S. Weather Bureau and with the help of a grant from the National Science Foundation.

The writer also wishes to acknowledge with gratitude the contribution of Mr. Joseph Levine upon whose work much of this endeavor is based, and that of the Director and Staff of the National Hurricane Research Project, who have generously supplied data, support, experience and encouragement at all stages.

The manuscript and drawings were ably prepared by Mrs. Mary C. Thayer and Miss Margaret Chaffee.

REFERENCES

1. H. R. Byers and R. R. Braham. *The Thunderstorm.* Govt. Printing Office, Washington, D.C. 287 pp. (1949).
2. H. R. Byers and E. C. Hull. Inflow patterns of thunderstorms as shown by winds aloft. *Bull. Amer. met. Soc.*, **30**, 90–96 (1949).
3. C. L. Jordan. *A Mean Atmosphere for the West Indies Area.* No. 6, National Hurricane Project Preprint Series (1957).
4. M. Koldovsky. Photographic observation of the development of a thunderstorm cloud. *Studia Geoph. et Geod.*, **3**, 93–97 (1959).
5. J. Levine. Spherical vortex theory of bubble-like motion in cumulus clouds. Manuscript accepted for publication in *J. Met.* Ref. No. 58–47 Woods Hole Oceanographic Institution (1959).
6. J. S. Malkus. Some results of a trade cumulus cloud investigation. *J. Met.*, **11**, 3, 220–237 (1954).
7. J. S. Malkus. *On the Thermal Structure of the Hurricane Core.* Proc. Tech. Conf. on Hurricanes, Miami Beach. D3, 1–2 (1958).
8. J. S. Malkus and C. Ronne. On the structure of some cumulonimbus clouds which penetrated the high tropical troposphere. *Tellus*, **6**, 351–366 (1954).
9. J. S. Malkus and R. S. Scorer. The erosion of cumulus towers. *J. Met.*, **12**, 43–57 (1955).

10. J. S. MALKUS and G. WITT. On the evolution of a connective element: a numerical experiment. Manuscript accepted for publication in Rossby Memorial Vol. (1959).
11. H. RIEHL. *Subtropical Flow Patterns in Summer.* Misc. Rep. No. 22 of the Univ. of Chicago. 64 pp. (1947).
12. H. RIEHL, W. S. GRAY, J. S. MALKUS and C. RONNE. *Cloud Structure and Distributions over the Tropical Pacific,* Part I. Unpublished report. W.H.O.I. Ref. No. 58–62 (1959).
13. C. RONNE. On a method of cloud measurements from aircraft motion pictures. Unpublished manuscript to be issued as Technical Report of the Woods Hole Oceanographic Institution (1959).
14. E. SCHACHT. A mean hurricane sounding for the Caribbean area. *Bull. Amer. met. Soc.,* **27,** 324–327 (1946).
15. R. S. SCORER and C. RONNE. Experiments with convection bubbles. *Weather,* **11,** 151–154 (1956).
16. H. STOMMEL. Entrainment of air into a cumulus cloud. *J. Met.,* **8,** 127–129 (1947).
17. B. VONNEGUT and C. B. MOORE. Giant electrical storms. Unpublished manuscript on file at the A.D. Little Co. (1958).
18. R. WEXLER and J. S. MALKUS. Observational Studies of Tropical Clouds: Results of 1956 Caribbean Aircraft Expedition. Unpublished report. W.H.O.I. Ref. No. 58–46 (1958).
19. B. WOODWARD. Penetrative convection in the sub-cloud régime. This Volume, p. 28 (1960).

Contribution No. 1046

Deep-Sea Research, 1960, Vol. 6, pp. 239 to 244. Pergamon Press Ltd., London. Printed in Great Britain

INSTRUMENTAL NOTE

The contouring temperature recorder

WILLIAM S. RICHARDSON and CHARLES J. HUBBARD

(*Received* 29 *April* 1959)

(1) INTRODUCTION

THE bathythermograph (BT) has been the standard instrument for the study of the thermal structure of the upper layers of the ocean for roughly 25 years. This very useful instrument provides a trace of temperature against depth (to either 450 or 900 ft, depending upon the type used) while the ship is under way. For some purposes this trace is the end result of the experiment, but to study the variations of structure in the horizontal, one commonly reads the BT traces, picks off the depths of various temperatures, and plots these on a curve of depth versus distance. The isotherms are then contoured and the resulting distribution is used as the data from which the physical processes are inferred. It is possible on a very arduous schedule to obtain BT's about every five minutes, but on most trips one is taken every hour or more. This provides sufficient data for many problems, and it may be easily supplemented by continuous surface temperature records to provide an indication of the location of some of the pronounced differences which often occur from one BT to the next. For many purposes the BT data even at its most rapid rate of acquisition is not sufficient; problems in sound transmission, internal waves and microstructure are examples.

The Contouring Temperature Recorder to be described in this paper is a device which takes data from temperature sensors (thermistors) located in a chain towed behind a ship and plots on a continuous record the vertical distribution of isotherms. The thermistors are electronically scanned in sequence from the top to the bottom of the chain, in a time interval adjustable from 2 to 20 secs. If it is desired to do so, the scan rate can be adjusted in relation to the speed of the ship so that the information is taken from a vertical column in the water. In the design to be described, the 1° isotherms from $-2°$ to 32°C can be contoured along with all 0·1° and 0·05°C isotherms between these limits. Also, selection can be made so only the 1°, the 0·1° (which of course include the 1°), or the 0·05°C are contoured. It is possible to accentuate the 1°C isotherms with respect to the others to aid in their identification. Provision is made for determining the depth of the tow (which is a function of ship's speed) and also for selecting the fastest possible scan rate consistent with the complexity of the water column. A straightforward method of isotherm identification is provided; this can be quite a difficult problem if there are many inversions within the water column.

(2) THE HOIST AND CHAIN–MOUNTING OF THERMISTORS AND DEPTH METER

The chain on which the thermistors are mounted is manufactured by Commercial Engineering Company, of Houston, Texas, (Fig. 1). The hoist is diesel-hydraulic powered and carries six hundred feet of chain. The chain consists of links about eleven inches long having a U-shaped cross section in the hotizontal plane. A rubber boot is contained inside the links into which a multi conductor electrical harness can be fitted. The rear portion of each link is then closed with a plastic fairing which holds the wire securely in place and completes the streamlining of the link. A 3400 lb ' fish ' is used on the end of the chain; the design of the hoist includes a simple means of launching and retrieving the fish.

The towing characteristics of the chain are shown in Fig. 2. The tow is very steady at speeds up to at least 15 knots and is normally used at about 10 knots to provide measurements to about 400 ft.

The electrical harness consists of about 100 leads of A.W.G. 26 hookup wire. This provides two leads to each of 23 thermistors, 3 leads to the depth meter and about 50 spare leads for other uses or repairs. The thermistors are mounted 25 ft apart in holes drilled in the plastic fairings and potted in place with an epoxy resin to insulate the electrical connection from the water. The depth meter, which is a commercial Bourdon type pressure potentiometer with 200 PSI full scale, is mounted in a stainless steel pressure case attached to a fairing 450 ft below the uppermost thermistor.

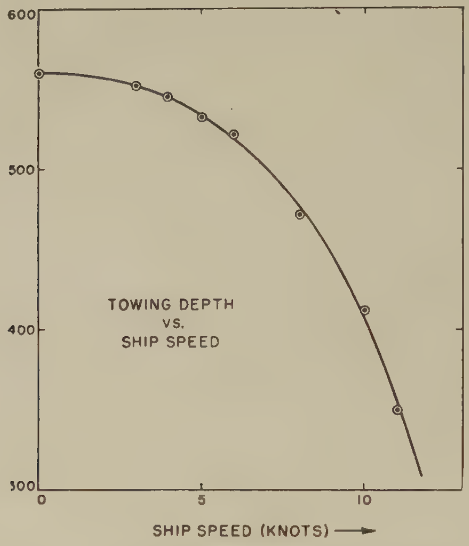

Fig. 2. Towing depth versus ship's speed.

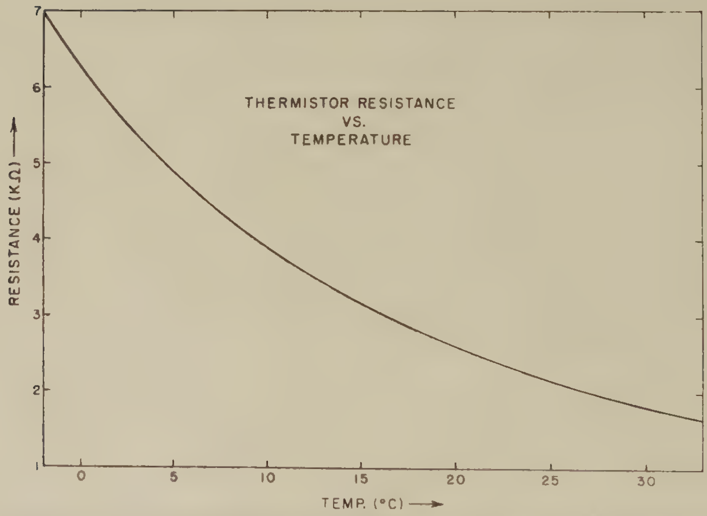

Fig. 3. Typical curve of temperature versus resistance for type 32A1 Thermistor.

(3) THE THERMISTORS

Type 32A1 Thermistors manufactured by Victory Engineering Company, of Union, New Jersey, are used in this equipment. Fig. 3 shows a typical curve of resistance versus temperature for these units. It is necessary that all units used are nearly identical. This condition is met as carefully as possible by procuring a large stock of thermistors from a single bead mix and culling them at a fixed temperature to find a set with the same resistance at this temperature. The set is then checked at

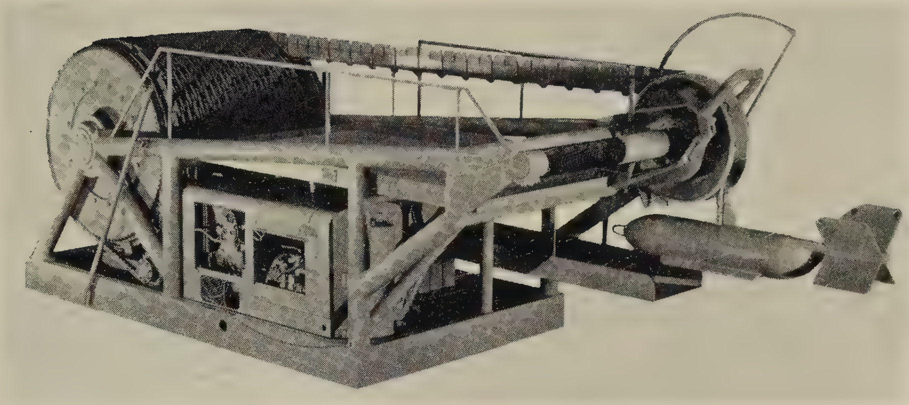

FIG. 1. The hoist with chain installed

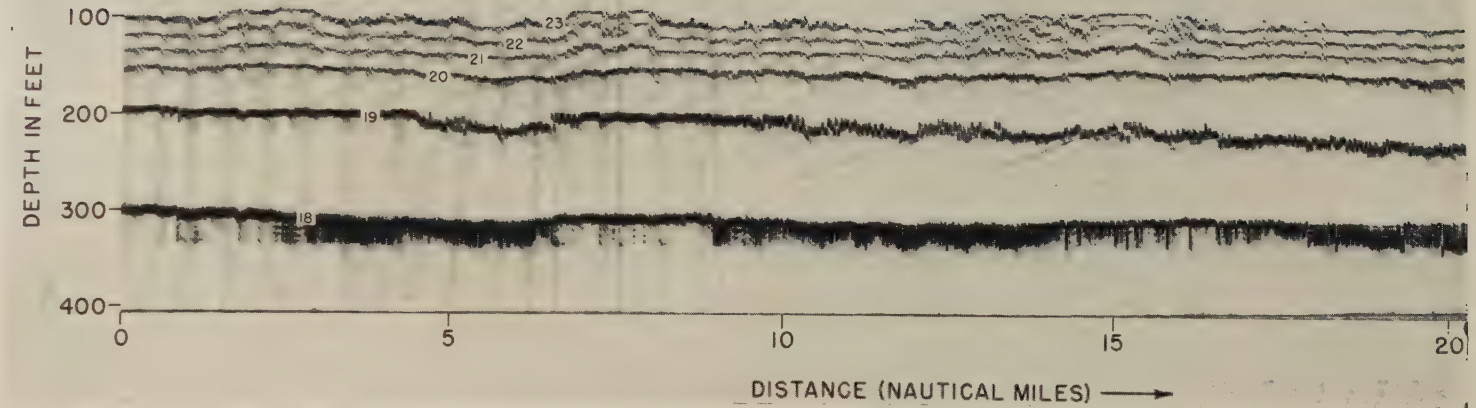

FIG. 7. Vicinity of 39°N 71°W ; 1 October 1958 ; Course 180°T ; Speed 10 knots ; 1°C isotherms.

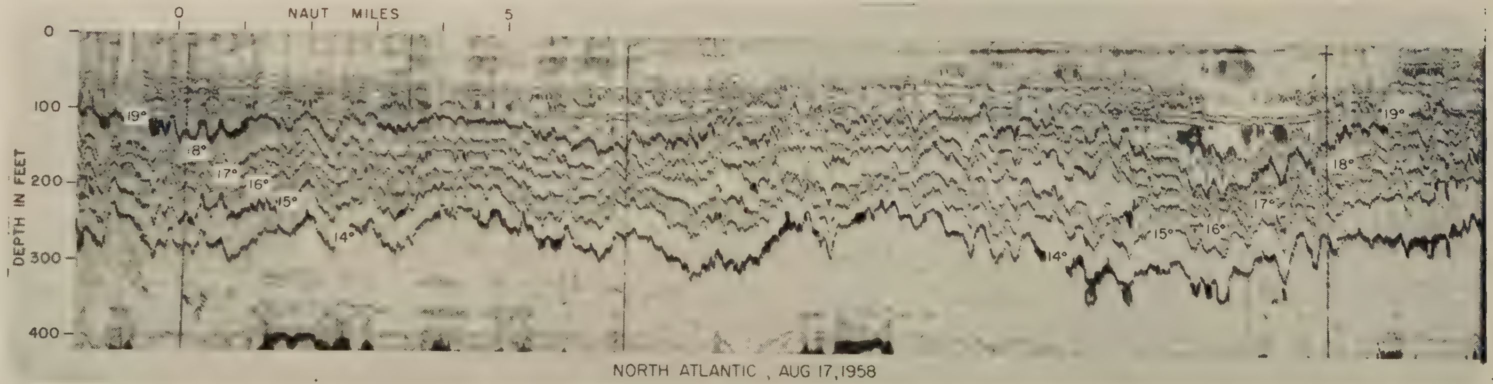

FIG. 8. Vicinity of 39°N 11°W ; 17 August 1958 ; Course 270°T ; Speed 10 knots ; 1°C and 0·1°C isotherms.

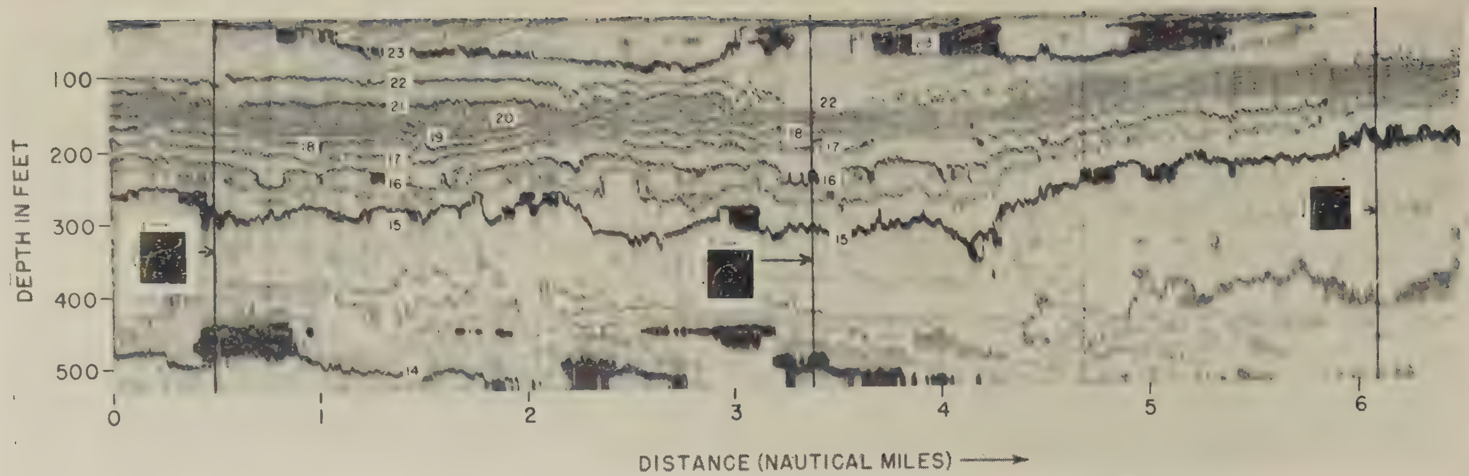

FIG. 9. Vicinity of 6°E 38°N ; 15 July 1958 ; Course 100°T ; Speed 3·3 knots ; 1°C and 0·1 C isotherms.

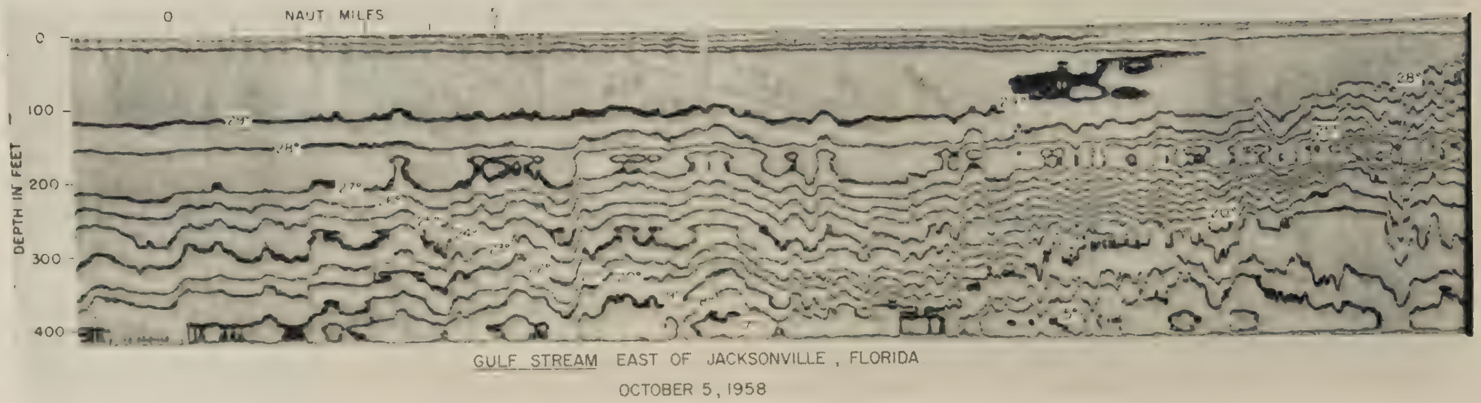
GULF STREAM EAST OF JACKSONVILLE , FLORIDA

OCTOBER 5, 1958

FIG. 10. Vicinity of 30·5°N 81°W ; 5 October 1958 ; Course 270°T ; Speed 10 knots ; 1 C isotherms.

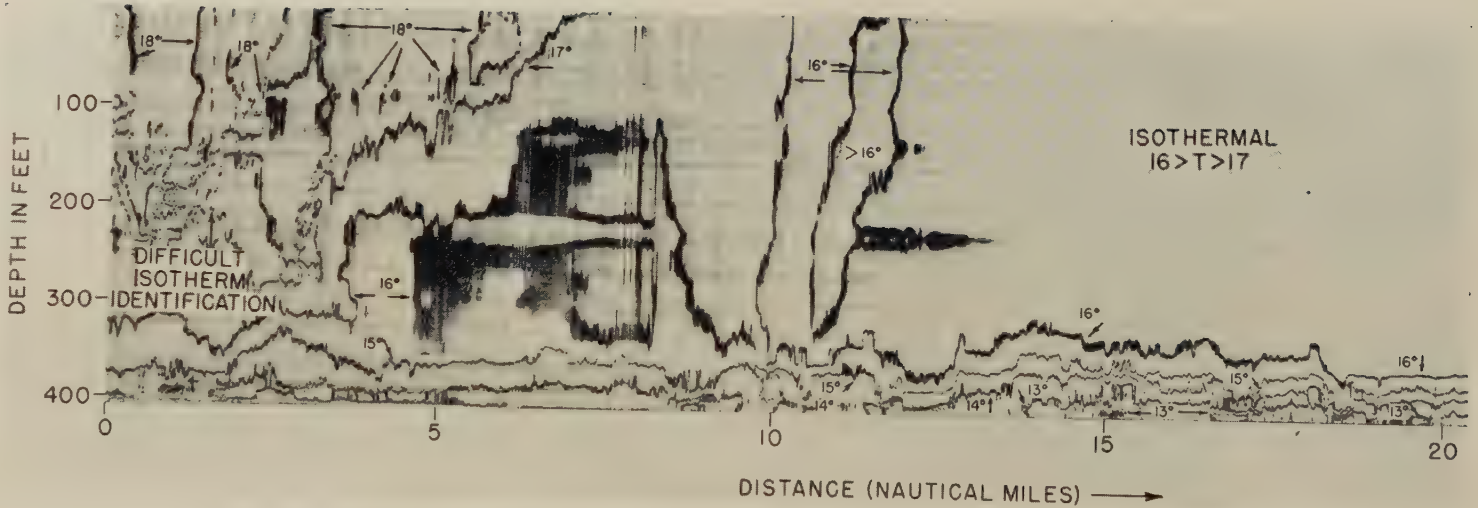

FIG. 11. Vicinity of 37°N 70°W ; 19 December 1958 ; Course 340°T ; Speed 10 knots ; 1°C isotherms.

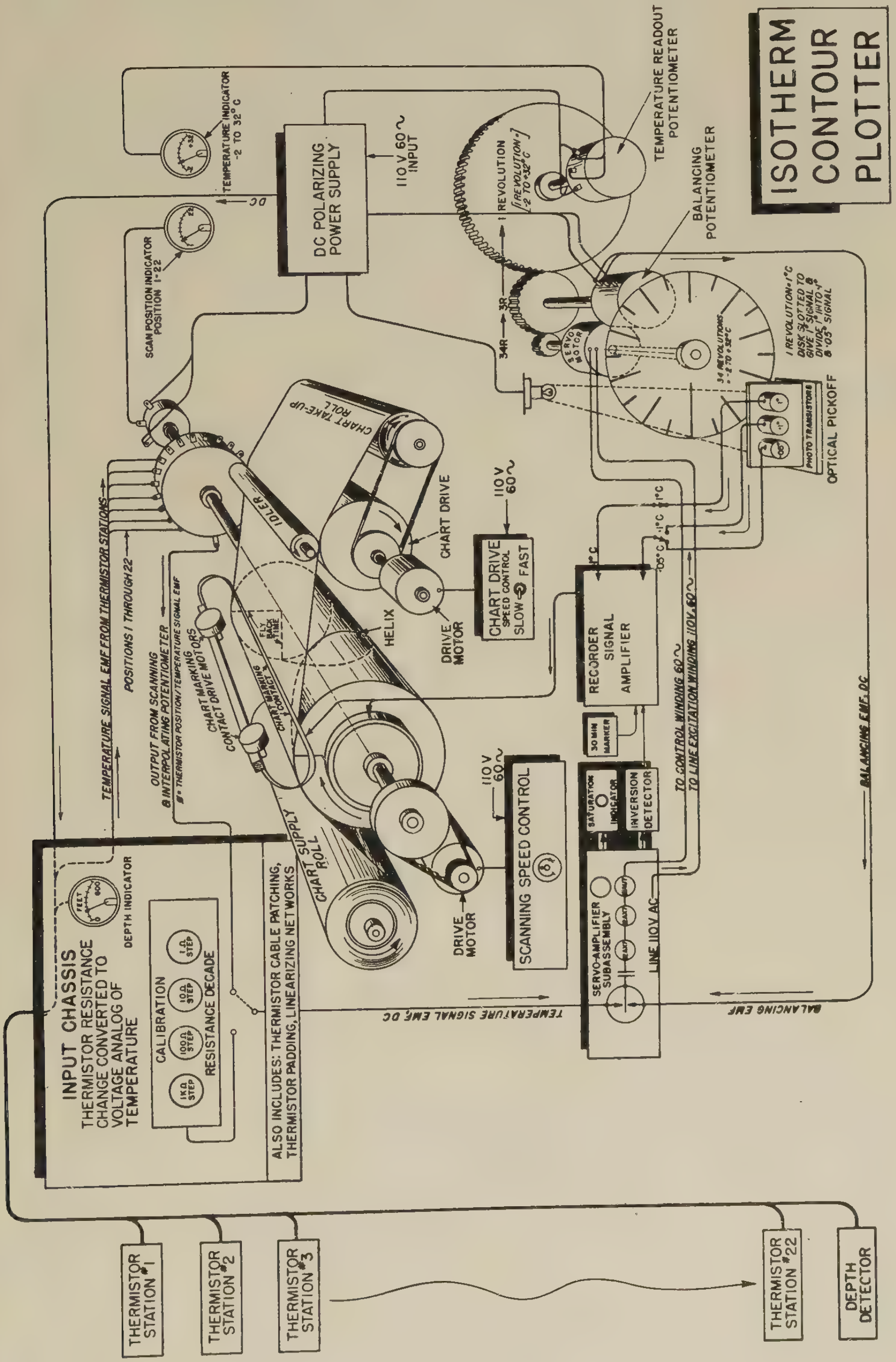
ISOTHERM
CONTOUR
PLOTTER
INPUT CHASSIS
THERMISTOR RESISTANCE CHANGE CONVERTED TO VOLTAGE ANALOG OF TEMPERATURE
DEPTH INDICATOR
FEET
CALIBRATION
1KΩ STEP
100Ω STEP
10Ω STEP
1Ω STEP
RESISTANCE DECADE
ALSO INCLUDES: THERMISTOR CABLE PATCHING, THERMISTOR PADDING, LINEARIZING NETWORKS
THERMISTOR STATION #1
THERMISTOR STATION #2
THERMISTOR STATION #3
THERMISTOR STATION #22
DEPTH DETECTOR
TEMPERATURE SIGNAL EMF FROM THERMISTOR STATIONS
POSITIONS 1 THROUGH 22
OUTPUT FROM SCANNING & INTERPOLATING POTENTIOMETER
# = THERMISTOR POSITION / TEMPERATURE SIGNAL EMF
CHART MARKING CONTACT DRIVE MOTORS
CHART MARKING CONTACT
FLY BACK TIME
HELIX
IDLER
CHART TAKE-UP ROLL
CHART SUPPLY ROLL
CHART DRIVE
DRIVE MOTOR
CHART DRIVE SPEED CONTROL SLOW FAST
110 V 60~
SCANNING SPEED CONTROL
DRIVE MOTOR
110 V 60~
SCAN POSITION INDICATOR POSITION 1-22
TEMPERATURE INDICATOR -2 TO 32° C
DC
DC POLARIZING POWER SUPPLY
110 V 60~ INPUT
1 REVOLUTION
[REVOLUTION = -2 TO +32°C]
TEMPERATURE READOUT POTENTIOMETER
BALANCING POTENTIOMETER
34R
3R
SERVO MOTOR
34 REVOLUTIONS = -2 TO +32°C
1 REVOLUTION = 1°C DISK SLOTTED TO GIVE 1° SIGNAL & DIVIDE 1° INTO .1° & .05° SIGNAL
PHOTO TRANSISTORS
OPTICAL PICKOFF
1°C
.1°C
.05°C
RECORDER SIGNAL AMPLIFIER
30 MIN MARKER
SATURATION INDICATOR
INVERSION DETECTOR
SERVO-AMPLIFIER SUBASSEMBLY
LINE 110V AC
TO CONTROL WINDING 60~
TO LINE EXCITATION WINDING 110V 60~
BALANCING EMF, DC
TEMPERATURE SIGNAL EMF, DC
BALANCING EMF

FIG. 4. System drawing of Contouring Temperature Recorder.

another temperature to determine that the curvatures are sufficiently identical and finally selected numbers of the set are calibrated against a Bureau of Standards thermometer calibrated to 0·01°C.

(4) GENERAL DESCRIPTION OF THE SYSTEM

Fig. 4 is a system drawing of the electronics, slightly simplified for clarity at certain points. The operation is as follows. Each thermistor is connected in a circuit like that shown in Fig. 5. The fixed resistance R_W is the lead resistance in the cable to the thermistor. Since this varies with the position of the thermistor in the chain, a second resistor R_P called padding is provided in each circuit.

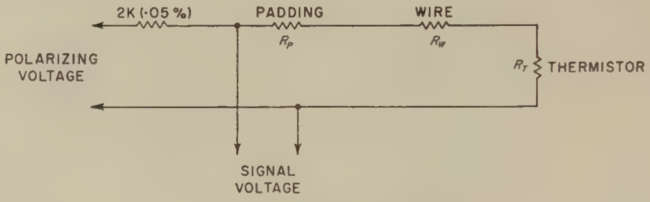

FIG. 5. Thermistor circuit.

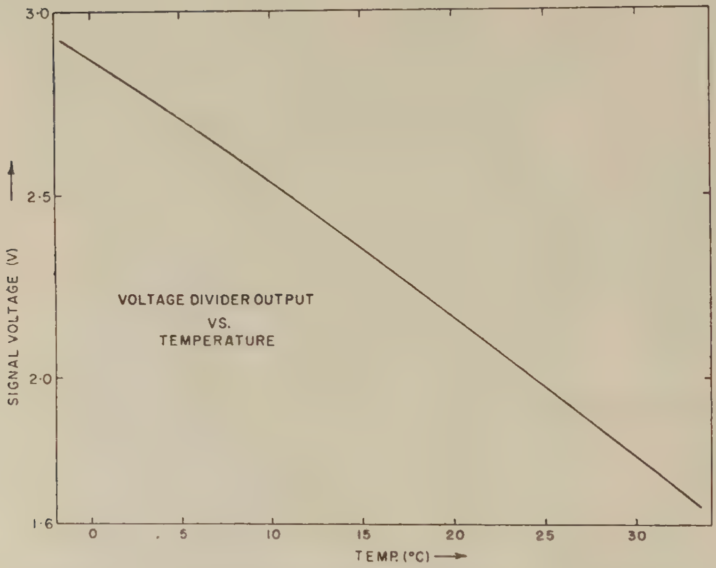

FIG. 6. Typical curve of temperature versus signal voltage from circuit shown in Fig. 5.

These are adjusted so that the sum of R_T, R_W, and R_P has the same value for each circuit at a selected temperature. All these circuits are powered by the same voltage source. These voltage dividers provide a signal output which is very nearly linear with temperature (Fig. 6), and there is one such voltage for each depth where a thermistor is located.

The voltage output from each of these dividers is cabled to a large potentiometer (interpolating and scanning potentiometer) where they are connected to equally spaced taps on the potentiometer winding in the order of their depths. The potentiometer has eighty thousand ohms between adjacent taps (total resistance 2·4 megohms). Therefore, each thermistor-voltage divider looks into an apparently open circuit, and the voltages impressed at the taps of the potentiometer remain proportional to temperature. As this potentiometer is rotated, the voltage on the slider is proportional to the temperature at the depth corresponding to its angle of rotation. When the slider is between taps, the voltage on the slider is a linear interpolation between the voltages impressed on the adjacent taps; i.e. the slider voltage varying with time ' looks like ' a curve of temperature versus depth.

In fact, this voltage may be impressed on one axis of an oscilloscope, the other axis of which is driven synchronously with the interpolating potentiometer, and a BT type trace occurs. Fig. 9 shows three such traces as insets.

The interpolating potentiometer is directly coupled to the shaft of a helical facsimile recorder and is driven by the helix drive motor at a steady (but selectable) rate. This recorder utilizes the rotation of a helix, mounted on a drum, to produce a uniform motion of a ' contact point ' between the helix and a straight edged electrode across the emerging chart paper. A voltage between the helix and this ' blade ' darkens the paper electrochemically.

The position of the contact point is then equivalent to the angle of rotation of the potentiometer, which is equivalent to depth, and it remains only to sample the potentiometer slider voltage and mark the record when this voltage corresponds to an integral temperature (or tenths or five hundredths thereof). This is accomplished by balancing the slider voltage against the voltage from another potentiometer which is driven to balance by a servo amplifier/motor combination (similar to a standard self-balancing potentiometer). This in effect converts the scanning potentiometer voltage (which is proportional to temperature) to a shaft rotation of the servo system. By proper design of the servo gearing and adjustment of the balance voltage it is possible to make one shaft rotation of the servomotor exactly equal to one degree centigrade. A disc is then attached to the servomotor shaft which has slots corresponding to the rotation equivalent to 1°C, 0·1°C and 0·05°C (Fig. 4). Light passing through these slots illuminates one of three phototransistors which provide pulse signals when isotherms are passed. These are amplified and used to mark the recorder.

The servomotor which drives the balance potentiometer is of special construction having very low inertia, with the result that it can attain full speed from a stopped condition in 0·05 secs. The associated servo amplifier is also of special design, as it must have a balanced differential input and present a very high impedance to the scanning potentiometer.

The balance potentiometer is a three-turn, high resolution, high linearity unit. It is energized by the same voltage source that polarizes the thermistor circuits (Fig. 5). Therefore, voltage drifts do not affect the accuracy of the system. The slight nonlinearity of the voltage divider output as a function of temperature is corrected in the balance circuit by adding four taps to the balancing potentiometer. By impressing certain voltages on these taps the voltage distribution along the winding of the balance potentiometer is forced to agree more closely to Fig. 6 than does a linear voltage distribution. While this correction is small it permits the servomotor shaft angle to follow the temperature distribution with an error of less than 0·02°C.

The servo balance system must ' snap back ' from the voltage equivalent to the temperature at the bottom of the chain to that of the surface, at the end of each sweep. Time for this 'snap back' is provided by using only 270° of the interpolating potentiometer winding for the thermistor taps and having the recorder helix made to record the full width of the paper with 270° of drum rotation.

The speed at which the servomotor must turn to follow a particular temperature structure is determined by the steepness of the structure and the selected speed of the recorder drum, the scan rate. There is, however, a maximum speed at which a servomotor can turn, and this determines the maximum allowable scan rate for a given temperature structure. A synchronous rectifier is provided that operates on the servomotor control voltage. This yields a d.c. voltage whose amplitude is proportional to motor speed and whose polarity is determined by direction of rotation. This voltage is used to light a neon bulb if the motor is near full speed, indicating that the scan speed must be reduced.

The same voltage is used to tint the recorder paper any time the servo system is moving in the ' hotter ' direction. Thus, a band appears on the chart that indicates the presence of the temperature inversion in the water column. With this feature, it is only necessary to know the identity of one isotherm appearing on the record. Both the scanning potentiometer and the servo balance system drive ' slave ' potentiometers whose outputs are put on meters. Thus, the scan can be stopped at the position on the paper corresponding to any line (isotherm) and the meters turned on to identify that isotherm and its depth.

(5) EXAMPLES OF DATA

The equipment described above (or some of its prototypes whose operation was essentially identical with it but lacked automatic inversion detection) has been towed extensively over the last two years. Many trips have been made along the East Coast of the United States and in the Caribbean

Sea. An Atlantic crossing from Newport, Rhode Island to Gibraltar via the Azores was made in July of 1958, and the equipment was used in the Mediterranean Sea during the summer of that year. The return crossing from Belfast, Ireland to Argentia, Newfoundland and thence to Boston, Masasachusetts was made in September, 1958. Following this, several other trips have been made in the Western Atlantic including a New England to Bermuda passage and return in December, 1958.

Fig. 7 shows a typical record for the slope water south of New England in the fall. Such a record is also typical of the Sargasso Sea (with, of course, different temperatures) during the months when a pronounced seasonal thermocline exists there. It may be noted that the isotherms are quite level and uncomplicated, which is in sharp contrast to the picture shown in Fig. 8. This recording was made about fifty miles east of Lisbon, Portugal, but is typical of most of the eastern North Atlantic during the summer and early fall. In this figure there are pronounced indications of periodicity which may be internal waves. However, without further data it is impossible to tell whether these are actually moving waves or stationary temperature structure. Fig. 9 shows a recording taken near the centre of the Western basin of the Mediterranean Sea, which is typical of the complexity encountered there. The three insets on the record are photographs of the BT-like trace obtained on an oscilloscope as mentioned above. It may be noted that a pronounced deepening of the isothermal layer and sharpening of the thermocline occurs at about three miles, and this is followed at five miles by a shallowing and further sharpening of the thermocline. Fig. 10 is a short section showing a passage out of the Gulf Stream into slope water east of Jacksonville, Florida. The slope of the warm water overlying cooler coastal water is apparent. The series of inversions which occur throughout this record at about 175 ft are caused by a thermistor which is slightly off calibration being towed at that depth. Fig. 11 is a similar crossing of the edge of the Gulf Stream south of New England in December. In this case the slope water to the north was isothermal to about 350 ft. The complex thermal structure which occurs just before leaving the stream presents a problem in isotherm identification and contouring which the prototype instrument could not handle.

Acknowledgements—The authors wish to acknowledge their indebtedness to their colleagues at the Woods Hole Oceanographic Institution who have assisted in the design, construction and use of this equipment. In particular, we are indebted to Mr. Charles H. Wilkins, who sorted and calibrated the thermistors and assisted in construction of the equipment. The work of Mr. Charles P. Cook in preparation of the figures is gratefully acknowledged. The patience and assistance of the officers and men of the U.S. Coast Guard Cutter *Yamacraw* and the USNS *Chain* are greatly appreciated.

Woods Hole Oceanographic Institution
Woods Hole, Massachusetts.

Woods Hole Oceanographic Institution Contribution No. 1046.

Printed in Great Britain by The Salisbury Press Ltd., Publicity House, Wilton Road, Salisbury, Wilts. (23091)

Contribution No. 1049

Reprinted from: THE ECOLOGY OF ALGAE (Special Publication Number 2)
A Symposium Held at the Pymatuning Laboratory of Field
Biology, University of Pittsburgh, June 18 and 19, 1959.

ORGANIC PRODUCTION BY PLANKTON ALGAE, AND ITS ENVIRONMENTAL CONTROL[1]

John H. Ryther
Woods Hole Oceanographic Institution

Roughly three quarters of the earth's surface is inhabited by an algal flora. Only on land and in a few shallow water areas do the higher plants prevail. Does it follow, then, that the non-vascular plants dominate the earth in terms of the biomass and productive capacity? In some coastal waters there are vast beds of giant seaweeds representing several thousands of grams of organic matter per square meter (i.e. Blinks, 1954), some of the densest stands of vegetation known. However, over 99% of the oceans are too deep to permit the growth of attached plants and the flora is represented almost entirely by the microscopic, unicellular algae, the so-called phytoplankton. The sole exception to this is the sporadic occurrence of floating seaweeds which may accumulate locally, as in the Sargasso Sea, but are quantitatively insignificant in the oceans as a whole.

There have been but few attempts to measure directly the standing crop, in terms of biomass, of the phytoplankton. But there have been a large number of measurements of their photosynthetic pigments, particularly during 1957 - 1958, as part of the oceanographic program of the International Geophysical Year. Chlorophyll a values for the upper, illuminated layers of the Atlantic Ocean were found to range usually between 0.1 and 0.5 mg/m^3, averaging perhaps 0.25. If we may assume a chlorophyll a:dry weight relationship of 1:100 in phytoplankton (Harris and Riley, 1956) the dry weight/m^2 of phytoplankton to a depth of 100 meters averages no more than 2.5 grams. Adding a generous 0.5 grams to allow for the richer coastal waters and to include the benthic algae, the oceans support an average standing crop of about 3.0 g/m^2 or, for the 361 x 10^{6}km^2 of the hydrosphere, a total weight of some 1.1 x 10^{12}kg.

From various sources (Schroeder, 1919; Fawcett, 1930; Show, 1949; Brown, 1956) we may divide the land surface into the following relative proportions:

1.	Wasteland (desert, artic regions, mountains)	50%
2.	Cultivated land, grasses, sedges, brush, etc.	20%
3.	Forests	30%

Let us assume that the first category, half of the land area, supports a negligible fraction of its vegetation. From various agricultural statistics, crop yields were found to average about 1000 g/m^2/year. According to Pearsall and Gorham (1956) natural stands of grasses, sedges, bracken, etc. produce from 400 to 1400 g/m^2/year, about the same as cultivated land. Since these crops are seasonal in most of the world, the average standing crop on an annual basis would be less, perhaps 50% of the annual production. The mean standing crop of this second category may be taken, then, as 500 g/m^2 over an area of roughly 30 x 10^{6}km^2 for a total biomass of 1.5 x 10^{13}kg.

Ovington and Pearsall (1956) have estimated the annual production of forest trees in Great Britain from the weight of selected samples and the age of the trees. Working backwards from their data, the standing crop of their forest trees was found to range from 10,000 to 40,000 g/m^2, an average of 25,000 g/m^2. Extropolating this to the 45 x 10^{6}km^2 of the world's forests, we may estimate a crop of trees of 1.1 x 10^{15}kg.

Summarizing these standing crop estimates, we have:

Oceans	1.1 x 10^{12}kg.
Land	
Wasteland	0
Crops, grasses, etc.	1.5 x 10^{13}kg.
Forest	1.1 x 10^{15}kg.

Thus it appears that the higher plants, occupying no more than 1/8 of the area inhabited by the algae, maintain a biomass more than 1,000 times greater. Crude though these figures may be, they probably minimize the contrast between the two plant groups, since the values for the aquatic plants, if anything, have been exaggerated, while the terrestrial stands were probably underestimated.

What of the productive capacity of the land and sea? Does it follow that the algae are equally insignificant in the annual production of the earth's organic matter? There have been several recent studies of organic production in restricted marine areas on an annual basis (Steemann Nielsen, 1937, 1951; Riley, 1956, 1958; Ryther and Yentsch, 1958; Menzel and Ryther, in press), and many more scattered single observations in different parts of the world's oceans (i.e. Riley et al, 1949; Steeman Nielsen and Jensen, 1957). From these sources, we may place the mean value for net oceanic production (that part of the plant's production in excess of its respiratory requirements) at approximately 100 g/m^2/year or 3.6 x 10^{13}kg/year for the oceans as a whole.

---

[1] Contribution No. 1049 from the Woods Hole Oceanographic Institution and Contribution No. 256 from the Bermuda Biological Station. Supported in part by contracts AT(30-1)-1918 and AT(30-1)-2078 with the U.S. Atomic Energy Commission and by NSF Research Grant G-3234.

Returning to our earlier consideration of land plants, it was estimated that the category of agricultural crops, grasses, etc. produce about 1000 g/m^2/year or 3.0 x 10^{13}kg/year over its alloted 30 x $10^6$$km^2$. Making another bold assumption that the average forest tree is 50 years old (actually, this could be halved or doubled without greatly affecting the end result) the crop of 1.1 x 10^{15}kg of trees would yield an annual production of 2.2 x 10^{13}kg/year. This is equivalent to about 500 g/m^2/year, roughly the lower limit of the values obtained by Ovington and Pearsall (1956) for 20 - 40 year-old forests.

Summarizing the production estimates, we have:

Ocean	3.6 x 10^{13}kg/year
Land	
Wasteland	0
Crops, grasses, etc.	3.0 x 10^{13}kg/year
Forests	2.2 x 10^{13}kg/year

Calculations of this second type have been made before, but it is of some interest and value to repeat them using independent methods and data. Schroeder's (1919) value for the land (3.8 x 10^{13} kg/year) and Steemann Nielsen and Jensen's (1957) value for the oceans (2.4 - 3.0 x 10^{13}kg/year) are both somewhat lower than those reported above, but are nevertheless in surprisingly good agreement with them.

The interesting fact which emerges from all this is that the annual rate of organic production on land and in the sea is about the same despite the fact that the latter is accomplished by a flora less than one thousandth the biomass of the terrestrial vegetation. The explanation for this is that most of the bulk of land plants is in the form of slowly growing, non-photosynthetic structural tissue. If we were to consider the relative quantities of photosynthetic pigments in the two environments, the results would be quite different. In fact, it has been proposed by Gessner (1949) that the highest concentration of chlorophyll that can be attained in nature (1 - 2 g/m^2) is actually the same for both water and land. What does this mean in terms of the photosynthetic potential of the land and sea? This depends not upon the amount of chlorophyll *per se*, but upon the amount of sunlight absorbed by this pigment. Steemann Nielsen (1957) correctly points out that the chlorophyll which lies below the illuminated or "euphotic" zone of lakes or oceans has no bearing on the productive potential of the area. In this connection, however, it would be difficult to estimate the chlorophyll in a comparable "euphotic zone" of a forest, where all of the pigment is probably never illuminated at any one time.

This difficulty can be circumvented if we look at the problem from another viewpoint and consider a situation in which all of the sunlight falling on a unit of the earth's surface is effectively absorbed by photosynthetic pigments. Stipulating these conditions in both a terrestrial and aquatic environment, how much of the solar energy will be converted to organic matter in each case? This, of course, depends upon the efficiency of the photochemical process, the quantum yield of photosynthesis.

The quantum yield of photosynthesis has been one of the most thoroughly studied aspects of plant physiology. Reviews by Rabinowitch (1951) and others reveal that, under similar conditions, approximately the same number of quanta of light are required to reduce one mole of CO_2 to carbohydrate by a wide variety of plant types; the process, in other words, seems to be largely species independent.

We have recently attempted to calculate the quantum yield of photosynthesis under completely natural conditions, considering the efficiency of utilization of light falling on a square meter of the earth's surface (Ryther, in press). The assumption was made that all of the light, except that lost by reflection and backscattering, was absorbed by photosynthetic pigments and that all other conditions for photosynthesis were optimal. In this treatment it was necessary to take into account the spectral composition of daylight and the photosynthetic utilization of light of this mean spectral composition. Particularly important was a consideration of the effects of light intensity. Photosynthesis is proportional to intensity up to about 1,000 foot candles, approximately 10% of full sunlight. Above this, the process becomes light saturated, and at still higher intensities may be actually depressed. Obviously, photosynthetic efficiencies decrease rapidly as plants are exposed to increasing intensities above the saturation point. At the same time, however, the higher intensities are effective in illuminating organisms deeper in the water of a planktonic community or the leaves farther down in a thick forest. Thus, while efficiencies are decreasing, production continues to increase with higher intensities of solar radiation. Individual algal cells or leaves become light saturated but entire plankton communities or forests do not. Figure 1 shows the striking similarity between plankton algae (Ryther, 1956a) and pine trees (Kramer and Clark, 1947) in this respect.

The resulting efficiencies which were obtained after corrections for respiratory loss, were equivalent to a yield ranging from 8 - 19 grams of dry organic matter/m^2/day for radiation values of 200 - 400 langleys/day (the range normally encountered over most of the earth). These theoretical

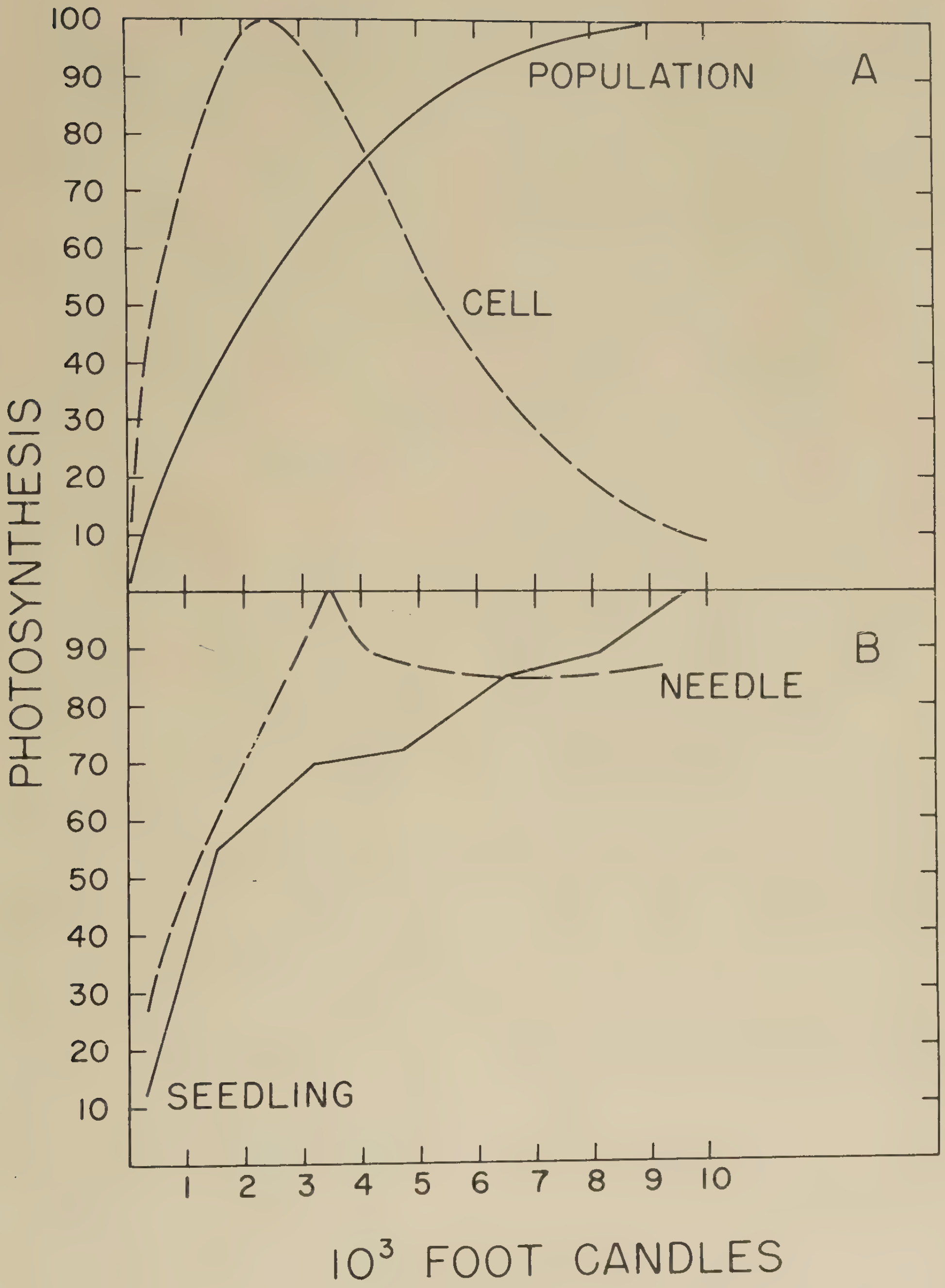

Figure Legends

Figure 1. Photosynthesis-light intensity curves for (A) individual phytoplankton organisms and entire phytoplankton populations (from Ryther, 1956) and (B) individual pine needles and entire seedlings (from Kramer and Clark, 1947).

Table I

Net organic production of various natural and cultivated systems in grams dry weight produced per square meter per day (from Ryther, in Press).

A. Theoretical potential	
average radiation (200 - 400 langleys/day)	8 - 19
maximum radiation (750 langleys/day)	27
B. Mass outdoor *Chlorella* culture (Tamiya, 1957)	
mean	12.4
maximum	28.0
C. Land (maxima for entire growing seasons) (Odum, 1959)	
sugar cane	18.4
rice	9.1
wheat	4.6
spartina marsh	9.0
pine forest (best growing years)	6.0
tall prairie	3.0
D. Marine (maxima for single days)	
coral reef (Odum and Odum, 1955)	9.6
turtle grass flat (Odum, 1954)	11.3
polluted estuary (Ryther, *et al*, 1958)	8.0
Grand Banks (April) (Ryther and Yentsch, unpublished)	6.5
continental shelf (May) (Ryther and Yentsch, 1958)	3.7
Sargasso Sea (April) (Ryther and Menzel, in press)	2.8

values were compared with some of the highest yields of organic matter which have been observed in nature. The data are reproduced here as Table I and they reveal that in cultivated crops and natural communities, on land or in the sea, in algae or in the higher plants, the maximum rate of production is very nearly the same and may closely approach the theoretical potential. As in laboratory quantum yield experiments, organic production in nature appears to be species independent and determined primarily by a photosynthetic potential common to all plants.

But the ideal conditions necessary for the attainment of this potential are seldom met in nature. Rather than producing 5 $kg/m^2/year$, the land averages no more than 10 - 20% of this, the sea perhaps 2 - 3%. The low mean production of the land is not hard to understand. Soils are frequently poor in quality or essential nutrients. Adequate moisture is often lacking. Carbon dioxide is thought to be usually, if not always, limiting to land plants, their yields being increased 2 - 3 fold when this gas is artificially introduced in greenhouse experiments (Maximov, 1930). Finally temperature, or climate, accounts for much of the discrepency between the potential and observed production of the land. A large portion of the culturable land on earth is found in temperate or semitropical climates where the plants have a limited growing season. An agricultural yield of 500 - 1000 g/m^2 may be achieved in such regions in 4 to 6 months.

But what of the ocean? Here there are no substrate problems; no lack of moisture. Carbon dioxide is probably never limiting due to the great reservoirs of dissolved carbonates and bicarbonates. Oceanic temperatures are always favorable for the growth of some species of phytoplankton. In the words of Henderson (1913) "No philosopher's or poet's fancy, no myth of a primitive people has ever exaggerated the importance, the usefulness, and above all the marvelous beneficence of the ocean for the community of living things." This ideal environment yields an average crop of organic matter which is almost two orders of magnitude less than the biotic potential of its producers. Only because of its vast area does the ocean equal the land in its over-all organic production.

The reasons for the apparent paradox lie in the restriction and limitations which the planktonic existence impose upon plants with respect to two basic requirements, light and nutrients. We shall consider these separately.

Though the oceans are some three miles deep, over 95% of their waters are in virtual darkness, uninhabitable by photosynthetic organisms. The light intensity at which photosynthesis balances respiration, the "compensation intensity", varies somewhat with the species and physiology of the plant, but is of the general order of 100 foot candles. This is equivalent to about 1% of full noon sunlight incident to the surface. Below this compensation intensity, no growth of plants is possible. Thus the oversimplified but useful concept has come into use of a "euphotic zone", the depth through which plant growth can occur, which has as its lower limit the depth of penetration of 1% of the incident surface radiation. In the clearest ocean water the euphotic zone extends to about 120 meters.

But this clearest ocean water contains no plants, so a euphotic zone of 120 meters is hypothetical. Let us introduce an algal population into this clear solution which we will further stipulate to be adequately enriched with all the vital plant nutrients. Immediately, the plants themselves will absorb and scatter the light, and the euphotic zone will become progressively shallower as the population grows. Thus, the phytoplankton, shutting out its own light, becomes self-limiting. But as the euphotic zone becomes shallower, a progressively larger fraction of the light is absorbed by the plants, a proportionately smaller fraction by the water itself. Consequently, organic production increases with a decreasing euphotic zone. However, this relationship holds only as long as the decreasing euphotic zone results from the increase of living plants. Not all turbid waters are highly productive, for the turbidity is frequently caused by non-living particulate or dissolved matter. In Long Island Sound, for example, Riley (1956) estimated that two thirds of the incident radiation was absorbed by such material.

We may conclude, then, that photosynthesis in the ocean is not only restricted to a shallow surface layer, no more than 100 meters deep, but that for the process to proceed at its maximum potential rate, the plants must be concentrated in the upper five meters or less of otherwise clear ocean water. Let us now turn to a consideration of the nutrients available to support this production. For a convenient example we shall take nitrogen.

The highest concentrations of inorganic nitrogen in the oceans are present as nitrate at intermediate depths of approximately 1000 meters, and range from about 40 to 60 µg A NO_3 - N/l or .56 - .84 gN/m^3. Water from this depth rarely reaches the surface. The highest known concentrations of nitrogen within the euphotic zone are found in restricted areas where upwelling or divergences of water masses bring water from several hundred meters of depth to the surface. Rudd (1930) for example, reports values of about 40 µg A NO_3 - N/l in the surface layers of the Antarctic, one of the most fertile oceanic regions.

In most temperate and northern waters, the surface layers are enriched by winter cooling and mixing to depths of some 300 - 500 meters. The highest concentrations of nitrogen brought to the surface in this way range from 10 to 20 µg A NO_3 - N/l (R. F. Vaccaro, unpublished data for the North Atlantic). Let us assume that winter mixing has resulted in a surface enrichment of 15 µg AN/l or 210 mg N/m^3. In clear ocean waters with a 100 meter euphotic zone, the phytoplankton will have a reservoir of 100 m x 210 mg N/m^3 or 21,000 mg of nitrogen per square meter to draw upon. However, as the population grows, it not only depletes this supply, but creates in the process a progressively shallower euphotic zone with a correspondingly smaller reservoir of nitrogen. By the time the phytoplankton have increased to a population containing 10 mg of chlorophyll/m^3, production is limited to a euphotic zone of about five meters (Riley, 1956). This water contained an initial amount of only 1050 mg N and, of that, 500 mg were utilized in producing the population (assuming the plants to contain about 1% chlorophyll and 10% nitrogen). We may calculate the daily rate of production from the chlorophyll and depth of the euphotic zone for a day of average incident radiation, (300 langleys) according to the equations of Ryther and Yentsch (1957). From these calculations it is estimated that 1.8 grams of organic matter will be produced and about 180 mg nitrogen concurrently consumed within the five meter euphotic zone each day. Thus, after a population equivalent to 10 mg chlorophyll/m^3 has developed, there is sufficient nitrogen remaining in the resulting shallow euphotic zone to sustain production for less than three days. Clearly in a static situation such as we have pictured, high levels of organic production approaching the potential discussed above can scarcely be attained, much less maintained.

The oceans as a whole are not, of course, a static environment, but their surface waters are highly variable in this respect. In certain restricted areas hydrographic or meteorological forces bring water from intermediate depths to the surface. This happens when two water masses diverge, as in the equatorial Pacific (Sette, 1955), and most notably along the West Coasts of continents, where prevailing offshore winds produce a surface current which moves seaward, this water being replaced with upwelling, rich, deep water. It is for this reason that the coastal waters off Peru and parts of West Africa are among the most fertile regions of the sea. However, if one were to follow a given parcel of water as it is brought to the surface and subsequently is transported horizontally, one would probably observe the same sequence of events which we discussed above. Steemann Nielsen and Jensen (1957) have described this for the coast of Africa, pointing out that the freshly upwelled water, though rich in nutrients, is poor in phytoplankton. It is "new" water, in which the plants have not had time to grow. As one moves seaward, following the path of the surface current, the plankton becomes more and more dense, passes through a maximum, and then decreases ultimately to a very sparse population by the time the water has reached mid-ocean. The time course of this sequence is probably not very different from that of a perfectly stable water mass which is enriched by winter mixing. The difference is that high production in an upwelling area is maintained at a given geographical location. Sette (1955) has described a similar geographical sequence "downstream" from the mid-Pacific equatorial divergence.

In contrast to these dynamic situations, which are comparatively rare in the oceans as a whole, we described above a static system in which the surface waters are enriched by winter mixing. The term "static" refers here to the absence or minor effects of horizontal advection, not to the absence of vertical water movements. Let us now return to this situation and consider it in more detail.

During the winter in temperate and northern regions, surface waters cool sufficiently to destroy the summer thermocline, and the waters become mixed to 300 - 500 meters, several times the depth of the euphotic zone. Not only are the nutrients from below the euphotic zone brought up and mixed with the impoverished surface layers, but the plankton algae are transported downward and spend a considerable fraction of their time in darkness. As a result, though nutrients are plentiful, production is severely curtailed due to the limitation of light.

With the return of spring, the surface waters begin to warm up, a seasonal thermocline develops, and the euphotic zone becomes stabilized against vertical mixing. At the same time, radiation increases. Those phytoplankton which find themselves in the euphotic zone are held there and suddenly have access to both light and nutrients. The stage is set for the "spring bloom", a feature characteristic of the temperate oceans. We have shown on the previous pages the succeeding events, terminating in the exhaustion of the nutrient supply. During a period of fine, calm weather in March or April, the whole process may run its course within a week or two. More typically, the formation of the summer thermocline is interrupted by storms, periods of cold weather, etc. and the spring flowering may then be prolonged, at a lower level, for a period of one or two months. But its days are numbered by the supplies of nitrogen, phosphorus, and the other essential elements which are limiting to plant growth in the sea. As we have seen, the amounts of these substances brought to the surface by mixing are small to begin with, and they are quickly consumed.

What happens next is a matter of some controversy. Some believe that most of the nutrient-deficient plants sink, their density increasing with old age. Evidence for this is the accumulation in summer of relatively high concentrations of chlorophyll at or near the lower limit of the euphotic zone. Others hold that the ultimate fate of the plants is to be eaten by the animal members of the planktonic community (i.e. Harvey et al, 1935; Cushing, 1958). Whatever happens, the spring maximum soon gives way to a summer minimum during which time production proceeds at a very low level which is probably maintained by the complete recycling (assimilation, death or consumption, and regeneration) of a small fraction of the winter nutrient budget within the surface layers.

In the fall, when cooling again destroys the seasonal thermocline, there may be minor and irregular outbursts of plant growth as the surface layers are alternatively cooled and mixed to a slight degree and then restabilized. These small blooms terminate with the final disappearance of thermal stratification and the return of winter conditions.

At the semi-tropical latitude of Bermuda, in the Sargasso Sea, the annual cycle of organic production is much the same as that pictured above, with the major difference that production persists at a relatively high level throughout most of the winter. This is due to the fact that winter cooling and mixing is less pronounced than in more northern waters, and never, in fact, extends below the depth of the permanent thermocline at 300 - 400 meters. In addition, incident radiation is higher at these latitudes, and the water is exceptionally clear. As a result of this combination of factors, the plants are never carried down out of the light for sufficiently long periods to prevent their growth. Figure 2 shows the seasonal cycle of organic production in the Sargasso Sea off Bermuda. The accompanying seasonal profile of temperature in the upper 700 meters will illustrate how hydrographic conditions influence plant growth. Note that high production is correlated with a well-mixed, largely isothermal layer in the upper 400 meters; low production, with the thermally-stratified summer conditions.

The nutrient supply available to the plants in this 400 meter deep reservoir in the Northern Sargasso Sea is extremely low--an order of magnitude less than that present in the temperate seas. Nitrate, for example, seldom exceeds 1.0 µg AN/l in the euphotic zone. Consequently, plant

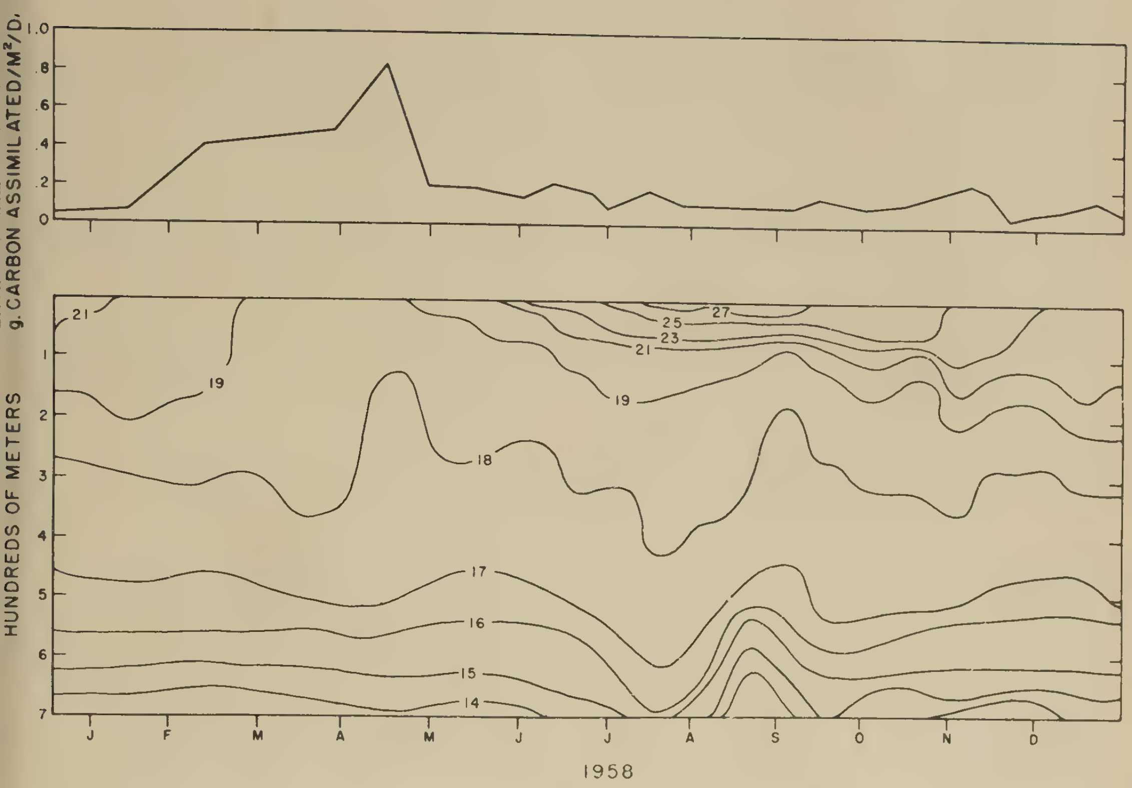

Figure 2. The seasonal profile of temperature to 700 meters and net organic production in the Sargasso Sea off Bermuda for the period January - July, 1958 (from Menzel and Ryther, in press).

production per unit volume is never high--the process cannot build up towards its biological potential. In contrast to a dense flowering in the upper five meters of temperate seas, the Sargasso Sea plankton grow over a euphotic zone which is never less than 50 - 100 meters deep. What maintains this organic production in the face of such poverty of nutrients? Low as they are, the concentrations of nitrate, phosphate, and silicate (to name a few essential elements which have been studied) never change appreciably in these surface waters. We don't yet understand this, but it appears that in these relatively warm waters the whole cycle of assimilation, consumption, death or excretion and remineralization occurs very rapidly. The amounts of plants and animals and minerals are small, but the metabolic wheels turn fast.

No study of the seasonal cycle of organic production has been made in tropical waters, but we can imagine what it must be like. In the true tropics there is no winter cooling of the surface waters, no mixing, no replenishment of the euphotic layer with rich aphotic waters. The seasonal thermocline of temperate and semi-tropical latitudes becomes a permanent, thermal barrier to vertical mixing.

On March 1, 1959, a short oceanographic section was made by Research Vessel Crawford between 24° and 35° North latitude at the longitude of Bermuda. At that time of year, the surface water temperatures in the North Atlantic Ocean are at their seasonal minimum; vertical mixing is most pronounced. Actually the 1959 season was somewhat early. Our seasonal study at Bermuda revealed the beginnings of warming and stratification by March 1, and the spring phytoplankton pulse was in full bloom on that date. Figure 3 shows the temperature profile and values of organic production for this section running from North to South. It is remarkably similar to the seasonal cycle at Bermuda. The well-mixed, almost isothermal, highly productive stations at the northern end of the section merge into stratified, low productive stations to the South much as the spring flowering

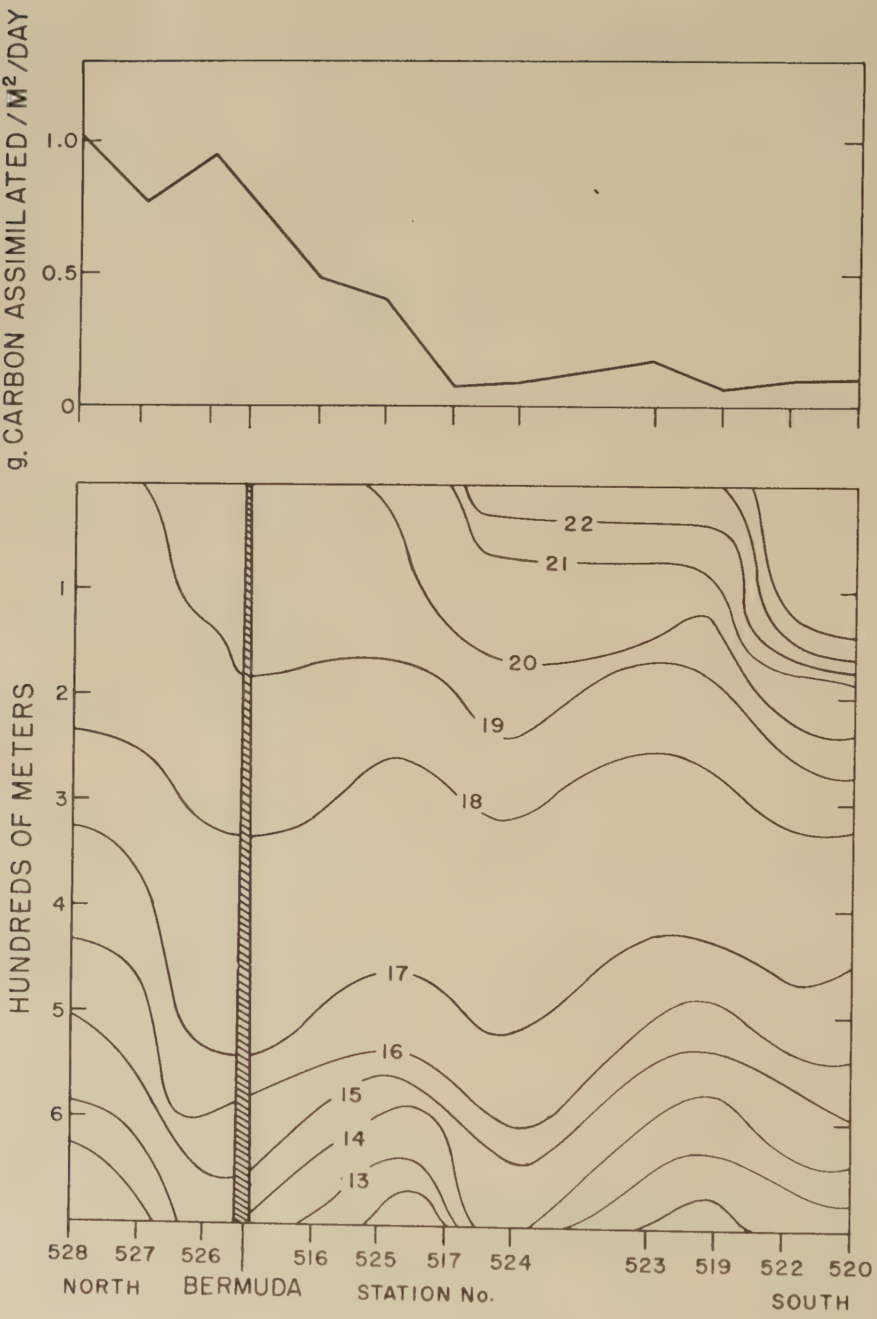

Figure 3. The profile of temperature to 700 meters and values for net organic production as measured on a section between 35° and 24° N. latitude at the longitude of Bermuda in March, 1959.

declines to the summer minimum at Bermuda. One can assume from this alone that organic production in the tropics is maintained at a low, rather steady rate throughout the year, probably maintained by the recycling of nutrients entirely within the euphotic zone, perhaps occasionally stimulated into brief minor outbursts of growth by the limited mixing action of storms.

It is clear, then, that organic production in the oceans is limited most of the time by either light or nutrients. Both are available in plentiful supply in the oceans as a whole, but both seldom occur together. At the few times and places where neither of these factors is limiting, production may proceed at rates comparable to the highest levels of production observed on land.

As mentioned earlier, the concentrations of nutrients in the tropics and semi-tropics are far less than those present in the high latitude seas. As a result much smaller populations of plants can develop. Yet, due to the rapid turnover of these materials, a low to moderate rate of production can be maintained throughout a deep euphotic zone. If one integrates production over the entire water column, the annual rate beneath a square meter of sea surface is as high or higher than that of presumably far richer waters. As an extreme example of this, let us compare the vertical profile of photosynthesis in the Sargasso Sea during a period of peak production (April 19, 1958) with that of a shallow, highly enriched sewage oxidation pond in South Dakota (from Bartsch and Allum, 1957). The chlorophyll concentration of the former averaged less than 1 mg/m^3, the latter some 450 mg/m^3. The oxygen production values of Bartsch and Allum have been converted to carbon fixation assuming an assimilatory quotient of 1.25 (Ryther, 1956b), and the depth curve of photosynthesis has been rather subjectively extrapolated to the surface. Examination of the depth profiles of daily production from the sewage oxidation pond and the Sargasso Sea (Figure 4) reveals an interesting fact. In the oxidation pond, the euphotic zone is two orders of magnitude smaller while production per unit volume is two orders of magnitude greater than in the Sargasso Sea. If one integrates the two curves, organic production beneath a square meter for the two areas is found to differ by less than 20%. Actually, the value for the oxidation pond is probably somewhat low, for the measurements were made from 10:00 a.m. to 3:00 p.m. rather than for an entire day. But even if this figure is increased by 25% - 50%, the similarity between the two situations is striking.

This may appear to contradict the earlier statement that production per unit area may be expected to increase with a decreasing euphotic zone. It should be reiterated here that such is true only in cases where living plants alone contribute to the turbidity of the water. In a pond receiving raw sewage wastes, this would hardly be the case.

But the point which I wish to make in comparing these two situations is this: that the daily rate of production of organic matter, as it is currently defined by ecologists, is very nearly the same in two bodies of water in which the amounts of living plant material are respectively of the order of 100 grams and 0.1 grams per cubic meter.

What, then, does this rate of primary production actually mean? One looks in vain for evidence of it in the clear, blue waters of the Sargasso Sea. The major fisheries of the world are located in the temperate or high latitudes, or in the few regions of divergences and upwellings which we discussed above, not in places like the Sargasso Sea. Is it realistic to compare fertility of northern and tropical seas, of the ocean and the land, of a plankton bloom and a cornfield, all on the basis of their relative rates of natural photosynthesis?

In modern, dynamic ecology, it has become unfashionable to speak of the "standing crop" of organisms. The important question is not "how much is there?" but "how fast is it being produced?" There is no doubt that this concept has opened up new and extremely interesting avenues of ecological research. But the population ecologist or fisheries biologist should beware of these values. The sociologist who compares the productive capacity of the land and sea may be sadly deluding himself. For animals eat food, not photosynthesis. What is the significance of organic matter which is produced, consumed, decomposed and remineralized almost simultaneously? Why add up a daily production which is daily expended into a non-existent annual total. Is this comparable to a barn full of corn? The study of the rate of organic production has already and will continue to reveal fundamental physiological and ecological principles. But the person who examines these data with the hope of feeding an overpopulated earth on marine resources would do well to remember, when he picks a pound of beans from his kitchen garden, that to get the same weight of rather undigestable and unappetizing plankton algae from the open sea, he would need to filter some five million gallons of water.

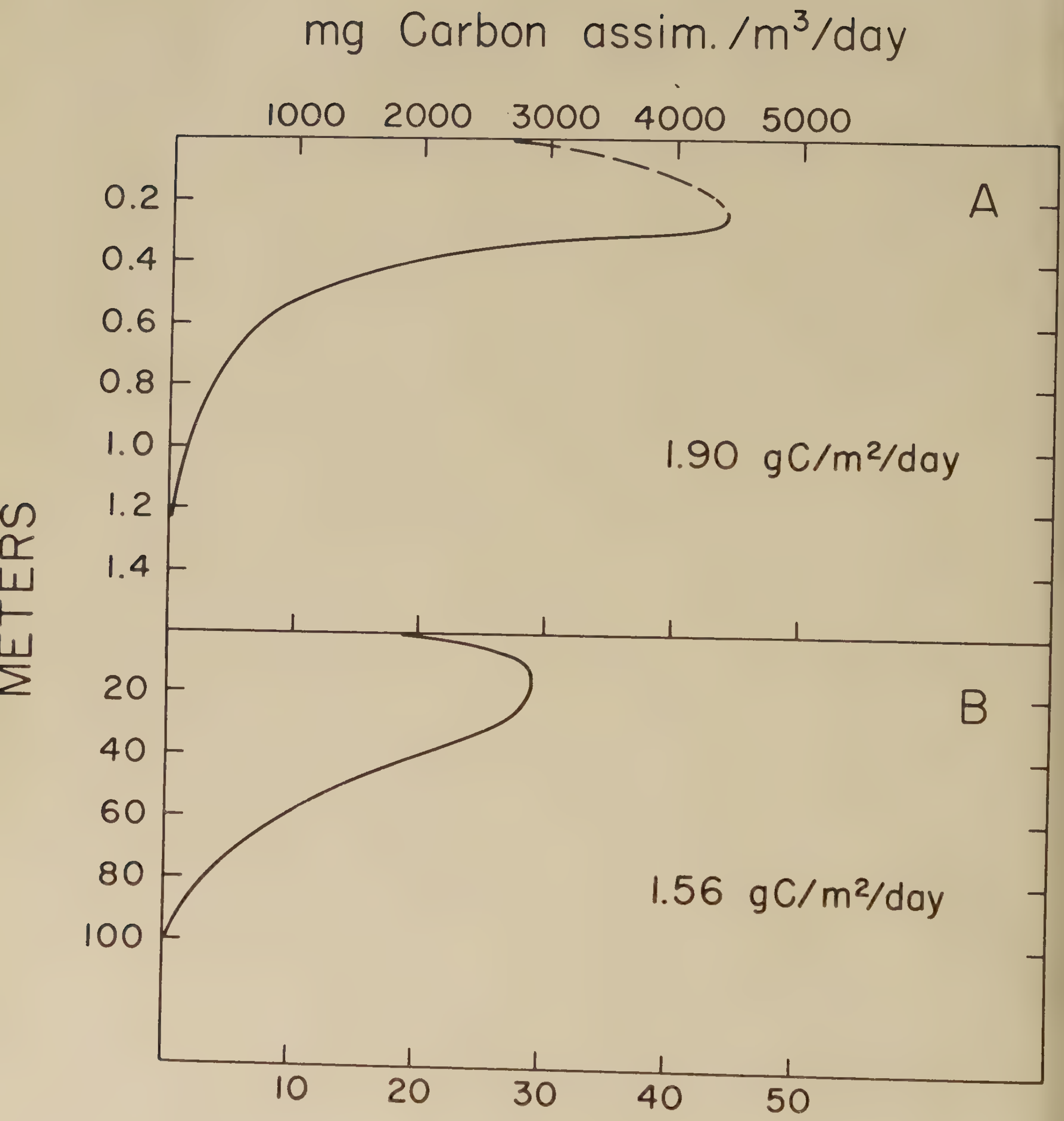

Figure 4. The vertical profile of daily photosynthesis in (A) a sewage oxidation pond in Lemmon, South Dakota (from Bartsch and Allum, 1957) and in the Northeastern Sargasso Sea (from Menzel and Ryther, in press).

References

Bartsch, A. F. and M. O. Allum. 1957. Biological factors in treatment of raw sewage in artificial ponds. Limnol. & Oceanogr., 2: 77-84.

Blinks, L. R. 1955. Photosynthesis and productivity of littoral marine algae. J. Mar. Res., 14: 363-373.

Brown, H. 1956. The challenge of man's future. The Viking Press, New York. 290 pp.

Cushing, D. H. 1958. The effect of grazing in reducing the primary production: a review. Rapp. et Proc. Verb. Cons. Internal. Explor. Mer., 144: 150-154.

Fawcett, C. B. 1930. The extent of the cultivable land. Geogr. Rev., 76: 504-509.

Gessner, F. 1949. Der Chlorophyllgehalt im See und seine photosynthetische Valenz als geophysikalisches Problem. Schw. Zeitschr. f. Hydrol, 11: 378-410.

Harris, E. and G. A. Riley. 1956. Oceanography of Long Island Sound, 1952 - 1954. VIII Chemical composition of plankton. Bull. Bing. Oceanogr. Coll., 15: 315-322.

Harvey, H. W., L. H. N. Cooper, M. V. Lebour and F S. Russell. 1953. Plankton production and its control. S. Mar. Biol. Assoc. U. K., 20: 407-442.

Henderson, L. J. 1913. The fitness of the environment. The Macmillan Co., New York.

Kramer, P. J. and W. S. Clark. 1947. A comparison of photosynthesis in individual pine needles and entire seedlings at various light intensities. Plant. Physiol., 22: 51-57.

Maximov, N. A. 1938. Plant physiology. 2nd. Eng. Ed. McGraw-Hill Book Co., Inc., New York.

Menzel, D. W. and J. H. Ryther. In press. The annual cycle of primary production in the Sargasso Sea off Bermuda. Deep-Sea Res.

Odum, E. P. 1959. Fundamentals of ecology. 2nd Ed. W. B. Saunders Co., Philadelphia.

Odum, H. T. 1957. Primary production measurements in eleven Florida springs and a marine turtle-grass community. Limnol. & Oceanogr., 2: 85-97.

Odum, H. T., and E. P. Odum. 1955. Trophic structure and productivity of a windward coral reef community on Eniwetok Atoll. Ecol. Monogr., 25: 291-320.

Ovington, J. D. and W. H. Pearsall. 1956. Production ecology II. Estimates of average production by trees. Oikos, 7: 202-205.

Pearsall, W. H. and E. Gorham. 1956. Production ecology I. Standing crops of natural vegetation. Oikos, 7: 193-201.

Rabinowitch, E. I. 1951. Photosynthesis and related processes. Vol. I. Interscience Publishers, Inc., New York.

Riley, G. A. 1956. Oceanography of Long Island Sound, 1952 - 1954. II Physical oceanography. Bull. Bing. Oceanogr. Coll., 15: 15-46.

Riley, G. A. 1958. Phytoplankton of the North Central Sargasso Sea, 1950 - 1952. Limnol. & Oceanogr., 2: 252-270.

Riley, G. A., H. Stommel and D. F. Bumpus. 1949. Quantitative ecology of the plankton of the western North Atlantic. Bull. Bing. Oceanogr. Coll., 12: 10-69.

Rudd, J. T. 1930. Nitrates and phosphates in the southern seas. J. Cons. Internat. Explor. Mer., 5: 347-360.

Ryther, J. H. 1956a. Photosynthesis in the ocean as a function of light intensity. Limnol. & Oceanogr., 1: 61-70.

Ryther, J. H. 1956b. The measurement of primary production. Limnol. & Oceanogr., 1: 72-84.

Ryther, J. H. In press. The potential productivity of the sea. Science.

Ryther, J. H., and C. S. Yentsch. 1957. The estimation of plankton production in the ocean from chlorophyll and light data. Limnol. & Oceanogr., 2: 281-286.

Ryther, J. H., and C. S. Yentsch. 1958. Primary production of continental shelf waters off New York. Limnol. & Oceanogr., 3: 327-335.

Ryther, J. H., and C. S. Yentsch, E. M. Hulburt and R. F. Vaccaro. 1958. The dynamics of a diatom bloom. Biol. Bull., 115: 257-268.

Schroeder, H. 1919. Die jährliche Gesamptproduktion der grünen Pflanzendecke der Erde. Naturwiss., 7: 23-29.

Sette, O. E. 1955. Consideration of mid-ocean fish production as related to oceanic circulatory systems. J. Mar. Res., 14: 398-414.

Show, S. B., 1949. The world forest situation. U.S. Dept. Agricult. Yearbook of Agriculture, Trees. 742-753.

Steemann Nielsen, E. 1937. The annual amount of organic matter produced by the phytoplankton in the Sound off Helsingør. Medd. Komm. Danmarks Fiskeri-og Havndenis Ser: Plankton., 3(3): 1-37.

Steemann Nielsen, E. The marine vegetation of the Isefjord--a study on ecology and production. Ibid., 5: 1-11.

Steemann Nielsen, E. 1957. The chlorophyll content and the light utilization in communities of plankton algae and terrestrial higher plants. Physiol. Plant., 10: 1009-1021.

Steemann Nielsen, E., and E. A. Jensen. 1957. Primary oceanic production, the autotrophic production of organic matter in the oceans. Galathea Repts., 1: 49-136.

Tamiya, H. 1957. Mass culture of algae. Ann. Nev. Plant Physiol., 8: 309-334.

Contribution No. 1051

Reprinted from MONOGRAPH NO. 5, AMERICAN GEOPHYSICAL UNION, 1960
Physics of Precipitation
Printed in U.S.A.

Cloud Distributions over the Tropical Oceans in Relation to Large-Scale Flow Patterns [1, 2]

JOANNE S. MALKUS AND CLAUDE RONNE

Woods Hole Oceanographic Institution, Woods Hole, Massachusetts

Introductory Remarks by Dr. Joanne Malkus—We will come down one step in the hierarchy of scale motions and discuss the relations between individual clouds and precipitation and traveling cloud systems. We enter now into the synoptic scale of motions over the tropical oceans. As Dr. Namias pointed out, these scales are associated with and certainly influenced by the large planetary scale. This next paper is a condensation of the results on the relationship of the clouds over the tropical Pacific Ocean to large-scale flow patterns.

Abstract—The relations between tropical cloud patterns and the three-dimensional synoptic structure have been studied by quantitative time-lapse photography from the regularly scheduled MATS aircraft in the North Pacific. From the films of three circuits of this oceanic area a 'Tropical Whole Sky Code' was devised. Its application proved relatively objective and reproducible; useful deductions concerning the large-scale flow from the code numbers and vice versa are possible. The code numbers were used as underlays in the synoptic analyses; in addition detailed cloud maps were constructed by simplified photogrammetry in particularly interesting areas. Preliminary results show first that in the tropics, large Cumulus clouds and precipitation are highly concentrated in convergent, or disturbed zones, and second that organization of clouds into rows parallel to the low-level flow is common, with increasing intensity and wider spacing between rows as the degree of disturbance increases. The importance of studying cloud physics and dynamics in the context of the overall synoptic situation is brought out.

Tropical Pacific clouds in relation to the large-scale structure of the atmosphere formed the subject of this investigation. The method employed was quantitative time-lapse photography from the scheduled military aircraft flying between Hawaii and the Phillipines, from which measurements and cloud maps were made by triangulation, together with a detailed synoptic analysis at all levels between the surface and 100 mb which was carried out at the University of Chicago by H. Riehl and William Gray.

Our results, as far as cloud physics is concerned, may be summarized in one sentence: In the tropics the precipitation process must be studied in the context of the synoptic patterns, which regulate the size, structure, development, and organization of the clouds and cloud groups observed. We plan to illustrate this point and our method of utilizing our photographic data quantitatively, by showing one small portion of the film, the corresponding synoptic charts and deductions drawn from these jointly, but first we must lead up to the questions we formulated by presenting some background material.

The classical picture of convection in the tropics might suggest a statistically both random and, on the average, invariant distribution of clouds over low-latitude oceans. In the vertical, the tropical atmosphere is usually conditionally unstable from cloud base upwards, frequently to the tropopause; buoyant energy would thus nearly always be available for a hypothetical non-interacting convective parcel. Horizontally, sharp air-mass contrasts are virtually non-existent; the low-level atmosphere is well-loaded with moisture and closely coupled by vertical

---

[1] This paper has been condensed from material developed in a joint investigation by the Woods Hole Oceanographic Institution and the University of Chicago and presented in preliminary form in a Technical Report (Woods Hole Rep. No. 58–62) by *Riehl, Gray, Malkus,* and *Ronne* [1959], which was distributed to all participants at the Conference and is referred to here simply as "the Report." Approximately one-third of the presentation at the Conference consisted in showing a selected portion of the aerial cloud motion picture films, which were the basic data of the study.

[2] Contribution No. 1051 of the Woods Hole Oceanographic Institution.

stirring with an almost infinite extent of homogeneous sea surface. One might expect, *a priori,* uniform or random bunching of tropical Cumulus clouds, with Cumulonimbus build-ups and precipitation distributed here, there, and everywhere, and cloud patterns which statistically show little diurnal, weekly or even seasonal variations. The organization, if any, might be expected to be the hexagonal or roll convection typical of laboratory experiments over a heated surface.

This classical picture of tropical convection has gradually faded. The first blow came with the Wyman-Woodcock trade-wind expedition, discussed by *Bunker* and others [1949] and the entrainment theory of *Stommel* [1947] evolved from its data. Clouds were found to exchange air with their surroundings and consequently the degree of instability of the temperature lapse rate lost its unique significance in determining cloud growth. The moisture distribution of the ambient air was found to affect in-cloud parameters, and most tropical Cumuli lost buoyancy by drying out well below the level where a stable layer was reached. Cumulonimbus towers reaching the high troposphere were, to be sure, occasionally observed but conditions permitting their growth proved rare. The evolution of the Woods Hole Studies (during the period 1947–1957) further emphasized the controlling effects of the environment and the inhibitory factors against penetrative development. Runaway cloud growth to the Cumulonimbus stage has been found to require special circumstances. Among these are a deep moist layer, a large horizontal dimension, and probably synoptic-scale convergence in the low levels. The correlation between vertical development and degree of conditional instability proves not just to be low but generally inverse; a more unstable lapse rate is found where our films show a sky of widely separated stunted trade Cumulus, than in easterly wave and hurricane, when Cumulonimbi are rampant.

The classical convection picture collapsed entirely with the work of Riehl and collaborators which carried tropical meteorology both upward and equatorward from the lower trades, where the synoptic disturbance is least evident. In contrast to the steadiness of the lower trades, the upper tropical atmosphere is characterized by extreme restlessness. Even in the upstream inversion-dominated portions, the constancy vanishes above the moist layer, and large space and time variations in wind, humidity, and stability aloft — governed by the dynamics and thermodynamics of phenomena on the synoptic scale. Equatorward from the trades, the inversion weakens and disappears and inconstancy at all levels becomes pronounced; the steady trade flow becomes perturbed into the deepening waves and vortices characteristic of the equatorial trough zone, which itself operates in a fluctuating manner. Throughout the tropics, over land and sea the reputed clockwork regularity of showers proved an erroneous myth. Nothing could be more unreliable than tropical rain. In fact, tropical rainfall studies revealed an enormously skewed distribution, with the major fraction of monthly precipitation falling on two or three days and being almost entirely concentrated in major disturbances, again pointing the finger toward a high degree of cloud, especially precipitating cloud, organization on the synoptic scale.

Our study was designed to pursue this point in terms of specific questions, for which it was hoped to gain quantitative answers. Three circuits of the North Pacific area were accomplished in July and August 1957 and 8000 ft of film successfully exposed, only about one-third of which has been analyzed to date because of the exorbitant labor involved. The three overall conclusions of most pertinence to cloud physics are:

(1) The degree of regulation and control upon cloud forms exerted by the synoptic scale of motion, which must be considered in its entire three-dimensional extent throughout the troposphere (including up to, at least, the 200 mb level).

(2) The extreme rarity and concentration of precipitating Cumulus and Cumulonimbus clouds, which on the first flight (which has been completely analyzed) never occurred except in a disturbance or a region where low-level synoptic-scale convergence could be readily inferred from the charts.

(3) The organization of Cumulus clouds into rows parallel to the low-level flow. On the 6300 km of Flight I, such organization was detected (and the angle determined by quantitative measurement on the films) 91% of the time; it was coded as moderate or strong 62% of the time. Organization was only absent in trade-inversion dominated circumstances and became more pronounced as the degree of disturbance increased. We have measured the orientation of

cloud lines wherever they occurred and their spacing on numerous occasions.

As a corollary to the above conclusions it was found possible to devise a code for the state of the tropical sky, with relatively few numbers, so that the code number chosen provides significant information about the synoptic pattern and physical processes at work. It consists of 17 basic sky types, ten for trade-wind skies and seven for disturbed skies. The code itself and an illustration of each number (a single frame chosen from our films) is contained in the Appendix. The code was used by us to characterize long strips of prints which were made from the movies at 15-min intervals; the appropriate code numbers are then plotted along maps of the flight path and used as underlays for the synoptic charts, as will be seen in the figures. A person can obtain a good visual image of the cloud forms during any portion of any flight by looking at the code number and referring to the sample print thereof, a result which is, in itself, of some interest. Conversely it may be hazarded that a meteorologist well acquainted with the three-dimensional synoptic picture could, with practice, enter in anticipation the code numbers along a projected flight path with little error.

We shall now illustrate our techniques, approaches, and some of our results by showing first the analysis and lastly the movies themselves of a small portion of Flight I. Figure 1 shows the path and times of this flight, which passed through an undisturbed trade regime from Hawaii to Johnston Island, into and through a moderate easterly wave just east of Kwajalein (in the Marshalls) where the first overnight stop was made. The wave passed Kwajalein during the night and thus was encountered again by the aircraft the following morning. After this the flight proceeded on to Guam and Manila, where on this last leg it passed through the typhoon Wendy. We shall be concerned here, however, only with the two passages through the easterly wave. The remainder of Flight I is analyzed in detail in the Report [*Riehl* and others, 1959]. Figure 2 shows the flight path of the first leg with the cloud code numbers entered along it used as an underlay for the low-level streamline chart. All code numbers entered refer to 'trade-wind skies' (code numbers 1–4) or 'trade-wind disturbance' (code numbers 6–9), the latter in this case associated with the moderate-strength Riehl-type easterly wave, whose trough line was centered between Majuro and Kwajalein, and which was moving westward at approximately ten knots, or more slowly than the trade flow.

We would thus expect the convection and precipitation zone to be located east of the troughline; the pictures confirmed this in a striking manner. Note the code numbers 8 and 9 (Cumulus congestus, high Cumulus tops and showers; the only difference between the two is that 9 contains upper clouds, broken to overcast) appearing up to the wave trough, and then cutting off sharply ahead, going over to ordinary or even suppressed trade-wind skies. The quantitative measurements from the films bring out even more clearly the effects of the disturbance upon the cloud structure. Figure 3 shows the cloud cross section of this leg constructed from the film analysis, superimposed upon a relative humidity cross section composited quite independently from the radiosondes and synoptic data.

The horizontal dimensions of the sketched Cumuli (as well as the hatched under curve below) gives the cloud amount, while the dashed cloud outline indicates the maximum height of tops; the average top height is shown by the darker outlines. The effects of the inversion domination near flight outset, its relief at about Johnston Island and gradual approach to the wave convergence zone are pronounced. Note the upper regions of high humidity in connection with the subtropical jet over Hawaii and with the level of maximum wave amplitude (15,000–20,000 ft) in the Marshalls area and the association of these with middle and upper cloudiness. It is worthwhile to remark here that Flights II and III crossed this area without a wave disturbance and only trade-wind or suppressed skies were photographed.

Figure 4 shows arrows denoting the orientation of the cloud lines, and vertical marks the number of which is proportional to the intensity of this organization into rows. We see that the cloud lines are parallel to the low-level streamlines, within the accuracy of our ability to draw these (except perhaps just west of the wave trough where the cloud lines were backed almost north-south and no wind information existed to test whether or not the flow was so oriented). We also see that the organization into rows is weak or absent in the inversion-dominated portions of the flight; namely, just out of Hawaii and just west (ahead) of the

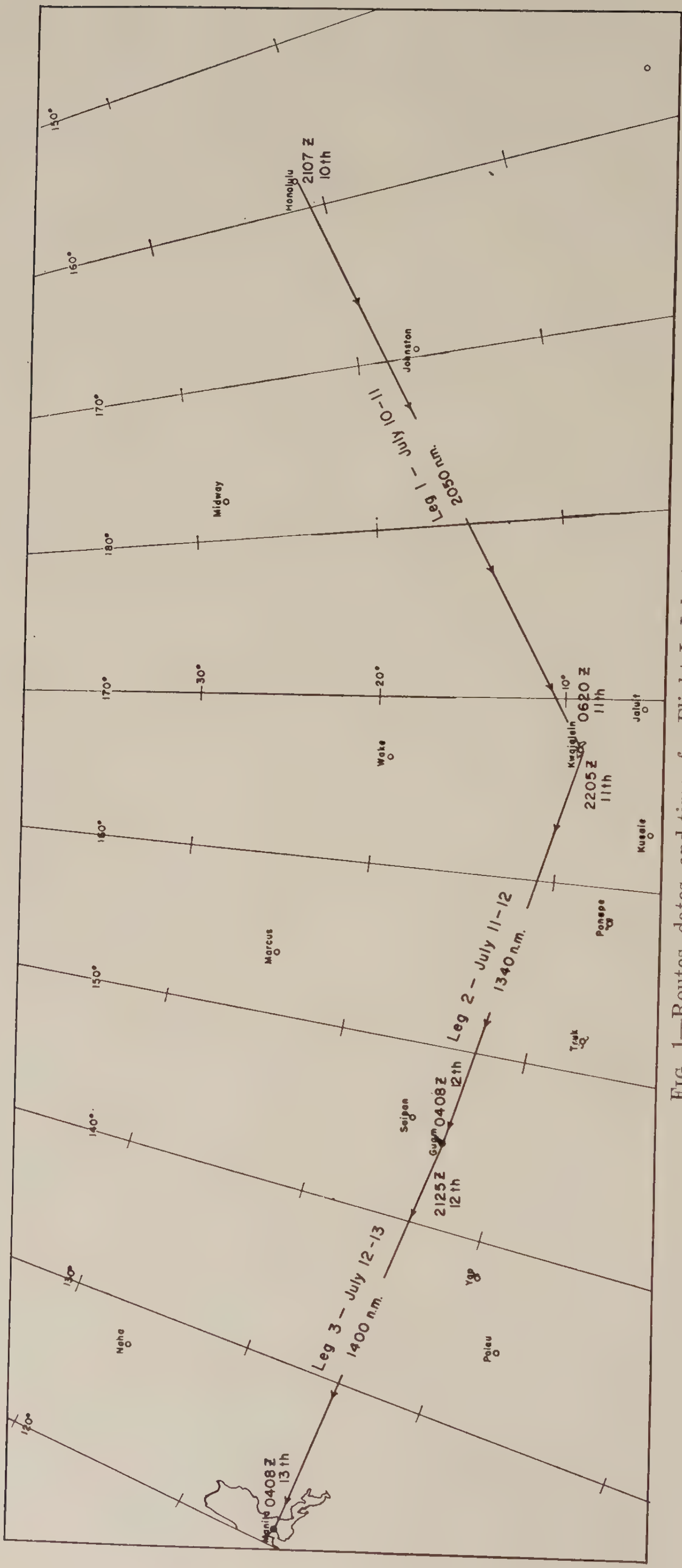
150°
160°
170°
180°
170°
160°
150°
140°
130°
120°
30°
20°
10°
Honolulu
2107 Z
10th
Johnston
Leg 1 – July 10–11
2050 n.m.
Midway
0620 Z
11th
Kwajalein
Jaluit
Wake
2205 Z
11th
Kusaie
Ponape
Marcus
Leg 2 – July 11–12
1340 n.m.
Truk
Saipan
Guam
0408 Z
12th
2125 Z
12th
Yap
Leg 3 – July 12–13
1400 n.m.
Naha
Palau
Manila
0408 Z
13th

FIG. 1—Routes, dates, and times for Flight I, July 10–13, 1957

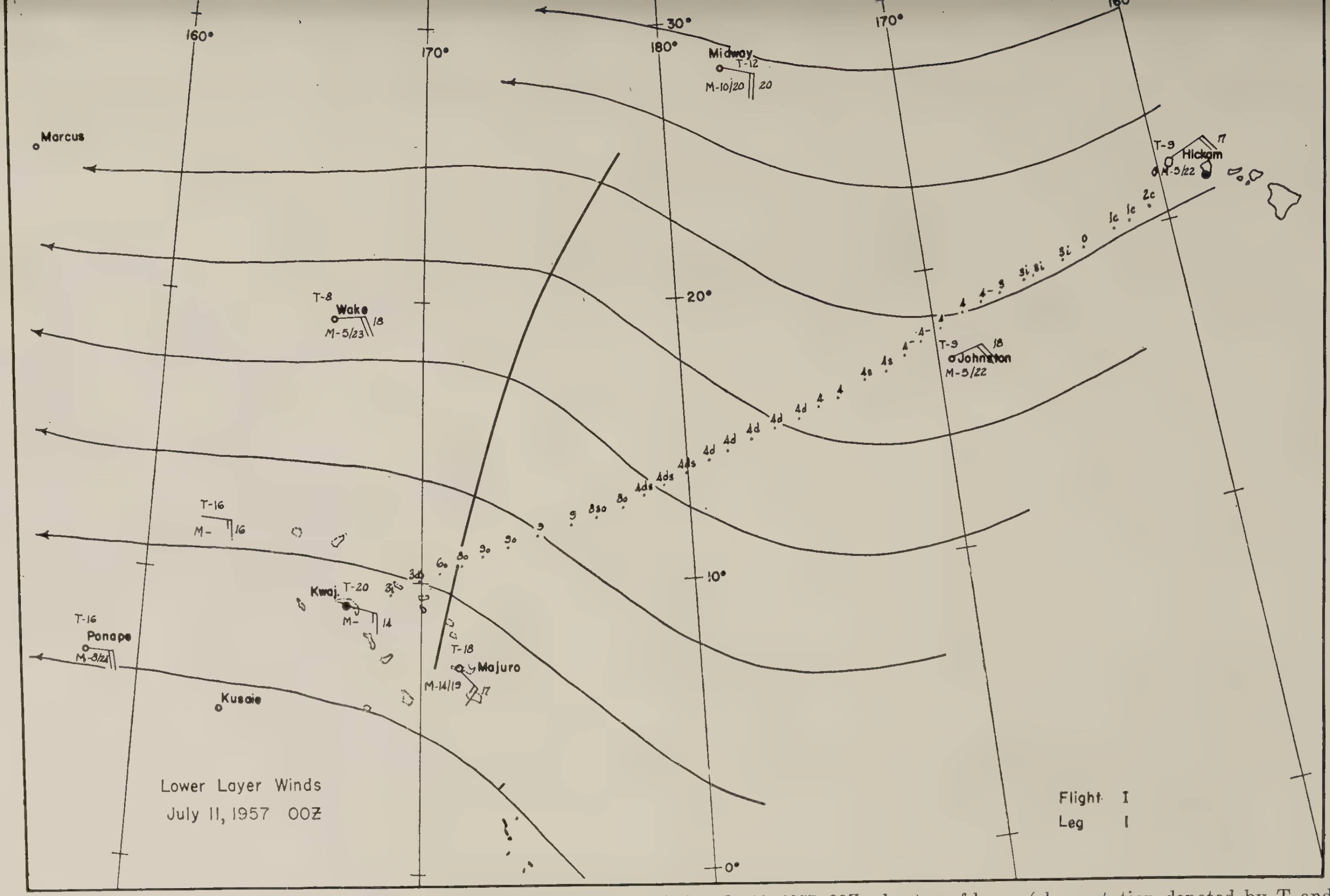
160°
170°
180°
30°
170°
20°
10°
0°
Marcus
Midway
T-12
M-10/20
20
T-9
Hickam
M-5/22
17
T-8
Wake
M-5/23
18
T-9
Johnston
M-5/22
18
T-16
M-
16
Kwaj.
T-20
M-
14
T-16
Ponape
M-8/24
T-18
Majuro
M-14/19
17
Kusaie
Lower Layer Winds
July 11, 1957 00Z
Flight I
Leg I

FIG. 2—Mean winds (knots) of lower layer with approximately uniform wind, July 11, 1957, 00Z; also top of layer (above station denoted by T and reported in 1000's of ft) and height of strongest wind in layer (below station denoted by M, height in 1000's of ft and maximum wind in knots); underlay is sky code (see Appendix); heavy solid line marks position of wave trough in easterlies; solid lines with arrows are low-level streamlines

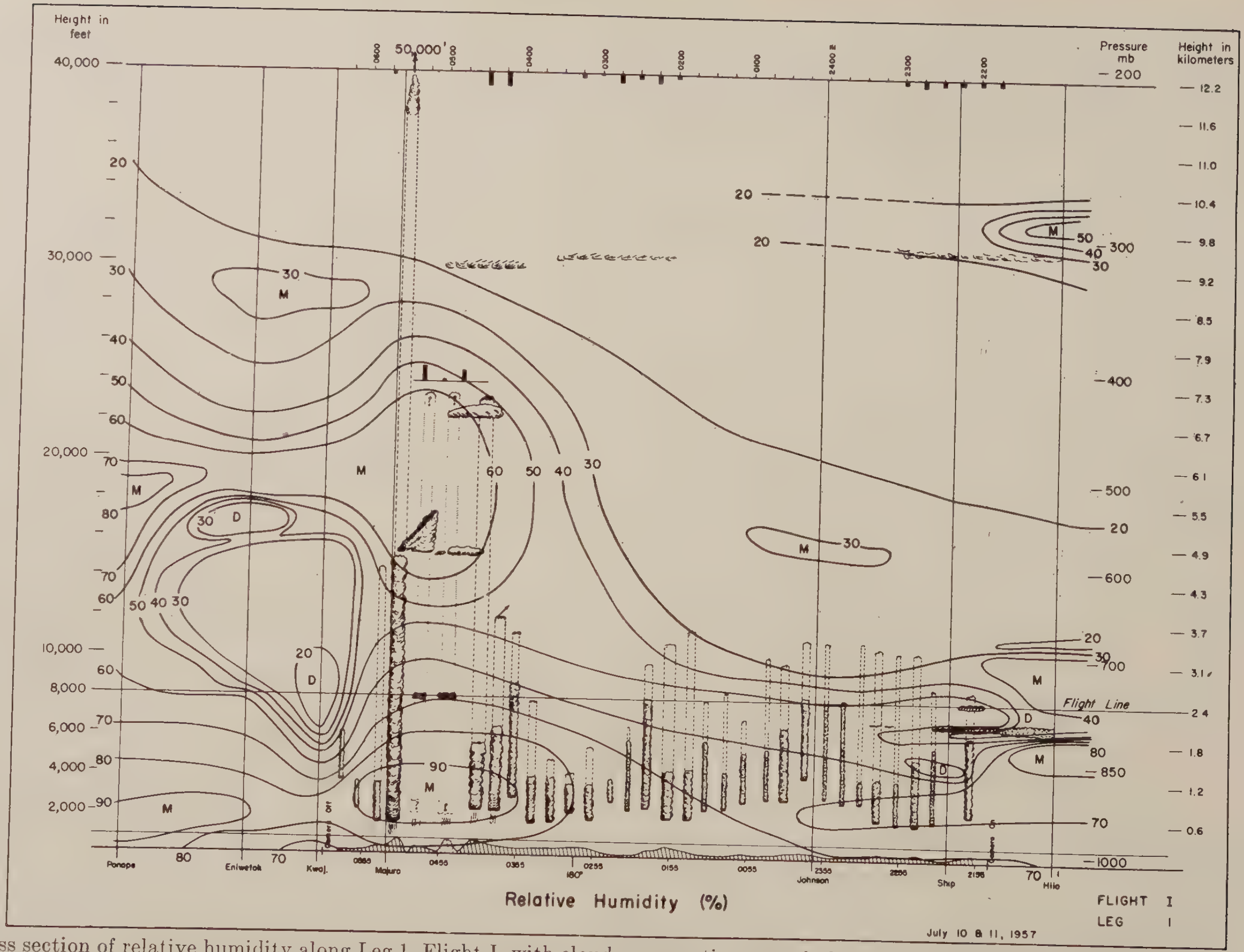

FIG. 3—Cross section of relative humidity along Leg 1, Flight I, with cloud cross section as underlay, isopleths are relative humidity in per cent; regions marked M are moister than the surroundings while regions marked D are drier; the wave disturbance in the easterlies lay between the longitudes of Majuro and Kwajalein; the cloud cross section was constructed from measurements on the motion picture film; lower cloudiness (Cumulus) amount indicated, to nearest one-quarter coverage, by bottom hatched under curve, middle cloudiness by black columns at mid-levels, and upper cloudiness by black columns at top; inversion Stratus is not included; width of schematic Cumuli indicate coverage (narrowest, one-quarter) not cloud size; arrows are direction of measured cloud shear (north upward); mean heights of Cumuli are solid clouds, maximum heights in the

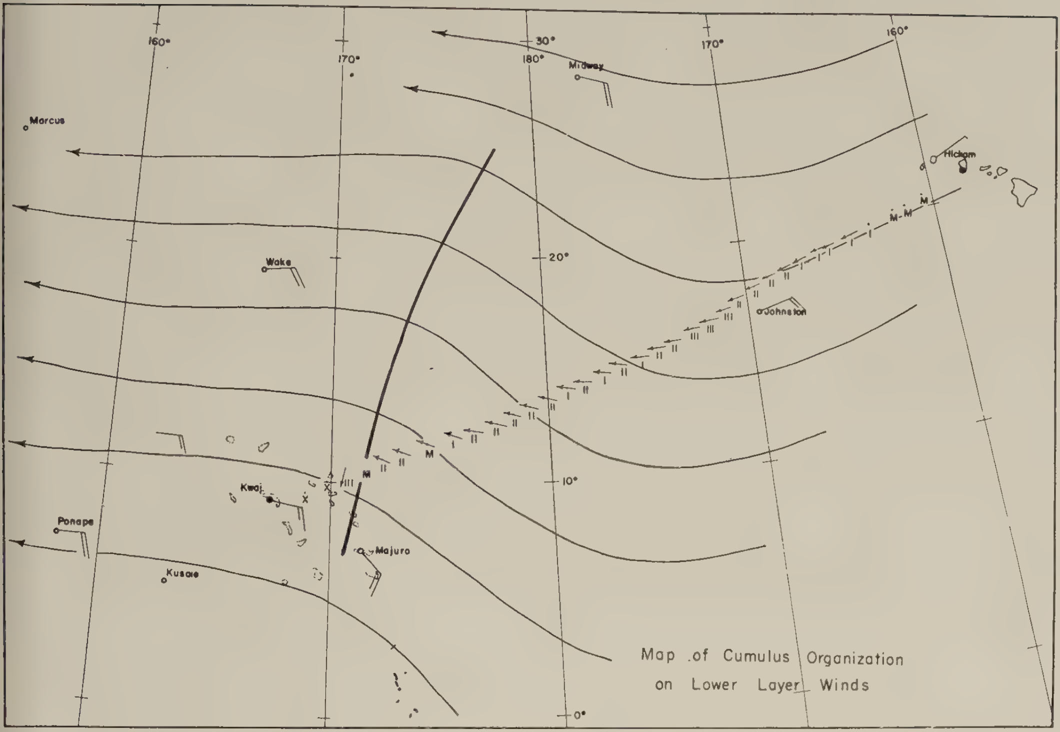
160°
170°
30°
180°
Midway
170°
160°
Marcus
Hickam
Wake
20°
Johnston
Kwaj.
Ponape
Majuro
Kusaie
10°
0°
Map of Cumulus Organization
on Lower Layer Winds

FIG. 4—Organization of Cumulus, Leg 1, Flight I, superposed on lower-layer winds; straight arrows give measured direction of cloud lines; code symbols are organization intensity: x absent, 1 weak, 11 moderate, 111 strong, M no measurement; solid wavy lines with arrowheads are streamlines

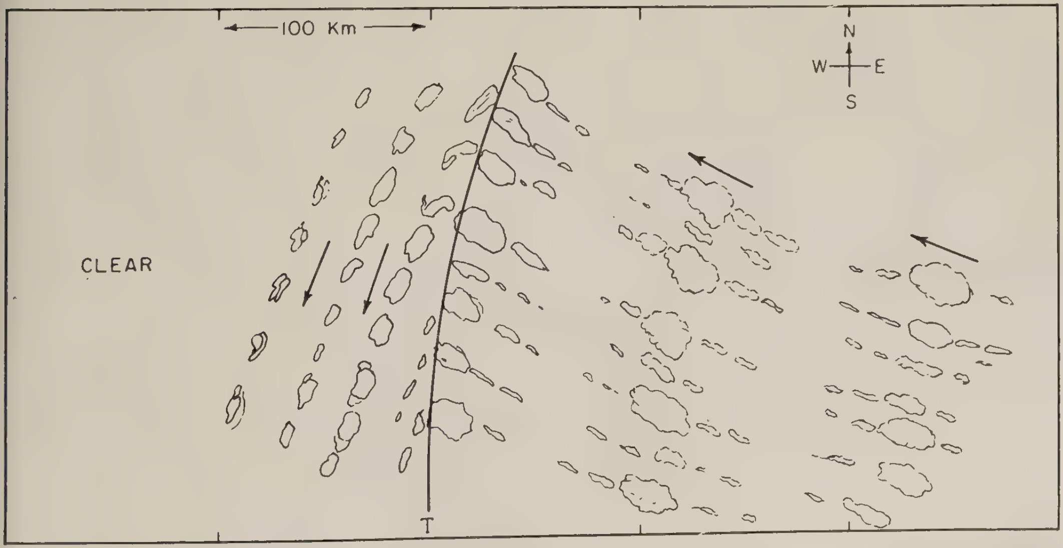
100 Km
N
W
E
S
CLEAR
T

FIG. 5—Schematic distribution of cumuliform clouds near wave trough in easterlies, Leg 1, Flight I; orientation of cloud rows and spacing between them was measured exactly from the film, as was the distance between the amplified cloud groups, denoted schematically in the figure as a single large cloud; individual clouds have not been entered nor drawn to scale

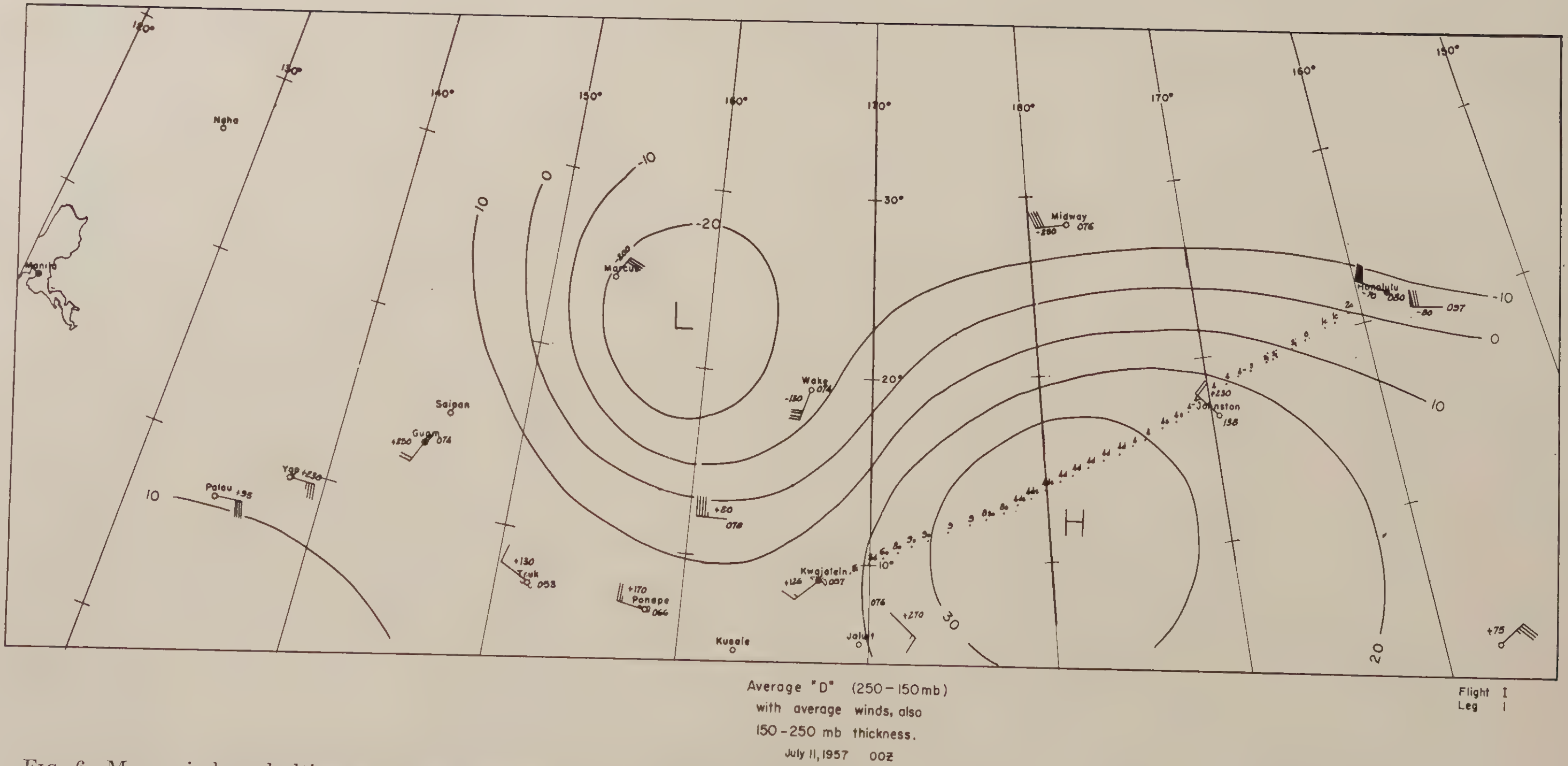
Average "D" (250 - 150 mb)
with average winds, also
150 - 250 mb thickness.
July 11, 1957 00Z
Flight I
Leg 1
120°
130°
140°
150°
160°
170°
180°
170°
160°
150°
30°
20°
10°
Naha
Manila
Saipan
Guam
Yap
Palau
Marcus
Truk
Ponape
Kusaie
Wake
Kwajalein
Jaluit
Midway
Johnston
Honolulu
L
H
-20
-10
0
10
20
30

FIG. 6—Mean winds and altimeter corrections with respect to mean tropical atmosphere for layer 250–150 mb, July 11, 1957, 00Z; isopleths are of the latter in tens of ft; the thickness of the layer in tens of ft (first digit omitted) is written to the right of the stations

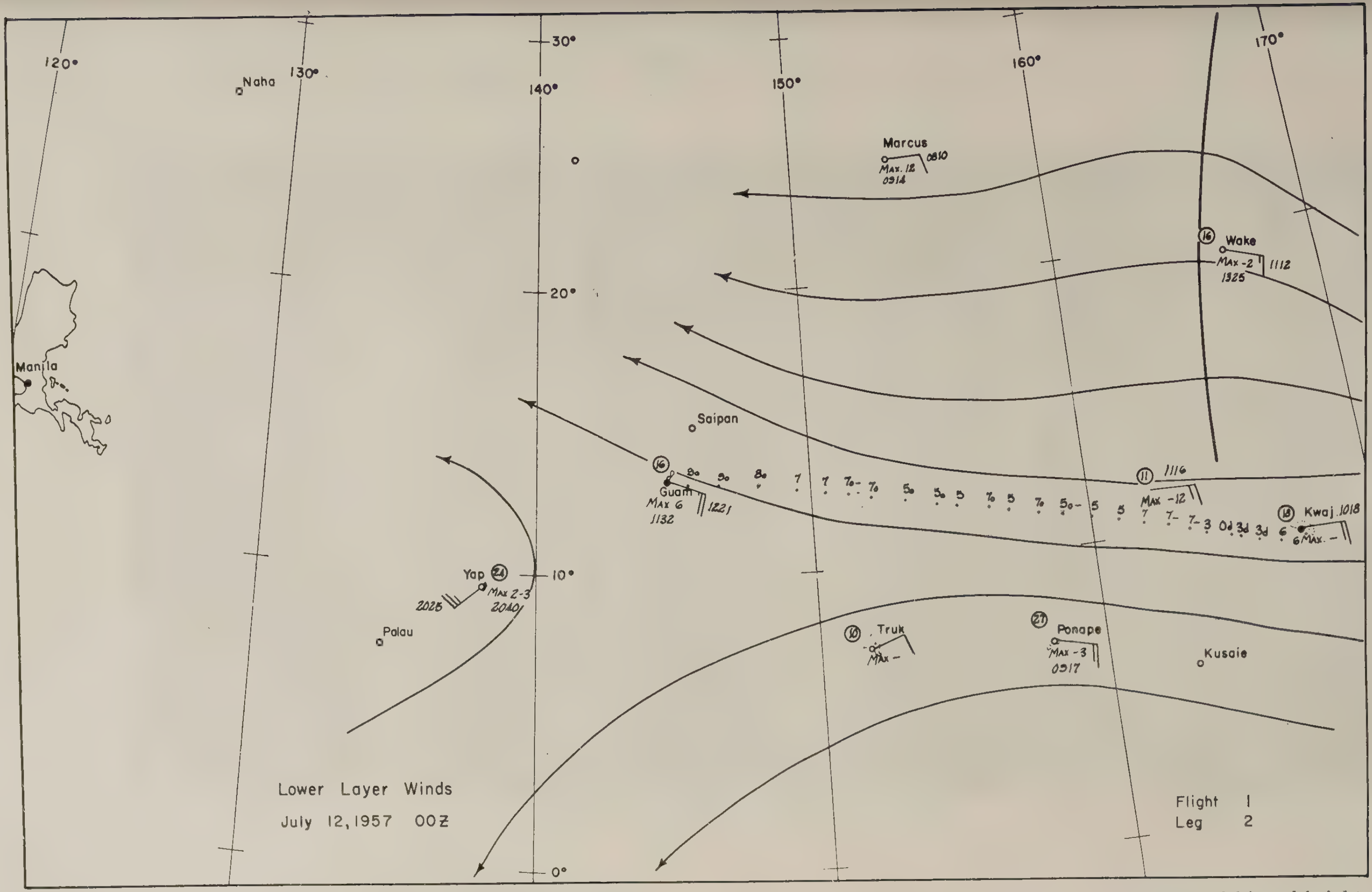
Lower Layer Winds
July 12, 1957 00Z
Flight 1
Leg 2
120°
130°
140°
150°
160°
170°
30°
20°
10°
0°
Naha
Manila
Marcus
Max. 12
0914
0810
Wake
⑯
Max -2
1325
1112
Saipan
Guam
⑯
Max 6
1132
1221
⑪
1116
Max -12
Kwaj 1018
⑱
6 Max. -
Yap
㉔
Max 2-3
2040
2025
Palau
Truk
⑩
Max -
Ponape
㉗
Max -3
0517
Kusaie

FIG. 7—Mean winds (knots) of lower layer with approximately uniform wind, July 12, 1957, 00Z; also top of layer (circled, in 1000's of ft) and height of strongest wind in layer (maximum height in 1000's of ft; direction and velocity of maximum in code); code notation at tail of arrow denotes mean wind

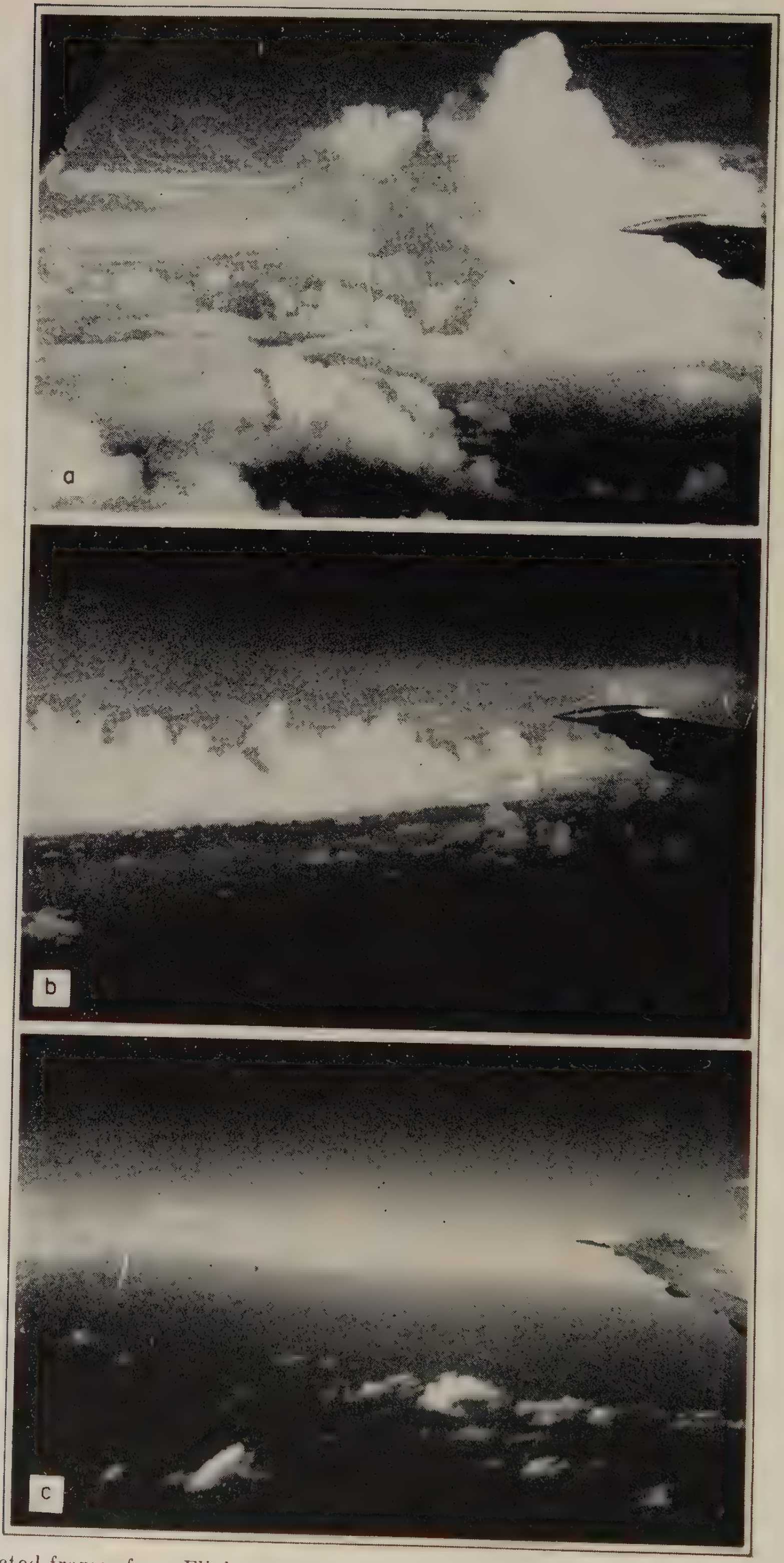

FIG. 8 –Selected frames from Flight I; camera aimed south from 8000 ft altitude; (a) frame just to east of wave trough, in active convection zone, Leg 1; (b) frame just to west of wave trough, Leg 1; cloud line same as that just to west of trough in Fig. 5; after the third of these, conditions became completely suppressed; (c) wave trough convection zone on following day after wave has passed under upper cold low; the second encounter of the aircraft with the wave took place 200 miles west of Kwajalein, on Leg 2; note contrast in clouds as compared with (a) and (b)

wave trough, while it is pronounced in the convection zone of the disturbance. A more detailed study of organization in the region of the easterly wave trough is shown in Figure 5 where we have mapped schematically the cloud lines ahead and to the rear of the disturbance. The spacing of the cloud lines is to scale, but not individual clouds. The large blobs located about 100 km apart in the convection zone are actually large groups of huge buildups which were regularly spaced at these intervals along the parallel cloud lines, giving the impression of a normal mode of organization. Beginning at about halfway between Honolulu and Kwajalein, we measured the spacing of these cloud lines; it began at about 4 km between rows, comparable to the depth of the moist layer. As the wave trough was approached, the row spacing became wider until it reached about 25 km just east of the wave trough and about 30 km just west of it. It appeared that the spacing was being widened by superposition of a larger-scale organization upon the smaller (4 km) scale and that some of the cloud rows were being enhanced while those between were being suppressed.

Finally, Figure 6 shows the high-level chart, the D-values and average winds for the 250-150-mb layer which prevailed at the time of Leg 1. The important point to note is that the easterly wave trough lies just to the west of the upper anticyclone and to the east of an upper cyclone, which was stationary. While the observer and aircraft spent the night at Kwajalein the wave trough passed by and moved underneath this upper cold low. On the next day's flight it should have been encountered about 200 miles out of Kwajalein, but only faint remnants of the previously vigorous wave were detected. There was hardly any trace of disturbance left along the path of the aircraft except five or six very distant Cumulonimbi on the southern horizon, which may have been associated with the equatorial trough. The synoptic study showed the air rounding the southern bend of the upper trough was likely to gain cyclonic relative and absolute vorticity. Upper level convergence and consequent sinking presumably destroyed the easterly wave and Figure 7 shows its total demise in the streamline field in the Marshall area. The cloud motion picture films showed its death far more dramatically, however, than any of our words or diagrams. Figure 8 shows three selected frames from the motion picture film; a and b were made to the west and east, respectively, of the wave trough on its first crossing on Leg 1. The cloud line seen in Figure 8b appears as the first one to the west of the trough line in Figure 5, and the large cloud build-up, in the distance reached 50,000 ft. Figure 8c shows the 'convection zone' of the trough on its second crossing by the aircraft on Leg 2 (after the overnight stop at Kwajalein). Note the complete disappearance of the disturbance, except for the very distant build-ups far to the south.

In conclusion, this work suggests that microphysical studies of tropical clouds and precipitation would be severely restricted if studied out of context with the synoptic scale flow patterns. If we wish eventually to predict, understand, or in any sense modify tropical rain, the interaction between large-scale flows, convection dynamics, and droplet formation and growth must be studied.

Note—At the Conference this paper was concluded by showing the portion of the cloud films from which the figures shown here were constructed. These films were made from military aircraft flying at 8000-ft altitude, and were taken in kodachrome at one frame per second. These films are on file at the Woods Hole Oceanographic Institution and at the Department of Meteorology, University of Chicago. The methods of photography and reduction are described in detail in the Report [*Riehl* and others, 1959] of which this paper is a partial condensation.

Acknowledgments—The writers wish to acknowledge the essential contribution made to this study by their colleagues at the University of Chicago, Herbert Riehl and William Gray, who carried out the synoptic analysis described herein. The work when completed is to be published under joint authorship with them.

This study was supported by the National Hurricane Project of the U. S. Weather Bureau and by the Office of Naval Research. Its execution was made possible through the kind cooperation of the Military Air Transport Service (Pacific Command) whose staff and crews went far beyond the call of duty to provide assistance.

REFERENCES

BUNKER, A. F., B. HAURWITZ, J. S. MALKUS, AND H. STOMMEL, Vertical distribution of temperature and humidity over the Caribbean Sea, *Pap. Phys. Ocean. and Met., Mass. Inst. of*

Tech. and Woods Hole Ocean. Inst., *11*, 1, 82 pp., 1949.

Riehl, H., W. S. Gray, J. S. Malkus, and C. Ronne, Cloud structure and distributions over the tropical Pacific, pt. I, unpublished manuscript, WHOI Ref. No. 58-62, 1959.

Stommel, H., Entrainment of air into a Cumulus cloud, *J. Met.*, **4**, 91–94, 1947.

Appendix

Tropical Whole Sky Code

Joanne S. Malkus and Herbert Riehl

This code is for use primarily in coding aerial photographs (or visual observations) over the open seas in the tropics far from land masses. Categories 0–4 denote undisturbed trade-wind skies. Categories 5–9 cover weak or trade-wind type disturbances, while categories 10–16 relate to strong disturbances (deep easterly waves, equatorial trough disturbances or convergence, through typhoons). The letters (to be placed after the appropriate numbers) permit some further refinements or sub-specifications.

Trade-Wind Skies

0 No clouds at all, or a few suppressed, or small numbers of very suppressed Cumulus. Upper cloud 1/10 or less.

1 Inversion-dominated: trade Cumulus spreading out into Stratocumulus, definite signs of stratiform but total sky cover less than about one-half.

2 Extensive Stratocumulus decks, more than about one-half total sky cover.

3 Average trade Cumulus sky, no particular organization into lines. No significant upper clouds. No marked shear. Tops 8000–10,000 or less, precipitation unlikely.

4 Average trade Cumulus sky, but with marked organization into rows or lines. No significant upper clouds. No marked shear. Tops 8000–10,000 or less. Precipitation unlikely.

5 Average trade Cumulus sky with upper sheet clouds up to broken. No marked organization or shear. No precipitation.

6 Marked concentration of convection, rather large convection clouds (not Cumulonimbus) in view, with extensive clear or almost clear areas. Upper sheets to broken may be present.

7 Suppressed trade Cumulus sky with upper sheets broken or overcast but not precipitating. No marked shear or organization in Cumulus.

8 Above average Cumulus activity, high tops, occasional Cumulus congestus. Showers suspected or seen. Upper cloudiness less than broken. No marked shear or organization of Cumulus.

9 Above average Cumulus activity, high tops, occasional Cumulus congestus. Showers suspected or seen. Upper cloudiness broken to overcast. No marked shear or organization.

10 Occasional Cumulonimbus, no obvious organization, no significant or extensive independent upper sheet clouds. Indicate component of shear in plane of film.

11 Rows or suspected organization of Cumulonimbus, no extensive or significant independent upper clouds. Indicate component of shear in plane of film.

12 Cumulonimbus and partial coverage of independent upper sheet clouds. Cirrus, Altostratus and/or Altocumulus.

13 Substantial upper cloud coverage, suppressed convection over wide clear areas, except some Cumulonimbus visible. Precipitation from upper clouds absent or unlikely.

14 Rain from upper sheets (overcast or almost overcast) Cumulonimbus indistinct, picture dark.

15 Rain from upper overcast, Cumulonimbus still suspected but not clearly visible, picture dark and disturbed.

16 Upper overcast raining, no Cumulonimbus seen or suspected, suppressed low convective activity; picture dark and disturbed.

Postscripts (Primarily for Trade-Wind Skies)

o Marked organization into rows or lines.

s Shear obvious; indicate component in plane of film.

c Apply to 1 or 2 if Cumulus tops are seen poking through the Stratus.

d Distant disturbance—evident from high clouds low on horizon.

— Weaker, more suppressed or less development than normal for category.

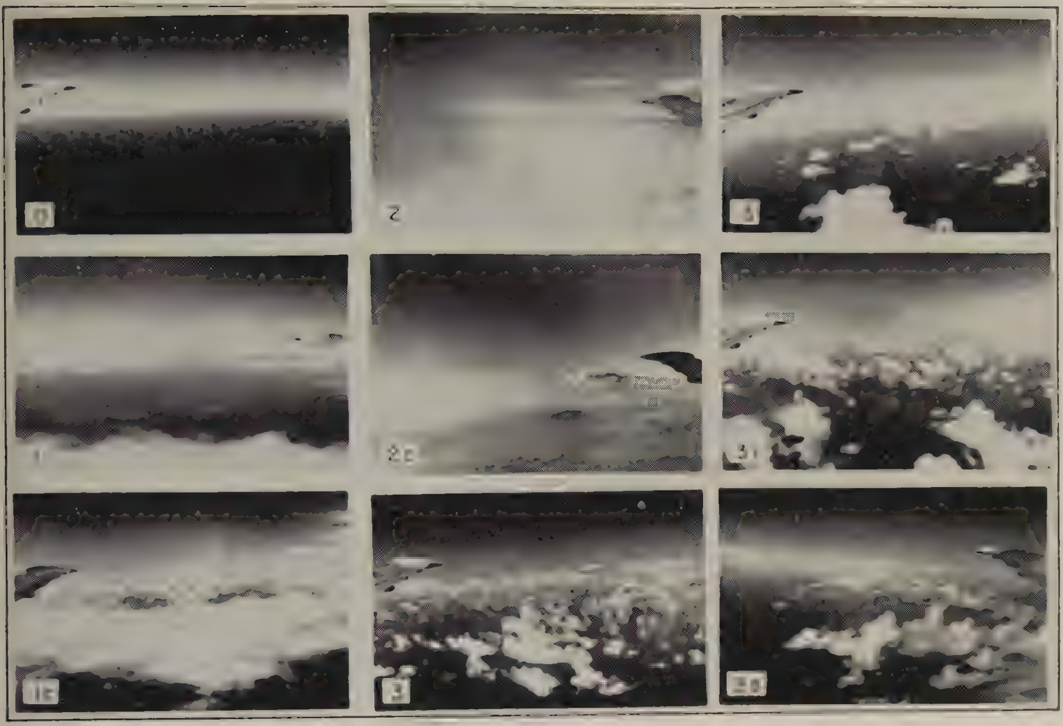

FIG. 9—Illustrations of sky code, undisturbed trade-wind skies

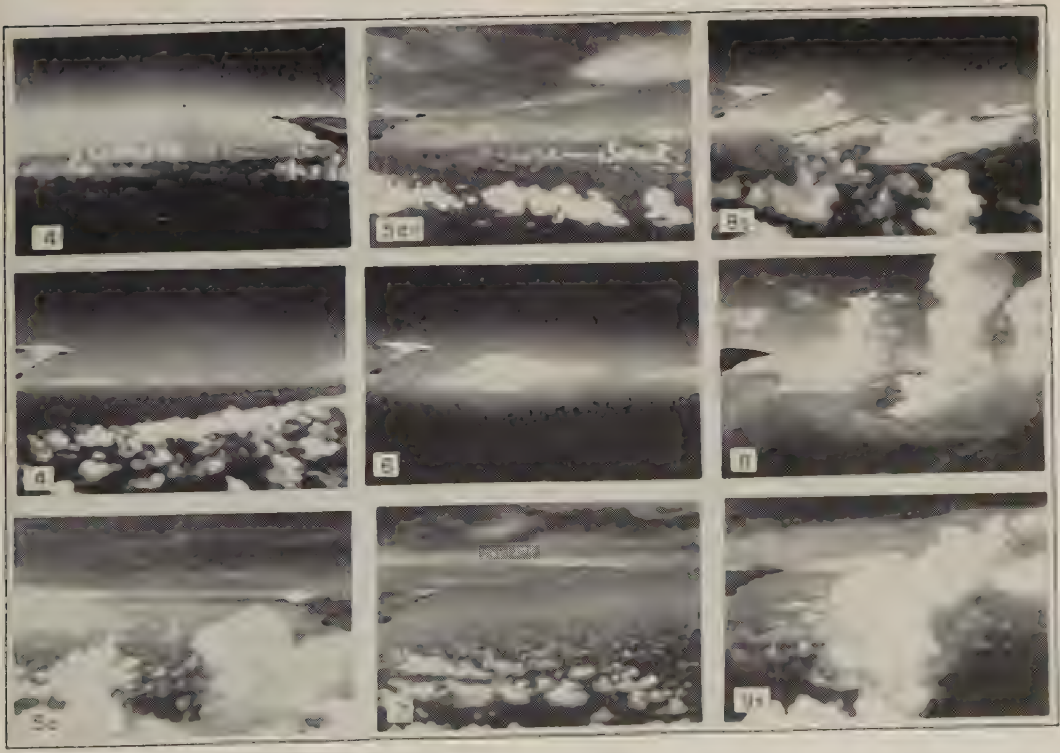

FIG. 10—Illustrations of sky code, organized or trade-wind disturbance or both

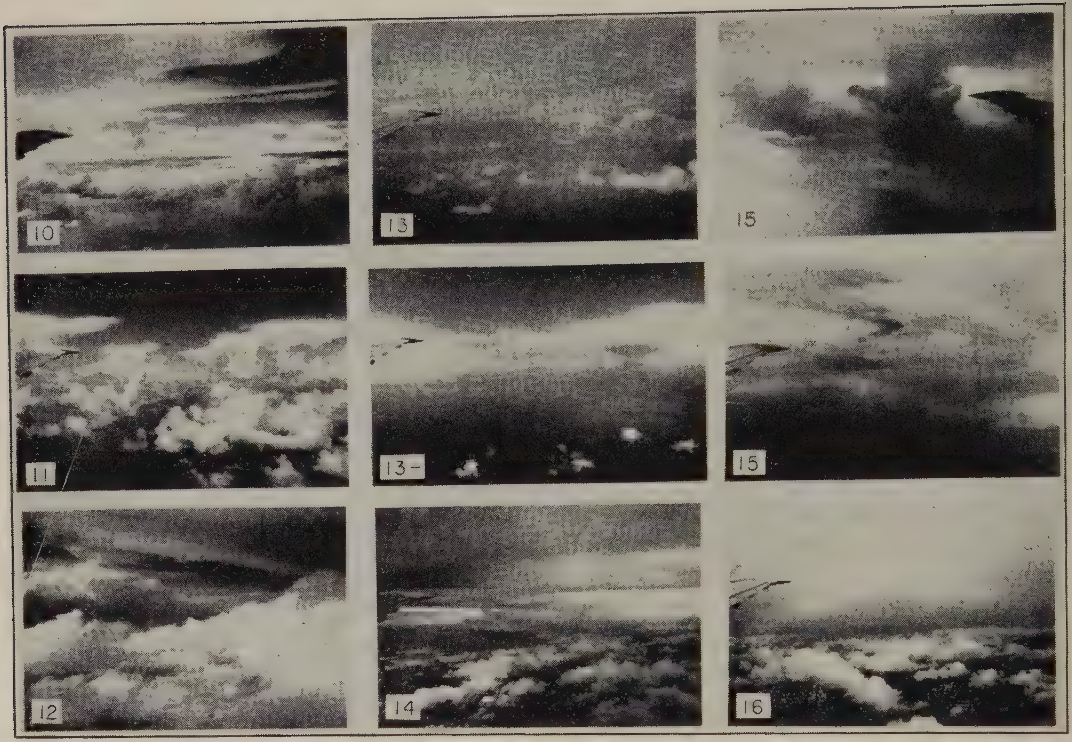

Fig. 11—Illustrations of sky code, tropical disturbance to typhoon

Typical illustrations of each sky type (and most of the postscript modifications thereof) are shown in Figs. 9–11. These were chosen from all the prints of the flight films for a combination of best representativeness and reproducible photographic quality.

Discussion

Dr. Malkus—I think this is an excellent illustration of how a picture can say much more than many words. It was with considerable surprise that we did not find the wave again after it had passed over us during the night and was presumably a hundred miles beyond Kwajalein. It simply was not there anymore. This illustrates, as we saw in Figure 8, that in order to make an analysis of precipitating systems in the tropics, we not only have to know about the synoptic patterns at all levels, but also about the intense coupling between the high tropic patterns and those in the low troposphere.

I will open the discussion by making one comment. It is a provoking question; namely, how well could we predict, understand, or even regulate the microphysics of tropical rain, if we were in an aircraft in the Marshall Islands area and, out of context, made a microstudy of the clouds? Other aircraft studies might be made in the area of Kwajalein and Majuro, which was on the other side of the wave. The result would probably be that one group of people says tropical clouds are less than 10,000 ft high and totally disorganized, while the other group says the observations are wrong, the clouds extend to 50,000 ft and are well organized. I have not heard any arguments quite that preposterous, but, of course, in the different sections and under the different conditions under which these observations were made, we would arrive at different conclusions.

Dr. Horace R. Byers—I think that the greatest sin that cloud physicists commit is to draw conclusions from small samples.

Dr. Morris Neiburger—Well, I will not say that what Drs. Malkus and Byers have just said may not be true, but it seems to me that the case is a rather different one. Rather than assuming that all clouds have the same micro-structure the cloud physicists have been attempting to determine what the differences are which decided whether a cloud will precipitate or not.

Synoptic meteorologists had been puzzled for many years as to why apparently similar situations under some circumstances gave rain and under other circumstances did not. Then Professor Bergeron came forward with his very remarkable explanation in terms of the ice-crystal theory. That handled a good many of the problems. People began to look at the temperatures and degree of supercooling of clouds, and to consider the possibility that the supply of ice-crystal nuclei might, under some conditions, be inadequate.

Then we became aware that there are many cases of rain when clouds are not supercooled; in these cases the ice-crystal theory could not explain the precipitation. There apparently are significant differences even in the micro-structure of warm clouds, and we are now trying to see what those differences are. Far from concluding that every cloud has the same structure, liquid content, or nuclei count, we are seeking to find out what are the critical differences in them.

In all this we are aware that it is necessary to seek the key to the differences in micro-structure, and that this key may be found in the larger scale air mass properties and flow patterns. Our hope is that by knowing what differences in micro-structure are involved, the synoptic and dynamic meteorologist will know what to look for in the large scale structure.

Dr. Henri Dessens—This is very interesting. Especially the organization of the cloud groups is striking. They have been observed and described in the equatorial region by V. Schaefer (*Transactions*, New York Academy of Science, *Oceanography and Meteorology*, pp. 535–540, 1958). In the Congo Basin the organization of clouds is one of the most remarkable facts. Observations regarding the vertical organization of the atmospheric layers in which these clouds form have recently been made at Lukoléla (1°S, 17°E) in the Belgian Congo. The basic very persistent fact in rainy or dry seasons is the existence of a moist layer at the ground. This layer is called the 'monsoon' and is in motion from WNW to ESE. It is topped by the trade-wind layer which moves from ESE to WNW. The trade-wind layer is very dry in the dry season and sometimes humid in the rainy season. During fine weather the humid layer is invariable in thickness at about 1200 meters; but during the rainy weather great variations are observed. Within a few hours one finds successively: 600 meters, 3200 meters, 600 meters, 2200 meters, etc. Deepening of the humid layer permits the formation of cumulus-type clouds. If Cumulonimbus clouds form, the layer may be as thick as 7000 meters. The word 'deepening' has been selected instead of 'wave' in order not to anticipate a wave mechanism for this phenomenon which appears so important in the equatorial region.

Mr. Richard G. Semonin—Incidentally, it also exists elsewhere; Dr. Fujita and I for instance, observed from the aircraft several of these streaks over central Michigan, so they are not limited to tropical regions.

Dr. Tor Bergeron—With respect to what Dr. Dessens said I wonder if he knows that British Colonel Keeling as early as 1908 made a pilot balloon expedition to Khartoum and Mongalla in Sudan. During a dry week in August at Mongalla (5°N) the monsoon formed a very shallow layer, only one to two kilometers thick, but otherwise it was six to seven kilometers deep. I have worked a little with these data and I have formed some ideas as to the structure of the southwest monsoon over Africa, and maybe I shall have an opportunity to come back to this thing during this conference. (See Dr. Bergeron's comments, pages 399–401—Ed.)

Dr. Malkus[a]—The skewed distribution of tropical rainfall is well known. The question remained in the minds of some investigators, however, as to whether this concentration of rainfall into disturbances would be equally pronounced over the much vaster tropical oceans as compared with that over the relatively restricted island and continental masses. The opportunity to make a fairly conclusive test was offered by the Pacific Marshall area data collected and distributed under 'Operation Redwing.' Our study was begun using the radiosonde and six-hourly rainfall data from the atoll of Kwajalein (8°43′N, 167°44′E) which extended in time from April 15 through July 24, 1956. It is interesting to note that the 'equatorial trough' had a mean position in July running right

---

[a] The above comments on tropical rainfall were omitted by Dr. Malkus during the conference because of the limited discussion period. As they are most fitting, Dr. Malkus has kindly contributed them in written form from a manuscript: *Studies of tropical rainfall* by J. Malkus and M. C. Thayer —Ed.

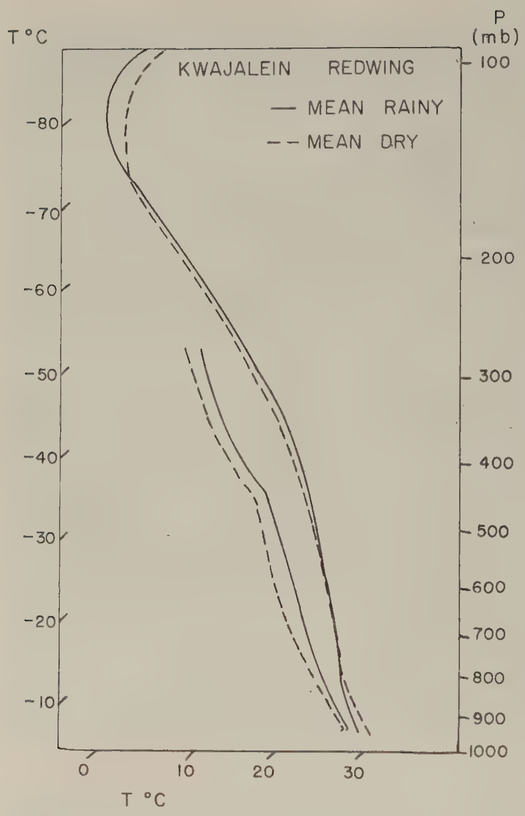

FIG. 12—Average soundings on the rainy and dry days

TABLE 1—*Rainy versus dry soundings for Kwajalein Atoll, April 15–July 24, 1956*

No. of days	24-hour rain	Aver. lapse	Aver. precipitable water	Standard deviation precipitable water
	Inch	°/100 m	gm	gm
Rainy days, 7	1.24	0.56	5.35	0.40
Dry days, 13	0	0.58	4.99	0.44

through Kwajalein, and although we have not yet determined it for April–June, it probably did not lie very far to the south of the Marshalls.

The procedure was first to calculate the 24-hr rainfall occurring between each midnight and the following, and arrange the days in a descending order.

In a total of 100 days, 87 experienced rain (from a trace upward) and a total of 35.21 inches of rain fell. The maximum rain falling in any 24-hr period was 3.26 inches on May 28, and a total of ten days (fairly evenly distributed throughout the period; only two consecutive) experienced more than one inch. On the highest seven of these (R = 1.24 inches) the rain fell fairly evenly around the clock, and these were designated for the remainder of the study as 'rainy' days. The thirteen days on which no rain at all fell were designated as 'dry' days. A mean sounding was then constructed for the rainy and dry days separately (shown in Fig. 12) with rather striking results. First, the soundings are fantastically similar, and day-to-day variations within the 'rainy' and 'dry' classes far exceeded the difference between the two averages. This clearly demonstrates the utter futility of attempting to forecast or explain rainfall in this area in terms of the stability or moisture structure of vertical soundings alone; we must look also either to large-scale dynamics or to microphysics, or to both in interaction. Table 1 summarizes some of the essential features of the soundings.

It will be noted that the tropospheric lapse rate (950 mb—tropopause) is five per cent steeper on the dry than on the rainy days, in good agreement with other findings in the tropics of an inverse relation between instability and penetrative clouds. The difference in average precipitable water (computed both from individual soundings, then averaging, and from the average soundings of Fig. 12) is very slight, and the standard deviation of this property within each category of days (last column) is greater than the difference in the averages, which suggests that the latter is not too meaningful.

Thus we must look for reasons for the enormous difference in rain in the two categories either in terms of the dynamics of the large-scale flows and their effects on penetrative cloud growth, or just possibly in terms of the differences in microfeatures of clouds (such as drop spectrum, nuclei count and spectrum, etc).

All evidence to date convinces us that the dynamics plays the controlling role, and if microphysical differences are at all significant they too are controlled by the large-scale dynamics and the convection itself by some as yet unknown 'feedback' mechanism.

In retrospect, it is not surprising that the concentration of rainfall may prove more pronounced over oceans, since islands and land masses, particularly mountainous ones, create both some large-scale convergence themselves (due to the diurnal heating-cooling cycle) and provide critical 'concentration points' for convergence which would locally intensify that of a very weak traveling disturbance.

Contribution No. 1052

Deep-Sea Research, 1960, Vol. 6, pp. 170 to 172. Pergamon Press Ltd., London. Printed in Great Britain

INSTRUMENTAL NOTE

Acoustically monitored bottom coring

(*Received* 29 *June* 1959)

Abstract—An adaptation of the sound pinger designed by EDGERTON to position an underwater camera for bottom photography has been used to monitor bottom coring operations with a Stetson corer. It is found that the pinger portrays the whole procedure in considerable detail, including the triggering of the corer for free-fall at the bottom. Cores have been taken successfully in water depths of 1912 and 2635 fathoms in the Ionian Sea.

INTRODUCTION

IN OPERATING instruments near the ocean floor in deep water one of the most demanding difficulties has been positioning the gear properly with respect to the bottom. Acoustical monitoring devices have been suggested several times in the past, and a few such devices have come into use. An example is the Scripps Institution's ball breaker (ISAACS and MAXWELL, 1952). Another more recent example is the EDGERTON pinger for monitoring bottom photography (EDGERTON, in preparation). In this note tests are described of an adaptation of the EDGERTON pinger for monitoring deep coring operations.

THE EDGERTON PINGER

The Edgerton Pinger is an ADP crystal array similar to the U.S. Navy's UQN-1b echo-sounding transducer manufactured by the Edo Corporation. The principal difference between the two is that the pinger is mounted in a much lighter aluminium case without the air cavity which houses the inductor of the UQN-1b. The transducer is shock-excited through a carefully tuned auto-transformer from battery power supply, so that no cabling to the surface is needed. The pinger radiates very short pulses of sound (pings) at a precisely controlled rate which is approximately one per second. It has been used by Edgerton and others to position underwater cameras above the bottom. His technique is to attach the transducer to the camera so that it points downward; then the ping and its bottom echo are recorded on an echo sounder recorder as the camera is lowered toward the bottom. The difference in travel time between the directly transmitted ping and the bottom echo is a measure of the height of the camera above bottom.

This instrument was tested by EDGERTON, R. H. BACKUS and the writer on USCGC *Yamacraw* in August 1957 using the Precision Graphic Recorder (PGR) (KNOTT and HERSEY, 1956). These tests were successful in permitting close control of an underwater camera within a few feet of the bottom in water depths up to 1500 fm. It occurred to the writer at the time that here at last was a sound source of adequate power and resolution to perform a similar service for bottom coring.

THE BOTTOM CORING TESTS

During the current cruise of USNS *Chain* to the Mediterranean the first opportunity presented itself for testing the pinger as monitor of a coring operation. At lat. 36° 55′N and long. 19° 50·2′E in the Ionian Sea we found a flat bottom at 1912 fm (assuming a sound velocity of 800 fm/sec). The bottom echo was followed by several later echo sequences suggesting the presence of several reflecting layers within 50 ft below the bottom. Some of these were well within reach of the 13-ft Stetson corer we had available at the time. A sample recording of the echo sequence over this flat area is shown in Fig. 1.

PROCEDURE AND RESULTS

The Stetson corer was rigged in the usual manner with 30 ft of suspension cable coiled at the trigger mechanism (Hvorslev and Stetson, 1946) but without its lead weights. Thirty feet above the releasing mechanism we attached the Edgerton pinger by means of a short wire rope pendant clamped to the suspension cable. Upon lowering this assembly we found immediately that the directly transmitted ping, and its echoes from the top of the corer, the trigger weight, and the sea bottom were all clearly recorded (Fig. 2). In addition there was a more faintly recorded echo which had been reflected first from the surface and then from the bottom before reaching the echo sounder.

Since the Edgerton pinger pings once a second the PGR was operated with a one second sweep (400 fm scale) so as to record one ping and one bottom reflexion per sweep. Knowing the approximate depth of the pinger and the depth of water a precise measure of the difference in acoustic travel time between the ping and its own echo may easily be read. If the suspension cable had been vertical the exact height of the pinger above bottom could also be measured. In this lowering, wire angles were small (about 30° at most) and in any event the exact height is of little consequence; the principal objective in coring is to lower the corer deep enough so that the trigger weight operates satisfactorily without at the same time paying out extra wire to tangle on the bottom.

Thus knowing the water depth to be approximately 1900 fm the ‘ height ’ of the pinger and corer above bottom is easily deduced by recalling that the echo recorded on a given sweep must be that corresponding to the ping recorded about 4·75 sweeps previously. As the lowering proceeds the ping and echo sequences cross and re-cross at times when the travel times differ by an integral number of seconds, or multiples of 400 fm. Thus the progress of the lowering could be followed with assurance (Fig. 3).

When the height above bottom became less than 100 fm the PGR sweep was changed to 0·25 sec (100 fm scale). Then much more detail was apparent (Fig. 4). The bottom echo which had appeared as double on the slower sweep was now resolved into four clear echoes, and after increasing the gain of the recorder the echo from the top of the corer was to be seen. As the corer reached a height of 5 fm its echo disappeared because the tripping weight had just struck bottom releasing the corer (Fig. 4). The suspension cable was then raised and the echo of the corer was seen separating from the bottom echo. The corer echo shows that the corer was sixty feet from the pinger in its proper position after coring. A third echo, probably that of the trigger mechanism was discernible thirty feet from the pinger (Fig. 4).

DISCUSSION

Some speculation can be made about the maximum depths to which Edgerton's present pinger can be used for coring. Since the first test described above a successful core has been taken in 2635 fm. In this water depth it was still possible to record the corer echo just before the tripping mechanism operated. Since it has proved to be the weakest sound of the sequence excepting only the echo from the lead tripping weight, one seems justified in supposing that the pinger is more than adequate for most ocean areas. Unfortunately it was not possible to obtain meaningful quantitative estimates of echo levels on this deeper lowering because of a bothersome electrical noise.

No preparations had been made for quantitative measurements during the first test, but judging from past experience with the PGR and the appearance of this recording the direct arrival and bottom echo were probably over 20 dB above the background noise throughout the test, while the other echoes were obviously fainter. With so favourable a signal-to-noise ratio in 1900 fm, useful operation should be possible in at least 3800 fm, since the additional transmission loss should be of the order of 14 dB (6 db spreading loss for doubling the distance and about 8 dB attenuation for the additional 3800 fm travel path). It appears to the writer that the signal-to-noise estimates above are conservative enough that the Edgerton pinger may well be loud enough to be useful for coring in all ocean depths, given expectably quiet receiving conditions at the echo sounder.

ACKNOWLEDGMENTS

The author is principally indebted to Prof. Harold Edgerton for his help and kindness in advising about his design and supplying auto transformers for the adaptation of his pinger to such purposes as reported here. Mr. Robert Cotell built the adaptations, and Mr. Thomas Stetson and

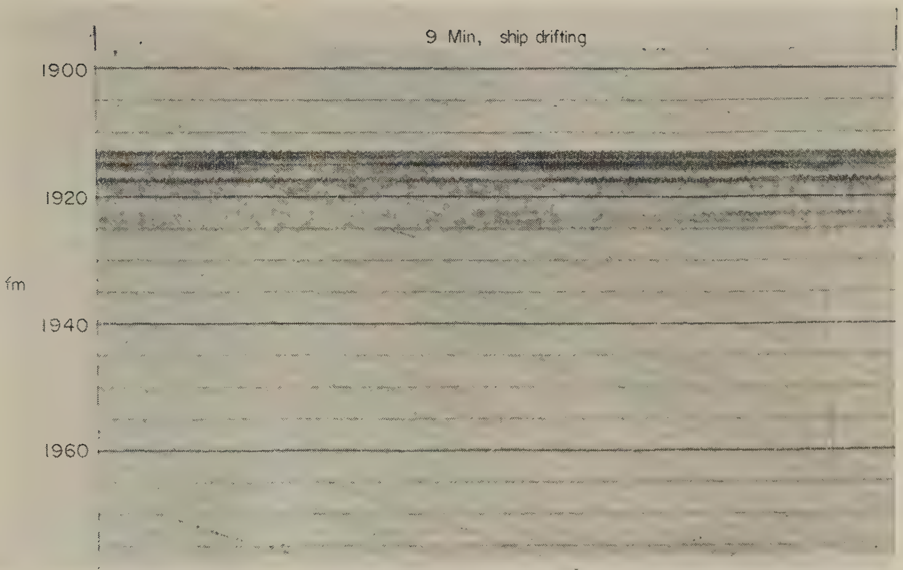

FIG. 1. High resolution bottom echo sequence at the core location, lat. 36° 55′N, long. 19°–50·2′E, from a drifting ship.

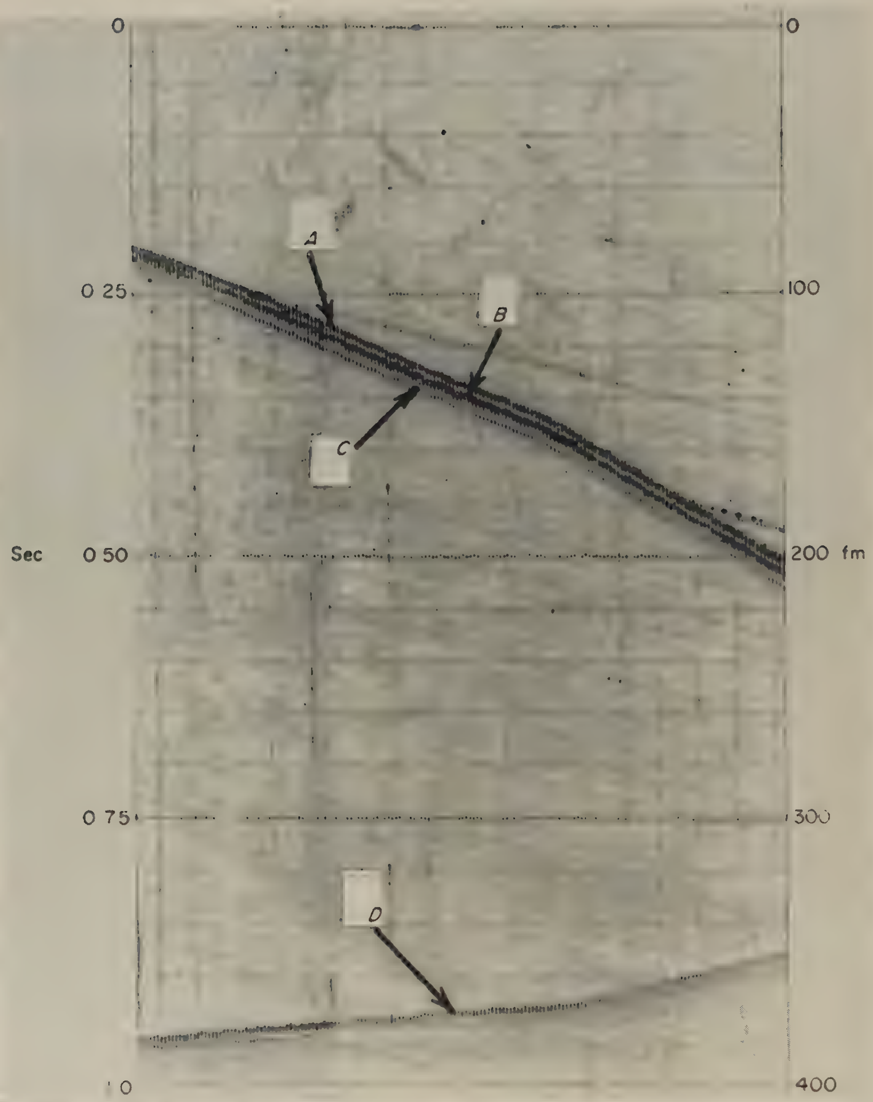

FIG. 2. Events recorded by the PGR when the corer and pinger are near the surface. A—the ping; *B*—the echo from the top of the corer; *C*—the echo from the trigger weight; and *D*—the bottom echo.

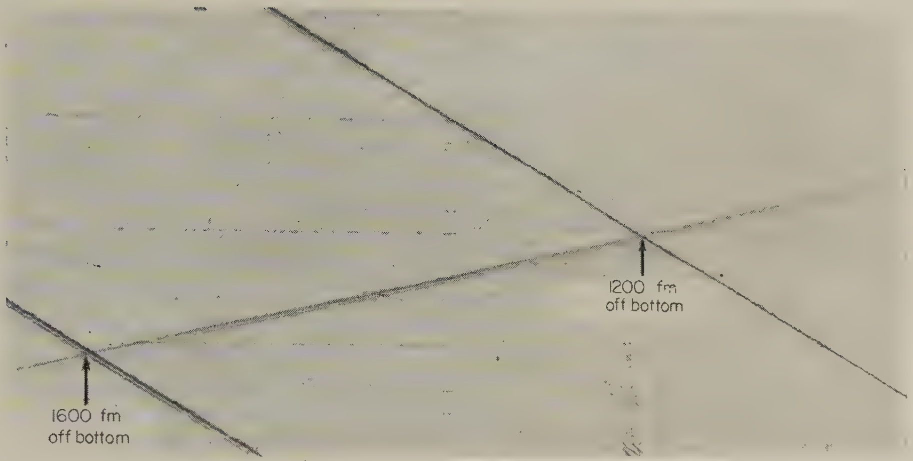

FIG. 3 The PGR record of part of the descent. Ping and bottom echo sequences crossed when the difference between their travel times was an integral number of seconds.

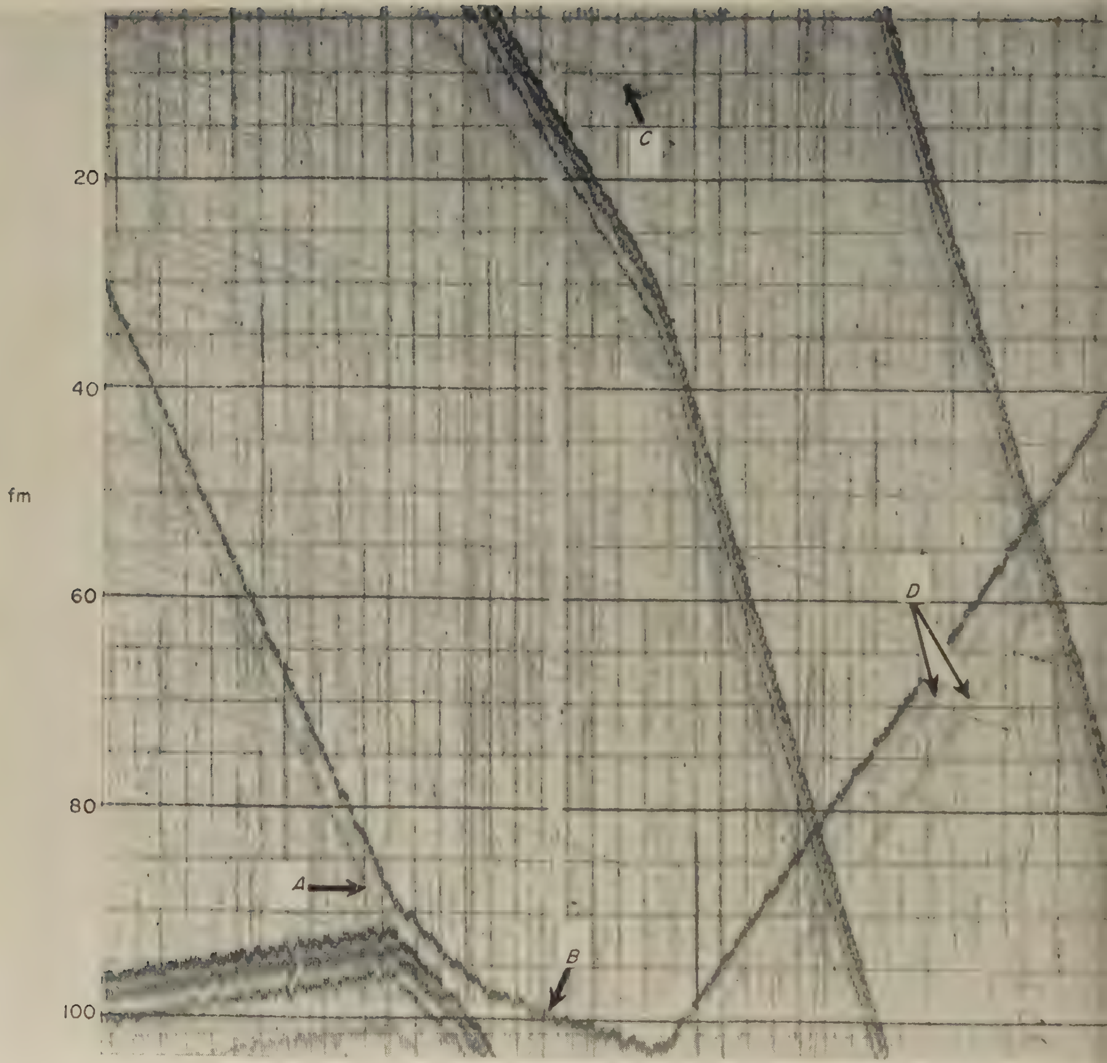

FIG. 4. Events recorded by the PGR when the corer is near the bottom. *A*—the echo of the top of the corer disappeared as the trigger released the corer for free-fall; *B*—the ascent commences; *C*—the echo of the corer appears as the corer is raised off bottom; *D*—during ascent echoes from both trigger mechanism and corer are recorded.

Dr. RICHARD PRATT rigged the corer. I am much indebted to Capt. OLIVEY and Boatswain LADZENSKI of the USNS *Chain* for valuable advice and assistance in the coring operations. This work was done under Contract Nonr-1367 with the Office of Naval Research, U.S. Navy Department.

J. B. HERSEY

Woods Hole Oceanographic Institution,
Woods Hole, Mass., U.S.A.

Contribution No. 1052 *of the Woods Hole Oceanographic Institution. This work was performed under Contract Nonr-*1367 *with the Office of Naval Research, U.S. Navy Department.*

REFERENCES

EDGERTON, H. E. In preparation.

HVORSLEV M. J. and STETSON H. C. (1946) Free-fall coring tube : A new type of gravity bottom sampler. *Bull. Geol. Soc. Amer.* **57**, 935-950.

ISAACS J. D. and MAXWELL A. E. (1952) The ball-breaker, a deep water bottom signalling device. *J. Mar. Res.* **11**, 63-68.

KNOTTS S. T. and HERSEY J. B. (1956) Interpretation of high-resolution echo-sounding techniques and their use in bathymetry, marine geophysics, and biology. *Deep-Sea Res.* **4**, 36-44.

Printed in Great Britain by The Salisbury Press Ltd., Publicity House, Wilton Road, Salisbury, Wilts. (20257)

Contribution No. 1053

Sonderdruck aus „Zoologischer Anzeiger“ Bd. 165, Heft 9/10, 1960
Akademische Verlagsgesellschaft Geest & Portig K.-G., Leipzig

2. Zoologisches Institut der Universität Wien und Woods Hole Oceanographic Institution, Woods Hole, Mass., U.S.A.

Vorschlag zum Anlegen einer „Stoffwechselkartei“ für marine Tiergemeinschaften

Von

WOLFGANG WIESER[1] und JOHN KANWISHER

Mit 1 Abbildung und 1 Tabelle

(Eingegangen am 2. November 1959)

Die systematische Erforschung der Tiergemeinschaften des Meeres hat für gewisse Lebensräume ein Stadium erreicht, in dem die Aufstellung weltweiter Besiedlungsschemata durchaus im Bereich des Möglichen liegt. Dies gilt vor allem für die felsigen Küsten des Gezeitengebietes (**SOUTHWARD** 1958) sowie für Sand- und Schlammböden (**THORSON** 1957). Alle bisherigen Versuche in dieser Richtung lassen vermuten, daß vergleichbare Biotope in sämtlichen Meeresregionen durch ähnliche Tiergemeinschaften besiedelt werden, wobei sich die Ähnlichkeit dadurch ausdrückt, daß die dominanten Formen derselben Gattung, derselben Familie oder zumindest derselben „Lebensform“ angehören. Es entsteht also ein Bild von der Tierbesiedlung der Weltmeere als einem Mosaik „paralleler“ oder „homologer“ Gemeinschaften, deren Übereinstimmung auf der Übereinstimmung gewisser physiographischer Merkmale der Biotope (vor allem des Substrates), deren Unterschiede auf den Unterschieden anderer Umweltsfaktoren (vor allem der Temperatur) beruhen. Diese Vorstellung wird im einzelnen noch modifiziert werden müssen, aber im Kern ist sie zweifellos richtig.

---

[1] Dr. Wolfgang Wieser, Wien I, Dr.-Karl-Lueger-Ring 1, 2. Zool. Institut der Universität.

[2] Contribution no. 1053 from the Woods Hole Oceanographic Institution.

Es ist nun von THORSON in mehreren Arbeiten (s. vor allem THORSON 1952) die Meinung ausgesprochen worden, daß die „parallelen Tiergemeinschaften" nicht nur vom systematischen, sondern auch vom physiologischen Gesichtspunkt aus vergleichbar seien, was auf die zum ersten Mal von ORTON (1923) festgestellte Tatsache zurückzuführen wäre, daß gewisse poikilotherme Meerestiere selbst unter sehr unterschiedlichen Temperaturverhältnissen ein relativ konstantes Stoffwechselniveau aufrechterhalten. Auf Grund dieser Temperaturanpassung der einzelnen Arten würden — nach THORSON — etwa innerhalb einer arktischen und einer tropischen Tiergemeinschaft dieselben Energieverhältnisse herrschen sowie dieselben interspezifischen Beziehungen aufrechterhalten werden, obwohl zwischen den Lebensräumen der beiden Gemeinschaften ein durchschnittlicher Temperaturunterschied von mehr als 20 °C bestehen mag.

Nun finden sich in der Literatur zahlreiche Beispiele sowohl für als auch gegen die Existenz von Temperaturanpassung bei poikilothermen Tieren (THORSON 1952, BULLOCK 1955). In allen Fällen sind bisher jedoch nur einzelne Arten, niemals eine ganze Tiergemeinschaft (oder auch nur sämtliche dominanten Repräsentanten einer Gemeinschaft) untersucht worden. Inwieweit die These von der physiologischen Vergleichbarkeit paralleler Tiergemeinschaften zutrifft, kann jedoch nur unter Berücksichtigung einer möglichst großen Anzahl von Vertretern dieser Gemeinschaften, nicht durch willkürliches Herausgreifen einzelner Arten entschieden werden.

Es sollte darum der Versuch gemacht werden, die physiologische Aktivität der Hauptformen paralleler Tiergemeinschaften aus den verschiedensten Meeresregionen zu erfassen. Als günstigster Ausdruck der physiologischen Aktivität bietet sich der Sauerstoffverbrauch an und die gewonnenen Daten mögen in Form einer „Stoffwechselkartei" zusammengefaßt werden. Ein Schema dieser Art ist in Abbildung 1 dargestellt. Es repräsentiert die Stoffwechselaktivität der Hauptvertreter der auf den großen Braunalgen um Woods Hole, Mass. (USA), lebenden Fauna. Die Charakterarten rekrutierten sich aus Nematoden (*Enoplus, Theristus*), Halacariden (*Rhombognathides, Halacarus*), Copepoden (*Harpacticus*), Amphipoden (*Calliopius, Hyale, Gammarus*), Chironomiden-Larven, Isopoden (*Idotea*) und Gastropoden (*Littorina*). Die Brauchbarkeit eines solchen Schemas hängt weitgehend von der Kontrolle der Bedingungen, unter denen die Messungen durchgeführt wurden, ab. Darum muß jedem „Karteiblatt" eine Legende mit möglichst detaillierten Informationen über die verschiedenen Variablen der Untersuchung beigegeben werden. Von besonderer Bedeutung sind Angaben über: Lokalität, Biotop, jährlichen Temperaturbereich des Wassers am Aufsammlungsort, Datum der Aufsammlung und Temperatur des Wassers zu diesem Zeitpunkt, verwendete Messungs-

Tab. Der Sauerstoffverbrauch (in mm³/g Trockengewicht/Stunde) der wichtigsten Komponenten einer auf Braunalgen lebenden Tiergemeinschaft.

Lokalität: Woods Hole, Massachusetts, USA. Jährlicher Temperaturbereich von 1,5 bis etwa 22 °C.

Biotop: Braunalgen auf Steinen (*Fucus vesiculosus*, *Ascophyllum nodosum*, mit Epiphyten (z. B. *Elachistea fucicola*) und anderen, kleineren Algen, z. B. *Chondrus crispus*). Nobska Beach, Little Harbor und kleiner Strand gegenüber MBL-Gebäude. Gezeitengebiet.

		Nematoden	Halacariden	*Harpacticus chelifer*	Amphipoden	Chironomiden-Larv.	*Idotea baltica*	*Littorina littorea*
Probenentnahme	Monat	I,II	IV	VI	IV—VI	VI	VI	VI
	Temperatur(C)	−1,5°	7—8°	18°	8—15°	15°	15—18°	18°
Experimente	Methode	←—— Cartesischer Taucher ——→			←—— SCHOLANDERS volumetrischer Respirometer ——→			
	Temperatur	←—— 20 °C ——→			←—— 10° ± 1° ——→			
	Zeitpunkt	unmittelbar nach Probenentnahme oder nach:						
		1—7tägiger Haltung bei 0°	1—4tägiger Haltung 2—7°	—	1—4tägiger Haltung bei 3—8°	1—3tägiger Haltung bei 7°	1tägiger Haltung bei 7°	—
Lebensphase der Versuchstiere		Erwachsene, ♀♀ eiertragend			späte Juvenilstadien, Erwachsene	große Larven	♀♀ mit Oostegiten, und ♂	Juvenilstadien und Erwachsene

Bemerkungen: 1. In keinem Fall ließ sich ein statistisch gesicherter Unterschied zwischen den gleich nach dem Aufsammeln und den nach mehrtägigem Halten bei vergleichbarer oder etwas niederer Temperatur gemessenen Tieren feststellen.

2. Die Nematoden zeigen zwischen −1,5° und 18° mit Sicherheit keine Temperaturanpassung.

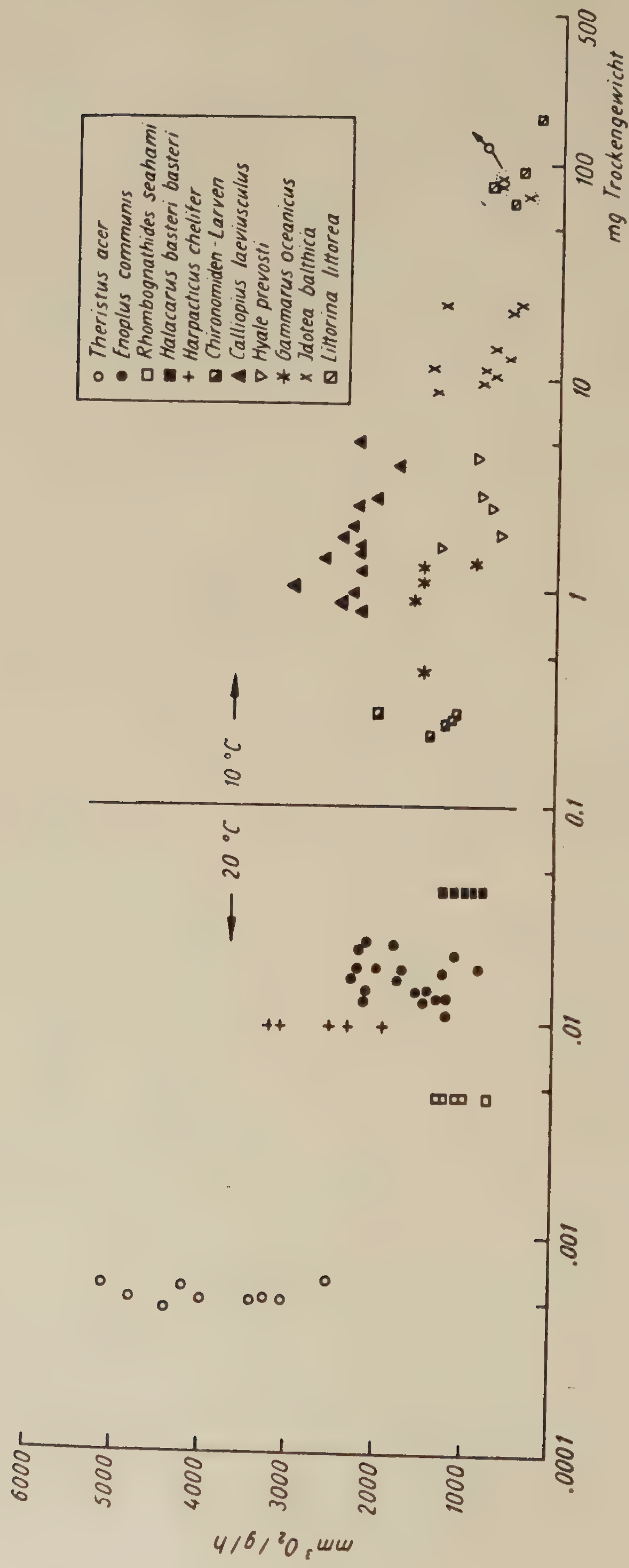
mm³ O₂/g/h
6000
5000
4000
3000
2000
1000
.0001
.001
.01
0.1
1
10
100
500
mg Trockengewicht
← 20 °C
10 °C →
○ Theristus acer
● Enoplus communis
□ Rhombognathides seahami
■ Halacarus basteri basteri
+ Harpacticus chelifer
▣ Chironomiden-Larven
▲ Calliopius laeviusculus
▽ Hyale prevosti
✱ Gammarus oceanicus
× Idotea balthica
⊠ Littorina littorea

Abb. 1

methode, Temperatur, bei der die Messungen durchgeführt wurden, Geschichte des untersuchten Materials, d. h. ob die Tiere unmittelbar nach dem Aufsammeln oder nach Haltung bei bestimmten Temperaturen gemessen wurden, Aktivität und Lebensphase der untersuchten Tiere. Weiterhin tragen alle zusätzlichen Informationen über eventuell festgestellte Temperaturanpassungen (jahreszeitliche und experimentelle) oder deren Abwesenheit zur Brauchbarkeit des Schemas bei. Eine genaue Berücksichtigung des Temperaturfaktors in all seinen Aspekten ist auf jeden Fall unerläßlich.

In Gebieten mit weitgehend konstanten Temperaturverhältnissen mag ein einziges Schema repräsentativ für die während des ganzen Jahres herrschenden Verhältnisse sein, obwohl auch hier die Entwicklungsphasen der einzelnen Tiere charakteristische Variationen in der Stoffwechselintensität verursachen mögen, die erfaßt werden sollten (Thorson 1936). In Gebieten mit wechselnden Temperaturverhältnissen müssen im Idealfall mehrere Schemata — jedes charakteristisch für eine bestimmte Jahreszeit — erstellt werden. Die Tabelle enthält Messungen, die zwischen Januar und Juni 1959 durchgeführt wurden, da aber jede Tiergruppe innerhalb eines Zeitraumes von nicht mehr als drei Monaten, meistens bloß innerhalb eines einzigen Monats gemessen wurde und die in diesen Zeiträumen herrschenden Temperaturverhältnisse keine großen Schwankungen aufwiesen, lassen sich die Daten für später aufzustellende jahreszeitliche Schemata verwenden.

Was die Form der Darstellung betrifft, so sind zwei Bedingungen besonders hervorzuheben: 1. Die Messungen müssen gewichtsbezogen sein, 2. die intraspezifische Variabilität der gewonnenen Werte muß aus dem Schema hervorgehen. Als Gewichtseinheit empfiehlt sich die Verwendung des Trockengewichtes (bei Mollusken unter Ausschluß der Schale); bezieht man jedoch auf Frischgewicht, dann sollte für die betreffende Tiergruppe das Verhältnis Frisch- : Trockengewicht bekannt sein (s. die Tabelle bei Thorson 1957). Die Gewichtskoordinate muß natürlich logarithmisch gewählt werden, da die untersuchten Tiere einen möglichst weiten Größenbereich umfassen sollen, während die Stoffwechselkoordinate arithmetisch sein kann.

Anzustreben wäre, viele „Karteiblätter“ von der Art, wie eines in Tab. 1 dargestellt ist, anzulegen, und erst auf dieser Basis ein Urteil über das Maß der physiologischen Ähnlichkeit paralleler Tiergemeinschaften zu fällen.

Schrifttum

Bullock, T. H.: Compensation for temperature in the metabolism and activity of poikilotherms. Biol. Rev. **30** (1955) 311—342.

Orton, J. H.: Some experiments on rate of growth in a polar region (Spitzbergen) and in England. Nature, London, **111** (1923) 146—148.

SOUTHWARD, A. J.: The zonation of plants and animals on rocky sea shores. Biol. Rev. **33** (1958) 137—177.

THORSON, G.: The larval development, growth and metabolism of arctic marine bottom invertebrates. Medd. Grønland 100, **6** (1936) 1—155.

— Zur jetzigen Lage der marinen Bodentier-Ökologie. Verh. Dt. Zool. Ges. Wilhelmshaven 1951 (1952) 276—327.

— Bottom Communities. In: Treatise on marine ecology and paleoecology. Geol. Soc. America, Mem. **67** (1957) 461—534.

Satz und Druck: Buchdruckerei Paul Dünnhaupt, Köthen

Contribution No. 1054

Made in United States of America
Reprinted from LIMNOLOGY AND OCEANOGRAPHY
Vol. 5, No. 2, April, 1960
pp. 121–137

BENTHIC STUDIES IN BUZZARDS BAY
II. THE MEIOFAUNA

BY WOLFGANG WIESER

ERRATA: The following corrections are required to Vol. V No. 2 of Limnology and Oceanography.

p. 137 The reference "Riedl, R. 1954" should read "RIEDL, R. 1956. Zur Kenntnis der Turbellarien adriatischer Schlammböden sowie ihrer geographischen und faunistischen Beziehungen. Thalassia Jugoslavica **1**: 69–184."

p. 144 The legend of Figure 1 should read—"Trellis diagram showing the degree of faunal similarity among the 24 samples from Station R.

pp. 151–152 The histograms in Figures 2 and 3 should be interchanged with their legends remaining on the pages as now printed.

BENTHIC STUDIES IN BUZZARDS BAY
II. THE MEIOFAUNA[1]

Wolfgang Wieser

Department of Zoology, University of Vienna, Austria
and Woods Hole Oceanographic Institution, Woods Hole, Mass.

ABSTRACT

During the summer of 1957 a study of the small metazoans (meiofauna), based on a series of Phleger core samples, was undertaken at three stations in Buzzards Bay, Massachusetts. The number of animals ranged from 1.69 x 10^5 to 1.86 x $10^6/m^2$, the dry weights varied from approximately 100 to 600 mg/m^2. The nematodes and kinorhynchs, which comprised between 89 and 99% of the total mieofauna, were studied in detail. The sandy localities (stations P and J) were characterized by a number of nematodes restricted to this habitat, particularly by three representatives of the genus *Odontophora* and by all representatives of the genus *Leptonemella.* The locality rich in fine deposits (station R) was characterized by the relative abundance of several nematodes, particularly of *Terschellingia longicaudata,* and the three kinorhynch species. It was possible to recognize an *Odontophora-Leptonemella* community in the sandy habitats, and a *Terschellingia longicaudata-Trachydemus mainensis* (kinorhynch) community in the silty habitat, the former being equivalent to the *Ampelisca* community, the latter to the *Nucula proxima-Nephthys incisa* community described for the macrofauna in the same area. However, these "communities" can also be considered as two ecological groups of species, the former dependent on the presence of sand, the latter on that of fine deposits, which actually live side by side, forming an intricate meshwork of faunal combinations. Each combination is determined by the relative amounts of sand and fine deposits present.

The uniformity of the nematode fauna within each station was greater than that between two different stations. Most important in determining the degree of faunal uniformity between paired samples is the similarity in their silt-clay content. However, other mechanical factors also play a role.

An analysis of the total species composition of the nematode fauna revealed that *Terschellingia longicaudata* was the most abundant species at station R, whereas at the stations P and J there were three or four equally dominant species. This is interpreted as indicating a splitting up of the sandy habitat into subhabitats. The simultaneous occurrence of closely related species in this environment further supports the conjecture.

The distribution of "buccal types" amongst nematodes is correlated with the distribution of sediments.

This is the second contribution to an investigation, initiated by Sanders (1958) which aims at as complete a picture as possible of the various vectors determining the structure and dynamics of a marine benthic community. It is concerned with the meiofauna, a term coined by Mare (1942) to characterize metazoans of medium size and which in the present paper includes the following groups: nematodes, kinorhynchs, ostracods, copepods, turbellarians, oligochaetes, halacarids, gastrotrichs and cephalocarideans. The former two groups (which together account for more than 90% of the meiofauna) are treated in detail, the others summarily without identification of species.

The area of investigation is Buzzards Bay, Massachusetts, the physiographic characters of which were described by Sanders

---

[1] Contribution No. 1054 from the Woods Hole Oceanographic Institution,

(1958). The samples on which the present study is based were taken by the author and H. Sanders between July and September 1957. I am indebted to H. Sanders for extensive discussions during preparation of this manuscript and also to him and to Jay Bercaw, the skipper of the R. V. "ASTERIAS", for assistance during sampling, and to the Woods Hole Oceanographic Institution for granting me a summer fellowship.

So far, studies of submarine benthic communities have been restricted to the macrofauna. Quantitative data on the density of the meiofauna below tidal level have been supplied by Moore (1931), Krogh and Sparck (1936), Mare (1942), Bougis (1946, 1950) and Purasjoki (1947). However, in none of these cases was the meiofauna identified to species. Numerical comparisons between meiofauna and macrofauna from the same locality were made only by Krogh and Sparck and by Mare. Recently, a very complete and thorough study of the sublittoral nematode fauna of the Bay of Kiel has been undertaken by Gerlach (1958) who delimited only qualitatively the fauna of different types of substrate. This holds also for Filipjev's classical work on the nematode fauna in the vicinity of Sebastopol (Filipjev 1918/21), for the author's investigation into the nematode fauna off the Chilean coast (Wieser 1958), and for the few studies dealing with the other meiofauna groups, *e.g.* ostracods (Elofson 1941), copepods (Lang 1948) and turbellarians (Riedl 1954).

METHODS

Collecting

The samples were taken with a Phleger core sampler, the plastic tubes of which have an inner diameter of 3.4 cm, circumscribing an area of 9.07 cm^2. In this paper, however, the area will be considered equivalent to 10 cm^2. In sand the core sampler did not work too well, but its efficiency could be slightly improved by attaching a brass core catcher to the opening of the tude. Only undisturbed cores were used. Samples were taken at three stations, the average sediment composition of which had been established earlier by Sanders (1958, Figure 1, Tables 1, 2). Station P comprised well sorted sand with little silt-clay, station J poorly sorted sand with much silt-clay and station R silt-clay with little sand. One sample, termed RA–1, was taken at station R but resembled a J-sample in appearance and sediment composition. In all, 5 single and 7 pairs of replicate samples were taken (Table 1). With each single and each pair of replicate samples an additional sample for sediment analysis was collected. This procedure introduced an uncertainty factor since the sample on which the faunal and the sediment analyses were based did not come from the same spot of substratum. This was not considered serious since the general sediment composition of the stations had already been established by Sanders, making it easy to distinguish macroscopically between the three types of substrate, and since the scope of the present investigation was to study the general structure of the meiofauna populations at the three stations rather than to elucidate in a detailed manner sediment-animal relationships.

The plastic tube containing the sample was taken to the laboratory, the water was siphoned off and the core was pushed upwards by means of a rubber plunger. The upper 7cm of the core, which had been shown previously to contain almost all the animals (see also Moore 1931, Mare 1942), were cut off and put into a 500 cc graduated cylinder which was then filled with filtered sea water and thoroughly shaken. After allowing sand to settle, the supernatant was poured through a screen with a mesh width of 160μ. The water with the fine particles that went through the screen was caught in a bucket. This procedure was repeated several times and resulted in separating the sample into three fractions: 1) the sand fraction in the cylinder 2) the medium fraction retained by the screen, and 3) the fine fraction that passed through the screen and was caught in the bucket.

Fraction 1 was discarded since repeated checks showed that a very thorough shaking

TABLE 1. *Grain size distribution and depth of samples taken in Buzzards Bay. Brackets unite samples which are considered replicates (see text)*

Sample No.	Date	Depth (m)	Grain size in mm Sand					Silt-clay <0.05	Ave. silt-clay content
			>1.0	1.0–0.5	0.5–0.25	0.25–0.12	0.12–0.05		
P-1	7/8	18	0.2	0.4	5.9	81.4	5.8	6.3	11.8
P-2	7/19	18	0.2	1.6	7.7	59.6	10.3	20.6	
P-3	8/9	18–20	0.1	0.6	8.6	78.6	6.6	5.5	
P-4	—	—							
P-5	8/30	30	2.8	6.6	3.17	39.1	5.1	14.7	
P-6	—	20							
RA-1	7/12	18	5.1	13.5	30.1	16.1	8.2	27.0	30.0
J-1	7/12	12	7.3	30.4	31.1	18.4	6.5	6.3	
J-2	—	—							
J-3	8/2	12	7.5	26.1	24.3	6.7	7.4	28.0	
J-4	—	—							
J-5	8/16	12	1.9	7.4	9.9	4.8	17.7	58.3	
J-6	—	—							
R-1	7/12	18	0.2	0.3	0.5	1.3	13.1	84.6	79.7
R-2	7/29	18	0.1	0.1	0.5	1.6	17.4	80.3	
R-3	—	—							
R-4	8/21	18	0.2	0.3	1.3	3.5	20.4	74.3	
R-5	—	—							
R-6	9/12	18	0.2	0.2	0.7	2.3	14.4	82.2	

tears loose all the animals and puts them into the supernatant. Fraction 2 was examined under the microscope, the animals being picked out and counted. Sometimes it was found necessary to divide this fraction and to examine only ½ or ¼ of it, extrapolating the results. The bucket with fraction 3 was left to stand in running sea water or in the refrigerator until the examination of fraction 2 had been completed. Then the water in the bucket was thoroughly stirred and 4 or 5 aliquots taken with a large pipette. Each aliquot was put into a Petri dish and allowed to settle. The fine deposits form a thin layer in which even very small nematodes can be seen under the microscope at strong illumination as long as they are alive and wriggle actively. The number of animals was extrapolated to the total volume of water present in the bucket.

Weight determinations

No meaning can be attached to the wet weight of small animals determined by direct weighing since evaporation through the body wall takes place too rapidly to allow the definition of a stable state. Thus dry weights only should be used. However, in order to allow comparisons with the macrofauna where very often only the wet weight is given, it would be desirable if wet weight values of the meiofauna were also available. It is fortunate in this respect that the most abundant meio-animals, the nematodes, due to their nearly cylindrical shape, lend themselves to weight determinations on the basis of volume and specific gravity measurement.

The nematodes before preparation were stretched in an oven at about 48°C, then fixed in 4% formaldehyde and transferred into pure glycerine by the evaporation method, a process which should take several days. The nematodes were mounted on slides, using glass rods or short pieces of nickel-chromium (Capstick 1956), tantalum or some other wire to support the coverslip. If the transfer into glycerine and the selection of the supporting rods is carried out carefully no significant shrinking or squashing of the animals occurs. At this stage the volume of the nematodes was determined by calculating $L \times (W/2)^2 \times \pi$, L being the length, W the body width at the middle of

TABLE 2. *Estimates of the ratio of dry weight to wet weight for various nematodes*

Number weighed	Species	Weight in mg Wet	Dry	Dry/Wet × 100	Type of Balance
124	*Enoplus communis*	5.44	1.42	26.1	quartz helix
28	*Enoplus communis*	1.48	0.41	27.7	quartz helix
48	*Enoplus communis*	2.14	0.60	28.0	analytical
73	*Enoplus* sp., *Sphaerolaimus dispar*, *Anticoma litoris*, etc.	2.43	0.50	20.6	analytical
49	*Metoncholaimus pristiurus*	0.725	0.196	27.0	quartz helix

the oesophagus. In species with a very long filiform tail, the length of the animal was taken from the anterior end to the end of the conical portion of the tail. In most species the diameter at the middle of the oesophagus corresponds reasonably well to the diameter of the imaginary cylinder, the volume of which is equivalent to that of the nematode. The same assumption was made by Nielsen (1951), who compared the results achieved by this method with those of another method and found good agreement. The values obtained do not differ significantly from those obtained with Andrassy's formula $a^2b/1.7$, in which a is the *maximum* width and b the length of the nematode (Andrassy 1956).

The volume multiplied by specific gravity gives the wet weight. The specific gravity of the marine nematode *Enoplus communis* Bast. was determined by flotation in a series of mixtures of kerosene and bromobenzene (suggested by Dr. J. Kanwisher). A value of 1.13 was obtained and taken as characteristic of all marine nematodes. Nielsen found a value of 1.02 and Andrassy of 1.084 for fresh water and terrestrial nematodes.

As every specimen could not be measured, an average volume was computed for the adults of each species; the juveniles were assumed to measure half that much. From the number of nematodes identified (ranging from 59 to 233 per sample) an average weight per specimen was calculated which, multiplied by the number of animals counted, gave the wet weight per sample or per 10 cm^2.

The mean wet weight of one nematode ranged from 0.0012 mg in sample R–3 to 0.0041 mg in sample RA–1, agreeing well with Mare's figures of 0.0017 to 0.003 mg which she determined by direct weighing of batches. This seems to invalidate the statement above that no meaning can be attached to the wet weight of small animals determined by direct weighing. However, as will be shown below, there is reason to assume that Mare's samples did not include the very small nematodes and that her values refer to the dry rather than to the wet weight of medium sized and large nematodes. The individual wet weights of the Buzzard Bay nematodes ranged from 0.0002 mg (several species) to 0.138 mg (*Enoplus behringicus*).

To determine the dry weight of nematodes, batches were weighed on an analytical balance (Becker, 0.1 mg) or on a "Misco" quartz helix (manufactured by Michrochemical Specialties Co., Berkeley, California) with a sensitivity of 1 mm per 10 mg. The specimens whose wet weight had been determined previously by the volume method were preserved in formalin, rinsed and oven dried. The weighing on the quartz helix was carried out by Dr. R. Conover. The results are given in Table 2. From these data a mean dry weight/wet weight ratio of 25% was adopted and the wet weight values per sample were converted into dry weight values accordingly (Table 4).

Representatives of all other meiofauna groups were preserved in formalin, rinsed and weighed in oven dried condition with the quartz helix. These weights are listed in Table 3. An average dry weight of 0.003, 0.018 and 0.0017 mg for one kinorhynch, one ostracod and one copepod respectively was adopted for these groups. The cope-

TABLE 3. *Average weights of meiofaunal groups*

	Number of specimens weighed	Total weight (mg)	Average weight per specimen
Kinorhyncha			
Pycnophyes frequens	50	0.167	0.0033
Ostracoda			
representatives of three species	12	0.221	0.018
Copepoda			
representatives of two species	20	0.035	0.0017

pods weighed by Mare (1942) possessed an average individual (wet?) weight of 0.0024 and 0.005 mg.

RESULTS

The numerical results of the present study are given in Table 4. The total numbers of specimens vary between 1.69 × 10^5 and 1.86 × 10^6/m², the calculated dry weights between 100 and 600 mg/m².

The average distribution of nematodes and kinorhynchs at the three stations investigated is set out in Table 5. Rare nematode species are not listed but will, together with the more abundant ones, be described in a later publication.

There is a considerable number of species confined to the sandy stations, amongst them some of the more abundant forms such as *Odontophora pugilator, O. papusi* and *Anticoma litoris.* Three of the four species of *Odontophora* and all three representatives of the genus *Leptonemella*, together with their associated blue-green algae, (*cf.* Wieser 1959c) are restricted to the sandy habitats. Few species occur at station J alone, the most abundant of these being *Nudora lineata. Neochromadora pistillata* is most abundant at station J although it also occurs at stations P and R. The soft bottom habitat, station R, can be characterized by the relative abundance of certain species, particularly of *Terschellingia longicaudata*, followed by *Odontophora loffleri, Sabatiera ornata, S. hilarula, S. vulgaris, Sphaerolaimus dispar* and all the kinorhynchs.

An analysis of the total species composition of the nematode fauna is shown in Figure 1. At the fine deposit station (R) the dominance of the most abundant species, *Terschellingia longicaudata*, is quite pronounced, whereas at the sandy stations J and P three or four equally dominant species occur. Station R also carries fewer species than either P or J.

The question may arise as to what extent the sampling sites represent homogeneous habitats and whether the animals living in these habitats represent homogeneous populations. The degree of uniformity, or affin-

TABLE 4. *Numbers and dry weights of the meiofauna groups in Buzzards Bay samples. The numbers are given per 10 cm², the dry weights in mg/m²*

Numbers/10 cm²:	P-1	P-2	P-3	P-4	P-5	P-6	RA-1	J-1	J-2	J-3	J-4	J-5	J-6	R-1	R-2	R-3	R-4	R-5	R-6
Nematoda	350	250	400	300	550	335	150	600	650	225	150	190	300	250	760	500	690	790	1800
Kinorhyncha			1	1	2		1	2	2	2	5		5	8	16	7	16	12	39
Ostracoda	4	25	?	2			6	1	1	2	2	1	5	16	3	4	1	6	4
Copepoda		4		4	4	6		10	6	6	7	4	11	2	8	2	3	9	12
Turbellaria		1	1	3	2		4		2	4	5	7	7		2	1	2	6	6
Halacaridae		2				1	3	7	3								1		
Gastrotricha							5												
Cephalocaridea		2																	
Total	354	284	402	310	558	342	169	620	664	239	169	202	328	276	789	514	713	823	1861
% nematodes	99	89	99	97	99	98	89	97	98	94	89	94	91	90	96	97	97	96	96
mean number of meiofauna/m²			380,000							340,000						838,000			
mean number of macrofauna/m² (Sanders 1958):																			
total			12,576							5,455						6,068			
deposit feeders			3,084							2,836						5,545			
weights mg/m²:																			
Nematoda	145	130	139	145	230	158	152	475	375	90	82	78	95	110	268	149	270	331	—
Kinorhyncha			3	3	6		3	6	6	6	15		15	24	48	21	48	36	—
Ostracoda	72	450	?	36			108	18	18	36	36	18	90	288	54	72	18	108	—
Copepoda		7		7	7	10		17	10	10	12	7	19	3	14	3	5	16	—
rest (estimated)		9	1	3	2	2	20	14	8	4	5	7	7		2	1	4	6	—
Total	217	596	143	194	245	170	283	530	417	146	150	110	226	425	386	246	345	497	—

TABLE 5. *Mean abundance of nematode and kinorhynch species (rare species not included) at stations P, J and R, in Buzzards Bay, Massachusetts. 'Frequency' refers to number of samples in which a given species was found (based on 6 samples at stations P and R respectively, 7 samples at Station J). * = less than 0.3%*

	Station P		Station J		Station R	
	Per cent abundance	Frequency	Per cent abundance	Frequency	Per cent abundance	Frequency
Nematoda						
Odontophora pugilator Wieser	9.6	6/6				
Odontophora calcarea Wieser	1.8	5/6				
Synonchiella bifaria Wieser	0.8	4/6				
Chromaspirina arietina Wieser	1.1	3/6				
Latronema macramphida Wieser	0.4	3/6				
Pomponema mirabilis Cobb	1.1	2/6				
Paracanthonchus spectabilis Allgen	1.1	2/6				
Odontophora papusi Wieser	9.7	6/6	5.9	7/7		
Anticoma litoris Chitwood	11.8	6/6	1.1	2/7		
Leptonemella aphanothecae Gerlach	2.2	6/6	*	1/7		
Viscosia sp.	3.2	5/6	*	1/7		
Mesacanthion sp.	1.6	5/6	*	2/7		
Leptonemella pellita Wieser	1.8	3/6	*	2/7		
Viscosia glabra (Bastian)	1.0	3/6	0.4	3/7		
Leptonemella cincta Cobb	0.6	3/6	*	1/7		
Monoposthia costata (Bastian)	1.2	5/6	1.8	4/7		
Halalaimus similerus Wieser	*	3/6	*	2/7		
Laimella quadrisetosa Chitwood	1.0	4/6	1.3	6/7		
Dichromadora cephalata (Steiner)	0.7	3/6	*	1/7		
Cobbia crenata Wieser	0.7	2/6	0.5	1/7		
Theristus multisetosus Wieser	0.6	3/6	1.1	4/7		
Bathylaimus tenuicaudatus (Allgen)	0.5	2/6	0.4	1/7		
Pareurystomina typicum Micoletzky	*	2/6	0.6	3/7		
Theristus sp.	0.6	1/6	0.6	3/7		
Dorylaimopsis metatypicus Chitwood	11.0	6/6	7.6	7/7	4.4	3/6
Neochromadora poecilosoma (de Man)	2.3	5/6	0.8	2/7	1.4	3/6
Neochromadora pistillata Wieser	2.3	5/6	9.5	7/7	1.8	4/6
Desmodora cephalata Cobb	0.8	5/6	1.3	4/7	1.5	5/6
Sabatiera hilarula (de Man)	1.4	5/6	1.2	5/7	4.3	6/6
Terschellingia longicaudata de Man	1.0	5/6	8.8	6/7	29.6	6/6
Desmodora devestita Wieser	0.7	4/6	1.9	6/7	*	2/6
Odontophora löffleri Wieser	0.6	4/6	1.2	3/7	7.7	6/6
Axonolaimus spinosus (Butschli)	1.6	3/6	*	1/7	*	1/6
Actinonema pachydermatum Cobb	1.0	3/6	0.6	3/7	3.6	5/6
Cervonema mediocris Wieser	0.5	3/6	0.8	3/7	1.3	4/6
Chromaspirina ciliata Wieser	0.4	3/6	1.1	4/7	1.4	4/6
Sabatiera ornata Ditlevsen	0.8	3/6	1.8	4/7	5.6	5/6
Oncholaimus sp.	0.7	3/6	*	3/7	0.5	3/6
Sabatiera tenuicaudata (Bastian)	1.0	3/6	0.5	4/7	0.5	1/6
Rhabdodemania minima Chitwood	1.1	3/6	0.8	1/7	2.0	6/6
Oxystomina elongata (Buetschli)	*	2/6	*	1/7	0.6	4/6
Metalinhomoeus additus Wieser	0.4	2/6	*	1/7	2.2	5/6
Halichoanolaimus robustus (Bastian)	*	2/6	1.1	4/7	1.4	4/6
Tripyloides gracilis (Ditlevsen)	0.5	2/6	1.5	5/7	*	1/6
Metalinhomoeus setosus Chitwood	0.7	3/6	0.6	3/7	0.6	4/6
Sabatiera vulgaris (de Man)	*	2/6	2.1	2/7	3.5	3/6
Parironus sandersi Wieser	0.6	2/6			1.0	4/6
Microlaimus sp.	*	1/6	0.4	3/7	0.5	2/6
Paramonhystera biforma Wieser	*	1/6	*	2/7	1.3	4/6
Chromadora axi Gerlach	*	1/6	1.1	4/7	*	1/6

TABLE 5. *(Continued)*

	Station P		Station J		Station R	
	Per cent abundance	Frequency	Per cent abundance	Frequency	Per cent abundance	Frequency
Hypodontolaimus patagiatus Wieser	*	2/6	0.7	3/7	*	1/6
Linhomoeus buculentus Wieser	*	2/6	1.0	3/7	1.7	3/6
Sphaerolaimus dispar Filipjev	*	1/6	2.7	5/7	3.5	5/6
Oxystomina beta Wieser	*	2/6	1.1	4/7	*	1/6
Lauratonema originale Gerlach	*	1/6	0.4	2/7	*	1/6
Monhystera parva (Bastian)	*	2/6	*	1/7	0.4	2/6
Neochromadora attenuata Gerlach	*	1/6	0.5	3/7	0.4	2/6
Metalinhomoeus dimorphus Wieser	0.4	2/6	1.5	5/7	0.9	2/6
Comesoma pararenae Wieser			0.8	3/7		
Nudora lineata Cobb			3.2	4/7		
Enoplus behringicus Filipjev			0.7	2/7		
Paramonhystera mystacoderma Wieser			1.5	2/7		
Linhomoeus iniquus Wieser			0.5	3/7		
Halalaimus sp.			0.6	3/7		
Filipjevinema potor Wieser			4.6	6/7	0.7	1/6
Sphaerolaimus margaritatus Wieser			0.5	3/7	*	1/6
Paralinhomoeus sp.			0.5	3/7	*	1/6
Sphaerolaimus nefastus Wieser			*	1/7	0.7	3/6
Pareurystomina flagellicaudata Stekh.			*	2/7	*	2/6
Prochromadorella sp.			0.4	2/7	1.0	3/6
Eleutherolaimus stenosoma (de Man)			*	1/7	1.0	4/6
Halalaimus anulatus Wieser					1.3	2/6
Number of rare species	45		35		21	
Total number of species	103		98		63	
Number of identified specimens	786		821		759	
Kinorhyncha						
Trachydemus mainensis Blake	*	1/6	0.3	4/7	0.6	6/6
Pycnophyes frequens Blake			*	4/7	0.4	6/6
Echinoderella remanei Blake			*	2/7	*	3/6
larvae	*	2/6			*	3/6
remaining groups of meiofauna	2.7%		5.2%		3.7%	
total number of counted specimens	2250		2391		4976	

ity, of a certain population can be established in the following way. The abundance of each species is expressed as a percentage of the total population. The percentages, or abundance values, of each species in two samples are compared and the smaller of the two is taken as the "common abundance value." The common abundance values are added up and the result represents in a quantitative way the faunal element common to the two samples. Thus, if three species, A, B and C, constitute the following percentages in two samples:

	sample I	sample II
species A	15%	76%
species B	27%	0
species C	58%	24%

The common abundance value for species A is 15%, for species B zero, and for species C it is 24%, which means that the two samples have 39% of their fauna in common.

If all possible pairs of samples are compared we arrive at a pattern of values which gives an idea of the degree of uniformity of the population from which the samples were derived. This is the so-called "trellis

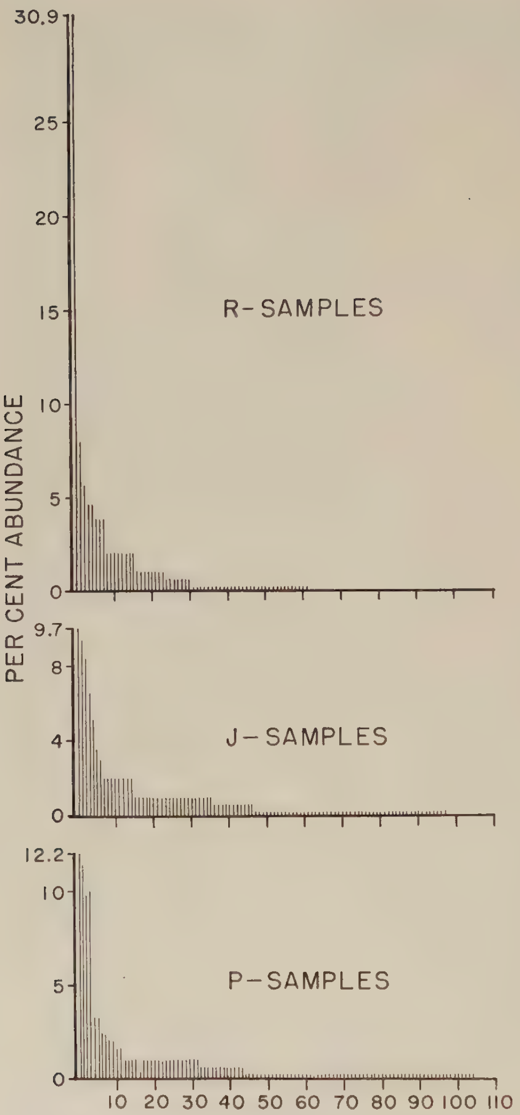

Fig. 1. Average species composition of the nematode fauna at the three stations studied. Each line represents one species, its height indicating the average abundance of the species in per cent of the total nematode population at the respective station.

diagram" which has been used widely by Scandinavian workers for delimitating communities of terrestral animals (*e.g.* Tenkonen 1944). The method has been criticized by Macfadyen (1954) but it seems to the writer that this criticism does not apply to the animal populations dealt with here. For a further discussion of the method see Sanders (1960).

Such an analysis of the nematode fauna at the three stations is shown in Figure 2. It is apparent that the uniformity of the fauna within each station is greater than that of two different stations. The two extreme stations, P with an average silt-clay content of 11.8% and R with a corresponding value of 79.7%, have relatively little in common, while station J with 30% silt-clay content assumes an intermediate position having about as much in common with P as with R.

DISCUSSION

Numbers

The most striking fact emerging from Table 4 is the dominance of the nematodes, which constitute between 89 and 99%. This is probably a feature characteristic of all marine shallow water substrates. If the data given in the literature are examined (Table 6) we find the nematodes varying between 43 and 100%.[1] However, the lower values are most probably due to sampling errors. In the present investigation both the material retained by and that passing through a 160μ screen was examined and it was found that between 10 and 60% of the living nematodes may go through the screen. Bougis (1946) estimated that with preserved material about 20% of the nematodes will pass a 200μ screen. Moore (1931), Mare (1942) and Purasjoki (1947) who worked with fresh material and counted only the animals, retained by a 200μ or a 100μ screen, probably missed considerable portions of the nematode populations.

In general it can be said that the samples rich in silt and clays (R) supported a larger number of meiofaunal animals than those poorer in fine deposits (J and P). The total macrofauna shows the opposite relationship, due to the abundance of filter

---

[1] These values refer to the meiofauna as defined in the first paragraph, which means that polychaetes are not included. Consequently, this group has been omitted in Table 6 and the figures given by the various authors have been recalculated.

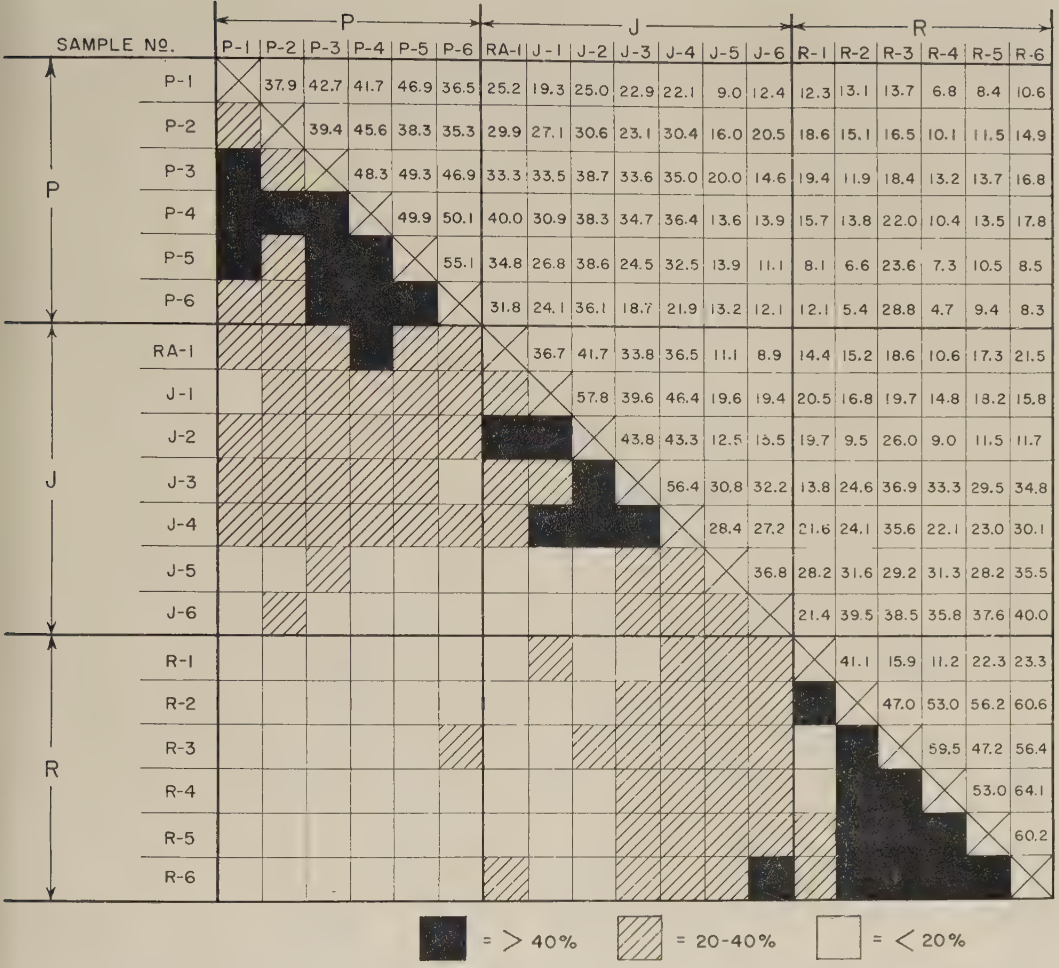

	SAMPLE NO.	P-1	P-2	P-3	P-4	P-5	P-6	RA-1	J-1	J-2	J-3	J-4	J-5	J-6	R-1	R-2	R-3	R-4	R-5	R-6
		P						J							R					
P	P-1	☒	37.9	42.7	41.7	46.9	36.5	25.2	19.3	25.0	22.9	22.1	9.0	12.4	12.3	13.1	13.7	6.8	8.4	10.6
	P-2	▨	☒	39.4	45.6	38.3	35.3	29.9	27.1	30.6	23.1	30.4	16.0	20.5	18.6	15.1	16.5	10.1	11.5	14.9
	P-3	■	▨	☒	48.3	49.3	46.9	33.3	33.5	38.7	33.6	35.0	20.0	14.6	19.4	11.9	18.4	13.2	13.7	16.8
	P-4	■	■	■	☒	49.9	50.1	40.0	30.9	38.3	34.7	36.4	13.6	13.9	15.7	13.8	22.0	10.4	13.5	17.8
	P-5	■	▨	■	■	☒	55.1	34.8	26.8	38.6	24.5	32.5	13.9	11.1	8.1	6.6	23.6	7.3	10.5	8.5
	P-6	▨	▨	■	■	■	☒	31.8	24.1	36.1	18.7	21.9	13.2	12.1	12.1	5.4	28.8	4.7	9.4	8.3
J	RA-1	▨	▨	▨	■	▨	▨	☒	36.7	41.7	33.8	36.5	11.1	8.9	14.4	15.2	18.6	10.6	17.3	21.5
	J-1		▨	▨	▨	▨	▨	▨	☒	57.8	39.6	46.4	19.6	19.4	20.5	16.8	19.7	14.8	18.2	15.8
	J-2	▨	▨	▨	▨	▨	▨	■	■	☒	43.8	43.3	12.5	13.5	19.7	9.5	26.0	9.0	11.5	11.7
	J-3	▨	▨	▨	▨	▨		▨	▨	■	☒	56.4	30.8	32.2	13.8	24.6	36.9	33.3	29.5	34.8
	J-4	▨	▨	▨	▨	▨	▨	▨	■	■	■	☒	28.4	27.2	21.6	24.1	35.6	22.1	23.0	30.1
	J-5			▨							▨	▨	☒	36.8	28.2	31.6	29.2	31.3	28.2	35.5
	J-6		▨								▨	▨	▨	☒	21.4	39.5	38.5	35.8	37.6	40.0
R	R-1								▨			▨	▨	▨	☒	41.1	15.9	11.2	22.3	23.3
	R-2										▨	▨	▨	▨	■	☒	47.0	53.0	56.2	60.6
	R-3						▨			▨	▨	▨	▨	▨		■	☒	59.5	47.2	56.4
	R-4										▨	▨	▨	▨		■	■	☒	53.0	64.1
	R-5										▨	▨	▨	▨	▨	■	■	■	☒	60.2
	R-6							▨			▨	▨	▨	■	▨	■	■	■	■	☒

■ = > 40% ▨ = 20-40% ☐ = < 20%

FIG. 2. "Trellis diagram" illustrating the degree of uniformity of the nematode fauna at the three stations investigated. Each number (and square) indicates the nematode fauna common to a pair of samples (see text).

feeders at station P (Sanders 1958). However, if we select the deposit-feeding component of the macrofauna the relationship displayed by the meiofauna is exactly paralleled (Table 4).

In comparing meio- and macrofauna, we find that the former exceeds the latter by a factor of 30–100, values around 100 probably being more common than lower ones.

The numbers of larger animals brought up by the Phleger core-samples conform well with the numbers obtained by dredging. For example, in six samples from R, the lamellibranch *Nucula proxima* was represented by 0, 2, 2, 3, 4 and 5 specimens respectively, yielding an extrapolated mean value of $2.5 \times 10^3/m^2$, while Sanders (1958, Table 6) reports a mean of $3.3 \times 10^3/m^2$ from the same station.

The meiofauna densities reported from various parts of the oceans are in good agreement with each other (Table 6), particularly if we take into account that the figures given by Moore and by Mare probably are too low. The low values found by Krogh and Sparck (1936) and by Purasjoki (1947) might be due to either the sampling method, or to the impoverishment of the brackish water habitats on which these authors worked.

Table 6. *Summary of quantitative results pertaining to the subtidal benthic meiofauna*

		Wieser (this paper)	Bougis 1946	Bougis 1950	Mare 1942	Moore 1931	Krogh & Sparck 1936 a)	Krogh & Sparck 1936 b)	Purasjoki 1947
meiofauna	specimens/m²	1.7–18.6×10⁵	4–11.3×10⁵	6.6×10⁵	1.5×10⁵	1.7–3.5×10⁵	5.1×10⁴	7×10⁴	1.0–10.0×10⁴
	wet weight/m²	0.4–2.5 g			1.15 g		7.1(!) g	7.0(!) g	
	% nematodes	89–99	70–80	66–76	59–66	75–91	92	100	43–83
macrofauna/m²		5–13 × 10³ (Sanders 1958)			2.3 × 10³				
locality		Buzzards Bay, Massachusetts	Bay of Lyon, Mediterranean		near Plymouth, England	Clyde Sea, Scotland	Oresund, Denmark reduced salinity		near Tvärminne, Finnland
depth (m)		12–30	30		45	24	26	54	9–55
screen, treatment		<, > 160µ, fresh material	> 200µ	> 100µ corrected for loss of small anim.	> 100µ	> 200µ	< 500µ		> 100µ
			preserved, stained material		fresh material		fresh material		

Weights

For the sake of comparison, the wet weights of the meiofauna can be calculated on the volume determinations of the nematodes and on the assumption that the dry weight of the other groups is 25% of the wet weight. A range of 0.4–2.5 g/m² is then obtained. In previous investigations only Mare (1942) and Krogh and Sparck (1936) have given wet weight values for the meiofauna. Mare's value of 1.15 g/m² is in good agreement with that found for Buzzards Bay, whereas the values given by Krogh and Sparck are much higher. However, in the latter paper an average weight of 0.1, 0.75 and 0.45 mg is assigned to one nematode, one turbellarian and one infusorian respectively, which as already noted by Mare is impossible. It is suggested that somewhere in the calculations an error of at least one order of magnitude must have occurred.

Species Distribution

In general it can be said that the sandy stations, P and J, are characterized by a number of stenotopic species, that is, species which do *not* occur at R. On the other hand, nearly all species occurring at R, also occur at J or P or both, but sometimes in much smaller numbers. This might reflect the distribution of the sediments. The 5 to 20% silt present at station P (see Table 1) probably provides sufficient interstitial space to permit the existence of a scarce "siltfauna," while the approximate 20% of sand found at R will be so thoroughly smothered by the abundance of silt and clay that animals dependent on a sandy substrate will only rarely be found there. A similar pattern of distribution can be inferred from the data provided by Gerlach (1958).

In addition to these two groups there exist many eurytopic species which seem to be able to thrive both in sandy and in silty substrates; the most important of these is *Dorylaimopsis metatypicus.*

The mechanical composition of the substrate is important in determining the distribution of the macro- and meiofauna (Sanders 1958, Webb and Hill 1958, Wieser 1959a). However, the sediment composition might effect these two faunal components somewhat differently. In one sense, the species assemblage listed for station P might be the meiofauna equivalent of the *Ampelisca* community reported by Sanders (1958) as being typical of sandy substrates in Buzzards Bay, and the species assemblage listed for station R might be equivalent to the *Nucula proxima-Nephthys incisa* community of fine deposits, with station J occupying an intermediate position between these two types. If so, the meiofauna equivalent of the *Ampelisca* community could be called the *Odontophora-Leptonemella* community, and the meiofauna equivalent of the *Nucula proxima-Nephythys incisa* community could be called the *Terschellingia longicaudata-Trachydemus mainensis* community.

However, as previously mentioned, the meiofauna of Buzzards Bay can also be regarded as consisting of three ecological groups: 1) species with affinity to sand, 2) species with affinity to fine deposits and 3) more eurytopic species. The fauna at each particular point of Buzzards Bay will be determined by the degree of mixing of sands and fine deposits, the three ecological groups actually living side by side and forming an intricate meshwork rather than the mosaic of patches, to which the community pattern usually is likened. The intricacy, and variability, of the meshwork is due to the fact that animals with a mean diameter of 30 μ and a mean length of 1.2 mm can exploit minute changes in the mechanical composition of the substrate much more thoroughly than the members of the macrofauna, and thus give rise to very gradual transitions from one extreme type of distribution to the other. The sensitivity of the nematode fauna to small changes in the composition of the substrate was also noticed by Gerlach (1958, p. 65).

Summarizing, it can be said that the meiofauna found in any sample represents a transect through at least three ecological groups of species. Each sample can be characterized by the degree of dominance of species belonging to these ecological groups, but to call any of them a "community" seems to be a misapplication of this term. On the other hand, to call the whole mixture a community would gloss over the fact that it consists of ecologically different components which combine to create a subtly graded series of faunal assemblages.

Too few data are available in the literature to correlate, even in a general way, the distribution of the shallow water meiofauna with the distribution of sediment types. Drawing on the studies by Gerlach (1950, 1958), Cobb (1920, 1933), and Wieser (1958a) it is suggested that the following nematode genera which occur at Buzzards Bay are characteristic of sandy substrates: *Synonchiella, Latronema, Pomponema, Leptonemella, Laimella,* to which may be added a great number of species of *Odontophora. Odontophora* is also one of the most important genera on the beaches of Puget Sound; (*cf.* Wieser 1959b).

Wieser (1958a), Gerlach (1958) and Filipjev (1918) show that *Terschellingia longicaudata* is one of the most characteristic representatives of the subtidal silt- or mudfauna. To this category can be added a great number of species of *Sabatiera* (*cf.* Wieser 1958a, b) *Sphaerolaimus, Metalinhomoeus,* and most representatives of the order Kinorhyncha.

In deeper water the composition of the nematode fauna of the soft bottom seems to change. Investigations in Chile (Wieser 1958a) suggest that at greater depths *Sabatiera* becomes the dominant genus, while *Terschellingia* and other linhomoeid genera decrease in importance.

The degree of uniformity of two samples, as defined above and shown in Figure 2, depends to a certain extent on the difference in silt-clay content between the two samples. If, choosing only one of each pair of replicates, the samples represented in Figure 2 are arranged according to their difference in silt-clay content, it can be inferred from Figure 3 that the faunal element common to two samples increases with decreasing difference in silt-clay content. It is nearly true to say that, if the difference in silt-clay content between two samples amounts to more than 40%, the two samples will have not more than 20% (mean 15%) of the fauna in common. If the difference in silt-clay content is less than 30%, the two samples will have more than 20% (mean 35%) of the fauna in common.

On the other hand, the variability of the values is considerable. This may be partly due to the fact that sediment and faunal analyses were carried out on replicate instead of the same samples, but it may also be because the faunal composition of a sample is not always, and not entirely, determined by its silt-clay content. If we

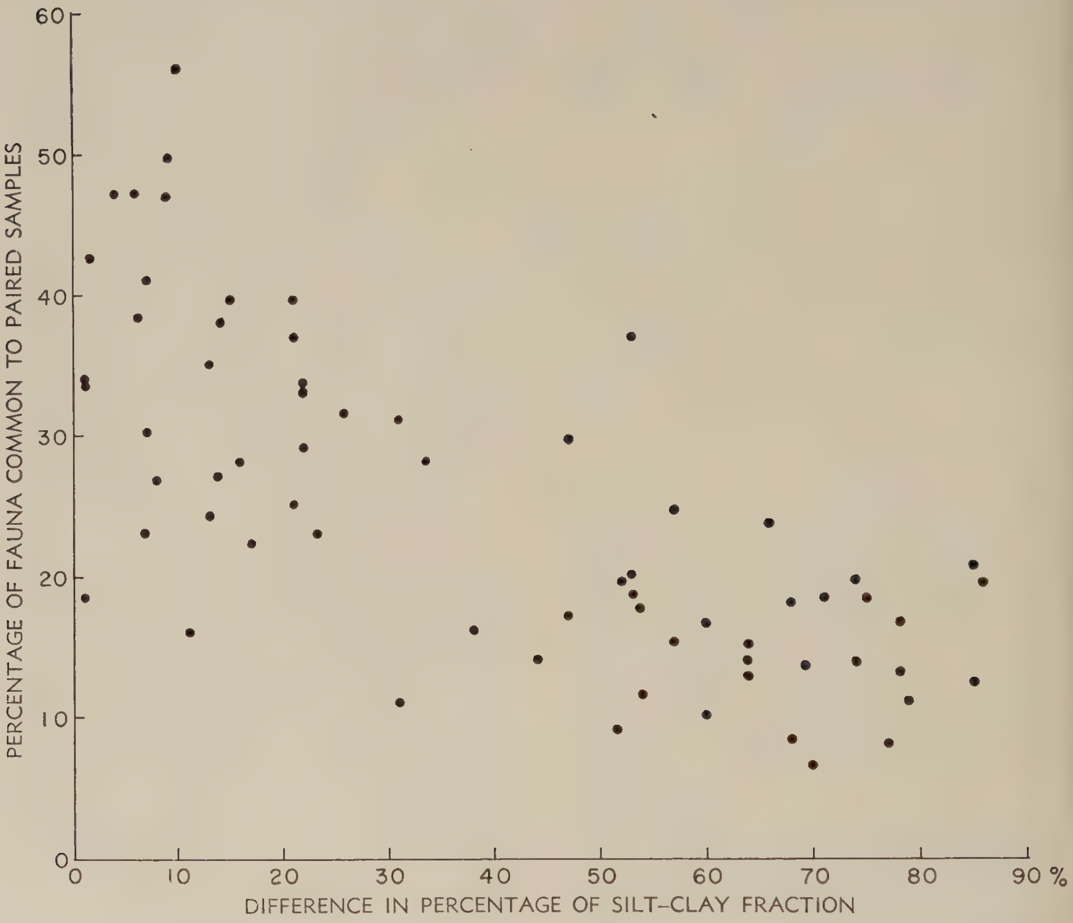

FIG. 3. Showing the dependence of the degree of uniformity of two samples on the sediment composition. The degree of uniformity (ordinate) is expressed as the per cent of the nematode fauna common to two samples, the sediment composition (abscissa) as the difference in the per cent silt-clay content between the two samples.

compare samples P–1 and J–1, we find that they have the same silt-clay content of 6.3% (Table 1), whereas the uniformity of their meiofauna is not high (19.3%). On closer inspection, however, it emerges that apart from the silt-clay content, the sediment composition of these two samples is quite different, P–1 representing a well-sorted fine sand habitat and J–1 a poorly-sorted medium or even coarse sand habit. It is conceivable that the lack of faunal conformity between the two samples has its basis in these differences of sediment composition. A similar effect of the sorting coefficient of the substrate on the fauna has been noted by Sanders (1958) with regard to the distribution of filter feeders.

Species dominance

Following Gause (1934) it has become generally accepted that two species with the same ecological requirements cannot live together in the same habitat; one of the two species will inevitably eliminate the other. Gause's contention was based in mathematical and experimental grounds, and in order to apply it to the natural environment

TABLE 7. *Per cent abundance of closely related species of nematodes in Buzzards Bay*

	P-1	P-2	P-3	P-4	P-5	P-6	RA-1	J-1	J-2	J-3	J-4	J-5	J-6	R-1	R-2	R-3	R-4	R-5
Odontophora pugilator	18.5	2.9	5.3	6.2	13.3	12.9	6.6	4.5	11.2	10.5	9.0	1.7	2.0					
O. papusi	10.8	6.8	14.4	12.3	8.5	7.1												
O. calcarea	2.3		2.6	1.5	2.4	2.9												
O. löffleri	0.8	1.9	0.5		0.6						1.1	5.1	2.9	13.9	4.3	4.5	11.8	6.2
Leptonemella pellita	8.5	1.3		1.5				0.5	0.6									
L. aphanothecae	4.6	3.9	1.1	1.5	1.2	1.4		1.0										
L. cincta	1.5			0.8		1.4		1.0										
Neochromadora pistillata	2.3	3.9	1.6	3.8	1.2		14.5	11.9	20.1	8.7	9.0	1.7	1.0	3.5			0.7	2.7
N. poecilosoma		1.0	6.4	3.1	1.2	2.9		2.0	4.5						0.6		2.2	
N. attenuata						1.4		0.5				1.7	2.0				1.5	0.7
N. sp.								2.5	0.6									
Sabatiera hilarula	3.1		2.1	2.3	0.6		1.3	1.0	1.1	0.9	4.5			13.9	1.9	0.7	0.7	1.4
S. ornata		1.9	1.6	1.5						6.1	2.2	3.4	2.0	0.9	4.3	7.1	17.0	5.5
S. tenuicaudata			0.5		4.2	1.4		1.0	0.6		1.1	1.7			3.1			
S. sp. 1		1.9	0.5								1.1	1.7						0.7
S. sp. 2			0.5		1.2			0.5										
Metalinhomoeus additus	0.8	1.9								0.9				4.3	0.6	1.3		3.4
M. setosus	1.5	2.0	0.5					1.0	1.1				2.9	1.7	0.6	0.7		0.7
M. dimorphus			1.6	0.8				0.5		0.9	1.1	8.5	1.0			4.5		0.7

the word "habitat," as was pointed out by Bagenal (1951), should be used in its narrowest sense and be equivalent to 'microhabitat.' Even so, natural conditions are rarely homogeneous and populations living in a well-defined habitat will deviate to a greater or lesser degree from the type of species composition requiredy by Gause's principle. Much depends on whether by "same" one implies "identical" or "similar." Riley (1953) has summarized the methods by which species with superficially identical, but in reality not quite identical ecological requirements, manage to live in what looks like the same habitat but what in reality is a mosaic of functional niches.

Therefore, if we believe Gause's principle to be valid in theory, deviations from it in nature can be considered as reflecting the degree of homogeneity of the habitat from which the examined population was derived. This is an application of the principle which seems to have attracted little attention yet it might prove to be of interest, particularly with respect to the benthic meio- and microfauna. These small animals live in an environment where the degree of homogeneity cannot readily be ascertained. We do not know beforehand what effect small physiographic differences of the environment may have on the animals. Thus the most convenient way to establish the presence or absence of ecological niches within an otherwise well defined habitat may be by studying the species composition within that habitat. If the population, or any important taxonomic group, is strongly dominated at a given time by one species then the habitat can be considered fairly homogeneous with respect to that population or taxonomic group. If there are several species of about equal dominance the presence of different niches within the habitat is indicated.

In aquatic environments the pelagial can be expected to offer homogeneous conditions over fairly large stretches. This is suggested by an analysis of the limnetic zooplankton (Pennak 1957) which revealed a very high abundance of the dominant species within each of the three major groups: copepods, cladocerans and rotifers. From 27 Colorado lakes Pennak found that the dominant species constituted 92.9% in copepods, 84.7% in cladocerans, 63.6% in rotifers while there were correspondingly low values for the next most abundant species.

A very different picture emerges if the nematode fauna of marine benthic habitats is compared. Figure 1 indicates that at none of the three stations does the nematode fauna possess a degree of homogeneity similar to that of the limnetic zooplankton. At each station there occurs a great number of species and the per cent abundance of

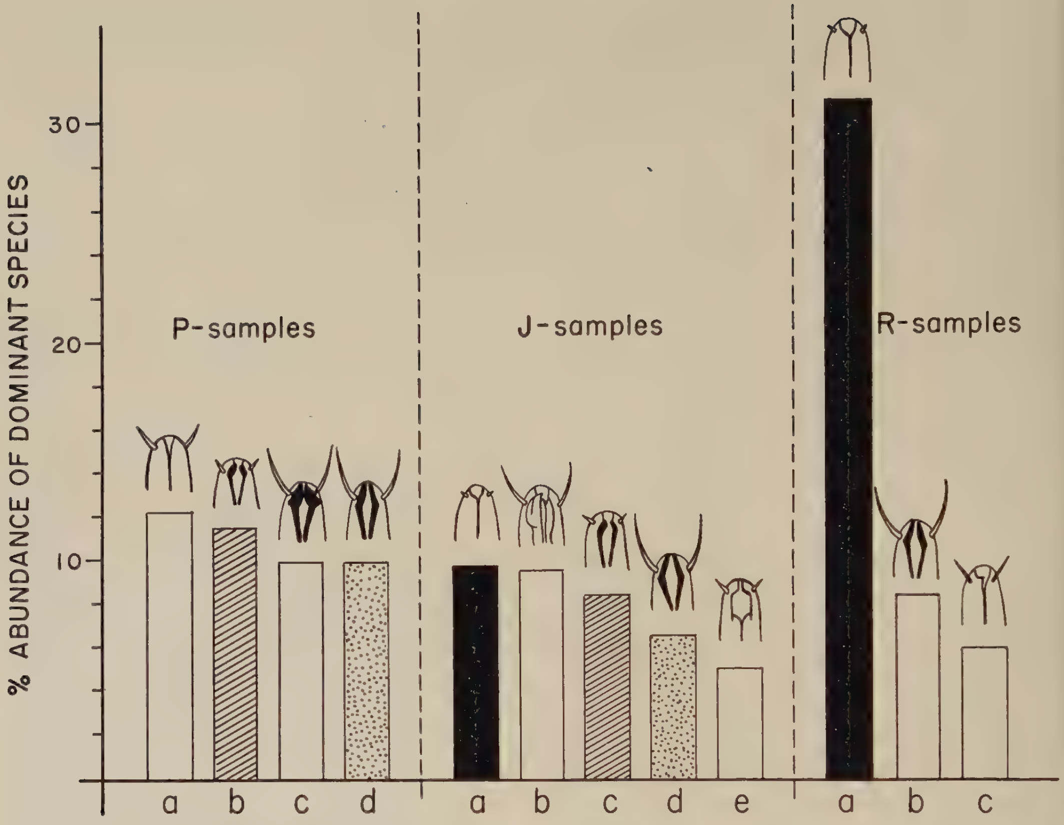

FIG. 4. The dominant nematode species at the three stations studied. The height of each column indicates the average abundance of each species at the respective station. Identical species are characterized by identical conventions. The species represented are the following:
P-samples: a: *Anticoma litoris*, b: *Dorylaimopsis metatypicus*, c: *Odontophora pugilator*, d: *O. papusi.*
J-samples: a: *Terschellingia longicaudata*, b: *Neochromadora pistillata*, c: *Dorylaimopsis metatypicus*, d: *Odontophora papusi*, e: *Filipjevinema potor.*
R-samples: a: *Terschellingia longicaudata*, b: *Odontophora löffleri*, c: *Sabatiera ornata.*

the dominant nematode does not approach that of the dominant copepod, cladoceran or rotifer in Pennak's investigation. However, there exist also significant differences between the three stations at Buzzards Bay. At the fine deposit station (R) the dominance of the most abundant species, *Terschellingia longicaudata*, is quite well pronounced, whereas at the sandy stations (J and P) there are three or four more or less equally dominant species. This indicates that, with respect to the nematode fauna, stations P and J represent a more heterogeneous habitat than station R. It might be speculated that in the sandy habitats the sand grains and the interstitial deposits represent two quite different sources of food, equivalent to two niches within the overall habitat. This is also suggested by the distribution of feeding types shown in Figure 4. Further splitting up of the habitats could be based on vertical layering of the substrate, accompanied by a segregation of the nematode fauna into vertically distinct components.

The existence of microhabitats within a more general habitat can also be inferred from the distribution of closely related species. Bagenal (1951) in clarifying the findings of Williams (1947) states "closely related species are more likely to be found in *similar*, though not identical, habitats." Thus it might very well be that microhabitats within a more general habitat will often be occupied by closely related species, or, conversely, if closely related species are found within one well-defined habitat, the segregation of the habitat into microhabitats is indicated.

In order to test this assumption, Table 7 lists all genera which were represented by more than two moderately abundant species. Within the genus *Odontophora* the occurrence of closely related species at station P is particularly striking. *O. pugilator* and *O. papusi* do not seem to compete for the same sort of food since both were about equally abundant in several samples although each sample covered an area of only 10 cm^2. As might be inferred from Figure 4, there is a clear difference in the structure of the buccal plates of these two species. *O. pugilator* has much more powerful plates than *O. papusi,* which may reflect the adaptation to different sources of food. On the other hand, the only case of simultaneous occurrence of closely related but moderately abundant species at station R seems to show that the representatives of the genus *Sabatiera* compete with each other, since when *S. hilarula* is abundant (R–1), *S. ornata* is rare, and, conversely, when *S. ornata* is abundant (R–3, R–4), *S. hilarula* is rare. The occurrence of several species of *Sabatiera* in one sample is common for marine mud bottoms and has been discussed before (Wieser 1958a, b).

Thus the distribution of closely related nematode species at the three stations again points toward the heterogeneity of the habitat with the highest percentage of sand (station P). The case for the intermediate habitat (station J) is not conclusive in this example. It is of interest that the macrofauna shows a pattern of distribution similar to that of the meiofauna; station P is dominated by three closely related species of amphipods, *Ampelisca spinipes, A. macrocephala* and *Byblis serrata,* while at station R the dominant species are not at all closely related (Sanders 1958). This parallelism is the more remarkable since the amphipods of station P are filter feeders whereas the nematodes are substrate feeders.

Feeding habits

Most representatives of the meiofauna feed on the substrate itself, either on the epigrowth on sandgrains, or by ingesting the fine deposits. Turbellarians, members of the subfamily Halacarinae and a number of nematodes have been considered predators but it becomes increasingly clear that many of the marine benthic animals that have been called "predators" actually behave as deposits feeders most of the time. This was shown by Sanders (1956) for the polychaete *Nephthys incisa* and by Thorson (1957) for the brittle star *Amphiura.* In a previous paper Wieser (1953) conjectured that a large portion of the nematode fauna were predators because of their strong buccal armature and the occasional appearance of metazoan remains in their guts. Possibly most of these forms are deposit feeders; Perkins (1958) found the gut content of 16 specimens with strong buccal armature to consist chiefly of diatoms, bacteria and "what were possibly minute flagellates."

As far as the feeding habits of the meiofauna are concerned, the main distinction seems to be between "epistrate feeders" and "deposit feeders" as supposed by Remane (1933). Both these types probably include species of various degrees of food specifity but there is insufficient evidence to permit any further sub-grouping. The predominance of species which have been reported to live on diatoms (*cf.* Remane 1933, Perkins 1958) may be somewhat misleading since diatoms are the most easily recognized food component. However, there can be no doubt that both sessile and vagile diatoms constitute one of the major food sources in marine shallow water substrates.

The two coarse bottom stations (P,J) are characterized by the more or less equal abundance of four or five species comprising four types of buccal structure. At station P we find on the one hand *Anticoma litoris,* a species with a minute buccal cavity, on the other hand *Dorylaimopsis metatypicus, Odonotophora papusi* and *O. pugilator*, three species equipped with fairly powerful buccal plates or mandibles. At station J we find two species with unarmed, cup-shaped or cylindrical buccal cavity, one species with relatively small buccal teeth and two of the more strongly armed species also occurring at station P. In contrast to this situation, the samples from the soft bottom station R are dominated by *Terschellingia longicaudata*, a species with unarmed, cup-shaped buccal cavity, and the third most abundant species is *Sabatiera ornata*, which has a buccal cavity of similar structure.

It may be assumed, therefore, that *Terschellingia longicaudata* and *Sabatiera ornata* with their buccal armature are "deposit feeders," while *Odontophora* spp. and *Dorylaimopsis metatypicus* are "epistrate feeders," scraping food off sand grains. However, it is not likely that every species of benthic animal can be assigned unequivocally to either of these two types, and as the so-called "predators" show, there exist also animals of more omnivorous habits. Similarly, some epistrate feeders may be able to feed on fine deposits and *vice versa*. A possible example of the first case is *Dorylaimopsis metatypicus* which occurred at all stations in relative abundance.

At station J the species without buccal armature (*Terschellingia* and *Filipjevinema*) are about as abundant as those with buccal armature (*Neochromadora, Dorylaimopsis* and *Odontophora*). This is in agreement with the intermediate position of station J on the silt-clay scale (Table 1).

Of the meiofauna groups less numerous than the nematodes, the kinorhynchs are pure deposit feeders. The ostracods have been considered as deposit feeders (Remane 1933, Mare 1942) while Perkins (1958) found the gut of many specimens of *Leptocythere pellucida* filled with diatoms. The harpacticoid copepods are either epistrate feeders or deposit feeders (Remane 1933). Perkins found in the guts of several species mainly diatoms, "vegetable matter of uncertain origin" and detritus. Turbellarians are generally regarded as predators but Webb (1956) observed rhabdocoeles feeding on diatoms and green flagellates in the laboratory.

REFERENCES

Andrassy, I. 1956. Die Rauminhalts- und Gewichtsbestimmung der Fadenwuermer (Nematoden). Acta Zool. (Budapest), **2**: 1–15.

Bagenal, T. B. 1951. A note on the papers of Elton and Williams on the generic relations of species in small ecological communities. J. Anim. Ecol., **20**: 242–245.

Bougis, P. 1946. Analyse quantitative de la microfaune d'une vase marine a Banyuls. C. R. Acad. Sci., **222**: 1122–1124.

———. 1950. Méthode pour l'étude quantitative de la microfaune des fonds marins (Meiobenthos). Vie et Milieu, **1**: 23–38.

Capstick, C. K. 1956. Lactophenol preparations for soil nematodes. Nature (London), **177**: 896–897.

Cobb, N. A. 1920. One hundred new nemas. Contributions to a Science of Nematology, IX: 217–343. Waverly Press, Baltimore.

———. 1933. New nemic genera and species, with taxonomic notes. J. Parasitol., **20**: 81–94.

Elofson, O. 1941. Zur Kenntnis der marinen Ostracoden Schwedens. Zool. Bidr. Uppsala, **19**: 215–534.

Filipjev, I. N. 1918/21. Svobodnozhivushchiya morskiya nematody okrestnosteij Sevastopolya. Trav. Lab. Zool. & Stat. biol. Sébastopol; Acad. Sci. Russ., (2) **4**: 1–614.

Gause, G. F. 1934. The struggle for existence. Williams and Wilkins Co., Baltimore, 163 pp.

Gerlach, S. 1950. Ueber einige Nematoden aus der Familie der Desmodoriden. N. Erg. Probl. Zool. (Klatt-Festschrift); 178–198. Leipzig.

———. 1958. Die Nematodenfuana der sublitoralen Region in der Kieler Bucht. Kieler Meeresf., **14**: 64–90.

Lang, K. 1948. Monographie der Harpacticiden. Lund, Håkan Ohlssons, 2 vol.

Krogh, A. and R. Spärck. 1936. On new bottom-sampler for investigation of the microfauna of the sea bottom. Kgl. Danske Vidensk. Selsk. Biol. Medd. XIII, **4**: 1–12.

Macfadyen, A. 1954. The invertebrate fauna of Jan Mayer Island (East Greenland) J. Anim. Ecol., **23**: 261–297.

Mare, M. 1942. A study of a marine benthic community with special reference to the micro organisms. J. Mar. Biol. Ass. U.K., **25**: 517–54.

Moore, H. B. 1931. The muds of the Clyde Sea area. J. Mar. Biol. Ass. U.K., **17**: 325–58.

Nielsen, C. O. 1949. Studies on the soil microfauna. II. The soil inhabiting nematodes. Natura Jutlandica, **2**: 1–131.

Pennak, R. W. 1957. Species composition of limnetic zooplankton communities. Limnol. Oceanogr., **2:** 222–232.

Perkins, E. J. 1958. The food relationships of the microbenthos, with particular reference to that found at Whitstable, Kent. Ann. Mag. Nat. Hist. ser. 13, **1:** 64–77.

Purasjoki, K. J. 1947. Quantitative Utersuchung ueber die Mikro-fauna des Meeresbodnes in der Umgebung der Zoologischen Station Tvärminne an der Südküste Finnlands. Soc. Scient. Fenn. Comm. Biol. IX, **14:** 1–24.

Remane, A. 1933. Verteilung und Organisation der benthonis-chen Mikro-fauna der Kieler Bucht. Wiss. Meeresunters. Kiel, N. F., **21:** 161–221.

Renkonen, O. 1944. Die Carabiden — und Staphylinidenbestaende eines Seeufers in SW-Finnland. Ann. Entom. Fenn., **10:** 33–104.

Riedl, R. 1954.

Riley, G. 1953. Theory of growth and competition in natural populations. J. Fish. Res. Bd. Canada., **10** (5): 211–223.

Sanders, H. L. 1956. Oceanography of Long Island Sound, 1952–1954. X. Biology of marine bottom communities. Bull. Bingham Oceanogr. Coll., **15:** 345–414.

———. 1958. Benthic studies in Buzzards Bay. I. Animal-sediment relationships. Limnol. Oceanogr., **3:** 245–258.

———. 1960. Benthic studies in Buzzards Bay. III. The structure of the soft bottom community. Limnol. Oceanogr., **5:** 138–153.

Thorson, G. 1957. Bottom communities. *In:* Treatise on marine ecology and paleoecology. Geol. Soc. Amer. Mem., 67, **1:** 461–534.

Webb, M. G. 1956. An ecological study of brackish water ciliates. J. Anim. Ecol., 25 (1): 149–175.

Webb, J. E. and M. B. Hill. 1958. The ecology of Lagos Lagoon. IV. On the reactions of *Branchiostoma nigeriense* Webb to its environment. Phil. Trans. Roy. Soc. Ser. B, **241:** 355–391.

Wieser, W. 1953. Die Beziehung zwischen Mundhöhlengestalt, Ernährungsweise und Vorkommen bei freilebenden marinen Nematoden. Ark. Zool., **2:** 439–484.

———. 1958. Free-living marine nematodes. IV. General part. Lunds Univ. Arsskr. N. F. Avd. 2, **54:** 1–111.

———. 1958b. Problems of species formation in the benthic micro-fauna of the deep sea. *In:* Perspectives in marine biology (A. A. Buzzati-Traverso, ed.), Univ. of Calif. Press, pp. 513–17.

———. 1959a. The effect of grain size on the distribution of small invertebrates inhabiting the beaches of Puget Sound, Washington. Limnol. Oceanogr., **4:** 181–194.

———. 1959b. The free-living nematodes and other small invertebrates of Puget Sound. Univ. Washington. Publ. Biol., **19:** 1–179.

———. 1959c. Eine ungewoehnliche Assoziation zwischen Blaualgen und freilebenden marinen Nematoden. Österr. Bot. Ztschr. **106:** 81–87.

Williams, C. B. 1947. The generic relations of species in small ecological communities. J. Anim. Ecol., **16:** 11–18.

Contribution No. 1055

Deep-Sea Research, 1960, Vol. 6, pp. 217 to 233. Pergamon Press Ltd., London. Printed in Great Britain

On the abyssal circulation of the world ocean – II. An idealized model of the circulation pattern and amplitude in oceanic basins

HENRY STOMMEL and A. B. ARONS

(*Received* 15 *August* 1959)

Abstract—Stationary planetary flow patterns driven by source sink distributions in an ocean on the rotating earth were developed in Part I. These theoretical results are now used to construct a highly idealized model of the general abyssal circulation of the world ocean. The model is based on the postulation of the existence of two concentrated sources of abyssal waters (one in the North Atlantic and another in the Weddell Sea) and on a uniformly distributed upward flux of water from the abyssal to the upper layers as part of the mechanism of the main oceanic thermocline. Order of magnitude calculations based on this model lead to a variety of estimates of the time in which the deep water is replaced (from every 200 to 1800 years). Comparison of leading terms in the dynamical equations and equation describing the flux divergence of a tracer shows that there is a large range of lateral eddy coefficient which will influence the distribution of the tracer but not affect the dynamically determined planetary flow patterns.

INTRODUCTION

IN Part I of this series of papers (STOMMEL and ARONS, 1959) we outlined the manner in which stationary flow patterns in oceanic basins on a spherical earth might be predicted for various source-sink distributions. These predictions were based on a previously published theory and interpretation of rotating basin experiments (STOMMEL *et al.*, 1958). In this paper we use the preceding results and a theory of the oceanic thermocline (ROBINSON and STOMMEL, 1959) to develop a model of the general abyssal circulation of the world ocean. The model, is of course, highly idealized, but we feel that it affords a plausible starting point for visualizing certain broad, qualitative features of the circulation, and that it may help generate suggestions for experiments and observations that will provide tests of the validity of the concepts which have been used.

OUTLINE OF THE MODEL

WÜST (1938) first presented a chart of the potential temperature at the bottom for the whole ocean, and showed that this clearly indicated that there was a powerful source of low temperature water in the Weddell Sea, and that this water spreads northwards along the western side of each ocean basin. This chart has become a standard exhibit in oceanographic textbooks, and, taken by itself, would suggest that on the basis of temperature alone all the deepest water in the ocean originates mainly in the Weddell Sea.

Of course, WÜST did not mean to suggest that there was only one source, and in a later paper (1951) he explicitly showed the great influence of the waters of the North Atlantic – through their high salinity – on the rest of the deep ocean water. This is also shown by the study of the T-S relations of deep water (STOMMEL, 1958) and by a study of the charts presented in Figs. 1(a) and 1(b), which we have compiled partly from WÜST's similar chart of the Atlantic, and partly from a new analysis of data in the Indian and Pacific Oceans. (The spacing of isohalines in Fig. 1(a) is not uniform, but is laid out in geometric progression to prevent extreme crowding of lines in the North Atlantic). One can see that there is a very high salinity tongue extending from the Straits of Gibraltar, down the Atlantic and then eastward around Antarctica, and finally extending up northward into the Indian and Pacific Oceans – the salinity falling all the way. This chart serves to emphasize the importance of the contribution of North Atlantic Deep Water to the general abyssal circulation. The Mediterranean outflow is not massive enough to warrant inclusion as a third mass source. Its high salinity, however, may be regarded as supplying a 'tracer' by means of which the flow of water from the greater North Atlantic mass source can be followed.

Another figure which helps to visualize the sources of the two abyssal water components and the way in which they sink down and flow around Antarctica and thence up into the Indian and Pacific Oceans is presented in Figs. 2(a) and 2(b)*. Thus in Fig. 2(a) several vertical profiles of salinity are sketched to show the spread and vertical extent of the water at the salinity maximum already depicted in Figs. 1(a) and 1(b). To emphasize the features under description only two isohalines are shown: 34·70‰ and 34·76‰, although of course the total range of salinity variation in the ocean is very much greater than this narrow range. In the North Atlantic profile in Fig. 2(a), the entire profile is filled with water of salinity greater than 34·76‰. The North Atlantic is the source of the high salinity Deep Water. In the South Atlantic the high salinity at the surface is separated from that in the Deep Water by a layer of fresh Antarctic Intermediate Water.

We can trace the high salinity Deep Water all around Antarctica – but we note it does not extend all the way to the bottom at the very foot of the Antarctic Continent. A somewhat diluted portion (between 34·70 and 34·76‰) extends up into the Indian and Pacific Oceans at depth. The high salinities shown at the surface in the Pacific Ocean do not connect anywhere with the deep maximum. In the Indian Ocean the picture is somewhat more complex. There is a flow of saline water from the Red Sea which influences the salinity in the Deep Water of Equatorial and North Indian Ocean, and masks the influence of the North Atlantic component on the salinity there.

In Fig. 2(b), two isotherms are plotted on the same profile: 0°C and 2°C. The very cold water, less than 0 °C, originates at the surface in the Weddell Sea, and extends eastward around Antarctica, vanishing about at the Ross Sea, and never extending very far north. A more dilute portion, between 0°C and 2°C reaches further northward: in the Atlantic it occupies only a small portion of the deepest part of the western trough of the South Atlantic, but does not extend into the North Atlantic. This cold water occupies all the deep regions of the Pacific and Indian Oceans. In the North Indian Ocean it is clear that the Red Sea Water does not extend into the Deep Water on account of the temperature – although the salinity profile in Fig. 2(a) is ambiguous on this point.

In making the above description of the distribution of properties we have purposely used words like 'extends' instead of 'flows,' and 'occupies' instead of 'fills up,' in order to avoid implying that a process of actual flow is occurring. Actually, of course, the inference we wish to draw from the distributions of salinity and temperature in

---

*Previously unpublished, but constructed by E. D. STROUP and H. STOMMEL in the summer of 1958.

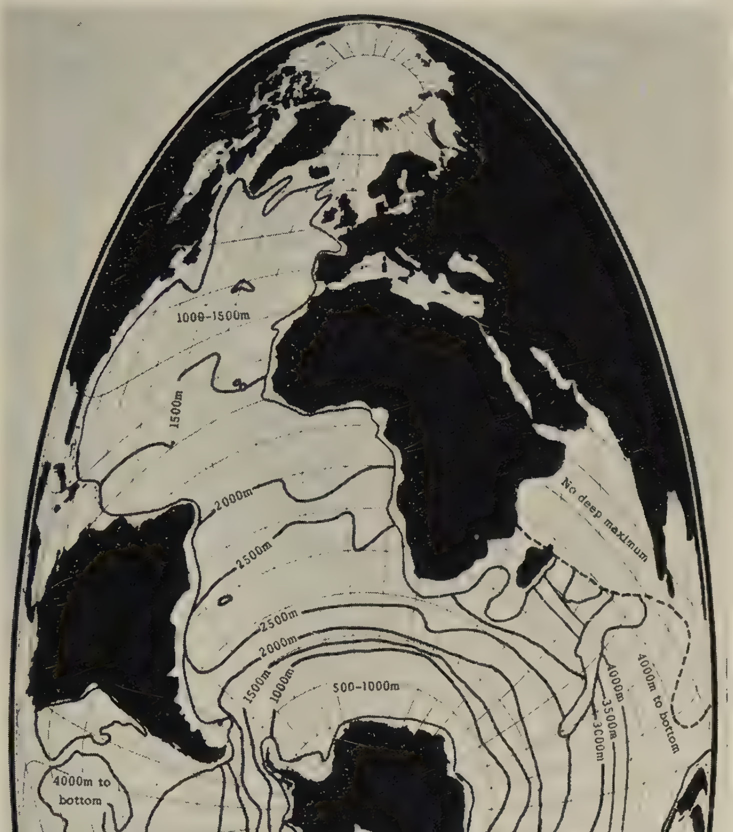
1000-1500m
1500m
2000m
2500m
No deep maximum
2500m
2000m
1500m
1000m
500-1000m
4000m
3500m
3000m
4000m to bottom
4000m to bottom
1000m
1500m
2000m
2500m
3000m
3500m
4000m
4000m to bottom

Fig. 1(a). Chart of the depth of the deep salinity maximum in the World Ocean, in metres. Aitoff equal-area projection.

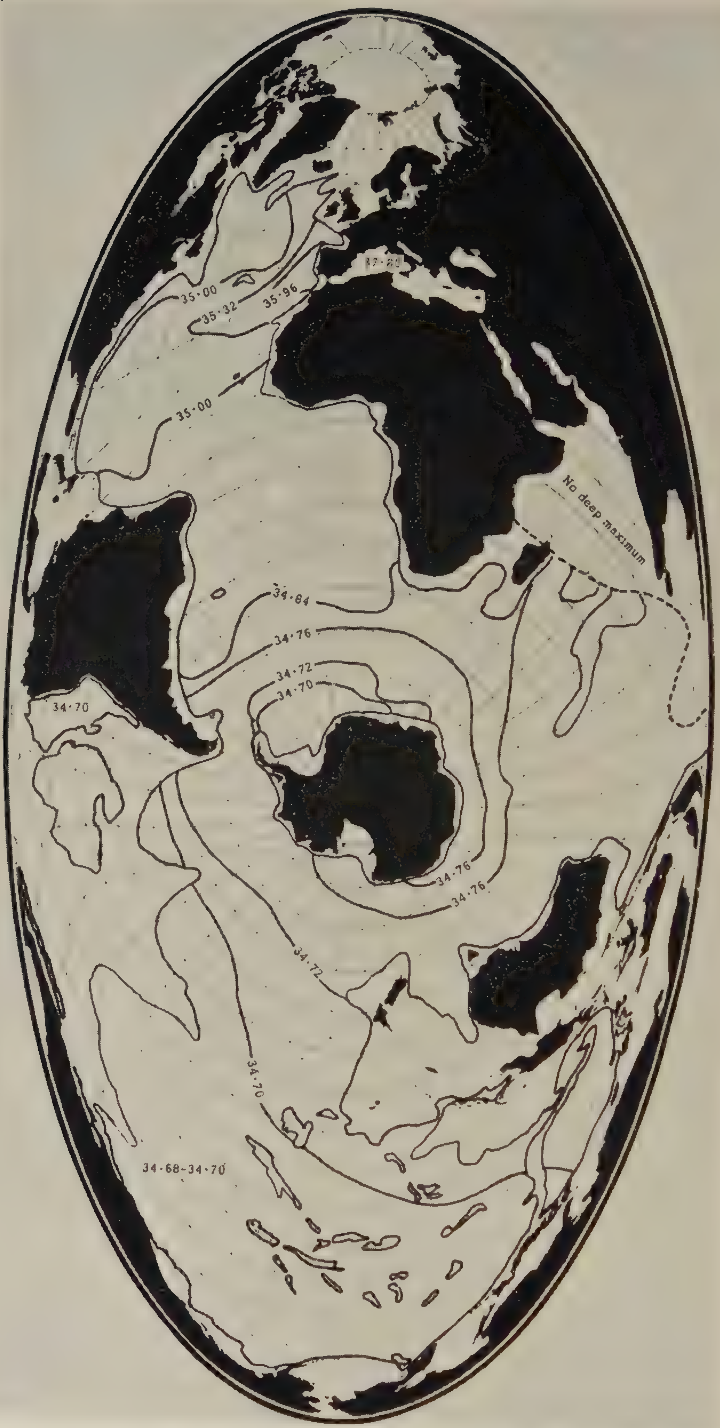
37·60
35·00
35·32
35·96
35·00
No deep maximum
34·84
34·76
34·72
34·70
34·70
34·76
34·76
34·72
34·70
34·68–34·70

FIG. 1(b). Chart of the salinity, in parts per mille, at the depth of the deep salinity maximum. The isohalines are not spaced at equal intervals; high values near the Mediterranean are spaced more widely.

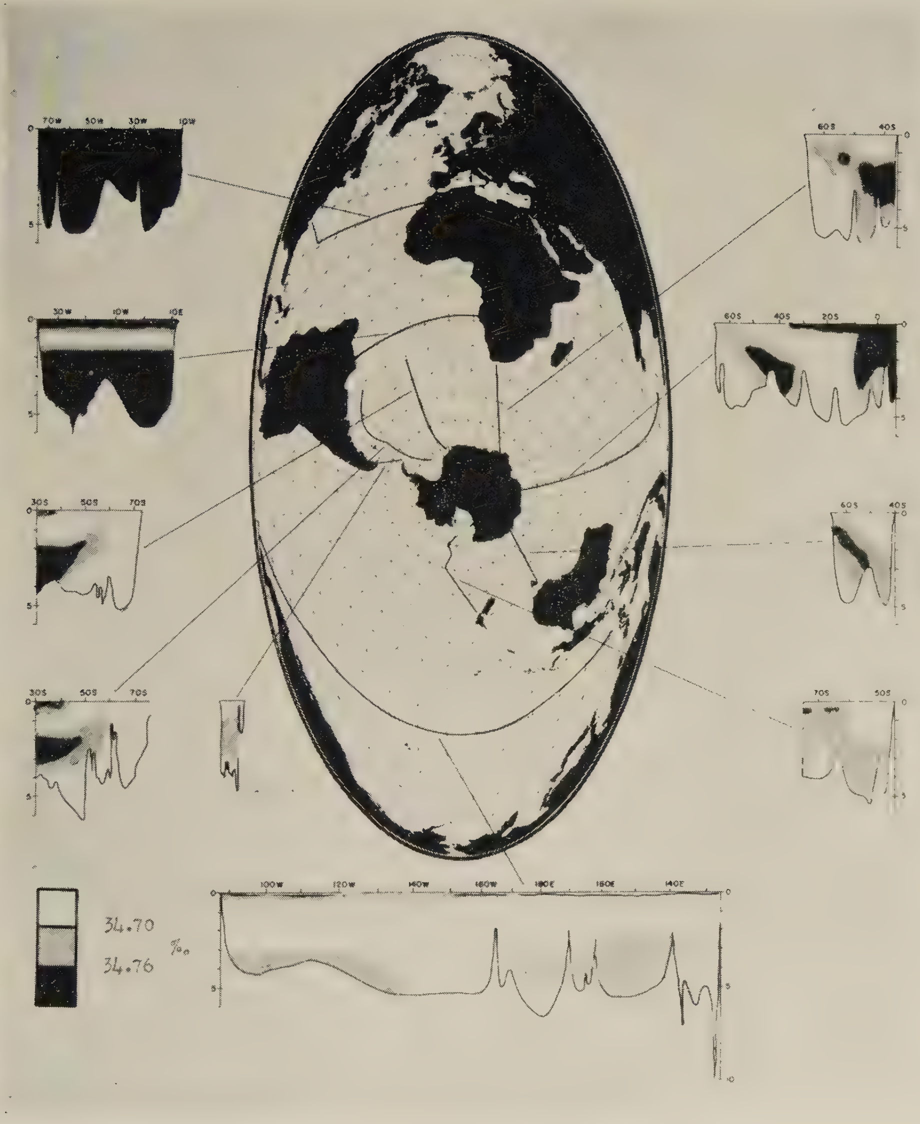
70W 50W 30W 10W
30W 10W 10E
30S 50S 70S
30S 50S 70S
60S 40S
60S 40S 20S 0
60S 40S
70S 50S
100W 120W 140W 160W 180E 160E 140E
0
5
10
34.70
34.76
‰

FIG. 2(a). Sketch of distribution of salinity on vertical profiles using only two selected isohalines chosen to depict in particular the influence of North Atlantic Deep Water on the Deep and Bottom Water characteristics of the rest of the World Ocean.

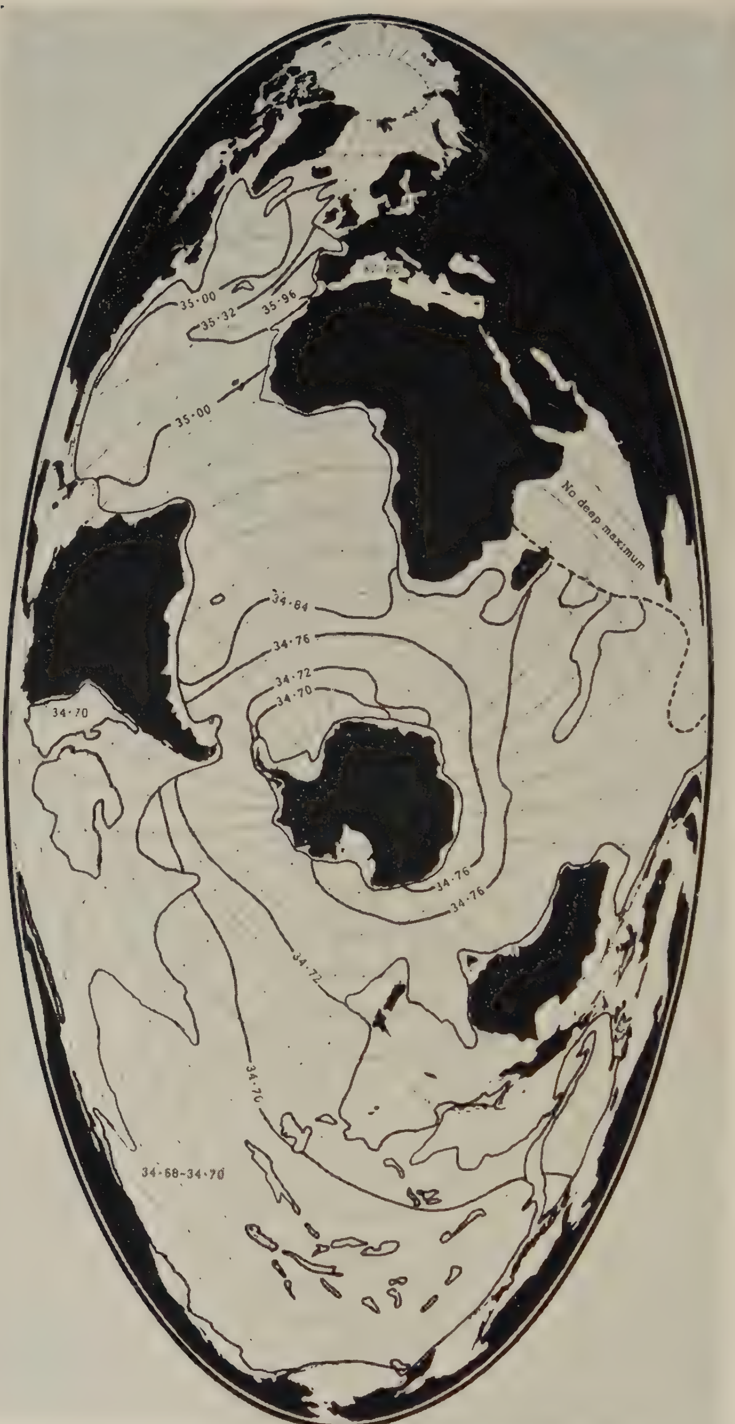
35·00
35·32
35·96
35·00
No deep maximum
34·84
34·76
34·72
34·70
34·70
34·76
34·76
34·72
34·70
34·68–34·70

FIG. 1(b). Chart of the salinity, in parts per mille, at the depth of the deep salinity maximum. The isohalines are not spaced at equal intervals; high values near the Mediterranean are spaced more widely.

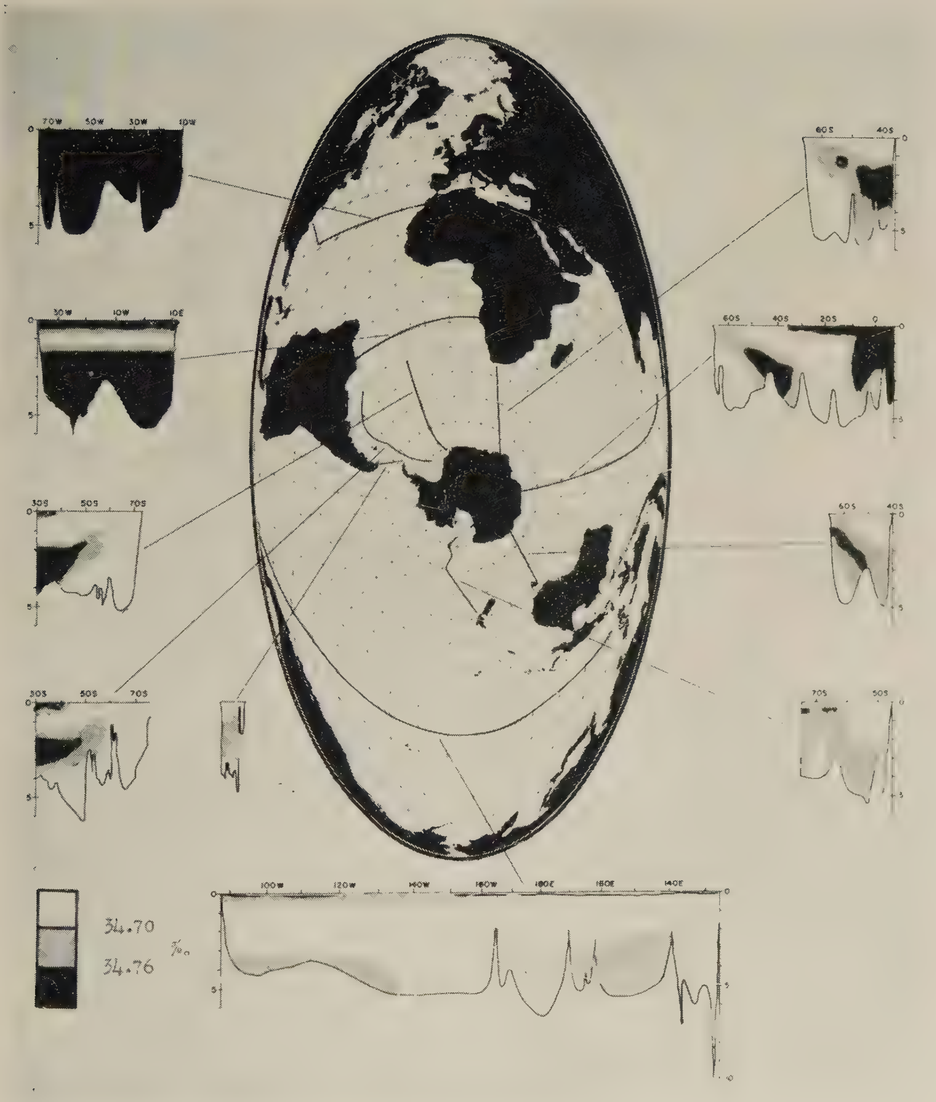
70W
50W
30W
10W
30W
10W
10E
30S
50S
70S
30S
50S
70S
60S
40S
60S
40S
20S
0
60S
40S
70S
50S
100W
120W
140W
160W
180E
160E
140E
0
5
34.70
34.76
‰

FIG. 2(a). Sketch of distribution of salinity on vertical profiles using only two selected isohalines chosen to depict in particular the influence of North Atlantic Deep Water on the Deep and Bottom Water characteristics of the rest of the World Ocean.

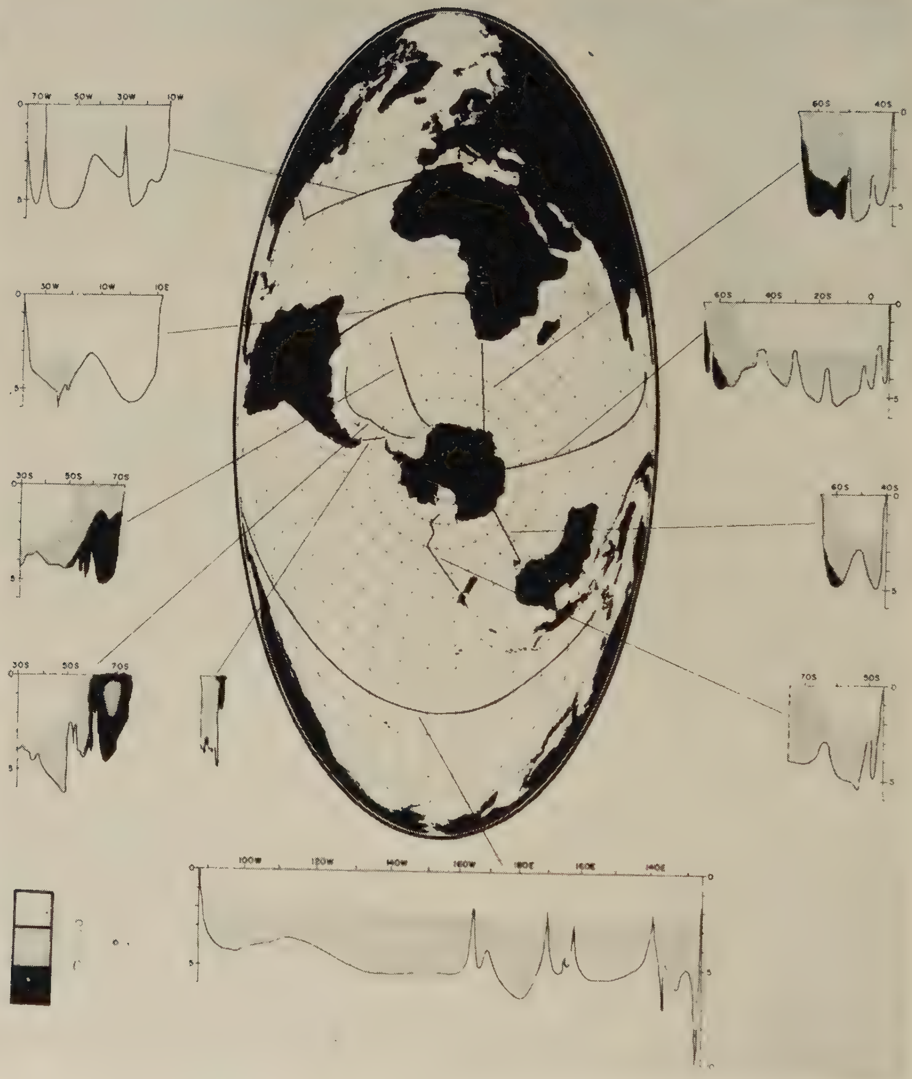
70W
50W
30W
10W
30W
10W
10E
30S
50S
70S
30S
50S
70S
60S
40S
60S
40S
20S
0
60S
40S
70S
50S
100W
120W
140W
160W
180E
160E
140E
0
5

FIG. 2(b). Sketch of distribution of temperature on vertical profiles using only two isotherms chosen to depict the influence of cold Bottom Water from the Weddell Sea on the temperature of the Deep and Bottom Waters of the World Ocean.

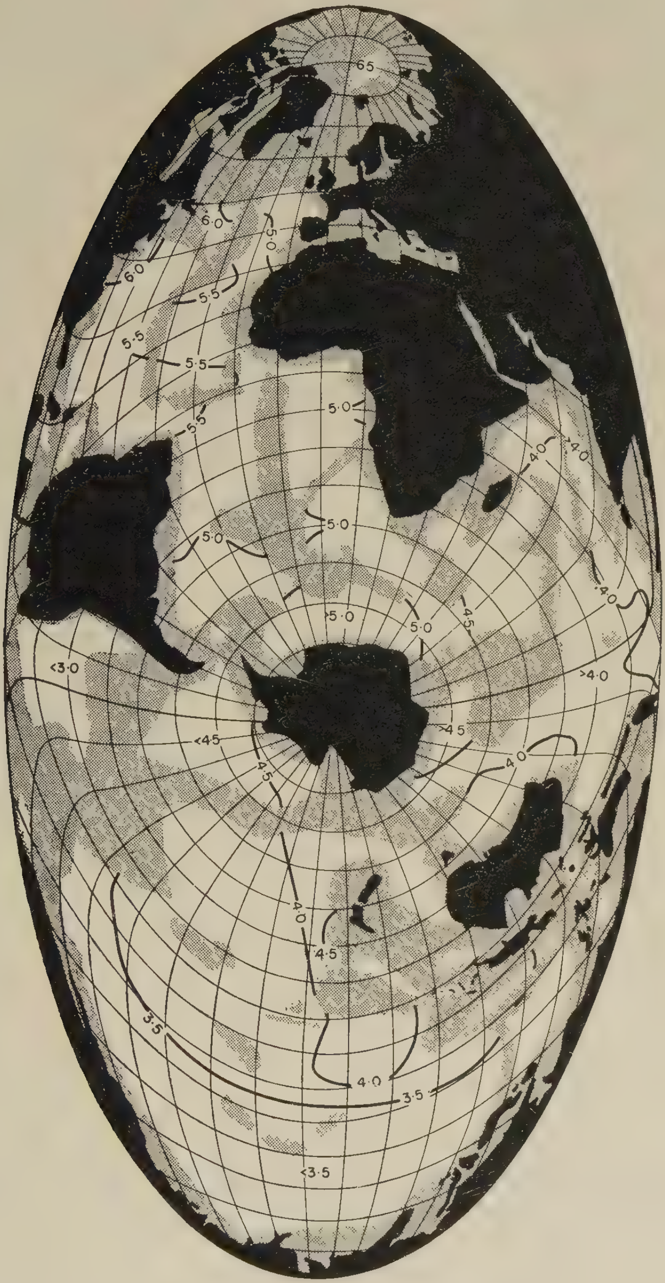
65
6·0
5·0
6·0
5·5
5·5
5·5
5·5
5·0
4·0
>4·0
5·0
5·0
4·0
>5·0
5·0
4·5
<3·0
>4·0
<4·5
>4·5
4·0
4·5
4·0
4·5
3·5
4·0
3·5
<3·5

Fig. 3. Sketch of the distribution of dissolved oxygen (ml/l) in the World Ocean at a depth of 4000 m., showing elevated oxygen values in the western North Atlantic and near the Weddell Sea. The oxygen is depleted in regions far removed from these two source areas.

the deep waters is that they are evidence of flow, and this is the inference oceanographers have traditionally made on the basis of the tongue-like distribution of properties. But, as we will see, the tongue-like distribution of properties indicates flow only in a very general way and not in detail. Thus we believe that the distribution of properties merely helps us to indicate the location of the sources of the deep water and general direction of flow from one ocean basin to another. However, we believe that the detailed structure of the mean currents in individual ocean basins – the strong western boundary currents, and large cyclonic gyres – is not shown clearly by the distribution of temperature and salinity because of a masking effect due to lateral mixing – a subject into which we will enquire further in Section 5 of this paper, and will take up *in extenso* in Part III.

A chart of the concentration of dissolved oxygen at 4000 m is presented in Fig. 3. This chart is a preliminary edition of a set of deep ocean charts now in preparation by E. D. STROUP and STOMMEL, and is based upon the totality of deep oxygen measurements available. It shows the high oxygen content of the North Atlantic Deep Water, and the secondary maximum of oxygen in the neighbourhood of the Weddell Sea. Throughout all the rest of the ocean, the deep water oxygen decreases. Quite evidently there is no source of deep water in the Indian or Pacific Oceans.

Thus, in the light of the oxygen data, we assume that bottom water is generated by cooling in only two locations: (a) in the North Atlantic, (b) in the Weddell Sea. If in addition we assume that the mechanism of the oceanic thermocline involves a general upward motion of water at mid-depths, the theory presented in Part I leads to a system of boundary currents and interior geostrophic flow of the qualitative pattern sketched in Fig. 4.

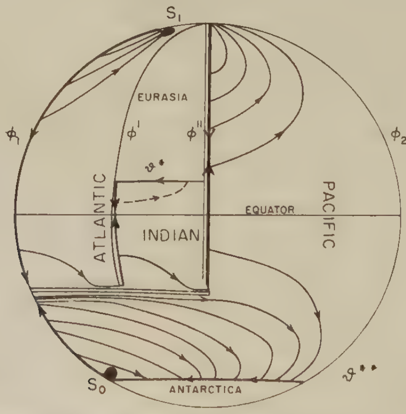

FIG. 4. A circulation diagram showing theoretical distribution of abyssal currents proceeding from the two sources S_0 and S_1 and flowing into a diffuse sink uniformly distributed over the whole ocean area.

Fig. 4 shows a sketch of a global ocean with meridional boundaries at ϕ_1, ϕ_2, ϕ' and ϕ'' and latitudinal boundaries at ϑ^*, ϑ^{**}. Thus we have very roughly a picture which looks like the real ocean basins. On the left is the Atlantic. The barrier ϕ' extending across the equator to mid-latitudes is the European-African land mass. The barrier ϕ'' is the East-Asian coast, extending down across the equator to Australia and New Zealand (in fact, of course this is not completely impermeable to water flow. The land mass bounded by ϕ', ϕ'' and ϑ^* is the Asian Continent. South of it we find the Indian Ocean. From ϕ'' to ϕ_2 we have the Pacific Ocean. The barriers ϕ_1 and ϕ_2 are the eastern and western edges of the North and South American Continental land mass drawn straight across Drake Passage to Antarctica. South of latitude ϑ^{**} lies Antarctica. Source S_0 is the source of Antarctic Bottom Water; Source S_1 is the source of North Atlantic Deep Water.

Isobars and schematic western boundary currents are sketched according to the principles described in Part I of this series – assuming a general upward motion over the entire ocean at mid-depths. From the North Atlantic source S_1 the water flows southward in a western boundary current. Part of this current feeds an interior geostrophic flow in the North Atlantic to the east and north-east. Some of this water rises vertically through the thermocline and the rest eventually rejoins the boundary current in higher latitudes nearer to the cource, thus forming a North Atlantic abyssal gyre.

It is well known that the existence of the southward flowing boundary current beneath the Gulf Stream was verified in the March–April 1957 *Discovery II – Atlantis* Expedition. Most of the North Atlantic Deep Water crosses the equator in the main strength of the western boundary current down the coast of South America past Brazil and Argentina to about 35 °S latitude. Along this course more water is lost to an interior geostrophic flow to the east and south-east, but we hypothesize that this water does not form a closed South Atlantic abyssal gyre, because upon reaching the latitude 35 °S it joins a zonal current flowing eastward toward the Cape of Good Hope. (See Section 7 and Fig. 16 of Part I). The zone bounded by 35°S and 55°S is marked by currents that flow all around the world; it is the zone in which communication between the Atlantic, Indian and Pacific Oceans is constrained to occur by the geographical distribution of the continents. We hypothesize that the Antarctic Bottom Water from the source S_0 flows northward along the western edge of the Weddell Sea to the 35 ° – 55 °S zone, where it veers eastward, joining the backing N Atlantic component, to form a great zonal stream that carries Atlantic water into both the Indian and Pacific Oceans. Upon passing the Cape of Good Hope some of this current flows northward in a narrow western boundary current that feeds the abyssal circulation of the entire Indian Ocean. The remainder of the zonal stream flows eastward, and after passing south of New Zealand, flows northward into the Pacific Ocean as a narrow western boundary current along the Tonga–Kermadec Trench. After crossing the equator the western boundary current flows northward to a latitude of about 30° ± 10°N where it exhausts itself. Analogy with the dynamical model shown in Fig. 8 of Part I suggests that further north in the N. Pacific there may actually be a southward directed western boundary current. South of latitude 55°S the pattern of flow seems to depend rather critically on what transport is permitted to flow through Drake Passage between the southern tip of South America and the northern tip of the Palmer Peninsula on the Antarctic Continent. It has been pointed out, however, in an earlier article (STOMMEL, 1957) that Drake Passage does not afford a free zonal passage for deep flows because of the position of the island arc on the eastern side. All except surface layers must (and indeed do) move northward in passing through. We do not have an adequate understanding of just what happens dynamically in this region, and as yet cannot introduce this complication theoretically in a quantitative manner. Therefore, in later sections the flow through

Drake Passage will have to be carried as an undetermined parameter. In Fig. 4 the rather drastic assumption that it vanishes has been made.

ESTIMATE OF THE AMPLITUDE OF THE ABYSSAL CIRCULATION ON THE BASIS OF TRADITIONAL OCEANOGRAPHIC INFORMATION

We have constructed in Fig. 4 a schema of the abyssal circulation, showing the patterns which would ensue if there is a general upward motion over the entire ocean at mid depths, fed by two equal point sources in the North and South Atlantic. We have not assigned an amplitude to this flow pattern. How much water is actually flowing in this pattern, in millions of cubic metres per second ? We now proceed to attempt to answer this question, first by comparison with the quantities of flow observed directly in the March – April 1957 *Discovery II – Atlantis* Expedition to the western boundary current in the North Atlantic, and secondly by a study and simplification of the dynamic calculations of the data recently published by Wüst (1955 and 1957). In the next section we shall determine the amplitude of the abyssal circulation by means of the new theory of the oceanic thermocline of Robinson and Stommel (1959).

We first consider the results of the joint British-American expedition to survey the deep currents under the Gulf Stream off Charleston, North Carolina, U.S.A., in the Spring of 1957. To date, only a short notice of the results has been published (Swallow and Worthington, 1957) and it is possible that estimates of deep flow will be rendered somewhat differently in the forthcoming more deliberate account of the survey which these authors are preparing, but if the depth of no axial motion in the western North Atlantic is about 1500 m., geostrophic calculations made on sections from Nova-Scotia to Bermuda and from Chesapeake Bay to Bermuda indicate that there are about 20×10^6 m^3/sec flowing southward in a narrow intense western boundary current along the coast of the United States. (However, when dynamic calculations of transport in the undercurrent off Charleston were made by Worthington and Swallow – as yet unpublished – much lower values were obtained : 3 to 6×10^6 m^3/sec). The transports computed by Wüst (1957) from the South Atlantic *Meteor* data show that the North Atlantic Deep Water flows southward along the Brazilian coast – riding over an intruding wedge of Antarctic Bottom Water – with about the same transport. Of course there is an arbitrary element in all dynamic current calculations based on hydrographic data alone – namely the choice of reference level – but the water mass characteristics in the South Atlantic are so very clear-cut that we are inclined to place confidence in Wüst's choice of reference level. We identify this narrow current of North Atlantic water with the western boundary current in our theoretical schema (Fig. 4) and think of it as merely being a somewhat attenuated continuation of the one under the Gulf Stream. Unfortunately we do not have reliable bases for estimating the deep flows in other oceanic areas, and so we cannot press this method further. From the T-S relations of deep water for the whole world it looks as though the contribution of flow from the Weddell Sea must be at least as much as that from the North Atlantic – at least another 20×10^6 m^{3}sec^{-1} so that the total rate of addition of water from the two sources S_0 and S_1 in Fig. 4 must be reckoned as at least 40×10^6 m^3/sec.

Having made reasonable guesses of the values for the two sources, we can now attach numerical values to all other parts of the circulation, and in so doing we naturally must make a crude allowance for the various dimensions of different oceanic basins. In Fig. 5 we have divided the world ocean into 14 portions :

North Atlantic into two sub-areas each of		2 unit areas
South Atlantic	2	2
North Indian	2	1
South Indian	2	3
North Pacific	2	5
South Pacific	2	5
Southern Ocean south of Africa	1	2
Southern Ocean south of Australia	1	2

The total area of the world ocean is thus divided into 40 unit areas. Inasmuch as the actual area of the 3000 m. surface in the world ocean is about 3 × 10⁸ km², we must associate 7·5 × 10⁶ km² with each of the above unit areas. Although the theory of the oceanic thermocline (ROBINSON and STOMMEL, 1959) indicates that the vertical velocities at mid-depths are functions of position we will, for simplicity, assume that the vertical velocity is nevertheless uniform over the ocean, in which case 1 × 10⁶ m³/sec flows upward through each unit area. The upward-bent arrows at the upper right hand corner of each box in Fig. 5 represent this upwelling. The figure associated with these arrows is the approximate total upward flux across the 3000 metre level out of each box. The meridionally directed arrows connecting boxes (such as the one labelled 15 between the two Northern Pacific sub-areas) is meant to represent the interior flow from one sub-area to another. The flow (in 10⁶ m³/sec) between the western boundary currents and each box is indicated by a zonally directed arrow on the left of the box. Thus there is a flux from the western boundary current to the southern sub-area in the Northern Pacific of 20 × 10⁶ m³/sec and a flow from the northern sub-area of the North Pacific into the western boundary

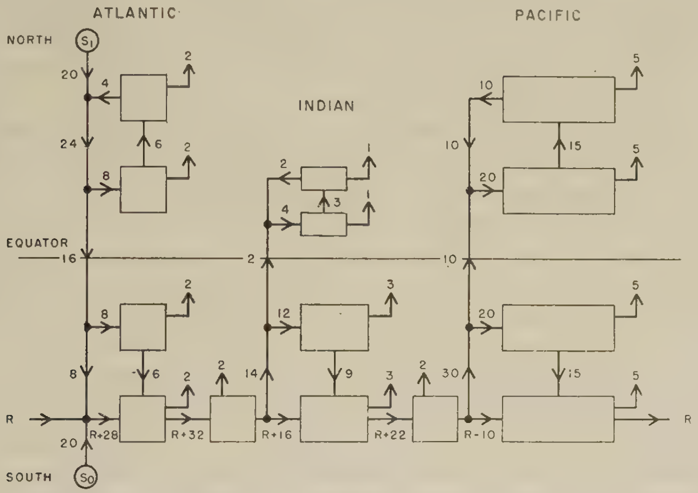

FIG. 5. Schematic budget of transports in various portions of the World Ocean (see text).

current of 10 × 10^6 m^3/sec. As we can see, only half of the water entering the interior of the North Pacific actually flows directly up through the thermocline, the other half recirculates through the western boundary current in accordance with the theory of Part I, section 3. The total flux of 10 × 10^6 m^3/sec up through the main thermocline in the Northern Pacific is supplied by a western boundary current across the equator, there being no mean flow across the equator at any distance from the western boundary. A similar picture prevails in the North Indian Ocean, but on a much smaller scale, the areas involved being so much smaller than those of the North Pacific. In the North Atlantic the interior flow patterns are much the same, but the strength of the western boundary current is much increased and flows toward the south and across the equator, the recirculation flow being amplified by one of the major deep water sources, S_1. The northern sub-areas of the major southern basins are similar to those just above the equator, but the flow pattern in the southernmost sub-areas (the bottom five in Fig. 5) are quite different. The flow through Drake Passage is not determined in our model so that we must assign it an arbitrary value R, which stands for another kind of recirculation, the amount of water which goes round and round the Antarctic Continent through Drake Passage. The rest of the numbers are obtained from simple continuity requirements. One of the most extraordinary features of this construction is the large flux (30 × 10^6 m^3/sec) in the western boundary current in the South Pacific, located we suppose, somewhere in the vicinity of the Tonga–Kermadec Trench. Other features of interest, though not so marked, are the reversals in directions of the deep western boundary currents in the Northern Pacific and Indian Oceans. Another feature, which we have also mentioned before (STOMMEL, 1958) is the fact that the cold deep waters flow away from the equator in the interior of the oceans.

Having described Fig. 5, let us now pause to interpret its meaning, and to review its implications. First, we have paid no attention to the probable disturbing effects of pronounced bottom topography within ocean basins. This will doubtless cause deviations from the extremely simple schema we have presented. However, it does not seem worthwhile to try to be more sophisticated than the present stage of our understanding and observational knowledge of the abyssal circulation demands. Similarly, since our main purpose is to imitate the grossest features of the abyssal circulation, we do not pursue the refinements of geographical variation of the upward flux of water to which the theory of the oceanic thermocline would naturally lead us: we simply take a constant and uniform upward velocity over the whole ocean. The pattern of flow in the interior of the deep ocean is thus fixed. Its amplitude remains to be determined. The flow in the interior is independent of the positions of the sources (S_0 and S_1). In a steady state the sum of the sources must be equal to the vertical flux over the entire ocean. Wherever the sources may be we can connect them to the interior solutions as necessary by a system of western boundary currents and the special zonal currents that connect western boundary currents at different boundaries.

We envisage the ultimate cause of the abyssal circulation to be the mechanism of the main thermocline which in effect, as a result of surface heating and applied wind stress, demands a certain upward flux at mid-depth. In the next section we will compute this upward flux from the theory of the oceanic thermocline (ROBINSON and STOMMEL, 1959).

The exact location of the sources is, according to our view, more or less a climatological accident. One could disappear and another appear somewhere else – for example, in the North Pacific – with changing climatic conditions, but these would be accompanied by no major modifications of the interior region of the abyssal circulation, and with no major change of the amplitude of the overall abyssal circulation. Of course any changes in the parametric mixing in the ocean would have effects on the rate of the abyssal circulation, and if the wind convergences were greatly intensified, this might also reduce the overall amplitude of the abyssal transports. This way of looking at the abyssal circulation is quite different from the traditional view which implies that the magnitude of the abyssal circulation is determined essentially by the amount of winter cooling at the polar regions and hence that a warming of polar regions of only a few degrees would largely stop the abyssal flow. From our point of view a warming of polar regions of one or two degrees would not affect deep transports except possibly to shift the location of the sources, and to reshuffle the western boundary currents. The deep temperatures would eventually rise a few degrees, and the distribution of oxygen might change – especially if sources shift position – but the overall transports, and the depth of the thermocline etc. would remain unchanged, providing the climatological factors which determine the thermocline remain unchanged.

ESTIMATE OF THE AMPLITUDE OF THE ABYSSAL CIRCULATION ON THE BASIS OF THE THEORY OF THE THERMOCLINE

A dynamical model of the thermocline in principle makes it possible to estimate the vertical component of velocity at mid-depths from the observed distribution of temperature (or more properly density) in the ocean. The calculation is only an estimate because there are simplifications and idealization in the theory which at best are only approximately true in nature and because there appear to be irregularities of a more or less short period observed in hydrographic data which make it impossible to obtain a sufficiently precise mean distribution of properties (in present day language, ‘ there is a high noise level ’), so that one can obtain only a rough estimate of various derivatives of the temperature and salinity fields.

The calculation may be made in a variety of ways.

(1) Pairs of hydrographic stations at the same latitude may be chosen, and a calculation of the depth of no meridional motion, and of the vertical component of velocity, made by the numerical integration of the linearized vorticity equation (STOMMEL 1956, equation 8). To make sure of this method it is necessary to have a good estimate of the mean curve of the wind-stress at the surface, to which unfortunately the results are quite sensitive. If the hydrographic station data contain short period variabilities (internal waves) the calculations of horizontal gradients of density can be made only very crudely. This difficulty has been encountered by most oceanographers employing ‘ dynamic calculations.’ In order to obtain even a fair representation of the currents the pairs of stations must be chosen fairly far apart, or else a line of stations must be smoothed in order to obtain a mean horizontal gradient. The method has one major advantage – it does not require hypothetical statements about relative magnitude of terms in the equation of density transport. Due to the uncertainties introduced through the hydrographic data and by the estimates of

curve of wind-stress the numerical results are doubtful – and it is impossible to state definitely even the range of doubt. STOMMEL'S 1956 calculations probably yield vertical velocities that are too high by a factor of ten.

(2) Alternatively, one may make a comparison with an idealized theoretical model such as that of ROBINSON and STOMMEL.

If we start with the same assumptions that ROBINSON and STOMMEL (1959) employ in their theory of the oceanic thermocline, except that we use spherical co-ordinates instead of a beta-plane, we have the following set of physical equations. First the dynamical equations are simplified (see Part I) by the traditional approximations used in spherical co-ordinates for a shallow fluid layer on a rotating globe to the linear geostrophic set :

$$-z\omega a\cos\theta\cdot u = -\partial p/\partial\theta \tag{4.1}$$

$$-z\omega a\cos\theta\cdot v = -\partial p/\partial\phi \tag{4.2}$$

$$g(1-\alpha T) = -\partial p/\partial z \tag{4.3}$$

The equation of continuity is :

$$a\sin\theta\frac{\partial w}{\partial z}+\frac{\partial}{\partial\theta}(u\sin\theta)+\frac{\partial v}{\partial\phi}=0 \tag{4.4}$$

and the equation for the temperature transfer is :

$$w\frac{\partial T}{\partial z}+\frac{u}{a}\frac{\partial T}{\partial\theta}+\frac{v}{a\sin\theta}\frac{\partial T}{\partial\phi}=\kappa\frac{\partial^2 T}{\partial z^2} \tag{4.5}$$

where T is temperature and κ is the parametric mixing coefficient which is discussed at length by FOBINSON and STOMMEL. Equations (4.1) to (4.5) lead to the following set of equations in u, w and T, which in fact are of the same form as the corresponding set in the beta-plane :

$$\frac{\partial^2 w}{\partial z^2}=\left[\frac{g\alpha}{2\omega a^2\cos^2\theta}\right]\frac{\partial T}{\partial\phi} \tag{4.6}$$

$$u\frac{\partial T}{a\,\partial\theta}+w\frac{\partial T}{\partial z}=\kappa\frac{\partial^2 T}{\partial z^2} \tag{4.7}$$

Hence there is no difficulty in immediately applying the same similarity transformation as before. In applying the theory to the real ocean the actual surface temperature cannot be used unless full account is also taken of the wind-stress distribution as well. However, if the origin ($z = 0$) is taken at the level where $w = 0$ – that is roughly at the inflexion point in the temperature sounding – the temperature boundary condition may be taken as

$$T = T_0\sin^n\theta$$

where of course T_0 is not the amplitude of observed temperature range at the surface, but at the centre of the main thermocline. We obtain the following expression for the vertical component of velocity just beneath the thermocline

$$w(-\infty)=T_0\sin^n\theta\left[\frac{4}{3}\frac{g\kappa^2}{2\omega T_0^{\,2}}\frac{\alpha}{a^2\phi}\frac{\sin^{1-2n}\theta}{\cos^2\theta}\right]^{\frac{1}{3}} \tag{4.8}$$

If we could neglect the influence of the wind we would probably set $n = 3$, which would give a pretty good fit to the observed surface temperature distribution in the oceans. However, as shown in ROBINSON and STOMMEL (1959), extensive regions of Ekman convergence produced by the wind at the surface force the level of no vertical component of velocity several hundred metres beneath the surface, and thereby reduce the amplitude of the temperature which should appear in the above expression for the vertical velocity to about one-half the surface amplitude. Instead of $T_0 = 30\,°\mathrm{C}$ we should use $T_0 = 15°$ as an approximation. This has very little influence on the thickness of the thermocline – since it affects it only by a multiplicative factor of the cube root of two, but the amplitude of the vertical component of velocity is directly proportional to this temperature amplitude so that it is reduced to a half of what it would be in the absence of the wind – other factors being equal.

We now wish to perform an integration of the above expression for the vertical component of velocity at mid-depth, over the surface of a single hemisphere globe completely covered with water and bounded by a complete meridian. This is not a bad approximation to the area of the 3000 m. level on the real ocean (about 60 per cent in fact). The limits of integration therefore will be

$$\theta = o, \qquad \theta = \pi/2, \qquad \phi = o, \qquad \phi = 2\pi$$

and the total integral I is :

$$I = \int_0^{\frac{\pi}{2}} \int_0^{2\pi} w\,(-\infty)\, a^2 \sin\theta \, d\theta \, d\phi$$

or

$$\doteq 11 \left[\frac{g\alpha T_0}{\omega} a^4 \kappa^2 \right]^{\frac{1}{3}} \tag{4.9}$$

Now setting in the following numerical values used by ROBINSON and STOMMEL :

$g = 10^3\ \mathrm{cm\ sec^{-2}}$ $\qquad \alpha = 2 \times 10^{-4}\ °\mathrm{C}^{-1}$

$\omega = 0{\cdot}7 \times 10^{-4}\ \mathrm{sec^{-1}}$ $\qquad \kappa = 0{\cdot}7\ \mathrm{cm^2\ sec^{-1}}$

$a = 0{\cdot}64 \times 10^9\ \mathrm{cm}$ $\qquad T_0 = 15\ °\mathrm{C}$

we obtain

$$I = 50 \times 10^6 \mathrm{m^3 sec^{-1}}$$

which is in reasonable agreement with the minimum value of $40 \times 10^6 \mathrm{m^3/sec}$ obtained in the previous section from estimates of flow from the cold sources S_0 and S_1. The average amplitude of the maximum vertical velocity is 4×10^{-5} cm/sec. Since the maximum upward velocity component is at a depth of about 1000 m. on the average, and there is on the average about 3000 m. of water beneath this depth, the deep water is replaced (in a very gross sense of course we have to allow for particular deviations) every 200 years. Although a calculation of this kind is simple because it uses a minimum of data – all the integrations are performed before comparison of the model with observation – it is rather misleading in its simplicity because it contains two implicit assumptions : Namely, that the eddy mixing parameter does not vary geographically (or with depth) and that horizontal mixing and the east-west component of density advection are negligible. These assumptions cannot be fully justified, and the numerical values of amplitude of the abyssal circulation obtained in the manner outlined above are thus subject to serious uncertainty.

(3) An intermediate approach is therefore indicated. Observational material is used to give an indication of the thickness of the thermocline at a number of different latitudes in the western sides of the interior of each ocean basin. The ROBINSON–STOMMEL theory for infinite depth model is used to compute the deep vertical component of velocity. If there are geographical variations in the mixing parameter they are thus taken into account (the hypotheses that the vertical eddy coefficient is constant in depth, and that horizontal mixing east-west advection are negligible, remain). In order to avoid calculation of too many quantities, zonal averages in each ocean can be calculated by direct x – integration using the analytical form introduced by the similarity transformation. The final summation is a simple numerical integration, where each zonal average of vertical component of velocity is multiplied by an appropriate area, so as to cover the whole ocean; the final sum is the total amplitude of the abyssal circulation. Considering the influence of errors in procedure (1) and of unsubstantiable hypothetical elements in the procedure (2), it seems to us that this intermediate procedure (3) is more likely to give good results, although one can hardly expect an accuracy of better than a factor of two or three.

Thus, using the notation and equation number of ROBINSON and STOMMEL (1959) we want to compute the average of w_∞ – the deep water asymptotic value of the vertical component of velocity along a latitude circle from one side to the other of the interior of a real ocean basin. One of the quantities which we want to avoid having to estimate is w_e, the vertical velocity just beneath the Ekman layer. Between equations (35) and (37) (of ROBINSON and STOMMEL 1959) the similarity transformation W_e of w_e can be eliminated to obtain the following form :

$$W_\infty = -\frac{L^2\,\theta_1}{4}$$

where θ_1, is the temperature near the middle of the thermocline, and L is a transformation of thermocline thickness z_t.

$$L = 2\,(\epsilon/x)^{\frac{1}{2}}\,z_t$$

where ϵ is the dimensionless small ratio $(\alpha\beta g)/(3f^2(y)$

Also $$W_\infty = (x/\epsilon)^{\frac{1}{2}}\,w_\infty$$

The calculations for which these formulae hold include the effect of wind-stress at the surface.

The thickness of the thermocline, z_t, is a function of distance from the eastern coast, — x and for a position far in the western side of the interior, $x = x_0$, is measured as $z_t\,(x_0)$. The quantity $z_t\,(x_0)$ is the vertical distance (in centimetres) over which the temperature decreases exponentially to e^{-1} of the mid-thermocline value. By eliminating W_∞ and L, the following expression is obtained :

$$w_\infty = -\,\epsilon\,[z_t\,(x_0)]^2\,(x - x_0)^{-\frac{1}{2}}\,\theta_1$$

The average of vertical velocity taken along a latitude circle between $x = 0$ and $x = x_0$ is :

$$\overline{w_\infty} = \frac{1}{x_0}\int_{x_0}^{0} w_\infty\,dx$$

The theoretical model uses the condition $z_t = 0$ at $x = 0$ as an eastern boundary condition. In the real ocean z_t is smaller is $x = 0$ than elsewhere but does not actually vanish.

$$\overline{w_\infty} = \frac{3}{2}\frac{1}{x_0}\left(\epsilon\,[z_t\,(x_0)]^2\,\theta_1\right)$$

If the depth of the thermocline does not vanish at $x = 0$, the factor 3/2 is replaced by unity.

For the North Pacific Ocean we might take very roughly the calculation as shown in Table 1. Evidently the zonal average of subthermoclinal vertical component of velocity cannot be calculated nearer to the equator than about 10° by the model proposed by Robinson and Stommel. This is obvious because the parameter ϵ is not small for latitudes less than 10° and because such observed features of the real ocean circulation as the Cromwell Current (Knauss 1959) are not shown when the theory is applied is this inadmissable range. If we can assume that the deep vertical velocity at the equator is not in some way quite singular we can compute averages

Table 1

Lat °*N*	$z_t\,(x_0)$ (cm)	ϵ (°C^{-1} cm^{-1})	θ_1 (°C)	$\theta_1\,\epsilon z^2$	x_0 (cm)	$\overline{w_\infty}$ (cm sec^{-1})
60	6×10^4	$0{\cdot}5 \times 10^{-6}$	5·0	$9{\cdot}0 \times 10^3$	4×10^8	$2{\cdot}5 \times 10^{-5}$
50	5	0·8	5·0	10·0	6	2·0
40	4	1·4	10·0	22·0	8	3·0
30	4	2·4	10·0	38·0	10	3·8
20	3	6·0	10·0	54·0	10	5·4
10	2	24·0	10·0	96·0	10	9·6
0	2	∞	10·0	∞	10	∞

Table 2

METHOD	*Total flux in world abyssal circulation* (10^6 m^3 sec^{-1})	*Vertical velocity under thermocline* (cm day^{-1})	*Replacement time of deep water* (years)
T-S diagram to establish proportions of North and South Atlantic water present; and direct deep current measurements off Charleston to give flux of North Atlantic component	15	0·5	1800
Same T-S analysis and Worthington's Nova Scotia section and 2000 metre reference level to establish flux of North Atlantic Component	40	1·3	650
Same T-S analysis and Wüst's dynamic calculations for South Atlantic Ocean for flux of North Atlantic component	50	1·6	550
Depth of the thermocline over the world ocean and theory of thermocline to establish total flux	90	3·0	300

and obtain thus a figure of abour 4×10^{-5} cm sec^{-1} as a North Pacific average (excluding a band of latitude south of 10 °N). This figure may be off by a factor of three, but at least the estimate of the mean wind-stress and the errors due to internal waves and details of hydrographic structure do not enter.

In a letter to the editor of *Deep-Sea Research*, STOMMEL (1958) gave a value of 3×10^{-5} cm sec^{-1} based on a much cruder thermo-convective model. Both of these are perhaps in fact too large by a factor of two or three. A figure more nearly in accord with WÜST'S (1957) geostrophic calculation is $1{\cdot}5 \times 10^{-5}$ cm sec^{-1}. A smaller value than this is obtained if we assume that the transport in the deep western boundary current in the North Atlantic is always the same as that measured in March–April 1957 by the joint British–American expedition (SWALLOW – WORTHINGTON 1957) 6×10^{12} cm^3/sec. Since the T-S properties of abyssal water (Section 3) indicate that the total flux of the abyssal circulation is from 2 to 3 times that of the western boundary current in the N Atlantic, we might choose 14×10^{12} cm^3/sec as the appropriate figure. To obtain the world average vertical velocity we divide this figure by the area of the ocean at 2000 m. (3×10^{18} cm^2) and obtain a figure of: $0{\cdot}5 \times 10^{-5}$ cm sec^{-1}. Table 2 summarizes these calculations.

EFFECT OF LATERAL MIXING ON THE DYNAMICS OF FLOW

In the preceding sections we have proposed a very highly idealized model of the abyssal circulation. The theoretically predicted flow patterns are based on the fundamental assumptions that (a) flow in the interior of the ocean is geostrophically balanced with negligible *dynamical* influence from frictional or eddy effects (b) significant departure from geostrophy occurs only in boundary currents along the edges of continental masses. Since it is clear that both lateral and vertical eddy diffusivity play a very important role in many oceanic processes and in the distribution of tracer properties of the water masses, it is important to inquire, at least in terms of orders of magnitude, as to whether Austausch coefficients large enough to be important in determining the distribution of oxygen, radio carbon, salinity, etc. are at the same time large enough to affect the dynamics of the postulated planetary motions driven by source-sink distributions.

To answer this question it is appropriate to assess the order of magnitude of the various terms appearing in the dynamical equations and in the diffusion equation.

Consider the dynamical problem in the form expressed by the vorticity equation for steady two-dimensional flow on a β-plane, retaining lateral friction terms :

$$u\frac{\partial \eta}{\partial x} + v\frac{\partial \eta}{\partial y} + \eta \operatorname{div}_H \mathbf{v} + f \operatorname{div}_H \mathbf{v} + \beta v = A_H\left[\frac{\partial^2 \eta}{\partial x^2} + \frac{\partial^2 \eta}{\partial y^2}\right]$$

In this notation :

x, y co-ordinates positive toward the east and north respectively,

u, v particle velocities corresponding to co-ordinates x, y respectively.

$\mathbf{v}$, total vector velocity

$$\eta = \frac{\partial v}{\partial x} - \frac{\partial u}{\partial y}$$

div_H, horizontal divergence

f, Coriolis parameter

β, $\partial f/\partial y$

A_H, horizontal (lateral) eddy coefficient.

Transforming Equations 3·1 of Part I to the β-plane as defined above, the zonal and meridional components of geostrophically balanced flow for a uniformly distributed sink Q_0 over the entire surface are :

$$u = 2Q_0\,(x_2 - x)/h \tag{2.2}$$

$$v = fQ_0/\beta h \tag{2.3}$$

$$\eta \doteqdot -\frac{2Q_0}{h}\frac{(x_2 - x)}{a} = -\frac{u}{a} \tag{2.4}$$

The order of magnitude of Q_0, estimated in section 4 is 4×10^{-5} cm/sec. We adopt the following values for various relevant quantities :

Horizontal distance scale : $\overline{X} \sim \overline{Y} \sim 6000$ km $= 6 \times 10^8$ cm

Thickness (depth) of abyssal layer : $h \sim 3$ km $= 3 \times 10^5$ cm

Coriolis parameter : $f \sim 10^{-4}$ sec^{-1}

$\beta \sim 2 \times 10^{-13}$ sec^{-1} cm^{-1}

Radius of the earth : $\sim 6{\cdot}5 \times 10^8$ cm

Vertical velocity at top of abyssal layer : $Q_0 \sim 4 \times 10^{-5}$cm/sec

From these assumed values we estimate the order of magnitude of the following :

$$u \sim 0{\cdot}16 \text{ cm/sec}$$

$$v \sim 0{\cdot}067 \text{ cm/sec}$$

$$\eta \sim +\,2{\cdot}5 \times 10^{-10} \text{ sec}^{-1}$$

$$\text{div}_{\text{H}}\,\mathbf{v} \sim -\,1{\cdot}3 \times 10^{-10} \text{ sec}^{-1}$$

$$\partial\eta/\partial x \sim -\,4{\cdot}1 \times 10^{-19} \text{ sec}^{-1} \text{ cm}^{-1}$$

$$\partial\eta/\partial y \sim +\,3{\cdot}8 \times 10^{-19} \text{ sec}^{3-1} \text{ cm}^{-1}$$

$$\frac{\partial^2 \eta}{\partial x} \sim \frac{\partial^2 \eta}{\partial y^2} \sim 7 \times 10^{-28} \text{ sec}^{-1} \text{ cm}^{-2}$$

(The magnitudes of the derivatives have been estimated by finding the appropriate derivates of Equations 3.1, Part I and then converting to the β-plane).

Thus we have the following orders of magnitude for the terms in Equation (2.1).

$$u\,\frac{\partial\eta}{\partial x} \sim -\,7 \times 10^{-2}{}_{0} \text{ sec}^{-2}$$

$$v\,\frac{\partial\eta}{\partial y} \sim 3 \times 10^{-20} \text{ sec}^{-2}$$

$$\eta\,\text{div}_{\text{H}}\,\mathbf{v} \sim -\,3 \times 10^{-20} \text{ sec}^{-2}$$

$$f\,\mathrm{div}_H\,\mathbf{v} \sim -\,1{\cdot}3 \times 10^{-14}\,\mathrm{sec}^{-2}$$

$$\beta v \sim +\,1{\cdot}3 \times 10^{-11}\,\mathrm{sec}^{-2}$$

It is clear that the dominant terms on the left-hand side of Equation (2.1) are $f\,\mathrm{div}_H\mathbf{v}$ and βv. It is, of course, the balance of these terms which represents the situation we describe as 'purely geostrophic flow.' We can now find values of the Austausch coefficient A_H which would make the right hand side of the equation assume magnitudes comparable with the dominant terms on the left. Noting that the latter are of the order of 10^{-14} and that the second derivatives on the right are of the order of 10^{-27}, it is apparent that A_H, must be of the order of 10^{12} cm^2/sec before the frictional terms on the right attain the order of one tenth of the planetary divergence terms.

Available estimates of the large scale lateral eddy coefficient for the ocean usually fall in the range 10^6 to 10^8 cm^2/sec. In the light of these results we feel that our fundamental assumption, that the very low velocity flows induced in the interior of the ocean are essentially geostrophically balanced, is a reasonable one. We not do expect lateral friction to affect seriously the purely geostrophic dynamical foundation of the basic circulation patterns. (It is interesting to note that BURGER (1958) obtains a similar result for large scale flows in his consideration of planetary motions in the atmosphere).

We now make a similar scale and order of magnitude analysis of diffusion of a tracer property of the water. The basic differential equation is of the form :

$$A_H\,\nabla^2_H\,c - \mathbf{v}\cdot\nabla_H\,c - \lambda\,c = 0 \qquad (2.5)$$

where c denotes concentration of a property (say oxygen) and λ is the reciprocal of the "half life" of decay. The three terms of Equation (2.5) represent a balance among diffusive transport, advective transport, and decay, the amplitude of the advective term being determined by the basic geostrophic flow.

To examine the relative significance at the planetary scale of the three terms in Equation (2.5) we re-write it in the following 'operator' form :

$$\left[A_H\,\nabla^2_H - \mathbf{v}\cdot\nabla_H - \frac{3{\cdot}17 \times 10^{-8}}{T}\right] c = 0 \qquad (2.6)$$

where T is the half-life of decay in years of the tracer property. Introducing the scale magnitudes used earlier, the orders of magnitude of the terms appearing in (2.6) are indicated by :

$$\left[2{\cdot}8\,(10^{-18})\,A_H - 2{\cdot}7\,(10^{-10}) - \frac{3{\cdot}17 \times 10^{-8}}{T}\right] c = 0 \qquad (2.7)$$

All three terms are of roughly comparable significance when A_H is of the order of $10^7 - 10^8$ cm^2/sec and T is of the order of $10^2 - 10^3$ years. If the half life becomes much less than 10^2 years, the distribution of the property is determined principally by diffusion in the immediate neighbourhood of the western boundary current, advective effects are insignificant, and appreciable concentrations do not extend very far into the interior of the ocean. If T and A_H are both large, the property becomes essentially uniformly distributed, the advective effects insignificant, and the concentration level determined by the relation between half life and rate of supply.

The amplitude of the basic geostrophic circulation in the model we have postulated is such that Austausch coefficients of the order of $10^7 - 10^8$ cm^2/sec will have a very marked diffusive effect on the distribution of tracer properties of the water masses. At the same time, as shown earlier in this section, coefficients of this magnitude would be expected to have a *negligible* effect on the dynamics of the basic flow. This rather paradoxical result arises from the very large scale and low velocity of the basic flow, the frictional force terms being proportional to third spatial derivatives of the geostrophic velocities. It is felt therefore that the fundamental model, in which an interior, large scale, geostrophically balanced circulation is driven by the mechanism of the thermocline, is basically reasonable. It is simultaneously to be pointed out that great caution must be exercised in drawing inferences about the basic flow from observed distributions of water mass properties; the latter probably being seriously affected by diffusion on a scale substantially smaller than that of the basic flow.

Woods Hole Oceanographic Institution
Woods Hole, Massachusetts

Contribution No. 1055 *from the Woods Hole Oceanographic Institution. Part of this work was done while one of us* (*A.B.A.*) *was the recipient of a Fellowship of the John Simon Guggenheim Memorial Foundation. The rest was done under contract with the Office of Naval Research.*

REFERENCES

BURGER A. P. (1958) Scale consideration of planetary motions of the atmosphere. *Tellus* **10**, 195-205.

ROBINSON A. and STOMMEL H. (1959) The oceanic thermocline and the associated thermohaline circulation. *Tellus.* In press.

STOMMEL H. (1956) On the determination of the depth of no meridional motion. *Deep Sea Res.* **3**, 273-278.

STOMMEL H. (1957) A survey of ocean current theory. *Deep Sea Res.* **4**, 149-184.

STOMMEL H. (1958) The abyssal circulation. *Deep Sea Res.* **5**, 80-82.

STOMMEL H. and ARONS A. B. (1959) On the abyssal circulation of the world ocean—I. Stationary planetary flow patterns on a sphere. *Deep Sea Res.* **6**, 140-154.

STOMMEL H., ARONS A. B. and FALLER A. J. (1958) Some examples of stationary flow patterns in bounded basins. *Tellus* **10**, 179-187.

SWALLOW J. C. and WORTHINGTON L. V. (1957) Measurements of deep currents in the western North Atlantic. *Nature, Lond.* **179**, 1183-1184.

WÜST G. (1938) Bodentemperatur und Bodenstrom in der Atlantischen, Indischen und Pazifischen Tiefsee. *Gerlands Beitrage zur Geophysik* **54** No. 1, 1-8.

WÜST G. (1951) Uber die Fernwirkungen Antarktischer und Nordatlantischer Wassermassen in den Tiefen des Weltmeeres. *Naturw. Rsch.* 3, 97–108.

WÜST G. (1955) Stromgeschwindigkeiten im Tiefen-und Bodenwasser des Atlantischen Ozeans auf Grund dynamischer Berechnung der *Meteor* – Profile der Deutschen Atlantischen Expedition 1925-1927. *Deep-Sea Res., Bigelow Volume,* 1955.

WÜST G. (1957) Strogeschwindigkeiten und Strommengen in den Tiefen des Atlantischen Ozeans. *Wiss. Ergeb. Deutsch. Atlant. Exped.* Meteor, 1925-27. Vol. VI, Part II. Gruyter, Berlin.

Printed in Great Britain by The Salisbury Press Ltd., Publicity House, Wilton Road, Salisbury, Wilts. (21934)

Contribution No. 1056

Made in United States of America
Reprinted from LIMNOLOGY AND OCEANOGRAPHY
Vol. 5, No. 3, July, 1960
pp. 291–300

OBSERVATIONS ON THE ECOLOGY OF THE SOFT CLAM, *MYA ARENARIA*, IN A SALT POND

BY GEORGE C. MATTHIESSEN

OBSERVATIONS ON THE ECOLOGY OF THE SOFT CLAM, *MYA ARENARIA*, IN A SALT POND[1]

George C. Matthiessen

Division of Marine Fisheries, Commonwealth of Massachusetts, Boston, Massachusetts

ABSTRACT

Observations were made on the ecology of the soft clam, *Mya arenaria*, in a salt water pond on Martha's Vineyard, Mass., during the summer and fall of 1958. Primary consideration was given to the tolerance of this species to low and fluctuating salinities, the effect of salinity upon rate of growth, and possible correlation between growth rate and the nature and abundance of phytoplankton.

Field observations supplemented by laboratory experimentation indicated that *Mya* longer than 2 mm can tolerate salinities less than 1‰ for at least 24 hrs and can withstand sudden salinity fluctuations of an order of 18‰. Tolerance of clams 2–25 mm in length to low salinities was found to be proportional to their size.

Growth rate of clams living under different salinity conditions ranging in mean value from 3.5‰ to 14‰ was found to vary directly with salinity. The fact that the pumping rate of clams was observed to vary directly with salinity within the limits 0–31‰ is considered significant in this respect.

Comparisons of growth rates with phytoplankton concentrations suggested that flagellates form an important source of nutrition for *Mya* and that diatoms may be of relatively little importance.

INTRODUCTION

The continued decline in abundance of clam and oyster populations in many coastal areas during the past decade has accentuated the need for more efficient methods of utilizing a potentially valuable marine resource. It has been suggested by certain investigators (Turner 1951; Loosanoff 1958) that shellfish might be raised quite profitably in enclosed or semi-enclosed salt water ponds in which optimum environmental conditions could be maintained. For example, it might be possible to exclude oceanic predators completely, to accelerate shellfish growth indirectly through the addition of fertilizer, and to eliminate the waste involved in the dispersal of shellfish larvae to inaccessible areas.

In certain respects the soft clam, *Mya arenaria,* might be ideally suited for pond culture. The ability of this species to thrive in brackish water has been recognized by shellfish investigators for many years (Belding 1930), and its tolerance to low and variable salinity conditions does not appear to be shared by its most significant and primarily oceanic predators, such as the green crab (*Carcinides maenas*), the horseshoe crab (*Limulus polyphemus*), or the boring snail (*Polinices heros*). However, the minimum salinity conditions required for a thriving, self-replenishing *Mya* population have not been established.

The objective of this investigation was to study certain factors influencing the survival and growth of members of a clam population in Oyster Pond, a salt water pond located on the south shore of Martha's Vineyard, Mass. Consideration was given primarily to the minimum salinity conditions under which this species is capable of survival, reproduction, and growth, and secondarily to its probable source of nutrition.

The author is sincerely grateful to Mr. Harry J. Turner of the Woods Hole Oceanographic Institute and Dr. George L. Clarke of Harvard University and the Woods Hole Oceanographic Institute for their advice during this project, to Mr. Anthony Provenzano of the U.S. Fish and Wildlife Service for his cooperation and suggestions, and to Mr. Thomas L. Flynn of Edgartown, Mass., for his permission to undertake re-

---

[1] Based upon data included in a thesis in biology submitted to the Graduate School of Arts and Sciences of Harvard University in partial fulfilment of the degree of Doctor of Philosophy.

Contribution No. 1056 from the Woods Hole Oceanographic Institute.

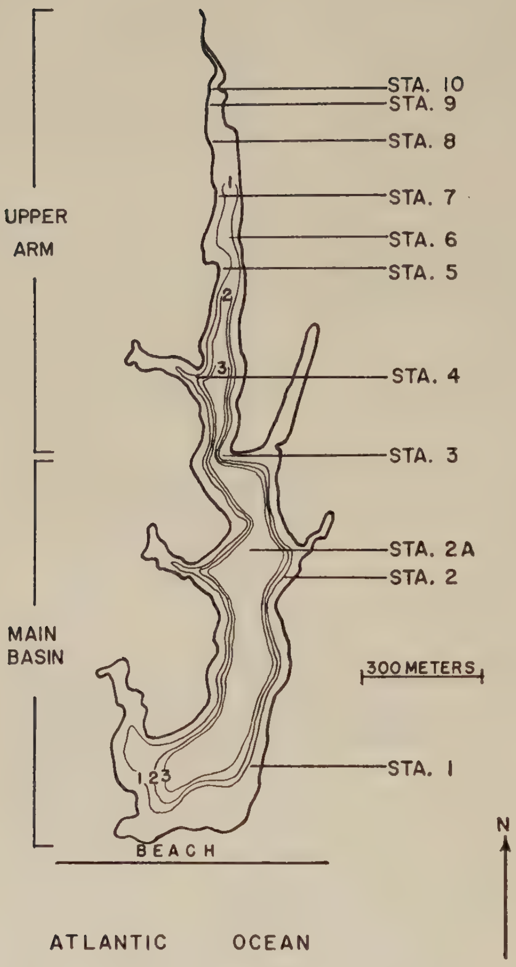

FIG. 1. Chart of Oyster Pond. Depth in meters.

search in Oyster Pond. Financial assistance in the form of a fellowship grant from the Woods Hole Oceanographic Institution is gratefully acknowledged.

DESCRIPTION OF OYSTER POND

Oyster Pond is usually separated from the Atlantic Ocean by a sand beach 50 to 100 m in width (Fig. 1). The pond is opened periodically by bulldozing a channel across the beach, resulting in a sharp increase in salinity throughout much of the pond. The pond seldom remains open for longer than two to three weeks, as wind-blown sand gradually fills the channel. Once closed, the pond water gradually freshens due to precipitation, seepage, and a stream at the extreme north end. The northern half of the pond, or upper arm (Fig. 1), is relatively shallow and bordered by wooded hills; the main basin is appreciably deeper and, due to the flat topography, is exposed to wind from all quarters.

The only species of bivalves of numerical significance inhabiting Oyster Pond are *Mya arenaria*, *Crassostrea virginica*, and *Macoma baltica*. The effect of the few potential predator species observed—the decapods *Callinectes* and *Panopeus* and the flatworm *Stylochus*—upon the bivalve population is uncertain but is not considered to be appreciable. A survey of the distribution of *Mya* was undertaken prior to June 16 when the pond was open and the water level low. It was observed that the population extended as far up the pond as Station 7 (Fig. 1) but no further. As no apparent change in sedimentary characteristics took place at this point, it was presumed that low salinity conditions prevented the population from advancing further.

Oyster Pond was open to the sea from June 3–June 16, 1958. After a strong southwest wind closed the inlet during the evening of June 16, it remained closed until August 27, 1958, when it was reopened by bulldozer. The strong salinity gradient that generally prevailed along the pond's axis during the period of June 16–August 27 provided a favorable opportunity to study the role of salinity in the ecology of a *Mya* population in a relatively small area, particularly as this period coincided with the population's major spawning period. After the pond closed on September 9, two northeast storms occurred in quick succession and destroyed the salinity gradient that had prevailed during the summer months. For reasons to be discussed below, homogeneity of both temperature and salinity throughout much of the pond during the autumn was accompanied neither by a homogeneous distribution of different planktonic species nor of phytoplankton abundance in general. Conditions were therefore considered ideal during the period September 18–November 6, 1958, for comparing the effects of different phytoplanktonic forms upon the growth rate of *Mya.*

METHODS

Clams were collected from the pond population near Station 1 and placed in shallow, sediment-filled trays, 40 clams to each tray. These clams, ranging in length from 13–25 mm, were measured with vernier calipers and numbered with finger-nail polish for future identification. The trays were placed at Stations 1–10 (Fig. 1) at a depth of about one meter. The clams were measured at approximately two-week intervals during the period June 16–August 26. At least three times each week the temperature and salinity at each station was determined to the nearest 0.1°C and 0.1‰, the latter by means of hydrometer.

To compare the ability of *Mya* of different sizes to survive under presumably adverse salinity conditions, small clams 2–4 mm long were collected and placed in quart jars, approximately 100 clams to each jar. The tops of the jars were covered with plastic screening. The jars were placed next to the wooden trays at Stations 4–8 for a six-day period, after which they were inspected to record any mortalities. The experiment was then repeated.

An attempt to determine whether clams native to Oyster Pond might have developed an unusually high tolerance to low salinity conditions was made in the following manner. A sample of 60 clams, ranging in length from 18–40 mm, were collected from a tidal flat along the Vineyard Sound shoreline in an area where the salinity would not be expected to vary appreciably from 28–32‰. These clams were placed in sediment-filled trays, 20 clams to each tray, at Stations 4, 6 and 8; their growth and survival rates were compared with native Oyster Pond clams in trays at the same stations.

Supplementary studies on the tolerance of clams of different sizes to low salinities were conducted under artificial conditions. A group of 125 clams, 2–4 mm in length, were collected from an area in Oyster Pond where the bottom salinity was 18‰ and had ranged from 18–30‰ during the previous month. They were placed in a polyethylene container of distilled water, temperature 20°C, for a period of 24 hr. Every 6 hr thereafter for the next 24 hr, groups of 25 clams were removed and placed in separate containers that had a layer of sand on the bottom and were filled with water of salinity 18‰. Mortality percentage was easily determined. Upon being returned to normal (18‰) salinity, the clams either dug into the sediment within 24 hr or remained on the surface of the sediment with shells agape and failed to respond to mechanical stimulation.

This experiment was repeated with groups of clams 5–10 mm and 15–25 mm in length. In another series of experiments salinities of 1, 2 and 4‰ were used instead of distilled water with clams in the 5–10 mm size range.

Determination of the relative pumping rates of clams under different salinity conditions was made by the method described by Cole and Hepper (1954). Six 3-liter polyethylene containers with a sand substratum were filled with water of 31, 15, 7.8, 3.9, 2.0 and 1‰. Six clams, averaging 27 mm in length, were placed in each container; the containers were placed in a thermostatically-controlled water bath at 21°C (± 1°). After a 24 hr acclimatization period, a dilute solution of Neutral Red was introduced into each container, and also into a seventh container serving as control, in sufficient amount to produce an initial Neutral Red concentration of 0.0003%.

At half-hour intervals, 10 ml samples of water were drawn from each container and acidified with three drops of concentrated HCl to restore coloration. The optical density of each sample was determined by means of a Beckman spectrophotometer and converted into per cent concentration by use of a calibration curve. In this way it was possible to determine the relative pumping rate at different salinities, the presumption being that Neutral Red would be removed from the water, by adsorption to the gills, at a rate directly proportional to the pumping rate of the clams.

To study the effects of different phyto-

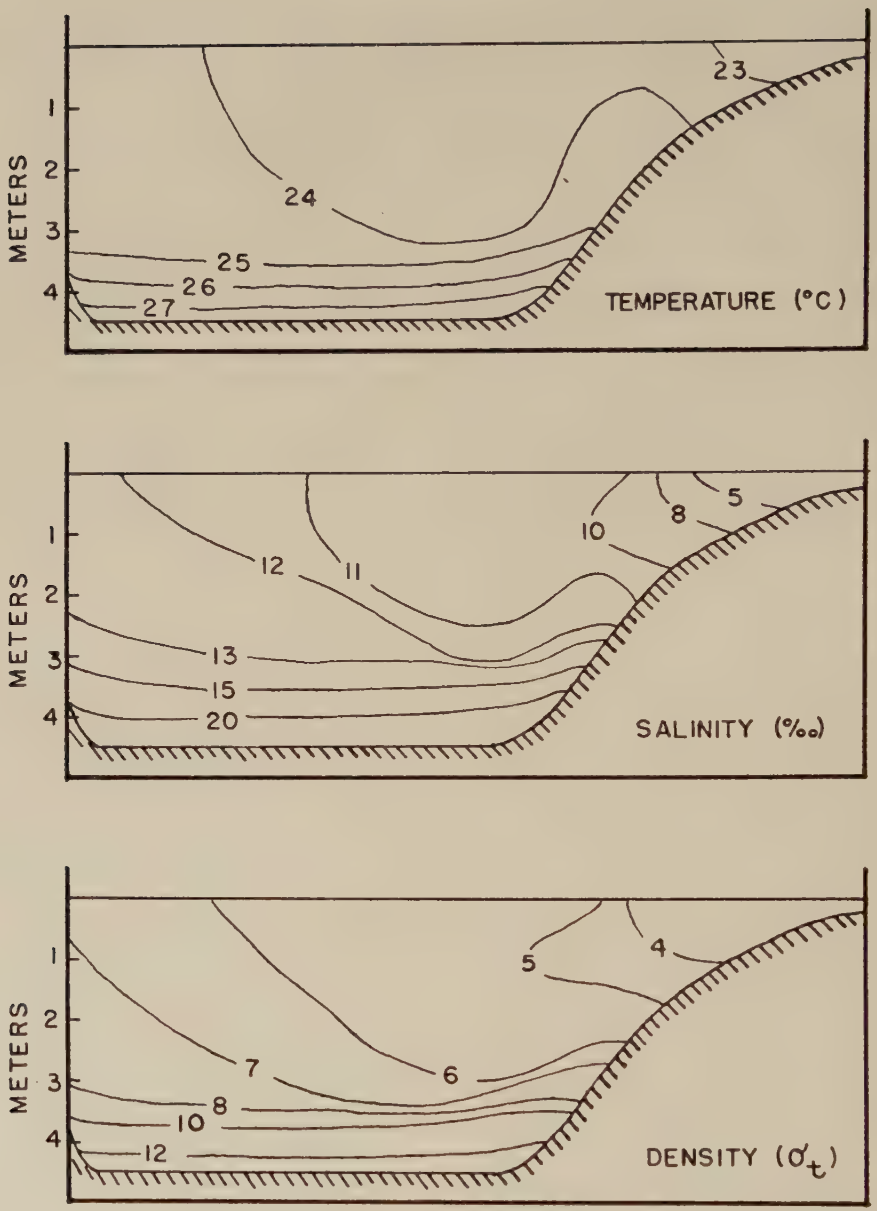

FIG. 2. Temperature, salinity and density distribution in Oyster Pond on August 22, 1958.

plankton upon the growth rate of *Mya*, 40 clams, averaging 17.5 mm in length, were placed in each of five wooden trays filled with sediment. The trays were placed at Stations 1, 2A, 3, 5 and 7 (Fig. 1). At approximately 10-day intervals the clams were measured with calipers to the nearest 0.1 mm. Temperature and salinity were from one-liter samples of water collected daily at each station at the level of the experiment trays.

The plankton population at each station was determined three times each week by analysis of the one-liter sample. A minimum of two Sedgwick-Rafter cell mounts were made from each sample, and the number of flagellated forms was estimated. After addition of formalin and after a 24-hr set-

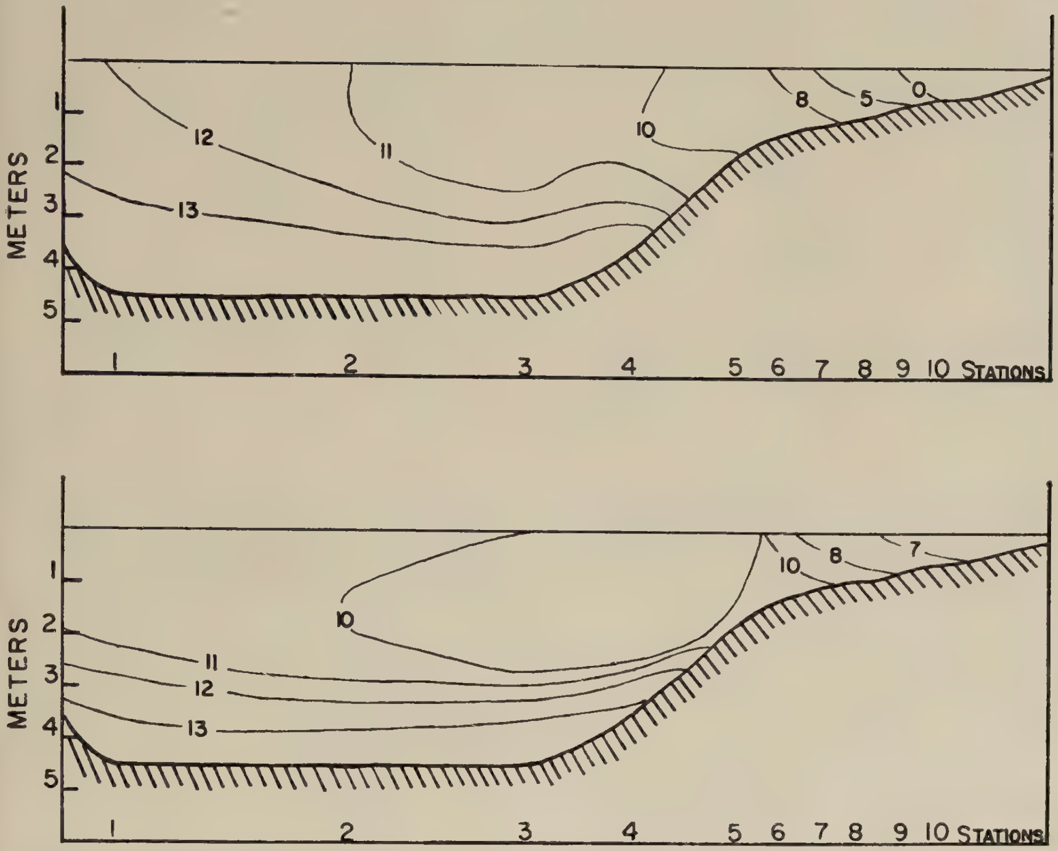

FIG. 3. Salinity distribution in Oyster Pond on August 22, 1958, with wind from the southwest (upper profile), and on August 24, 1958, with wind from the north (lower profile).

tling period, each sample was concentrated to 100 ml by siphoning off the excess liquid with a U-shaped tube. After reshaking, at least two Sedgwick-Rafter cell mounts were made from each, and the nature and abundance of the diatom population was determined.

The samples were then further concentrated to 15 ml, and each was examined under 50 high power microscope fields to give a proportionate estimate by volume of inorganic material, phytoplankton cells, and organic detritus. The remainder of the sample was centrifuged for a 20-min period and the approximate total volume of particulate matter determined.

RESULTS

Certain hydrographic features of Oyster Pond, in particular the salinity distribution during the period when the pond was closed, should be mentioned. Fresh water entering the pond formed a layer over the saline water entrapped by the pond's closing and mixed only very slowly with the subsurface layers. This stability resulted in a positive thermal gradient between surface and bottom layers during the summer (Fig. 2). As Figure 2 also indicates, water of comparatively high salinity was generally confined to the deeper portions of the main basin of the pond.

Northerly winds blew fresh surface water down the upper arm of the pond into the main basin. In compensation, bottom water of high salinity moved into the upper arm, being easily detectable as far as Station 10 within a few hours after a wind shift to the north (Fig. 3). Certain benthic forms such as *Mya* must be able to tolerate ap-

Table 1. *Temperature, salinity, and clam growth at Stations 1–10 in Oyster Pond during the period June 17–August 27, 1958*

Station number	Temperature (°C)		Salinity (‰)		Mean weekly growth increments (mm)
	Range	Mean	Range	Mean	
1	16.4–27.0	23.1	9.8–30.5	15.5	1.4
2	17.2–27.4	23.2	10.2–30.0	14.7	1.4
3	19.6–27.0	23.4	8.8–29.0	13.6	1.2
4	15.0–26.9	23.4	7.8–28.8	14.0	1.5
5	19.2–26.9	23.4	5.9–21.0	11.0	1.2
6	18.3–26.8	23.3	3.6–18.5	9.6	1.1
7	16.4–26.6	22.4	1.1–12.8	7.6	1.1
8	15.6–26.9	21.8	0.0–12.0	5.3	0.7
9	12.0–26.2	21.3	0.0–12.0	4.2	0.2
10	11.4–26.2	19.7	0.0–11.8	3.5	0.0

preciable and sudden fluctuations in salinity and temperature as great as the extremes presented in Table 1.

As mentioned previously, Oyster Pond was closed to the sea during the period June 17–August 27; no mortality was recorded among the clams that had been placed in experimental trays at Stations 1–10 during this time. Therefore, although the native population extended no further up the pond than Station 7, clams longer than 12 mm (the smallest clams placed in the trays were 13 mm) were capable of tolerating the salinity that prevailed at Stations 8, 9 and 10 during this period (Table 1). Similarly, clams obtained from an area characterized by constantly high salinities survived as well and grew at the same rate at Stations 4, 6 and 8 as did the native clams at the same stations.

However small *Mya* (2–4 mm in length) were unable to survive above Station 7. Moreover, no clams resulting from the summer spawning succeeded in setting above Station 7, even though it is probable that larvae were carried well above Station 7 in the subsurface layers during the occurrence of northerly winds.

Results from laboratory studies on the ability of *Mya* of different sizes to tolerate immersion in water free of salt for various lengths of time are presented in Figure 4. These results substantiate the evidence obtained from field observations that the larger members of this species are more tolerant to low salinity conditions than the juveniles. The number of days that clams in the 5–10 mm size range can be exposed to various low salinities and resume normal behavior when returned to more favorable conditions are as follows: in 0‰, 2–3 days; in 1‰, 3–4 days; in 2‰, 5–6 days; in 4‰, indefinitely. No clam, regardless of size, appeared capable of survival after immersion in distilled water for a period exceeding 72 hr at about 20°C.

As indicated in Table 1, rate of growth appeared to be directly related to salt concentration within the limits given. As the experiment with Neutral Red suggests (Fig. 5), the pumping rate of *Mya* varies only slightly in water between 15.5–31‰, is sharply reduced when the salinity has dropped to approximately 8‰, and appears to cease altogether at salinities of 4‰ or below. Therefore, even though the water of low salinity at the upper stations may have been deficient in nutritive material, it would seem that the inhibiting effect of low salinities upon the feeding processes satisfactorily explains the different growth rates observed. The fact that growth rate also appears to be directly related to temperature in Table 1 is not considered significant in this case, as further investigations during the fall established that not until the temperature had dropped to 15°C or below did growth rate show a decline from its midsummer value.

The growth rate of clams in experimental

TABLE 2. *Temperature, salinity, and clam growth at Stations 1, 2A, 5 and 7 in Oyster Pond during the period September 18–November 6, 1958*

Station number	Temperature (°C)		Salinity (‰)		Mean weekly growth increments (mm)
	Range	Mean	Range	Mean	
1	14.1–19.8	16.7	15.7–20.7	18.2	1.0
2A	9.5–21.7	14.6	12.0–27.3	16.5	1.0
5	10.1–20.2	14.6	10.8–19.5	14.0	1.5
7	10.0–19.6	14.5	8.2–18.2	13.1	1.5

trays at four stations during the period September 18–November 6 are given in Table 2. During the first week of this experiment, the clams at Station 3 were washed from the tray and lost; those at Station 1 were lost in similar fashion after three weeks.

Contrary to the temperature and salinity distributions, which remained fairly constant during this time, there was a distinct difference in the nature and abundance of phytoplankton in the upper arm of the pond and in the main basin. Diatoms were consistently more numerous at Station 2A, whereas flagellates were considerably more abundant at Station 7 (Table 3). The volume of organic detritus in the water was also found to be greater in the upper arm at Station 7.

DISCUSSION

Turner (1953) states that *Mya arenaria* is fundamentally a creature of the upper estuarine, as opposed to the oceanic, environment. The present results illustrate

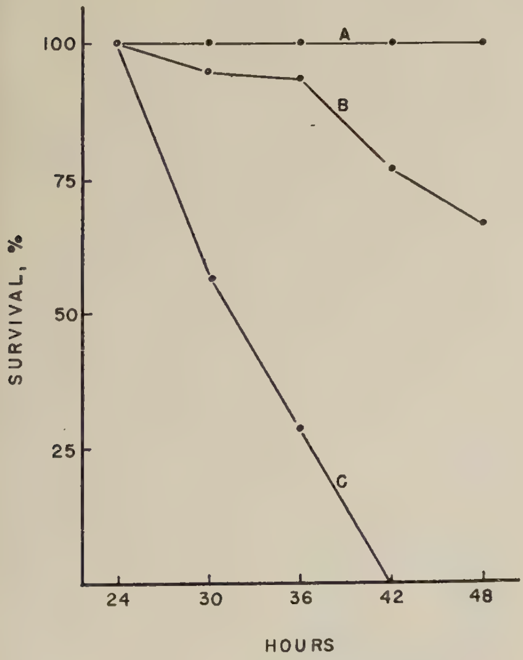

FIG. 4. Percentage of survival of clams of different sizes after immersion in distilled water for given periods of time. A = 15–25 mm; B = 5–10 mm; C = 2–4 mm.

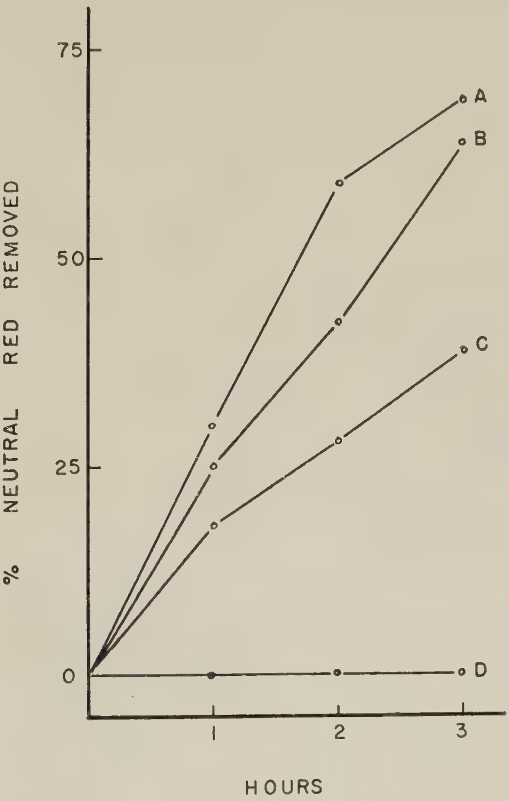

FIG. 5. Relative pumping rates of clams at different salinities. A = 31‰; B = 15.5‰; C = 7.8‰; D = 0–4‰.

TABLE 3. *A comparison of the abundance of diatoms, flagellates, and organic detritus at Stations 2A and 7 in Oyster Pond during the period September 18–November 6, 1958*

	Diatoms Cells/L × 10^6		Flagellates Cells/L × 10^6		Organic detritus cc/L	
	Sta. 2A	Sta. 7	Sta. 2A	Sta. 7	Sta. 2A	Sta. 7
Sept. 18	0.2	0.4	1.9	2.2	0.10	0.35
Sept. 22	1.0	0.5	1.3	3.9	0.30	0.20
Sept. 24	2.1	1.2	1.3	5.8	0.15	0.30
Sept. 26	1.8	1.4	1.7	10.0	0.05	0.35
Sept. 29	1.1	0.9	2.4	6.0	0.05	0.10
Oct. 1	1.0	0.9	1.8	6.5	0.02	0.15
Oct. 3	0.9	0.7	3.2	6.5	0.05	0.05
Oct. 6	0.7	0.6	3.3	5.5	0.02	0.05
Oct. 8	0.9	0.6	2.2	6.8	0.01	0.25
Oct. 10	4.4	2.1	1.8	6.3	0.02	0.10
Oct. 13	1.0	0.4	2.9	6.6	0.10	0.05
Oct. 15	1.0	0.5	2.9	11.6	0.02	0.35
Oct. 17	0.8	0.1	4.5	6.0	0.02	0.05
Oct. 20	0.7	0.2	1.3	2.0	0.05	0.05
Oct. 22	0.4	0.1	1.8	5.7	0.10	0.05
Oct. 24	0.4	0.3	2.2	5.3	0.05	0.20
Oct. 26	0.2	0.2	2.5	3.0	0.05	0.05
Oct. 28	0.3	0.3	4.1	6.0	0.05	0.20
Oct. 30	0.1	0.1	4.6	4.8	0.03	0.15
Nov. 1	0.2	0.1	5.1	5.7	0.02	0.20
Nov. 3	0.1	0.1	4.9	8.2	0.05	0.10
Nov. 5	0.1	0.1	3.4	4.7	0.02	0.03
Mean values	0.9	0.5	2.8	5.9	0.06	0.15

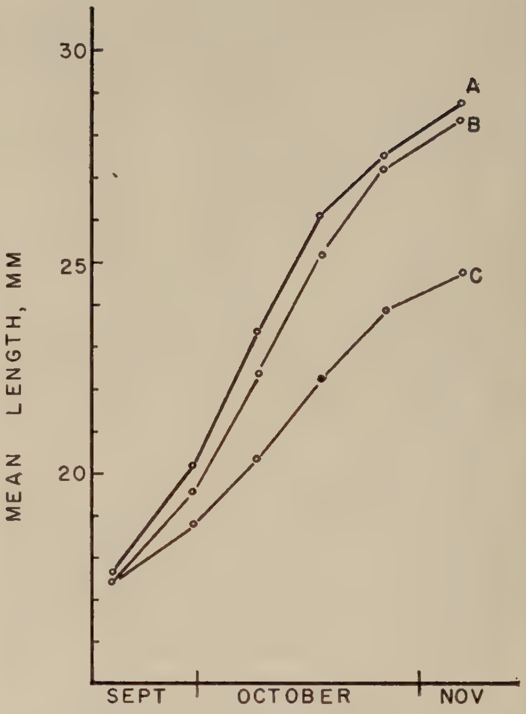

FIG. 6. Comparison of clam growth rates at Stations 2A, 5 and 7 in Oyster Pond during period of September 18 to November 5, 1958. A = Station 7; B = Station 5; C = Station 2A.

again the ability of this species to tolerate sudden and appreciable changes in salinity, a condition common to most estuaries. The fact that the adult clam can withstand sudden salinity fluctuations of an order of 18‰ and apparently can survive for considerable periods of time in salinities as low as 4‰ provides it with a distinct advantage over its less tolerant predators.

With respect to feeding behavior at low salinities, these studies appear to indicate that the salinity may drop as low as 15‰ before the pumping rate is significantly reduced. Moreover, as indicated in Table 1, the weekly growth increment at Station 4 during the summer months averaged 1.5 mm, even though the salinity at this station then averaged only 14‰. This growth rate compares favorably with that determined for a *Mya* population in Quincy Bay during the previous summer, which averaged 1.1 mm per week at a salinity of 28–32‰.

The results also suggest that the greater sensitivity of the juvenile clams will inhibit the establishment of populations in areas subject to sharp fluctuations in salinity. Chanley (1958) found that the young of *Venus mercenaria* were less tolerant to subminimal salt concentrations than adults, and it is probable that the larvae are equally, or perhaps even more, sensitive. It now appears unlikely that the soft clam can successfully reproduce where the salinity averages less than 7‰ and occasionally drops below 1‰, and it is quite possible that its requirements for propagation are even more rigorous.

There are at least two possible reasons why the young of this or any other species of mollusk are more sensitive to low salinities than the adult. Firstly, if Prosser *et al.* (1952) are correct in assuming that death in a hypotonic medium occurs as a result of the breakdown of the enzymatic system, it may be that excessive dilution of the tissues and body fluids is accomplished at a

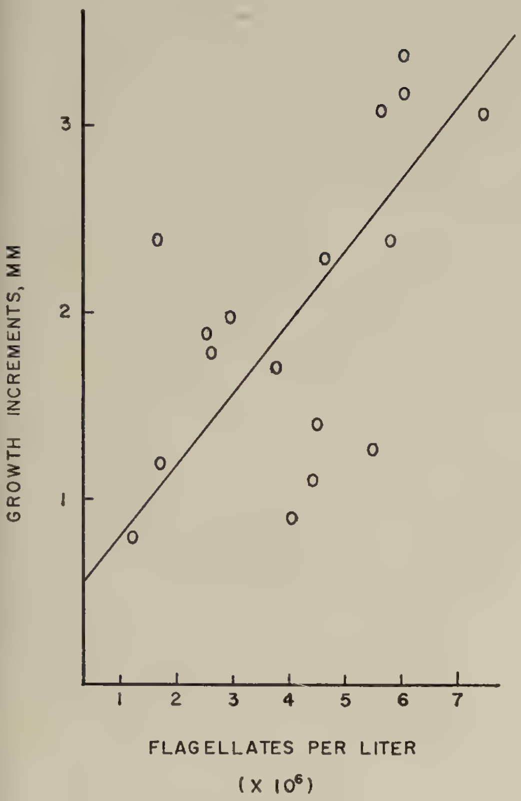

FIG. 7. Increments of clam growth at Stations 1, 2A, 5 and 7 in Oyster Pond, determined at 10-day intervals during fall of 1958, plotted against average flagellate abundance at each station during the corresponding interval.

faster rate in the smaller individuals due to their greater surface area to volume ratio. Secondly, any factor that temporarily interferes with the feeding processes, such as low salinity, may be indirectly lethal to the rapidly developing juvenile but not to the adult. For example, the larvae of *Venus* cultured to the early umbo stage die within 24 hr if food is withheld (Turner and George 1955), whereas the adult may survive for long periods without food.

During the fall the growth of *Mya* was considerably more rapid in the upper arm of the pond where the plankton population was composed almost entirely of flagellates than in the main basin where diatoms comprised a significant portion of the plankton. The growth rates at Stations 2A, 5 and 7 are contrasted in Figure 6. A T-test shows the difference in growth at the upper and lower stations to be significant. Moreover, when the average number of flagellates collected at each station during each of five 10-day growth periods is plotted against mean growth increments at each station for the corresponding periods (Fig. 7), the derived correlation coefficient is significant at the 1% level.

It seems paradoxical that wind-induced mixing was sufficient to destroy the salinity gradient along the axis of the pond but not sufficient to cause homogeneity of phytoplankton. However, an explanation of an analogous situation in Great Pond, Mass., has already been given by Hulburt (1956). It should also be mentioned that a dinoflagellate, believed to be *Kryptoperidinium,* which was abundant in the entering stream water, was often responsible for the larger numbers of flagellates at Station 7 than at Station 2A. Slobodkin (1953) states that the reproductive rate of several species of dinoflagellates is favored by low salinities. The combined effect of these two processes —low reproductive rate among the nonmotile diatoms at the upper stations (Hulburt 1956) and the influx of flagellated forms at the head of the pond—would result in the observed distribution.

The conclusion that flagellates are more readily utilized by clams than are diatoms may appear to conflict with the observations of Pratt and Campbell (1956), who found a negative correlation between flagellate abundance and the growth rate of *Venus mercenaria* but a significant positive correlation between growth and the abundance of diatoms less than 15 μ in size. However, *Venus* occurs most abundantly in the lower estuary (Turner 1953), where diatoms are generally the dominant phytoplanktonic form (Nash 1947; Hulburt 1956). *Mya,* on the other hand, is frequently most abundant in the upper estuary, where flagellates are more likely to outnumber diatoms. The nutritive requirements of the two species, or the relative ability to utilize different phytoplankton, may be correspondingly different.

Organic detritus, also more abundant at

a factor influencing the more rapid growth of the clams there. However, microscopic examination indicated that a fair percentage of it was composed of fragments of crustacean exoskeletons and other refractory substances, of probably no nutritive value to the clam.

REFERENCES

BELDING, D. A. 1930. The soft-shelled clam fishery of Massachusetts. Commonwealth of Mass., Dept. of Conservation, Marine Fisheries Series No. 1: 65 pp.

CHANLEY, P. 1958. Survival of some juvenile bivalves in water of low salinity. Proc. Natl. Shellfish Assoc., **48**: (in press).

COLE, H. A. AND B. T. HEPPER. 1954. The use of Neutral Red solution for the comparative study of filtration rates of lamellibranchs. Jour. Cons., Int. Explor. Mer, **20**: 197–203.

HULBURT, E. M. 1956. The phytoplankton of Great Pond, Massachusetts. Biol. Bull., **110**: 157–168.

LOOSANOFF, V. L. 1958. Challenging problems in shellfish biology. *In*: Perspectives in Marine Biology. A symposium held at Scripps Institute of Oceanography, Univ. of Calif., March 24–April 2, 1956. Univ. of Calif. Press.: 483–493.

NASH, C. B. 1947. Environmental characteristics of a river estuary. Chesapeake Biology Laboratory, **64**: 27 pp.

PRATT, D. M. AND D. A. CAMPBELL. 1956. Environmental factors affecting growth in *Venus mercenaria*. Limnol. and Oceanogr., **1**: 2–17.

PROSSER, C. L., D. W. BISHOP, F. A. BROWN, T. L. JAHN, AND V. J. WULFF. 1952. Comparative Animal Physiology. W. B. Saunders and Co., New York. 888 pp.

SLOBODKIN, L. B. 1953. A possible initial condition for red tides on the coast of Florida. Jour. Mar. Res., **12**: 148–155.

TURNER, H. J. 1951. Fifth Report on Investigations of the Shellfisheries of Massachusetts. Div. Mar. Fish., Dept. of Conservation, Commonwealth of Mass., Boston: 9–10.

———. 1953. A review of the biology of some commercial molluscs of the east coast of North America. Sixth Report on Investigations of the Shellfisheries of Massachusetts. Div. Mar. Fish., Dept. of Conservation, Commonwealth of Mass., Boston: 39–74.

——— AND C. J. GEORGE. 1955. Some aspects of the behavior of the quahog, *Venus mercenaria*, during the early stages. Eighth Report on Investigations of the Shellfisheries of Massachusetts, Div. Mar. Fish., Dept. of Conservation, Commonwealth of Mass., Boston: 5–14.

Contribution No. 1058

Deep-Sea Research, 1960, Vol. 7, pp. 1 to 9. Pergamon Press Ltd., London. Printed in Great Britain

The influence of phytoplankton pigments on the colour of sea water

CHARLES S. YENTSCH

(*Received* 15 *July* 1959)

Abstract—By summing the absorbency of phytoplankton pigments with that of pure water, the absorption of the blue portion of the spectrum is markedly increased. As the concentration of phytoplankton pigments increases, the diminution of blue light gradually shifts the wave length of maximum transmission toward the green. At the concentration of phytoplankton pigments normally found in the open ocean, the red chlorophyll band has little influence on water colour.

Inadequacies in present methods for detection of absorption bands in natural waters is attributed to wide band widths of filters used in submarine photometers. Poor spectral curves applicable to colour analysis in particulate systems are obtained by conventional spectrophotometric techniques because a large portion of the scattered light never reaches the photo-detector. Improvements for spectral analysis are suggested.

INTRODUCTION

THE clearest ocean waters are deep blue, those near coasts usually are green, while many inshore estuarine waters may be brown or red, the colour generally varying with the proximity of sources of land run-off. These differences in colour can be attributed to variations in the magnitude of scattering and absorption of daylight.

KALLE (1937, 1938, 1939) and JERLOV (1951a, 1951b, 1953, 1955) have concluded, consistent with earlier theories of ocean water colour, that the blue colour of the clearest oceans arises from the selective scattering of short wave lengths by water molecules and small particles, while the change from blue to the green of coastal waters is the result of selective absorption by dissolved yellow materials in the water.

Recently, ATKINS and POOLE (1958) and YENTSCH and RYTHER (1959) have indicated the importance of absorption in the blue regions of the spectrum by the photosynthetic pigments of phytoplankton. The present report is an attempt to evaluate the effects of this absorbency on the colour of natural waters.

COMPARATIVE TRANSPARENCY OF PURE AND NATURAL OCEAN WATERS AND THEORIES WITH REGARD TO COLOUR

A number of investigators have measured the transmission spectrum of ' purified ' natural waters (see SVERDRUP *et al.*, 1942, Chap. 3; HUTCHINSON, 1958, Chap. 6). Although these measurements have served to demonstrate a general similarity of transmission spectra, considerable discrepancy exists between individual sets of measurements in the blue violet region of the spectrum. Because of techniques involved and the extensive nature of the studies, the investigations by JAMES and BIRGE (1938) must be considered to be the most representative of light absorption by pure water. Their measurements do not differ greatly from the previous ones made in the red region of the spectrum, but the transmission maximum extends farther into the blue than previously reported, (Fig. 1). CLARKE and JAMES (1939) obtained a similar spectrum for ' fine ' filtered coastal water which was significantly less transparent in the blue region. According to JERLOV, the clearest sea water

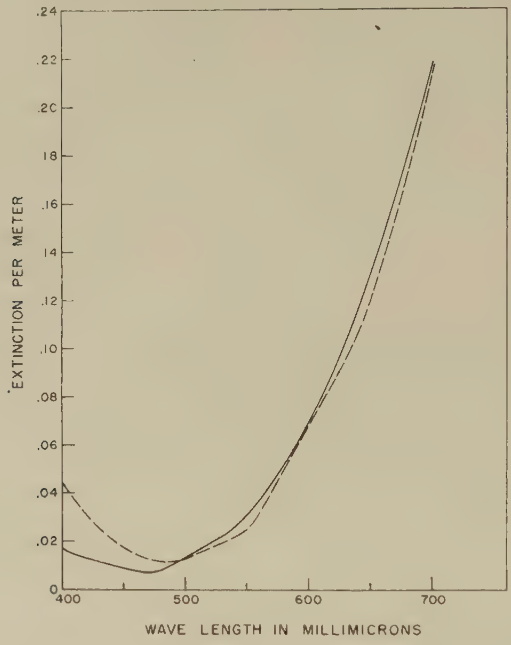

FIG. 1. Comparative extinction of pure water (JAMES and BIRGE 1937) solid line, and filtered sea water (CLARKE and JAMES 1939) dotted line.

Table 1. Wavelength of maximum transmission and the percentage of light of this colour transmitted in five different types of ocean, from (JERLOV 1951a)

Types of ocean water	*Wavelength of maximum transmission*	*Percent transmission per metre*
Clearest oceans	470	98·1
Average oceans	475	89·0
Clearest coastal	500	88·6
Average coastal	550	72·4
Average inshore	600	60·8

does not differ markedly from JAMES and BIRDGE's pure water. He prepared transmission curves for ocean waters of different transparency, using his own observations, data of POOLE and ATKINS (1937) and of UTTERBACH (1936). Table 1 shows the wavelength of maximum transparency in different types of coastal and ocean water designated by JERLOV. The clearest ocean water has a transmission maximum at

470 millimicrons, while in less transparent ocean water the maximum lies between 475 and 500 millimicrons. In turbid coastal waters, maximum transmission is between 550 and 600 millimicrons. This ' shift ' in the wavelength of maximum transmission, equivalent to changes in colour of different types of ocean water, has been attributed to the combined effects of selective scattering and absorption by dissolved yellow substance (KALLE, 1938, 1939).

The following discussion demonstrates that the absorption of light by living phytoplankton can selectively influence the absorption of submarine light, and spectral shifts, comparable to those in Table 1, can be produced by increasing the concentrations of phytoplankton.

ABSORPTION SPECTRA OF LIVING PHYTOPLANKTON

The combined absorbencies of natural populations of phytoplankton could be expected to vary from population to population; however, there is no evidence of great variations in the pigment composition of groups normally found in abundance in natural marine populations. For example, spectral curves for cultures of dinoflagellates, diatoms, green flagellates and a natural population sampled from Woods Hole waters (Fig. 2) all show an absorption minimum in the green, strong combined chlorophyll and carotenoid absorption in the blue, and the red absorption by chlorophyll *a*. These spectra were determined by the cleared millipore filter method (YENTSCH, 1957), and hence represent principally the absorption of the pigment

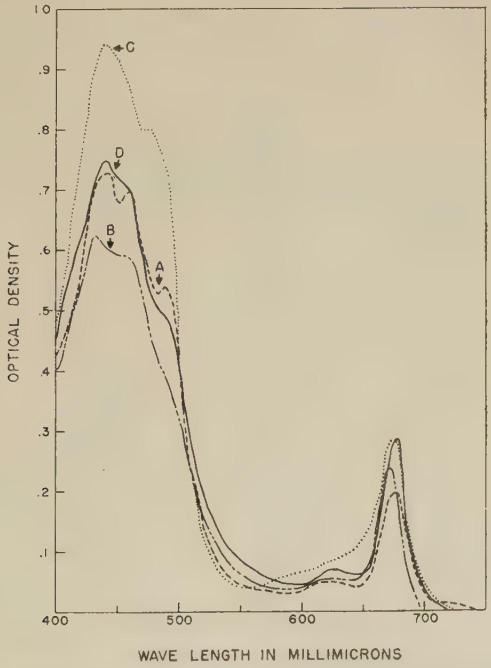

FIG. 2. Pigment spectra of living phytoplankton, *A*. Diatom *Cyclotella sp.*, *B*. Dinoflagellate, *Amphidium sp.*, *C*. green Flagellate *Chlamydomonas*, *D*. Natural population sampled from Woods Hole waters.

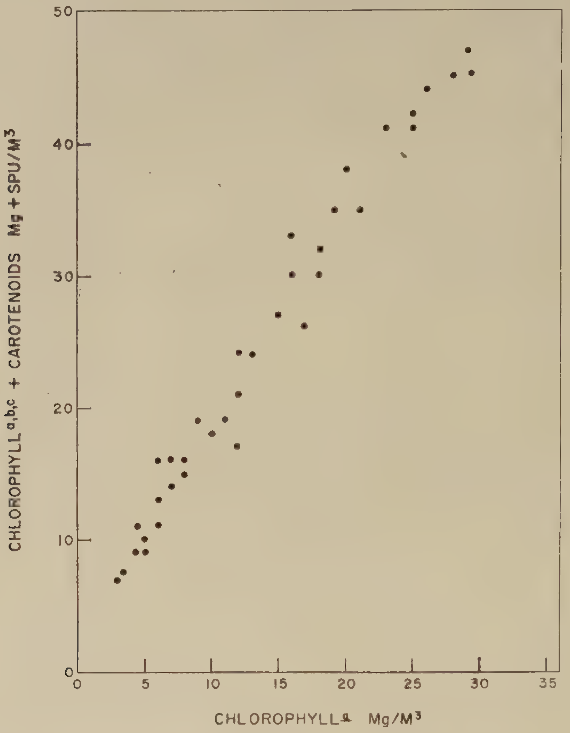

FIG. 3. Relationship between Chlorophyll *a* and total fat soluble pigments in natural populations of phytoplankton sampled from coastal waters and inshore waters.

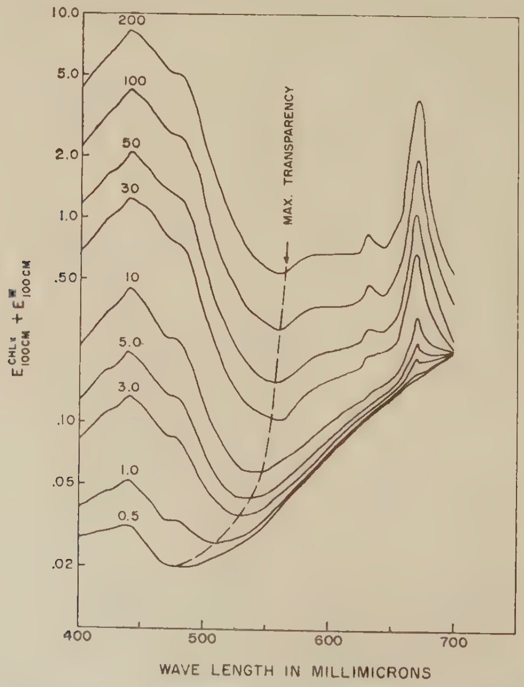

FIG. 4. Combined absorption coefficients for pure water and plant pigments. Numbers adjacent the curves indicate the chlorophyll concentration in mgs./m³.

within the plant.* Particularly important in this discussion is the intense pigment absorption in the blue region (400–500 mμ) where pure water has a minimum absorption (Fig. 1). Thus, the maximum transmission by pure water coincides with the maximum absorption of algal pigments, whereas the red chlorophyll absorption band falls in the range of high absorption by water.

THE EFFECTS OF DIFFERENT QUANTITIES OF PHYTOPLANKTON PIGMENTS ON THE ABSORPTION SPECTRA OF PURE WATER

The total effects of absorption by phytoplankton pigments and by pure water is estimated by summing their respective absorption coefficients. The assumption is made that the quantity of chlorophyll can be used as an index of total plant pigment. Data shown in Fig. 3 supports this assumption throughout a wide range of pigment values in natural populations. Optical density (E) was measured at every ten millimicrons throughout visible wavelengths in a Beckman DU spectrophotometer. Using the filter method chlorophyll concentrations are expressed in terms of a 10 cm light path, thus for given wavelengths an extinction coefficient $E^{1\,\text{mg Chl}}_{100\,\text{cm}}$ can be obtained (Table 2). The absorption by different concentrations of chlorophyll may be obtained by multiplying these values by appropriate concentrations. The combined absorption of phytoplankton pigments and of water is computed by summing the specific absorbence by chlorophyll, $E^{\text{Chl}x}_{100\,\text{cm}}$ at x concentration and

Table 2. Specific absorption coefficients (E) *for Chlorophyll and pure water*

Wavelength in millimicrons	$E^{1\,\text{mg Chl}}_{100\,\text{cm}}$	$E^{\text{W}}_{100\,\text{cm}}$ *
400	0·0220	0·0160
410	0·0260	0·0150
420	0·0320	0·0130
430	0·0350	0·0110
440	0·0420	0·0100
450	0·0380	0·0090
460	0·0320	0·0080
470	0·0260	0·0070
480	0·0250	0·0080
490	0·0190	0·0100
500	0·0110	0·0150
510	0·0075	0·0180
520	0·0050	0·0210
540	0·0031	0·0260
560	0·0025	0·0360
580	0·0030	0·0500
600	0·0030	0·0700
625	0·0030	0·0950
630	0·0038	0·1000
645	0·0030	0·1230
650	0·0035	0·1300
655	0·0040	0·1360
660	0·0060	0·1440
665	0·0100	0·1520
670	0·0180	0·1590
675	0·0107	0·1670
700	0·0018	0·2150

* JAMES and BIRGE (1938)

*Spectral analysis of *in vivo* pigment systems of plant cells has been extensively used in connection with other physiological studies.

the specific absorption values of pure water, $E^{\text{w}}_{100\text{ cm}}$ (JAMES and BIRGE, 1938). Visible spectra representative of combined absorbencies are shown in Fig. 4. The intense blue absorption by phytoplankton pigments increases the total absorption in this region. Increases in chlorophyll concentration changes the wavelength of minimum absorption from blue toward green, a shift analogous to the shift observed in ocean waters of decreasing transparency. Because of the intense absorption by water in the red region, the chlorophyll peak at 675 millimicrons imparts almost no selective absorption when pigment concentrations are low. Therefore, in the open oceans where chlorophyll concentrations are generally below $1{\cdot}0\ \text{mg/m}^3$ the absorption by the red band of chlorophyll is small, relative to that of water.

The absorption of blue light by phytoplankton is similar to the absorption by KALLE's 'yellow substance,' hence the combined effects of these would produce a residual absorbency in this region. Further evaluation of the relative importance of phytoplankton and of yellow substance must await the comparison of submarine spectral curves in water masses containing different concentrations of phytoplankton pigments.

DISCUSSION

JOSEPH (1949), TYLER (1958) and BURT (1958) have emphasized the importance of using narrow band filters when making light measurements underwater. When measurements are made in conventional spectrophotometers such as BURT's 1955a, 1955b, 1958 observations, the dominance of parallel light passing through suspensions of particles can lead at times to poor results. Measurements of optical density in dilute suspensions of phytoplankton generally yield spectral curves with little or no absorptive definition (Fig. 5). This is because the light transmitted to the phototube after passing through the sample cell is composed of both parallel and scattered light. In most spectrophotometers the geometric relationship between the sample and the phototube allows a considerable fraction of the scattered light to go undetected, so that the detected light is largely parallel light whose attenuation is independent of wavelength, since ratio measurements are made. SHIBATA (1958) has referred to this type of measurement as quasi-attenuance and gives the characteristics of the E units as $p^1\,Epdf$ where the p^1 to the left of E is the parallel light of the reference beam, whereas symbols to the right refer to the type of light passing through the sample, that is, parallel and diffuse (scattered). The magnitude of the diffuse light reaching the photocell is a function of the amount of scattering and the geometry of the spectrophotometer.

SHIBATA (1957, 1958) has obtained sharp absorption bands by placing opal glass between sample and photocell. In this manner, light reaching the photodetector is completely diffuse. Identical fractions, or nearly so, of diffuse and parallel light strike the phototube after passing through opal glass. The optical density measured in three ways on a suspension of *Skeletonema* culture are given in Fig. 5. Curve *A* is the direct measurement on the cell suspension; Curve *B* was obtained by using SHIBATA's opal glass techniques; Curve *C* was obtained by the cleared millipore filter method. Sharp absorption bands were obtained by using the opal glass or the cleared millipore filter method. In the latter method the portions of diffused and parallel light are kept nearly constant by concentrating the absorptive materials on a millipore filter, scattering is reduced by narrowing the light path, and the filter is rendered transparent by applying cedar oil. Spectral curves obtained by either of these two improved methods show much sharper absorption peaks than conventional measurements on dilute suspensions.

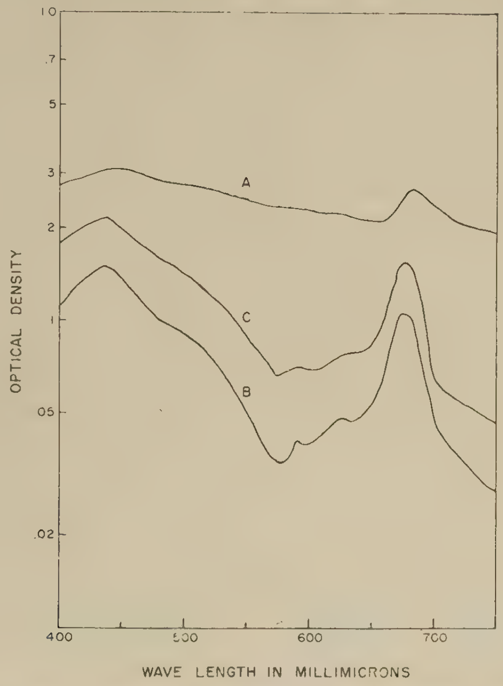

FIG. 5. Attenuation spectra of sea water suspension of *Phaeodactylum tricornutum* by different techniques, Curve *A*, conventional spectrophotometry, Curve *B*, opal glass technique, Curve *C*, cleared millipore filter technique.

Fig. 6 further illustrates the inadequacies of determining spectral curves of natural waters using conventional spectrophotometric techniques. Water samples were collected from a small estuary off Great South Bay, Long Island, New York (see RYTHER *et al.*, 1958). The colour of the estuary at this time was yellow-brown, and chlorophyll measurements revealed concentrations in excess of 100 mg/m^3. Microscopic examination by Dr. E. M. HULBURT revealed that the dominant phytoplankton was the dinoflagellate *Prorocentrum minimum*. Optical density measurements were made immediately on the raw water sample. A Beckman DU spectrophotometer was used with a 10 cm light path. For a reference, AA millipore filtered water from the estuary was used. Comparison with distilled water revealed no selective attenuation in the reference. Curve *A*, Fig. 6, shows the quasi-attenuance by the suspension, Curve *B* the attenuance of the suspension on a ' cleared ' millipore filter, and Curve *C* an acetone extract of the filtrate. The much greater absorptive definition gained by the cleared filter, as compared to optical density measurements made directly on the suspension, is quite apparent. Even when chlorophyll concentrations are larger, as was the case later during the same day of sampling, the absorptive ' bumps ' observed in the measurement of the suspension are by no means as clearly defined as are the measurements by the ' cleared ' filter technique.

Spectral measurements on natural waters containing suspended particles such as phytoplankton can probably be greatly improved by using Shibata's opal glass or the cleared filter technique. In clearest ocean waters, however, the light path must be sufficiently long to gain necessary sensitivity. Submarine spectrophotometers may obviate the technical difficulties of long light paths. However, one may still question whether or not quasi-attenuance is obscuring true extinction. Submarine measurements conducted well below the sea surface probably are representative of true extinction because of the diffuse light at these depths resulting from multiple scattering.

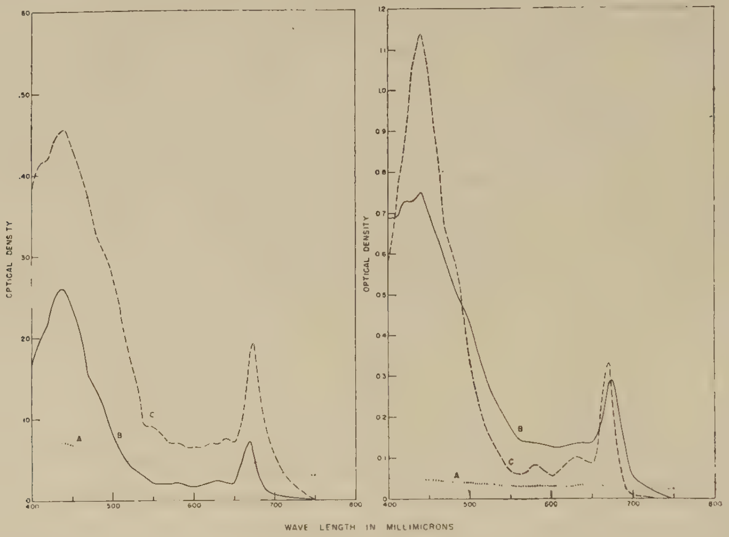

Fig. 6. Visible spectrum of water sampled from Senix Creek estuary, June 15th, 1958, by different techniques. Curve *A*, conventional spectrophotometry, Curve B, cleared millipore filter, Curve *C*, Acetone extract.

Acknowledgements—The writer expresses gratitude for the counsel provided by W. S. Richardson, C. H. Hubbard, F. A. Richards and B. H. Ketchum.

Woods Hole Oceanographic Institution, Woods Hole, Mass., U.S.A.

Contribution No. 1058 *from the Woods Hole Oceanographic Institution. This work was supported in part by the Atomic Energy Commission, Contract* AT (30–1)–1918.

REFERENCES

Atkins W. R. G. and Poole H. H. (1958) Cube measurements of the angular distribution of submarine daylight and the total submarine illumination. *J. du Cons.* **23**, (3) 327–337.

Burt W. V. (1955a) Interpretation of spectrophotometer readings on Chesapeake Bay waters. *J. Mar. Res.* **14** No. 1, 33–46.

Burt W. V. (1955b) Distribution of suspended materials in Chesapeake Bay. *J. Mar. Res.* **14** No 1, 47–62.

Burt W. V. (1958) Selective transmission of light in tropical Pacific waters. *Deep-Sea Res.* **5**, No. 1 51–62.

Clarke G. L. and James H. R. (1939) Laboratory analysis of the selective absorption of light by sea water. *J. Opt. Soc., Amer.* **29**, 43.

HUTCHINSON G. E. (1957) *A treatise on Limnology*. Vol. 1, Geography, Physics and Chemistry. 1013 pp. John Wiley and Sons, New York.

JAMES H. R. and BIRGE E. A. (1938) A laboratory study of the absorption of light by lake waters. *Trans. Wisconsin Acad.* **31**, 11–154.

JERLOV N. G. (1951a) Optical studies of ocean waters. *Reports of the Swedish Deep-Sea Expedition* **3**, No. 1, 3–57.

JERLOV N. G. (1951b) Optical measurements of particle distribution. *Tellus* **3**, No. 3, 122–128.

JERLOV N. G. (1953) Influence of suspended and dissolved matter on the transparency of sea water. *Tellus* **5**, No. 1, 59–65.

JERLOV N. G. (1955) The particulate matter in the sea as determined by means of the Tyndall meter. *Tellus* **7**, No. 2, 218-225.

JOSEPH J. (1949) Uber die Messung des Vertickalen Extinctionskoefficienten. *Deutsche Hydr. Zeitschr.* **2**, No. 6, 255-267.

KALLE K. (1937) Meereskundliche chemische Untersuchungen mit Hilfe des Zeisschen Pulfrich Photometers. *Am. d. Hydr. u. Mar. Meteor*, H. VI. 276–282.

KALLE K. (1938) Zum problem der Meereswasserfarbe. *Ann. d. Hydrogr. u. Mar. Meteor*, **66**, 1–3.

KALLE K. (1939) Die Farbe des Meeres. *Cons. Perm. Int. Explor. de la Mer, Rapp. et Proc.-Verb.* **109**, 98–105

POOLE H. H. and ATKINS W. R. G. (1937) The penetration into the sea of various wave lengths as measured by emission of rectifier cells. *Proc. Roy. Soc. London*, (B) **123**, 151.

RYTHER J. H., YENTSCH C. S., HULBURT E. M. and VACCARO R. F. (1958) The dynamics of a diatom bloom. *Biol. Bull.* **115**, No. 2, 257–268.

SHIBATA K. (1958) Spectrophotometry of intact biological materials. Absolute and relative measurements of their transmission, reflection and absorption spectra. *J. Biochem.* **45**, No. 8, 599–623.

SVERDRUP H. U., JOHNSON M. W. and FLEMING R. H. (1946) *The Oceans*. 1087 pp. Prentice-Hall, New York.

TYLER J. E. (1959) Natural water as a monochromator. *Limnol. and Oceanogr.* **4**, No. 1, 102–105.

UTTERBACK C. L. (1936) Spectral bands of submarine solar radiation in the North Pacific and adjacent inshore waters. *Cons. Perm. Int. Explor. de la Mer, Rapp. et. Proc.-Verb.* **101**, (2) No. 4, 15 pp.

YENTSCH C. S. (1957) A non-extractive method for the quantitative estimation of chlorophyll in algal cultures. *Nature, Lond.* **179**, 1302–1304.

YENTSCH C. S. and RYTHER J. H. (1959) Absorption curves of acetone extracts of deep water particulate matter. *Deep-Sea Res.* **6**, 72–74.

Printed in Great Britain by The Salisbury Press Ltd., Publicity House Wilton Road, Salisbury, Wilts. (24149)

Contribution No. 1059

Zeitschrift für vergleichende Physiologie 43, 29—36 (1960)

From the Dept. of Zoology, Univ. of Vienna, Austria
and Woods Hole Oceanographic Institution, Mass. U.S.A.

GROWTH AND METABOLISM IN A MARINE NEMATODE, *ENOPLUS COMMUNIS* BASTIAN*, **

By

Wolfgang Wieser and John Kanwisher

With 4 Figures in the Text

(Received November 20, 1959)

Although nematodes represent the most diversified and most abundant group of metazoans living at the bottom of the sea (Wieser 1960) there is not a single marine species in which the life span and the rate of growth is known. Smidt (1951), trying to estimate the productivity of nematode populations in the Danish Waddensea, had to rely on figures given by Overgaard Nielsen (1949) for terrestrial nematodes which indicate for many species an average life span (from egg to adult female) in the order of one month at an experimental temperature of 15° C.

It seemed desirable to provide a better basis for speculations on the productivity of marine nematode populations. In connection with this aim an attempt was made to investigate the metabolism of one species of marine nematodes during its whole life span. Since nematodes do not have special respiratory organs and since they maintain throughout their life history a nearly constant ratio of suface to volume these animals are ideally suited to show whether or whether not in poikilotherms the metabolism/size relationship can be expressed by a simple function. So far there exist only data by Overgaard Nielsen (1949) on the oxygen consumption of a marine nematode, *Pontonema vulgare*, within a size range of 70 and 500 μg. A few single data on the oxygen consumption of unidentified marine nematodes were published by Zeuthen (1947).

Material and methods

Enoplus communis Bastian was chosen as a convenient object since it is of large size and easily obtained the year round from large brown algae *(Fucus, Ascophyllum)* in the intertidal and shallow sublittoral. Algae from Nobska Beach or near the Woods Hole Oceanographic Institution were collected in a bucket and vigorously shaken in the laboratory. The water was filtered through a screen with a mesh width of 160 μ. Checks showed that after this treatment only few

---

* Contribution no. 1059 from the Woods Hole Oceanographic Institution, Woods Hole, Mass.

** Supported by NSF grant G-4813.

nematodes remained in the algae and not even small larvae passed through the screen. Fifty to 100 specimens were picked out at random under the dissecting microscope and their weight determined by assuming the volume of a nematode to be very nearly comparable to that of a cylinder (see Overgaard Nielsen 1949 and Wieser 1960). The eggs could be found in batches of 4—7 attached to branches of seaweeds, or they were dissected out of gravid females. Their weight is based on measurements of their diameter, excluding the membranes. The specific gravity of adult specimens has been found to be 1.13 by Wieser (1960) and this figure was assumed to hold for all stages — which assumption, as will be shown later, is probably unjustified. The samples were collected in October 1958, January, February, April, May, June and July 1959.

Determinations of oxygen consumption were made by the Cartesian diver method as described, amongst others, by Holter and Linderstrøm-Lang (1943) and by Zeuthen (1947). The divers used had a volume from 6.5 to 37.4 μl and volume changes could be read to 0.001 μlO_2/hr in the smallest and 0.006 μl/hr in the largest diver. The divers were filled with seawater and the nematode(s) transferred by means of a fine steel needle (Kerr pulp files no. 1). After the nematode(s) had sunk to the bottom of the diver, the superfluous water was sucked out with a fine pipette. Consequently, the volume of the water drop was not exactly controlled. Most of the experiments were performed on single individuals, some on two. The eggs were measured in batches of four or five. The experimental temperature was usually 20° C, in some cases 21 and 22°. In the following diagrams all values are corrected for 20°, assuming the temperature/metabolism relationship as expressed in Krogh's standard curve (Krogh 1941). A few oxygen measurements with batches of adult *Enoplus communis* were made employing the microvolumetric respirometer of Scholander (Scholander et al. 1952). The data obtained by this method were in agreement with those obtained by the Cartesian diver technique.

Results

1. Growth. If the random batches of nematodes collected between October 1958 and July 1959 are arranged according to arbitrarily chosen weight classes, the picture shown in Fig. 1 emerges. It is evident that *E. communis* has an annual life cycle, spawing setting in around the beginning of April. Unfortunately, it cannot be stated when most of the animals have reached sexual maturity since it was omitted to note in the October sample the frequency of mature animals. However, it is certain that mature animals can be found in October; and in the January sample, most of the animals are sexually mature. The female/male ratio rises from January to May quite regularly, suggesting higher death rates of the males after copulation. In the June and July samples the number of adults has dropped so much that the ♀♀/♂♂ ratio has no biological meaning.

By determining for each month the average weight of one year class and by plotting the obtained values on arithmetic graph paper (Fig. 2), one obtains the growth curve of the nematode population (or, rather, of an idealized "average" individual). This curve agrees well with the sigmoid growth curve which, according to v. Bertalanffy (1957 and previously) is typical for animals in which anabolism varies with the 2/3 power of the weight.

2. *Metabolism.* The main purpose of this part of the investigation was to establish the metabolism/size relationship in *E. communis* from egg to adult stage. Since, however, juveniles and adults appear at different times of the year the possible effect of temperature compensation in the different stages had to be taken into account. Fig. 3 summarizes measurements on larger specimens collected at —1.5 to 0° C, at 6 to 16° C and at 18° C. The experimental temperature always was 20° C and the animals were measured on the day of collecting or after spending a number of days in a refrigerator or culture room at either the habitat or a lower temperature. None of these variables seems to have had an effect on the oxygen consumption of the larger specimens and it is assumed that this situation is characteristic of all stages of the species. In addition, no difference in respiration rate could be detected between the two sexes.

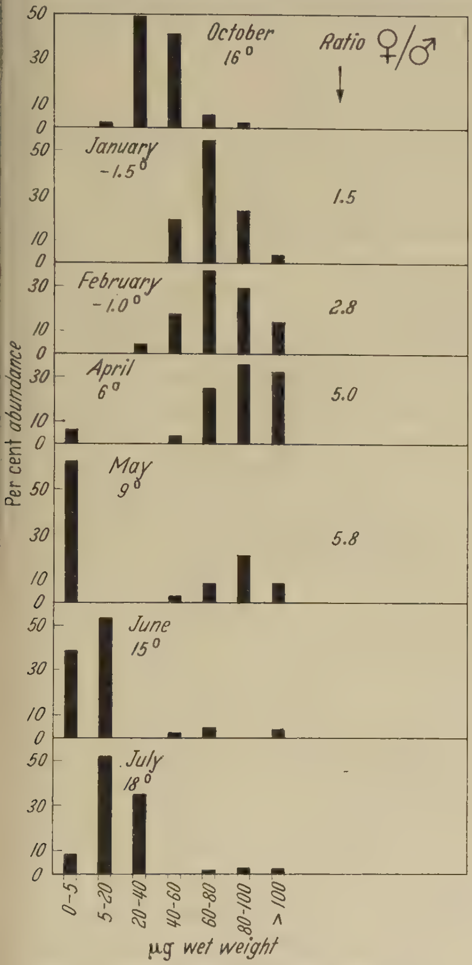

Fig. 1. Histogram showing distribution of size classes of *E. communis* from October through July. The water temperature prevailing on collecting day is indicated under each month

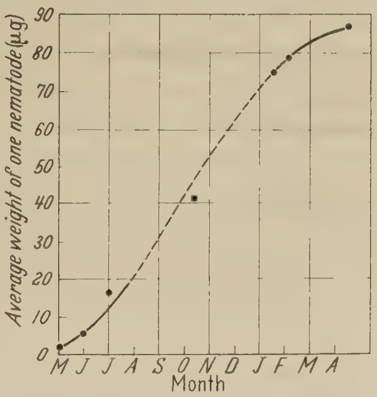

Fig. 2. Growth curve of an "average" individual of *E. communis* from first larval stage to maturity. The weight figures represent averages of one year class from the samples shown in Fig. 1

When all the experimental values from egg to adult are plotted on semi-log paper (Fig. 4, solid circles) it becomes clear that no simple

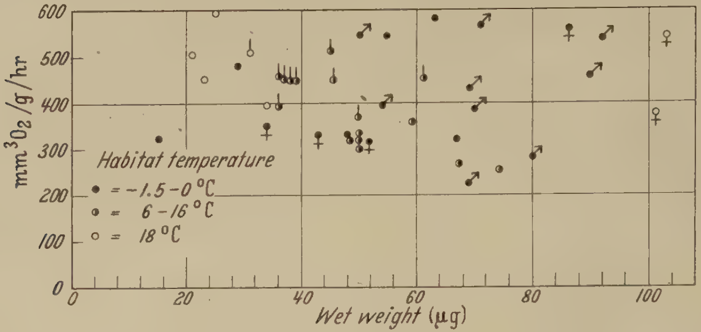

Fig. 3. The oxygen consumption of *E. communis* collected at different times of year. Circles with dashes indicate animals that were kept for one to several days before measurement at about half the habitat temperature. The other specimens were measured right after collecting or after having been kept at the habitat temperature for one to several days. Each circle represents the oxygen consumption of one specimen. All measurements at 20° C

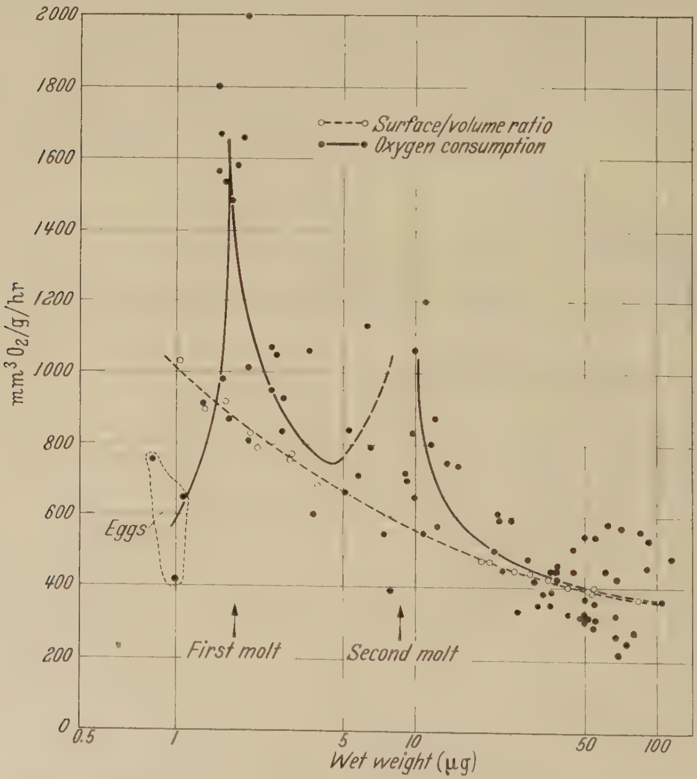

Fig. 4. Oxygen consumption (solid circles) and surface/volume ratio (open circles) of *E. communis* from egg to adult stage. The regression lines are eye-fitted

relationship exists between the oxygen consumption and the size of the animals as expressed by the wet weight. The (fertilized and uncleaved) eggs have a fairly low value of consumption. Right after hatching the metabolism increases sharply to a value three times that of the eggs. Then it drops quickly, but in animals weighing between 6 and 10 μg the distribution of the points forces one to assume another rise in respiration rate, followed by another sudden drop and subsequent leveling of the curve. As will be discussed later, these changes in respiration rate are probably correlated with the processes of molting occurring in this species. The polyphasic metabolism-weight relationship may be contrasted with the simple surface/volume relationship of the animals (Fig. 4, open circles) as based on actual measurements of surface and volume of randomly selected specimens.

Discussion

E. communis spends its whole life cycle on the large seaweeds. Spawning takes place in early spring when the water temperature has risen to approximately 5° C. The fertilized eggs are deposited in batches of not more than 10 and stick to branches of the algae where they undergo cleavage. After hatching, the juveniles molt four times until they reach maturity (FILIPJEV and MICHAJLOVA 1924), but there also takes place a gradual increase in body weight and volume between the molts. Due to this continuous growth between molts, body weight is not a good basis for distinguishing the five instars of the species. In specimens from the Arctic, studied by FILIPJEV and MICHAJLOVA (1924), which reach a final size about 3.5 times that of the Woods Hole specimens, the five instars cover the following (wet) weight ranges: Instar I ÷ 1.5—4.3 μg; instar II ÷ 2.7—25.0 μg; instar III ÷ 24.0—188.0 μg; instar IV ÷ 150.0 to 250.0 μg; instar V (mature) ÷ 174—350 μg. Growth is fastest in the early stages of the life cycle. When — in Woods Hole — the individuals weigh between 2 and 10 μg, a population doubles its weight within 20 days, whereas between 30 and 70 μg doubling of weight takes nearly four months (Fig. 2). Maturity is reached sometime in fall or early winter and the cold season is spent with gonads fully developed and with the females carrying eggs in the uterus. The slow growth prevailing in a time of year when the water temperature lies between —1.5 and 0° C is only what one would expect of a species which does not possess the ability of temperature compensation (Fig. 3) and in which, therefore, low temperatures must depress all metabolic processes. On the other hand, the leveling of the growth curve in its last third can also be regarded as reflectting a simple law of growth, quite independent of any relationship between temperature and metabolism. If, for example, the growth equation $dW/dt = \eta W^m - \varkappa W^n$ (v. BERTALANFFY 1957) is solved, assuming anabolism (ηW^{m}) to vary with the 2/3 power of the weight, catabolism ($\varkappa W^{n}$) to vary linearly with the weight, a sigmoid curve results of the same type as found in *E. communis.*

The relationship between respiration and animal weight can be expressed by the equation $O_2/W = a W^{(b-1)}$ (Zeuthen 1953, v. Bertalanffy 1957). Fig. 4 shows that in the present investigation the values of the exponent *b* vary with the size of the animals. Zeuthen (1953) pointed out that changes in the *b*-values occur during development of many animals, with the *b*-value being close to 1 during a middle phase of the life cycle and lower during an initial and an end phase. In this consideration the step from the fertilized eggs to the first larval stages was not included. The few investigations in which this was done show a characteristically steep increase in the respiratory rate during this first developmental phase, so in *Nassa reticulata, Mytilus edulis* (Zeuthen 1947) and in *Lymnaea stagnalis* (Horstmann 1958), which agrees well with the present data on *E. communis.* Such an increase in respiratory rate may be due to the activation of enzymes or other metabolically important constituents.

After the first maximum of oxygen consumption is reached, the metabolism/size relationship in *E. communis* seems to indicate further changes in the *b*-value and at least up to a weight of 40 μg no simple relationship of the oxygen consumption to the surface/volume ratio of the animals can be postulated. An indication as to what might lie at the root of this seemingly complicated relationship is afforded by the fact that the two peaks of the oxygen consumption coincide with the first two molts of the juveniles.

As already mentioned, body weight is not a good characteristic to delimit the five instars in this species but as far as the first two molts are concerned it is accurate enough to say that ecdysis takes place in animals weighing about 2 μg and 8—10 μg respectively. This checks with the data by Filipjev and Michajlova if it is kept in mind that the Arctic specimens grew to a much larger size. The last two molts take place in animals weighing from 40 to 90 μg and cannot be pinpointed with any accuracy on the basis of wet weight alone.

The irregularities in the respiratory rate/weight relationship, as well as the great variability of the oxygen consumption in specimens differing little in weight, could easily be explained if in this species changes in water content were assumed to take place in connection with the molting processes. If the relative water content of the animals were low just before molting and increased by rapid water uptake after ecdysis, the respiratory rates based on *volume* determinations would be expected to fluctuate just in the manner shown in Fig. 4.

That such changes in water content do occur in connection with molting and that they influence the determination of respiratory rates has recently been shown by Edwards (1958) in *Chironomus riparius*. The same phenomenon could also account for the sudden changes in the metabolism/size relationship as observed by Overgaard Nielsen (1949) in *Pontonema vulgare* and by Krüger (1936) in *Ascaris suilla.*

In *E. communis* the separation of specimens into groups of exactly defined developmental stage, the measurement of their oxygen consumption and the subsequent determination of dry body weight or total nitrogen was not possible.

However, the large fluctuations in respiration rate despite a constant surface/volume ratio (Fig. 4) shows one thing, namely, that in this species body surface proper cannot be a limiting factor for respiratory activity. This means that for normal tensions diffusion suffices in supplying all tissues with the required oxygen. This is in agreement with the calculation by Krogh (1941) for animals measuring less than 1 mm in diameter.

Summary

The life history and metabolism of a marine nematode, *Enoplus communis* Bastian, was studied. The species has an annual life cycle, spawning taking place in early spring. Maturity is reached in fall and early winter, and both sexes overwinter with their gonads fully developed.

The metabolism is not temperature-compensated and there is no difference in respiration between the two sexes.

The respiration rate is fairly low in the fertilized, uncleaved eggs (about 600 mm^3 O_2/g/hr). Right after hatching, the oxygen consumption increases sharply to a value about three times that of the eggs. Then it drops quickly, but in animals weighing between 6 and 10 μg, another sudden rise occurs, followed by a second drop and subsequent leveling of the curve. The first increase in metabolic rate from egg to first juvenile stage might be due to the activation of metabolically important substances. The following changes, however, are most likely correlated with the process of molting and are probably due to changes in the percentage of dry tissue matter in animals prior to and after ecdysis.

The large fluctuations in respiration rate occuring in animals of different size, despite a constant surface/volume ratio, suggest that body surface proper does not control oxygen consumption in this species.

Literature cited

Bertalanffy, L. v.: Quantitative laws in metabolism and growth. Quart. Rev. Biol. **32**, 217—231 (1957). — Edwards, R. W.: The relation of oxygen consumption to body size and to temperature in the larvae of *Chironomus riparius* Meigen. J. exp. Biol. **35**, 383—395 (1958). — Filipjev, I. N., u. E. Michajlova:

Zahl der Entwicklungsstadien bei *Enoplus communis* Bastian. Zool. Anz. **59**, 212—219 (1924). — Holter, H., and K. Linderstrøm-Lang: On the Cartesian Diver. C. R. Lab. Carlsberg, Sér. chim. **24**, 333—478 (1943). — Horstmann, H. J.: Sauerstoffverbrauch und Trockengewicht der Embryonen von *Lymnaea stagnalis* L. Z. vergl. Physiol. **41**, 390—404 (1958). — Krogh, A.: The comparative physiology of respiratory mechanisms. Philadelphia: University Pennsylvania Press 1941, 172 p. — Krüger, F.: Untersuchungen zur Kenntnis des aeroben und anaeroben Stoffwechsels des Schweinespulwurmes *(Ascaris suilla)*. Zool. Jb., Abt. allg. Zool. u. Physiol. **57**, 1—56 (1936). — Overgaard Nielsen, C.: Studies on the soil micro-fauna. II. Natura Jutlandica **2**, 1—131 (1949). — Scholander, P. F., C. L. Claff, J. R. Andrews and D. F. Wallach: Microvolumetric respirometry. Methods for measuring O_2 consumption and CO_2 production by cells and enzymic reactions. J. gen. Physiol. **35**, 375—395 (1952). — Smidt, E.: Animal production in the Danish Waddensea. Medd. Komm. Danmark. Fisk. Havunders, Ser. Fisk. **11 6**, 1—151 (1951). — Wieser, W.: Benthic studies in Buzzards Bay. II. The meiofauna. Limnol. Oceanogr. (1960 in press). — Zeuthen, E.: Body size and metabolic rate in the animal kingdom, with special regard to the marine micro-fauna. C. R. Lab. Carlsberg, Sér. chim. **26**, 17—161 (1947). — Oxygen uptake as related to body size in organisms. Quart. Rev. Biol. **28**, 1—12 (1953).

Dr. Wolfgang Wieser, Wien 1 (Österreich),
II. Zoologisches Institut der Universität, Dr. Karl Lueger-Ring 1

Druck der Universitätsdruckerei H. Stürtz AG., Würzburg

Contribution No. 1062

AUXOTROPHY AND HETEROTROPHY IN MARINE LITTORAL DIATOMS[1]

Joyce C. Lewin and Ralph A. Lewin

Abstract

Forty-four pure cultures of marine littoral diatoms (43 pennate and 1 centric) have been studied to determine (*a*) whether any accessory organic factors (vitamins) are essential for growth in light, and (*b*) whether the cells can grow in darkness using glucose, acetate, or lactate as substrates.

Six isolates were shown to require thiamine as sole growth factor; eleven require cobalamin only; and three require both thiamine and cobalamin. Sixteen are capable of heterotrophic growth using glucose but not acetate or lactate; eight can use glucose or lactate; one uses glucose or acetate; one uses glucose, acetate, or lactate; and two use only lactate.

By the classical criteria of valve structure, the clones fall into about 25 different species, belonging to nine genera. However, it is evident that light microscopy is inadequate for the specific descriptions of many small diatoms. Electron micrographs of acid-cleaned frustules of each isolate served as an aid to specific identifications. Nutritional studies have demonstrated the existence of a range of distinct physiological races within the "species" *Amphora coffaeiformis*, *Nitzschia closterium*, and *N. frustulum*.

Introduction

The density of phytoplankton in the ocean has generally been observed to increase around the littoral margins, where the shallowness of the water and the propinquity of land provide conditions more favorable for plant growth than in the open ocean. This littoral flora consists largely of diatoms. These comprise not only centric species, which for the most part are truly planktonic, but also an abundance of pennate forms, usually associated with growth on solid substrata. Although the brown, slimy layer of diatoms on sand, mud, and attached algae in shallow waters and rock pools is a familiar feature of the shore, this littoral flora is taxonomically less well known than the diatoms of the oceanic plankton. As an example of our lack of knowledge of these pennate forms, Hustedt (13) described 89 new species out of a total of 369 species identified in two mud samples sent to him from Beaufort, North Carolina. The richness of this flora must be attributable at least in part to the variety of organic and inorganic substances derived from the nearby land and from decaying seaweeds and other organic matter in the mud.

---

[1] Manuscript received August 12, 1959.

Contribution No. 1062 from the Woods Hole Oceanographic Institution, Woods Hole, Massachusetts. These studies were aided by a contract between the Office of Naval Research, Department of the Navy, and the Woods Hole Oceanographic Institution, NR-104-392.

As a preliminary contribution to our understanding of the ecology of marine littoral diatoms, a study of the physiology of such forms is needed. The present investigation deals with the requirement of certain species for accessory organic growth factors, namely vitamins (i.e. auxotrophy), and with their ability to use glucose, acetate, or lactate for growth in darkness (i.e. heterotrophy). The range of species was limited to tolerant forms capable of growing well under the empirical conditions of laboratory culture. This accounts largely for the recurrence of similar species from different localities.

Materials and Methods

Unless otherwise indicated, the diatoms were collected and isolated free from bacterial contaminants by R.A.L. Many of the strains were isolated from crude selective cultures in sea water enriched with mineral supplements, as given below. Most were purified by streaking on enriched sea water agar; a few were isolated by micromanipulation.

Specific identification of the species was facilitated by the use of electron micrographs of cleaned frustules. However, additional complications were introduced thereby, since many fine structural details, revealed by electron microscopy but not perceptible otherwise, could not have been taken into consideration in the original descriptions of the species. Moreover, the examination of clonal cultures has provided considerable information on intraspecific variation, not hitherto available to taxonomists working with field collections. In spite of our conviction that many diatom species are inadequately described, we have endeavored to assign a binomial to each isolate.[2] The following works were consulted for this purpose: Boyer (1), Cholnoky (5), Cleve-Euler (6), Helmcke and Krieger (11), Hustedt (12, 13), Peragallo and Peragallo (19), Schmidt (21), Van Heurck (22).

Stock cultures were maintained in 125-ml Erlenmeyer flasks containing 50 ml of filtered sea water enriched with 0.1 g/l. $Ca(NO_3)_2.4H_2O$; 0.02 g/l. K_2HPO_4; 0.05 g/l. $Na_2SiO_3.9H_2O$; 0.5 mg/l. Fe; 0.3 mg/l. Zn; 0.1 mg/l. each of B, Co, Cu, Mn, Mo; 1 μg per liter of vitamin B_{12}; and 1.0 g/l. Tryptone (Difco). Stock cultures were also maintained in test tubes on 1.0% agar slants of the same medium.

For determination of the vitamin requirements of these diatoms, sea water was first treated with decolorizing carbon, Norit A (Pfanstiehl), at a concentration of 1 g per 100 ml for $\frac{1}{2}$–1 hour at room temperature, and then filtered. This treatment removed cobalamin (2, 17) and other vitamins originally present. To determine whether cobalamin was required, the growth of each diatom was tested in Norit-treated sea water (50 ml in a 125-ml Erlenmeyer flask) with and without cobalamin addition, but otherwise enriched as above. It was found that Tryptone, a rich source of most organic nutrilites including thiamine, supplies no detectable cobalamin to the medium. For the

[2] Cultures of the diatoms used in this investigation have been deposited in the Algal Culture Collection, Botany Department, Indiana University, Bloomington, Indiana. Permanent slide mounts of the cleaned silica walls have been deposited at the Smithsonian Institution, Washington, D. C.

determination of other vitamin requirements, Tryptone was omitted, and growth was tested with and without the addition of a vitamin mixture containing 1 mg each of thiamine, niacin, and biotin per liter. Essential vitamins were identified by the use of single supplements. A vitamin was evidently required in those cases where growth in the absence of a nutrilite was negligible, or where a short period of growth was followed after a few days by bleaching of the cells. In the presence of the required vitamins, the cells were capable of sustained growth, and bleaching did not occur. No attempt was made to reveal additional vitamin requirements by a second transfer, since carry-over with the first inoculum was considered negligible. Inoculum was transferred with a bacteriological loop; in the case of vitamin B_{12}, it was estimated that vitamin contamination by carry-over did not exceed 10^{-4}–10^{-5} μg per liter.

For determination of heterotrophic growth, each species was tested in light and in darkness on agar medium: (*a*) as in the preceding paragraph, i.e., control without carbon source, (*b*) with 0.5% glucose, autoclaved separately, (*c*) with 0.1% Na acetate, and (*d*) with 0.2% Na lactate. Heterotrophic growth was confirmed in liquid media.

Results

In Table I are presented data on the following points: (1) vitamins, if any, found to be essential for autotrophic growth in light, using carbon dioxide as the sole major carbon source; and (2) the ability of the strain to grow heterotrophically in darkness, using glucose, acetate, or lactate as sole carbon source, in the presence of requisite vitamins. Since in many cases the specific determination was in some doubt, information is also given on the size range observed in our cultures and on the number of striae per unit length. These data, together with electron micrographs of cleaned frustules (Figs. 1–30), serve further to identify the species in case of question.

The two groups of diatom strains classified as *Nitzschia frustulum* (Kütz.) Grun. (6 isolates) and *Amphora coffaeiformis* Ag. (10 isolates) exhibited considerable intraclonal variation, and intergradation between clones did not permit clear separation into recognized varieties. Evidently each of these species comprises several physiological races (see Table I). One isolate classified as *Nitzschia closterium* W. Sm. (No. 54) differed considerably from the other three strains of this species both in cell size and in physiological characteristics, although the fine structure of the silica walls appeared identical.

The numbers of isolates exhibiting requirements for vitamins and ability to grow heterotrophically are summarized in Table II. All diatoms capable of heterotrophic growth were pigmented when grown in the dark. No correlation between auxotrophy and facultative heterotrophy was observed.

Discussion

The diatoms reported on in this paper were isolated from inshore littoral habitats and probably include no planktonic species. Since centric diatoms generally do not grow well on agar, only pennate forms were obtained by the

TABLE I

Auxotrophy and heterotrophy in various diatom strains

Isolate No.	Fig. No.	Name	Size of valve, μ	Striae in 10 μ	Origin	Requires vitamin:		Grows in dark on:		
						B₁	B₁₂	Gl.	Ac.	La.
—	1	*Achnanthes brevipes* (Ag.) Cl.	40–50×9–11	16	Great Pond, Mass. (from S. Watson, No. 7)	−	+	−	−	−
40	7	*Amphipleura rutilans* (Trentepohl) Cl.	11–16×4	24	Herring Cove, N.S. (rock pool)	+	+	−	−	−
73	30	*Amphiprora paludosa* W. Sm. var. *duplex* (Donk.) Cl.	25×10	36	Woods Hole, Mass. (tank)	+	−	−	−	−
34	11	*Amphora coffaeiformis* Ag.	12–22×4	27	Lehave Islands, N.S. (brackish ditch)	−	−	+	−	−
45	—	*Amphora coffaeiformis* Ag.	6–14×4	33	Halifax, N.S. (inlet)	−	+	−	−	−
47	—	*Amphora coffaeiformis* Ag.	12–18×4	30	Woods Hole, Mass. (brackish pond)	−	+	+	−	+
51	9	*Amphora coffaeiformis* Ag.	25×5	26	San Diego, Cal. (mud)	−	−	+	−	−
56	—	*Amphora coffaeiformis* Ag.	4–10×2.5	—	La Jolla, Cal. (tidal rock)	+	+	+	−	−
64	—	*Amphora coffaeiformis* Ag.	5–6×2	27	San Francisco, Cal. (saline pool)	−	−	+	−	−
—	—	*Amphora coffaeiformis* Ag.	13–18×5	32	Sapelo Is., Georgia (shore) (from T. Starr, D 2)	+	−	+	−	−
—	—	*Amphora coffaeiformis* Ag.	13–19×4	24	Galveston, Texas (from T. Starr, D 106)	+	−	+	+	−
—	—	*Amphora coffaeiformis* Ag.	8–13×4	27	Beaufort, N.C. (from T. Rice)	−	−	+	−	−
—	10	*Amphora coffaeiformis* Ag.	6–13×4	30	Rockaway Beach, N.Y. (sea water) (from L. Provasoli)	−	+	−	−	+
59	8	*Amphora lineolata* Ehr.	30–45×10–18	23	Pacific Beach, Cal. (mud)	−	+	−	−	−
44	3	*Navicula menisculus* Schum.	12–17×6–7	20	Eagle Pt., N.S. (mud)	−	−	−	−	−
78	6	*Navicula* sp.	5–6×2.5	20–25	Sandwich, Mass. (marine canal)	−	−	−	−	−
66	2	*Navicula incerta* Grun.	8–16×5–6	14	San Francisco, Cal. (saline pool)	−	−	+	−	−
69	—	*Navicula incerta* Grun.	12–16×5	16	Salton Sea, Cal. (shore)	−	−	+	−	−
35	24	*Nitzschia angularis* var. *affinis* (Grun.) Perag.	30×3.5	67	Herring Cove, N.S. (on *Chondrus*)	−	−	+	−	−

36	28	*N. filiformis* W. Sm.	60×6	36	Lehave Islands, N.S. (brackish ditch)	—	—	+	—	—
8	—	*N. frustulum* (Kütz.) Grun.	6×3	34	New Haven, Conn. (shore)	—	—	—	—	—
13	17	*N. frustulum* (Kütz.) Grun.	7–16×3	36–41	Prospect, N.S. (rock pool)	—	—	+	—	+
39	—	*N. frustulum* (Kütz.) Grun.	5–12×4	28	Lehave Islands, N.S. (brackish ditch)	—	—	—	—	—
53	18	*N. frustulum* (Kütz.) Grun.	7–16×4–5	23–32	La Jolla, Cal. (tidal rock)	—	+	+	—	—
58	19	*N. frustulum* (Kütz.) Grun.	5–12×4	41	San Diego, Cal. (tidal mud)	—	+	—	—	—
68	—	*N. frustulum* (Kütz.) Grun.	6–28×5	22–24	Salton Sea, Cal. (water sample)	—	—	+	—	—
71	14	*N. hybridaeformis* Hust.	44×8	32	Woods Hole, Mass. (tank)	—	—	—	—	—
72	23	*N. laevis* Hust.	11–18×5	52	Woods Hole, Mass. (tank)	—	—	+	—	+
—	—	*N. laevis* Hust.	8–11×3.5	57	(from S. Watson, No. 5)	—	—	+	—	+
5	15	*N. curvilineata* Hust.	38×9	39	New Haven, Conn. (shore)	—	—	—	—	+
—	12	*N. marginata* Hust.	27–67×1.5–2	54	(from S. Watson, No. 10)	—	—	+	—	—
63	16	*N. obtusa* W. Sm. var. *scalpelliformis* Grun.	75×9	27–31	San Diego, Cal. (shore)	—	—	—	—	—
49	22	*N. ovalis* Arnott	8–10×3–4	52–66	Vineyard Sound, Mass. (water sample)	—	+	—	—	—
—	21	*Nitzschia* sp. (cf. *N. ovalis* Arnott)	8–12×5–7	44	(from S. Watson, No. 18)	—	—	—	—	—
52	27	*N. punctata* (W. Sm.) Grun.	10×7	20	San Diego, Cal. (tidal mud)	—	+	+	—	—
—	20	*N. tenuissima* Perag.	9–33×3	50–55	Beaufort, N.C. (from T. Rice)	?	?	+	+	+
—	13	*Nitzschia* sp.	12–17×2	52	(from S. Watson, No. 12)	—	?	—	—	—
—	—	*N. closterium* (Ehr.) W. Sm.	26–60×7	—	Galveston, Texas (from T. Starr, D 105)	+	—	+	—	+
—	—	*N. closterium* (Ehr.) W. Sm.	45–60×7	—	Sapelo Is., Georgia (from T. Starr)	+	—	+	—	+
—	26	*N. closterium* (Ehr.) W. Sm.	40–45×7	—	Beaufort, N. C. (from T. Rice)	+	—	+	—	+
54	25	*N. closterium* (Ehr.) W. Sm.	18–36×7	—	San Diego, Cal. (mud)	+	+	—	—	—
27	5	*Synedra affinis* Kütz.	50×6	12	Herring Cove, N.S. (rock pool)	—	+	—	—	—
11	4	*Stauroneis amphoroides* Grun.	13–30×5	27	Herring Cove, N.S. (rock pool)	—	—	—	—	—
—	29	*Cyclotella* sp.	4–18	—	Martha's Vineyard, Mass. (from R. Guillard)	—	+	+	—	—

TABLE II

Numbers of isolates exhibiting auxotrophy or heterotrophy

Vitamins required	No. of isolates	Growth in dark on:	No. of isolates
Thiamine only	6	Glucose only	16
Cobalamin only	11	Glucose or lactate	8
Thiamine + cobalamine	3	Glucose or acetate	1
None	24	Glucose, acetate, or lactate	1
		Lactate only	2
Total	44	No growth in dark on any	16
		Total	44

ordinary bacteriological techniques employed, and only one centric species was included in this study.

It should be pointed out that the range of physiological features among the species investigated here is not necessarily representative of the littoral flora, because diatoms with certain growth-factor requirements may have been eliminated by the methods of isolation. The proportion of vitamin-requiring species among those examined here is certainly an underestimate of that in nature. The fact that about a third of the strains required cobalamin reflects the abundance of this vitamin in marine muds (3, 4); in inshore waters it may rarely fall below limiting values (9). There have apparently been no comparable studies on the free thiamine in sea water, but since nine diatom strains were found to require this vitamin for growth, thiamine, too, may often be in adequate supply in littoral sea water. The absence of strains requiring other vitamins, such as biotin and niacin, may be a consequence of inadequate supplies of these substances in nature and in the media employed for preliminary isolations. Vitamin requirements by diatoms, in all cases marine, have been previously reported by Hutner and Provasoli (14), Droop (7, 8, 10), and Lewin (18). (It is our present opinion that the organism referred to as "*A. perpusilla*" by Hutner and Provasoli (14) should be designated *A. coffaeiformis*, and that "*Fragilaria brevistriata*" of Lewin (18) should be *Synedra affinis* Kütz. These organisms have been listed by their preferred names in Table I.)

Several species of fresh-water diatoms are capable of heterotrophic growth using glucose (15). Among 60 carbon sources tested, glucose was the only one which supported growth of *Navicula pelliculosa* in darkness (15). In order to limit the range of substrates to be tested here for heterotrophic growth, a representative sugar and two acids were selected. Glucose and acetate were chosen, since virtually all algae shown to be capable of heterotrophy can utilize at least one of these substrates. In addition, lactate was tested since it is actively respired by *N. pelliculosa*, although it does not support heterotrophic growth (15, 16). Since three of the marine diatoms studied here (strains 13, 36, 53) were capable of digesting agar, as indicated by the formation of pits at the site of individual colonies, it appeared possible that galactose might also support growth in darkness. However, in a preliminary test with the 15 species then available, including strains 5, 8, 11, 13, 27, and others not included in Table I, none was able to use galactose for growth. The fact that approximately half of the isolates were able to grow heterotrophically is of some ecological significance, indicating a means of nutrition other than photosynthesis if suitable carbon sources are available. Plunkett (20) has demonstrated free sugars (sucrose, glucose, fructose, galactose, arabinose, xylose) in deep-sea sediments; presumably littoral muds would be even richer in such compounds.

Acknowledgments

A great deal of difficulty was encountered in the identification of some of the small diatoms employed in this study. Dr. Paul S. Conger (Smithsonian Institution, Washington, D.C.) spent considerable time and effort in checking some of our tentative identifications and in certain cases suggested more appropriate designations, for which we are very grateful.

Acknowledgment is also extended to the following for supplying certain strains as indicated in Table I. Dr. R. R. G. Guillard (Woods Hole, Mass.), Dr. L. Provasoli (Haskins Laboratories, N.Y.), and Dr. S. W. Watson (Woods Hole, Mass.) provided pure cultures. Dr. T. Rice (Beaufort, N.C.) and Dr. T. Starr (Galveston, Texas) supplied unialgal cultures from which pure strains were isolated.

For the electron microscopy we are indebted to A. W. Tickner (National Research Council, Ottawa) and to D. E. Philpott (Woods Hole, Mass.).

References

1. Boyer, C. S. Synopsis of North American Diatomaceae. Proc. Acad. Nat. Sci. Phila. **78**, Suppl. (1927).
2. Buchholz, C. H. Concentration of vitamin B_{12} from urine by adsorption on carbon. J. Lab. Clin. Med. **52**, 653–656 (1958).
3. Burkholder, P. R. and Burkholder, L. M. Vitamin B_{12} in suspended solids and marsh muds collected along the coast of Georgia. Limnology and Oceanog. **1**, 202–208 (1956).
4. Burkholder, P. R. and Burkholder, L. M. Studies on B vitamins in relation to productivity of the Bahia Fosforescente, P. R. Bull. Marine Science Gulf and Caribbean, **8**, 201–223 (1958).
5. Cholnoky, B. J. Neue und seltene Diatomeen aus Africa. IV. Diatomeen aus der Kaap-Provinz. Österr. Botan. Z. **106**, 1–69 (1959).
6. Cleve-Euler, A. Die Diatomeen von Schweden und Finnland. I–V. K. Svenska Vetenskapsakad. Handl. Fjärde Serien. **2** (1), (1951); **3** (3), (1952); **4** (1), (1953); **4** (5), (1954); **5** (4), (1955).
7. Droop, M. R. A pelagic marine diatom requiring cobalamin. J. Marine Biol. Assoc. United Kingdom, **34**, 229–231 (1955).
8. Droop, M. R. Auxotrophy and organic compounds in the nutrition of marine phytoplankton. J. Gen. Microbiol. **16**, 286–293 (1957).
9. Droop, M. R. Vitamin B_{12} in marine ecology. Nature, **180**, 1042–1043 (1957).
10. Droop, M. R. Requirement for thiamine among some marine and supra-littoral protista. J. Marine Biol. Assoc. United Kingdom, **37**, 323–330 (1958).
11. Helmcke, J.-G. and Krieger, W. Diatomeenschalen in Elektronenmikroskopischen Bild. Teil I, 1953; Teil II, 1954.
12. Hustedt, F. Bacillariophyta. *In* Pascher, Die Süsswasserflora Mitteleuropas, 10. Fischer, Jena. 1930.
13. Hustedt, F. Marine littoral diatoms of Beaufort, North Carolina. Duke Univ. Marine Station Bull. No. 6 (1955).
14. Hutner, S. H. and Provasoli, L. A pigmented marine diatom requiring vitamin B_{12} and uracil. News Bull. Phycological Soc. Am. **6**, 7–8 (1953).
15. Lewin, J. C. Heterotrophy in diatoms. J. Gen. Microbiol. **9**, 305–313 (1953).

16. Lewin, J. C. Silicon metabolism in diatoms. III. Respiration and silicon uptake in *Navicula pelliculosa*. J. Gen. Physiol. **39**, 1–10 (1955).
17. Lewin, R. A. A marine Stichococcus sp. which requires vitamin B_{12} (cobalamin). J. Gen. Microbiol. **10**, 93–96 (1954).
18. Lewin, R. A. Vitamin-bezonoj de algoj. Sciencaj Studoj. Copenhagen. 1958. pp. 187–192.
19. Peragallo, H. and Peragallo, M. Diatomées marines de France et des districts maritimes voisins. M. J. Tempere, Grez-sur-Loing (S. et M.). 1897–1908.
20. Plunkett, M. A. The qualitative determination of some organic compounds in marine sediments. Deep-Sea Research, **5**, 259–262 (1957).
21. Schmidt, A. Atlas der Diatomaceen-Kunde. Reisland, Leipzig. 1874–1944.
22. Van Heurck, H. Synopsis des diatomées de Belgique. Anvers. 1880–1885.

Explanation of Figures

Fig. 1. *Achnanthes brevipes* (Ag.) Cl. ×1200
Fig. 2. *Navicula incerta* Grun. ×3850
Fig. 3. *Navicula menisculus* Schum. ×5610
Fig. 4. *Stauroneis amphoroides* Grun. ×2600
Fig. 5. *Synedra affinis* Kütz. ×3000
Fig. 6. *Navicula* sp. ×5610
Fig. 7. *Amphipleura rutilans* (Trentepohl) Cl. ×3000
Fig. 8. *Amphora lineolata* Ehr. ×2400
Fig. 9. *Amphora coffaeiformis* Cl. ×2400
Fig. 10. *Amphora coffaeiformis* Cl. ×2400
Fig. 11. *Amphora coffaeiformis* Cl. ×3000
Fig. 12. *Nitzschia marginata* Hust. ×7200
Fig. 13. *Nitzschia* sp. ×4800
Fig. 14. *Nitzschia hybridaeformis* Hust. ×2400
Fig. 15. *Nitzschia curvilineata* Hust. ×3000
Fig. 16. *Nitzschia obtusa* W. Sm. var *scalpelliformis* Grun. A, ×1200; B, ×7720
Fig. 17. *Nitzschia frustulum* (Kütz.) Grun. ×3000
Fig. 18. *Nitzschia frustulum* (Kütz.) Grun. ×3850
Fig. 19. *Nitzschia frustulum* (Kütz.) Grun. ×3850
Fig. 20. *Nitzschia tenuissima* Perag. ×7200
Fig. 21. *Nitzschia* sp. (cf. *N. ovalis* Arnott) ×5610
Fig. 22. *Nitzschia ovalis* Arnott ×5610
Fig. 23. *Nitzschia laevis* Hust. ×3850
Fig. 24. *Nitzschia angularis* var. *affinis* (Grun.) Perag. ×6000
Fig. 25. *Nitzschia closterium* (Ehr.) W. Sm. ×3600
Fig. 26. *Nitzschia closterium* (Ehr.) W. Sm. ×3850
Fig. 27. *Nitzschia punctata* (W. Sm.) Grun. ×5610
Fig. 28. *Nitzschia filiformis* W. Sm. ×3000
Fig. 29. *Cyclotella* sp. A, ×5610; B, ×3850
Fig. 30. *Amphiprora paludosa* W. Sm. var. *duplex* (Donk.) Cl. ×5610

Note: Figs. 1–30 follow.

PLATE I

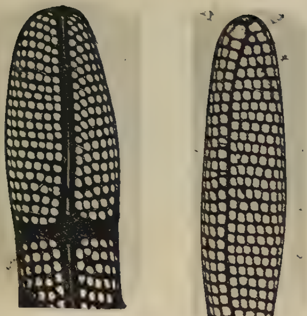
A B

1

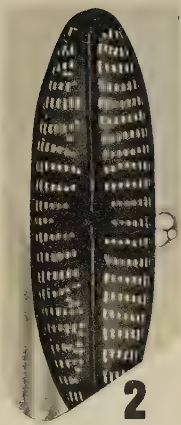
2

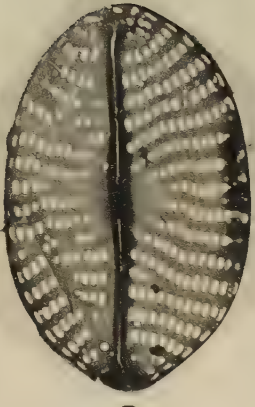
3

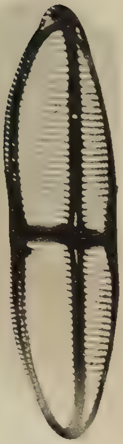
4

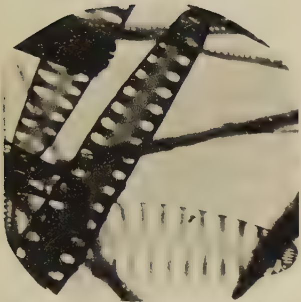
5

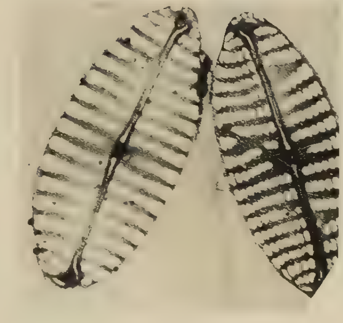
6

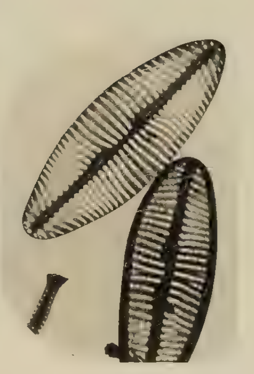
7

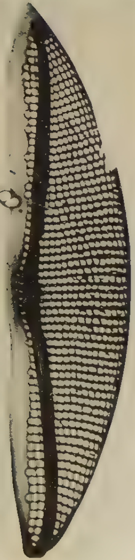
8

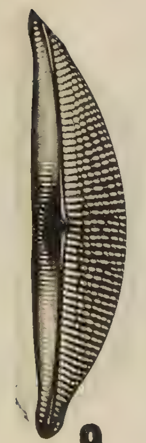
9

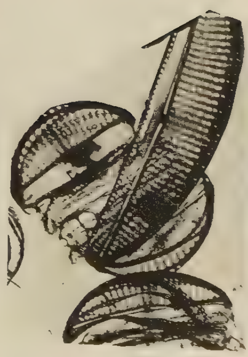
10

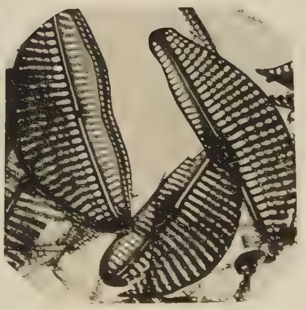
11

PLATE II

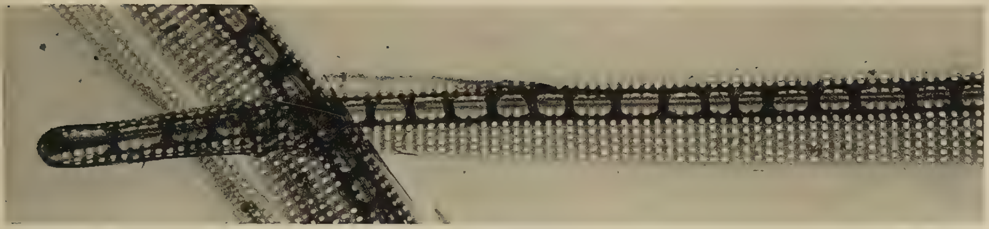

12

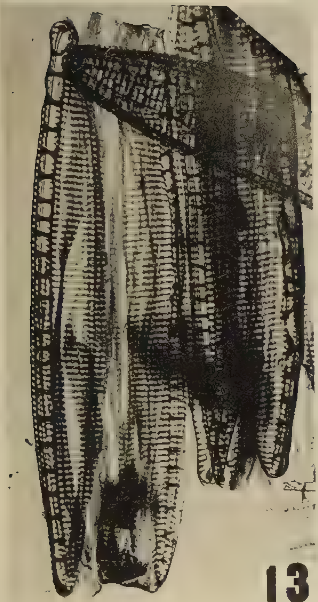

13

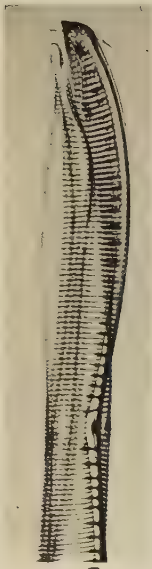

14

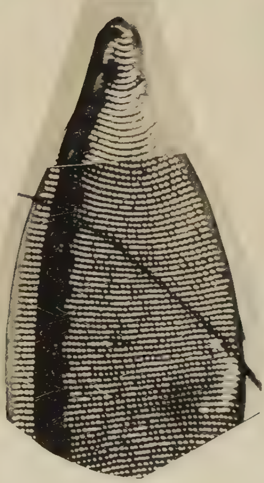

15

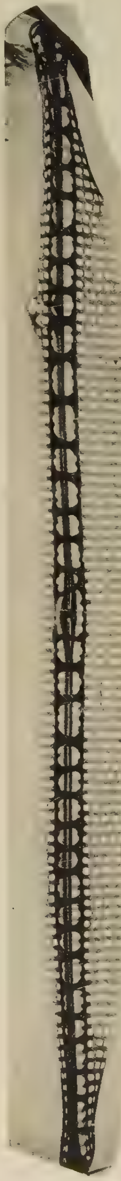

20

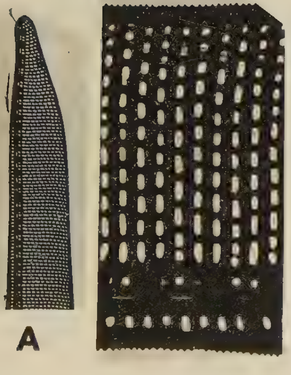

16 B

17

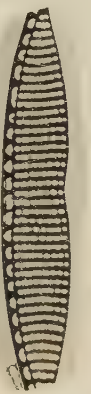

18

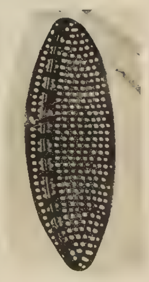

19

Plate III

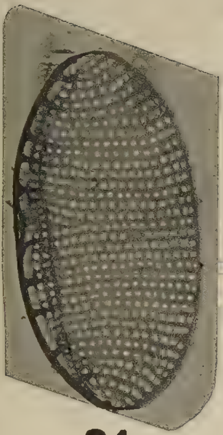
21

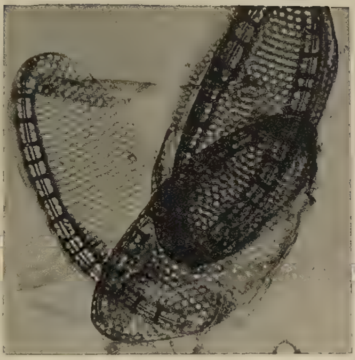
22

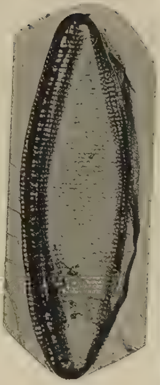
23

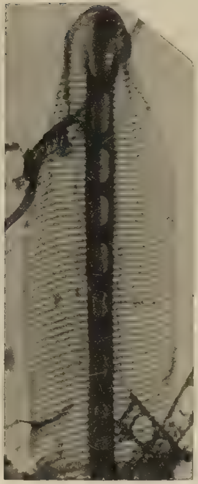
24

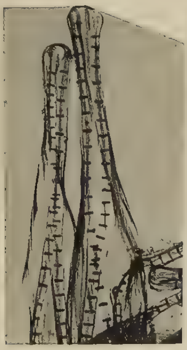
25

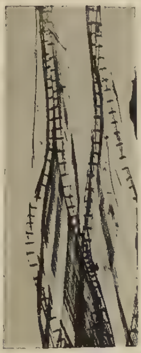
26

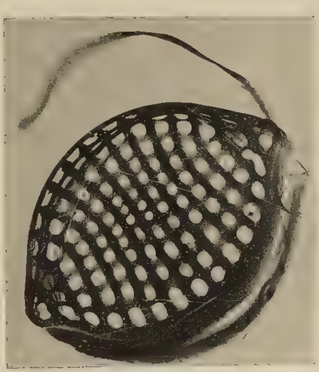
27

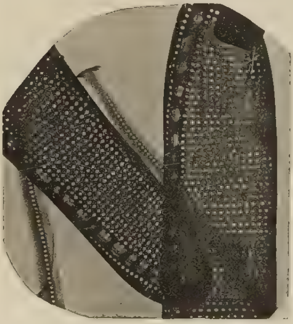
28

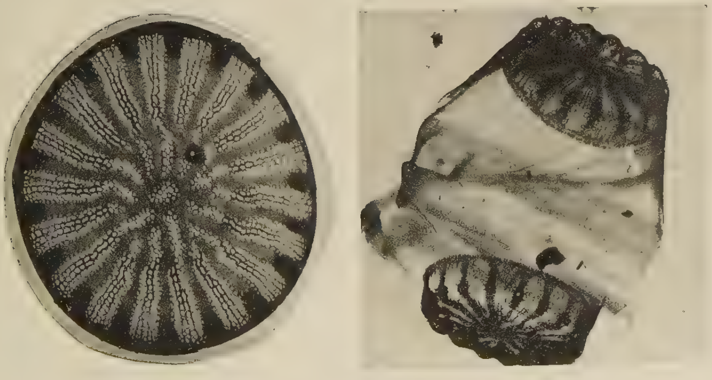
A

B

29

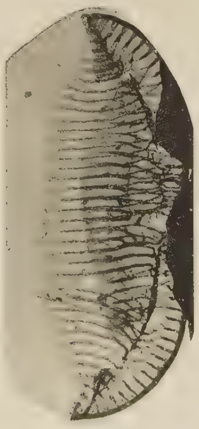
30

Contribution No. 1064

Made in United States of America
Reprinted from Limnology and Oceanography
Vol. 5, No. 2, April, 1960
pp. 232–235

PROCEDURE FOR AND COMMENTS ON ICE POINT TESTS OF DEEP SEA REVERSING THERMOMETERS

by G. G. Whitney, Jr.

PROCEDURE FOR AND COMMENTS ON ICE POINT TESTS OF DEEP SEA REVERSING THERMOMETERS[1]

One of the most basic and important tools of the physical oceanographer is the deep-sea reversing thermometer. The soundness of theories on the behavior of the oceans, and the validity of proof supporting or refuting such theories depends, in no small part, upon the accuracy of hydrographic observations obtained by means of these instruments.

Reversing thermometers are constructed with great care and precision but a calibration of each instrument is necessary before it can be properly used.

The purpose of this calibration is to determine for each instrument: 1) the corrections necessary at each of a number of selected points along the scales of the main and auxiliary thermometers, so as to reduce the thermometer reading to actual temperature; 2) the volume of the small bulb of the main thermometer to the zero degree mark ($V_\circ$), and 3) in the case of an unprotected thermometer, the pressure factor (Q) which is needed to determine the depth of the instrument at the time of reversal.

The scale corrections are determined by comparing the readings of the main and auxiliary thermometers of each instrument with the corrected reading of a "standard" thermometer of known accuracy at a series of selected points. These points are generally not more than 50 scale divisions apart for the main thermometer, and every 10° for the auxiliary. To prove reproducibility and determine a mean or average correction at each calibration point, several successive reversals should be made at each temperature point. With proper care and equipment, the correction determined at each such calibration point on the main scale of a good instrument should be accurate to within about 0.05 of a scale division. Auxiliary corrections are usually determined only to the nearest 0.1°C.

$V_\circ$ is determined by reversing and reading the main thermometer at an accurately known temperature, changing the temperature of the reversed thermometer to another accurately known temperature, about 30–40°C different from the first reading, and then dividing the difference between the two main readings ($T''-T'$) by the actual temperature change (t) times the glass constant (k)

$$V_\circ = \frac{T''-T'}{t \times k}$$

Several such tests should be made to determine an average value, which should be accurate to about one part in 100.

Q is determined in the laboratory by a series of reversals at accurately known pressures, 100 Kg/cm^2 or greater, and accurately known temperatures, generally at or near 0°C. The corrected reading of the unprotected thermometer (T_u), less the actual temperature (T_w), divided by the pressure in Kg/cm^2 gives the pressure factor

$$Q = \frac{T_u - T_w}{P}$$

A number of such tests at different pressures should be made to determine an average for each depth (pressure) and to determine linearity of pressure response. Q should be accurate to about one or two meters per thousand.

All of this calibration procedure is exacting, time-consuming, and requires a rather extensive and elaborate array of equipment to attain the desired degree of accuracy; it is therefore also relatively expensive, from 20% to 40% of the cost price of the instrument, depending upon the type and range. Without such calibration, however, the instrument is relatively valueless to the oceanographer.

Once such calibration has been accomplished, certain characteristics of the instrument are known and fixed. Barring the necessity for major glass repairs or the opening or changing by heat of the dimensions of the main capillary system, $V_\circ$ and the relation of the established scale corrections, one to another, will not change. Many laboratory rechecks of Q indicate that this value does not change with age or use within the pressure endurance capabilities of the instrument.

---

[1] Contribution No. 1064 from the Woods Hole Oceanographic Institution.

The ice point (reading at 0°C) can, and generally does, change with age. The amount of such change, the rapidity with which it may occur, and the period of time during which change may continue will vary greatly from one instrument to another. The direction of such change is most often in the direction of higher readings but may be downward, and may even be first in one direction and later in the other. There are two principal factors involved in such change; the shrinkage, with age, of the glass of the thermometer bulb, and in the case of a protected thermometer the gradual diffusion of a superatmospheric pressure around the bulb, initially created by the driving down of the cork plug during assembly.

Proper artificial "ageing" of the thermometer glass in the course of manufacture of the instrument minimizes the subsequent bulb shrinkage and consequent upward zero point shift resulting from natural ageing. It is possible to relieve any excess pressure below the cork plug by venting the area below the plug with a fine hypodermic needle. When these things have been done, the zero point shift with age is generally very slight, and may not become apparent for a year or more, and after two or three years the zero reading will, in most cases, have become stabilized. Where the bulb has not been artifically "aged," or when superatmospheric pressure exists around the bulb, the zero point may shift slowly but continuously for years.

It is always possible that there may exist in the bulb unrelieved stress just below the relief threshold. In such case, a severe jar or vibration, or exposure to extremes of temperature may cause ice point shift. It is probable that most ice point shifts resulting from bulb shrinkage are quite sudden, a shift from one level to another occurring at some particular moment in time, the ice point then remaining stable for a period until the stress relief threshold may once again be reached.

If he wants accurate data, the oceanographer must see that the accuracy of the original calibration is verified from time to time and that proper adjustment of the scale corrections are made in the event of ice point shift. If the ice point reading (and hence correction) changes, the corrections determined at all other points on the thermometer scale will change in the same direction by the same amount.

It is recommended that all reversing thermometers should be given an ice point check not more than six months after the time of initial calibration, and then rechecked every six months until the ice point appears to have become essentially stabilized. Thereafter an ice point check perhaps once a year is desirable. An ice point check should always be made after the thermometer has undergone any factory repairs, major or minor.

While all calibration laboratories can and do perform these checks, such tests are somewhat expensive, and there is the risk to the thermometers of damage or breakage during transportation to and from the testing laboratory.

The method for checking the ice point is relatively simple and can be undertaken by any organization using reversing thermometers as follows:

A. *Requirements*

1. Finely crushed fresh water ice must be used. (100% through 1" square screen; 50% through ½" square screen.)
2. Ice must be physically clean and chemically free from any dissolved substance that might lower the melting point. Most good commercial ice satisfies this requirement, and distilled water ice generally need not be used. (The melting point of distilled water ice at atmospheric pressure is 0.000°C. While a depression of a few thousandths of a degree may occur in essentially "clean" commercial ice, this is generally not significant. How-

ever, commercial ice that is chemically or physically impure may have a melting point down to several hundreths of a degree below 0.000°C. A check on the purity, and hence the "accuracy," of the ice should be made by including in each group of thermometers tested a thoroughly reliable protected reversing thermometer, the ice point of which is known and has become stable. It is perhaps desirable to have more than one of these so-called "standard" or "check" thermometers, the ice points of which can be verified by the use of distilled water ice in the procedure described below.)

3. Ice must be in melting condition. Melting can be promoted by sprinkling with distilled water.
4. The thermometers must be entirely free from any trace of salt. Rinse well in fresh water before test series.

B. *Procedure*

1. Thermometers are placed upright in ice in a container about 18″ deep. The container should have drainage in the bottom. If the container is insulated the thermometers should be not closer than 1″ to the sides; if uninsulated they should be not closer than 2″ to the sides. The lower ends of the thermometers should be not closer than 3″ to the bottom of the vessel. There should be not less than 3″ of ice over the top of the thermometers, and this should be covered to prevent air circulation.
2. The thermometers should stand in the ice for approximately one hour, after which each thermometer in turn should be carefully and quickly uncovered enough to permit the grasping of the upper end. The thermometer is then quickly withdrawn from the ice, instantly reversed, returned to the hole in the ice from which it was withdrawn, and recovered with ice.
3. When all the thermometers have been thus reversed, they should be allowed to stand about 15 minutes to ensure that all parts of the instrument, internally and externally, have lost the small amount of heat absorbed in the process of reversal and have returned to a temperature of 0.00°C.
4. Each reversed thermometer in turn should then be carefully uncovered enough to permit grasping its upper end. The thermometer is then quickly withdrawn from the ice only far enough to make visible the top of the mercury column of the auxiliary. Using a viewer or loupe of about 5× magnification, first the auxiliary, and then, withdrawing the instrument further, the main thermometer is read. This should be done as quickly as possible in order to avoid the effect of the ambient temperature. The time from the beginning of withdrawal of the thermometer until completion of both readings should be not more than 10 seconds. During all of this operation the extreme lower end of the reversed thermometer should remain surrounded by ice.
5. Care should be taken to avoid error due to parallax. A mask on the eyepiece with an orifice of about 3⁄16″ diameter centered on the optical axis is extremely helpful in this regard. A tube or other stand-off device on the objective end of the viewer, which can be placed against the outside of the thermometer shell to maintain the proper focus of the image, is also helpful.
6. In humid weather, fogging on the outside of the thermometer shells can be controlled by wiping a slight film of substance such as saddle soap on the shells in the vicinity of the zero points. Internal fogging of unprotected thermometer shells and stems can be controlled by rinsing the inside of the instruments with a little liquid detergent solution prior to placing the instruments in the ice.
7. It is preferable to pre-chill the reservoir ends of the thermometers

prior to each test by standing them upright in about 6" of clean ice mixed with water for a few minutes. This ensures that the reservoir end will not melt an air space around itself.

8. If a double-ended ice vessel with removable end caps is provided for the tests, after the thermometers have stood for one hour in the ice, the entire vessel can be reversed, thus reversing all the thermometers at once and eliminating the necessity for the steps outlined in paragraphs 2 and 3.
9. It is not safe to determine the ice point correction of the main thermometer based on one test (reversal) only. At least two tests should be made, and if these do not agree, a third test should be made and an average taken to determine the main ice point correction. If readings are several hundredths of a degree apart, additional tests should be made until a good average can be obtained, discarding readings which are apparently aberrant. The only condition under which one reversal is adequate would be when it agreed with the ice point reading previously determined in a proper manner, in which case it is safe to assume that no change in the ice point has occurred since the last determination. One reading of the auxiliary is generally satisfactory, as the correction is normally stated only to the nearest 0.1°C.

G. G. WHITNEY, JR.
Woods Hole Oceanographic Institution
Woods Hole, Mass.

Contribution No. 1065

Deep-Sea Research, 1960, Vol. 6, pp. 311 to 317. Pergamon Press Ltd., London. Printed in Great Britain

The general thermal circulation in equatorial regions

Allan R. Robinson

(*Received* 20 *August* 1959)

Abstract—An approximation valid near the equator is developed for a model of the general thermal circulation. The existence of equatorial effects is related to the vanishing of the Coriolis parameter, and the equatorial approximation is related to the mid-latitude circulation. Qualitative features of the solutions are discussed.

1. INTRODUCTION

A recent study (Robinson and Stommel, 1959) has been made of a fluid system on the β-plane, thermally driven by imposed boundary temperatures. The surface temperature imposed varied with latitude only. The fluid considered, although inviscid, possessed a vertical coefficient of heat conductivity. The system was bounded on the east by a meridional plane, and was of infinite depth. This model was proposed as related to the general thermal circulation of the oceans.

In the previous study, solutions for the non-linearly coupled temperature and velocity fields were obtained, the validity of the solutions being limited to mid-latitude regions away from the eastern coast. In particular, the solutions became singular as they approached the equator. It is the purpose of the present work to remove this singularity by developing an approximation appropriate to the equatorial region. To do so, it is necessary to restate the assumptions which define the model in a more formal manner. This allows additional implications to be deduced. In addition, the inviscid but conducting condition is relaxed. It is replaced by the more physically plausible assumption of a unit eddy Prandtl number.

(2) THE MID-LATITUDE APPROXIMATION

Since the physical basis of an approximation scheme lies in order of magnitude considerations, non-dimensional variables and parameters are introduced. In the following, primed variables have dimensions and unprimed do not. x' is positive eastward, y' northward, and z' upward. p' is the actual pressure minus the hydrostatic pressure due to the mean density ρ_0. The mean temperature of the surface is T_0, and the asymptotic value of the temperature is zero. The vertical eddy conductivity, the vertical eddy viscosity, the thermal expansion coefficient, a typical horizontal dimension, the magnitude of the earth's rotation, and gravitational acceleration are denoted respectively by κ, ν, α, L, Ω, g.

Let

$$(x', y', z') = L(x, y, z)$$

$$(u', v', w') = [\alpha T_0 g (2\Omega)^{-1}] (u, v, w)$$

$$P' = [\rho_0 L \alpha T_0 g] P$$

$$T' = T_0 T$$

Then, under the Boussinesq approximation, the equations of conservation of momentum, mass, and heat appropriate to this model are

$$- n\sigma\epsilon\, u_{zz} - fv + p_x + n\,(uu_x + vu_y + wu_z) = 0 \tag{1}$$

$$- n\sigma\epsilon\, v_{zz} + fu + p_y + n\,(uv_x + vv_y + wv_z) = 0 \tag{2}$$

$$- n\sigma\epsilon\, w_{zz} - T + p_z + n\,(uw_x + vw_y + ww_z) = 0 \tag{3}$$

$$u_x + v_y + w_z = 0 \tag{4}$$

$$- \epsilon T_{zz} + (uT_x + vT_y + wT_z) = 0 \tag{5}$$

where

$$\epsilon = K2\Omega\,(\alpha T_0\, gL)^{-1}, \quad n = \alpha T_0\, g\,(4\Omega^2 L)^{-1}, \quad \sigma = \nu\kappa^{-1}$$

and f is the Coriolis parameter divided by 2Ω, a smooth* function of y.

Although full non-dimensional variables have been introduced, the variables will not in general be order unity quantities, except for the horizontal coordinates and the temperature. Amplitudes and scales will depend on the three parameters ϵ, n, σ.

For $T_0 = 25\,C^\circ$, $L = 10^8\,cm$, $\Omega = \cdot 7 \times 10^{-4}\,\text{sec}^{-1}$, $g = 10^3\,\text{cm-sec}^{-2}$,

$\alpha = 2 \times 10^{-4}\,(^\circ C)^{-1}$, $\nu = \kappa = 1\,\text{cm}^2\text{-sec}^{-1}$,

$\epsilon = 3 \times 10^{-13}$, $n = 2$, $\sigma = 1$.

ϵ is extremely small while n and σ are of order unity. Therefore ϵ will have the major effect in setting all scales and amplitudes. To exploit the smallness of ϵ in order to derive approximate equations, it is necessary to use the techniques of singular perturbation theory. In ordering the equations by this method, the amplitudes and scales of all quantities are initially determined, that is, before the integration of the still mathematically complicated approximate equations.

Proceeding, we introduce explicitly the ϵ-dependence of all the variables. This is done in terms of as yet unknown exponents, viz. $\zeta = \epsilon^a z$, $u = \epsilon^b U$, $v = \epsilon^c V$, $w - \epsilon^d W$, $p = \epsilon^e P$. These new variables are substituted into equations (1) – (5), and it is assumed that all variables approach close to their asymptotic ($z = -\infty$) values within unit range of ζ, and that all dependent variables are smooth functions of x, y, ζ. Thus all the ϵ-dependence of each term of each equation is now exhibited explicitly in the coefficient of the term. The five exponents are determined by the following five assumptions:

(1) and (2) In equations (1) and (2), the pressure gradient and Coriolis terms are of the same order in ϵ.

(3) In equation (3), the pressure gradient and the buoyancy terms are of the same order in ϵ.

(4) In equation (4), the vertical divergence is the same order as the horizontal divergences.

(5) In equation (5), the vertical diffusion and the vertical advection are the same order in ϵ.

These five conditions yield $a = -1/3$, $b = c = e = 1/3$, $d = 2/3$.

---

*i.e., the scale of y is order of unity, and $f(y)$ itself and all its derivatives are upper bounded by unity.

In terms of these exponents, the coefficient in ϵ of each term in all five equations can be computed. The equations can now be expanded by keeping in each only the lowest order ϵ-terms. The resulting approximate equations are

$$-fV+P_x=0 \tag{6}$$

$$fV+P_y=0 \tag{7}$$

$$-T+P_\zeta=0 \tag{8}$$

$$U_x+V_y+W_\zeta=0 \tag{9}$$

$$-T_{\zeta\zeta}+UT_x+VT_y+WT_\zeta=0 \tag{10}$$

It should be noted that n and σ do not appear in these equations, so that to this approximation, all quantities of interest are independent of these parameters. In the momentum equations the amplitude ratios in ϵ, of the first neglected terms compared to the retained terms are:

(1) $O(\epsilon^{1/3})$, viscous and inertial terms

(2) $O(\epsilon^{1/3})$, viscous and inertial terms

(3) $O(\epsilon)$, viscous and inertial terms

Note also that all terms are important in the continuity and heat equations even to the lowest order of this approximation, and that the system is much more highly hydrostatic than geostrophic.

Equations physically identical to (6)–(10) were the assumed starting point of the previous study, and a full discussion of their solutions is given in that paper. The formal discussion of the assumptions leading to these equations given here serves two purposes. Firstly, the relative size of neglected effects can be numerically estimated i.e., a range of validity of the theory in ϵ is obtained. Secondly, in regions where the solutions of these approximate equations break down, the nature of the breakdown can be related to the assumptions violated. An appropriately modified approximation scheme can then be derived.

(3) THE EQUATORIAL APPROXIMATION

The behaviour of the solutions obtained from equations (6)–(10) is such as to invalidate their application near the equator. There the thermocline depth approaches zero, and all fields approach zero, except for W which diverges. In particular the asymptotic value of the vertical velocity, W_∞, is inversely proportional to the two-thirds power of the non-dimensional Coriolis parameter,

$$W_\infty \propto f^{-2/3} \tag{11}$$

Thus as $f \to o$, W is no longer a smooth function of y. Terms involving W in our original equations (1)–(5) may no longer be negligible compared to terms retained in equations (6)–(10).

This lack of smoothness is associated with amplitude changes, which must be considered in obtaining the approximation appropriate to the region about $f=0$.*

---

*The mathematical technique which is being employed here may be found in an article by CARRIER (1954).

Furthermore, in addition to allowing for new ϵ-dependence of quantities whose amplitudes and scales were found in the mid-latitude regions, a new quantity of primary interest enters. This is the scale of y in which equatorial effects occur, i.e. the width of the singular region. As above. we introduce . .

$$\eta = \epsilon^{A}\, y, \quad \xi = \epsilon^{B}\, z, \quad \mu = \epsilon^{C}\, u, \quad \nu = \epsilon^{D}\, v, \quad \omega = \epsilon^{E}\, w, \quad p = \epsilon^{F}\, \varpi,$$

substitute in equations (1)–(5), and assume μ, ν, ω, ϖ, T to be smooth functions of x, η, ξ. The following set of assumptions is used to determine the six exponents and thereby to order the equations in the equatorial region.

(1) In equation (1), the vertical momentum advection and the pressure gradient terms are of the same order in ϵ.

(2) In equation (2) the pressure gradient and Coriolis terms are of the same order in ϵ.

(3) In equation (3), the pressure gradient and the buoyancy terms are of the same order.

(4) All terms in the continuity equation, (4), are of the same order in ϵ.

(5) In equation (5), the vertical diffusion and vertical advection are the same order.

(6) In the region where the mid-latitude and equatorial approximations overlap in validity, the same amplitude of W must be given by the two approximations.

Assumptions (1) and (5) are requirements consistent with the apparent equatorial divergence of the vertical velocity. The form of (1) is also consistent with the mathematical requirement that some term from the old approximation remain to balance the newly required term. This is necessary in order that the same solution to the original full equations may be obtained from the two approximations valid in different regions. p_x is chosen instead of fv because of the equatorial asymmetry of v. Assumption (2) differs from (1) because $\partial/\partial y$ becomes large as well as w, because of the equatorial symmetry of u and p, and because of the anticipation that a large linear term will dominate a large non-linear term. Assumption (4) is the only one containing D, the amplitude of v. Thus A, B, C, E, F are determined independently of (4), which is then the only assumption which yields five consistent approximate equations necessary for the five dependent fields.*

The joining condition, assumption (6), which relates amplitudes in the two regions by matching the ϵ-dependence of w at the as yet undefined ' edge ' of each region, is mathematically realized as follows. Approaching the region of overlap from the equator, we recall that everywhere in the equatorial region $w = \epsilon^{E}\, \omega$. Since ω is smooth in η, $\omega_{\infty} = \omega\,(\eta \to \infty)$ is independent of ϵ; furthermore, ω_{∞} is closely approached in order unity range of η. Approaching from mid-latitudes, we insist that when y becomes sufficiently small so that η is of order unity, the amplitude of w given by the mid-latitude approximation must also be ϵ^{E}. Taking the origin of y and η at the equator, let $f = \beta y = \beta \epsilon^{-A}\, \eta$, where β is 0 (1). Using equation (11), and recalling that in mid-latitudes $w \quad \epsilon^{2/3}\, W$, assumption (6) is found to require that

---

*This paragraph is, of course, a discussion and not a justification of our assumptions. The assumptions are a formal way of stating our physical model. The only logical justification lies in the internal consistency of the ordered equations implied by the assumptions. This consistency must be examined *a posteriori*. Any real justification lies in a comparison with nature.

$\epsilon^{2/3}\,\epsilon^{2/3A} = \epsilon^{E}$, or $\frac{2}{3}(1 + A) = E$. Together with (1)–(5), the exponents are determined as

$$A = -\tfrac{1}{10},\quad B = -\tfrac{2}{5},\quad C = \tfrac{1}{5},\quad D = \tfrac{3}{10},\quad E = \tfrac{3}{5},\quad F = \tfrac{2}{5}.$$

In terms of these exponents, the equations expanded to lowest order take the approximate forms,

$$-\sigma n\mu_{\xi\xi} - \beta\eta v + \varpi_x + n(\mu\mu_x + v\mu_\eta + \omega\mu_\xi) = 0 \tag{12}$$

$$\beta\eta\mu + \varpi_\eta = 0 \tag{13}$$

$$-T + \varpi_\xi = 0 \tag{14}$$

$$\mu_x + \nu_\eta + \omega_\xi = 0 \tag{15}$$

$$-T_{\xi\xi} + (\mu T_x + \nu T_\eta + \omega T_\xi) = 0 \tag{16}$$

Thus the equations for the new scaled variables differ from the old approximate equations only in the first momentum equation. There, all non-linear terms as well as the frictional term are necessarily of the same order of magnitude as the geostropic terms. Compared to the retained terms the neglected terms in the second and third momentum equations are

(2) $O(\epsilon^{1/5})$, viscous and inertial terms.

(3) $O(\epsilon^{4/5})$, viscous and inertial terms.

Thus the system is less geostrophic and hydrostatic than it was at mid-latitudes.

Furthermore, for a system which is driven by wind stress as well as thermal forces, the appearance of the viscous term in (12) is important. It implies a much stronger coupling of wind-driven and thermal circulations than occurred at mid-latitudes. Thus in this region we can no longer relate our model to a real ocean by imposing a non-zero vertical velocity at the surface, i.e. by imposing the divergence of a wind-driven Ekman layer. The additional boundary condition required by the higher order z-term in (12) may be taken as a specification of the surface stress. Specification of zero surface stress now corresponds to a purely thermally-driven system; however, to make any realistic comparison with a real ocean, a non-zero stress must be applied.

Equations (12)–(16) are of course independent of ϵ, and serve to determine the form of μ, ν, ω, T, ϖ, as well as the amplitude dependence of these fields on η and σ. However, as mentioned above, since (6)–(12) and their boundary conditions contain only order unity parameters and variables, they can yield only order unity amplitude factors. Thus, in obtaining the ϵ-dependence of the amplitudes and scales we have in fact obtained the numerical order of magnitude of the variables. Using the numerical values given in section (1), we obtain: the scale of equatorial effects as the order of 100 km, the magnitude of the east–west velocity in the equatorial region as the order of 100 cm sec^{-1}, and the equatorial thermocline as almost an order of magnitude shallower than at mid-latitudes. In addition, the equatorial amplitudes of the vertical and north–south velocities are found to be slightly greater than at mid-latitudes, $O(\epsilon^{.60})$ compared to $O(\epsilon^{.67})$, and $O(\epsilon^{.30})$ compared to $O(\epsilon^{.33})$, respectively.

(4) DISCUSSION

That the main features of the Cromwell current may indeed be related to the general thermal circulation is apparent from the above numerical results. The Cromwell current is observed to have a maximum amplitude of about 150 cm sec^{-1}, and a width of about 200 km. The dense packing of isothermal surfaces near the equator obtained from our analysis is also compatible with observations on real oceans. However to make a meaningful comparison of our model with a real ocean, at least one additional qualitative result is needed. This is the sign of the strong equatorial current, or the latitudinal slope of the isothermal surfaces just north or south of the equator. This information is contained in equations (6)–(12) and in their boundary conditions. Since these equations are highly non-linear and involve many coupled variables, it is difficult to obtain even the gross features of their solutions.

However, dimensional equations physically equivalent to (6)–(12) form the assumed starting point for a study of the equatorial undercurrent by VERONIS (1960). In a paper appearing elsewhere in this issue, power series solutions of these equations in the latitudinal coordinate are developed about the equator. These solutions are for a longitudinally varying imposed surface temperature distribution. Associated with this boundary condition, a special type of longitudinal dependence is allowed, viz. u', p', T' are linear in x', and v' w' are independent of x'. The solutions obtained do contain an eastward flowing Cromwell current. Veronis' results do not strictly apply to our problem because of the different surface temperature condition imposed, but it is possible to reformulate simply our original problem to eliminate this difference. We consider therefore the general thermal circulation subject to the condition that $T(x, y, o) = T_0(y) + T_1 x$ where $T_0(y)$ is a prescribed function and T_1 a prescribed constant. Considering first the fields at mid-latitudes, solutions are sought with the special x-dependence stated above, rather than with the x-dependence given by our previous similarity transformation. In this case it can easily be shown that the asymptotic value of the vertical velocity remains inversely proportional to the two-thirds power of the Coriolis parameter, equation (11) is maintained. Since this is the feature of the mid-latitude solution used in deriving the equatorial approximation, all the results of section (2) are unaltered, including numerical results. Thus a qualitative resemblance, both in order of magnitudes and in signs, is seen to exist between the results of our model and oceanic observations.

Emphasis has been placed on the gross features of the solution to these equations not only because of the mathematical difficulty of obtaining exact solutions, but also because a comparison is made with average observations on a real ocean. The crude model proposed, containing constant eddy parameters, can in no sense be expected to bear a precise quantitative relation to the fundamentally turbulent geophysical situation. It is, however, meaningful to make a qualitative or semi-quantitative comparison. What has been studied is the effect of the driving forces and rotational constraints on the mean fields. The turbulent transfer processes are essential and must be included. In terms of eddy parameters, they are included in a crude and hypothetical way. The approach is a meaningful one only because there is a large number of terms in our equations, other than the eddy parameter terms, which govern the gross features of the solutions.

Acknowledgments—I am grateful to Professor HENRY STOMMEL for interesting discussions, and to the Woods Hole Oceanographic Institution for a fellowship held during the time of this research.

*Woods Hole Oceanographic Institution, Woods Hole, Mass., U.S.A.**

Woods Hole Oceanographic Institution Contribution No. 1081.

*Present address: The Cavendish Laboratory, Cambridge University.

REFERENCES

CARRIER G. F. (1954) Boundary Layer Problems in Applied Mathematics, *Comm. on Pure and Applied Math.*, **7** 11.

ROBINSON A. and STOMMEL H. (1959) The Oceanic Thermocline and the Associated Thermohaline Circulation, *Tellus* **11**.

VERONIS G. (1960) An Approximate Theoretical Analysis of the Equatorial Undercurrent. *Deep-Sea Res.* **6**, 287-296.

Printed in Great Britain by The Salisbury Press Ltd., Publicity House, Wilton Road, Salisbury, Wilts. (22849)

Contribution No. 1067

Deep-Sea Research, 1960, Vol. 6, pp. 235 to 238. Pergamon Press Ltd., London. Printed in Great Britain

SHORTER COMMUNICATION

The seasonal and geographical range of primary production in the Western Sargasso Sea

JOHN H. RYTHER and DAVID W. MENZEL

(*Received* 3 *September*, 1959)

IN a recent publication (MENZEL and RYTHER, in press) the annual cycle of primary production was discussed for the North-western Sargasso Sea as observed from a single hydrographic station (Station 'S') located 15 miles SE of Bermuda in 1500 fm of water. The values for net daily organic production (g carbon assimilated/m^2/day) for 1958 are shown in Fig. 1. These values were obtained by *in situ* or simulated *in situ* ^{14}C measurements. The latter consisted of exposing samples, collected from several depths within the euphotic zone and inoculated with $^{14}CO_3^{=}$, to light intensities comparable to those occurring at the depths from which the samples were taken. This was accomplished by means of neutral density filters covering a water-cooled incubator which was mounted on the deck of the oceanographic vessel. The *in situ* measurements lasted for half the daylight portion of a day; the modified *in situ* measurements, for 24 hrs.

There was a definite seasonal cycle of production, comparable to but of less magnitude than the cycle in temperate and boreal waters. The values ranged from a maximum of 0·85 g C/m^2/day in April to 0·05 g C/m^2/day in November. Also shown in Fig. 1 is the seasonal temperature profile to 700 m, which illustrates the relationship between vertical stability of the surface waters and productivity. Minimum levels of production occurred throughout the summer and early fall when the seasonal thermocline was well developed. Moderately high levels persisted throughout the late fall, winter, and early spring when the water was more or less isothermal and mixed to or nearly to the depth of the permanent thermocline (about 400 m). The highest values for the year occurred briefly in April when thermal stratification of the surface layers first began to develop.

The relatively high production throughout the winter is in contrast to the situation further north, where in deep water there are both winter and summer minima (RYTHER and YENTSCH, 1958). This is due to the conditions in the Bermuda region of (1) greater incident radiation in winter, (2) more transparent water and (3) less extensive vertical mixing. As a result of this combination of factors, the ratio euphotic zone/mixed zone is greater at Bermuda than further north permitting plant growth in winter in the former but not the latter region.

The latitude of Bermuda may be considered a semi-tropical area where surface water conditions differ markedly from those further south in the true tropics. There, no winter cooling and mixing of the surface layers occurs and the 'seasonal thermocline' of more northern waters persists in the tropics throughout the year and merges more or less continuously into the permanent thermocline. The wide band of 18° water, characteristic of the Sargasso Sea (WORTHINGTON, 1959), becomes thinner and thinner southward from Bermuda as the westerly drifting equatorial current is approached. Just 100 miles south of the island, surface temperatures seldom, if ever, drop below 20 °C.

Since high production is so obviously dependent upon winter mixing and its enrichment of the surface layers (60 per cent of the annual production at Bermuda occurred between January and April, 1958) it follows that the productivity of tropical waters where no such mixing occurs must be low throughout the year. There has been no study made of the annual cycle of primary production in the tropics comparable to that described above for the semi-tropical Sargasso Sea. But the results of a short oceanographic section north and south of Bermuda do much to confirm the hypothesis presented above.

This section, made during the first week of March, 1959 on Cruise No. 24 of the Research Vessel *Crawford*, consisted of two stations north-west of Bermuda and nine stations approximately 50 miles

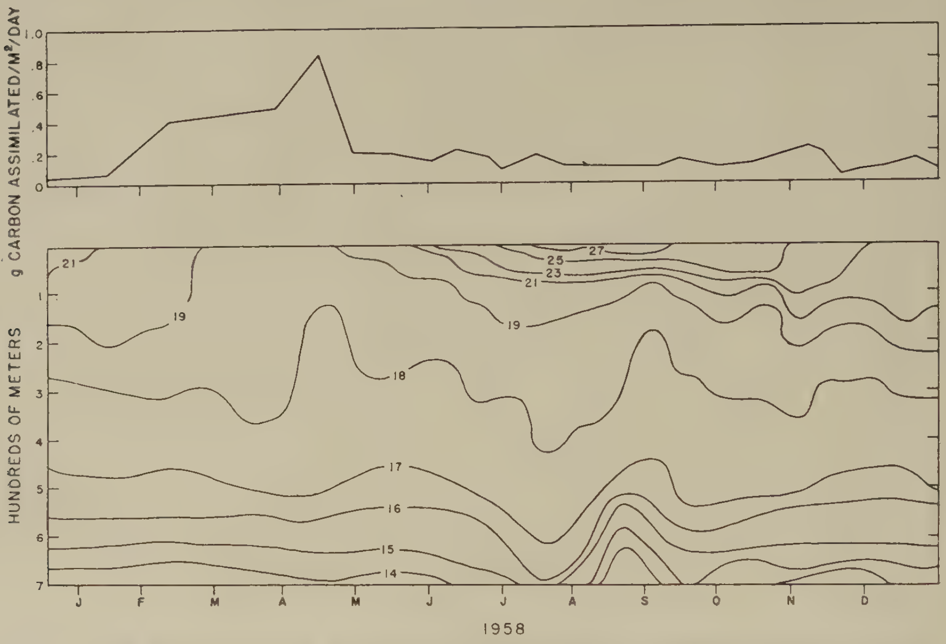

FIG. 1. The seasonal cycle of net primary production and the seasonal temperature profile at Station S for 1958.

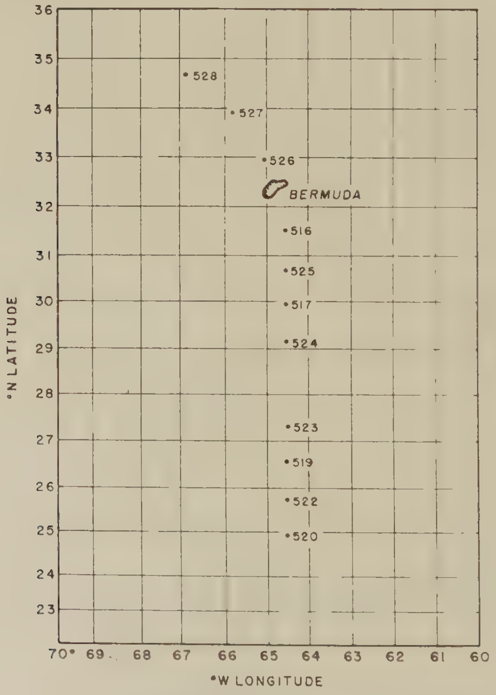
36
35
34
33
32
31
30
29
28
27
26
25
24
23
°N LATITUDE
• 528
• 527
• 526
BERMUDA
• 516
• 525
• 517
• 524
• 523
• 519
• 522
• 520
70° 69 68 67 66 65 64 63 62 61 60
°W LONGITUDE

FIG. 2. Station locations for the oceanographic section south of Bermuda made during *Crawford* cruise No. 24 in March, 1959.

apart in a line due south of the island extending to 24° 53′N latitude. The location of these stations is shown in Fig. 2. It was intended to extend this section across the Sargasso Sea to the north-eastern coast of the United States, but a severe winter storm prevented further working during the passage.

Winter cooling and mixing in the North Atlantic ocean are usually most extreme during early March. Actually, the winter of 1959 was rather mild and the season somewhat early. The first indications of seasonal thermal stratification of the surface water had begun to appear in the Bermuda region by March 1.

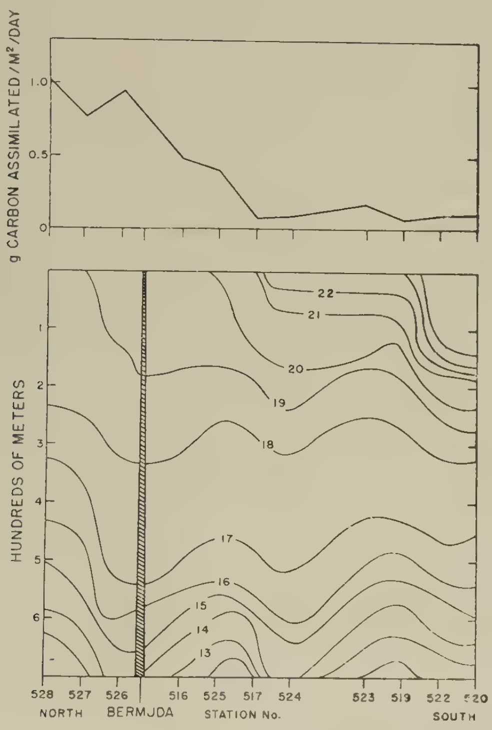

FIG. 3. Net primary production and temperature profile observed on the section illustrated in Fig. 2.

Fig. 3 shows the values for net primary production, as measured by the simulated *in situ* ^{14}C technique, on this section. Below this is shown the temperature profile to 700 m. It is remarkably similar to the seasonal cycle at Bermuda as shown in Fig. 1. Production at the northern end of the section averaged about 1·0 g C/m^2/day, the highest ever observed in the Sargasso Sea and about comparable to the seasonal maximum at Station *S* in 1958. Production dropped off rapidly south of Bermuda reaching a low, rather constant level at the six southernmost stations of the section of about 0·1 g C/m^2/day. Across a distance of less than 200 miles production differed by an order of magnitude.

So, too, does the north-south temperature profile mirror the seasonal trend at Station *S*. The broad band of isothermal water, some 300 m deep, at the northern end of the section merges into a well stratified water mass to the south much the same as the development in time of the seasonal thermocline *in situ* at Bermuda.

No other time of year and no other set of conditions can be envisaged which would cause primary production in the tropical Sargasso Sea to exceed the level shown here. Until a seasonal study of the region has been made, it may be assumed that the process proceeds at a low rather constant level, with an annual rate of some 25–50 gC/m^2/year (net production), perhaps one third of that in the semi-tropical waters to the North.

Acknowledgments—The authors wish to acknowledge the assistance of L. V. WORTHINGTON and W. G. METCALF in making the hydrographic measurements on *Crawford* cruise No. 24.

Woods Hole Oceanographic Institution,
Woods Hole, Massachusetts

Contribution No. 1067 *from the Woods Hole Oceanographic Institution, Woods Hole, Mass., U.S.A. Contribution No.* 1067 *from the Woods Hole Oceanographic Institution and Contribution No.* 240 *from the Bermuda Biological Station, under contracts AT* (30–1)–1918 *and* AT (30–1)–2078 *with the U.S. Atomic Energy Commission and with partial support of N.S.F. Grant* B–3234.

REFERENCES

MENZEL D. W. and RYTHER J. H. The annual cycle of primary production in the Sargasso Sea off Bermuda. *Deep-Sea Res.* In press.

RYTHER J. H. and YENTSCH C. S. (1958) Primary production of continental shelf waters off Bermuda. *Limnol. & Oceanogr.* 3, 327-335.

WORTHINGTON L. V. (1959) The 18° water in the Sargasso Sea. *Deep-Sea Res.* 5, 297-305.

Printed in Great Britain by The Salisbury Press Ltd., Publicity House, Wilton Road, Salisbury, Wilts. (22277)

Contribution No. 1068

The Phytoplankton of the Sargasso Sea off Bermuda*)

By

E. M. Hulburt, J. H. Ryther, and R. R. L. Guillard

Introduction and Methods

A standard oceanographic station in the north-western Sargasso Sea has been occupied at two weekly intervals since November, 1957. This station (Station S) is located fifteen miles SE of Bermuda in 1,500 fathoms of water. Routine observations have included measurements of temperature, salinity, dissolved oxygen, plant nutrients (N, P, Si), phytoplankton pigments, rates of primary production, zooplankton standing crops, light penetration, and incident solar radiation. These aspects of the programme are reported elsewhere and will be referred to here only where pertinent. In addition, each time Station S has been occupied, a series of 250 ml samples has been taken, initially from 0, 10, 25, 50, and 100 metres, later from just 0, 50, and 100 metres. These were preserved with 2% neutral formalin for subsequent examination and enumeration of the phytoplankton organisms. After the sample bottles were received in the laboratory, the cells were allowed to settle, the supernatant was decanted and an aliquot of the remaining concentrate was counted under "high-dry" magnification. For the most part these counts include only the microorganisms down to the size of 5–10 μ. The smaller organisms were largely unidentifiable by the counting technique, their systematics are unknown or uncertain and many of the delicate forms were probably destroyed or made unrecognizable by the method of preservation. This fraction of the phytoplankton will be discussed briefly at the end of the paper.

In this report we shall consider primarily the species composition, abundance, diversity, and the seasonal variation of these properties as revealed by routine counts of surface (0–10 m) samples collected each month for the period November 1957–November 1958 and of selected samples from 50 m collected within the same period.

---

*) Contribution No. 258 from the Bermuda Biological Station and Contribution No. 1068 from the Woods Hole Oceanographic Institution under Contract AT(30-1)–2078 and AT(30-1)–1918 with the U.S. Atomic Energy Commission with partial support of NSF Research Grant G-3234.

Results

The complete listing of species and numbers of organisms counted in this annual series is given in Tables 1 and 2. In each case the species found only at the surface or only at 50 m are indicated by asterisks. In addition, counts have been lumped into the three major algal groups present (Coccolithophoridaceae, diatoms, and dinoflagellates) to show their relative importance (Table 3). The one dominant in the region, *Coccolithus huxleyi*, is shown separately in this table. Also shown are values for chlorophyll *a*, determined from the same water that provided the phytoplankton samples, and temperatures (from MENZEL and RYTHER, in press).

Species composition and abundance

The most striking feature of the phytoplankton in the Bermuda area is the predominance of the Coccolithophoridaceae throughout the year, with a single exception, and the dominance of one species, *Coccolithus huxleyi*, for at least half the year. The latter occurred in greatest abundance in the late autumn or early winter (December, 1957 and November, 1958), but was dominant, exceeding in number all the other species combined, throughout the spring with the exception of April. It was about equally abundant at both the surface and 50 m, and appears to be associated with temperatures between 20° and 24°C (Table 3), its midsummer decline probably resulting from high temperatures. It has been shown by experiments with this species in culture that its optimum temperature for growth is about 20°C and that it will not grow above 25°C (MJAALAND, 1956).

In April, a spring flowering of moderate magnitude took place. Chlorophyll *a* values at that time were two to three times as great as were present throughout the late autumn and winter, and an order of magnitude greater than the summer values. The hydrographic features responsible for this flowering are discussed in detail elsewhere (MENZEL and RYTHER, in press), but in essence the bloom coincided with the onset of thermal stratification of the surface waters following a period of winter and early spring cooling and mixing to 300–400 m. Figure 1, from RYTHER and MENZEL (in press), shows net primary production, as measured by a simulated *in situ* ^{14}C technique, and the temperature structure of the upper 700 m, which illustrates the dependence of plant growth upon the hydrography of the surface waters.

The spring flowering was remarkable for the fact that it consisted predominantly of diatoms, this group being numerically abundant only at that one time of the year. At the surface, no single species of diatom was dominant. Of the 19 species observed, ten were present at concentrations between 1,000 and 10,000 cells/litre. At 50 m, on the other hand, there were ten times as many cells present as at the surface, and of these 86% were a small unidentified centric diatom which was not even observed in the surface sample. Unfortunately, our sampling programme did not anticipate the rapid changes which occurred at that time of year, and we have only a single observation of this diatom bloom. At best, however, it was short-lived, for by the middle of May the diatoms were outnumbered by both Coccolithophoridaceae and dinoflagellates.

The dinoflagellates were never dominant in the phytoplankton except in September when the entire population numbered only 1575 cells/litre. They

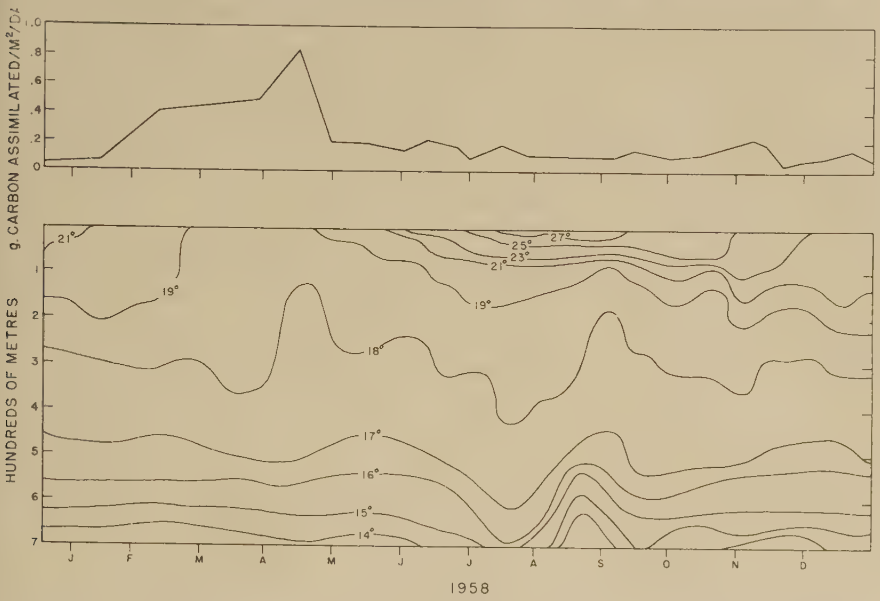

Figure 1. The annual cycle of net primary production and the temperature profile to 700 m in the Sargasso Sea off Bermuda (from RYTHER and MENZEL, in press).

were least abundant in the November–March winter period, and most numerous in the summer and early autumn. Again temperature appears to be the most likely factor controlling their presence.

In the late autumn of both 1957 and 1958 there were minor flowerings which coincided with the breakdown of the summer thermocline and the subsequent enrichment of the surface waters. In contrast to the spring diatom bloom, the autumn outburst was due entirely to an increase of one species of Coccolithophoridaceae, *C. huxleyi*.

The 50 m samples always contained a greater density of phytoplankton than the surface waters (Table 3). The difference was slight during the autumn, winter, and early spring and most pronounced when the surface waters were thermally stratified and vertical mixing presumably negligible. Of 67 species of phytoplankton observed in the surface samples, 31 or 47% were never observed at 50 m. This figure is biased, however, by the fact that more surface samples were counted. But of the 48 species observed in the 50 m samples, 14 or 29% were never seen in the more numerous surface samples. Table 4 shows, for the six times when both surface and 50 m samples were counted, the number of species found only at the surface, those found only at 50 m, and those found at both depths. While some of these differences probably resulted from inadequate counting, there being only a statistical chance of encountering rare species at both depths, there were also cases of species numerically abundant at one depth and absent from the other. Again this occurred most frequently in the summer period when vertical mixing was minimal. Under such conditions, there may be a seasonal succession of species in the upper waters, the older cells settling out and accumulating at greater depths, or mobile organisms may select depths where they are best adapted.

Table 1

Phytoplankton species and numbers in the surface waters (0–10 m) of the Sargasso Sea off Bermuda, November 1957/November 1958 (cells/litre)

	4. Nov.	3. Dec.	21. Jan.	22. Feb.	25. Mar.	15. Apr.	19. May	20. June	26. July	18. Aug.	15. Sept.	18. Oct.	14. Nov.
Bacillariophyceae:													
Bacteriastrum delicatulum	–	60	–	80	300	5800	–	–	–	–	–	–	–
**B. hyalinum*	–	–	–	–	–	1800	–	–	–	–	–	–	–
Cerataulina bergonii	–	–	–	–	–	3000	–	–	–	–	–	–	–
**Chaetoceros affinis*	–	–	–	–	–	200	–	–	–	–	–	–	–
**C. danicus*	–	–	–	–	–	–	–	–	–	15	–	–	–
**C. decipiens*	–	–	–	–	–	1000	–	–	–	–	–	–	–
**C. didymus*	–	–	–	–	–	200	–	–	–	–	–	–	–
C. laciniosus	–	–	–	–	–	1000	–	–	–	–	–	–	–
C. spp.	–	–	30	–	40	1400	–	–	–	–	–	–	–
Eucampia zoodiacus	–	–	–	–	–	1500	–	–	–	–	–	–	–
**E.* sp.	–	–	–	–	–	400	–	–	–	–	–	–	–
Hemiaulus hauckii	–	–	–	–	–	–	–	–	15	–	30	40	–
H. membranaceus	–	–	–	–	–	–	–	–	–	–	45	–	–
**Lauderia borealis* (?)	–	–	–	–	120	–	–	–	–	–	–	–	–
Leptocylindrus danicus	–	–	–	–	–	2300	–	–	–	–	–	–	–
**Nitzschia closterium* v. *recta*	–	–	–	–	–	200	–	–	–	–	–	–	–
N. delicatissima	–	–	–	–	–	1000	–	–	–	–	–	–	–
**N. seriata*	–	–	–	–	–	700	102	–	–	–	–	–	–
**Planktoniella sol*	–	–	30	–	–	–	–	–	–	–	–	–	–
**Rhabdosphaera stylifer*	–	–	–	–	–	–	–	–	–	–	–	20	–
Rhizosolenia alata	–	–	–	–	–	–	220	–	–	–	–	–	–
R. calcar avis	–	–	–	–	–	100	34	–	–	–	–	–	–
R. imbricata v. *shrubsolei*	–	30	–	–	–	–	–	–	–	–	–	–	–
R. stolterfothii	–	150	60	140	20	6500	–	–	–	–	–	–	–
**Stephanopyxis palmeriana*	–	–	–	–	40	–	–	–	–	–	–	–	–
Stigmophora rostrata	–	–	–	–	–	–	–	–	65	–	75	–	–
**Thalassionema nitzschioides*	–	210	–	–	–	–	–	–	–	–	–	–	–
**Thalassiothrix frauenfeldii*	–	–	–	–	–	300	–	–	–	–	–	–	–
**T. mediterranea*	–	–	–	–	–	600	–	–	–	–	–	–	–
Thalassiosira rotula	–	–	–	–	–	1200	–	–	–	–	–	–	–
Unidentified pennate diatoms	–	90	30	–	–	100	–	24	65	180	60	100	135
Unidentified centric diatoms	–	–	–	–	20	–	–	–	–	–	–	–	–
Chrysophyceae (Coccolithophoridaceae):													
**Braarudosphaera bigelowii*	–	–	–	–	–	–	34	–	–	–	–	–	–
Calciosolenia granii	15	–	–	–	–	–	34	–	13	–	–	–	–
**C. granii* v. *closterium*	–	–	–	–	–	–	–	–	–	–	–	–	30
Calyptrosphaera globosa (?)	–	–	–	–	80	–	612	24	[illegible]	[illegible]	[illegible]	[illegible]	[illegible]

C. leptoporus	90	60	600	20	–	–	–	192	26	15	60	160	150
**C. wallichii*	–	30	–	–	–	–	–	–	–	–	–	–	15
Deutschlandia anthos	45	–	–	–	–	–	–	–	–	–	–	–	–
Discosphaera tubifer	105	210	–	–	–	–	34	288	260	60	210	220	165
Heyneckia barkowii	–	–	–	–	–	–	–	–	13	–	–	40	–
Michaelsarsia elegans	–	30	30	–	–	–	–	–	–	–	–	–	–
M. falklandia	–	30	–	–	–	–	–	–	–	–	–	–	–
Ophiaster hydroideus	–	–	60	–	–	–	–	–	–	–	–	–	–
**Pontosphaera nigra*	–	–	–	–	–	–	–	–	–	15	–	–	–
Rhabdosphaera hispida	–	30	–	–	–	–	68	–	–	–	–	–	–
Syracosphaera heimii	–	–	90	–	20	–	374	96	–	30	–	–	120
S. pulchra	90	90	–	–	–	–	102	120	13	75	45	–	–
Umbilicosphaera mirabilis	–	30	–	–	–	–	–	–	–	–	–	–	30
Unidentified	–	–	180	–	–	–	–	48	–	45	–	–	–
Dinophyceae and Desmokontae:													
**Ceratium extensum*	–	–	30	–	–	–	–	–	–	–	–	–	–
**C. fusus*	–	–	–	–	–	–	–	–	–	–	15	–	–
**C. teres*	–	–	–	–	–	–	34	24	13	15	45	–	–
Cladopyxis setifera	–	–	–	–	–	–	–	–	–	–	–	–	30
**Dinophysis ovum*	–	–	–	–	–	300	–	–	–	–	–	–	–
**Goniodoma polyedricum*	–	–	–	–	–	–	–	–	–	–	15	–	–
Gymnodinium punctatum	–	–	30	–	–	–	–	24	–	–	–	–	–
Katodinium rotundatum	–	–	–	–	–	102	–	120	26	120	330	160	–
Oxytoxum scolopax	–	–	–	–	–	–	–	–	–	–	15	–	–
O. sphaeroideum	–	30	–	–	–	–	–	24	13	60	195	100	–
O. variabile	45	–	90	20	20	102	–	96	52	15	135	60	15
**Peridinium globulus*	15	–	–	–	–	–	–	–	–	–	–	–	–
**Podolampus palmipes*	–	–	–	–	–	–	–	–	–	15	–	–	–
**Porella perforata*	–	–	–	–	–	–	34	–	–	–	–	–	–
**Pyrocystis obtusa*	–	–	–	–	–	–	–	–	–	–	–	20	–
Unidentified	30	–	–	–	–	200	306	48	143	90	75	20	–
Chlorophyceae:													
**Carteria excavata*	–	–	30	–	–	–	–	–	–	–	–	20	–
Cryptophyceae:													
**Chilomonas marina*	–	–	–	–	–	–	–	–	–	–	–	30	–
Euglenophyceae:													
**Eutreptia* sp.	–	–	–	20	–	–	·	·	26	–	30	–	–
Myxophyceae:													
**Trichodesmium thiebaudii*	–	–	–	–	–	–	–	–	13	–	–	–	–

* Not observed at 50 m.

Table 2

Phytoplankton species and numbers at 50 m in the surface waters of the Sargasso Sea off Bermuda, November 1957/November 1958 (cells/litre)

	3. Dec.	21. Jan.	25. Mar.	15. Apr.	20. June	18. Aug.
Bacillariophyceae:						
Bacteriastrum delicatulum	–	–	180	–	–	–
Cerautulina bergonii	–	–	60	–	–	–
**Chaetoceros densus*	–	–	–	620	–	–
C. laciniosus	–	–	40	1860	–	–
Eucampia zoodiacus	–	–	–	620	–	–
Hemiaulus hauckii	–	–	–	–	–	13
H. membranaceus	180	–	–	–	88	–
Leptocylindrus danicus	–	–	–	620	–	–
**Nitzschia closterium*	30	–	–	620	–	–
N. delicatissima	80	–	–	7440	–	–
**Rhabdosphaera hispida*	–	–	–	–	–	104
Rhizosolenia alata	–	–	–	–	22	–
R. calcar avis	120	–	–	–	–	–
R. imbricata v. *shrubsolei*	30	–	20	–	–	–
R. stolterfothii	30	–	40	11780	–	–
**Skeletonema costatum*	–	–	–	5580	–	–
Stigmophora rostrata	–	–	–	–	22	–
Thalassiosira rotula	–	–	–	1240	–	–
Unidentified pennate diatoms	90	–	20	620	22	78
Unidentified centric diatoms	–	–	–	197160	–	–
Chrysophyceae (Coccolithophoridaceae):						
**Acanthoica acanthifera*	–	20	20	–	–	–
Calciosolenia granii	30	40	–	–	–	–
Calyptrosphaera globosa (?)	30	40	–	–	–	–
**C.* sp.	–	–	–	–	22	–
Coccolithus huxleyi	12900	2820	7540	5580	1390	–
C. leptoporus	270	540	200	620	264	64
Deutschlandia anthos	–	–	–	–	22	-
Discosphaera tubifera	210	–	–	–	396	–
Heyneckia barkowii	–	–	–	–	198	26
Michaelsarsia elegans	–	20	–	–	–	–
M. falklandia	30	80	–	–	–	–
Ophiaster hydroideus	–	240	–	–	–	–
**Pontosphaera syracusana*	–	20	–	–	–	–
Rhabdosphaera hispida	–	–	–	–	220	–
**Syracosphaera cornifera*	–	–	–	–	–	156
**S. dentata*	–	–	–	–	66	–
S. heimii	–	120	60	–	–	–
S. pulchra	120	–	–	–	220	130
Umbilicosphaera mirabilis	60	–	–	–	–	–
Unidentified	30	120	100	–	–	13
Dinophyceae and Desmokontae:						
**Ceratium pentagonium*	–	–	–	–	66	–
**C. trichoceros*	–	20	–	–	–	–
Cladopyxis setifera	–	–	–	–	88	13
**Exuviella baltica*	–	20	–	–	–	–
Gymnodinium punctatum	–	20	20	–	22	–
Katodinium rotundatum	–	–	–	–	110	234
Oxytoxum scolopax	–	–	–	–	66	–
O. sphaeroideum	–	–	–	–	44	130
O. variabile	–	-		-	242	91
**Prorocentrum dentatum*		-		–	22	-
**P. gracile*	–	–	–	–	22	–
Unidentified	–	–	20	620	176	39

* Not observed at surface.

Table 3

Relative proportions of the major groups of phytoplankton (cells/litre), chlorophyll *a* concentrations (μg/l), chlorophyll *a*/cell (mg), and water temperature (°C) at the surface and at 50 m in the Sargasso Sea off Bermuda

	4. Nov.	3. Dec.	21. Jan.	22. Feb.	25. Mar.	15. Apr.	19. May	20. June	26. July	18. Aug.	15. Sept.	18. Oct.	14. Nov.
Diatoms													
surface	–	540	150	220	540	30200	357	24	130	210	210	160	134
50 m	–	480	80	–	360	228160	–	154	–	91	–	–	–
Dinoflagellates													
surface	90	30	120	20	20	500	578	336	275	315	825	360	45
50 m	–	–	60	–	40	620	–	912	–	507	–	–	–
Coccolithophoridae (excl. *C. huxleyi*)													
surface	335	510	1020	40	100	–	1258	768	364	300	345	480	525
50 m	–	780	1270	–	380	620	–	1958	–	502	–	–	–
C. huxleyi													
surface	4740	12900	2700	720	6400	200	917	1010	234	60	195	800	12600
50 m	–	12900	2820	–	7540	5580	–	1390	–	–	–	–	–
Total cells													
surface	5165	13980	3990	1000	7060	30900	3110	2138	1003	885	1575	1800	13305
50 m	–	14160	4230	–	8320	234980	–	4260	–	1100	–	–	–
Ratio, no. cells													
surface/50 m	–	·99	·95	–	·85	·13	–	·50	–	·80		–	–
% dominance of most abundant single species													
surface	92	93	71	72	91	23	33	56	30	21	23	48	96
50 m	–	92	69	–	90	85	–	36	–	24	–	–	–
Chlorophyll *a*													
surface	·70	·38	·37	·34	·45	·88	·09	·07	·11	·16	·08	·24	·34
50 m	–	·47	·39	–	·48	1·00	–	·19	–	·13	–	–	–
Chlorophyll *a*/cell ($\times 10^{-8}$)													
surface	14·0	2·7	9·5	34·0	6·5	2·8	2·9	3·3	11·0	20·0	4·8	13·0	2·5
50 m	–	3·3	9·5	–	5·8	0·5	–	4·7	–	12·0	–	–	–
Temperature													
surface	24·35	22·0	20·5	18·5	18·3	18·5	21·3	24·1	28·0	28·5	27·0	25·9	23·1
50 m	–	21·6	20·4	–	18·3	18·2	–	21·5	–	24·3	–	–	–

Indeed the restriction to one or the other depth appears to be most pronounced in the dinoflagellates which are known to be migratory and depth selective in response to light (Hasle, 1950). Both Steemann Nielsen (1934) and Graham and Bronikovsky (1944) were able to differentiate between surface- and deep-dwelling species of the dinoflagellate *Ceratium*. Finally, under conditions of thermal stratification, entire populations, differing in their environmental requirements from the surface forms, mày develop at these greater depths. It is impossible to decide which of these is the correct explanation without more intensive studies than we have attempted so far. The problems of vertical stratification of phytoplankton populations, settling rates in nature, depth selectivity, and vertical migration obviously need more attention. Until such time, it is difficult to conclude whether physiological differences between surface and deep-water phytoplankton, such as their responses to light (i. e. Steemann Nielsen and Hansen, 1959; Ryther and Menzel, 1959) are due to the presence of different endemic populations at these depths or to adaptation to the different environments by the same species.

Diversity

Between May and October, the total cell concentration at both the surface and at 50m was 4,000/litre or less. The ratio of concentration of the most abundant species to the total cell concentration was usually less than 0·5 or, in other words, there was less than 50% dominance. From November through March the number of cells per litre, with one exception, was greater than 4,000 and dominance by a single species was 70% or more. During the May–October, or summer period the coccolithophorid, *Discosphaera tubifer*, was dominant once and the dinoflagellate, *Katodinium rotundum* (ex *Massartia rotunda*), three times. All other summer samples and all winter samples were dominated by *Coccolithus huxleyi*. The percentage dominance by the most abundant single species is shown for each sample in Table 3.

In the counting of a phytoplankton sample, the number of species encountered normally increases at a rate roughly proportional to the logarithm of the number of individuals enumerated. If, in counting progressively larger aliquots of a given sample, the numbers of species and individuals are separately recorded, the relationship between these variables may be described by the index of diversity (α), as obtained from an expression derived by Fisher, Corbett and Williams (1943)

$$S = \alpha \log \left(\frac{N}{\alpha} + 1 \right)$$

where S is the number of species and N, the number of individuals. The diversity index (α) is constant for a given population, or true sample of a population, and differs only as the number of species for a given number of individuals changes from sample to sample. Thus within a single sample, if the number of species encountered increases with the number of individuals counted, as predicted from theory, the plot of species against individuals should fall on a line of constant α. Figure 2 shows that this was the case for samples taken between May and October. If the number of species does not increase as expected, the plot of species against individuals cuts across lines of constant α. In samples taken between November and May, the observed points always cut across lines of constant α in the same way; as the number

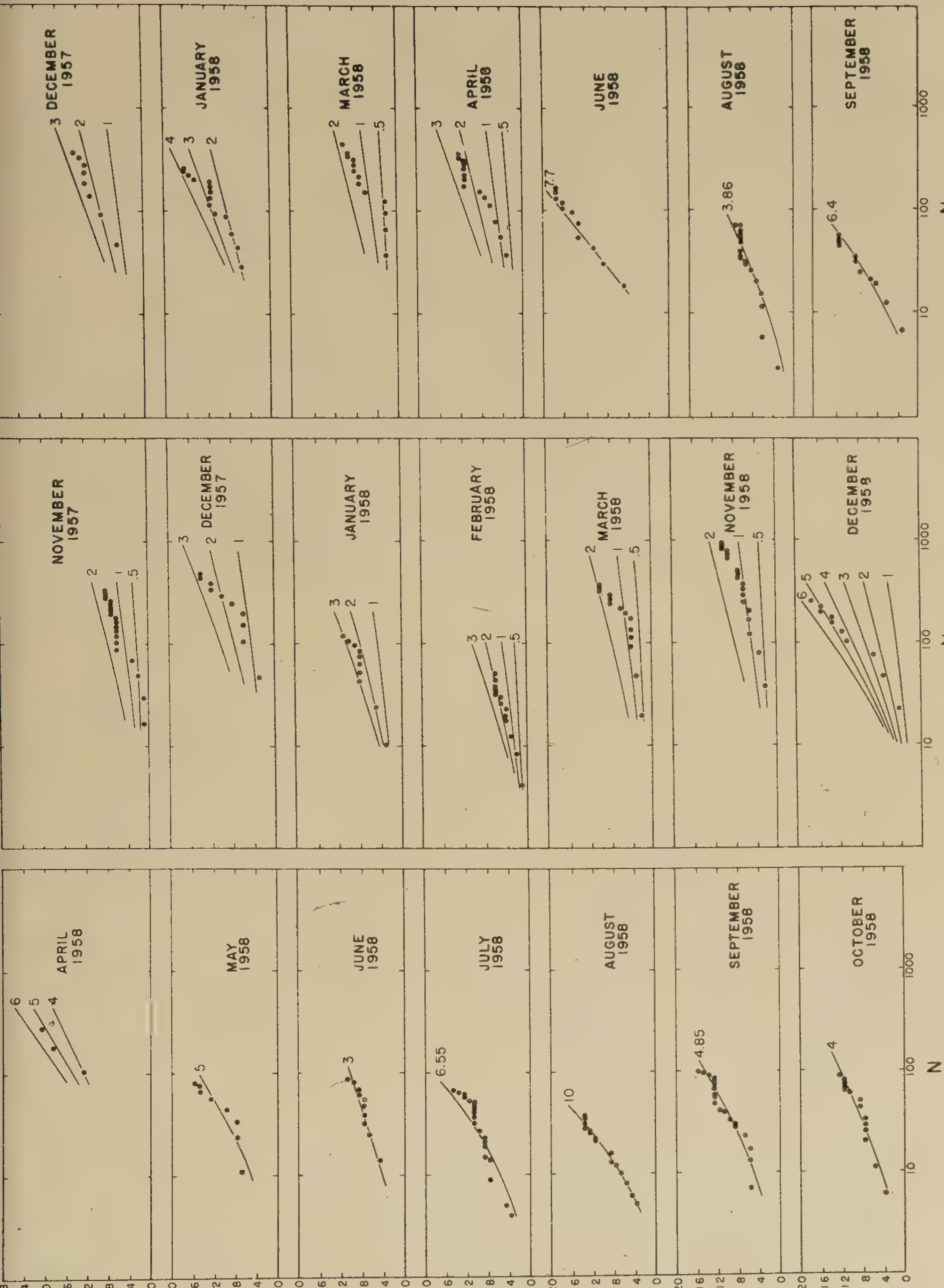

Figure 2. The index of diversity (α) of summer surface samples, winter surface samples, and 50m samples of the phytoplankton in the Sargasso Sea off Bermuda. Values of constant α are shown as numbered lines. Points show observed species-numbers relations.

of individuals counted increased, there was in every case a progressively larger number of species than expected (Figure 2).

The final value of α achieved in the winter samples ranged from three, the lower limit of the summer values, to five, well within the summer range. Thus, one is led to suspect that, if really large numbers of cells had been counted during the winter period, all the final values of α would have fallen within the summer range. The departure from theory during the winter months, then, seems to have resulted from the disproportionate growth of a single species, the same number of less abundant forms persisting from summer to winter.

Consider now the radically different situation in April. At the surface many of the species appearing in the counts were rare enough previously to have been undectectable, while many which had been prevalent at other times were now too scarce to be recorded. There were still a large number of minor species, those rarities that turn up as counting proceeds. But dominance, rather than being restricted to a single species, was shared by a dozen diatoms whose cell concentrations differed by less than an order of magnitude. At the same time, at 50 m there was a high degree of dominance (85%) by a small centric diatom not recorded at the surface or at either depth at any other time of year. Clearly, the surface and 50 m populations were quite distinct, and at both depths, different from those present throughout the rest of the year.

Discussion

From the three criteria which we have discussed, abundance, species composition, and diversity, we can describe the effects of the changing environment upon the phytoplankton community. It is probably only because these changes are gradual and relatively slight in the semi-tropical Bermuda region that we can detect and evaluate them. In any case, we see what may be interpreted as three stages in phytoplankton succession. The first, encountered during the May–October "summer" period, is characterized by a meagre population with the "normal" distribution of abundant and rare species. The physical environment may change during this period and exert selective pressure on species composition. Thus dominance passes from the Coccolithophoridaceae to the dinoflagellates as the summer progresses, probably as a result of rising temperature. But the biological environment controlling the growth of the plants (i.e. nutrients) is constant and, thus, abundance and diversity remain the same.

The second stage of succession began with the breakdown of the summer thermocline in November. The resulting enrichment of the surface waters was a slow and intermittent process; at the same time radiation was decreasing. The growth potential of the phytoplankton increased only to a limited extent, the population increasing in abundance by 2–3 fold. This increase was confined to the growth of a single species, *C. huxleyi*, which attained dominance in November and maintained it throughout the winter. Why this species was favoured over others present in nearly equal numbers in the early autumn cannot be explained. The point is, however, that the increase in the growth potential was slow enough and the environment rigorous enough to permit the selective action of some one or more chemical or physical factors upon this one species. Furthermore, throughout the ensuing winter period, growth conditions were never favourable enough to remove this selective pressure and thereby permit the general growth of the population.

Table 4

The numbers of species found only at the surface, only at 50 m, and at both depths

	Surface only	50 m only	Surface and 50 m
13. December	6	6	8
21. January	5	7	6
25. March	4	6	3
15. April	15	6	5
20. June...........	4	13	8
18. August.........	8	5	5

This situation changed abruptly in April with the onset of thermal stratification and the development of the third stage of succession. The phytoplankton in the euphotic zone had sudden access to nutrients and light, the growth potential increasing 10 fold over its summer level. Conditions became favourable for an entire group of plants, the diatoms. Undoubtedly, the environment favoured the growth of some species more than others, but competition and selection were unimportant for this brief period; at least a dozen diatoms could grow at rates limited mainly by their intrinsic growth potentials.

This was not the case at 50 m, however, where one species of diatom, absent from the surface, was strongly dominant. Perhaps at that depth, reduced illumination exerted sufficient selective pressure to prevent the general augmentation of the diatom population which appeared to take place at the surface.

Thus we have observed in the Bermuda waters three different types of phytoplankton communities, one consisting of sparse populations existing under marginal conditions, with the "normal" distribution of abundant and rare species; the second, living under improved but still limiting conditions, in which selective pressure favours the dominance of a single species with the minor species continuing to exist at a subsistence level; and the third, under optimal growth conditions, in which selection is largely inoperative and dominance is shared by several species. We have referred to these community types as representative of three stages of phytoplankton succession. This has the unfortunate implication that the three stages should follow each other in some regular way, and that they are interrelated. This is probably not true. It appears more likely that the communities we have described are dependent entirely upon their physical-chemical environment, and that they may follow each other in any order.

Nanoplankton

Our discussion would not be complete without some consideration of the nanoplankton or "μ"-plankton. However, the separation of this group from the phytoplankton, wholly unsatisfactory for ecological consideration to begin with, is also rather arbitrary. Thus many of the small flagellates and Coccolithophoridaceae which have been enumerated and included in our counts, as for example the dominant *Coccolithus huxleyi*, might well be included in the nanoplankton. We can only say, therefore, that we have not included in our counts a vast array of tiny microorganisms of the general size of 1–5 μ which, when looked for, are always found at a high level of numerical abundance in our samples. Of uncertain taxonomic position and mode of existence, these organisms play an unknown but almost certainly an important role in marine ecology. In recent years many investigators have emphasized the quantitative significance of this group in the marine plankton, one of the most recent of such references by RILEY (1957) relating to the north central Sargasso Sea. Our preliminary observations of nanoplankton in the Bermuda region confirm RILEY's conclusions concerning the importance of this group.

While we have not attempted routine examination and enumeration of the nanoplankton (which will refer henceforth to those organisms not included in Tables 1 and 2) we have made cursory examinations of samples collected for this purpose at various times of the year. Duplicate 250 ml samples were preserved with 2% formalin and with I_2-KI in acetic acid. These were concentrated to 40 ml by sedimentation, and a 10 ml aliquot of the concentrate was placed in a Zeiss sedimentation chamber, the organisms allowed to settle again, and the concentrated organisms were then examined under 1350× magnification with a water immersion lens. One such pair of samples, collected on 2. December 1958, will be discussed briefly below.

While we could not identify most of the organisms, or frequently even place them into major taxonomic groups, we could separate the majority of the nanoplankton into the following three categories: (1) naked flagellates, small Coccolithophoridaceae, and diatoms, (2) coccoid cells about 3·5 μ in diameter, and (3) colourless filaments about $0{\cdot}5 \times 10\text{–}20\ \mu$.

The first group consisted mainly of flagellates and were recognizable by their flagellae and their irregular shape. This group was better preserved by the I_2-KI except for the Coccolithophoridaceae, whose coccoliths were destroyed by the acid. The second group of thick-walled spherical cells were very uniform in size (3·5 μ) and were the most abundant form in these samples. They occurred singly or, more commonly, in clusters or sporangia-like "heads". One complete fungus-like organism observed in this sample bore a cluster of the same coccoid cells, which leads us to suspect that they are fungal spores. However, remarkably similar forms have been recently reported from the Pacific and other oceanic regions by KRISS and MITZKEVICH (1958) who described them as a new class of microorganisms. The third group, the filaments, were not enumerated because they were frequently clumped. Since many of them were branched, they are suspected of being fungal mycelia. They appeared to be more abundant in the I_2-KI preservative, perhaps because the iodine-staining made them more visible.

Omitting the filaments, the counts on this one pair of samples are summarized below.

	Formalin	I_2-KI
Flagellates, small phytoplankton ..	290,000/litre	800,000/litre
"Spores"......................	2,900,000/litre	1,080,000/litre

Counts of this general order of magnitude have been obtained from samples collected at other times of the year in the Bermuda region. Organisms in the first category alone are thus 100 times more numerous than the phytoplankton listed in Tables 1 and 2. If the average nanoplankton were 4 μ in diameter as compared with perhaps 25 μ for the larger phytoplankton, the biomass of the two groups would be about the same. Unfortunately we do not know what fraction of the nanoplankton is autotrophic, but there is further evidence that the photosynthetic activity of this group may be far more important than that of the larger cells.

If we divide the total cell count into the chlorophyll concentration of the water, we obtain values for chlorophyll per cell ranging from 10^{-8} to 10^{-7} mg (Table 3). The lower limit is about comparable to the chlorophyll content of large diatoms, such as *Rhizosolenia alata* and *Ditylum brightwellii* (FLEMING, 1940) and one or two orders of magnitude greater than that of smaller diatoms, such as *Skeletonema costatum* and *Phaeodactylum tricornutum* (YENTSCH and RYTHER, 1959). Yet a great majority of the cells counted were *Coccolithus huxleyi*, which is smaller than any of these diatoms. If the chlorophyll values have any validity, this would indicate that our total cell counts reported in Table 3 include but a small fraction, in terms of biomass as well as numbers, of the autotrophic organisms. Thus while consideration of the larger phytoplankton alone may provide information concerning community structure and change, quantitative ecological evaluation of the autotrophic level in the sea must include all photosynthetic forms, of which the nanoplankton may be of prime importance.

Summary

1. Seasonal changes in the abundance, species composition, and diversity of the phytoplankton in the Sargasso Sea have been examined and discussed. The data are based upon a series of samples collected at monthly intervals from the surface and from 50 m at a station 15 miles SE of Bermuda.

2. Total cell counts ranged from approximately 1000 to 200,000 per litre, with lowest numbers observed in the summer (May–October), a small flowering in November, and a larger bloom in April. The population was dominated by Coccolithophoridceae during most of the year, and by a single species, *Coccolithus huxleyi*, for more than half the year. The absence of this species in summer is presumed to have resulted from high temperatures, other coccolithophorids and dinoflagellates dominating the plankton during that period. Diatoms were relatively insignificant except during the spring flowering, which lasted for no more than one month. At least 10 species of diatoms were about equally abundant in the surface waters during this bloom, while at 50 m one diatom species accounted for 85% of the total population.

3. Higher cell concentrations were invariably found at 50 m rather than at the surface, the difference being most pronounced in summer. At any one time, over half the species found either at the surface or at 50 m were not present at both depths simultaneously.

4. Three different types of community structure, as revealed by abundance, species composition, and diversity, are considered as representing three stages of phytoplankton succession.

5. The nature and significance of the nanoplankton are discussed briefly.

References

FISHER, R. A., CORBETT, A. S., & WILLIAMS, C. B., 1943. "The relation between the number of species and the number of individuals in a random sample of an animal population". J. Anim. Ecol., **12**: 42–58.

FLEMING, R. H., 1940. "Composition of plankton and units for reporting populations and production". Proc. Pacif. Sci. Congr. Calif., **3**: 535–40.

GRAHAM, H. W., & BRONIKOVSKY, N., 1944. "The genus *Ceratium* in the Pacific and North Atlantic Oceans". Publ. Carneg. Instn., No. 565: 209 pp.

Hasle, G. R., 1950. "Phototactic vertical migration in marine dinoflagellates". Oikos, **2**: 162–75.

Kriss, A. E., & Mitzkevich, I. N., 1958. "Krassilnikoviae: A new class of micro-organisms found in the sea and ocean depths". J. gen. Microbiol., **19**: 1–12.

Menzel, D. W., & Ryther, J. H. (in press). "The annual cycle of primary production in the Sargasso Sea off Bermuda". Deep-Sea Res.

Mjaaland, G., 1956. "Some laboratory experiments on the coccolithophorid *Coccolithus huxleyi*". Oikos, **7**: 251–55.

Riley, G. A., 1957. "Phytoplankton of the North Central Sargasso Sea, 1950–1952". Limnol. Oceanogr., **2**: 252–70.

Ryther, J. H., & Menzel, D. W., 1959. "Light adaptation by marine phytoplankton". Limnol. Oceanogr., **4**: 492–97.

Ryther, J. H., & Menzel, D. W. (in press). "The seasonal and geographical range of primary production in the Western Sargasso Sea". Deep-Sea Res.

Steemann Nielsen, E., 1934. "Untersuchungen über die Verbreitung, Biologie und Variation der Ceratien im südlichen Stillen Ozean". Dana-Rep., **4**: 1–67.

Steemann Nielsen, E., & Hansen, V. Kr., 1959. "Measurements with the carbon-14 technique of the respiration rates in natural populations of phytoplankton". Deep-Sea Res., **5**: 222–33.

Yentch, C. S., & Ryther, J. H., 1959. "Relative significance of the net phytoplankton and nanoplankton in the waters of Vineyard Sound". J. Cons. int. Explor. Mer, **24**: 231–38.

Contribution No. 1069

Särtryck ur Tellus nr 2, 1960

Further Examples of Stationary Planetary Flow Patterns in Bounded Basins[1]

By ALAN J. FALLER, Woods Hole Oceanographic Institution, Woods Hole, Massachusetts

(Manuscript received August 28, 1959)

Abstract

Laboratory experiments which supplement those presented by Stommel, Arons and Faller (1958) are described. Extension of the analysis to include the effects of bottom friction shows that the characteristic spreading of zonal currents, apparent in the original experiments, is due to bottom friction combined with the radial depth variation. The experiments confirm the theoretical prediction of an intense "recirculation" from the western boundary (similar to the "wind-spun vortex" of Munk, 1950) when a localized interior source or sink is present. Application of the basic concepts of the earlier paper to the geometrically more complicated case with a partial radial barrier gave good agreement between theory and experiment, but the limiting effects of bottom friction were made evident in other examples.

An eastern boundary current was found to occur in a situation geometrically similar to the intrusion of Mediterranean water into the Atlantic Ocean. Simple transformations illustrate the application of the equations developed in polar coordinates to the flow of a uniform fluid on a sphere, and examples of "recirculation" and the spread of zonal flow are worked out for a barotropic ocean of uniform depth.

. Introduction

A recent paper by Stommel, Arons, and ALLER (1958) hereafter referred to as (A) set orth qualitative and quantitative *a priori* pre-ictions of the circulation in a bounded basin in vhich the source of energy for the flow was he pressure head set up by the introduction nd/or extraction of mass at various locations n the fluid. Specifically the analysis pertained o the circulation of a homogeneous layer of uid in a pie-shaped basin rotating about the pex of the sector. Because of the rotational onstraint the flow could be considered geo-trophic and two-dimensional except for certain oundary regions in which the viscous and/or nertia forces could produce appreciable departures from geostrophic flow. The predictions of the simple theory were borne out by subsequent laboratory experiments.

This paper presents the results of some additional related experiments and expands upon details of the flow patterns of the earlier work. As in (A) the experiments are restricted to depths of fluid and rotation rates such that the flow is primarily geostrophic, but in addition to departures from geostrophy near the side boundaries the specific effects of the bottom frictional boundary layer are considered. It is shown that bottom friction is a most important consideration for situations where there are no unbroken radial barriers, and indeed the effects of bottom friction may be observed and are of some significance in all of the experiments.

The analysis described in (A) is extended here to somewhat more complicated regimes of geophysical interest, namely the circulation with a partial radial barrier and the "recirculation" associated with localized interior sources or sinks of fluid.

---

[1] This work was supported by a contract with the Office f Naval Research and is Contribution No. 1069 from the Voods Hole Oceanographic Institution.

An unanticipated development was the occurrence of *eastern* boundary currents in certain circumstances. It was asserted in (A) that only *western* boundary currents would occur and this assertion seemed to be a justified one on the basis of the original experiments. It now appears that eastern boundary currents of inertial character are possible when fluid is introduced through a slot in the eastern boundary in such a manner that viscosity may generate negative absolute vorticity.

Finally the theory for the flat rotating tank is extended to a spherical shell of fluid. The recirculation phenomenon and the spread of zonal flow are computed as examples of what might be expected for barotropic flow in an ocean basin of constant depth.

2. Equations for the Interior Circulation

The polar equations of motion and the continuity equation for a uniform fluid with an arbitrary distribution of sources (or sinks) are (Dryden, Murnaghan, and Bateman, 1956):

$$\frac{dv_r}{dt} - \frac{v_\Theta^2}{r} - \underline{2\Omega v_\Theta} = \underline{-\frac{1}{\varrho}\frac{\partial p}{\partial r}} +$$

$$+\nu\left\{\underline{\frac{\partial^2 v_r}{\partial z^2}} + \frac{1}{r}\frac{\partial^2 r v_r}{\partial r^2} - \frac{v_r}{r^2} + \frac{1}{r^2}\frac{\partial^2 v_r}{\partial \Theta^2} - \frac{2}{r^2}\frac{\partial v_\Theta}{\partial \Theta}\right\} \quad (1)$$

$$\frac{dv_\Theta}{dt} + \frac{v_r v_\Theta}{r} + \underline{2\Omega v_r} = \underline{-\frac{1}{\varrho r}\frac{\partial p}{\partial \Theta}} +$$

$$+\nu\left\{\frac{\partial^2 v_\Theta}{\partial z^2} + \frac{1}{r}\frac{\partial^2 r v_\Theta}{\partial r^2} - \frac{v_\Theta}{r^2} + \frac{1}{r^2}\frac{\partial^2 v_\Theta}{\partial \Theta^2} + \frac{2}{r^2}\frac{\partial v_r}{\partial \Theta}\right\} \quad (2)$$

$$\frac{dw}{dt} = \underline{-\frac{1}{\varrho}\frac{\partial p}{\partial z}} - g +$$

$$+\nu\left\{\frac{\partial^2 w}{\partial z^2} + \frac{\partial^2 w}{\partial r^2} + \frac{1}{r}\frac{\partial w}{\partial r} + \frac{1}{r^2}\frac{\partial^2 w}{\partial \Theta^2}\right\} \quad (3)$$

$$\underline{\frac{\partial w}{\partial z}} + \underline{\frac{1}{r}\frac{\partial r v_r}{\partial r}} + \underline{\frac{1}{r}\frac{\partial v_\Theta}{\partial \Theta}} = P \quad (4)$$

where the r direction is radially outward, Θ is in direction of rotation (counterclockwise) and z is vertically upward. P is a source of fluid per unit of volume. Dimensional arguments may be used to show that for: 1) small flow rates, 2) small horizontal shear, 3) a steady state, and 4) large radius the equations reduce to those terms which are underlined and which were the equations used by Ekman (1905) in his studies of wind driven ocean currents. Again from dimensional arguments or from the solutions given below one may see that the depth of a viscous boundary layer at a rigid horizontal surface should be characterized by the Ekman depth $D_E = \pi\left(\frac{\nu}{\Omega}\right)^{\frac{1}{2}}$, so that far from the boundaries $(z \gg D_E)$ we may omit the vertical derivatives in 1) and 2) to obtain the geostrophic equations

$$v \equiv v_{\Theta g} = \frac{1}{2\Omega\varrho}\frac{\partial p}{\partial r} \quad (5)$$

$$u \equiv v_{rg} = -\frac{1}{2\Omega\varrho r}\frac{\partial p}{\partial \Theta} \quad (6)$$

$$\frac{\partial r u}{\partial r} + \frac{\partial v}{\partial \Theta} = 0. \quad (7)$$

Therefore for a total depth of fluid $h \gg D_E$ with a free surface the following lower and upper boundary conditions apply:

at $z = 0$: $v_{r_0} = v_{\Theta_0} = w_0 = 0$

at $z = h$: $v_{\Theta_h} = v$

$v_{r_h} = u$

$$w_h = u\frac{\partial h}{\partial r} + \frac{v}{r}\frac{\partial h}{\partial \Theta} + \frac{\partial h}{\partial t} \quad (8)$$

where $\frac{\partial h}{\partial t}$ is the depth variation associated with a steady rise or fall of the free surface. The depth variation h' due to the steady geostrophic currents need not be considered in the expression for w_h since $\vec{V}_g \cdot \nabla h' = 0$.

Since the boundary layer circulation decreases exponentially with height, we may safely take the upper limit of integration in exponential expressions as $h = \infty$ and so obtain as solutions to 1) and 2):

$$v_r = u - e^{-\pi\frac{z}{D_E}}\left(u\cos\pi\frac{z}{D_E} + v\sin\pi\frac{z}{D_E}\right) \quad (9)$$

$$v_\Theta = v - e^{-\pi\frac{z}{D_E}}\left(u\sin\pi\frac{z}{D_E} - v\cos\pi\frac{z}{D_E}\right). \quad (10)$$

By substitution of these expressions into equation 4) we find:

$$\frac{\partial w}{\partial z} + e^{-\pi\frac{z}{D_E}}\sin\pi\frac{z}{D_E}\left(\frac{1}{r}\frac{\partial u}{\partial\Theta} - \frac{1}{r}\frac{\partial rv}{\partial r}\right) = P. \quad (11)$$

Vertical integration of (11) from $z=0$ to $z=h(\infty)$ together with the boundary conditions (8) yields the following equation for the geostrophic flow:

$$u\frac{\partial h}{\partial r} + \frac{v}{r}\frac{\partial h}{\partial\Theta} + \frac{\partial h}{\partial t} + \frac{D_E}{2\pi}\left(\frac{\partial u}{r\partial\Theta} - \frac{\partial rv}{r\partial r}\right) = Q \quad (12)$$

where $Q = \int_0^h P dz$ is the source of fluid per unit area. Equations (7) and (12) are sufficient to solve for the geostrophic flow given Q, $\frac{\partial h}{\partial r}$, $\frac{\partial h}{\partial\Theta}$, $\frac{\partial h}{\partial t}$ and suitable lateral boundary conditions. Introduction of a stream function defined by $u = \frac{\partial\psi}{r\partial\Theta}$, $v = -\frac{\partial\psi}{\partial r}$ into (7) and (12) and considering only radial depth variations yields:

$$\frac{\partial h}{\partial r}\frac{1}{r}\frac{\partial\psi}{\partial\Theta} + \frac{D_E}{2\pi}\nabla^2\psi = Q - \frac{\partial h}{\partial t}. \quad (13)$$

Equation (13) is of the same form as that derived by STOMMEL (1948) with the following differences: 1) the radial depth variation enters in place of the latitudinal variation of the Coriolis parameter, 2) the effects of bottom friction have been derived more completely rather than to assume a linear friction law, and 3) no specific functional form for the source term has been considered here, whereas STOMMEL assumed a specific wind stress distribution in order to obtain an analytical solution. The above equations will now be specialized for specific examples of interest.

3. Transport across an Annular Ring

As a first test of the adequacy of the Ekman theory as developed above a circular channel with inner radius 50 cm and outer radius 100 cm was set up on the same rotating apparatus as had been used in the earlier experiments. Provision was made for a source of mass continuously distributed around the outer rim and a sink at the inner wall as indicated in Figure 1. In this manner a steady mass transport (S_0) across the channel was forced, and since it was anticipated that this transport would take place entirely in an Ekman layer, the source and sink were arranged to feed the bottom boundary layer directly. If we assume circular symmetry ($u=0$) and take $Q = \frac{\partial h}{\partial t} = \frac{\partial h}{\partial\Theta} = 0$ we immediately obtain from (12) the solution $rv = C$ where the constant C must be determined by the condition on the total mass transport,

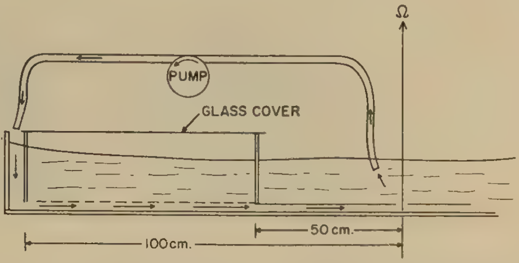

Fig. 1. A schematic diagram of a source-sink experiment in an annular ring with the source continuously distributed around the outer rim and the sink at the inner rim. For relatively slow flow rates the radial mass transport occurs entirely in an Ekman layer.

$$\int_0^{2\pi}\int_0^h r v_r d\Theta\, dz = S_0. \quad (14)$$

Substitution of equation (9) into (14) gives directly:

$$rv = \frac{S_0}{D_E}. \quad (15)$$

The accuracy of this expression, which implies a zonal flow inversely proportional to radius, was examined experimentally with a source strength $S_0 = 8.67$ cm³/sec. The following values of the zonal geostrophic flow were obtained from successive photographs showing the displacements of patches of dye at various radii:

Table 1.

Radius	v	S_p
62.5 cm	.272 cm/sec	7.35 cm³/sec
74	.232	7.31
87	.194	7.45

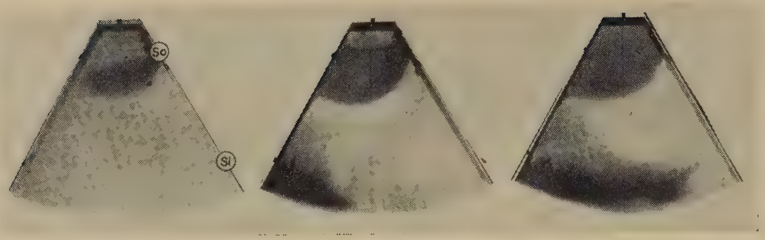

Fig. 2. Reproduced from Stommel, Arons and Faller (1958) to illustrate the spread of zonal flow from the source S_0 as it moved westward and the convergence of the flow as it moved eastward toward the sink S_i.

Values of transport predicted from the zonal flow (S_p) averaged 15 % below the imposed transport $S_0 = 8.67$ cm³/sec.

Estimates of the neglected terms of the equations of motion show these to be three orders of magnitude lower than those of the Ekman equations, (2) and (3), which fact is indicated directly by the Rossby number, $R_0 = \frac{\nu}{\Omega r} \approx .004$. Possible explanations of the discrepancy are: 1) that the bottom boundary surface which was a painted metal surface had some roughness elements which tended to introduce irregular flow and an eddy viscosity above the molecular value $\nu = .01$ at 20° C; 2) that a free surface stress existed because of some properties of the surface film. Other possibilities such as a wind stress or a thermal circulation were eliminated by a sealed glass cover and insulation of the tank. A systematic study of the effects of boundary roughness is planned for the near future, but it is believed that a surface film could easily have caused the observed discrepancy between theory and experiment. Several cases have been observed where contaminants have caused the surface to act as a stationary membrane even in the presence of active (1 cm/sec) circulations within the fluid. Other experiments have shown that flow at the free surface is always somewhat slower than the interior flow. In the present example the Ekman transport produced by a membrane would be radially inward and would augment the transport due to the bottom boundary layer with the result that the required values of ν would be less than with the bottom boundary layer alone.

More extensive experiments of a similar nature have recently been performed by ARONS and BRYAN at the Institute of Meteorology in Stockholm (personal communication) and by GREEN and ARONS (Green, 1959) at Amherst College.

4. The Spread of Zonal Flow from a Point Source due to Bottom Friction.

Some of the experiments illustrated in (A) and subsequent work have shown a rather peculiar spreading of westward flowing zonal currents. Conversely, currents directed eastward toward a point sink seem to broaden near the western boundary where they originate and then converge smoothly toward the sink. Figure 2 reproduced from (A) illustrates the spread of the westward flowing current from the source at the eastern wall near the apex and an orderly convergence of the eastward flow toward the sink. In Figure 6b the stream from the western boundary to the tip of the partial barrier definitely indicated radial spread near the western boundary and convergence as it moved eastward. Other experiments have shown this phenomenon more strikingly.

We consider the flow from a point source in the eastern wall toward the western boundary where we regard the western boundary current as a sink. The circulation in the immediate vicinity of a source is exceedingly complicated and the analytical solution to be obtained can be valid only some distance from the source itself. Equations (7) and (12) are specialized by letting

$$Q = \frac{\partial h}{\partial t} = \frac{\partial h}{\partial \Theta} = 0, \quad \frac{\partial h}{\partial r} = \text{const.},$$

$$\frac{\partial}{\partial y} \equiv \frac{\partial}{r \partial \Theta}, \; \frac{\partial}{\partial x} \equiv \frac{\partial}{\partial r}.$$

These conditions represent 1) no interior sources or sinks of fluid, 2) a constant radial depth variation, and 3) conversion to rectangular coordinates. Then after cross-differentiation to eliminate u we obtain:

$$\frac{\partial h}{\partial x}\frac{\partial v}{\partial y}+\frac{D_E}{2\pi}\left(\frac{\partial^2 v}{\partial y^2}+\frac{\partial^2 v}{\partial x^2}\right)=0\,\cdot \quad (19)$$

The term $\frac{\partial^2 v}{\partial y^2}$ will be omitted since it may be shown in terms of the resultant solution that $\frac{\partial^2 v}{\partial y^2}$ is comparable to $\frac{\partial^2 v}{\partial x^2}$ only near the source.

The equation to be considered is therefore:

$$\frac{\partial^2 v}{\partial x^2}+\frac{2\pi}{D_E}\frac{\partial h}{\partial x}\frac{\partial v}{\partial y}=0 \qquad (20)$$

subject to the integral condition that the transport be constant at any value of y,

$$\int_{-\infty}^{+\infty}\int_{0}^{h}-v\,dz\,dx=S_0. \qquad (21)$$

In this integration we take h as independent of x as a first approximation.

Equation (20) is similar to the one-dimensional heat flow equation $\frac{\partial^2 T}{\partial x^2}-K\frac{\partial T}{\partial t}=0$ where K is the thermometric conductivity. Correspondingly, the integral condition on mass transport (21) is equivalent to supplying a given amount of heat in a pulse at $t=0$ and $x=0$ and thereafter allowing the heat to spread along the rod toward $x=+\infty$ and $x=-\infty$. By analogy, the solution to (20) and (21) is (Carlslaw and Jaeger, 1947):

$$v=\pm\frac{S_0}{h(2\pi)^{\frac{1}{2}}(2Ay)^{\frac{1}{2}}}e^{-\left[\frac{x^2}{2(2Ay)}\right]} \qquad (22)$$

where $A=-\dfrac{D_E}{2\pi\dfrac{\partial h}{\partial x}}$. Inasmuch as A is negative, this solution has meaning only for negative values of y although v may be positive or negative corresponding to a sink or a source respectively at $x=0$, $y=0$. Equation (22) represents a Gaussian distribution of v in x for any distance y from the source and with a standard deviation $\sigma_x=(2Ay)^{\frac{1}{2}}$.

Figure 3 illustrates the derived distribution of zonal and radial flow, of Ekman flow, and the vertical motions for a case with $A=-1$.

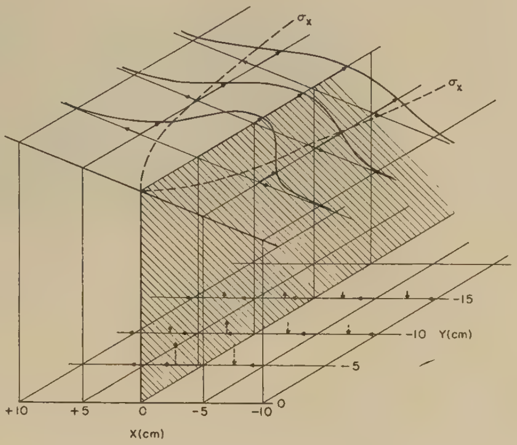

Fig. 3. The theoretical circulation associated with the spread of a westward flowing current from a source at $x=0$, $y=0$ for the value of the parameter $A=-1$.

For negative values of x there exists divergence in the Ekman layer and a loss of mass to the fluid directly above, so that in accordance with the depth variation the interior geostrophic current must have a component toward negative x. The opposite is true for positive values of x, and as a result there is a systematic spreading of the flow. Along the axis of the stream there is clearly a net transport of mass toward positive x by the Ekman flow. Qualitatively this mass is absorbed on the left hand side of the current which is spreading to greater depths and therefore progressively transporting a greater fraction of the mass than the right hand side which is spreading to shallower depths. However, this balance is not quantitatively correct because of the approximation $h=$const. in equation (21) which led to a symmetrical solution. Inspection of $\frac{\partial^2 v}{\partial y^2}$ in comparison with $\frac{\partial^2 v}{\partial x^2}$ indicates that inclusion of this term would tend to retard the divergence of the stream although the effect is already small 10 cm from the source for $A=-1$ (an average value for the experiments).

Quantitative experimental data to support these conclusions are not yet available, but we may estimate the spread of the westward flowing current in Figure 2 and compare this with the theory. The equation of the free surface is:

$$h=h_0\left(1+l\frac{r^2}{a^2}\right) \qquad (23)$$

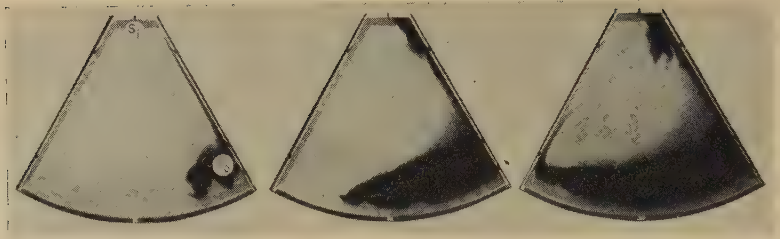

Fig. 4. Photographs at 20, 80 and 136 minutes after the introduction of dye showing the existence of both eastern and western boundary currents for the case where the source water was injected through a slot in the eastern wall.

where $l = \frac{\Omega^2 a^2}{2gh_0}$ and for the experimental values $h_0 = 5$ cm, $l = 1$, $a = 100$ cm, $\Omega = 1$ sec^{-1}, and $\nu = .01$ cm^2 sec^{-1} it is found that $A = -\frac{50}{r}$. The radius of the source in Figure 2 is approximately $r = 20$ cm which gives $A = -2.5$ and $\sigma_x = (5y)^{\frac{1}{2}}$. If we consider that most of the dyed source water will be contained within the region $\pm 2\,\sigma_x$ the rimward limit of the dye outline is in quite good agreement for various distances y from the eastern wall. Dye fronts are not adequate for quantitative comparison for several reasons including the fact that the cross stream Ekman flow causes the dye to be systematically displaced toward the left of the axis of the flow.

5. Eastern Boundary Currents

In (A) it was asserted as one of the essential elements which defined the regime to be considered that departures from geostrophic flow were to be permitted only at western boundaries where narrow and rapidly flowing currents could occur. The function of these currents was to preserve continuity of mass in the basin as a whole by providing means for radial transport but the dynamics of the boundary currents were not explicitly considered. In nearly all experiments the above assertion was found to be a justified one, but in one particular situation a pronounced *eastern* boundary current was observed.

Figure 4 is a sequence of photographs at 20, 80, and 136 minutes after dye was introduced into the source water, there being a source (S_0) through a slot in the eastern boundary near the rim and a sink (S_i) at the apex of the sector. As in the previous experiments, the radius was $a = 100$ cm, rotation rate $\Omega = 1.05$ sec^{-1}, the mean depth $h = 8$ cm, and the ratio of the depth at the rim to that at the center h_a/h_0 was 2. The volume rate of flow was $S_0 = 110$ cm^3/min. As may be noted from the photographs there existed an obvious eastern boundary current transporting perhaps 10 % S_0, and repeated experiments showed this phenomenon to be reproducible. The hypothesis is advanced that a small portion of the fluid received negative absolute vorticity by means of the viscous forces at the edge of the source slot, and that this portion of the fluid could take part in an eastern boundary current.

Several theoretical models of boundary current circulations in the ocean have been summarized by STOMMEL (1958). It is clear from the various studies that for linear viscous models significant mass transports may occur only at western boundaries where it is possible to have a balance of changes of relative vorticity (ζ) due to latitudinal (or depth) variation with those caused by lateral or vertical viscous stresses. In addition, MORGAN (1956) has shown for the simplest non-linear models that only western boundary currents can be of significance. However, inasmuch as the possibility of negative absolute vorticity has not been considered and since complete non-linear solutions including viscosity have not been available for examination, there is no reason to rule out all possibilities of inertio-viscous eastern boundary currents.

The simplest physical arguments suggest that if the fluid next to the eastern boundary had negative absolute vorticity ($\zeta + 2\Omega < 0$) it would again be possible to balance vorticity changes due to the depth variation with those due to

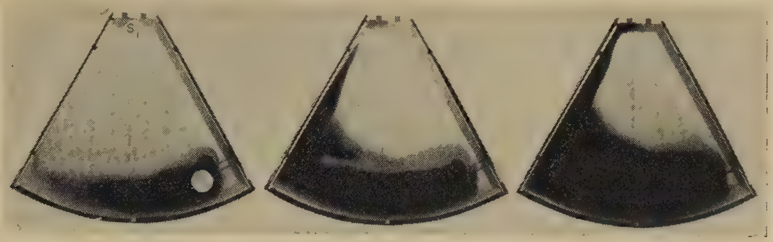

Fig. 5. Photographs at 10, 20, and 40 minutes illustrating the absence of an eastern boundary current when an interior source was used (compare with Figure 4) and the existence of strong "recirculation" from the western boundary.

lateral viscous stresses. However, in such an event many non-linear terms would become important and the simple arguments would be invalid. It is suggestive that for the experiment of Figure 4 6 % of the source fluid would enter with $\zeta + 2\Omega < 0$ given a slot width of 1/4 in., the flow rate of 110 cm³/sec, and assuming a parabolic velocity profile for the flow through the slot. More critical experiments with various slot widths and flow rates are suggested as means of varying the percentage of fluid entering with negative absolute vorticity.

As a first test of the above hypothesis, the experiment illustrated in Figure 5 was conducted. Conditions were identical to those of Figure 4 except that the source water was introduced through a tube just away from the boundary so that there would be no opportunity for the fluid to obtain negative absolute vorticity. As may be seen, no eastern boundary current occurred.

6. Recirculation about an Interior Source or Sink

Introduction of the source water in the manner shown in Figure 5 eliminated the eastern boundary current but caused other interesting circulations. It is shown below that with an interior point source (distributed over a small area by turbulent mixing) an amplification of flow toward the western boundary is required. The sequence of Figure 5 shows a return flow from the western boundary current to the source, a circulation which is required by continuity in the vicinity of the source and the geostrophic constraints in the system with variable depth. To analyze this phenomenon we now consider the circulation about an interior source in the absence of bottom friction.

From equation (12) setting $\frac{\partial h}{\partial \Theta} = \frac{\partial h}{\partial t} = 0$ and $v = 0$ we obtain:

$$ru \frac{\partial h}{\partial r} - rQ = 0 \qquad (24)$$

and by elimination of u with equation (7) we find:

$$\frac{\partial v}{\partial \Theta} = \frac{\frac{\partial^2 h}{\partial r^2}}{\left(\frac{\partial h}{\partial r}\right)^2} rQ - \frac{1}{\frac{\partial h}{\partial r}} \frac{\partial (rQ)}{\partial r}. \qquad (25)$$

Integration of (25) from longitude Θ_0 to the eastern wall $\Theta = \Theta_E$ such that the entire source is included in this region gives:

$$v_{\Theta_0} = -\frac{\frac{\partial^2 h}{\partial r^2}}{\left(\frac{\partial h}{\partial r}\right)^2} Q_S + \frac{1}{\frac{\partial h}{\partial r}} \frac{\partial}{\partial r} Q_S \qquad (26)$$

where we have taken $v_{\Theta_E} = 0$ (no zonal flow at the eastern boundary) and have written $Q_S = \int_{\Theta_0}^{\Theta_E} Q r d\Theta$, the zonally integrated source per unit of radius. Using the equation for the free surface (23) we obtain:

$$v_{\Theta_0} = \frac{a^2}{2h_0 l r^2} \frac{\partial}{\partial r}\left(\frac{Q_S}{r}\right). \qquad (27)$$

Equation (27) shows that there should, in general, be both positive and negative values for v_{Θ_0} and that inflection points $v_{\Theta_0} = 0$ occur where $\frac{\partial}{\partial r}\left(\frac{Q_S}{r}\right) = 0$. For a smoothly varying source with a single maximum at r_0 we define the radius r $(v_{\Theta_0} = 0) = r'$ and write:

$$\underbrace{\int_0^{r'} hv\,dr}_{T(+)} + \underbrace{\int_{r'}^{a} hv\,dr}_{T(-)} = \int_0^a Q_S\,dr = S_0. \quad (28)$$

The integrals on the left of (28) represents transports toward and away from the source. We define $\frac{T(+)}{S_0}$ as the "recirculation" and find:

$$\frac{T(+)}{S_0} = \frac{1}{S_0} \int_0^{r'} \left(\frac{a^2 + lr^2}{2l}\right) \left[\frac{\partial}{\partial r}\left(\frac{Q_S}{r}\right)\right] dr. \quad (29)$$

Interpretation of (29) is facilitated by considering a specific functional form, say the Gaussian distribution $\frac{Q_S}{r} = \frac{S_0}{(2\pi)^{\frac{1}{2}} r_0 \sigma} e^{-\frac{(r-r_0)^2}{2\sigma^2}}$ so that $r' = r_0$, the radius of maximum source strength, and where σ is the radial spread of the source. Therefore for a source with small radial spread we may write approximately:

$$\frac{T(+)}{S_0} \approx \left(\frac{a^2 + lr^2}{2lS_0}\right) \int_0^{r_0} d\left(\frac{Q_S}{r}\right) =$$

$$= \left(\frac{a^2}{lr_0^2} + 1\right) \frac{r_0}{(2\pi)^{\frac{1}{2}}\, 2\sigma}. \quad (30)$$

We see that for small σ the recirculation is inversely proportional to σ. In any physical situation a lower limit on the practical size of σ probably occurs because of mixing associated with the source and with the increased circulation.

From Figure 5 we estimate $r_0 = 85$ cm and $\sigma = 5$ cm, and using the values $a = 100$ cm and $l = 1$, we obtain a theoretical recirculation $\frac{T(+)}{S_0} = 7.5$. This surprisingly large value was checked by evaluations from Figure 5. The total volume of dyed fluid which had been introduced by the time of the first picture was 1100 cm^3 (110 cm^3/min for 10 min). The volume of dyed water as evaluated from the photograph was 10,440 cm^3 or 9.5 $S_0 \triangle t$, which indicates that the source water was diluted by mixing at the source of 8.5 parts of recirculated clear water. This result is in good agreement with the theoretical recirculation considering the arbitrary specification of the form and width of the source region. Confirmation of these figures was obtained from the second photograph of Figure 5 which shows a volume of dyed fluid 10 times the total source input at 20 minutes. Comparison of Figures 4 and 5 shows the very large differences in the speeds of the zonal flow without recirculation (Figure 4) and with the additional flow produced by recirculation (Figure 5).

One may well inquire why the phenomenon of recirculation did not occur when the source water was injected through the slot in the wall. Formally the difference lies in the assumption following equation (26) where we have taken for the case of an interior source $v_{\Theta E} = 0$, i.e., no geostrophic flow through the eastern wall and consequently no radial pressure gradient. For flow through the wall and with $Q = 0$ we would immediately obtain the solution to (25) $v_{\Theta_0} = v_{\Theta E}$. Qualitatively we observe that for an interior source no isobars intersect the eastern wall but instead they form a region of high pressure extending to the western boundary with the source at the extreme eastern end. Having in mind this pattern the associated geostrophic recirculation and southward flow through the source region is obvious.

7. Partial Barrier Experiments

At the suggestion of Stommel, some experiments were performed to test the simple hypotheses proposed in (A) under somewhat more complicated conditions having geophysical interest. Figure 6a illustrates the anticipated circulation and Figure 6b the observed circulation in the 60 degree sector described in (A) but modified by a partial radial barrier 30 cm long extending inward from the midpoint of the rim. The barrier thus divided the sector into three portions referred to as the N, SW, and SE basins. Conditions of the experiment were $S_0 = 100$ cm^3/sec, $\bar{h} = 8$ cm, $h_0/h_a = 2$, $\Omega = 1$ sec^{-1} and since no water was removed from the tank the sink is represented by the uniform rise of the free surface.

The water budget of the predicted circulation is based upon the considerations developed in

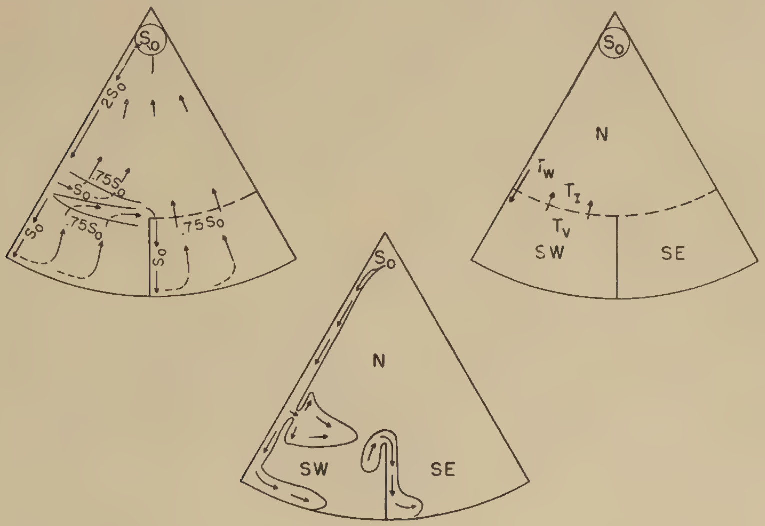

Fig. 6. The circulation obtained with a source at the apex of the sector and a uniform rise of the free surface in the presence of a partial radial barrier extending inward from the center of the rim. a) The theoretically predicted circulation; b) a sketch of the observed circulation; c) a schematic diagram for the definitions of N, SE, SW, T_W, T_I, T_V.

A) as follows: we consider continuity in either he SW or the SE basin as indicated in Figure c where T_w is the transport of the western oundary current into the basin, T_I is the nterior geostrophic transport out of the basin, nd T_V is the upward flux due to the filling of he entire sector by the source. Continuity in W requires $T_W = T_I + T_V$. $T_V = \frac{S_0}{2}\left(\frac{a^2 - r^2}{a^2}\right)$ s the fraction of S_0 used to fill the SE or the W basin. T_I may be obtained from $T_I = \int_{\Theta} \int_{0}^{h+h'} ur \, d\Theta \, dz$ where h is the basic height at adius r and h' is the departure from h due to he steady geostrophic current. From equation 12) setting $v = Q = \frac{\partial h}{\partial \Theta} = 0$ we obtain $u = -\frac{\partial h/\partial t}{\partial h/\partial r}$ which permits evaluation of u. Using $\frac{h}{r} = \frac{2h_0 lr}{a^2}$ and $\frac{\partial h}{\partial t} = \frac{6S_0}{\pi a^2}$ we obtain $u = -\frac{3S_0}{\pi h_0 lr}$ nd ignoring h' compared to h we find $T_I = \frac{S_0}{2l}\left(1 + \frac{lr^2}{a^2}\right)$. From the above expressions or T_I and T_V we obtain $T_W = \frac{S_0}{2}\left(1 + \frac{1}{l}\right)$. Therefore for $l = 1$ we find $T_W = S_0$, and for $r = 70$ cm we obtain $T_V = +.25\, S_0$ and $T_I = +.75\, S_0$ for either the SW or the SE basin.

Of particular interest is the origin of the source water for the SE basin, for according to the simple theory 75 % of this water would be recirculated through the SW basin and 25 % would come zonally across from the western boundary current. This type of circulation was confirmed in the experiment by inserting crystals of dye in the SW basin to observe the flow around the end of the barrier as illustrated. Of further interest is the difference in history of the water in the western and eastern sides of the N basin; that on the west side having come directly from the western boundary current and 75 % of that on the eastern side having passed through both the SW and SE basins before flowing northward in the interior.

8. The Limiting Role of Bottom Friction

Figure 7a illustrates a partial barrier experiment similar to that of Figure 6 but with a localized sink near the rim as indicated and with the western and eastern walls coincident half way around the tank. The circulation performed in the expected fashion carrying the

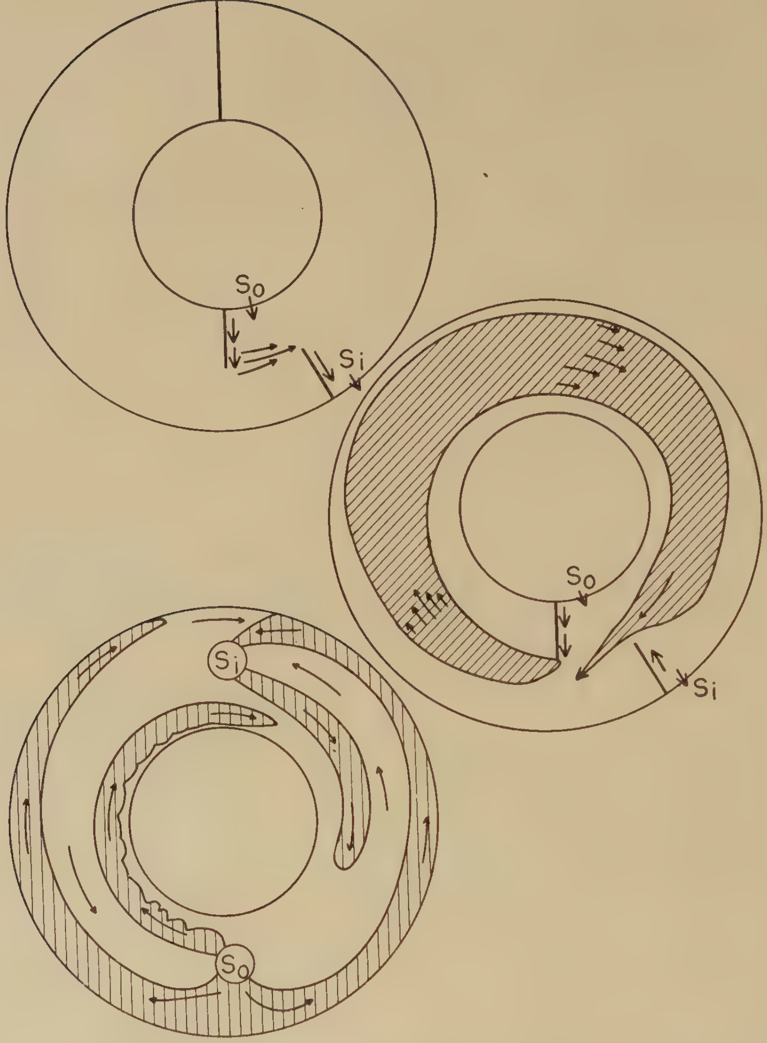

Fig 7. A series of experiments illustrating the progressive domination of bottom friction as radial barriers are removed. a) A partial radial barrier experiment similar to that of figure 6; b) the same experiment as in a) but with the complete radial barrier removed; c) a spiral circulation pattern required to transport mass from S_0 to S_i; with no radial barriers.

source water directly to the sink along the western boundaries.

Removal of the radial wall (Figure 7b) left an annular ring with partial barriers, a geometry somewhat similar to the geography of the antarctic circumpolar seas. For this case the boundary current from the inner barrier moved westward and proceeded around the tank at the same time spreading in accordance with the theory presented in section IV. After 1 circumference the dyed source water by-passed the outer barrier and the sink as indicated. Injection of dye beside the outer barrier clearly showed a boundary current flowing away from the sink. The interpretation is that the Ekman transport toward the rim was oversupplying the sink so that an inward flowing boundary current was required by continuity.

An extreme example of the domination of the flow by bottom friction in the absence of radial barriers is that illustrated in Figure 7c. The source and sink were at mid radii and 180 degrees apart. The complex spiraling pattern is evidence of the importance of the bottom boundary layer in the absence of radial barriers.

9. Applications to a Barotropic Ocean Circulation

The example of recirculation about an interior source is closely related to the "wind-spun vortex" suggested by MUNK (1950). In fact the theory of STOMMEL (1948) which includes a simple form of bottom friction and that of MUNK (1950) which includes lateral friction at the western boundary together contain nearly all of the essential elements of the theory and experiments presented above.

A striking feature of the recirculation about a source region is the extent of the large scale lateral mixing which may involve volumes of fluid several times the strength of the source itself. Also, the circulation of Figure 6 indicates significant mixing processes associated with the larger scale recirculations and the radial barriers. From this viewpoint it should be expected that the circulation of the deep ocean, which is now known to have some fairly strong currents (SWALLOW, personal communication), should be markedly affected by the large scale topography of the ocean floor. Accordingly, the distribution of properties may be significantly affected by localized mixing processes of large magnitude.

The amplitude of the recirculated zonal currents is of considerable interest especially in connection with the results recently published by ROBINSON and STOMMEL (1959). These authors described the localized amplification of the speed of barotropic currents of the oceans (VERONIS and STOMMEL, 1956) by relatively small scale irregularities in the ocean bottom. In a specific example, an amplification factor of 8 was suggested. Neither of the above named papers was concerned with nor implicitly included the recirculation phenomenon described here, and an additional amplification factor for barotropic currents should be considered. As in the model, the magnitude of the recirculation is primarily dependent upon the scale of the source-sink distribution as will be shown.

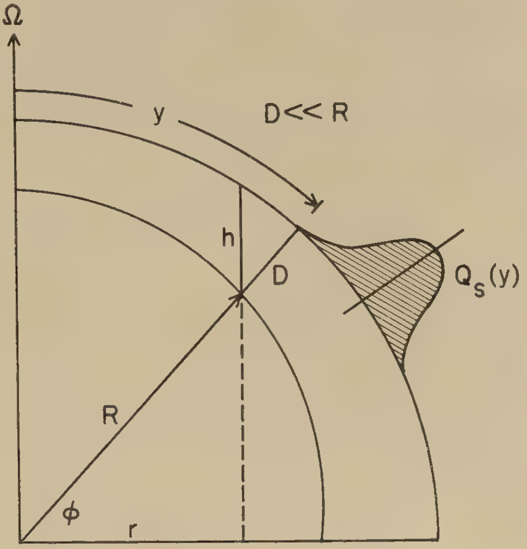

Fig 8. Conversion from polar to spherical geometry.

The barotropic theory for an ocean of constant depth D is readily obtained by conversion from polar coordinates according to the geometry of the sphere as in Figure 8. Into equations (19) and (20) we introduce the following relations for the sphere:

$$r = R \cos \varphi, \quad h = \frac{D}{\sin \varphi}$$

$$Q_S(r) = \frac{Q_S(y)}{\sin \varphi}, \quad \frac{\partial}{\partial \varphi} = -R \frac{\partial}{\partial y}$$

We then obtain:

$$v_\Theta = -\frac{Q_S(y)}{D} + \frac{R}{D} \frac{\partial}{\partial y} (Q_S(y) \tan \varphi) \qquad (31)$$

and

$$T(+) = -\int_0^{y'} Q_S(y)\, dy + R \int_0^{y'} d(Q_S(y) \tan \varphi) \qquad (32)$$

which may be evaluated for any given latitudinal distribution of the source. For a source of small latitudinal extent and symmetrical with a maximum at the mean position y_0 we may approximate equation (32) by letting $\tan \varphi = \tan \varphi_0$ to obtain:

$$T(+) = -\frac{S_0}{2} + R \tan \varphi_0 Q_S(y_0) \qquad (33)$$

where $Q_S(y_0)$ is the maximum value of $Q_S(y)$. As was done for the model we consider a normal distribution $Q_S = \frac{S_0}{(2\pi)^{\frac{1}{2}}\sigma} e^{-\frac{(y-y_0)^2}{2\sigma^2}}$ and obtain $Q_S(y_0) = \frac{S_0}{(2\pi)^{\frac{1}{2}}\sigma}$ so that the recirculation is:

$$\frac{T(+)}{S_0} = -\frac{1}{2} + \frac{R \tan \varphi_0}{(2\pi)^{\frac{1}{2}}\sigma}. \qquad (34)$$

$\frac{T(+)}{S_0}$ depends inversely upon the spread of the source region when $\sigma \ll R$. To take an extreme example we consider an idealized source due to precipitation or the wind stress convergence associated with a stationary hurricane having $\sigma = 20$ km at latitude $\varphi = 25$ degrees. The second term of (32) is dominant and gives a recirculation $\frac{T(+)}{S_0} = 59$! As another example, we consider a large-scale stationary system with $\sigma = 500$ km at $\varphi = 60$ degrees, and we obtain $\frac{T(+)}{S_0} = 10$ from the approximate formula (33). These figures suggest that the estimates of barotropic flow given by Veronis and Stommel (1956) and the partition of energy between barotropic and baroclinic currents (Veronis, 1956) should be reexamined in a framework which permits the recirculation phenomenon.

It is of some interest to estimate the spread of zonal barotropic flow due to bottom friction for the scale of an actual ocean. From section IV the formula for the standard deviation of the spread is $\sigma_x = (2Ay)^{\frac{1}{2}}$. For conversion to the spherical case we use

$$\sigma_y = \frac{\sigma_x}{\sin \varphi}, \; \frac{\partial h}{\partial r} = \frac{D \cos \varphi}{R \sin^3 \varphi}, \quad \Omega \rightarrow \Omega \sin \varphi$$

in the Ekman equations, and $\nu \rightarrow \nu_e$ (an eddy coefficient of viscosity). We then obtain

$$A = -\frac{R \sin^3 \varphi}{\sqrt{2}\, D \cos \varphi} \left(\frac{\nu_e}{2\Omega \sin \varphi} \right)^{\frac{1}{2}}$$

For $\nu_e = 1$ cm²/sec, $\Omega = .729 \times 10^{-4}/\text{sec}^{-1}$, $\varphi = 45$ degrees, $D = 5$ km, and $R = 6400$ km, we find $A = -45 \times 10^3$ cm, so that at a distance $x = 1000$ km from a point source $\sigma_y = 42$ km. We may take the total width of the current as $4\sigma_y = 168$ km. This width is latitude dependent, but it is reasonable to take 100 km as the minimum width of a barotropic zonal current except where local concentration due to bottom topography may be important. σ_y varies as $\nu_e^{\frac{1}{4}}$ so that only order of magnitude variations of ν_e can be of significance here.

10. Concluding Remarks

From time to time the uses and applications of model experiments are seriously questioned, particularly with respect to inability to improve our knowledge of real geophysical problems. The work described here contains a variety of experiments which suggest various possibilities and limitations for studies of the ocean circulation.

In the first place, the experiments have confirmed the qualitative predictions of the general ocean current theory suggested by STOMMEL (1957), and insofar as dimensional arguments can show that the same equations apply to the geophysical scale, the experiments represent confirmation of that theory.

Secondly, laboratory studies using a real fluid (as opposed to an idealized frictionless fluid) are sometimes capable of resolving incomplete or inconsistent theoretical analyses such as those proposed by HOUGH (1897) and by GOLDSBOROUGH (1933) each of whom considered source-sink circulations on a sphere. As has been pointed out by STOMMEL (1957) Hough had neither bottom friction nor meridional boundaries and could not obtain steady state solutions, whereas Goldsborough (having meridional boundaries) could obtain solutions only in certain restricted circumstances and did not conceive of boundary currents for the resolution of the general problem. The experiments described here and in (A) clearly resolve the difficulties of the above authors by means of experiments which would have been ideally suited to examination of their theoretical analyses.

Finally, laboratory experiments may suggest circulations of possible oceanographic significance which have heretofore been overlooked. Such is the case for the recirculation phenomenon and the spread of barotropic zonal flow each of which are contained within the elementary theory.

The eastern boundary current is an example of a circulation which may be of some geophysical interest but which is not contained within the elementary theories and deserves special attention. It is tempting to suggest on the basis of our experimental results that inertial eastern boundary currents may occur where there is a sufficiently strong discharge of water from a river or other source at an eastern boundary of an ocean. A geographical situation which resembles the experiment of Figure 4 is the saline discharge of approximately 1,680,000 m^3/sec (Sverdrup, 1943) through the Straits of Gibraltar and into the Atlantic Ocean. It appears to be well established on the basis of observations of salinity (Nielsen, 1912) that at least a small portion of the Mediterranean discharge moves in a narrow current northward along the coast of Spain, and a diagram of salinity would appear similar to the distribution of dyed source water in Figure 4.

Complete velocity profiles are not available, but direct observations of currents using Swallow floats at the salinity maximum (1,100 meters depth) off the south coast of Spain have shown on one occasion an average speed toward the West of 25 cm/sec at the closest observational distance 7.5 km from the coast (F. C. Fuglister, private communication). A shear of 25 cm/sec/3 km would equal the vertical component of the earth's vorticity at that latitude, therefore it seems probable that some small fraction of the Mediterranean discharge may have sufficient shear to realize negative absolute vorticity.

REFERENCES

Carlslaw, H. J. and Jaeger J. C., 1947: *Conduction of heat in solids*. Oxford, Clarendon Press. 386 pp.

Dryden, H. L., Murnaghan F. P., and Bateman H., 1956: *Hydrodynamics*. New York, Dover, 634 pp.

Ekman, V. W., 1905: On the influence of the earth's rotation on ocean currents. *Arkiv. f. Matem., Astr. o. Fysik*, Stockholm, Bd. 2, No. **11**, 53 pp.

Goldsborough, G. R., 1933: Ocean currents produced by evaporation and precipitation. *Proc. Roy. Soc. A* **141**, pp. 512—517.

Green, T. R., 1959: Qualitative and quantitative observations of fluid flows in rotating tanks. B. A. Thesis, Amherst College.

Hough, S. S., 1897: On the application of harmonic analysis to the dynamical theory of the tides. Part I: On Laplace's "Oscillation of the first species", and on the dynamics of ocean currents. *Phil. Trans.* (*A*) **189**, pp. 201—258.

Morgan, G. W., 1956: On the wind-driven ocean circulation. *Tellus*, **8**, pp. 301—320.

Munk, W. H., 1950: On the wind-driven ocean circulation. *J Meteor.*, **7**, pp. 79—93.

Nielsen, J. N., 1912: Hydrography of the Mediterranean and adjacent waters. *Rep. on the Danish Ocean. Exp. 1908—10*, Johs. Schmidt Ed., **1**, pp. 77—191.

Robinson, A., and Stommel, H. 1959: Amplification of transient response of the ocean to storms by the effect of bottom topography. *Deep-Sea Res.*, **5**, pp. 312—314.

Stommel, H., 1948: The westward intensification of wind-driven ocean currents. *Trans. Amer. Geophys. Union*, **29**, pp. 202—206.

Stommel, H., 1957: A survey of ocean current theory. *Deep-Sea Res.*, **4**, pp. 149—184.

Stommel, H., 1958: *The Gulf Stream*. London, Cambridge University Press, 201 pp.

Stommel, H., Arons A. B., and Faller A. J., 1958: Some examples of stationary planetary flow patterns in bounded basins. *Tellus*, **10**, pp. 179—187.

Sverdrup, H. U., 1942: *Oceanography for meteorologists*. New York, Prentice-Hall, 235 pp.

Veronis, G., 1956: Partition of energy between geostrophic and nongeostrophic oceanic motions. *Deep-Sea Res.*, **3**, pp. 157—177.

Veronis, G. and Stommel, H. 1956: The action of variable wind stresses on a stratified ocean. *J. of Mar. Res.*, **15**, pp. 43—75.

PRINTED IN SWEDEN
ESSELTE, STHLM 60

Contribution No. 1070

(*Reprinted from Nature, Vol.* 188, *No.* 4752, *pp.* 700–703,
November 26, 1960)

PORPOISES AND THE BOW-RIDING OF SHIPS UNDER WAY*

By ANDREW A. FEJER
Woods Hole Oceanographic Institution and Illinois Institute of Technology, Chicago
AND
RICHARD H. BACKUS
Woods Hole Oceanographic Institution, Mass.

IN recent years there has been a controversy concerning the phenomenon of porpoises dwelling almost motionless near the bows of ships under way while obtaining propulsive power from the moving vessel. In reading the papers[1–5,7] that have been published relative to this matter it is evident that certain observational facts have been overlooked by earlier investigators. In view of this, and on the basis of some new observations made by one of us, we would like to offer an explanation of the phenomenon of bow-riding based on a model which differs from those proposed earlier.

Since Woodcock reported his observations on 'wave-riding' porpoises in *Nature* twelve years ago[1] the several papers published concerning this subject have offered explanations given in terms of the forward-sloping surface of the bow wave—hence the term 'wave-riding'. Woodcock[1] and Woodcock and McBride[2] showed that the component of the submerged weight taken along the wave slope was scarcely sufficient to balance the resistance that the animal experiences as it is moved through the water. Hayes[3] pointed out that near the wave surface the isobars are not horizontal and that the force due to the buoyancy (B) must therefore be normal to the slope of the wave (Fig. 1); consequently the hydrodynamic resistance (D) of the porpoise can be balanced by the component of the body-weight parallel to the wave surface ($W \sin \theta$). Scholander[4], on the other hand, refutes this argument on the basis of drag measurements made on small, streamlined, neutrally buoyant models that were towed in the waves of a vessel. He believes[5] that the porpoise places itself ahead of the bow wave with the tail flukes buried in the forward-facing portion of the wave (Fig. 2) in order to provide the thrust ($L_f \sin \theta$).

Observations by one of us (R.H.B.) of porpoises and their swimming and bow-riding have been

---

* Contribution No. 1070 from the Woods Hole Oceanographic Institution.

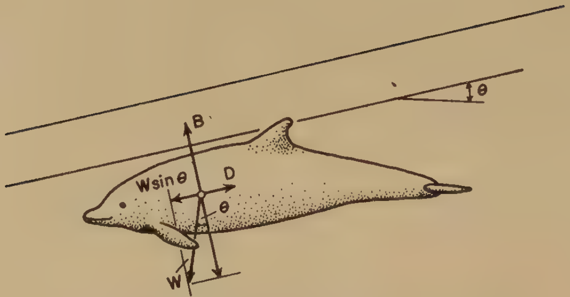

Fig. 1. Model of bow-riding porpoise according to Hayes (ref. 3). *B*, buoyant force; *D*, hydrodynamic drag force; *W*, weight of porpoise; θ, slope of wave

distributed over the period of the past ten years, although it is only during about the last two that we have watched these charming animals with the present problem particularly in mind. These observations have been made from vessels having lengths of 100–214 ft. and speeds of 7–14 knots. None of these relatively small vessels generates conspicuous bow waves.

The animals concerned in these observations are the bottlenose porpoise, *Tursiops truncatus*; the saddleback porpoise, *Delphinus delphis*; the white-sided porpoise, *Lagenorhynchus acutus*; *Stenella styx*; and other unsuccessfully identified porpoises including several of the poorly known genus *Stenella*. The largest of these animals is *Tursiops*, which may attain a length of about 11 ft. The others are smaller, generally being, in adulthood, from six to eight feet long. These small cetaceans all belong to the sub-family Delphininae of the family Delphinidae (the 'duodecimo' whales of Herman Melville's classification). It is interesting to note that the next sort of cetacean in point of size (Melville's 'octavo' whales), the Orcinae of the family Delphinidae, most of which reach lengths

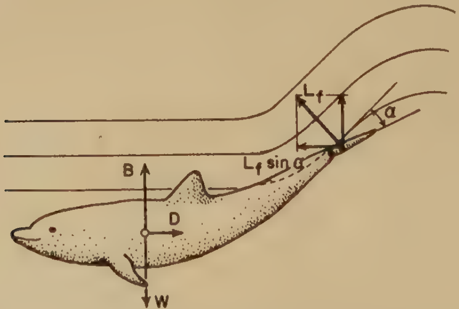

Fig. 2. Model of bow-riding porpoise according to Scholander (ref. 5). *Lf*, hydrodynamic lift force on flukes; *D*, hydrodynamic drag force

of 15–20 ft. at maturity—the potheads or pilot whales, *Globicephala* spp.; the killer whale, *Orcinus*; the false killer, *Pseudorca*; *Grampus*; and the like —are not known to be bow-riders nor are cetaceans of still larger size. (The most famous of all individual bow-riders is the porpoise 'Pelorus Jack', which escorted vessels in and out of Pelorus Sound, New Zealand, during the years 1880–1912 and was granted special protection by the New Zealand Government. This animal is supposed to have been a grampus (*G. griseus*), but this is not certain. In our experience grampuses avoid close approaches to a vessel, generally not coming nearer than about 50 or 75 ft.)

Would-be bow-riders, when first observed at a distance of several hundred yards, seem to swim purposefully towards the ship for taking their stations. Sometimes porpoises thus approaching come to within 30 or 40 ft. of the ship but no nearer. On a number of occasions we have watched porpoises approach on a nearly reciprocal heading from that of the ship, then turn sharply on to the ship's heading when the range between ship and animal was 20 or 30 ft., and be gently overtaken by the ship as they assume a bow-riding station 1–5 ft. ahead of the ship's stem.

Once at a position at the bow the animals may remain only for seconds or for as long as an hour or more. Often a group of eight or ten porpoises may join the ship together and spend 10–15 min. riding at the bow. Then the group may diminish slowly over the period of 5 min. or so as the animals drop away by ones and twos.

The distance between the ship's stem and the porpoise's flukes is usually between less than a foot to five feet. The lateral spread of bow-riders is generally about 3 ft. to either side of the stem. Sometimes when the porpoise is riding very close to the ship and is to the side of the ship's midline the flukes may be up to a foot or 18 in. behind the ship's stem. The animals are between one or two and five or six feet below the surface and may be arranged in two or even three layers. The animals rise to the surface, of course, as it becomes necessary to breathe and often leap clear, or partly clear, of the water at these times.

While one may detect the swimming motions of porpoises at close range from the ship's side, it is often very difficult to see these motions in bow-riding animals. A novice observer often suggests that this is because of the high frequency and low amplitude of the tail beats; but it appears that it is really due to the facts that: (1) at times the porpoise is not swimming at all; (2) at times the animal is swimming easily with low-frequency and low-amplitude strokes;

(3) that the common vantage point of the observer at the top of the ship's stem is a poor one for detecting the vertical swimming motions of an upright porpoise.

Often one sees individuals proceeding on a sinuous course, repeatedly swerving from right to left and back across the very bow while rolling from side to side. Bow-riders may go along on their sides or even upside down and we have seen individuals proceed while slowly revolving about their long axis. One posture assumed by the bow-rider, which we have only recently noticed, seems of particular significance. This was first observed in *Tursiops* from *Chain* on November 20 and 21, 1958, in the ocean area known as the Blake Plateau. From time to time individuals swimming on their side were seen to throw the tail into a strong downward flexure and hold it in this extreme position for two to four seconds. At these times it was hard to observe the angle of attack of the flukes but it was noticed that such porpoises were generally, if not always, so oriented that the back was towards the long axis of the vessel, that is, a porpoise on the starboard bow coasted on its left side and vice versa. It might be assumed that these animals coast in this posture while belly-down or -up; but this, of course, would be less easily seen from the top of the ship's stem. Wrinkles in the skin were noticed on several occasions when the tail was flexed downwards. These were located at the point of flexure and probably do not have a dynamic significance such as the skin folds reported for this species by Essapian[6] may have. On May 12, 1959, off Cádiz, Spain, about two dozen *Tursiops* were observed from *Chain*, and tail-down coasting the same as that described above was seen.

On May 16, 1959, just west of the Strait of Gibraltar and on May 26, 1959, in the Malta Channel this activity was observed in *Delphinus*, animals that are for the most part about 6 ft. long. The tail-down coasting posture of *Delphinus* does not appear to differ from that observed in *Tursiops*; however, it has been observed less frequently in *Delphinus* than in *Tursiops*. That is, after first noticing this bow-riding attitude in *Tursiops*, we saw it in the next two encounters with *Tursiops* but only in two of the next eight meetings with *Delphinus*. Since *Delphinus* is in general smaller and of quicker movement than *Tursiops*, the details of its motion may be more difficult to discern; on the other hand, it may assume this particular posture less frequently. Furthermore, varying states of the sea and the heading of the ship relative to the sea probably affect the behaviour of the animals. In neither species can this activity be described as continuous. Individuals can be watched for periods of many seconds riding close to the ship's bow, but assuming the tail-down attitude only at irregular intervals and then for only a few seconds at a time. On August 27, 1960, tail-down coasting was observed in an unidentified species of the genus *Stenella* from *Bear* near 38° 30′ N., 78° 00′ W. It was noted on this occasion in a porpoise riding on its side at a depth of 5 or 6 ft. in the deeper of two layers of bow-riding animals.

It is readily apparent that some of the observations reported above are not compatible with the bow-riding model proposed by Hayes[3]. The propulsive force required by the porpoise depends in that case on the magnitude of the angle θ between the streamline and the horizontal (Fig. 1). As this angle decreases exponentially with depth, the explanation offered by Hayes is clearly incomplete when the porpoise is not located in the immediate vicinity of the surface and when small and relatively slow vessels are involved that do not produce bow waves of sufficient size for wave-riding, that is, waves of slopes of 15° or more and large enough to contain the body of the porpoise. It should be pointed out, however, that hydrodynamically, Hayes's explanation, while limited in scope, appears to be correct and that the contradictory data reported by Scholander[4] seem to be the consequence of limitations pertaining to the latter's apparatus, which did not permit him to control and maintain the position and orientation of the model relative to the wave surface.

Considering next the model proposed by Scholander[5], one can determine readily that a propulsive force of sufficient magnitude can result when the animal places its tail flukes in a bow wave in the manner shown in Fig. 2. However, the objection raised by Hayes[7], that the forces and moments do not balance and that consequently the porpoise is not in equilibrium, appears to be sound. Indeed our calculations show that in Scholander's model equilibrium is not attainable : the force on the tail flukes contributes a large moment around the centre of mass and because of the shape of the porpoise and the fact that the pectoral fins are located too near the centre of mass (maximum girth is at the point of insertion of the pectoral fins) it seems impossible that the animal could generate an opposing moment of equal magnitude.

In order to arrive at a model which is consistent with our observations it is proposed to focus attention on the pressure distribution in a horizontal plane ahead of the bow. If one neglects the effect of the surface and keel, that is, considers the flow to be two-dimensional, one can readily determine the pressure field ahead of the bow with the aid of

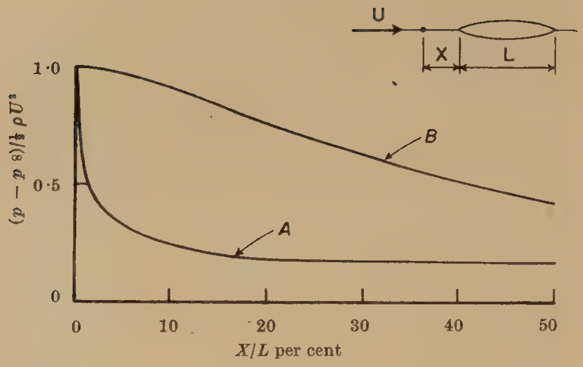

Fig. 3. Pressure distribution in a two-dimensional flow past cylindrical shapes. A, ship's water-line profile ; B, circular cylinder ; p, pressure at point X ; p_∞, pressure at a great distance from profile ; ρ, density of water ; U, velocity of flow

potential theory. Fig. 3 shows the pressure distribution along the centre-line ahead of the bow, obtained in this manner, for a cylinder having a cross-section of the shape of an ordinary ship's water line as taken from ref. 8. For the sake of comparison the distribution for a cylinder with a circular cross-section is also shown. A streamlined body placed in this region experiences a force which is approximately equal to the negative of the average pressure gradient in the field times the volume of the body[9]. It is apparent from the pressure distribution in Fig. 3 that this

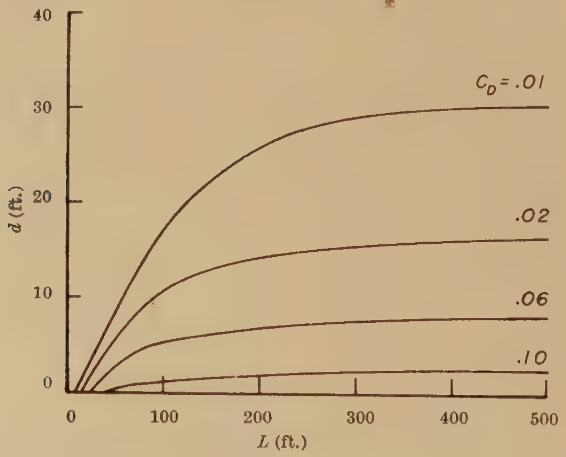

Fig. 4. Dependence of distance between tail of bow-riding porpoise and the bow on length of vessel for various values of the drag. Drag $D = 1/2\ \rho U^2 A\ C_D$; A, frontal area of porpoise ; C_D, drag coefficient

force is maximum at the bow and decreases gradually as the distance between the bow and the object increases. At a location where the force due to the pressure field equals the drag experienced by the body from the flow around it, the conditions appear to be right for bow-riding. This situation was considered using the dimensions and shape of a female *Stenella styx* which was harpooned from *Bear* on July 27, 1959, at 37° 42′ N., 73° 34′ W.[10]. The resulting curves are presented in Fig. 4 showing the distance d between the bow and the tail of the porpoise as a function of the length L of the vessel for the waterline profile used in preparing Fig. 3. It should, of course, be understood that the distances shown in the figure are larger than one would expect and that this is due primarily to the assumption of two-dimensional flow. Furthermore, it should be pointed out that it is within the power of the porpoise to vary the distance by appropriate changes in posture that will influence its drag, and that the presence of vertical and lateral pressure gradients in addition to those along the centre-line will make it necessary for the porpoise to assume some of the curious positions that have been described above. These positions remind us of the attitude assumed by the sausage-like object employed by G. I. Taylor[9] to demonstrate the equilibrium position of a body in a flow field in which the streamlines are curved. In reading Dr. Taylor's paper it becomes clear that, due to the complexity of the situation, intuition will be of little help in arriving at the posture and position the porpoise must assume in order to remain motionless in the pressure field ahead of the bow.

In turning sharply on to the ship's heading for bow-riding in the manner described earlier the porpoise could, of course, be guided visually or by echo-location, but it seems most plausible that in manœuvring into bow-riding position and during the bow-riding itself, the animal is responding directly in a tactile way to the pressure field generated by the vessel.

In viewing our results it is of course necessary to realize that the situation to which our calculations pertain is a highly stylized one. In reality the porpoises are now coasting, now swimming to make adjustments in their position relative to the ship or to change their posture, now coasting again. These changes seem to be necessary to counteract fluctuations of the pressure field due to the state of the sea and the resultant motions of the ship, and to correct any mismatch between propulsive force and drag occurring, at times, as the result of a change in the animal's posture. The resulting picture is quite involved, and a more complete and accurate analysis of the bow-riding activity would require detailed information regarding the shapes assumed by the animal and the field of flow ahead of the vessel.

Recently, near 38° 30′ N., 73° 00′ W. on August 26, 1960, we observed what appeared to be the riding of wind waves five to six feet high by a porpoise of the genus *Stenella* the length of which was about 6 ft. In the best-observed instance two porpoises rode side by side in exactly the same posture for several seconds near the top of the forward slope of the wave. Little, if any, of the porpoises' bodies were exposed (possibly the dorsal fins). The heads were down and the tail portions were raised but seemingly not quite to the extent that the long axes of the bodies were parallel to the forward slope of the wave. After proceeding with the wave for several seconds the porpoises fell behind it. This observation is similar to those recently reported by Caldwell and Fields[11] of 'surf-riding' porpoises. They report that the animals rode the top front of the wave with their heads down and only their dorsal fins and a small part of their backs exposed. In these cases Hayes's model is not only appropriate but it seems to be the only feasible one. Our calculations show that even shallow wind waves having slopes of 10–18° and travelling at velocities in the vicinity of 5–6 m./sec. could be utilized for this purpose by porpoises in minimum drag posture ; and based on this observation it seems not unreasonable to conclude with the speculation that in regions of the oceans where steady, strong winds are known to raise large waves that move steadily over long distances, even large cetaceans could very well use wave-riding techniques for migratory travel.

[1] Woodcock, A. H., *Nature*, **161**, 602 (1948).

[2] Woodcock, A. H., and McBride, A. T., *J. Exp. Biol.*, **28**, 215 (1951).

[3] Hayes, W. D., *Nature*, **172**, 1060 (1953).

[4] Scholander, P. F., *Science*, **130**, 1658 (1959).

[5] Scholander, P. F., *Science*, **129**, 1085 (1959).

[6] Essapian, F. S., *Breviora*, **43** (1955).

[7] Hayes, W. D., *Science*, **130**, 1657 (1959).

[8] Horn, F., "Handbuch der Physikalischen und Technischen Mechanik", 5, Sect. 2 (Auerbach and Hort).

[9] Taylor, G. I., *Proc. Roy. Soc.*, A, **120**, 260 (1928).

[10] For these data and for other help we are indebted to our friend, W. E. Schevill, of this Institution. A. H. Woodcock has also offered many useful criticisms.

[11] Caldwell, D. K., and Fields, H. M., *J. Mamm.*, **40**, 454 (1959).

Printed in Great Britain by Fisher, Knight & Co., Ltd., St. Albans.

Contribution No. 1073

WOODS HOLE RAPID SEDIMENT ANALYZER

BY

JOHN M. ZEIGLER, GEOFFREY G. WHITNEY, JR.,
AND CARLYLE R. HAYES

Reprinted from the Journal of Sedimentary Petrology for September, 1960

JOURNAL OF SEDIMENTARY PETROLOGY, VOL. 30, NO. 3, PP. 490–495
FIGS. 1–4, SEPTEMBER, 1960

WOODS HOLE RAPID SEDIMENT ANALYZER[1]

JOHN M. ZEIGLER, GEOFFREY G. WHITNEY, JR., AND CARLYLE R. HAYES
Woods Hole Oceanographic Institution, Woods Hole, Massachusetts

ABSTRACT

A recording rapid sediment analyzer has been developed at the Woods Hole Oceanographic Institution from the method and technique described by Appel (1953). The system measures pressure changes induced in a column of water by sediment settling through a measured distance. Mechanical analysis of sediment samples whose sizes are between coarse silts and fine gravels can be made. The authors estimate that one operator could complete curves for a maximum of 150 sand samples in a day.

Reproducibility of results is excellent. In some of the tests there was no variation of the standard deviation around an average particle diameter, at least to the fourth decimal place. A comparison of mechanical analysis by sieving and settling is given, and a method for determining shape is described.

Studies which required size frequency analysis of many hundreds of sand samples stimulated development of a rapid sediment analyzer at Woods Hole Oceanographic Institution. This device has been completed since March 1958, and many size frequency analyses have been made and examined. The writers believe that this procedure has had a reasonable test and wish to present both the technique and an analysis of the method at this time.

Excellent summaries of the development of size frequency analyses by sedimentation methods can be found in reports 4 and 7 prepared by a group of collaborating agencies (U. S. Engineer District, St. Paul, and Hydraulic Laboratory, S.U.I., 1941 and 1943) as well as in various text books (Krumbein and Pettijohn, 1938 for example). Therefore, the writers will not attempt a historical survey of the literature on this subject but leave it to the reader to compare the operation of this device with others of interest to him.

The sediment analyzer developed at Woods Hole (figs. 1 and 2) was designed and built by Mr. Geoffrey G. Whitney, Jr. to exploit a piezometric measuring method developed by Appel (1953). In brief, the pressure of a column of water is measured at two points one meter apart by a bellows within a pressure-tight case.

When a charge of sediment is introduced at the top of the water column, the pressure will increase at the bottom of the column' and as the sediment settles past the pressure sensing hole 1m down the tube, the pressure measured at the bottom hole will return to its original value before sediment was added. If a population of sediment sizes is present, then the rate of change of pressure represents the frequency distribtuion of sediment velocities in the population because the largest grains or the most spherical grains settle fastest and pass out of the measured column first.

DESCRIPTION AND OPERATION

Two tubes have been developed at Woods Hole. One tube measures sediment fall velocity over a 2 m fall and the other over a 1 m fall. Two holes through each tube either 1 m or 2 m apart transmit the pressure difference by means of glass and rubber tubing to a bellows enclosed in a case (fig. 2). The top hole transmits pressure to the inside of the pressure case (outside of the bellows) and the bottom hole to the inside of the bellows. When pressure at the bottom hole is increased, the bellows is extended. A very sensitive differential transformer mounted on the bottom of the bellows measures the amount of bellows movement, and the signal is sent through an amplifier to a recording device. Either a Sanborn recorder or a Speedomax recorder is used at Woods Hole. It would be possible to have holes at various levels down the tube for shorter fall courses if so desired.

The sediment is introduced into the

---

[1] Contribution No. 1073 from the Woods Hole Oceanographic Institution. Manuscript received October 26, 1959.

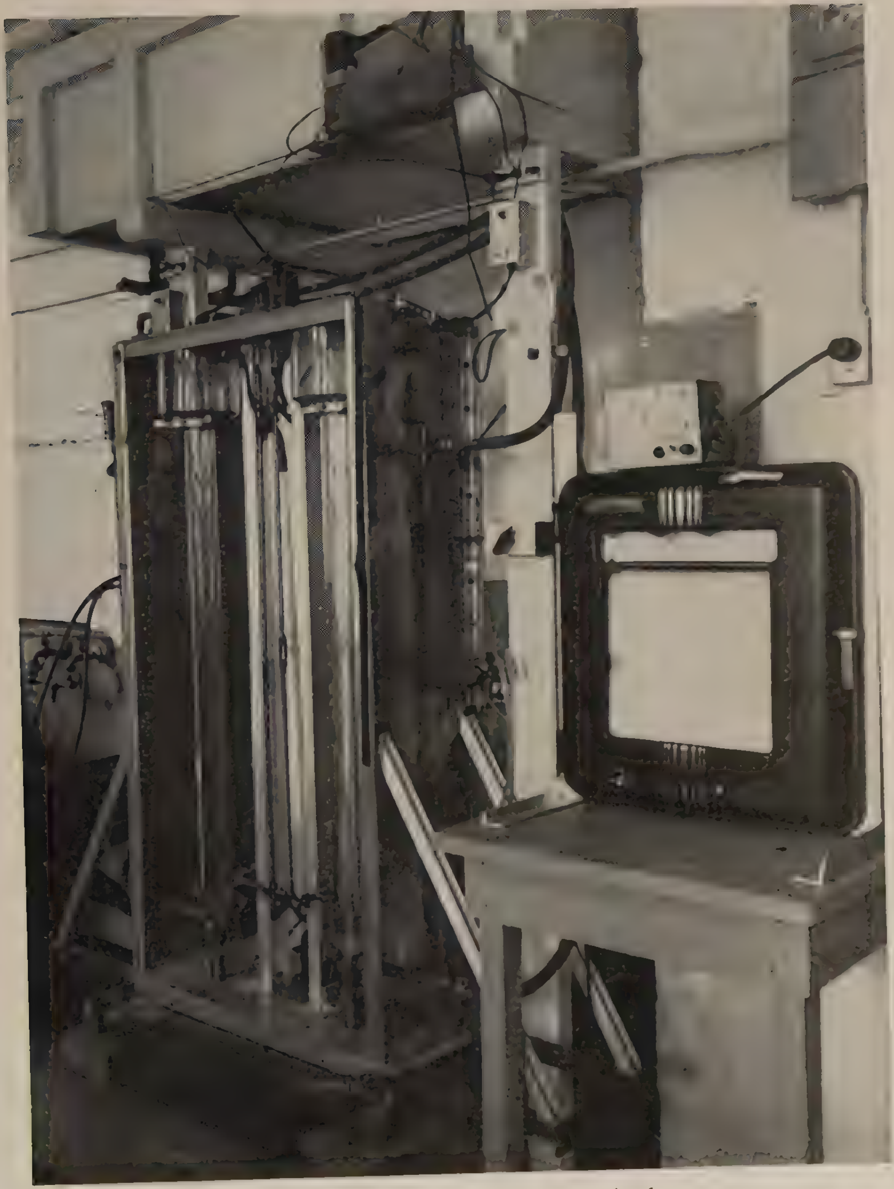

FIG. 1.—Woods Hole Rapid Sediment Analyzer.

column by first placing the charge on a closed knife gate which is submerged at the level of the top hole. After the sediment is wetted, it can be released by opening the gate. The sediment is pushed off or wiped off the gate by a rubber ring as the gates open. The gates are held closed against a spring by a charged solenoid. When the circuit is broken, the gates are opened smoothly and a timing mark put on the record at the same time.

The hot water storage tank permits dissolved gas in the water to be driven off, the room temperature storage tank is simply a

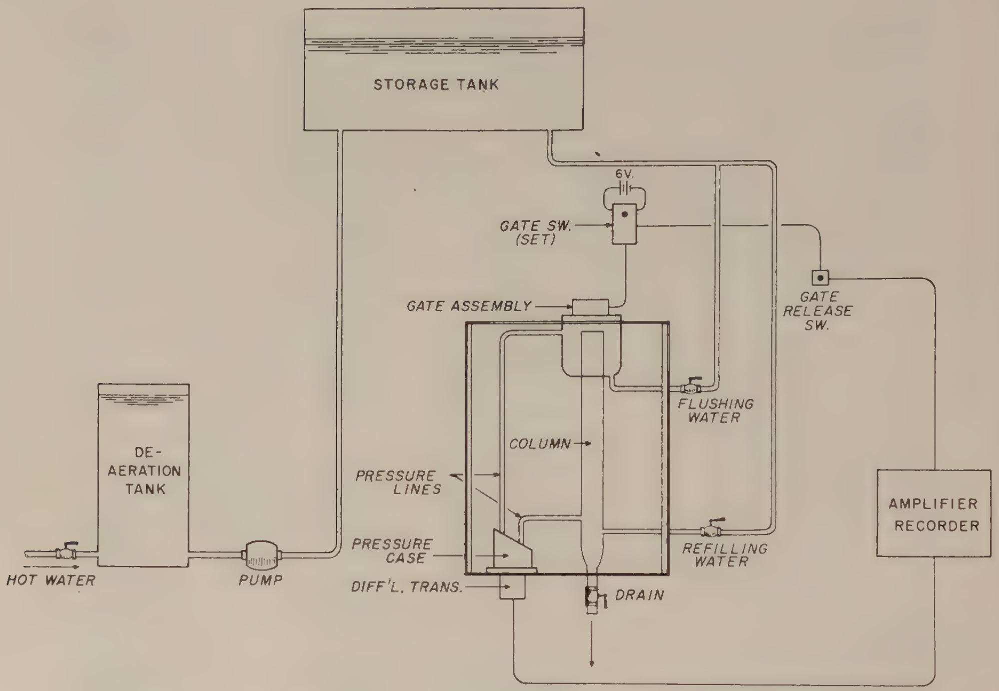
STORAGE TANK
6V.
GATE SW. (SET)
GATE ASSEMBLY
GATE RELEASE SW.
FLUSHING WATER
COLUMN
PRESSURE LINES
DE-AERATION TANK
AMPLIFIER RECORDER
PRESSURE CASE
REFILLING WATER
HOT WATER
PUMP
DIFF'L. TRANS.
DRAIN

Fig. 2.—Schematic diagram of Woods Hole Rapid Sediment Analyzer.

reservoir needed to fill the tube. This tank is not necessary if one is willing to wait for the hot water to cool in the storage tank.

The writers recommend either lucite or some other plastic for tubing because glass tubes prepared for us, required the skill of an optical company in drilling the holes and making the top edge exactly normal to the axis of the tube. The 2 m tube was developed to measure sediments with a maximum diameter of 2 to 3 mm. Ordinarily, the system is not expected to be useful for analyzing sediment finer than 0.04 mm.

No particular care is required to prepare the samples for analysis. Splits of approximately 5 gm are optimum size, but charges as large as 25 or 30 gm and as small as 2 gm can be used. One does not need to know the sample weight. Small charges of sediment were introduced into the tube in order to find the smallest sample which would cause the marking pen to register. The recorder showed a deflection when 0.05 gm were dropped as the initial charge. If, however, the system was already recording and the

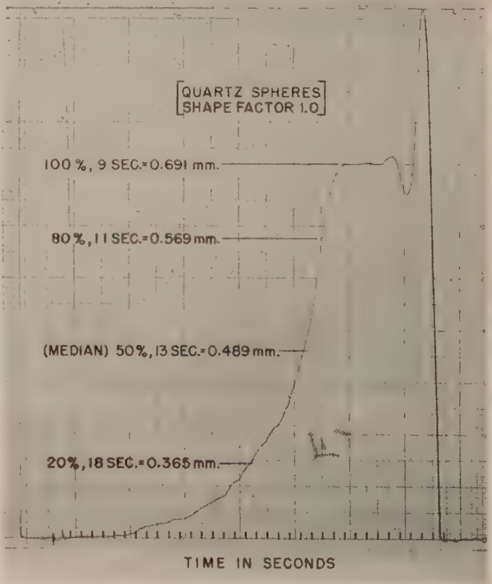

Fig. 3.—Record from Woods Hole Rapid Sediment Analyzer.

TABLE 1.—*Data pertinent for evaluation of the reproducibility of the method*

Sample No.	Number of times analysis was repeated	20th percentile		50th percentile		80th percentile	
		$\bar{x}_{20}$	σ_{20}	$\bar{x}_{50}$	σ_{50}	$\bar{x}_{80}$	σ_{80}
91-1	8	0.941	0.0262	0.893	0.0169	0.81	0.0154
E-106	9	0.837	0.0123	0.789	0.0126	0.741	0.0088
B-103	8	0.718	0.0093	0.667	0.0000	0.402	0.0161
A-26	10	0.573	0.0047	0.524	0.0109	0.300	0.0080
A-25	15	0.570	0.0116	0.520	0.0105	0.312	0.0115
D-98	8	0.408	0.0047	0.345	0.0056	0.294	0.0039
D-97	8	0.407	0.0050	0.342	0.0000		0.0000
F-107	8	0.152	0.0039	0.124	0.0025		0.0000

Samples arranged in descending order of size.

Where $\bar{x}_{20}$ is the arithmetic mean for the 20th percentile in millimeters, and σ_{20} is the standard deviation around the mean for the number of runs made.

original inertia overcome, the recorder reacted to 0.01 gm. Inasmuch as the average charge used is approximately 5 gm, it is believed that the system will detect pressure changes caused by 0.2 percent by weight of 5 gm samples.

The record obtained (fig. 3) can be treated in a variety of ways. Time is measured on the ordinate, and from this one can compute velocity or look up size in tables (Zeigler and Gill, 1959). Percentiles are determined by use of a Gerber variable scale, which can select 100 equal divisions of a line by a single setting.

REPRODUCIBILITY OF THE METHOD

An effort to discover the reproducibility of the method was made. A single operator completed all phases of the following procedure. Eight different samples having median diameters between 0.893 mm and 0.124 mm were chosen. Each sample was dropped through the settling tube, collected, and dropped again from eight to fifteen times. The samples were weighed after each collection to determine if material was lost. Each run was graphed by the recorder and the various percentiles computed and compared. The results (table 1) indicate that the standard deviation around the same percentiles nowhere exceeds 0.0262, and that the standard deviation is often negligible to the fourth decimal place.

No attempts have been made to determine the maximum speed at which samples can be analyzed by a single operator or by a combination of operations. However, Mrs. Barbara Gill completed 80 curves of beach sand and computed the median diameters and sorting coefficients on 60 of these in a normal working day. The system is certainly faster than any other known to the authors.

This procedure for determining particle size is subject to many uncertainties and limitations. The usefulness of a mechanical analysis depends on what is required of it. The reliability of mechanical analyses by sedimentation methods in general is dependent upon several assumptions and upon either estimation of or tolerance of certain sources of error. Uniform viscosity and uniform density throughout the settling column and lack of convection currents within the column are generally assumed. These assumptions are reasonably met with the Woods Hole Rapid Sediment Analyzer unless the machine is placed where severe temperature gradients form in the settling column.

Sources of error arising from mass properties of the sediment are more difficult to assess. One may apply a correction for wall proximity to the fall velocity of a single particle (Krumbein and Pettijohn, 1938, p. 91; Schulz, Wilde, and Albertson, 1954, p. 40), but it is difficult to apply this correction to a population of particles settling at the same time. In general, the correction is omitted because it is thought to be small. The same philosopy applies to hindered settling, that is, interference between the grains within a settling population. Ordinarily this correction is omitted, but in certain engineering problems such as sewage settling it is imper-

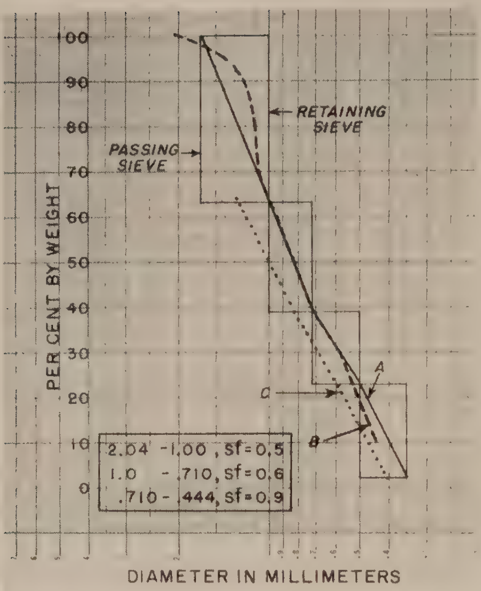

FIG. 4.—Comparison of curve from WHRSA and sieving.

ative to estimate hindered settling (Camp 1946, figs. 3 and 4); also corrections are applied in some clinical measurements (Kermack, McKendrick and Ponder, 1928) and in biological measurements in the centrifuge. Effects of concentration may influence sediment size to a greater degree than is usually supposed, particularly where the sediment is fine and well sorted. This effect, of course, is not unique to the Woods Hole Analyzer but would affect the results of any analysis made by settling. A few preliminary experiments indicate that the effects of concentration should be examined further. Results tabulated on Table 1 indicate that the variation caused by all of the above errors taken together for any one sample is small.

More serious errors arise which are related to other properties of a sediment population, such as sediment samples having a spectrum of specific gravities, that is, being multimineralic. In general, our settling velocities are analyzed as if the sediment samples have the specific gravity of quartz, 2.65. One does not usually attempt to make settling analyses of sediment samples which have noticeably large quantities of heavy minerals, yet this decision depends upon the investigator. One might, for example speculate on the effect of a spectrum of specific gravities on the number of modes.

Most analyses are made as if all fractions of a sediment sample have the same hydrodynamic shape. This assumption, perhaps, leads to more serious difficulties than assuming a monomineralic assemblage, and some readily useful system for determining shape spectra is well worth developing. One way to make an evaluation of the spectrum of shapes present in a sample is to compare the results of a settling analysis with the results obtained by screening the same sample.

One knows that the intermediate axis of sediment caught on a screen is coarser than the retaining screen size but finer than the screen which passed it. Therefore, the sizes of sediment caught on any one screen should fall between the sizes of the retaining and passing screens (fig. 4, line A). If one assumes a uniform distribution of sediment size within any one sieve interval and if one also assumes that the size of the screen opening rather than some function of the diagonal of the opening is a true measure of the size, then curve A on figure 4, connecting the screen sizes, represents the mechanical analysis of that sample determined by screens.

It is possible to fit the cumulative frequency curve obtained by settling for this same sample to the curve obtained by sieving by choosing shape factors to adjust the settling velocity curve to the assumed correct position obtained by screening.

Corey (1949) shape factors of 0.5, 0.6 and 0.9 are needed to fit the settling Curve B to the Curve A of the same sample obtained by screening. The Corey factor[2] $c/\sqrt{ab}$ is used because of the availability of drag coefficients and Reynolds numbers in terms of this factor (Shultz, Wilde, and Albertson, 1954, table 15) and because of the availability of settling velocities prepared in terms of shapes from these drag coefficients and Reynolds numbers (Zeigler and Gill, 1959).

One could likewise fit a curve obtained by settling to other assumptions concerning screening; for example, that any one screen can pass material whose intermediate axis is as much as 1.414 times the screen opening

---

[2] a = the long axis of a grain, "b" the intermediate axis, and "c" the short axis.

(the diagonal). Perhaps the mid-point of the screen interval is a better estimate of size, Curve C. In this particular case, a Corey factor of about 0.6 will adjust the curves for the entire sample.

At any rate, some assumption of shape is necessary in the procedure for determining sediment size from settling velocities where Reynolds Numbers are less than 0.1. It has been found that Cape Cod sands are very rough and tend to have much lower shape factors than one would get by direct measurement of the axial ratio. Roughness was not included in the computations for particle settling velocity; therefore particles which are rough fall slower than predicted and appear to be less spherical (as defined) than they are. Not only does this point to another source of uncertainty in mechanical analysis determined from settling velocity, but it illustrates that experience with a region helps the investigator choose reasonable values for shape.

In spite of the sources of uncertainty in obtaining sediment sizes from settling velocities, the technique will probably continue to be used. There is a whole class of problems in sediment transport or deposition where the settling velocity itself is a necessary parameter. In problems where sedimentation techniques are valid and desired, the Woods Hole Rapid Sediment Analyzer will be useful.

ACKNOWLEDGMENTS

The authors wish to express their thanks to Mr. Robert Walden of the Electronics Department and Mr. James Gifford of the Machine Shop for their contribution in development of this instrument.

REFERENCES

Appel, D. W., 1953, An instrument for rapid size-frequency analysis of sediment: unpublished Ph.D. thesis, State University of Iowa, 45 p.

Camp, T. R., 1946, Sedimentation and the design of settling tanks: Am. Soc. Civil Engineers Trans., v. 3, paper 2285, p. 895–958.

Corey, A. T., 1949, Influence of shape on the fall velocity of sand grains: unpublished M.S. thesis, Colorado A & M College, 102 p.

Kermack, W. O., McKendrick, A. G. and Ponder, E., 1928, The stability of suspensions III. The velocities of sedimentation and cataphoresis of suspensions in a viscous fluid: Proceedings of the Royal Soc. Edinburgh Proc., v. 49, p. 170–177.

Krumbein, W. C., and Pettijohn, F. J., 1938, Manual of sedimentary petrography. Appleton-Century Co., New York, 549 p.

Schulz, E. F., Wilde, R. H., and Albertson, M. L., 1954, Influence of shape on the fall velocity of sedimentation particles: Colorado A & M Research Foundation report to the Missouri Research Division. Corps. of Engineers, U. S. Army, Omaha, Nebraska, M. D. Sediment Series, No. 5, 161 p.

U. S. Army Engineers and Hydraulic Laboratory, State University of Iowa, 1941, Methods of Analyzing Sediment Samples: Report No. 4, St. Paul, U. S. Engineer District Sub-Office, 203 p.

U. S. Army Engineers and Hydraulic Laboratory, State University of Iowa, 1943, A study of new methods for size analysis of suspended sediment samples: Report No. 7, St. Paul, U. S. Engineer District Sub-Office, 102 p.

Zeigler, J. M., and Gill. Barbara, 1959, Tables and graphs for the settling velocity of quartz in water, above the range of Stoke's Law: References No. 59–36, Woods Hole Oceanographic Institution, Woods Hole, Mass., 13 p. 55 tables and graphs.

Contribution No. 1074

Reprinted from JOURNAL OF APPLIED PHYSICS, Vol. 31, No. 3, 474–478, March, 1960
Copyright 1960 by the American Institute of Physics
Printed in U. S. A.

Optical Studies of the Diffraction of Water Waves by Circular and Thin Elliptic Cylinders*

RICHARD BARAKAT, *Research Laboratory, Itek Corporation, Boston, Massachusetts*

AND

ROBERT BARAKAT, *Suffolk University, Boston, Massachusetts*
(Received June 5, 1959)

By using the optical grid method the diffraction of water waves from circular and elliptic cylinders were measured and compared with theory. The scattered wave intensity S and the total energy scattered per sec per unit intensity Q were measured and the results bear out the well-known fact that for angles less than 30 deg or in the vicinity of 180 deg, one cannot separate out the scattered wave and the incident plane wave.

The optical grid method is described in detail and the advantage of its being able to measure the instantaneous field emphasized.

I. INTRODUCTION

THE diffraction of water waves by rigid obstacles has been a subject of some interest recently from both an experimental[1] and a theoretical[2] point of view. The authors have used a variant of the optical grid method to study the diffraction of water waves by a variety of bodies. Both two-dimensional (circular and elliptic cylinders, wedge-shaped bodies) and three-dimensional (sphere, prolate spheroid) objects were investigated with the intention of comparing with theory wherever possible. One of the advantages of the optical grid method lies in the fact that the instantaneous diffracted field can be measured whereas the probe techniques used in acoustics or microwave optics must necessarily deal with average fields.

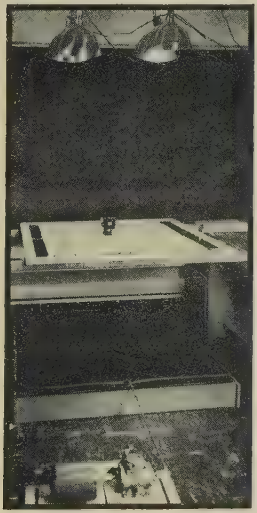

FIG. 1. Photograph of experimental setup.

Mogi[3] has already made an experimental study of water wave diffraction by a semi-infinite screen (Sommerfeld's problem), slits, and circular cylinders. However, his results are somewhat questionable as the waves generated in his tank were short enough to have appreciable viscous damping for which the present diffraction theory makes no provision.

The purpose of the present paper is to restudy the case of the circular cylinder and examine the diffraction from elliptic cylinders whose minor axes are perpendicular to the wave front, and also at an angle to the major axis. A further paper, in preparation, will deal with diffraction from ship-shaped bodies, with a view toward comparing the experiments and the approximate solutions by the source technique.[4]

II. DESCRIPTION OF THE APPARATUS

The experimental arrangement is illustrated in Fig. 1. The far end of the wave tank has a beach of 15° inclination made of layers of black felt tacked on the wooden incline. Sufficient percolation was provided by the felt layers to insure practically no reflection. The water was blackened by ink as demanded by the optical grid method. Figure 2 shows a schematic of the wave tank and lighting setup.

The waves are generated by an oscillating plate pivoted about an axis located 0.5 cm above the bottom of the tank. A long connecting rod was attached at one end to the plate and at the other end to the output shaft of a variable speed unit via an adjustable eccentric. The amplitude of the incident wave was controlled by adjusting the eccentric; the wavelength could be varied by changes in the variable speed unit. In this manner a wide variety of reproducible waves could easily be obtained. The variable speed unit was a Graham variable speed transmission unit, Model 20BE, capable of an output rpm range of 0–325 (gear setting on unit, 0–20). The motor was a 0.25 hp electric motor. Figure 3 illustrates the change in wavelength as a function of gear setting. The wave generating apparatus is not capable of producing exactly the desired wave motion because the method of wave generation cannot reproduce the exponential decrease of wave height with depth, although motion imparted to the water is zero near the bottom. Nevertheless this method gives reasonably good results provided the water is deep.

The chief effect of viscosity is to diminish wave height and this in turn effects the form of the wave.

---

* Research performed while the authors were on the staff of the Woods Hole Oceanographic Institution and is Contribution No. 1074 from the Woods Hole Oceanographic Institution.

[1] "Gravity waves," Natl. Bur. Standards Circ. No. 521 (1952)

[2] J. J. Stoker, *Water Waves* (Interscience Publishers, Inc., New York, 1958).

[3] K. Mogi, Bull. Earthquake Research Inst. 34, 267 (1956).

[4] F. Ursell, Quart. J. Mech. Appl. Math. 7, 427 (1954).

Mogi was faced with viscous damping of his waves as they progressed down his tank; however, his waves were only 5 cm long and one expects large damping in this range. In order to avoid this complication, waves of 9.5 cm were used as a standard; now these waves are capillary-gravity waves, but to within an error of less than 4% they can be considered as pure gravity waves. It is known that the modulus of decay T (time for the wave amplitude to decay to $1/e$ of its original value) for a clean surface of water is $0.712\ \lambda^2$ where λ is the wavelength expressed in centimeters.[5] Waves take about 4 sec to travel down the tank and it is easy to show there is only a 6% diminution in wave amplitude down the tank. Our optical measurements are good to about 5% so that any change in wave amplitude arising from viscosity is within the limits of error of our own measurements. In order to test this neglect of wave height attenuation, a series of wave height measurements down the tank were made and the results averaged at various points along the tank. When the averaged results were plotted as a function of distances from the face of the wave generator, an almost straight line of zero slope was obtained except very near the generator where complications due to higher harmonics, standing waves, etc., manifested themselves.

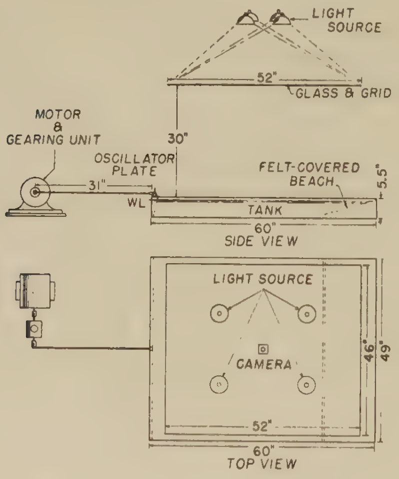

Fig. 2. Diagramatic sketch of wave tank.

The test objects were made of laminated wood and sanded down to the correct dimensions. They were then attached by screws to a thin brass plate which could be laid on the floor of the tank.

III. OPTICAL GRID METHOD

The principle underlying the optical grid method is quite simple. A grid of lines is placed above the tank, the image of which photographed in the mirror formed by the water surface. When the surface is calm there is no distortion of the grid lines; however, when the surface is disturbed by waves there is a distortion of the image of the grid. The wave height can then be calculated by an analysis of the distorted grid.

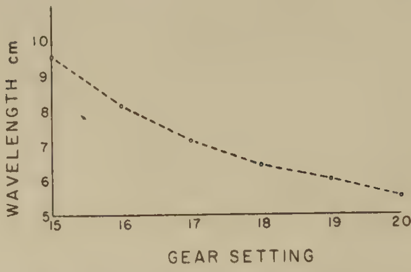

Fig. 3. Change in wavelength of incident waves as a function of gear setting on wave generator.

It is probably of interest to describe in detail the working formulae used in the method since we cannot find any accounts in the literature. We are indebted to Professor Mogi of the University of Tokyo for informative correspondence concerning the method, especially in its two-dimensional form. If we knew the slope $\Delta\alpha$ at every point we could reconstruct the wave and from this find the wave height. The slope $\Delta\alpha$ can be obtained from the simple relation $\Delta\alpha = d/2L$ [see Fig. 4(a)] provided that $\Delta\alpha \ll 1$ and the angle β in the figure is not too large. The symbol d represents the change of scale due to the distortion of the water surface. The grid of Fig. 4(b) represents the photograph of the undisturbed grid. Locate at position R the grid point (a,b). When the surface is covered with waves, the image of the grid will deform and another point of the grid, say (a', b'), will appear at position R. The slope can be obtained from

$$\Delta\alpha = \frac{d}{2L} = \frac{1}{2L}[(a-a')^2+(b-b')^2]^{\frac{1}{2}}. \tag{1}$$

The difference in the height between any two positions can be evaluated numerically as follows. Let $\eta(x,y)$ represent the surface profile; then η is expressed in

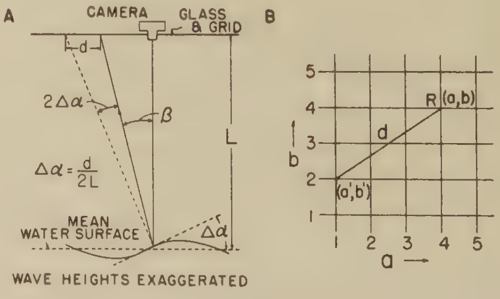

Fig. 4. Diagram showing the principles of the optical grid method; (a) relation between the wave slope and change in scale of grid; (b) relation between undistorted and distorted grid.

---

[5] H. Lamb, *Hydrodynamics* (Dover Publications, New York, 1945), p. 624.

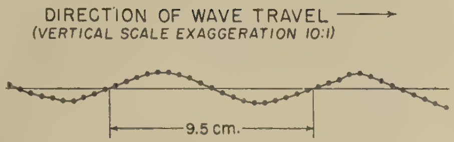

FIG. 5. Reconstruction of wave profile using one-dimension numerical integration of Eq. 3.

terms of the gradient $g(x,y)$ via the expression

$$\eta(x,y)=\int_{S_1}^{S_2} g(x,y)dS, \qquad (2)$$

where S is the arc length. Therefore, the difference in wave height is simply

$$\eta(x_2,y_2)-\eta(x_1,y_1)=\int_{S_1}^{S_2} g(x,y)dS$$

$$=\sum_i g(x_i,y_i)\Delta S_i. \qquad (3)$$

From this expression we can calculate $\eta(x,y)$ by numerical integration if necessary. Provided that we have a one-dimensional sine wave, the formulas simplified considerably and, in fact, the foregoing integration can be carried out analytically. If $\eta(x,y,t)=A\sin(kx-\omega t)$ where A is the amplitude and k the wave number, then the amplitude A is given by

$$A=\frac{1}{k}(d\eta/dx)_{x=\lambda/2}=\frac{\lambda}{4\pi L}(d)_{x=\lambda/2} \qquad (4)$$

since $(d\eta/dx)=d/2L$. Thus the wave height H is given by

$$H=2A=\frac{\lambda}{2\pi L}(d)_{x=\lambda/2}. \qquad (5)$$

This is the basic equation. Therefore, we can obtain the wave height by simply measuring d (at the position $x=\lambda/2$) directly from the photograph. Or looking at it another way, the change of gradation of the grid image at the position $x=\lambda/2$ is sufficient to allow us to measure wave height. This method fails if the wave height is such as to violate the condition $(H\sim\lambda)$.

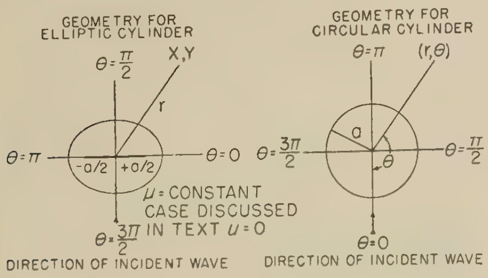

FIG. 6. Geometry of the scattering for both types of cylinders.

The assumption that the waves are essentially sine waves was tested by actually carrying out the one-dimensional numerical integration and reconstructing the wave profile. Figure 5 shows a section of the wave profile located about 2 ft from the face of the wave generator. We concluded that for most of the work the sine wave analysis was sufficient.

The grid was a translucent black-line print ruled with black lines drawn at 1 cm intervals in both directions. The use of this material greatly facilitated our work since we could easily make copies of the master grid and mark on the copies as desired.

IV. CIRCULAR CYLINDERS

All measurements are normalized by division of the incident wave height H_0 so that our measure of the diffraction effect H/H_0 will be a pure number.

An examination of Mogi's experimental data on circular cylinders reveals that the theoretical solution is always larger than the experimental answer. The reason for this is simple enough; the waves are being damped for which the theory makes no provision. Mogi's attempt to correct for this via normalizing by the incident wave height at the point in question is partially successful, but nevertheless agreement is to some extent circumspect. In view of this, we decided to repeat as closely as possible Mogi's experiment for a circular cylinder of radius $a=1.6\lambda\,(ka=10)$. See Fig. 6 for geometry of circular cylinder.

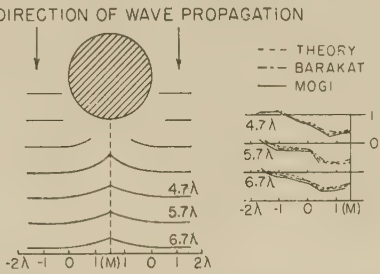

FIG. 7. Comparison of experimental data of Mogi and Barakat with theoretical values for $ka=10$. The left-hand side of the figure shows the position of the wave fronts, while the graph illustrates the computed and experimental normalized wave heights along the wave fronts at 4.7λ, 5.7λ, and 6.7λ.

Figure 7 shows the positions of the wave fronts according to Mogi; a considerable amount of trial and error was necessary before we could obtain comparable geometric relationships implied in the figure. The right-hand side of the figure summarizes the theory and observation. The theoretical result was obtained by summing the Hankel function series for $ka=10$ using eleven terms in the series. Our measurements seem to overestimate the wave heights along the horizontal scale 0 to (M) while Mogi's data underestimate the heights. The results seem to agree quite well with theory along the rest of the horizontal scale, although slightly under the theoretically predicted heights.

When kr is large, we can obtain a measure of the scattered intensity at a point (r,θ) from the well-known formula[6]

$$S(\theta)=\frac{2}{\pi kr}\sum_{m,n=0}^{\infty}\epsilon_m\epsilon_n \sin\delta_n' \sin\delta_m' \times\cos(\delta_m'-\delta_n')\cos m\theta \cos n\theta, \quad (6)$$

expressing the ratio of the scattered intensity at (r,θ) to the intensity of the incident wave. The measure of intensity is the height of the wave squared at the point in question. By fixing the angle θ we measured the wave heights at a series of fixed distances (kr) from the center of the cylinder and repeated the procedure every 10 deg from 30 to 150 deg. Any attempt to measure $S(\theta)$ at smaller angles than 30 deg or much larger than 150 deg is illusory since we can only measure the total of plane and scattered wave in these angular regions. We refer the reader to Morse and Feshbach[7] for a full discussion of the condition under which we can separate the scattered wave and plane wave.

TABLE I. Comparison of theoretical and experimental values of $S(\theta)$ for $ka=3$ and $kr=18$.

	Theoret.	Exptl.
30°	0.0978	0.110
40	0.1181	0.135
50	0.1351	0.139
60	0.1321	0.128
70	0.1031	0.095
80	0.0596	0.050
90	0.0222	0.020
100	0.0059	0.007
110	0.0102	0.010
120	0.0384	0.040
130	0.0535	0.053
140	0.1331	0.130
150	0.1446	0.145

Table I gives the results of theory and experiment for a cylinder of $ka=3$ and a field point $kr=18$; the field point condition does not represent exactly the far field constraint ($kr\gg1$) upon $S(\theta)$, yet is sufficient to permit comparison. Since we have to square the experimental wave heights and thereby introduce an even larger error into the problem, we should not expect to get close quantitative agreement with theory. Nevertheless the comparison was excellent. The experimental results are the average of 5 different measurements.

The relative intensity $S(\theta)$ was also measured for $ka=1.5$ and $ka=2$ at $kr=18$ essentially the same agreement with theory was obtained. We have not thought it necessary to reproduce this data.

The long wavelength or Rayleigh scattering limit ($ka\ll1$) for $S(\theta)$ can be shown to be given by[8]

$$S(\theta)\underset{ka\to0}{\sim}(\pi a/8r)(ka)^3(1-2\cos\theta)^2. \quad (7)$$

TABLE II. Comparison of theoretical and experimental values of $S(\theta)$ using Rayleigh scattering approximation with $ka=0.5$ and $kr=10$.

θ	Theoret.	Exptl.	θ	Theoret.	Exptl.
0°	2.39	2.95	100°	4.34	4.45
10	2.26	2.55	110	6.78	6.85
20	1.86	2.10	120	9.55	10.00
30	1.29	1.40	130	12.50	12.25
40	0.68	0.70	140	15.35	15.40
50	0.20	0.18	150	17.85	18.00
60	0.00	0.10	160	19.80	20.00
70	0.24	0.30	170	21.10	21.50
80	1.00	1.00	180	21.50	22.00
90	2.39	2.45			

Note here that there is a linear dependence of $S(\theta)$ upon the ratio (a/r) entirely independent of the incident wave number k. It is important to study this limiting case as most circular piles in practical problems would be subsumed under this category.

Table II gives a summary of the results using the Rayleigh scattering approximation. The table represents the average results of 10 measurements; the individual measurements fluctuated considerably but the average experimental values tend to confirm the theoretical values. Note the wide departure of theory and experiment for angles close to 0° to 180°. This confirms the well-known result that for angles close to 0° and 180°, we cannot separate out the scattered and plane waves but only measure the combination.

Finally there is one other quantity of interest which we can measure via the optical grid method; this is the total energy scattered, per second, per unit intensity which in the Rayleigh scattering range assumes the simple form[9]

$$Q\sim\tfrac{3}{4}\pi a(ka)^3. \quad (8)$$

We note that Q has dimensions of a length. We chose to

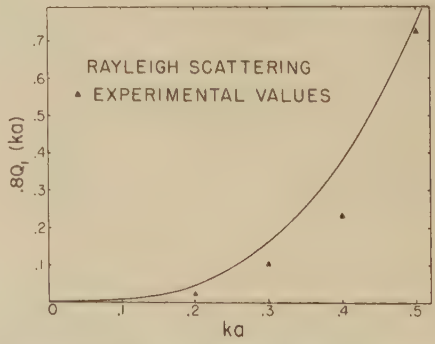

FIG. 8. Normalized measure of energy scattered in the Rayleigh scattering range for circular cylinder.

---

[6] P. M. Morse and H. Feshbach, *Methods of Mathematical Physics* (McGraw-Hill Book Company, Inc., New York, 1953), Part II, p. 1378

[7] See reference 6, p. 1378–1382.

[8] See reference 6, p. 1382.

[9] See reference 6, p. 1379.

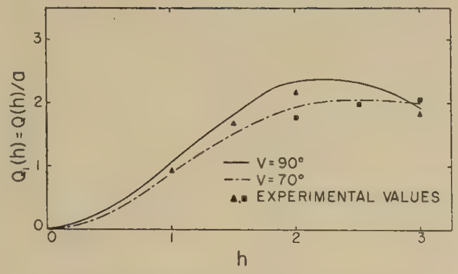

FIG. 9. Normalized measure of energy scattered for thin elliptic cylinder.

measure the dimensionless quantity $Q_1(ka)=Q/a$ which is simply the total area under $S(\theta)$. Figure 8 illustrates the dependence of Q_1 on (ka) in the longwave approximation. The experimental points again represent the average of 10 measurements. The experimental values all lie considerably below the predicted values as we would expect. As (ka) becomes very small, the scattered intensity $S(\theta)$ develops a very narrow peak in the forward direction, where we cannot separate out scattered and plane waves. When (ka) is sufficiently small we will not be able to measure any part of the forward peak at all; consequently our measured values are less than theory.

V. THIN ELLIPTIC CYLINDERS

We have a situation equivalent to diffraction by a finite lamina when an elliptic cylinder has an eccentricity near unity and is placed such that the major axis is parallel to the wave crests (see Fig. 6 for the geometry).

The dimensionless parameter governing the scattering is $h=ka/2$ where a is the interfocal distance. Reference is made to Morse and Feshbach[10] for the appropriate notation for the various Mathieu functions used. The boundary condition on the cylinder is that the gradient of the total velocity potential is zero. The relative intensity scattered at large distances from the strip is given by

$$S \to \frac{8\pi}{kr}\sum_{m,n}\frac{\sin\delta_m{}^0\sin\delta_n{}^0}{M_m{}^0M_n{}^0}\cos(\delta_m{}^0-\delta_n{}^0)\cdot So_m(h,\cos v)So_n(h,\cos v)\times So_m(h,\cos\theta)So_n(h,\cos\theta) \qquad (14)$$

where v is the angle of incident of the plane wave with respect to the major axis of the ellipse. Two cases are studied: (1) $v=90°$, (2) $v=70°$. Case 1 (normal incidence) simplifies since $So_{2n}(h,0)=0$. Table III shows contrasts for the theoretical results for a cylinder of eccentricity unit with the experimental results of a cylinder having an eccentricity of 0.9. The experimental values represent the average of 5 observations. Table IV summarizes the results for case 2. Again the experimental values represent averages of 5 measurements. Note that the curve decreases in magnitude as the angle v decreases; in fact as v approaches zero, Q_1 also goes to zero.

TABLE III. Comparison of theoretical and experimental values of S for $h=3$ and $h=2$ at $kr=20$ for normal wave incidence.

	$h=3$		$h=2$	
θ	Theoret.	Exptl.	Theoret.	Exptl.
30°	0.016	0.020	0.023	0.025
40	0.036	0.040	0.044	0.050
50	0.073	0.075	0.074	0.075
60	0.128	0.130	0.110	0.110
70	0.193	0.195	0.147	0.150
80	0.247	0.255	0.175	0.180
90	0.269	0.265	0.185	0.195

TABLE IV. Comparison of theoretical and experimental values of S for $h=3$ and $h=2$ at $kr=20$ for wave incident at 70°.

	$h=3$		$h=2$	
θ	Theoret.	Exptl.	Theoret.	Exptl.
30°	0.068	0.075	0.032	0.040
40	0.126	0.130	0.058	0.065
50	0.193	0.195	0.089	0.090
60	0.250	0.250	0.121	0.120
70	0.271	0.275	0.146	0.145
80	0.245	0.255	0.155	0.160
90	0.188	0.195	0.146	0.150

VI. CONCLUSION

The optical grid method is described in detail and the importance of its being able to measure the instantaneous diffracted field emphasized. The scattered wave intensity and the scattering cross section were determined experimentally and compared with theory. The experimental values agreed very well with theory for large distances from the object.

Much work remains to be done on bodies that are not simple and here the combination of optical grid method and source technique should provide adequate tools for future work.

ACKNOWLEDGMENTS

The research reported in this paper was supported by the Office of Naval Research. We wish to thank Dr. Paul Fye for making available to us all necessary facilities. We also wish to thank Mr. John Stimpson who made the translucent grid as well as helping us with a number of photographic problems that occurred.

---

[10] See reference 6, p. 1407.

Contribution No. 1075

KIELER MEERESFORSCHUNGEN

Institut für Meereskunde der Universität Kiel
Herausgegeben vom Direktor G. DIETRICH
unter Mitwirkung von A. REMANE (Zoologisches Institut),
G. WÜST, C. SCHLIEPER und R. KÄNDLER und J. KREY
(Institut für Meereskunde)

Band XV 1959 Heft 2

Sonderdruck S. 242—251

The effect of temperature on the oxygen uptake and rate of development of the egg-masses of two common cirripedes, *Balanus balanoides* (L.) and *Pollicipes polymerus* J. B. Sowerby.

H. Barnes and Margaret Barnes

Kommissionsverlag Walter G. Mühlau, Kiel

The effect of temperature on the oxygen uptake and rate of development of the egg-masses of two common cirripedes, *Balanus balanoides* (L.) and *Pollicipes polymerus* J. B. Sowerby.

H. Barnes and Margaret Barnes

The Marine Station, Millport, Scotland.

The egg-masses in many cirripedes take the form of two compact lamellae occupying much of the adult mantle cavity in which they are incubated until the ripe embryos are hatched. Under optimal conditions, this period of incubation in a typical warm water species, may be quite short (10—15 days) as one brood follows another in rapid succession. By contrast, incubation in some arctic or boreo-arctic species may occupy several months. For example, in the Arctic, the eggs of *Balanus balanoides* are fertilized in the late summer and remain in the mantle cavity until the following June-July; during much of this time the animals may be frozen under the ice foot. Further south, for example, at Millport, Scotland, the embryos are retained from November to the following spring. At Woods Hole, Mass., U.S.A., where planktonic conditions are somewhat atypical for a north temperate coastal region (Fish, 1925), incubation may last only from October to December (Barnes 1958; Barnes and Barnes, 1959a).

In view of these facts the respiratory activity of the egg-masses of two intertidal cirripedes namely *B. balanoides* (L.) and *Pollicipes polymerus* J.B Sowerby has been investigated The former, common on both sides of the Atlantic and recorded from the Alaskan coast, is a typical boreo-arctic operculate and the latter, common on the Pacific coast of both North and South America, a temperate and possibly sub-tropical pedunculate.

Development of the embryos.

The embryology of a number of common barnacles has been examined in some detail by Groom (1895); the earlier stages of embryogenesis in *Balanus balanoides* was given particular attention by Delsman (1917) and Batham (1946) has given an account of the formation and development of the egg-mass of *Pollicipes spinosus* Quoy and Gaimard. Embryonic development appears to be very similar in many cirripedes; the following stages are recognised by Groom (loc. cit):

Stage A. Formation of polar bodies and first blastomere; the freshly laid ovum consists of granular protoplasm, coarse and fine yolk granules, together with oil globules of various sizes. The first polar body is soon formed and the egg is probably fertilized prior to the formation of the second polar body.

Stage B. Formation of blastomeres and growth of blastoderm over yolk; blastoderm, formed by repeated division, gradually extends from the anterior to the posterior pole until it eventually comes to cover the whole yolk. The position of the blastopore appears to be variable.

Stage C. Formation and extension of mesoblast and hypoblast; closure of the blastopore is followed by division of the yolk within the single layered epiblast.

Stage D. Formation of naupliar segments.

---

1) Contribution No. 1075 from The Woods Hole Oceanographic Institution. I wish to acknowledge a Research Fellowship from this Institution, support from the National Science Foundation (Grant No. G 3235, to Professor T. H. Bullock, Department of Zoology, University of California, Los Angeles) and the Office of Naval Research (Contract No. N. R. 165/142, to Dr. D. L. Ray, Department of Zoology, University of Washington, Seattle), as well as leave of absence granted by the Council of the Scottish Marine Biological Association.

Stage E. Marking out of naupliar appendages; this stage differs from the preceding only in that the epiblast and mesoblast are traversed by the dorsal longitudinal groove.

Stage F. Origin of labrum, oesophagus and intestine; the furrows on the dorsal side of the embryo become more marked forming very considerable depressions.

Stage G. Appendages long with short setae; the embryo at this stage is much transparent; various organs and body cavity can be distinguished.

Stage H. Development of the ultimate naupliar form ready for hatching; the appendages lengthen, the spines become very distinct and the embryo is even more transparent than in the preceding stage. It is particularly characterized by the development of a single median eye which in the later phases becomes deeply pigmented. The yolk endoderm, at first forming a solid mass, later separates and eventually yolk endoderm surrounds a wide cavity.

The Material and Methods

The animals were collected and brought to the laboratory as quickly as possible while still attached to substrata such as rock, stones or shells. Where they had to be transported for some distance, delay was reduced to a minimum and the material kept at ambient air temperature and immersed at intervals in sea water. For each set of experiments, egg lamellae were carefully removed from adult mantle cavities, transferred to a dish of sea water, and each lamella examined under a binocular microscope. The lamellae were then graded according to GROOM's classification; the required numbers in any given stage of development were lightly dried on filter paper and quickly weighed before being transferred to a manometer vessel containing a measured volume of sea water.

The oxygen uptake was measured using standard Warburg constant volume respirometers. The vessels (volume 15—21 ml.) had 3 or 5 ml. of sea water containing 1 mg/l of choloromycetin to prevent bacterial action but had no addition of any substrate; 10% KOH and filter papers were used in the centre cups. The gas phase was air. Preliminary experiments showed that, under the conditions employed, oxygen uptake was not affected by the presence of chloromycetin and that O_2 uptake/g. wet tissue/hr. (or $\mu l\ O_2$/mg. N/hr.) was independant of the duration of the experiment and amount of material used. 30 minutes were allowed for equilibration. Experiments were run for 2—4 hrs. (depending upon the temperature) at 0^0, 5^0, 10^0, 15^0 and 20^0 C, and check readings were taken at intervals.

After the oxygen uptake had been determined the lamellae were transferred to a Kjeldahl flask wet ashed and their nitrogen contents determined by a standard semimicro technique.

The results are expressed ether as μlO_2/g. wet tissue/hr. or μlO_2/mg N/hr.

As stated above each lamella was characterized according to GROOM's scheme; however, because this grading was done as rapidly as possible to avoid deterioration of the material and because lamellae had often to be pooled in order to obtain adequate manometer readings, the results from the various stages have been pooled into four categories, namely GROOM's A+B, C+D+E, F+G and H. These are relatively natural divisions in development and except for the last stage, take about equal times at moderate temperatures; stage H takes longer than the others and includes several phases of development prior to hatching.

All the experiments on *Balanus balanoides* were done at Woods Hole; much of the material was collected either from the nearby Institution pier or from Rocky Beach — a small stoney shore at the entrance to Buzzards Bay. In addition animals were investigated from two points in Maine some 200 miles (latitudinal) to the north — collections being made at Cundy's Harbor, a relatively well sheltered inlet several miles from the open coast, and at Small Point on the outer exposed coast. A single series of comparisons was also made on lamellae taken from animals collected further to the south (150 miles, latitudinal) at Sandy Hook, New Jersey. The experiments on *Pollicipes polymerus* were made on material collected at Will Rogers State Beach, near Santa Monica, California and at Friday Harbor, Washington some 1000 miles (latitudinal) further north.

The Results

It was possible to obtain sufficient numbers of embryos in different stages from these widely separated places to compare their oxygen uptake even although for *Balanus balanoides* their initial fertilization had taken place more or less synchronously. The results are shown in Tables 1 and 2. (In the limited time available and in view of the fact that some of the material had to be transported several hundred miles, a comparison of all stages at all the selected temperatures was not possible). Irrespective of the stage of development or the temperature at which the estimations were made there is no

Table 1

Balanus balanoides: oxygen uptake (µl/g/hr) of lamellae in different stages of development at different temperatures. Animals from Maine (Small Point S.P.M.; Cundy's Harbor C.H.M.) and Woods Hole (Pier, W.H.P.; Rocky Beach, W.H.R.B.).

T°C. / Stage	5	10	15	20
D	—	—	—	S.P.M. 107 W.H.P. 109 W.H.R.B. 98
E	C.H.M. 23 W.H.P. 27 W.H.R.B. 41	—	S.P.M. 85 C.H.M. 79	C.H.M. 126 W.H.P. 126
F	S.P.M. 29 W.H.P. 34	W.H.P. 58 W.H.R.B. 57	W.H.P. 103 S.P.M. 100	—
G	—	S.P.M. 79 W.H.R.B. 67	—	—

Table 2.

Pollicipes polymerus: oxygen uptake (µl/g/hr) of lamellae in different stages of development at different temperatures. Animals from Los Angeles, California (L.A.) and Friday Harbor, Washington (F.H.)

T°C. / Stage	15	20	25
C	—	—	L.A. 237 F.H. 245
G	—	L.A. 342 F.H. 323	L.A. 375 F.H. 410
H	L.A. 190 F.H. 188	L.A. 282 F.H. 305	—

indication in the case of either species of any significant regional difference in regard to oxygen uptake. For *Balanus balanoides* this is further evidence in support of a previous suggestion that is little indication of any sub-speciation adequate to separate physiologically distinct races in this area (Barnes and Barnes, 1959 a). The orgin of the animals will, therefore, be neglected in the further treatment of the results that follows.

The results are shown in Figure 1, in which log. oxygen uptake/mg. N/hr. for the several pooled stages of development described above has been plotted against the reciprocal of the absolute temperature. They are plotted in this conventional form for convenience of discussion; nothing is thereby implied regarding any theoretical interpretation of such curves in relation to the energy of activation of complex biological processes. Although discrete breaks are shown, the curves may in reality be continous curves with constantly changing slope. In both species, as is commonly the case when embryos cannot be (or are not) separated from yolk, the earlier stages with their smaller quantity of active protoplasm give the lower respiratory rates at any given temperature. With *B. balanoides* the initial stages of the curves are of similar slope, but with rising temperature there is a marked 'inflexion' (change of slope if the curves are continuous) which occurs at a successively higher temperature with advancing stage of development. The effect of increase in temperature on the rate of respiration is greatest at low temperatures on the early stages. It may be noted that there is an indication that a rise of temperature from 15—20° C. has a deleterious effect on the late stage (H) embryos. Between 0—5° C. there is little difference in oxygen uptake between the stages of development up to that in which the nauplii appendages are marked out (CDE). Elsewhere over the temperature range investigated *B. balanoides* shows a marked increase in respiratory rate from stage to stage. The slope of the lower parts of these curves approximates to a Q_{10} value of 4.2 and of the upper parts above the 'inflexion' of 2.2.

No data are available for the early stages of *Pollicipes polymerus*. For the later stages (CDE onwards) the curves show a marked change of slope at 10° C, this change taking place at the same temperature for all the stages in contrast to the situation found in *Balanus balanoides*. The most striking difference, however, is the relative independence of temperature (above 10°) of the CDE stage in *Pollicipes*; changes in respiratory rate as one passes from this to the next are, therefore, very marked at the higher temperatures. Below 10° C. the slope corresponds to a Q_{10} of 4.2, as in *Balanus*, but above 10° C. for all the stages except CDE the value approximates to 2.5.

Because the inflexion varies with the embryonic stage in *Balanus balanoides* the relative rates at which the two species take up oxygen will change with the temperature at which the comparison is made, although *Pollicipes* embryos always respire at a higher rate over the range investigated. At 15° the rate for the latter species is 1.25 times that of the former, but at 5° the differences are greater in the earlier stages (2.2 for CDE). However the eggs of *Pollicipes* are much smaller than those of *Balanus*, the former averaging 0.08 × 0.15 mm. and the latter 0.19 × 0.31 mm. The volume of a single egg of *Pollicipes* is about $^1/_{12}$ that of a *Balanus* egg. However, the ratio of wet weight to nitrogen is somewhat greater, (1.5 times) in *Pollicipes* so that on the basis of a single egg corrected for the difference in nitrogen content the rate of oxygen uptake of a *Pollicipes* egg approximates to $^1/_6$ to $^1/_3$ that of a *Balanus* egg. (The densities of these similar eggs are presumed equal).

Development of the embryos in vitro

The in vitro development of cirripede embryos has not often been reported although Batham (1946) has given an account of the culture of *Pollicipes spinosus* embryos. A number of species have now been reared including *Balanus balanoides*. As indicated by the work of Oppenheimer (1955) success would seem to depend upon keeping the growth of bacteria and fungi in check; adequate aeration is also essential. The following method has been found satisfactory for barnacles. Two or three egg-masses are placed in a series of small containers through which a continuous flow of sea water at the selected temperature is maintained. Over the outlet tube of each container a piece of fine plankton gauze is fastened to prevent the escape of nauplii after they have hatched. This gauze may be changed at intervals to prevent clogging. The sea water is adjusted to the selected temperature before reaching the containers and the latter are maintained in a constant temperature bath. At the inlet to the train a two-way tap allows the system to be cut off from the main supply and to be put into connection with a vessel containing a bactericide. After cutting off the main supply the system was flushed out daily with 2 litres of sea water containing 1 mg. chloromycetin per litre. Embryos treated in this way were inspected frequently, and after passing through all the sequence of colour changes observed when they are incubated in the adult mantle cavity, normal and fully viable nauplii were hatched out. There was no apparent arrest in the eyed stage consequent upon the lamellae being outside the mantle cavity (for discussion, see Barnes, 1954; Barnes and Barnes, 1959b; Crisp and Spencer, 1958). *Balanus balanoides* took 32 days at 5^0 and 11 days at 15^0 C. to hatch, the original material being in the 8—16 cell stage. This is equivalent to a Q_{10} of almost 3.0, and is similar to the value found by Crisp and Davies (1955) for *Elminius modestus*, an Australian barnacle now common in Britain. Between 5^0—15^0 C the Q_{10} of oxygen uptake is 2.2 for the first and in part the second stages, and 4.2 for the two later stages. Since each of these pooled stages takes about the same time for complete development, it is evident that the Q_{10} for total development time is similar to the overall value for the rate of respiration obtained experimentally.

Development of the embryos on the shore

In addition to following the development of *Balanus balanoides* embryos in vitro, shore populations at Millport, Scotland, and Woods Hole, have been investigated. Samples were taken at fortnightly intervals and again staged according to Groom's classification. Careful check had been kept on the state of the animals so that at any particular collecting locality the time when they fertilized was known to within a few days.

It has already been stressed that naupliar release is related to the spring diatom increase in the eastern Atlantic and Arctic regions (Barnes, 1957; Crisp and Spencer, 1958). At Woods Hole with a considerable winter diatom population it might be expected that with constant feeding activities nauplii would be released as soon as embryonic development is complete. This is the case as regards a proportion of the population — but a considerable number delay release which takes place over several weeks. The samples taken from the Woods Hole Institution pier will be first considered. Here the whole population behaved similarly. The animals were fertilized during the second half of October. Within three-four days all the animals in the samples were found to

Legenden zu den nebenstehenden Abbildungen (Tafel 49)

Fig. 1: Oxygen uptake (μlO^2/mg.N/hr.) for *Balanus balanoides* and *Pollicipes polymerus* eggmasses at various temperatures and stages of development; logarithmic scales.

Fig. 2: *Balanus balanoides* at Woods Hole; development of egg lamellae at various levels on the shore during the latter part of the season: e = empty, nauplii released.

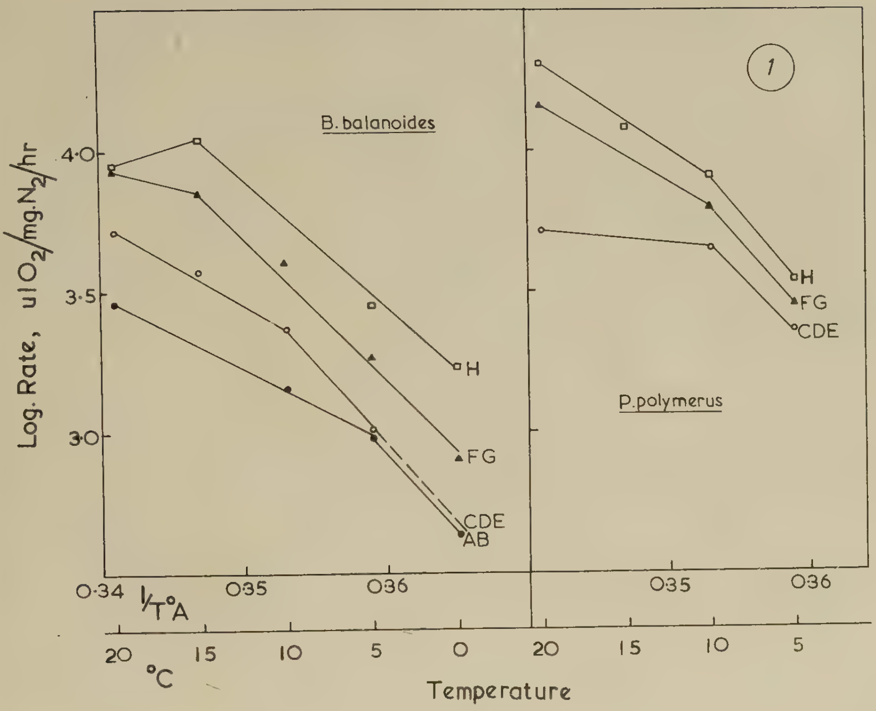
1
B. balanoides
P. polymerus
Log. Rate, ul O_2/mg. N_2/hr
4·0
3·5
3·0
H
FG
CDE
AB
0·34
0·35
0·36
1/T°A
20
15
10
5
0
°C
Temperature

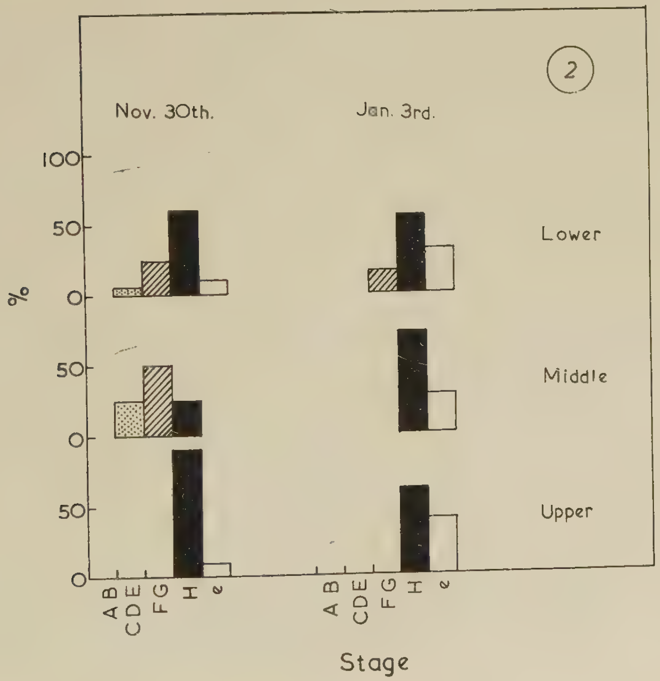
2
Nov. 30th.
Jan. 3rd.
100
50
0
%
Lower
Middle
Upper
AB
CDE
FG
H
e
Stage

Tafel 49

contain embryos; on 30th October 100% were in the AB stage. By 11th December 99% were in Stage H and 1% had released their nauplii. This gives a period of about 45 days for development; this is in good agreement with the in vitro results when it is remembered that during November both sea and air temperatures were falling rapidly. For these months the mean sea surface temperature is 11° falling to 6.6° C (mean max. 10.1° C, mean min. 3.1° C) and reaching 3.5° C. (mean max. 6.7° C; mean min. 1.5° C.) in December. Although hardly affecting the pier population the shores were often frozen during the mornings but no ice cover was formed during this period. The pier population in stage H, however, released nauplii for two months, some 3% still containing stage H embryos on 4th February. During this period, however, air temperatures were around zero — (January, mean max. 3.7° C.: mean min. —2.9° C: February, mean max. 4.2° C: mean min. — 3.1° C.) and the mean water temperatures were 1.7° C. and 0.7° C. for the two months. The shores during this period in 1957 both at Woods Hole and elsewhere in the Buzzards Bay region were frozen up.

Detailed continuous observations on the shore, where samples were taken at several levels, were started later and the early stages of development of the population missed. The animals began to be fertilized earlier (Oct. 11th—15th) than on the pier. Even so, certain features are worthy of comment. On 16th November only 18% of the population of the upper shore had lamellae in stage FG, the remainder being at early stage H, and yet at the lowest levels of the shore 10% were still at stage AB, 80% at CDE, and 10% at stage FG and none had reached the eyed stage. Evidence has been presented (Crisp, 1957; Barnes, 1958, 1959) that there is a temperature bar to the processes associated with the fertilization or final maturation of the gametes; at Woods Hole these are well developed during the late summer. It is considered that the upper shore will be released from this temperature barrier sooner than the lower shore since although water temperatures even in October are still high, air temperatures are falling very rapidly. On the upper shore the period of development appears again to be of the order of 40 days; Moreover, although by 15th December some 10% had released their nauplii — entire release of the population was not completed until February to March. During much of this time the shores were iced-up. At the lowest levels of the shore not only was fertilization much delayed but it was much less synchronous. However, once initiated, development was more rapid. The interpretation placed upon these facts is that once the temperature barrier has been removed at the lower levels of the shore which happens somewhat later in the season than at the upper levels, the higher sea temperatures and freedom from ice will not only allow development to proceed more rapidly but will also allow naupliar release to take place once development is completed.

At Millport the eggs are not usually fertilized until November; it is initiated fairly regularly during the first fortnight. Development to Stage H occupies some 50—60 days and in 1957 samples (100%) taken from the pier remained in this stage during the whole of February. There is, therefore, a delay either in the final stages of development or in the actual release of the nauplii. Release was, however, fairly synchronous being completed during March and indeed over 50% of it during the early part of the month. Temperatures — both sea and air — are much higher at Millport during this period of embryonic development than at Woods Hole (the mean air temperature lying between 6.5° and 4° C and mean sea temperatures between 10.5° and 7.0° C). The long time of development to stage H is, quite apart from the delayed release, therefore, unexpected and as has been suggested previously, may be due to inadequate ventilation of the mantle cavity consequent upon inactivity resulting not from low sea temperatures but from the absence of diatoms in the water (Barnes, 1957).

Rather less precise data is available for the development under natural conditions of *Pollicipes polymerus* lamellae and none for in vitro development. Batham (1946) has given a period of 30 days for development of *P. spinosus* in the laboratory at an unspecified temperature. Since breeding is continous during the warmer months and since the state of the lamellae in a single animal cannot be followed through the whole period of development, an estimate of this period cannot be made by examination of a series of random samples from the population. An estimation of the proportion of the time spent in each stage is, however, readily obtained by regular sampling.

At weekly intervals, collections were made at Friday Harbor and Los Angeles and lamellae graded according to the previous scheme; this was done throughout the summer. Since sampling was carried out at regular intervals and the same number (20) of animals staged on each occasion the fraction of the total generation time spent in any stage is given by the percentage of animals in that stage over the whole sampling period. The following results were obtained.

Table 3.

Percentage animals (*Pollicipes polymerus*) in given stage of development. Samples (20 animals taken) weekly throughout the summer; Los Angeles and Friday Harbor.

Stage	AB	CDE	FG	H	Empty
Los Angeles (July—September	2.7	6.5	5.2	15.0	70.6
Friday Harbor (July—August)	3.7	6.9	5.6	25.7	58.1

There are two notable features of these results; first the relatively long time spent in the "empty" phase and secondly the relatively longer time in stage H at Friday Harbor. The prolonged time during which the animals have no lamellae indicates that in any animal one brood does not succeed another in rapid succession. It is suggested that this is in keeping with the known sluggish behaviour of the animal; for example, Batham (1946) has pointed out that growth in the related *P. spinosus* is extremely slow, and it may be assumed that in view of a generally low metabolic activity this long period in between broods is required for building up of the ovary. This would also be in accord with the observed low rate of oxygen uptake when expressed on an egg basis (p. 245).

Discussion

There are few references in the literature to the oxygen consumption of crustacean eggs over the whole period of embryonic development and indeed relatively few Q_{10} values during this process for marine invertebrates other than echinoderms. Needham (1931) determined the oxygen consumption of *Carcinus maenas* embryos at 17° and 35° C — pointing out, however, that the latter temperature was lethal to the adult. His results are expressed in terms of weight of eggs and on this basis, as in the present experiments, the earliest stages with the smallest amount of active protoplasm showed the least respiratory activity. Between 15° and 37° C Needham found some — though not a great — variation of Q_{10} with the stage of development; all his values lay between 2.03 and 2.5. It is of interest to note that Melvin (1928) found that in the development of a number of insects temperaure had very little effect on oxygen uptake during the early stages but its influence was considerable during the late stages; it is evident from his figures that, while in the early stages Q_{10} was little more than unity, in the late stages it reached values greater than 3.0.

Apart from the apparent insensitivity of the CDE stage to temperature in *Pollicipes polymerus*, the major difference between it and *Balanus balanoides* is that in the former the Q_{10} for all stages above 10° C. approximates to 2.2, whereas in the latter such a value is only found at the higher temperatures. Now although it is well known that under certain experimental conditions respiratory activity and morphological development can be dissociated, the available evidence suggests that, as regards the effect of temperature, they are closely linked in these two cirripedes. This is particularly indicated by the fact that similar values of oxygen uptake are obtained for a particular stage of development whatever its previous temperature history (pp. 244 and 245). This may not be the case outside the temperature range investigated or under natural or experimental stresses other than temperature. *B. balanoides* is a northern form and the development of the egg-masses takes place at a relatively low temperature (below 10° C.) since this development succeeds a phase (the final stages of the maturation of the gametes) which has an upper critical temperature. With the exception of the early stages (AB) a Q_{10} of about 4.0 will be applicable to animals in their natural environment. If the respiratory and developmental processes are closely linked with respect to their Q_{10} values, the high value of the latter would seem to be of ecological significance. It has previously been stressed (BARNES, 1957) that the time available for development in artic regions is an important determinant in the distrioution of the species; in such places, once released from ice-cover under which the embryos, within the mantle cavity, have spent the winter, a high value of Q_{10} allows development to be accelerated with the rising temperatures during the artic spring so that the embryos are ripe early during the diatom bloom. Falling temperatures during the autumn subsequent to fertilization will similarly tend to retard embryonic development so that the animals will become frozen under the ice foot when the embryos are in a relatively early stage. There is some evidence (personal, unpublished) that early stages are better able to withstand the freezing and melting that occurs at the onset of winter than are the late stages. In contrast it may be noted that, except in Stage H, between 15° and 20° C there is apparently little deleteriouse ffect of tempratures above the normal habitat range on respiratory activity during embryonic develop-ment.

The time of development on the shore at Woods Hole agrees reasonably well with that estimated from the in vitro experiments on *B. balanoides*. At Millport, however, the time required to reach the H stage is somewhat longer than expected from the temperature conditions; BARNES (1957) has suggested that this may be due to somewhat inadequate ventilation of the mantle cavity during the winter months when feeding is minimal. There is then a further delay at Millport in the H stage and this is associated with processes concerned in the hatching of the embryos that lead to liberation at the time of the spring diatom increase.

There has recently been much interest in homeostasis in poikilothermous animals (SEGAL, RAO and JAMES, 1953; BULLOCK, 1955; SEGAL, 1956; DEHNEL, 1956). There is much evidence that animals living in colder regions have, at the temperature of their environment, a relatively higher metabolic rate than animals in warmer regions have at the same low temperature.

Relatively little is known concerning the mechanism of homeostasis and some discussion has centred round the effect of temperature on Q_{10} values since a low value of Q_{10} clearly results in homeostatic tendencies. RAO and BULLOCK (1954) have maintained that there is a tendency for lower values of Q_{10} to play a part in homeostatis whereas SCHOLANDER, FLAGG, WALTERS and IRVING (1953) consider changes in sensitivity to temperature play no part in climatic adaptation which, they believe, is brought about by a shift in the metabolism (or activity) — temperature curve and not a change in its slope. One of the objects of the current work was to compare the metabolism of egg lamellae of the two different species as well as the same species over a range of latitude. On the one hand, it might be expected that in a sessile animal acclimation would be more marked since there is no possibility of retreat to a more favourable micro-habitat; on the oher, the great changes in the environment to which intertidal animals are constantty subjected might be expected to mitigate against such a hypothesis. However, acclilmation has been indicated with regard to a number of rate functions in intertidal species and KIRBERGER's work (1953) indicates that some animals can 'average' temperature fluctuations.

In the present instance, as far as it was possible to test, there is no acclimation as regards the oxygen uptake of embryos in either *B. balanoides* or *Pollicipes polymerus.* At each temperature employed and with all the stages tested the oxygen uptake was the same for animals taken over a wide range (see Tables 1 and 2) although there were considerable variations in habitat temperature. Furthermore, there is no evidence of a reduction in Q_{10} at low temperatures. It is clear that any acclimation in embryonic development would have to take place at the metabolic rather than the behavioural level and as PROSSER (1956) has pointed out there is general evidence that activity acclimation is more common than that of basal metabolic processes.

Summary.

1. Data are presented on the oxygen uptake, determined by the Warburg technique, of the isolated egg-masses of *Balanus balanoides* and *Pollicipes polymerus.*

2. Oxygen uptake of egg-nasses from widely separated places (latitudinal) showed no significant differences at any of the stages of development tested.

3. The earlier stages of development give low respiratory rates.

4. In *Balanus balanoides* the Q_{10} changes with stage and temperature whereas above 10° C all stages of *Pollicipes polymerus,* except CDE, have the same value of Q_{20}.

5. The oxygen uptake (on a per egg basis) of the pedunculate is $^1/_3$ rd. to $^1/_6$ th. that of the northern operculate.

6. The in vitro development of egg-masses is described.

7. An account of development in some natural shore populations and the effect of temperatures on them is presented.

8. The ecological significance of the results is discussed.

We wish to acknowledge the critical comments of a number of friends particularly those of Dr. PETER TUFT and to thank Mr. D.M. FINLAYSON for assistance with the nitrogen estimation.

References

BARNES, H.: Processes of restoration and synchronization in marine ecology; the spring diatom increase and the 'spawning' of the common barnacles, *Balanus balanoides* (L.). Ann. Biol., 33, 67—85, 1957. — BARNES, H.: Regarding the southern limits of *Balanus balanoides* (L.). Oikos, 9, 139—157, 1958. — BARNES, H.: Temperature and the life cycle of *Balanus balanoides* (L.). Friday Harbor Symposia in Marine Biology; I. Marine Boring and Fouling Organisms. Univ. Wash. Press, 234—245, 1959. — BARNES, H. and BARNES, M.: A comparison of the annual growth patterns of *Balanus balanoides* (L.) with particular reference to the effect of food and temperature. Oikos, 10, 1-18 1959a. — BARNES, H. and BARNES, M.: Stimulation of hatching in cirripede nauplii. Oikos, 10. 19-23, 1959b. — BATHAM, E. J.: *Pollicipes spinosus* Quoy and Gaimard. II. Embryonic and larval development. Trans. Proc. Roy. Soc. N. Z., 74, 405 —418, 1946. — BULLOCK, T. H.: Compensation for temperature in the metabolism and activity of poikilotherms. Biol. Rev., 30, 311—342, 1955. —

Crisp, D. J.: Effect of low temperature on the breeding of marine animals. Nature, Lond., 179, 1138—1139, 1957. — Crisp, D. J. and Davies, P. A.: Observations *in vivo* on the breeding of *Elminius modestus* grown on glass slides. J. mar. biol. Ass. U. K., 34, 357—380, 1955. — Crisp, D. J. and Spencer, C. P.: The control of the hatching process in barnacles. Proc. Roy. Soc. Ser. B, 149, 278—299, 1958. — Dehnel, P. A.: Growth rates in latitudinally and vertically separated populations of *Mytilus californianus*. Biol. Bull., 110, 43—53, 1956. — Delsman, H. C.: Die Embryonalentwicklung von *Balanus balanoides* Linn. Tidj. Nederland. Dierkung. Ver., Ser. 2, 15, 419—520, 1917. — Fish, C. J.: Seasonal distribution of the plankton of the Woods Hole region. Bull. Bur. Fish, 41, 91—179, 1925. — Groom, T. T.: On the early development of cirripedia. Phil. Trans. Roy. Soc. B, 185, 119—232, 1894. — Kirberger, C.: Untersuchungen über die Temperaturabhängigkeit von Lebensprozessen bei verschiedenen Wirbellosen. Zeitschr. vergl. Physiol., 35, 175—198, 1953. — Melvin, R.: Oxygen consumption of insect eggs. Biol. Bull., 55, 135—142, 1928. — Needham, J.: 'Chemical Embryology'. Vol. II. Cambridge Univ. Press, 1931. — Oppenheimer, C. H.: The effect of marine bacteria on the development and hatching of pelagic fish eggs, and the control of such bacteria by antibiotics. Copeia, No. 1, 43—49, 1955. — Prosser, C. L.: Physiological variation in annimals. Biol. Rev., 30, 229—262, 1955. — Rao, K. P. and Bullock, T. H.: Q_{10} as a function of size and habitat temperature in poikilotherms. Amer. Nat., 88, 33—44, 1954. — Scholander, P. F., Flagg, W., Walters, V. and Irving, L.: Climatic adaptation in arctic and tropical poikilotherms. Physiol. Zool., 26, 67—92, 1953. — Segal, E.: Microgeographic variation as thermal acclimation in an intertidal mollusc. Biol. Bull., 111, 129—152, 1956. — Segal, E., Rao, K. P. and James, T. W.: Rate of activity as a function of intertidal height within populations of some littoral molluscs. Nature, Lond., 172, 1108—1109, 1953.

Contribution No. 1076

Reprinted from COPEIA, 1960, No. 3, pp. 243–245, September 26
Printed in U. S. A.

NOTES ON WESTERN NORTH ATLANTIC SHARKS, No. 2.—The data reported here chiefly bear on the distribution of western North Atlantic sharks. They come from a variety of sources and the author is indebted to the following people for help in accumulating them: Mr. Norman Benson, Vineyard Haven, Mass.; Mr. George Berglund, U. S. Fish and Wildlife Service, Provincetown, Mass.; Mr. Russell Boardman, Mattapoisett, Mass.; Dr. Robert L. Edwards, USFWS, Woods Hole, Mass.; Dr. Robert H. Gibbs, Boston University; Mr. Robert Leahy, Woods Hole, Mass.; Capt. Norbert Macara, Provincetown, Mass.; Mr. James L. Squire, Jr., USFWS, Gloucester, Mass.; Mr. Samuel Vincent, now of Lewes, Delaware; Mr. Milton Welt, S. Harwich, Mass.; and Messrs. Frank J. Mather, III, Stanley E. Poole, William E. Schevill, and William C. Schroeder all of the Woods Hole Oceanographic Institution. I would also thank the officers and crews of the Research Vessels ATLANTIS, ASTERIAS, BEAR and CRAWFORD of W.H.O.I. and of the USFWS vessel DELAWARE. This note is Contribution No. 1076 from the Woods Hole Oceanographic Institution.

Lamna nasus (Bonnaterre), mackerel shark. The following longline captures were made on exploratory fishing cruises of the R/V DELAWARE of the United States Fish and Wildlife Service. Depth of capture could have been at any depth from about 100 meters to near the surface. The identifications were made by F. J. Mather, III.

On January 23, 1959, at 37°30′N, 71°33′W, a female, 112 cm. in total length, and on May 20, 1959, at 38°42′N, 68°32′W, a male, 98 cm. in total length were taken. Both of these records, which came from near the 2000-fathom curve, are of interest since *Lamna nasus* is generally considered to be a shark of the continental shelves, there being no records of it in the western North Atlantic from deep water, save one just off the shelf near Sable Island Bank (Bigelow and Schroeder, 1948, *Fishes of the western North Atlantic, 1:118–9*). The rather small size of these specimens is also of interest.

Isurus oxyrinchus Rafinesque, mako shark. Since the distribution of this shark is not well understood, a summary of seven long-line captures made during exploratory fishing cruises by the R/V DELAWARE is given in Table I. Depth of capture could have been at any depth from about 100 meters to near the surface. Cephalopod and fish remains (including an *Alepisaurus*), and in one case some pieces of salps, were found in the stomachs.

Carcharodon carcharias (Linnaeus), white shark. To recent records of this species for the New England coast (Scattergood and Coffin, 1957, Copeia: *155*; Backus, 1957, Copeia: *246*; Bigelow

Table I

Records of *Isurus oxyrinchus* Made on R/V Delaware Cruises

Position	Date	Sex	Total Length (cm.)
38°58′N, 66°26′W	June 9, 1957	M	166
37°45′N, 66°32′W	June 10, 1957	M	131
37°30′N, 68°10′W	June 12, 1957	F	205
42°18′N, 64°02′W	Sept. 11, 1957	F	176
40°34′N, 64°02′W	Sept. 12, 1957	M	200
38°49′N, 68°00′W	May 21, 1959	M	201
38°37′N, 68°24′W	May 24, 1959	M	158

and Schroeder, 1958, Copeia: *54*; and Scattergood and Goggins, 1958, *Marine Field Naturalist, 14:40*) the following may be added. A male, 188 cm. in total length, was taken in a fish trap off Quisset Harbor, Woods Hole, Mass. on May 29, 1958. According to Mr. Robert Leahy, Marine Biological Laboratory, Woods Hole, another specimen of the same kind and of about like size was taken in the same trap on May 31, 1958.

On July 6, 1959, an immature female 278 cm. in total length was taken in the same trap. The dressed weight of the animal was about 115 kg. The head, fins, and viscera were estimated as weighing from 35 to 45 kg. so that the total weight was likely between 150 and 160 kg. The stomach contained fish remains including an intact menhaden about 30 cm. long.

On September 2, 1959, an immature male, 189 cm. in total length, was harpooned at the surface about two miles south-southeast of West I., Buzzards Bay, Mass. by Mr. Russell Boardman of Mattapoisett, Mass. The claspers were about 17 cm. long and extended about 10 mm. past the tips of the pelvic fins. This animal weighed 78.4 kg.

On September 5, 1959, a newly-dead male specimen, 169 cm. in total length, was found on Red River Beach, South Harwich, Mass. The claspers were about 12 cm. long and extended about 10 mm. beyond the tips of the pelvic fins. The stomach contained a few pieces of eel grass (*Zostera*) and a few ounces of a clear, yellow, oily fluid. The weight was estimated to be between 40 and 45 kg.

Cetorhinus maximus (Gunnerus), basking shark. Bigelow and Schroeder (1948, *Fishes of the western North Atlantic, 1:154–5*) say: "In colonial days the southern and western parts of the Gulf of Marine appear to have supported a considerable population . . . But the local stock soon went . . . into the try pot". These authorities can cite only 16 records (a few records involve more than one specimen) for this species from waters north of Cape Cod during the period from 1840 to the writing of their book. Some recent observations seem to temper this melancholy history and suggest a healthy population of this species in New England waters. At Cape Porpoise, Maine this animal is regarded as common enough by the fisherman there and is known as "nurse fish". In the spring months the mackerel-netters working out of this harbor commonly carry a saw which is used to untail such nurse fish and other large sharks (presumably mostly or wholly *Lamna*) as become entangled in their nets. A 20-footer was thus dispatched by fishermen about 10 miles southeast of Cape Porpoise on June 1, 1958. Another of this size was seen by W. E. Schevill and myself on the previous day a few miles northeast of Cape Porpoise. In the same area as the latter, two specimens between 15 and 20 feet in length were seen by Schevill on June 3, 1958. On June 5, 1958, we harpooned one of the same size here but lost him at the end of an hour. The animals seen by us were all swimming slowly at the surface with parts of the dorsal fin or dorsal and caudal fins showing and were feeding (mouth open and buccal region greatly expanded). They are easy to approach as other authors have noted. The one struck immediately sounded and never again showed itself.

The R/V CRAWFORD encountered a basking shark, estimated at 30 feet in length, on June 26, 1959 off the coast of Nova Scotia in 44°24′N, 62°20′W and on June 27, 1959 reported about 30 of these animals up to 30 feet in length during an hour's steam near 42°15′N, 64°46′W. Two individuals were almost run down by the vessel.

On August 3, 1959, W. E. Schevill and R. G. Weeks spotted a specimen 20 to 25 feet long from the air over the southwest edge of Stellwagen Bank about 10 miles northwest of Provincetown, Mass. On August 30, 1956, W. E. Schevill threw a harpoon at an eight– to nine–foot specimen in Menemsha Bight, Martha's Vineyard, Mass.

Sphyrna lewini (Griffith), a hammerhead shark. (This is the animal called *S. diplana* Springer by Bigelow and Schroeder, 1948, *Fishes of the western North Atlantic, 1:415*. According to Fraser-Brunner, 1950, *Rec. Austral. Mus., 22:213–4*, *S. diplana* must be regarded as a synonym of *S. lewini*, a possibility suggested by Bigelow and Schroeder). Since the Atlantic distribution of this shark is poorly known, the species having been confused with *S. zygaena* for many years, the following record is of interest.

A female, 304 cm. in total length (214 cm. from snout to anterior margin of precaudal pit), was harpooned on July 26, 1959, from the R/V BEAR at 37°55′N, 73°55′W. The animal was swimming at the surface with parts of the dorsal and caudal fins showing. The upper parts are a warm, olive-drab color as seen underwater. The fish was easily approached and struck but after a 10-minute struggle the harpoon-head withdrew. The shark surfaced nearby and was struck again and shot and landed after 25 minutes more fight. The stomach of this specimen contained unidentified fish remains and cephalopod beaks. Some of the latter, judging from their size, belonged to animals 50 to 75 cm. long. About two liters of eggs (up to about 40 mm. in size) were present in one ovary. The stretched oviducts and their supporting mesenteries suggested that this animal had previously borne young. The flesh of this animal is deep orange-red in color. A raw sample taken from the nape was very bland in taste and so soft as to be easily macerated by squeezing it between the tongue and the roof of the mouth.

On 25 July 1959, in 37°50′N, 73°50′W, a hammerhead shark of about the same size and appearance was seen. It was likely this species. This specimen sounded at the approach of the vessel, resurfaced, was approached a second time, sounded again and was seen no more.

On 30 July 1959, in 39°50′N, 70°50′W, two hammerheads swimming close together were seen which, judging from head and dorsal fin shape as well as general appearance, seemed to be this species. One was about 10 to 11 feet, the other about seven to eight feet long. These were approached numerous times. They sounded when disturbed but quickly reappeared at the surface. When swimming undisturbedly at the surface, the tail strokes were about one cycle per three seconds and about 75 cm. in amplitude.

Isistius brasiliensis (Quoy and Gaimard). Previous western Atlantic records are three: off Rio de Janeiro, from among the Bahamas and 160 miles north of the Bahamas (Bigelow and Schroeder, 1948, *Fishes of the western North Atlantic, 1:512*). A female specimen about 16.5 cm. in total length was taken at night in an Isaacs-Kidd midwater trawl between the surface and 415 meters on March 4, 1954, within a few miles of 19°N, 66°W. When removed from the net this specimen showed no signs of the brilliant luminescence for which the species is noted; however, the animal was near death.

Squatina dumerili (LeSueur), angel shark. Massachusetts records where summarized by Backus (Copeia, *1957:248*). Additional records are given which suggests that this animal is more common in southern New England waters than previously supposed.

A male specimen, 109 cm. in total length, was trawled in 60 meters off Race Point, Provincetown, Mass., sometime during the first week of December 1957 by Captain Norbert Macara of Provincetown.

A male specimen about 110 cm. in total length was trawled in 120 meters of water at about 40°10′N, 70°05′W on February 1 or 2, 1957, by the vessel R. W. GRIFFIN.

A specimen, about 115 cm. in total length, was trawled in Menemsha Bight, Martha's Vineyard, Mass. sometime between August 15 and 20, 1959.

Attention is called to the photograph of a specimen published in the *New Bedford Standard-Times* on October 24, 1957. The animal was trawled in 48 meters of water about 25 miles southeast of Noman's Land, Mass.

The following records were kindly furnished by Mr. William C. Schroeder:

A male, 112 cm. long, was taken in 133 meters of water at 39°55′N, 71°45′W by the dragger PRINCESS on March 21, 1957.

The dragger GROWLER caught a "large one" near Veatch Canyon (about 40°N, 69°30′W) in 125 meters of water on March 27, 1957.

A dragger took a male about 110 cm. long in Menemsha Bight, Martha's Vineyard, Mass. on August 15, 1957.—RICHARD H. BACKUS, *Woods Hole Oceanographic Institution, Woods Hole, Massachusetts.*

Contribution No. 1077

THE INSTABILITY OF A TWO-LAYERED SYSTEM ENCLOSED BETWEEN HORIZONTAL, COAXIALLY ROTATING PLATES

Kirk Bryan

Woods Hole Oceanographic Institution[1]

(Manuscript received 5 November 1959)

ABSTRACT

The motion of two homogeneous layers of fluid enclosed between horizontal plates, which rotate coaxially at slightly different angular velocities, has been investigated. The solution for the zonally symmetric forced motion is only a slight modification of a solution of Stewartson's (1953) for a single fluid between rotating disks. Experiments with the two-layer system confirmed the existence of symmetric motion, but for a certain range of parameters it was unstable. A criterion for instability of the symmetric flow was developed from appropriate inviscid, quasi-geostrophic frequency equations, using an approximate variational method. A comparison with experiment indicated stability for somewhat greater shear across the interface of the two layers than predicted.

Exploratory experiments in the unstable range demonstrated that the number of disturbances tended to increase directly as the rotation rate and inversely with the density difference. A steady wave pattern was observed only when the horizontal dimensions of the disturbance were comparable to the diameter of the cylindrical container. The shape of the steady disturbance was such as to give a strong transport of momentum inward.

Certain analogies are drawn between eddy circulation observed in the experiments and low-level cyclones in the atmosphere and meanders of upper-level ocean currents.

1. Introduction

In the broadest sense, waves of the second class (Lamb, 1932) are oscillations in a rotating fluid in which the motions are primarily geostrophically balanced. They are also characterized by periods which are long compared to the period of rotation. In the troposphere, these waves fall into two categories: very long planetary waves (or Rossby waves) and lower-level cyclone waves. Evidence for meanders in ocean currents, which also appear to be second-class waves on a much smaller scale, has been obtained in surveys of the Gulf Stream (Fuglister and Worthington, 1951; Stommel, 1959).

A great deal of the research on these waves has been done in order to formulate appropriate mathematical models for numerical weather prediction. Partly in connection with studies of the general circulation of the atmosphere, considerable attention has been devoted to laboratory models of second-class waves (Fultz, 1956a,b; Hide, 1958). One of the very simplest experiments is the "polar front" experiment performed by Fultz (1952). Two shallow, immiscible layers of fluid were brought into solid rotation in a cylindrical container. The rotation rate was then changed slightly. Due to bottom friction, the lower layer is slowed down more rapidly than the upper layer, creating a shear at the interface. For certain ranges of the basic rotation rate and density contrast between the layers, waves developed which could be easily observed in the topography of the interface between the layers. The phase speed and shape of these waves indicated that they were baroclinic second-class waves rather than Helmholtz shear waves modified by rotation.

This basic experiment has received relatively little attention, probably because it was considered to have less relevance to the over-all thermodynamic problem of the general circulation than rotating models with differential heating. However, a detailed study of its kinematics may have a direct bearing on relatively small cyclones in the lower troposphere and on the meanders in upper-level ocean currents. In these two cases, disturbances occur in flows which are already strongly stratified. The experiment also has intrinsic value as a simple illustration of baroclinic instability that can be reproduced in a laboratory.

A theoretical study of this experiment has been carried out by Lowell (1958). By using slightly modified inviscid perturbation equations, he calculated the phase speed and wave number for different values of shear and Froude number. The theory is somewhat idealized and may not actually apply to Fultz's experiments for which the assumptions that the angular velocity is constant along the radius and that the disturbance is "small" are only partially fulfilled. The physically important second-class waves are altered in the analysis by a neglect of the perturbation pressure in the upper layer.

---

[1] Contribution No. 1077 from the Woods Hole Oceanographic Institution.

The object of this experimental investigation is to reformulate the problem in a more tractable way. Attention is focused on the stability of the system, to which the perturbation equations are strictly relevant. To eliminate the strong time dependence of the basic zonal motion in the "polar front" experiment of Fultz, the two-layer system was enclosed between two horizontal glass plates rotating at slightly different angular velocities. In this way, a uniform shear at the interface could be maintained or slowly changed at will. Two significant dimensionless parameters for this investigation are a Rossby number and an Ekman (or a Taylor) number. The Rossby number is a measure of the ratio of inertia terms to Coriolis terms in the equations of motion. The square of the Ekman number (the square root of the inverse Taylor number) is a measure of the ratio of viscous terms to Coriolis terms. The experiments have been confined to cases in which both of these parameters are much less than unity, since this is the range of greatest interest from the standpoint of large-scale planetary flows.

2. The zonally symmetric forced motion

For convenience, the equations will be written in terms of a coordinate system rotating with the mean angular velocity of the two horizontal plates containing the two-layered system. This mean angular velocity is designated by $\bar{\Omega}$. In the case of no relative motion, the pressure distribution in each layer will be governed by the relations

$$\frac{\partial p_0}{\partial r} = \rho_0 r\bar{\Omega}^2, \quad \text{and} \quad \frac{\partial p_0}{\partial z} = -\rho_0 g.$$

In order to write the equations for relative motion in non-dimensional form, the following substitutions will be made:

$$\frac{dr}{dt} = \bar{\Omega} a R_0 U, \qquad \frac{dz}{dt} = \bar{\Omega} h_0 R_0 W, \qquad r\frac{d\theta}{dt} = \bar{\Omega} a R_0 V,$$

$$p = g h_0 \rho_0 R_0 \Phi, \qquad r = ar', \qquad z = h_0 \xi,$$

and

$$Ek^2 = \frac{\nu}{h_0{}^2\bar{\Omega}}, \qquad R_0 = \frac{\Omega_1 - \Omega_2}{2\bar{\Omega}}, \qquad \beta = \frac{\bar{\Omega}^2 a^2}{g h_0}.$$

U, V, and W are the non-dimensional velocity components of order unity directed radially outward, in the azimuthal direction, and in the vertical respectively. a is the outer diameter, and h_0 is a standard depth. R_0 is a Rossby number, and Ek is the Ekman number. β is another important non-dimensional number for the system and is not to be confused with the usual meteorological notation for the gradient of the Coriolis parameter on a spherical earth. Ω_1 and Ω_2 are the angular velocities of the upper and lower plates respectively. In what follows, r will be understood to designate r'.

The non-dimensional equations specialized for stationary, zonally symmetric flow in a rotating cylindrical coordinate system are

$$R_0LU - \left(\frac{R_0 V}{r} + 2\right)V = \frac{-1}{\beta}\frac{\partial\Phi}{\partial r} + Ek^2\left[\gamma\left(\frac{\partial^2}{\partial r^2} + \frac{1}{r}\frac{\partial}{\partial r} - \frac{1}{r^2}\right) + \frac{\partial^2}{\partial\xi^2}\right]U, \tag{1}$$

$$R_0LU + \left(\frac{R_0 V}{r} + 2\right)U = Ek^2\left[\gamma\left(\frac{\partial^2}{\partial r^2} + \frac{1}{r}\frac{\partial}{\partial r} - \frac{1}{r^2}\right) + \frac{\partial^2}{\partial\xi^2}\right]V, \tag{2}$$

$$R_0LW = \frac{-1}{\beta\gamma}\frac{\partial\Phi}{\partial\xi} + Ek^2\left[\gamma\left(\frac{\partial^2}{\partial r^2} + \frac{1}{r}\frac{\partial}{\partial r}\right) + \frac{\partial^2}{\partial\xi^2}\right]W, \tag{3}$$

and

$$0 = \frac{1}{r}\frac{\partial}{\partial r}(Ur) + \frac{\partial W}{\partial\xi}. \tag{4}$$

L and γ are defined by

$$L \equiv U\frac{\partial}{\partial r} + W\frac{\partial}{\partial\xi}, \quad \text{and} \quad \gamma \equiv \frac{h_0{}^2}{a^2}.$$

The forced motion of a homogeneous fluid between two rotating coaxial disks has been considered by Stewartson (1953). An expansion is made in terms of the Rossby number. The first-order solution, valid for $R_0 \ll 1$, is of the form

$$V + iU = -r\frac{\sin h\left[\dfrac{(1-i)(1-2\xi)}{2Ek}\right]}{\sin h\left(\dfrac{1-i}{2Ek}\right)}. \tag{5}$$

Zonally symmetric, laminar flow in the two-layer case is very similar provided that the interface is nearly horizontal so that lateral viscous terms do not have to be taken into account. In a range for which $Ek_{1,2} \ll 1$, the solution takes on an even simpler exponential form. Let $H_1 = h_0[1 - f(r)]$ and $H_2 = h_0[1 + f(r)]$, where H_1 and H_2 are the depths of the upper and lower layers respectively. $f(r)$ expresses the radial dependence of the depth. The solution for motions relative to a frame moving with the angular

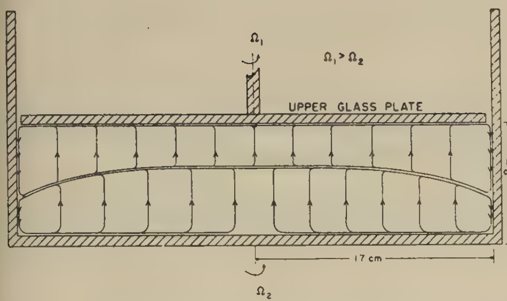

FIG. 1. A schematic diagram of the experimental model. The meridional component of the forced, zonally symmetric circulation is indicated by arrows. The interface is convex if the upper layer has a greater angular velocity than the lower layer and the ratio of the basic rotation to the density difference is sufficiently great.

velocity, $\bar{\Omega}$, is

$$V_1 + iU_1 = \frac{(\Omega_1 - \Omega_i)}{2\bar{\Omega}R_0} r\{1 + \exp[-\alpha_1(\xi_1 - 1 + f(r))] - e^{\alpha_1\xi_1}\} \quad (6)$$

$$V_2 + iU_2 = \frac{(\Omega_i - \Omega_2)}{2\bar{\Omega}R_0} r\{-1 + \exp[-\alpha_2(\xi_2 - 1 - f(r))] - e^{\alpha_2\xi_2}\}. \quad (7)$$

ξ_1 and ξ_2 are zero at the interface and at the lower disk respectively. The coefficients,

$$\alpha_1 = \frac{i-1}{Ek_1},$$

and

$$\alpha_2 = \frac{i-1}{Ek_2}.$$

The angular velocity of the interface may be determined by the condition that the stress must be continuous across the interface of the two fluids. For a nearly flat interface, surface tension effects may be neglected and

$$\epsilon Ek_1^2 \frac{\partial V_1}{\partial \xi_1} = Ek_2^2 \frac{\partial V_2}{\partial \xi_2}, \quad \text{and} \quad \xi_1 = 0.$$

Here, $\epsilon = \rho_1/\rho_2$, the ratio of the densities in the two fluids. By substituting from (6) and (7) and by differentiating,

$$\Omega_i = \frac{\epsilon Ek_1\Omega_1 + Ek_2\Omega_2}{\epsilon Ek_1 + Ek_2}.$$

If surface tension effects can be neglected so that pressure is continuous across the interface,

$$\vec{s}\cdot\nabla p_1 = \vec{s}\cdot\nabla p_2.$$

Here $\vec{s}$ is a unit vector parallel to the interface in the meridional plane. By substituting non-dimensional expressions for the pressure, p and p_0, in each layer,

$$\frac{\partial f(r)}{\partial r} = \beta r - \frac{R_0}{1-\epsilon}\left[\epsilon\frac{\partial \Phi_1}{\partial r} - \frac{\partial \Phi_2}{\partial r}\right]. \quad (8)$$

The first term represents the effect of solid rotation. The other terms give the effect of relative motion and are analogous to the Margules formula for the slope of a frontal surface in the atmosphere.

The development up to this point gives a solution consistent with small values of the Ekman and Rossby numbers for the region away from the vertical outer wall. The flow is principally solid rotation in each layer at different relative angular velocities. Superimposed on this is a uniform rising or sinking motion fed by ageostrophic flow in relatively thin boundary layers adjacent to the interface and the plates. The appropriate boundary-layer equations for the region near the outer vertical boundary cannot be simplified in any logical way as is the case in the interior. Solutions obtained by Robinson (1959) for a similar vertical boundary layer indicate that this region contains a narrow meridional cell. Whatever the detailed structure of this boundary flow is, the experiments indicate that it is confined to a very narrow region whose width is of the same order as the Ekman depth. It adjusts itself to provide the connecting link between the ageostrophic flow in the upper and lower boundary layers of each fluid. A schematic diagram of the flow is given in fig. 1.

3. The stability of the zonally symmetric flow

The question of stability of the frictionally driven, two-layer vortex is investigated by means of frequency equations which ignore the effect of viscosity on the disturbed motion. The only way in which the viscous boundary layer will enter is implicitly through the choice of boundary conditions. The justification for this procedure is that, unless the disturbances are of small horizontal extent, almost all the dissipation will be concentrated in the boundary layers. For small Ekman numbers, these viscous boundary layers will occupy only a small fraction of the total volume. The possibility of Couette instability in the vertical boundary layer near the outer wall may be excluded for all practical purposes since this layer is thin and the velocity of the basic flow is small relative to the walls of the container.

The equations of motion for inviscid flow in the two *shallow*, homogeneous layers, in a coordinate frame rotating with an angular velocity $\bar{\Omega}$, are

$$\left[\frac{\partial}{\partial T} + R_0\left(U_{1,2}\frac{\partial}{\partial r} + V_{1,2}\frac{\partial}{r\partial\theta}\right)\right]U_{1,2} - \left(\frac{R_0V_{1,2}}{r} + 2\right)V_{1,2} = \frac{-1}{\beta}\frac{\partial\Phi_{1,2}}{\partial r}$$

and

$$\left[\frac{\partial}{\partial T} + R_0\left(U_{1,2}\frac{\partial}{\partial r} + V_{1,2}\frac{\partial}{r\partial\theta}\right)\right]V_{1,2} + \left(\frac{R_0 V_{1,2}}{r} + 2\right)U_{1,2} = \frac{-1}{\beta}\frac{\partial\Phi_{1,2}}{r\partial\theta}.$$

In these equations, T is a non-dimensional measure of time, defined by $T \equiv \bar{\Omega}t$. Let c be the angular velocity of a wave with respect to t; then

$$c \equiv \bar{\Omega}S_0\sigma.$$

σ is a non-dimensional wave speed of order unity, and S_0 is a non-dimensional number characterizing the flow, analogous to the Rossby number. Let

$$U_{1,2} = u_{1,2}(r)\exp[im(\theta - S_0\sigma T)],$$
$$V_{1,2} = \omega_{1,2}r + v_{1,2}(r)\exp[im(\theta - S_0\sigma T)],$$

and

$$\Phi_{1,2}' = \phi_{1,2}(r)\exp[im(\theta - S_0\sigma T)].$$

ω_1 and ω_2 are the relative angular velocities of the basic zonal flow in the upper and lower layers respectively.

$$\omega_1 = \frac{\Omega_i - \Omega_2}{2\bar{\Omega}R_0}, \quad \text{and} \quad \omega_2 = \frac{\Omega_i - \Omega_1}{2\bar{\Omega}R_0}.$$

If the zonally symmetric component of the flow is taken to be large compared to the non-symmetric components, linearized equations are

$$im(S_0\sigma - R_0\omega_{1,2})u_{1,2} + (R_0\omega_{1,2} + 2)v_{1,2} = -\frac{1}{\beta}\frac{d\phi_{1,2}}{dr} \qquad (9)$$

and

$$im(S_0\sigma - R_0\omega_{1,2})v_{1,2} - (R_0\omega_{1,2} + 2)u_{1,2} = -\frac{im}{\beta}\phi_{1,2}. \qquad (10)$$

The equation of continuity is

$$im(S_0\sigma - R_0\omega_1)H' = -u_1\frac{dH}{dr} + H_1(r)\left[\frac{1}{r}\frac{dru_1}{dr} + \frac{imv_1}{r}\right] \qquad (11)$$

$$im(S_0\sigma - R_0\omega_2)H' = -u_2\frac{dH}{dr} - H_2(r)\left[\frac{1}{r}\frac{dru_2}{dr} + \frac{imv_2}{r}\right] \qquad (12)$$

where $H'\exp[im(\theta - S_0\sigma T)]$ is the disturbed height of the interface due to the non-symmetric motion.

$$\frac{dH}{dr} \equiv -\frac{dH_1}{dr} = \frac{dH_2}{dr}.$$

Hydrostatic balance of the disturbed motion requires that

$$(1 - \epsilon)H' = \epsilon\phi_1 - \phi_2 + \text{constant}. \qquad (13)$$

By combining (9) and (10) with (11), (12), and (13), two equations can be formed in ϕ_1 and ϕ_2 only—

$$\frac{\beta}{1-\epsilon}[(S_0\sigma - R_0\omega_1)^2m^2 - (R_0\omega_1 + 2)^2](\epsilon\phi_1 - \phi_2) - \frac{dH}{dr}\left[\frac{d}{dr} - \frac{R_0\omega_1 + 2}{r(S_0\sigma - R_0\omega_1)}\right]\phi_1 = -H_1(r)L\phi_1 \qquad (14)$$

and

$$\frac{\beta}{1-\epsilon}[(S_0\sigma - R_0\omega_2)^2m^2 - (R_0\omega_2 + 2)^2](\epsilon\phi_1 - \phi_2) - \frac{dH}{dr}\left[\frac{d}{dr} - \frac{R_0\omega_2 + 2}{r(S_0\sigma - R_0\omega_2)}\right]\phi_2 = H_2(r)L\phi_2. \qquad (15)$$

L stands for the operator,

$$L \equiv \frac{d^2}{dr^2} + \frac{1}{r}\frac{d}{dr} - \frac{m^2}{r^2}.$$

These two equations may be combined to form a single differential equation. Of the four roots of σ, two will correspond to inertial-gravitational oscillations and two will correspond to second-class waves.

To formulate the problem in a more tractable way, an approximation is introduced to reduce the order. If the two roots corresponding to inertial-gravitational oscillations are orders of magnitude greater than the other two roots, it is possible to form two second-order frequency equations, which are quite accurate. This method was introduced in dealing with the meteorological equations by Charney (1949). In all that follows, the range of validity will be defined by

$$R_0 \ll 1, \qquad \beta \ll 1, \qquad \text{and} \qquad 1 - \epsilon \ll 1.$$

From (8), it may be seen that dH/dr can range from βr in the case of no relative motion to an extreme of $\pm 4r$ when the interface just touches the upper or lower plates.

As a first case, consider mS_0 to be larger than one. In this case, the radial variation in depth is relatively unimportant. A consistent approximation of (14) and (15) is then

$$\frac{\beta}{1-\epsilon}[(S_0\sigma - R_0\omega_1)^2m^2 - 4](\epsilon\phi_1 - \phi_2) + L\phi_1 = 0 \qquad (16a)$$

and

$$\frac{\beta}{1-\epsilon}[(S_0\sigma - R_0\omega_2)^2m^2 - 4](\epsilon\phi_1 - \phi_2) - L\phi_2 = 0. \qquad (16b)$$

For normal flow to be zero at the boundaries,

$$u_{1,2} \cong \left(\frac{d}{dr} - \frac{2}{S_0\sigma r}\right)\frac{\phi_{1,2}}{\beta} = 0, \qquad r = 0,1.$$

Let

$$\epsilon\phi_1 - \phi_2 = a_1 J_m(\mu r),$$

where μ is chosen to satisfy the boundary conditions. By substituting in the frequency equation above,

$$S_0\sigma = \frac{R_0(\epsilon\omega_1 + \omega_2)}{1 + \epsilon} \pm \left[\frac{(1-\epsilon)\mu^2}{(1+\epsilon)\beta m^2} + \frac{4}{m^2} - \frac{\epsilon R_0{}^2}{(1+\epsilon)^2}(\omega_1 - \omega_2)^2\right]^{\frac{1}{2}}.$$

This relation indicates the criterion for shear instability of gravitational-inertial waves. Note that they are very stable except for large values of the wave number, m. Due to the dominating effect of the second term in the radical,

$$|S_0\sigma m| \geq 2.$$

In a coordinate frame moving with the angular velocity $\bar{\Omega}$, the term on the left outside the radical would be small and the maximum period of oscillation would be nearly one-half the period of rotation. This result gives an *a posteriori* justification of the approximations in (16a, b).

For waves of the second class, $S_0 \ll 1$. In this case, all terms quadratic in S_0, R_0, $1 - \epsilon$ and β are very small. Also,

$$R_0\omega_{1,2} + 2 \cong 2.$$

Provided that the wave number, m, is not too large, eq (14) and (15) may be written as

$$H_1(r)L\phi_1 - \frac{4\beta}{1-\epsilon}(\phi_1 - \phi_2) - \frac{dH}{dr} \times \left[\frac{d}{dr} - \frac{2}{r(S_0\sigma - R_0\omega_1)}\right]\phi_1 \equiv M_1 = 0 \quad (17)$$

and

$$H_2(r)L\phi_2 + \frac{4\beta}{1-\epsilon}(\phi_1 - \phi_2) + \frac{dH}{dr} \times \left[\frac{d}{dr} - \frac{2}{r(S_0\sigma - R_0\omega_2)}\right]\phi_2 \equiv M_2 = 0. \quad (18)$$

M_1 and M_2 are defined for later reference. These frequency equations are almost equivalent to the set that would be obtained through a systematic use of the quasi-geostrophic approximation (Phillips, 1951). The depth in each layer is ordinarily taken to be a constant, however, and the third term in (17) and (18) is not included.

Eq. (17) and (18) with appropriate boundary conditions still pose a difficult characteristic value problem. To circumvent this, a corresponding variational problem may be formulated and approximate characteristic values calculated by the Raleigh-Ritz method. If the condition is imposed that the geostrophic flow normal to the outer boundary be zero,

$$\phi_1, \phi_2 = 0, \qquad \text{and} \qquad r = 0, 1. \qquad (19)$$

Free slip parallel to the outer wall is physically consistent with the neglect of viscous boundary layers in the analysis. If (17) is multiplied by $\phi_1 rdr$ and integrated from 0 to 1 to form I_1, and if (18) is multiplied by $\phi_2 rdr$ and integrated to form I_2,

$$I_1 + I_2 = I_a - \frac{I_b}{S_0\sigma - R_0\omega_1} + \frac{I_c}{S_0\sigma - R_0\omega_2} = 0 \quad (20a)$$

where

$$I_a = \int_0^1 \left\{H_1\left[\left(\frac{d\phi_1}{dr}\right)^2 + \left(\frac{m\phi_1}{r}\right)^2\right] + H_2 \times \left[\left(\frac{d\phi_2}{dr}\right)^2 + \left(\frac{m\phi_2}{r}\right)^2\right] + \frac{4\beta}{1-\epsilon}(\phi_1 - \phi_2)^2\right\} rdr,$$

$$I_b = 2\int_0^1 \frac{dH}{dr}\phi_1{}^2 dr, \quad \text{and} \quad I_c = 2\int_0^1 \frac{dH}{dr}\phi_2{}^2 dr.$$

By solving (20a) for $S_0\sigma$,

$$S_0\sigma = \frac{I_c - I_b + I_a R_0(\omega_1 + \omega_2) \pm \Delta^{\frac{1}{2}}}{2I_a} \quad (20b)$$

and

$$\Delta = [I_c - I_b + I_a R_0(\omega_1 + \omega_2)]^2 - 4I_a R_0(R_0 I_a \omega_1\omega_2 + I_b\omega_2 - I_c\omega_1).$$

By taking the variation of (20a) and making use of (20b),

$$\delta(I_1 + I_2) = (S_0\sigma - R_0\omega_1)(S_0\sigma - R_0\omega_2) \times \int_0^1 (M_1\delta\phi_1 + M_2\delta\phi_2)rdr \pm \Delta^{\frac{1}{2}}\delta\sigma = 0. \quad (21)$$

Thus, M_1 and M_2 with the boundary conditions (19) are differential equations associated with a variational problem as long as ϕ_1 and ϕ_2 are real. Under these circumstances, the Ritz method is applicable (Hildebrand, 1952) for approximating the true solution.

As a first approximation, the variable may be set equal to the leading term of a Bessel series—

$$(\phi_{1,2})_I = a_{1,2}J_m(\mu r).$$

In this case, μ is chosen to satisfy (19). This function is the exact characteristic function for the case in

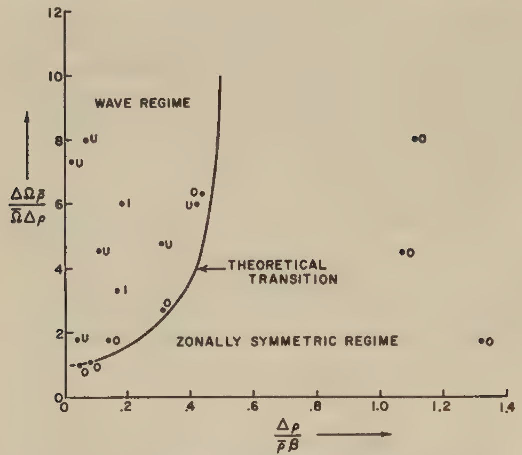

Fig. 2. A comparison of the experimental results with the inviscid stability criterion. *U* indicates unsteady patterns, while the numbers indicate the number of standing eddies in steady cases as determined by ink patterns in the upper layer.

which the radial variation of depth in each layer is neglected, except when divided by S_0 or R_0. Therefore, it should be quite close to the "true" characteristic function when the slope of the interface is not too large. By substituting $(\phi_{1,2})_I$ in I_1 and I_2, two simultaneous equations are obtained:

$$\begin{bmatrix} c_1+1-\dfrac{2B}{S_0\sigma-R_0\omega_1} & -1 \\ -1 & c_2+1+\dfrac{2B}{S_0\sigma-R_0\omega_2} \end{bmatrix} \begin{bmatrix} a_1 \\ a_2 \end{bmatrix} = 0. \quad (22)$$

The constants

$$c_{1,2} \equiv \frac{1-\epsilon}{4\beta} \times \frac{\displaystyle\int_0^1 \left\{ \mu^2 H_{1,2}(r) J_m{}^2(\mu r) - \frac{dH_{1,2}}{dr}\frac{dJ_m}{dr}(\mu r) J_m(\mu r) \right\} r\,dr}{\displaystyle\int_0^1 J_m{}^2(\mu r)\,r\,dr}, \quad (23)$$

and, by using (1) and (8),

$$B \equiv \frac{1-\epsilon}{4\beta r}\frac{dH}{dr} = \frac{1-\epsilon}{4}\left[1 - \frac{2R_0(\omega_1-\omega_2)}{1-\epsilon}\right]. \quad (24)$$

Since the determinant of the coefficients must be zero for non-trivial solutions to exist, the phase speed may be determined from the characteristic equation. Thus,

$$S_0\sigma = \frac{R_0(\omega_1+\omega_2)}{2} - \frac{(c_1-c_2)[1-\epsilon-2R_0(\omega_1-\omega_2)] \pm \Delta^{\frac{1}{2}}}{4(c_1c_2+c_1+c_2)} \quad (25)$$

and

$$\Delta = R_0{}^2(\omega_1-\omega_2)^2\{(c_1c_2)^2 - 4c_1c_2\} + \frac{R_0(\omega_1-\omega_2)(1-\epsilon)}{2}\{2c_1c_2[c_1+c_2+2] - 4(c_1+c_2)\} + \left(\frac{1-\epsilon}{2}\right)^2\{(c_1+c_2)^2 + 4(c_1+c_2)\}.$$

The system is unstable if

$$\Delta < 0.$$

An examination of the discriminant in the range in which

$$\frac{2R_0(\omega_1-\omega_2)}{1-\epsilon} < 1$$

indicates that the system is stable for all possible values of the coefficients c_1 and c_2. Thus, as positive shear $(\Omega_1 > \Omega_2)$ is increased from zero, stability is assumed until the interface passes from a convex downward configuration to a convex upward one. The stabilizing effect of the centrifugal term becomes negligible, however, when this ratio becomes much larger than one. The criterion for stability in this range becomes

$$\frac{\lambda^2}{a^2} \geq \frac{2}{\mu^2\left[1 - k_m\left(\dfrac{1}{r}\dfrac{dH}{dr}\right)^2\right]^{\frac{1}{2}}}$$

where

$$\lambda^2 = \frac{gh_0(1-\epsilon)}{4\bar{\Omega}^2}$$

and k_m is a constant, depending only on m, from (23). This result is almost the same as that derived in previous meteorological studies of baroclinic instability. The effect was first pointed out by Eady (1949), who gave an excellent physical explanation of it. The principal difference, other than that of the cylindrical geometry, in the result obtained here is the term containing the slope of the interface. From this expression, it is clear that the disturbance of the largest scale, for which μ^2 takes on a minimum value, will be the most unstable.

In order to make a comparison with experiments, the curve for marginal stability has been plotted for $m = 1$ in fig. 2. Since, in the experiments,

$$Ek_1 = Ek_2,$$

from the theory in the previous sections,

$$\frac{2(\omega_1-\omega_2)R_0}{1-\epsilon} \cong \frac{\bar{\rho}\Delta\Omega}{\bar{\Omega}\Delta\rho}.$$

$\Delta\Omega$ is the difference in angular velocity of the upper and lower plates enclosing the system. With the coordinate system used in fig. 2, the curves for marginal stability for different values of β coincide almost exactly. Note that a curve has been drawn only for positive shear; *i.e.*, $\Omega_1 > \Omega_2$. The case of negative shear also has a great deal of physical interest but has not been treated in this investigation.

As stated previously, the approximate trial function,

$$(\phi_{1,2})_I = a_{1,2}J_1(\mu r),$$

should be a close approximate to the "true" characteristic function as long as the radial variation in depth is weak. To obtain some idea of the reliability of the approximation as the slope of the interface increases, another trial function is chosen—

$$(\phi_{1,2})_{II} = b_{1,2}r(1 - r).$$

This function has a similar shape in the range $r = 0$ to $r = 1$, but it differs in detail. The criterion for marginal stability for a fixed value of β calculated on the basis of the two trial functions is shown in fig. 3. The two estimates of marginal stability are within 2 per cent as long as R_0 is small. According to this test, where the difference exceeds 5 per cent little confidence can be placed in either criterion. This takes place when the difference between the height of the interface at the center and at the outer boundary exceeds a third of the total distance between the plates. Calculations of marginal stability could be extended further by an iterative method, using a series expansion for the trial function, but the computations would be extremely laborious. Fortunately, agreement is indicated over the range of the experiments. For this range, the criterion does not appear to be sensitive to the exact shape of the characteristic function. $\beta = 0.07$ corresponds for the particular dimensions of the apparatus to a rotation rate of one radian per second, an average value for the experiments.

4. The experimental work

The experiments were carried out on a low turntable driven by an AC motor. A 50:1 reduction gear box and a combination of step pulleys allowed the turntable to be driven at seven fixed speeds ranging from one-half to two radians per second. The two fluids were contained between two horizontal, circular glass plates in a straight-sided glass basin 34 cm in diameter. The lower glass plate was fixed as a false bottom in the container. The upper glass plate was fastened to the end of a short vertical shaft. This shaft was connected to a small DC motor supported by a plexiglass cross bar across the top of the container. A small gap between the upper plate and the walls of the container allowed it to turn freely (see fig. 1).

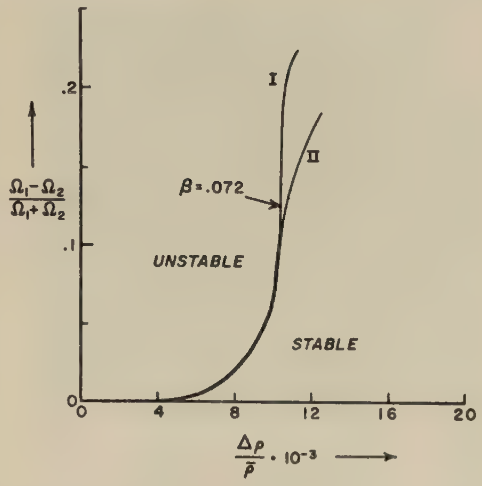

FIG. 3. The condition of marginal stability for the two approximations of the characteristic function for $\beta = 0.072$. Agreement is within 2 per cent over the lower part of the range.

In all the experiments, the vertical spacing between the plates was eight centimeters. While the system was at rest, each fluid layer had a depth of four centimeters. In preliminary trials, several combinations of immiscible fluids were tried, but they were discarded because of the troublesome problems caused by a surface film developing at the interface. Instead, a uniform salt-water solution was used for the lower layer, and fresh water was used for the upper one. In order to form the two layers, tap water was first put into the basin to a depth of four centimeters. Then salt water at the desired concentration was introduced through a thin tube under this layer. With care, the inflow could be kept very nearly laminar and a clear-cut separation obtained between the two layers. Precautions were taken to keep the fluids and the container at a uniform temperature. Once rotation began, the frictionally-driven circulation tended to keep each layer uniform, although their densities gradually approached one another through molecular diffusion across the interface. As an example, in one experiment lasting twenty minutes, an initial density difference of 0.55 per cent changed to 0.50 per cent. In another run of about the same length, it decreased from 2.2 to 2.05 per cent.

Thirty-eight runs in all were made. The speed settings, density differences, and the pattern of flow are summarized in table 1. Density determinations were accurate to only 0.1 per cent, and consequently there is an uncertainty in the measurement of $\Delta\rho/\rho$ ranging from 5 to 20 per cent. The experimental procedure was as follows: as soon as the salt layer built up to a thickness of four centimeters under the fresh water, the tube coming from the salt-water

Table 1. Summary of the experiments.

Ω_2	R_0	$\Delta\rho/\rho \times 10^3$	E_h	Remarks
0.42	0.126	4	0.12	0
0.42	0.126	2	0.12	2
0.42	0.126	30	0.12	0
0.42	0.034	15	0.12	0
0.52	0.104	4	0.11	1
0.52	0.104	3	0.11	1
0.55	0.098	5	0.11	U
0.55	0.098	2	0.11	U
0.55	0.026	30	0.11	0
0.79	0.071	4	0.09	2
0.79	0.071	4	0.09	2
0.79	0.071	4	0.09	2
0.79	0.071	5	0.09	1
0.79	0.071	3	0.09	3
0.79	0.071	6	0.09	1
0.79	0.071	3	0.09	1
0.79	0.071	2	0.09	3
0.79	0.071	8	0.09	1
0.79	0.036	30	0.09	0
0.79	0.071	22	0.09	0
0.79	0.036	15	0.09	U
0.79	0.060	20	0.09	U
0.79	0.125	20	0.09	U
0.97	0.057	5	0.08	2
0.97	0.057	4	0.08	U
0.97	0.057	6	0.08	U
0.97	0.057	6	0.08	U
0.97	0.020	5	0.08	U
0.97	0.020	8	0.08	U
0.97	0.009	10	0.08	0
0.97	0.030	22	0.08	0
1.36	0.042	6	0.07	2
1.36	0.011	3	0.07	U
1.36	0.093	30	0.07	1
1.36	0.006	11	0.07	0
1.36	0.042	25	0.07	1
1.71	0.034	5	0.06	U
1.71	0.034	4	0.06	2
1.71	0.008	9	0.06	U
1.71	0.005	10	0.06	0

reservoir was removed. Then the upper plate was put in position and leveled just in contact with the upper surface. The turntable was gradually accelerated to a given speed. After equilibrium was established, the upper disk was set into motion to create a shear. Diluted ink was then introduced with an eye dropper into the upper layer through the narrow gap between the edge of the top plate and the walls of the container. Three different types of patterns were observed. In many cases, the ink was drawn into the center in long bands. The ink indicated the existence of primarily two-dimensional flow in eddies which varied from four to ten centimeters in length. The eddies were unsteady with a "lifetime" ranging from one to ten rotations. A photograph of this type of regime is shown in fig. 4. In a few cases, the flow pattern went through repeated cycles, alternating from one number of primary disturbances to another and back again.

The second type of pattern observed was that of steady disturbances. Generally, a steady pattern occurred only in cases where one or two disturbances predominated. The disturbances were accompanied by rather marked topography of the interface which could be seen looking through the glass walls of the container. Steady waves of this type are indicated by numbers in the remarks column of table 1.

The third type of pattern was one in which no disturbances amplified to any extent, and the ink was drawn into a long band around the outer rim of the basin. An example of this type of flow is shown in fig. 4C. Cases in which this occurred are indicated by 0 in table 1. The speeds with which this band was drawn around the periphery of the system were in good agreement with the solutions derived in the section on the zonally symmetric flow.

In fig. 2, sixteen runs have been plotted. All runs made over the range of coordinates shown have been included. Points are marked by the same symbols used in the remarks column of table 1. Only a very general agreement between the inviscid theory and the experi-

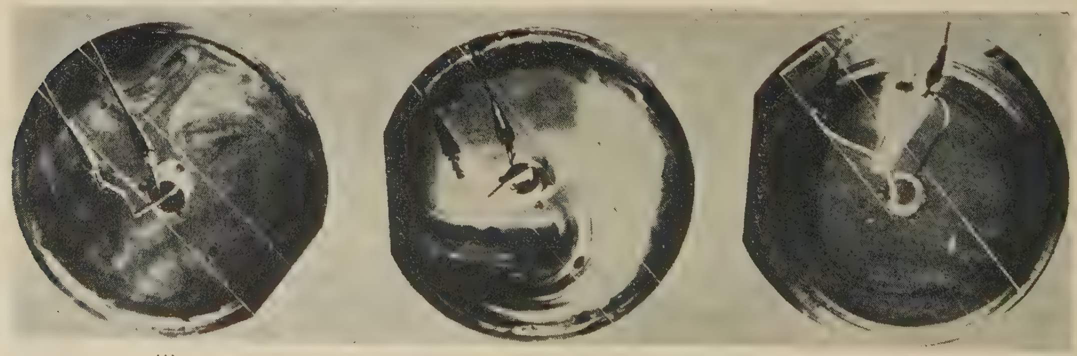

(A) (B) (C)

Fig. 4. Photographs taken through the top disk of ink patterns in the upper layer. The basic rotation was counter-clockwise in all three cases.

(A) $\bar{\Omega} = 1.7$ rad./sec., $\Delta\rho/\rho = 5 \times 10^{-3}$, $R_0 = 0.034$.
(B) $\bar{\Omega} = 1.0$ rad./sec., $\Delta\rho/\rho = 5 \times 10^{-3}$, $R_0 = 0.06$.
(C) $\bar{\Omega} = 0.67$ rad./sec., $\Delta\rho/\rho = 29 \times 10^{-3}$, $R_0 = 0.11$.

ment can be claimed for transition from the symmetric to the wave regime. Friction may account for the discrepancy. In the course of the experiments, an interesting finite amplitude effect was very evident. If, at a given rotation rate, a relative shear was introduced rather suddenly, the number of disturbances to appear initially would gradually decrease until a steady wave pattern was established with a smaller number of cells. Previously, a similar effect has been noted by Fultz (1956a) in the course of his "polar front" experiments.

In all cases in which a steady disturbance was present in the upper layer, the flow pattern was very much the same. The trough line of the disturbance was very strongly bent back. That is, its phase angle decreased markedly with increasing radius. This shows up very strongly in the photographs shown in figs. 3b and 4. The dark area in the photographs is a region of anticyclonic motion just behind the trough. The phase speeds of steady disturbances could be measured easily by simply timing the movement of ink patterns. Measurements indicated that the disturbances were practically stationary with respect to a coordinate system moving with an angular velocity $\bar{\Omega}$. This confirms that the observed disturbances are the geostrophic modes. Since precise agreement between the phase speed of finite disturbances and the phase speed of linear theory could not be expected, more refined measurements were not undertaken.

5. Conclusions

This study has attempted to lay the groundwork for quantitative study of baroclinic instability in a system in which the baroclinicity is entirely concentrated at the interface of two homogeneous fluids. The model is essentially the same as Fultz's "polar front" model except that the time dependence is removed by enclosing the fluid between two horizontal plates rotating at slightly different angular velocities.

Experiments indicate two regimes, as is the case in the thermal experiments with rotating fluids carried out by Fultz and Hide. Examination of the inviscid frequency equations indicates that, for the range of interest, the system is quite stable to disturbances of the inertio-gravitational type but unstable to low-frequency, second-class waves. The criterion for this latter type of instability is calculated from simplified equations, only slightly different from the quasi-geostrophic frequency equations. Calculations of the stability indicate that replacing the depth of each layer by a constant where it appears as a coefficient has little effect on the criterion as long as the total variation of depth is less than 30 per cent. Comparison with a rather small number of experiments suggests that the inviscid criterion gives a minimum value. Flow is stable below the criterion value of shear, but it may or may not be stable above it.

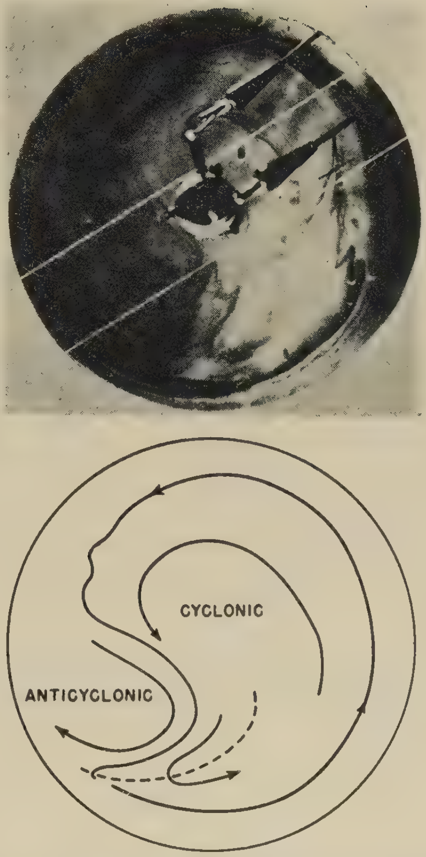

FIG. 5. A photograph of the ink pattern as seen through the upper disk, and a sketch of the corresponding flow. This was a steady pattern like fig. 4b, but the ink has settled to the vicinity of the interface. The basic rotation is counter-clockwise, and $\bar{\Omega} = 0.82$ rad./sec., $\Delta\rho/\rho = 8 \times 10^{-3}$, $R_0 = 0.071$.

In the experiments, a series of steady sub-regimes was indicated in which either one or two disturbances dominated the flow in the upper layer. For more disturbances than two, the flow was generally unsteady. The shape of the steady wave patterns invariably indicated a strong flow of momentum radially inward in the upper layer.

The experimental system is far from a realistic model of any natural, large-scale phenomena, but it does illustrate some important points in regard to them. It demonstrates that rather simple kinematic considerations can give a first-order approximation of a baroclinic instability criterion. The success of inviscid, laminar models has strongly indicated that the same is true of the atmosphere, but the relative complexity of natural conditions makes interpretation more difficult. The frequency equations used in this study are remarkably similar to those used in many investigations of large-scale flows, since the two-layered model is often used as an approximation of a more complicated dependence on the vertical coordinate. With the exception of numerical investigations, the potential vorticity is usually taken to be independent of position where it appears as a coefficient in the equations. A slightly more detailed analysis was made in this study to account for the slope of the interface. As long as the percentage variation of the depth was not great, the criterion is the same as that which would have been obtained without this refinement. Apparently, the principal effect of the slope of the interface is to make the characteristic function representing the shape of the disturbance more complicated than it would be otherwise. The methods used in this study may be useful in determining whether this finding has any general application in models which more closely approximate actual conditions.

Acknowledgments. The author is very grateful to Drs. Alan Faller, Melvin Stern and George Veronis for suggestions during the course of this study and to Mrs. L. A. Thayer for assistance in preparing the manuscript.

REFERENCES

Charney, J., 1949: On a physical basis for numerical prediction of large-scale motions in the atmosphere. *J. Meteor.*, **6**, 371–385.

Eady, E. T., 1949: Long waves and cyclone waves. *Tellus*, **1**, 33–52.

Fultz, D., 1952: On the possibility of experimental models of the polar-front wave. *J. Meteor.*, **9**, 379–384.

Fultz, D., 1956a: *A survey of certain thermally and mechanically driven fluid systems of meteorological interest.* Fluid Models in Geophysics, Proc. 1st Sympos. Geophys. Fluid Dynam., Baltimore, 27–36.

Fultz, D., 1956b: *Studies in experimental hydrodynamics applied to large-scale meteorological phenomena.* Final Rep., Part II, Contract AF 19(122)–160 A.F.C.R.C.

Fuglister, F. C., and L. V. Worthington, 1951: Some results of the multiple ship, survey of the Gulf Stream. *Tellus*, **3**, 1–14.

Hide, R., 1958: An experimental study of thermal convection in a rotating fluid. *Philosoph. Trans. r. Soc.*, **250**, Series A, 441–478.

Hildebrand, F. B., 1952: *Methods of applied mathematics.* New York, Prentice-Hall, 523 pp.

Lamb, H., 1932: *Hydrodynamics*, sixth ed. New York, Dover Publ., 738 pp.

Lowell, S. C., 1958: *Shear waves in stratified, rotating liquids.* NYU Inst. Math. Sci., Res. Rep., IMM 251.

Phillips, N. A., 1951: A simple three-dimensional model for the study of large-scale extratropical flow patterns. *J. Meteor.*, **8**, 381–394.

Robinson, A. R., 1959: *Thermal convection in rotating systems.* Ph.D. Thesis, Harvard Univ.

Stewartson, K., 1953: On the flow between two rotating coaxial disks. *Proc. Camb. Philosoph. Soc.*, **49**, 333–341.

Stommel, H., 1959: *The gulf stream.* Berkeley and Los Angeles, Univ. Calif. Press, 202 pp.

Contribution No. 1078

J. mar. biol. Ass. U.K. (1960) 39, 217–226
Printed in Great Britain

THE VERTICAL DISTRIBUTION OF CHLOROPHYLL[1]

By J. H. Steele[2] and C. S. Yentsch
Woods Hole Oceanographic Institution

(Text-figs. 1–7)

The vertical distribution of chlorophyll in the sea generally shows a maximum concentration at a depth which may vary from at or just below the surface, to near or below the bottom of the euphotic zone. The easiest distributions to explain are those where the maximum chlorophyll concentration is at or very near the surface. These are found when a population is photosynthesizing actively during the first stages of an outburst, and the distribution corresponds roughly with the change with depth of the photosynthetic rate (Steele, 1957). However, these form a small proportion of observations, probably because outbursts are usually restricted to comparatively short periods of time. The more usual distributions show a maximum in the chlorophyll concentrations well below the surface and below the depth of maximum photosynthesis.

Such features are normally explained by the sinking of plants and a sinking rate constant with depth is used in the mathematical models of Riley, Stommel & Bumpus (1949) to explain some observed patterns of vertical distribution. However, on the basis of their model, the chlorophyll maximum must occur above the compensation depth. Although many of the maxima are of this type, there are as many which occur below or just at the compensation point and so are not explicable by a constant sinking rate. In particular, this feature is the dominant one in the distributions found during summer by the Woods Hole Oceanographic Institution in waters off New York (Ketchum, Ryther, Yentsch & Corwin, 1957; Ryther & Yentsch, 1958; Yentsh & Vaccaro, 1958). This work is concerned with a possible explanation for such distributions.

THE OBSERVED DISTRIBUTIONS

Two examples of chlorophyll distribution in which the maximum concentration was found near the compensation depth are given in Table 1, which includes simultaneous observations of the ^{14}C *in situ* rate of photosynthesis, and the concentrations of nitrate and phosphate in water. Crawford station

---

[1] Contribution no. 1078 from the Woods Hole Oceanographic Institution. This work was supported in part by A.E.C. Contract AT (30–1) 1918.

[2] Marine Laboratory, Aberdeen, Scotland. Visiting investigator under a W.H.O.I. fellowship during the autumn of 1958.

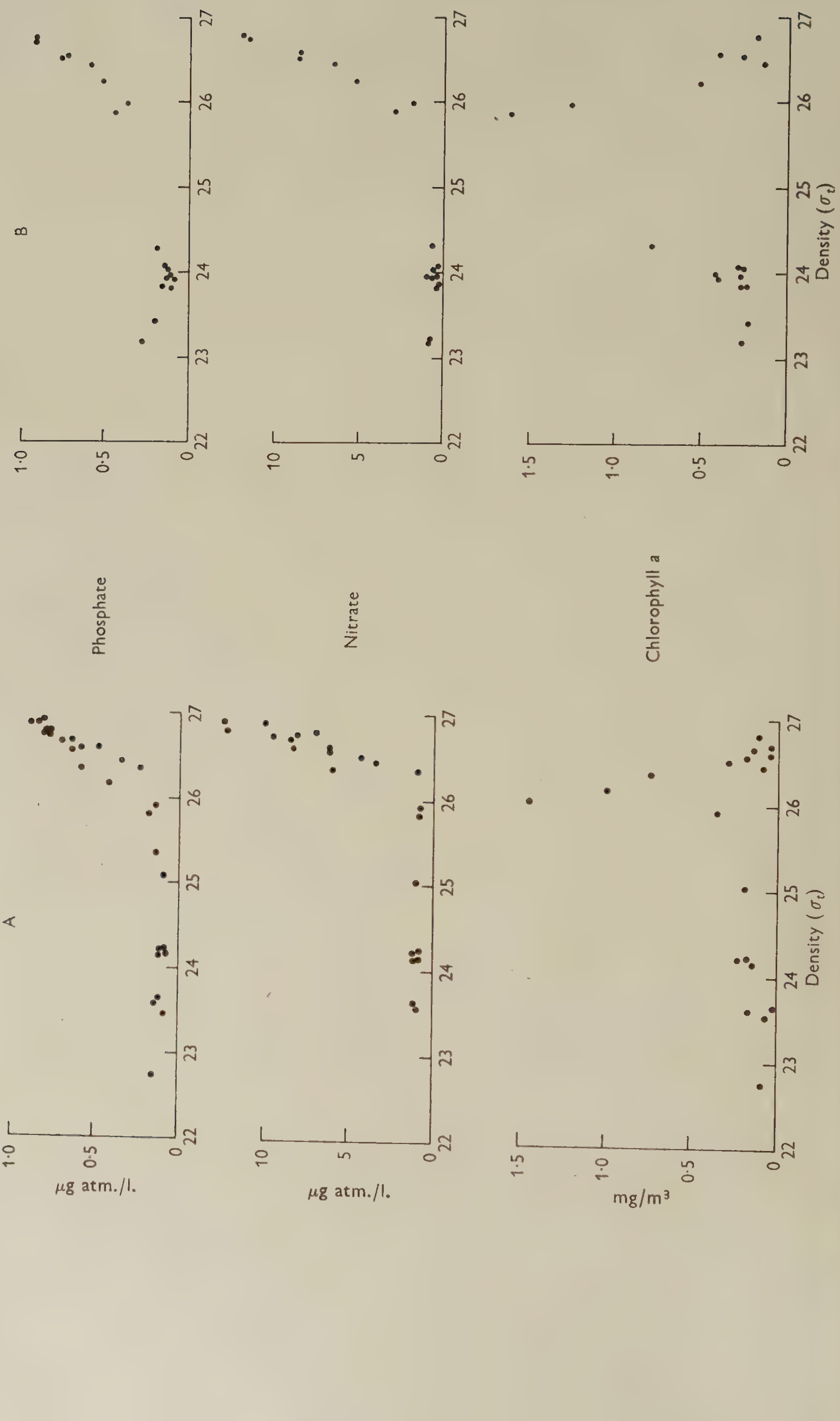

Fig. 1. Observed conditions in July (A) and September (B) 1957.

no. 194 was occupied where the total depth was 3000 m and the other station (Crawford no. 209) was in water with a depth of 40 m.

For four offshore stations in depths greater than 1000 m the relations between nitrate, phosphate and chlorophyll in July and September 1957 are shown in Fig. 1 by plotting these against density. The July chlorophyll values suggest a very sharp peak at $\sigma_t = 26$, but the September values do not have enough observations in the middle range of density to determine the sharpness. In all cases the high values are found at 50 m, although there are some stations at which no pronounced peak is found; this is probably due to the wide spacing of the sampling depths and the comparative sharpness of the peak. The occurrence of the peak in both July and September and the similarity of the nutrient distributions suggest that conditions during this interval can be considered to approximate a steady state. Perhaps the most convincing evidence that the depth of the mean daily euphotic zone is near these peaks is shown by the concentrations of nutrients which increase sharply at about the same depth. The ^{14}C data can be used to define the depth distribution of production. It appears that the compensation point at station 194 must be just below 50 m and the 1 % light level was found at 58 m. At the shallower station the compensation depth was between 20 and 30 m and the 1 % level was at 19 m.

THEORETICAL DISTRIBUTIONS

The purpose of these theoretical considerations is to show how the sinking rate interacts with other factors affecting vertical distribution of plants, and how a variable sinking rate can produce idealized distributions similar to those described above. These concepts do not explain how this decreasing sinking rate could be brought about and since the main possible explanation is in terms of the effect of density, the theoretical relations between size, shape and density will be considered.

Since sinking is only one factor which can affect the vertical distributions of plants, the effects of variations in this rate must be linked with other factors —photosynthesis and respiration of the plants, grazing by herbivores and vertical mixing of the water. These five variables have been combined in a mathematical form by Riley *et al.* (1949). Assuming a sinking rate that is constant with depth, z, the equation for a steady state is

$$A\frac{\partial^2 p}{\partial z^2} - v\frac{\partial p}{\partial z} + (w-h)\,p = 0, \tag{1}$$

where p is the plant concentration, A is the coefficient of eddy diffusivity, v is the sinking rate, w is the photosynthetic rate and h is the combined effect of grazing and plant respiration. For a maximum concentration of plants, p

$$\frac{\partial p}{\partial z} = 0 \quad \text{and} \quad \frac{\partial^2 p}{\partial z^2} = \left(\frac{h-w}{A}\right) p < 0.$$

The latter holds only for $w > h$, that is when the photosynthetic rate exceeds the combined loss due to respiration and grazing. Thus for a constant sinking rate the maximum must occur above the mean daily compensation depth. This conclusion is independent of variations with depth in grazing or mixing. (Although it can be seen from this how decreased mixing tends to increase the sharpness of the maximum.)

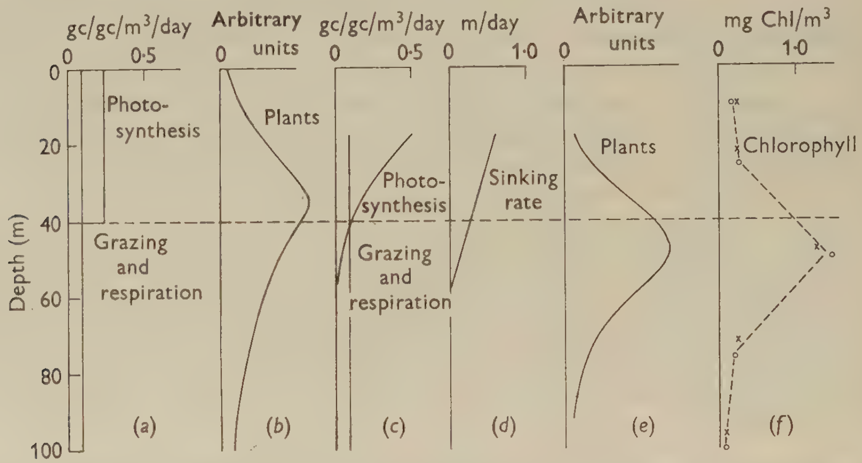

Fig. 2. (*a* and *b*) Conditions from the theory of Riley *et al.* (1949), using a constant sinking rate. (*c, d, e*) Conditions with a variable sinking rate. (*f*) Data from Station 194.

On this basis, Riley *et al.* (1949) constructed profiles of vertical plant distributions. With their solution, the deepest possible maximum will be given when a constant photosynthetic rate throughout the euphotic zone is assumed, Fig. 2(*a*). Constant sinking, grazing and respiration rates throughout the water column are assigned. With a sinking rate of 3 m/day and numerical values for the other factors corresponding roughly to the offshore conditions, the example in Fig. 2(*b*) is obtained. Its disadvantage is that the form of the photosynthetic coefficient is unrealistic and biases the plant maximum downwards.

If a variable sinking rate is introduced, (1) takes the form

$$A\frac{\partial^2 p}{\partial z^2} - v\frac{\partial p}{\partial z} + (w - h - v^1)\,p = 0, \qquad (2)$$

where v^1 is the rate of change of the sinking rate. Then a maximum occurs when

$$\frac{\partial p}{\partial z} = 0 \text{ and } \frac{\partial^2 p}{\partial z^2} = \left(\frac{h + v^1 - w}{A}\right) p < 0,$$

i.e. when $-v^1 > h - w$. This permits a maximum below the foot of the euphotic zone.

Thus a decreasing sinking rate is not only a possible means of securing a maximum at or below the compensation depth, which is fairly obvious; it is also the only way it can be achieved in terms of the variables considered here.

As an example of the kind of profile that can be obtained in the thermocline region offshore, a solution of (2) was constructed with a linearly decreasing sinking rate and a more realistic photosynthetic rate as shown in Fig. 2(*c*) and (*d*). The zero sinking rate has been set at 58 m so that the balance between photosynthesis and grazing plus respiration, the compensation depth of the community, occurs at nearly the same depth as in Fig. 2(*a*) and is indicated by a dashed line. This leads to the profile given in Fig. 2(*e*). The data from station 194 are shown for comparison in Fig. 2(*f*). This example shows how a decreasing sinking rate depresses the chlorophyll maximum to below the compensation depth of the community. It also provides a value for the decrease in sinking rate that is required to give a profile similar to those observed.

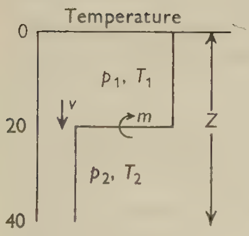

Fig. 3

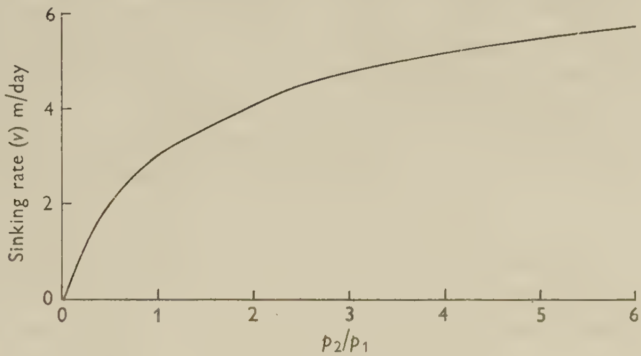

Fig. 4

Fig. 3. Idealized inshore distribution of temperature (T_1, T_2), plants (p_1, p_2), zooplankton (Z) with mixing (m) and sinking (v) between the layers.

Fig. 4. Relation between sinking rate and ratio of plant concentrations in lower and upper layers.

A second theoretical example corresponding to inshore conditions can be constructed by considering a sea 40 m deep divided into two equal layers, Fig. 3, with a positive sinking rate v in the upper layer and zero rate in the lower; this gives the relation between v and the ratio p_2/p_1 shown in Fig. 4. It can be seen that ratios of three to six which is around the observed range are obtained for a sinking rate of 5–6 m/day which is about the same value as that deduced for the upper layers in the offshore example. These values are realistic in terms of previously calculated sinking rates (Riley *et al.* 1949; Steele, 1956, 1957; Steemann-Nielsen & Jensen, 1957).

In both areas the density increase across the thermocline is in the range

0·002–0·003. From Munk & Riley (1952) the relations between the sinking rates, size of the plants, and the density difference between the plants and the water, for the simple shapes, spheres and cylinders, can be expressed approximately as

$$v_s = \frac{\Delta p d_s^2}{10} \quad \text{for a sphere (Stokes Law),}$$

$$v_c = \Delta p d_c^2 \quad \text{for a cylinder,}$$

where v_s, v_c are the sinking rates (m/day) and d_s, d_c are the diameters (μ) of spheres and cylinders, respectively; Δp is the density difference between the cell and the water.

Assuming the extreme case considered earlier, when the cells are neutrally buoyant in the lower layers, then the approximate sinking rates are obtained by putting $\Delta p = 0{\cdot}0025$. For a sinking rate of 5 m/day the required diameters are $d_s = 140\ \mu$, $d_c = 45\ \mu$. These values are high for generally observed sizes (Munk & Riley, 1952, Fig. 6) and they appear to be very much higher than those found in the areas studied. From information kindly provided by Dr E. M. Hulburt, the diameter of the main species found during the summer is generally about 5 μ and usually less than 10 μ. A value of 5 μ would give sinking rates of $v_s = 0{\cdot}006$ m/day, $v_c = 0{\cdot}06$ m/day. This is between two and three orders of magnitude less than the values calculated from the models.

THE EFFECT OF LIGHT AND NUTRIENTS ON SINKING RATES

This gross difference between the two estimates of sinking rates suggested that a change in water density alone was not a satisfactory explanation of decreasing sinking rates.[1] Thus it seemed necessary to look for changes in the density of the cells themselves as a possible explanation. It seemed probable that a decrease in sinking rate could be produced as a result of recovery of the plant cells from nutrient deficiencies. The depth at which maximum chlorophyll is observed is frequently within the thermocline, where nutrient concentrations increase with increasing depth. Gross & Zeuthen (1948) have observed variations in the sinking rates of diatoms under different culture conditions. It is a common phenomenon for the algal culturist to observe that old cultures settle out more rapidly than do young actively growing cultures.

To examine the effects of light and nutrients on the sinking rate we have conducted the following experiments. Cultures of the diatom *Skeletonema costatum* (Grev.) were grown in 4B media (Yentsch & Vaccaro, 1958) at 18° C in constant optimal light intensity. Periodically this culture was sampled and the sinking rate of the cells measured. Approximately 30 c.c. of well-agitated culture were placed in a 5 cm, large volume, optical cuvette. In the first experiment clumping was removed with a Potter–Eluehjehm homogenizer using a Teflon pestle. Optical density measurements were made in a Beckman DU spectrophotometer at a wave-length of 750 mμ. Decreases in the optical density at this wave-length, resulting from cells settling out of the light path, were measured at regular intervals over a period of 1 h (Fig. 5). The percentage decrease of the optical density during the hour is used as a measure of relative sinking rate.

---

[1] Jerlov (1959) by the same reasoning given earlier noted the necessity of decreasing sinking rates to explain deep particle maxima. However, he had no information on the particle sizes and accepted density changes in the water as sufficient explanation.

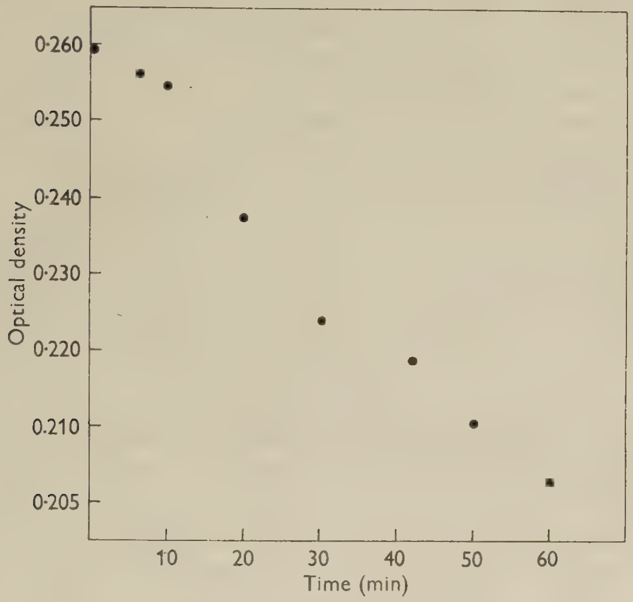

Fig. 5. Changes in optical density of a culture in a cuvette, resulting from cells settling.

The results of two experiments show that the settling rate of actively dividing cells was approximately one-half the rate of slowly dividing, senescent cells. In the first experiment, Fig. 6, an aliquot of the culture was removed between the seventh and eighth day, enriched with nutrients, and placed in the dark. During the first half day the cells in the dark settled more slowly than the illuminated cells, after which the settling rate increased.

In the second experiment three aliquots of the illuminated culture were removed between the third and fourth day of growth. Two of these were enriched, one was darkened, the other illuminated. The third aliquot was not enriched but was placed in the dark. In all three aliquots the settling rate of cells was decreased relative to that of the original culture. The lowest settling

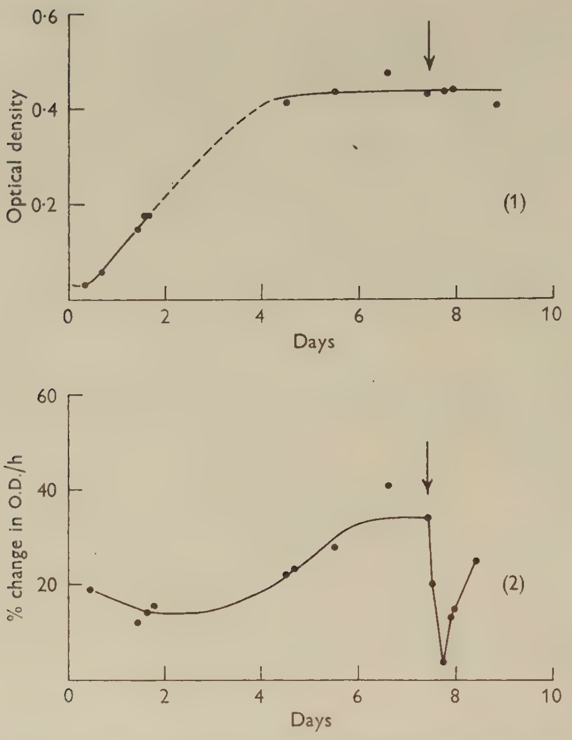

Fig. 6. Experiment I, changes with time in culture density (1) and the relative sinking rate (2). The arrows indicate the time at which 300 c.c. of 4B media was added to 150 c.c. aliquot of the culture and placed in the dark.

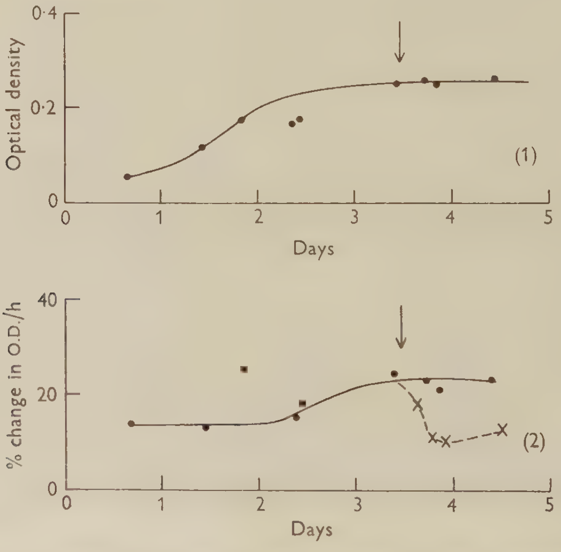

Fig. 7. Experiment II, changes with time in culture density (1) and relative sinking rate (2). The arrows indicate the time at which 300 c.c. of 4B media was added to 150 c.c. aliquot of the culture and placed in the dark.

rate occurred in the enriched darkened aliquot, Fig. 7, broken line, with the others intermediate between this and the control.

The results of these experiments show that older cells settle faster than do rapidly growing cells. Furthermore, when old cells are enriched in the dark, the settling rate is considerably reduced.

DISCUSSION

From a mathematical model which used as parameters of the phytoplankton environment, photosynthesis, respiration, grazing and eddy diffusion, we have concluded that a decreased sinking rate is needed to produce chlorophyll maxima at or below the base of the euphotic zone. Density differences observed throughout the water column appeared unable to explain these vertical distributions, and so we postulated the concept that the chlorophyll maxima are due to a decrease in sinking rate of the plants themselves caused by their entry into the dark, nutrient-rich waters found at the foot of the euphotic zone. The justification of this rather tentative hypothesis is that it predicted an experimental result.

Our experimental results show that as growth slows down, the cells sink more rapidly. When the deficient cells are re-enriched and placed in the dark, their sinking rate decreases rapidly. The picture that emerges is one where the general physiological condition of the cell and its buoyancy are closely related, as Gross & Zeuthen (1948) have also suggested. On this basis, seasonal variations in the vertical distribution of chlorophyll can be explained. For example, during early spring when nutrients are sufficient, phytoplankton cells would tend to have a low sinking rate, and populations undergoing rapid growth would tend to accumulate near the surface. In late summer when nutrients are depleted in the surface waters, phytoplankton would sink and accumulate in the nutrient rich water at the base of the euphotic zone. Here the assimilation of nutrients which can proceed in the dark (Ketchum, 1939) would, as our experiments show, decrease the sinking rate of the phytoplankton cells.

SUMMARY

Theoretical considerations of the occurrence of chlorophyll maxima at the foot of the euphotic zone show that a decreasing sinking rate is necessary to explain this feature but that the required decrease could not be obtained from density changes in the water alone. It is thought that the cells themselves might increase their buoyancy when they reach dark, nutrient-rich waters, and this has been confirmed by two experiments in which deficient laboratory cultures of *Skeletonema costatum* were re-enriched in the dark and decreased their sinking rate considerably.

REFERENCES

Gross, F. & Zeuthen, E., 1948. The buoyancy of plankton diatoms; a problem of cell physiology. *Proc. Roy. Soc.* B, Vol. 135, pp. 382–9.

Jerlov, N. G., 1959. Maxima in the vertical distribution of particles in the sea. *Deep-Sea Res.*, Vol. 5, pp. 173–84.

Ketchum, B. H., 1939. The development and restoration of deficiencies in the phosphorus and nitrogen composition of unicellular plants. *J. cell. comp. Physiol.*, Vol. 13, pp. 373–81.

Ketchum, B. H., Ryther, J. H., Yentsch, C. S. & Corwin, N., 1957. Productivity in relation to nutrients. *Rapp. Cons. Explor. Mer*, Vol. 144, pp. 132–41.

Munk, W. H. & Riley, G. A., 1952. Absorption of nutrients by aquatic plants. *J. mar. Res.*, Vol. 11, pp. 215–40.

Riley, G. A., Stommel, H. & Bumpus, D. F., 1949. Quantitative ecology of the plankton of the western North Atlantic. *Bull. Bingham oceanogr. Coll.*, Vol. 12, No. 3, pp. 1–169.

Ryther, J. H. & Yentsch, C. S., 1958. Primary production of continental shelf waters off New York. *Limnol. and Ocean.*, Vol. 3, pp. 327–35.

Steele, J. H., 1956. Plant production on the Fladen ground. *J. mar. biol. Assoc. U.K.*, Vol. 35, pp. 1–33.

—— 1957. Production studies in the northern North Sea. *Rapp. Cons. Explor. Mer*, Vol. 144, pp. 79–83.

Steemann-Nielsen, E. & Jensen, A., 1957. Primary oceanic production. The autotrophic production of organic matter in the ocean. *'Galathea' Rep.*, Vol. 1, pp. 49–136.

Yentsch, C. S. & Vaccaro, R. F., 1958. Phytoplankton nitrogen. *Limnol. and Ocean.*, Vol. 3, pp. 443–8.

TABLE 1. EXAMPLES OF THE VERTICAL DISTRIBUTION OF CHLOROPHYLL, OF THE RATE OF PHOTOSYNTHESIS AND CONCENTRATION OF NUTRIENTS AT STATIONS WHERE THE MAXIMUM CHLOROPHYLL CONCENTRATIONS OCCURRED AT OR NEAR THE COMPENSATION DEPTH

Depth (m)	Chl *a* mg/m^3	^{14}C *in situ* measurements mg C/m^3/day	NO_3—N µg atm./l.	PO_4—P µg atm./l.
		Crawford station 194, July 1957		
10	0·18	1·8	0·53	0·09
25	0·24	5·2	0·39	0·11
50	1·46	5·6	0·43	0·19
75	0·19	0	6·00	0·59
100	0·09	0	6·20	0·66
		Crawford station 209, July 1957		
0	0·40	24·0	0·96	0·48
10	0·57	9·3	0·50	0·36
20	1·62	8·7	1·17	0·54
30	0·25	0	4·50	0·41

Contribution No. 1079

Reprinted from Monograph No. 5, American Geophysical Union, 1960
Physics of Precipitation
Printed in U.S.A.

Differences in Coalescence Tendencies in Computed Condensation Cloud Droplet Spectra[a]

W. A. Mordy

International Meteorological Institute, Stockholm, Sweden

Abstract—Four numerically computed cases of the growth of a population of cloud droplets by condensation are analyzed in terms of coalescence tendencies. Following the suggestions of Hitschfeld, 1957; Telford, 1955; and Welander, 1959, particular attention has been given to the stochastic influence on the coalescence-produced cloud-droplet spectrum. The evidence taken from the numerically computed cases strongly supports the contention that collisions between small droplets readily produce a wider spectrum than the condensation-produced spectrum. The transition time for a condensation-produced spectrum to change to a predominantly coalescence-produced spectrum depends strongly on the maximum supersaturation and resulting cloud droplet concentration produced at cloud base.

In a recently published paper [*Mordy*, 1959] the writer described a theoretical investigation on the effects of vertical motion and condensation nucleus spectra on cloud droplet spectra. The purpose of the present paper is to evaluate the differences in cloud droplet spectra which resulted in these cases in terms of some important factors which lead to the subsequent changing of these spectra by the coalescence of droplets.

The coalescence of droplets is mainly dependent on three factors. These factors are the size spectrum, the concentration, and the coalescence (collision times collection) efficiencies of the droplets. An equation which gives the number of contacts between two droplet sizes is frequently given as [for example, *Telford*, 1955]

$$n = EN_1N_2\pi(r_1 + r_2)^2v \qquad (1)$$

where E = collision efficiency between r_1 and r_2 radius droplets
N_1 and N_2 are the concentrations per unit vol of the r_1 and r_2 size droplets respectively
$\pi(r_1 + r_2)^2$ = the area surrounding a droplet in which a contact could be made
v = relative velocity between the r_1 and r_2 droplets

Customarily the coalescence of droplets has been described by following the growth of a larger droplet as it sweeps up smaller droplets in a cloud with certain assumed characteristics of droplet size and vertical velocity [*Houghton*, 1950; *Mason*, 1957; *Bowen*, 1950; *Ludlam*, 1951; *Langmuir*, 1948]. The growth of the larger droplet in these cases is assumed to be continuous, that is

$$\frac{1}{\rho}\frac{dm}{dt} = 4\pi r_1^2\frac{dr}{dt} = E\pi N_2(r_1 + r_2)^2v\frac{4\pi r^3}{3} \qquad (2)$$

where r_1 and r_2 are the radii of the collecting and collected droplets respectively. In fact of course it is discontinuous, each unit of growth being one cloud droplet.

If one adopts the practice of thinking of the coalescence of cloud droplets as in (2) above, then it is the *initial* drop size spectrum which largely determines the initial and subsequent relative velocities between the droplets. Thus droplets which are initially slightly larger, will remain larger throughout the coalescence process and there will be no tendency for smaller droplets to overtake them, except that they may follow different trajectories in the cloud [*Bowen*, 1950]. Such reasoning has been followed in the work of *Houghton* [1950], *Woodcock* [1952], *Fournier d'Albe* [1955], and others. In this line of thought Woodcock has reported measuring a correspondence between the size distributions of sea salt particles and raindrops measured in the same localities and at the same time.

As exceptions to the above treatment of this problem there have been three very interesting investigations to date [*Telford*, 1955; *Hitschfeld*, 1957; *Welander*, 1959], which study the importance of statistical aspects of the coalescence process.

This statistical process in its simplest form may be illustrated by the following example. Suppose a group of 100 large droplets is falling through a cloud of randomly spaced, uniform size, small cloud droplets. Because of the random spacing of the cloud droplets, each of the large droplets will have a different collision experience with the cloud droplets and after some time will represent not a uniform-size group but a spectrum of droplets located at different levels in the cloud.

---

[a] Contribution No. 1079 from the Woods Hole Oceanographic Institution.

If such reasoning is applied to an initial spectrum of cloud droplet sizes instead of an initially uniform-size group, a question arises as to whether, after some time has elapsed, the resulting drop size spectrum is more dependent on this statistical process than on the initial drop size spectrum. In other words one may ask the question; do more of the large droplets present represent initially large nucleus droplets or do collisions between the smaller sizes of droplets ultimately produce more large droplets?

A complete mathematical investigation of this problem has not been made but the evidence offered by the three investigators above indicates that the statistical nature of the problem is very important.

One way of approaching this question is to examine the differences in drop sizes and drop concentrations which may result from condensation with a view toward assessing their coalescence tendencies, that is, how will n (the number of first collisions) change in (1) as r grows by condensation? It seems that the assumptions which are necessary to make such an appraisal are not too gross to prevent an examination of important aspects of this process.

As a model for such investigation, assume a constantly rising current of air containing a given frequency distribution of salt particles. The condensation conditions attending are then fixed by the initial conditions such as temperature, pressure, rate of rise, and the above assumptions such that, until the process of coalescence becomes important, we can describe the cloud droplet spectrum at each time and altitude above base [*Mordy*, 1959]. We shall then investigate, as time elapses, the characteristics of these changing spectra which are conducive to coalescence.

We shall therefore look first at the way n varies with time or height if the growth of the particles is controlled only by the condensation conditions.

The fall velocity of the drops we consider is satisfactorily described by Stokes law (that is, for $r < 40\mu$) so that

$$v = \frac{2g\rho r^2}{gn} \approx kr^2 \; (k = \text{constant})$$

If the above expression is substituted in (1) and the terms rearranged the equation can be written

$$n = E\pi N_1 N_2 k (r_1 + r_2)^3 (r_1 - r_2) \tag{3}$$

Only that part of the condensation process that occurs above the zone of maximum supersaturation (where N_1 and N_2 are determined in this model) need be considered here so that $\pi N_1 N_2 k$ may be considered as a constant. The variation of E is uncertain and therefore for the moment will be included in a new variable $n' = n/E$.

If the ln n' is differentiated with respect to time the equation becomes

$$\frac{1}{n'}\frac{dn'}{dt} = \frac{3}{r_1 + r_2}\frac{d(r_1 + r_2)}{dt} + \frac{1}{r_1 + r_2}\frac{d(r_1 - r_2)}{dt} \tag{4}$$

The time derivatives of the radii can now be obtained from the equation for drop growth by condensation. Here we shall for the moment consider only droplets which have grown until they are dilute enough to neglect the hygroscopic effect of the nucleus. We shall see in the discussion below that this makes very little difference in the conclusions we draw from our results. If a is the ratio of the radius r_1 to r_2 or $r_1 = ar_2$ ($= a\bar{r}$, see (6b) below) the drop growth equations for the two drop sizes which appear in equation (4) can be written [*Mordy*, 1959]

$$\begin{aligned} \frac{dr_1}{dt} &= \frac{\alpha}{a^2\bar{r}^2}(as\bar{r} - A) \\ \frac{dr_2}{dt} &= \frac{\alpha}{\bar{r}^2}(s\bar{r} - A) \end{aligned} \tag{5}$$

where

$s = (e - e_s)/e_s$ = supersaturation

$$\alpha = \frac{\epsilon^2 e L^2 DJe}{R^2T^3}\left[\frac{1}{1 + \dfrac{\epsilon^2L^2DJe}{kR^2T^3}}\right]$$

$\approx$ const $\approx 8 \times 10^{-7}$ cgs at 800mb, $10^\circ\ C$

$A = 2\sigma T/JL\rho$

= capillarity term coefficient $\approx 1.7 \times 10^{-6}$ cgs

T = temp of drop

σ = surface tension
J = mech equiv. of heat
L = latent heat of water
ρ = density of water
k = heat diffusion coefficient
e = vapor pressure
e_s = saturation vapor pressure

When (5) is substituted in (4) the equation becomes

$$\frac{1}{n'}\frac{dn'}{dt} = \frac{2\alpha}{r^3}\frac{1}{a}\left[s\bar{r} - A + \frac{A(2a-1)}{a(a+1)}\right] \quad (6)$$

The objective now is to see how the terms in (6) vary as time proceeds. In the writer's previous study it was shown how the bulk of the liquid water lies in the smallest one or two categories of cloud droplets in such a model (see Fig. 1), hence the mean volume radius will represent nearly the radius of droplets which contain the largest part of the liquid water. It will serve as a good index, therefore, for this discussion to consider collisions between this volume mean radius ($\bar{r}$) and larger or smaller droplets in the spectrum. The volume mean radius is defined by

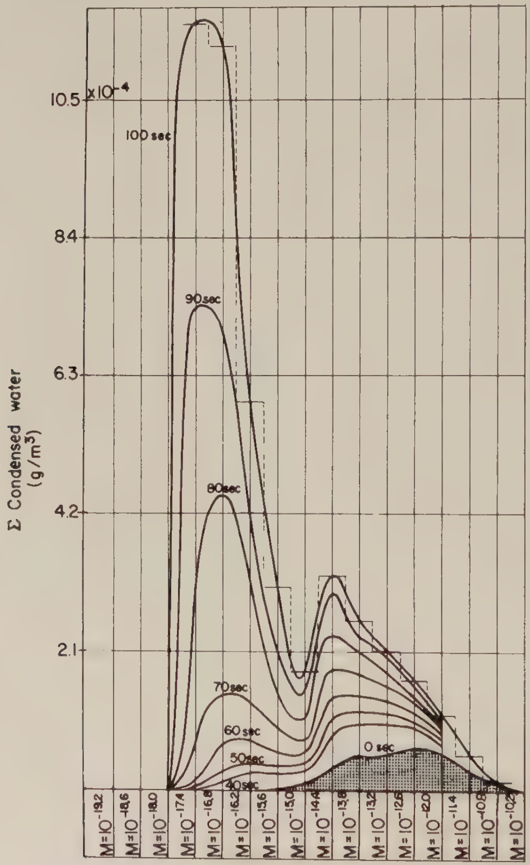

FIG. 1—The concentration of liquid water on droplets growing by condensation on a spectrum of different size condensation nuclei; the spectrum was characteristic of spectra measured by Woodcock at cloud base over the open sea in a Beaufort Force 4 wind; note how quickly the liquid water is concentrated on the smallest one or two size categories of droplets; the mean radius derived from the total liquid water content therefore does not differ much from the minimum droplet radius as used in the present calculations [*Mordy*, 1959]

$$\begin{aligned} \tfrac{4}{3}\pi\bar{r}^3\rho &= \bar{m} \\ &= \text{mean mass of the droplets} \end{aligned} \quad (6b)$$

In the model we are considering, the liquid water is very nearly equal to a constant times the height above cloud base, which is to say

$$N\frac{4}{3}\pi\bar{r}^3\rho = \frac{dx}{dz}\cdot z \approx cz \quad (7)$$

where dx/dz = the change in mixing ratio in a moist adiabatic expansion ($\sim 2 \times 10^{-5}$ cgs at 800mb and 10°C)
z = *ht* above cloud base
$N = \Sigma(N_1 + N_2 \cdots)$ = const.

By differentiating, (7) can be written

$$\frac{d\bar{m}}{dt} = 4\pi\bar{r}^2\rho\frac{d\bar{r}}{dt} = 4\pi\alpha(s\bar{r} - A)\rho = \frac{cv}{N} \quad (8)$$

where $z = vt$ in the model.

The term containing $(s\bar{r} - A)$ here has been substituted from the condensation growth equation (5). If these expressions in (7) and (8) are used to replace $\bar{r}^3$ and $(s\bar{r} - A)$ in (6) the equation becomes:

$$\frac{1}{n'}\frac{dn'}{dt} = \left(\frac{2}{3a}\right)\left(\frac{1}{t}\right)\left[1 + \frac{A(2a-1)}{a(a+1)}\cdot\frac{4\pi\alpha N}{cv}\right] \quad (9)$$

when it is assumed that $\rho = 1$

If the two equations for drop growth (5) are subtracted the following equation may be obtained in quite an analogous way

$$\frac{1}{r_1 - \bar{r}}\frac{d(r_1 - \bar{r})}{dt} = \frac{-1}{3at}\left[1 - \frac{A4\pi\alpha N}{acv}\right] \quad (10)$$

Now putting

$$y = \frac{cv}{4\pi\alpha NA}$$

and

$$\Delta r = r_1 - \bar{r}$$

and combining (9) and (10) the following equation is obtained.

$$\frac{1}{n'}\frac{dn'}{dt} = \frac{-2}{\Delta r}\frac{d\Delta r}{dt}\left[1 + \frac{3}{\left(1+\frac{1}{a}\right)(ay-1)}\right] \tag{11}$$

Note: $c = dx/dz$ (see Eq. 7); A is defined in (5).

Values of y are given in Table 1 for cases from the writer's previous condensation study. Choosing four representative values of y and computing the value of the coefficient in (11) for all radii larger than one half the mean radius one can see that a good approximation for this quantity is $y' = 2 + 6/y$ for the given values of y. Hence the time dependence of a can be rather safely neglected in integrating (11).

Putting

$$y' = 2\left[1 + \frac{3}{\left(1+\frac{1}{a}\right)(ay-1)}\right] \approx 2$$

when $60 > y > 4$, (11) may be integrated to give

$$n' = n_0'\left(\frac{\Delta r_0}{\Delta r}\right)^{y'} \qquad 2 < y' < 2.75 \tag{12}$$

Eq. (12) indicates that if Δr remains $<\Delta r_0/2$, n' will be only from 4 to 16 times greater than n_0'.

It is useful now to examine the variations in Δr which occur as a result of condensation. Eq. (10) shows that as long as $1 \gg 1/ay$ that $\Delta r_0/\Delta r$ varies approximately as $t^{-(1/3a)}$. In this range all values of Δr are converging. By the time that 300 sec have elapsed Δr has a time constant

$$T = \left(\frac{1}{\Delta r}\frac{d\Delta r}{dt}\right)^{-1}$$

of more than 1000 sec. In fact when one includes the effect of the salt nuclei in the drops this time constant is appreciably lengthened so that Δr may be treated as nearly constant in the time interval of 1000 sec or so which we consider here. If variations of two in the values of $\Delta r_0/\Delta r$ are allowed for, an error in the estimation of n' by a factor as large as 16 may occur. We shall see, however, that this variation is small compared to the several orders of magnitude variation in n' computed in the cases of different droplet spectra.

Eq. (12) shows effectively that the most important factors (n_0, y) which determine n' are determined very near the cloud base and are influenced by the strength of the vertical current and the nucleus distribution on which the droplets form.

If Δr is considered a constant then with the aid of (7), $\bar{r}$ is known and the spectrum of condensation produced droplets can be estimated at each altitude (or liquid water content). Once the spectrum is determined an estimate can be made from Eq. (3) of the number of 'potential' first collisions ($n' = n/E$) per unit time between any size category and the mean radius.

Such calculations of n' are given in Tables 2–5 for four cases from the condensation study. The drop size distributions for these cases are shown in Figure 2. The calculations were made for a cloud liquid water content of 1g/m³ which by (8)

TABLE 1—*Values of y for various nucleus distributions and vertical velocities*

Case	vertical velocity (v)	No. of drops (N)	$y = \frac{cv}{4\pi\alpha NA}$
	cm/sec		
I–100	100	2.5×10^7	56.2
II–15	15	4.7×10^7	4.57
III–5	5	1.6×10^7	4.47
III–100	100	1.4×10^8	10.2

TABLE 2—*Case III, 100 cm/sec*

N	r	n'	a
10^8	11.9		
3×10^7	12.1	6760	0.98
10^7	12.3	3930	0.96
3×10^6	12.4	1780	0.958
10^6	12.6	835	0.945
9×10^5	12.9	1167	0.922
7×10^5	13.3	1495	0.895
5×10^5	13.8	1581	0.862
3×10^5	14.4	1407	0.826
9×10^4	15.7	870	0.758
3.2×10^4	18.7	943	0.636
9×10^3	20.0	376	0.595
2×10^3	24.0	211	0.496

TABLE 3—*Case II, 15 cm/sec*

N	r	n'	a
3×10^7	17.5		
10^7	17.85	3760	0.980
3×10^6	18.10	2005	0.966
10^6	18.4	1000	0.951
4×10^5	18.7	578	0.935
2.5×10^5	19.2	563	0.911
2×10^5	19.9	698	0.880
10^5	20.8	570	0.841

TABLE 4—*Case I, 100 cm/sec*

N	r	n'	a
1.28×10^7	21.2		
6.4×10^7	22.2	2710	0.954
3.2×10^6	22.4	1950	0.946
1.6×10^6	22.7	1195	0.933
8×10^5	23.2	730	0.912
4×10^5	23.6	436	0.897
2×10^5	24.2	285	0.875
10^5	25.2	203	0.840
5×10^4	26.2	134	0.809
2×10^4	27.3	70	0.790
3×10^3	29.9	18	0.708
3×10^2	33.7	3	0.628
10	38.6	1.8	0.548

TABLE 5—*Case III, 5 cm/sec*

N	r	n	a
10^7	24.6		
3×10^6	26.1	232	0.943
10^6	27.0	133	0.910
9×10^5	28.0	175	0.878
7×10^5	29.2	197	0.842
5×10^5	30.6	199	0.803
3×10^5	33.1	192	0.743

determines $\bar{r}$. Because of the very skew nature of the droplet distribution the mean radius and the minimum radius were assumed to be the same, an assumption which could lead to an error of a few per cent in the estimate of n' at most. The four cases chosen were representative of the range of differences in nucleus spectra which resulted from different nucleus distributions and vertical velocities.

In all of these cases except one there is a markedly higher number of potential collisions among the smallest cloud droplets. The exception is the case where there is an extremely slow rate of rise, 5 cm/sec, and a dense nucleus distribution (which was taken from Woodcock's data as characteristic of the distributions of salt particles produced at cloud base by a Beaufort Force 7 wind at the sea surface).

The fact that there are a higher number of potential collisions between small droplets, however, is not enough to determine whether collisions between the smallest droplets are of comparable importance to those between the larger and smaller droplets. It must be determined whether in a reasonable time a comparable number of larger droplets are originating by combining smaller droplets as from condensation on large salt particles. To test whether this is true the resulting radius and number of the droplets produced by the combination of the smallest droplets in a reasonably short time, must be compared with the total number of condensation produced droplets which have about the same radius as the combined droplets ($r = 2^{1/3}\bar{r} = 1.26r$). If these figures are close to the same value then one must assume that collisions between the smaller droplets are more important than between large nucleus drops and small drops. The larger droplets are then being increased in number at a sufficiently rapid rate so that the number of originally large particles is relatively insignificant.

A useful index therefore as to the importance of these collisions is the time of replacement of large nucleus droplets (droplets formed on large nuclei) by smaller coalescing droplets. If this is computed for the cases in Table 6 one finds that the number of coalescences between the smallest two categories of droplets replace

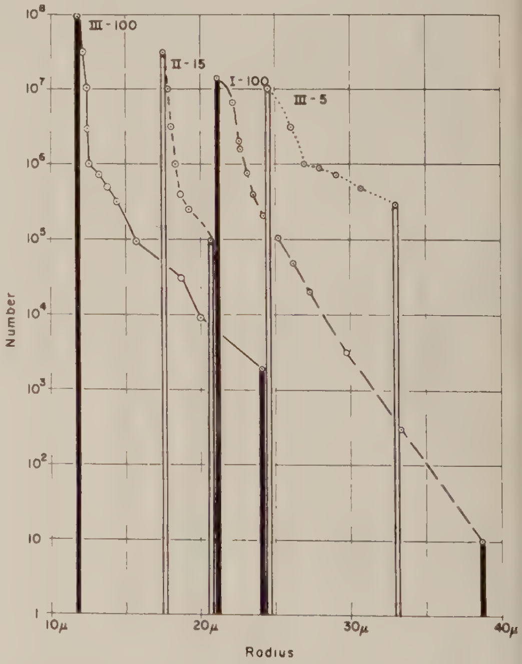

FIG. 2—The distribution of cloud droplet sizes used in the computations; these distributions are derived from *Mordy* [1959] and represent the extreme differences in droplet concentration and spectrum width obtained in the different assumed cases of nucleus spectra and vertical velocities; the spectra represent the sizes of droplets expected if the liquid water content is $1 g/m^3$ and is assumed constant (see text); the figures at the top give the distribution type and the vertical velocity in cm/sec

TABLE 6—*Values of T for the four cases*

Distribution	Vertical velocity	A = no. nuclei drops with $r = 2^{1/3}\bar{r}$	n/E	$T = A/(N/E)$
	cm/sec		sec $^{-1}$	sec
I	100	3×10^4	2.7×10	0.10
II	15	10^5	3.8×10	26.
III	5	3×10^5	2.3×10^2	1.3×10^3
III	100	4×10^5	6.7×10	60.

those with a radius $r = 2^{1/3}\bar{r} = 1.26r$ in periods ranging from less than one second for the distribution Case I at 100 cm/sec to more than 1000 sec in the distribution Case III at 5 cm/sec. These values for the four cases are given in Table 6.

The values for T in Table 6 only give a comparison between the two smallest categories of droplets and the number of existing, condensation-produced droplets which have a radius roughly equal to that of the droplets produced by combining the two small droplets. Actually it would be better perhaps to compare all coalescences between the smallest categories having a radius not more than about ten per cent larger than the minimum value with the number of condensation produced large droplets. If this is done, values of T are decreased by a factor of 3 to 5.

If these computations are made for a larger liquid water content then the collisions between the small droplets become relatively more important. To see how this proceeds a useful diagram can be constructed as in Figure 3. Here the

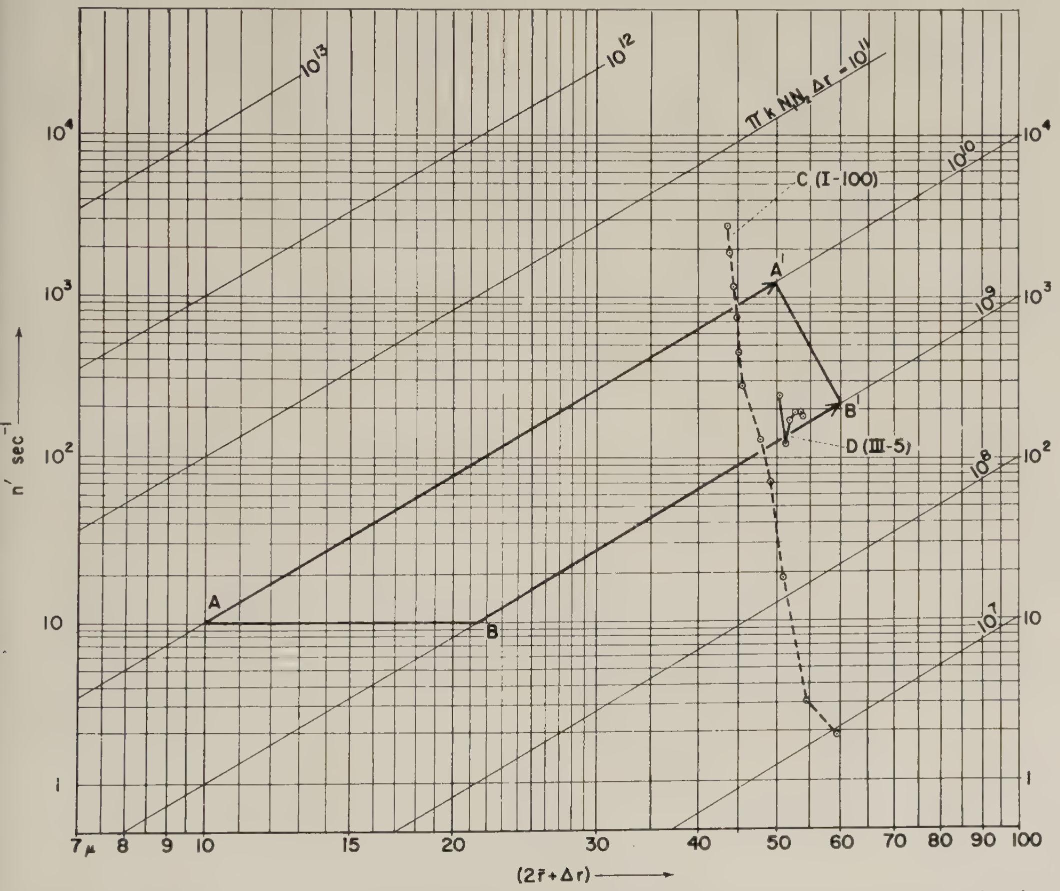

FIG. 3—The number of potential collisions n' per unit time between two size categories of droplets of radius $(\bar{r})$ and $(\bar{r} + \Delta r)$ as computed from Eq. (13); as $\bar{r}$ increases the points in the curves move along the diagonal lines ($\pi k N_1 N_2 \Delta r$ = constant) hence tend to line up vertically as $\Delta r/\bar{r} \to 0$ and thus demonstrates the increasing importance of collisions between the smaller size categories as $\bar{r}$ increases with time or liquid water content; curve AB becomes $A'B'$ as $2\bar{r} + \Delta r$ increases; the curves marked C and D represent two cases computed in Table 6 and demonstrate how different the collision expectancy can be for the different condensation conditions assumed.

terms in (3) have been expressed as

$$\ln n' = \ln \frac{n}{E} = \ln \pi N_1 N_2 k \Delta r + 3 \ln (2\bar{r} + \Delta r) \qquad (13)$$

where $r_1 = \bar{r}$

$$r_2 = \bar{r} + \Delta r$$

$$\Delta r = \text{const}$$

Since for any pair of droplet sizes N_1N_2 is considered constant in the model, then the variation of $\ln n'$ depends only on n_0' and $\bar{r}$. Hence if one plots the number of collisions between two categories of droplets as given in Tables 2 to 5 it is possible to extrapolate how the relative number of collisions change with time or with different liquid water contents. As $\Delta r/r$ becomes small the points representing the number of collisions tend to line up more vertically as the points move along the diagonal lines (curve AB becomes curve $A'B'$) showing that as time elapses the relative importance of the small droplet collisions increases. The diagram also shows how important the initial droplet spectra radii are in determining the relative importance of large and small droplets, for these show up as the separation of points in the curves in the diagram. When satisfactory information about E is available as a plot of $\ln E$ vs. $\ln (2\bar{r} + \Delta r)$ and Δr, this will allow a more complete diagrammatic treatment.

The calculations and reasoning in this paper have been made with the assumption that the collection efficiency of the droplet was 100%. Research and theory on the collection efficiency of droplets unfortunately does not yet converge on values which can be substituted into these equations to provide more conclusive arguments. However, if one follows the reasoning of *Hocking* [1959], it seems that few if any collisions occur before the droplets reach radii of 18μ or more. At this point the collection efficiency rises rapidly to values exceeding unity. If these values were to be inserted in the present study an almost explosive effect on the numbers of droplets coalescing should occur at the point where the mean drop size exceeds this value, independently of whether one has a wide spectrum of cloud condensation produced droplets or not. Here the most important consideration would be the concentration of droplets per unit volume. This is largely fixed by the supersaturation conditions and nucleus concentrations at cloud base. With different droplet concentration, considerable differences in liquid water content or cloud depth are required to produce the large mean droplet size which Hocking states is necessary for coalescence.

Acknowledgments—The writer wishes to acknowledge with thanks the helpful discussions of the work described in this paper with B. Bolin, P. Welander, and most especially with Mr. Claes Rooth of the International Meteorological Institute in Stockholm. The work has been supported by the U. S. Office of Naval Research and the Woods Hole Oceanographic Institution.

REFERENCES

BOWEN, E. G., The formation of rain by coalescence, *Austr. J. Sci. Res.*, A **3**, 193–212, 1950.

FOURNIER D'ALBE, E. M., A. M. A. LATEEF, L. I. RASOOL, AND I. H. ZAIDI, The cloud seeding trials in the central Punjab, July–September 1954, *Q. J. R. Met. Soc.*, **81**, 574–581, 1955.

HITSCHFELD, WALTER, Size distribution generated by a random process, *Artificial Stimulation of Rain*, Pergamon Press, pp. 224–229, 1957.

HOCKING, L. M., The collision efficiency of small drops, *Q. J. R. Met. Soc.*, **85**, 44–50, 1959.

HOUGHTON, H. G., A preliminary quantitative analysis of precipitation mechanisms, *J. Met.*, **7**, 363–369, 1950.

LANGMUIR, I., The production of rain by chain reaction in Cumulus clouds at temperatures above freezing, *J. Met.*, **5**, 175–192, 1948.

LUDLAM, F. H., The production of showers by the coalescence of droplets, *Q. J. R. Met. Soc.*, **76**, 52–58, 1951.

MASON, B. J., *The Physics of Clouds*, Oxford Univ. Press, 481 pp., 1957.

MORDY, W. A., Computations of the growth by condensation of a population of cloud droplets, Tellus, **11**, 16–44, 1959.

TELFORD, J. W., A new aspect of coalescence theory, *J. Met.*, **12**, 436–444, 1955.

WELANDER, P., A theoretical power law for the distribution of small particles or drops falling through the atmosphere, *Tellus*, **11**, 197–201, 1959.

WOODCOCK, A. H., Atmospheric salt particles and raindrops, *J. Met.*, **9**, 200–212, 1952.

Discussion

(Note: The discussion of this paper is combined with that following the next paper.)

Contribution No. 1080

A METHOD FOR PREPARING THE MARINE POLYCHAETE, *PECTINARIA GOULDI* (VERRILL), FOR HISTOLOGICAL STUDY[1]

JAMES E. HANKS
Woods Hole Oceanographic Institution

Prior to cutting sections of the deposit-feeding polychaete annelid, *Pectinaria* (*Cistenides*) *gouldi* (Verrill), for histological study, it was necessary to remove the sand grains from the digestive tract to prevent injury to the edge of the microtome knife. This note reports a method by which this was accomplished in the hope it may be of use to other investigators.

Worms placed in finger-bowls of standing sea water were observed to eliminate a portion of the sand as faecal pellets. After a period of 48 hours, however, no further faecal material was passed. After removing the worm from its sand-tube, microscopic examination indicated that sufficient sand was still present to prevent cutting of sections.

Attempts to remove the digestive tract intact by dissecting both living and fixed specimens were unsuccessful. Some sand was always discharged into the body cavity during dissection. Although a portion of this sand could be flushed away, it was impossible to remove enough to make sectioning feasible.

This suggested the use of a substance which the worms would ingest to replace the sand in the digestive tract in a natural manner. Sand can be removed from the digestive tract of oligochaete annelids such as *Lumbricus terrestris* Linnaeus by allowing them to feed on agar or gelatin. Following this procedure, specimens of *P. gouldi* were offered agar or corn-meal which had been mixed with sea water to form a soft substratum. Worms were unable to maintain themselves in their normal, upright position in these substratums, however, and neither substance was ingested.

These results indicated that the artificial substratum would have to be of the approximate consistency of the natural substratum. This eliminated most substances that could themselves be sectioned. The requirements of such a substratum are: 1) it must be easily ingested by the worm, and 2) it must be removable by a solvent which will not injure the tissues of the worm. It seemed possible that calcium carbonate might suit this purpose, for, if it were ingested, it could be removed by decalcification during the fixation of the tissue.

Calcium carbonate was prepared by grinding dried, quahog shells (*Mercenaria mercenaria* (Linnaeus)) in a ballmill. The ground material was seived to remove particles larger than course sand grains, mixed with sea water, and the finer material, which did not settle readily, washed away. The wet calcium carbonate was then packed into a glass vial and the vial placed in a container of sea water. A worm was then introduced into the vial.

The worm burrowed quickly into this substratum. It was left un-

---

[1] Contribution No. 1080 from the Woods Hole Oceanographic Institution. This research was supported by National Science Foundation Grant G–8905.

Reprinted from TRANSACTIONS OF THE AMERICAN MICROSCOPICAL SOCIETY
Vol. LXXIX (4): 470–471, October 1960.

disturbed overnight and then removed to a finger-bowl of sea water. After breaking the sand-tube away from the worm, examination under the microscope showed that the digestive tract was completely filled with calcium carbonate. Within ten minutes faecal pellets of this substance were observed discharging from the anal opening.

The worm was fixed in a saturated mercuric bichloride solution acidified to five percent with acetic acid for decalcification. In order to expose the calcium carbonate directly to the acidified fixative and to permit the escape of the carbon dioxide bubbles as they were formed, the worm was cut into three pieces. As decalcification progressed, a vacuum was applied to the tissue at intervals to remove entrapped bubbles. The solution was changed frequently until decalcification was completed. Sections of the tissue cut at ten microns thickness and stained with hematoxylin and eosin were completely satisfactory.

Contribution No. 1081

ON THE BOUSSINESQ APPROXIMATION FOR A COMPRESSIBLE FLUID

E. A. SPIEGEL AND G. VERONIS

Reprinted for private circulation from
THE ASTROPHYSICAL JOURNAL
Vol. 131, No. 2, March 1960
Copyright 1960 by the University of Chicago
PRINTED IN U.S.A.

ON THE BOUSSINESQ APPROXIMATION FOR A COMPRESSIBLE FLUID

E. A. Spiegel* and G. Veronis
Woods Hole Oceanographic Institution, Woods Hole, Massachusetts

Received September 28, 1959

ABSTRACT

The full, non-linear equations governing thermal convection in a compressible fluid have been re-examined in order to determine the conditions under which the Boussinesq approximation is applicable. These conditions are (*a*) the vertical dimension of the fluid is much less than any scale height, and (*b*) the motion-induced fluctuations in density and pressure do not exceed, in order of magnitude, the total static variations of these quantities. Under these conditions the equations are formally equivalent to those for an incompressible system when the temperature gradient is replaced by its excess over the adiabatic and C_p replaces C_v.

INTRODUCTION

In the study of problems of thermal convection it is a frequent practice to simplify the basic equations by introducing certain approximations which are attributed to Boussinesq (1903). The Boussinesq approximations can best be summarized by two statements: (1) The fluctuations in density which appear with the advent of motion result principally from thermal (as opposed to pressure) effects. (2) In the equations for the rate of change of momentum and mass, density variations may be neglected except when they are coupled to the gravitational acceleration in the buoyancy force.

For a liquid the approximations are quite natural ones to apply and Rayleigh (1916) used them in a formal analysis of Bènard cells. For the case of a compressible fluid Boussinesq attempted to justify the first assertion by noting that atmospheric pressure fluctuations are much too small to produce the observed density changes. But Jeffreys (1930) went further and suggested a formal justification for the applicability of the Boussinesq-Rayleigh equations. However, Jeffreys restricted his discussion to the study of infinitesimal, steady motions.

In the present note we re-examine the simplifying assumptions and restrictions which lead to the set of equations applicable to the study of convection in a narrow layer of compressible fluid. In order to make explicit order-of-magnitude comparisons, we have confined our analysis to the case where the equation of state may be adequately represented by the perfect gas law.

EQUATIONS

The equations of motion are

$$\rho \frac{\partial \boldsymbol{v}}{\partial t} + \rho \boldsymbol{v} \cdot \nabla \boldsymbol{v} = -\nabla p - g \rho \boldsymbol{k} + \mu \nabla^2 \boldsymbol{v} + \frac{\mu}{3} \nabla (\nabla \cdot \boldsymbol{v}) \tag{1}$$

and

$$\frac{\partial \rho}{\partial t} + \boldsymbol{v} \cdot \nabla \rho + \rho \nabla \cdot \boldsymbol{v} = 0 , \tag{2}$$

where $\boldsymbol{k}$ is a unit vector in the vertical (z) direction. In obtaining equation (1) the second coefficient of viscosity has been related to μ by asserting that it is independent of the rate of compression. The coefficient μ is taken as constant.

---

[*] Woods Hole Oceanographic Institution Fellow, Summer, 1959.

The equation for the rate of change of energy is

$$\rho C_v \left(\frac{\partial}{\partial t} + \boldsymbol{v} \cdot \nabla\right) T + p \nabla \cdot \boldsymbol{v} = k \nabla^2 T + Q + \mu \nabla \cdot (\boldsymbol{v} \cdot \nabla \boldsymbol{v}) - \tfrac{2}{3} \mu (\nabla \cdot \boldsymbol{v})^2 , \tag{3}$$

where Q represents the radiation source and the coefficients, C_v and k, have been taken as constant.

The viscous dissipation terms contribute negligibly to the energy balance. This can be seen by noting that the convection of internal energy, $\rho \boldsymbol{v} \cdot \nabla e$, is large compared with $\mu \nabla \cdot (\boldsymbol{v} \cdot \nabla \boldsymbol{v})$. Since the internal energy is of order v_k^2, where v_k is the kinetic velocity and $\mu \sim \rho l |v_k|$, where l is the mean free path, we must compare terms like $\rho(|v| v_k^2/L)$ and $\rho(l |v_k| v^2/L^2)$, where L is some macroscopic scale. Thus the ratio of the viscous dissipation term to the rate of change of internal energy is of the order of $|v| \, l/ |v_k| \, L$, and we conclude that viscous dissipation will play no significant role in convection problems.

The equation of state for a homogeneous sytem (in the thermodynamic sense) is of the form

$$\rho = \rho (p, T) \tag{4}$$

THE BASIC APPROXIMATION

Let f represent any one of the state variables: density (ρ), temperature (T), or pressure (p). We shall express these in the form

$$f(x, y, z, t) = f_m + f_0(z) + f'(x, y, z, t) , \tag{5}$$

where f_m is the (constant) space average of f; f_0 is the variation in the absence of motion; and f' is the fluctuation resulting from motion. (For simplicity we have omitted cases where f_m and f_0 depend on t, which would occur if boundary conditions were time-dependent.) We may also introduce the scale heights,

$$D_f = \left| \frac{1}{f_m} \frac{d f_0}{d z} \right|^{-1} . \tag{6}$$

The basic approximation which we shall apply is that the fluid be confined to a layer whose thickness, d, is much less than the smallest scale height, D_f. Thus if $D = (D_f)_{\min}$, we have

$$d \ll D \tag{7}$$

throughout the fluid.

In particular, condition (7) implies that $d/D\rho \ll 1$. On integrating this latter condition from the level of minimum to the level of maximum density within the layer, we conclude that

$$\frac{\Delta \rho_0}{\rho_m} \equiv \epsilon \ll 1 , \tag{8}$$

where $\Delta\rho_0$ is the maximum variation of ρ_0 across the layer. Condition (8) is often the basic restriction imposed at the outset of convection studies.

The basic approximation, condition (7), is sufficient to produce the simplified Boussinesq-Rayleigh equations if only motions of infinitesimal amplitudes are considered. However, in non-linear investigations it is necessary to make the additional restriction that the motion-induced fluctuations do not exceed, in order of magnitude, the static variation. Thus we require that

$$\left| \frac{\rho'}{\rho_m} \right| \leq 0 (\epsilon) . \qquad (9$$

Condition (9) must be verified a posteriori from solutions of the problem. However, there seems to be no experimental evidence to indicate that ρ' ever exceeds $\Delta\rho_0$, so that, if the original restriction on $\Delta\rho_0$ is satisfied, one may generally proceed to apply the equations and expect to satisfy condition (9).

THERMODYNAMIC RELATIONS

Equation (4) may be expanded about ρ_m, p_m, T_m in a Taylor series, to yield

$$\rho = \rho_m\left[1 - \alpha_m (T - T_m) + K_m (p - p_m) + \frac{1}{2}\left(\frac{1}{\rho}\frac{\partial^2\rho}{\partial T^2}\right)_m \frac{(T - T_m)^2}{p} + \frac{1}{2}\left(\frac{1}{\rho}\frac{\partial^2\rho}{\partial p\,\partial T}\right)_m (p - p_m)(T - T_m) + \frac{1}{2}\left(\frac{1}{\rho}\frac{\partial^2\rho}{\partial p^2}\right)_m (p - p_m)^2 + \ldots\right], \tag{10}$$

where

$$\alpha_m = -\left(\frac{1}{\rho}\frac{\partial\rho}{\partial T}\right)_m, \qquad K_m = \left(\frac{1}{\rho}\frac{\partial\rho}{\partial p}\right)_m. \tag{11}$$

If the fluid is an ideal gas, the series expansion becomes

$$\rho = \rho_m\left[1 - \frac{T - T_m}{T_m} + \frac{p - p_m}{p_m} + \left(\frac{T - T_m}{T_m}\right)^2 - \frac{1}{2}\left(\frac{p - p_m}{p_m}\right)\left(\frac{T - T_m}{T_m}\right) + \ldots\right], \tag{12}$$

where, for brevity, we have omitted the (ordinarily) small corrections required by variation in mean molecular weight and by the effect of the radiation pressure.

From the restriction imposed in the preceding section, it follows that $[(T - T_m)/T_m]^2$ and $[(p - p_m)/p_m]\,[(T - T_m)/T_m]$ cannot be greater than $0(\epsilon^2)$. Hence, to order ϵ, we may write

$$\begin{aligned}\frac{\rho - \rho_m}{\rho_m} &= -\frac{T - T_m}{T_m} + \frac{p - p_m}{p_m} \\ &= -\alpha_m (T - T_m) + K_m (p - p_m)\end{aligned} \tag{13}$$

with the further consequence that

$$\rho_0 = \rho_m (K_m p_0 - \alpha_m T_0) \tag{14}$$

and

$$\rho' = \rho_m (K_m p' - \alpha_m T'). \tag{15}$$

EQUATIONS OF MOTION

In the absence of motion, the vertical component of equation (1) becomes

$$\frac{\partial p_0}{\partial z} = -g\rho_m - g\rho_0. \tag{16}$$

If we introduce the hydrostatic relation into equation (1), we have

$$\rho\left(\frac{\partial v}{\partial t} + v\cdot\nabla v\right) = -\nabla p' - g\rho' k + \rho\nu\nabla^2 v + \tfrac{1}{3}\rho\nu\nabla(\nabla\cdot v). \tag{17}$$

We may introduce equations (5) and (8) into the continuity equation to obtain

$$\nabla\cdot v = -\left(\frac{\partial}{\partial t} + v\cdot\nabla\right)\left(\epsilon\frac{\rho_0}{\Delta\rho_0} + \epsilon\frac{\rho'}{\Delta\rho_0}\right) + 0(\epsilon^2). \tag{18}$$

Hence, to order ϵ, equations (17) and (18) may be written

$$\frac{\partial \boldsymbol{v}}{\partial t}+\boldsymbol{v}\cdot\nabla\boldsymbol{v}=-\frac{1}{\rho_m}\nabla p'-g\epsilon\frac{\rho'}{\Delta\rho_0}\boldsymbol{k}+\nu\nabla^2\boldsymbol{v}\,, \tag{19}$$

$$\nabla\cdot\boldsymbol{v}=0\,. \tag{20}$$

In equation (19) we have retained the term $g\epsilon(\rho'/\Delta\rho_0)\boldsymbol{k}$ even though it contains ϵ as a factor. This procedure is clearly necessary if we are to study convection problems in the present approximation, and the following justification may be made.

The quantity $\partial\boldsymbol{v}/\partial t$ measures the characteristic acceleration of the fluid. Now the system is driven by fluctuations of the density field, and hence we must insist that the characteristic acceleration be of order $(g\epsilon\rho'/\Delta\rho_0)\boldsymbol{k}$. This in turn forces the conclusion that the acceleration of gravity is always much greater than the characteristic acceleration. We note that this is a statement concerning the relative size of the accelerations which occur in a convecting fluid and is not an assumption about the magnitude of g.

Equation (19) can be further simplified in the following way. The vertical component of equation (19) is

$$\frac{\partial w}{\partial t}+\boldsymbol{v}\cdot\nabla w=-\frac{1}{\rho_m}\frac{\partial p'}{\partial z}-g\epsilon\frac{\rho'}{\Delta\rho_0}+\nu\nabla^2 w\,, \tag{21}$$

where w is the vertical velocity component. Using equation (15) we may write

$$\begin{aligned}-\frac{1}{\rho_m}\frac{\partial p'}{\partial z}-g\epsilon\frac{\rho'}{\Delta\rho_0}&=-\frac{1}{\rho_m}\frac{\partial p'}{\partial z}-g\frac{p'}{p_m}+g\frac{T'}{T_m}\\&=-\frac{1}{\rho_m}\left(\frac{\partial p'}{\partial z}+\frac{1}{H}p'\right)+g\frac{T'}{T_m},\end{aligned} \tag{22}$$

where

$$H=\frac{p_m}{g\rho_m}. \tag{23}$$

The quantity H is the thickness of a layer with uniform density and pressure varying from p_m at the bottom to zero at the top. From the definition of scale height and equation (16) it is readily seen that

$$H=D_p+0(\epsilon)\,; \tag{24}$$

and, since $\partial p'/\partial z\geq p'/d$, we conclude that p'/H is negligible compared to $\partial p'/\partial z$ in equation (23).

Therefore, equation (21) becomes

$$\frac{\partial \boldsymbol{v}}{\partial t}+\boldsymbol{v}\cdot\nabla\boldsymbol{v}=-\frac{1}{\rho_m}\nabla p'+g\alpha T'\boldsymbol{k}+\nu\nabla^2\boldsymbol{v}\,. \tag{25}$$

The considerations leading to equation (25) have an interesting consequence. We have seen that the fluctuation buoyancy term is a necessary part of the convection problem. However, the contribution of p' to this term is of $0(d/H)$ as compared to the contribution of the temperature fluctuation. Therefore to $0(d/H)$ we may approximate equation (15) by

$$\frac{\rho'}{\rho_m}=-\frac{T'}{T_m}=-\alpha_m T'\,, \tag{26}$$

which is equivalent to the first of the approximations mentioned in the introduction. It is of interest to note that equation (26) is a consequence of the dynamical argument.

We also note here that a similar argument does not apply to equation (14), since p_0 provides a major contribution to hydrostatic balance.

THE HEAT EQUATION

In the absence of motion, equation (3) becomes

$$k\nabla^2 T_0 + Q_0 = 0 \ . \qquad (27$$

Hence the equation for the temperature fluctuation is

$$\rho_v C_v \left(\frac{\partial T'}{\partial t} + v \cdot \nabla T\right) + p \nabla \cdot v = k \nabla^2 T' + Q' \ , \qquad (28)$$

where

$$Q' = Q - Q_0 \ . \qquad (29)$$

The term $p\nabla \cdot v$ is retained here because it is of the same order as the other terms in equation (28).

To verify this, we first note that p_0/p_m is of order d/H. Further, as mentioned earlier, we expect that $|p'/p_m| = 0(\Delta p_0/p_m)$. Hence $p = p_m + 0(d/H)$. Now, using equations (14), (18), and (26), we may write

$$p\nabla \cdot v = p_m \left(\frac{\partial}{\partial t} + v \cdot \nabla\right)\left(\frac{T_0 + T'}{T_m} - \frac{p_0}{p_m}\right) , \qquad (30)$$

where we have neglected terms of order d/H. But, as a consequence of equation (16),

$$\left(\frac{\partial}{\partial t} + v \cdot \nabla\right) \frac{p_0}{p_m} = -\frac{w}{p_m} g \rho_m + 0\left(\frac{d}{H}\right) , \qquad (31)$$

so that equation (30) becomes

$$p\nabla \cdot v = \frac{p_m}{T_m}\left(\frac{\partial}{\partial t} + v \cdot \nabla\right)(T_0 + T') + w g \rho_m \ . \qquad 32)$$

Thus equation (28) is reduced to the form

$$\rho_m C_p \left(\frac{\partial T'}{\partial t} + v \cdot \nabla T\right) + w g \rho_m = k \nabla^2 T' + Q' \ , \qquad (33)$$

where $C_p = C_v + p_m/\rho_m T_m \equiv C_v + R$. Equation (33) simplifies to the equation suggested by Jeffreys when non-linear terms and time derivatives are neglected. A more familiar form of the equation is

$$\left(\frac{\partial}{\partial t} + v \cdot \nabla\right) T' + w \left(\frac{\partial T_0}{\partial z} + \frac{g}{C_p}\right) = K \nabla^2 T' + \frac{Q'}{\rho_m C_p} , \qquad (34)$$

where $-g/C_p$ is the adiabatic gradient and

$$K = \frac{k}{\rho_m C_p} . \qquad (35)$$

SUMMARY

It has been shown that the equations governing convection in a perfect gas are formally equivalent to those for an incompressible fluid if the static temperature gradient is replaced by its excess over the adiabatic, C_v is replaced by C_p, and the following approximations are valid: (*a*) the vertical dimension of the fluid is much less than any scale height, and (*b*) the motion-induced fluctuations in density and pressure do not exceed, in order of magnitude, the total static variations of these quantities.

With these restrictions, the final system of equations is given by equations (20), (25), (26), and (34).

We wish to thank the National Science Foundation for its interest in and support of the summer geophysical hydrodynamics program at W.H.O.I. We have discussed this problem with W. V. R. Malkus on several occasions and wish to thank him for his interest. The research was supported in part by the Office of Naval Research and is *Contribution No. 1081* from the Woods Hole Oceanographic Institution.

REFERENCES

Boussinesq, J. 1903, *Théorie analytique de la chaleur* (Paris: Gathier-Villars), Vol. 2.
Jeffreys, H. 1930, *Proc. Cambridge Phil. Soc.*, 26, 170.
Rayleigh, Lord. 1916, *Phil. Mag.*, 32, 529; *Collected Papers*, 6, 432.

Contribution No. 1082

Deep-Sea Research, 1960, Vol. 6, pp. 318 to 327. Pergamon Press Ltd., London. Printed in Great Britain

An approximate theoretical analysis of the equatorial undercurrent

G. VERONIS

(*Received* 25 *August* 1959)

INTRODUCTION AND SUMMARY

THE EQUATORIAL Undercurrent in the Pacific Ocean is a narrow (2° wide) subsurface current flowing to the east. The prevailing winds in this equatorial region are toward the west. CROMWELL, *et. al.*, (1954) made the first oceanographic observations of the current in 1952. KNAUSS (1960) later undertook a more extensive observational programme and confirmed the original observation. The current has a maximum eastward velocity of 150 cm/sec at a depth of about 100 m. At the surface and at depths greater than 300 m the flow is relatively weak and toward the west.

A simple physical argument can be put forth to explain the existence of the undercurrent. A wind blowing westward over a non-rotating, bounded basin will pile up water on the western ride and thus give rise to a pressure gradient which drives the subsurface water back toward the east (Fig. 1). When the water is vertically stratified, the depth to which the current extends may be limited by the adjustment of the stratified layers. At the equator where the effect of the earth's rotation is essentially negligible the above picture obtains. In regions away from the equator the Coriolis force becomes appreciable and, indeed, dominates the system.

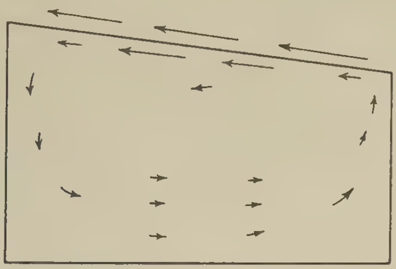

FIG. 1. A sketch of the overturning cellular motion in a confined non-rotating basin when the surface is subjected to a tangential shear stress acting to the left. The pile-up of water toward the left forces a slow return circulation in the deeper parts of the basin.

The present paper is a study of the dynamics of the system in the immediate vicinity of the equator. The investigation is restricted to an analysis of the vertical structure of the current. No attempt has been made to determine the parameters which control the width of the current. ROBINSON (1960) has investigated this phase of the problem and has, by dimensional arguments, deduced a width of approximately 100 km. The system of equations which he deduces as the equations which control the motion, coincide with those treated in this paper and which are arrived at by a physical argument. He also shows that this system of equations joins with those of the thermocline model of Robinson and Stommel (1959) at about 1° latitude.

The non-linear equations are treated approximately by replacing parts of the non-linear convective terms by average values.* For example, W, an average value of the vertical velocity, is substituted for w in the terms $w \frac{\partial T}{\partial z}$ and $w \frac{\partial u}{\partial z}$. The quantity W is determined by averaging the final solution for w.

In addition the various quantities are expanded in a power series in y, the north–south coordinate. Solutions are derived for the coefficients of y^0, y^1 and y^2 only, since the essential behaviour of the fluid system near the equator is then immediately available. A final simplification is the choice of a very specific dependence of the variables on the east-west co-ordinate, x. Essentially, the latter implies a treatment of the system away from coastal or other barriers at points along the equator. A boundary-layer solution would have to be added to satisfy boundary conditions at the east-west boundaries.

The model treated requires a knowledge of the temperature (or the heat flux) at the surface of the ocean. The method of solution allows one to fix only that part of the surface temperature which is independent of y. The part of the surface temperature which varies with y is then deduced. In one sense this inability to fix the surface temperature completely is desirable since the final results can then represent a test of the model.

The first conclusion from this analysis is that the depth of penetration of the current system is proportional to $\sqrt{-\frac{\tau L}{g \alpha \bar{T}}}$, where τ is the east – west wind-stress (positive toward the east), L is the east-west scale of the system, g is the gravitational acceleration, α is the coefficient of thermal expansion and $\bar{T}$ is the difference in surface temperatures between the western and eastern edges of the system. It is important to note that the above expression is independent of any internal parameters such as eddy coefficients etc. Using $\tau = -0{\cdot}2\ \mathrm{cm^2/sec}$*, $L = 10^9$ cm, $g = 10^3\ \mathrm{cm/sec^2}$, $\alpha = 2{\cdot}5 \times 15^{-4}/°\mathrm{C}$ and $\bar{T} = 5\ °\mathrm{C}$†, one finds that the scale depth is 125 m. This is also the depth of the core of the undercurrent and it agrees reasonably well with Knauss' measurement of 100 m.

Fig. 2 shows a vertical profile of the east-west current at the equator (u is independent of longitude in this analysis). The *shape* of the profile is given by the present theory but the *surface value* depends strongly on the depth over which the vertical averages for W etc. are made. In Fig. 2 the surface value has been chosen as — 15 cm/sec. The remaining values are then completely determined. The agreement with Knauss' measurement is quite good. The maximum velocity of the undercurrent is 170 cm/sec toward the east as compared to the observed value of 150 cm/sec.

In Fig. 3 the temperature at the eastern and western extremities along the equator is plotted as a function of the vertical co-ordinate z. The absence of a sharp thermocline near the equator appears in the observations also. However, the water near

*One cannot expect precise quantitative results with this model unless the non-linear terms are actually unimportant. However, in that case the equations could be linearized from the outset.

†The value $\tau = -0{\cdot}2\ \mathrm{cm^2/sec}$ was suggested by Knauss for the average value of the east-west wind stress component. The value $\bar{T} = 5\ °\mathrm{C}$ was taken from Муромцев, А. М., 1958, Основные Черты Гидрологии Тихого Океана, Приложениед, Атлас Вертикальных Разрезов и Карт Температуры, Солености, Плотности и Содержания Кислорода, Ленинград.

the surface (upper 100 m) is more nearly water of constant temperature than one deduces from this analysis.

An east-west profile of temperature vs. depth is shown in Fig. 4. The qualitative agreement with observation is again reasonable considering the restrictions imposed by the specific east-west dependence chosen here.

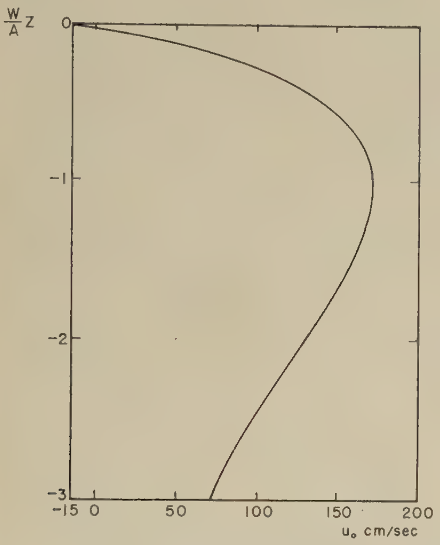

FIG. 2. The vertical profile for u_0.

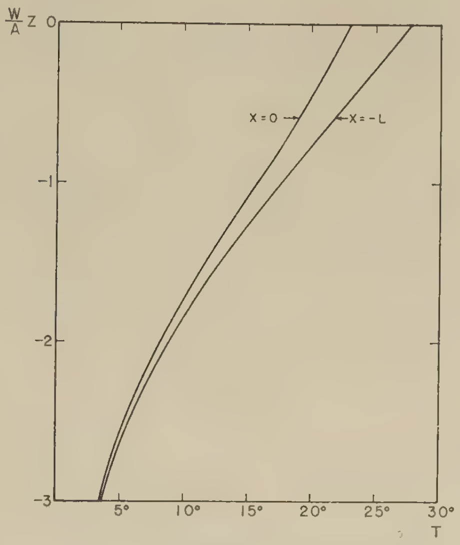

FIG. 3. Vertical profiles of the temperature T_0 at $x = 0$ and at $x = -L$.

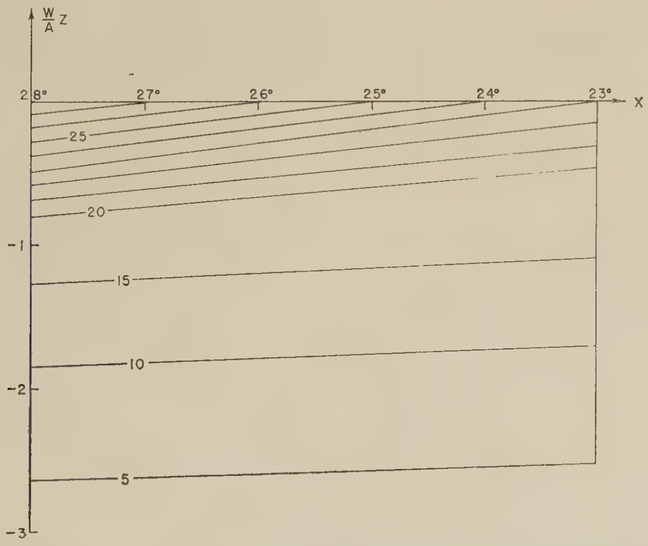

FIG. 4. A vertical cross-section along the equator of the theoretically determined temperature distribution.

One cannot extend the analysis to include much more quantitative information than that discussed up to this point. Qualitatively, one can see that the temperature above the core increases with latitude and the temperature below the core decreases.

REPRINT

This gives rise to the relative vertical spreading of the isotherms at the equator. For further quantitative results one would have to include the east-west convective terms in the second order equations but, as discussed in the next section, the iterative approach hinges on an averaging process which cannot lead to quantitative results.

It should be emphasized that the model described here is oriented toward solving a specific problem. One can see this most readily if one tries the same approach for the purely thermal model of ROBINSON and STOMMEL (1959) near the equator. Since the prescribed surface temperature is intimately connected with the presence of a wind-stress at the surface, one cannot impose the same simple east-west dependance of the variables for the analysis of the purely thermal equatorial problem.

There are other approaches to this problem which are oriented toward explaining features other than the vertical structure. FOFONOFF and MONTGOMERY (1954) have shown that the existence of the undercurrent is consistent with conservation of potential vorticity. STOMMEL (1960) and CARRIER (1960) each look at the undercurrent in the light of the Ekman layer, near the equator. LONG (1960) treats the undercurrent as one example of eastward moving jets in the atmosphere-ocean system. ROBINSON'S (1960) approach has already been mentioned. Finally, there is the ever-present problem of the stability of the undercurrent. What are the factors which limit the current to a 2° band centred on the equator ? C. C. LIN, during a seminar in which the undercurrent was discussed at M.I.T., suggested the interesting possibility that an eastward moving jet may be stabilized by the Coriolis effect. He notes that if the jet is pushed toward the north or south, the Coriolis force acts on the current to return it to its equatorial position. For a westward moving jet the same force causes it to become unstable.

ANALYSIS

The system of equations which is taken to be descriptive of the Equatorial Undercurrent is

$$u\frac{\partial u}{\partial x} + v\frac{\partial u}{\partial y} + w\frac{\partial u}{\partial z} - fv = -\frac{1}{\rho}\frac{\partial p}{\partial x} + A\frac{\partial^2 u}{\partial z^2} \tag{1}$$

$$fu = -\frac{1}{\rho}\frac{\partial p}{\partial y} \tag{2}$$

$$\frac{1}{\rho}\frac{\partial p}{\partial z} = g\alpha T \tag{3}$$

$$\frac{\partial u}{\partial x} + \frac{\partial v}{\partial y} + \frac{\partial w}{\partial z} = 0 \tag{4}$$

$$u\frac{\partial T}{\partial x} + v\frac{\partial T}{\partial y} + w\frac{\partial T}{\partial z} = A\frac{\partial^2 T}{\partial z^2} \tag{5}$$

where x, y, z are co-ordinates which are positive eastward, northward and upward respectively; α is the coefficient of thermal expansion. The constants A in (1) and (5) is an eddy coefficient. The assumption is that heat and momentum mixing is generated by the same type of small scale motion and that the effects of this mixing can be parameterized by a constant coefficient. The remaining variables are the usual ones.

This system of equations is based on the Boussinesq approximation where the variation of density $\rho = \rho_0(1 - \alpha T)$ is taken into account only in the gravitational term. Terms have been neglected not only on the basis of a formal expansion but simply on the basis of physical arguments. For example, the non-linear terms have been kept in equation (1) where at the equator the familiar geostrophic approximation fails completely. However, in equation (2) the neglected terms vanish at the equator (as do the terms retained) and the geostrophic approximation is therefore kept as a reasonable first approximation. Horizontal mixing has been neglected throughout since attention is confined primarily to the vertical structure. An *a posteriori* check of the above equations shows that the neglected terms are never larger than 10 per cent of those kept.

The problem as it stands now is to solve the above system of equations together with appropriate boundary conditions. There are obvious difficulties in trying to solve this general problem and certain approximations will therefore be made.

First the vertical velocity, w, is replaced by an average value $W =$ constant* in the convective terms. Equations (1) and (5) then become

$$u\frac{\partial u}{\partial x} + v\frac{\partial u}{\partial y} + W\frac{\partial u}{\partial z} - fv = -\frac{1}{\rho}\frac{\partial p}{\partial x} + A\frac{\partial^2 u}{\partial z^2} \tag{6}$$

$$u\frac{\partial T}{\partial x} + v\frac{\partial T}{\partial y} + W\frac{\partial T}{\partial z} = A\frac{\partial^2 T}{\partial z^2} \tag{7}$$

For the y-- dependence we assume symmetry about the equator for u, w, p and T and anti-symmetry for v. We can then write

$$(u, w, p, T) = \sum_0^\infty (u_{2n}, w_{2n}, p_{2n}, T_{2n})\, y^{2n} \tag{8}$$

$$v = \sum_0^\infty v_{2n+1}\, y^{2n+1} \tag{9}$$

The Coriolis parameter f will be written

$$f = \beta y \tag{9.a}$$

If (8), (9) and (9.a) be substituted into (2), (3), (4), (6), (7) and if the coefficients of the various powers of y be equated, the following system of equations obtains:

$$u_0\frac{\partial T_0}{\partial x} + W\frac{\partial T_0}{\partial z} = A\frac{\partial^2 T_0}{\partial z^2} \tag{10}$$

$$\frac{1}{\rho}\frac{\partial p_0}{\partial z} = g\alpha T_0 \tag{11}$$

$$u_0\frac{\partial u_0}{\partial x} + W\frac{\partial u_0}{\partial z} = -\frac{1}{\rho}\frac{\partial p_0}{\partial x} + A\frac{\partial^2 u_0}{\partial z^2} \tag{12}$$

$$\frac{\partial u_0}{\partial x} + v_1 + \frac{\partial w_0}{\partial z} = 0 \tag{13}$$

*This value of W must, of course, be deduced from the final solution and, therefore, it is not an 'available' parameter.

$$\beta u_0 = -\frac{2}{\rho} p_2 \tag{14}$$

$$u_2 \frac{\partial T_0}{\partial x} + u_0 \frac{\partial T_2}{\partial x} + 2 v_1 T_2 + W \frac{\partial T_2}{\partial z} = A \frac{\partial^2 T_2}{\partial z^2} \tag{15}$$

$$\frac{1}{\rho} \frac{\partial p_2}{\partial z} = g\alpha T_2 \tag{16}$$

$$u_0 \frac{\partial u_2}{\partial x} + u_2 \frac{\partial u_0}{\partial x} + (2u_2 - \beta) v_1 + W \frac{\partial u_2}{\partial z} = -\frac{1}{\rho} \frac{\partial p_2}{\partial x} + A \frac{\partial^2 u_2}{\partial z^2} \tag{17}$$

$$\frac{\partial u_2}{\partial x} + 3 v_3 + \frac{\partial w_2}{\partial z} = 0 \tag{18}$$

$$\beta u_2 = -\frac{4}{\rho} p_w \tag{19}$$

etc.

Now the surface temperature at the equator is approximately a linear function of x. This suggests a substitution of the form

$$T = T_{00} + T_{01}\, x, \qquad p_0 = p_{00} + p_{01}\, x \tag{20}$$

where the form of p_0 comes from the hydrostatic relation. The remaining variables can be chosen consistently to be independent of x (since the wind-stress is also taken independent of x). One can look upon the present restricted form for the variables as appropriate away from the coastal boundaries. To satisfy such conditions as zero flow through the x– boundaries, it is necessary to add a boundary-layer solution to the present system.

We now propose to solve the equations to order y^2 with the specific x– dependence described above and with the boundary conditions

$$z = 0: \quad T_0 = \bar{T}\left(c - \frac{x}{L}\right), \qquad A \frac{\partial u_0}{\partial z} = \tau = \text{constant}$$

$$z = \infty: \quad T_i = u_i = v_i = p_i = 0$$

The condition on T_0 at the surface simply prescribes the surface temperatures as a linear function of x. In the Equatorial Pacific $\bar{T} \approx 5\,°\mathrm{C}$ and $c\bar{T}$, the temperature at the eastern edge ($x = 0$) of the ocean is abour 23°. Therefore $C = 4{\cdot}6$.

Substituting (20) into (10), one has

$$u_0 T_{01} + W \frac{\partial T_{00}}{\partial z} = A \frac{\partial^2 T_{00}}{\partial z^2} \tag{21}$$

$$W \frac{\partial T_{01}}{\partial z} = A \frac{\partial^2 T_{01}}{\partial z^2} \tag{22}$$

Equation (12) becomes (since $\frac{\partial u_0}{\partial x} = 0$)

$$W \frac{\partial u_0}{\partial z} = -\frac{1}{\rho} \frac{\partial p_0}{\partial x} + A \frac{\partial^2 u_0}{\partial z^2} \tag{23}$$

Integrating (22) and applying the condition that $T_{01} \to 0$ as $z \to -\infty$ gives

$$T_{01} = -\frac{\bar{T}}{L} e^{\frac{W}{A}z} \tag{24}$$

where $-L \leqslant x \leqslant 0$ and $\bar{T}$ is the total amplitude of the east west temperature variation ($\approx 5°$ at the equator in the Pacific).

From (11)

$$\frac{p_{01}}{\rho} = -\frac{g\alpha\bar{T}A}{LW} e^{\frac{W}{A}z} \tag{25}$$

where we have taken $p_{01} \to 0$ as $z \to -\infty$.

Substitution (25) into (23), we have as a solution for u_0,

$$u_0 = \frac{\tau}{w}\left[1 + \frac{g\alpha\bar{T}}{L\tau}\frac{A^2}{W^2}\left(1 - \frac{W}{A}z\right)\right] e^{\frac{W}{A}z} \tag{26}$$

where the conditions

$$A\frac{\partial u_0}{\partial z}\bigg|_{z=0} = \tau = \text{constant}, \qquad u_0\bigg|_{z=-\infty} = 0$$

have been used. In the Pacific $\tau \approx -0{\cdot}2$ cm²/sec near the equator. The quantities u_0 and T_{01} can be substituted into (21) to yield T_{00} which is

$$T_{00} = 4\bar{T}e^{\frac{W}{A}z} + \frac{\tau\bar{T}A}{2LW^2}\left\{\left(1 + \frac{5}{2}\frac{g\alpha\bar{T}}{\tau L}\frac{A^2}{W^2}\right)\left(e^{\frac{W}{A}z} - e^{2\frac{W}{A}z}\right) + \frac{g\alpha T}{\tau L}\frac{A}{W} z\, e^{2\frac{W}{A}z}\right\} \tag{27}$$

In (27) the condition $T_0 = 4{\cdot}6\,\bar{T}$ at $z = o$, $x = o$ has been satisfied. This condition merely states that the surface temperature at the eastern edge of the basin is 23 °C. Equations (24) and (27) which together give the temperature at the equator satisfy the condition that the surface temperature at the equator varies between 23° at the eastern edge and 28° at the western edge.

From (14) and (16)

$$g\alpha T_2 = -\frac{\beta}{2}\frac{\partial u_0}{\partial z}$$

or

$$T_2 = \frac{\beta\bar{T}}{2LW}\left(-\frac{\tau LW}{g\alpha\bar{T}A} + z\right) e^{\frac{W}{A}z} \tag{28}$$

The second order temperature, T_2, is automatically prescribed everywhere and one cannot satisfy any boundary conditions for T_2. We shall propose therefore to investigate the surface values of T_2 in the final solution and if the values deviate very much from the observed boundary values, the present method of solution must be discarded. We shall see, however, that fairly reasonable results are deduced from (28).

To proceed one must solve equations (15) and (17) for u_2 and v_1 with $\frac{\partial p_2}{\partial x} = 0$, $\frac{\partial T_2}{\partial x} = 0$, $\frac{\partial u_2}{\partial x} = 0$, $\frac{\partial u_0}{\partial x} = 0$. The second of these is non-linear and no general solution to the system has been found. Approximate solutions can be found in the following way:

Replace $2T_2$ by an average value $\theta =$ const. and $2U_2$ by an average value $s =$ const. Furthermore $u_2 \dfrac{\partial T_0}{\partial x}$ will be taken into account by an iteration procedure, i.e., first one solves

$$\vartheta v_1 = A\frac{\partial^2 T_2}{\partial x^2} - W\frac{\partial T_2}{\partial x} \tag{29}$$

for v_1, then

$$(S - \beta)\, v_1 = A\frac{\partial^2 u_2}{\partial z^2} - W\frac{\partial u_2}{\partial z} \tag{30}$$

for u_2. One can then substitute the u_2 solution into the term $u_2 \dfrac{\partial T_0}{\partial x}$ of (15), solve for a corrected v_1 which can replace the old v_1 in (17) to correct u_2 etc.

The first step in this procedure gives

$$v_1 = \frac{\beta\bar{T}}{2L\vartheta}\, e^{\frac{W}{A}z} \tag{31}$$

and

$$u_2 = -\frac{(s-\beta)\,\beta\bar{T}}{2L\vartheta W}\left(\frac{A}{W} - z\right) e^{\frac{W}{A}z} \tag{32}$$

where $\dfrac{\partial u_2}{\partial z} = 0$ at $z = 0$.

Rather than proceed with the iteration procedure we can return to (13) to solve for w_0 using (31) for the value of v_1. This yields

$$w_0 = \frac{\beta\bar{T}A}{2L\vartheta W}\left(1 - e^{\frac{W}{A}z}\right) \tag{33}$$

where $w_0 = 0$ at $z = 0$.

If one now returns to the definition of W one can deduce W from (33). Integrating (33) from a depth $z = -\dfrac{cA}{W}$ (where c is some constant) to $z = 0$, one has

$$W^2 = \frac{\beta T}{2L\vartheta C}\left[c - (1 - e^{-c})\right] \tag{34}$$

Similarly integrating T_2 in (28) from $-\dfrac{cA}{W}$ to 0,

$$\vartheta = -\frac{\beta\tau}{g\alpha Ac}(1 - e^{-c}) - \frac{\beta\bar{T}A}{LcW^2}\left[1 - (1 + c)\, e^{-c}\right] \tag{35}$$

Solving (34) and (35) jointly yields

$$\frac{W^2}{A^2} = -\frac{g\alpha\bar{T}}{2L\tau}\,\frac{\left[c + 1 - (1 + \alpha c)\, e^{-c}\right]}{1 - e^{-c}} \tag{36}$$

$$\vartheta = -\frac{\beta\tau}{g\alpha A}\,\frac{(1 - e^{-c})(c - 1 + e^{-c})}{c\left[c + 1 - (1 + 2c)\, e^{-c}\right]} \tag{37}$$

From (36) and (37) one can immediately see the qualitative dependence of θ and W/A (the reciprocal of the scale depth) on the given parameters of the problem. It is interesting to note first that A/W is independent of all internal parameters of the problem. Specifically, the scale depth does not depend on the internal mixing parameter, A. The remaining parameters g, α, $\overline{T}$, L, τ are all well defined (τ may be difficult to deduce quantitatively in practice but the only pertinent point is that it has a single value).

Before proceeding further I should like to mention a simple, qualitative argument proposed by L. N. Howard by which one can deduce the same parametric dependence for the scale depth. Consider a bounded non-rotating basin where the average temperature above a scale depth, h, varies from $T + \Delta T$ at the western edge to T at the eastern edge. If the horizontal pressure gradient vanishes at the depth, h, the level $h + \Delta h$, of the surface at the warmer end will be higher than that at the cooler end. The pressure at the depth $h + \Delta h$ in the warmer region is $(h + \Delta h)\ (\rho_0 - \Delta\rho)g$ where $\rho_0 - \Delta\rho$ is the average density of the water there. In the cooler region the corresponding pressure is $\rho_0\, gh$. Since the horizontal pressure gradient vanishes $\rho_0 gh = (h + \Delta h)\ (\rho_0 - \Delta\rho)\, g$. Hence, to first order in $\Delta\rho$ and Δh, $\rho_0\Delta h = h\Delta\rho$. At depths less than h the change in pressure along a horizontal surface is of order $\Delta p = \rho_0 g\Delta h = gh\Delta\rho = gh\rho_0\alpha\Delta T$ where we have used the relation $\Delta\rho = \rho_0\alpha\Delta T$. Thus

$$\frac{\partial p}{\partial x} = -\, gh\rho_0\, \alpha\, \frac{\Delta T}{L}$$

where $\Delta T/L$ approximates the horizontal temperature gradient $\partial T/\partial x$. If the horizontal pressure gradient is approximately balanced by the vertical mixing, we have

$$\frac{\partial p}{\partial x} = -\, gh\rho_0\, \alpha\, \frac{\Delta T}{L} \sim \rho_0\, A\, \frac{\partial^2 u}{\partial z^2}$$

Integrating from $z = h$ to $z = 0$, we get

$$-\, gh\alpha\, \frac{\Delta T}{L}\, h \sim A\, \left.\frac{\partial u}{\partial z}\right|_{z=0} = \tau$$

where we assume $\dfrac{\partial u}{\partial z} = 0$ at $z = -\, h$. Thus

$$h^2 \sim \frac{-\,\tau}{g\alpha\Delta T/L} = \frac{-\,\tau L}{g\alpha\Delta T}\Bigg]$$

Returning to (36) we chose c so that the integration ranges over the depth of interest, viz., about 2 scale depths. The qualitative results are unaffected by the explicit value of c but the quantitative results are. Quite arbitrarily therefore we choose $c = 1{\cdot}5$ which gives the surface value $u_0 = -\ 16$ cm/sec. Other choices for c yield quite different surface values for u_0.

However, the scale depth A/W which has the value 125 m for $c = 1{\cdot}5$ changes only by 20 per cent when c is halved or doubled. The $u_0 vs.z$ profile is also qualitatively unchanged by changes in c.

The results presented thus far are discussed in the introduction and summary. We shall now discuss the possibility of refining these results by taking into account higher order terms and by extending the iteration procedure discussed in the paragraphs following equation (28).

In the first place it should be noted that T_2 as given by (28) goes through zero at the depth $z_0 = \dfrac{\tau LW}{g\alpha\overline{T}A}$. Hence, the approximation introduced by taking the average

θ = const. for $2T_2$ is not generally a good one. (Since the positive part of T_2 is of greater amplitude than the negative part, the approximation may be acceptable for the region $z > z_0$). It can be seen that by this procedure v_1 must always be positive, a fact which is clearly at odds with both observation and the physics of the model. Furthermore, since u_2 is determined from v_1, it is also of one sign. Therefore, the procedure leads to inconsistent information regarding the higher order velocities.

One cannot alter the qualitative results by the iteration procedure proposed to provide higher order corrections to v_1 and u_2. The only appropriate procedure is to solve the non-linear system consisting of equations (15) and (17) for v_1 and u_2. This I have not been able to do. However, it should be noted that the analysis leading to the expressions for p_0, T_0, u_0, T_2, p_2 is independent of the subsequent procedure. The only necessary information which requires a knowledge of the quantities v_1 and v_2 is the parametric dependence of A/W, an evaluation which does not depend on the *form* of u_2 and v_1. Furthermore, since one can derive the same parametric dependence by means of Howard's argument there is some justification for keeping the limited results obtainable from this model.

The calculation for the temperature $T_0 + y^2T_2$ at the surface shows that the temperature increases by 0·4° at a distance of 50 km north or south of the equator. (This distance represents the limit of validity of the second-order solution. Higher order terms must be taken into account for larger values of y). This value of the temperature increase is approximately twice the observed value.

* *Contribution No.* 1082 *from the Woods Hole Oceanographic Institution. The research reported in this paper was conducted under the auspices of the Office of Naval Research.*

REFERENCES

Carrier G. F. (to be published).
Cromwell T., Montgomery R. B. and Stroup E. D. (1954) Equatorial Undercurrent in Pacific Ocean Revealed by New Methods. *Science* **119**, 648-649.
Fofonoff N. and Montgomery R. B. (1955) The Equatorial Undercurrent in the Light of the Vorticity Equation, *Tellus*, **7** No 4, 518-521.
Knauss J. A. (1960) Measurements of the Cromwell Current. *Deep-Sea Res.* **6**, 265-286.
Long R. (to be published).
Robinson A. R. (1960) The General Thermal Circulation in Equatorial Regions. *Deep-Sea Res.* **6**, 297-303.
Robinson A. R. and Stommel H. (1959) The Oceanic Thermocline and the Associated Thermocline Circulation, *Tellus*, **11** No. 4, (in press).
Stommel H. (1960) Wind-drift near the Equator. *Deep-Sea Res.* **6**, 304-308.

Printed in Great Britain by The Salisbury Press Ltd., Publicity House Wilton Road, Salisbury, Wilts. (22848)

Contribution No. 1083

COLD CLOUDS OVER TROPICAL OCEANS*

RAYMOND WEXLER
Allied Research Associates, Inc., Boston, Massachusetts

and **RUTH WEXLER**†
Woods Hole Oceanographic Institution

INTRODUCTION

Observations in clear air over the tropical oceans showed fluctuations in temperature and humidity which indicate the existence of areas warm or cold with respect to the environment (Langwell[1]). In general, the warm areas coincided with low humidity, indicating subsidence, while the cold areas coincided with high humidity, indicating lifting.‡

According to Hubert[2] the formation of a cold tropical cyclone was the result of convergence throughout a deep layer of the troposphere beneath a region of subsidence in the stratosphere. The middle troposphere of the cyclone subsequently warmed due to ascent of air initially near the surface but to the north of the cold low.

Mesoscale convergence, responsible for the formation of groups of cumulus clouds, was indicated by observations over the Caribbean made by the Woods Hole Oceanographic Institution with a PBY aircraft during August 1956 (Wexler and Malkus[3]). In addition, their data showed that the cold cloud is a rather frequent phenomenon and may represent a significant portion of the life history of many cumulus clouds over the ocean. In this paper the results of their observations are summarized and compared with a theoretical model, based on "bubble" experiments, which attempts to show how the temperature and moisture within a cloud may be expected to vary during its life history.

RESULTS OF AIRCRAFT OBSERVATIONS AUGUST 1956

The aircraft observations in the Caribbean on a few days during August 1956 indicated that changes in convective activity were largely controlled by mesoscale synoptic features. On 15 August 1956, with a developing wave approaching the observation area, the increased convective activity from morning to afternoon could be ascribed to widespread convergence in the lower troposphere which, according to computations by Riehl and Malkus, was of the order of 10^{-5} sec^{-1}. During this period the moist layer below cloud actually became drier while conditional instability increased above cloud base. On 25 August the air was extremely moist and conditionally unstable up to 800 mb; nevertheless with no essential change in the sounding, cloud activity decreased from morning to afternoon due to the fact that a wave disturbance was receding from

---

* Contribution No. 1083 of the Woods Hole Oceanographic Institution.

† Now with Allied Research Associates, Inc.

‡ A different interpretation was made by Langwell: warm areas were considered to be thermals (despite low humidity) and cold areas residues of clouds.

the area. Hence on these days the moist layer near the surface had little to do with changes in convective activity.

Comparative temperatures also showed the effect of convergence. Temperatures in the cloudy region (in the clear spaces between clouds) were always somewhat colder than in the clear areas. Temperatures within cloud were colder than in the cloudy region. Thus convergence from clear area to cloudy area and from cloudy area to cloud was indicated. In addition most of the soundings within cloud could be derived from the soundings outside cloud by the lifting of a column of air by about 40 mb.

Flights through clouds indicated the following characteristics of most clouds:

(1) In a growing cloud maximum temperature occurred in peak updraughts which were usually associated with maximum liquid water contents.

(2) Minimum temperatures occurred along the cloud edge.

(3) In about the lower third of the cloud average virtual temperatures slightly exceeded those of the environment, but in the upper two-thirds they were less.

(4) The lapse rate within the cloud was generally much steeper than that of the environment.

(5) The temperature excess of the environment over the minimum temperature in the cloud tended to increase as the relative humidity of the environment decreased.

An analysis of four successive runs through a cloud over a twenty minute period on 7 August 1956 indicated the following:

(6) During the growing stage of the cumulus maximum updraughts increased with time, while downdraughts, although increasing, remained relatively small. At the beginning of the dissipation stage the cloud was characterized by a succession of evenly spaced updraughts and downdraughts, with the latter apparently gaining in ascendancy.

The analysis of 7 August 1956 data and the data from clouds in different stages of development on 25 August 1956 also indicated these tentative results:

(7) Maximum temperatures were lowest relative to the environment during the early stages of the cloud but increased to almost the environment temperature at the time of the maximum intensity of the updraught and continued to warm during the dissipating stage. Maximum virtual temperatures were less than those of the environment during the early stages but became equal to or exceeded them within peak updraughts at the time of maximum cloud development.

(8) Minimum temperatures appeared to be lowest at the time of maximum intensity of the updraught.

It is to be emphasized that cloud development is frequently a pulsating process so that some of the characteristics associated with different stages of development do not necessarily occur in sequence.

CLOUD DEVELOPMENT MODEL

It was originally shown by Stommel that the entrainment of dry air from the surroundings into a cloud leads to a steeper lapse rate within the cloud. The role of the dry air is to cause ascent of the thermals at a lapse rate between the dry and the wet adiabats. Therefore, the greater the percentage of dry air entrained into the thermals the colder will be the rising air, and the smaller the liquid water content of the cloud.

A more realistic model is indicated by the experiments of Woodward[4] who showed that the increase in volume of a thermal came 60 per cent from the fluid ahead (although entry was made from the rear) and 40 per cent from the sides. The application of this experiment to the atmosphere would mean that the first thermal traversing a path in the atmosphere would serve to modify the air that is entrained into succeeding thermals traversing the same path. The moistening of the air by the first thermals would allow the cloud to penetrate successively to greater heights. Of equal importance, however, is the temperature sequence. Since the later thermals tend to entrain relatively moist air, they would ascend closer to the wet adiabat which would result in a warming trend in the cloud.

A simple application of the model was applied to the soundings of 15 and 16 August 1956, which represent two days of considerable contrast (Fig. 1). On 15 August a conditionally unstable moist layer extended to 870 mb above which there was a sharp drop in humidity and a nearly isothermal lapse rate to 800 mb. On 16 August the lapse rate was conditionally unstable to 800 mb above which it approximated the wet adiabat. The air was extremely moist; the spread between temperature and dewpoint was 1 to 2°C up to 860 mb and about 3°C at 800 mb.

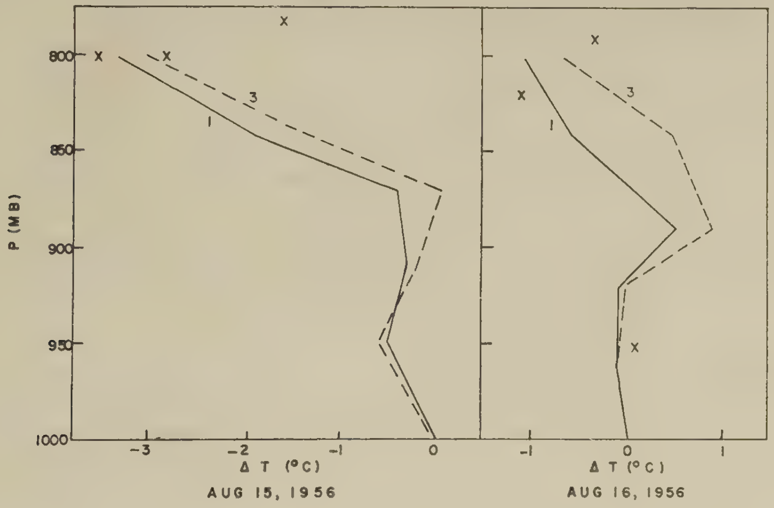

Fig. 1—Aircraft soundings of temperature and dewpoint outside clouds for 15 and 16 August 1956. The slopes of the dry (*D*) and wet (*W*) adiabats are shown.

In the procedure (using an adiabatic chart) a parcel of air at 1000 mb was allowed to rise in steps of 40 or 50 mb mixing completely with an equal parcel of air consisting of 60 per cent of the air ahead and 40 per cent of the air from the sides. For the first parcel the air ahead is identical with environment air but for succeeding thermals it is different.

The result of the analysis is shown in Fig. 2 which shows the temperature in the rising thermals relative to the environment at the same level. On 15 August the temperatures within the bubbles are slightly colder than the environment near 950 mb and about equal at 870 to 900 mb. The dryness of the air above 870 mb results in sharply colder temperatures above that level by about 3 to 3.5°C at 800 mb. For 16 August, with a comparatively moist sounding, the minimum temperature near 800 mb is only about 1°C below environment. Near 880 mb temperatures are warmer than the environment by almost 1°C. A warming trend at upper levels between bubbles *1* and *3* is indicated on both days but it is most pronounced on 15 August.

The difference between maximum temperatures observed by the aircraft within the cloud and the environment on 15 and 16 August are shown by crosses and are in excellent agreement with the computed values for the rising bubbles. The two values at 800 mb on 15 August were observed on the same run through two different updraughts. The minimum temperatures (not shown) observed near 800 mb were about 5°C lower than environment temperature on 15 August as compared to less than 2°C lower on 16 August.

It is possible to compute liquid water contents of the cloud in the analysis, but the computations are more intricate and the results are not presented here. The computed liquid water contents tend to increase with height and with time.

After about the fourth bubble there is little change in temperature or moisture due to the fact that the continued entrainment of dry air from the surroundings limits the amount of warming and the liquid water content of the cloud. Further warming and an increase in the liquid water content could occur in an enlarged cloud in which the air entrained into the bubble from the environment is saturated.

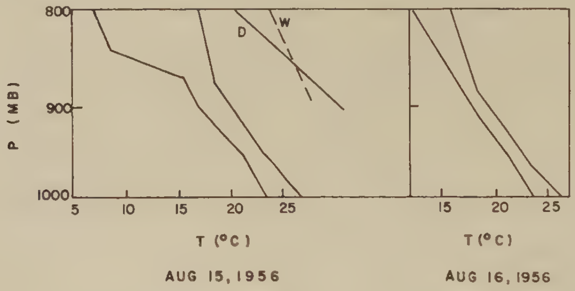

Fig. 2—Computed cloud temperatures relative to the environment after passage of successive thermals which entrain air from ahead and from sides. The environment conditions are shown in Fig. 1. The crosses give the temperature differences between cloud and environment observed by aircraft. Negative values indicate relatively cold cloud.

The above results are not dependent on a bubble theory or the application of Woodward's experiment to the atmosphere. If entrainment is a process in the rising air within the cumulus, whether it is in the form of bubbles, plumes or draughts, then if the environment air is relatively dry, the lifting of this air will result in relatively cold cloud temperatures in the early stages of the cumulus followed by a warming trend as the entrained air is moistened.

CONCLUDING DISCUSSION

The formation of clear areas and cloudy areas over the tropical oceans depends essentially on macroscale or mesoscale synoptic features, which determine regions of convergence in the lower troposphere. The result is the formation of relatively cold cloudy regions due to lifting, and to warm clear areas due to subsidence.

The location of the individual cumulus clouds in the cloudy area probably is a chance phenomenon dependent on small perturbations in the wind field. The lifting which causes the formation of the cloud also initiates the cold temperatures aloft due to the dry adiabatic ascent of air in a stable environment. Once formed the cloud becomes a favored place for the generation or the entry of thermals which may be formed in the cloudy region by the field of convergence. The thermals have excess buoyancy in the lower portion of the cloud and their rise is facilitated by the steepened lapse rate above.

Because of the entrainment of dry air, the rise of air in cumulus may be initially closer to the dry adiabat than to the wet adiabat, thereby causing further cooling. Subsequent thermals may be warm with respect to the cloud but cold with respect to clear air outside. In fact, the maintenance of a cold sink above the warm source near cloud base thermodynamically favors continued cloud growth. Hence the existence of cold temperatures (outside the thermals) in the upper portion of the cloud is indicative of the growing stage of a cumulus and not of a dissipation stage.

The continued flow of thermals causes an increase in the liquid water of the cloud and may also cause a warming trend due to the entrainment of moister air from ahead and from the sides of an enlarged cloud, thereby causing an ascent closer to the wet adiabat. If the warming occurs primarily at upper levels the increased stability may actually be a factor in the dissipation of many clouds. However, under favorable conditions, which probably includes the existence of a mesoscale divergent region aloft, the cloud may survive this period of increased stability and eventually transform into a warm cloud in which positive buoyancy over a deep layer is responsible for continued cloud growth to thunderstorm proportions. The process is believed to be similar to the transformation of a cold tropical cyclone to a warm hurricane.

The question arises as to the origin of the energy which causes the rising air to be colder than the environment. This energy comes from two sources: first the channeling of the convergent mechanism into the individual cumulus clouds, and second, the inertia of the motion due to the positive buoyancy in the lower portion of the cloud. The question is also asked: if the cloudy air is colder than the environment why does it not sink? Sinking motion probably does take place and would cause the cloud to dissipate if no new thermals replenished the supply of moisture. The sinking motion is at first in the form of gentle downdraughts, which are small compared to the updraughts, but which may increase with time.

Since the temperature of the upper portion of the cloud was generally intermediate between the environment temperature and dewpoint, cooling by evaporation from the cloud sides would be counteracted by mixing with the warmer environment air. The temperature minimum which was generally observed in downdraughts along cloud edge cannot therefore be explained entirely by evaporation. This air had probably been lifted with the thermals partially along the dry adiabat and acquired sufficient liquid water to descend in downdraughts along the wet adiabat. The original ascent of this air was probably greater than its later descent. Cumulus clouds are seldom homogeneous and pockets of unsaturated air are frequently encountered. The origin of this dry air is undoubtedly environment air dragged up with the thermals, thus accounting for their cold temperature.

The cumulus cloud with cold temperatures aloft and warm temperatures below represents the release of convective instability in the atmosphere. A spectacular example of such release was given by Cunningham in this conference, who observed the upper half of a cloud, with temperatures considerably colder than the environment, extending through the trade wind inversion.

REFERENCES

1. P. A. LANGWELL. Inhomogeneities of turbulence, temperature and moisture in the West Indies trade-wind region. *J. Met.*, **5,** 243–246 (1945).
2. L. F. HUBERT. A case study of hurricane formation. *J. Met.*, **12,** 486–492 (1955).
3. R. L. WEXLER and J. S. MALKUS. Observational Studies of Tropical Clouds : Results of 1956 Caribbean Aircraft Expedition Woods Hole Ocean. Inst. (Unpublished manuscript) Ref. No. 58–46, 122 pp. (1958).
4. B. WOODWARD. The motion in and around isolated thermals. *Quart. J. Roy. Met. Soc.*, **85,** 144–151 (1959).

Contribution No. 1084

Deep-Sea Research, 1960, Vol. 6, pp. 298 to 302. Pergamon Press Ltd., London. Printed in Great Britain

Wind-drift near the Equator

HENRY STOMMEL

(*Received* 20 *July* 1959)

Abstract—The principal result of the model is to show that a linear theory constructed from Ekman spiral and geostrophic current does not suffer singularities at the equator and even exhibits some qualitative similarity to the Equatorial Undercurrent, but that in order to account for the observed amplitude of the phenomenon, non-linearities are not altogether negligible.

(1) INTRODUCTION

IN EKMAN's well-known solution of drift of water in a rotating homogeneous ocean of infinite depth when acted upon by a steady stress applied at the surface, the depth of the spiral, and amplitude of the currents increase without limit as the vertical component of rotation (or latitude) approaches zero. It is possible to add an arbitrary infinitesimal deformation of the free surface to Ekman's homogeneous model and an associated pattern of geostrophic flow – independent of depth – whose Coriolis force just balances the arbitrary pressure gradient. In fact, Ekman uses such additional geostrophic velocities to satisfy conditions of no flow through coastal barriers. The one-dimensional nature of the simplified equations used by Ekman does not permit satisfying the true boundary condition at a vertical coastal barrier : namely, that the velocity normal to the barrier shall vanish at all depths. Instead of trying to solve the details of this more complicated problem, which evidently would involve a higher-order set of dynamical equations, Ekman simply adds a pressure field sufficient to cause the total vertically integrated component of velocity normal to the coast to vanish. When the ocean is of finite depth, a finite geostrophic current is required, and when the bottom is rigid it is necessary to allow for a second frictional boundary layer, or current spiral at the bottom. This latter complication can be avoided by asserting that the bottom boundary condition is one of no stress – such as can be achieved by letting the viscosity become very small near the bottom.

In these ways Ekman is able to avoid the indeterminacy of additive geostrophic motion in his simple one-dimensional (vertical) dynamical system, to make an approximate allowance for the influence of lateral boundaries, and also to compute patterns of flow in homogeneous ocean models under various distributions of wind and coasts.

The purpose of the present paper is to show that this simple type of analysis can be extended across the equator, and that there is indeed no singularity at the equator. Thus, in principle, there is no reason to suppose that Ekman's solution ' blows up ' at the equator, as is sometimes asserted in qualitative discussions. However, it will be shown that the model is consistent only when the amplitude of the velocity is kept at an unrealistically low value by imposing a very small value of wind stress, or a large eddy viscosity. When realistic values are introduced and the solution for the velocity field is used to compute the magnitude of the neglected inertia terms it is found that they are not truly negligible and that the model presented here becomes inconsistent. Therefore it seems that the model does not apply as it stands to the Pacific Equatorial Undercurrent (Cromwell Current). From a pedagogical point of view however the model may be of some value because it exhibits qualitative features similar to the Cromwell Current, because in an ocean where mean wind stress along the equator is less (Indian Ocean) it might actually apply, and because it embraces the very simplest linear type of dynamical scheme which one is bound to investigate before pursuing more complex models including lateral friction, inertial terms, etc.

At one time Dr. VERONIS and I considered introducing the heat-transport equation in a linearized form such as used by LINEYKIN (1955, 1957) and STOMMEL and VERONIS (1957) and developing the temperature, pressure and velocity fields about the equator in a power series in latitude (y), but such an analysis is also inapplicable to the actual Cromwell Current because of the neglect of inertial terms, and we decided that it did not reveal enough additional information to publish. In this same issue Dr. CHARNEY shows how the inertial terms can be included in the simple homogeneous model, and in the paper after that Dr. VERONIS shows how the thermal field can also be included.

(2) THE SOLUTION OF THE LINEAR PROBLEM

The model consists of a homogeneous layer of water of uniform depth h straddling the equator. Acting upon the upper surface there is a westward wind stress τ. It does not appear likely that a current like the Cromwell Current is caused by a detailed structure of the wind stress as a function of latitude, so the wind stress is assumed to be uniform. The x-axis is direct toward the east, the y-axis northward, the z-axis upward and $z = 0$ at the bottom of the layer. The eddy viscosity is a constant A.

The linearized equations of motion, in which latitude enters only parametrically through the vertical component of the earth's angular velocity ω are of the form :

$$-2\omega v = A\frac{\partial^2 u}{\partial z^2} - \frac{1}{\rho}\frac{\partial p}{\partial x}$$

$$2\omega u = A\frac{\partial^2 v}{\partial z^2} - \frac{1}{\rho}\frac{\partial p}{\partial y}$$

where p is pressure, ρ density, and u, v the x and y components of velocity. We assume the water to be homogeneous in density so that $\partial p/\partial x$ and $\partial p/\partial y$ are independent of depth. The solutions are of the form

$$u + iv = \sum_1^4 c_i e^{\alpha_i z} + G_1 + i\,G_2$$

where

$$\alpha_1 = r(1 + i), \quad \alpha_2 = r(1 - i), \quad \alpha_3 = r(-1 + i), \quad \alpha_4 = r(-1 - i)$$

$$r = \sqrt{\omega/A}$$

G_1 and G_2 are real constants. We take $z = 0$ at the bottom where we assume $A\frac{\partial u}{\partial z} = A\frac{\partial v}{\partial z} = 0$. Making the bottom a plane of no stress has the virtue of avoiding the necessity of calculating an additional functional layer at the bottom, thus simplifying the analysis.

At the top surface, $z = h$, the stress τ is taken to be only in the x-direction. These boundary conditions are enough to fix the four constants c_i. The additive constants G_1, G_2 corresponding to geostrophic flow, are evaluated by taking the vertically integrated transports equal to zero. This might at first seem to be a very arbitrary step. It can be perhaps justified by stating first that since we will eventually allow ω to vary parametrically ($\omega = \beta y$) the well-known 'curl' equation

$$\beta \int_0^h v dz = \text{curl}\,(\tau/\rho)$$

hence, since curl $(\tau/\rho) = 0$, the vertical integral of v must also vanish everywhere. The continuity equation

$$\frac{\partial}{\partial x}\int_0^h u dz + \frac{\partial}{\partial y}\int_0^h v dz = 0$$

reduces to the form

$$\frac{\partial}{\partial x}\int_0^h u dz = 0$$

If, therefore, $\int_0^h u dz$ is set equal to zero at an eastern meridional boundary it also must vanish everywhere. The solution of the problem can now be written in the form :

$$u + iv = \frac{\tau}{\mu\alpha_1\rho}\left(\frac{\cosh \alpha_1 z}{\sinh \alpha_1 h} - \frac{1}{\alpha_1 h}\right)$$

In order to evaluate the velocity components u and v as functions of z and ω it is necessary to separate real and imaginary parts of the right hand side. Writing $Z = rz$ and $H = rh$ we obtain the following expressions :

$$\begin{aligned}\frac{u}{\left(\dfrac{\tau h}{2A\rho}\right)} = \frac{1}{H(\sinh^2 H + \sin^2 H)}\{&\cosh Z \cos Z \sinh H \cos H \\ &+ \sinh Z \sin Z \cosh H \sin H \\ &+ \sinh Z \sin Z \sinh H \cos H \\ &- \cosh Z \cos Z \cosh H \sin H\}\end{aligned}$$

$$\begin{aligned}\frac{v}{\left(\dfrac{\tau h}{2A\rho}\right)} = \frac{1}{H^2} + \frac{1}{H(\sinh^2 H + \sin^2 H)}\{&\sinh Z \sin Z \sinh H \cos H \\ &- \cosh Z \cos Z \cosh H \sin H \\ &- \cosh Z \cos Z \sinh H \cos H \\ &- \sinh Z \sin Z \cosh H \sin H\}\end{aligned}$$

We can regard the H as containing the essential parametric variation of the quantities with latitude. The following table gives some computed values

			H			
			0	$\pi/2$	π	$\to \infty$
z/h	1·0	$\frac{2A\rho}{\tau h}\cdot u$	0·666	0·584	0·285	$1/H$
		$\frac{2A\rho}{\tau h}\cdot v$	0·000	$-$ 0·180	$-$ 0·186	$-$ $1/H$
	0·5	$\frac{2A\rho}{\tau h}\cdot u$	$-$ 0·083	$-$ 0·081	$-$ 0·063	0
		$\frac{2A\rho}{\tau h}\cdot v$	0·000	0·013	0·038	$1/H^2$
	0·0	$\frac{2A\rho}{\tau h}\cdot u$	$-$ 0·333	$-$ 0·254	$-$ 0·027	0
		$\frac{2A\rho}{\tau h}\cdot v$	0·000	0·151	0·128	$1/H^2$

At $H = 0$, which corresponds to the equator, the expressions can be reduced to the following form,

$$u + iv = \frac{\tau h}{2A\rho}\left(\frac{z^2}{h^2} - \frac{1}{3}\right) + i\,0$$

a simple parabolic velocity profile, with no north-south component. The case $H \to \infty$ corresponds to the combination of a thin surface Ekman layer underlain by an equatorward meridional geostrophic component. The figure shows the velocity vectors on either side of the equator. Quantitatively, the mean stress τ at the equator is about $-$ 0·2 dynes cm^{-2} in the Pacific, and the layer depth (core of undercurrent) is $h = 10^4$ cm. The observed amplitude of the undercurrent at $H = 0$ and $z/h = 0$, is about 150 cm sec^{-1}, so that eddy viscosity A is 2·2 $\text{cm}^2\ \text{sec}^{-1}$. According to the model the undercurrent vanishes at a latitude where $H = \pi$, so that using these values the northern border of the undercurrent is at a latitude corresponding to $\omega = A \times 10^{-7}\ \text{sec}^{-1}$, or about 0·15°N. The observed boundary is more nearly at 1·5° latitude, so this agreement is not good. If the eddy viscosity is increased to 22·0 $\text{cm}^2\ \text{sec}^{-1}$, the computed northern boundary of the undercurrent agrees with that observed, but the velocities in the core of the undercurrent are reduced to 15 cm sec^{-1}, which is much too low. Therefore, it appears that this linearized model does *not* apply to the Pacific Equatorial Undercurrent. Furthermore, using the above values of the wind stress and the two choices of eddy viscosity, a calculation shows that the non-linear inertial terms are of the same order of magnitude as the other terms in the neighbourhood of the equator, and should not be neglected.

A reviewer has indicated several obscurities in the presentation which need to be cleared up. First, strictly speaking, the homogeneous layer lies upon a deeper resting layer of greater density. If there are pressure gradients in the homogeneous upper layer, but none in the lower layer, there must be a slope in the interface between them.

Therefore the upper layer cannot be of precisely uniform depth. Also it is worthwhile to emphasize that there is a local balance of pressure-gradient force on the layer and wind stress, and the uniformity of one guarantees that of the other. And finally,

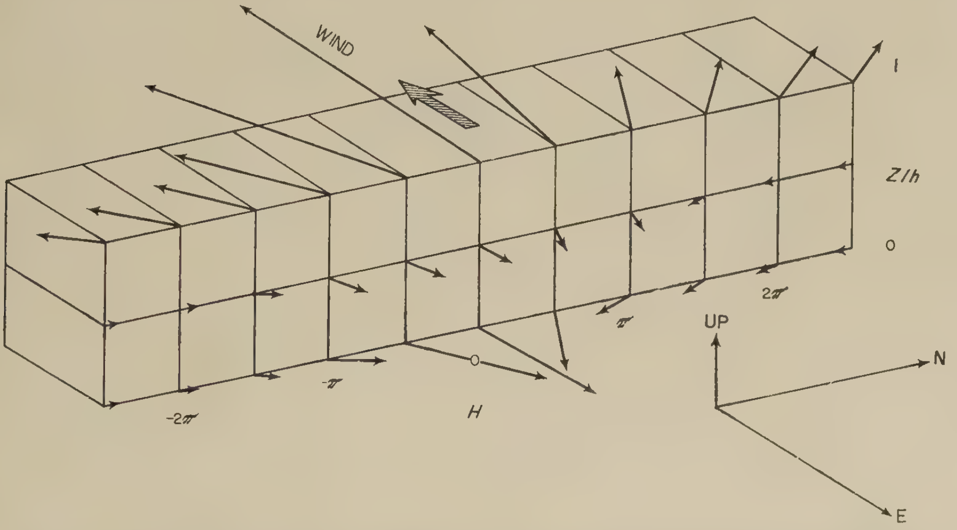

FIG. 1. Schematic three-dimensional diagram of the combined frictional and geostrophic flow field in the neighbourhood of the equator, not showing the vertical component of velocity (which can in principle be determined from continuity).

the current transport field obtained in this model is very similar to that pictured by CROMWELL (1953, Fig. 6), and we might regard the present model as a mathematical analysis of Cromwell's dynamical description of the currents produced by an east wind at the equator.

Woods Hole Oceanographic Institution, Woods Hole, Mass., U.S.A.

Contribution No. 1084 *from Woods Hole Institution.*

REFERENCES

CROMWELL TOWNSEND (1953) Circulation in a meridional plane in the central equatorial Pacific. *J. Mar. Res.* **12**, 196-213.

Printed in Great Britain by The Salisbury Press Ltd., Publicity House, Wilton Road, Salisbury, Wilts. (22850)

Contribution No. 1086

Sources of Water Contributed to the Bay of Fundy by Surface Circulation[1]

By Dean F. Bumpus[2,3]

Woods Hole Oceanographic Institution
Woods Hole, Mass., U.S.A.

ABSTRACT

The returns from the 35,000 drift bottles launched in the Gulf of Maine area since 1919 have been analyzed to determine the annual cycle of surface drift. The source of surface flow into the Bay of Fundy expands from a minimum during January in the offing of the eastern side of the bay to a maximum in May which includes most of Georges Bank, the Gulf of Maine and the southwestern Scotian Shelf, then commencing in September gradually contracts toward the minimum.

Secular variations in the removal of surface water from the Bay of Fundy, indicative of changes in the Maine eddy, were noted during 1957 and 1958.

INTRODUCTION

The circulation of water into an area, through it and out of it has much to do with the distribution of fishes in the area. Pelagic fish feeding at random may be effectively transported many scores of miles, particularly where they encounter non-tidal drifts of up to 10 miles (16 km) per day with no significant change in their environment to cause them to modify their random movements. The distribution of other fishes may result from the effects of non-tidal drift during the planktonic stages of their existence. Cod and haddock eggs float in the upper few meters of water for several weeks as do the larval cod and haddock hatched from these eggs. The resulting non-tidal drift during this period may disperse and remove this stock of fish from the spawning grounds to other places. Stormy winds for extended periods may be effective modifiers of the drift and may affect the survival of a year class (Chase, 1955). Herring larvae hatch from eggs adhering to the bottom and for several months thereafter are planktonic in the superficial waters. What are the current systems relative to the spawning grounds? How do these systems change with time? More specifically, do herring larvae spawned on Georges Bank during the autumn reach the Bay of Fundy?

The area under discussion and the names of places referred to in the text are indicated in Fig. 1.

---

[1] Received for publication October 20, 1959.

[2] Contribution No. 1086 from the Woods Hole Oceanographic Institution. This research was sponsored by the U.S. Fish and Wildlife Service under Contract No. 14–17–008–62.

[3] International Passamaquoddy Fisheries Board, 1956–1959. Scientific Report No. 11.

J. Fish. Res. Bd. Canada, 17(2), 1960.
Printed in Canada.

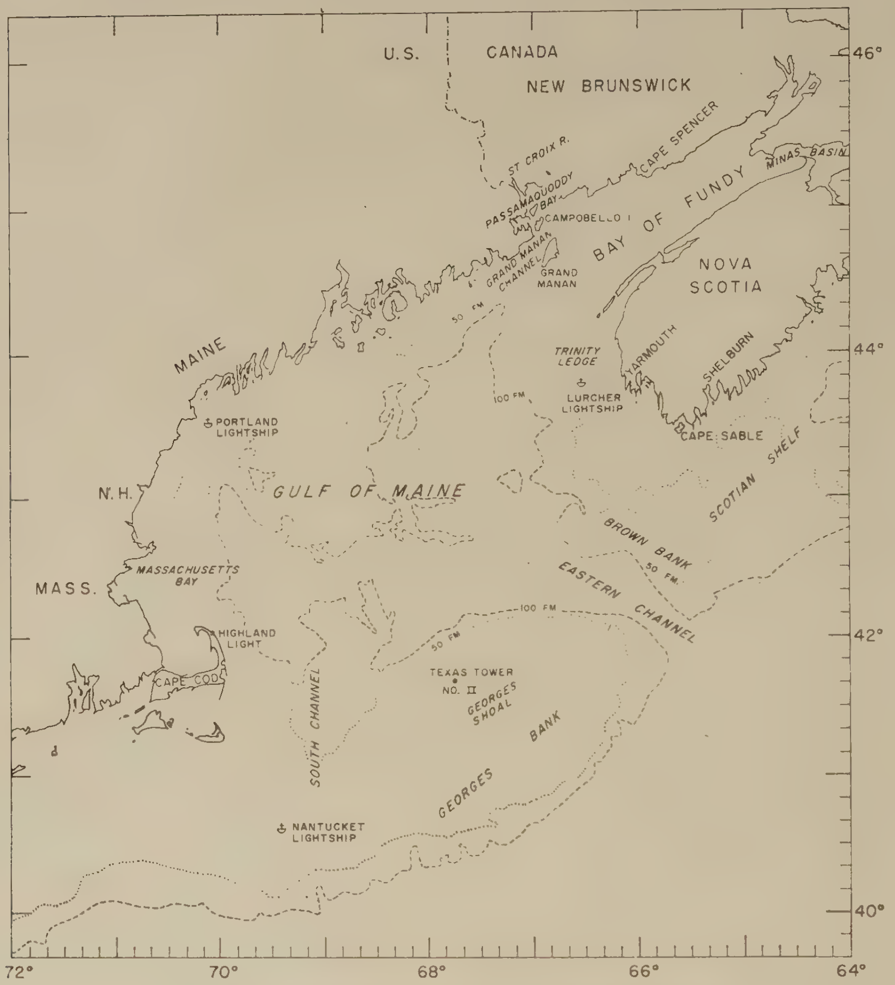
U.S.
CANADA
NEW BRUNSWICK
ST CROIX R.
PASSAMAQUODDY BAY
CAMPOBELLO I
CAPE SPENCER
BAY OF FUNDY
MINAS BASIN
GRAND MANAN CHANNEL
GRAND MANAN
NOVA SCOTIA
MAINE
50 FM
100 FM
TRINITY LEDGE
LURCHER LIGHTSHIP
YARMOUTH
SHELBURN
CAPE SABLE
SCOTIAN SHELF
PORTLAND LIGHTSHIP
N. H.
GULF OF MAINE
BROWN BANK
EASTERN CHANNEL
MASSACHUSETTS BAY
MASS.
HIGHLAND LIGHT
CAPE COD
SOUTH CHANNEL
TEXAS TOWER NO. II
GEORGES SHOAL
GEORGES BANK
NANTUCKET LIGHTSHIP
46°
44°
42°
40°
72°
70°
68°
66°
64°

FIG. 1. Orientation chart of area under discussion.

PREVIOUS INVESTIGATIONS

Much of the information presently available stems from the results of international co-operation initiated by the North American Council on Fishery Investigations in 1922 and is discussed in detail by Bigelow (1927). Investigations have continued sporadically until the autumn of 1956 when co-operation between several laboratories in the United States and Canada was resumed.

CIRCULATION IN THE BAY OF FUNDY

Mavor (1922 and 1923) examined Dawson's (1908) current-meter data and his own drift-bottle experiments (June, August and September, 1919) together with the findings of Bigelow and concluded: " . . . that there is a movement of water into the Bay of Fundy from the Gulf of Maine and the southern end of the Nova Scotia coast and along the eastern side of the Bay of Fundy." This had been surmised by Craigie and Chase (1918): "This movement is most marked at a depth of 50 meters but can be recognized from the surface to a depth of 100 meters. It extends into the Bay of Fundy on the Nova Scotian side at least 12 miles (19 km) below the Gulf of Digby. A portion of this water probably moves across the bay toward St. John Harbour." He also mentioned that there was a flow out of the bay to the east of Grand Manan and an inward movement in the Grand Manan Channel.

Returns from bottles set out by Huntsman in a line off Yarmouth, N.S., in July, August, September and October, 1926, (A.O.G., 1958) and summarized by Bigelow (1927) "demonstrate the northerly drift along western Nova Scotia into the southern side of the Bay of Fundy, and up it. The New Brunswick recoveries show the anti-clockwise movements brought out by Mavor's experiments."

Fish and Johnson (1937) set out several series of drift bottles in May and June 1932 in the northwestern part of the Gulf of Maine and in the southern part of the Bay of Fundy. They reported that numerous bottles from the northern part of the Gulf of Maine entered the Bay of Fundy. Many proceeded toward Minas Basin, others appeared to have followed the route suggested by Mavor and stranded in the Passamaquoddy Bay region or on Grand Manan. Those released in the Bay of Fundy gave similar results. There was also evidence that bottles released in the southwest portion of the bay proceeded across its mouth to the eastern side, suggesting a closed circulation at the surface at this time of the year.

Watson (1936) has described in detail the oceanographic observations made during 1932 and presents some dynamical evidence for the residual current systems mentioned above.

Hachey and Bailey (1952) report several drift-bottle experiments commenced in May 1930. They summarized their results as follows:

> "All of the drift bottles indicated a tendency of the waters to circulate the island of Grand Manan in a clockwise direction.
>
> "The movements of the bottles suggest a cyclonic circulation about the basin determined by the 50 fathoms (91 m) contour in the Bay of Fundy.
>
> "An intense movement towards the mouth of Passamaquoddy Bay is definitely illustrated, while it will be noted that the water movement along the coast of Campobello Island is outward.
>
> "An inward movement in the main waters between Grand Manan and the mainland is noted in keeping with the clockwise circulation about Grand Manan. However, the waters in contact with the coast of Maine have an outward movement."

Bumpus *et al.* (1957) launched radio drift buoys in the Trinity Ledge area off Yarmouth, in Grand Manan Channel and off Cape Spencer in the autumn of 1956. These experiments added some detail to the earlier descriptions of the circulation in the Bay of Fundy and confirmed the existence of the same general pattern for the autumn period. There were no previous drift experiments at this time of year in that region. The inflowing drift, restricted to the southeasterly side of the bay, averaged about 10 miles (16 km) per day, and the outflowing drift was restricted to the northwest side at comparable speeds. The inflowing drift was about 10 miles wide off Digby and the outflowing drift was about 6 miles (10 km) off Cape Spencer. While some of the water from the Lurcher Shoal–Trinity Ledge region may penetrate well up into the bay, perhaps even to its head, cyclonic rotations with speeds of 2 to 4 miles (3 to 6 km) per day between the two drifts may shorten the route and allow transfer of water from one side of the bay to the other. These speeds are greater than those observed by the earlier investigators using drift bottles. Mavor (1922) and Fish and Johnson (1937) have tended to restrict the routes of drift bottles reaching New Brunswick to the vicinity of the 50-fathom (91-m) curve. We believe that the transfer from the inflowing to the outflowing drift can take place all along the centre portion well up into the bay.

The residual current in the Grand Manan Channel may be variable depending on the tidal range and meteorological condition (MacGregor and McLellan, 1952).

Circulation on the Southwestern Scotian Shelf

The circulation on the Scotian Shelf appears to be complex and variable. The efforts of the Canadian Fisheries Expedition of 1914–15, Bjerkan (1919), Huntsman (1924), Bigelow (1927) and Hachey (1947) reveal how complex the circulation may be.

A southwesterly flow along the Nova Scotia coast may prevail during the spring months, fed by the icy waters and ice flows debouching from the Gulf of St. Lawrence. This water may regularly be traced to the offing of Shelburne, and in some years on into the Gulf of Maine. This drift appears to cease by June at the latest. With the retrogression of the Nova Scotian current an eddy pattern may set up with cyclonic eddies about the basins and anticyclonic eddies about the banks. Hence inflow into the northern Gulf of Maine and the Bay of Fundy during the summer appears to be, not from the Nova Scotian current, which by this time has turned offshore and eastward off Shelburne, but from across Browns Bank. The area between Cape Sable and Shelburne evidently becomes a "dead area".

Only 3 of the 800 drift bottles released by Trites and Banks (1958) during August 1954 over the Scotian Shelf reached the Bay of Fundy. The circulation deduced from the bottle returns and distribution of salinity indicated a cyclonic circulation centered northeast of Sable Island. Only a narrow filament of the southwesterly drift, close to the shore, rounded Cape Sable into the Bay of Fundy.

Circulation in the Gulf of Maine

Bigelow (1927) has documented his many years of work in the Gulf of Maine in his extensive monograph on the "Physical Oceanography of the Gulf of Maine." The dominant non-tidal circulation comprises a cyclonic circulation in the Gulf of Maine and an anticyclonic circulation around Georges Bank and other shoals with seasonal and annual variations. Redfield (1939, 1941) has examined the time variation in the concentration of the pteropod *Limacina retroversa* and the crustacean plankton throughout the Gulf of Maine together with concurrent oceanographic data. He ascribed the principal factor influencing the distribution of these population densities to the inflow of water poor in these species from over the Nova Scotian banks in winter. The inflow is compensated by the escape of water to the south and east across the end of Georges Bank. The populations are able to grow and maintain themselves in the recurrent cyclonic eddy which commences in the spring. Unfortunately Redfield's field work did not extend into the Bay of Fundy where the application of his theory would have been fruitful.

Day (1958) has examined the drift-bottle experiments conducted in the Gulf of Maine from 1931 to 1956 (Bumpus and Day, 1957) consisting of releases from late February through June.

Commencing in the autumn of 1956 drift-bottle experiments have been conducted in the Gulf of Maine on a nearly year-round basis. The results of Day's report and the still more recent experiments are summarized as follows:

Bigelow's (1927) July–August circulation pattern (Fig. 2), a relatively closed circulation and hence a highly conservative one, seems to be the climax of a seasonal evolution, possibly the result of vernal warming and river runoff and

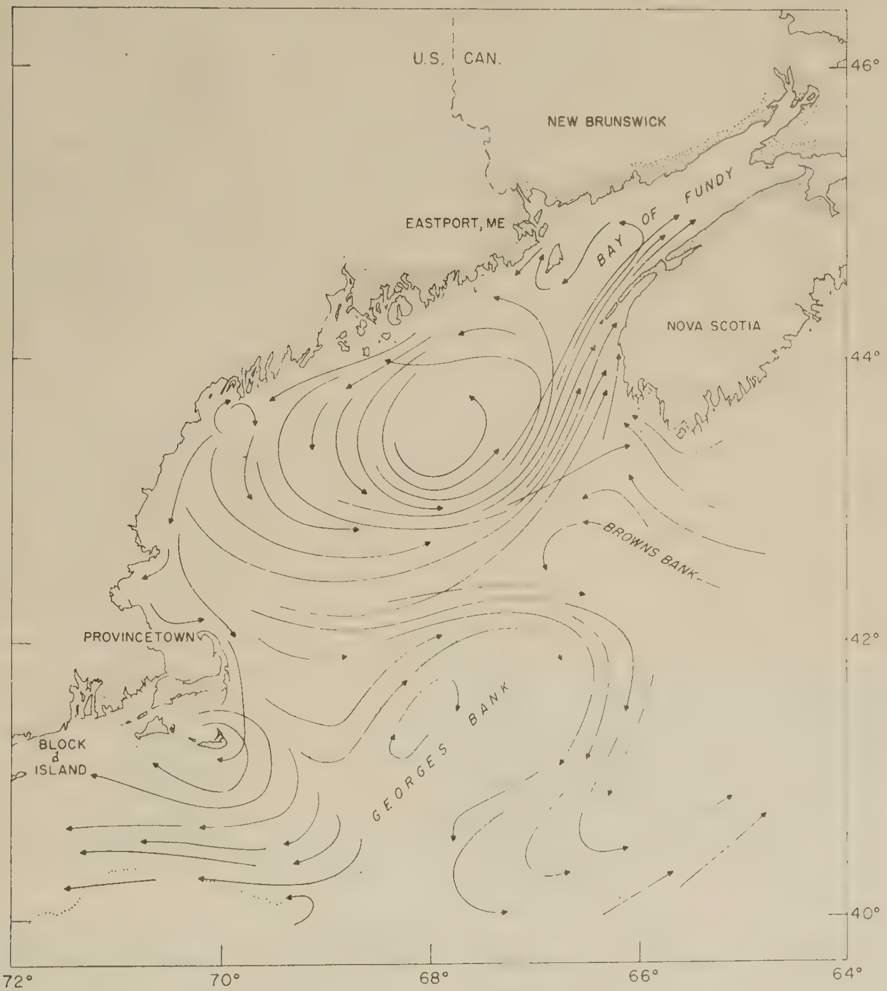
U.S.
CAN.
NEW BRUNSWICK
EASTPORT, ME
BAY OF FUNDY
NOVA SCOTIA
BROWNS BANK
PROVINCETOWN
BLOCK ISLAND
GEORGES BANK
46°
44°
42°
40°
72°
70°
68°
66°
64°

FIG. 2. Schematic representation of the dominant non-tidal circulation of the Gulf of Maine, July to August. (After Bigelow, 1927).

the consequent build-up of a dynamic structure conducive to the production of these motions.

In February and March, the Gulf of Maine eddy is ill defined on the south as water from Massachusetts Bay moves southward out South Channel. The Georges eddy is not apparent at this time, the net movement across Georges Bank being southwest. By late April, the two counter-rotating eddies are taking form with the appearance of a northeasterly movement along the northern edge of Georges Bank where the two eddies become confluent. A branch of the gulf eddy develops, penetrating into the eastern side of the Bay of Fundy. This dual eddy system continues throughout the summer. Beginning in September the Georges eddy breaks down as does the southern side of the gulf eddy. The indraft into the Bay of Fundy is limited to north of 43°, i.e. from over Eastern Channel and Browns Bank but not from Georges Bank. The western side of the gulf eddy weakens as winter sets in and the Georges eddy gives way by December to an easterly offshore drift. Just when this reverses to the southwesterly drift previously noted in February or March remains to be determined.

At any time during the year, the prevailing circulation may be modified by winds or river runoff. Offshore winds from the northwest quadrant have a pronounced effect on the Georges region tending to destroy the Georges eddy. Northeasterly winds, even of short duration, speed up the northern segment of the gulf eddy and increase the flow out South Channel. Winds from the west and southwest seem to give a strong onshore component to the waters south of Cape Cod and to accentuate the northward flow from Brown's Bank to the Bay of Fundy. A prolonged drought may weaken the western side of the gulf eddy, restricting the eddy to the northern half of the Gulf of Maine. Abundant river runoff will strengthen the western side of the gulf eddy.

COMBINED ANALYSIS OF ALL AVAILABLE DRIFT BOTTLE DATA

Over 35,000 drift bottles have been launched in the Gulf of Maine area over the 40-year period 1919 to December 1958, and more than 11% of them have been recovered. An attempt has been made to treat these data statistically. The number of bottles launched in each 30- by 30-minute rectangle of latitude and longitude by month, irrespective of year, has been recorded. Then the percentage of these bottles which reached the following shores has been determined, i.e.:

A. Southeast coast of Nova Scotia including Sable Island.
B. Eastern shore of the Bay of Fundy.
C. Western shore of the Bay of Fundy.
D. Coast of Maine, New Hampshire, and Massachusetts to Highland Light.
E. Highland Light southwestward.
F. Overseas.

The resulting tabulations have been plotted on charts (Bumpus, 1959) and the circulation deduced therefrom. The distribution of bottles released throughout the area is fairly good except for January, July, August and December. There is a paucity of data on the southwestern part of the Scotian Shelf except for south of Cape Sable.

SEASONAL PROGRESSION

For the purposes of this paper two contours have been drawn for each month (Fig. 3). One contour encloses lightly shaded areas from which bottles have moved into the Bay of Fundy, limiting the "possible" sources of water which may reach the bay through surface circulation. The heavily shaded portions delineate the areas month by month from which 5% or more of the drift

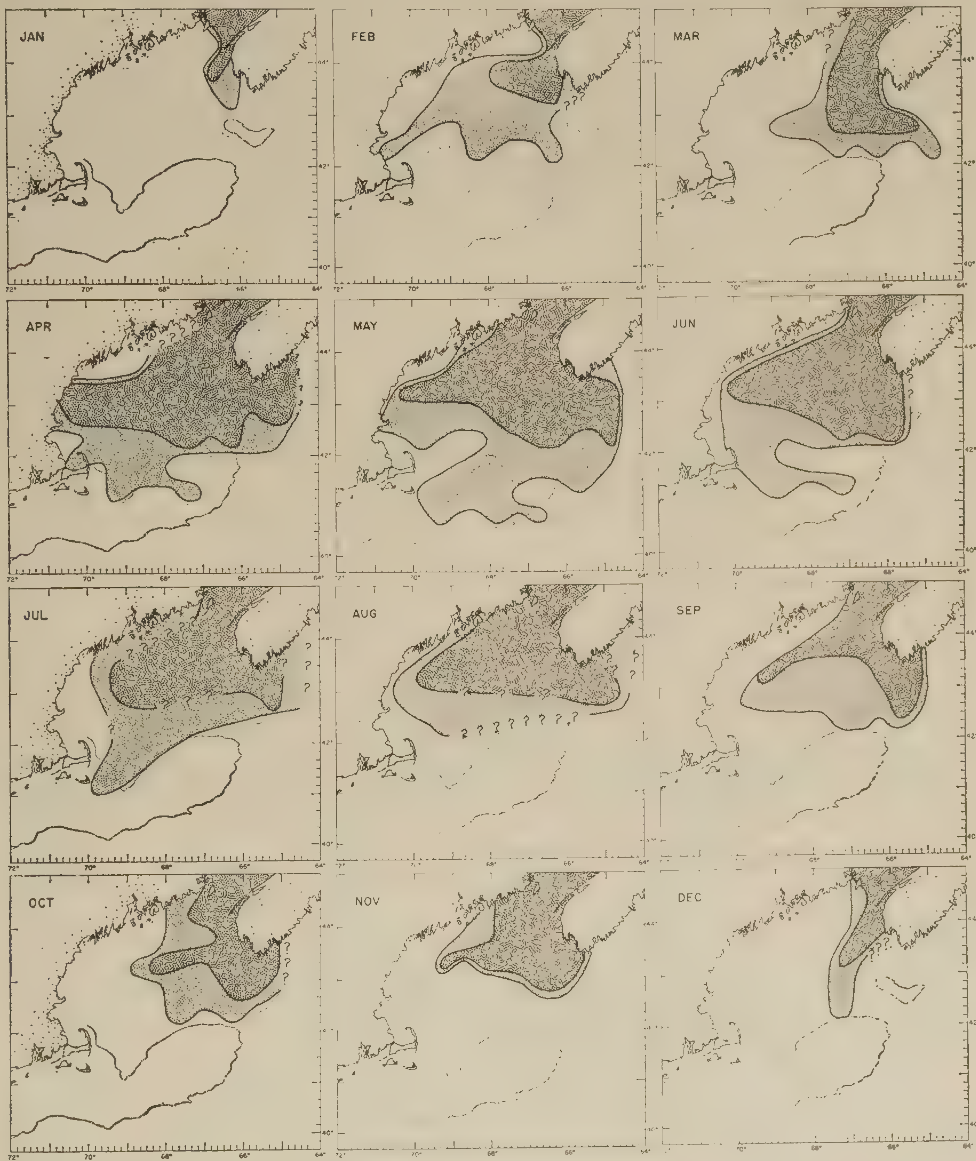
JAN
FEB
MAR
APR
MAY
JUN
JUL
AUG
SEP
OCT
NOV
DEC
72°
70°
68°
66°
64°
44°
42°
40°

FIG. 3. Sources of water contributed to the Bay of Fundy by surface circulation. See text for explanation.

bottles have consistently reached the Bay of Fundy. These charts indicate a restricted source of surface drift into the bay in January, i.e. its southeastern approaches, gradually increasing during February and March parallel with the development of the Gulf of Maine eddy to a maximum during April, May and June, and concurrent with the development of the Georges eddy. Undoubtedly the source area continues near the maximum throughout July and August, but the drift bottle data for these two months are insufficient to delineate this, as indicated by question marks. By September the eddy systems have commenced to slow down with the consequent restriction in the area of water reaching the Bay of Fundy. The area is further withdrawn from Georges Bank during the autumn and early winter to the minimum in January. Note that the eastern boundary of the source area is annotated in some instances with question marks, indicating no data. Hence the Nova Scotian herring spawning ground may be within the limits of the Fundian circulation during the early autumn.

SECULAR CHANGES

Further demonstrations of the seasonal cycle in the southern part of the Bay of Fundy together with one spectacular secular change are available from the return of drift bottles launched at *Lurcher* Lightship and from those bottles launched during 1957 and 1958 which escaped from the Passamaquoddy Bay region.

The sequence of probable drift from *Lurcher* Lightship is indicated, month by month, in Fig. 4 and 5. The flow was generally either into St. Mary's Bay or slightly to the westward past Brier Island and thence northeasterly toward the head of the Bay of Fundy.

Following their release in May, June and July some bottles drifted across to the western side of the Bay of Fundy and so into Passamaquoddy Bay, much the same as has previously been observed by Mavor (1922) and Fish and Johnson (1937). We believe this to be characteristic of the summer circulation pattern.

During November 1957, the drift appeared to be directly to the Yarmouth area.

With regard to secular changes, the majority of bottles recovered following their release in January, February and March, 1958, had drifted to Massachusetts Bay with speeds as great as 8 miles (13 km) per day. This is in distinct contrast to the results observed subsequent to releases in January and March, 1957.

Bottles have been released regularly in large numbers in Passamaquoddy Bay and approaches since January 1957. Those which escaped from the Passamaquoddy region (Fig. 6 and 7) moved for the most part across to the western shore of Nova Scotia and thence northeasterly toward Minas Basin. A few bottles worked to the westward along the coast of Maine during May and June. This circulation continued, with minor variations, until December 1957; following

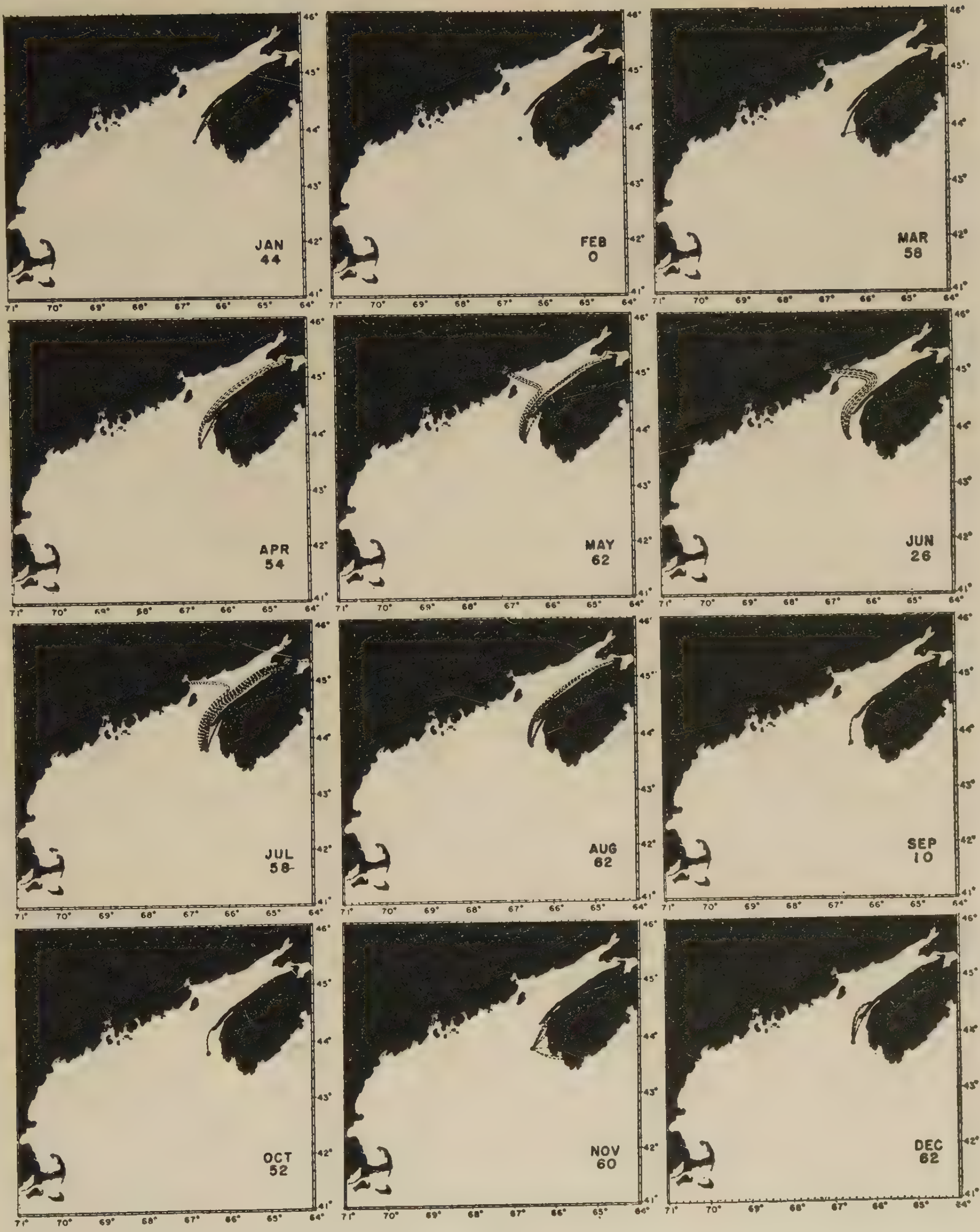
JAN
44
FEB
0
MAR
58
APR
54
MAY
62
JUN
26
JUL
58
AUG
62
SEP
10
OCT
52
NOV
60
DEC
62
71°
70°
69°
68°
67°
66°
65°
64°
46°
45°
44°
43°
42°
41°

FIG. 4. Returns of drift bottles released at *Lurcher* Lightship during 1957. Number of bottles released each month indicated in lower right of each diagram.

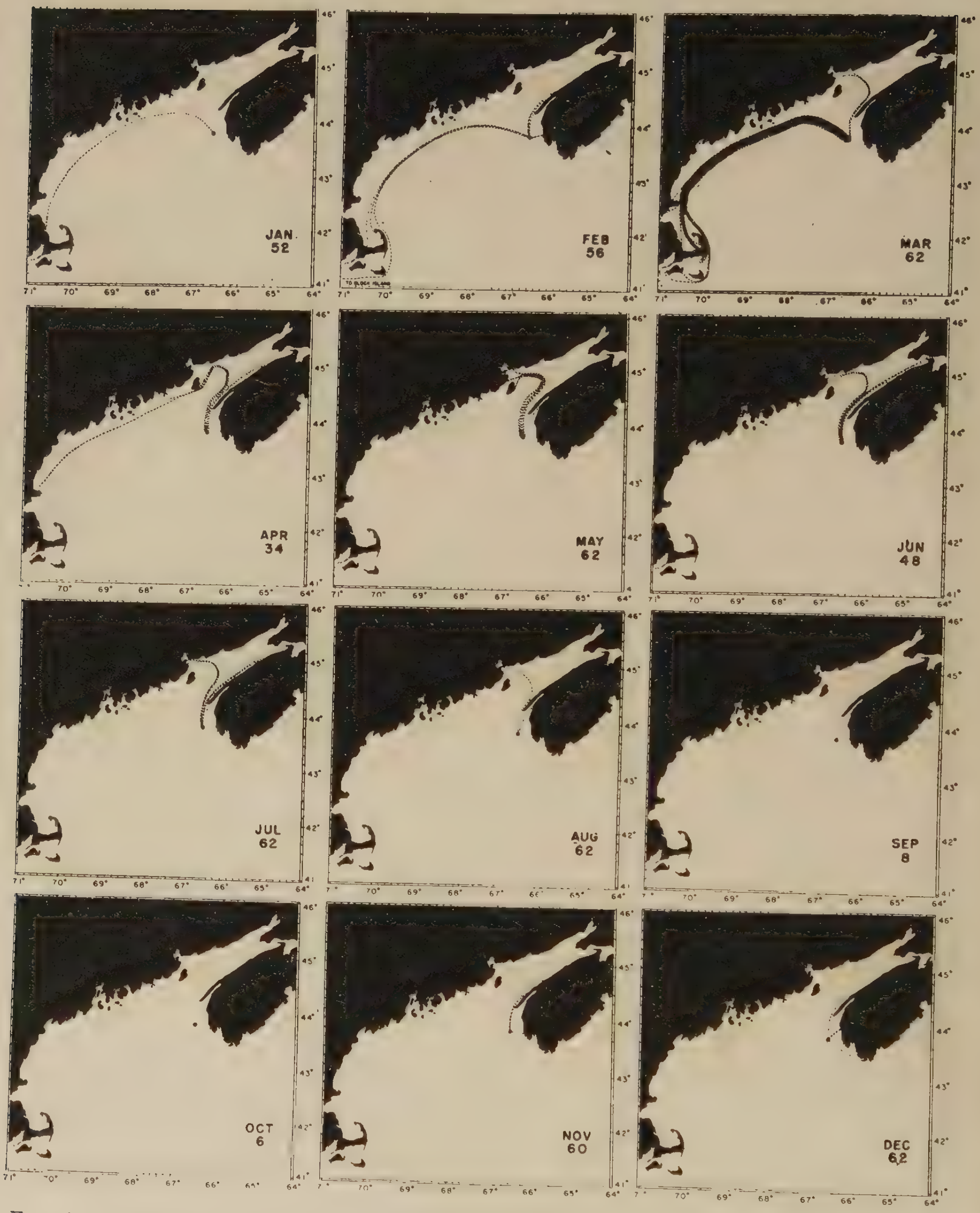
JAN. 52
FEB 56
MAR 62
APR 34
MAY 62
JUN 48
JUL 62
AUG 62
SEP 8
OCT 6
NOV 60
DEC 62
TO BLOCK ISLAND
71° 70° 69° 68° 67° 66° 65° 64°
41° 42° 43° 44° 45° 46°

FIG. 5. Returns of drift bottles released at *Lurcher* Lightship during 1958. Number of bottles released each month indicated in lower right of each diagram.

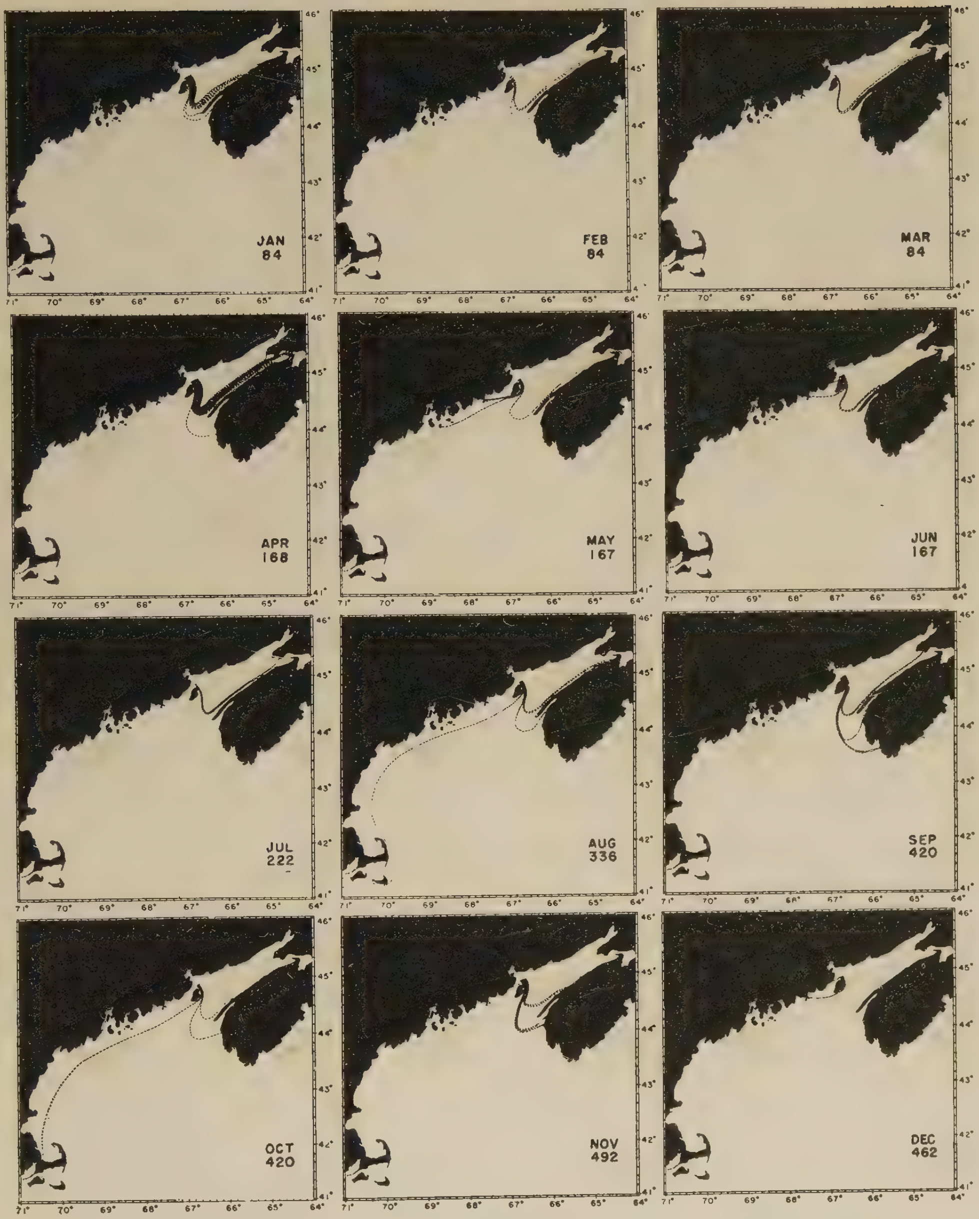
JAN
84
FEB
84
MAR
84
APR
168
MAY
167
JUN
167
JUL
222
AUG
336
SEP
420
OCT
420
NOV
492
DEC
462
46°
45°
44°
43°
42°
41°
71°
70°
69°
68°
67°
66°
65°
64°

FIG. 6. Returns of drift bottles released during 1957 which escaped from the Passamaquoddy Area. Number of bottles released each month indicated in lower right of each diagram.

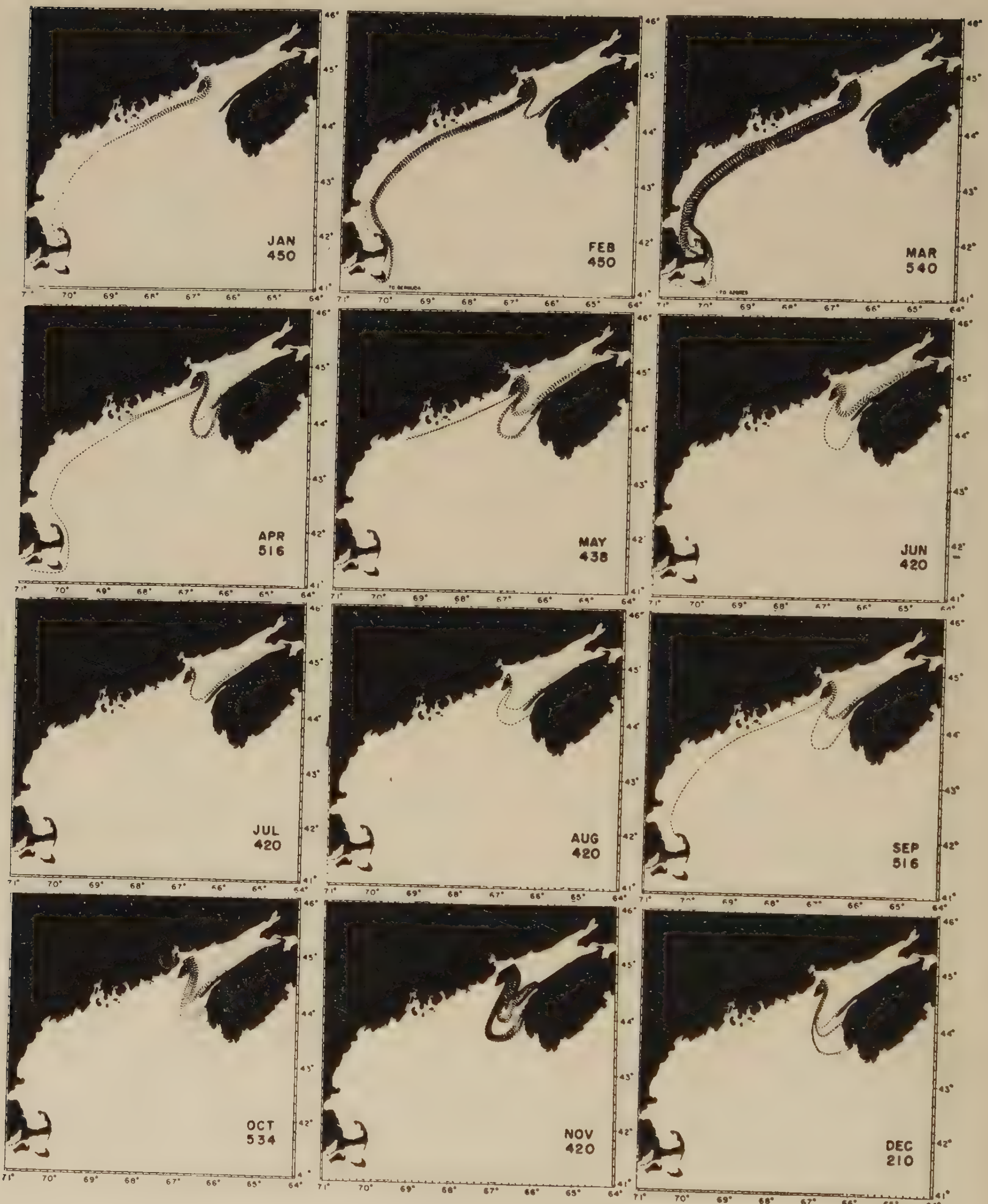
JAN
450
FEB
450
TO BERMUDA
MAR
540
TO AZORES
APR
516
MAY
438
JUN
420
JUL
420
AUG
420
SEP
516
OCT
534
NOV
420
DEC
210
71°
70°
69°
68°
67°
66°
65°
64°
41°
42°
43°
44°
45°
46°

FIG. 7. Returns of drift bottles released during 1958 which escaped from the Passamaquoddy Area. Number of bottles released each month indicated in lower right of each diagram.

which time the set was toward the southwest, as evidenced by the stranding of bottles along the coast of Maine and ultimately Cape Cod. The usual drift across to Nova Scotia was resumed in April. These drift bottle returns are summarized in Table I.

There seems to be no doubt that there was a real difference in the circulation during the first three months of 1958 in contrast to the rather limited circulation during the first month of 1957. This is further substantiated by the releases from the fields of bottles launched in the Gulf of Maine immediately preceding or during these same periods.

TABLE I.

	Percentage of *Lurcher* Lightship bottles which went to:				Percentage of Passamaquoddy project bottles which went to:			
	Passamaquoddy Area	Grand Manan	Nova Scotia	Maine, Mass.	Passamaquoddy Area	Grand Manan	Nova Scotia	Maine, Mass.
1957								
Jan.	0	0	14	0	13.1	1.2	10.7	0
Feb.	...	...	...	...	28.6	0	3.6	0
Mar.	0	0	7	0	21.4	0	2.4	0
Apr.	0	0	13	0	20.2	0	7.7	0
May	5	0	11	0	31.1	0	0.6	1.8
June	15	4	4	0	44.9	1.2	1.2	1.2
July	3	0	14	0	50.0	0	1.4	0
Aug.	0	0	11	0	29.2	0.3	0.9	0.3
Sept.	0	0	10	0	22.2	0.7	1.0	0
Oct.	0	0	2	0	26.0	0.2	0.5	0.2
Nov.	0	0	13	0	27.0	0.4	1.4	0.2
Dec.	0	0	6	0	17.6	0.9	0	0.4
1958								
Jan.	0	0	0	2	14.4	0	0	1.1
Feb.	0	0	9	5	7.1	0.7	0.7	1.9
Mar.	0	0	3	18	17.8	0.4	0	3.7
Apr.	0	6	9	6	13.0	1.0	1.4	0.6
May	6	2	2	0	19.6	0.2	2.0	0.7
June	4	0	4	0	21.6	0.5	1.4	0
July	3	0	3	0	28.1	0.5	0.5	0
Aug.	2	0	2	0	27.2	0.5	0	0.2
Sept.	0	0	12	0	25.8	0.6	0.6	0.2
Oct.	0	0	0	0	22.5	0.6	1.7	0
Nov.	0	0	5	0	10.7	1.9	4.5	0
Dec.	0	0	5	0	8.0	0	1.9	0

DISCUSSION

The factors which may contribute to the non-tidal drift are:

a. The introduction of river runoff at the periphery of the area,

b. the dynamic pressure gradients resulting from unequal heating or cooling of the water over the area,

c. the frictional drag of the wind, and

d. the effect of the Coriolis force on tidal motions in restricted waters.

The runoff has an annual cycle on the average, but departures from the average are common in time and amplitude. The thermal cycle undergoes a regular annual progression. Departures from the mean are restricted to small changes in amplitude or time of occurrence. The wind systems likewise undergo a seasonal cycle but are subject to great departures from the mean in direction and force. Only the tidal motions are truly predictable. Huntsman (1924) has emphasized how the Coriolis force affects the tidal oscillations as an "imperfect valve" in producing stronger currents on the right side of the incoming flood into an embayment, and on the right side of the outgoing ebb. This effect results in a cyclonic eddy. Superimposed on this "Coriolis drift" are the seasonal effects of runoff and wind. The temperature effects are less easily demonstrated as secular effects and are probably less common and much less vigorous than the others.

Important wind effects in the Gulf of Maine have been detected (Day, 1958). Strong northerly winds of extended duration may accentuate the drift on the western side of the gulf or disrupt the southern side of the Maine eddy. One would expect such winds to have an impeding effect on any northerly directed drift. The runoff effect may be demonstrated by the returns from drift bottles launched at *Lurcher* Lightship and in Passamaquoddy Bay during January, February and March 1958 in contrast to the same time the previous year. The mean monthly discharge for the St. Croix River for December 1957 and January and February 1958 is substantially higher than for the same period a year before (Fig. 8); but more important, this higher-than-normal runoff occurred after 9 months of below-normal runoff, a condition common to the whole of the western side of the Gulf of Maine. The sea surface salinities were substantially higher than usual (*Albatross III* Cruise 106 data, 3–19 December 1957) as a result of the prolonged drought and resultant deficit in runoff from the land. The sudden increase in runoff commencing in December along the western side of the Gulf of Maine appears to have given impetus to the western side of the Gulf of Maine eddy at that time. This is further substantiated by the returns from bottles set adrift in the Gulf of Maine and Bay of Fundy in January and February 1958.

We are not able at this time to detail the normal sequence of circulation

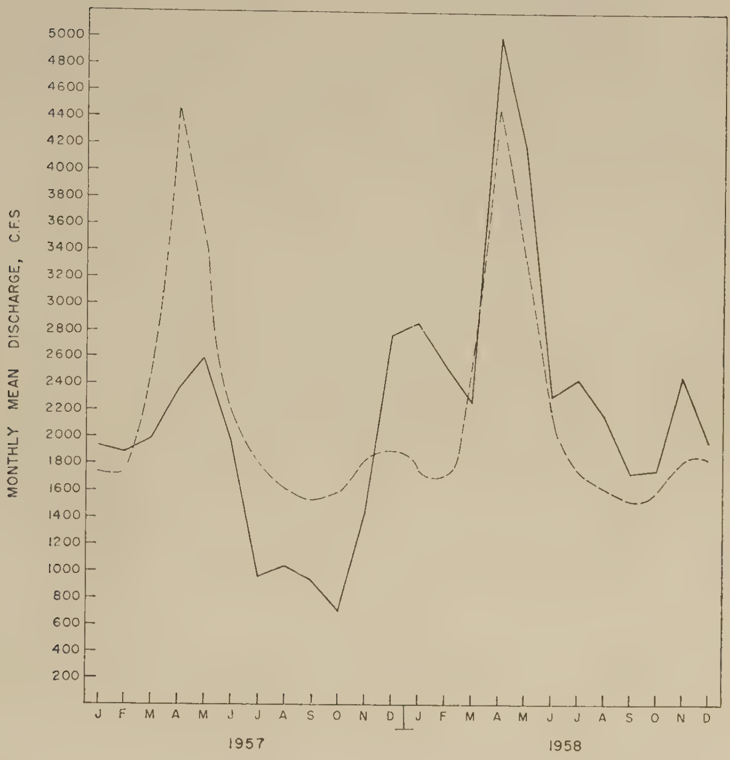

FIG. 8. Mean monthly discharge of St. Croix River at Baileyville for 1957 and 1958. Dashed line represents mean for period of record.

into the Bay of Fundy from east and south of Cape Sable. Bigelow's and Huntsman's data indicate that water from the Scotian Shelf does enter the Gulf of Maine during late spring. This appears to be an area where the current system is markedly unstable, moving into the gulf at one time but turning offshore at another. One might expect at least a slow drift from the inshore waters of southeastern Nova Scotia past Cape Sable at all seasons of the year, with a marked increase in speed and volume and distance offshore during the spring.

According to our present knowledge it would appear that herring spawned inshore on the Scotian Shelf during the autumn have a better chance of drifting into the Bay of Fundy than those spawned on Georges Bank.

SUMMARY

The surface circulation in the Bay of Fundy, Gulf of Maine and southwestern Scotian Shelf has been reviewed. The sources from which drift bottles have reached the Bay of Fundy have been demonstrated, outlining the month-by-month progression. The area from which drift bottles at the surface enter the

Bay of Fundy is restricted during January to the immediate approaches to the bay. It gradually expands during the spring to a maximum in early summer, encompassing most of the Gulf of Maine and part of Georges Bank as the result of the confluence of the Georges and Maine eddies. The source area gradually retracts during the autumn to the eastern side of the Gulf of Maine and northward away from Georges Bank. Some evidence of important secular departure from the normal circulation has been given.

ACKNOWLEDGMENTS

The author gratefully acknowledges the basic data collected over the years by the authors mentioned, together with the more recent efforts of the U.S. Bureau of Commercial Fisheries Laboratories at Woods Hole and Boothbay Harbor and workers at the Fisheries Research Board of Canada's Biological Station, St. Andrews, N.B., chiefly John B. Colton, Leslie Scattergood and S. Noel Tibbo, who have directed the field programs.

REFERENCES

A.O.G. (Atlantic Oceanographic Group, Fish. Res. Bd. Canada). MS, 1958. Canadian drift bottle data, Atlantic Coast. *Fish. Res. Bd. Canada, MS Rept. Series (Oceanog. and Limnol.)*, No. 15, 80 pp.

BIGELOW, H. B. 1927. Physical oceanography of the Gulf of Maine. *Bull. U.S. Bur. Fish.*, **40** (1924) Pt. II. Doc. No. 969: 511–1027.

BJERKAN, P. 1919. Results of the hydrographical observations made by Dr Johan Hjort in the Canadian Atlantic waters during the year 1915. Canadian Fisheries Expedition, 1914–15. Canada Department of Naval Service, pp. 349–403. Ottawa.

BUMPUS, D. F. MS, 1959. Investigations of climate and oceanographic factors influencing the environment of fish. Third Quarterly Report W.H.O.I., Ref. No. 59–10. (Unpublished.)

BUMPUS, D. F., J. CHASE, C. G. DAY, D. H. FRANTZ, JR, D. D. KETCHUM AND R. G. WALDEN. 1957. A new technique for studying non-tidal drift with results of experiments off Gay Head, Mass., and in the Bay of Fundy. *J. Fish Res. Bd. Canada*, **14**(6): 931–944.

BUMPUS, D. F., AND C. G. DAY. 1957. Drift bottle records for Gulf of Maine and Georges Bank, 1931–1956. U.S. Dept. of Int. Fish and Wildlife Serv. *Spec. Sci. Rept.–Fish.*, No. 242, 61 pp.

CHASE, J. 1955. Winds and temperatures in relation to the brood-strengths of Georges Bank haddock. *J. du Cons.*, **21**(1): 17–24.

CRAIGIE, E. H., AND W. H. CHASE. 1918. Further hydrographic investigations in the Bay of Fundy. *Contr. Canadian Biol.* (1917–1918), (7): 125–147.

DAWSON, W. B. 1908. Tables of the hourly direction and velocity of the currents and time of slack water in the Bay of Fundy and its approaches, as far as Cape Sable. Department of Marine and Fisheries, Canada, 15 pp. Ottawa.

DAY, C. G. 1958. Surface circulation in the Gulf of Maine as deduced from drift bottles. *Fishery Bull. of the U.S. Fish and Wildlife Serv.*, **58**(14): 445–472.

FISH, C. J., AND M. W. JOHNSON. 1937. The biology of the zooplankton population in the Bay of Fundy and Gulf of Maine with special reference to production and distribution. *J. Biol. Bd. Canada*, **3**(3): 189–322.

HACHEY, H. B. 1947. Water transports and current patterns for the Scotian Shelf. *J. Fish. Res. Bd. Canada*, **7**(1): 1–16.

HACHEY, H. B., AND W. B. BAILEY. MS, 1952. The general hydrography of the waters of the Bay of Fundy. Revision. *Fish. Res. Bd. Canada MS Rept. Biol. Sta.*, No. 455, 62 pp.

HUNTSMAN, A. G. 1924. Oceanography. Handbook of the British Association for the Advancement of Science, pp. 274–290. Toronto.

MACGREGOR, D. C., AND H. J. MCLELLAN. 1952. Current measurements in the Grand Manan Channel. *J. Fish. Res. Bd. Canada*, **9**(5): 213–222.

MAVOR, J. W. 1922. The circulation of the water in the Bay of Fundy. Pt. I. Introduction and drift bottle experiments. *Contr. Canadian Biol.* N.S., **1**(8): 101–124.

1923. The circulation of the water in the Bay of Fundy. Pt. II. The distribution of temperature, salinity and density in 1919, and the movements of the water which they indicate in the Bay of Fundy. *Ibid.*, **1**(18): 355–375.

REDFIELD, A. C. 1939. The history of a population of *Limacina retroversa* during its drift across the Gulf of Maine. *Biol. Bull.*, **76**(1): 26–47.

1941. The effect of the circulation of water on the distribution of the calanoid community in the Gulf of Maine. *Ibid.*, **80**(1): 26–110.

TRITES, R. W., AND R. E. BANKS. 1958. Circulation on the Scotian shelf as indicated by drift bottles. *J. Fish. Res. Bd. Canada*, **15**(1): 79–89.

WATSON, E. E. 1936. Mixing and residual currents in tidal waters as illustrated in the Bay of Fundy. *J. Biol. Bd. Canada*, **2**(2): 141–208.

Contribution No. 1087

OIKOS 11:2 1960

LETHAL HIGH TEMPERATURES FOR THREE MARINE INVERTEBRATES: *LIMULUS POLYPHEMUS, LITTORINA LITTOREA* AND *PAGURUS LONGICARPUS*[1][2]

BY

G. FRAENKEL

(Department of Entomology, University of Illinois, Urbana and
Oceanographic Institution, Woods Hole)

It is well known that different poikilothermic animals differ very widely in their tolerance of high temperatures. The literature abounds in data about high temperatures that certain animals can or cannot tolerate. However, as pointed out variously by compilers of such data [UVAROV (1931), BELEHRADEK (1935), HEILBRUNN (1937)] much of this information is useless owing to the neglect by the authors to consider the time factor. Even since this criticism was made, data continued to be published in which the time of exposure to a particular temperature was either not mentioned, or a criterion for a time-temperature relationship was chosen which does not allow a proper interpretation of the data. As pointed out by Heilbrunn and others, a full set of data should be concerned with the length of time each particular temperature can be tolerated. However, again and again, and up to very recently, authors have followed a course by which an animal is submitted to a *rising* temperature. The lethal temperatures, thus determined, have been affecting the subject for a very short period only, possibly only a matter of seconds, while it was previously exposed to a series of rising temperatures for periods depending on the rate of heating.

Another difficulty arises in the exact definition of the term "lethal". There may be a wide span between the temperatures or periods of an exposure at which an organism may either be killed outright, or may still exhibit signs of life of various degrees before dying eventually. Authors have used different criteria, and in many cases have not even stated their criteria.

In recent years much interest has been concentrated upon the adaptation of

---

[1] This research was supported by a research grant from the Office of Naval Research NONR-1834(07). The author is much indebted to Dr. PAUL M. FYE and Dr. HARRY J. TURNER for the hospitality he enjoyed at the Oceanographic Institution, Woods Hole, Massachusetts.

[2] Contribution No. 1087 from the Woods Hole Oceanographic Institution.

different geographical races of a species, or that of individual animals, to high temperatures (Scholander *et al.* (1953), Prosser (1955), Bullock (1955)). This line of work has been almost exclusively concerned with the metabolism or certain functions of animals that had been exposed before to different temperatures, and it was silently assumed that an animal that has successfully adapted its metabolism to a higher temperature would also be better able to tolerate high temperatures. There is no proof that this is necessarily so. Such a correlation has been successfully demonstrated for fishes (Fry 1957, and the lobster (McLeese 1956), but most of the existing investigations on temperature adaptation of invertebrates were not concerned with lethal high temperatures.

The literature on heat death of poikilothermic animals is rich in data on insects and fishes, while there is an almost complete lack of reliable information concerning marine invertebrates. A recent compilation of such data (Spector 1956) includes tables concerning insects and fishes, but omits the vast field of aquatic invertebrates, owing apparently to lack of data. The author's interest in the present work arose from chance observations made during the summer of 1953 at Woods Hole on *Limulus*, and led, during the summer of 1959 to an investigation of the heat death of three marine invertebrates: the horseshoe crab, *Limulus polyphemus* L.; the common periwinkel, *Littorina littorea* L; and the small hermit crab, *Pagurus longicarpus* Say.

Method adopted

Throughout this work the animals concerned were exposed to high temperatures by immersing them in a constant temperature bath, containing about 10 liters of sea water, for varying periods and at different temperatures. It was aimed to determine the temperature at which half the number of animals died after an exposure of one hour. The definition of death will be discussed below for each of the three species separately.

Results

Limulus polyphemus

The Orleans bay of Cape Cod is a vast expanse of very shallow water which runs dry over large areas at low tide. On a hot day in July 1953 I observed limuli left by the receding tide high and dry on top of the mudflats and fully exposed to the sun and air. These limuli felt very warm to the touch and had obviously reached a body temperature considerably above that of the water and air. They were entirely motionless, yet recovered completely and instantaneously when transferred into open water. Subsequently limuli were kept in a heated seawater aquarium in the laboratory. On one occasion, when the temperature regulation had broken down overnight, they were found in the morning lying motionless on the bottom of the tank at a temperature of 40°, but recovered completely when transferred to cooler water. Mayer (1914) had previously reported that limuli at Woods Hole could stand temperatures of 41°, and in Florida of even 46°. These temperatures appeared exceptionally high for an aquatic animal, and prompted the present investigation.

The experiments were performed with limuli measuring 6 to 7.5 cm across the cephalothorax (11–14 cm total length) which had been collected early in August 1959 in the Orleans Bay of Cape Cod. They were chosen with hard cuticles and probably had moulted earlier in the year. No differences were found between individuals according to the differences of size.

Healthy limuli, when kept on a surface of mud or fine sand, rapidly dig in. This proved to be the most reliable criterion for successful tolerance of a particular temperature. However, under certain conditions of exposure *Limulus* recovered from heat coma within a few seconds, and appeared active and normal, while failing to dig in. Such animals were never observed to recover completely after 24 hours' observation (Table 1). They frequently died after several days (Table 1) or longer periods, and although the time was too short to determine the life span of every individual until death, it was assumed that they would all eventually die.

For the purpose of quick reference and tabulation of results, the following classification of graded responses to temperature exposures was used:

A. The animals seem normal in every respect, and dig into the mud or sand.
B. The animals seem normal in every respect, and may remain so for at least several days, but for their failure to dig in.
C. The animals show less spontaneous activity, but still react strongly to handling by bending the cephalothorax and abdomen ventralwards, to form an angle of about 90°, and by leg and spine movements. Respiratory movements of the gills are vigorous.
D. The animal shows essentially only weak respiratory movements of the gills.
E. No visible movements, but the heart may still beat. The animals are dying or dead.

This classification is admittedly somewhat arbitrary and could be almost indefinitely expanded and more finely graded.

A summary of the results of the tests is given in Table 1. In this table the effect of heat treatment is expressed by the above explained symbols A-E, as it manifested itself 24, 48, and 72 hours after the end of the exposure. A 24 hour period appeared to give the most significant results, since a shorter time after exposure recovery may not have been optimal, and those adversely affected by the exposure tended to deteriorate subsequently, as seen in some of the tests.

Table 1. The effect of high temperatures on *Limulus polyphemus* after various periods of exposure. A: normal and dig in; B: apparently normal, do not dig in; C: reduced activity; D: immobile, but for respiratory movements; E: totally immobile, dying or dead.

Date	Temperature	Exposure in minutes	Number of animals affected														
			after 24 hours					after 48 hours					after 72 hours				
			A	B	C	D	E	A	B	C	D	E	A	B	C	D	E
9- 5-1959	40°	840	5	1	–	–	4	6	–	–	–	4	–	–	–	–	–
8- -1959	41.5°	315	3	2	–	–	–	–	–	–	–	–	–	–	–	–	–
9- 5-1959	42°	300	4	4	–	–	2	4	2	1	–	3	–	–	–	–	–
8-12-1959	43°	90	10	–	–	–	–	–	–	–	–	–	–	–	–	–	–
8-31-1959	43°	180	–	–	3	–	2	–	2	1	–	2	–	–	–	–	5
9- 5-1959	43°	120	–	4	–	–	1	–	4	–	–	1	–	–	–	–	–
		210	–	–	4	–	1	–	3	–	–	2	–	–	–	–	–
8-12-1959	44°	30	10	–	–	–	–	–	–	–	–	–	–	–	–	–	–
		60	–	3	–	–	2	–	3	–	–	2	–	1	–	–	4
8-19-1959	44°	60	–	2	1	–	–	–	–	–	–	–	–	1	–	–	2
8-28-1959	44°	60	–	6	2[1]	2[1]	–	–	6	–	–	–	–	3	–	–	3
9- 2-1959	44°	60	–	13	–	–	–	–	13	–	–	–	–	6	1	2	4
8-14-1959	45°	15	5	–	–	–	–	5	–	–	–	–	5	–	–	–	–
		30	–	–	–	5	–	–	–	–	3	2	–	–	–	–	5
		40	–	–	–	4	1	–	–	–	3	2	–	–	–	–	5
8-31-1959	45°	30	–	–	2	1	2	–	–	–	2	3	–	–	–	1	4
9- 3-1959	45°	30	–	–	–	4	1	–	–	–	–	–	–	–	–	–	–
9- 7-1959	45°	20	3	3	–	–	–	–	–	–	–	–	–	–	–	–	–
		30	–	2	2	2	–	–	–	–	–	–	–	–	–	–	–
		40	–	3	–	1	1	–	–	–	–	–	–	–	–	–	–
9- 7-1959	46°	7	5	–	–	–	–	–	–	–	–	–	–	–	–	–	–
		15	–	3	1	1	–	–	–	–	–	–	–	–	–	–	–

[1] Killed.

At all the temperatures concerned in the tests of table 1 the limuli became immobile sooner or later, if left in that temperature continually, depending on the temperature. Those of class A and B recovered almost instantaneously in cooler water. They recovered completely from an exposure to 43° for 90 minutes. One hour at 44° left them in a state in which the majority appeared normal, but for the failure to dig in; yet these crabs died eventually (test of 9-2-1959). An exposure at 45° was well tolerated for 15 or 20 minutes only, and one at 46° for 7 minutes. At the other end of the scale, 42° were tolerated for 5 hours, and 40° for 14 hours.

Littorina littorea

The heat death of various marine mollusks, and in particular tidal gastropods has been investigated by a number of authors, working in Canada (Huntsman

& SPARKS 1924, HENDERSON 1929, HAYES 1929), Britain (EVANS 1948), and South Africa (BROECKHUYSEN 1940). Some of this work has been reviewed by GUNTHER (1958). Inasfar as the heat tolerance of gastropods from intertidal zones is concerned, these investigations arose from the idea that the higher the place of an animal was in a tidal zone, and consequently the longer the exposure to air and sun at low tides, the more resistant to high temperature the snail was expected to be. The investigations to some degree bore out this contention. In order to obtain comparable data for species from so widely distant geographical areas, the authors followed closely the same procedure, which would have all been to the good, had this method not possessed serious drawbacks. This method devised by HUNTSMAN and SPARKS (1924) consisted of heating the animals in water, at the rate of a rise in temperature of 1°/5 minutes, and removing them when they showed signs of heat coma. If they recovered they were submitted to higher temperatures, until recovery did no longer occur. Thus the animals were exposed for only a few minutes to the temperature considered the highest that was tolerated. The criterion for survival or death was whether or not they responded to prodding once they had become immobile and were allowed to recover in colder water for 1 hour. The authors aimed to control the rate of raising the temperature to 1°/5 minutes, but did not entirely succeed in this, so that the time interval per one degree tended to become longer with increasing temperature. This renders the data by the several authors not strictly comparable. The thermal death point for *Littorina littorea*, thus determined, was of the astonishingly high figure of 46–47° (HAYES 1929) or 46° EVANS (1948).

The specimens of *Littorina littorea* used in our experiments were collected at low tide on the shores of the "big" harbor of Woods Hole, and submitted to several constant temperatures for various periods. The results of exposures to temperatures between 39 and 41° are summarized in Table 2. At these temperatures, the snails became immobile, and were usually entirely withdrawn into their shells long before the end of the periods stated. They frequently remained so for many hours, after transfer to cooler water, even in cases where recovery was complete. A result of some significance required a recovery period of at least 24 hours, preferably one of 48 hours. A normal *Littorina* attaches itself almost immediately to a substrate, crawls up the vertical sides of a container and out of the water, to become fixed usually 2 to 4 cm above water level. For the purpose of the present investigation specimens were considered as fully recovered when they crawled out of the water. At a lower stage of recovery the snails become attached to a substrate, without leaving the water. At a still lower stage the snails extend their bodies out of the shell to a lesser or greater degree without becoming attached. The least active ones in this category open the operculum very slightly, but like more active ones, withdraw completely

Table 2. The effect of high temperatures on *Littorina littorea*, after various periods of exposures. A: normal, crawl out of the water; B: attached to a surface, but do not crawl out of the water; C: Operculum open and body stretched out of shell to a varying degree; D: withdrawn into the shell, dying or dead.

Date	Temperature	Exposure in minutes	Number of animals affected							
			after 24 hours				after 48 hours			
			A	B	C	D	A	B	C	D
9- 3-1959	39°	180	15	–	–	–	–	–	–	–
		330	18	–	1	15	–	–	–	–
8-18-1959	40°	30	9	–	–	1	–	–	–	–
		45	4	5	–	1	7	–	1	2
		60	8	1	1	–	8	1	–	1
		90	4	–	3	3	5	–	3	2
		120	1	–	9	–	2	–	–	8
9- 4-1959	40°	120	9	–	–	6	–	–	–	–
		270	3	–	30	2	3	–	1	31
8-27-1959	40.5°	60	11	1	2	6	12	–	–	8
8-17-1959	41°	15	10	–	–	–	–	–	–	–
		30	10	–	–	–	–	–	–	–
		45	6	1	3	–	6	–	3	1
		60	–	–	8[1])	1	–	–	–	9[1])
		75	2	2	4	1	2	–	1	6
8-25-1959	41°	60	5	–	4	11	8	2	–	10

[1]) Water very smelly.

Table 3. The effect of raising the temperature from 35° to 45° on *Littorina littorea*. A: normal, crawl out of the water; B: attached to surface, do not crawl out of the water; C: Body stretched out of shell to a varying degree, not attached to a surface; D: withdrawn into shell, dying or dead.

Time	Temperature	Time	Temperature	Number of animals affected							
				after 24 hours				after 48 hours			
				A	B	C	D	A	B	C	D
10.00	35°	10.32	41°	9	1	–	–	10	–	–	–
10.05	36°	10.37	42°	9	1	–	–	10	–	–	–
10.10	37°	10.42	43°	8	1	–	–	9	–	–	–
10.15	38°	10.48	44°	10	–	–	–	10	–	–	–
10.20	39°	10.56	45°	1	–	4	5	1	–	–	9
10.25	40°	–	–	–	–	–	–	–	–	–	–

upon being prodded with a pin. Those most affected are entirely withdrawn into the shell, with the operculum firmly closed. After a recovery period of 24 hours or less, it was not possible to ascertain death, except by breaking the shell. But snails which had not opened the operculum after 48 hours were always dead.

On the basis of these findings the following scale of response to high temperatures was adopted:

A. Normal, the snails crawl out of the water.
B. They become fixed to the walls of the vessel under water, but usually show little activity.
C. They stretch out of the shell, without becoming fixed to a substrate. In this category is included a wide variety of activities from barely opening of the operculum to extensive stretching and moving out of the shell.
D. The operculum is firmly closed. In this stage, after 24 hours or more, the snails are usually dead or dying.

It is obvious from this description that a recovery period of 1 hour allowed by some of the previous authors is far too short for judging survival, and that a response to prodding in no way indicates whether the snails are going to recover or die. As is seen in Table 2, snails from category B at 24 hours frequently recovered completely subsequently, and those from category C usually died.

Table 2 indicates, that about 50% mortality on a 24–48 hours criterion occurs at 39° after 5½ hours exposure, at 40° after between 90 and 120 minutes, and at 41° after 1 hour. By way of comparison with results reported by previous authors an experiment was set up in which their procedure was followed as closely as was possible, namely raising the temperature at the rate of 1°/5 minutes, starting at 35° and removing 10 snails at each degree between 41 and 45° (Table 3). Those withdrawn up to 44° recovered completely, while at 45° they were greatly affected and eventually died. This agrees fairly well with the figure of 46° reported by HAYES (1929) and EVANS (1948), especially considering differences in geographical locality.

Pagurus longicarpus

The small hermit crab, *Pagurus longicarpus* was chosen as an organism which lives in similar habitats to the other two, near the shore. At low tide it is sometimes trapped in tidal pools which may considerably heat up, but never leaves the water. When heated to an appropriate level, the crabs become overactive and frequently voluntarily wiggle out of the shell. It was then found that those which had left the shell tolerated high temperatures much better than those which had not done so. Subsequently in all experiments some of the crabs were taken out from the shell (by cautiously breaking the shell with a nut cracker) before exposure to the high temperature. After exposure to temperatures between 34 and 36° for suitable periods, the crabs were in a heat coma, but usually recovered within several hours. During the recovery period those without shells were provided with empty snail shells of which they took possession readily once they had completely recovered.

Table 4. The effect of high temperatures on *Pagurus longicarpus* after various periods of exposure. A: normal, in shell; B: apparently normal, but outside shell; C: greatly reduced activity, outside shell; D: dead.

Date	Temperature	Exposure in minutes	In relation to shell	Number of animals affected: within a few hrs. of exposure A	B	C	D	after 24 hours A	B	C	D
8-11-1959	34°	60	12 stayed inside	12	–	–	–	–	–	–	–
8-26-1959	35°	60	10 taken out	10	–	–	–	–	–	–	–
			5 wiggled out	2	–	3	–	–	–	–	–
			15 stayed inside	12	–	3	–	–	–	–	–
8-26-1959	35.5°	60	10 taken out	9	1	–	–	10	–	–	–
			9 wiggled out	4	3	–	2	5	–	–	4
			11 stayed inside	4	–	–	7	4	–	–	7
8-10-1959	36°	45	4 wiggled out	3	–	–	1	3	–	–	1
			8 stayed inside	–	–	–	8	–	–	–	8
8-25-1959	36°	60	11 taken out	2	1	–	8	–	–	–	–
			8 wiggled out	2	–	–	6	–	–	–	–
			12 stayed inside	–	–	–	12	–	–	–	–
8-27-1959	36°	60	10 taken out	3	3	–	4	4	2[1]	–	4
			9 wiggled out	2	5	–	2	5	1[2]	–	3
			10 stayed inside	–	–	–	10	–	–	–	10
8-20-1959	37°	60	10 taken out 10 wiggled out	–	5	–	15	–	–	–	–
			8 stayed inside	–	–	–	8	–	–	–	–
8- 8-1959	40°	10–30	became almost immediately immobile, none recovered								

[1] occupied shell after 120 hours, 1 dead after 48 hours.

[2] occupied shell after 144 hours.

The following criteria were adopted, in judging the results of heat treatments:

A. Complete recovery: The crabs had re-entered a shell, and showed normal activity.

B. The crabs appear normal, but have not re-entered a shell.

C. The crabs show signs of activity of various degrees, but are not normal.

D. The crabs are motionless or dead.

Table 4 gives a summary of the results of exposure for periods of mostly one hour, at temperatures between 34 and 36°. At 34° they were little affected, but for increased activity at the beginning, and reduced activity later during the exposure. They did not voluntarily leave the shell. At 35° some left the shell, but most of the shells were reoccupied subsequently. At 35.5 and 36° a large percentage of the crabs, sometimes half of them, wiggled out of the shells during the period of excessive activity shortly after beginning of the exposure. Of those which had left their shells, or were previously taken out, a variable number, roughly 50%, recovered completely, while the rest either died outright, or eventually, within 24 hours. In two cases only, crabs survived for several days and reoccupied a shell after 120 and 144 hours, respectively. Nearly all those which remained in the shell during exposure died soon afterwards. Of those treated at 37°, most died soon, but of 5 which were active none had reentered a shell within 8 hours. The reason why crabs out of their shells survived so much better than those inside was assumed to be the restriction of respiratory exchanges in the latter.

The observation of hermit crabs abandoning their shell voluntarily, except for the purpose of entering another one, is somewhat remarkable in view of the fact that it is normally wellnigh impossible to pull them out of their shells without tearing them apart. BRIGHTWELL (1951) reported difficulties in removing them from the shell without injury. I observed that *Pagurus longicarpus* would eventually leave their shell, if the shell had been fixed to some object so that it could not be moved.

Discussion

What criteria for death or recovery should be used in experiments on exposure to high temperatures? This question is difficult to answer unambiguously. It is obvious that the indication of any signs of life, as it was used by most of the authors working with tidal mollusks, is a very uncertain criterion, since in many instances the animals are dying, and a response may have been elicited to a direct mechanical stimulation of musculature. On the other hand, a criterion of complete recovery would imply observation of the animals for long periods after the exposure, and would then also have to take into account normal feeding, growth and reproduction. Such a procedure is obviously not practical, considering the excessive expenditure of time, space and labor involved. In the 3 species of animals under observation, critical and clear-cut indices of normal behavior were recognized. In *Limulus* it was the habit to dig into mud or sand, in *Littorina* the tendency to crawl up a vertical surface and out of the water, and in *Pagurus* the urge and ability to reoccupy a snail shell. These indices of normal activity were manifest in animals that had been only little affected within a few hours after exposure, and in those more affected usually within 24 hours. Those which did not regain these typical activities within one day usually died eventually, *Limulus* within several days or even weeks, and *Littorina* and *Pagurus* within another day. It, therefore, appears that a certain manifestation of normal behavior, which is typical for the organism under investigation, constitutes a most valuable index for viability. This does not solve the problem entirely, because it leaves out of consideration the more long-range activities listed above. In any investigation which includes the interpretation of such experimental data in terms of population ecology, under temperature conditions in the field, entirely different procedures have to be followed. Not only has the effect of the exposure on all activities, up to the natural death of the individual, to be taken into consideration, but exposure periods have to be greatly lengthened, to correspond to periods potentially encountered in the natural environment of the animal.

In this investigation the experiments were primarily designed to determine the temperature which gives approximately 50% survival after exposure of one hour, one hour being considered a sufficiently substantial period to render the period of equilibration to the required temperature relatively insignificant. Much of the previous research on heat death deals with the effect of very high temperatures after very short exposures of a few minutes only. In the case of terrestrial animals, like insects, such short exposures do not allow for sufficient equilibration with the temperature of the environment. On the other hand, the tolerance of high temperatures for very long periods, even indefinitely, poses entirely different problems of metabolic and behavioral adaptations which are not under consideration at exposure times of one hour.

Much of the recent physiological literature about the effect of high temperatures on animals deals with this entirely different problem of adaptation. Starting from the premises that the normal activity of one and the same, or closely related species, living at widely divergent temperatures at different periods of the year, or in different geographical regions, may not be too dissimilar at these different environmental temperatures, a metabolic adaptation to temperature was postulated. In most of the extensive work in this area (SCHOLANDER *et al.* 1953, BULLOCK 1955, PROSSER 1955) the oxygen uptake was used as the criterion for adaptation, and the occurrence of such adaptations was demonstrated for many poikilothermal animals. It may seem reasonable to assume that such adaptation would also change the temperature of heat death. This angle was, however, not considered in most of the relevant literature.

Reliable data on upper lethal temperatures for marine invertebrates are almost non-existent. All data obtained by a sliding-temperature method must be considered as several degrees higher than those obtained with fixed temperatures, the differences depending also on the rate of heating; and the absence of, or difference in, criteria adopted in judging mortality makes a comparison of existing data wellnigh impossible.

VERNON (1899) working with many different invertebrates from the Bay of Naples, and using a method of quickly raising the temperature (within 15 minutes) recorded death temperatures of mostly between 36 and 42°. Most of the extensive data by MAYER (1914), which include those already mentioned for *Limulus* of 46.2° for Florida and 41° at Woods Hole and others about *Aurelia aurita* (38.5° Florida, 20–30° Halifax), *Lepas fascicularis* (42.3°), *Beroe cucumis* (30°), *Cassiopea frondosa* (40°) are almost meaningless owing to the failure by the author to state the methods and criteria adopted. The death temperature of various reef corals in the Florida-Bahamas region is given as 36–37°, determined by raising the temperature by 2° per hour. It is not stated whether the same method was used in the results elsewhere stated in the investigation. In HUNTSMAN and SPARKS (1924) tests with many marine invertebrates and fishes from Canadian waters, undertaken with slowly rising temperatures (about 2 hours) at the rate of 1° per 5 minutes, death occurred usually around 30°. As an example of exposure for a far more extended period the investigations by MCLEESE (1956) on the American lobster may be quoted. With an exposure period of 48 hours and the criterion of a 50% kill, the figures were 26.5° (acclimated to 9°), and 29–30° (acclimated to 25°).

By comparison with the data quoted by these various authors, and making due allowance for the difference in the methods employed, the lethal temperature reported in this paper about *Limulus* and *Littorina* are very high. This would seem to constitute a very striking example of temperature adaptation by an organism which is habitually exposed to high temperatures. *Limulus* has been observed stranded at low tide and fully exposed to air and sun, and the exposure of *Littorina* on rocks above the water surface under similar conditions is a familiar sight. There can be no doubt that a considerable rise in the body temperature of the animals, above that of the air or water temperature, must take place, which may have to be tolerated during several hours. It would be most desirable to have measurements of the actual body temperatures of these and similarly exposed animals.

Summary

The lethal high temperatures were determined for three marine invertebrates, *Limulus polyphemus*, *Littorina littorea*, and *Pagurus longicarpus*, employing constant exposure temperatures, exposure times between several minutes and several hours, and survival after 24 hours as a criterion. For one-hour exposure they were found to be 44° for *Limulus*, 40–41° for *Littorina*, and 36° for *Pagurus*. The importance of considering the time factor, using constant temperatures, and choosing proper criteria for judging survival has been stressed. The best criteria for survival were considered to be certain indices for normal behavior, in *Limulus* the habit to dig into sand, in *Littorina* the tendency to crawl up vertical surfaces, and in *Pagurus* the urge to reoccupy a snail shell when out of the shell. By comparison with the results for other marine invertebrates from other authors, the lethal temperatures found for *Limulus* and *Littorina* were very high. This is considered as examples of temperature adaptation in organisms which are habitually exposed to high temperatures.

Made in United States of America
Reprinted from LIMNOLOGY AND OCEANOGRAPHY
Vol. 5, No. 3, July, 1960
pp. 337–338

ON WINTER MIXING AND THE VERTICAL DISTRIBUTION OF PHYTOPLANKTON[1]

During winter in the North Atlantic Ocean, the vertical distributions of temperature, salinity and other properties indicate that the surface waters are homogeneous, unstable and presumably well mixed to depths ranging from one to several hundred meters. Phytoplankton is seldom abundant at that time of year and under those conditions. Its paucity is usually attributed to the organisms being continually mixed through a column of water several times greater than that within which photosynthesis can occur (*i.e.* 25–75 m) and hence receiving insufficient light to grow. A number of authors have considered as a factor controlling plant growth, and particularly the onset of vernal flowering, the relationship between the depths of the euphotic and mixed layers. Vertical instability is identified with vertical turbulence, and hence the organisms are considered to be exposed to the average light intensity within the mixed layer, an intensity which must exceed some threshhold (*i.e.* compensation level) before growth may occur.

On March 27, 1957 an oceanographic station was occupied by R. V. Crawford at 39°27′N, 71°28′W, about 100 miles off New York City, in 1200 fathoms of water. Table 1 shows the vertical distribution to 200 m of temperature, salinity, density, dissolved oxygen, phosphate, nitrite, nitrate and total phosphorus. By all of these criteria the upper 100 m would be considered completely homogeneous. Such variations as exist in the data are irregular and inconsistent from one parameter to the next, and must therefore have resulted from sampling or analytical error. There are indications in the phosphorus analyses of a discontinuity at 150 m, and there is sharp break in the values of all properties at 200 m.

Examine now the vertical distribution of the phytoplankton within the upper 100 m of the same water column (Fig. 1). Only the five most abundant species (those with concentrations exceeding 1,000 cells/L at one or more depths) are shown. Not only is their vertical distribution uneven, but the pattern is different for each of the five species. We will not attempt to estimate how much of the observed variability in the phytoplankton may have resulted from counting error. Great as it may have been, no conceivable error could distort vertical homogeniety to the observed discontinuous distribution of the small, unidentified diatom, found only 10 m in a concentration of 12,300 cells/L.

Only one of the five species, *Coccolithus huxleyi,* is a motile organism. The other four species, all centric diatoms, had peaks of abundance respectively at 0, 10, 75 and 100 m. It seems doubtful that those found

TABLE 1. *The vertical distribution of physical and chemical properties in the upper 200 m at CRAWFORD Station 136 (39°27′N, 71°28′W) on March 23, 1957*

Depth (m)	Temperature (°C)	Salinity (‰)	Density (σt)	O_2 (ml/L)	$PO_4^{\equiv} - P$ µgA/L	$NO_2 - N$ µgA/L	$NO_3^{-} - N$ µgA/L	Total P µgA/L
0	15.26	36.10	26.80	5.27	.36	.24	4.9	.50
10	15.24	36.10	26.79	5.18	.48	.28	6.0	.50
25	15.28	36.07	26.74	5.14	.48	.23	4.3	.51
50	15.23	36.07	26.76	5.09	.42	.26	4.2	.59
75	15.27	36.07	26.76	5.09	.48	.26	7.4	.53
100	15.23	36.05	26.76	5.14	.46	.26	6.0	.56
150	15.28	36.05	26.74	5.04	.68	.26	4.9	.69
200	13.33	35.71	26.90	3.97	1.02	.04	9.6	1.10

---

[1] Contribution No. 1088 from the Woods Hole Oceanographic Institution.

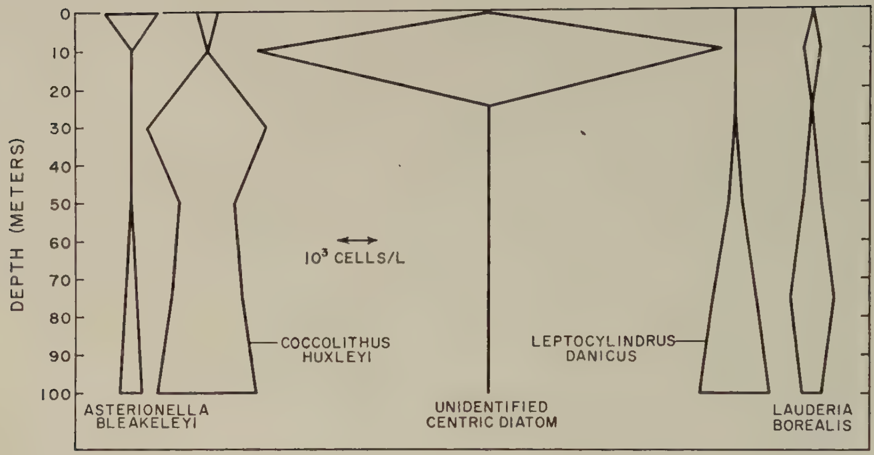

FIG 1. Vertical distribution of the five most abundant species of phytoplankton.

concentrated at 75 and 100 m grew at those depths. Indeed, the extinction coefficient ($k = .07$) indicates an euphotic zone of less than 75 m. Despite the appearance of a well mixed layer of over 100 m, vertical turbulence was apparently weak enough, for a long enough period, to permit not only the growth of populations of *Asterionella bleakeleyi* and the unidentified diatom in the upper 10 m, but also the growth and subsequent settling out of the euphotic zone of populations of *Leptocylindrus danicus* and *Lauderia borealis*. Thus a "mixed layer" by physical or chemical criteria is not necessarily mixed with respect to its phytoplankton, nor does it provide any indication of the occurrence or degree of mixing at the time of observation.

J. H. RYTHER AND E. M. HULBURT
Woods Hole Oceanographic Institution,
Woods Hole, Mass.

Contribution No. 1089

CONSEIL PERMANENT INTERNATIONAL
POUR L'EXPLORATION DE LA MER
CHARLOTTENLUND SLOT — DANEMARK

JOURNAL DU CONSEIL

VOL. XXV · NO. 3

PUBLIÉ PAR LE BUREAU DU CONSEIL

RÉDIGÉ PAR
F. R. HARDEN JONES

EN COMMISSION CHEZ
ANDR. FRED. HØST & FILS
COPENHAGUE

AOÛT 1960

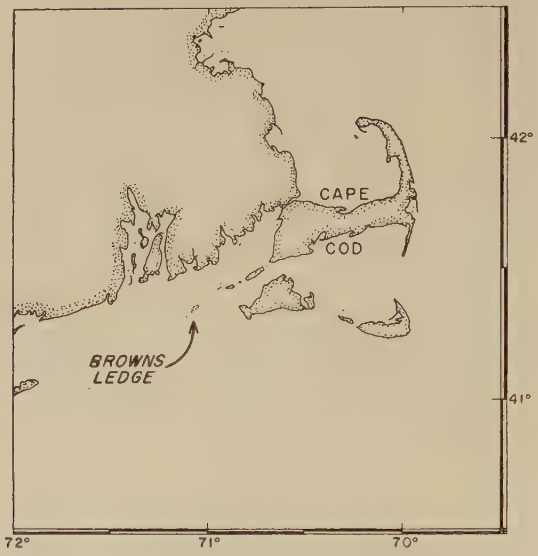

Figure 1. Chart to show the position of Browns Ledge.

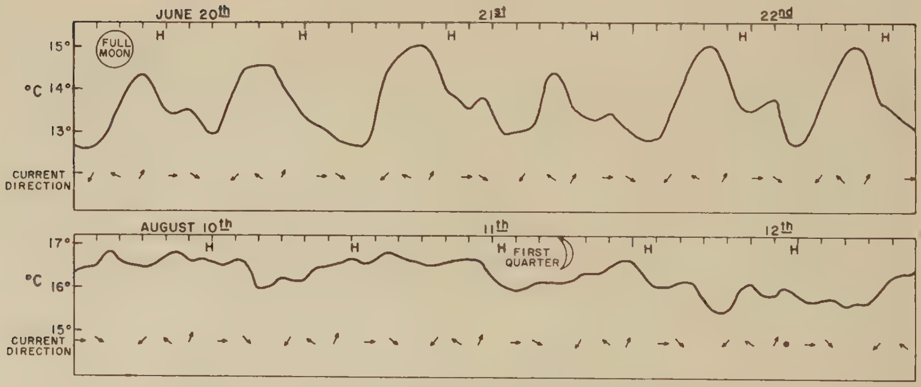

Figure 2. Excerpts from temperature record, showing extremes in fluctuation. The letter H indicates high water at Cuttyhunk. Arrows show current direction at 13 m.

Results

The record was read for each hour of the 56-day period and plotted as a curve. The resulting pattern suggested a 28-day periodicity; at the time of spring tides temperature variations of nearly 3°C showed strong semidiurnal periodicity.

Excerpts from the plot are shown in Figure 2. The arrows below the temperature curves indicate direction of flow at a depth of 13 m. These directions were extrapolated, using as a reference the time of high water at Cuttyhunk, from measurements made on Browns Ledge by the U. S. Coast and Geodetic Survey from 17.–21. June 1959. Tidal influence on temperature is indicated.

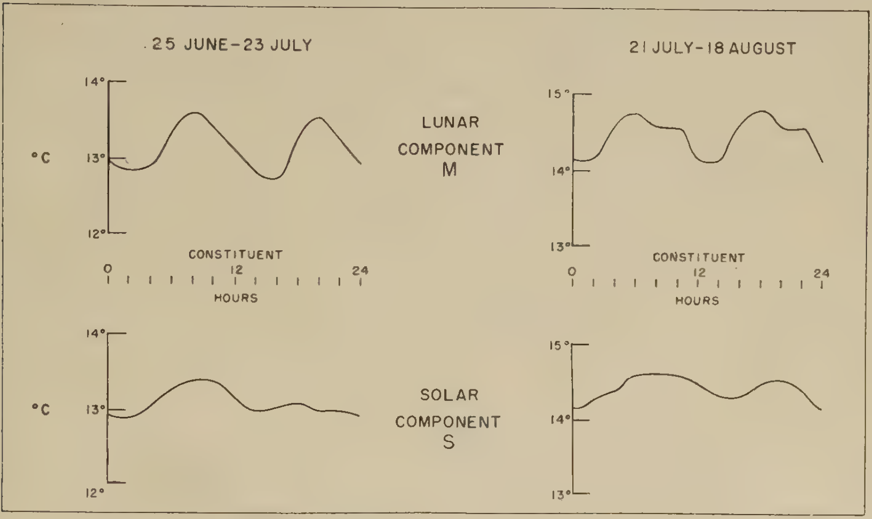

Figure 3. Harmonic lunar and solar components of temperature values for two overlapping 29-day periods.

To demonstrate the extent of this influence, harmonic analysis was carried out, using hourly temperature readings in place of the hourly tidal heights ordinarily employed in tidal analysis. This was done for M (lunar) and S (solar) components for two overlapping 29-day periods. The resulting curves, shown in Figure 3, reflect the tidal nature of the temperature fluctuations found in the raw data. (Similar semidiurnal oscillations in temperature were found in a 67-day record obtained by another recorder placed at a depth of 43 m under Texas Tower 4, off New York.)

It is apparent that advection through tidal action caused the short-term changes in bottom temperature. Data in the files of the Woods Hole Oceanographic Institution show a closely spaced series of bathythermograph lowerings made on 20. August 1952, in the area of Browns Ledge. Figure 4 A is a plan plot of temperature at a depth of 18 m drawn from these data. It shows a temperature structure which, under tidal action, could produce oscillations such as those observed by the recorder. Figure 4 B is a north-south profile passing less than 0·2 miles to the east of the Ledge, from these same data. It is expected that the amplitude of temperature fluctuation will show seasonal characteristics since the temperature difference between adjacent water masses will vary seasonally. One would expect little fluctuation at the time of the autumn overturn and possibly a reversal in phase during the winter, when inshore waters will be colder than those offshore.

To determine the net change in temperature for the period of record, the data were filtered by the Doodson averaging process ordinarily used to eliminate the effect of tidal periodicity on sea level. Four values per day at 0100, 0700, 1300, and 1900 hrs. were used. These values were then averaged to derive a daily mean which was plotted (Figure 5).

The abrupt temperature rise during the first 10 days of August is the most striking feature. The daily record of air temperature and cloud cover from

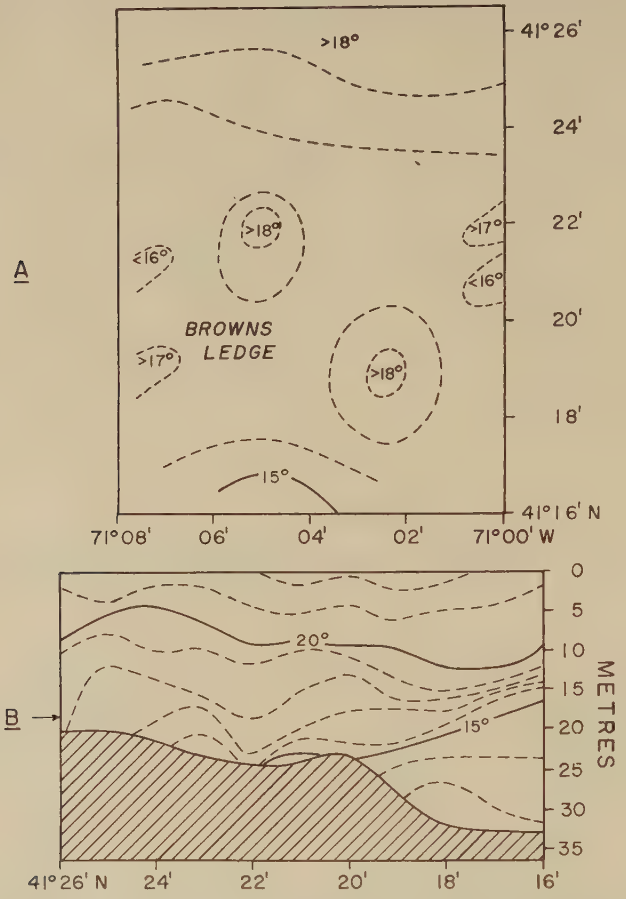

Figure 4. A. Plan plot of temperature at 18 m, 20. August 1952.
B. North to south temperature-depth profile near Browns Ledge from the same data.

Buzzards Lightship, 4 miles north-east of Browns Ledge, in no way suggested that the rise in bottom temperature was the result of local warming, and it was assumed that a change in the circulation had occurred. Consequently, winds for the period in question were read from the daily weather map. On the assumption that the warmer water would be coming from inshore, probably from Buzzards Bay, the daily wind values were vectored to show north-east and south-west components. These wind components are plotted below the temperature curve in Figure 5. The implication is that strong or persistent north-easterly winds at this time of year result in rising temperature when the warmer inshore water of the Bay is moved out over the Ledge, dominating the temperature regime.

Apparently the wind effect is felt throughout the water column, or at least as deep as 18 m. Had the north-east winds of early August moved only the surface layers, upwelling and consequent cooling should have occurred (see Figure 4 B), and the temperature reaction to the north-east/south-west wind components seen in Figure 5 would have been reversed.

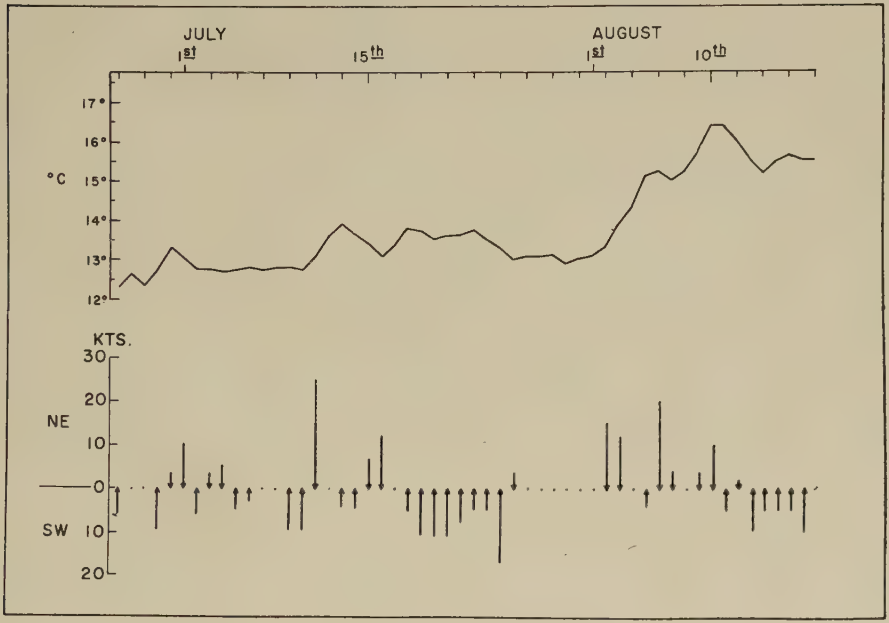

Figure 5. Mean daily bottom water temperature with tidal periodicity removed. Arrows show north-easterly/south-westerly components of daily winds.

By extension these results are of interest from the point of view of fisheries ecology. They demonstrate that in areas along the continental shelf where waters of different characteristics are juxtaposed, marked changes in a given physical parameter may be expected to occur with tidal periodicity. It is indicated that such abrupt changes are the result of advection rather than the modification of the local waters *in situ*, and that prevailing winds can contribute to the dominance of one water type over others for appreciable periods.

Acknowledgements

The writer is indebted to Harris B. Stewart, Jr., of the U.S. Coast and Geodetic Survey for putting the recorder in place and for making available the tidal current data used. The assistance and criticism of Arthur R. Miller, Joseph Chase, and Dean F. Bumpus is also gratefully acknowledged. This study was done under contract No. 14–17–008–62 with the U.S Bureau of Commercial Fisheries.

Summary

Hourly readings of bottom water temperature obtained on Browns Ledge off southern Massachusetts over a 56-day period were subjected to harmonic analysis. Tidal influence on temperature is demonstrated. The effect of winds on the temperature regime is shown.

Contribution No. 1090

Studies of Luminescent Flashing in Phosphorescent Bay, Puerto Rico, and in the Gulf of Naples using a Portable Bathyphotometer

BY

GEORGE L. CLARKE and LLOYD R. BRESLAU

Harvard University and Woods Hole Oceanographic Institution[*]

---

[*] Contribution N° 1090 from the *Woods Hole Oceanographic Institution.*

Bull. Inst. océanogr. Monaco, N° 1171, 4 mars 1960.

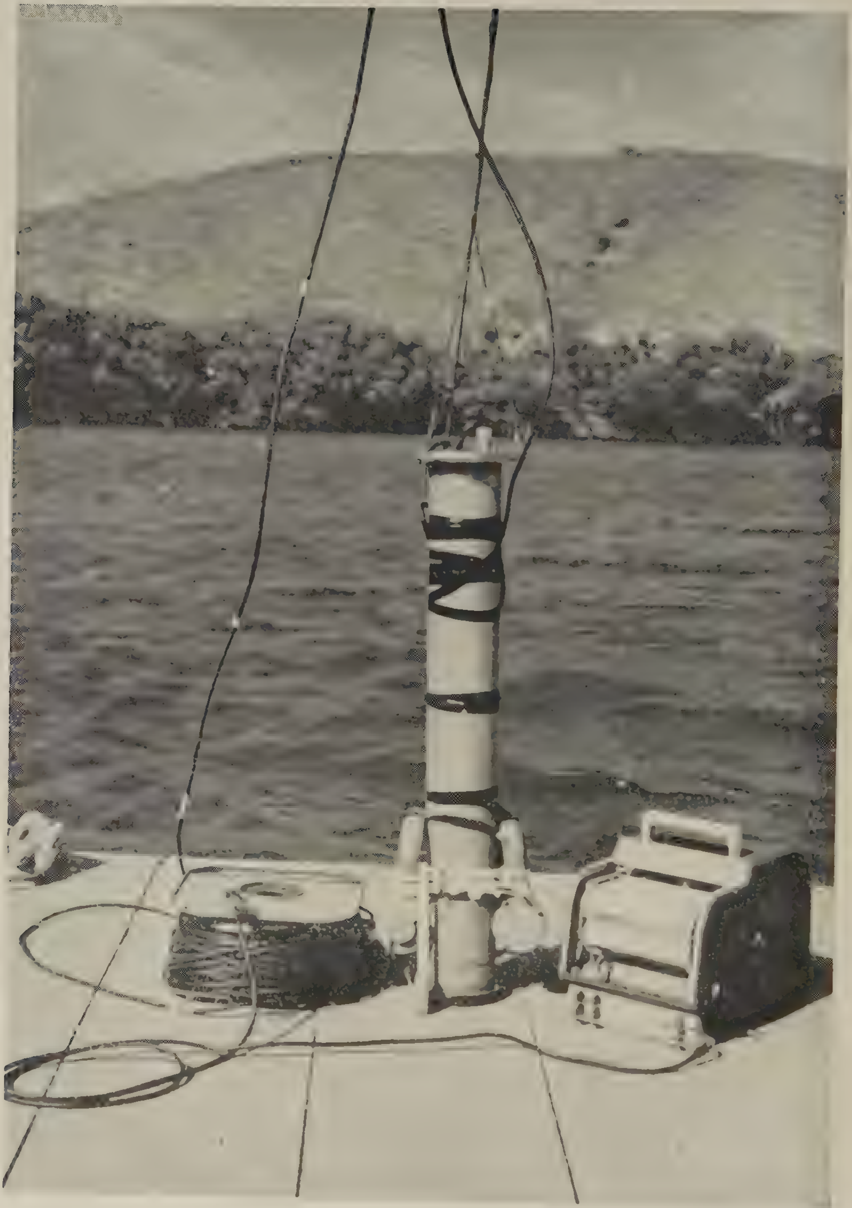

Fig. 1. — Portable bathyphotometer showing the underwater unit in the center (receiving window down) and the recorder on the right. Extra weights have been attached to the photometer tube and a 6-inch scale stands to the left.

Previous measurements of underwater illumination in the Atlantic and in the Mediterranean revealed the occurrence of unexpected amounts of bioluminescence at all depths below those at which light penetrating from the surface interferred, and demonstrated the wide variation in intensity and pattern of luminescent flashing at different levels in the water (Clarke and Backus, 1956; Clarke and Hubbard, 1959; and Clarke and Breslau, 1959). It was desired to extend the study of the production of bioluminescence and of its significance as an environmental influence to other areas, particularly those known to be especially rich in luminescent organisms. In order that such investigations need not be confined to situations in which a large research vessel was available, a bathyphotometer was constructed that can be transported by hand and operated to moderate depths from a boat without electric power supply or winch. In the present study, using the new portable bathyphotometer with 70 m of cable (Fig. 1), measurements of bioluminescence were carried out under a variety of circumstances in Phosphorescent Bay and adjacent waters of southwestern Puerto Rico, and in the Gulf of Naples on the southwestern coast of Italy.

We are greatly indebted to Dr. Juan A. Rivero, Director of the Institute of Marine Biology, University of Puerto Rico, for inviting us to use the laboratory and boat facilities at Maguey Island, La Parguera. We also wish to thank Dr. Rivero and his staff for valuable assistance given us during the progress of our work. We are obliged to Dr. Arturo Benavent, Jr., of Mayaguez and to Mr. Donald Erdman of the U. S. Fish & Wildlife Service for providing their personal boats for measurements at off-shore localities. Mr. W. A. Dawson kindly carried out the identification and enumeration of the plankton.

Indebtedness is similarly acknowledged to Dr. Peter Dohrn, Director of the Zoological Station at Naples, for his invitation to use the facilities and the collecting boats of the Station for the studies in the Gulf of Naples. Thanks are due to Dr. Dohrn, Mr. Andrew Packard, and other members of the Station, and to the boat crews for their kind help in the arrangements and in the execution of the measurements.

The authors wish to thank H. E. Edgerton for the use of facilities in the Stroboscopic Laboratory of the Massachusetts Institute of Technology and also V. MacRoberts and L. Hoadley for assistance in the construction and pressure testing of the instrument. We are indebted to Henry H. Fuller, Jr. for assistance in preparing the figures. The investigations in both localities were supported in part by funds from Research Grant N° 3838 of the U. S. National Science Foundation.

DESCRIPTION OF PORTABLE BATHYPHOTOMETER

The portable bathyphotometer is a modification of the underwater photomultiplier photometer described by HUBBARD (1956) and CLARKE and HUBBARD (1959) which in turn had been redesigned from the original model (WERTHEIM, 1954; CLARKE and WERTHEIM, 1956). The present instrument, like its immediate predecessor, records over a wide range of light intensity with great speed and on a single galvanometer scale. Low light levels and weak flashes are measured with the same accuracy as bright light due to the logarithmic response of the instrument.

The underwater housing is no stronger than necessary to withstand pressures down to 200 m, the maximum depth for which it was designed, and is supported by its own rubber-covered cable which is lowered by hand. A mechanically wound, field-type strip chart recorder is used without separate amplifier since a transistor amplifier stage has been added to the photomultiplier circuit. All circuitry, including high voltage elements, and batteries, are contained in the underwater unit so that only the final signal travels up the cable to the recorder. The instrument is extremely stable with respect to temperature since feedback circuitry and a thermistor have been employed. The provision of mercury switches and an external filter holder, together with the low battery drain, and very little drift or sensitivity variation, eliminates the necessity of opening the underwater photometer housing during normal operation at sea.

The Circuit employed.

The light receiver used is the RCA photomultiplier tube 5819. When the anode current is fixed at .01 μa, the total irradiancy range of 10^{-7} to 10μw/cm² implies a voltage variation of from 1150 v to 100 v respectively. The anode current is maintained by a vacuum tube in series with the high voltage supply which samples the anode current and adjusts the voltage across the photomultiplier bleeder chain. The type 959 « acorn » pentode employed is capable of cutting off 1000 v, and draws very little grid current.

One decade of direct current amplification is required to drive the chart recorder located on the deck. This is obtained by using a pair of type 2N117 transistors in the compound connected manner known as the « Darlington configuration ». The stabilization of such a circuit is excellent, owing to the nonlinear compensation of one stage by the other. Furthermore, as a consequence of the inherently large amounts of feedback involved, the circuit is relatively insensitive to changes in transistor parameters. The 2N117 is a N-P-N grown junction silicon transistor with a collector cutoff current of less than 1 μa at room temperature.

A Veco 43R1 thermistor was added for further temperature stabilization. A shunt resistance from base to ground vs. ambient temperature curve was empirically determined so as to give excellent temperature compensation. The thermistor effect was then shaped by a series parallel resistance network into the rectangular hyperbola which most approximated the desired resistance vs. temperature curve. The complete unit, when tested between 0° and 38° C, was found to experience a total sensitivity change of less than 1 %. The high voltage batteries (Eveready 493) and the transistor collector mercury batteries (Mallory TR-153R) will give at least 400 hrs of use. The filament mercury battery (Mallory RM-42R) will give at least 250 hrs of use. The circuit employed (Fig. 2) is the same as that described by Clarke and Hubbard (1959) except for the added transistor amplifier stage.

The calibration curve of the instrument (Fig. 3) shows the cable

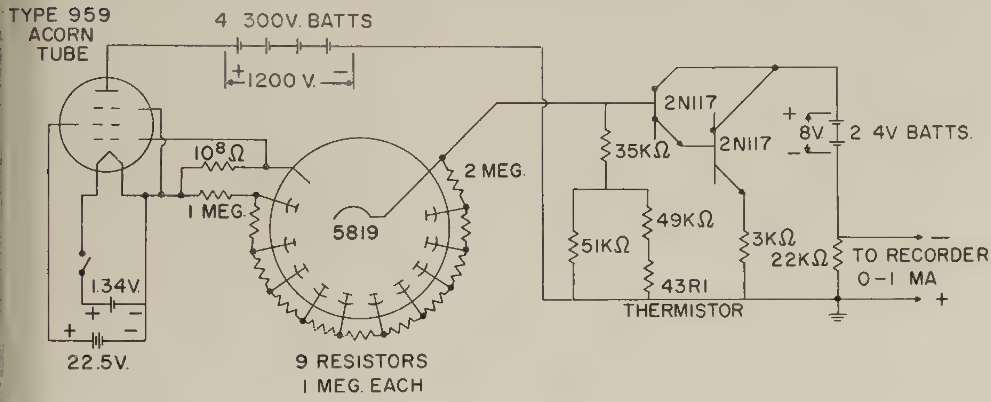
TYPE 959
ACORN
TUBE
4 300V. BATTS
+1200 V. −
$10^8\Omega$
1 MEG.
5819
2 MEG.
1.34V.
+ −
+ −
22.5V.
9 RESISTORS
1 MEG. EACH
2N117
2N117
35KΩ
49KΩ
51KΩ
43R1
THERMISTOR
3KΩ
22KΩ
+
8V.
2 4V BATTS.
−
TO RECORDER
0−1 MA
−
+

Fig. 2. — Circuit employed in the portable bathyphotometer.

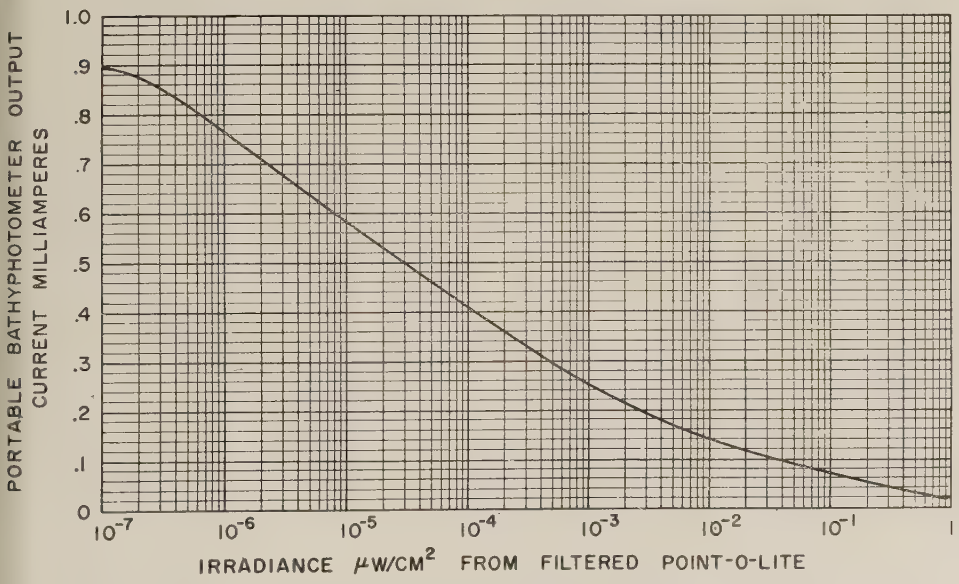

Fig. 3. — Calibration curve for the portable bathyphotometer.

current plotted against the incident energy flux from a « Point-o-lite » bulb, filtered by a Corning Blue-Green filter N° 4303. As stated in previous reports, this calibration is only valid for incident light of the same spectral character, and for a circuit employing a similar phototube. The RCA 5819 tube was chosen since it has low dark current and a spectral response peaked in the region of maximum transmission of sea water, namely, between wavelengths 400 and 500 μm (CLARKE and WERTHEIM, 1956), which is also the chief region of the bioluminescent emission of most pelagic organisms according to present evidence (BODEN and KAMPA, 1957; KAMPA and BODEN, 1957; NICOL, 1958).

Mechanical design.

The electronic units are built on a half cylinder of linen bakelite which slides into the underwater housing. The high voltage supply consists of four 300 v photoflash batteries. The 959 tube is mounted in a special socket located just ahead of the battery pack and behind the phototube socket. A mu-metal magnetic shield fits around the photomultiplier tube. The transistor amplifier and its batteries are completely contained in a test tube which is secured along side the photoflash batteries.

The underwater housing consists of a 30-inch length of type 304 stainless steel, welded tubing of outside diameter 4 inches and wall thickness 1/12 inch. Flanges have been welded on each end and upon these the end caps are bolted and sealed with « O » rings. The front end cap, made of 3/8 inch plexiglass, serves as the photometer window, and provides a 90° field of view. The rear end cap, made of 3/8 inch stainless steel, is provided with a Conax packing gland through which the conducting cable is led in. In measurements subsequent to the present ones the underwater unit has been operated down to 200 m without leak or failure.

Since the intensity of full sunlight is 4 decades above the upper limit of the useful response of the photomultiplier tube, a watertight filter holder containing a Kodak series 9 neutral filter of density 4 is placed over the receiving window of the photometer when it is to be used near the sea surface in daytime. The filter holder is made of plexiglass provided with an « O » ring seal which allows it to be mounted on the outside of the window, without opening the main tube of the photometer.

Four-conductor shielded microphone cable (Belden 8424) with outside diameter of .295 inch is used for electrical conduction and mechanical support. Although only two electrical conductors are required, the four-conductor type was selected as stronger. A sample of this cable, tested in the laboratory, broke at 240 lbs. The underwater unit of the photometer weighs 20 lbs in air and is almost weightless in water. In use at sea additional weights of about 20 lbs are fastened around the lower end of the tube to keep it in a vertical position. The underwater unit may be hung from either end by means of a bridle connected to a loop in the cable provided with a metal thimble. In the upright position the photometer is used to measure downward passing light from the surface (from which transparency may be determined). The inverted position is ordinarily used for the investigation of bioluminescence since the effect of surface light is then minimized.

The Deck Recorder.

A Texas Instruments, Inc. single channel rectilinear galvanometric recorder called the « Recti/Riter » is used. This high-speed strip-chart recorder weighs only 30 lbs, and contains a spring clock mechanism wound by hand. The instrument is galvanometer actuated with a 1,500 ohm input resistance and it requires a source resistance of 20,000 ohms for critical damping. Since the input current required for a full scale deflection of 4.5 inches is 1 ma, the signal emanating from the underwater photometer may be employed directly. The pen speed for full scale deflection under critical damping conditions is .25 sec. With the usual chart speed of one foot a minute, frequencies associated with luminescent flashing are adequately resolved. A more detailed account of the portable bathyphotometer has been given by Breslau (1959).

OBSERVATIONS AT PHOSPHORESCENT BAY, PUERTO RICO

Phosphorescent Bay is located on the south coast of Puerto Rico about 2 miles east of Maguey Island and the village of La Parguera, which is 15 miles SE of the city of Mayaguez (Fig. 4). The bay has an approximate area of 19 hectares (46 acres), an average depth of 3.5 m, and an outlet to the sea about 100 m wide. The brilliant luminescence, for which the bay is famous and which persists throughout the year, is due chiefly to the flashing of myriads of dinoflagellates. In abundant populations these luminescent microorganisms flash spontaneously to some extent (perhaps due to collisions with each other), and when agitated by waves or solid objects, produce showers of tiny lights in a

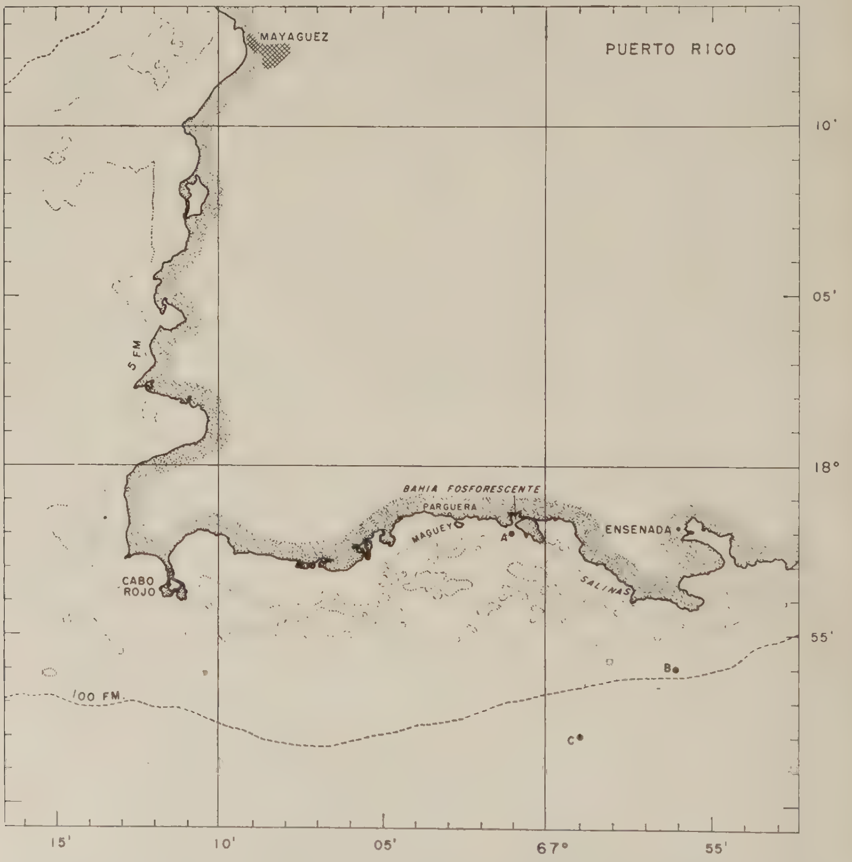
MAYAGUEZ
PUERTO RICO
10'
05'
18°
55'
5 FM
BAHIA FOSFORESCENTE
PARGUERA
MAGUEY
A
ENSENADA
SALINAS
CABO ROJO
B
100 FM
C
15'
10'
05'
67°
55'

FIG. 4. — Southwest portion of Puerto Rico showing the location of Maguey Island, Phosphorescent Bay (Bahia Fosforescente), and of the stations occupied outside the bay.

remarkable display of underwater fireworks. If the water is stirred slowly, as by moving the hand through it, the luminous discharges of individual organisms can easily be distinguished with the naked eye and appear like shining grains of wheat. If the water is moved rapidly, the points of light blur into bright sheets and bands. When a motor boat enters Phosphorescent Bay on a dark night, the bow waves look like billows of snow. Rapidly swimming fishes cause the organisms which they disturb to luminesce, thus outlining their bodies with light and leaving behind a trail of sparks. A school of fishes darting away from the boat gives the appearance of a volley of underwater rockets.

Investigation of the phytoplankton of Puerto Rican waters by MARGALEF (1957) has indicated that whereas blooms of diatoms occur irregularly off shore, rich populations of dinoflagellates are characteristic of the coastal waters, especially in the mangrove areas. *Pyrodinium bahamense* (Fig. 5) has generally been found to be the most abundant dinoflagellate in Phosphorescent Bay and chiefly responsible for its luminescence.

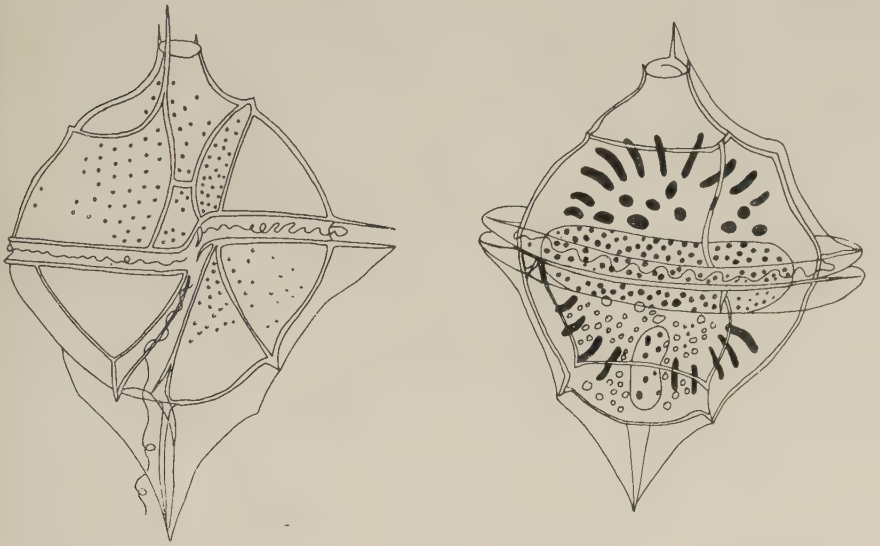

FIG. 5. — *Pyrodinium bahamense*, a very abundant luminescent dinoflagellate in Phosphorescent Bay. Left : ventral side with flagellum groove lying in the middle; right : dorsal side. (Modified from PLATE, 1906)

Intriguing questions arise as to what factors underlie the great abundance of the phytoplankton and why this particular species continues to predominate in relatively constant numbers throughout the year. No doubt, as has been suggested by MARGALEF and GONZALEZ (unpublished Ms), the vertical circulation of the water in conjunction with the active swimming of certain species is partly responsible. Increased water density in shallow areas due to high rate of evaporation may cause the water to sink and flow out at the bottom while the inflow is chiefly at the surface. Those dinoflagellates which maintained themselves near the surface would tend to become concentrated in the bay. Whether or not such a « plankton trap » is effective in this instance, explanation is needed for the source of nutrients to permit the production and maintenance of the observed high standing crop. BURKHOLDER and BURKHOLDER (1958)* reported that the phytoplankton in Phosphorescent Bay was about 10 times as abundant as in the waters outside. They suggest that this rich standing crop is supported by mineral nutrients and vitamins supplied by drainage from the surrounding land, plus some vitamin B_{12} synthesized *in situ*. As long as this exogenous supply of nutrients remains relatively high and constant, a continuing abundant standing crop of phytoplankton could be maintained. The particular circumstance which favors the continuing predominance of *Pyrodinium bahamense* remains to be discovered. The species and abundance of dinoflagellates in Phosphorescent Bay on one day of the present study are given in Table 1.

TABLE 1

Dinoflagellates in 1 liter of surface water.
Phosphorescent Bay, Puerto Rico, Feb. 9, 1959 at 2200 hours.

Pyrodinium bahamense	7600
Peridinium breve	7000
Prorocentrum micans	2600
Ceratium hircus	1700
Pyrophacus horologicum	210
Peridinium divergens	120
Ceratium fusus	105
Gymnodinium sp. (*?splendens*)	50
Dinophysis caudata	25
Gymnodinium lohmanni	25

Transparency.

Measurements of transparency in Phosphorescent Bay and at two stations outside the bay were made near the middle of the day using the Clarke marine photometer containing a Weston photronic cell. This older instrument is convenient for the very shallow depths and high light intensities involved, although the new portable bathyphotometer with neutral density filter of value D = 4 could have been used. The water in the bay was found to be optically homogeneous with an average extinction coefficient of $k = 0.43$ from the surface to the bottom at 4 m (Fig. 6). About 18 % of the incident light reached the bottom. Just outside the bay, at Station A, the water was somewhat more transparent near the surface and very much more transparent in the lower stratum,

---

* Another report, now in press, is: « Measurements of productivity on the coral reefs, turtle grass flats, and the Bahia Fosforescente of Southern Puerto Rico », by H.T. ODUM, P. BURKHOLDER, and J. RIVERO. *Publication of the Institute of Marine Science of Texas*, vol. 6, 1959.

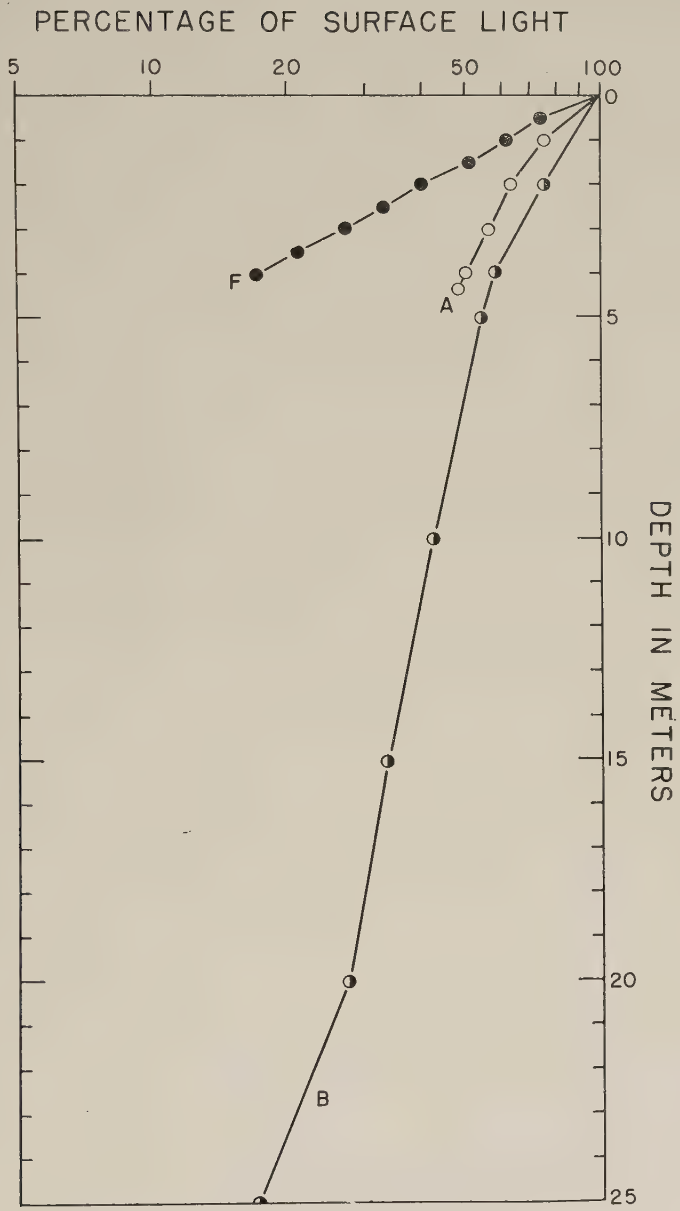

Fig. 6. — Transparency measurements : (F) in Phosphorescent Bay, (A) outside entrance at Station A, Feb. 7, 1959, both near noon, bright sun, cumulus clouds, wind force 2; and (B) outside reefs at Station B, Feb. 8, 1959, 1400 hrs, bright sun, cumulus clouds, wind force 4.

with an extinction coefficient of k = 0.11 from 2 m to the bottom at 4.5 m. At Station B, about 1.8 miles south of Point Brea, the coefficient changed from k = 0.13 in the surface stratum to k = 0.053 from 5 m to 20 m, with somewhat lower transparency near the bottom at 25 m. The clarity of the water thus varies tremendously within short distances. The transparency in Phosphorescent Bay was lower than Woods Hole Harbor, that outside the bay was comparable to values on the Continental Shelf farther north, and the clearest water at Station B approached the value reported for the Caribbean Sea (CLARKE, 1954, Table 14).

Bioluminescence at surface.

Bioluminescence at the surface at night as measured from above the water will first be described. The bow wave of the *Physalia* (a 6 m flat-bottomed, outboard motor boat), when travelling at fixed speeds, was used as providing standard amounts of agitation of the surface water for this series of measurements. The portable bathyphotometer, directed vertically downward, was lashed to the gunwale of the boat in such a position that its receiving surface was 50 cm above the breaking portion of the bow wave. The radiation received consisted of the luminescence emanating from the disturbed organisms plus weak skylight reflected from the water surface (there was no moon). A continuous record was taken from a point outside the bay, through the narrow entrance, into the middle of the bay, and out again. Subsequently the boat reentered the bay and ran up one of the canals leading inland through the thick stand of mangroves along the inner shore of the bay.

The record (Fig. 7) shows the intensity of the upward-passing light outside Phosphorescent Bay before the start (a), when the water surface was unbroken, and its subsequent increase as the boat accelerated to half-speed (b) and then entered the bay at the same speed. The rise in intensity was partly due to the greater reflection of skylight from the foam of the bow wave and partly due to increased luminescence. The amount of radiation contributed by reflected skylight remained the same thereafter but patches of intensified luminescence, which also could be discerned by the eye, were encountered at (c) and (d). At (e) the boat reached the beginning of the narrows and at (f) entered the bay itself where a further sharp increase in brilliance occurred. Advance of the engine throttle at (g), bringing the boat to its full speed of about 10 knots at (h), resulted in a maximal emission of light from the bow wave of 3×10^{-2} μw, or about $4 \times 10^{-7} \times$ full sunlight. Since this value is just below the threshold for human color vision, the light appeared whitish to the eye, although its spectrum may have been peaked in the blue, as shown for certain other dinoflagellates (NICOL, 1958). This amazing display of luminescence was more brilliant than the moonlight recorded a few nights later with the photometer in the air, oriented directly toward the quarter moon. On leaving the bay the luminescence again dropped off to the previous value (i) and the record showed irregular fluctuations of greater amplitude, indicating the presence of a different type of luminescent organism (j). In the canal among the mangroves luminescence produced at half-speed (k) was only one-tenth as intense as in the middle of the bay. When the boat was slowed (ℓ) and stopped (m), the upward-passing light was recorded as 3 × 10^{-5} μw, or about the same as outside the bay before the start.

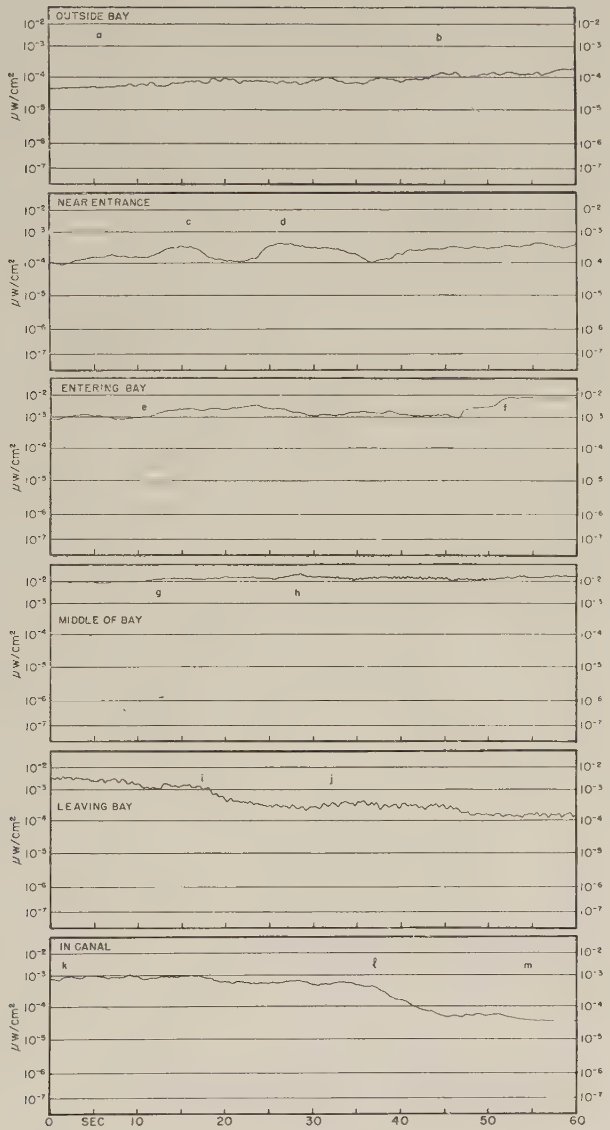

FIG. 7.—Light recorded by portable bathyphotometer, receiving surface downward, 50 cm above bow wave of motorboat, while entering Phosphorescent Bay, Feb. 6, 1959, 2030 to 2100 hrs, no wind, clear, bright stars, no moon. For explanation see text.

Bioluminescence in water.

Excerpts from the first series of measurements extending into the water in Phosphorescent Bay, made on Feb. 5 about two hours after sunset, are presented in Fig. 8. The intensity of skylight received by the bathyphotometer directed vertically upward in air (a) was 7×10^{-4} $\mu w/cm^2$. When inverted and held with the receiving window 2 cm over the water surface, a luminous flux of about 1×10^{-4} μw was recorded (b). Since this value for the upward light is greater, relative to the downward light, than could be accounted for by reflection alone from the unbroken water surface, or by reflected plus upward-scattered light from beneath the surface (POWELL and CLARKE, 1936), a large part of it must be due to light of luminescent origin passing out from the water. This interpretation was substantiated by lowering the photometer until its head was just under water (thus eliminating reflection) and finding only a trivial reduction in light, as recorded just before (c). When lowered to 1 m and held as still as possible, following (c), light was reduced somewhat at first, but increased as slight motion stimulated numbers of luminescent organisms to discharge sporadically. Extra stimulation of the organisms was brought about at (d) by raising and lowering the photometer rapidly about 25 cm. This procedure was followed at other depths and on other occasions in order that the intensity of luminescent discharge could be compared during a standard amount of agitation. At a depth of 2 m there was more spontaneous luminescence (e), but during agitation (f) the same maximal light was recorded. At 3 m intensities were generally lower when the photometer was still (g), agitated (h), or moved by the wake of a passing boat (i), indicating a lower concentration of luminescent organisms. Illumination was greatly reduced at 4 m when the photometer was still, due to the nearness of the bottom, but when organisms were stirred up from the bottom (j), flashes 1000 × the background were recorded. The response dropped to the dark level of the photometer when it struck the bottom mud at 4.2 m (k).

A second study of the light conditions in Phosphorescent Bay made on Feb. 9 (Fig. 9) revealed similar values for downward-passing (a) and upward-passing light over the water surface (b) and for upward-passing light under the surface (c). When the photometer was being lowered from one depth to another, the resulting turbulence caused a strong discharge of luminescence, as at (d). At the 2 m level the instrument was raised about 30 cm, held steady for about 5 sec, and then lowered again. This procedure was carried out three times as indicated by the broken line below the record which represents the motion of the photometer. Raising the photometer evoked an immediate and strong increase in light received (e) because the turbulence, and resulting luminescence, was produced immediately below the receiving window. Since the turbulence and the response of the organisms are short-lived, luminescence soon decays once the motion of the photometer is stopped. Lowering the photometer (f) resulted in a smaller and delayed peak in the record (g) because the turbulence was then produced above the photometer

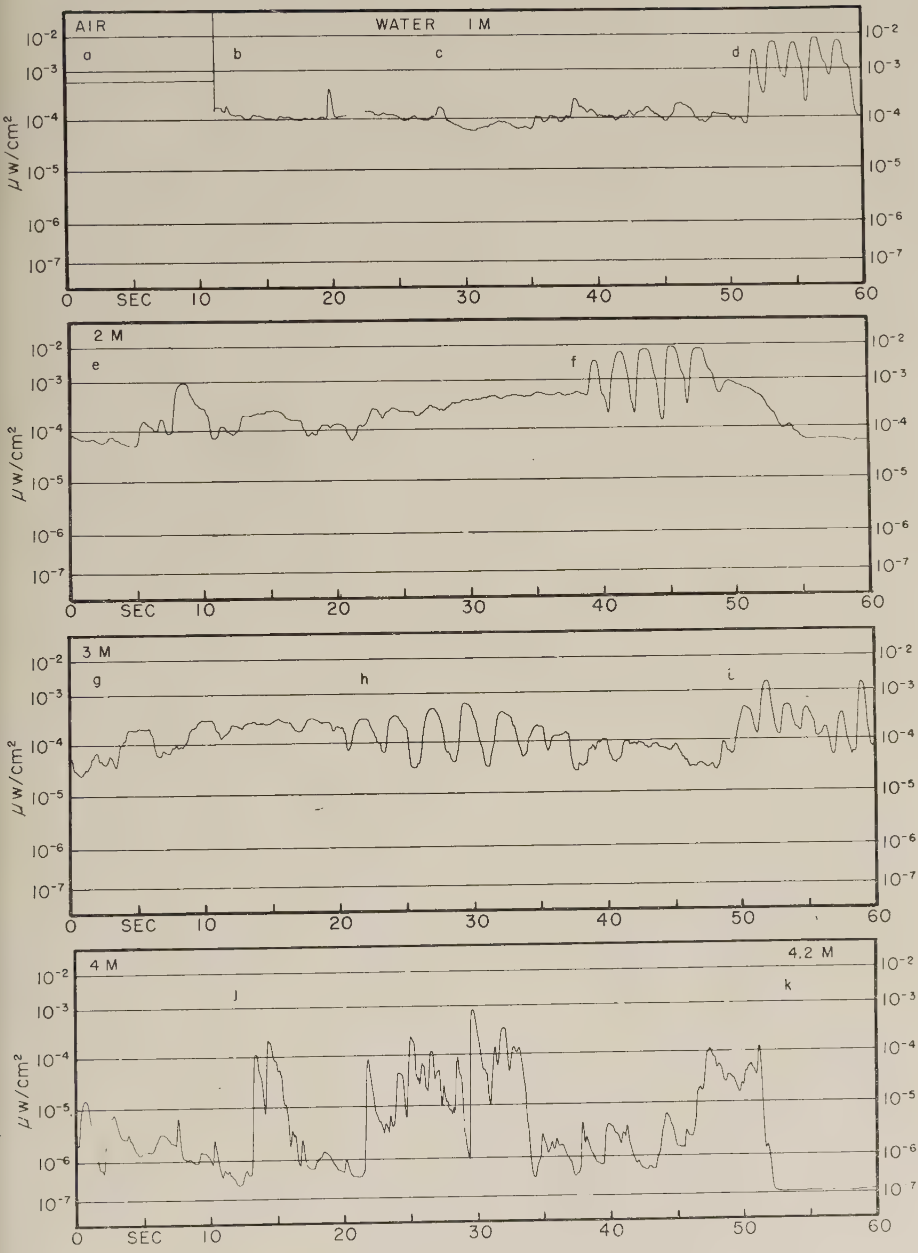

FIG. 8. — Light records in Phosphorescent Bay, Feb. 5, 1959, 2030 hrs, wind force 2, clear, no moon. For explanation see text.

and more time was required for the disturbance of the organisms to reach a point where their light could enter the window. The intensity of background light, when the photometer was still, dropped off regularly

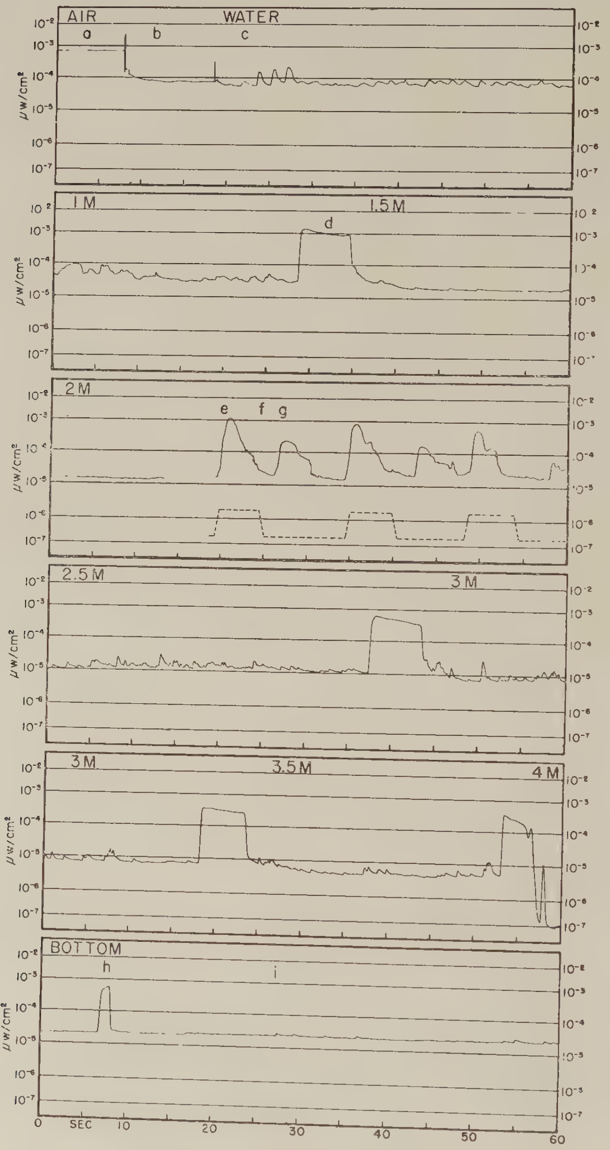

Fig. 9. — Light records in Phosphorescent Bay, Feb. 9, 1959, 2045 hrs, wind force 1, clear, no moon.

until at 3.5 m it was less than 0.1 × that just under the surface. Since this is a greater reduction than would be accounted for solely by the extinction of scattered skylight by 3.5 m of water, a smaller amount of spontaneous luminescence is indicated in the lower strata. At 4 m the head of the photometer touched the bottom and the response dropped to the dark level. The last record in Fig. 9 was made with the photometer lying horizontally in a cradle on the bottom. The response at (h) was produced by the beam of a flashlight directed into the water from the boat. The succession of small peaks beginning at (i) resulted from the spontaneous flashes of organisms living on or near the bottom.

For comparison with the foregoing, excerpts from records made about 0.5 mile outside the entrance to Phosphorescent Bay at Station A are presented in Fig. 10. The night skylight measured in air with the upright photometer (a) was the same, but the upward-passing light reaching the window of the inverted instrument 20 cm above the water (b) and 3 cm below the surface (c) was weaker due to the smaller amount of spontaneous luminescence. The records obtained at this level and at greater depths differ also in indicating the occurrence of more widely spaced and longer flashes (d and e), presumably emitted by larger animals. At 2 m depth the standard agitation was given the photometer, but the resulting luminescence (f) was far weaker and less sustained than that recorded inside the bay. When the instrument touched bottom (g), light was reduced, but the coarser bottom material at this more exposed location prevented the photometer from making light-tight contact with the bottom as had been the case with the mud in the Bay. Movement of the photometer near the bottom evoked the brightest flashes (after g and h) observed at this locality.

Exploration was made three nights later of Moncio Jose Bay, another shallow body of water largely cut off from the outside water by reefs and small islands and located about 2 miles west of La Parguera. This bay is also known for its remarkable luminescence but the display was not believed to occur as regularly nor to be as brilliant as in Phosphorescent Bay. The first-quarter moon was visible at an altitude of about 20° during the measurements in Moncio Jose Bay (Fig. 11). This fact accounts for the higher radiation value reported by the photometer when held vertically upright (a). When oriented directly toward the moon (b), an intensity of 6×10^{-3} μw was recorded. The intensity of upward-passing light received by the inverted photometer just over the water (c) and shaded from the moon was about the same as in Phosphorescent Bay. A somewhat smaller value was obtained when the photometer head was lowered beneath the surface due probably to the lower amount of luminescence in the water. Rapid agitation of the photometer at 1 m depth (f) and slow agitation at 1.5 m (h and i) resulted in luminescent discharges, as before, but the peak intensities were mostly much lower than in Phosphorescent Bay. The last record shows that the intensity of light received by the inverted photometer from the bow wave, including the reflection of moonlight, after starting (j) and accelerating to full speed (k) was also much less than had been observed with the same technique in Phosphorescent Bay with no moon.

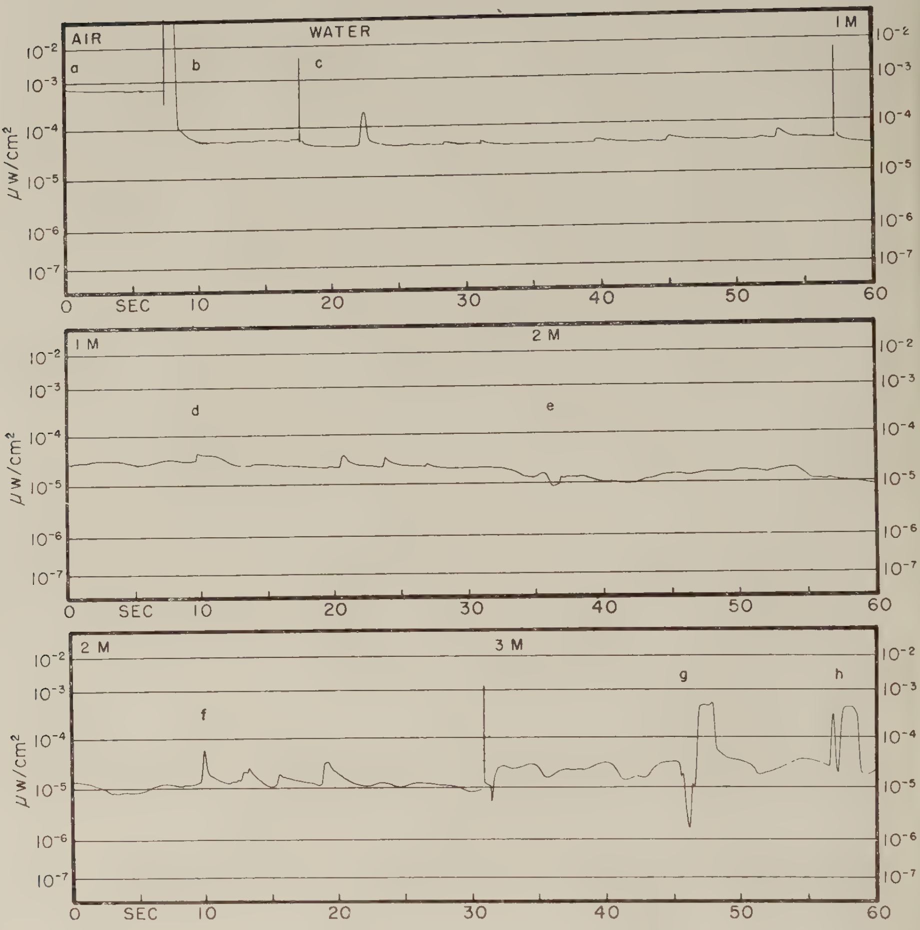

FIG. 10. — Light records at Station A outside Phosphorescent Bay, Feb. 4, and 9, 1959, 2040 to 2200 hrs, wind force 1-2, clear, no moon.

For comparison with the foregoing studies in and near shallow bays, records of bioluminescence were made from 5 m to 50 m at Station C, 5 miles south of Salinas Cove, in the clear water beyond the 100 fathom curve (Fig. 12). The heavy rolling of the sloop *Booby*, from which the observations were conducted, caused by steep wind waves, provided continuous agitation of the photometer by moving the supporting cable up and down with a period of about 4 sec. The close correspondence between bursts of luminescence and the motion of the photometer is indicated in the record at 10 m on which the ship's roll, traced at the time, is represented by the broken line below the curve for light. The ambient light between flashes, as recorded by the inverted photometer, had an intensity of about 4 × 10^{-5} µw/cm² at a depth of 5 m. The background light level dropped regularly at successively greater depths to a value of 1 × 10^{-5} µw at 50 m. This small change is consistent with the high transparency of the water. The intensity of the luminescent discharges varied over a range of more than 10 × at all levels, but the

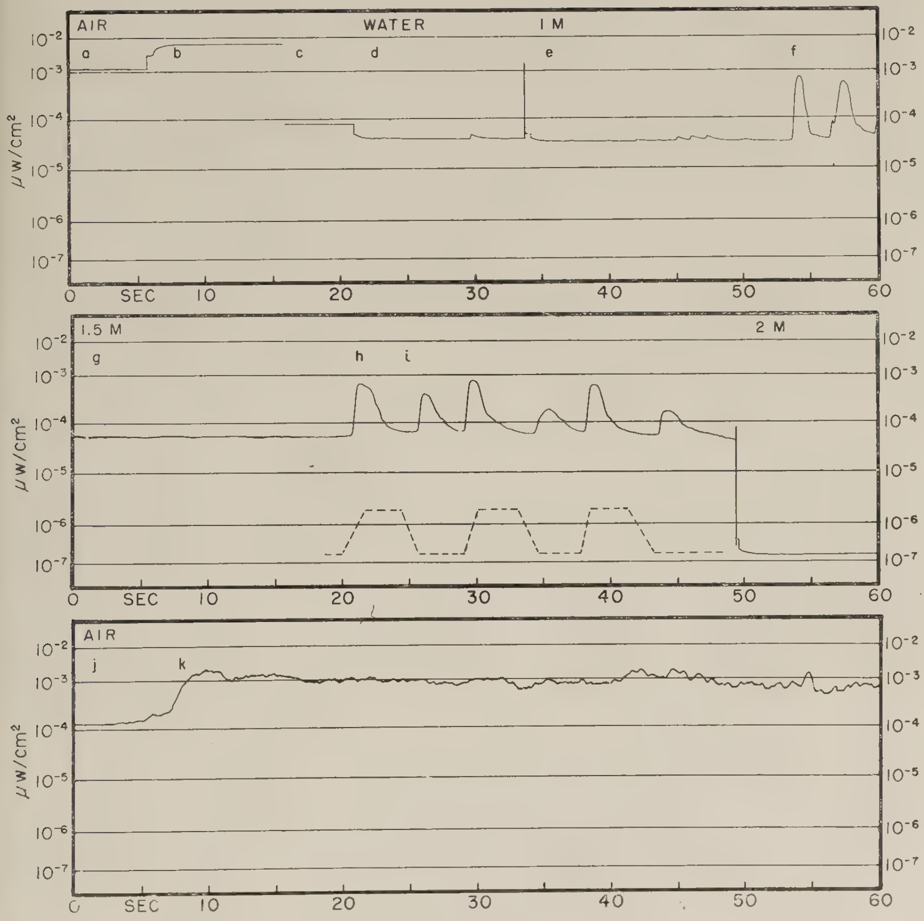

FIG. 11. — Light records in Moncio Jose Bay, Feb. 12, 1959, 2040 to 2110 hrs, no wind, clear, first quarter moon.

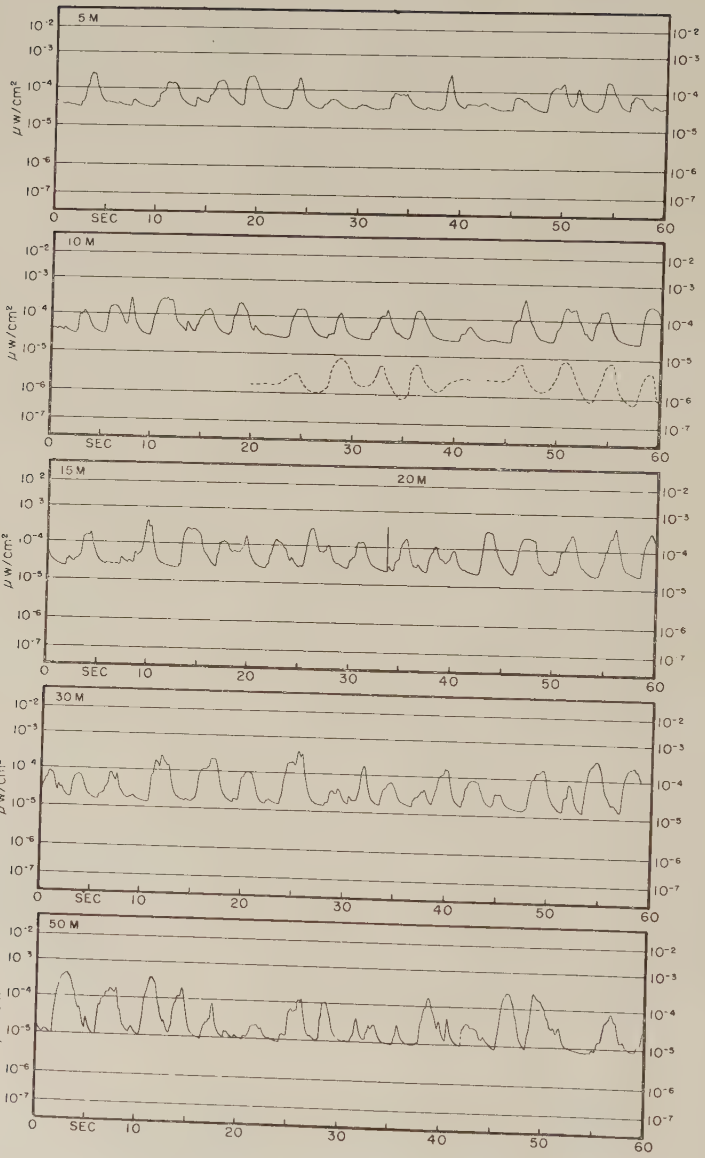

FIG. 12. — Light records at Station C about 5 miles south of Salinas Cove, Feb. 11, 1959. Depth more than 200 m, 0525 to 0530 hrs, wind force 3, sea moderate, clear, no moon.

maximum values at each level were near 4 × 10^{-4} μw. These observations indicate the presence of a relatively uniform population of luminescent organisms in the upper 50 m at this station with maximum intensity only about 0.04 × of that in Phosphorescent Bay.

OBSERVATIONS IN THE GULF OF NAPLES

The Gulf of Naples presents a sharp contrast to the bays of Puerto Rico discussed above, as it is much larger and deeper with clearer water penetrating well into the inner portion. Quantitative records of bioluminescence were made by the senior author during April, 1959, using the same portable bathyphotometer, at four stations southwest of the city of Naples in water ranging from 50 to 300 m deep (Fig. 13). Although no daytime measurements of transparency were made in the present study, the water in the Gulf is known to be highly transparent, particularly at localities away from commercial harbors. South of Capri (at J in Fig. 13) JERLOV and PICCARD (1959) found an extinction coefficient of k = 0.048 for the depth interval 100-300 m with even clearer water nearer the surface. Off Monaco a value of k = 0.072 for the stratum above 80 m and much lower values for the deeper levels were reported by CLARKE and BRESLAU (1959).

During the month following the present study IVANOFF (1959) carried out preliminary measurements of the light-scattering and polarizing properties of water in the Gulf of Naples. At a point near our Station 2 he found the coefficient of diffusion to decrease from the surface to about 40 m and then to increase at greater depths, whereas polarization reached a minimum at 10 m. However, since considerable variation existed, a more extensive investigation must be made before the biological or hydrographic factors controlling these properties can be identified. During the period of the present study little thermal stratification occurred in the upper layers where bioluminescence was measured. At Station 3, for example, on April 24 at 2120 hrs the temperature dropped at a constant rate from 14.7° C at the surface to 14.0° C at 60 m, then more rapidly to 13.6° C at 70 m, but more slowly thereafter to 13.4° C at 100 m.

Measurements of bioluminescence.

The first series of measurements was made on April 23 at Station 1, on Benda Palummo Bank, beginning about 2 hrs after the time of moonrise, but the moon, although full on that day, was obscured first by hills to the east and then by overcast sky. The light received by the upright photometer in air had an intensity of about 1 × 10^{-2} μw/cm² (a in Fig. 14). The fact that this is more than 10 × the corresponding value obtained in Puerto Rico is probably accounted for partly by moonlight penetrating through the cloud cover and partly by sky glare from lights in Naples and other settlements along the shore. When the photometer was inverted and held just over the surface (at b), the intensity of the upward-passing light was 4×10^{-4} μw, or about 4 % of the downward-passing light. In the water at 2 m the inverted photometer reported an upward luminous flux of about 2×10^{-4} μw on which sporadic luminescent flashes were superimposed (c). The intensity of the upward light dropped steadily with increasing depth to a value just over 1×10^{-5} μw at 40 m. A large number of flashes, ranging in intensity from just above the background to as high as 10^{-3} μw/cm², was recorded at each depth. In addition to irregularly occurring spontaneous flashes, the tracings clearly show a periodicity due to the luminescent discharge of organisms disturbed by the movement of the photometer as the boat rolled. The dark level for the instrument was at 10^{-7} μw/cm² for all measurements in the Gulf of Naples.

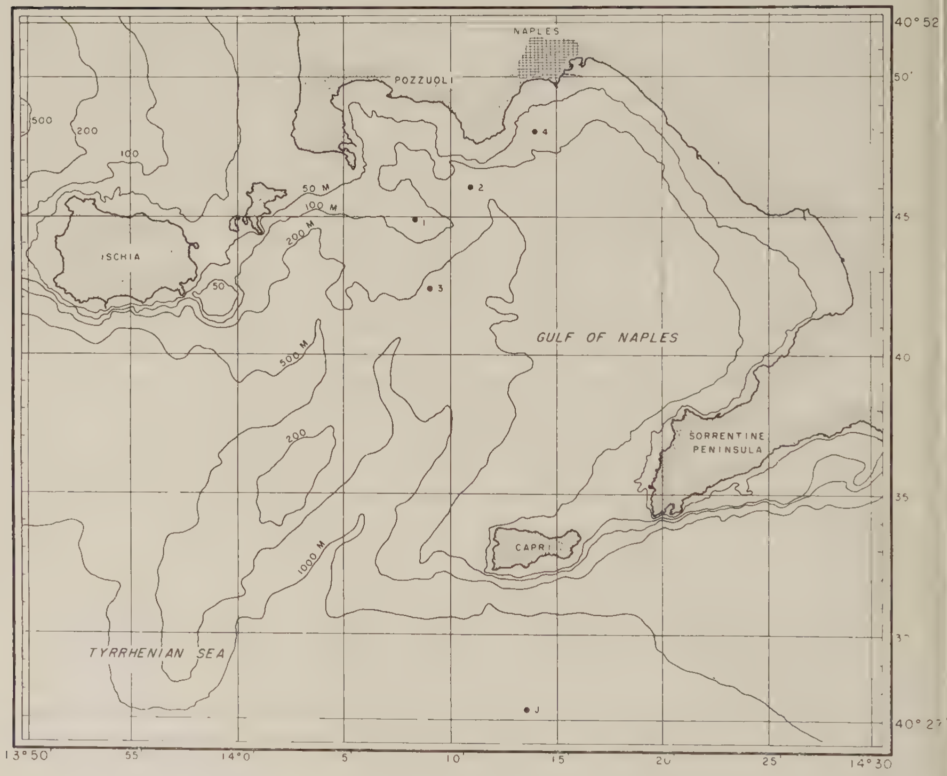
NAPLES
POZZUOLI
500
200
100
50 M
100 M
200 M
ISCHIA
50
• 4
• 2
• 1
• 3
GULF OF NAPLES
500 M
SORRENTINE PENINSULA
200
1000 M
CAPRI
TYRRHENIAN SEA
• J
40° 52'
50'
45
40
35
30
40° 27'
13° 50'
55'
14° 0'
5'
10'
15'
20'
25'
14° 30

FIG. 13. — Gulf of Naples showing the location of Stations 1-4 in the present study and Station J occupied by JERLOV and PICCARD (1959).

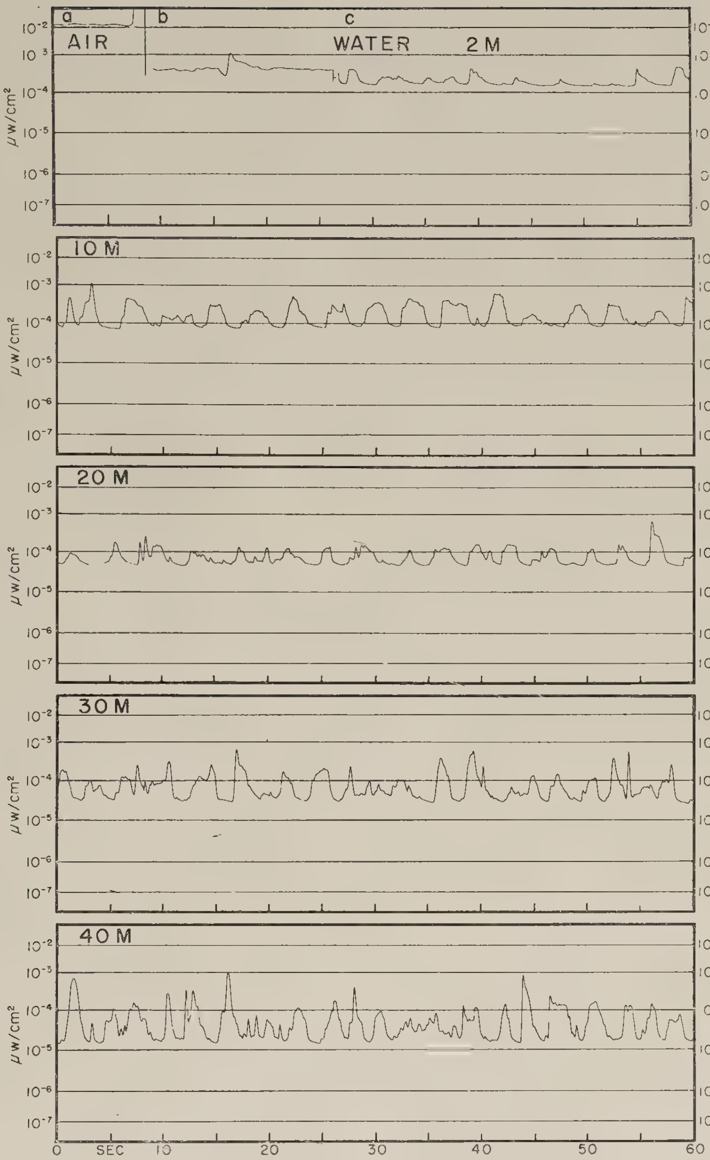

Fig. 14. — Light records at Station 1, Gulf of Naples, April 23, 1959, 2015-2040 hrs, wind force 1, sea slight, overcast, moon not visible. Bottom depth 50 m. For explanation see text.

Observations were continued later the same evening at Station 2, about 1 mile south of La Gaiola Light, in deeper water. Ambient light at all levels was considerably higher than at Station 1 due to the greater altitude of the moon and the thinning of the clouds. The intensity of upward-passing light at 5 m (a in Fig. 15) was 4×10^{-4} μw-cm and agitation of the photometer by rapid vertical movements with amplitude of about 50 cm (at b) evoked luminescent discharges stronger than 1×10^{-3} μw. In air just over the surface the upward light (c) was 2×10^{-3} μw and the downward light (d) was 4×10^{-2} μw. At 10 m the inverted photometer moved only by the slight rolling of the boat (e), reported an ambient flux of 3×10^{-4} μw above which a few sporadic flashes were recorded. Standard agitation (f) resulted in luminescent discharges reaching an intensity of 2×10^{-3} μw. At successively greater depths the background illumination dropped off to a minimum flux of 4×10^{-6} μw at 70 m. Standard agitation produced flashes of slightly lower intensity at 30 m (h) and at 50 m (i), and considerably lower values at 70 m (i'). In the sections of the records made without added agitation the frequency of flashing increased with depth to a maximum of about 60 per minute at 60 m, but the intensity of the maximum flashes remained just short of 10^{-3} μw at most depths.

Observations made in much deeper water at the head of the eastern branch of Ammontatura Canyon (Station 3) consisted of one series made before and one after the appearance of the moon on April 24 under conditions of slight sea, and a third series on April 27 with moderately rough sea. Records from the first of these (Fig. 16 a) revealed a considerable amount of luminescence at all depths with no agitation of the photometer beyond that produced by the slight motion of the boat.

Strata of noticeably less luminescence were detected at 10 m and 60 m. One of the brightest flashes with intensity of 7×10^{-4} μw/cm^2 was recorded at 70 m. The second series (Fig. 16 b) made from 60 m to the surface shows the effect of the moon in strengthening the upward-scattered light at every depth. At 60 m, for example, the intensity rose from 3×10^{-6} to 6×10^{-6} μw/cm^2, and at 5 m it rose from 4×10^{-5} to 2×10^{-4} μw/cm^2. During the second series considerable luminescent activity was recorded at 60 m but at shallower depths the rise in background illumination apparently obscured many of the smaller flashes. The fact that luminescent animals were still present and capable of flashing at all levels is demonstrated in the last 10 or 15 sec of each excerpt when standard agitation was given to the photometer (as at f). The intensity of the upward light just under the water surface (a) and just above it (b) may be compared with the luminous flux received by the photometer directed toward the zenith (c) and toward the moon (d). In the third series the ambient light in air (intensity 1×10^{-3} μw/cm^2) and in the water at all depths (Fig. 17) was lower because of the absence of the moon, but more luminescence was recorded at all levels, probably due chiefly to the stronger movement of the photometer caused by rougher sea conditions, but possibly due to the presence of a different planktonic population. Adding the standard agitation at the end of the observation

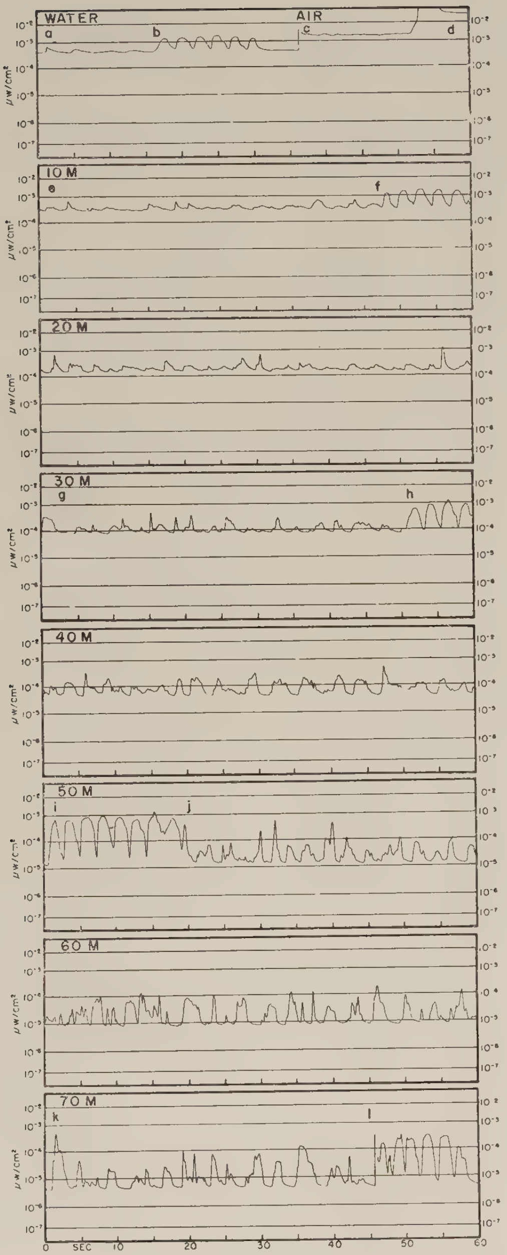

FIG. 15. — Light records at Station 2, Gulf of Naples, April 23, 1959, 2151-2237 hrs, wind force 1, sea slight, mostly overcast, moon occasionally visible through clouds. Bottom depth 180 m.

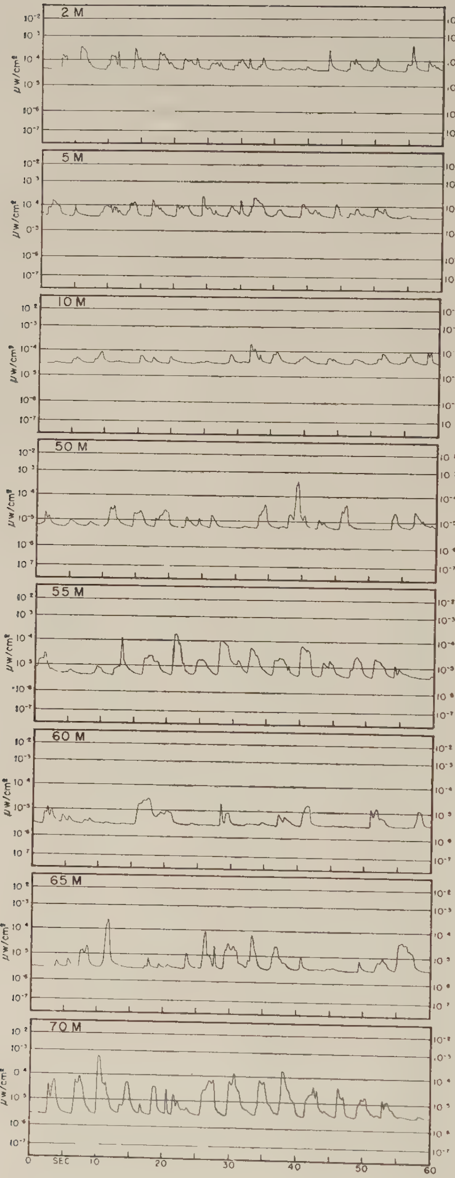

Fig. 16 a. — Light records at Station 3, Gulf of Naples, April 24, 1959, 2026-2045 hrs, wind force 0, sea slight, clear with haze on horizon, moon not visible. Bottom depth 300 m.

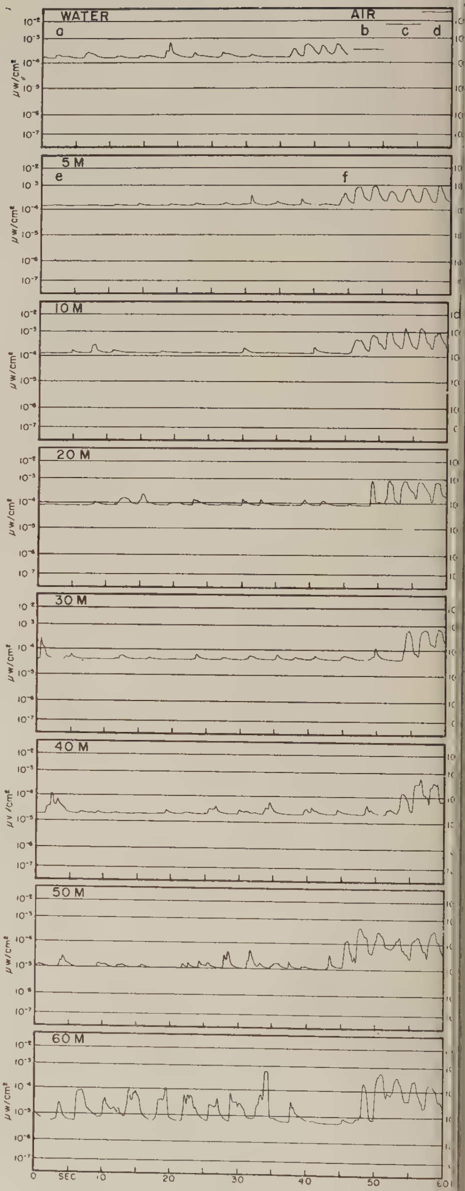

Fig. 16 b. — Continuation of records at Station 3, April 24, 1959, 2050-2110 hrs, moon clear. Photometer in water: directed downward (a); in air : directed downward (b), upward (c), at moon (d).

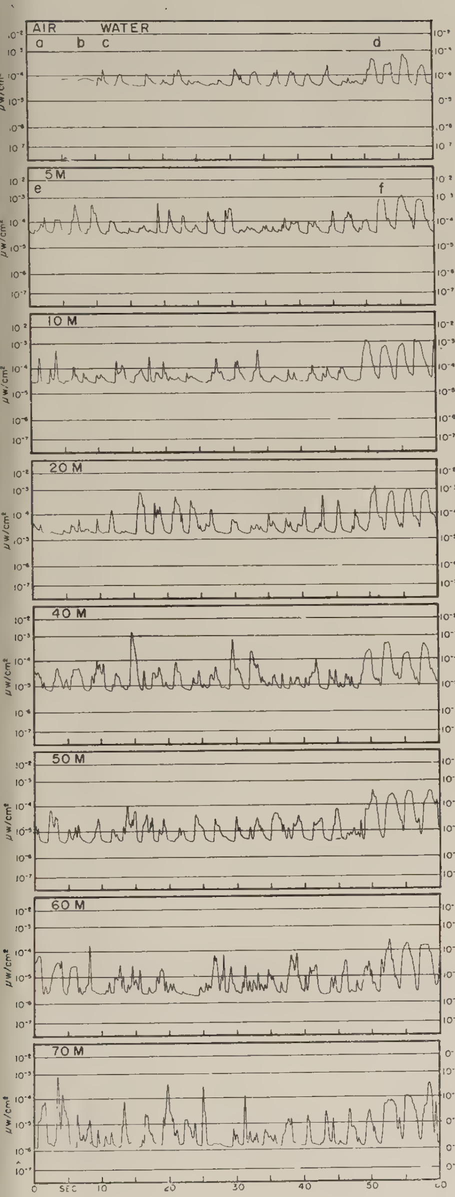

FIG. 17. — Light records at Station 3, April 27, 1959, 2022-2055 hrs, wind force 2, sea moderate, clear with haze on horizon, moon not visible. Bottom depth 300 m. Photometer in air : directed upward (a), downward (b) ; in water : directed downward, with no added agitation (c) and (e), with standard agitation (d) and (f).

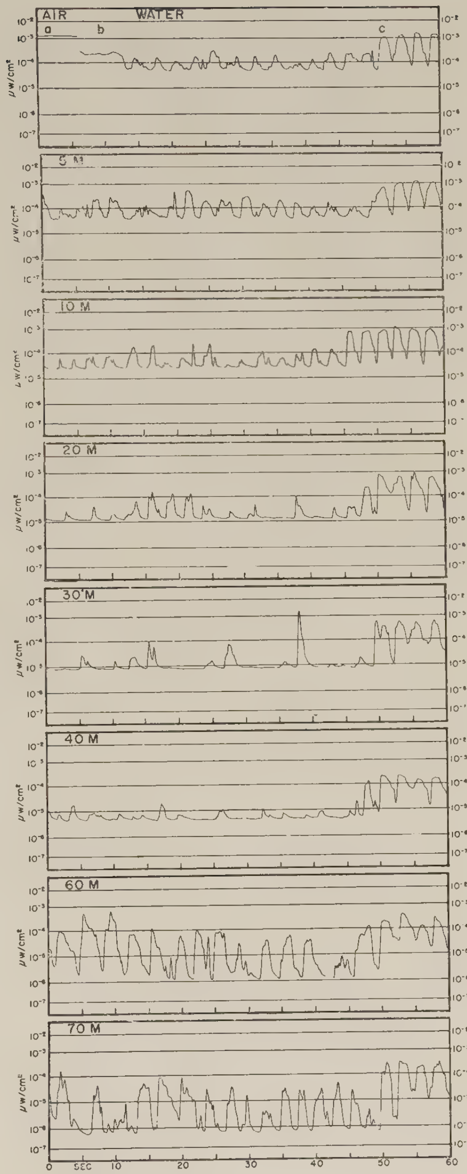

FIG. 18. — Light records at Station 4, Gulf of Naples, April 27, 1959, 2220-2240 hrs, wind force 0, sea slight, clear, moon not visible. Bottom depth 80 m. Photometer in air : directed upwards (a), downward (b); in water: at 2 m (following b), with standard agitation (c).

period at each depth produced more regular and sustained discharges, but not always with higher intensities. At 70 m a large amount of luminescent activity took place throughout the period of observation with some flashes almost 1000 × the intensity of the background illumination.

The last series of measurements, made east of La Gaiola Light (Station 4) under conditions of slight sea, no wind, and no moon, indicated slightly higher ambient flux in air due to greater influence of light from the shore (Fig. 18). Without extra agitation the frequency and intensity of luminescence diminished with increasing depth (with the exception of one flash of more than 1×10^{-3} μw/cm^2) until at 40 m few flashes brighter than 10^{-5} μw were recorded. However, standard agitation at the end of each observation period elicited luminescent responses ranging in intensity between 10^{-3} and 10^{-4} μw/cm^2. At 60 m and 70 m much larger numbers of bright flashes were encountered than at any other depth. Furthermore, during added agitation at these depths, as well as at 30 m and 40 m, the luminous discharges were so prolonged that the light level remained high between peaks. The presence of quite different populations of luminescent organisms at these various depths is thus indicated.

At very depth at each of the four stations in the Gulf of Naples luminescent flashes were detected above the background illumination. The intensity of the flashes as they reached the photometer ranged chiefly between 10^{-3} and 10^{-5} μw/cm^2 although weaker flashes could be and were recorded at the greater depths. Since boat roll or added agitation of the photometer always produced an increase in luminescent discharge, the frequency of flashing was related, often to a large extent, to the rate of movement of the instrument. However, the intensity of the spontaneous discharges was sometimes as high as that resulting from agitation. Differences in the spontaneous luminescence when the photometer was quiet were recorded and indicated quantitative or qualitative changes in the luminescent plankton with location, depth, or time.

The present measurements may be compared with those made in the Mediterranean in 1958 (Clarke and Breslau, 1959), although the previous observations were carried out in much deeper water. Records for the upper 75 m in the central portion of the Ligurian Sea (Station C) showed ranges for the ambient light and for bioluminescence which are about the same as in the present study, but the flashing displayed a higher frequency and was more irregular. The differences are only partially assignable to the longer period of roll of the larger ship and the fact that a different photometer was used. The conclusion seems inescapable that the plankton at this station had very different characteristics of luminescence. The earlier observations made northeast of Corsica (Station E) similarly revealed the same range of intensities for light conditions in the upper layers for records taken both with and without added agitation, but the presence of a population with a somewhat different type of flashing is indicated. Thus, as far as may be judged from these initial studies, in the regions investigated bioluminescence is widespread in its occurrence and is superimposed upon a background illumination which varies regularly with depth. Luminescent flashes fall within the same extreme range of intensities, but differ greatly in frequency, duration and degree of regularity.

SUMMARY

Investigations of light conditions with special reference to bioluminescence, were conducted in Phosphorescent Bay and neighboring areas, working from the Institute of Marine Biology, University of Puerto Rico, and at four stations in the Gulf of Naples, working from the Zoological Station at Naples.

The new portable bathyphotometer used consists of an underwater unit, containing a photomultiplier tube with transistor amplifier, and a mechanically wound, field-type strip chart recorder connected by an insulated cable. This photometer may be operated by hand without an outside electric power source and is sensitive to light intensities down to about 10^{-7} μw/cm^2.

The intensity of upward-passing light from the bow wave of the Institute's motor boat at night, due chiefly to the luminescence of the disturbed organisms, increased more than 100 × (to a value of 3×10^{-2} μw/cm^2) when the boat entered Phosphorescent Bay, as a result of the concentration therein of luminescent dinoflagellates, principally *Pyrodinium bahamense*. The extinction coefficient in the Bay averaged $k = 0.43$ in contrast to values running to $k = 0.053$ outside the reefs.

At all stations in Puerto Rican waters and in the Gulf of Naples the intensity of light received at night in air by the upright photometer ranged between slightly less than 10^{-3} μw/cm^2 and slightly more than 10^{-2} μw/cm^2. Upward light measured by the inverted photometer over the surface was a small percentage of the downward light. In the water the upward background light dropped in intensity at successively greater depths to about 10^{-6} μw/cm^2 at 4 m in Phosphorescent Bay and to 10^{-5} μw/cm^2 at 50 m off the Puerto Rican coast, and to slightly more than 10^{-6} μw/cm^2 at 70 m in the Gulf of Naples.

In Phosphorescent Bay spontaneous luminescent flashing was rather weak but agitation evoked discharges approaching 10^{-2} μw/cm^2 in intensity. Offshore the larger flashes ranged between 10^{-4} and 10^{-3} μw/cm^2. In the Gulf of Naples spontaneous flashes varied between 10^{-5} and 10^{-3} μw/cm^2, according to circumstances, and discharges resulting from added agitation ranged between 10^{-4} and 10^{-3} μw/cm^2. The investigation demonstrates the widespread occurrence of organisms producing different types of luminescence either spontaneously or when stimulated. The variations in the intensity, frequency, and duration of luminescent flashing, which have been recorded quantitatively, are discussed in relation to locality, time, and depth.

RÉSUMÉ

Des recherches sur la pénétration de la lumière se rapportant plus particulièrement à la bioluminescence ont été entreprises dans la Baie phosphorescente (Bahia fosforescente) et les zones avoisinantes, à partir de l'Institut de biologie marine de l'Université de Porto Rico, et à quatre stations de la Baie de Naples, à partir de la Station zoologique de Naples.

Le nouveau bathyphotomètre portatif comporte une partie sous-marine contenant le tube photomultiplicateur avec amplificateur à transistors, et un enregistreur portatif sur bande, reliés par un câble isolé. Ce photomètre peut être utilisé sans source d'énergie électrique extérieure; il est sensible aux intensités lumineuses jusqu'à un niveau d'environ 10^{-7} µw/cm².

Pendant la nuit, l'intensité de la lumière transmise vers le haut par la lame d'étrave du canot automobile de l'Institut, provenant principalement de la luminescence des organismes dérangés, était multipliée par plus de 100, quand le bateau entrait dans la Baie phosphorescente, atteignant une valeur de 3×10^{-2} µw/cm², par suite de la concentration dans ces parages de dinoflagellés luminescents, surtout *Pyrodinium bahamense*. Le coefficient d'extinction dans la Baie était, en moyenne, $k = 0{,}43$ alors que cette valeur atteignait $k = 0{,}053$ au-delà des récifs.

A toutes les stations dans les eaux de Porto Rico et dans la Baie de Naples, l'intensité de la lumière reçue la nuit par le photomètre tourné vers le zénith dans l'air se tenait entre un peu moins de 10^{-3} µw/cm² et un peu plus de 10^{-2} µw/cm². La lumière transmise vers le haut au-dessus de la surface et mesurée par le photomètre dirigé vers le bas n'était qu'un faible pourcentage de la lumière incidente. Dans l'eau, la lumière ambiante dirigée vers le haut diminuait en intensité à mesure que la profondeur augmentait jusqu'à environ 10^{-6} µw/cm² à 4 m dans la Baie phosphorescente, 10^{-5} µw/cm² à 50 m au large de la côte de Porto Rico, et légèrement plus que 10^{-6} µw/cm² à 70 m dans la Baie de Naples.

Dans la Baie phosphorescente, la luminescence due aux éclairs spontanés était assez faible, mais l'agitation provoquait des décharges dont l'intentisé approchait 10^{-2} µw/cm². Au large, les décharges les plus puissantes atteignaient de 10^{-4} à 10^{-3} µw/cm². Dans la Baie de Naples, la luminescence due aux éclairs spontanés variait, suivant les circonstances, entre 10^{-5} et 10^{-3} µw/cm², et les décharges provoquées par l'agitation atteignaient 10^{-4} à 10^{-3} µw/cm².

Ces recherches montrent la vaste répartition d'organismes produisant différents types de luminescence, soit spontanément, soit quand on les stimule. Les variations dans l'intensité, la fréquence et la durée des éclairs qui ont été enregistrées quantitativement sont étudiées en fonction du lieu, du temps et de la profondeur.

REFERENCES

BODEN, B. P. & KAMPA, E. M. 1957. Records of Bioluminescence in the ocean. *Pacific Science*, **2** : 229-235.

BRESLAU, L. R. 1959. The Portable Bathyphotometer. *Unpublished Manuscript, Woods Hole Oceanographic Institution.* Reference N° 59-28.

BURKHOLDER, P. R. & BURKHOLDER, L. M. 1958. Studies on B vitamins in relation to productivity of the Bahia fosforescente, Puerto Rico. *Bull. Mar. Sci. of the Gulf & Caribbean*, **8** (3) : 201-223.

CLARKE, G. L. 1954. Elements of Ecology. John Wiley & Sons, New York (534 pp).

CLARKE, G. L. & BACKUS, R. H. 1956. Measurements of light penetration in relation to vertical migration and records of luminescence of deep sea animals. *Deep-sea Res.*, **4** : 1-14.

CLARKE, G. L. & BRESLAU, L. R. 1959. Measurements of Bioluminescence off Monaco and Northern Corsica. *Bull. Inst. océanogr., Monaco*, N° 1147.

CLARKE, G. L. & HUBBARD, C. J. 1959. Quantitative Records of the Luminescent Flashing of oceanic animals at great depths. *Limnology and Oceanography*, **4** : 163-180.

CLARKE, G. L. & WERTHEIM, G. K. 1956. Measurements of illumination at great depths and at night in the Atlantic Ocean by means of a new bathyphotometer. *Deep-sea Res.*, **3** : 189-205.

HUBBARD, C. J. 1956. A wide-range, high-speed, bathyphotometer. *Unpublished Manuscript, Woods Hole Oceanographic Institution.* Reference N° 56-68.

IVANOFF, A. 1959. Introduction à une étude des propriétés diffusantes des eaux de la Baie de Naples. *Publ. Staz. Zool. Napoli*, **31** : 33-43.

JERLOV, N. G. & PICCARD, J. 1959. Bathyscaph measurements of daylight penetration into the Mediterranean. *Deep-sea Res.*, **5** : 201-204.

KAMPA, E. M. & BODEN, B. P. 1957. Light generation in a sonic-scattering layer. *Deep-sea-Res.*, **4** (2); 73-92.

MARGALEF, R. 1957. Fitoplancton de las costas de Puerto Rico. *Investigacion Pesquera*, Tomo VI. Publicado en enero de 1957. Barcelona.

NICOL, J. A. C. 1958. Observations on luminescence in pelagic animals. *J. Mar. Biol. Assoc. U.K.*, **37** : 705-752.

PLATE, L. 1906. *Pyrodinium bahamense* n.g., n.sp. die Leucht-Peridinee des « Feuersees » von Nassau, Bahamas. *Archiv für Protistenkunde*, **7** : 411-429.

POWELL, W. M. & CLARKE, G. L. 1936. The reflection and absorption of daylight at the surface of the ocean. *J. Opt. Soc. Am.*, **26** : 111-120.

WERTHEIM, G. K. 1954. Design and operation of a bathyphotometer. *Unpublished Manuscript, Woods Hole Oceanographic Institution.* Reference N° 54-65.

Contribution No. 10

(Extract from Coast Guard Bulletin No. 45)

PHYSICAL OCEANOGRAPHY OF THE GRAND BANKS REGION AND THE LABRADOR SEA IN 1959[1]

By Floyd M. Soule and P. A. Morrill

(U. S. Coast Guard)

The 180-foot tender class cutter U.S.C.G.C. *Evergreen* served again as the oceanographic vessel of the International Ice Patrol for 1959. No marked alterations affecting the oceanographic work were made in the vessel since the 1958 season.

The *Evergreen* departed Argentia, Newfoundland, on 4 April to conduct the first survey of the 1959 season. This survey covered the waters over and immediately seaward of the southern and eastern slopes of the Grand Banks from westward of the Tail-of-the-Banks northward to the latitude of Flemish Cap. The work of collection of data began on 5 April at station 6890 located off the southwestern slope of the Banks and progressed from south to north without major interruption. On 18 April the final station, 6976, was completed and the *Evergreen* proceeded to Argentia arriving there the following afternoon.

A second survey, stations 6977 to 7064, made between 30 April and 12 May, and a third survey, stations 7065 to 7149, made between 27 May and 6 June, covering the same general area as the first survey, were completed without major interruptions.

On 14 June the *Evergreen* departed Argentia to conduct the fourth survey over and immediately seaward of the northeastern slope of the Grand Banks, including an occupation of the Bonavista triangle. The work of collection of data began during the late evening of 15 June at station 7150, located at the northern corner of the triangle. Again there were no major interruptions or delays, the work progressed in a counterclockwise direction around the triangle and thence southeasterly to the latitude of Flemish Cap where the last station, 7229, was completed on 24 June.

From 7 to 14 July the *Evergreen* assumed the duties of Surface Ice Patrol Vessel, during which time studies were conducted by Lt. (jg.) Thomas F. Budinger of the Ice Patrol staff, on iceberg detection and iceberg disintegration. The results of the detection study may be found in the preceding section of this bulletin. During the disintegration studies a number of oceanographic observations were made and these will be published at a later date.

---

[1] To be reprinted as Contribution No. 1091 in the Collected Reprints of the Woods Hole Oceanographic Institution.

On the afternoon of 26 July the *Evergreen* departed Boston on a post-season cruise which included an occupation of the Bonavista triangle and a section across the Labrador Sea from South Wolf Island, Labrador, to Cape Farewell, Greenland. In addition to the regularly assigned personnel, Mr. Saul Friedman from the Lamont Geological Observatory was aboard to conduct a limited collection program of geochemical and biological samples in the area of the Labrador Sea.

The work of collection of data began in the early morning of 1 August at station 7230, the northern corner of the triangle. As expected, considerable difficulty was encountered in lowering the L. G. O. 50-gallon sampler and the 150-pound bottom pinger which were to be used at eight selected stations. After several unsuccessful attempts to launch and retrieve the equipment, it was decided to proceed with the stations of the triangle in a counterclockwise direction and make another attempt with the L. G. O. equipment at station 7259 again located at the northern corner of the triangle. During the intervening stations the ship's personnel devised a successful system of lowering and raising the drum and pinger to the waters edge and casts were made to 602 and 1826 meters at station 7259 without further difficulties.

Upon completion of the station the *Evergreen* proceeded to within 5 miles of South Wolf Island and commenced the Labrador Sea Section. Stations proceeded without major interruptions until station 7270. While attempting to obtain a drum and small coring samples, the pinger, with corer attached, and drum were being lowered when the pinger gave an uncertain signal of bottom at a meter wheel reading 3047 meters. As the pinger was again signaling free of bottom, lowering was continued to a meter wheel reading of 3081. The cast was then hauled in to 3030 meters to wait for the thermometers to reach equilibrium and allow for messengers to travel to the deepest gear. Hauling in was difficult and with about 2000 meters of wire out the unloading valves stopped the winch. After a wait of 10 minutes hoisting was resumed, but about every 100–200 meters the winch would again fail. Finally, with a reading of 833 meters the wire broke at a bad kink just below the surface resulting in the loss of the drum sampler, pinger, corer, three Nansen bottles, and eight reversing thermometers. After that disastrous station the remainder of the survey was completed without major interruption and at station 7283, located 5 miles off Cape Farewell, the survey was completed on 9 August 1959.

In addition to the 54 stations taken on the postseason cruise, four deep and nine surface large volume radiocarbon water samples, six atmospheric and three surface water equilibrated carbon dioxide samples, and six vertical tow and eight surface tow samples were taken for the Lamont Geological Observatory.

The oceanographic work was under the supervision of Oceanographer Floyd M. Soule for the first, second and postseason surveys, and Lt R. M. Morse for the third and fourth surveys with Lt. P. A. Morrill assisting on all surveys. Other assistants in the observational work were

Elwood C. Gray and Richard C. Norris, aerographer's mates first class, William G. Carpenter, yeoman second class, Lynn E. Dawson and Donald P. Wagner, aerographer's mates third class. Temperature and salinity observations were made at each of the 394 stations. At the 24 stations forming the section across the Labrador Sea the observations extended from the surface to as near the bottom as was practicable. At the remaining stations the observations were limited to the upper 1500 meters. The intended depths of observations, in meters, were 0, 25, 50, 75, 100, 150, 200, 300, 400, 600, 800, 1,000, and thence by 500-meter intervals.

Temperatures were measured with protected deep sea reversing thermometers, mostly of Richter & Wiese manufacture but with some manufactured by Negretti & Zambra, G. M. Manufacturing Co. and Kahl Scientific Inst. Corp. Depths of observation are based on unprotected reversing thermometers made by Richter & Wiese and by Kahl. As in other years, a program of intercomparison of protected thermometers was carried out in the field measurements. The thermometers were used in pairs and one of each pair was shifted periodically so that the same thermometer was eventually paired with a number of other thermometers. From a total of 2,668 intercomparisons, the probable difference between the corrected readings of a pair of protected thermometers was 0.01°C. Of these comparisons, 343 involved thermometers having a range of +3° to +13° with a probable difference of 0.006°, 1,587 comparisons between thermometers of range −2° to +8° and gave a probable difference of 0.009°, and 738 comparisons were between thermometers with a range of −2° to +20° or greater and gave a probable difference of 0.014°. As most of the temperatures listed in the Table of Oceanographic Data are the means of the corrected readings of a pair of thermometers and since many of the thermometers used had recent laboratory comparisons with thermometers tested by the National Bureau of Standards, it is considered that the tabulated observed temperatures are good to 0.01°C.

As in previous years, routine salinity measurements were made with a Wenner salinity bridge. Prior to the 1959 season it was planned to construct a new calibration curve by titration of a number of large volume water samples collected at sea and then make a series of runs on the salinity bridge. Unfortunately, the water froze in its containers before this could be done. Consequently, a single carboy of water, designated C–1–59, was titrated 12 times with the result that when a series of comparisons was made on the salinity bridge between the water of C–1–59 and Copenhagen standard water of batch P23, a new reading for the P23 was determined. By using the new reading, a discrepancy of $+0.03_1$‰ is introduced between the 1959 and 1958 salinity values. It is noted that this discrepancy is the same that existed between the WHOI and the CGOU salinity bridges, as reported in Bulletin No. 44 of this series; however, until a number of titrations can be made on a series of large-volume water samples, covering the salinity range of the bridge, and a

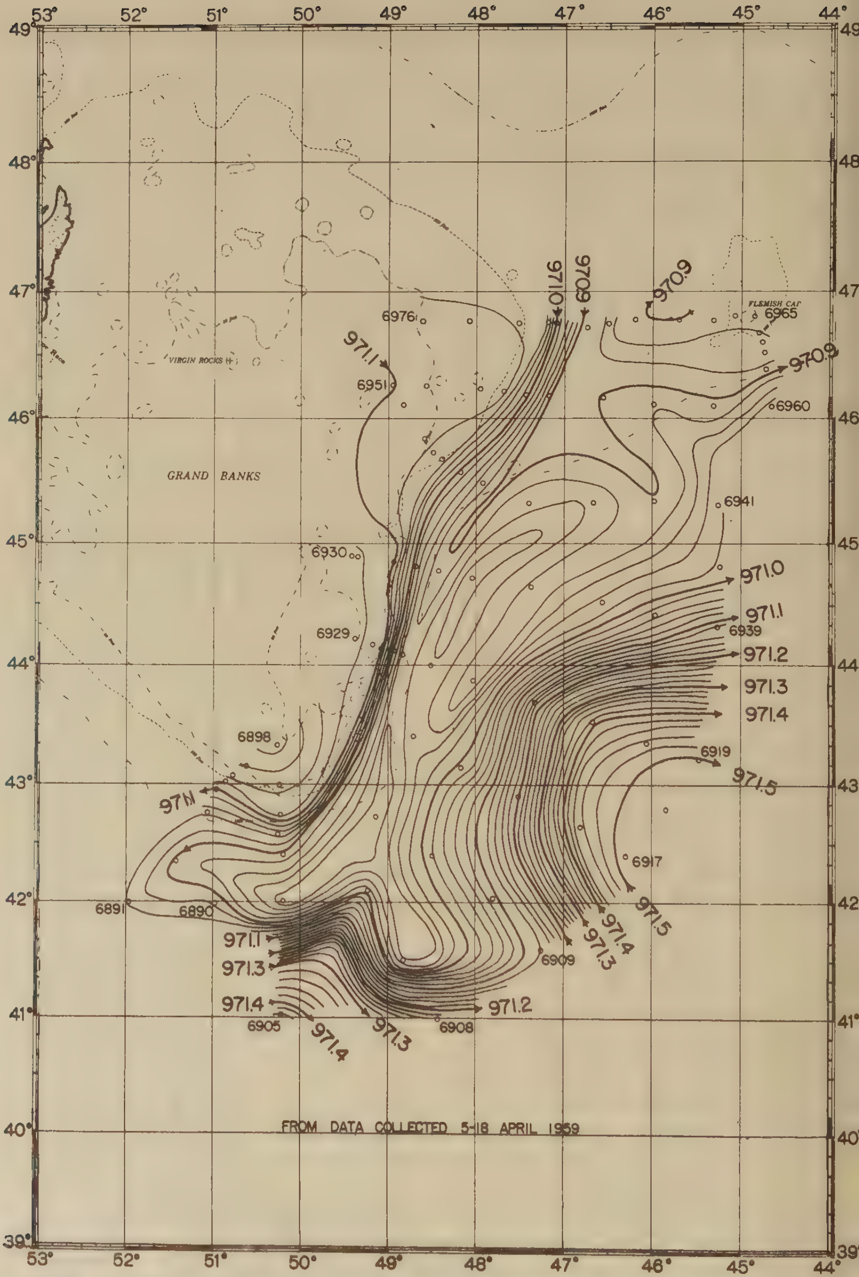

53°
52°
51°
50°
49°
48°
47°
46°
45°
44°
49°
48°
47°
46°
45°
44°
43°
42°
41°
40°
39°
FLEMISH CAP
6965
970.9
971.0
970.9
6976
971.1
6951
VIRGIN ROCKS
6960
GRAND BANKS
6941
6930
971.0
971.1
6939
6929
971.2
971.3
971.4
6898
6919
971.5
971.1
6917
6891
6890
971.5
971.1
971.4
971.3
971.3
6909
971.4
971.2
6905
6908
971.4
971.3
FROM DATA COLLECTED 5-18 APRIL 1959

Figure 44.—Dynamic topography of the sea surface relative to the 1000-deciba surface from data collected 5–18 April 1959. Oceanographic statio positions are indicated and the station numbers given at turning points

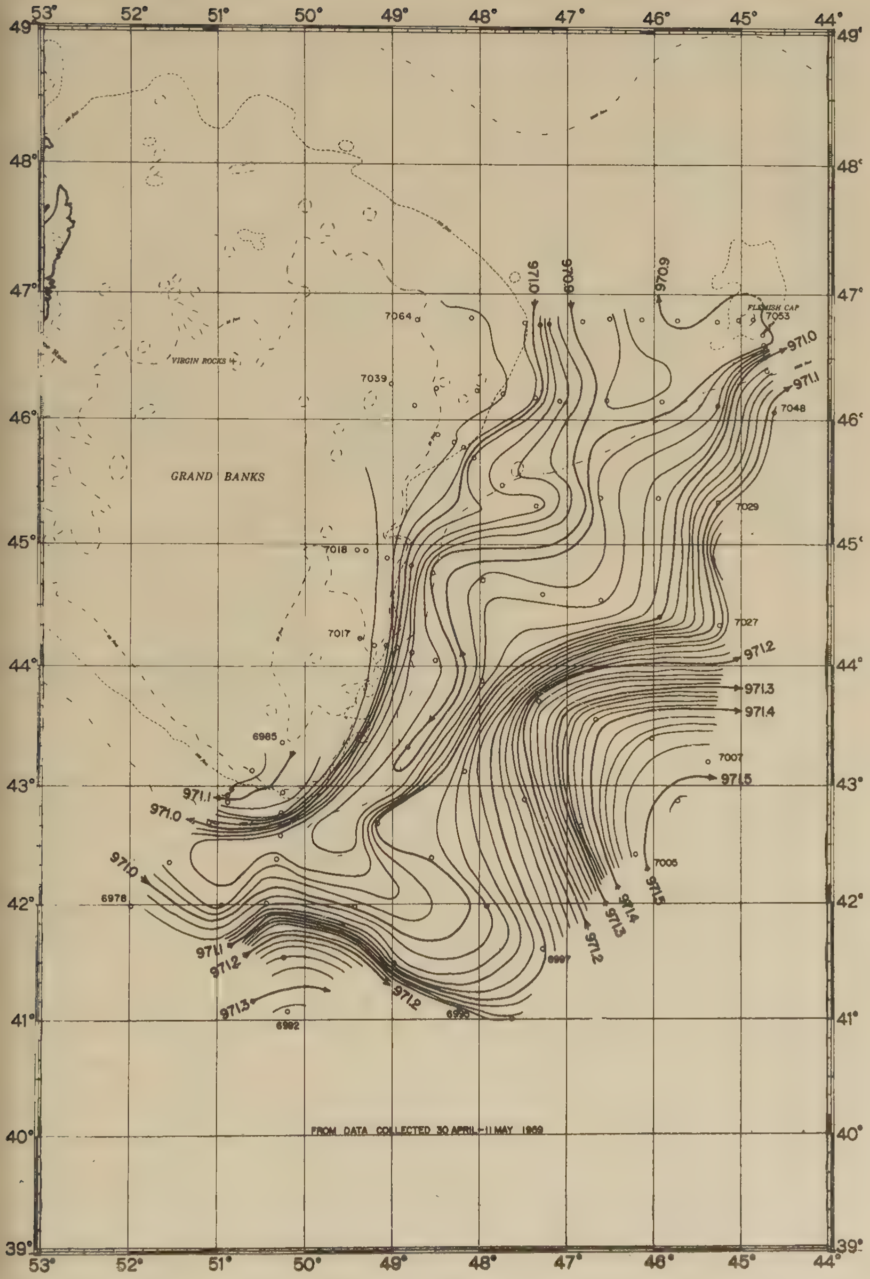
53°
52°
51°
50°
49°
48°
47°
46°
45°
44°
49°
48°
47°
46°
45°
44°
43°
42°
41°
40°
39°
FLEMISH CAP
VIRGIN ROCKS
GRAND BANKS
971.6
970.8
970.9
971.0
971.1
971.2
971.3
971.4
971.5
7064
7039
7053
7048
7029
7018
7027
7017
6985
7007
7005
6978
6997
6992
6995
FROM DATA COLLECTED 30 APRIL–11 MAY 1959

FIGURE 45.—Dynamic topography of the sea surface relative to the 1000-decibar surface from data collected 30 April to 11 May, 1959. Oceanographic station positions are indicated and the station numbers given at turning points.

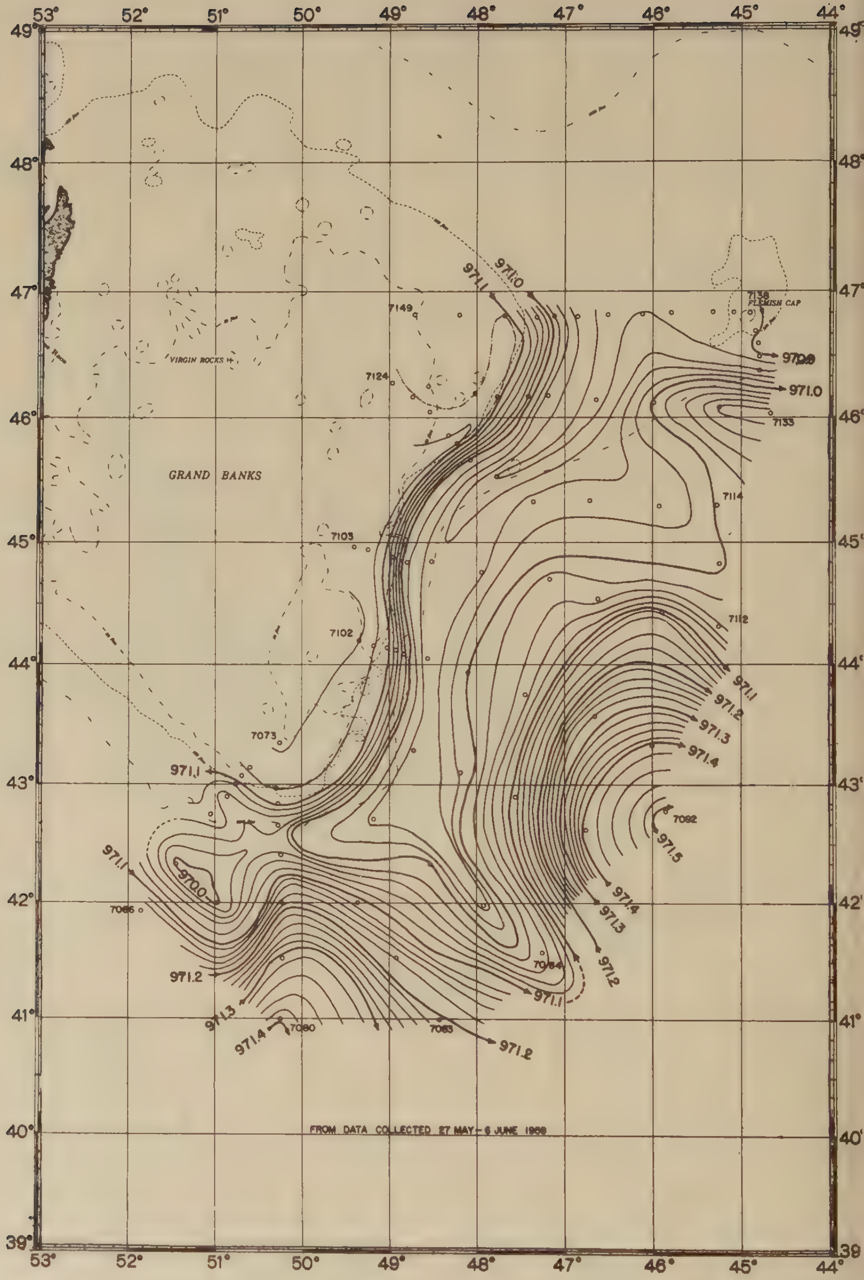
53°
52°
51°
50°
49°
48°
47°
46°
45°
44°
49°
48°
47°
46°
45°
44°
43°
42°
41°
40°
39°
GRAND BANKS
VIRGIN ROCKS
FLEMISH CAP
7138
7149
7124
7133
7114
7103
7102
7112
7073
7092
7066
7064
7060
7063
971.0
971.1
970.9
971.0
971.1
971.2
971.3
971.4
971.5
971.4
971.3
971.2
971.1
971.1
970.0
971.2
971.3
971.4
971.2
FROM DATA COLLECTED 27 MAY – 6 JUNE 1959

FIGURE 46.—Dynamic topography of the sea surface relative to the 1000-decibar surface from data collected 27 May to 6 June, 1959. Oceanographic stations are indicated and the station numbers given at turning points.

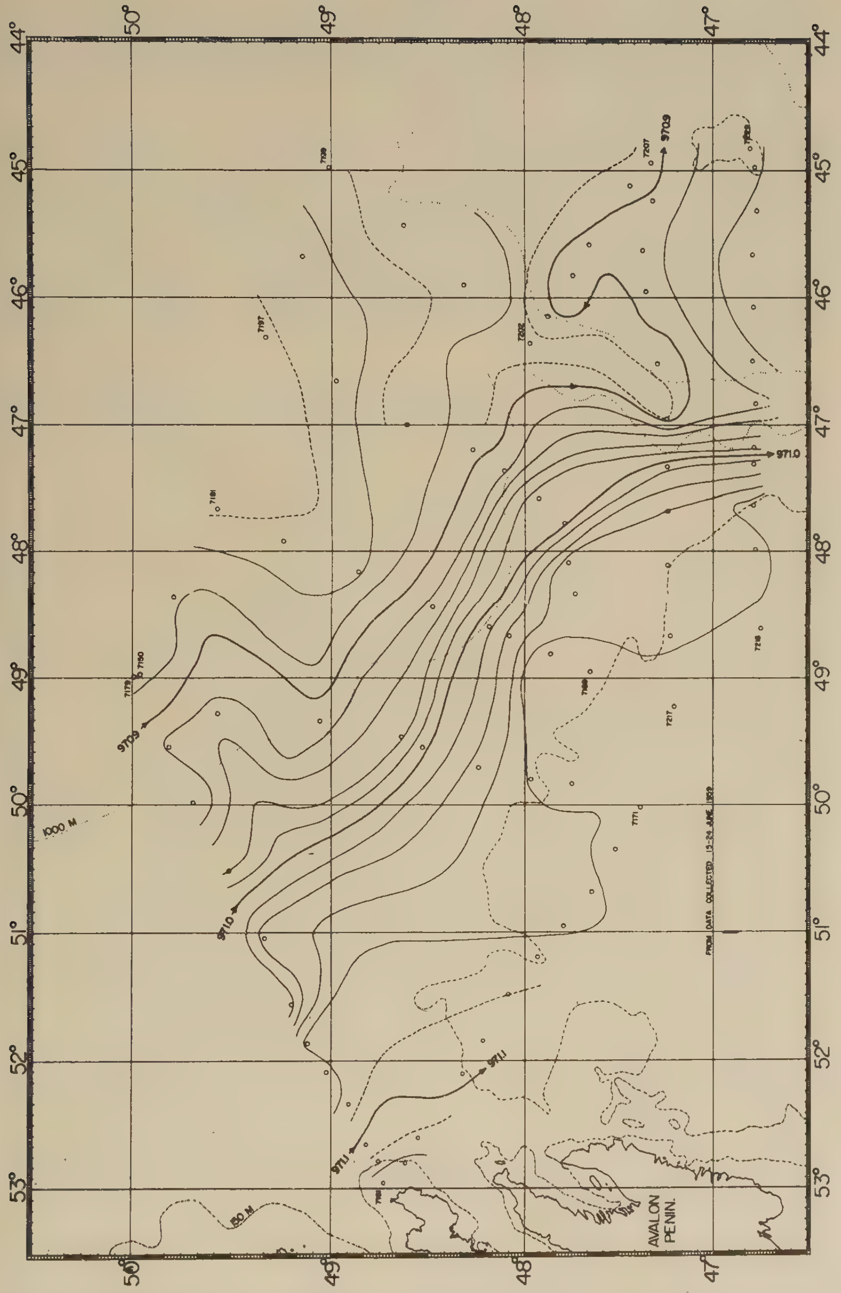
44°
45°
46°
47°
48°
49°
50°
51°
52°
53°
50°
49°
48°
47°
9709
9710
9711
1000 M
50 M
AVALON PENIN.
FROM DATA COLLECTED 15-24 JUNE 1959
7179
7190
7181
7197
7202
7207
7217
7216
7171

FIGURE 47.—Dynamic topography of the sea surface relative to the 1000-decibar surface from data collected 15–24 June, 1959. Oceanographic station positions are indicated and the station numbers given at turning points.

new calibration curve constructed, no positive statement can be made as to which values are correct. To this end, a number of water drum samples, varying from 31.5‰ to 36.5‰, were collected during the season and it is planned that a new calibration curve will be constructed prior to the 1960 season. The precision with which salinities were measured is considered to be about ±0.005‰.

Figures 44 through 48 show, in chronological order, the dynamic topography found during the four surveys made during the season and one during the occupation of the Bonavista triangle on the postseason cruise. As in the past, the reference surface used was 1,000 decibars for the four season cruises and the postseason triangle. It would appear that, especially in the case of the fourth survey triangle, a different reference level should have been used.

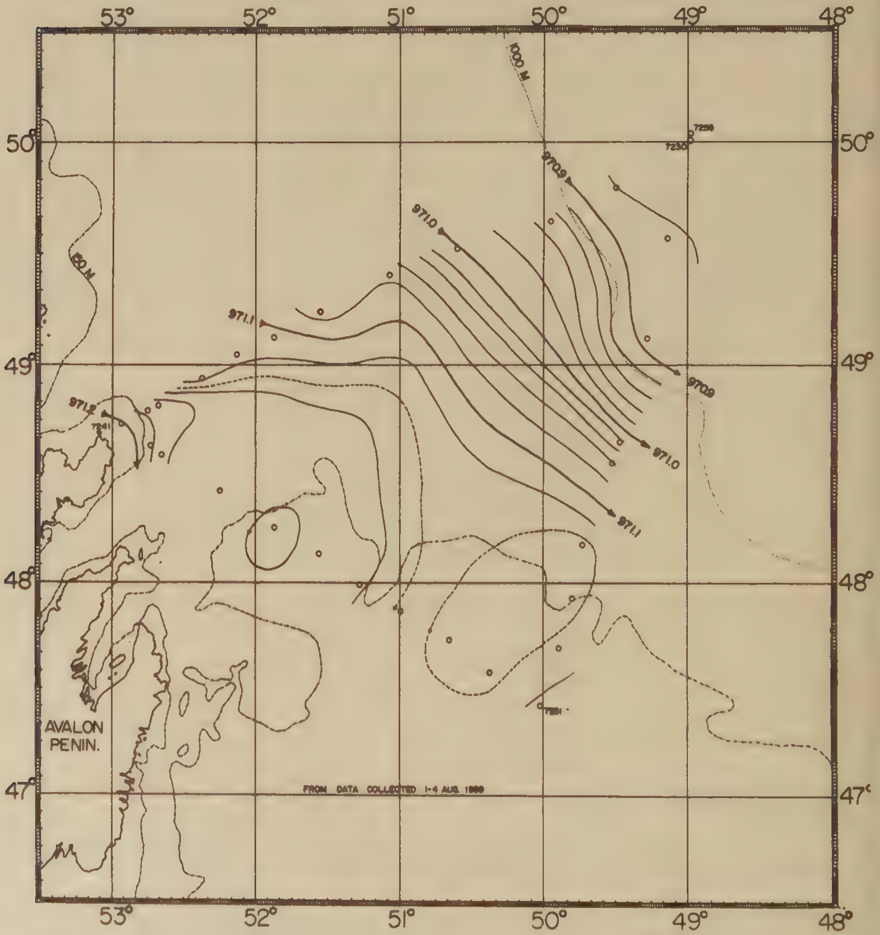

FIGURE 48.—Dynamic topography of the sea surface relative to the 1000-decibar surface from data collected 1–4 August, 1959. Oceanographic station positions are indicated and the station numbers given at turning points.

The first survey, figure 44, shows a very well defined Labrador Current but a rather small pool of quiet water off the southeastern side of the Tail-of-the-Banks and a poorly defined section of the North Atlantic Current in the Flemish Cap area. In the second survey, figure 45, we see that the Labrador Current becomes confused above latitude 45° N., a more developed pool of quiet water off the Tail-of-the-Banks and a rather well defined North Atlantic Current developing south of Flemish Cap. Third survey, figure 46, again shows a well defined Labrador Current but the quiet water pool extends northward to 45° N. Again the well developed North Atlantic Current off Flemish Cap is in evidence. It is noted that the main core of the Labrador Current moves off the Banks, near 44° N., and widens with a corresponding decrease of the maximum surface velocity as the season progresses. The average minimum temperature for the Labrador Current in the valley between the Grand Banks and Flemish Cap for the three surveys was −1.40°C which is colder than the 9-year average minimum of −1.26°C.

Comparing the two occupations of the Bonavista triangle, figures 47 and 48, we see a much more concentrated surface current flowing across the northwestern leg of the triangle during the postseason occupation than during the fourth survey. This might be a false representation as, in the fourth survey, there appears to be a possible movement at and below 1000 meters which was taken as the depth of no motion. In both cases the eastern branch of the current, which is the current flowing out across the southeastern side of the triangle, comprises more than 90 percent of the volume of water flowing into the triangle. Also on the fourth survey, figure 47, the main body of the Labrador Current lies westward of 47° W. and eastward of that longitude, at about 47° N., there is some loss of water to the east as it recurves northward.

Figure 49 shows a comparison of the temperature-salinity characteristics of water masses on the first three surveys of 1959 with the mean T–S characteristics from 1948 to 1959. Labrador Current water and Atlantic Current water are water masses found in this region and these two water masses usually mix in a sufficiently constant proportion to produce a mixed water which may be regarded as a virtual water mass. Of the three, the mixed water is the least definite and over the years there have been greater changes in the yearly shape of the curves representing this water mass than those for the other two. Every year there are some stations where the mixing is atypical and the individual station curves do not fall into any of the three categories. The data from these stations are excluded in determining the water mass characteristics. As has happened in the past, the majority of these stations showed mixtures between typical mixed water and the Atlantic Current water. Since the surveys do not normally include sections which completely cross the Atlantic Current, the curve for the 12-year mean does not accurately represent that water. It is noted that in both the Labrador Current and mixed waters both the temperature and salinity are lower than the 12-year mean

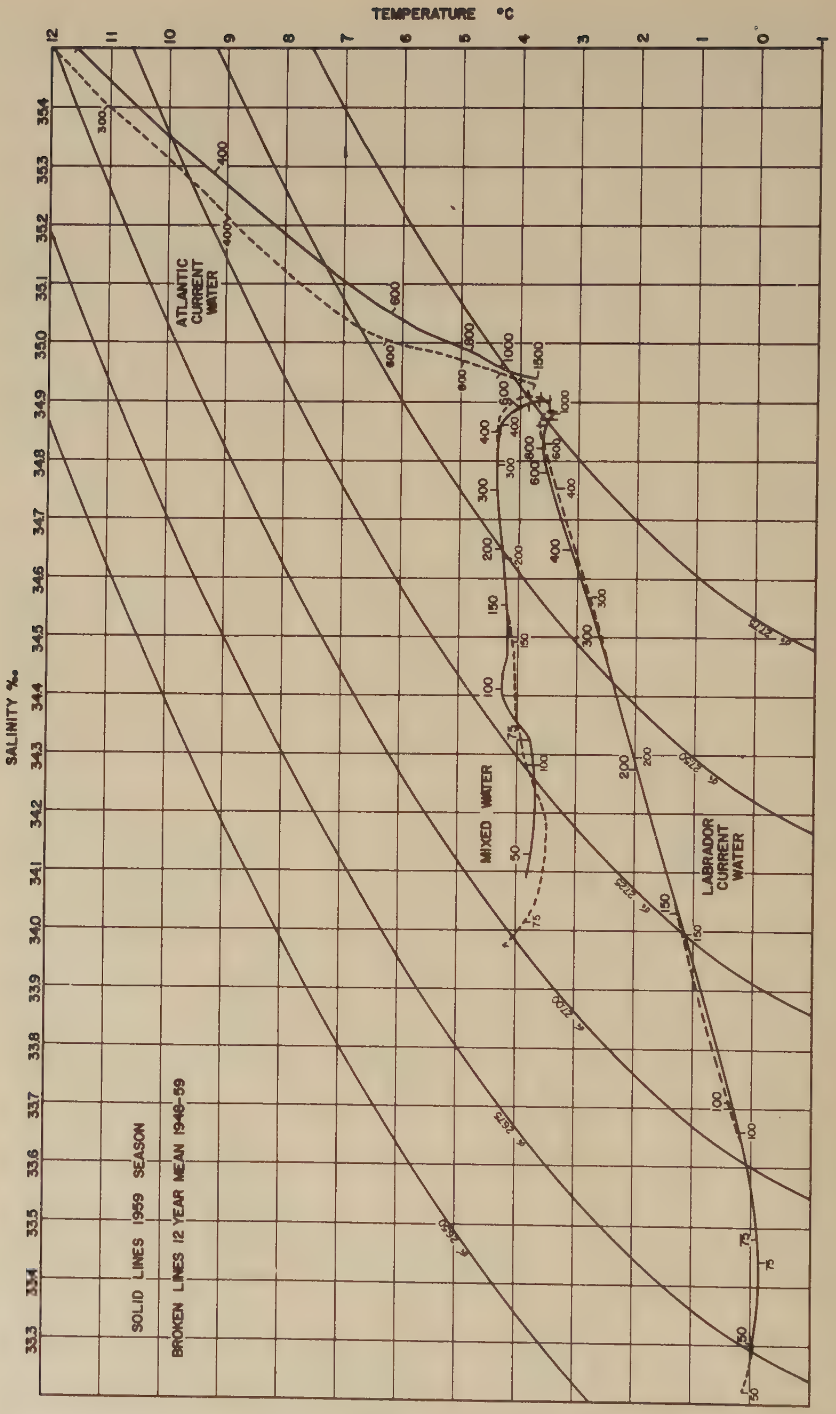

FIGURE 49.—Temperature-salinity relationships for Labrador Current water, Atlantic Current water and mixed water found in the Grand Banks region. Solid lines show conditions found during 1959 and broken lines represent the 12-year means for the period 1948–1959. An approximate depth scale in meters is given.

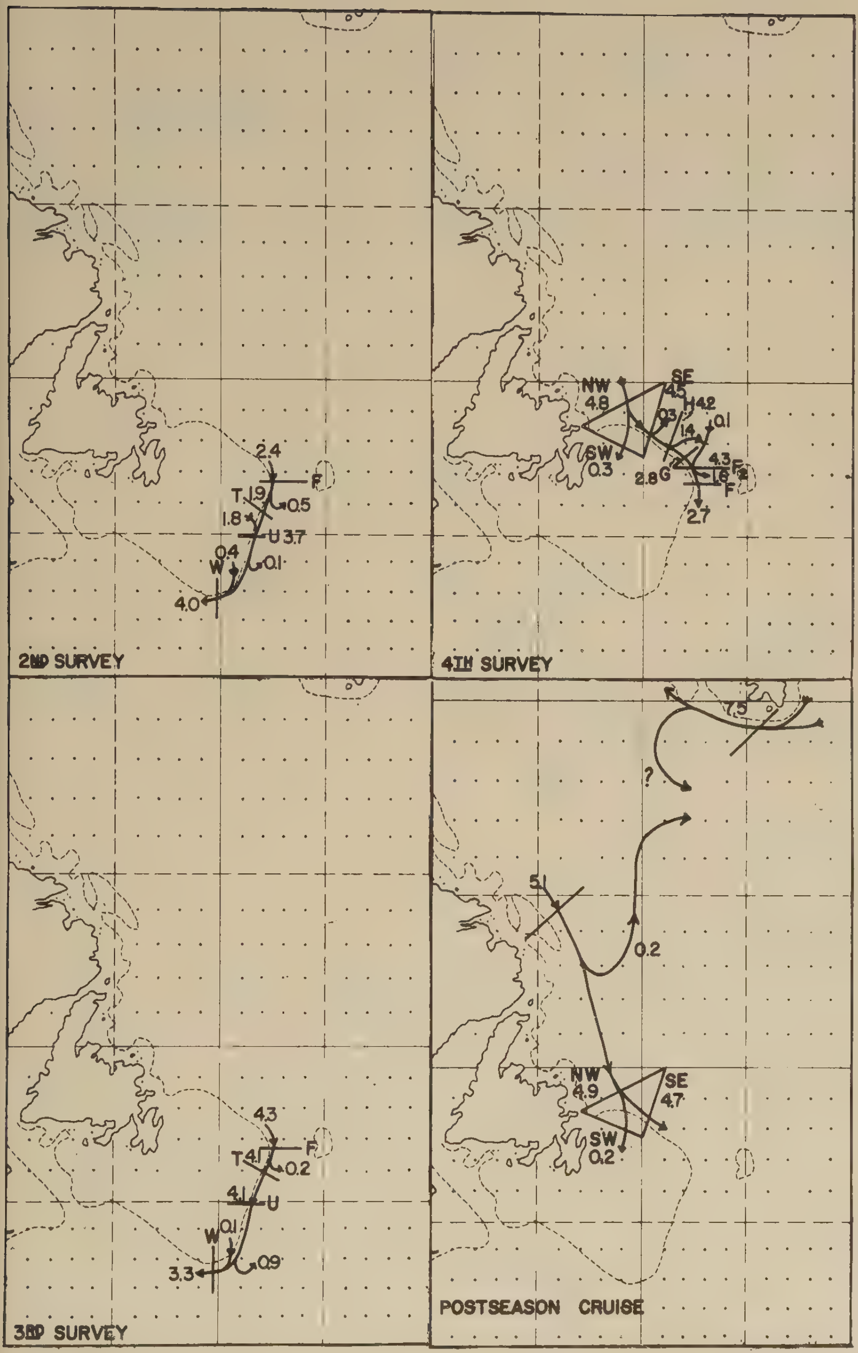
2ND SURVEY
2.4
F
T
1.9
0.5
1.8
U 3.7
0.4
W
0.1
4.0
4TH SURVEY
NW
4.8
SE
4.5
H 4.2
0.3
0.1
1.4
SW
0.3
2.8 G
2
4.3
F
1.6
2
F
2.7
3RD SURVEY
4.3
F
T 4.1
0.2
4.1
U
W
0.1
3.3
0.9
POSTSEASON CRUISE
7.5
?
5.1
0.2
NW
4.9
SE
4.7
SW
0.2

Figure 50.—Schematic representation of the circulation deduced from sections occupied on the 2nd, 3rd, 4th, and postseason cruises in 1959. Numerals indicate approximate volume transport in units of m³ x 10⁶ sec.

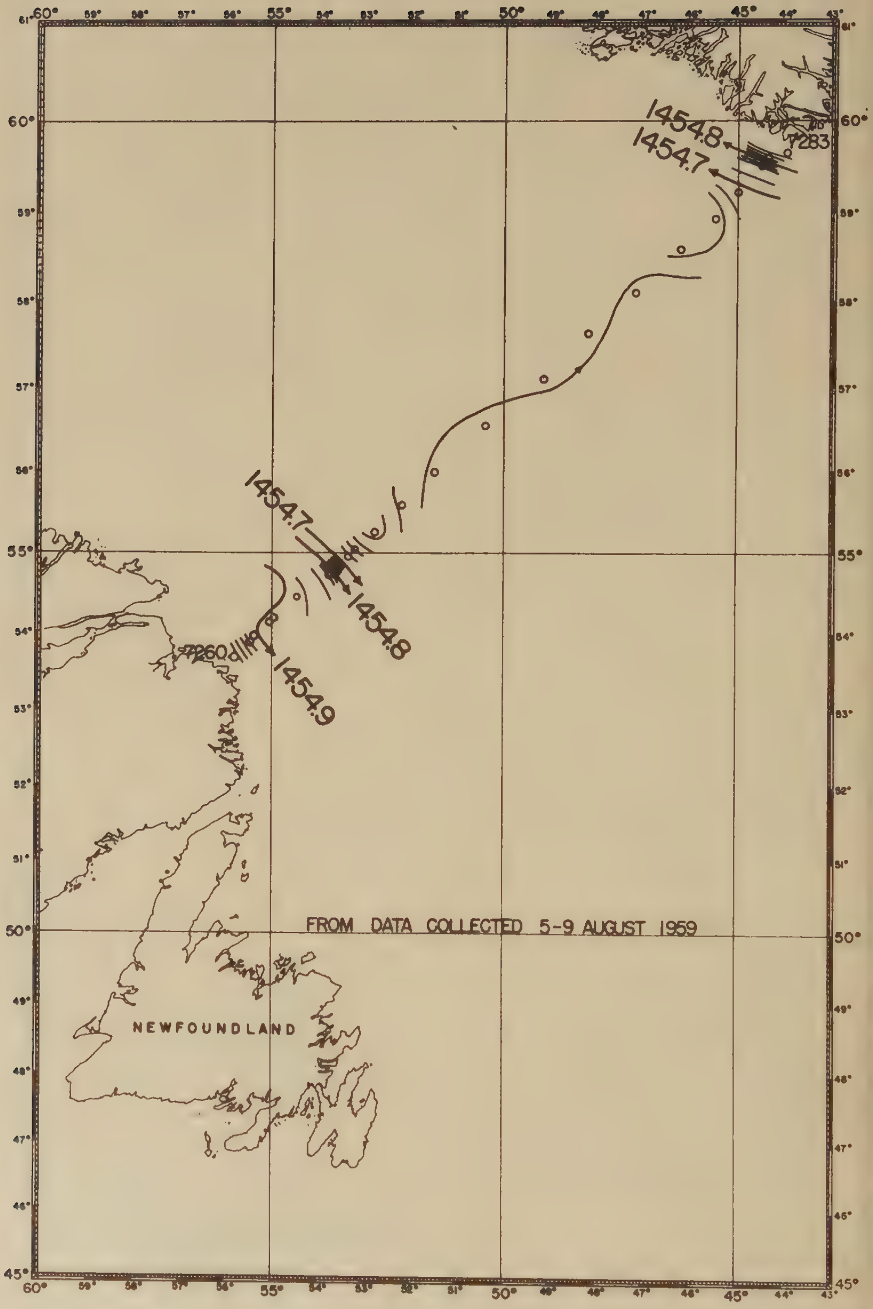
60°
55°
50°
45°
43°
61°
60°
59°
58°
57°
56°
55°
54°
53°
52°
51°
50°
49°
48°
47°
46°
45°
1454.8
1454.7
1283
1454.7
1454.8
1260
1454.9
FROM DATA COLLECTED 5-9 AUGUST 1959
NEWFOUNDLAND

FIGURE 51.—Dynamic topography of the sea surface relative to the 1500-decibar surface from data collected 5–9 August, 1959. Oceanographic station positions are indicated by circles.

below 200 meters with the salinity being the controlling factor as the density is lower. In the Atlantic Current, the salinity is again the controlling factor but in the opposite direction as both the salinity and density are higher below 200 meters.

Figures 51, 52, and 53 show respectively, the topography of the sea surface relative to the 1500-decibar surface, the temperature distribution, and the salinity distribution along the section between South Wolf Island, Labrador, and Cape Farewell, Greenland. In figure 51, the effect of the

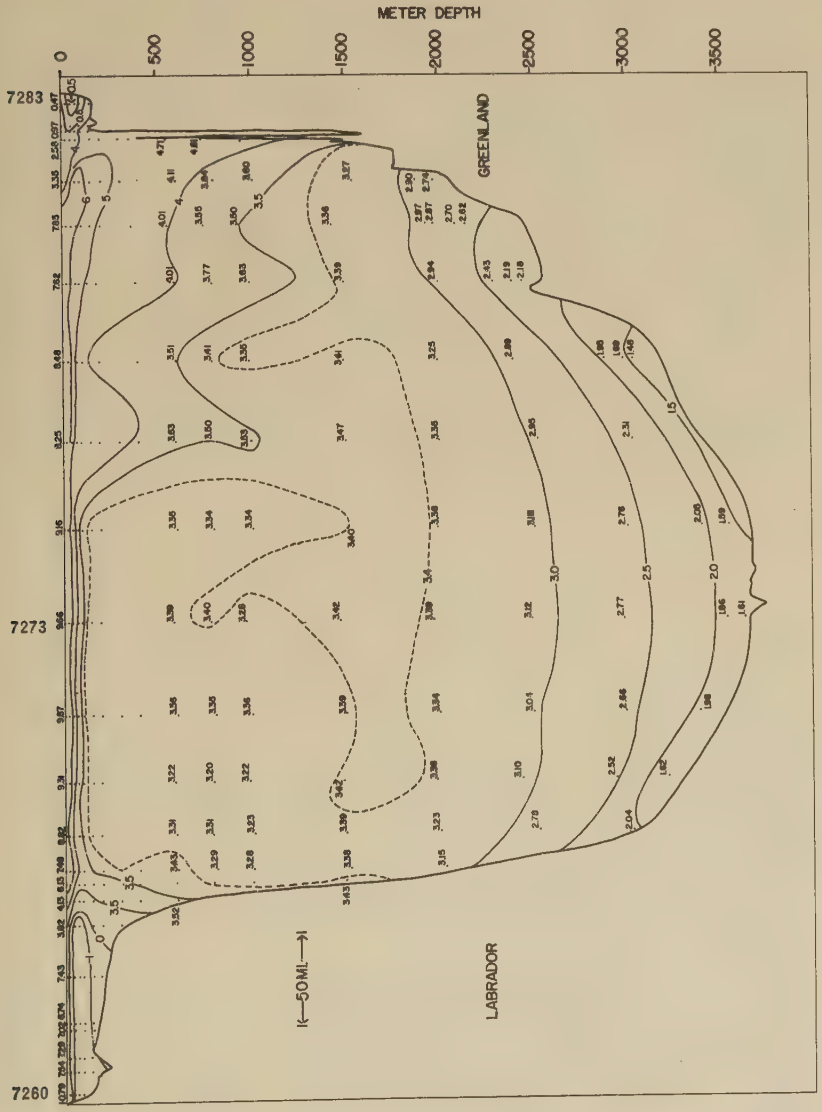

FIGURE 52.—Temperature distribution along section between South Wolf Island, Labrador and Cape Farewell, Greenland 5–9 August, 1959.

shoal off Hamilton Inlet is apparent in the current pattern off South Wolf Island. On the Greenland side, the Irminger Current component and the East Greenland Current component of the West Greenland Current are not distinguishable in figure 51. The contributions of each of these components, however, can be seen in figures 52 and 53, the temperature and salinity distributions. The temperature distribution appears to be normal but the salinity distribution in the deep water at station 7277 shows an anomalous condition with an intrusion of 34.84‰ water

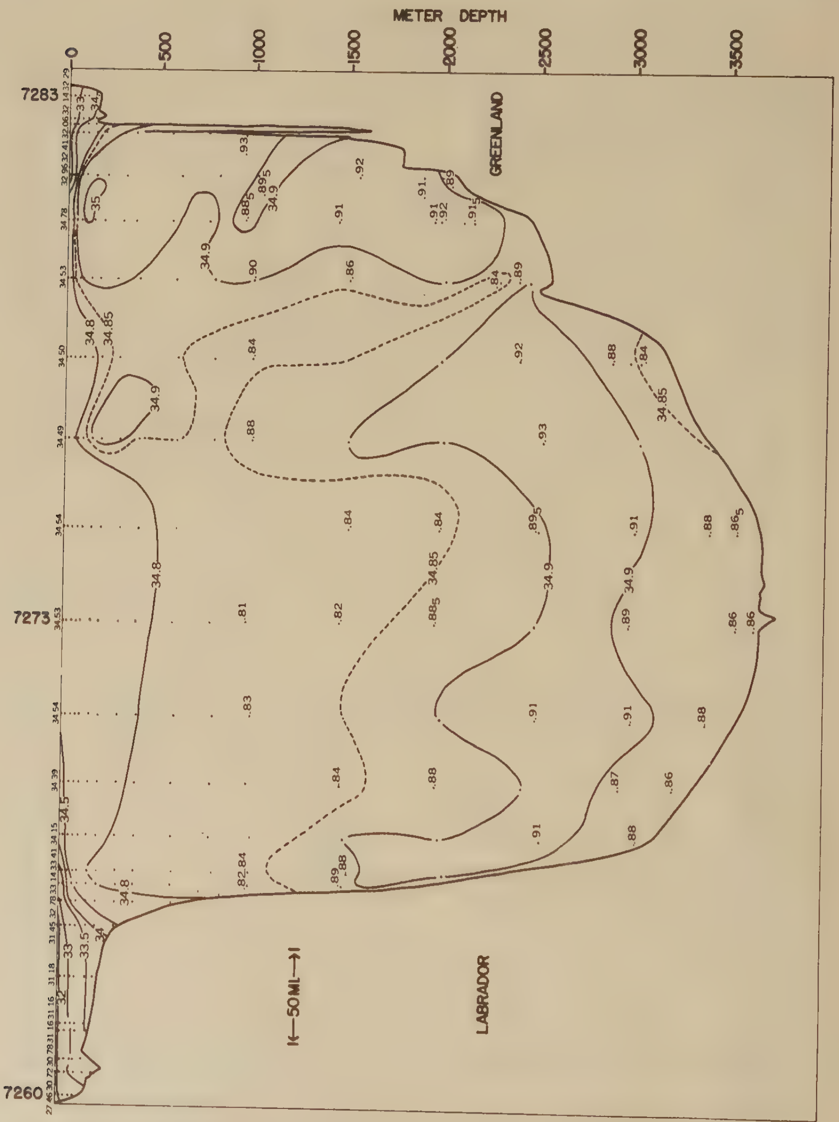

FIGURE 53.—Salinity distribution along section between South Wolf Island, Labrador and Cape Farewell, Greenland 5–9 August, 1959.

into an area where water of 34.90‰ is predominant. Figure 52 does not show a corresponding distortion of the isotherms in this vicinity.

Figure 50 shows a schematic representation of approximate volume transport in millions of cubic meters per second for the second, third, fourth, and postseason cruises. Time has not yet permitted a full evaluation of the volume transport. A more complete analysis of volume and heat transports will be reported in a subsequent bulletin of this series.

TABLE OF OCEANOGRAPHIC DATA

The data collected in 1959 are tabulated below. The individual station headings give the station number, date, geographical position, depth of water and dynamic height of the sea surface used in the construction of the dynamic topographic charts shown in figures 44, 45, 46, 47, 48, and 51. The depths of water are rough approximations being the uncorrected sonic soundings based on a sounding velocity of 800 fathoms per second and containing an additional mechanical speed error of about 1/60. Where the depths of scaled values are enclosed in parentheses, the data are based on extrapolated vertical distribution curves of temperature or salinity or both. Asterisks appearing before observed temperatures indicate that these temperatures were determined from the depth of reversal and the corrected reading of an unprotected thermometer. The symbol σ_t signifies 1,000 (density − 1) at atmospheric pressure and temperature t.

TABLE OF OCEANOGRAPHIC DATA
STATIONS OCCUPIED IN 1959

Station 6890; 5 April; 41°59′N., 50°58′W.; depth 3,200 m.; dynamic height 971.016.

Observed values			Scaled values			
Depth, meters	Temperature, °C.	Salinity, ‰	Depth, meters	Temperature, °C.	Salinity, ‰	σ_t
0	3.65	33.18	0	3.65	33.18	26.39
26	3.03	33.20	25	3.05	33.20	26.47
51	2.57	33.22	50	2.60	33.22	26.52
77	2.18	33.37	75	2.20	33.35	26.65
103	1.58	33.70	100	1.60	33.63	26.92
153	3.33	34.30	150	3.25	34.29	27.31
205	2.43	34.26	200	2.50	34.26	27.36
308	3.92	34.77	300	3.80	34.74	27.62
338	4.38	34.855	400	4.60	34.92	27.68
514	4.73	34.99	600	4.60	34.99	27.73
695	4.45	34.995	(800)	4.25	34.98	27.76
			(1,000)	3.90	34.93	27.76

Station 6891; 6 April; 42°00′N., 51°57′W.; depth 3,731 m.; dynamic height 971.036.

Observed values			Scaled values			
Depth, meters	Temperature, °C.	Salinity, ‰	Depth, meters	Temperature, °C.	Salinity, ‰	σ_t
0	3.47	33.26	0	3.47	33.26	26.47
25	4.60	33.52	25	4.60	33.52	26.57
51	6.23	33.93	50	6.15	33.92	26.70
76	7.98	34.45	75	7.90	34.45	26.88
102	10.44	35.15	100	10.35	35.14	27.02
152	8.44	34.96	150	8.45	34.96	27.19
204	7.69	34.94	200	7.70	34.94	27.29
306	6.50	35.015	300	6.55	35.01	27.51
423	5.42	35.00	400	5.60	35.00	27.62
634	4.29	34.945	600	4.40	34.95	27.72
845	4.14	34.96	800	4.15	34.96	27.76
1,057	4.03	34.965	1,000	4.05	34.96	27.77

STATIONS OCCUPIED IN 1959—Continued

Observed values			Scaled values			
Depth, meters	Temperature, °C.	Salinity, ‰	Depth, meters	Temperature, °C.	Salinity, ‰	σ_t
Station 6892; 6 April; 42°20.5′N., 51°25′W.; depth 2,834 m.; dynamic height 970.995.						
0	2.93	33.23	0	2.93	33.23	26.50
25	2.84	33.34	25	2.84	33.34	26.60
52	2.82	33.52	50	2.85	33.52	26.74
77	0.03	33.53	75	0.10	33.53	26.93
103	4.78	34.26	100	4.35	34.20	27.13
154	1.75	34.21	150	1.80	34.21	27.38
205	4.64	34.66	200	4.40	34.62	27.46
308	4.82	34.83	300	4.80	34.82	27.58
424	4.64	34.91	400	4.70	34.90	27.65
630	4.49	34.965	600	4.50	34.96	27.72
831	4.20	34.96	800	4.25	34.96	27.75
1,035	3.91	34.94	1,000	3.95	34.94	27.76
1,553	3.54	34.92				
Station 6893; 6 April; 42°45.5′N., 51°04′W.; depth 1,829 m.; dynamic height 971.044.						
0	1.48	33.19	0	1.48	33.19	26.58
19	−0.12	33.34	25	−0.15	33.25	26.72
38	−0.26	33.36	50	−0.35	33.40	26.85
57	−0.38	33.42	75	−0.45	33.47	26.92
77	−0.38	33.48	100	3.20	34.10	27.14
114	5.80	34.50	150	0.90	33.96	27.24
152	0.78	33.95	200	1.50	34.10	27.31
229	1.95	34.18	300	2.40	34.34	27.43
389	2.83	34.53	400	2.90	34.55	27.56
585	3.93	34.83	600	3.95	34.83	27.67
782	3.91	34.85	800	3.90	34.86	27.71
979	4.14	34.935	1,000	4.15	34.93	27.73
1,479	3.54	34.90				
Station 6894; 6 April; 42°57.5′N., 50°58′W.; depth 1,024 m.; dynamic height 971.095.						
0	0.69	33.22	0	0.69	33.22	26.65
26	0.56	33.24	25	0.60	33.24	26.68
52	0.00	33.33	50	0.00	33.33	26.78
78	−0.31	33.41	75	−0.30	33.40	26.85
104	−0.38	33.44	100	−0.40	33.43	26.88
155	−0.34	33.58	150	−0.35	33.56	26.98
208	0.00	33.72	200	−0.10	33.70	27.08
312	3.42	34.52	300	2.90	34.42	27.46
406	2.73	34.54	400	3.55	34.53	27.47
609	3.70	34.78	600	3.70	34.77	27.66
812	3.78	34.86	800	3.80	34.85	27.71
1,015	3.73	34.88	1,000	3.75	34.88	27.73
Station 6895; 6 April; 43°01.5′N., 50°52′W.; depth 439 m.; dynamic height 971.130.						
0	2.75	32.22	0	2.75	32.22	25.71
24	0.74	33.12	25	0.65	33.12	26.58
47	0.12	33.20	50	0.05	33.22	26.69
71	−0.37	33.38	75	−0.40	33.39	26.85
95	−0.39	33.44	100	−0.40	33.46	26.91
142	−0.20	33.64	150	−0.15	33.66	27.06
189	0.10	33.76	200	0.20	33.79	27.14
284	1.06	34.06	300	1.15	34.09	27.32
331	1.29	34.13	(400)	1.70	34.23	27.39

Observed values			Scaled values			
Depth, meters	Temperature, °C.	Salinity, ‰	Depth, meters	Temperature, °C.	Salinity, ‰	σ_t
Station 6896; 6 April; 43°04.5′N., 50°47′W.; depth 168 m.; dynamic height 971.152.						
0	2.76	32.18	0	2.76	32.18	25.68
27	0.80	32.64	25	0.85	32.61	26.17
53	1.37	32.98	50	1.35	32.96	26.40
80	−0.22	33.35	75	−0.05	33.30	26.75
107	−0.26	33.41	100	−0.30	33.39	26.84
159	0.23	33.78	150	0.10	33.72	27.09
Station 6897; 6 April; 43°09.5′N., 50°36′W.; depth 91 m.; dynamic height 971.161.						
0	2.68	32.22	0	2.68	32.22	25.71
25	0.70	32.54	25	0.70	32.54	26.11
50	0.53	32.78	50	0.53	32.78	26.31
75	−0.15	33.22	75	−0.15	33.22	26.70
Station 6898; 6 April; 43°20′N., 50°16′W.; depth 64 m.; dynamic height 971.192.						
0	2.38	32.21	0	2.38	32.21	25.73
25	1.91	32.20	25	1.91	32.20	25.76
51	1.31	32.24	50	1.35	32.24	25.83
Station 6899; 6 April; 43°00′N., 50°14′W.; depth 95 m.; dynamic height 971.149.						
0	1.81	32.46	0	1.81	32.46	25.97
24	0.77	32.56	25	0.70	32.57	26.14
47	0.04	33.07	50	−0.05	33.11	26.60
71	−0.20	33.32	75	−0.20	33.32	26.78
Station 6900; 7 April; 42°44′N., 50°14′W.; depth 327 m.; dynamic height 971.123.						
0	1.76	32.54	0	1.76	32.54	26.05
25	0.12	33.23	25	0.12	33.23	26.70
50	−0.31	33.30	50	−0.31	33.30	26.76
75	−0.35	33.40	75	−0.35	33.40	26.85
100	−0.34	--------	100	−0.34	33.43	26.87
150	−0.26	33.50	150	−0.26	33.50	26.93
200	0.03	33.68	200	0.03	33.68	27.06
300	0.91	34.01	300	0.91	34.01	27.28
Station 6901; 7 April; 42°34.5′N., 50°16′W.; depth 2,058 m.; dynamic height 971.046.						
0	1.31	32.95	0	1.31	32.95	26.40
25	0.07	33.22	25	0.07	33.22	26.69
50	−0.45	33.37	50	−0.45	33.37	26.83
75	−0.31	33.44	75	−0.31	33.44	26.88
99	−0.31	33.57	100	−0.30	33.57	26.99
149	0.27	33.82	150	0.30	33.83	27.16
199	1.34	34.20	200	1.35	34.20	27.40
298	2.40	34.46	300	2.40	34.46	27.53
404	2.94	34.58	400	2.90	34.57	27.58
606	3.86	34.79	600	3.85	34.78	27.64
808	3.94	34.86	800	3.95	34.86	27.70
1,010	3.72	34.88	1,000	3.75	34.88	27.73
1,516	3.74	34.93				

TABLE OF OCEANOGRAPHIC DATA—Continued
STATIONS OCCUPIED IN 1959—Continued

Station 6902; 7 April; 42°24.5′N., 50°11′W.; depth 2,651 m.; dynamic height 970.989.

Observed values			Scaled values			
Depth, meters	Temperature, °C.	Salinity, ‰	Depth, meters	Temperature, °C.	Salinity, ‰	σ_t
0	0.41	33.27	0	0.41	33.27	26.71
25	−0.40	33.34	25	−0.40	33.34	26.81
51	−0.55	33.42	50	−0.55	33.42	26.88
76	−0.14	33.68	75	−0.15	33.68	27.07
102	0.40	33.87	100	0.35	33.86	27.19
152	0.97	34.09	150	0.95	34.09	27.33
203	1.47	34.25	200	1.45	34.24	27.42
305	2.75	34.55	300	2.65	34.54	27.57
414	------	34.72	400	3.50	34.70	27.62
621	3.89	34.865	600	3.90	34.85	27.70
829	3.76	34.88	800	3.75	34.88	27.73
1,033	3.64	34.88	1,000	3.65	34.88	27.74
1,540	3.50	34.90				

Station 6903; 7 April; 42°00.5′N., 50°12′W.; depth 3,566 m.; dynamic height 970.911.

Observed values			Scaled values			
Depth, meters	Temperature, °C.	Salinity, ‰	Depth, meters	Temperature, °C.	Salinity, ‰	σ_t
0	4.05	33.23	0	4.05	33.23	26.39
25	2.64	34.07	25	2.64	34.07	27.20
51	3.87	34.49	50	3.85	34.48	27.41
76	3.95	34.60	75	3.95	34.60	27.49
102	4.20	34.66	100	4.20	34.66	27.52
152	4.23	34.72	150	4.20	34.72	27.57
202	4.36	34.76	200	4.35	34.76	27.58
304	4.55	34.82	300	4.55	34.82	27.61
482	4.54	34.94	400	4.55	34.89	27.66
679	4.20	34.95	600	4.30	34.94	27.72
880	4.21	34.98	800	4.20	34.97	27.77
1,077	4.01	34.98	1,000	4.10	34.98	27.78
1,476	3.67	34.96				

Station 6904; 7 April; 41°31′N., 50°12′W., depth 3,749 m.; dynamic height 971.275.

Observed values			Scaled values			
Depth, meters	Temperature, °C.	Salinity, ‰	Depth, meters	Temperature, °C.	Salinity, ‰	σ_t
0	15.26	35.89	0	15.26	35.89	26.62
25	15.24	35.89	25	15.24	35.89	26.63
48	15.08	35.90	50	15.00	35.90	26.68
73	14.29	35.77	75	14.30	35.77	26.74
97	14.10	35.73	100	14.10	35.72	26.74
146	13.54	35.56	150	13.50	35.56	26.74
195	13.26	35.62	200	13.15	35.62	26.86
292	11.41	35.38	300	11.05	35.35	27.05
267	11.56	35.42	400	8.80	35.11	27.26
384	9.06	35.14	600	6.40	34.97	27.50
491	7.41	34.98	800	4.40	34.85	27.64
594	6.43	34.975	(1,000)	3.90	34.90	27.74
812	4.35	34.85				

Station 6905; 7 April; 41°05.5′N., 50°12′W.; depth 3,749 m.; dynamic height 971.445.

Observed values			Scaled values			
Depth, meters	Temperature, °C.	Salinity, ‰	Depth, meters	Temperature, °C.	Salinity, ‰	σ_t
0	17.75	36.29	0	17.75	36.29	26.33
25	17.76	36.30	25	17.76	36.30	26.34
51	17.71	36.29	50	17.70	36.29	26.35
76	17.41	36.25	75	17.45	36.24	26.37
102	16.81	36.22	100	16.85	36.22	26.50
152	16.29	36.16	150	16.30	36.16	26.59
203	15.34	36.00	200	15.35	36.01	26.69
305	14.09	35.79	300	14.15	35.80	26.79
417	12.32	35.55	400	12.65	35.59	26.93
625	7.64	35.07	600	8.20	35.12	27.36
836	4.88	34.935	800	5.10	34.95	27.64
1,046	4.66	35.00	1,000	4.70	34.99	27.72
1,573	3.86	34.96				

Station 6906; 8 April; 42°07′N., 49°14′W.; depth 3,200 m.; dynamic height 970.995.

Observed values			Scaled values			
Depth, meters	Temperature, °C.	Salinity, ‰	Depth, meters	Temperature, °C.	Salinity, ‰	σ_t
0	3.92	33.23	0	3.92	33.23	26.41
25	2.44	33.34	25	2.44	33.34	26.63
51	2.25	33.45	50	2.25	33.44	26.73
76	6.43	34.50	75	6.30	34.45	27.10
102	7.05	34.69	100	7.00	34.67	27.18
152	7.07	34.83	150	7.05	34.83	27.29
202	4.67	34.59	200	4.70	34.59	27.40
304	5.22	34.87	300	5.20	34.87	27.57
407	4.24	34.84	400	4.25	34.84	27.65
611	4.47	34.96	600	4.45	34.96	27.73
816	4.07	34.95	800	4.10	34.95	27.76
1,019	3.95	34.95	1,000	3.95	34.95	27.77
1,528	3.56	34.935				

Station 6907; 8 April; 41°31′N., 48°51′W.; depth 3,292 m.; dynamic height 970.942.

Observed values			Scaled values			
Depth, meters	Temperature, °C.	Salinity, ‰	Depth, meters	Temperature, °C.	Salinity, ‰	σ_t
0	4.98	33.19	0	4.98	33.19	26.27
25	8.39	34.76	25	8.39	34.76	27.04
50	3.62	34.29	50	3.62	34.29	27.28
75	1.84	34.28	75	1.84	34.28	27.43
100	4.18	34.60	100	4.18	34.60	27.47
150	3.42	34.54	150	3.42	34.54	27.50
200	3.63	34.62	200	3.63	34.62	27.54
300	3.66	34.66	300	3.66	34.66	27.57
407	4.58	34.87	400	4.55	34.87	27.65
572	3.92	34.84	600	3.95	34.86	27.70
738	4.26	34.94	800	4.30	34.97	27.75
913	4.34	34.99	1,000	4.15	34.97	27.77
1,282	3.59	34.91				

Station 6908; 8 April; 40°59.5′N., 48°26′W.; depth 3,658 m.; dynamic height 971.245.

Observed values			Scaled values			
Depth, meters	Temperature, °C.	Salinity, ‰	Depth, meters	Temperature, °C.	Salinity, ‰	σ_t
0	12.51	35.22	0	12.51	35.22	26.68
26	12.83	35.35	25	12.80	35.35	26.72
52	13.03	35.51	50	13.00	35.51	26.81
78	12.78	35.45	75	12.80	35.46	26.81
104	12.58	35.40	100	12.60	35.41	26.81
155	12.26	35.34	150	12.25	35.34	26.82
206	12.25	35.40	200	12.25	35.40	26.87
310	11.18	35.38	300	11.30	35.38	27.03
390	9.44	35.20	400	9.25	35.18	27.24
587	6.18	35.00	600	6.05	34.99	27.56
786	4.78	34.975	800	4.75	34.98	27.70
984	4.41	34.985	1,000	4.40	34.98	27.74
1,486	3.78	34.95				

Station 6909; 9 April; 41°35′N., 47°16′W.; depth 4,390 m.; dynamic height 971.122.

Observed values			Scaled values			
Depth, meters	Temperature, °C.	Salinity, ‰	Depth, meters	Temperature, °C.	Salinity, ‰	σ_t
0	6.56	33.61	0	6.56	33.61	26.41
24	9.21	34.40	25	9.20	34.41	26.65
48	8.92	34.52	50	8.95	34.52	26.77
73	9.23	34.62	75	9.40	34.65	26.80
97	10.87	35.04	100	10.85	35.03	26.84
145	10.49	35.01	150	10.50	35.03	26.90
193	10.59	35.25	200	10.40	35.23	27.08
290	6.88	34.79	300	6.50	34.78	27.33
384	5.01	34.72	400	4.95	34.73	27.48
579	4.59	34.90	600	4.60	34.91	27.67
775	4.50	34.97	800	4.45	34.97	27.74
972	4.03	34.95	1,000	4.00	34.95	27.77
1,469	3.79	34.96				

TABLE OF OCEANOGRAPHIC DATA—Continued
STATIONS OCCUPIED IN 1959—Continued

Station 6910; 9 April; 42°02.5′ N., 47°49′ W.; depth 3,828 m.; dynamic height 971.090.

Observed values			Scaled values			
Depth, meters	Temperature, °C.	Salinity, ‰	Depth, meters	Temperature, °C.	Salinity, ‰	σ_t
0	6.00	33.53	0	6.00	33.53	26.41
24	6.25	33.82	25	6.30	33.84	26.62
49	7.62	34.17	50	7.75	34.18	26.68
73	8.50	34.40	75	8.45	34.40	26.75
98	7.89	34.46	100	7.95	34.48	26.89
147	9.47	34.97	150	0.45	34.97	27.04
195	8.98	35.00	200	8.80	34.99	27.16
293	5.85	34.71	300	5.80	34.71	27.37
412	5.41	34.89	400	5.45	34.88	27.54
621	4.24	34.92	600	4.35	34.92	27.71
831	4.11	34.93	800	4.10	34.93	27.74
1,037	4.05	34.96	1,000	4.05	34.95	27.76
1,549	3.57	34.925				

Station 6911; 9 April; 42°24′ N., 48°30′ W.; depth 3,365 m.; dynamic height 971.017.

Observed values			Scaled values			
Depth, meters	Temperature, °C.	Salinity, ‰	Depth, meters	Temperature, °C.	Salinity, ‰	σ_t
0	4.14	33.18	0	4.14	33.18	26.34
25	5.22	33.61	25	5.22	33.61	26.57
51	5.50	33.85	50	5.45	33.84	26.73
76	6.72	34.40	75	6.70	34.38	26.99
102	6.65	34.55	100	6.65	34.53	27.11
152	8.33	35.00	150	8.25	34.99	27.25
202	5.12	34.57	200	5.25	34.58	27.33
304	3.27	34.56	300	3.25	34.56	27.53
393	3.57	34.71	400	3.60	34.72	27.63
595	4.72	34.99	600	4.70	34.99	27.72
800	4.15	34.995	800	4.15	34.96	27.76
1,001	3.85	34.94	1,000	3.85	34.94	27.77
1,503	3.55	34.935				

Station 6912; 9 April; 42°44′ N., 49°08′ W.; depth 2,524 m.; dynamic height 970.909.

Observed values			Scaled values			
Depth, meters	Temperature, °C.	Salinity, ‰	Depth, meters	Temperature, °C.	Salinity, ‰	σ_t
0	2.79	33.73	0	2.79	33.73	26.91
26	1.41	33.92	25	1.40	33.91	27.16
52	1.63	34.08	50	1.65	34.07	27.28
78	1.81	34.24	75	1.80	34.21	27.38
104	3.51	34.48	100	3.15	34.44	27.44
155	4.92	34.77	150	4.85	34.74	27.51
208	5.36	34.92	200	5.35	34.90	27.57
312	5.10	34.96	300	5.15	34.96	27.65
400	4.85	34.98	400	4.85	34.98	27.69
599	4.52	34.99	600	4.55	34.99	27.74
799	4.22	34.98	800	4.20	34.98	27.27
1,000	3.83	34.94	1,000	3.85	34.94	27.77
1,507	3.44	34.91				

Station 6913; 9 April; 43°24′ N., 48°42′ W.; depth 1,829 m.; dynamic height 970.957.

Observed values			Scaled values			
Depth, meters	Temperature, °C.	Salinity, ‰	Depth, meters	Temperature, °C.	Salinity, ‰	σ_t
0	−0.18	33.24	0	−0.18	33.24	26.72
25	0.73	33.44	25	0.73	33.44	26.83
51	2.63	33.97	50	2.65	33.96	27.11
76	2.30	34.01	75	2.30	34.00	27.17
102	2.16	34.06	100	2.15	34.05	27.22
152	3.30	34.40	150	3.25	34.39	27.39
203	3.72	34.57	200	3.70	34.56	27.49
305	4.47	34.84	300	4.45	34.82	27.62
404	4.36	34.88	400	4.35	34.88	27.67
608	3.97	34.89	600	4.00	34.89	27.72
813	3.71	34.89	800	3.75	34.89	27.74
1,013	3.52	34.885	1,000	3.55	34.89	27.76
1,511	3.41	34.90				

Station 6914; 10 April; 43°09′ N., 48°10′ W.; depth 3,017 m.; dynamic height 971.009.

Observed values			Scaled values			
Depth, meters	Temperature, °C.	Salinity, ‰	Depth, meters	Temperature, °C.	Salinity, ‰	σ_t
0	5.81	33.55	0	5.81	33.55	26.45
25	5.72	33.56	25	5.72	33.56	26.47
51	6.26	33.97	50	6.20	33.95	26.72
76	9.33	34.88	75	9.30	34.87	26.99
102	8.16	34.83	100	8.30	34.84	27.12
152	5.55	34.64	150	5.55	34.63	27.33
204	6.47	34.83	200	6.40	34.82	27.38
306	3.87	34.63	300	3.90	34.63	27.52
425	5.09	34.98	400	4.90	34.92	27.65
638	4.54	34.99	600	4.60	34.99	27.73
853	4.21	34.97	800	4.25	34.97	27.76
1,064	3.92	34.95	1,000	4.00	34.96	27.78
1,586	3.43	34.915				

Station 6915; 10 April; 42°54′ N., 47°32′ W.; depth 3,603 m.; dynamic height 971.196.

Observed values			Scaled values			
Depth, meters	Temperature, °C.	Salinity, ‰	Depth, meters	Temperature, °C.	Salinity, ‰	σ_t
0	11.67	34.99	0	11.67	34.99	26.67
25	11.74	35.00	25	11.74	35.00	26.66
51	13.67	35.62	50	13.65	35.62	26.76
77	13.70	35.65	75	13.70	35.65	26.77
103	13.53	35.63	100	13.55	35.63	26.78
153	13.13	35.55	150	13.15	35.55	26.80
205	13.08	35.61	200	13.10	35.61	26.86
308	9.97	35.24	300	10.15	35.26	27.15
377	8.64	35.15	400	8.20	35.13	27.36
566	5.65	34.995	600	5.40	35.00	27.65
756	4.86	35.00	800	4.70	35.00	27.73
948	4.26	34.98	1,000	4.30	34.97	27.75
1,433	3.79	34.95				

Station 6916; 10 April; 42°39′ N., 46°49′ W.; depth 3,932 m.; dynamic height 971.456.

Observed values			Scaled values			
Depth, meters	Temperature, °C.	Salinity, ‰	Depth, meters	Temperature, °C.	Salinity, ‰	σ_t
0	15.16	36.02	0	15.16	36.02	26.74
25	15.22	36.02	25	15.22	36.02	26.73
50	15.21	36.02	50	15.21	36.02	26.73
76	15.23	36.02	75	15.20	36.02	26.73
101	15.23	36.02	100	15.25	36.02	26.72
151	15.28	36.04	150	15.25	36.04	26.73
201	15.29	36.07	200	15.30	36.07	26.75
302	15.02	36.04	300	15.00	36.04	26.79
405	13.27	35.72	400	13.35	35.74	26.91
609	9.50	35.26	600	10.05	35.28	27.18
813	6.79	35.17	800	6.90	35.17	27.50
1,017	5.78	35.16	1,000	5.85	35.16	27.72
1,535	3.86	34.95				

Station 6917; 10 April; 42°24′ N., 46°17′ W.; depth 4,481 m.; dynamic height 971.503.

Observed values			Scaled values			
Depth, meters	Temperature, °C.	Salinity, ‰	Depth, meters	Temperature, °C.	Salinity, ‰	σ_t
0	15.36	36.00	0	15.36	36.00	26.68
26	15.38	36.00	25	15.35	36.00	26.68
52	15.38	36.00	50	15.40	36.00	26.67
78	15.34	35.98	75	15.35	35.99	26.67
104	14.70	35.83	100	14.80	35.85	26.68
155	14.36	35.77	150	14.35	35.78	26.73
207	15.05	35.99	200	14.95	35.98	26.76
311	14.72	35.945	300	14.80	35.96	26.77
399	13.61	35.75	400	13.60	35.75	26.87
602	10.58	35.36	600	10.60	35.36	27.15
807	6.92	35.04	800	7.00	35.04	27.47
1,009	6.27	35.20	1,000	6.35	35.20	27.68
1,514	4.01	34.96				

TABLE OF OCEANOGRAPHIC DATA—Continued
STATIONS OCCUPIED IN 1959—Continued

Station 6918; 10 April; 42°48′ N., 45°52′ W.; depth 4,618 m.; dynamic height 971.510.

Observed values			Scaled values			
Depth, meters	Temperature, °C.	Salinity, ‰	Depth, meters	Temperature, °C.	Salinity, ‰	σ_t
0	14.53	35.89	0	14.53	35.89	26.78
24	14.57	35.89	25	14.55	35.89	26.77
49	14.57	35.89	50	14.55	35.89	26.77
73	14.56	35.89	75	14.55	35.89	26.77
98	14.59	35.89	100	14.60	35.89	26.76
146	14.76	35.95	150	14.75	35.95	26.78
195	14.79	35.97	200	14.75	35.97	26.79
293	14.75	--------	300	14.75	35.97	26.79
343	14.77	35.98	400	14.35	35.90	26.82
519	12.55	35.62	600	10.90	35.39	27.11
700	8.91	35.14	800	6.90	34.99	27.44
879	5.82	34.93	1,000	5.10	34.93	27.62
1,334	4.16	34.945				

Station 6919; 10 April; 43°12.5′ N., 45°28′ W.; depth 4,663 m., dynamic height 971.496.

Observed values			Scaled values			
Depth, meters	Temperature, °C.	Salinity, ‰	Depth, meters	Temperature, °C.	Salinity, ‰	σ_t
0	14.65	35.95	0	14.65	35.95	26.80
24	14.68	35.96	25	14.65	35.96	26.81
48	14.67	35.955	50	14.65	35.95	26.80
73	14.67	35.95	75	14.65	35.95	26.80
97	14.70	35.95	100	14.70	35.95	26.79
145	14.70	35.95	150	14.70	35.95	26.79
193	14.75	35.96	200	14.75	25.96	26.78
290	14.79	36.00	300	14.75	36.00	26.82
394	14.72	35.99	400	14.70	35.99	26.82
592	11.26	35.45	600	11.10	35.48	27.15
791	7.39	35.05	800	7.20	35.04	27.44
989	4.88	34.905	1,000	4.85	34.91	27.64
1,480	4.04	34.95				

Station 6920; 11 April; 43°21′ N., 46°04′ W.; depth 4,572 m.; dynamic height 971.470.

Observed values			Scaled values			
Depth, meters	Temperature, °C.	Salinity, ‰	Depth, meters	Temperature, °C.	Salinity, ‰	σ_t
0	14.61	35.90	0	14.61	35.90	26.77
23	14.67	35.90	25	14.65	35.90	26.76
46	14.68	35.91	50	14.70	35.91	26.76
70	14.71	35.92	75	14.70	35.92	26.77
93	14.78	35.92	100	14.75	35.93	26.76
139	14.91	36.03	150	14.90	36.03	26.81
185	14.91	36.03	200	14.90	36.03	26.81
278	14.88	36.03	300	14.85	36.03	26.82
338	14.84	36.02	400	14.35	35.91	26.83
521	12.17	35.58	600	10.55	35.36	27.16
715	8.20	35.12	800	6.70	35.07	27.54
905	5.83	35.025	1,000	5.35	35.02	27.67
1,405	4.31	34.985				

Station 6921; 11 April; 43°31′ N., 46°41′ W.; depth 4,207 m.; dynamic height 971.390.

Observed values			Scaled values			
Depth, meters	Temperature, °C.	Salinity, ‰	Depth, meters	Temperature, °C.	Salinity, ‰	σ_t
0	14.98	35.97	0	14.98	35.97	26.74
22	14.99	35.97	25	15.00	35.97	26.74
44	15.01	35.97	50	15.00	35.97	26.74
66	15.02	35.97	75	15.05	35.97	26.73
87	15.04	35.98	100	15.05	35.98	26.73
132	15.06	35.99	150	15.15	36.02	26.74
176	15.36	36.08	200	15.30	36.05	26.73
263	14.87	35.95	300	14.25	35.87	26.82
420	11.82	35.50	400	12.20	35.56	27.00
643	7.27	35.06	600	8.15	35.11	27.36
875	5.55	35.05	800	5.90	35.05	27.62
1,101	4.38	34.955	1,000	4.75	34.99	27.71
1,676	3.81	34.95				

Station 6922; 11 April; 43°41′ N., 47°19′ W.; depth 4,115 m.; dynamic height 971.166.

Observed values			Scaled values			
Depth, meters	Temperature, °C.	Salinity, ‰	Depth, meters	Temperature, °C.	Salinity, ‰	σ_t
0	9.29	34.45	0	9.29	34.45	26.66
28	9.35	34.45	25	9.35	34.45	26.65
57	9.70	34.67	50	9.60	34.61	26.74
85	10.51	34.88	75	10.20	34.80	26.78
113	11.23	35.09	100	10.90	35.00	26.81
183	12.16	35.40	150	11.85	35.28	26.85
226	9.57	34.94	200	11.15	35.26	26.97
339	8.63	35.10	200	9.00	35.05	27.18
424	5.96	34.84	400	6.65	34.91	27.42
639	4.37	34.89	600	4.45	34.87	27.66
859	4.47	34.975	800	4.45	34.95	27.72
1,073	4.12	34.965	1,000	4.25	34.97	27.76
1,608	3.45	34.91				

Station 6923; 11 April; 43°52′ N., 48°02′ W.; depth 3,676 m.; dynamic height 970.906.

Observed values			Scaled values			
Depth, meters	Temperature, °C.	Salinity, ‰	Depth, meters	Temperature, °C.	Salinity, ‰	σ_t
0	3.09	33.92	0	3.09	33.92	27.04
24	3.13	33.92	25	3.15	33.92	27.03
48	3.19	34.14	50	3.25	34.15	27.20
72	4.32	34.40	75	4.50	34.44	27.31
97	5.54	34.67	100	5.50	34.67	27.38
144	3.00	34.44	150	3.05	34.46	27.47
192	4.36	34.77	200	4.35	34.78	27.59
289	4.16	34.84	300	4.15	34.85	27.67
390	4.02	34.88	400	4.00	34.87	27.71
592	3.85	34.90	600	3.85	34.90	27.74
799	3.88	34.93	800	3.90	34.93	27.76
999	3.62	34.92	1,000	3.60	34.92	27.79
1,500	3.42	34.905				

Station 6924; 11 April; 44°00′ N., 48°30′ W.; depth 3,292 m.; dynamic height 970.957.

Observed values			Scaled values			
Depth, meters	Temperature, °C.	Salinity, ‰	Depth, meters	Temperature, °C.	Salinity, ‰	σ_t
0	3.38	33.99	0	3.38	33.99	27.06
26	3.40	34.00	25	3.40	34.00	27.07
52	2.25	33.98	50	2.25	33.98	27.15
78	2.24	34.00	75	2.25	34.00	27.17
104	2.38	34.04	100	2.35	34.04	27.19
155	2.48	34.24	150	2.45	34.21	27.32
208	4.05	34.59	200	3.90	34.55	27.46
312	4.45	34.80	300	4.45	34.78	27.58
419	4.26	34.87	400	4.30	34.86	27.66
626	3.96	34.885	600	4.00	34.88	27.71
831	3.76	34.905	800	3.80	34.90	27.75
1,037	3.58	34.91	1,000	3.60	34.91	27.78
1,549	3.35	34.91				

Station 6925; 11–12 April; 44°05′ N., 48°50′ W.; depth 1,646 m.; dynamic height 970.928.

Observed values			Scaled values			
Depth, meters	Temperature, °C.	Salinity, ‰	Depth, meters	Temperature, °C.	Salinity, ‰	σ_t
0	0.05	33.39	0	0.05	33.39	26.83
27	−0.34	33.49	25	−0.35	33.49	26.92
53	0.60	33.94	50	0.40	33.91	27.23
80	2.79	34.28	75	2.45	34.25	27.35
106	3.04	34.36	100	3.00	34.34	27.38
158	2.32	34.46	150	2.35	34.45	27.52
212	2.49	34.52	200	2.45	34.51	27.56
318	3.32	34.69	300	3.25	34.68	27.62
331	3.52	34.69	400	3.75	34.79	27.66
502	3.92	34.86	600	3.80	34.87	27.73
674	3.75	34.87	800	3.80	34.89	27.74
853	3.82	34.905	1,000	3.75	34.90	27.75
1,310	3.58	34.90				

TABLE OF OCEANOGRAPHIC DATA—Ctoninued

STATIONS OCCUPIED IN 1959—Continued

Station 6926; 12 April; 44°07.5′ N., 48°56′ W.; depth 631 m.; dynamic height 970.999.

Observed values			Scaled values			
Depth, meters	Temperature, °C.	Salinity, ‰	Depth, meters	Temperature, °C.	Salinity, ‰	σ_t
0	−0.60	33.22	0	−0.60	33.22	26.71
26	−0.60	33.21	25	−0.60	33.21	26.71
52	−0.19	33.38	50	−1.15	33.37	26.86
79	−0.85	33.53	75	−0.90	33.51	26.97
104	−0.38	33.64	100	−0.45	33.63	27.04
157	1.37	34.05	150	1.15	34.00	27.25
209	2.07	34.33	200	2.00	34.30	27.43
313	2.63	34.56	300	2.60	34.54	27.57
375	2.80	34.60	400	2.90	34.62	27.62
604	3.58	34.83	600	3.60	34.82	27.71

Station 6927; 12 April; 44°09″ N., 49° 04′ W.; depth 183 m.; dynamic height 971.107.

Observed values			Scaled values			
Depth, meters	Temperature, °C.	Salinity, ‰	Depth, meters	Temperature, °C.	Salinity, ‰	σ_t
0	−0.81	33.14	0	−0.81	33.14	26.66
26	−0.80	33.14	25	−0.80	33.14	26.66
53	−0.87	33.31	50	−0.85	33.29	26.77
79	−1.04	33.42	75	−1.00	33.41	26.89
106	−0.96	33.44	100	−1.00	33.43	26.90
158	−0.41	33.59	150	−0.50	33.57	27.00

Station 6928; 12 April; 44.10.5′ N., 49°11′ W.; depth 91 m.; dynamic height 971.115.

Observed values			Scaled values			
Depth, meters	Temperature, °C.	Salinity, ‰	Depth, meters	Temperature, °C.	Salinity, ‰	σ_t
0	−0.63	33.16	0	−0.63	33.16	26.67
26	−0.62	33.16	25	−0.60	33.16	26.66
53	−0.74	33.17	50	−0.75	33.17	26.68
79	−0.65	33.23	75	−0.65	33.22	26.72

Station 6929; 12 April; 44°13′ N., 49°23′ W.; depth 48 m.; dynamic height 971.124.

Observed values			Scaled values			
Depth, meters	Temperature, °C.	Salinity, ‰	Depth, meters	Temperature, °C.	Salinity, ‰	σ_t
0	1.16	33.02	0	1.16	33.02	26.47
25	0.03	33.21	25	0.03	33.21	26.69
40	−0.10	33.25				

Station 6930; 12 April; 44°54′ N., 49°25′ W.; depth 80 m.; dynamic height 971.126.

Observed values			Scaled values			
Depth, meters	Temperature, °C.	Salinity, ‰	Depth, meters	Temperature, °C.	Salinity, ‰	σ_t
0	0.26	33.06	0	0.26	33.06	26.55
25	−0.24	33.20	25	−0.24	33.20	26.69
51	−0.34	33.26	50	−0.35	33.26	26.73
71	−0.34	33.26	(75)	−0.35	33.26	26.73

Station 6931; 12 April; 44°53.5′ N., 49°22′ W.; depth 90 m.; dynamic height 971.129.

Observed values			Scaled values			
Depth, meters	Temperature, °C.	Salinity, ‰	Depth, meters	Temperature, °C.	Salinity, ‰	σ_t
0	0.18	33.07	0	0.18	33.07	26.56
26	−0.03	33.10	25	0.00	33.10	26.59
51	−0.37	33.24	50	−0.35	33.23	26.71
77	−0.52	33.26	75	−0.50	33.26	26.74

Station 6932; 12 April; 44°50.5′ N., 48°55′ W.; depth 732 m.; dynamic height 971.101.

Observed values			Scaled values			
Depth, meters	Temperature, °C.	Salinity, ‰	Depth, meters	Temperature, °C.	Salinity, ‰	σ_t
0	−0.89	33.15	0	−0.89	33.15	26.67
25	−0.99	33.16	25	−0.94	33.16	26.68
50	−1.13	33.22	50	−1.13	33.22	26.74
76	−1.31	33.33	75	−1.30	33.33	26.83
101	−1.04	33.46	100	−1.05	33.45	26.92
151	−0.39	33.58	150	−0.40	33.58	27.00
201	−0.15	33.66	200	−0.15	33.66	27.06
302	1.45	34.16	300	1.40	34.15	27.36
407	2.08	34.38	400	2.05	34.37	27.49
617	3.20	34.69	600	3.15	34.67	27.63

Station 6933; 12 April; 44°49′ N., 48°41′ W.; depth 1,554 m.; dynamic height 970.975.

Observed values			Scaled values			
Depth, meters	Temperature, °C.	Salinity, ‰	Depth, meters	Temperature, °C.	Salinity, ‰	σ_t
0	−0.55	33.39	0	−0.55	33.39	26.85
25	−0.57	33.40	25	−0.57	33.40	26.86
50	−0.46	33.64	50	−0.46	33.64	27.05
75	0.56	33.93	75	0.56	33.93	27.23
100	2.31	34.20	100	2.31	34.20	27.33
150	2.62	34.26	150	2.62	34.26	27.35
199	3.32	34.38	200	3.30	34.39	27.39
299	2.50	34.49	300	2.50	34.49	27.54
390	2.96	34.64	400	3.00	34.65	27.63
584	3.97	34.85	600	3.95	34.85	27.69
778	3.70	34.87	800	3.70	34.87	27.74
971	3.62	34.88	1,000	3.60	34.88	27.75
1,450	3.55	34.89				

Station 6934; 12 April; 44°46.5′ N., 48°26′ W.; depth 2,012 m.; dynamic height 970.906.

Observed values			Scaled values			
Depth, meters	Temperature, °C.	Salinity, ‰	Depth, meters	Temperature, °C.	Salinity, ‰	σ_t
0	1.31	33.82	0	1.31	33.82	27.10
25	1.32	33.84	25	1.32	33.84	27.11
51	3.11	34.38	50	3.10	34.38	27.40
76	3.29	34.46	75	3.30	34.46	27.45
102	3.10	34.47	100	3.10	34.47	27.48
152	3.62	34.62	150	3.60	34.61	27.54
204	3.70	34.70	200	3.70	34.69	27.59
306	4.08	34.82	300	4.05	34.82	27.66
403	3.92	34.84	400	3.90	34.83	27.68
605	3.94	34.88	600	3.95	34.88	27.71
809	3.66	34.875	800	3.65	34.88	27.74
1,008	3.58	34.88	1,000	3.60	34.88	27.75
1,503	3.45	34.91				

Station 6935; 12–13 April; 44°43′ N., 48°03′ W.; depth 3,384 m.; dynamic height 970.973.

Observed values			Scaled values			
Depth, meters	Temperature, °C.	Salinity, ‰	Depth, meters	Temperature, °C.	Salinity, ‰	σ_t
0	3.11	33.99	0	3.11	33.99	27.09
24	3.19	33.99	25	3.20	33.99	27.08
49	3.20	33.99	50	3.20	33.99	27.08
73	2.97	34.01	75	2.95	34.01	27.12
98	2.71	34.04	100	2.70	34.04	27.16
146	2.84	34.11	150	2.85	34.12	27.22
195	3.18	34.30	200	3.25	34.33	27.34
293	4.45	34.76	300	4.45	34.77	27.58
378	4.26	34.85	400	4.20	34.85	27.67
570	3.91	34.875	600	3.90	34.88	27.72
764	3.77	34.895	800	3.75	34.89	27.74
959	3.55	34.89	1,000	3.55	34.89	27.76
1,456	3.42	34.90				

TABLE OF OCEANOGRAPHIC DATA—Continued
STATIONS OCCUPIED IN 1959—Continued

Station 6936; 13 April; 44°38.5′ N., 47°22′ W.; depth 3,768 m.; dynamic height 970.913.

Observed values			Scaled values			
Depth, meters	Temperature, °C.	Salinity, ‰	Depth, meters	Temperature, °C.	Salinity, ‰	σ_t
0	3.42	34.03	0	3.42	34.03	27.09
25	3.42	34.03	25	3.42	34.03	27.09
50	3.36	34.05	50	3.36	34.03	27.10
75	2.19	34.09	75	2.19	34.09	27.25
100	1.81	34.16	100	1.81	34.16	27.34
149	4.72	34.70	150	4.70	34.70	27.49
199	4.28	34.72	200	4.30	34.73	27.56
299	4.46	34.87	300	4.45	34.87	27.66
398	4.17	34.88	400	4.15	34.88	27.69
			(600)	3.85	34.90	27.74
			(800)	3.80	34.91	27.76
			(1,000)	3.65	34.91	27.77

Station 6937; 13 April; 44°21′ N., 46°33′ W.; depth 3,786 m.; dynamic height 970.965.

Observed values			Scaled values			
Depth, meters	Temperature, °C.	Salinity, ‰	Depth, meters	Temperature, °C.	Salinity, ‰	σ_t
0	4.69	33.79	0	4.69	33.79	26.77
26	4.73	33.80	25	4.75	33.80	26.77
51	2.99	33.92	50	3.00	33.91	27.04
77	8.22	34.93	75	8.20	34.93	27.20
102	6.32	34.65	100	6.45	34.65	27.24
153	5.45	34.64	150	5.50	34.65	27.36
204	5.16	34.75	200	5.15	34.74	27.47
306	5.44	34.96	300	5.45	34.95	27.60
406	5.28	35.00	400	5.30	35.00	27.66
612	4.67	35.00	600	4.70	35.00	27.73
821	3.75	34.90	800	3.80	34.90	27.75
1,026	3.76	34.92	1,000	3.75	34.92	27.77

Station 6938; 13 April; 44°25′ N., 45°58′ W.; depth 3,841 m.; dynamic height 971.034.

Observed values			Scaled values			
Depth, meters	Temperature, °C.	Salinity, ‰	Depth, meters	Temperature, °C.	Salinity, ‰	σ_t
0	5.41	33.79	0	5.41	33.79	26.69
26	5.63	33.79	25	5.65	33.79	26.66
51	5.68	33.91	50	5.70	33.91	26.76
77	5.97	33.94	75	5.95	33.94	26.75
102	4.15	33.94	100	4.20	33.95	26.95
153	6.75	34.60	150	6.70	34.59	27.15
204	6.38	34.71	200	6.40	34.71	27.29
306	5.20	34.82	300	5.25	34.82	27.53
402	5.04	34.92	400	5.05	34.92	27.63
609	4.00	34.88	600	4.00	34.88	27.71
818	3.96	34.92	800	3.95	34.92	27.75
1,022	3.71	34.90	1,000	3.75	34.90	27.75
1,529	3.50	34.91				

Station 6939; 13 April; 44°19.5′ N., 45°15′ W.; depth 4,390 m.; dynamic height 971.123.

Observed values			Scaled values			
Depth, meters	Temperature, °C.	Salinity, ‰	Depth, meters	Temperature, °C.	Salinity, ‰	σ_t
0	5.60	33.66	0	5.60	33.66	26.57
27	5.65	33.68	25	5.65	33.67	26.57
53	8.64	34.41	50	8.35	34.33	26.71
80	10.05	34.98	75	9.90	34.80	26.83
106	10.36	34.98	100	10.30	34.95	26.88
158	------	35.05	150	10.60	35.05	26.90
212	10.50	35.03	200	10.55	35.04	26.90
318	5.53	34.70	300	6.25	34.73	27.32
414	4.27	34.73	400	4.30	34.72	27.56
619	4.32	34.90	600	4.30	34.89	27.68
821	4.09	34.925	800	4.15	34.92	27.73
1,025	3.92	34.925	1,000	3.95	34.92	27.75
1,530	3.58	34.91				

Station 6940; 13 April; 44°50′ N., 45°14′ W.; depth 4,155 m.; dynamic height 970.986.

Observed values			Scaled values			
Depth, meters	Temperature, °C.	Salinity, ‰	Depth, meters	Temperature, °C.	Salinity, ‰	σ_t
0	5.22	34.02	0	5.22	34.02	26.89
25	5.20	34.02	25	5.20	34.02	26.90
49	5.14	34.02	50	5.20	34.03	26.90
74	6.89	34.57	75	6.95	34.58	27.11
98	7.16	34.66	100	7.15	34.66	27.15
147	4.83	34.54	150	4.80	34.54	27.35
196	4.51	34.52	200	4.50	34.52	27.37
294	4.44	34.77	300	4.45	34.78	27.58
406	4.49	34.88	400	4.50	34.88	27.65
612	4.02	34.89	600	4.05	34.89	27.71
823	3.78	34.88	800	3.80	34.88	27.73
1,030	3.61	34.89	1,000	3.65	34.89	27.75
1,551	3.52	34.91				

Station 6941; 14 April; 45°18.5′ N., 45°15′ W.; depth 4,155 m.; dynamic height 970.975.

Observed values			Scaled values			
Depth, meters	Temperature, °C.	Salinity, ‰	Depth, meters	Temperature, °C.	Salinity, ‰	σ_t
0	5.17	33.90	0	5.17	33.90	26.81
28	5.24	33.91	25	5.20	33.90	26.81
55	5.96	34.28	50	5.80	34.22	26.99
83	6.18	34.46	75	6.10	34.39	27.08
110	6.74	34.60	100	6.60	34.61	27.19
166	3.85	34.42	150	4.55	34.48	27.33
220	4.31	34.62	200	4.10	34.54	27.43
330	4.75	34.86	300	4.70	34.81	27.58
421	4.40	34.88	400	4.45	34.88	27.66
633	4.40	34.96	600	4.40	34.96	27.73
847	3.82	34.90	800	3.95	34.91	27.74
1,058	3.68	34.905	1,000	3.70	34.90	27.76
1,582	3.48	34.91				

Station 6942; 14 April; 45°20.5′ N., 45°59′ W.; depth, 3,475 m.; dynamic height 970.905.

Observed values			Scaled values			
Depth, meters	Temperature, °C.	Salinity, ‰	Depth, meters	Temperature, °C.	Salinity, ‰	σ_t
0	3.17	34.29	0	3.14	34.29	27.32
24	3.18	34.29	25	3.20	34.29	27.32
49	3.17	34.31	50	3.15	34.31	27.34
73	3.32	34.34	75	3.30	34.34	27.35
98	3.20	34.38	100	3.20	34.38	27.39
147	3.10	34.50	150	3.10	34.51	27.51
196	3.14	34.57	200	3.15	34.57	27.55
294	3.26	34.69	300	3.30	34.70	27.64
406	3.95	34.86	400	3.95	34.85	27.69
610	3.82	34.87	600	3.85	34.87	27.72
815	3.75	34.90	800	3.75	34.90	27.75
1,019	3.64	34.90	1,000	3.65	34.90	27.76
1.528	3.39	34.90				

Station 6943; 14 April; 45°19.5′ N., 46°40′ W.; depth 3,396 m.; dynamic height 970.944.

Observed values			Scaled values			
Depth, meters	Temperature, °C.	Salinity, ‰	Depth, meters	Temperature, °C.	Salinity, ‰	σ_t
0	3.37	34.23	0	3.37	34.23	27.25
26	3.37	34.23	25	3.40	34.23	27.25
52	3.39	34.24	50	3.40	34.23	27.25
79	3.37	34.28	75	3.35	34.27	27.29
105	3.41	34.33	100	3.40	34.32	27.33
156	4.32	34.51	150	4.25	34.48	27.36
209	4.39	34.64	200	4.40	34.62	27.46
314	3.80	34.72	300	3.85	34.71	27.59
391	3.85	34.78	400	3.85	34.79	27.65
587	4.28	34.93	600	4.25	34.93	27.72
784	3.63	34.86	800	3.65	34.86	27.73
978	3.71	34.88	1,000	3.70	34.88	27.74
1,458	3.45	34.91				

STATIONS OCCUPIED IN 1959—Continued

Observed values			Scaled values			
Depth, meters	Temperature, °C.	Salinity, ‰	Depth, meters	Temperature, °C.	Salinity, ‰	σ_t
Station 6944; 14 April; 45°19.5′ N., 47°24′ W.; depth 2,926 m.; dynamic height 970.933.						
0	2.41	34.00	0	2.41	34.00	27.16
25	2.50	34.00	25	2.50	34.00	27.15
52	2.49	34.00	50	2.50	34.00	27.15
77	2.55	34.10	75	2.55	34.09	27.22
103	2.69	34.22	100	2.60	34.21	27.31
154	3.48	34.43	150	3.40	34.41	27.40
205	4.22	34.66	200	4.15	34.64	27.50
308	4.48	34.83	300	4.45	34.82	27.62
399	4.45	34.90	400	4.45	34.90	27.68
604	4.01	34.91	600	4.00	34.91	27.74
811	3.63	34.88	800	3.65	34.88	27.74
1,014	3.49	34.88	1,000	3.50	34.88	27.76
1,528	3.38	34.91				
Station 6945; 14 April; 45°29.5′ N., 47°55′ W.; depth 1,591 m.; dynamic height 970.930.						
0	0.42	33.75	0	0.42	33.75	27.10
26	9.50	33.76	25	0.50	33.76	27.10
51	0.64	33.90	50	0.60	33.90	27.20
77	0.95	34.07	75	0.95	34.06	27.31
103	1.45	34.16	100	1.35	34.15	27.36
153	2.48	34.45	150	2.45	34.45	27.51
204	2.34	34.49	200	2.35	34.48	27.54
307	2.46	34.57	300	2.45	34.56	27.60
389	3.31	34.72	400	3.35	34.73	27.65
586	3.81	34.85	600	3.80	34.85	27.71
786	3.80	34.89	800	3.80	34.89	27.74
983	3.58	34.88	1,000	3.60	34.88	27.75
1,492	3.48	34.885				
Station 6946; 15 April; 45°35.5′ N., 48°10′ W.; depth 832 m.; dynamic height 970.993.						
0	−0.92	33.33	0	−0.92	33.33	26.82
23	−0.79	33.33	25	−0.80	33.33	26.81
47	−0.71	33.35	50	−0.65	33.36	26.83
70	0.03	33.64	75	0.10	33.66	27.04
94	0.32	33.75	100	0.40	33.78	27.12
141	0.96	34.03	150	1.10	34.07	27.32
188	1.75	34.26	200	1.85	34.30	27.44
282	2.42	34.53	300	2.50	34.56	27.60
362	2.84	34.65	400	2.95	34.67	27.65
546	3.22	34.73	(600)	3.25	34.74	27.67
Station 6947; 15 April; 45°40.5′ N., 48°23′ W.; depth 174 m.; dynamic height 971.069.						
0	−1.28	33.21	0	−1.28	33.21	26.73
26	−1.23	33.22	25	−1.20	33.22	26.74
52	−1.33	33.34	50	−1.30	33.33	26.83
78	−0.75	33.50	75	−0.80	33.48	26.93
105	−0.42	33.54	100	−0.45	33.53	26.96
156	−0.36	33.56	150	−0.35	33.56	26.98
Station 6948; 15 April; 45°44′ N., 48°29′ W.; depth 115 m.; dynamic height 971.076.						
0	−1.23	33.20	0	−1.33	33.20	26.72
26	−1.23	33.20	25	−1.20	33.21	26.73
52	−1.17	33.31	50	−1.15	33.30	26.80
78	−1.16	33.32	75	−1.15	33.32	26.82
104	−1.15	33.33	100	−1.15	33.33	26.83

Observed values			Sclaed values			
Depth, meters	Temperature, °C.	Salinity, ‰	Depth, meters	Temperature, °C.	Salinity, ‰	σ_t
Station 6949; 15 April; 45°50.5′ N., 48°35′ W.; depth 89 m.; dynamic height 971.085.						
0	−1.14	33.12	0	−1.14	33.12	26.65
26	−1.16	33.12	25	−1.15	33.12	26.66
51	−1.15	33.12	50	−1.15	33.12	26.66
77	−1.09	33.22	75	−1.10	33.21	26.73
Station 6950; 15 April; 46°06′ N., 48°49′ W.; depth 69 m.; dynamic height 971.087.						
0	−0.17	32.98	0	−0.17	32.98	26.51
26	−0.17	33.02	25	−0.15	33.02	26.54
52	−0.77	33.24	50	−0.75	33.22	26.72
Station 6951; 15 April; 46°16′ N., 48°58′ W.; depth 66 m.; dynamic height 971.104.						
0	−0.11	32.67	0	−0.11	32.67	26.25
28	−0.13	32.67	25	−0.10	32.67	26.25
57	−0.86	33.06	50	−0.70	33.97	26.52
Station 6952; 15 April; 46°15′ N., 48°35′ W.; depth 88 m.; dynamic height 971.082.						
0	−0.37	33.19	0	−0.37	33.19	26.68
25	−0.39	33.19	25	−0.39	33.19	26.69
51	−0.73	33.24	50	−0.75	33.24	26.74
76	−0.72	33.24	75	−0.70	33.24	26.74
Station 6953; 15 April; 46°13.5′ N., 47°58′ W.; depth 112 m.; dynamic height 971.083.						
0	−1.22	33.10	0	−1.22	33.10	26.64
26	−1.21	33.10	25	−1.20	33.10	26.64
51	−1.34	33.14	50	−1.35	33.14	26.68
77	−0.99	33.30	75	−1.00	33.30	26.79
103	−0.88	33.32	100	−0.90	33.32	26.81
Station 6954; 15 April; 46°13′ N., 47°42′ W.; depth 172 m.; dynamic height 971.088.						
0	−1.32	33.09	0	−1.32	33.09	26.63
22	−1.32	33.09	25	−1.30	33.09	26.63
43	−1.32	33.09	50	−1.30	33.09	26.63
65	−1.33	33.10	75	−1.35	33.14	26.68
87	−1.35	33.22	100	−1.15	33.30	26.80
130	−0.18	33.55	(150)	0.85	33.73	27.05
Station 6955; 15 April; 46°12′ N., 47°28′ W.; depth 677 m.; dynamic height 971.005.						
0	−1.21	33.27	0	−1.21	33.27	26.78
27	−1.19	33.27	25	−1.15	33.27	26.78
54	−1.18	33.30	50	−1.15	33.28	26.78
81	−0.74	33.53	75	−0.95	33.47	26.94
108	0.81	33.82	100	0.35	33.74	27.09
162	1.57	34.20	150	1.45	34.13	27.33
216	2.17	34.36	200	2.00	34.32	27.45
324	2.62	34.55	300	2.50	34.51	27.56
508	3.76	34.82	400	3.10	34.67	27.64
618	3.79	34.83	600	3.80	34.83	27.69

TABLE OF OCEANOGRAPHIC DATA—Continued
STATIONS OCCUPIED IN 1959—Continued

Observed values			Scaled values			
Depth, meters	Temperature, °C.	Salinity, ‰	Depth, meters	Temperature, °C.	Salinity, ‰	σ_t
Station 6956; 15 April; 46°11′ N., 47°10′ W.; depth 1,518 m.; dynamic height 970.901.						
0	2.12	34.31	0	2.12	34.31	27.43
27	2.09	34.32	25	2.10	34.32	27.44
53	2.18	34.34	50	2.20	34.34	27.45
80	2.30	34.43	75	2.25	34.41	27.50
106	2.58	34.51	100	2.50	34.49	27.54
160	2.75	34.59	150	2.75	34.58	27.59
213	2.87	34.63	200	2.85	34.62	27.62
319	3.09	34.68	300	3.05	34.68	27.64
362	3.13	34.70	400	3.25	34.73	27.66
543	3.80	34.84	600	3.80	34.84	27.70
724	3.77	34.85	800	3.75	34.84	27.70
915	3.70	34.83	1,000	3.65	34.84	27.71
1,411	3.47	34.87				
Station 6957; 16 April; 46°10′ N., 46°33′ W.; depth 503 m.; dynamic height 970.901.						
0	2.61	34.09	0	2.61	34.09	27.21
28	2.61	34.09	25	2.65	34.09	27.21
54	2.28	34.23	50	2.55	34.20	27.31
82	3.21	34.43	75	3.05	34.40	27.42
109	3.42	34.54	100	3.40	34.49	27.46
164	2.51	34.54	150	2.70	34.53	27.55
218	2.95	34.65	200	2.75	34.61	27.62
327	3.86	34.81	300	3.75	34.78	27.65
413	3.88	34.86	400	3.90	34.86	27.71
Station 6958; 16 April; 46°06.5′ N., 45°59′ W.; depth 1,371 m.; dynamic height 970.918.						
0	3.16	34.24	0	3.16	34.24	27.28
26	3.14	34.24	25	3.15	34.24	27.28
51	3.13	34.25	50	3.15	34.25	27.29
77	3.15	34.26	75	3.15	34.26	27.30
103	3.27	34.30	100	3.25	34.29	27.31
153	4.09	34.58	150	4.10	34.57	27.46
204	3.83	34.65	200	3.85	34.64	27.53
307	4.13	34.83	300	4.10	34.82	27.66
442	3.89	34.85	400	3.95	34.85	27.69
663	3.70	34.84	600	3.75	34.85	27.71
887	3.59	34.88	800	3.65	34.87	27.74
1,104	3.47	--------	(1,000)	3.55	34.88	27.75
Station 6959; 16 April; 46°06′ N., 45°18′ W.; depth 2,698 m.; dynamic height 970.907.						
0	3.93	34.41	0	3.93	34.46	27.38
26	3.66	34.47	25	3.65	34.47	27.42
52	3.60	34.48	50	3.60	34.48	27.43
78	3.57	34.49	75	3.60	34.49	27.44
103	3.56	34.48	100	3.55	34.48	27.43
154	3.72	34.60	150	3.70	34.59	27.51
206	3.58	34.62	200	3.60	34.62	27.55
309	3.80	34.76	300	3.80	34.75	27.63
391	3.74	34.78	400	3.75	34.78	27.65
586	3.87	34.855	600	3.85	34.86	27.71
781	3.71	34.875	800	3.70	34.87	27.74
979	3.58	34.875	1,000	3.60	34.88	27.75
1,480	3.49	34.90				

Observed values			Scaled values			
Depth, meters	Temperature, °C.	Salinity, ‰	Depth, meters	Temperature, °C.	Salinity, ‰	σ_t
Station 6960; 16 April; 46°05′ N., 44°39′ W.; depth 3,658 m.; dynamic height 970.973.						
0	5.45	33.93	0	5.45	33.93	26.80
25	5.55	33.97	25	5.55	33.97	26.82
51	7.49	34.74	50	7.50	34.75	27.17
76	5.07	34.48	75	5.15	34.49	27.27
102	3.75	34.40	100	3.75	34.40	27.35
152	3.82	34.44	150	3.80	34.44	27.38
203	3.35	34.51	200	3.35	34.51	27.48
305	3.06	34.69	300	3.05	34.59	27.57
377	2.88	34.58	400	2.90	34.60	27.60
569	3.90	34.83	600	3.90	34.84	27.69
762	3.80	34.86	800	3.75	34.86	27.72
956	3.63	34.855	1,000	3.60	34.85	27.73
1,450	3.42	34.895				
Station 6961; 16 April; 46°23.5′ N., 44°43′ W.; depth 2,280 m.; dynamic height 970.885.						
0	3.56	34.45	0	3.56	34.45	27.41
26	3.49	34.49	25	3.50	34.49	27.45
53	3.30	34.50	50	3.35	34.50	27.47
79	2.99	34.51	75	3.05	34.51	27.51
106	2.81	34.51	100	2.80	34.51	27.53
158	2.88	34.59	150	2.85	34.57	27.58
211	3.30	34.67	200	3.20	34.66	27.62
317	3.26	34.72	300	3.25	34.71	27.65
411	3.59	34.77	400	3.60	34.76	27.66
616	3.73	34.86	600	3.75	34.86	27.72
796	3.63	34.85	800	3.60	34.85	27.73
1,030	3.43	34.865	1,000	3.45	34.87	27.76
1,555	3.43	34.88				
Station 6962; 17 April; 46°31′ N., 44°44′ W.; depth 896 m.; dynamic height 970.863.						
0	2.73	34.46	0	2.73	34.44	27.50
22	2.68	34.47	25	2.70	34.47	27.51
45	2.51	34.48	50	2.60	34.47	27.52
67	2.56	34.46	75	2.55	34.47	27.53
90	2.57	34.48	100	2.55	34.49	27.54
135	2.70	34.52	150	2.80	34.56	27.57
180	3.00	34.65	200	3.15	34.70	26.65
270	3.57	34.40	300	3.60	34.80	27.69
395	3.72	34.82	400	3.70	34.83	27.70
601	3.69	34.86	600	3.70	34.86	27.73
Station 6963; 17 April; 46°35.5′ N., 44°46′ W.; depth 229 m.; dynamic height 970.873.						
0	2.62	34.36	0	2.62	34.36	27.43
22	2.61	34.36	25	2.60	34.36	27.43
45	2.49	34.35	50	2.50	34.35	27.43
67	2.52	34.40	75	2.55	34.41	27.48
90	2.57	34.45	100	2.60	34.47	27.52
134	2.77	34.55	150	2.85	34.57	27.58
179	2.98	34.59	(200)	3.05	34.60	27.58

TABLE OF OCEANOGRAPHIC DATA—Continued

STATIONS OCCUPIED IN 1959—Continued

Station 6964; 17 April; 46°40′ N., 44°48′ W.; depth 165 m.; dynamic height 970.886.

Observed values			Scaled values			
Depth, meters	Temperature, °C.	Salinity, ‰	Depth, meters	Temperature, °C.	Salinity, ‰	σ_t
0	2.63	34.30	0	2.63	34.30	27.38
26	2.64	34.33	25	2.60	34.33	27.40
53	2.53	34.33	50	2.55	34.33	27.41
79	2.54	34.33	75	2.55	34.33	27.41
105	2.53	34.32	100	2.55	34.33	27.41
157	2.62	34.42	150	2.60	34.41	27.47

Station 6965; 17 April; 46°48′ N., 44°51′ W.; depth 137 m.; dynamic height 970.890.

Observed values			Scaled values			
Depth, meters	Temperature, °C.	Salinity, ‰	Depth, meters	Temperature, °C.	Salinity, ‰	σ_t
0	2.68	34.31	0	2.68	34.31	27.38
26	2.66	34.31	25	2.70	34.31	27.38
52	2.57	34.30	50	2.60	34.30	27.38
79	2.56	34.30	75	2.55	34.30	27.39
105	2.57	34.32	100	2.55	34.31	27.40
131	2.45	34.40				

Station 6966; 17 April; 46°48′ N., 45°04′ W.; depth 172 m.; dynamic height 970.889.

Observed values			Scaled values			
Depth, meters	Temperature, °C.	Salinity, ‰	Depth, meters	Temperature, °C.	Salinity, ‰	σ_t
0	2.60	34.32	0	2.60	34.32	27.40
25	2.62	34.30	25	2.62	34.30	27.38
50	2.56	34.30	50	2.56	34.30	27.39
74	2.50	34.31	75	2.50	34.31	27.40
99	2.49	34.32	100	2.50	34.32	27.41
148	2.50	34.42	150	2.50	34.42	27.49

Station 6967; 17 April; 46°45.5′ N., 45°19′ W.; depth 220 m.; dynamic height 970.889.

Observed values			Scaled values			
Depth, meters	Temperature, °C.	Salinity, ‰	Depth, meters	Temperature, °C.	Salinity, ‰	σ_t
0	2.61	34.31	0	2.61	34.31	27.39
24	2.62	34.29	25	2.65	34.29	27.37
48	2.61	34.29	50	2.60	34.29	27.37
72	2.57	34.31	75	2.55	34.31	27.40
96	2.54	34.32	100	2.55	34.33	27.41
143	3.15	34.51	150	3.20	34.52	27.51
191	3.37	34.60	200	3.40	34.61	27.56

Station 6968; 17 April; 46°46′ N., 45°42′ W.; depth 262 m.; dynamic height 970.900.

Observed values			Scaled values			
Depth, meters	Temperature, °C.	Salinity, ‰	Depth, meters	Temperature, °C.	Salinity, ‰	σ_t
0	2.71	34.27	0	2.71	34.27	27.35
26	2.71	34.29	25	2.70	34.29	27.36
51	2.71	34.28	50	2.70	34.28	27.35
77	2.70	34.27	75	2.70	34.27	27.35
102	2.69	34.28	100	2.70	34.28	27.35
153	2.85	34.41	150	2.80	34.40	27.37
204	3.86	34.69	200	3.80	34.67	27.57
248	3.77	34.74				

Station 6969; 17 April; 46°46′ N., 46°12′ W.; depth 320 m.; dynamic height 970.899.

Observed values			Scaled values			
Depth, meters	Temperature, °C.	Salinity, ‰	Depth, meters	Temperature, °C.	Salinity, ‰	σ_t
0	2.74	34.26	0	2.74	34.26	27.34
26	2.72	--------	25	2.75	34.26	27.34
52	2.70	34.27	50	2.70	34.27	27.35
78	2.68	34.27	75	2.70	34.27	27.35
104	2.60	34.29	100	2.60	34.28	27.36
155	2.62	34.39	150	2.60	34.37	27.44
207	3.66	34.65	200	3.60	34.61	27.54
311	3.74	34.83	300	3.75	34.81	27.68

Station 6970; 17 April; 46°44.5′ N., 46°30′ W.; depth 686 m.; dynamic height 970.879.

Observed values			Scaled values			
Depth, meters	Temperature, °C.	Salinity, ‰	Depth, meters	Temperature, °C.	Salinity, ‰	σ_t
0	2.32	34.28	0	2.32	34.28	27.39
26	2.33	34.26	25	2.35	34.26	27.37
52	2.33	34.28	50	2.35	34.28	27.38
78	2.53	34.44	75	2.75	34.42	27.47
104	2.83	34.61	100	3.40	34.59	27.54
155	4.05	34.74	150	4.05	34.72	27.58
208	3.95	34.79	200	3.95	34.78	27.63
312	4.20	34.84	300	4.20	34.83	27.65
376	4.06	34.87	400	4.00	34.87	27.71
572	3.64	34.84	(600)	3.60	34.85	27.73

Station 6971; 17 April; 46°43′ N., 46°44′ W.; depth 1,244 m.; dynamic height 970.886.

Observed values			Scaled values			
Depth, meters	Temperature, °C.	Salinity, ‰	Depth, meters	Temperature, °C.	Salinity, ‰	σ_t
0	2.41	34.31	0	2.41	34.31	27.41
26	2.42	34.31	25	2.45	34.31	27.40
52	2.41	34.31	50	2.45	34.31	27.40
78	2.28	34.41	75	2.30	34.40	27.49
104	2.46	34.52	100	2.45	34.51	27.56
157	2.44	34.56	150	2.45	34.56	27.60
209	2.56	34.61	200	2.55	34.60	27.63
313	2.94	--------	300	2.90	34.66	27.65
424	3.60	34.78	400	3.50	34.76	27.67
636	3.71	34.85	600	3.70	34.84	27.71
850	3.61	--------	800	3.65	34.86	27.73
1,064	3.51	34.875	1,000	3.55	34.87	27.75

Station 6972; 18 April; 46°45′ N., 47°05′ W.; depth 631 m.; dynamic height 970.993.

Observed values			Scaled values			
Depth, meters	Temperature, °C.	Salinity, ‰	Depth, meters	Temperature, °C.	Salinity, ‰	σ_t
0	−1.17	33.16	0	−1.17	33.16	26.69
27	−1.19	33.19	25	−1.15	33.18	26.70
53	−0.78	33.40	50	−0.90	33.38	26.86
80	0.65	33.74	75	0.40	33.68	27.04
106	1.32	34.01	100	1.25	33.97	27.22
160	1.60	34.14	150	1.55	34.11	27.31
212	2.18	34.33	200	2.05	34.28	27.41
318	2.90	34.61	300	2.85	34.58	27.58
410	2.86	34.66	400	2.85	34.65	27.64
607	3.66	34.81	600	3.65	34.81	27.69

Station 6973; 18 April; 46°45.5′ N., 47°10′ W.; depth 327 m.; dynamic height 971.058.

Observed values			Scaled values			
Depth, meters	Temperature, °C.	Salinity, ‰	Depth, meters	Temperature, °C.	Salinity, ‰	σ_t
0	−0.30	33.14	0	−0.30	33.14	26.67
25	−1.30	33.15	25	−1.31	33.15	26.68
50	−1.33	33.16	50	−1.33	33.16	26.69
75	−1.17	33.31	75	−1.17	33.31	26.81
101	−0.69	33.41	100	−0.75	33.41	26.88
151	1.58	33.96	150	1.60	33.95	27.18
201	1.49	34.04	200	1.50	34.04	27.26
302	2.02	34.28	300	2.00	34.28	27.41

Station 6974; 18 April; 46°45.5′ N., 47°33′ W.; depth 172 m.; dynamic height 971.077.

Observed values			Scaled values			
Depth, meters	Temperature, °C.	Salinity, ‰	Depth, meters	Temperature, °C.	Salinity, ‰	σ_t
0	−1.27	33.08	0	−1.27	33.08	26.62
24	−1.29	33.08	25	−1.30	33.08	26.62
47	−1.29	33.08	50	−1.30	33.08	26.62
70	−1.27	33.22	75	−1.25	33.24	26.75
94	−0.81	33.31	100	−0.60	33.36	26.82
141	0.86	33.72	(150)	1.15	33.80	27.09

TABLE OF OCEANOGRAPHIC DATA—Continued
STATIONS OCCUPIED IN 1959—Continued

Station 6975; 18 April; 46°46′ N., 48°05′ W.; depth 119 m.; dynamic height 971.085.

Observed values			Scaled values			
Depth, meters	Temperature, °C.	Salinity, ‰	Depth, meters	Temperature, °C.	Salinity, ‰	σ_t
0	−1.19	33.09	0	−1.19	33.09	26.63
26	−1.20	33.10	25	−1.20	33.10	26.64
51	−1.19	33.08	50	−1.15	33.08	26.62
77	−1.12	33.13	75	−1.15	33.13	26.66
103	−0.89	33.30	100	−0.90	33.27	26.77

Station 6976; 18 April; 46°46′ N., 48°37′ W.; depth 97 m.; dynamic height 971.084.

Observed values			Scaled values			
Depth, meters	Temperature, °C.	Salinity, ‰	Depth, meters	Temperature, °C.	Salinity, ‰	σ_t
0	−0.58	33.17	0	−0.58	33.17	26.67
28	−0.59	33.135	25	−0.60	33.14	26.65
55	−0.60	33.17	50	−0.60	33.16	26.66
83	−0.59	33.21	75	−0.60	33.20	26.70

Station 6977; 30 April; 41.59.5′ N., 50°58′ W.; depth 3,392 m.; dynamic height 970.949.

Observed values			Scaled values			
Depth, meters	Temperature, °C.	Salinity, ‰	Depth, meters	Temperature, °C.	Salinity, ‰	σ_t
0	2.81	33.33	0	2.81	33.33	26.59
25	2.81	33.32	25	2.81	33.32	26.58
49	1.61	33.71	50	1.61	33.73	27.80
74	3.04	34.18	75	3.05	34.18	27.24
98	2.98	34.21	100	3.00	34.21	27.28
147	3.73	34.52	150	3.70	34.52	27.46
196	3.49	34.52	200	3.50	34.52	27.48
294	5.53	34.98	300	5.50	34.99	27.62
357	4.97	34.95	400	4.70	34.95	27.69
539	4.36	34.94	600	4.35	34.96	27.74
724	4.38	34.99	800	4.10	34.97	27.78
910	3.79	34.93	1,000	3.75	34.94	27.78
1,384	3.66	34.94				

Station 6978; 1 May; 41°59′ N., 51°59′ W.; depth 3,932 m.; dynamic height 971.054.

Observed values			Scaled values			
Depth, meters	Temperature, °C.	Salinity, ‰	Depth, meters	Temperature, °C.	Salinity, ‰	σ_t
0	3.72	33.12	0	3.72	33.12	26.33
24	3.70	33.13	25	3.70	33.13	26.35
48	2.36	33.17	50	2.45	33.18	26.50
72	9.17	34.52	75	9.55	34.73	26.83
97	11.15	35.17	100	11.15	35.16	26.89
144	4.55	34.26	150	4.55	34.27	27.17
192	4.55	34.46	200	4.50	34.48	27.34
289	4.62	34.69	300	4.65	34.72	27.52
396	5.35	34.94	400	5.35	34.95	27.61
595	4.48	34.95	600	4.45	34.95	27.72
795	3.87	34.89	800	3.90	34.89	27.73
994	3.90	34.935	1,000	3.90	34.93	27.76
1,492	3.57	34.92				

Station 6979; 1 May; 42°21.5′ N., 51°33′ W.; depth 3,109 m.; dynamic height 970.954.

Observed values			Scaled values			
Depth, meters	Temperature, °C.	Salinity, ‰	Depth, meters	Temperature, °C.	Salinity, ‰	σ_t
0	2.81	33.40	0	2.81	33.40	26.65
25	2.37	33.48	25	2.37	33.48	26.75
50	1.34	33.70	50	1.34	33.70	27.00
75	1.66	33.87	75	1.66	33.87	27.11
99	2.25	34.11	100	2.30	34.14	27.28
149	5.47	34.68	150	5.45	34.68	27.38
199	4.88	34.74	200	4.85	34.74	27.51
298	3.66	34.74	300	3.65	34.74	27.63
393	4.00	34.84	400	4.00	34.85	27.69
592	3.94	34.88	600	3.95	34.89	27.72
793	3.72	34.895	800	3.70	34.89	27.75
991	3.56	34.895	1,000	3.55	34.90	27.77
1,484	3.52	34.92				

Station 6980; 1 May; 42°41′ N., 51°06′ W.; depth 1,810 m.; dynamic height 971.012.

Observed values			Scaled values			
Depth, meters	Temperature, °C.	Salinity, ‰	Depth, meters	Temperature, °C.	Salinity, ‰	σ_t
0	−0.45	33.14	0	−0.45	33.14	26.65
24	−0.60	33.16	25	−0.60	33.17	26.67
50	−0.58	33.48	50	−0.55	33.48	26.92
74	0.65	33.79	75	0.65	33.79	27.11
100	0.78	33.85	100	0.80	33.85	27.15
149	1.03	33.94	150	1.05	33.94	27.21
198	1.62	34.14	200	1.65	34.15	27.34
298	2.73	34.54	300	2.75	34.51	27.54
337	3.05	34.56	400	3.15	34.63	27.59
509	3.29	34.71	600	3.60	34.80	27.69
683	3.93	34.87	800	3.90	34.89	27.73
867	3.88	34.895	1,000	3.80	34.90	27.75
1,351	3.56	34.90				

Station 6981; 1 May; 42°52′ N., 50°53′ W.; depth 1,090 m.; dynamic height 971.098.

Observed values			Scaled values			
Depth, meters	Temperature, °C.	Salinity, ‰	Depth, meters	Temperature, °C.	Salinity, ‰	σ_t
0	1.46	33.08	0	1.46	33.08	26.49
25	0.67	33.16	25	0.67	33.16	26.61
50	0.26	33.23	50	0.26	33.23	26.69
75	−0.07	33.28	75	−0.07	33.28	26.74
100	−0.43	33.33	100	−0.43	33.33	26.80
150	−0.28	33.50	150	−0.28	33.50	26.93
200	0.45	33.78	200	0.45	33.78	27.11
300	1.81	34.25	300	1.81	34.25	27.41
404	2.59	34.50	400	2.55	34.49	27.54
607	3.67	34.77	600	3.65	34.76	27.65
811	3.88	34.88	800	3.90	34.87	27.72
1,010	3.67	34.885	1,000	3.70	34.88	27.74

Station 6982; 1 May; 42°56′ N., 50°53′ W.; depth 635 m.; dynamic height 971.139.

Observed values			Scaled values			
Depth, meters	Temperature, °C.	Salinity, ‰	Depth, meters	Temperature, °C.	Salinity, ‰	σ_t
0	2.02	32.67	0	2.02	32.67	26.13
23	1.28	32.90	25	1.25	32.92	26.38
48	0.66	33.12	50	0.60	33.12	26.58
71	0.01	33.21	75	−0.10	33.22	26.69
96	−0.52	33.29	100	−0.55	33.30	26.77
143	−0.70	33.38	150	−0.65	33.40	26.87
190	−0.11	33.58	200	0.00	33.62	27.02
286	1.20	34.00	300	1.40	34.06	27.28
394	2.49	34.42	400	2.55	34.43	27.49
596	3.68	34.78	600	3.70	34.78	27.66

Station 6983; 1 May; 42°58.5′ N., 50°50′ W.; depth 174 m.; dynamic height 971.117.

Observed values			Scaled values			
Depth, meters	Temperature, °C.	Salinity, ‰	Depth, meters	Temperature, °C.	Salinity, ‰	σ_t
0	2.54	32.52	0	2.54	32.52	25.97
25	1.47	32.76	25	1.47	32.76	26.24
52	−0.46	33.24	50	−0.40	33.22	26.71
78	−0.63	33.32	75	−0.60	33.31	26.78
104	−0.62	33.44	100	−0.60	33.43	26.88
155	−0.40	33.52	150	−0.45	33.51	26.95

Station 6984; 1 May; 42°08′ N., 50°35′ W.; depth 90 m.; dynamic height 971.133.

Observed values			Scaled values			
Depth, meters	Temperature, °C.	Salinity, ‰	Depth, meters	Temperature, °C.	Salinity, ‰	σ_t
0	2.41	32.67	0	2.41	32.67	26.10
26	1.99	32.68	25	2.00	32.68	26.14
51	1.73	32.70	50	1.75	32.70	26.17
77	−0.50	33.28	75	−0.40	33.26	26.74

STATIONS OCCUPIED IN 1959—Continued

Station 6985; 1 May; 43°21′ N., 50°15′ W.; depth 64 m.; dynamic height 971.115.

Observed values			Scaled values			
Depth, meters	Temperature, °C.	Salinity, ‰	Depth, meters	Temperature, °C.	Salinity, ‰	σ_t
0	1.59	32.87	0	1.59	32.87	26.32
25	1.15	32.94	25	1.15	32.94	26.41
50	0.44	33.08	50	0.44	33.08	26.56

Station 6986; 1 May; 42°56.5′ N., 50°15′ W.; depth 99 m.; dynamic height 971.094.

Observed values			Scaled values			
Depth, meters	Temperature, °C.	Salinity, ‰	Depth, meters	Temperature, °C.	Salinity, ‰	σ_t
0	0.43	33.24	0	0.43	33.24	26.69
25	0.15	33.28	25	0.15	33.28	26.73
50	−0.46	33.32	50	−0.45	33.32	26.79
75	−0.30	33.34	75	−0.30	33.34	26.80

Station 6987; 2 May; 42°47′ N., 50°16′ W.; depth 293 m.; dynamic height 971.077.

Observed values			Scaled values			
Depth, meters	Temperature, °C.	Salinity, ‰	Depth, meters	Temperature, °C.	Salinity, ‰	σ_t
0	−0.34	33.13	0	−0.34	33.13	26.63
22	−0.56	33.14	25	−0.55	33.14	26.65
44	−0.64	33.14	50	−0.70	33.15	26.66
66	−0.94	33.22	75	−0.95	33.29	26.78
88	−0.94	33.38	100	−0.80	33.44	26.90
132	−0.27	33.53	150	−0.15	33.57	26.99
176	−0.02	33.62	200	0.20	33.68	27.05
264	0.81	33.88				

Station 6988; 2 May; 42°35.5′ N., 50°16′ W.; depth 1,719 m.; dynamic height 970.934.

Observed values			Scaled values			
Depth, meters	Temperature, °C.	Salinity, ‰	Depth, meters	Temperature, °C.	Salinity, ‰	σ_t
0	1.57	33.56	0	1.57	33.56	26.87
25	1.49	33.62	25	1.49	33.62	26.93
50	1.25	33.78	50	1.25	33.78	27.06
75	1.31	33.96	75	1.31	33.96	27.21
100	1.70	34.12	100	1.70	34.12	27.31
150	2.23	34.33	150	2.23	34.33	27.44
200	2.67	34.54	200	2.67	34.54	27.57
300	3.46	34.74	300	3.46	34.74	27.65
392	3.62	34.79	400	3.65	34.79	27.67
592	3.82	34.86	600	3.80	34.86	27.72
793	3.61	34.875	800	3.60	34.87	27.75
991	3.66	34.88	1,000	3.65	34.88	27.75

Station 6989; 2 May; 42°22′ N., 50°18′ W.; depth 2,671 m.; dynamic height 970.954.

Observed values			Scaled values			
Depth, meters	Temperature, °C.	Salinity, ‰	Depth, meters	Temperature, °C.	Salinity, ‰	σ_t
0	1.47	33.36	0	1.47	33.36	26.72
25	2.00	33.56	25	2.00	33.56	26.85
51	2.47	33.96	50	2.50	33.94	27.10
76	2.00	33.98	75	2.00	33.97	27.17
102	3.05	34.20	100	2.90	34.18	27.26
152	5.11	34.64	150	5.00	34.62	27.40
203	5.54	34.80	200	5.55	34.80	27.47
305	4.78	34.85	300	4.80	34.85	27.60
401	4.38	34.85	400	4.40	34.88	27.66
600	3.90	34.89	600	3.90	34.89	27.73
798	3.82	34.915	800	3.80	34.91	27.76
997	4.02	34.96	1,000	4.00	34.96	27.78
1,489	3.47	34.915				

Station 6990; 2 May; 42°00′ N., 50°17′ W.; depth 3,612 m.; dynamic height 971.033.

Observed values			Scaled values			
Depth, meters	Temperature, °C.	Salinity, ‰	Depth, meters	Temperature, °C.	Salinity, ‰	σ_t
0	4.29	33.20	0	4.29	33.20	26.35
24	3.88	33.31	25	3.85	33.32	26.48
49	4.44	33.76	50	4.45	33.78	26.79
73	5.32	34.16	75	5.25	34.15	26.99
98	3.00	33.91	100	3.05	33.92	27.04
147	5.35	34.47	150	5.30	34.45	27.22
196	1.59	34.08	200	1.60	34.08	27.28
294	2.95	34.44	300	3.10	34.48	27.48
317	3.92	34.64	400	4.75	34.92	27.66
471	5.10	34.97	600	4.55	34.94	27.70
622	4.44	34.94	800	4.00	34.91	27.74
789	4.00	34.91	1,000	3.85	34.91	27.75
1,224	3.72	34.92				

Station 6991; 2 May; 41°31.5′ N., 50°14′ W.; depth 3,841 m.; dynamic height 971.263.

Observed values			Scaled values			
Depth, meters	Temperature, °C.	Salinity, ‰	Depth, meters	Temperature, °C.	Salinity, ‰	σ_t
0	10.97	34.79	0	10.97	34.79	26.64
26	10.85	34.88	25	10.85	34.87	26.72
52	11.21	35.02	50	11.15	35.01	26.78
78	11.69	35.17	75	11.65	35.16	26.80
104	11.67	35.18	100	11.65	35.17	26.81
155	11.87	35.26	150	11.80	35.25	26.84
206	12.20	35.38	200	12.15	35.37	26.87
310	12.21	35.48	300	12.20	35.48	26.94
420	9.35	35.18	400	9.85	35.23	27.17
630	5.45	34.93	600	5.80	34.95	27.56
840	3.96	34.86	800	4.05	34.86	27.69
1,050	4.24	34.955	1,000	4.20	34.93	27.73
1,578	3.79	34.95				

Station 6992; 2 May; 41°04.5′ N., 50°12′ W.; depth 3,658 m.; dynamic height 971.328.

Observed values			Scaled values			
Depth, meters	Temperature, °C.	Salinity, ‰	Depth, meters	Temperature, °C.	Salinity, ‰	σ_t
0	14.86	35.90	0	14.86	35.90	26.71
25	14.61	35.87	25	14.61	35.87	26.75
51	14.44	35.85	50	14.45	35.85	26.76
76	14.33	35.83	75	14.35	35.83	26.77
102	14.27	35.82	100	14.25	35.82	26.78
152	14.20	35.80	150	14.20	35.80	26.78
202	13.54	35.64	200	13.55	35.64	26.79
304	13.22	35.69	300	13.25	35.69	26.89
413	10.91	35.38	400	11.20	35.42	27.09
609	6.35	34.91	600	6.60	34.91	27.42
796	4.54	34.89	800	4.55	34.89	27.66
1,004	4.33	34.95	1,000	4.35	34.95	27.73
1,542	3.80	34.945				

Station 6993; 3 May; 41°59′ N., 49°25′ W.; depth 3,292 m.; dynamic height 970.990.

Observed values			Scaled values			
Depth, meters	Temperature, °C.	Salinity, ‰	Depth, meters	Temperature, °C.	Salinity, ‰	σ_t
0	3.55	33.29	0	3.55	33.29	26.48
24	2.96	33.36	25	2.85	33.36	26.61
49	0.31	33.46	50	0.30	33.46	26.87
73	0.59	33.62	75	0.60	33.63	26.98
97	0.71	33.80	100	0.75	33.83	27.14
145	2.46	34.19	150	2.90	34.25	27.32
194	6.01	34.84	200	5.90	34.84	27.46
291	2.61	34.52	300	2.65	34.52	27.56
386	3.70	34.73	400	3.80	34.75	27.63
577	4.14	34.90	600	4.15	34.91	27.72
766	4.03	34.94	800	4.00	34.94	27.76
958	3.82	34.925	1,000	3.80	34.92	27.77
1,436	3.50	34.91				

TABLE OF OCEANOGRAPHIC DATA—Continued
STATIONS OCCUPIED IN 1959—Continued

Observed values			Scaled values			
Depth, meters	Temperature, °C.	Salinity, ‰	Depth, meters	Temperature, °C.	Salinity, ‰	σ_t
Station 6994; 3 May; 41°30′ N., 48°60′ W., depth 3,292 m.; dynamic height 971.051.						
0	2.52	33.03	0	2.52	33.03	26.39
24	2.98	33.38	25	2.95	33.38	26.61
50	−0.10	33.38	50	−0.10	33.38	26.82
75	−0.25	33.48	75	−0.25	33.48	26.91
99	−0.07	33.58	100	−0.05	33.58	26.98
148	0.60	33.82	150	0.70	33.84	27.15
198	3.11	34.25	200	3.15	34.28	27.31
297	4.18	34.61	300	4.15	34.61	27.48
368	3.07	34.53	400	3.35	34.59	27.54
553	4.80	34.96	600	4.60	34.93	27.68
738	3.92	34.89	800	3.80	34.89	27.74
929	3.70	34.89	1,000	3.65	34.89	27.75
1,417	3.56	34.91				
Station 6995; 3 May; 41°06′ N., 48°14′ W.; depth 3,567 m.; dynamic height 971.166.						
0	12.13	35.27	0	12.13	35.27	26.79
25	11.93	35.29	25	11.93	35.29	26.85
50	11.92	35.29	50	11.92	35.29	26.85
75	11.95	35.30	75	11.95	35.30	26.85
100	12.20	35.39	100	12.20	35.39	26.87
150	11.93	35.32	150	11.93	35.32	26.87
200	9.86	34.88	200	9.86	34.88	26.90
300	7.43	34.79	300	7.43	34.79	27.21
360	4.98	34.54	400	5.00	34.59	27.37
549	5.10	34.87	600	5.00	34.91	27.63
745	4.65	34.965	800	4.50	34.96	27.72
937	4.17	34.94	1,000	4.10	34.94	27.75
1,431	3.85	34.955				
Station 6996; 3 May; 41°00′ N., 47°37′ W.; depth 3,383 m.; dynamic height 971.149.						
0	3.59	33.28	0	3.59	33.28	26.48
24	10.61	34.95	25	10.60	34.95	26.82
49	10.51	35.00	50	10.45	35.00	26.89
73	9.54	34.81	75	9.50	34.80	26.90
98	9.09	34.72	100	9.05	34.71	26.90
147	7.19	34.39	150	7.00	34.37	26.95
196	5.06	34.20	200	5.10	34.20	27.05
294	8.88	35.11	300	8.85	35.11	27.25
351	8.43	35.11	400	7.40	35.03	27.40
547	4.68	34.80	600	4.50	34.82	27.61
760	4.34	34.90	800	4.15	34.90	27.71
950	3.81	34.885	1,000	3.80	34.89	27.74
1,424	3.71	34.94				
Station 6997; 3 May; 41°35.5′ N., 47°17′ W.; depth 4,390 m.; dynamic height 971.090.						
0	6.26	33.42	0	6.26	33.42	26.29
25	5.80	33.46	25	5.80	33.46	26.38
51	7.31	34.14	50	7.20	34.11	26.71
77	10.60	35.12	75	10.60	35.11	26.95
103	8.19	34.67	100	8.50	34.72	27.00
153	6.98	34.58	150	7.00	34.59	27.11
205	7.77	34.84	200	7.75	34.83	27.19
308	3.99	34.50	300	4.10	34.51	27.41
426	4.30	34.72	400	4.25	34.67	27.52
637	4.55	34.92	600	4.55	34.90	27.67
849	4.29	34.95	800	4.35	34.95	27.73
1,059	3.99	34.93	1,000	4.05	34.94	27.75
1,579	3.53	34.91				

Observed values			Scaled values			
Depth, meters	Temperature, °C.	Salinity, ‰	Depth, meters	Temperature, °C.	Salinity, ‰	σ_t
Station 6998; 4 May; 41°58.5 N., 47°56′ W.; depth 3,932 m.; dynamic height 971.015.						
0	6.25	33.34	0	6.25	33.34	26.23
25	5.72	33.46	25	5.72	33.36	26.31
49	5.60	33.59	50	5.60	33.60	26.52
74	6.57	34.00	75	6.55	34.02	26.73
98	4.30	34.15	100	4.30	34.18	27.12
147	6.18	34.70	150	6.15	34.70	27.32
196	4.67	34.60	200	4.70	34.60	27.41
294	5.10	34.86	300	5.15	34.87	27.58
383	5.40	34.99	400	5.40	35.00	27.65
575	5.08	35.06	600	4.95	35.05	27.74
768	4.23	34.97	800	4.20	34.97	27.77
958	4.04	34.97	1,000	4.00	34.97	27.79
1,431	3.56	34.93				
Station 6999; 4 May; 42°23′ N., 48°33′ W.; depth 3,410 m.; dynamic height 971.005.						
0	9.07	34.40	0	9.07	34.40	26.66
25	9.35	34.57	25	9.35	34.57	26.75
51	10.18	34.80	50	10.15	34.80	26.79
76	3.83	33.87	75	4.00	33.93	26.95
102	1.69	33.75	100	1.70	33.75	27.01
152	2.92	34.09	150	2.90	34.08	27.18
202	2.37	34.32	200	2.40	34.31	27.41
304	3.85	34.68	300	3.75	34.66	27.56
408	4.56	34.86	400	4.50	34.85	27.63
609	4.68	35.00	600	4.70	35.00	27.73
809	4.52	35.01	800	4.55	35.01	27.76
1,010	4.07	34.97	1,000	4.10	34.97	27.78
1,514	3.46	34.93				
Station 7000; 4 May; 42°42′ N., 49°10′ W.; depth, 2,652 m.; dynamic height 971.003.						
0	7.15	33.92	0	7.15	33.92	26.57
25	10.57	34.98	25	10.57	34.98	26.85
52	10.15	34.96	50	10.15	34.96	26.91
77	11.15	35.34	75	11.10	35.34	27.04
103	10.10	35.26	100	10.25	35.27	27.14
154	8.49	35.04	150	8.60	35.06	27.25
206	6.27	34.80	200	6.35	34.81	27.38
309	6.21	35.03	300	6.25	35.01	27.55
341	6.03	35.05	400	5.50	35.00	27.63
517	4.09	34.89	600	4.30	34.93	27.71
697	4.46	35.00	800	4.15	34.96	27.76
884	3.93	34.92	1,000	3.85	34.92	27.76
1,378	3.53	34.92				
Station 7001; 4 May 43°19.5′ N., 48°49′ W.; depth 2,103 m.; dynamic height 970.904.						
0	3.14	33.72	0	3.14	33.72	26.87
25	1.79	33.78	25	1.79	33.78	27.03
50	1.82	33.90	50	1.82	33.90	27.12
75	2.55	34.29	75	2.55	34.29	27.38
100	2.74	34.41	100	2.74	34.41	27.46
150	2.68	34.52	150	2.68	34.52	27.55
199	2.81	34.58	200	2.80	34.58	27.58
299	3.98	34.81	300	4.00	34.81	27.66
384	4.05	34.88	400	4.05	34.88	27.70
583	3.94	34.90	600	3.90	34.90	27.74
786	3.66	34.90	800	3.65	34.90	27.76
984	3.51	34.90	1,000	3.50	34.90	27.78
1,484	3.40	34.90				

Observed values			Scaled values			
Depth, meters	Temperature, °C.	Salinity, ‰	Depth, meters	Temperature, °C.	Salinity, ‰	σ_t
Station 7002; 4 May; 43°07′ N., 48°10′ W.; depth 3,383 m.; dynamic height 971.049.						
0	6.05	33.44	0	6.05	33.44	26.33
25	9.11	34.26	25	9.11	34.26	26.54
50	7.23	34.35	50	7.23	34.35	26.90
75	9.33	34.92	75	9.33	34.92	27.02
100	10.53	35.24	100	10.53	35.24	27.07
150	9.60	35.17	150	9.60	35.17	27.17
199	8.29	35.03	200	8.30	35.03	27.27
299	5.85	34.83	300	5.85	34.83	27.45
388	5.80	34.99	400	5.70	34.99	27.60
584	4.37	34.90	600	4.35	34.90	27.69
782	4.38	34.97	800	4.35	34.97	27.75
976	3.74	34.90	1,000	3.75	34.90	27.75
1,460	3.46	34.89				
Station 7003; 4 May; 42°53′ N., 47°30′ W.; depth 3,749 m.; dynamic height 971.152.						
0	6.23	33.28	0	6.23	33.38	26.26
25	5.70	33.77	25	5.70	33.77	26.64
50	9.88	34.80	50	9.88	34.80	26.84
75	11.17	35.12	75	11.17	35.12	26.86
99	12.23	35.40	100	12.23	35.40	26.87
150	10.63	35.16	150	10.63	35.16	26.98
200	7.14	34.56	200	7.14	34.56	27.07
299	8.46	35.04	300	8.45	35.04	27.25
386	7.34	35.05	400	7.25	35.05	27.44
580	5.00	34.91	600	4.90	34.91	27.64
774	4.47	34.93	800	4.45	34.93	27.70
968	4.31	34.94	1,000	4.25	34.94	27.73
1,458	3.66	34.93				
Station 7004; 5 May; 42°39.5′ N., 46°51′ W.; depth 4,051 m.; dynamic height 971.355.						
0	14.27	35.74	0	14.27	35.74	26.72
23	14.27	35.74	25	14.25	35.74	26.72
45	14.72	35.92	50	14.70	35.92	26.77
68	14.69	35.92	75	14.50	35.90	26.79
90	14.15	35.79	100	13.95	35.74	26.78
136	13.53	35.62	150	13.40	35.60	26.79
182	13.20	35.56	200	13.05	35.53	26.81
272	12.35	35.38	300	12.20	35.36	26.85
361	12.00	35.52	400	11.25	35.27	26.96
546	8.15	35.08	600	7.35	35.05	27.43
735	5.82	35.00	800	5.35	34.99	27.64
923	4.71	34.98	1,000	4.55	34.98	27.73
1,400	4.09	34.975				
Station 7005; 5 May; 42°24.5′ N., 46°12′ W.; depth 4,663 m.; dynamic height 971.486.						
0	15.60	35.99	0	15.60	35.99	26.61
25	15.58	35.99	25	15.58	35.99	26.62
51	15.50	35.99	50	15.50	35.99	26.64
76	15.19	35.96	75	15.20	35.97	26.70
101	14.98	35.94	100	15.00	35.94	26.71
151	14.92	35.94	150	14.90	35.94	26.74
202	14.12	35.76	200	14.10	35.77	26.78
303	14.68	35.98	300	14.65	35.97	26.82
413	13.57	35.79	400	13.80	35.82	26.88
617	9.73	35.23	600	10.05	35.26	27.16
820	7.12	35.14	800	7.30	35.14	27.50
1,024	5.36	35.05	1,000	5.50	35.06	27.68
1,532	4.03	34.97				

Observed values			Scaled values			
Depth, meters	Temperature, °C.	Salinity, ‰	Depth, meters	Temperature, °C.	Salinity, ‰	σ_t
Station 7006; 5 May; 42°52′ N., 45°43′ W.; depth 4,755 m.; dynamic height 971.523.						
0	16.42	36.20	0	16.42	36.20	26.59
23	15.43	36.04	25	15.35	36.04	26.71
45	15.17	36.05	50	15.05	36.04	26.78
68	14.71	35.93	75	14.55	35.90	26.78
90	14.45	35.88	100	14.50	35.90	26.79
135	14.91	36.03	150	14.90	36.03	26.81
180	14.82	36.02	200	14.70	36.00	26.83
270	14.38	35.93	300	14.25	35.91	26.85
394	13.92	35.87	400	13.90	35.86	26.89
591	12.22	35.59	600	12.05	35.56	27.03
788	8.24	35.13	800	8.05	35.13	27.38
984	6.32	35.14	1,000	6.20	35.14	27.66
1,473	4.13	34.97				
Station 7007; 5 May; 43°11′ N., 45°23′ W.; depth 4,663 m.; dynamic height 971.492.						
0	15.15	35.99	0	15.15	35.99	26.72
24	15.04	35.98	25	15.05	35.98	26.73
48	14.71	35.94	50	14.65	35.94	26.79
72	14.45	35.88	75	14.45	35.88	26.79
97	14.52	35.90	100	14.55	35.91	26.79
145	14.66	35.96	150	14.65	35.96	26.81
193	14.68	35.97	200	14.65	35.97	26.82
290	14.56	35.95	300	14.55	35.95	26.82
383	14.46	35.96	400	14.35	35.94	26.86
576	11.32	35.46	600	10.90	35.39	27.11
772	7.71	35.07	800	7.20	35.05	27.45
968	5.36	34.98	1,000	5.05	34.98	27.67
1,466	4.05	34.95				
Station 7008; 5 May; 43°24.5′ N., 46°01′ W.; depth 4,663 m.; dynamic height 971.469.						
0	15.63	36.02	0	15.63	36.02	26.63
26	15.58	36.03	25	15.55	36.03	26.66
51	15.16	35.96	50	15.15	35.96	26.70
77	14.91	35.92	75	14.90	35.92	26.72
102	15.07	35.97	100	15.05	35.97	26.73
152	14.65	35.88	150	14.65	35.88	26.74
204	14.73	35.91	200	14.70	35.91	26.76
306	14.15	35.81	300	14.20	35.82	26.79
424	12.71	35.63	400	13.05	35.67	26.92
634	9.50	35.24	600	10.10	35.30	27.19
844	5.64	34.905	800	6.20	34.96	27.52
1,054	5.06	35.01	1,000	5.20	34.99	27.66
1,579	3.97	34.955				
Station 7009; 5 May; 43°33.5′ N., 46°41′ W.; depth 4,463 m.; dynamic height 971.385.						
0	14.89	35.75	0	14.89	35.75	26.59
24	15.44	36.02	25	15.45	36.02	26.68
49	15.21	36.00	50	15.20	36.00	26.72
73	15.20	36.01	75	15.20	36.01	26.73
98	15.19	36.01	100	15.20	36.01	26.73
147	15.09	36.00	150	15.10	36.00	26.74
196	15.24	36.02	200	15.20	36.01	26.73
294	14.18	35.90	300	14.10	35.89	26.87
388	12.87	35.66	400	12.60	35.62	26.97
584	8.34	35.10	600	8.00	35.07	27.35
780	5.35	34.94	800	5.25	34.94	27.62
978	4.71	34.96	1,000	4.70	34.96	27.70
1,478	3.91	34.945				

TABLE OF OCEANOGRAPHIC DATA—Continued

STATIONS OCCUPIED IN 1959—Continued

Observed values			Scaled values			
Depth, meters	Temperature, °C.	Salinity, ‰	Depth, meters	Temperature, °C.	Salinity, ‰	σ_t
Station 7010; 6 May; 43°43′ N., 47°19′ W.; depth 4,024 m.; dynamic height 971.220.						
0	10.22	34.44	0	10.22	34.44	26.50
25	14.43	35.75	25	14.43	35.75	26.70
51	14.76	35.88	50	14.75	35.88	26.72
76	14.31	35.81	75	14.35	35.81	26.76
102	13.99	35.76	100	14.05	35.77	26.79
152	13.06	35.53	150	13.05	35.53	26.81
202	13.22	35.62	200	13.20	35.62	26.85
304	10.72	35.31	300	10.85	35.32	27.07
406	8.28	35.10	400	8.45	35.11	27.31
610	5.20	34.94	600	5.25	34.94	27.62
816	4.52	34.965	800	4.55	34.96	27.72
1,017	4.35	34.99	1,000	4.40	34.99	27.75
1,516	3.74	34.95				
Station 7011; 6 May; 43°53′ N., 47°58′ W.; depth 3,658 m.; dynamic height 970.943.						
0	4.60	33.72	0	4.60	33.72	26.73
25	4.06	33.85	25	4.06	33.85	26.88
51	3.67	34.06	50	3.70	34.05	27.08
76	3.29	34.13	75	3.30	34.13	27.18
102	2.98	34.23	100	3.00	34.21	27.28
152	3.82	34.48	150	3.80	34.47	27.41
202	3.96	34.61	200	3.95	34.61	27.50
304	4.41	34.84	300	4.40	34.83	27.62
400	4.01	34.86	400	4.00	34.86	27.70
600	3.93	34.89	600	3.95	34.89	27.72
802	3.81	34.91	800	3.80	34.91	27.76
1,002	3.72	34.92	1,000	3.70	34.92	27.78
1,501	3.42	34.91				
Station 7012; 6 May; 44°02.5′ N., 48°30′ W.; depth 4,017 m.; dynamic height 970.931.						
0	0.71	33.43	0	0.71	33.43	26.82
25	0.14	33.52	25	0.14	33.52	26.93
50	0.26	33.60	50	0.26	33.60	26.99
75	1.09	33.98	75	1.09	33.98	27.24
101	1.54	34.16	100	1.50	34.15	27.35
151	2.72	34.44	150	2.70	34.44	27.48
201	3.64	34.64	200	3.65	34.64	27.55
302	4.28	34.84	300	4.20	34.84	27.65
393	4.04	34.86	400	4.05	34.86	27.69
592	3.82	34.88	600	3.80	34.88	27.73
795	3.89	34.915	800	3.90	34.91	27.75
995	3.67	34.90	1,000	3.65	34.90	27.76
1,499	3.42	34.92				
Station 7013; 6 May; 44°07′ N., 48°47′ W.; depth 1,628 m.; dynamic height 970.936.						
0	1.19	33.50	0	1.19	33.50	26.85
25	1.58	33.69	25	1.58	33.69	26.97
50	1.38	33.88	50	1.38	33.88	27.14
75	1.21	33.96	75	1.21	33.96	27.22
100	1.38	34.06	100	1.38	34.06	27.29
150	2.05	34.33	150	2.05	34.33	27.45
201	2.58	34.55	200	2.60	34.55	27.58
301	2.80	34.62	300	2.80	34.62	27.62
392	3.22	34.73	400	3.25	34.73	27.66
587	3.77	34.86	600	3.75	34.86	27.72
781	3.67	34.87	800	3.63	34.87	27.74
978	3.59	34.885	1,000	3.60	34.88	27.75
1,478	3.49	34.905				

Observed values			Sclaed values			
Depth, meters	Temperature, °C.	Salinity, ‰	Depth, meters	Temperature, °C.	Salinity, ‰	σ_t
Station 7014; 6 May; 44°09′ N., 48°57′ W.; depth 715 m.; dynamic height 970.990.						
0	0.01	33.24	0	0.01	33.24	26.71
25	0.22	33.42	25	0.22	33.42	26.85
49	0.56	33.56	50	0.55	33.56	26.94
74	0.43	33.69	75	0.45	33.69	27.04
99	0.69	33.78	100	0.70	33.78	27.10
148	1.17	33.93	150	1.20	33.94	27.20
197	1.66	34.22	200	1.70	34.24	27.40
296	2.80	34.60	300	2.80	34.61	27.61
387	3.21	34.71	400	3.25	34.72	27.66
590	3.59	34.80	600	3.60	34.80	27.69
Station 7015; 6 May; 44°10′ N., 49°04′ W.; depth 169 m.; dynamic height 971.051.						
0	0.18	33.30	0	0.18	33.30	26.74
25	-0.35	33.38	25	-0.35	33.38	26.83
50	-0.40	33.41	50	-0.40	33.41	26.87
75	-0.41	33.43	75	-0.41	33.43	26.88
101	-0.38	--------	100	-0.35	33.45	26.89
151	-0.20	33.51	150	-0.20	33.51	26.94
Station 7016; 6 May; 44°11′ N., 49°12′ W.; depth 80 m.; dynamic height 971.057.						
0	-0.18	33.16	0	-0.18	33.16	26.65
26	-0.36	33.34	25	-0.36	33.33	26.79
52	-0.45	33.37	50	-0.45	33.37	26.83
78	-0.45	33.37	75	-0.45	33.37	26.83
Station 7017; 6 May; 44°14′ N., 49°23′ W.; depth 55 m.; dynamic height 971.069.						
0	0.45	33.11	0	0.45	33.11	26.58
25	-0.30	33.11	25	-0.30	33.11	26.61
50	-0.30	--------	50	-0.30	33.11	26.61
Station 7018; 6 May; 44°58′ N.. 49°24′ W.; depth 71 m.; dynamic height 971.066.						
0	0.14	33.13	0	0.14	33.13	26.61
24	-0.22	33.25	25	-0.25	33.25	26.72
48	-0.57	33.28	50	-0.60	33.28	26.76
Station 7019; 6 May; 44°75′ N., 49°18′ W.; depth 146 m.; dynamic height 971.065.						
0	-0.32	33.23	0	-0.32	33.23	26.71
26	-0.48	33.23	25	-0.50	33.23	26.72
52	-0.67	33.26	50	-0.65	33.26	26.75
77	-0.72	33.27	75	-0.70	33.27	26.76
103	-0.75	33.28	100	-0.75	33.28	26.77

STATIONS OCCUPIED IN 1959—Continued

Station 7020; 7 May; 44°53′ N., 49°03′ W.; depth 677 m.; dynamic height 971.058.

Observed values			Scaled values			
Depth, meters	Temperature, °C.	Salinity, ‰	Depth, meters	Temperature, °C.	Salinity, ‰	σ_t
0	−0.11	33.25	0	−0.11	33.25	26.72
25	−0.39	33.28	25	−0.39	33.28	26.75
49	−0.78	33.32	50	−0.80	33.32	26.80
74	−0.85	33.32	75	−0.85	33.32	26.80
98	−0.80	33.33	100	−0.80	33.33	26.81
148	−0.65	33.39	150	−0.65	33.39	26.86
197	−0.20	33.54	200	−0.15	33.58	26.99
295	2.08	34.34	300	2.20	34.38	27.48
400	3.39	34.76	400	3.40	34.76	27.68
601	3.66	34.85	600	3.65	34.85	27.72

Station 7021; 7 May; 44°50′ N., 48°46′ W.; depth 1,728 m.; dynamic height 970.982.

Observed values			Scaled values			
Depth, meters	Temperature, °C.	Salinity, ‰	Depth, meters	Temperature, °C.	Salinity, ‰	σ_t
0	0.31	33.14	0	0.31	33.14	26.61
25	−0.72	33.40	25	−0.72	33.40	26.87
50	−0.44	33.49	50	−0.44	33.49	26.93
75	0.87	33.76	75	0.87	33.76	27.08
100	0.75	33.82	100	0.75	33.82	27.14
150	1.26	34.02	150	1.26	34.02	27.26
199	1.66	34.24	200	1.65	34.25	27.42
299	2.47	34.52	300	2.50	34.52	27.57
347	2.58	34.55	400	2.85	34.63	27.62
521	3.56	34.82	600	3.70	34.87	27.74
695	3.76	34.89	800	3.75	34.89	27.74
876	3.71	34.88	1,000	3.65	34.88	27.74
1,339	3.58	34.89				

Station 7022; 7 May; 44°46′ N., 48°32′ W.; depth 2,241 m.; dynamic height 970.899.

Observed values			Scaled values			
Depth, meters	Temperature, °C.	Salinity, ‰	Depth, meters	Temperature, °C.	Salinity, ‰	σ_t
0	1.96	33.63	0	1.96	33.63	26.90
25	2.63	33.84	25	2.63	33.84	27.01
51	1.91	33.92	50	1.90	33.92	27.14
76	2.84	34.26	75	2.70	34.25	27.33
102	2.51	34.35	100	2.55	34.34	27.42
153	3.77	34.64	150	3.70	34.62	27.54
204	4.68	34.82	200	4.65	34.81	27.59
306	3.97	34.83	300	4.00	34.83	27.67
397	3.93	34.88	400	3.95	34.88	27.71
596	3.78	34.90	600	3.70	34.90	27.76
795	3.59	34.885	800	3.60	34.89	27.76
993	3.51	34.895	1,000	3.50	34.90	27.78
1,484	3.42	34.93				

Station 7023; 7 May; 44°42.5′ N., 47°57′ W.; depth 3,292 m.; dynamic height 970.932.

Observed values			Scaled values			
Depth, meters	Temperature, °C.	Salinity, ‰	Depth, meters	Temperature, °C.	Salinity, ‰	σ_t
0	2.10	33.58	0	2.10	33.58	26.85
25	3.83	34.03	25	3.83	34.03	27.05
50	3.31	34.01	50	3.31	34.01	27.09
75	2.41	34.08	75	2.41	34.08	27.22
101	3.19	34.30	100	3.15	34.30	27.33
151	3.55	34.47	150	3.55	34.46	27.42
201	4.01	34.64	200	4.00	34.64	27.52
302	4.10	34.80	300	4.10	34.80	27.64
484	3.91	34.86	400	4.00	34.84	27.68
682	3.73	34.89	600	3.80	34.88	27.73
881	3.60	34.89	800	3.65	34.89	27.75
1,079	3.48	34.90	1,000	3.50	34.90	27.78
1,478	3.44	34.91				

Station 7024; 7 May; 44°36′ N., 47°17′ W.; depth 3,841 m.; dynamic height 970.927.

Observed values			Scaled values			
Depth, meters	Temperature, °C.	Salinity, ‰	Depth, meters	Temperature, °C.	Salinity, ‰	σ_t
0	6.18	33.95	0	6.18	33.95	26.72
25	3.24	33.98	25	3.24	33.98	27.07
49	3.35	34.02	50	3.35	34.02	27.09
74	2.84	34.13	75	2.85	34.13	27.22
99	3.15	34.29	100	3.15	34.29	27.32
148	3.63	34.50	150	3.65	34.50	27.44
197	4.06	34.69	200	4.05	34.69	27.55
296	3.55	34.72	300	3.55	34.72	27.63
415	4.10	34.87	400	4.05	34.86	27.69
617	3.98	34.92	600	4.00	34.92	27.75
816	3.89	34.92	800	3.90	34.92	27.76
1,021	3.62	34.91	1,000	3.65	34.91	27.77

Station 7025; 7 May; 44°32′ N., 46°38′ W.; depth 3,841 m.; dynamic height 970.935.

Observed values			Scaled values			
Depth, meters	Temperature, °C.	Salinity, ‰	Depth, meters	Temperature, °C.	Salinity, ‰	σ_t
0	6.22	33.77	0	6.22	33.77	26.58
25	3.97	33.92	25	3.97	33.92	26.95
51	3.69	33.97	50	3.70	33.97	27.02
76	2.99	34.10	75	3.00	34.09	27.18
102	3.00	34.25	100	3.00	34.24	27.30
152	3.25	34.50	150	3.20	34.49	27.48
204	5.19	34.88	200	5.10	34.87	27.58
306	4.22	34.82	300	4.25	34.82	27.64
406	4.13	34.87	400	4.15	34.87	27.69
610	3.86	34.89	600	3.90	34.89	27.73
816	3.67	34.89	800	3.70	34.89	27.75
1,018	3.54	34.895	1,000	3.55	34.89	27.76
1,518	3.43					

Station 7026; 7 May; 44°24.5′ N., 45°56′ W.; depth 3,649 m.; dynamic height 970.999.

Observed values			Scaled values			
Depth, meters	Temperature, °C.	Salinity, ‰	Depth, meters	Temperature, °C.	Salinity, ‰	σ_t
0	6.40	33.31	0	6.40	33.31	26.19
25	3.71	33.52	25	3.71	33.52	26.67
50	5.58	34.24	50	5.58	34.24	27.03
74	3.20	33.98	75	3.20	33.98	27.07
99	7.85	34.86	100	7.80	34.85	27.20
149	3.37	34.29	150	3.40	34.29	27.30
198	6.30	34.83	200	6.30	34.83	27.40
297	5.30	34.85	300	5.25	34.85	27.55
378	4.37	34.88	400	4.40	34.89	27.67
563	4.71	34.99	600	4.70	34.98	27.71
746	4.11	34.935	800	3.95	34.91	27.74
937	3.70	34.88	1,000	3.65	34.88	27.74
1,422	3.47	34.90				

Station 7027; 8 May; 44°20.5′ N., 45°15′ W.; depth 3,851 m.; dynamic height 971.111.

Observed values			Scaled values			
Depth, meters	Temperature, °C.	Salinity, ‰	Depth, meters	Temperature, °C.	Salinity, ‰	σ_t
0	11.11	34.74	0	11.11	34.74	26.57
25	11.90	35.20	25	11.90	35.20	26.78
51	11.86	35.46	50	11.85	35.45	26.98
75	12.10	35.57	75	12.20	35.57	27.03
101	12.18	35.62	100	12.15	35.62	27.06
150	12.16	35.62	150	12.15	35.62	27.06
201	12.10	35.61	200	12.10	35.61	27.06
302	8.58	35.12	300	8.65	35.13	27.29
320	8.05	35.07	400	6.90	35.01	27.46
491	6.08	34.985	600	5.30	34.99	27.65
668	4.95	34.995	800	4.60	35.00	27.74
854	4.52	35.00	1,000	4.15	34.98	27.77
1,351	3.60	34.91				

TABLE OF OCEANOGRAPHIC DATA—Continued

STATIONS OCCUPIED IN 1959—Continued

Observed values			Scaled values			
Depth, meters	Temperature, °C.	Salinity, ‰	Depth, meters	Temperature, °C.	Salinity, ‰	σ_t
Station 7028; 8 May; 44°52′ N., 45°18′ W.; depth 4,115 m.; dynamic height 971.168.						
0	12.30	35.24	0	12.30	35.24	26.74
23	12.26	35.24	25	12.25	35.24	26.75
46	12.41	35.43	50	12.45	35.44	26.86
69	12.51	35.47	75	12.50	35.47	26.88
93	12.50	35.47	100	12.45	35.46	26.88
139	12.01	35.37	150	11.95	35.38	26.91
185	11.87	35.46	200	11.85	35.47	27.00
278	11.75	35.53	300	11.20	35.47	27.13
417	7.20	35.01	400	7.65	35.05	27.38
628	5.26	34.985	600	5.40	34.99	27.64
842	4.44	34.97	800	4.55	34.97	27.73
1,051	4.09	34.96	1,000	4.15	34.96	27.76
1,572	3.61	34.925				
Station 7029; 8 May; 45°21′ N., 45°15′ W.; depth 4,253 m.; dynamic height 971.100.						
0	11.89	34.92	0	11.89	34.92	26.57
25	11.85	35.16	25	11.85	35.16	26.76
51	11.54	35.26	50	11.55	35.25	26.89
76	11.61	35.34	75	11.60	35.33	26.94
102	11.81	35.43	100	11.80	35.42	26.98
152	10.40	35.19	150	10.45	35.19	27.04
203	10.51	35.33	200	10.50	35.33	27.14
305	8.44	35.12	300	8.55	35.13	27.31
401	5.23	34.78	400	5.25	34.78	27.49
602	5.02	34.985	600	5.05	34.98	27.67
803	4.63	35.005	800	4.65	35.00	27.74
1,001	4.00	34.95	1,000	4.00	34.95	27.77
1,493	3.55	34.92				
Station 7030; 8 May; 45°22.5′ N., 45°57′ W.; depth 3,512 m.; dynamic height 970.969.						
0	7.26	33.62	0	7.36	33.62	26.32
25	5.36	33.91	25	5.36	33.91	26.80
51	4.46	34.09	50	4.50	34.09	27.03
76	4.21	34.20	75	4.20	34.19	27.14
102	5.20	34.46	100	5.15	34.43	27.22
152	5.31	34.64	150	5.30	34.63	27.36
204	5.05	34.74	200	5.05	34.74	27.48
306	5.21	34.93	300	5.20	34.92	27.61
410	4.38	34.88	400	4.40	34.88	27.66
613	4.14	34.93	600	4.15	34.93	27.73
815	3.93	34.92	800	3.95	34.92	27.75
1,017	3.91	34.945	1,000	3.90	34.94	27.77
1,518	3.52	34.94				
Station 7031; 8 May; 45°23.5′ N., 46°37′ W.; depth 3,146 m.; dynamic height 970.925.						
0	6.49	33.84	0	6.49	33.84	26.59
25	3.82	34.02	25	3.82	34.02	27.05
50	3.24	34.26	50	3.24	34.26	27.29
75	2.95	34.35	75	2.95	34.35	27.39
100	3.62	34.49	100	3.62	34.49	27.44
150	4.28	34.65	150	4.28	34.65	27.50
199	4.81	34.83	200	4.80	34.83	27.58
299	3.55	34.73	300	3.55	34.73	27.63
396	3.80	34.795	400	3.85	34.80	27.66
580	3.88	34.865	600	3.85	34.87	27.72
774	3.74	34.88	800	3.70	34.88	27.74
970	3.57	34.875	1,000	3.55	34.88	27.75
1,461	3.46	34.91				
Station 7032; 9 May; 45°19′ N., 47°21′ W.; depth 2,469 m.; dynamic height 970.968.						
0	4.81	33.99	0	4.81	33.99	26.92
24	3.58	34.04	25	3.60	34.05	27.09
48	3.80	34.13	50	3.80	34.14	27.14
73	3.48	34.21	75	3.45	34.22	27.24
97	3.51	34.28	100	3.50	34.28	27.28
146	3.15	34.28	150	3.15	34.28	27.31
194	3.61	34.43	200	3.70	34.45	27.40
291	4.50	34.77	300	4.50	34.78	27.57
393	4.45	34.88	400	4.45	34.88	27.66
591	3.87	34.85	600	3.85	34.85	27.70
789	3.66	34.85	800	3.65	34.85	27.72
987	3.55	34.88	1,000	3.55	34.88	27.75
1,481	3.38	34.87				
Station 7033; 9 May; 45°28.5′ N., 47°44′ W.; depth 1,554 m.; dynamic height 970.953.						
0	4.55	33.885	0	4.55	33.88	26.85
24	3.14	33.94	25	3.10	33.94	27.05
48	2.50	33.94	50	2.50	33.95	27.11
73	3.04	34.05	75	3.05	34.06	27.15
97	3.17	34.22	100	3.20	34.24	27.28
146	3.53	34.40	150	3.60	34.43	27.39
194	4.51	34.66	200	4.50	34.68	27.49
291	4.03	34.76	300	4.05	34.77	27.62
367	4.35	34.84	400	4.30	34.85	27.66
554	3.92	34.87	600	3.90	34.87	27.72
743	3.17	34.88	800	3.75	34.88	27.73
936	3.60	34.88	1,000	3.60	34.88	27.75
1,430	3.46	34.89				
Station 7034; 9 May; 45°41.5′ N., 48°04′ W.; depth 637 m.; dynamic height 970.976.						
0	0.20	33.11	0	0.20	33.11	26.59
25	0.27	33.46	25	0.27	33.46	26.87
51	0.32	33.64	50	0.30	33.64	27.01
75	1.17	33.86	75	1.15	33.86	27.14
100	1.36	33.94	101	1.35	33.94	27.19
151	1.53	34.18	150	1.50	34.17	27.37
202	1.93	34.34	200	1.90	34.33	27.46
303	2.44	34.47	300	2.40	34.46	27.53
404	2.77	34.63	400	2.75	34.62	27.63
609	3.63	34.84	600	3.60	34.83	27.71
Station 7035; 9 May; 45°46.5′ N., 48°11′ W.; depth 180 m.; dynamic height 971.034.						
0	−0.29	32.88	0	−0.29	32.88	26.43
25	−1.27	33.00	25	−1.27	33.00	26.56
50	−1.41	33.20	50	−1.41	33.20	26.73
75	−1.20	33.34	75	−1.20	33.34	26.84
100	0.21	33.58	100	0.21	33.58	26.97
149	0.68	33.73	150	0.70	33.73	27.06
Station 7036; 9 May; 45°49′ N., 48°18′ W.; depth 115 m.; dynamic height 971.041.						
0	0.13	32.92	0	0.13	32.92	26.44
25	−0.67	33.02	25	−0.67	33.02	26.56
51	−1.36	33.21	50	−1.35	33.20	26.73
76	−1.21	33.30	75	−1.20	33.20	26.80
102	−0.97	33.37	100	−1.00	33.37	26.85

STATIONS OCCUPIED IN 1959—Continued

Observed values			Scaled values			
Depth, meters	Temperature, °C.	Salinity, ‰	Depth, meters	Temperature, °C.	Salinity, ‰	σ_t
Station 7037; 9 May; 45°53′ N., 48°30′ W.; depth 89 m.; dynamic height 971.046.						
0	0.81	32.99	0	0.81	33.99	26.47
25	−0.57	33.10	25	−0.57	33.10	26.56
51	−0.69	33.14	50	−0.70	33.14	26.66
76	−0.98	33.15	75	−0.95	33.15	26.68
Station 7038; 9 May; 46°07′ N., 48°45′ W.; depth 68 m.; dynamic height 971.046.						
0	0.75	33.06	0	0.75	33.06	26.52
26	−0.20	33.12	25	−0.15	33.11	26.61
52	−0.35	33.11	50	−0.35	33.11	26.61
Station 7039; 9 May; 46°17′ N., 49°01′ W.; depth 64 m.; dynamic height 971.051.						
0	1.15	33.00	0	1.15	33.00	26.46
25	0.66	33.04	25	0.26	33.04	26.51
50	0.23	33.06	50	0.23	33.06	26.55
Station 7040; 9 May; 46°15′ N., 48°30′ W.; depth 89 m.; dynamic height 971.047.						
0	0.55	33.06	0	0.55	33.06	26.53
24	−0.24	33.10	25	−0.25	33.10	26.60
49	−0.43	33.11	50	−0.45	33.11	26.62
73	−0.54	33.11	75	−0.55	33.11	26.62
Station 7041; 9 May; 46°14′ N., 48°02′ W.; depth 115 m.; dynamic height 971.054.						
0	0.24	32.90	0	0.24	32.90	26.42
25	−0.18	32.96	25	−0.18	32.86	26.49
51	−0.97	33.00	50	−0.95	33.01	26.56
76	−0.86	33.02	75	−0.85	33.02	26.56
102	−1.37	33.20	100	−1.30	33.18	26.70
Station 7042; 9 May; 46°12.5′ N., 47°44′ W.; depth 169 m.; dynamic height 971.047.						
0	0.08	32.86	0	0.08	32.86	26.40
26	−0.65	32.98	25	−0.65	32.97	26.52
52	−1.15	33.04	50	−1.15	33.02	26.58
77	−1.37	33.21	75	−1.35	33.18	26.71
103	−1.07	33.30	100	−1.10	33.28	26.78
155	−0.62	33.45	150	−0.65	33.43	26.89
Station 7043; 9 May; 46°10′ N., 47°22′ W.; depth 659 m.; dynamic height 971.016.						
0	0.27	32.86	0	0.27	32.86	26.39
25	−1.48	33.06	25	−1.48	33.06	26.61
50	−1.28	33.32	50	−1.28	33.28	26.74
75	−0.57	33.44	75	−0.57	33.44	26.89
100	−0.06	33.56	100	−0.06	33.56	26.97
150	1.56	34.10	150	1.56	34.10	27.30
199	2.01	34.22	200	2.05	34.22	27.37
299	2.66	34.55	300	2.70	34.55	27.57
398	3.15	34.705	400	3.15	34.71	27.66
597	3.66	34.82	600	3.65	34.83	27.70

Observed values			Scaled values			
Depth, meters	Temperature, °C.	Salinity, ‰	Depth, meters	Temperature, °C.	Salinity, ‰	σ_t
Station 7044; 10 May; 46°09′ N., 47°05′ W.; depth 1,463 m.; dynamic height 970.947.						
0	0.53	33.26	0	0.53	33.26	26.69
24	−0.03	33.34	25	0.00	33.35	26.80
49	0.74	33.76	50	0.75	33.79	27.11
73	1.49	34.00	75	1.55	34.03	27.24
98	2.19	34.26	100	2.20	34.27	27.40
146	2.17	34.39	150	2.20	34.40	27.50
195	2.60	34.51	200	2.60	34.52	27.56
292	2.92	34.66	300	2.95	34.67	27.65
382	3.24	34.72	400	3.30	34.73	27.66
573	3.78	34.84	600	3.80	34.84	27.70
764	3.70	34.84	800	3.70	34.84	27.71
958	3.59	34.84	1,000	3.60	34.84	27.72
1,351	3.48	34.87				
Station 7045; 10 May; 46°09′ N., 46°32′ W.; depth 494 m.; dynamic height 970.876.						
0	3.28	34.06	0	3.28	34.06	27.13
24	3.29	34.06	25	3.29	34.06	27.13
51	2.51	34.18	50	2.50	34.18	27.29
76	2.29	34.29	75	2.30	34.29	27.40
102	3.09	34.60	100	3.05	34.59	27.57
152	3.32	34.68	150	3.35	34.67	27.61
204	3.27	34.73	200	3.30	34.73	27.66
306	3.67	34.80	300	3.65	34.80	27.68
351	3.81	34.86	400	3.85	34.87	27.72
397	3.83	34.87				
Station 7046; 10 May; 46°08.5′ N., 45°54′ W.; depth 1,646 m.; dynamic height 970.886.						
0	5.22	34.27	0	5.22	34.27	27.09
25	5.12	34.26	25	5.12	34.26	27.09
52	3.68	34.41	50	3.75	34.40	27.35
77	3.51	34.46	75	3.50	34.45	27.42
103	2.96	34.51	100	3.00	34.50	27.51
154	3.00	34.58	150	3.00	34.57	27.57
206	3.13	34.65	200	3.10	34.64	27.61
309	3.67	34.79	300	3.65	34.78	27.66
397	3.67	34.84	400	3.65	34.84	27.71
594	3.73	34.875	600	3.70	34.87	27.74
792	3.58	34.89	800	3.60	34.89	27.76
991	3.48	34.90	1,000	3.45	34.90	27.78
1,493	3.37	34.91				
Station 7047; 10 May; 46°06′ N., 45°16′ W.; depth 3,410 m.; dynamic height 970.938.						
0	6.00	34.36	0	6.00	34.36	27.07
25	5.28	34.42	25	5.28	34.42	27.20
49	3.97	34.49	50	3.95	34.49	27.40
74	3.67	34.48	75	3.65	34.48	27.42
99	3.41	34.47	100	3.40	34.47	27.45
148	3.41	34.56	150	3.40	34.56	27.52
197	3.62	34.64	200	3.60	34.64	27.56
296	3.39	34.68	300	3.40	34.68	27.61
380	3.38	34.69	400	3.40	34.69	27.62
575	3.59	34.775	600	3.55	34.78	27.67
764	3.74	34.815	800	3.80	34.83	27.69
970	3.88	34.90	1,000	3.90	34.90	27.74
1,468	------	34.91				

TABLE OF OCEANOGRAPHIC DATA—Continued
STATIONS OCCUPIED IN 1959—Continued

Station 7048; 10 May; 46°03.5′ N., 44°37′ W.; depth 3,841 m.; dynamic height 971.122.

Observed values			Scaled values			
Depth, meters	Temperature, °C.	Salinity, ‰	Depth, meters	Temperature, °C.	Salinity, ‰	σ_t
0	9.72	34.29	0	9.72	34.29	26.47
25	10.04	34.53	25	10.04	34.53	26.60
52	11.60	35.11	50	11.40	35.08	26.78
77	11.96	35.26	75	11.90	35.24	26.81
103	12.54	35.44	100	12.50	35.43	26.84
154	10.14	35.06	150	10.30	35.08	26.98
206	9.44	35.07	200	9.50	35.07	27.11
310	8.16	35.02	300	8.30	35.02	27.27
412	6.47	35.01	400	6.65	35.01	27.50
617	5.11	35.02	600	5.20	35.02	27.69
821	4.57	35.00	800	4.60	35.00	27.74
1,026	4.11	34.955	1,000	4.15	34.96	27.76
1,536	3.61	34.935				

Station 7049; 10 May; 46°24′ N., 44°42′ W.; depth 1,646 m.; dynamic height 971.025.

Observed values			Scaled values			
Depth, meters	Temperature, °C.	Salinity, ‰	Depth, meters	Temperature, °C.	Salinity, ‰	σ_t
0	7.42	33.82	0	7.42	33.82	26.45
25	10.01	34.85	25	10.01	34.85	26.85
50	10.20	34.95	50	10.20	34.95	26.90
75	10.89	35.20	75	10.89	35.20	26.97
101	11.31	35.40	100	11.30	35.40	27.05
151	8.67	35.02	150	8.70	35.03	27.20
201	6.28	34.73	200	6.30	34.73	27.32
302	5.58	34.94	300	5.60	34.94	27.57
388	5.12	34.86	400	5.05	34.85	27.57
581	3.65	34.82	600	3.65	34.82	27.70
773	3.70	34.87	800	3.70	34.87	27.74
964	3.60	34.885	1,000	3.60	34.86	27.74
1,437	3.47	34.89				

Station 7050; 10 May; 46°30′ N., 44°44′ W.; depth 677 m.; dynamic height 971.000.

Observed values			Scaled values			
Depth, meters	Temperature, °C.	Salinity, ‰	Depth, meters	Temperature, °C.	Salinity, ‰	σ_t
0	6.89	33.74	0	6.89	33.74	26.46
25	9.16	34.66	25	9.16	34.66	26.85
50	10.30	35.00	50	10.30	35.00	26.92
75	6.98	34.50	75	6.98	34.50	27.05
101	4.94	34.30	100	4.95	34.30	27.15
151	6.13	34.65	150	6.10	34.64	27.27
201	6.14	34.78	200	6.10	34.78	27.38
302	5.13	34.82	300	5.15	34.82	27.54
400	4.95	34.93	400	4.95	34.93	27.64
601	3.84	34.86	600	3.85	34.86	27.71

Station 7051; 10 May; 46°35.5′ N., 44°44′ W.; depth 224 m.; dynamic height 970.896.

Observed values			Scaled values			
Depth, meters	Temperature, °C.	Salinity, ‰	Depth, meters	Temperature, °C.	Salinity, ‰	σ_t
0	4.56	34.28	0	4.56	34.28	27.17
25	3.79	34.29	25	3.79	34.29	27.26
49	3.07	34.35	50	3.05	34.35	27.38
74	2.86	34.36	75	2.85	34.36	27.41
99	2.69	34.39	100	2.70	34.39	27.44
148	2.75	34.52	150	2.75	34.52	27.55
197	3.04	34.63	200	3.05	34.63	27.60

Station 7052; 10 May; 46°40.5′ N., 44°44′ W.; depth 169 m.; dynamic height 970.895.

Observed values			Scaled values			
Depth, meters	Temperature, °C.	Salinity, ‰	Depth, meters	Temperature, °C.	Salinity, ‰	σ_t
0	4.45	34.28	0	4.45	34.28	27.18
25	4.02	34.28	25	4.02	34.28	27.23
50	3.06	34.37	50	3.06	34.37	27.40
75	2.98	34.39	75	2.98	34.39	27.42
101	2.79	34.40	100	2.80	34.40	27.44
151	2.93	34.52	150	2.90	34.52	27.54

Station 7053; 10 May; 46°48′ N., 44°51′ W.; depth 143 m.; dynamic height 970.898.

Observed values			Scaled values			
Depth, meters	Temperature, °C.	Salinity, ‰	Depth, meters	Temperature, °C.	Salinity, ‰	σ_t
0	4.16	34.26	0	4.16	34.26	27.20
25	3.44	34.28	25	3.44	34.28	27.28
50	2.88	34.30	50	2.88	34.30	27.36
76	2.83	34.31	75	2.85	34.31	27.37
101	2.72	34.33	100	2.75	34.33	27.39
126	2.57	34.42				

Station 7054; 10 May; 46°47.6′ N.; 45°01′ W.; depth 172 m.; dynamic height 970.892.

Observed values			Scaled values			
Depth, meters	Temperature, °C.	Salinity, ‰	Depth, meters	Temperature, °C.	Salinity, ‰	σ_t
0	4.30	34.26	0	4.30	34.26	27.19
25	3.78	34.28	25	3.78	34.28	27.26
51	3.00	34.35	50	3.00	34.35	27.39
76	2.76	34.35	75	2.75	34.35	27.41
101	2.66	34.38	100	2.65	34.38	27.44
152	2,92	34.55	150	2.90	34.54	27.55

Station 7055; 11 May; 46°47′ N., 45°17′ W.; depth 220 m.; dynamic height 970.894.

Observed values			Scaled values			
Depth, meters	Temperature, °C.	Salinity, ‰	Depth, meters	Temperature, °C.	Salinity, ‰	σ_t
0	4.09	34.24	0	4.09	34.24	27.19
25	2.94	34.25	25	2.94	34.25	27.31
49	2.80	34.30	50	2.80	34.30	27.37
74	2.82	34.34	75	2.80	34.34	27.40
98	2.69	34.36	100	2.70	34.36	27.42
148	2.78	34.48	150	2.80	34.48	27.50
197	3.38	34.66	200	3.40	34.66	27.60

Station 7056; 11 May; 46°47.5′ N., 45°44′ W.; depth 274 m.; dynamic height 970.905.

Observed values			Scaled values			
Depth, meters	Temperature, °C.	Salinity, ‰	Depth, meters	Temperature, °C.	Salinity, ‰	σ_t
0	4.32	34.21	0	4.32	34.21	27.15
22	3.97	34.21	25	3.85	34.21	27.20
44	3.28	34.27	50	3.15	34.27	27.31
67	2.92	34.28	75	2.90	34.28	27.34
89	2.88	34.28	100	3.00	34.31	27.36
133	3.50	34.48	150	3.35	34.51	27.48
177	3.12	34.55	200	3.20	34.61	27.58
266	3.74	34.79				

Station 7057; 11 May; 46°47.5′ N., 46°08′ W.; depth 320 m.; dynamic height 970.896.

Observed values			Scaled values			
Depth, meters	Temperature, °C.	Salinity, ‰	Depth, meters	Temperature, °C.	Salinity, ‰	σ_t
0	3.80	34.22	0	3.80	34.22	27.21
25	3.69	34.22	25	3.69	34.22	27.22
50	3.00	34.27	50	3.00	34.27	27.33
75	2.95	34.28	75	2.95	34.28	27.33
99	2.70	34.36	100	2.70	34.37	27.43
149	3.01	34.51	150	3.00	34.51	27.52
199	3.52	34.67	200	3.55	34.68	27.59
298	3.83	34.81	300	3.85	34.81	27.67

TABLE OF OCEANOGRAPHIC DATA—Continued

STATIONS OCCUPIED IN 1959—Continued

Station 7058; 11 May; 46°47.5′ N., 46°32′ W.; depth 640 m.; dynamic height 970.883.

Observed values			Scaled values			
Depth, meters	Temperature, °C.	Salinity, ‰	Depth, meters	Temperature, °C.	Salinity, ‰	σ_t
0	2.05	33.59	0	2.05	33.59	26.87
25	3.18	34.08	25	3.18	34.08	27.15
50	2.40	34.22	50	2.40	34.22	27.34
74	2.18	34.32	75	2.20	34.32	27.44
99	2.53	34.50	100	2.55	34.51	27.56
149	2.77	34.60	150	2.75	34.61	27.62
198	2.80	34.65	200	2.80	34.65	27.64
297	3.05	34.72	300	3.05	34.72	27.68
393	3.45	34.79	400	3.45	34.79	27.69
590	3.64	34.875	600	3.60	34.88	27.75

Station 7059; 11 May; 46°47′ N., 46°49′ W.; depth 1,244 m.; dynamic height 970.885.

Observed values			Scaled values			
Depth, meters	Temperature, °C.	Salinity, ‰	Depth, meters	Temperature, °C.	Salinity, ‰	σ_t
0	1.95	33.49	0	1.95	33.49	26.79
25	3.06	34.05	25	3.05	34.04	27.13
50	2.90	34.24	50	2.90	34.24	27.31
75	2.52	34.29	75	2.52	34.29	27.38
100	2.68	34.53	100	2.68	34.53	27.56
200	2.90	34.68	150	2.78	34.64	27.64
300	3.20	34.74	200	2.90	34.68	27.66
380	3.42	34.78	300	3.20	34.74	27.68
556	3.77	34.86	400	3.50	34.79	27.69
721	3.66	34.88	600	3.75	34.87	27.73
882	3.55	34.88	800	3.60	34.88	27.75
1,002	3.45	34.89	1,000	3.45	34.89	27.77

Station 7060; 11 May; 46°45.5′ N., 47°11′ W.; depth 612 m.; dynamic height 970.940.

Observed values			Scaled values			
Depth, meters	Temperature, °C.	Salinity, ‰	Depth, meters	Temperature, °C.	Salinity, ‰	σ_t
0	1.32	33.10	0	1.32	33.10	26.52
25	0.45	33.40	25	0.45	33.40	26.81
50	0.36	33.60	50	0.36	33.60	26.98
75	0.99	33.91	75	0.99	33.91	27.19
101	1.68	34.10	100	1.65	34.09	27.29
151	2.16	34.34	150	2.15	34.33	27.44
201	2.52	34.50	200	2.50	34.49	27.54
302	2.89	34.65	300	2.90	34.64	27.63
387	3.22	34.76	400	3.30	34.77	27.70
579	3.69	34.86	600	3.70	34.86	27.73

Station 7061; 11 May; 46°45.5′ N., 47°17′ W.; depth 331 m.; dynamic height 970.981.

Observed values			Scaled values			
Depth, meters	Temperature, °C.	Salinity, ‰	Depth, meters	Temperature, °C.	Salinity, ‰	σ_t
0	0.02	32.95	0	0.02	32.95	26.48
24	0.38	33.17	25	0.35	33.18	26.64
49	−0.56	33.40	50	−0.55	33.40	26.86
73	−0.19	33.51	75	−0.15	33.51	26.94
97	0.44	33.75	100	0.50	33.78	27.11
146	1.49	34.12	150	1.50	34.14	27.34
195	1.88	34.32	200	1.95	34.33	27.46
292	2.73	34.58	300	2.80	34.59	27.59

Station 7062; 11 May; 46°46′ N., 47°30′ W.; depth 183 m; dynamic height 971.025.

Observed values			Scaled values			
Depth, meters	Temperature, °C.	Salinity, ‰	Depth, meters	Temperature, °C.	Salinity, ‰	σ_t
0	0.34	32.92	0	0.34	32.92	26.43
25	−0.40	33.06	25	−0.40	33.06	26.61
49	−1.47	33.19	50	−1.45	33.19	26.72
74	−1.34	33.28	75	−1.35	33.28	26.79
98	−0.80	33.40	100	−0.80	33.41	26.88
147	0.89	33.79	150	1.00	33.82	27.12

Station 7063; 11 May; 46°49′ N., 48°05′ W.; depth 119 m.; dynamic height 971.043.

Observed values			Scaled values			
Depth, meters	Temperature, °C.	Salinity, ‰	Depth, meters	Temperature, °C.	Salinity, ‰	σ_t
0	0.49	33.03	0	0.49	33.03	26.51
25	0.41	33.04	25	0.41	33.04	26.53
50	−0.55	33.08	50	−0.55	33.08	26.60
75	−0.72	33.09	75	−0.72	33.09	26.61
100	−0.84	33.34	100	−0.84	33.34	26.82

Station 7064; 11 May; 46°47.5′ N., 48°43′ W.; depth 95 m.; dynamic height 971.044.

Observed values			Scaled values			
Depth, meters	Temperature, °C.	Salinity, ‰	Depth, meters	Temperature, °C.	Salinity, ‰	σ_t
0	0.16	33.11	0	0.16	33.11	26.59
25	0.12	33.11	25	0.12	33.11	26.60
50	−0.13	33.13	50	−0.13	33.13	26.62
75	−0.32	33.16	75	−0.32	33.16	26.65
95	−0.30	33.16	100	−0.30	33.16	26.65

Station 7065; 27 May; 42°00′ N., 50°58′ W.; depth 3,383 m.; dynamic height 971.001.

Observed values			Scaled values			
Depth, meters	Temperature, °C.	Salinity, ‰	Depth, meters	Temperature, °C.	Salinity, ‰	σ_t
0	4.37	33.18	0	4.37	33.18	26.32
24	4.36	33.19	25	4.35	33.19	26.33
47	2.20	33.38	50	2.20	33.42	26.72
71	2.24	33.72	75	2.60	33.78	26.96
94	3.05	34.02	100	3.10	34.06	27.15
141	3.41	34.30	150	3.55	34.35	27.33
189	4.20	34.58	200	4.35	34.64	27.48
283	5.79	34.98	300	5.60	34.96	27.59
347	4.90	34.89	400	4.60	34.89	27.65
526	4.19	34.89	600	4.20	34.91	27.72
708	4.30	34.96	800	4.15	34.95	27.75
894	3.95	34.94	1,000	3.90	34.94	27.77
1,377	3.70	34.94				

Station 7066; 27 May; 41°55.5′ N., 51°52′ W.; depth 3,932 m.; dynamic height 971.159.

Observed values			Scaled values			
Depth, meters	Temperature, °C.	Salinity, ‰	Depth, meters	Temperature, °C.	Salinity, ‰	σ_t
0	6.89	33.32	0	6.89	33.32	26.13
25	9.33	34.04	25	9.33	34.04	26.33
50	13.56	35.57	50	13.56	35.57	26.74
75	11.73	35.19	75	11.73	35.19	26.80
101	12.33	35.38	100	12.30	35.37	26.84
150	12.53	35.46	150	12.55	35.46	26.86
201	9.21	34.92	200	9.20	34.92	27.04
302	8.35	35.07	300	8.35	35.07	27.30
380	6.34	34.86	400	6.15	34.86	27.44
577	4.81	34.92	600	4.75	34.92	27.66
778	4.29	34.91	800	4.25	34.91	27.71
973	4.16	34.95	1,000	4.15	34.95	27.75
1,466	3.61	34.915				

Station 7067; 27 May; 42°20.5′ N., 51°26′ W.; depth 2,916 m.; dynamic height 970.991.

Observed values			Scaled values			
Depth, meters	Temperature, °C.	Salinity, ‰	Depth, meters	Temperature, °C.	Salinity, ‰	σ_t
0	4.61	33.14	0	4.61	33.14	26.26
25	4.26	33.16	25	4.26	33.16	26.31
51	2.20	33.70	50	2.20	33.69	26.92
76	3.44	34.14	75	3.40	34.13	27.17
102	4.90	34.42	100	4.80	34.42	27.26
152	4.76	34.54	150	4.75	34.54	27.36
204	5.29	34.76	200	5.25	34.74	27.46
306	4.41	34.78	300	4.45	34.78	27.58
403	5.31	35.01	400	5.30	35.00	27.66
604	4.28	34.93	600	4.30	34.93	27.71
804	4.18	34.95	800	4.20	34.95	27.75
1,005	3.86	34.94	1,000	3.85	34.94	27.77
1,509	3.59	34.935				

TABLE OF OCEANOGRAPHIC DATA—Continued
STATIONS OCCUPIED IN 1959—Continued

Station 7068; 27 May; 42°44.5′ N., 51°02′ W.; depth 1,646 m.; dynamic height 971.074.

Observed values			Scaled values			
Depth, meters	Temperature, °C.	Salinity, ‰	Depth, meters	Temperature, °C.	Salinity, ‰	σ_t
0	2.53	33.04	0	2.53	33.04	26.39
25	2.16	33.04	25	2.16	33.04	26.41
52	−0.63	33.24	50	−0.60	33.22	26.71
77	−1.06	33.43	75	−1.05	33.41	26.89
103	0.49	33.64	100	0.30	33.62	27.00
154	1.52	33.81	150	1.45	33.80	27.07
206	4.62	34.43	200	4.30	34.36	27.27
309	3.40	34.53	300	3.50	34.52	27.48
415	2.99	34.63	400	3.05	34.60	27.58
620	3.63	34.79	600	3.55	34.73	27.63
824	3.81	34.85	800	3.80	34.84	27.70
1,030	3.74	34.88	1,000	3.75	34.87	27.73

Station 7069; 27 May; 42°54′ N., 50°52′ W.; depth 1,097 m.; dynamic height 971.049.

Observed values			Scaled values			
Depth, meters	Temperature, °C.	Salinity, ‰	Depth, meters	Temperature, °C.	Salinity, ‰	σ_t
0	2.93	32.91	0	2.93	32.91	26.24
24	1.40	33.13	25	1.40	33.13	26.54
48	0.96	33.195	50	0.95	33.20	26.63
72	4.08	33.835	75	4.05	33.84	26.87
96	2.93	33.865	100	2.85	33.87	27.02
144	2.23	33.925	150	2.15	33.93	27.12
192	1.60	33.99	200	1.60	34.01	27.23
288	2.79	34.50	300	2.85	34.54	27.55
389	3.19	34.66	400	3.25	34.67	27.62
587	3.76	34.825	600	3.75	34.83	27.69
787	3.80	34.86	800	3.80	34.86	27.72
982	3.74	34.875	1,000	3.75	34.88	27.73

Station 7070; 27 May; 43°00′ N., 50°45′ W.; depth 649 m.; dynamic height 971.079.

Observed values			Scaled values			
Depth, meters	Temperature, °C.	Salinity, ‰	Depth, meters	Temperature, °C.	Salinity, ‰	σ_t
0	2.93	32.94	0	2.93	32.94	26.27
26	1.68	33.225	25	1.70	33.22	26.59
51	6.53	34.115	50	6.35	34.09	26.81
77	8.26	34.64	75	8.25	34.63	26.96
103	5.76	34.27	100	6.10	34.31	27.02
153	1.61	33.945	150	1.75	33.96	27.18
205	4.42	34.37	200	4.25	34.35	27.26
308	3.42	34.35	300	3.50	34.35	27.34
402	2.88	34.525	400	2.90	34.52	27.54
598	3.56	34.76	(600)	3.55	34.76	27.66

Station 7071; 27 May; 43°04.5′ N., 50°41′ W.; depth 169 m.; dynamic height 971.113

Observed values			Scaled values			
Depth, meters	Temperature, °C.	Salinity, ‰	Depth, meters	Temperature, °C.	Salinity, ‰	σ_t
0	3.07	32.83	0	3.07	32.83	26.17
25	1.93	33.01	25	1.93	33.01	26.41
50	0.53	33.25	50	0.53	33.25	26.68
75	0.32	33.49	75	0.32	33.49	26.89
101	0.56	33.57	100	0.55	33.57	26.95
151	0.64	33.61	150	0.70	33.61	26.97

Station 7072; 27 May; 43°08.5′ N., 50°35′ W.; depth 93 m. dynamic height 971.128.

Observed values			Scaled values			
Depth, meters	Temperature, °C.	Salinity, ‰	Depth, meters	Temperature, °C.	Salinity, ‰	σ_t
0	3.37	32.82	0	3.37	32.82	26.14
25	1.94	33.00	25	1.94	33.00	26.40
50	0.58	33.18	50	0.58	33.18	26.62
75	−0.05	33.24	75	−0.05	33.24	26.71

Station 7073; 28 May; 43°21.5′ N., 50°15′ W.; depth 68 m.; dynamic height 971.144.

Observed values			Scaled values			
Depth, meters	Temperature, °C.	Salinity, ‰	Depth, meters	Temperature, °C.	Salinity, ‰	σ_t
0	3.65	32.51	0	3.65	32.51	25.86
22	3.36	32.51	25	3.35	32.55	25.92
45	1.35	32.98	(50)	1.00	33.10	26.54

Station 7074; 28 May; 42°58′ N., 50°18′ W.; depth 95 m.; dynamic hegiht 971.120.

Observed values			Scaled values			
Depth, meters	Temperature, °C.	Salinity, ‰	Depth, meters	Temperature, °C.	Salinity, ‰	σ_t
0	2.10	33.05	0	2.10	33.05	26.42
25	1.47	33.08	25	1.47	33.08	26.49
49	0.56	33.22	50	0.55	33.22	26.66
74	0.18	33.38	(75)	0.20	33.37	26.80

Station 7075; 28 May; 42°51′ N., 50°16′ W.; depth 364 m.; dynamic height 971.107.

Observed values			Scaled values			
Depth, meters	Temperature, °C.	Salinity, ‰	Depth, meters	Temperature, °C.	Salinity, ‰	σ_t
0	2.39	33.03	0	2.39	33.03	26.39
25	0.94	33.17	25	0.94	33.17	26.59
50	0.36	33.25	50	0.36	33.25	26.69
75	−0.14	33.38	75	−0.14	33.38	26.82
100	0.08	33.44	100	0.08	33.44	26.86
150	0.91	33.75	150	0.91	33.75	27.06
200	1.40	33.94	200	1.40	33.94	27.17
300	2.11	34.28	300	2.11	34.28	27.40

Station 7076; 28 May; 42°39′ N.; 50°16′ W.; depth 1,735 m.; dynamic height 971.035.

Observed values			Scaled values			
Depth, meters	Temperature, °C.	Salinity, ‰	Depth, meters	Temperature, °C.	Salinity, ‰	σ_t
0	1.88	33.21	0	1.88	33.21	26.58
25	1.40	33.21	25	1.40	33.21	26.60
50	0.83	33.53	50	0.83	33.53	26.89
75	1.18	33.67	75	1.18	33.67	26.98
100	1.77	33.78	100	1.77	33.78	27.03
150	2.49	33.97	150	2.49	33.97	27.13
199	2.45	34.15	200	2.45	34.14	27.26
299	2.75	34.49	300	2.75	34.49	27.52
402	2.92	34.62	400	2.90	34.62	27.62
601	3.53	34.78	600	3.50	34.77	27.68
800	3.92	34.88	800	3.95	34.87	27.71
1,000	4.02	34.94	1,000	4.00	34.94	27.76

Station 7077; 28 May; 42°24.5′ N., 50°14′ W.; depth 2,561 ,.; dynamic height 971.048.

Observed values			Scaled values			
Depth, meters	Temperature, °C.	Salinity, ‰	Depth, meters	Temperature, °C.	Salinity, ‰	σ_t
0	5.40	33.10	0	5.40	33.10	26.14
25	5.20	33.13	25	5.20	33.13	26.19
50	6.24	33.74	50	6.24	33.74	26.54
74	6.34	34.22	75	6.35	34.21	26.91
99	5.56	34.34	100	5.55	34.33	27.10
149	7.15	34.81	150	7.15	34.81	27.27
198	7.20	34.96	200	7.20	34.95	27.37
297	2.98	34.50	300	3.00	34.50	27.51
396	4.35	34.81	400	4.40	34.80	27.60
592	4.48	34.94	600	4.45	34.93	27.70
785	3.87	34.895	800	3.85	34.89	27.73
982	3.66	34.89	1,000	3.65	34.88	27.74
1,476	3.49	34.90				

TABLE OF OCEANOGRAPHIC DATA—Ctoninued

STATIONS OCCUPIED IN 1959—Continued

Station 7078; 28 May; 42°00.5′N., 50°14′ W.; depth 3,470 m.; dynamic height 971.168.

Observed values			Scaled values			
Depth, meters	Temperature, °C.	Salinity, ‰	Depth, meters	Temperature, °C.	Salinity, ‰	σ_t
0	6.90	33.22	0	6.90	33.22	26.05
25	8.34	33.83	25	8.34	33.83	26.32
50	10.71	34.84	50	10.71	34.84	26.71
75	11.48	35.08	75	11.48	35.08	26.76
100	11.84	35.22	100	11.84	35.22	26.80
150	12.55	35.47	150	12.55	35.47	26.86
200	11.51	35.42	200	11.51	35.42	27.02
300	7.92	34.96	300	7.92	34.96	27.27
399	6.96	34.92	400	6.95	35.01	27.46
599	4.06	34.80	600	4.05	34.79	27.63
799	4.83	35.025	800	4.85	35.02	27.73
1,001	4.40	35.00	1,000	4.40	35.00	27.76
1,510	3.72	34.94				

Station 7079; 28 May; 41°31.5′ N., 50°13′ W.; depth 3,932 m.; dynamic height 971.313.

Observed values			Scaled values			
Depth, meters	Temperature, °C.	Salinity, ‰	Depth, meters	Temperature, °C.	Salinity, ‰	σ_t
0	10.80	34.40	0	10.80	34.40	26.36
25	12.40	35.02	25	12.40	35.02	26.55
50	14.18	35.64	50	14.18	35.64	26.65
74	13.25	35.69	75	14.25	35.68	26.67
99	14.13	35.68	100	14.15	35.68	26.70
149	13.56	35.61	150	13.55	35.60	26.76
199	12.75	35.47	200	12.75	35.47	26.83
288	12.43	35.44	300	12.40	35.43	26.87
390	10.45	35.32	400	10.20	35.29	27.16
583	6.61	35.05	600	6.45	35.03	27.53
775	5.24	35.00	800	5.10	34.99	27.67
970	4.59	34.99	1,000	4.55	34.98	27.73
1,458	3.87	34.95				

Station 7080; 29 May; 41°00′ N., 50°15′ W.; depth 3,566 m.; dynamic height 971.394.

Observed values			Scaled values			
Depth, meters	Temperature, °C.	Salinity, ‰	Depth, meters	Temperature, °C.	Salinity, ‰	σ_t
0	15.40	36.03	0	15.40	36.03	26.69
25	15.33	36.03	25	15.33	36.03	26.70
50	15.21	36.01	50	15.21	36.01	26.72
75	15.21	36.01	75	15.21	36.01	26.72
101	15.24	36.02	100	15.25	35.91	26.72
151	14.75	35.91	150	14.75	35.91	26.74
202	13.71	35.66	200	13.75	35.66	26.77
303	13.51	35.63	300	13.50	35.63	26.79
399	12.45	35.56	400	12.45	35.55	26.94
597	8.08	35.10	600	8.00	35.09	27.36
794	5.07	34.93	800	5.05	34.92	27.63
991	4.37	34.93	1,000	4.35	34.92	27.71
1,484	3.86	34.95				

Station 7081; 29 May; 42°00.5′ N., 49°23′ W.; depth 2,880 m.; dynamic height 971.114.

Observed values			Scaled values			
Depth, meters	Temperature, °C.	Salinity, ‰	Depth, meters	Temperature, °C.	Salinity, ‰	σ_t
0	8.94	33.82	0	8.94	33.83	26.23
25	11.60	34.68	25	11.60	34.68	26.43
50	14.19	35.67	50	14.19	35.67	26.68
75	12.76	35.42	75	12.76	35.42	26.78
100	12.27	35.34	100	12.27	35.34	26.82
150	12.67	35.54	150	12.67	35.54	26.90
201	10.13	35.22	200	10.20	35.22	27.11
301	7.33	34.98	300	7.30	34.98	27.38
380	4.49	34.74	400	4.30	34.73	27.56
567	3.43	34.76	600	3.50	34.76	27.67
752	3.81	34.865	800	3.85	34.88	27.72
940	3.89	34.91	1,000	3.85	34.91	27.75
1,410	3.78	34.94				

Station 7082; 29 May; 41°31.5′ N., 48°55′ W.; depth 3483 m.; dynamic hiehgt 971.181.

Observed values			Sclaed values			
Depth, meters	Temperature, °C.	Salinity, ‰	Depth, meters	Temperature, °C.	Salinity, ‰	σ_t
0	9.27	33.67	0	9.27	33.67	26.04
25	10.87	34.55	25	10.87	34.55	26.46
49	11.86	35.05	50	11.85	35.05	26.68
74	11.64	35.08	75	11.65	35.08	26.73
98	11.92	35.23	100	11.95	35.23	26.80
147	12.58	35.46	150	12.55	35.45	26.85
197	12.18	35.44	200	12.15	35.43	26.91
295	8.74	35.06	300	8.55	35.04	27.24
383	6.67	34.87	400	6.40	34.87	27.42
573	4.55	34.88	600	4.50	34.88	27.65
762	4.26	34.92	800	4.15	34.91	27.72
963	3.72	34.88	1,000	3.70	34.88	27.74
1,482	3.68	34.93				

Station 7083; 29 May; 41°00′ N., 48°26′ W.; depth 3,182 m.; dynamic height 971.206.

Observed values			Sclaed values			
Depth, meters	Temperature, °C.	Salinity, ‰	Depth, meters	Temperature, °C.	Salinity, ‰	σ_t
0	8.73	33.46	0	8.73	33.46	25.97
24	13.68	35.40	25	13.65	35.39	26.58
49	13.44	35.52	50	13.45	35.51	26.72
73	13.28	35.52	75	13.25	35.52	26.76
97	13.08	35.52	100	13.05	35.51	26.80
146	12.70	35.46	150	12.70	35.45	26.82
195	12.68	35.50	200	12.65	35.50	26.87
292	10.50	35.30	300	10.30	35.28	27.13
391	8.06	35.08	400	7.90	35.06	27.36
592	5.58	35.04	600	5.50	35.04	27.66
776	4.42	34.95	(800)	4.35	34.95	27.72
			(1,000)	4.05	34.94	27.74

Station 7084; 29 May; 41°34.5′ N., 47°15′ W.; depth 4,280 m.; dynamic height 971.035.

Observed values			Sclaed values			
Depth, meters	Temperature, °C.	Salinity, ‰	Depth, meters	Temperature, °C.	Salinity, ‰	σ_t
0	8.24	33.67	0	8.24	33.67	26.21
25	4.08	33.55	25	4.08	33.55	26.64
49	3.50	33.61	50	3.50	33.61	26.75
74	3.32	33.75	75	3.30	33.75	26.88
99	0.89	33.77	100	0.90	33.77	27.09
148	5.71	34.56	150	5.70	34.56	27.26
197	5.37	34.59	200	5.35	34.58	27.32
296	3.99	34.59	300	4.00	34.59	27.48
395	5.53	34.01	400	5.50	35.00	27.63
592	4.39	34.92	600	4.35	34.91	27.70
789	4.41	34.98	800	4.40	34.98	27.74
985	4.18	34.96	1,000	4.20	34.96	27.76
1,471	3.66	34.93				

Station 7085; 30 May; 41°59′ N., 47°55′ W.; depth 3,731 m.; dynamic height 970.943.

Observed values			Sclaed values			
Depth, meters	Temperature, °C.	Salinity, ‰	Depth, meters	Temperature, °C.	Salinity, ‰	σ_t
0	7.35	33.67	0	7.35	33.67	26.35
24	6.02	33.77	25	5.90	33.78	26.62
48	4.08	34.06	50	4.05	34.06	27.06
72	3.87	34.26	75	3.90	34.29	27.25
96	4.25	34.46	100	4.30	34.47	27.36
144	4.51	34.62	150	4.50	34.63	27.45
192	4.52	34.72	200	4.60	34.73	27.52
288	5.57	35.02	300	5.55	35.02	27.65
400	5.23	35.04	400	5.25	35.04	27.70
596	4.36	34.97	600	4.35	34.97	27.75
791	4.08	34.96	800	4.05	34.95	27.76
988	3.92	34.96	1,000	3.90	34.95	27.78
1,480	3.55	34.94				

TABLE OF OCEANOGRAPHIC DATA—Continued
STATIONS OCCUPIED IN 1959—Continued

Station 7086; 30 May; 42°20′ N., 48°31′ W.; depth 3,017 m.; dynamic height 971.001.

Observed values			Scaled values			
Depth, meters	Temperature, °C.	Salinity, ‰	Depth, meters	Temperature, °C.	Salinity, ‰	σ_t
0	7.57	33.62	0	7.57	33.62	26.26
25	7.35	33.82	25	7.35	33.82	26.46
51	6.89	34.17	50	6.90	34.16	26.79
76	7.43	34.66	75	7.40	34.64	27.10
101	7.40	34.75	100	7.40	34.74	27.18
152	6.01	34.66	150	6.05	34.67	27.31
203	4.23	34.54	200	4.30	34.54	27.41
304	5.04	34.86	300	5.00	34.85	27.58
400	5.19	34.98	400	5.20	34.98	27.65
600	4.53	34.97	600	4.55	34.96	27.72
800	4.17	34.97	800	4.15	34.96	27.76
999	4.03	34.97	1,000	4.05	34.96	27.77
1,494	3.58	34.93				

Station 7087; 30 May; 42°42′ N., 49°10′ W.; depth 2,122 m.; dynamic height 970.957.

Observed values			Scaled values			
Depth, meters	Temperature, °C.	Salinity, ‰	Depth, meters	Temperature, °C.	Salinity, ‰	σ_t
0	6.71	33.58	0	6.71	33.58	26.36
25	4.33	33.64	25	4.33	33.64	26.70
50	3.07	33.78	50	3.07	33.78	26.92
74	2.31	34.16	75	2.30	34.16	27.30
99	2.40	34.25	100	2.35	34.25	27.36
149	4.44	34.64	150	4.45	34.64	27.47
199	4.36	34.71	200	4.35	34.71	27.54
298	4.67	34.88	300	4.70	34.87	27.63
390	4.78	34.94	400	4.89	34.89	27.63
585	4.84	34.03	600	4.80	34.02	27.74
779	4.17	34.96	800	4.10	34.94	27.75
974	3.80	34.92	1,000	3.80	34.92	27.77
1.463	3.48	34.90				

Station 7088; 30 May; 43°17.5′ N., 48°44′ W.; depth 2,103 m.; dynamic height 970.945.

Observed values			Scaled values			
Depth, meters	Temperature, °C.	Salinity, ‰	Depth, meters	Temperature, °C.	Salinity, ‰	σ_t
0	5.94	33.74	0	5.94	33.74	26.58
24	4.15	33.74	25	4.10	33.73	26.79
49	3.45	33.89	50	3.45	33.90	26.98
73	2.84	34.07	75	2.85	34.10	27.20
98	3.14	34.29	100	3.15	34.30	27.33
145	3.40	34.52	150	3.40	34.52	27.49
193	3.24	34.60	200	3.25	34.60	27.56
292	4.06	34.81	300	4.10	34.82	27.66
377	4.14	34.87	400	4.10	34.86	27.69
566	3.68	34.86	600	3.65	34.85	27.72
756	3.61	34.84	800	3.60	34.84	27.72
949	3.55	34.87	1,000	3.55	34.87	27.75
1,439	3.43	34.89				

Station 7089; 30 May; 43°08 N., 48°11′ W.; depth 3,109 m.; dynamic height 970.980.

Observed values			Scaled values			
Depth, meters	Temperature, °C.	Salinity, ‰	Depth, meters	Temperature, °C.	Salinity, ‰	σ_t
0	7.86	33.78	0	7.86	33.78	26.35
23	5.28	33.68	25	5.15	33.67	26.63
46	3.84	33.65	50	3.70	33.66	26.78
69	3.19	34.03	75	3.20	34.08	27.15
92	3.52	34.23	100	3.55	34.26	27.26
138	3.43	34.39	150	3.55	34.39	27.36
184	3.92	34.44	200	4.00	34.48	27.39
276	4.34	34.79	300	4.25	34.81	27.63
377	4.24	34.86	400	4.25	34.86	27.67
565	4.11	34.91	600	4.05	34.91	27.73
753	3.68	34.86	800	3.65	34.86	27.73
947	3.65	34.905	1,000	3.60	34.90	27.77
1,444	3.42	34.91				

Station 7090; 31 May; 42°54′ N., 47°33′ W.; depth 3,676 m.; dynamic height 971.111.

Observed values			Scaled values			
Depth, meters	Temperature, °C.	Salinity, ‰	Depth, meters	Temperature, °C.	Salinity, ‰	σ_t
0	11.99	34.37	0	11.99	34.37	26.12
24	11.32	34.65	25	11.35	34.66	26.47
48	12.65	35.22	50	12.70	35.23	26.65
72	12.78	35.42	75	12.75	35.41	26.78
96	12.04	35.34	100	11.75	35.27	26.87
144	7.62	34.62	150	7.25	34.56	27.06
192	5.43	34.30	200	5.40	34.31	27.10
288	5.43	34.59	300	5.35	34.60	27.34
408	4.33	34.72	400	4.40	34.70	27.52
609	4.70	34.965	600	4.70	34.95	27.69
809	4.22	34.96	800	4.25	34.95	27.74
1,007	3.95	34.94	1,000	3.95	34.93	27.75
1,485	3.67	34.935				

Station 7091; 31 May; 42°38′ N., 46°46′ W.; depth 4,207 m.; dynamic height 971.404.

Observed values			Scaled values			
Depth, meters	Temperature, °C.	Salinity, ‰	Depth, meters	Temperature, °C.	Salinity, ‰	σ_t
0	17.54	36.34	0	17.54	36.34	26.43
25	17.52	36.34	25	17.52	36.34	26.43
49	17.26	36.31	50	17.25	36.30	26.47
74	16.97	36.26	75	16.95	36.25	26.50
98	16.56	36.23	100	16.50	36.22	26.59
146	15.30	35.94	150	15.25	35.93	26.65
196	14.67	35.84	200	14.60	35.86	26.74
294	12.60	35.45	300	12.50	35.44	26.85
413	11.54	35.45	400	11.70	35.44	27.01
617	7.60	35.09	600	7.90	35.11	27.40
819	5.58	35.04	800	5.75	35.04	27.63
1,024	4.58	34.985	1,000	4.65	34.98	27.72
1,534	3.81	34.95				

Station 7092; 31 May; 42°47′ N., 45°51′ W.; depth 4,663 m.; dynamic height 971.516.

Observed values			Scaled values			
Depth, meters	Temperature, °C.	Salinity, ‰	Depth, meters	Temperature, °C.	Salinity, ‰	σ_t
0	16.53	36.11	0	16.53	36.11	26.48
25	16.50	36.22	25	16.50	36.22	26.59
50	16.36	36.19	50	16.36	36.19	26.59
75	16.24	36.16	75	16.24	36.16	26.60
100	15.33	35.97	100	15.33	35.97	26.65
148	15.06	35.89	150	15.05	35.89	26.66
198	14.89	35.94	200	14.85	35.93	26.74
298	13.41	35.61	300	13.40	35.60	26.79
396	12.96	35.60	400	12.95	35.59	26.87
586	10.89	35.39	600	10.70	35.37	27.14
770	7.90	35.17	800	7.50	35.14	27.47
963	5.93	35.09	1,000	5.70	35.07	27.67
1,451	4.18	34.97				

Station 7093; 31 May; 43°20′ N., 46°00′ W.; depth 3,932 m.; dynamic height 971.423.

Observed values			Scaled values			
Depth, meters	Temperature, °C.	Salinity, ‰	Depth, meters	Temperature, °C.	Salinity, ‰	σ_t
0	15.44	35.94	0	15.44	35.94	26.61
25	15.42	35.98	25	15.42	35.98	26.65
49	15.35	35.99	50	15.35	35.98	26.66
74	15.35	35.98	75	15.35	35.98	26.66
98	15.32	35.98	100	15.30	35.98	26.67
147	14.60	35.82	150	14.55	35.80	26.70
196	13.91	35.68	200	13.85	35.66	26.75
294	12.80	35.49	300	12.75	35.49	26.84
386	12.56	35.57	400	12.45	35.44	26.86
575	8.99	35.20	600	8.50	35.16	27.34
762	5.97	34.98	800	5.50	34.95	27.60
953	4.34	34.89	1,000	4.20	34.89	27.70
1,433	3.99	34.94				

STATIONS OCCUPIED IN 1959—Continued

Station 7094; 31 May; 43°34.5′ N., 46°40′ W.; depth 3,948 m.; dynamic height 971.290.

Observed values			Scaled values			
Depth, meters	Temperature, °C.	Salinity, ‰	Depth, meters	Temperature, °C.	Salinity, ‰	σ_t
0	10.99	34.26	0	10.99	34.26	26.21
25	15.19	35.90	25	15.19	35.90	26.64
50	15.07	35.90	50	15.07	35.89	26.65
74	15.04	35.89	75	15.05	35.89	26.66
99	14.38	35.77	100	14.35	35.76	26.72
149	13.39	35.58	150	13.35	35.37	26.78
199	12.80	35.50	200	12.80	35.50	26.88
298	11.85	35.48	300	11.80	35.47	27.91
396	9.68	35.22	400	9.60	35.21	27.20
588	5.83	34.89	600	5.75	34.89	27.52
777	4.72	34.94	800	4.90	34.93	27.65
973	4.30	34.93	1,000	4.25	34.92	27.72
1,466	3.88	34.95				

Station 7095; 1 June; 43°45.5′ N., 47°27′ W.; depth 4,006 m.; dynamic height 971.048.

Observed values			Scaled values			
Depth, meters	Temperature, °C.	Salinity, ‰	Depth, meters	Temperature, °C.	Salinity, ‰	σ_t
0	7.88	33.82	0	7.88	33.82	26.38
25	7.68	33.83	25	7.68	33.83	26.41
51	7.03	34.22	50	7.05	34.21	26.81
76	7.17	34.47	75	7.20	34.46	26.99
102	7.02	34.54	100	7.05	34.53	27.06
152	6.95	34.75	150	6.95	34.74	27.24
202	5.98	34.65	200	5.80	34.65	27.32
304	5.52	34.84	300	5.55	34.82	27.49
405	4.75	34.85	400	4.80	34.85	27.60
602	4.69	34.95	600	4.70	34.94	27.68
796	4.23	34.94	800	4.20	34.93	27.73
995	3.99	34.93	1,000	4.00	34.92	27.75
1,496	3.65	34.905				

Station 7096; 1 June; 43°56.5′ N., 48°06′ W.; depth 3,749 m.; dynamic height 970.999.

Observed values			Scaled values			
Depth, meters	Temperature, °C.	Salinity, ‰	Depth, meters	Temperature, °C.	Salinity, ‰	σ_t
0	7.64	33.81	0	7.64	33.81	26.41
25	7.64	33.92	25	7.64	33.92	26.50
50	6.52	34.32	50	6.52	34.32	26.96
75	7.03	34.57	75	7.03	34.57	27.09
100	8.29	34.94	100	8.29	34.94	27.20
150	6.90	34.82	150	6.90	34.82	27.31
200	5.59	34.68	200	5.59	34.68	27.37
300	4.30	34.70	300	4.30	34.70	27.53
384	5.14	34.93	400	5.15	34.94	27.64
577	4.55	34.97	600	4.50	34.96	27.72
771	4.04	34.945	800	3.95	34.93	27.75
966	3.59	34.905	1,000	3.55	34.90	27.77
1,458	3.39	34.89				

Station 7097; 1 June; 44°03′ N., 48°33′ W.; depth 3,109 m. dynamic height 970.943.

Observed values			Scaled values			
Depth, meters	Temperature, °C.	Salinity, ‰	Depth, meters	Temperature, °C.	Salinity, ‰	σ_t
0	2.97	33.37	0	2.97	33.37	26.60
25	2.49	33.54	25	2.49	33.54	26.78
50	2.20	33.87	50	2.20	33.87	27.06
75	2.77	34.13	75	2.77	34.13	27.23
100	2.51	34.23	100	2.51	34.23	27.33
150	2.52	34.40	150	2.52	34.40	27.46
200	3.23	34.59	200	3.23	34.59	27.54
300	4.33	34.86	300	4.33	34.86	27.66
404	4.17	34.88	400	4.20	34.87	27.69
602	3.97	34.90	600	4.00	34.89	27.72
798	3.65	34.885	800	3.65	34.88	27.74
997	3.62	34.91	1,000	3.60	34.90	27.77
1,491	3.39	34.90				

Station 7098; 1 June; 44°06′ N., 48°50′ W.; depth 1,600 m.; dynamic height 971.030.

Observed values			Scaled values			
Depth, meters	Temperature, °C.	Salinity, ‰	Depth, meters	Temperature, °C.	Salinity, ‰	σ_t
0	2.02	32.99	0	2.02	32.99	26.38
25	1.07	33.04	25	1.07	33.04	26.49
50	−0.56	33.17	50	−0.56	33.17	26.66
75	−0.95	33.33	75	−0.95	33.33	26.81
100	−0.03	33.60	100	−0.03	33.60	26.99
150	1.25	33.90	150	1.25	33.90	27.16
199	1.95	34.22	200	1.95	34.22	27.38
299	2.51	34.48	300	2.55	34.47	27.53
410	3.14	34.68	400	3.10	34.66	27.63
609	3.53	34.84	600	3.55	34.82	27.71
803	3.69	34.87	800	3.70	34.86	27.73
1,002	3.65	34.87	1,000	3.65	34.86	27.73
1,495	3.55	34.88				

Station 7099; 1 June; 44°07′ N., 48°55′ W.; depth 903 m.; dynamic height 971.070.

Observed values			Scaled values			
Depth, meters	Temperature, °C.	Salinity, ‰	Depth, meters	Temperature, °C.	Salinity, ‰	σ_t
0	1.89	32.97	0	1.89	32.97	26.37
25	0.90	32.97	25	0.90	32.97	26.43
50	−0.77	33.15	50	−0.77	33.15	26.66
74	−0.66	33.40	75	−0.65	33.39	26.86
99	−0.26	33.51	100	−0.25	33.50	26.93
148	0.23	33.66	150	0.25	33.50	26.93
197	0.92	33.85	200	0.95	33.86	27.15
296	2.29	34.31	300	2.35	34.31	27.41
400	3.12	34.68	400	3.10	34.67	27.64
598	3.59	34.80	(600)	3.60	34.80	27.69

Station 7100; 1 June; 44°07′ N., 48°55′ W.; depth 192 m ; dynamic height 971.108.

Observed values			Scaled values			
Depth, meters	Temperature, °C.	Salinity, ‰	Depth, meters	Temperature, °C.	Salinity, ‰	σ_t
0	1.15	32.98	0	1.15	32.98	26.44
24	0.49	33.04	25	0.45	33.05	26.54
49	−0.84	33.22	50	−0.85	33.22	26.72
73	−0.86	33.32	75	−0.85	33.32	26.80
97	−0.76	33.35	100	−0.75	33.34	26.82
146	−0.68	33.39	(150)	−0.65	33.38	26.85

Station 7101; 1 June; 44°10′ N., 49°11′ W.; depth 89 m.; dynamic height 971.120.

Observed values			Scaled values			
Depth, meters	Temperature, °C.	Salinity, ‰	Depth, meters	Temperature, °C.	Salinity, ‰	σ_t
0	1.52	33.03	0	1.52	33.03	26.45
25	0.59	33.03	25	0.59	33.03	26.51
49	−0.09	33.12	50	−0.10	33.12	26.61
74	−0.44	33.22	75	−0.45	33.22	26.71

Station 7102; 1 June; 44°11.5′ N., 49°21′ W.; depth 48 m.; dynamic height 971.114.

Observed values			Scaled values			
Depth, meters	Temperature, °C.	Salinity, ‰	Depth, meters	Temperature, °C.	Salinity, ‰	σ_t
0	2.78	33.16	0	2.78	33.16	26.46
26	1.24	33.185	25	1.35	33.18	26.59
42	0.79	33.22	50	0.60	33.24	26.68

Station 7103; 1 June; 44°58′ N., 49°24′ W.; depth 71 m.; dynamic height 971.124.

Observed values			Scaled values			
Depth, meters	Temperature, °C.	Salinity, ‰	Depth, meters	Temperature, °C.	Salinity, ‰	σ_t
0	1.37	32.90	0	1.37	32.90	26.34
26	0.49	32.915	25	9.50	32.90	26.40
52	−1.01	33.15	50	−0.95	33.12	26.65

TABLE OF OCEANOGRAPHIC DATA—Continued

STATIONS OCCUPIED IN 1959—Continued

Station 7104; 1 June; 44°57′ N., 49°14′ W.; depth 119 m.; dynamic height 971.132.

Observed values			Scaled values			
Depth, meters	Temperature, °C.	Salinity, ‰	Depth, meters	Temperature, °C.	Salinity, ‰	σ_t
0	1.48	32.89	0	1.48	32.89	26.34
25	1.00	32.90	25	1.00	32.90	26.37
51	−0.32	33.02	50	−0.25	33.01	26.54
76	−0.82	33.05	75	−0.80	33.05	26.58

Station 7105; 2 June; 44°52.5′ N., 48°58′ W.; depth 694 m.; dynamic height 971.088.

Observed values			Scaled values			
Depth, meters	Temperature, °C.	Salinity, ‰	Depth, meters	Temperature, °C.	Salinity, ‰	σ_t
0	1.24	32.92	0	1.24	32.92	26.38
25	0.74	32.94	25	0.74	32.94	26.43
50	1.04	33.12	50	−1.04	33.12	26.64
76	−1.07	33.28	75	−1.05	33.27	26.77
101	−0.85	33.35	100	−0.85	33.33	26.81
151	−0.44	33.50	150	−0.45	33.49	26.93
202	0.17	33.66	200	−0.20	33.65	27.05
303	2.27	34.40	300	2.20	34.38	27.48
388	2.81	34.60	400	2.85	34.60	27.60
579	3.33	34.75	(600)	3.35	34.75	27.67

Station 7106; 2 June; 44°51′ N., 48°47′ W.; depth 2,012 m.; dynamic height 970.981.

Observed values			Scaled values			
Depth, meters	Temperature, °C.	Salinity, ‰	Depth, meters	Temperature, °C.	Salinity, ‰	σ_t
0	2.00	33.10	0	2.00	33.10	26.46
24	1.49	33.22	25	1.45	33.22	26.61
48	0.31	33.39	50	0.35	33.41	26.83
72	0.71	33.73	75	0.80	33.75	27.07
97	1.86	33.97	100	1.90	33.98	27.18
146	1.93	34.22	150	2.00	34.23	27.37
194	2.49	34.43	200	2.60	34.45	27.50
291	3.93	34.74	300	3.90	34.73	27.60
400	3.50	34.76	400	3.50	34.75	27.66
595	3.75	34.83	600	3.75	34.82	27.69
788	3.69	34.88	800	3.70	34.88	27.74
984	3.62	34.895	1,000	3.60	34.89	27.76
1,472	3.45	34.90				

Station 7107; 2 June; 44°50.5′ N., 48°31′ W.; depth 2,431 m.; dynamic height 970.951.

Observed values			Scaled values			
Depth, meters	Temperature, °C.	Salinity, ‰	Depth, meters	Temperature, °C.	Salinity, ‰	σ_t
0	2.97	33.38	0	2.97	33.38	26.61
25	2.76	33.40	25	2.76	33.40	26.64
50	3.68	34.05	50	3.68	34.05	27.07
76	1.98	34.06	75	2.00	34.05	27.23
101	1.82	34.15	100	1.80	34.14	27.32
151	2.10	34.32	150	2.10	34.30	27.42
202	2.98	34.52	200	2.95	34.50	27.51
303	3.88	34.77	300	3.85	34.76	27.64
402	4.01	34.85	400	4.00	34.84	27.68
599	3.82	34.88	600	3.85	34.88	27.72
794	3.81	34.905	800	3.80	34.90	27.75
992	3.56	34.895	1,000	3.55	34.89	27.76
1,489	3.41	34.895				

Station 7108; 2 June; 44°45.5′ N., 45°57′ W.; depth 3,109 m.; dynamic height 970.957.

Observed values			Scaled values			
Depth, meters	Temperature, °C.	Salinity, ‰	Depth, meters	Temperature, °C.	Salinity, ‰	σ_t
0	1.37	33.14	0	1.37	33.14	26.55
25	0.74	33.30	25	0.74	33.30	26.70
50	0.35	33.58	50	0.35	33.58	26.96
75	1.71	33.96	75	1.71	33.96	27.18
99	3.64	34.32	100	3.70	34.33	27.30
149	5.46	34.73	150	5.45	34.73	27.42
199	5.37	34.84	200	5.30	34.84	27.53
298	3.82	34.78	300	3.80	34.77	27.65
375	4.23	34.87	400	4.25	34.87	27.68
559	4.12	34.89	600	4.05	34.89	27.71
739	3.84	34.89	800	3.80	34.89	27.74
935	3.76	34.905	1,000	3.75	34.90	27.75
1,444	2.97	34.90				

Station 7109; 2 June; 44°42′ N., 47°11′ W.; depth 3,749 m.; dynamic height 971.030.

Observed values			Scaled values			
Depth, meters	Temperature, °C.	Salinity, ‰	Depth, meters	Temperature, °C.	Salinity, ‰	σ_t
0	8.72	34.19	0	8.72	34.19	26.54
25	9.39	34.59	25	9.39	34.59	26.75
50	9.38	34.80	50	9.38	34.80	26.91
75	9.53	34.92	75	9.53	34.92	26.99
99	10.16	35.11	100	10.15	35.10	27.02
149	8.99	35.07	150	8.95	35.06	27.20
199	7.48	34.94	200	7.45	34.94	27.32
298	5.38	34.80	300	5.40	34.80	27.49
368	5.57	34.94	400	5.30	34.93	27.60
552	4.27	34.895	600	4.20	34.89	27.70
737	3.98	34.895	800	3.90	34.90	27.74
926	3.71	34.91	1,000	3.65	34.91	27.77
1,405	3.44	34.89				

Station 7110; 2 June; 44°33′ N., 46°37′ W.; depth 3,832 m.; dynamic height 971.031.

Observed values			Scaled values			
Depth, meters	Temperature, °C.	Salinity, ‰	Depth, meters	Temperature, °C.	Salinity, ‰	σ_t
0	8.02	33.83	0	8.02	33.83	26.36
25	5.74	33.79	25	5.75	33.79	26.65
52	6.11	34.12	50	6.10	34.11	26.86
77	4.52	34.09	75	4.74	34.09	27.00
104	4.16	34.18	100	4.20	34.15	27.11
154	5.83	34.58	150	5.75	34.55	27.25
206	5.26	34.60	200	5.30	34.60	27.34
310	5.03	34.78	300	5.05	34.76	27.50
411	5.37	34.98	400	5.40	34.96	27.62
617	4.38	34.93	600	4.45	34.93	27.70
823	4.34	34.97	800	4.40	34.96	27.73
1,030	3.70	34.87	1,000	3.75	34.88	27.73
1,552	3.47	34.90				

Station 7111; 2 June; 44°26′ N., 45°54′ W.; depth 3,834 m.; dynamic height 971.139.

Observed values			Scaled values			
Depth, meters	Temperature, °C.	Salinity, ‰	Depth, meters	Temperature, °C.	Salinity, ‰	σ_t
0	10.99	34.36	0	10.99	34.36	26.29
25	10.63	34.36	25	10.55	34.36	26.38
47	10.19	34.70	50	10.30	34.73	26.70
70	12.82	35.43	75	12.85	35.45	26.79
94	12.87	35.51	100	12.70	35.46	26.83
141	11.06	35.19	150	10.75	35.17	26.98
187	9.77	35.12	200	9.55	35.09	27.11
281	8.22	34.99	300	7.65	34.93	27.29
337	6.50	34.85	400	5.95	34.89	27.49
503	5.33	34.95	600	4.90	34.93	27.65
669	4.59	34.92	800	4.05	34.90	27.72
844	3.95	34.90	1,000	3.70	34.89	27.75
1,294	3.51	34.87				

TABLE OF OCEANOGRAPHIC DATA—Continued
STATIONS OCCUPIED IN 1959—Continued

Station 7112; 3 June; 44°19′ N.; 45°18′ W.; depth 4,481 m.; dynamic height 971.043.

Observed values			Scaled values			
Depth, meters	Temperature, °C.	Salinity, ‰	Depth, meters	Temperature, °C.	Salinity, ‰	σ_t
0	7.45	33.76	0	7.45	33.76	26.40
24	7.53	33.96	25	7.55	33.97	26.55
48	9.46	34.55	50	9.65	34.60	26.72
73	12.01	35.52	75	12.05	35.53	27.01
97	12.15	35.61	100	12.15	35.61	27.05
145	10.99	35.42	150	10.80	35.35	27.10
193	7.36	34.86	200	7.00	34.84	27.31
290	4.91	34.73	300	4.95	34.74	27.49
400	5.20	34.94	400	5.20	34.93	27.61
596	4.56	34.96	600	4.55	34.96	27.72
789	4.38	34.97	800	4.35	34.97	27.75
984	3.97	34.945	1,000	3.95	34.94	27.76
1,463	3.57	34.92				

Station 7113; 3 June; 44°50′ N., 45°15′ W.; depth 4,024 m.; dynamic height 970.996.

Observed values			Scaled values			
Depth, meters	Temperature, °C.	Salinity, ‰	Depth, meters	Temperature, °C.	Salinity, ‰	σ_t
0	8.74	33.96	0	8.74	33.96	26.37
25	8.34	33.92	25	8.34	33.92	26.40
49	5.32	34.04	50	5.25	34.04	26.90
74	4.54	34.14	75	4.55	34.13	27.05
98	4.81	34.36	100	4.80	34.37	27.22
147	4.80	34.50	150	4.75	34.50	27.33
196	4.10	34.52	200	4.10	34.52	27.42
294	4.78	34.81	300	4.85	34.82	27.57
400	5.00	34.97	400	5.00	34.96	27.67
598	4.34	34.95	600	4.35	34.93	27.71
794	4.22	34.97	800	4.20	34.96	27.76
996	3.98	34.95	1,000	4.00	34.94	27.76
1,498	3.52	34.92				

Station 7114; 3 June; 45°18′ N., 45°17′ W.; depth 4,024 m.; dynamic height 971.004.

Observed values			Scaled values			
Depth, meters	Temperature, °C.	Salinity, ‰	Depth, meters	Temperature, °C.	Salinity, ‰	σ_t
0	8.44	33.99	0	8.44	33.99	26.43
25	8.34	33.98	25	8.34	33.98	26.45
51	6.60	34.10	50	6.65	34.09	26.77
76	4.99	34.26	75	5.00	34.25	27.10
102	5.94	34.53	100	5.90	34.51	27.20
152	5.44	34.60	150	5.45	34.59	27.31
204	5.01	34.645	200	5.00	34.64	27.41
306	4.36	34.75	300	4.40	34.73	27.54
410	4.46	34.88	400	4.50	34.87	27.65
610	4.05	34.89	600	4.10	34.88	27.70
806	3.89	34.92	800	3.90	34.91	27.75
1,007	3.90	34.945	1,000	3.90	34.94	27.77
1,505	3.53	34.92				

Station 7115; 3 June; 45°18.5′ N.; 45°56′ W.; depth 3,475 m.; dynamic height 970.967.

Observed values			Scaled values			
Depth, meters	Temperature, °C.	Salinity, ‰	Depth, meters	Temperature, °C.	Salinity, ‰	σ_t
0	5.92	33.52	0	5.92	33.52	26.41
25	3.37	33.53	25	3.37	33.53	26.70
50	3.96	34.10	50	3.96	34.10	27.10
75	1.94	33.99	75	1.94	33.99	27.18
101	4.44	34.41	100	4.40	34.41	27.30
151	6.20	34.80	150	6.15	34.80	27.40
202	5.03	34.74	200	5.05	34.74	27.48
303	5.52	34.97	300	5.50	34.96	27.60
406	4.56	34.90	400	4.65	34.90	27.66
605	3.88	34.88	600	3.90	34.88	27.72
80[illegible]	3.69	34.88	800	3.70	34.88	27.74
1,002	3.83	34.94	1,000	3.85	34.94	27.77
1,502	3.49	34.92				

Station 7116; 3 June; 45°20′ N., 46°43′ W.; depth 3,164 m.; dynamic height 970.970.

Observed values			Scaled values			
Depth, meters	Temperature, °C.	Salinity, ‰	Depth, meters	Temperature, °C.	Salinity, ‰	σ_t
0	7.52	33.82	0	7.52	33.82	26.43
25	6.14	33.86	25	6.14	33.86	26.66
50	4.96	33.96	50	4.96	33.96	26.88
74	4.46	34.21	75	4.45	34.20	27.12
99	4.36	34.37	100	4.35	34.37	27.27
149	4.17	34.52	150	4.15	34.52	27.41
198	4.58	34.67	200	4.60	34.68	27.48
297	5.03	34.92	300	5.05	34.92	27.63
400	4.79	34.95	400	4.80	34.94	27.67
596	4.04	34.905	600	4.05	34.90	27.72
789	3.95	34.93	800	3.95	34.92	27.75
987	3.61	34.885	1,000	3.60	34.88	27.75
1,483	3.43	34.92				

Station 7117; 3 June; 45°20.5′ N., 47°21′ W.; depth 2,743 m.; dynamic height 970.967.

Observed values			Scaled values			
Depth, meters	Temperature, °C.	Salinity, ‰	Depth, meters	Temperature, °C.	Salinity, ‰	σ_t
0	5.83	33.64	0	5.83	33.64	26.51
25	5.45	33.79	25	5.45	33.79	26.68
50	3.33	33.86	50	3.33	33.86	26.96
76	3.17	34.40	75	3.15	34.30	27.33
101	3.45	34.32	100	3.45	34.39	27.37
151	4.33	34.57	150	4.35	34.57	27.43
201	4.39	34.71	200	4.40	34.70	27.52
302	4.36	34.82	300	4.35	34.82	27.63
393	3.66	34.75	400	3.70	34.75	27.64
586	3.88	34.85	600	3.90	34.84	27.69
777	3.72	34.85	800	3.70	34.84	27.71
969	3.69	34.91	1,000	3.65	34.90	27.76
1,448	3.42	34.89				

Station 7118; 3 June; 45°31.5′ N., 47°46′ W.; depth 1,554 m.; dynamic height 970.920.

Observed values			Scaled values			
Depth, meters	Temperature, °C.	Salinity, ‰	Depth, meters	Temperature, °C.	Salinity, ‰	σ_t
0	4.18	33.44	0	4.18	33.44	26.55
25	4.44	33.70	25	4.44	33.70	26.73
50	3.02	34.14	50	3.02	34.14	27.22
75	3.58	34.46	75	3.58	34.46	27.42
100	4.05	34.59	100	4.05	34.59	27.47
150	4.83	34.79	150	4.83	34.79	27.54
201	4.32	34.78	200	4.35	34.77	27.59
301	3.43	34.74	300	3.45	34.74	27.65
391	3.22	34.76	400	3.25	34.76	27.69
590	3.84	34.88	600	3.85	34.88	27.72
789	3.65	34.89	800	3.65	34.89	27.75
992	3.50	34.89	1,000	3.50	34.88	27.76
1,510	3.43	34.90				

Station 7119; 4 June; 45°40′ N., 48°04′ W.; depth 677 m.; dynamic height 970.997.

Observed values			Scaled values			
Depth, meters	Temperature, °C.	Salinity, ‰	Depth, meters	Temperature, °C.	Salinity, ‰	σ_t
0	2.20	33.23	0	2.20	33.23	26.55
25	1.80	33.24	25	1.80	33.24	26.59
50	0.06	33.42	50	0.06	33.42	26.85
75	0.13	33.69	75	0.13	33.69	27.06
100	0.87	33.89	100	0.87	33.89	27.10
150	1.77	34.15	150	1.77	34.14	27.32
199	1.98	34.30	200	2.00	34.30	27.43
299	2.58	34.50	300	2.60	34.50	27.54
386	2.83	34.61	400	2.90	34.61	27.61
592	3.45	34.80	(600)	3.30	34.79	27.71

TABLE OF OCEANOGRAPHIC DATA—Continued
STATIONS OCCUPIED IN 1959—Continued

Station 7120; 4 June; 45°48′ N., 48°14′ W.; depth 162 m.; dynamic height 971.120.

Observed values			Scaled values			
Depth, meters	Temperature, °C.	Salinity, ‰	Depth, meters	Temperature, °C.	Salinity, ‰	σ_t
0	1.38	32.88	0	1.38	32.88	26.34
25	1.34	32.88	25	1.34	32.88	26.34
50	0.18	32.91	50	0.18	32.91	26.43
75	−1.31	33.10	75	−1.31	33.10	26.64
100	−1.41	33.15	100	−1.41	33.15	26.68
150	−0.77	33.41	150	−0.77	33.40	26.87

Station 7121; 4 June; 45°52′ N., 48°19′ W.; depth 114 m.; dynamic height 971.119.

Observed values			Scaled values			
Depth, meters	Temperature, °C.	Salinity, ‰	Depth, meters	Temperature, °C.	Salinity, ‰	σ_t
0	1.85	32.86	0	1.85	32.86	26.28
25	0.64	32.84	25	0.64	32.84	26.35
50	−0.93	32.92	50	−0.93	32.92	26.49
75	−1.53	33.08	75	−1.53	33.08	26.62
100	−1.42	33.17	100	−1.42	33.17	26.70

Station 7122; 4 June; 46°03′ N., 48°32′ W.; depth 91 m.; dynamic height 971.114.

Observed values			Scaled values			
Depth, meters	Temperature, °C.	Salinity, ‰	Depth, meters	Temperature, °C.	Salinity, ‰	σ_t
0	1.63	32.95	0	1.63	32.95	26.37
26	1.53	32.95	25	1.55	32.95	26.38
54	−0.22	33.04	50	0.05	33.02	26.53
80	−0.97	33.19	75	−0.90	33.15	26.68

Station 7123; 4 June; 46°11′ N., 48°44′ W.; depth 77 m.; dynamic height 971.112.

Observed values			Scaled values			
Depth, meters	Temperature, °C.	Salinity, ‰	Depth, meters	Temperature, °C.	Salinity, ‰	σ_t
0	1.61	33.04	0	1.61	33.04	26.45
26	1.58	33.02	25	1.60	33.02	26.44
53	0.46	33.08	50	0.65	33.06	26.53
74	−0.70	33.25	(75)	−0.75	33.25	26.74

Station 7124; 4 June; 46°17′ N., 48°58′ W.; depth 64 m.; dynamic height 971.109.

Observed values			Scaled values			
Depth, meters	Temperature, °C.	Salinity, ‰	Depth, meters	Temperature, °C.	Salinity, ‰	σ_t
0	1.63	33.07	0	1.63	33.07	26.47
27	1.59	33.08	25	1.60	33.08	26.49
55	0.43	33.14	50	0.70	33.13	26.58

Station 7125; 4 June; 48°15.5′ N., 48°33′ W.; depth 89 m.; dynamic height 971.115.

Observed values			Scaled values			
Depth, meters	Temperature, °C.	Salinity, ‰	Depth, meters	Temperature, °C.	Salinity, ‰	σ_t
0	1.55	32.94	0	1.55	32.94	26.38
26	1.47	32.98	25	1.45	32.97	26.41
53	0.60	33.00	50	0.75	32.99	26.47
79	−0.90	33.19	75	−0.70	33.16	26.67

Station 7126; 4 June; 46°12.5′ N., 48°01′ W.; depth 118 m.; dynamic height 971.110.

Observed values			Scaled values			
Depth, meters	Temperature, °C.	Salinity, ‰	Depth, meters	Temperature, °C.	Salinity, ‰	σ_t
0	1.63	32.90	0	1.63	32.91	26.33
25	0.89	32.90	25	0.89	32.90	26.38
50	0.34	33.10	50	0.34	33.10	26.57
76	−0.69	33.27	75	−0.65	33.26	26.75
101	−1.16	33.28	100	−1.15	33.27	26.78

Station 7127; 4 June; 46°11′ N; 47°47′ W.; depth 169 m.; dynamic height 971.112.

Observed values			Scaled values			
Depth, meters	Temperature, °C.	Salinity, ‰	Depth, meters	Temperature, °C.	Salinity, ‰	σ_t
0	1.26	32.84	0	1.26	32.84	26.32
25	0.73	32.88	25	0.73	32.87	26.37
50	−1.41	33.06	50	−1.41	33.06	26.61
74	−1.49	33.12	75	−1.50	33.12	26.66
99	−1.25	33.24	100	−1.25	33.25	26.76
149	−0.57	33.44	150	−0.55	33.44	26.89

Station 7128; 4 June; 46°11.5′ N., 47°25′ W.; depth 672 m.; dynamic height 971.012.

Observed values			Scaled values			
Depth, meters	Temperature, °C.	Salinity, ‰	Depth, meters	Temperature, °C.	Salinity, ‰	σ_t
0	1.56	33.11	0	1.56	33.11	26.50
24	1.71	33.22	25	1.70	33.23	26.60
43	1.76	33.39	50	1.75	33.42	26.75
65	1.66	33.50	75	1.25	33.56	26.89
87	0.42	33.71	100	0.70	33.80	27.12
130	1.39	33.96	150	1.70	34.05	27.25
173	1.93	34.14	200	2.05	34.23	27.37
260	2.34	34.41	300	2.65	34.51	27.55
407	3.18	34.68	400	3.15	34.66	27.62
609	3.67	34.82	600	3.65	34.81	27.69

Station 7129; 4 June; 46°11′ N., 47°11′ W.; depth 1,317 m.; dynamic height 970.947.

Observed values			Scaled values			
Depth, meters	Temperature, °C.	Salinity, ‰	Depth, meters	Temperature, °C.	Salinity, ‰	σ_t
0	1.92	33.25	0	1.92	33.25	26.59
25	2.47	33.50	25	2.47	33.50	26.76
50	4.12	34.03	50	4.12	34.03	27.02
75	3.76	34.14	75	3.76	34.14	27.15
99	2.53	34.26	100	2.50	34.26	27.36
148	2.31	34.41	150	2.30	34.42	27.51
198	2.70	34.55	200	2.70	34.55	27.57
297	3.01	34.68	300	3.05	34.67	27.64
396	3.24	34.75	400	3.25	34.75	27.68
596	3.49	34.80	600	3.50	34.80	27.70
797	3.67	34.86	800	3.70	34.85	27.72
999	3.56	34.87	1,000	3.55	34.87	27.75
1,317	3.47	34.86				

Station 7130; 4 June; 46°09′ N., 46°39′ W.; depth 969 m.; dynamic height 970.909.

Observed values			Scaled values			
Depth, meters	Temperature, °C.	Salinity, ‰	Depth, meters	Temperature, °C.	Salinity, ‰	σ_t
0	4.43	33.58	0	4.43	33.58	26.64
25	4.04	34.00	25	4.04	34.00	27.01
50	2.93	34.28	50	2.93	34.28	27.33
75	3.62	34.53	75	3.62	34.53	27.46
100	3.94	34.60	100	3.94	34.60	27.49
150	3.46	34.63	150	3.46	34.63	27.57
201	3.39	34.68	200	3.40	34.68	27.61
301	4.09	34.83	300	4.10	34.82	27.66
395	4.06	34.87	400	4.05	34.87	27.70
594	3.88	34.90	600	3.85	34.89	27.73
793	3.75	34.90	800	3.75	34.88	27.73
901	3.76	34.89				

TABLE OF OCEANOGRAPHIC DATA—Continued

STATIONS OCCUPIED IN 1959—Continued

Station 7131; 5 June; 46°05′ N., 45°15′ W.; depth 1,328 m.; dynamic height 971.010.

Observed values			Scaled values			
Depth, meters	Temperature, °C.	Salinity, ‰	Depth, meters	Temperature, °C.	Salinity, ‰	σ_t
0	9.09	34.27	0	9.09	34.27	26.54
25	9.07	34.27	25	9.07	34.27	26.55
50	8.14	34.47	50	8.14	34.47	26.85
75	7.38	34.66	75	7.38	34.66	27.11
100	8.50	34.91	100	8.50	34.91	27.15
149	6.96	34.75	150	6.95	34.75	27.25
199	6.66	34.85	200	6.65	34.84	27.36
299	4.90	34.77	300	4.90	34.76	27.52
397	4.26	34.81	400	4.30	34.81	27.63
600	4.41	34.94	600	4.40	34.94	27.71
807	3.57	34.88	800	3.60	34.87	27.75
1,011	3.62	34.90	1,000	3.60	34.89	27.76
1,217	3.52	34.89				

Station 7132; 5 June; 46°05′ N., 45°15′ W.; depth 2,347 m.; dynamic height 971.083.

Observed values			Scaled values			
Depth, meters	Temperature, °C.	Salinity, ‰	Depth, meters	Temperature, °C.	Salinity, ‰	σ_t
0	9.35	34.29	0	9.35	34.29	26.52
25	10.75	34.74	25	10.75	34.74	26.64
51	10.60	34.89	50	10.60	34.88	26.77
76	10.97	35.04	75	10.95	35.04	26.83
102	10.30	34.99	100	10.35	34.99	26.90
152	9.74	35.12	150	9.75	35.11	27.10
203	7.59	34.80	200	7.75	34.80	27.17
305	6.83	34.94	300	6.90	34.94	27.40
402	4.85	34.82	400	4.90	34.81	27.56
605	4.95	35.00	600	4.95	35.00	27.70
806	4.48	34.99	800	4.50	34.98	27.73
1,003	4.03	34.94	1,000	4.05	34.95	27.76
1,484	3.93	34.92				

Station 7133; 5 June; 46°02′ N.; 44°40′ W.; depth 3,749 m.; dynamic height 971.094.

Observed values			Scaled values			
Depth, meters	Temperature, °C.	Salinity, ‰	Depth, meters	Temperature, °C.	Salinity, ‰	σ_t
0	9.87	34.34	0	9.87	34.34	26.47
25	9.99	34.43	25	9.99	34.43	26.52
49	10.62	34.84	50	10.65	34.85	26.74
74	11.42	35.17	75	11.45	35.17	26.85
98	11.58	35.29	100	11.55	35.28	26.91
147	8.71	34.87	150	8.45	34.84	27.10
197	5.66	34.41	200	5.65	34.41	27.15
295	5.50	34.67	300	5.55	34.68	27.37
405	6.04	34.98	400	6.05	34.96	27.54
608	4.95	35.00	600	5.00	35.00	27.70
810	4.33	34.97	800	4.35	34.96	27.74
1,000	4.00	34.95	1,000	4.00	34.94	27.76
	3.53	34.92				

Station 7134; 5 June; 46°23′ N.; 44°48′ W.; depth 2,433 m.; dynamic height 970.940.

Observed values			Scaled values			
Depth, meters	Temperature, °C.	Salinity, ‰	Depth, meters	Temperature, °C.	Salinity, ‰	σ_t
0	6.39	33.88	0	6.39	33.88	26.63
25	5.19	33.96	25	5.19	33.96	26.85
50	4.65	34.17	50	4.65	34.17	27.08
75	4.14	34.26	75	4.14	34.26	27.20
100	3.21	34.27	100	3.21	34.27	27.31
150	3.00	34.42	150	3.00	34.42	27.45
200	3.18	34.60	200	3.18	34.60	27.57
300	4.66	34.91	300	4.66	34.91	27.65
398	3.47	34.79	400	3.50	34.78	27.68
596	3.65	34.84	600	3.65	34.83	27.70
795	3.69	34.86	800	3.70	34.85	27.72
997	3.61	34.86	1,000	3.60	34.85	27.73
1,506	3.50	34.89				

Station 7135; 5 June; 46°29′ N.; 44°48′ W.; depth 690 m.; dynamic height 970.908.

Observed values			Scaled values			
Depth, meters	Temperature, °C.	Salinity, ‰	Depth, meters	Temperature, °C.	Salinity, ‰	σ_t
0	5.94	34.28	0	5.94	34.28	27.01
25	5.43	34.28	25	5.43	34.28	27.07
50	5.03	34.34	50	5.03	34.34	27.16
75	4.14	34.44	75	4.14	34.44	27.34
100	3.40	34.48	100	3.40	34.48	27.45
150	3.41	34.62	150	3.41	34.62	27.57
199	3.29	34.71	200	3.35	34.70	27.63
299	3.53	34.80	300	3.55	34.79	27.68
403	3.58	34.82	400	3.60	34.81	27.70
607	3.68	34.85	600	3.70	34.84	27.71

Station 7136; 5 June; 46°35′ N., 44°48′ W.; depth 227 m.; dynamic height 970.884.

Observed values			Scaled values			
Depth, meters	Temperature, °C.	Salinity, ‰	Depth, meters	Temperature, °C.	Salinity, ‰	σ_t
0	5.77	34.21	0	5.77	34.21	26.97
24	4.84	34.30	25	4.80	34.30	27.16
48	3.25	34.42	50	3.20	34.43	27.43
72	2.86	34.50	75	2.85	34.50	27.52
96	2.69	34.53	100	2.65	34.52	27.56
144	2.54	34.58	150	2.55	34.59	27.62
191	3.50	34.75	(200)	3.70	34.78	27.66

Station 7137; 5 June; 46°40′ N., 44°49′ W.; depth 172 m.; dynamic height 970.905.

Observed values			Scaled values			
Depth, meters	Temperature, °C.	Salinity, ‰	Depth, meters	Temperature, °C.	Salinity, ‰	σ_t
0	5.92	34.19	0	5.92	34.19	26.94
25	5.17	34.22	25	5.17	34.22	27.06
50	4.62	34.26	50	4.62	34.26	27.16
75	2.89	34.38	75	2.89	34.38	27.42
99	2.92	34.49	100	2.95	34.48	27.49
149	3.12	34.60	150	3.15	34.60	27.57

Station 7138; 5 June; 46°50′ N., 44°54′ W.; depth 144 m.; dynamic height 970.904.

Observed values			Scaled values			
Depth, meters	Temperature, °C.	Salinity, ‰	Depth, meters	Temperature, °C.	Salinity, ‰	σ_t
0	5.74	34.23	0	5.74	34.23	26.99
25	5.24	34.22	25	5.24	34.22	27.05
49	3.53	34.31	50	3.50	34.30	27.30
74	2.98	34.34	75	2.95	34.34	27.38
98	2.79	34.42	100	2.80	34.42	27.46
128	2.81	34.43				

Station 7139; 5 June; 46°50′ N., 45°04′ W.; depth 183 m.; dynamic height 970.905.

Observed values			Scaled values			
Depth, meters	Temperature, °C.	Salinity, ‰	Depth, meters	Temperature, °C.	Salinity, ‰	σ_t
0	5.83	34.21	0	5.83	34.21	26.89
25	5.18	34.23	25	5.18	34.23	27.06
50	3.22	34.30	50	3.22	34.30	27.33
75	2.79	34.36	75	2.79	34.36	27.41
99	2.79	34.42	100	2.80	34.42	27.46
149	2.93	34.54	(150)	2.95	34.54	27.54

Station 7140; 5 June; 46°50′ N., 45°19′ W.; depth 222 m.; dynamic height 970.912.

Observed values			Scaled values			
Depth, meters	Temperature, °C.	Salinity, ‰	Depth, meters	Temperature, °C.	Salinity, ‰	σ_t
0	5.54	34.13	0	5.54	34.13	26.94
25	4.93	34.15	25	4.93	34.15	27.02
49	3.44	34.25	50	3.45	34.24	27.25
74	2.85	34.26	75	2.85	34.26	27.33
98	2.70	34.35	100	2.70	34.35	27.41
148	3.03	34.53	150	3.10	34.53	27.52
197	3.60	34.695	(200)	3.65	34.70	27.60

TABLE OF OCEANOGRAPHIC DATA—Continued
STATIONS OCCUPIED IN 1959—Continued

Station 7141; 5 June; 46°49.5′ N., 45°48′ W.; depth 295 m.; dynamic height 970.916.

Observed values			Scaled values			
Depth, meters	Temperature, °C.	Salinity, ‰	Depth, meters	Temperature, °C.	Salinity, ‰	σ_t
0	5.54	34.19	0	5.54	34.19	26.99
25	5.14	34.18	25	5.14	34.18	27.02
50	4.96	34.20	50	4.96	34.20	27.07
75	3.78	34.38	75	3.78	34.38	27.33
100	3.52	34.50	100	3.52	34.80	27.45
149	3.76	34.64	150	3.75	34.63	27.53
199	3.62	34.68	200	3.60	34.68	27.59
249	3.93	34.75				

Station 7142; 6 June; 46°49.5′N., 46°06′ W.; depth 324 m.; dynamic height 970.923.

Observed values			Scaled values			
Depth, meters	Temperature, °C.	Salinity, ‰	Depth, meters	Temperature, °C.	Salinity, ‰	σ_t
0	4.48	34.00	0	5.48	34.00	26.84
24	4.97	34.14	25	4.95	34.14	27.02
48	4.76	34.17	50	4.75	34.16	27.06
73	3.71	34.245	75	3.65	34.25	27.25
97	3.11	34.365	100	3.10	34.37	27.40
145	3.28	34.53	150	3.30	34.54	27.51
193	3.34	34.64	200	3.35	34.64	27.58
290	3.80	34.82	(300)	3.85	34.84	27.69

Station 7143; 6 June; 46°49.5′ N.; 46°31′ W.; depth 667 m. dynamic height 970.912.

Observed values			Scaled values			
Depth, meters	Temperature, °C.	Salinity, ‰	Depth, meters	Temperature, °C.	Salinity, ‰	σ_t
0	4.74	33.89	0	4.74	33.89	26.83
25	4.27	33.94	25	4.27	33.94	26.97
50	2.28	34.12	50	2.28	34.12	27.27
75	2.25	34.31	75	2.25	34.31	27.42
100	3.44	34.56	100	3.44	34.56	27.51
150	4.79	34.82	150	4.79	34.82	27.58
200	3.68	34.70	200	3.68	34.70	27.60
300	3.56	34.76	300	3.56	34.76	27.65
379	3.79	34.82	400	3.80	34.82	27.69
576	3.85	34.88	(600)	3.85	34.87	27.72

Station 7144; 6 June; 46°48′ N., 46°52′ W.; depth 1,262 m.; dynamic height 970.931.

Observed values			Scaled values			
Depth, meters	Temperature, °C.	Salinity, ‰	Depth, meters	Temperature, °C.	Salinity, ‰	σ_t
0	3.05	33.48	0	3.05	33.48	26.69
25	2.19	33.50	25	2.19	33.50	26.78
50	3.94	34.09	50	3.94	34.09	27.09
75	3.06	34.21	75	3.06	34.21	27.26
100	2.81	34.31	100	2.81	34.31	27.37
150	2.52	34.45	150	2.52	34.45	27.50
201	3.08	34.58	200	3.10	34.57	27.56
301	3.13	34.73	300	3.15	34.72	27.67
404	3.23	34.75	400	3.25	34.75	27.68
607	3.65	34.86	600	3.70	34.85	27.72
809	3.59	34.87	800	3.65	34.87	27.74
1,015	3.50	34.885	1,000	3.50	34.88	27.76
1,129	3.43	34.88				

Station 7145; 6 June; 46°48′ N., 47°07′ W.; depth 682 m.; dynamic height 971.005.

Observed values			Scaled values			
Depth, meters	Temperature, °C.	Salinity, ‰	Depth, meters	Temperature, °C.	Salinity, ‰	σ_t
0	2.39	33.26	0	2.39	33.26	26.57
25	1.86	33.32	25	1.86	33.32	26.66
50	1.65	33.36	50	1.65	33.36	26.70
75	0.19	33.60	75	0.19	33.60	26.99
100	0.72	33.78	100	0.72	33.78	27.10
150	1.50	34.11	150	1.50	34.11	27.31
200	2.14	34.31	200	2.14	34.31	27.42
300	2.63	34.53	300	2.63	34.53	27.56
403	3.12	34.70	400	3.10	34.68	27.64
605	3.41	34.79	600	3.40	34.78	27.69

Station 7146; 6 June; 46°48 N., 47°19′ W.; depth 329 m.; dynamic height 971.049.

Observed values			Sclaed values			
Depth, meters	Temperature, °C.	Salinity, ‰	Depth, meters	Temperature, °C.	Salinity, ‰	σ_t
0	2.18	33.18	0	2.18	33.18	26.52
25	1.41	33.20	25	1.41	33.20	26.60
50	0.83	33.35	50	0.83	33.35	26.74
76	−0.48	33.44	75	−0.45	33.44	26.89
101	0.42	33.72	100	0.35	33.71	27.07
151	1.31	34.03	150	1.30	34.02	27.26
202	2.02	34.26	200	2.00	34.25	27.39
303	2.23	34.36	300	2.25	34.35	27.45

Station 7147; 6 June; 46°48.5′ N., 47°42′ W.; depth 172 m.; dynamic height 971.110.

Observed values			Sclaed values			
Depth, meters	Temperature, °C.	Salinity, ‰	Depth, meters	Temperature, °C.	Salinity, ‰	σ_t
0	1.89	32.83	0	1.89	32.83	26.26
25	1.01	32.87	25	1.01	32.87	26.35
50	−1.41	33.10	50	−1.41	33.10	26.63
75	−1.34	33.19	75	−1.34	33.19	26.71
99	−1.01	33.31	100	−1.00	33.31	26.80
149	0.74	33.82	(150)	0.80	33.82	27.13

Station 7148; 6 June; 46°49′ N., 48°12′ W.; depth 114 m.; dynamic height 971.116.

Observed values			Sclaed values			
Depth, meters	Temperature, °C.	Salinity, ‰	Depth, meters	Temperature, °C.	Salinity, ‰	σ_t
0	2.19	33.00	0	2.19	33.00	26.37
25	1.83	32.99	25	1.83	32.99	26.39
51	1.47	33.01	50	1.50	33.01	26.44
76	−0.52	33.10	75	−0.50	33.10	26.60
102	−0.81	33.24	100	−0.80	33.23	26.73

Station 7149; 6 June; 46°49.5′ N.; 48°42′ W.; depth 89 m ; dynamic height 971.116.

Observed values			Sclaed values			
Depth, meters	Temperature, °C.	Salinity, ‰	Depth, meters	Temperature, °C.	Salinity, ‰	σ_t
0	2.29	33.02	0	2.29	33.02	26.39
26	1.59	33.01	25	1.60	33.01	26.44
52	1.22	33.02	50	1.25	33.01	26.46
78	−0.49	33.14	75	−0.10	33.11	26.60

Station 7150; 15 June; 49°58′ N.,48°58′ W ; depth 1,847 m.; dynamic height 970.869.

Observed values			Sclaed values			
Depth, meters	Temperature, °C.	Salinity, ‰	Depth, meters	Temperature, °C.	Salinity, ‰	σ_t
0	4.55	33.86	0	4.55	33.86	26.84
25	3.57	34.08	25	3.57	34.08	27.12
50	3.73	34.30	50	3.73	34.30	27.28
75	3.54	34.44	75	3.54	34.44	27.40
100	2.37	34.48	100	2.34	34.48	27.54
150	3.05	34.68	150	3.05	34.68	27.64
199	3.11	34.74	200	3.10	34.74	27.69
299	3.27	34.80	300	3.25	34.80	27.72
394	3.25	34.81	400	3.25	34.81	27.73
590	3.37	34.85	600	3.40	34.85	27.75
787	3.47	34.86	800	3.45	34.86	27.75
987	3.38	34.87	1,000	3.40	34.87	27.77
1,488	3.41	34.90				
1,801	3.24	34.92				

TABLE OF OCEANOGRAPHIC DATA—Continued
STATIONS OCCUPIED IN 1959—Continued

Station 7151; 16 June; 49°49′ N., 49°32′ W.; depth 1,234 m.; dynamic height 970.923.

Observed values			Scaled values			
Depth, meters	Temperature, °C.	Salinity, ‰	Depth, meters	Temperature, °C.	Salinity, ‰	σ_t
0	4.32	33.48	0	4.32	33.48	26.57
24	2.86	33.57	25	2.80	33.57	26.79
48	1.62	33.66	50	1.50	33.66	26.96
72	0.95	34.03	75	1.00	34.04	27.29
96	1.43	34.14	100	1.50	34.16	27.36
144	2.03	34.40	150	2.10	34.42	27.52
193	2.50	34.54	200	2.55	34.57	27.61
289	3.11	34.72	300	3.15	34.73	27.67
390	3.29	34.79	400	3.35	34.79	27.70
585	3.23	34.81	600	3.25	34.81	27.73
780	3.45	34.85	800	3.45	34.85	27.74
984	3.49	34.87	1,000	3.50	34.87	27.76
1,190	3.41	34.90				

Station 7152; 16 June; 49°42′ N., 49°59′ W.; depth 635 m.; dynamic height 970.904.

Observed values			Scaled values			
Depth, meters	Temperature, °C.	Salinity, ‰	Depth, meters	Temperature, °C.	Salinity, ‰	σ_t
0	3.93	33.39	0	3.93	33.39	26.53
25	2.64	33.40	25	2.64	33.40	26.66
49	2.26	33.67	50	2.25	33.68	26.92
74	2.03	34.23	75	2.05	34.24	27.38
99	2.13	34.38	100	2.15	34.39	27.49
148	2.59	34.52	150	2.60	34.53	27.56
197	2.73	34.60	200	2.75	34.61	27.62
296	3.36	34.75	300	3.35	34.76	27.68
393	3.53	34.82	400	3.55	34.82	27.71
592	3.46	34.84	(600)	3.45	34.84	27.73

Station 7153; 16 June; 49°31′ N., 50°31′ W.; depth 336 m.; dynamic height 970.960.

Observed values			Scaled values			
Depth, meters	Temperature, °C.	Salinity, ‰	Depth, meters	Temperature, °C.	Salinity, ‰	σ_t
0	3.15	32.81	0	3.15	32.81	26.16
24	1.79	33.04	25	1.75	33.05	26.46
47	0.86	33.17	50	0.60	33.19	26.64
71	−1.05	33.34	75	−1.05	33.37	26.85
94	−0.84	33.55	100	−0.70	33.61	27.04
141	0.56	33.92	150	0.90	33.99	27.26
189	1.84	34.26	200	2.05	34.34	27.46
283	3.31	34.79	(300)	3.55	34.85	27.73

Station 7154; 16 June; 49°20′ N., 51°02′ W.; depth 334 m.; dynamic height 971.049.

Observed values			Scaled values			
Depth, meters	Temperature, °C.	Salinity, ‰	Depth, meters	Temperature, °C.	Salinity, ‰	σ_t
0	3.04	32.86	0	3.04	32.86	26.20
26	1.65	32.86	25	1.65	32.86	26.30
51	−0.40	33.00	50	−0.25	32.99	26.52
77	−1.41	33.11	75	−1.40	33.10	26.64
103	−1.33	33.18	100	−1.35	33.17	26.70
153	−1.03	33.38	150	−1.05	33.36	26.84
205	0.35	33.76	200	0.15	33.73	27.09
308	2.16	34.34	300	2.05	34.31	27.44

Station 7155; 16 June; 49°12′ N.; 51°33′ W.; depth 334 m.; dynamic height 971.015.

Observed values			Scaled values			
Depth, meters	Temperature, °C.	Salinity, ‰	Depth, meters	Temperature, °C.	Salinity, ‰	σ_t
0	3.34	32.87	0	3.34	32.87	26.18
25	2.04	32.87	25	2.04	32.87	26.29
51	0.58	33.06	50	0.65	33.06	26.53
76	0.03	33.18	75	0.05	33.17	26.65
102	−0.99	33.24	100	−0.95	33.23	26.74
151	0.05	33.67	150	0.00	33.66	27.05
202	1.40	34.00	200	1.35	33.99	27.23
304	2.93	34.64	300	2.90	34.62	27.62

Station 7156 16 June; 49°07′ N., 51°52′ W.; depth 295 m dynamic height 971.082.

Observed values			Scaled values			
Depth, meters	Temperature, °C.	Salinity, ‰	Depth, meters	Temperature, °C.	Salinity, ‰	σ_t
0	3.22	32.18	0	3.22	32.18	25.64
25	1.51	32.52	25	1.51	32.52	26.04
49	−1.49	32.97	50	−1.50	32.98	26.55
74	−1.68	33.07	75	−1.70	33.07	26.63
99	−1.71	33.10	100	−1.70	33.10	26.65
148	−1.57	33.17	150	−1.55	33.17	26.71
197	−0.98	33.45	200	−0.90	33.43	26.90
271	1.40	34.05	(300)	2.45	34.20	27.31

Station 7157; 16 June; 49°01.5′ N., 52°05′ W.; depth 295 m.; dynamic height 971.076.

Observed values			Scaled values			
Depth, meters	Temperature, °C.	Salinity, ‰	Depth, meters	Temperature, °C.	Salinity, ‰	σ_t
0	3.21	32.25	0	3.21	32.25	25.70
25	1.21	32.72	25	1.21	32.72	26.22
50	−1.39	32.97	50	−1.39	32.97	26.54
75	−1.67	33.06	75	−1.67	33.06	26.62
100	−1.69	33.11	100	−1.69	33.11	26.66
151	−1.61	33.15	150	−1.60	33.15	26.69
201	−0.92	33.47	200	−0.95	33.46	26.93
276	1.53	34.06				

Station 7158; 16 June; 48°55′ N., 52°20′ W.; depth 357 m. dynamic height 971.081.

Observed values			Scaled values			
Depth, meters	Temperature, °C.	Salinity, ‰	Depth, meters	Temperature, °C.	Salinity, ‰	σ_t
0	2.60	31.94	0	2.60	31.94	25.50
25	1.46	32.58	25	1.46	32.58	26.09
50	−0.82	32.86	50	−0.82	32.86	26.43
75	−1.49	33.04	75	−1.49	33.04	26.60
100	−1.60	33.10	100	−1.60	33.10	26.65
150	−1.59	33.16	150	−1.59	33.16	26.70
200	−1.21	33.40	200	−1.21	33.40	26.89
300	2.17	34.29	300	2.17	34.29	27.41

Station 7159; 16 June; 48°49.5′ N., 52°38′ W.; depth 224 m. dynamic height 971.104.

Observed values			Scaled values			
Depth, meters	Temperature, °C.	Salinity, ‰	Depth, meters	Temperature, °C.	Salinity, ‰	σ_t
0	3.47	31.28	0	3.47	31.28	24.90
25	0.04	32.71	25	0.04	32.71	26.28
50	−1.11	32.92	50	−1.11	32.92	26.49
76	−1.60	33.02	75	−1.60	33.02	26.59
101	−1.69	33.06	100	−1.70	33.06	26.62
152	−1.70	33.13	150	−1.70	33.13	26.68
202	−1.33	33.27	200	−1.35	33.26	26.77

Station 7160; 16 June; 48°45.5′ N., 52°47′ W.; depth 146 m dynamic height 971.112.

Observed values			Scaled values			
Depth, meters	Temperature, °C.	Salinity, ‰	Depth, meters	Temperature, °C.	Salinity, ‰	σ_t
0	3.68	31.59	0	3.68	31.59	25.13
25	1.87	32.51	25	1.87	32.51	26.01
50	−1.30	32.84	50	−1.30	32.84	26.43
75	−1.48	33.00	75	−1.48	33.00	26.57
99	−1.57	33.04	100	−1.60	33.05	26.61
124	−0.61	33.08				

Station 7161; 17 June; 48°44′ N., 52°57′ W.; depth 93 m. dynamic height 971.135.

Observed values			Scaled values			
Depth, meters	Temperature, °C.	Salinity, ‰	Depth, meters	Temperature, °C.	Salinity, ‰	σ_t
0	3.67	31.00	0	3.67	31.00	24.66
25	0.68	32.16	25	0.68	32.16	25.82
51	−0.53	32.54	50	−0.50	32.54	26.17
76	−1.17	32.82	75	−1.15	32.82	26.41

STATIONS OCCUPIED IN 1959—Continued

Observed values			Scaled values			
Depth, meters	Temperature, °C.	Salinity, ‰	Depth, meters	Temperature, °C.	Salinity, ‰	σ_t
Station 7162; 17 June; 48°37.5′ N., 52°47′ W.; depth 172 m.; dynamic height 971.123.						
0	3.82	31.14	0	3.82	31.14	24.76
25	1.26	32.42	25	1.26	32.42	25.98
49	−1.11	32.70	50	−1.10	32.71	26.32
74	−1.21	32.82	75	−1.20	32.82	26.42
99	−1.61	33.04	100	−1.60	33.04	26.60
148	−1.60	33.15	(150)	−1.60	33.16	26.70
Station 7163; 17 June; 48°33.5′ N., 52°36′ W.; depth 265 m; dynamic height 971.111.						
0	3.25	32.06	0	3.25	32.06	25.54
25	0.98	32.48	25	0.98	32.48	26.05
50	−1.10	32.84	50	−1.10	32.84	26.43
75	−1.34	32.93	75	−1.34	32.93	26.51
100	−1.62	33.03	100	−1.62	33.03	26.59
150	−1.65	33.07	150	−1.65	33.07	26.63
			(200)	−1.60	33.15	26.69
Station 7164; 17 June; 48°19.5′ N., 52°05′ W.; depth 174 m.; dynamic height 971.099.						
0	2.86	32.69	0	2.86	32.69	26.07
25	1.75	32.75	25	1.75	32.75	26.22
49	1.09	32.79	50	1.05	32.80	26.31
74	−1.07	33.00	75	−1.10	33.00	26.56
98	−1.47	33.06	100	−1.50	33.06	26.61
147	−1.51	33.14	(150)	−1.50	33.15	26.68
Station 7165; 17 June; 48°13′ N., 51°50′ W.; depth 181 m.; dynamic height 970.091.						
0	2.60	32.74	0	2.60	32.74	26.14
25	1.38	32.73	25	1.38	32.73	26.22
50	−0.06	32.85	50	−0.06	32.85	26.40
75	−1.20	33.04	75	−1.20	33.04	26.59
100	−1.34	33.06	100	−1.35	33.06	26.61
151	−1.28	33.25	150	−1.25	33.25	26.76
Station 7166; 17 June; 48°05′ N., 51°29′ W.; depth 174 m.; dynamic height 971.090.						
0	2.78	32.80	0	2.78	32.80	26.18
25	1.60	32.83	25	1.60	32.83	26.29
51	0.43	32.86	50	0.45	32.86	26.38
76	−0.89	32.98	75	−0.85	32.97	26.52
101	−1.36	33.11	100	−1.35	33.10	26.64
142	−1.20	33.23	(150)	−1.15	33.25	26.76
Station 7167; 17 June; 47°56′ N., 51°11′ W.; depth 159 m.; dynamic height 971.086.						
0	2.48	32.80	0	2.48	32.80	26.20
25	1.67	32.80	25	1.67	32.80	26.26
50	1.37	32.83	50	1.37	32.83	26.30
74	−0.99	33.02	75	−1.00	33.02	26.57
99	−1.46	33.14	100	−1.45	33.15	26.68
139	−1.13	33.25	(150)	−1.00	33.27	26.85

Observed values			Scaled values			
Depth, meters	Temperature, °C.	Salinity, ‰	Depth, meters	Temperature, °C.	Salinity, ‰	σ_t
Station 7168; 17 June; 47°47.5′ N., 50°56′ W.; depth 128 m.; dynamic height 971.079.						
0	2.79	32.90	0	2.79	32.90	26.25
25	1.48	32.92	25	1.48	32.92	26.36
50	0.55	32.95	50	0.55	32.95	26.44
76	−0.76	33.08	75	−0.75	33.07	26.60
101	−1.17	33.12	100	−1.15	33.12	26.66
Station 7169; 17 June; 47°39′ N., 50°40′ W.; depth 110 m.; dynamic height 971.079.						
0	2.61	32.86	0	2.61	32.86	26.23
25	2.30	32.87	25	2.30	32.87	26.27
50	1.28	32.89	50	1.28	32.89	26.35
75	−0.64	33.13	75	−0.64	33.13	26.64
100	−1.18	33.22	100	−1.18	33.32	26.82
Station 7170; 17 June; 47°31.5′ N., 50°21′ W.; depth 146 m.; dynamic height 971.083.						
0	2.85	32.89	0	2.85	32.89	26.23
25	2.07	32.96	25	2.07	32.96	26.36
50	1.35	32.97	50	1.35	32.97	26.41
75	0.01	33.12	75	0.01	33.12	26.61
101	−0.24	33.15	100	−0.25	33.15	26.64
141	−0.40	33.16	150	−0.45	33.16	26.66
Station 7171; 17 June; 47°23.5′ N., 50°01′ W.; depth 95 m.; dynamic height 971.082.						
0	2.58	32.94	0	2.58	32.94	26.30
26	1.86	32.95	25	1.90	32.95	26.36
53	1.79	32.96	50	1.80	32.96	26.37
79	−0.42	33.18	75	0.05	33.16	26.64
Station 7172; 17 June; 47°45′ N., 49′50′ W.; depth 114 m.; dynamic height 971.083.						
0	2.39	32.86	0	2.39	32.86	26.25
26	1.86	32.85	25	1.85	32.85	26.28
52	1.19	32.88	50	1.20	32.88	26.35
78	−0.55	33.16	75	−0.40	33.13	26.64
104	−0.73	33.38	100	−0.70	33.35	26.82
Station 7173; 18 June; 47°58′ N., 49°47′ W.; depth 174 m.; dynamic height 971.083.						
0	1.50	32.87	0	1.50	32.87	26.32
25	0.71	32.89	25	0.71	32.89	26.38
50	1.17	33.07	50	1.17	33.07	26.51
76	0.45	33.06	75	0.50	33.06	26.53
101	−1.42	33.14	100	−1.20	33.14	26.67
152	−0.79	33.42	150	−0.80	33.40	26.87

TABLE OF OCEANOGRAPHIC DATA—Continued

STATIONS OCCUPIED IN 1959—Continued

Station 7174; 18 June; 48°14.5′ N., 49° 42′ W.; depth 220 m.; dynamic height 971.048.

Observed values			Scaled values			
Depth, meters	Temperature, °C.	Salinity, ‰	Depth, meters	Temperature, °C.	Salinity, ‰	σ_t
0	2.52	33.03	0	2.52	33.03	26.38
25	1.78	33.09	25	1.78	33.09	26.47
50	1.70	33.10	50	1.70	33.10	26.49
75	0.27	33.26	75	0.27	33.26	26.71
100	−0.97	33.43	100	−0.97	33.43	26.90
150	0.27	33.78	150	0.27	33.78	27.13
200	1.04	33.985	200	1.04	33.98	27.24

Station 7175; 18 June; 48°32′ N., 49°33′ W.; depth 638 m.; dynamic height 970.997.

Observed values			Scaled values			
Depth, meters	Temperature, °C.	Salinity, ‰	Depth, meters	Temperature, °C.	Salinity, ‰	σ_t
0	2.88	33.04	0	2.88	33.04	26.36
25	2.01	33.13	25	2.01	33.13	26.50
50	1.07	33.12	50	1.07	33.12	26.55
74	−0.88	33.47	75	−0.85	33.48	26.93
99	0.16	33.78	100	0.20	33.79	27.14
149	1.23	34.05	150	1.25	34.05	27.29
199	1.96	34.29	200	2.00	34.29	27.42
298	2.96	34.64	300	3.00	34.64	27.62
392	3.65	34.82	400	3.65	34.83	27.70
591	3.65	34.84	(600)	3.65	34.84	27.71

Station 7176; 18 June; 48°38.5′ N., 49°27′ W.; depth 1,024 m.; dynamic height 970.956.

Observed values			Scaled values			
Depth, meters	Temperature, °C.	Salinity, ‰	Depth, meters	Temperature, °C.	Salinity, ‰	σ_t
0	2.90	32.88	0	2.90	32.88	26.23
25	1.43	33.09	25	1.43	33.09	26.50
50	−0.01	33.42	50	−0.01	33.42	26.86
75	−0.11	33.67	75	−0.11	33.67	27.06
100	0.26	33.83	100	0.26	33.83	27.17
150	2.02	34.34	150	2.02	34.34	27.46
200	2.57	34.54	200	2.57	34.54	27.58
300	3.17	34.70	300	3.17	34.70	27.65
390	3.63	34.82	400	3.65	34.82	27.70
587	3.61	34.84	600	3.60	34.85	27.73
785	3.59	34.88	800	3.60	34.88	27.75
992	3.51	34.88	(1,000)	3.50	34.88	27.76

Station 7177; 18 June; 49°03′ N., 49°20′ W.; depth 1,628 m.; dynamic height 970.913.

Observed values			Scaled values			
Depth, meters	Temperature, °C.	Salinity, ‰	Depth, meters	Temperature, °C.	Salinity, ‰	σ_t
0	3.41	33.37	0	3.41	33.37	26.56
25	3.21	33.39	25	3.21	33.39	26.60
49	0.51	33.76	50	0.55	33.77	27.11
74	1.34	34.11	75	1.35	34.12	27.34
98	1.84	34.28	100	1.85	34.29	27.43
147	2.49	34.48	150	2.50	34.49	27.54
197	2.74	34.58	200	2.75	34.59	27.60
295	3.27	34.75	300	3.25	34.76	27.69
385	3.18	34.805	400	3.20	34.81	27.74
576	3.26	34.82	600	3.30	34.82	27.74
766	3.30	34.83	800	3.30	34.83	27.74
960	3.46	34.84	1,000	3.45	34.845	27.74

Station 7178; 18 June; 49°34.5′ N., 49°17′ W.; depth 1,646 m.; dynamic height 970.926.

Observed values			Scaled values			
Depth, meters	Temperature, °C.	Salinity, ‰	Depth, meters	Temperature, °C.	Salinity, ‰	σ_t
0	3.05	33.06	0	3.05	33.06	26.35
25	2.67	33.52	25	2.67	33.52	26.76
50	0.99	33.86	50	0.99	33.86	27.15
76	1.00	34.05	75	1.00	34.05	27.30
101	1.26	34.15	100	1.25	34.14	27.36
151	2.32	34.43	150	2.30	34.42	27.51
202	2.60	34.56	200	2.60	34.55	27.58
303	3.08	34.70	300	3.05	34.70	27.66
390	3.24	34.78	400	3.25	34.78	27.70
591	3.29	34.81	600	3.30	34.81	27.73
795	3.39	34.84	800	3.40	34.84	27.74
1,000	3.46	34.86	1,000	3.45	34.86	27.75
1,524	3.28	34.90				

Station 7179; 18 June; 49°59.5′ N., 49°00′ W.; depth 1,920 m.; dynamic height 970.871.

Observed values			Scaled values			
Depth, meters	Temperature, °C.	Salinity, ‰	Depth, meters	Temperature, °C.	Salinity, ‰	σ_t
0	4.00	33.78	0	4.00	33.78	26.84
25	3.76	34.08	25	3.76	34.08	27.10
50	3.29	34.25	50	3.29	34.25	27.28
76	3.53	34.52	75	3.55	34.51	27.46
101	2.87	34.56	100	2.85	34.56	27.57
151	3.11	34.69	150	3.10	34.69	27.65
202	3.27	34.74	200	3.25	34.74	27.67
303	3.33	34.80	300	3.35	34.80	27.71
410	3.32	34.82	400	3.35	34.81	27.72
616	3.50	34.86	600	3.50	34.86	27.75
823	3.37	34.86	800	3.40	34.86	27.76
1,031	3.46	34.87	1,000	3.45	34.87	27.76
1,553	3.43	34.90				
1,859	3.23	34.90				

Station 7180; 19 June; 49°48′ N., 48°22′ W.; depth 2,350 m.; dynamic height 970.878.

Observed values			Scaled values			
Depth, meters	Temperature, °C.	Salinity, ‰	Depth, meters	Temperature, °C.	Salinity, ‰	σ_t
0	6.56	34.62	0	6.56	34.62	27.20
25	6.04	34.63	25	6.04	34.63	27.27
50	5.76	34.63	50	5.76	34.63	27.31
76	5.18	34.64	75	5.20	34.64	27.39
101	3.63	34.67	100	3.65	34.67	27.58
151	3.29	34.71	150	3.30	34.71	27.65
201	3.55	34.78	200	3.55	34.77	27.67
302	3.47	34.81	300	3.45	34.81	27.71
389	3.53	34.83	400	3.55	34.83	27.71
585	3.53	34.85	600	3.55	34.85	27.73
781	3.32	34.83	800	3.35	34.83	27.73
984	3.45	34.88	1,000	3.45	34.88	27.76
1,504	3.32	34.90				

Station 7181; 19 June; 49°35′ N., 47°40′ W.; depth 2,743 m.; dynamic height 970.849.

Observed values			Scaled values			
Depth, meters	Temperature, °C.	Salinity, ‰	Depth, meters	Temperature, °C.	Salinity, ‰	σ_t
0	5.06	34.30	0	5.06	34.30	27.14
25	5.05	34.36	25	5.05	34.36	27.19
50	5.23	34.56	50	5.23	34.56	27.32
74	4.61	34.59	75	4.60	34.59	27.41
99	3.47	34.67	100	3.40	34.67	27.61
148	3.22	34.75	150	3.20	34.75	27.69
198	3.36	34.78	200	3.40	34.78	27.69
297	3.58	34.86	300	3.55	34.86	27.74
378	3.49	34.86	400	3.50	34.86	27.75
576	3.44	34.87	600	3.45	34.87	27.76
779	3.49	34.90	800	3.50	34.89	27.77
982	3.44	34.90	1,000	3.45	34.90	27.78
1,504	3.32	34.91				

TABLE OF OCEANOGRAPHIC DATA—Continued

STATIONS OCCUPIED IN 1959—Continued

Station 7182; 19 June; 49°15′ N., 47°55′ W.; depth 2,451 m.; dynamic height 970.855.

Observed values			Scaled values			
Depth, meters	Temperature, °C.	Salinity, ‰	Depth, meters	Temperature, °C.	Salinity, ‰	σ_t
0	4.42	34.25	0	4.42	34.25	27.17
25	4.44	34.33	25	4.44	34.33	27.22
50	2.56	34.35	50	2.56	34.35	27.43
76	2.62	34.50	75	2.65	34.50	27.54
101	2.62	34.55	100	2.60	34.55	27.58
151	3.03	34.68	150	3.05	34.68	27.64
202	3.30	34.76	200	3.30	34.76	27.69
303	3.33	34.80	300	3.30	34.80	27.72
410	3.31	34.82	400	3.30	34.82	27.74
617	3.46	34.85	600	3.45	34.85	27.74
827	3.41	34.86	800	3.45	34.86	27.76
1,035	3.42	34.88	1,000	3.45	34.88	27.76
1,553	3.29	34.92				

Station 7183; 19 June; 48°52′ N., 48°09′ W.; depth 2,405 m.; dynamic height 970.858.

Observed values			Scaled values			
Depth, meters	Temperature, °C.	Salinity, ‰	Depth, meters	Temperature, °C.	Salinity, ‰	σ_t
0	5.17	34.24	0	5.17	34.24	27.07
25	5.17	34.28	25	5.17	34.28	27.10
50	3.28	34.35	50	3.28	34.35	27.36
75	2.93	34.54	75	2.93	34.54	27.54
100	2.93	34.62	100	2.93	34.62	27.61
150	3.17	34.74	150	3.17	34.74	27.67
201	3.19	34.76	200	3.20	34.75	27.69
301	3.29	34.82	300	3.30	34.82	27.74
391	3.26	34.82	400	3.25	34.82	27.74
590	3.28	34.82	600	3.30	34.83	27.74
792	3.53	34.87	800	3.55	34.87	27.75
993	3.49	34.87	1,000	3.50	34.87	27.76

Station 7184; 19 June; 48°20′ N., 48°25′ W.; depth 1,739 m.; dynamic height 970.926.

Observed values			Scaled values			
Depth, meters	Temperature, °C.	Salinity, ‰	Depth, meters	Temperature, °C.	Salinity, ‰	σ_t
0	2.95	33.08	0	2.95	33.08	26.38
25	1.90	33.33	25	1.90	33.33	26.66
50	0.29	33.70	50	0.29	33.70	27.06
76	0.51	33.85	75	0.50	33.84	27.16
101	1.28	34.11	100	1.25	34.10	27.33
151	2.40	34.44	150	2.40	34.44	27.51
202	2.98	34.64	200	2.95	34.64	27.62
303	3.22	34.76	300	3.20	34.75	27.69
404	3.29	34.78	400	3.30	34.78	27.70
606	3.27	34.82	600	3.30	34.82	27.74
807	3.44	34.84	800	3.40	34.84	27.74
1,012	3.51	34.87	1,000	3.50	34.87	27.76
1,523	3.39	34.88				

Station 7185; 19 June; 48°11′ N., 48°36′ W.; depth 688 m.; dynamic height 971.013.

Observed values			Scaled values			
Depth, meters	Temperature, °C.	Salinity, ‰	Depth, meters	Temperature, °C.	Salinity, ‰	σ_t
0	3.12	33.11	0	3.12	33.11	26.38
25	2.05	33.05	25	2.05	33.05	26.43
50	0.50	33.24	50	0.50	33.24	26.68
76	−1.08	33.44	75	−1.05	33.43	26.90
101	0.04	33.70	100	0.00	33.70	27.08
151	1.23	34.09	150	1.20	34.08	27.31
202	1.89	34.27	200	1.85	34.26	27.41
303	2.74	34.56	300	2.70	34.55	27.57
402	2.85	34.58	400	2.85	34.58	27.58
601	3.57	34.84	600	3.55	34.84	27.72

Station 7186; 19 June; 48°05′ N., 48°40′ W.; depth 316 m.; dynamic height 971.041.

Observed values			Scaled values			
Depth, meters	Temperature, °C.	Salinity, ‰	Depth, meters	Temperature, °C.	Salinity, ‰	σ_t
0	2.58	32.96	0	2.58	32.96	26.32
25	1.41	33.04	25	1.41	33.04	26.47
50	−1.52	33.10	50	−1.52	33.10	26.64
76	−1.44	33.19	75	−1.45	33.18	26.71
101	−1.03	33.35	100	−1.05	33.34	26.83
151	0.00	33.78	150	0.00	33.77	27.14
201	0.61	33.98	200	0.60	33.98	27.26
302	2.48	34.46	300	2.40	34.45	27.52

Station 7187; 19 June; 47°51.5′ N., 48°49′ W.; depth 220 m.; dynamic height 971.089.

Observed values			Scaled values			
Depth, meters	Temperature, °C.	Salinity, ‰	Depth, meters	Temperature, °C.	Salinity, ‰	σ_t
0	2.04	32.85	0	2.04	32.85	26.28
25	1.87	32.85	25	1.87	32.85	26.28
50	1.82	33.08	50	1.82	33.08	26.47
75	−1.20	33.05	75	−1.20	33.05	26.60
100	−1.57	33.12	100	−1.57	33.12	26.67
150	−1.07	33.29	150	−1.07	33.29	26.78
200	−0.41	33.54	200	−0.41	33.54	26.97

Station 7188; 19 June; 47°39′ N., 48°57′ W.; depth 167 m.; dynamic height 971.083.

Observed values			Scaled values			
Depth, meters	Temperature, °C.	Salinity, ‰	Depth, meters	Temperature, °C.	Salinity, ‰	σ_t
0	2.21	32.86	0	2.21	32.86	26.26
25	0.99	32.84	25	0.99	32.84	26.34
50	−0.35	32.96	50	−0.35	32.96	26.49
76	−1.29	33.05	75	−1.25	33.04	26.59
101	−1.52	33.12	100	−1.50	33.11	26.65
151	−0.95	33.37	150	−1.00	33.36	26.84

Station 7189; 20 June; 47°44.5′ N., 48°20′ W.; depth 227 m.; dynamic height 971.076.

Observed values			Scaled values			
Depth, meters	Temperature, °C.	Salinity, ‰	Depth, meters	Temperature, °C.	Salinity, ‰	σ_t
0	2.05	32.82	0	2.05	32.82	26.25
25	2.08	32.87	25	2.08	32.87	26.28
50	1.24	32.94	50	1.24	32.94	26.40
75	1.19	32.96	75	1.19	32.96	26.41
100	0.36	33.20	100	0.36	33.20	26.66
149	−0.42	33.53	150	−0.40	33.54	26.97
199	0.77	33.86	(200)	0.80	33.87	27.17

Station 7190; 20 June; 47°46′ N., 48°05′ W.; depth 254 m.; dynamic height 971.064.

Observed values			Scaled values			
Depth, meters	Temperature, °C.	Salinity, ‰	Depth, meters	Temperature, °C.	Salinity, ‰	σ_t
0	2.68	32.98	0	2.68	32.98	26.33
25	0.83	32.88	25	0.83	32.88	26.38
51	−1.44	33.08	50	−1.40	33.07	26.62
76	−1.55	33.13	75	−1.55	33.13	26.67
101	−1.45	33.18	100	−1.45	33.18	26.71
152	−0.86	33.43	150	−0.90	33.42	26.90
203	0.41	33.78	200	0.35	33.76	27.11
228	0.79	33.88				

TABLE OF OCEANOGRAPHIC DATA—Continued
STATIONS OCCUPIED IN 1959—Continued

Station 7191; 20 June; 47°47′ N., 47°47′ W.; depth 293 m.; dynamic height 970.990.

Observed values			Scaled values			
Depth, meters	Temperature, °C.	Salinity, ‰	Depth, meters	Temperature, °C.	Salinity, ‰	σ_t
0	2.79	33.14	0	2.79	33.14	26.45
25	2.60	33.13	25	2.60	33.13	26.45
50	1.66	33.13	50	1.66	33.13	26.52
74	0.95	33.59	75	0.95	33.61	26.95
99	0.73	33.86	100	0.70	33.87	27.18
149	1.54	34.18	150	1.55	34.19	27.37
198	2.13	34.39	200	2.15	34.40	27.50
248	2.61	34.52				

Station 7192; 20 June; 47°56′ N., 47°34′ W.; depth 340 m.; dynamic height 970.989.

Observed values			Scaled values			
Depth, meters	Temperature, °C.	Salinity, ‰	Depth, meters	Temperature, °C.	Salinity, ‰	σ_t
0	2.64	33.11	0	2.64	33.11	26.43
25	2.67	33.14	25	2.67	33.14	26.45
50	2.23	33.32	50	2.23	33.32	26.63
75	2.95	33.88	75	2.95	33.88	27.01
100	0.56	33.74	100	0.56	33.74	27.08
150	1.56	34.12	150	1.56	34.12	27.32
200	1.99	34.30	200	1.99	34.30	27.43
300	3.33	34.76	300	3.33	34.76	27.68

Station 7193; 20 June; 48°06.5′ N., 47°22′ W.; depth 613 m.; dynamic height 970.914.

Observed values			Scaled values			
Depth, meters	Temperature, °C.	Salinity, ‰	Depth, meters	Temperature, °C.	Salinity, ‰	σ_t
0	4.51	33.64	0	4.51	33.64	26.68
25	4.66	33.82	25	4.66	33.82	26.80
50	4.13	33.99	50	4.13	33.99	26.99
75	4.14	34.22	75	4.14	34.22	27.18
100	2.80	34.42	100	2.80	34.42	27.46
150	2.92	34.58	150	2.92	34.58	27.58
200	3.10	34.69	200	3.10	34.69	27.65
300	3.46	34.80	300	3.46	34.80	27.70
400	3.59	34.84	400	3.60	34.84	27.72
604	3.55	34.87	600	3.55	34.87	27.75

Station 7194; 20 June; 48°16′ N., 47°12′ W.; depth 1,655 m.; dynamic height 970.884.

Observed values			Scaled values			
Depth, meters	Temperature, °C.	Salinity, ‰	Depth, meters	Temperature, °C.	Salinity, ‰	σ_t
0	5.35	33.68	0	5.35	33.68	26.61
25	4.04	34.01	25	4.04	34.01	27.02
50	3.75	34.34	50	3.75	34.34	27.31
76	2.99	34.51	75	3.00	34.51	27.52
101	3.10	34.63	100	3.10	34.63	27.60
151	3.22	34.72	150	3.20	34.72	27.67
202	3.28	34.74	200	3.30	34.74	27.67
303	3.29	34.78	300	3.30	34.78	27.70
402	3.34	34.80	400	3.35	34.80	27.71
605	3.24	34.79	600	3.25	34.79	27.71
810	3.48	34.85	800	3.45	34.85	27.74
1,012	3.50	34.88	1,000	3.50	34.88	27.76
1,514	3.36	34.89				

Station 7195; 20 June; 48°36.5′ N., 47°00′ W.; depth 2,469 m.; dynamic height 970.876.

Observed values			Scaled values			
Depth, meters	Temperature, °C.	Salinity, ‰	Depth, meters	Temperature, °C.	Salinity, ‰	σ_t
0	5.00	33.98	0	5.00	33.98	26.89
25	4.90	34.17	25	4.90	34.17	27.05
50	3.34	34.32	50	3.34	34.32	27.33
75	3.02	34.56	75	3.02	34.56	27.55
101	3.04	34.61	100	3.05	34.61	27.59
151	3.14	34.70	150	3.15	34.70	27.65
201	3.22	34.73	200	3.20	34.73	27.67
302	3.32	34.79	300	3.30	34.79	27.71
397	3.37	34.80	400	3.40	34.80	27.71
598	3.26	34.80	600	3.25	34.80	27.72
800	3.47	34.86	800	3.45	34.86	27.75
1,000	3.50	34.86	1,000	3.50	34.86	27.75
1,502	3.38	34.91				

Station 7196; 20 June; 48°58′ N., 46°39′ W.; depth 2,743 m.; dynamic height 970.859.

Observed values			Scaled values			
Depth, meters	Temperature, °C.	Salinity, ‰	Depth, meters	Temperature, °C.	Salinity, ‰	σ_t
0	6.44	34.48	0	6.44	34.48	27.11
25	5.88	34.48	25	5.88	34.48	27.18
51	4.43	34.60	50	4.50	34.60	27.43
76	3.59	34.65	75	3.60	34.65	27.57
101	3.30	34.70	100	3.30	34.70	27.64
152	3.34	34.74	150	3.35	34.73	27.65
203	3.40	34.79	200	3.40	34.79	27.70
304	3.39	34.81	300	3.40	34.81	27.72
400	3.44	34.82	400	3.45	34.82	27.72
600	3.67	34.87	600	3.70	34.87	27.74
799	3.55	34.88	800	3.55	34.88	27.75
999	3.50	34.88	1,000	3.50	34.88	27.76
1,502	3.36	34.90				

Station 7197; 20 June; 49°20′ N., 46°19′ W.; depth 3,109 m.; dynamic height 970.849.

Observed values			Scaled values			
Depth, meters	Temperature, °C.	Salinity, ‰	Depth, meters	Temperature, °C.	Salinity, ‰	σ_t
0	6.53	34.38	0	6.53	34.38	27.01
25	5.52	34.52	25	5.52	34.52	27.25
50	4.13	34.62	50	4.13	34.62	27.49
75	3.46	34.70	75	3.46	34.70	27.62
99	3.25	34.72	100	3.25	34.72	27.66
149	3.21	34.74	150	3.20	34.74	27.68
199	3.33	34.80	200	3.35	34.80	27.71
298	3.32	34.82	300	3.30	34.82	27.74
397	3.30	34.82	400	3.30	33.83	27.74
595	3.43	34.85	600	3.45	34.85	27.74
794	3.47	34.85	800	3.50	34.85	27.74
993	3.47	34.88	1,000	3.45	34.88	27.76
1,493	3.37	34.90				

Station 7198; 21 June; 49°09′ N., 45°41′ W.; depth 2,671 m.; dynamic height 970.957.

Observed values			Scaled values			
Depth, meters	Temperature, °C.	Salinity, ‰	Depth, meters	Temperature, °C.	Salinity, ‰	σ_t
0	5.64	34.15	0	5.64	34.15	26.95
25	5.58	34.21	25	5.58	34.21	27.00
50	3.41	34.48	50	3.41	34.48	27.45
75	3.09	34.65	75	3.09	34.65	27.62
100	3.45	34.76	100	3.45	34.76	27.67
150	3.44	34.76	150	3.44	34.76	27.67
200	3.52	34.81	200	3.52	34.81	27.70
300	3.36	34.81	300	3.36	34.81	27.72
398	3.30	34.81	400	3.30	34.81	27.73
598	3.34	34.84	600	3.35	34.84	27.74
798	3.50	34.87	800	3.50	34.87	27.76
998	3.45	34.88	1,000	3.45	34.88	27.76
1,499	3.38	34.90				

TABLE OF OCEANOGRAPHIC DATA—Continued

STATIONS OCCUPIED IN 1959—Continued

Station 7199; 22 June; 49°02′ N., 44°58′ W.; depth 1,728 m.; dynamic height 970.865.

Observed values			Scaled values			
Depth, meters	Temperature, °C.	Salinity, ‰	Depth, meters	Temperature, °C.	Salinity, ‰	σ_t
0	5.01	33.95	0	5.01	33.95	26.86
25	2.54	34.21	25	2.54	34.21	27.32
50	2.36	34.38	50	2.36	34.38	27.46
75	2.68	34.54	75	2.68	34.54	27.57
100	2.74	34.57	100	2.74	34.57	27.59
150	2.86	34.64	150	2.86	34.64	27.63
201	3.03	34.69	200	3.05	34.69	27.65
301	3.27	34.76	300	3.25	34.75	27.68
398	3.30	34.79	400	3.30	34.79	27.71
598	3.49	34.84	600	3.50	34.85	27.74
797	3.50	34.87	800	3.50	34.87	27.76
997	3.49	34.88	1,000	3.50	34.89	27.77
1,500	3.34	34.92				

Station 7200; 21 June; 48°37′ N., 45°26′ W.; depth 1,040 m.; dynamic height 970.876.

Observed values			Scaled values			
Depth, meters	Temperature, °C.	Salinity, ‰	Depth, meters	Temperature, °C.	Salinity, ‰	σ_t
0	6.54	34.26	0	6.54	34.26	26.92
25	6.23	34.29	25	6.23	34.29	26.98
50	3.77	34.46	50	3.77	34.46	27.40
76	3.13	34.54	75	3.15	34.54	27.52
101	2.79	34.605	100	2.80	34.60	27.60
151	2.79	34.63	150	2.80	34.63	27.62
201	3.01	34.72	200	3.00	34.71	27.68
302	3.28	34.77	300	3.30	34.77	27.70
392	3.43	34.80	400	3.45	34.80	27.70
590	3.58	34.85	600	3.60	34.85	27.73
790	3.57	34.88	800	3.60	34.88	27.75
988	3.41	34.90	(1,000)	3.40	34.90	27.79

Station 7201; 21 June; 48°19′ N., 45°54′ W.; depth 1,169 m.; dynamic height 970.971.

Observed values			Scaled values			
Depth, meters	Temperature, °C.	Salinity, ‰	Depth, meters	Temperature, °C.	Salinity, ‰	σ_t
0	6.58	34.24	0	6.58	34.24	26.90
25	4.49	34.23	25	4.49	34.23	27.14
50	4.71	34.53	50	4.71	34.53	27.35
76	3.92	34.53	75	3.95	34.53	27.43
101	3.07	34.59	100	3.10	34.59	27.57
151	3.06	34.68	150	3.05	34.68	27.64
201	3.20	34.72	200	3.20	34.72	27.67
302	3.28	34.79	300	3.30	34.79	27.71
398	3.31	34.80	400	3.30	34.80	27.72
597	3.33	34.82	600	3.35	34.82	27.73
795	3.50	34.86	800	3.50	34.86	27.75
1,000	3.50	34.88	1,000	3.50	34.88	27.76

Station 7202;21 June; 47°59′ N., 46°21′ W.; depth 1,188 m.; dynamic height 970.885.

Observed values			Scaled values			
Depth, meters	Temperature, °C.	Salinity, ‰	Depth, meters	Temperature, °C.	Salinity, ‰	σ_t
0	6.23	34.20	0	6.23	34.20	26.83
25	5.16	34.31	25	5.16	34.31	27.13
50	4.09	34.48	50	4.09	34.48	27.59
76	3.59	34.53	75	3.60	34.53	27.47
101	3.25	34.60	100	3.25	34.59	27.55
151	3.10	34.69	150	3.10	34.69	27.65
201	3.22	34.73	200	3.20	34.73	27.67
302	3.29	34.79	300	3.30	34.79	27.71
396	3.29	34.79	400	3.30	34.79	27.71
594	3.27	34.79	600	3.30	34.79	27.71
793	3.46	34.83	800	3.50	34.83	27.72
995	3.51	34.85	(1,000)	3.50	34.85	27.74

Station 7203; 21 June; 47°53′ N., 46°09′ W.; depth 1,024 m.; dynamic height 970.899.

Observed values			Scaled values			
Depth, meters	Temperature, °C.	Salinity, ‰	Depth, meters	Temperature, °C.	Salinity, ‰	σ_t
0	5.98	33.77	0	5.98	33.77	26.61
25	5.29	33.81	25	5.29	33.81	26.72
50	3.09	34.34	50	3.09	34.34	27.37
75	2.63	34.46	75	2.63	34.46	27.51
100	2.87	34.55	100	2.87	34.55	27.57
150	2.96	34.62	150	2.96	34.62	27.61
201	2.99	34.66	200	3.00	34.65	27.63
301	3.28	34.72	300	3.30	34.72	27.66
399	3.40	34.76	400	3.40	34.76	27.68
598	3.70	34.87	600	3.70	34.87	27.74
797	3.57	34.86	800	3.60	34.86	27.74
996	3.42	34.89	(1,000)	3.45	34.90	27.78

Station 7204; 21 June; 47°45′ N., 45°50′ W.; depth 434 m.; dynamic height 970.911.

Observed values			Scaled values			
Depth, meters	Temperature, °C.	Salinity, ‰	Depth, meters	Temperature, °C.	Salinity, ‰	σ_t
0	5.93	33.78	0	5.93	33.78	26.62
24	3.41	33.82	25	5.35	33.82	26.73
48	3.57	34.27	50	3.50	34.28	27.28
72	3.11	34.36	75	3.15	34.36	27.38
96	3.64	34.49	100	3.70	34.51	27.45
144	4.56	34.72	150	4.45	34.71	27.53
193	3.27	34.62	200	3.30	34.63	27.58
289	3.67	34.75	300	3.70	34.76	27.65
387	3.77	34.81	(400)	3.80	34.82	27.69

Station 7205; 21 June; 47°40′ N., 45°35′ W.; depth 320 m. dynamic height 970.905.

Observed values			Scaled values			
Depth, meters	Temperature, °C.	Salinity, ‰	Depth, meters	Temperature, °C.	Salinity, ‰	σ_t
0	5.36	33.65	0	5.36	33.65	26.59
25	4.67	33.72	25	4.67	33.72	26.72
50	3.13	34.15	50	3.13	34.15	27.21
75	2.69	34.26	75	2.69	34.26	27.34
99	2.84	34.36	100	2.85	34.36	27.41
149	2.92	34.52	150	2.95	34.52	27.53
199	3.38	34.68	200	3.40	34.68	27.61
298	3.80	34.84	(300)	3.80	34.85	27.71

Station 7206; 22 June; 47°26.5′ N., 45°07′ W.; depth 238 m.; dynamic height 970.898.

Observed values			Scaled values			
Depth, meters	Temperature, °C.	Salinity, ‰	Depth, meters	Temperature, °C.	Salinity, ‰	σ_t
0	6.44	33.96	0	6.44	33.96	26.69
25	6.08	34.00	25	6.08	34.00	26.77
50	4.07	34.17	50	4.07	34.17	27.14
75	3.29	34.34	75	3.29	34.34	27.35
100	2.79	34.46	100	2.79	34.46	27.49
150	3.15	34.60	150	3.15	34.60	27.57
200	3.61	34.75	200	3.61	34.75	27.65

Station 7207; 22 June; 47°20′ N., 41°57′ W.; depth 208 m.; dynamic height 970.891.

Observed values			Scaled values			
Depth, meters	Temperature, °C.	Salinity, ‰	Depth, meters	Temperature, °C.	Salinity, ‰	σ_t
0	6.56	34.00	0	6.56	34.00	26.72
25	4.86	34.06	25	4.86	34.06	26.97
50	3.70	34.20	50	3.70	34.20	27.20
75	3.68	34.35	75	3.68	34.35	27.32
100	2.97	34.50	100	2.97	34.50	27.51
150	3.29	34.64	150	3.29	34.64	27.59
180	3.52	34.70	(200)	3.70	34.75	27.64

Station 7208; 22 June; 47°19′ N., 45°14′ W.; depth 231 m.; dynamic height 970.902.

Observed values			Scaled values			
Depth, meters	Temperature, °C.	Salinity, ‰	Depth, meters	Temperature, °C.	Salinity, ‰	σ_t
0	6.03	33.86	0	6.03	33.86	26.67
25	5.72	33.93	25	5.72	33.93	26.77
50	3.40	34.06	50	3.40	34.06	27.12
75	2.80	34.28	75	2.80	34.28	27.35
100	2.68	34.37	100	2.68	34.37	27.43
149	3.00	34.57	150	3.00	34.57	27.57
199	3.44	34.70	(200)	3.45	34.70	27.62

Station 7209; 22 June; 47°23′ N , 45°38′ W.; depth 276 m.; dynamic height 970.911.

Observed values			Scaled values			
Depth, meters	Temperature, °C.	Salinity, ‰	Depth, meters	Temperature, °C.	Salinity, ‰	σ_t
0	5.47	33.66	0	5.47	33.36	26.33
25	5.08	33.70	25	5.08	33.70	26.66
50	2.55	33.98	50	2.55	33.98	27.13
75	2.35	34.21	75	2.35	34.21	27.33
100	2.60	34.36	100	2.60	34.36	27.43
150	2.77	34.50	150	2.77	34.50	27.52
200	3.21	34.65	200	3.21	34.65	27.61
250	3.71	34.76	300	4.15	34.84	27.66

Station 7210; 22 June; 47°22′ N., 45°57′ W.; depth 324 m.; dynamic height 970.908.

Observed values			Scaled values			
Depth, meters	Temperature, °C.	Salinity, ‰	Depth, meters	Temperature, °C.	Salinity, ‰	σ_t
0	5.94	33.82	0	5.94	33.82	26.66
25	5.95	33.82	25	5.95	33.82	26.66
50	3.55	34.17	50	3.55	34.17	27.20
75	2.88	34.29	75	2.88	34.29	27.35
100	2.73	34.38	100	2.73	34.38	27.43
150	3.14	34.56	150	3.14	34.56	27.54
199	3.38	34.64	200	3.40	34.64	27.58
299	3.77	34.84	(300)	3.80	34.84	27.70

Station 7211; 22 June; 47°18.5′ N., 46°31′ W.; depth 668 m.; dynamic height 970.894.

Observed values			Scaled values			
Depth, meters	Temperature, °C.	Salinity, ‰	Depth, meters	Temperature, °C.	Salinity, ‰	σ_t
0	5.51	33.64	0	5.51	33.64	26.56
25	4.11	33.92	25	4.11	33.92	26.93
50	2.63	34.23	50	2.63	34.23	27.32
75	2.49	34.40	75	2.49	34.40	27.47
99	3.53	34.60	100	3.55	34.61	27.54
149	4.27	34.76	150	4.30	34.76	27.59
199	4.26	34.76	200	4.25	34.82	27.64
298	3.88	33.81	300	3.90	34.81	27.67
390	3.68	34.81	400	3.70	34.81	27.69
591	3.68	34.87	600	3.70	34.87	27.74

Station 7212; 22 June; 47°15′ N., 46°57′ W.; depth 1,143 m.; dynamic height 970.890.

Observed values			Scaled values			
Depth, meters	Temperature, °C.	Salinity, ‰	Depth, meters	Temperature, °C.	Salinity, ‰	σ_t
0	5.18	33.84	0	5.18	33.84	26.76
25	4.95	33.88	25	4.95	33.88	26.81
51	3.17	34.29	50	3.25	34.27	27.30
76	3.02	34.46	75	3.05	34.45	27.46
103	2.93	34.59	100	2.95	34.58	27.57
153	2.97	34.64	150	3.00	34.63	27.61
104	3.14	34.72	200	3.15	34.72	27.67
307	3.26	34.75	300	3.30	34.75	27.68
401	3.44	34.79	400	3.45	34.79	27.69
601	3.51	34.85	600	3.50	34.85	27.74
801	3.59	34.87	800	3.60	34.87	27.75
1,008	3.44	34.89	1,000	3.45	34.89	27.77

Station 7213; 22 June; 47°15′ N., 47°20′ W.; depth 302 m.; dynamic height 971.018.

Observed values			Sclaed values			
Depth, meters	Temperature, °C.	Salinity, ‰	Depth, meters	Temperature, °C.	Salinity, ‰	σ_t
0	2.71	33.03	0	2.71	33.03	26.36
24	2.41	33.18	25	2.40	33.18	26.51
48	1.10	33.35	50	1.05	33.37	26.76
73	0.73	33.62	75	0.75	33.66	27.01
97	1.36	33.86	100	1.40	33.90	27.15
146	1.73	34.20	150	1.75	34.22	27.39
194	2.10	34.33	200	2.15	34.34	27.45
291	2.68	34.52	(300)	2.70	34.53	27.55

Station 7214; 22 June; 47°15′ N., 47°41′ W.; depth 220 m.; dynamic height 971.060.

Observed values			Sclaed values			
Depth, meters	Temperature, °C.	Salinity, ‰	Depth, meters	Temperature, °C.	Salinity, ‰	σ_t
0	3.37	33.02	0	3.37	33.02	26.30
25	2.32	33.05	25	2.32	33.05	26.41
51	0.27	33.07	50	0.45	33.06	26.54
76	−1.34	33.27	75	−1.30	33.26	26.77
102	−0.60	33.46	100	−0.70	33.45	26.91
153	0.82	33.89	150	0.75	33.87	27.18
204	1.35	34.02	200	1.30	34.01	27.25

Station 7215; 22 June; 47°15′ N., 48°06′ W.; depth 172 m.; dynamic height 971.067.

Observed values			Sclaed values			
Depth, meters	Temperature, °C.	Salinity, ‰	Depth, meters	Temperature, °C.	Salinity, ‰	σ_t
0	2.68	33.00	0	2.68	33.00	26.34
25	2.39	32.96	25	2.39	32.96	26.34
50	1.42	33.22	50	1.42	33.22	26.61
76	−1.06	33.22	75	−1.05	33.22	26.73
101	−0.72	33.42	100	−0.70	33.41	26.88
151	0.55	33.78	150	0.50	33.77	27.11

Station 7216; 22 June; 47°13.5′ N., 48˘40′ W.; depth 123 m.; dynamic height 971.079.

Observed values			Sclaed values			
Depth, meters	Temperature, °C.	Salinity, ‰	Depth, meters	Temperature, °C.	Salinity, ‰	σ_t
0	2.59	32.88	0	2.59	32.88	26.25
25	1.97	32.92	25	1.97	32.92	26.33
50	0.17	32.97	50	0.17	32.97	26.48
75	−1.40	33.12	75	−1.40	33.12	26.66
100	−1.07	33.28	100	−1.07	33.28	26.78

Station 7217; 23 June; 47°12.5′ N., 49°13′ W.; depth 91 m.; dynamic height 971.086.

Observed values			Sclaed values			
Depth, meters	Temperature, °C.	Salinity, ‰	Depth, meters	Temperature, °C.	Salinity, ‰	σ_t
0	3.00	32.86	0	3.00	32.86	26.20
26	2.83	32.85	25	2.85	32.85	26.20
51	1.94	32.96	50	2.00	32.95	26.36
77	−0.74	33.22	75	−0.55	33.19	26.69

Station 7218; 23 June; 46°45′ N., 48°36′ W.; depth 106 m.; dynamic height 971.082.

Observed values			Sclaed values			
Depth, meters	Temperature, °C.	Salinity, ‰	Depth, meters	Temperature, °C.	Salinity, ‰	σ_t
0	3.12	32.80	0	3.12	32.80	26.15
25	3.07	32.81	25	3.07	32.81	26.16
51	−0.41	33.05	50	−0.30	33.04	26.56
76	−0.87	33.25	75	−0.85	33.24	26.74

TABLE OF OCEANOGRAPHIC DATA—Continued
STATIONS OCCUPIED IN 1959—Continued

Station 7219; 23 June; 46°47′ N., 47°59′ W.; depth 124 m.; dynamic height 971.075.

Observed values			Scaled values			
Depth, meters	Temperature, °C.	Salinity, ‰	Depth, meters	Temperature, °C.	Salinity, ‰	σ_t
0	2.64	32.91	0	2.64	32.91	26.27
25	2.43	32.96	25	2.43	32.96	26.33
51	−1.11	32.94	50	−1.10	32.95	26.52
76	−1.05	33.30	75	−1.05	33.29	26.78
102	−0.89	33.36	100	−0.90	33.35	26.84

Station 7220; 23 June; 46°48′ N., 47°39′ W.; depth 166 m ; dynamic height 971.084.

Observed values			Scaled values			
Depth, meters	Temperature, °C.	Salinity, ‰	Depth, meters	Temperature, °C.	Salinity, ‰	σ_t
0	2.49	32.92	0	2.49	32.92	26.29
25	2.30	32.92	25	2.30	32.92	26.31
51	1.18	33.03	50	1.25	33.03	26.47
76	−0.32	33.09	75	−0.25	33.09	26.59
101	−0.92	33.21	100	−0.90	33.20	26.72
152	0.44	33.77	150	0.35	33.75	27.10

Station 7221; 23 June; 46°47.5′ N., 47°18′ W.; depth 327 m.; dynamic height 971.029.

Observed values			Scaled values			
Depth, meters	Temperature, °C.	Salinity, ‰	Depth, meters	Temperature, °C.	Salinity, ‰	σ_t
0	3.12	33.07	0	3.12	33.07	26.36
24	2.90	33.09	25	2.85	33.09	26.39
49	−0.73	33.24	50	−0.75	33.25	26.74
73	−0.86	33.40	75	−0.85	33.42	26.89
97	−0.23	33.67	100	−0.15	33.70	27.09
146	1.64	34.14	150	1.65	34.15	27.34
195	1.87	34.23	200	1.90	34.24	27.39
292	2.51	34.46	(300)	2.55	34.47	27.53

Station 7222; 23 June; 46°47.5′ N., 47°11′ W.; depth 640 m.; dynamic height 970.972.

Observed values			Scaled values			
Depth, meters	Temperature, °C.	Salinity, ‰	Depth, meters	Temperature, °C.	Salinity, ‰	σ_t
0	3.47	33.12	0	3.47	33.12	26.36
25	2.78	33.26	25	2.78	33.26	26.54
50	1.00	33.56	50	1.00	33.56	26.91
75	0.85	33.75	75	0.85	33.75	27.07
100	0.85	33.91	100	0.85	33.91	27.20
150	1.96	34.26	150	1.96	34.26	27.41
199	2.72	34.46	200	2.75	34.46	27.50
299	3.15	34.66	300	3.15	34.66	27.62
385	3.32	34.77	400	3.35	34.78	27.69
581	3.54	34.82	(600)	3.55	34.82	27.71

Station 7223; 23 June; 46°47′ N., 46°50′ W.; depth 1,244 m.; dynamic height 970.915.

Observed values			Scaled values			
Depth, meters	Temperature, °C.	Salinity, ‰	Depth, meters	Temperature, °C.	Salinity, ‰	σ_t
0	5.71	33.88	0	5.71	33.88	26.73
25	5.10	33.90	25	5.10	33.90	26.82
50	3.03	34.30	50	3.03	34.30	27.34
75	2.16	34.36	75	2.16	34.36	27.47
100	2.39	34.43	100	2.39	34.43	27.50
150	2.72	34.54	150	2.72	34.54	27.56
200	3.22	34.66	200	3.22	34.66	27.61
300	3.21	34.73	300	3.21	34.73	27.67
403	3.23	34.75	400	3.25	34.75	27.68
605	3.64	34.84	600	3.65	34.84	27.71
807	3.62	34.85	800	3.65	34.85	27.72
1,011	3.52	34.86	1,000	3.55	34.86	27.74
1,196	3.45	34.87				

Station 7224; 23 June; 46°48′ N., 46°30′ N.;depth 626 m.; dynamic height 970.937.

Observed values			Scaled values			
Depth, meters	Temperature, °C.	Salinity, ‰	Depth, meters	Temperature, °C.	Salinity, ‰	σ_t
0	6.73	33.64	0	6.73	33.64	26.41
25	6.06	33.64	25	6.06	33.64	26.49
50	3.13	34.16	50	3.13	34.16	27.22
75	2.48	34.26	75	2.48	34.26	27.36
100	3.51	34.51	100	3.51	34.51	27.47
150	4.24	34.73	150	4.24	34.73	27.57
200	4.84	34.85	200	4.84	34.85	27.59
300	4.07	34.82	300	4.07	34.82	27.66
401	3.67	34.81	400	3.70	34.81	27.69
603	3.88	34.86	600	3.90	34.86	27.71

Station 7225; 23 June; 46°48′ N., 46°04′ W.; depth 320 m.; dynamic height 970.949.

Observed values			Scaled values			
Depth, meters	Temperature, °C.	Salinity, ‰	Depth, meters	Temperature, °C.	Salinity, ‰	σ_t
0	6.54	33.66	0	6.54	33.66	26.45
25	5.70	33.71	25	5.70	33.71	26.59
50	3.44	34.05	50	3.44	34.05	27.11
75	3.68	34.34	75	3.68	34.34	27.31
100	4.41	34.57	100	4.41	34.57	27.42
150	4.96	34.76	150	4.96	34.76	27.51
200	3.58	34.64	200	3.58	34.64	27.56
300	3.80	34.75	300	3.80	34.75	27.63

Station 7226; 23 June; 46°48′ N., 45°40′ W.; depth 256 m.; dynamic height 970.950.

Observed values			Scaled values			
Depth, meters	Temperature, °C.	Salinity, ‰	Depth, meters	Temperature, °C.	Salinity, ‰	σ_t
0	6.79	33.89	0	6.79	33.89	26.59
25	6.12	33.91	25	6.12	33.91	26.71
49	4.89	34.09	50	4.85	34.05	26.96
74	3.31	34.28	75	3.30	34.28	27.30
98	3.04	34.35	100	3.05	34.36	27.39
147	3.95	34.60	150	3.95	34.60	27.49
197	3.75	34.66	200	3.60	34.64	27.56

Station 7227; 23 June; 46°46.5′ N., 45°19′ W.; depth 220 m.; dynamic height 970.944.

Observed values			Scaled values			
Depth, meters	Temperature, °C.	Salinity, ‰	Depth, meters	Temperature, °C.	Salinity, ‰	σ_t
0	7.01	33.90	0	7.01	33.90	26.57
25	6.36	33.96	25	6.36	33.96	26.71
49	4.35	34.17	50	4.30	34.17	27.12
74	3.61	34.31	75	3.60	34.31	27.30
99	4.44	34.53	100	4.45	34.53	27.38
148	2.88	34.50	150	2.90	34.50	27.52
197	3.44	34.63	(200)	3.45	34.63	27.56

Station 7228; 24 June; 46°47′ N., 44°59′ W.; depth 170 m.; dynamic height 970.937.

Observed values			Scaled values			
Depth, meters	Temperature, °C.	Salinity, ‰	Depth, meters	Temperature, °C.	Salinity, ‰	σ_t
0	7.03	34.12	0	7.03	34.12	26.74
25	6.48	34.14	25	6.48	34.14	26.83
50	4.98	34.18	50	4.98	34.18	27.05
74	3.22	34.30	75	3.22	34.31	27.33
99	2.85	34.37	100	2.85	34.37	27.42
149	3.05	34.54	150	3.05	34.54	27.53

TABLE OF OCEANOGRAPHIC DATA—Ctoninued

STATIONS OCCUPIED IN 1959—Continued

Station 7229; 24 June; 46°48.5′ N., 44°50′ W.; depth 143 m.; dynamic height 970.929.

Observed values			Scaled values			
Depth, meters	Temperature, °C.	Salinity, ‰	Depth, meters	Temperature, °C.	Salinity, ‰	σ_t
0	6.99	34.12	0	6.99	34.12	26.75
25	6.48	34.14	25	6.48	34.14	26.83
50	3.54	34.26	50	3.54	34.26	27.26
75	2.81	34.32	75	2.81	34.32	27.38
100	2.76	34.36	100	2.76	34.36	27.42
125	2.76	34.40				

Station 7230; 1 August; 50°00′ N., 48°59′ W.; depth 1,911 m.; dynamic height 970.867.

Observed values			Scaled values			
Depth, meters	Temperature, °C.	Salinity, ‰	Depth, meters	Temperature, °C.	Salinity, ‰	σ_t
0	9.66	32.49	0	9.66	32.49	25.06
24	4.40	34.39	25	4.30	34.40	27.30
48	3.49	34.56	50	3.40	34.57	27.53
73	3.21	34.65	75	3.20	34.65	27.61
97	3.24	34.73	100	3.25	34.73	27.66
146	3.22	34.76	150	3.25	34.76	27.69
194	3.29	34.79	200	3.30	34.79	27.71
291	3.32	34.82	300	3.35	34.82	27.73
376	3.33	--------	400	3.35	34.83	27.73
565	3.34	34.84	600	3.35	34.84	27.74
755	3.28	34.85	800	3.30	34.85	27.76
950	3.31	34.86	1,000	3.30	34.86	27.77
1,447	3.38	34.90	1,500	3.40	34.90	27.79

Station 7231; 1 August; 49°48′ N., 49°30′ W.; depth 1,388 m.; dynamic height 970.880.

Observed values			Scaled values			
Depth, meters	Temperature, °C.	Salinity, ‰	Depth, meters	Temperature, °C.	Salinity, ‰	σ_t
0	8.99	31.98	0	8.99	31.98	24.78
25	2.98	34.36	25	2.98	34.36	27.40
51	2.76	34.48	50	2.75	34.48	27.51
75	2.69	34.57	75	2.70	34.57	27.59
101	2.80	34.62	100	2.75	34.62	27.63
151	3.13	34.70	150	3.15	34.70	27.65
202	3.29	34.76	200	3.30	34.76	27.69
303	3.32	34.80	300	3.35	34.80	27.71
386	3.31	34.81	400	3.30	34.81	27.73
580	3.35	34.84	600	3.35	34.84	27.74
774	3.32	--------	800	3.35	34.84	27.74
976	3.31	34.84	1,000	3.30	34.84	27.75
1,388	3.64	34.87				

Station 7232; 1 August; 49°39′ N., 49°57′ W.; depth 631 m.; dynamic height 970.952.

Observed values			Scaled values			
Depth, meters	Temperature, °C.	Salinity, ‰	Depth, meters	Temperature, °C.	Salinity, ‰	σ_t
0	9.46	31.77	0	9.46	31.77	24.54
25	−0.29	33.26	25	−0.29	33.26	26.73
50	−0.26	33.65	50	−0.26	33.65	27.05
75	0.50	33.94	75	0.50	33.94	27.24
101	1.32	34.16	100	1.30	34.15	27.36
151	2.26	34.44	150	2.25	34.43	27.51
201	2.63	34.57	200	2.60	34.57	27.60
302	3.20	34.72	300	3.20	34.72	27.67
403	3.31	34.78	400	3.30	34.78	27.70
607	3.37	34.82	600	3.40	34.82	27.73

Station 7233; 1 August; 49°31.5′ N., 50°36′ W.; depth 342 m.; dynamic height 971.002.

Observed values			Scaled values			
Depth, meters	Temperature, °C.	Salinity, ‰	Depth, meters	Temperature, °C.	Salinity, ‰	σ_t
0	10.34	32.34	0	10.34	32.34	24.84
24	0.91	32.74	25	0.60	32.80	26.33
47	−0.88	33.21	50	−0.90	33.25	26.76
71	−0.82	33.50	75	−0.70	33.54	26.98
94	−0.08	33.72	100	0.05	33.76	27.13
141	0.94	34.00	150	1.15	34.05	27.29
188	1.94	34.30	200	2.10	34.55	27.46
282	2.92	34.64	300	3.05	34.69	27.65
323	3.23	34.77				

Station 7234 1 August; 49°24.5′ N., 51°05′ W.; depth 351 m.; dynamic height 971.077.

Observed values			Scaled values			
Depth, meters	Temperature, °C.	Salinity, ‰	Depth, meters	Temperature, °C.	Salinity, ‰	σ_t
0	11.24	32.02	0	11.24	32.02	24.44
24	7.11	32.23	25	6.65	32.26	25.33
49	−0.33	32.98	50	−0.40	32.99	26.53
73	−1.21	33.19	75	−1.20	33.20	26.72
98	−0.46	33.58	100	−0.45	33.60	27.02
147	0.66	33.96	150	0.70	33.98	27.26
195	1.75	34.23	200	1.85	34.25	27.40
293	2.91	34.65	300	2.95	34.66	27.64
336	3.07	34.70				

Station 7235; 1 August; 49°14′N., 51°33′ W.; depth 312 m.; dynamic height 971.075.

Observed values			Scaled values			
Depth, meters	Temperature, °C.	Salinity, ‰	Depth, meters	Temperature, °C.	Salinity, ‰	σ_t
0	11.39	31.22	0	11.39	31.22	23.79
24	0.65	32.41	25	0.60	32.43	26.03
49	−0.14	32.92	50	−0.20	32.93	26.47
73	−1.50	33.17	75	−1.50	33.18	26.71
99	−1.12	33.31	100	−1.10	33.31	26.80
147	−0.18	33.70	150	−0.10	33.72	27.10
196	0.62	33.95	200	0.70	33.97	27.26
295	2.81	34.53	(300)	2.95	34.56	27.56

Station 7236; 1 August; 49°07.5′ N., 51°52′ W.; depth 295 m.; dynamic height 971.110.

Observed values			Scaled values			
Depth, meters	Temperature, °C.	Salinity, ‰	Depth, meters	Temperature, °C.	Salinity, ‰	σ_t
0	11.24	31.18	0	11.24	31.18	23.78
25	1.15	32.63	25	1.15	32.63	26.16
50	−1.21	32.89	50	−1.21	32.89	26.47
75	−1.62	33.04	75	−1.62	33.04	26.60
100	−1.66	33.05	100	−1.66	33.05	26.61
149	−1.31	33.31	150	−1.30	33.31	26.81
199	−0.21	33.68	200	−0.20	33.69	27.08
280	2.25	34.33				

Station 7237; 2 August; 49°02.5′ N., 52°08′ W.; depth 302 m.; dynamic height 971.112.

Observed values			Scaled values			
Depth, meters	Temperature, °C.	Salinity, ‰	Depth, meters	Temperature, °C.	Salinity, ‰	σ_t
0	10.87	32.26	0	10.87	31.26	23.91
24	0.38	32.44	25	0.15	32.45	26.06
49	−1.16	32.84	50	−1.20	32.85	26.44
74	−1.52	33.02	75	−1.55	33.02	26.59
99	−1.61	33.10	100	−1.60	33.10	26.65
147	−1.16	33.28	150	−1.15	33.30	26.80
197	−0.25	33.62	200	−0.15	33.65	27.05
276	2.23	34.31	(300)	2.95	34.52	27.53

TABLE OF OCEANOGRAPHIC DATA—Continued

STATIONS OCCUPIED IN 1959—Continued

Station 7238; 2 August; 48°56.5′ N., 52°22′ W.; depth 302 m.; dynamic height 971.119.

Observed values			Scaled values			
Depth, meters	Temperature, °C.	Salinity, ‰	Depth, meters	Temperature, °C.	Salinity, ‰	σ_t
0	10.86	30.84	0	10.86	30.84	23.59
25	1.21	32.44	25	1.21	32.44	26.01
50	−1.07	32.95	50	−1.07	32.95	26.52
75	−1.60	33.05	75	−1.60	33.05	26.61
100	−1.64	33.06	100	−1.64	33.06	26.62
149	−1.39	33.28	150	−1.35	33.28	26.79
199	−0.67	33.55	200	−0.65	33.56	27.00
280	2.44	34.39	(300)	3.00	34.55	27.55

Station 7239; 2 August; 48°56.5′ N., 52°22′ W.; depth 227 m.; dynamic height 971.168.

Observed values			Scaled values			
Depth, meters	Temperature, °C.	Salinity, ‰	Depth, meters	Temperature, °C.	Salinity, ‰	σ_t
0	10.25	30.95	0	10.25	30.95	23.78
24	1.05	32.08	25	0.95	32.10	25.74
49	−0.80	32.55	50	−0.85	32.57	26.20
73	−1.18	32.79	75	−1.20	32.80	26.40
97	−1.36	32.96	100	−1.35	32.98	26.55
145	−1.60	33.11	150	−1.60	33.13	26.67
194	−0.85	33.44	(200)	−0.70	33.49	26.94

Station 7240; 2 August; 48°47.5′ N., 52°45′ W.; depth 185 m.; dynamic height 971.171.

Observed values			Scaled values			
Depth, meters	Temperature, °C.	Salinity, ‰	Depth, meters	Temperature, °C.	Salinity, ‰	σ_t
0	11.10	30.92	0	11.10	30.92	23.62
25	−0.16	32.19	25	−0.16	32.19	25.87
51	−1.04	32.66	50	−1.05	32.65	26.28
76	−1.26	32.82	75	−1.25	32.82	26.42
102	−1.42	32.96	100	−1.40	32.95	26.52
152	−1.55	33.14	150	−1.55	33.13	26.67

Station 7241; 2 August; 48°44′ N., 52°56′ W.; depth 110 m.; dynamic height 971.203.

Observed values			Scaled values			
Depth, meters	Temperature, °C.	Salinity, ‰	Depth, meters	Temperature, °C.	Salinity, ‰	σ_t
0	12.72	30.89	0	12.72	30.89	23.29
28	1.01	32.00	25	2.25	31.88	25.48
55	−0.52	32.41	50	−0.35	32.36	26.01
83	−0.94	32.58	75	−0.85	32.53	26.17
106	−1.20	32.78	100	−1.15	32.73	26.33

Station 7242; 2 August; 48°38′ N., 52°43′ W.; depth 251 m.; dynamic height 971.183.

Observed values			Scaled values			
Depth, meters	Temperature, °C.	Salinity, ‰	Depth, meters	Temperature, °C.	Salinity, ‰	σ_t
0	11.87	30.80	0	11.87	30.80	23.37
25	1.39	31.96	25	1.39	31.96	25.61
51	−0.94	32.52	50	−0.90	32.50	26.15
76	−1.30	32.89	75	−1.30	32.89	26.47
101	−1.52	32.98	100	−1.50	32.98	26.55
152	−1.61	33.04	150	−1.60	33.04	26.60

Station 7243; 2 August; 48°36′ N., 52°39′ W.; depth 265 m.; dynamic height 971.166.

Observed values			Scaled values			
Depth, meters	Temperature, °C.	Salinity, ‰	Depth, meters	Temperature, °C.	Salinity, ‰	σ_t
0	11.90	30.90	0	11.90	30.90	23.45
25	0.87	32.06	25	0.87	32.06	25.72
49	−1.02	32.58	50	−1.05	32.60	26.24
74	−1.32	32.92	75	−1.35	32.93	26.51
99	−1.54	33.01	100	−1.55	33.01	26.58
148	−1.61	33.10	150	−1.60	33.10	26.65
198	−1.32	33.24	200	−1.30	33.25	26.76
247	0.49	33.75				

Station 7244; 2 August; 48°25′ N., 52°14′ W.; depth 198 m.; dynamic height 971.150.

Observed values			Scaled values			
Depth, meters	Temperature, °C.	Salinity, ‰	Depth, meters	Temperature, °C.	Salinity, ‰	σ_t
0	12.12	31.06	0	12.12	31.06	23.53
25	1.78	32.50	25	1.78	32.50	26.00
50	−0.09	32.91	50	−0.09	32.91	26.44
75	−1.28	33.02	75	−1.28	33.02	26.58
99	−1.49	33.05	100	−1.50	33.05	26.60
149	−1.64	33.11	150	−1.65	33.11	26.66
184	−1.42	33.21	200	−1.25	33.27	26.78

Station 7245; 2 August; 48°15′ N., 51°52′ W.; depth 198 m.; dynamic height 971.135.

Observed values			Scaled values			
Depth, meters	Temperature, °C.	Salinity, ‰	Depth, meters	Temperature, °C.	Salinity, ‰	σ_t
0	12.60	31.11	0	12.60	31.11	23.49
24	−0.36	32.57	25	−0.45	32.59	26.21
49	−1.30	32.90	50	−1.35	32.91	26.49
73	−1.55	33.03	75	−1.55	33.04	26.60
98	−1.63	33.08	100	−1.60	33.08	26.63
147	−1.37	33.22	150	−1.35	33.23	26.75
186	−0.99	33.40				

Station 7246; 2 August; 48°08′ N., 51°33′ W.; depth 245 m.; dynamic height 971.144.

Observed values			Scaled values			
Depth, meters	Temperature, °C.	Salinity, ‰	Depth, meters	Temperature, °C.	Salinity, ‰	σ_t
0	12.55	31.14	0	12.55	31.14	23.52
25	2.27	32.66	25	2.27	32.66	26.10
50	−0.65	32.94	50	−0.65	32.94	26.50
75	−1.38	33.02	75	−1.38	33.02	26.58
100	−1.60	33.08	100	−1.60	33.08	26.63
150	−1.27	33.22	150	−1.27	33.22	26.74
200	−1.08	33.28	200	−1.08	33.28	26.78
225	−1.09	33.27				

Station 7247; 2 August; 47°59.5′ N., 51°17′ W.; depth 170 m.; dynamic height 971.143.

Observed values			Scaled values			
Depth, meters	Temperature, °C.	Salinity, ‰	Depth, meters	Temperature, °C.	Salinity, ‰	σ_t
0	12.86	31.28	0	12.86	31.28	23.56
25	3.28	32.74	25	3.28	32.74	26.08
51	−0.12	32.93	50	−0.05	32.92	26.45
76	−1.13	33.04	75	−1.10	33.03	26.58
101	−1.44	33.10	100	−1.45	33.09	26.58
152	−1.07	33.28	150	−1.10	33.27	26.77

Station 7248; 2 August; 47°52′ N., 51°00′ W.; depth 125 m.; dynamic height 971.129.

Observed values			Scaled values			
Depth, meters	Temperature, °C.	Salinity, ‰	Depth, meters	Temperature, °C.	Salinity, ‰	σ_t
0	12.80	31.92	0	12.80	31.92	24.08
25	3.02	32.81	25	3.02	32.81	26.17
50	0.59	32.95	50	0.59	32.95	26.44
76	−1.19	33.13	75	−1.20	33.12	26.66
101	−1.21	33.20	100	−1.20	33.20	26.72

Station 7249; 3 August; 47°44′ N., 50°40′ W.; depth 150 m.; dynamic height 971.134.

Observed values			Scaled values			
Depth, meters	Temperature, °C.	Salinity, ‰	Depth, meters	Temperature, °C.	Salinity, ‰	σ_t
0	12.51	32.07	0	12.51	32.07	24.25
25	4.86	32.79	25	4.86	32.79	25.97
51	1.12	32.88	50	1.30	32.88	26.35
76	−0.66	33.10	75	−0.60	33.09	26.60
102	−0.91	33.26	100	−0.90	33.25	26.76

TABLE OF OCEANOGRAPHIC DATA—Continued

STATIONS OCCUPIED IN 1959—Continued

Observed values			Scaled values			
Depth, meters	Temperature, °C.	Salinity, ‰	Depth, meters	Temperature, °C.	Salinity, ‰	σ_t
Station 7250; 3 August; 47°35′ N., 50°22′ W.; depth 110 m.; dynamic height 971.133.						
0	11.98	32.46	0	11.98	32.46	24.64
25	5.27	32.77	25	5.27	32.77	25.90
51	1.38	32.88	50	1.40	32.88	26.34
76	−0.21	33.10	75	−0.20	33.09	26.59
102	−0.64	33.18	100	−0.60	33.18	26.68
Station 7251; 3 August; 47°25.5′ N., 50°02′ W.; depth 104 m.; dynamic height 971.118.						
0	10.77	32.71	0	10.77	32.71	25.05
25	4.75	32.86	25	4.75	32.86	26.03
51	0.57	33.04	50	0.60	33.03	26.51
76	−0.72	33.18	75	−0.70	33.17	26.68
			(100)	−1.05	33.27	26.77
Station 7252; 3 August; 47°42′ N., 49°54′ W.; depth 119 m.; dynamic height 971.124.						
0	11.41	32.59	0	11.41	32.59	24.85
25	4.42	32.83	25	4.42	32.83	26.05
50	0.72	33.00	50	0.72	33.00	26.48
75	−0.67	33.09	75	−0.67	33.09	26.61
100	−1.04	33.24	100	−1.04	33.24	26.75
Station 7253; 3 August; 47°56′ N., 49°48′ W ; depth 172 m.; dynamic height 971.131.						
0	11.59	32.22	0	11.59	32.22	24.53
25	2.98	32.72	25	2.98	32.72	26.09
50	−0.70	32.91	50	−0.70	32.91	26.47
74	−1.25	33.08	75	−1.25	33.08	26.62
99	−1.37	33.12	100	−1.35	33.12	26.66
124	−0.88	33.29	(150)	−0.20	33.56	26.98
Station 7254; 3 August; 48°10′ N., 49°43′ W.; depth 218 m.; dynamic height 971.136.						
0	11.36	31.68	0	11.36	31.68	24.16
25	2.44	32.38	25	2.44	32.38	25.87
51	−0.09	32.95	50	−0.05	32.94	26.47
76	−1.23	33.11	75	−1.20	33.10	26.64
101	−1.44	33.24	100	−1.45	33.24	26.76
152	−0.57	33.56	150	−0.60	33.55	26.98
203	0.62	33.88	200	0.55	33.86	27.18
Station 7255; 3 August; 48°33.5′ N., 49°31′ W.; depth 659 m.; dynamic height 971.065.						
0	11.69	31.32	0	11.69	31.32	23.82
25	2.55	32.78	25	2.55	32.78	26.18
49	−0.52	33.07	50	−0.55	33.08	26.60
74	−1.21	33.29	75	−1.20	33.30	26.80
98	−0.55	33.60	100	−0.45	33.62	27.04
148	1.08	33.98	150	1.15	34.00	27.25
197	2.15	34.28	200	2.20	34.30	27.42
295	2.91	34.61	300	2.95	34.61	27.60
390	3.07	34.68	400	3.10	34.68	27.64
591	3.25	34.74	600	3.25	34.74	27.67
Station 7256; 3 August; 48°39′ N., 49°28′ W.; depth 1,106 m.; dynamic height 971.028.						
0	11.91	31.38	0	11.91	31.38	23.82
25	2.37	32.52	25	2.37	32.52	25.98
50	−0.85	33.13	50	−0.85	33.13	26.65
75	−0.69	33.50	75	−0.69	33.50	26.95
101	−0.09	33.74	100	−0.10	33.74	27.11
151	1.55	34.12	150	1.55	34.11	27.31
201	2.18	34.40	200	2.15	34.39	27.49
302	2.92	34.64	300	2.90	34.64	27.63
378	3.43	34.76	400	3.45	34.78	27.68
569	3.37	34.82	600	3.35	34.81	27.72
765	3.37	34.81	800	3.40	34.82	27.73
965	3.48	34.85	1,000	3.50	34.85	27.74
Station 7257; 3 August; 49°07′ N., 49°17′ W.; depth 1,746 m.; dynamic height 970.894.						
0	9.84	31.69	0	9.84	31.69	24.42
25	1.44	33.92	25	1.44	33.92	27.17
74	2.12	34.35	50	1.65	34.20	27.38
99	2.45	34.46	75	2.15	34.35	27.46
149	2.89	34.62	100	2.45	34.47	27.53
198	3.30	34.70	150	2.90	34.62	27.62
297	3.39	34.78	200	3.30	34.70	27.64
409	3.41	34.83	300	3.40	34.83	27.73
615	3.37	....	400	3.40	34.83	27.73
822	3.32	34.84	600	3.35	34.83	27.73
1,029	3.37	....	800	3.30	34.84	27.75
1,549	3.38	34.885	1,000	3.40	34.85	27.75
			1,500	3.55	34.88	27.77
Station 7258; 3 August; 49°34′ N., 49°09′ W.; depth 1,792 m.; dynamic height 970.884.						
0	9.94	32.18	0	9.94	32.18	24.78
25	4.30	34.29	25	4.30	34.29	27.21
50	3.46	34.54	50	3.46	34.54	27.49
75	3.26	34.65	75	3.26	34.65	27.60
100	3.19	34.70	100	3.19	34.70	27.65
150	3.31	34.76	150	3.31	34.76	27.69
200	3.37	34.80	200	3.37	34.80	27.71
300	3.40	34.81	300	3.40	34.81	27.72
392	3.50	34.82	400	3.50	34.82	27.72
589	3.44	....	600	3.45	34.83	27.72
788	3.34	34.84	800	3.35	34.84	27.74
986	3.38	34.87	1,000	3.40	34.87	27.77
1,482	3.37	34.87	1,500	3.35	34.87	27.77
Station 7259; 4 August; 50°02.5′ N., 48°58′ W.; depth 1,920 m.; dynamic height 970.882.						
0	10.06	33.11	0	10.06	33.11	25.49
25	4.90	34.15	25	4.90	34.15	27.03
49	3.55	34.56	50	3.50	34.56	27.51
74	3.23	34.66	75	3.20	34.66	27.62
98	3.22	34.70	100	3.20	34.70	27.65
148	3.37	34.76	150	3.35	34.76	27.68
198	3.28	34.75	200	3.30	34.75	27.68
296	3.29	34.78	300	3.30	34.78	27.70
472	3.40	34.79	400	3.40	34.81	27.72
670	3.34	34.835	600	3.40	34.83	27.73
867	3.26	34.83	800	3.25	34.83	27.74
1,358	3.38	34.88	1,000	3.30	34.85	27.76
1,707	3.29	....	1,500	3.35	34.88	27.77
1,750	3.29	34.88				
1,758	3.29	34.88				

TABLE OF OCEANOGRAPHIC DATA—Continued
STATIONS OCCUPIED IN 1959—Continued

Station 7260; 5 August; 53°44′ N., 55°47′ W.; depth 123 m.; dynamic height 1454.991.

Observed values			Scaled values			
Depth, meters	Temperature, °C.	Salinity, ‰	Depth, meters	Temperature, °C.	Salinity, ‰	σ_t
0	10.79	27.46	0	10.79	27.46	20.98
25	0.14	32.21	25	0.14	32.21	25.87
50	−1.24	32.60	50	−1.24	32.60	26.24
74	−1.42	32.69	75	−1.40	32.69	26.31
99	−1.47	32.75	100	−1.45	32.75	26.36

Station 7261; 5 August; 53°52′ N., 55°33′ W.; depth 205 m.; dynamic height 1454.920.

Observed values			Scaled values			
Depth, meters	Temperature, °C.	Salinity, ‰	Depth, meters	Temperature, °C.	Salinity, ‰	σ_t
0	7.54	30.72	0	7.54	30.72	24.01
25	−0.69	32.38	25	−0.69	32.38	26.05
50	−1.34	32.82	50	−1.34	32.82	26.42
75	−1.29	33.00	75	−1.29	33.00	26.56
100	−1.22	33.10	100	−1.22	33.10	26.64
150	−1.16	33.20	150	−1.16	33.20	26.72
190	−1.09	33.29	(200)	−1.05	33.31	26.80

Station 7262; 5 August; 53°56.5′ N., 55°24′ W.; depth 181 m.; dynamic height 1454.905.

Observed values			Scaled values			
Depth, meters	Temperature, °C.	Salinity, ‰	Depth, meters	Temperature, °C.	Salinity, ‰	σ_t
0	7.29	30.78	0	7.29	30.78	24.08
24	−0.34	32.31	25	−0.50	32.35	26.02
48	−1.35	32.84	50	−1.35	32.85	26.44
73	−1.29	32.98	75	−1.30	32.99	26.55
97	−1.20	33.15	100	−1.20	33.17	26.70
145	−1.01	33.39	150	−1.00	33.41	26.89

Station 7263; 5 August; 54°06.5′ N., 55°04′ W.; depth 165 m.; dynamic height 1454.905.

Observed values			Scaled values			
Depth, meters	Temperature, °C.	Salinity, ‰	Depth, meters	Temperature, °C.	Salinity, ‰	σ_t
0	7.02	31.16	0	7.02	31.16	24.42
25	−0.69	32.46	25	−0.69	32.46	26.12
50	−1.24	32.80	50	−1.24	32.80	26.40
75	−1.30	32.98	75	−1.30	32.98	26.54
101	−1.34	33.15	100	−1.35	33.14	26.68
(151)	−0.88	33.50	150	−0.90	33.49	26.95

Station 7264; 5 August; 54°09′ N., 54°59′ W.; depth 174 m.; dynamic height 1454.894.

Observed values			Scaled values			
Depth, meters	Temperature, °C.	Salinity, ‰	Depth, meters	Temperature, °C.	Salinity, ‰	σ_t
0	6.74	31.16	0	6.74	31.16	24.45
25	−0.54	32.45	25	−0.54	32.45	26.10
50	−1.26	32.93	50	−1.26	32.93	26.50
75	−1.26	33.07	75	−1.26	33.07	26.62
100	−1.18	33.20	100	−1.18	33.20	26.72
150	−0.86	33.49	150	−0.86	33.49	26.94

Station 7265; 5 August; 54°26′ N., 54°26′ W.; depth 212 m.; dynamic height 1454.895.

Observed values			Scaled values			
Depth, meters	Temperature, °C.	Salinity, ‰	Depth, meters	Temperature, °C.	Salinity, ‰	σ_t
0	7.43	31.18	0	7.43	31.18	24.38
25	−0.74	32.54	25	−0.74	32.54	26.18
50	−1.38	32.82	50	−1.38	32.82	26.42
75	−1.26	33.04	75	−1.26	33.04	26.59
100	−1.19	33.18	100	−1.19	33.18	26.70
149	−0.94	33.42	150	−0.95	33.43	26.90
189	−0.19	33.77	(200)	0.05	33.88	27.22

Station 7266; 6 August; 54°43.5′ N., 53°53′W.; depth 322 m.; dynamic height 1454.843.

Observed values			Sclaed values			
Depth, meters	Temperature, °C.	Salinity, ‰	Depth, meters	Temperature, °C.	Salinity, ‰	σ_t
0	3.82	31.45	0	3.82	31.45	25.00
25	−0.48	32.74	25	−0.48	32.74	26.33
50	−1.21	33.06	50	−1.21	33.06	26.61
75	−1.09	33.34	75	−1.09	33.34	26.83
99	−0.67	33.44	100	−0.65	33.44	26.90
149	0.12	33.83	150	0.15	33.84	27.20
199	0.93	34.05	200	0.95	34.05	27.30
298	2.68	34.46	300	2.75	34.47	27.51

Station 7267; 6 August; 54°51′ N., 53°32′ W.; depth 644 m.; dynamic height 1454.714.

Observed values			Sclaed values			
Depth, meters	Temperature, °C.	Salinity, ‰	Depth, meters	Temperature, °C.	Salinity, ‰	σ_t
0	4.13	32.78	0	4.13	32.78	26.03
25	3.92	33.35	25	3.92	33.35	26.50
50	2.73	34.25	50	2.73	34.25	27.33
75	2.18	34.33	75	2.18	34.33	27.44
100	2.85	34.44	100	2.85	34.44	27.47
149	3.45	34.64	150	3.45	34.64	27.57
199	3.81	34.73	200	3.80	34.73	27.61
299	3.87	34.78	300	3.90	34.78	27.64
397	3.81	34.81	400	3.80	34.81	27.68
597	3.52	34.80	600	3.50	34.80	27.70

Station 7268; 6 August; 54°55.5′ N., 53°19′ W.; depth 1,719 m.; dynamic height 1454.685.

Observed values			Sclaed values			
Depth, meters	Temperature, °C.	Salinity, ‰	Depth, meters	Temperature, °C.	Salinity, ‰	σ_t
0	6.13	33.14	0	6.13	33.14	26.09
25	5.26	33.36	25	5.26	33.36	26.36
51	3.93	33.44	50	3.95	34.40	27.34
76	3.53	34.62	75	3.55	34.61	27.54
102	3.57	34.72	100	3.55	34.71	27.62
152	3.73	34.76	150	3.75	34.76	27.64
203	3.65	34.80	200	3.65	34.80	27.68
305	3.51	34.82	300	3.55	34.82	27.71
391	3.46	34.82	400	3.45	34.82	27.72
588	3.46	34.82	600	3.45	34.82	27.72
788	3.38	34.82	800	3.35	34.82	27.73
988	3.27	34.82	1,000	3.25	34.82	27.74
1,493	3.43	34.89	1,500	3.45	34.89	27.77

Station 7269; 6 August; 55°01.5′ N., 53°10′ W.; depth 2,186 m.; dynamic height 1454.662.

Observed values			Sclaed values			
Depth, meters	Temperature, °C.	Salinity, ‰	Depth, meters	Temperature, °C.	Salinity, ‰	σ_t
0	7.48	33.41	0	7.48	33.41	26.12
25	7.58	33.78	25	7.58	33.78	26.40
50	4.72	34.63	50	4.72	34.63	27.54
75	3.98	34.69	75	3.98	34.69	27.56
100	3.63	34.77	100	3.63	34.77	27.66
150	3.48	34.80	150	3.48	34.80	27.70
199	3.44	34.80	200	3.45	34.80	27.70
299	3.40	34.81	300	3.40	34.81	27.72
401	3.41	34.83	400	3.40	34.83	27.73
603	3.43	34.84	600	3.45	34.84	27.73
806	3.29	--------	800	3.30	34.84	27.75
1,009	3.28	34.84	1,000	3.30	34.84	27.75
1,517	3.38	34.88	1,500	3.40	34.88	27.77
2,026	3.15	34.90	2,000	3.15	34.90	27.81
2,078	3.10	34.91				
2,123	3.03	34.92				

TABLE OF OCEANOGRAPHIC DATA—Continued
STATIONS OCCUPIED IN 1959—Continued

Station 7270; 6 August; 55°14′ N., 52°45′ W.; depth 3,072 m.; dynamic height 1454.623.

Observed values			Scaled values			
Depth, meters	Temperature, °C.	Salinity, ‰	Depth, meters	Temperature, °C.	Salinity, ‰	σ_t
0	8.82	34.15	0	8.82	34.15	26.50
25	4.45	34.46	25	4.45	34.46	27.33
49	3.92	34.66	50	3.90	34.66	27.55
74	3.64	34.71	75	3.65	34.71	27.61
98	3.45	34.71	100	3.45	34.71	27.63
147	3.33	34.77	150	3.30	34.77	27.70
196	3.19	34.76	200	3.20	34.76	27.70
294	3.35	34.82	300	3.35	34.82	27.73
393	3.35	34.84	400	3.35	34.84	27.74
591	3.31	--------	600	3.30	34.84	27.75
791	3.31	--------	800	3.30	34.84	27.75
992	3.23	--------	1,000	3.25	34.84	27.75
1,494	3.39	--------	1,500	3.40	34.90	27.79
2,002	3.23	34.90	2,000	3.25	34.90	27.80
2,529	2.78	34.91	2,500	2.80	34.91	27.85
3,025	2.04	34.88	3,000	2.10	34.88	27.88

Station 7271; 6 August; 55°34′ N., 52°13′ W.; depth 3,310 m.; dynamic height 1454.644.

Observed values			Scaled values			
Depth, meters	Temperature, °C.	Salinity, ‰	Depth, meters	Temperature, °C.	Salinity, ‰	σ_t
0	9.31	34.39	0	9.31	34.39	26.61
25	5.79	34.50	25	5.79	34.50	27.20
50	4.01	34.67	50	4.01	34.67	27.54
75	3.73	34.71	75	3.73	34.71	27.60
100	3.47	34.71	100	3.47	34.71	27.63
150	3.25	34.75	150	3.25	34.75	27.68
201	3.30	34.75	200	3.30	34.75	27.68
301	3.25	34.79	300	3.25	34.78	27.70
393	3.27	34.81	400	3.25	34.81	27.73
590	3.22	--------	600	3.20	34.81	27.74
787	3.20	34.82	800	3.20	34.82	27.745
984	3.22	--------	1,000	3.25	34.83	27.745
1,489	3.42	34.84	1,500	3.40	34.84	27.74
1,981	3.38	34.88	2,000	3.40	34.88	27.77
2,436	3.10	34.90	2,500	3.05	34.90	27.82
2,938	2.52	34.87	3,000	2.40	34.87	27.86
3,216	1.62	34.86				

Station 7272; 7 August; 55°59′ N., 51°28′ W.; depth 3,530 m.; dynamic height 1454.665.

Observed values			Scaled values			
Depth, meters	Temperature, °C.	Salinity, ‰	Depth, meters	Temperature, °C.	Salinity, ‰	σ_t
0	9.87	34.54	0	9.87	34.54	26.64
25	9.62	34.54	25	9.62	34.54	26.68
50	4.31	34.70	50	4.31	34.70	27.54
76	3.90	34.71	75	3.95	34.71	27.58
101	3.40	34.72	100	3.40	34.72	27.65
151	3.21	34.74	150	3.20	34.74	27.65
202	3.17	--------	200	3.15	34.76	27.70
303	3.21	34.79	300	3.20	34.79	27.72
400	3.29	34.80	400	3.30	34.80	27.72
600	3.36	--------	600	3.35	34.82	27.73
801	3.35	34.83	800	3.35	34.83	27.73
1,001	3.36	34.83	1,000	3.35	34.83	27.73
1,502	3.39	34.85	1,500	3.40	34.85	27.75
2,003	3.34	34.90	2,000	3.35	34.90	27.79
2,498	3.04	34.91	2,500	3.05	34.91	27.83
2,994	2.66	34.91	3,000	2.65	34.91	27.87
3,390	1.98	34.885	(3500)	1.60	34.87	27.92

Station 7273; 7 August; 56°32′ N., 50°21′ W.; depth 3,658 m.; dynamic height 1454.678.

Observed values			Scaled values			
Depth, meters	Temperature, °C.	Salinity, ‰	Depth, meters	Temperature, °C.	Salinity, ‰	σ_t
0	9.66	34.53	0	9.66	34.53	26.66
25	9.21	34.53	25	9.21	34.53	26.73
50	4.30	34.64	50	4.30	34.64	27.49
75	3.86	34.69	75	3.86	34.69	27.57
99	3.51	34.73	100	3.50	34.73	27.64
149	3.26	--------	150	3.25	34.74	27.67
199	3.24	34.75	200	3.25	34.75	27.68
298	3.22	--------	300	3.25	34.76	27.69
389	3.29	34.78	400	3.30	34.78	27.70
583	3.39	34.82	600	3.40	34.82	27.73
778	3.40	34.82	800	3.40	34.82	27.73
972	3.28	34.81	1,000	3.30	34.81	27.73
1,464	3.42	34.82	1,500	3.40	34.82	27.73
1,962	3.39	34.885	2,000	3.40	34.89	27.78
2,491	3.12	34.90	2,500	3.10	34.90	27.82
2,982	2.77	34.89	3,000	2.75	34.89	27.84
3,476	1.86	34.86	3,500	1.75	34.86	27.90
3,573	1.61	34.86				

Station 7274; 7–8 August; 57°05′ N., 49°10′ W.; depth 3,678 m.; dynamic height 1454.658.

Observed values			Scaled values			
Depth, meters	Temperature, °C.	Salinity, ‰	Depth, meters	Temperature, °C.	Salinity, ‰	σ_t
0	9.16	34.54	0	9.16	34.54	26.75
25	5.40	34.62	25	5.40	34.62	27.35
50	4.05	34.67	50	4.05	34.67	27.54
75	3.59	--------	75	3.59	34.67	27.59
100	3.41	34.72	100	3.41	34.72	27.64
150	3.20	34.74	150	3.20	34.74	27.68
199	3.22	34.745	200	3.20	34.75	27.69
299	3.24	34.79	300	3.25	34.79	27.71
400	3.28	34.79	400	3.30	34.79	27.71
601	3.35	34.81	600	3.35	34.81	27.72
802	3.34	34.81	800	3.35	34.81	27.72
1,005	3.34	--------	1,000	3.35	34.83	27.73
1,508	3.40	34.84	1,500	3.40	34.84	27.74
1,990	3.38	34.84	2,000	3.40	34.84	27.74
2,507	3.15	34.895	2,500	3.15	34.89	27.80
3,006	2.76	34.91	3,000	2.75	34.91	27.86
3,403	2.05	34.88	3,500	1.75	34.87	27.91
3,551	1.59	34.865				

Station 7275; 8 August; 57°37.5′ N., 48°06′ W.; depth 3,383 m.; dynamic height 1454.658.

Observed values			Scaled values			
Depth, meters	Temperature, °C.	Salinity, ‰	Depth, meters	Temperature, °C.	Salinity, ‰	σ_t
0	8.25	34.49	0	8.25	34.49	26.85
25	8.06	34.54	25	8.06	34.54	26.92
50	5.01	34.72	50	5.01	34.72	27.47
75	4.87	34.84	75	4.87	34.84	27.58
100	4.29	34.82	100	4.29	34.82	27.63
150	4.57	34.90	150	4.57	34.90	27.67
200	4.42	34.915	200	4.42	34.915	27.69
300	4.25	34.925	300	4.25	34.925	27.72
400	3.73	34.85	400	3.73	34.85	27.715
599	3.63	34.85	600	3.65	34.85	27.72
798	3.50	--------	800	3.50	34.83	27.72
995	3.53	34.875	1,000	3.55	34.88	27.75
1,497	3.47	34.90	1,500	3.45	34.90	27.78
2,001	3.35	34.90	2,000	3.35	34.90	27.79
2,523	2.95	34.93	2,500	2.95	34.93	27.85
3,028	2.31	34.90	3,000	2.35	34.90	27.88

TABLE OF OCEANOGRAPHIC DATA—Continued
STATIONS OCCUPIED IN 1959—Continued

Station 7276; 8 August; 58°07′ N., 47°06′ W.; depth 3,182 m.; dynamic height 1454.664.

Observed values			Scaled values			
Depth, meters	Temperature, °C.	Salinity, ‰	Depth, meters	Temperature, °C.	Salinity, ‰	σ_t
0	8.48	34.50	0	8.48	34.50	26.82
24	8.27	34.59	25	8.15	34.59	26.95
49	5.49	34.64	50	5.35	34.64	27.37
73	4.15	34.66	75	4.15	34.65	27.51
97	4.26	34.78	100	4.25	34.79	27.61
146	3.93	34.81	150	3.95	34.81	27.66
195	4.10	34.87	200	4.10	34.87	27.70
292	3.99	34.87	300	3.95	34.87	27.71
394	3.71	34.86	400	3.70	34.86	27.73
592	3.51	--------	600	3.50	34.84	27.73
790	3.41	34.83	800	3.40	34.83	27.73
989	3.35	34.84	1,000	3.35	34.84	27.74
1,488	3.41	34.85	1,500	3.40	34.85	27.75
1,987	3.25	34.90	2,000	3.25	34.90	27.80
2,392	2.89	34.92	2,500	2.75	34.92	27.87
2,883	1.95	34.875	3,000	1.60	34.85	27.90
2,982	1.69					
3,032	1.48	34.84				

Station 7277; 8 August; 58°35′ N., 46°07′ W.; depth 2,561 m.; dynamic height 1454.637.

Observed values			Scaled values			
Depth, meters	Temperature, °C.	Salinity, ‰	Depth, meters	Temperature, °C.	Salinity, ‰	σ_t
0	7.62	34.53	0	7.62	34.53	26.98
22	7.47	34.58	25	7.15	34.61	27.11
45	5.46	34.85	50	5.30	34.86	27.55
68	5.14	34.89	75	5.15	34.91	27.61
91	5.21	34.95	100	5.15	34.95	27.64
135	4.98	34.95	150	4.90	34.96	27.68
180	4.79	34.97	200	4.70	34.96	27.70
271	4.41	34.915	300	4.30	34.905	27.695
392	4.05	34.885	400	4.05	34.89	27.71
590	4.01	--------	600	4.00	34.90	27.73
789	3.77	34.905	800	3.75	34.90	27.75
990	3.63	34.90	1,000	3.60	34.90	27.77
1,494	3.39	34.86	1,500	3.40	34.90	27.79
2,002	2.94	34.90	2,000	2.95	34.90	27.83
2,290	2.43	34.84	(2,500)	1.90	34.88	27.90
2,389	2.19	34.89				
2,438	2.18	34.90				

Station 7278; 9 August; 58°56.5′ N., 45°24′ W.; depth 2,451 m.; dynamic height 1454.633.

Observed values			Scaled values			
Depth, meters	Temperature, °C.	Salinity, ‰	Depth, meters	Temperature, °C.	Salinity, ‰	σ_t
0	7.85	34.78	0	7.85	34.78	27.15
26	7.84	34.77	25	7.85	34.77	27.14
51	6.95	34.90	50	7.00	34.90	27.56
77	6.03	34.98	75	6.05	34.97	27.55
102	5.78	35.03	100	5.80	35.03	27.62
154	5.21	34.99	150	5.25	34.99	27.66
204	4.90	34.98	200	4.95	34.98	27.68
306	4.49	34.945	300	4.50	34.98	27.705
372	4.28	34.915	400	4.25	34.91	27.71
560	4.01	34.915	600	3.95	34.90	27.73
751	3.55	34.86	800	3.55	34.86	27.74
944	3.50	34.885	1,000	3.50	34.89	27.77
1,435	3.36	34.91	1,500	3.30	34.91	27.81
1,935	2.97	34.91	2,000	2.85	34.91	27.85
1,976	2.87	34.92				
2,089	2.70					
2,148	2.62	34.915				

Station 7279; 9 August; 59°13.5′ N., 44°53′ W.; depth 2,058 m.; dynamic height 1454.689.

Observed values			Scaled values			
Depth, meters	Temperature, °C.	Salinity, ‰	Depth, meters	Temperature, °C.	Salinity, ‰	σ_t
0	3.35	32.96	0	3.35	32.96	26.25
25	3.72	33.10	25	3.72	33.10	26.31
51	6.83	34.79	50	6.80	34.75	27.27
77	6.56	34.95	75	6.60	34.94	27.44
103	6.14	34.98	100	6.20	34.97	27.53
153	5.76	34.99	150	5.75	34.99	27.59
205	5.46	34.99	200	5.50	34.99	27.62
308	4.93	34.96	300	5.00	34.96	27.67
402	4.62	34.95	400	4.65	34.95	27.70
604	4.11	34.91	600	4.15	34.91	27.72
806	3.84	34.91	800	3.85	34.91	27.75
1,010	3.60	34.895	1,000	3.60	34.90	27.77
1,538	3.27	34.92	1,500	3.30	34.92	27.82
1,875	2.90	34.91	(2,000)	2.70	34.88	27.83
1,977	2.74	34.89				

Station 7280; 9 August; 59°30.5′ N., 44°24′ W.; depth 951 m.; dynamic height 1454.759.

Observed values			Scaled values			
Depth, meters	Temperature, °C.	Salinity, ‰	Depth, meters	Temperature, °C.	Salinity, ‰	σ_t
0	2.58	32.41	0	2.58	32.41	25.88
25	3.11	33.82	25	3.11	33.82	26.95
50	3.29	34.30	50	3.29	34.30	27.32
75	3.65	34.49	75	3.65	34.49	27.43
101	4.04	34.62	100	4.05	34.62	27.50
150	4.68	34.80	150	4.70	34.80	27.57
200	4.94	34.89	200	4.95	34.89	27.61
301	4.90	34.90	300	4.90	34.90	27.63
363	4.81	34.95	400	4.80	34.95	27.68
552	4.78	--------	600	4.75	34.94	27.67
746	4.61	34.93	800	4.55	34.93	27.69
943	4.53	34.93				

Station 7281; 9 August; 59°34.5′ N., 44°21′ W.; depth 187 m.; dynamic height 1454.806.

Observed values			Scaled values			
Depth, meters	Temperature, °C.	Salinity, ‰	Depth, meters	Temperature, °C.	Salinity, ‰	σ_t
0	0.97	32.06	0	0.97	32.06	25.71
23	0.55	32.40	25	0.55	32.53	26.61
47	3.24	33.92	50	3.30	34.00	27.08
70	3.48	34.29	75	3.65	34.36	27.33
95	4.10	--------	100	4.10	34.60	27.48
141	4.22	34.605	150	4.25	34.61	27.47

Station 7282; 9 August; 59°37′ N., 44°17′ W.; depth 165 m.; dynamic height 1454.840.

Observed values			Scaled values			
Depth, meters	Temperature, °C.	Salinity, ‰	Depth, meters	Temperature, °C.	Salinity, ‰	σ_t
0	0.96	32.14	0	0.96	32.14	25.77
25	−0.99	32.88	25	−0.99	32.88	26.45
50	−1.00	33.08	50	−1.00	33.08	26.61
75	0.51	33.49	75	0.51	33.49	26.88
101	1.60	33.76	100	1.60	33.75	27.02
150	4.42	34.47	150	4.43	34.47	27.34

Station 7283; 9 August; 59°40′ N., 43°53′ W.; depth 165 m.; dynamic height 1454.861.

Observed values			Scaled values			
Depth, meters	Temperature, °C.	Salinity, ‰	Depth, meters	Temperature, °C.	Salinity, ‰	σ_t
0	0.46	32.29	0	0.46	32.29	25.92
25	0.04	32.44	25	0.04	32.44	26.07
50	−0.71	32.98	50	−0.71	32.98	26.53
75	−0.90	33.16	75	−0.90	33.16	26.68
100	−0.21	33.43	100	−0.21	33.43	26.87
150	2.50	34.14	150	2.50	34.14	27.26

U.S. GOVERNMENT PRINTING OFFICE : 1960 O—551829

Contribution No. 1092

Reprinted from COPEIA, 1960, No. 2, pp. 149–151, June 29
Printed in U. S. A.

RECAPTURES OF TUNA, MARLIN AND SAILFISH TAGGED IN THE WESTERN NORTH ATLANTIC.—For some years, the Woods Hole Oceanographic Institution has been conducting a program of marking pelagic gamefishes with the cooperation of many sport fishermen and their organizations and also of the U. S. Fish and Wildlife Service, the Marine Laboratory of the University of Miami, and other research establishments. Small scale experiments with marked hooks and opercular strap tags in 1951–1953 were unsuccessful. In 1954, plastic dorsal loop tags (Type G, Wilson, *Cal. Fish and Game, 39 (4):429–442,* 1953.) were used to mark small bluefin tuna, *Thunnus thynnus* (Linnaeus), off Massachusetts. Additional small bluefin tuna as well as some very large ones, and a few Atlantic sailfish, *Istiophorus albicans* (Latreille), and white marlin, *Makaira albida* (Poey), were marked with dart tags. These, first designed by the author in that year and subsequently refined in several ways, consist of a plastic streamer attached to a harpoon-like stainless steel dart which is set in the flesh of the fish. In subsequent years, dart tags, including since 1958 the all-plastic FT-1 type produced by the Floy Tag and Manufacturing Co., Seattle, Washington, have been used almost exclusively. By May, 1959, approximately 600 bluefin tuna, 750 white marlin, and 115 Atlantic sailfish had been marked, as well as many fish of other species. Tags from 5 bluefin tuna, 3 Atlantic sailfish, and 2 white marlin had been recovered up to the end of 1959 (Table 1). Those from the 3 tuna marked in 1954 were of the dorsal loop type; the others were dart tags.

The most important result is the proof of the trans-Atlantic migration of 2 bluefin tuna. It has been widely believed that the eastern and western Atlantic populations of bluefin tuna were distinct, due to slight differences in proportions and counts

TABLE 1

TAG RETURNS OF TUNA, MARLIN AND SAILFISH OBTAINED UP TO JANUARY 1, 1960
(Numbers in Parentheses Estimated)

Species	Date and Locality of		Years at Large	Size When	
	Tagging	Recapture		Tagged	Recaptured
Bluefin tuna	July 5, 1954 Martha's Vineyard, Mass. (40°54′N-70°45′W)	Aug. 18, 1954 Provincetown, Mass. (42°02′N-70°08′W)	0.1	35¾″	Not reported
Bluefin tuna	July 27, 1954 Martha's Vineyard, Mass. (41°02N-70°53′W)	Aug. 16, 1959 Bay of Biscay (43°55′N-3°25′W)	5.1	28½″	(150 lbs.)
Bluefin tuna	July 25, 1954 Martha's Vineyard, Mass. (41°02′N-70°53′W)	July, 1959 Bay of Biscay	5	30″	Not reported
Bluefin tuna	Aug. 11, 1957 Chatham, Mass. (41°36′N-69°50′W)	Aug. 30, 1959 Stellwagen Bank, Mass. (42°26′N-70°24′W)	2	(65 lbs.)	130 lbs.
Bluefin tuna	May 24, 1959 (38°37′N-68°24′W)	Aug. 20, 1959 Provincetown, Mass. (41°58′N-70°13′W)	0.25	(150 cms.)	Not reported
White marlin	Not reported[1]	April 30, 1957 Havana, Cuba (23°10′N-82°20′W)		Not reported	60 lbs.
White marlin	July 11, 1955 Ocean City, Md. (38°05′N-74°35′W)	July 18, 1959 Ocean City, Md. (38°05′N-74°35′W)	4	(7′2″)	(55 lbs.)
Atlantic sailfish	Dec. 15, 1954–Jan. 28, 1955 Stuart, Fla. (27°10′N-80°05′W)	Jan. 12, 1956 Islamorada, Fla. (24°45′N-80°30′W)	1	Not reported	6′9″
Atlantic sailfish	Jan. 28, 1958 Palm Beach, Fla. (26°45′N-79°55′W)	Jan. 14, 1959 Stuart, Fla. (27°10′N-80°05′W)	1	(7′2″)	7′2″ 40 lbs.
Atlantic sailfish	Feb. 5, 1958 Palm Beach, Fla. (26°45′N-79°55′W)	Apr. 19, 1959 Hillsboro Inlet, Fla. (26°15′N-80°00′W)	1.2	(7′) (46 lbs.)	6′11″ 51½ lbs.

---

[1] This tag was issued to a local charter boat at Ocean City, Md., in the summer of 1956. It is highly probable that the fish was tagged there in that summer.

(Ginsburg, Copeia 1953, *(1):1–10*; Rivas, *Final Report 54–1, Charles F. Johnson Found., Mar. Lab., Univ. of Miami: 1–5 mimeo,* 1954.). Much more tagging will be required to determine the extent to which the populations intermingle. Next in importance is the return connecting the newly-discovered offshore wintering grounds for medium-sized (60–300 pounds) bluefin tuna *(Reports of M/V DELAWARE Cruises, Comm. Fish. Rev., 19(5):28–29; 19(8):27–29,* 1957.; *20(7):35–36,* 1958.; *21(4):46–47, 21(7):40–41,* 1959.), with their usual summering area off Cape Cod. Two returns give interesting data on the growth of bluefin tuna although, unfortunately, exact size data were obtained at one end of each experiment only.

Page 151

The returns for marlin and sailfish are of value mainly in showing the survival of the fish and the holding power of the tags. The life span of the sailfish has been reported to be very short (de Sylva, *Bull. Mar. Sci. Gulf and Carib. 7(1):1–20,* 1957.), and it has been implied that this may also be so for the white marlin (Voss and Robins, *57–15, The Charles F. Johnson Oceanic Gamefish Investigations, Prog. Rept. No. 3, Mar. Lab. Univ. of Miami: 1–11 mimeo,* 1957.). The latter authors also questioned the value of tagging any istiophorids other than very small individuals. Sizes estimated by experienced fishermen indicate that a white marlin which was of average size (7 feet 2 inches) when tagged was not much larger (55 pounds) when recaptured 4 years later. Likewise 2 Atlantic sailfish estimated by an experienced fishing guide to have been about 7 feet long when marked were each recaptured about a year later. These results suggest that the life span of the white marlin may be fairly long, as the species attains weights of over 100 pounds, and that adult Atlantic sailfish may be tagged with a reasonable chance of recapture. The probable movement of a white marlin from off Ocean City, Maryland, to off Habana, Cuba, is of great interest, but due to the unfortunate negligence of the tagger in failing to report the necessary data, this cannot be considered as entirely certain.

This program has been directed by the author under the supervision of William C. Schroeder except during 1956–1957, when Dr. Robert H. Gibbs, Jr., now of Boston University, took over its direction while the author was on leave of absence. The excellent facilities of the Lerner Marine Laboratory were utilized during several field trips to the Bahamas. The valued assistance of these and of the many other individuals who and organizations which have cooperated is most gratefully acknowledged.—Frank J. Mather, III, *Woods Hole Oceanographic Institution, Woods Hole, Massachusetts.* Contribution No. 1092. Work supported by grants of the National Science Foundation starting in 1956.

Contribution No. 1093

(Extract from U.S. Coast Guard Bulletin No. 45, pages 49–97. Reprinted as Contribution No. 1093 to the Collected Reprints of the Woods Hole Oceanographic Institution.)

ICEBERG DETECTION BY RADAR[1]

by Thomas F. Budinger

(U.S. Coast Guard)

ABSTRACT

The behavior of ice to electromagnetic radiation is analyzed to determine the reliability of radar as an iceberg detection instrument. From absolute quantitative measurements, quantitative generalizations, and theoretical considerations the following results were obtained:

1. Iceberg ice on the Grand Banks has a reflection coefficient of approximately 0.33 and reflects radar waves 60 times less than a ship of equivalent physical cross-sectional area.
2. The maximum range of radar contact is proportional to the fourth root of the physical cross-sectional area of icebergs. A statistical relation derived from 152 observations shows that growlers normally cannot be detected at ranges over 4 miles.
3. The Grand Banks and contiguous areas of the North Atlantic Ocean exhibit conditions of subnormal radar propagation during the spring months when fog and ice hazards are most prevalent.
4. Waves over 4 feet in height might obscure a dangerous growler even with the expert use of the FTC and STC anticlutter devices. If an ice target is not picked up beyond the sea return, it will not be detected at all and a fatal collision might result.
5. Ice is not frequency sensitive. The response of ice to S- and X-bands is the same. Furthermore, there is practically no difference in the response of sea water to S- and X-bands.
6. The use of sector scan, trained radar operators, and constant surveillance of the radar scope increases the probability of detecting ice by radar.
7. Commercial radar in common use on the ships of the world today cannot be relied upon for the detection of all dangerous icebergs or fragments thereof drifting in the North Atlantic Ocean. This instrument definitely is an aid, but it does not provide an assurance against the presence of all floating ice which might sink a ship upon collision.

INTRODUCTION

Objectives

Since the inception of radar as a means for providing safe passage at sea, there have been many conflicting reports on the behavior of this navigational aid as an instrument for ice detection. These reports together with the increased speed of merchant ships and increased usage of radar have emphasized the need for precise and trustworthy information on the reliability of radar as an ice detection instrument. The primary objective of this investigation is to determine the behavior of floating ice to electromagnetic irradiation and thereby assess the efficiency of radar in providing safe navigation through potential ice areas of the North Atlantic Ocean. To attain this goal both field and theoretical research were conducted in a controlled quantitative analysis of the various parameters of radar characteristics, target characteristics, meteorology, and sea conditions.

---

[1] To be reprinted as Contribution No. 1093 in the Collected Reprints of the Woods Hole Oceanographic Institution.

Shipboard X-band radars of known overall performance were tested on icebergs and berg fragments of different sizes and shapes under varying conditions of sea and weather. Quantitative measurements of reflected power from icebergs and sea waves were made on board the U.S. Coast Guard Cutters *Acushnet, Androscoggin* and *Evergreen*; and qualitative observations of the maximum range of detection were made by participating merchant, U.S. Naval, and U.S. Coast Guard vessels. The results and interpretations of these observations together with an evaluation of the effectiveness of anticlutter devices in the discrimination of ice echoes from sea return are presented in this report.

Previous Work

The method for quantitative analysis of the ability of radar as an ice detection instrument was devised and field work carried out on the Grand Banks and adjacent iceberg areas during 1945 by the Ice Information Group, Task Group 24.7 [*1*]. This work was supplemented by investigations in 1946 by the International Ice Patrol [*2*]. The reports of these investigations were recently declassified and have been revised and consolidated by the International Ice Patrol in May 1959 [*3*]. Qualitative analyses of radar ice reports submitted by Hudson Bay shipping were made by the National Research Council of Canada during 1953 to 1957 [*4*]. The results of these surveys and additional reports from merchant ships transiting ice areas indicate that growlers are inconsistent targets, and that vessels relying on radar for safe navigation through ice infested areas might, in so doing, compromise their safety. It has been established that in calm or slight seas dangerous ice formations of all types should be detected at ranges varying from 10–15 miles for icebergs to 2–3 miles for small growlers and sea ice; however, during moderate and rough sea conditions when sea clutter extends beyond 2 miles on the PPI presentation, growlers large enough to cause serious damage to ships might not be detected. In view of the recent advances in radar systems and anticlutter circuitry and the need for a quantitative evaluation of radar reliability and anticlutter device effectiveness which could be promulgated to the marine world, the present investigation was undertaken.

Acknowledgments

This investigation was initiated by the Commandant of the United States Coast Guard and its performance came under the auspices of the International Ice Patrol, U.S. Coast Guard. The formative planning was accomplished through the efforts of Lt. Comdr. Paul A. Lutz, USCG, and Lt. Kermit R. Meade, USCG. These individuals together with Lt. Comdr. Robertson P. Dinsmore, Commanding Officer of the Office of the International Ice Patrol, provided the initial logistic support. Through the efforts of LCDR Dinsmore, who made arrangements for ship support and enlisted aid from various sea-going agencies, the field program progressed with a high caliber of organization. The writer is deeply grateful for the encouragement and facilities provided by the U.S. Coast Guard headquarters, the International Ice Patrol, and the First Coast Guard District. Without the cooperation from Coast Guard Ocean Station Vessels, military and merchant ships, this program could not have progressed. In particular, the cooperation of the Commanding Officers and the conscientious observations of the officers and men of the USCGC *Acushnet*, USCGC *Androscoggin*, USCGC *Evergreen*, and USCGC *Westwind* are acknowledged. The suggestions and criticisms of Comdr. George C. Fleming, USCG, Lt. Comdr. Paul A. Lutz, USCG, and Lt. Kermit R. Meade, USCG aided in the preparation of the manuscript.

COLLECTION OF DATA

Field Observations

There were two data collection programs:

1. Quantitative observations of the reflected power from ice targets of varying sizes and shapes under known overall radar performance and radar propagation conditions, and evaluations of the effectiveness of the common anticlutter devices documented by PPI photographs were made by International Ice Patrol vessels.
2. Qualitative observations of the maximum range of detection of icebergs and growlers were submitted in the form of completed data forms by U.S. Coast Guard, U.S. Naval, and merchant ships which frequented the ice areas of the North Atlantic Ocean in 1959.

The first program was considered critical for the thoroughness of the investigation because it provided the detailed quantitative data necessary for an objective evaluation. The Ice Patrol vessels were furnished Radar Test sets for the measurements of radar overall performance and reflected power from targets. A captive balloon instrument for recording the detailed vertical temperature and humidity distribution of the atmosphere was obtained from the U.S. Navy and a Polaroid camera PPI scope mount was fabricated. In addition to 26 usable target runs and numerous sea return measurements, an extensive evaluation of the effectiveness of anticlutter devices was accomplished. The second program was expedited by the promulgation of reporting forms to ships which

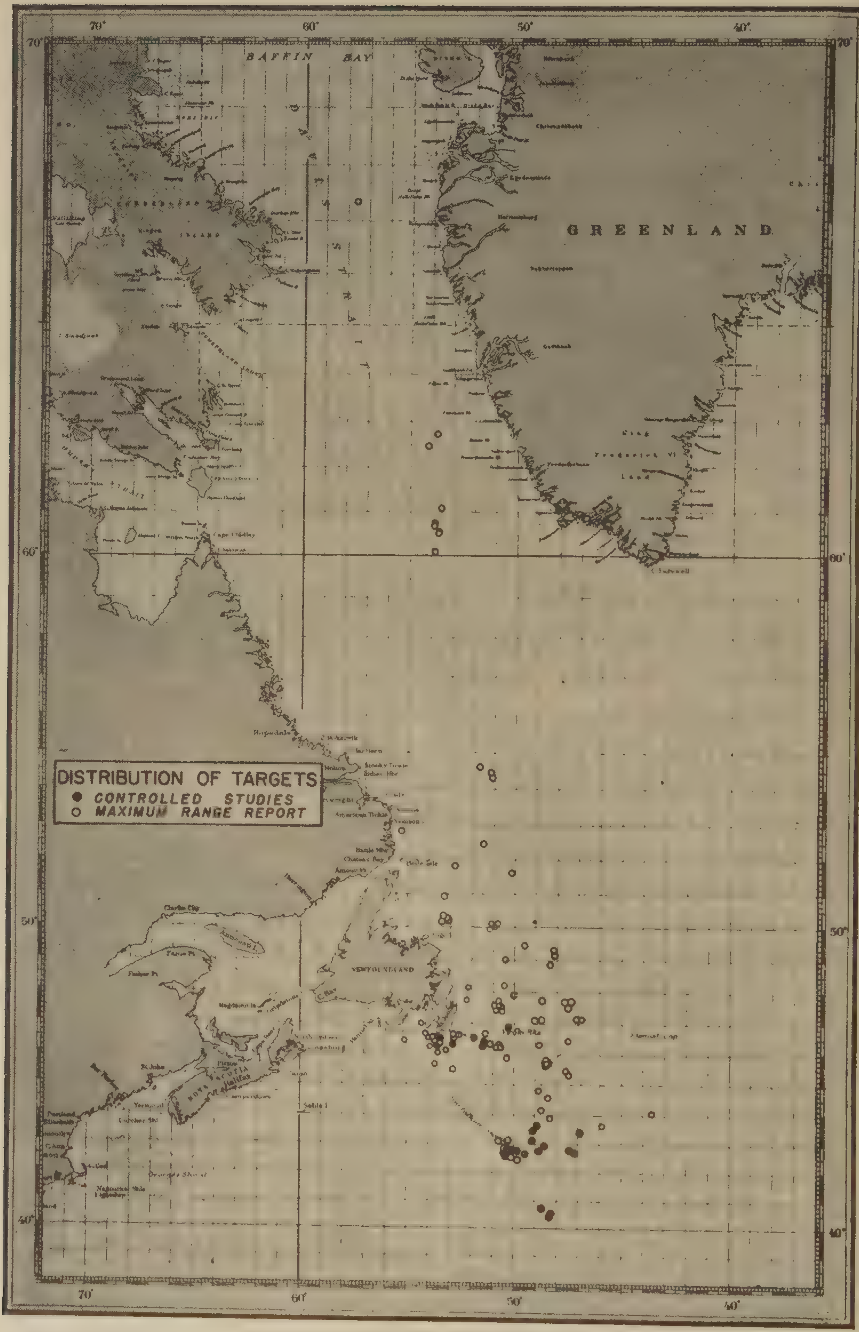
70°
60°
50°
40°
BAFFIN BAY
GREENLAND
DISTRIBUTION OF TARGETS
● CONTROLLED STUDIES
○ MAXIMUM RANGE REPORT
NEWFOUNDLAND
NOVA SCOTIA
Halifax
St. John
Portland
Sable I.
Cape Chidley
Belle Isle

FIGURE 22.—Locations of iceberg and berg fragments studied. Nineteen locations in Melville Bay and Kane Basin are not shown

operate in potential iceberg areas. These forms required the maximum range of detection and the physical measurements of height and length together with a photograph or sketch of the aspect seen by the radar at the recorded range. Of the 191 reports submitted 138 were sufficiently complete for use in this investigation. In addition, 24 observations from 1945 were utilized resulting in a total of 152 iceberg observations included in this discussion.

Location of Targets

The locations of the ice targets studied this year are shown in figure 22. Nineteen icebergs, included in this study, which were investigated by the icebreaker, USCGC *Westwind*, north of 70° North latitude are not shown. It is important to note that most of the ice targets were in the Grand Banks region or the North Atlantic shipping lanes. The controlled quantitative studies made by the Ice Patrol cutters are distinguished by the solid circles. These observations were made from March to October 1959.

Instrumentation

The X-band Radar, model AN/SPS-23, on the Coast Guard cutters *Acushnet* and *Androscoggin* was used for the bulk of the controlled reflectivity measurements and anticlutter device evaluation. The measurements of overall radar performance and the measurements of reflected power were made by use of the Radar Test set, type TS–147D/UP. This portable, microwave signal generator provided measurements of power output, transmitter and receiver frequency, and echo signal strength of reflected power from the radar targets. The reflected power measurements were made by matching an internally generated signal of known adjustable power with the target signal on an "A" scan. A block diagram of the equipment set up is shown in figure 23. The accuracy of

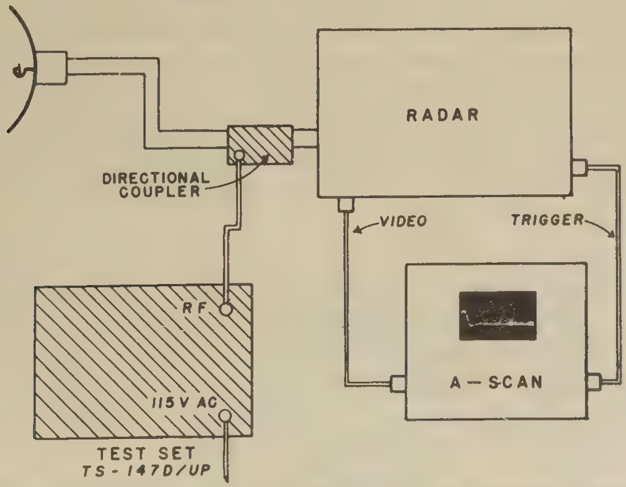

FIGURE 23.—Block diagram showing the linkage of test equipment to radar components (test set RF triggered).

power measurements was within 1.5 db and that of frequency measurements was within 2.5Mc/s. The instrument precision is considerably better than ±0.5 db and far better than the operator's judgment.

Observation Technique

The signal strength measurements were made from the maximum range of detection to the nearest practical approach (usually the upper range of the signal generator). After an iceberg target was selected, the ship steamed away from the berg on a course whose reciprocal would take it back to the target on a bearing determined by the berg aspect desired during the actual test-run. During this period the overall performance of the radar system was measured and a synthetic signal generated on the "A" scan (oscilloscope or "M" scope). When the target could no longer be discerned, the ship proceeded on the same course for a few minutes and then turned to approach the target at reduced speed (usually 6 knots). The first instant the target was painted on the PPI scope the range was recorded as the maximum range of detection and the radar antenna stopped and held on the target by manual training as necessary. For several reasons the target echo was constantly varying in amplitude and at times the scintillations were over 10 decibels in magnitude. The recorded values of reflected power are not instantaneous readings but rather the maximum signal strength observed at any time during the half minute interval ending with the time and range for which the reading was recorded. This method was inaugurated in 1945 and it is believed that a reasonable record of echo strength versus range was thus made. Continuous surveillance of the radar performance was made by test set measurements and ringing time checks. Either before or immediately after the test runs a photograph, sketch, physical dimensions and description of the berg surface were obtained. This data was used to obtain the cross-sectional area of the target presented to the radar during the test runs and to interpret the importance of morphology on signal strength. Although there was little calving noted, there was considerable change in aspect during some of the runs. Some icebergs, reaching a point of instability, rocked to and fro through an appreciable angle while others rotated. The indeterminate error of aspect change was eliminated when grounded bergs were studied.

The photographs of the PPI scope were taken with a Polaroid Land camera. Transparency film was used and the exposure time was 11 seconds. It is believed this longer exposure time on the PPI scope results in a picture which better depicts what the radar operator actually sees than the synchronized short exposures usually used.

Preparation of Results

As an investigation of this sort involves many different approaches and as many different sciences some mention of the data handling methods is necessary. The 191 observations received from all types of vessels and competencies of observers were first examined to determine if the established criteria for usuable data were met. These criteria vary with the type of measurement; however, basically all accepted reports had the maximum range of detection, and sketch and/or photograph of the maximum range aspect appropriately dimensioned. Comments on anticlutter devices were neglected for the most part as the conflicting reports indicated a good deal of subjectivity. An extensive examination of the anticlutter devices documented by radar scope photographs was made by the writer on three different Ice Patrol vessels. The evaluation of the effect of sea return is based on these controlled observations on different types of ice formations under varying sea conditions and on the writers experience with three radars in the Arctic and Antarctic while in the capacity of Combat Information Center Officer on the Coast Guard Icebreaker, USCGC *Westwind*. The photographs or sketches of the 152 accepted targets were enlarged and the physical cross sections determined. The reflected power measurements and maximum range measurements were treated statistically by the method of least squares, and throughout an effort has been made to view the data objectively.

The following discussion moves from a consideration of the maximum range of iceberg detection to a discussion of iceberg reflectivity, radar propagation over the Grand Banks area, the danger of sea return, and finally an evaluation of anticlutter device effectiveness. The observational results are compared with the theoretical in each case to allow an evaluation of the conclusions. It is hoped that the reader will not be burdened by the presentation of basic concepts which underlie the many disciplines applicable to this study.

MAXIMUM RANGE OF ICEBERG DETECTION

Empirical Expression

The maximum ranges of detection for the 152 targets studied are shown in figure 24. The best fit locus of these observations by least squares analysis is the curve:

$$R^{4.06}=3.78\times 10^{13}A \qquad (1)$$

where R is the maximum range of detection in yards and A is the physical cross-sectional area in square feet illuminated by the radar at maximum range. This fourth power relationship is in remarkable agreement with the theoretical expression for the relation of maximum range to actual area for some geometric shapes as derived from the free space radar equation:

$$R^4=K\times A$$

where K is a function of receiver sensitivity, antenna gain, and transmitter power output. Because the characteristics of all the radars used were very similar, this grouping of observations from various types of radars was justified. Equation (1) is an expression which relates the maximum range to be expected to the physical cross-sectional area of an

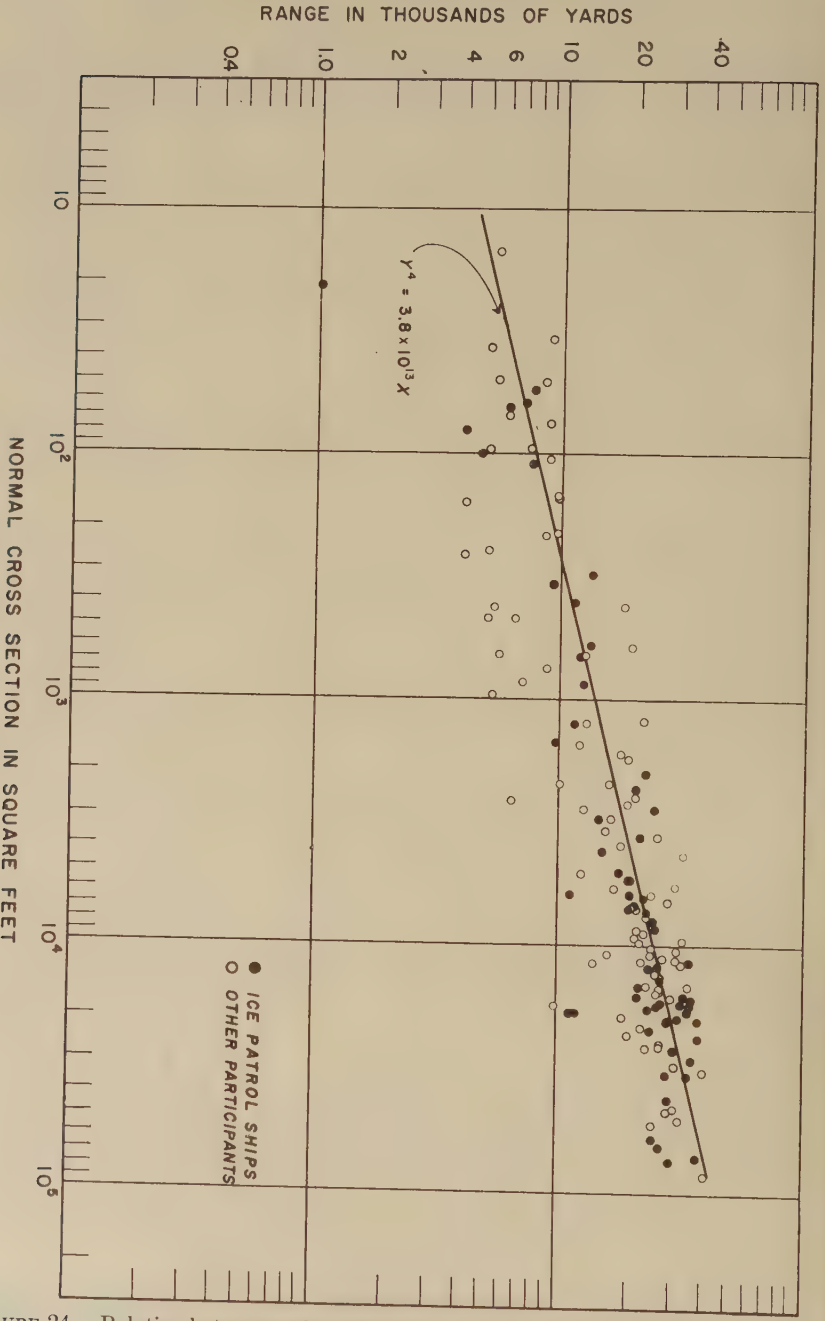

FIGURE 24.—Relation between radar maximum range of detection and iceberg physical cross-sectional area illuminated at the maximum range.

iceberg. Although the index of correlation (rho) is 0.81, the standard deviation is ±5,600 yds. A poor deviation is to be expected considering the diversified sources of information and the fact that the geometric shape and therefore target gain of icebergs changes considerably from target to target. Furthermore, from considerations to be presented later, the value of the constant 3.78×10^{13} may change considerably with the dielectric constant of the ice surface. In this respect it is important to note that 80 percent of the observations were made on icebergs which were in or approaching the shipping lanes. As will be seen later, the air temperature near a floating ice formation materially effects the range of detection; and the constant, K, should decrease with a decrease in temperature, and therefore with an increase in latitude. In figure 24 the Ice Patrol vessels' controlled observations are distinguished by solid circles. The radar overall performance during these maximum range observations was measured and found to be practically the same for all cases.

Theoretical Detection Range of Growlers

Based on equation (1) we can determine the magnitude of the maximum detection range for the most dangerous of all ice formations, growlers. Dangerous growlers from the exposed size of 10 sq. feet to 100 sq. feet (usually about 10 feet high and approximately 250 tons) can be detected at approximately 2 and 4 miles, respectively. Immediately, the danger to a fast moving vessel becomes apparent. The possibility that the curve presented in figure 24 might flatten out for the lower cross sections was precluded by examination of 26 growler observations made by Hudson Bay shipping [4] and 18 growler observations by the icebreaker *Northwind*. These indicate that the expected range is even lower than that presented here.

REFLECTIVITY OF ICEBERGS

Reflected Power Measurements

The behavior of ice as a reflector can best be measured by either laboratory or field observations of the quantity of power returned from an iceberg. As laboratory procedures obviate evaluation of the many parameters of reflection interference, iceberg shape, propagation, etc., it was decided to make the quantitative study of iceberg reflection on actual targets in the vicinity of the shipping lanes or similar environs where possible. The method devised in 1945, mentioned earlier, was used with few modifications. The echo signal strengths from the maximum range of detection to the upper limit of the test set were measured on 26 approaches to targets of various sizes and shapes. A typical run is illustrated in figure 25. On this large target (165 by 380 feet) duplicate runs were made to determine the precision of the observation technique. These two series of observations, indicated by open and solid circles on figure 25, show close agreement and similar results were observed on another duplicate set. The ordinate is the power received in decibels above minimum discernible signal. This method of presentation provides the best graphic illustration of what the radar operator sees while approaching a target. The slope of the least squares best fit for the two runs is −4.3 in both cases. This is in good agreement with the theoretical given by the free space radar equation.

$$\frac{P_r}{P_t}=\frac{G^2\lambda^2\sigma}{(4\pi)^3R^4} \tag{2}$$

Where P_r is the reflected power received, P_t the power output, G the antenna gain, λ the wave length, σ the radar cross-section, and R the range. This equation indicates that the power received should follow an inverse fourth power law. The validity of this equation is well known for most targets, and was first demonstrated to be approximately true for ice targets in 1945 and 1946. To provide a means of observational comparison between iceberg reflected power and ship reflected power, the echo signal strength from the retreating stern of the *Evergreen* was also measured (fig. 25). In remarkable agreement with the theoretical, the best fit locus for that run has a slope of −4.0 to 18,000 yds and then changes abruptly to approximately a −8 slope. This slope change in attenuation rate is also in conformance with the theoretical. If perfect reflection from the sea is assumed at low grazing angles, then the free space radar equation (2) becomes

$$\frac{P_r}{P_t}=\frac{4\pi G^2(h_1h_2)^4\sigma}{\lambda^2R^8} \tag{3}$$

for targets at low angles (i.e. $2h_1h_2/R\lambda<1$) where the terms have the same meaning as in (2) and h_1 and h_2 are the heights of the antenna and target, respectively. This effect is also quite apparent on most of the iceberg echo strength observations of this year and of 1945 and 1946. The few cases where the change is not noticeable can be attributed to the rough sea surface and concomitant diminished reflection reinforcement when the iceberg echo measurements were made.

The free space radar equation (2) can be further modified by a path-gain factor which is a function of the geometry of the transmission path, the electromagnetic properties of the sea, the reflective and refractive properties of the atmosphere, frequency, etc. This factor is dependent upon the specific conditions at a particular time, and in view of the generalized approach of this paper, dealing with a wide variation of propagation and sea conditions, no further consideration will be given to the path-gain factor. However, a treatment of the prevalent meteorological conditions and expected anomalies in radar propagation over the Grand Banks will be given in a later section.

Fluctuating Echoes

There was considerable concern over the rapidly fluctuating signal and early in the field work a study was made to determine the time variations

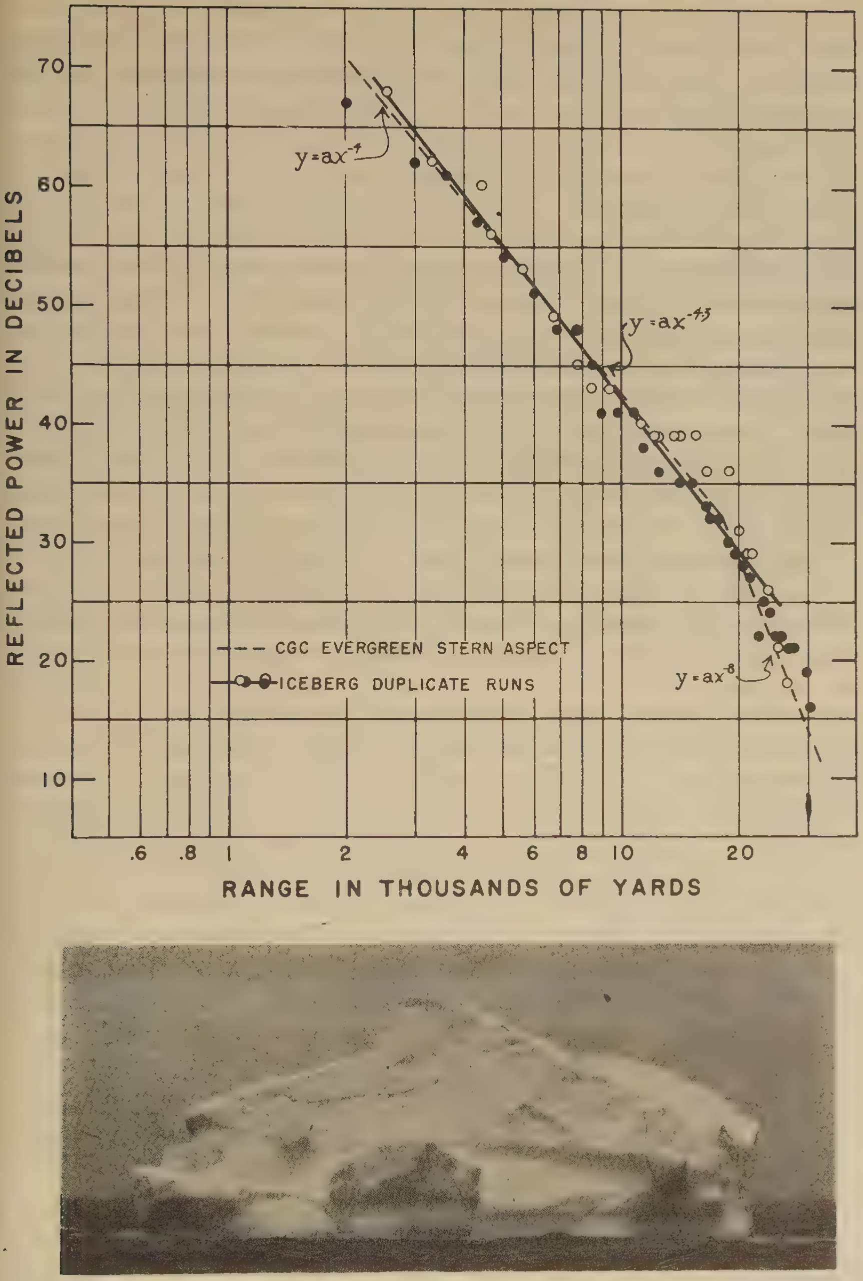

FIGURE 25.—Reflected power expressed in decibels above minimum discernible signal plotted as a function of range, logarithmic scale, for a large iceberg (43,900 sq. feet) and the stern of the CGC *Evergreen* (740 sq. feet). The agreement between duplicate runs on the same aspect (165 by 380 feet) and the similarity of iceberg attenuation rate with that observed on a ship target are illustrated by least squares, best fit curves.

of the maximum echo strength received at a constant range. Measurements were made both on the first field trip by the writer and again during the latter part of the field work by personnel experienced with the procedure. The fluctuation amplitude of these measurements agreed in both cases and the results of the latter observations are shown in figure 26. The bottom curve is the top curve normalized to a constant range of 13,150 yards by equation (2). The mean deviation, regardless of sign, for these 24 normalized observations is 1.9 decibels. During the observation period the wind increased from 16 kts at 1230 to 20 kts at 1400, and decreased to 8 kts at 1500. There is a slight correlation between the weather conditions and the trend of the fluctuations and it is believed that a change in the path-gain factor can partly account for the increased amplitude of fluctuations between 1400 and 1500. A comparison of the observations of figure 26 with those made by the Radiation Laboratory, Massachusetts Institute of Technology, indicates that these fluctuations are certainly within the expected magnitudes. It is concluded that, although the measurement procedure is at best rather coarse, major trends in propagation anomalies and changes should be detected by the technique of matching the echo observed over a 30-second period. This time series indicates, also, that the time-space fluctuation of an iceberg echo is comparable to that from a ship. The micro scintillations were not measured.

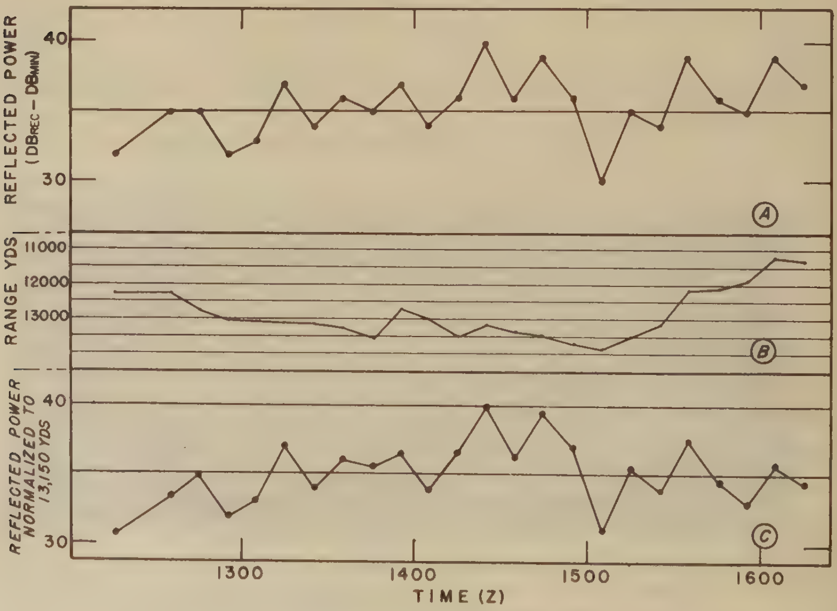

FIGURE 26.—Time series observations of reflected power at near constant range and aspect from an ice formation. Curve A is the actual observation, B the change in station on the target, and C the power curve normalized to constant range.

Iceberg Effective Echoing Area

In the free space radar equation:

$$\frac{P_r}{P_t}=\frac{G^2\lambda^2\sigma}{(4\pi)^3R^4} \tag{2}$$

The term σ is defined as the effective echoing area or the radar cross section and has the dimensions of length squared. This parameter may be thought of as the area of a perfectly conducting sphere which is equivalent to the echoing strength of the target; or, as the effective scattering cross section which a target would have if it scattered as much energy in all directions as it actually does scatter in the direction of the radar receiver. The dependence of the radar cross section on the shape of a target is best illustrated by considering that the radar cross section of a large metallic plate placed perpendicular to incident radiation is 1,200 times that of a sphere of equivalent area. The radar cross section of a battleship is approximately 3.2×10^7 sq. feet and that for a 10,000 g.r.t. merchant ship approximately 1.2×10^4 sq. feet. The value of σ, for a given shaped target may not vary in direct proportion with its projected area; in fact, the direct variation is true only for a few simple geometric forms (i.e. sphere, curved surface).

Seemingly the task of analyzing the aspect of the iceberg targets is an insurmountable one in view of the fact that the micro and macro morphology of icebergs varies considerably from berg to berg and unquestionably no two bergs are alike. The theoretical computation of the effective echoing area based on the geometrical shapes involved is neither meaningful nor feasible for icebergs. However, as the effective echoing area does provide an excellent means of evaluating ice as a radar reflector it was desirable to determine the magnitude of this parameter. Not until the empirical relation between the maximum range of detection and the physical cross-sectional area was derived was it possible to attempt this.

Iceberg Ice Reflection Coefficient

Because the correlation ratio for the empirical relation (1):

$$R^4=3.8\times10^{13}A \tag{1}$$

is 0.81, we may assume that the theoretical fourth power relation between range and actual cross-sectional area is true for icebergs. However, as mentioned earlier, only a few geometrical shapes show a direct variation of the effective echo area with the actual area. The sphere segment has a radar cross section given by

$$\sigma=\pi r^2 \tag{4}$$

where σ is the radar cross section and r is the radius of the perfect conductor. The segment may be viewed either on the concave or convex side.

Equation (4) is also valid for a nonspherical curved surface, in which case r is the geometric mean of the two principal radii of curvature. These shapes adhere to this direct relationship if the diameter of the shape perpendicular to the incident beam is greater than the incident wave length. A direct relationship also exists between the disc at random orientation and its radar cross section and it can be shown [5] that the average effective echoing area of simple shapes in random orientation is given by:

$$\sigma = 0.5A$$

where A is the total physical cross-sectional area of the aggregate of surfaces. It is not difficult to imagine the face of an iceberg as being shaped similar to an aggregate of concave and convex curved surfaces of diameter greater than 1.3 inches (X-band wave length); in fact, the processes of melting leave an iceberg with a pocked-like micro morphology. Based on these arguments an idealized iceberg model surface may be defined as an aggregate of perfectly conducting surfaces larger than 1.3 inches in diameter. The reflection coefficient of these conducting shapes is 1.0 and the ratio of effective echoing area to cross-sectional area is given by:

$$\frac{\sigma}{A} = 0.5 \tag{5}$$

These considerations lead to the computation of iceberg effective area coefficient and reflection coefficient. At the maximum range of detection the free space radar equation becomes:

$$\frac{P_{\min}}{P_t} = \frac{G^2\lambda^2\sigma}{(4\pi)^3 R^4_{\max}} \tag{6}$$

where $P_{\min}$ is the minimum discernible signal. Substituting equation (1) for $R_{\max}$ and transposing we have the expression for the ratio of effective echoing area to actual area:

$$\frac{\sigma}{A} = \frac{P_{\min}(4\pi)^3 K}{P_t G^2 \lambda^2} \tag{7}$$

By substitution of the following average values for terms:

Absolute Antenna Gain $= 10^3$
Wave length $= .032$ meters
$P_{\min}$ $= 10^{-12}$ watts
P_t $= 10^{+4}$ watts
K $= 3.8 \times 10^{13}$ yd^4/ft^2
$= 2.85 \times 10^{14} m^2$

this expression becomes

$$\frac{\sigma}{A} = 0.056. \tag{8}$$

It is immediately apparent that the reflectivity of icebergs is indeed poor as the same ratio for a flat metal plate is equal to 1,200.

The reflection coefficient (ratio of reflected energy to incident energy) can be computed as follows. The effective echo area is proportional to the power ratio as seen from equation (7). But the power ratio is proportional to the square of the field intensity; therefore, we can write:

$$\frac{\dfrac{\sigma_i}{A_i}}{\dfrac{\sigma_m}{A_m}}=\frac{|R_i|^2}{|R_m|^2} \tag{9}$$

where R_i and R_m are the reflection coefficients of the real and idealized icebergs, respectively. Taking into account the average aspect reflection for the model conducting iceberg and the Grand Banks icebergs, and substituting 1.0 for R_m, equation (9) becomes

$$R=0.33$$

where R is the average reflection coefficient of Grand Banks and North Atlantic Ocean iceberg ice. Confidence in the arguments used to arrive at this coefficient is given by its close agreement with the theoretical values of 0.25 for a dry iceberg and 0.32 for a melting iceberg derived below.

Theoretical Reflection Coefficient

As has been shown the computed reflection coefficient from various arguments based on field observations is 0.33. It remains to compute the reflection coefficient based on theoretical considerations. Either by consideration of Fresnel's equations or the intrinsic impedance derived therefrom, the reflection coefficient at normal incidence becomes

$$\frac{\sqrt{\epsilon_2}-\sqrt{\epsilon_1}}{\sqrt{\epsilon_2}+\sqrt{\epsilon_1}}=R=\frac{Z_2-Z_1}{Z_2+Z_1} \tag{10}$$

where ϵ is the dielectric constant, Z the intrinsic impedance, and R the reflection coefficient modulus. The electromagnetic properties of a medium are completely described by the complex dielectric constant:

$$\epsilon_c=\epsilon_r-j\epsilon_i=\epsilon_r-2j\frac{K}{f}=(n-j\zeta)^2 \tag{11}$$

where

ϵ_c = the complex dielectric constant or complex relative permittivity
K = conductivity in electrostatic units
f = frequency in cycles per second
n = refractive index
ζ = absorption coefficient

The anomalous dispersion of radio frequencies exhibited by polar molecules has been discussed by Debye [*6*] and others; and it has been shown that the water molecule shows anomalous dispersion in the frequency range 10^3 to 10^6 Mc/s [*7*]. However for ice, the maximum dispersion is near 6 Kc/s at a temperature of -2°C. and occurs at even lower frequencies as the temperature decreases; and the observations of Errera [*8*] in the frequency range between about 0.4 Kc/s to 37.5 Kc/s indicate that ice behaves as if it were a polar liquid with very high internal friction. However, by use of the formulae Debye [*6*] presented to calculate the generalized dielectric constant (liquid formula) we find that the imaginary part of the complex dielectric constant, ϵ_i, becomes nearly zero in the frequency range above 1000 Mc/s. As Saxton [*9*] has summarized, the most recent observations of Lamb [*10*] together with those of Smyth and Hitchcock [*11*] indicate that the dielectric constant of pure ice is 3.05, and as no absorption band exists between 30 Mc/s and 30,000 Mc/s (the upper limit of observations) this value may be assumed constant and equal to 3.05 in the radar bands. It is therefore easily derived from equation (11) that there should be no difference in the behavior of S- and X-band frequencies on ice. By equation (10) the reflection coefficient of pure ice is 0.272.

However, iceberg ice is far from pure, being composed of up to 15 percent co-volume of air and varying amounts of melt water depending on the meteorological conditions. As far as the writer is aware, there are no direct measurements of the dielectric properties of aerated ice, iceberg ice, or snow. It is important to determine the importance of the air and melt water effects on the magnitude of the reflection coefficient in order to assess the most probable theoretical value for icebergs. In order to do this it is necessary to make certain assumptions concerning the characteristics of the ice-air-water mixture on the surface of a Grand Banks iceberg. First, it is assumed that the mixture of ice and air is homogeneous and the internal force of the "particles" is zero; the latter is true in the case of a cubic crystal or non-associated liquids [*12*]. Based on the assumption that the internal force is negligible and that Mosotti's computations are correct; i.e., the relation between the dielectric constant and molecular polarizability is given by

$$\frac{\epsilon-1}{\epsilon+2}=N\frac{4\alpha}{3\pi} \qquad (12)$$

where N is Avagadro's number, and α is the molecular polarizability, Debye [*6*] derived an expression for the relation of the dielectric constant to the polarization of the components of a binary solution:

$$\frac{\epsilon-1}{\epsilon+2}\cdot\frac{M_1 f_1+M_2 f_2}{p}=P_1 f_1+P_2 f_2 \qquad (13)$$

where M_1 and M_2 are the molecular weights of the two components, f_1

and f_2 the mole fractions, p the density, and P_1 and P_2 the polarizability From equation (12) we can derive

$$P=\frac{M(\epsilon-1)}{p(\epsilon+2)};$$

therefore,

$$\frac{\epsilon-1}{\epsilon+2}\cdot\frac{M_1 f_1+M_2 f_2}{p}=\frac{M_1 f_1}{p_1}+\frac{M_2 f_2}{p_2} \tag{14}$$

which is an expression for the relation of the resultant dielectric of a mixture to the concentration of two components. This equation is applied below to the two-phase system of air-ice and to the three-phase system of air-ice-water. The latter, of course, predominates on the surface of Grand Banks and North Atlantic Ocean icebergs. The assumptions prohibit a precise quantitative determination of the reflection coefficient, and the results of computations based upon equation (14) can be expected to indicate only the magnitudes of the effects of air and water contamination of pure ice. The values for the terms in equation (14) are known with some degree of accuracy however. The entrapped air is known to have the same composition as the atmosphere, and is normally under a slight pressure. The sublimation of the ice surrounding an air "particle" would provide the maximum vapor pressure of moisture and at 0°C the density of the entrapped air becomes 0.00132 gms/cc and the "molecular weight" very nearly 30. The density of pure ice is 0.9167 gms/cc and the relative permittivity is 3.05. Based on these quantities and equations (10) and (14), the lower portion of the curve presented in figure 27 was constructed. As the second-right term of equation (14) becomes zero for all practical purposes in the case of air and ice mixture, examination of the curve reveals the relation between ice density and reflection coefficient is very approximately given by

$$R=0.029p \tag{15}$$

The measurements of iceberg density by Barnes [*13*], Smith [*14*], the writer, and others indicate that a density of 0.86 gms/cc is close to the mean. At this density the reflection coefficient is 0.26 (slightly lower than that for pure ice). This simple relation between reflection coefficient and density seems to fit the observations for snow covered forests, and frozen muskeg and gravel measured from aircraft [*15*]. However, the simple mixture of ice and air is rarely met on an iceberg approaching or in the shipping lanes. As the ice begins to melt the presence of even a small amount of liquid water becomes of considerable importance. The problem of melt water was handled by the same arguments used for the air-ice system. The upper portion of the curve in figure 27 was derived using aerated ice of 0.86 density as one component and pure water as the other in equation (14), and a modulus of 80 for the complex dielectric constant

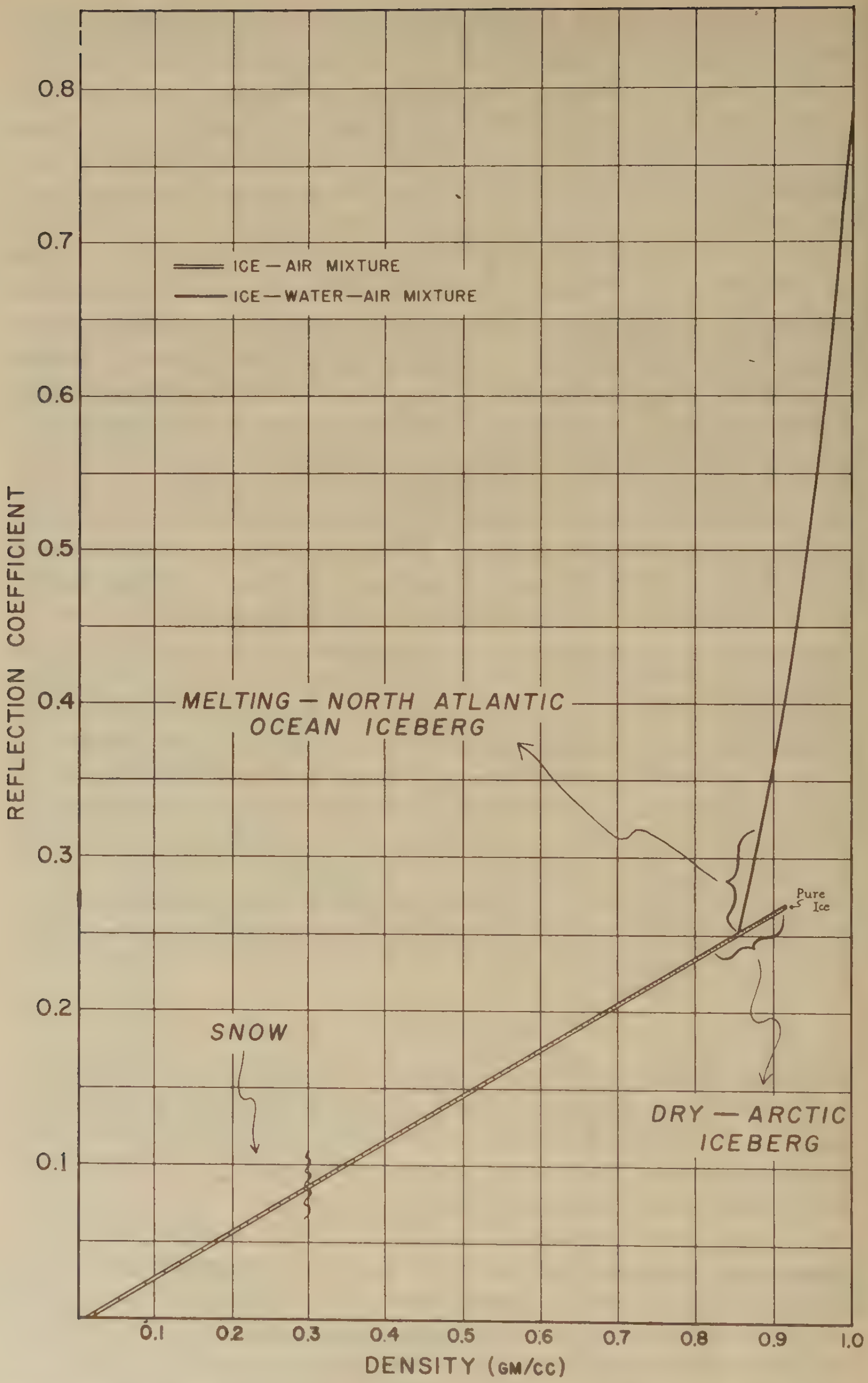

Figure 27. Relation between ice density and reflection coefficient. Lower curve represents ice-air mixture and upper curve represents ice-air-water mixture.

of fresh water. From the upper portion of figure 27 it is readily apparent that the reflection coefficient increases rapidly with addition of melt water. A wet iceberg might be considered to have a surface consisting of approximately 15 percent water by volume. This corresponds to a reflection coefficient of 0.32. In the above arguments the reflection from the surface veneer of melt water is neglected as field observations indicate that the thickness of this melt water rarely exceeds that of $\frac{1}{4}$ wave length (0.3 inches for X-band and 1.0 inches for S-band). The theoretical results shown in figure 27 are in good agreement with the computed value of 0.33 based on the maximum range of detection.

It follows from the foregoing that insofar as the mean temperature is considered a function of latitude the reflection coefficient and therefore the maximum range of detection might decrease with increasing latitude and cloud cover. It should be noted, also, that the precipitation of moisture from fog on a cold iceberg might lead to increased ranges.

Qualitative Comparison Between Iceberg and Ship Reflection

Both approaches to the determination of the reflection coefficient presented above either are purely theoretical or make assumptions which cannot readily be proved valid or otherwise. The most straightforward approach is to compare the reflection from a ship to that from an iceberg, the comparison being made under identical atmospheric or propagation path conditions. On three occasions the echo from a ship and an iceberg at nearly the same range were photographed on the PPI presentation. Two of these occasions are shown in figure 28.

Figure 28 (top) illustrates the relative intensities of an echo from an iceberg (010°T; 18,200 yds) and a merchant ship, SS *Mormacpenn* (047°T; 19,000 yds) on the 20-mile range scale. The illuminated cross section of the iceberg (90 by 460 feet; 22,680 sq. feet) was approximately 46 times that of the ship, however the blip intensity was considerably less. On another occasion shown by figure 28 (bottom), the USNS *Alatna* (341°T; 6,000 yds) was photographed with a large iceberg (150°T; 7,000 yds). Here again, although the area of the iceberg (150 by 400 feet; 20,600 sq. feet) was 34 times that illuminated on the *Alatna* (6,000 sq. feet), the berg blip was less intense.

Quantitative Comparison Between Berg and Ship

Although the qualitative evidence supports the reflection coefficient computations it remained to make a quantitative measurement of the comparison between an iceberg and a merchant vessel. The reflection coefficient could not be determined due to the difference in geometry and therefore gain of the two types of targets; however, direct measurement of reflected power from a ship and iceberg would afford a means of comparing the radar cross sections of the two objects.

ceived from the ship to that received from the iceberg was 200 but because the illuminated ship cross-sectional area was 3.2 times that of the iceberg (c.f. fig. 29) and because a linear relation has been shown to exist

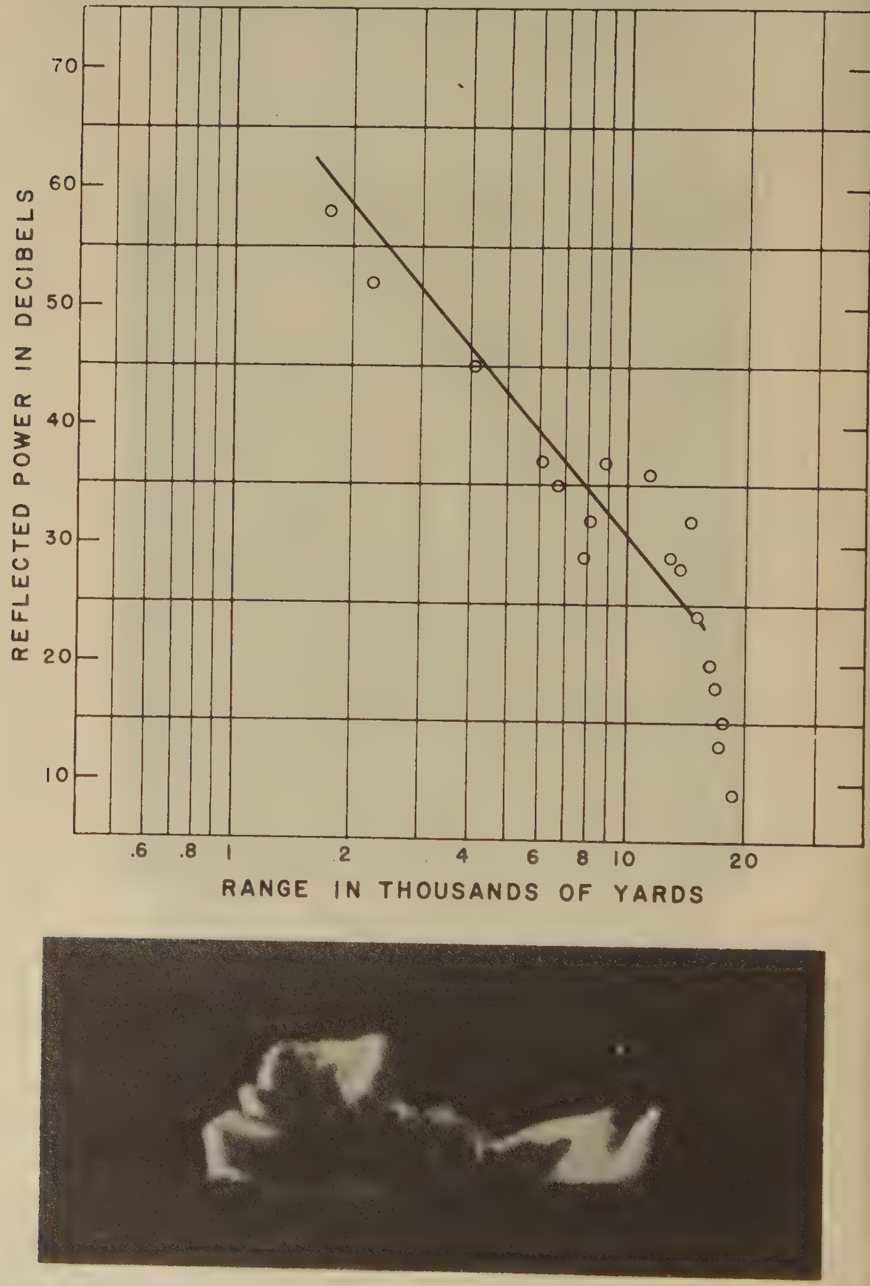

Figure 30.—Reflected power expressed in decibels above minimum discernible signal plotted as a function of range for a small iceberg (27 by 84 feet; 1,460 sq. feet). Locus is least squares best fit.

between iceberg radar cross section and actual cross section, this power ratio becomes 62.5 for equivalent area targets. By consideration of equation (2) it is evident that this ratio represents the ratio of effective echoing areas for equivalent-sized ship and iceberg targets. In other words this ship reflected 62 times better than an equivalent size iceberg. Although this value seems high a similar approach to the comparison of effective echoing areas by more reliable observations gives similar results. Examination of figure 25 reveals that the reflected power curves for both the stern of the CGC *Evergreen* (740 sq feet) and the large iceberg (43,900 sq. feet) are practically identical. The ratio of areas is 59.

Reflectivity Summary

From the above considerations we can arrive at the conclusions that iceberg ice has a low reflection coefficient very approximately 0.33 and that this coefficient might increase with the addition of melt water; and that Grand Banks icebergs appear to reflect 60 times (16 decibels) less than a ship of equivalent area.

ASPECT

The fraction of the power incident upon a target which will be returned to the radar antenna is dependent on a parameter involving the dimensions and orientation of the target, and usually the wavelength of radiation. In this discussion we shall speak of both the radar cross section (equivalent echoing area) and the target gain. Target gain may be thought of as the degree to which a target directs the radar beam back to the receiver and is proportional to the radar cross section, i.e.:

$$G_r = \frac{\sqrt{4\pi\sigma}}{3\lambda}$$

The dependence of these parameters, and therefore the reflected power, on target orientation or aspect is very great, and the reflected power from less complex targets than icebergs has been reported to change as much as 20 decibels with a change of orientation of only few degrees. The computation of radar cross sections for targets of complicated geometric design is one that has repeatedly defied attempts of thorough analysis, although recently the use of computers has allowed the problem to become feasible. As no two icebergs or iceberg orientations are similar it would be fruitless to compute the theoretical radar cross section for one or many icebergs. Fortunately, as shown earlier the complex nature of the iceberg aspect problem was simplified by the discovery of the direct relation between the radar cross section and the actual cross section. The quantitative generalization of this problem has many exceptions. An iceberg with a smooth and vertical face (c.f. fig. 31) normally conforms to the relations derived earlier; however, the icebergs of complex configuration show deviations which at times are quite remarkable, but in general conform qualitatively to what might be expected. Of interest in this respect is the large pinnacled iceberg whose shape might lead to di-

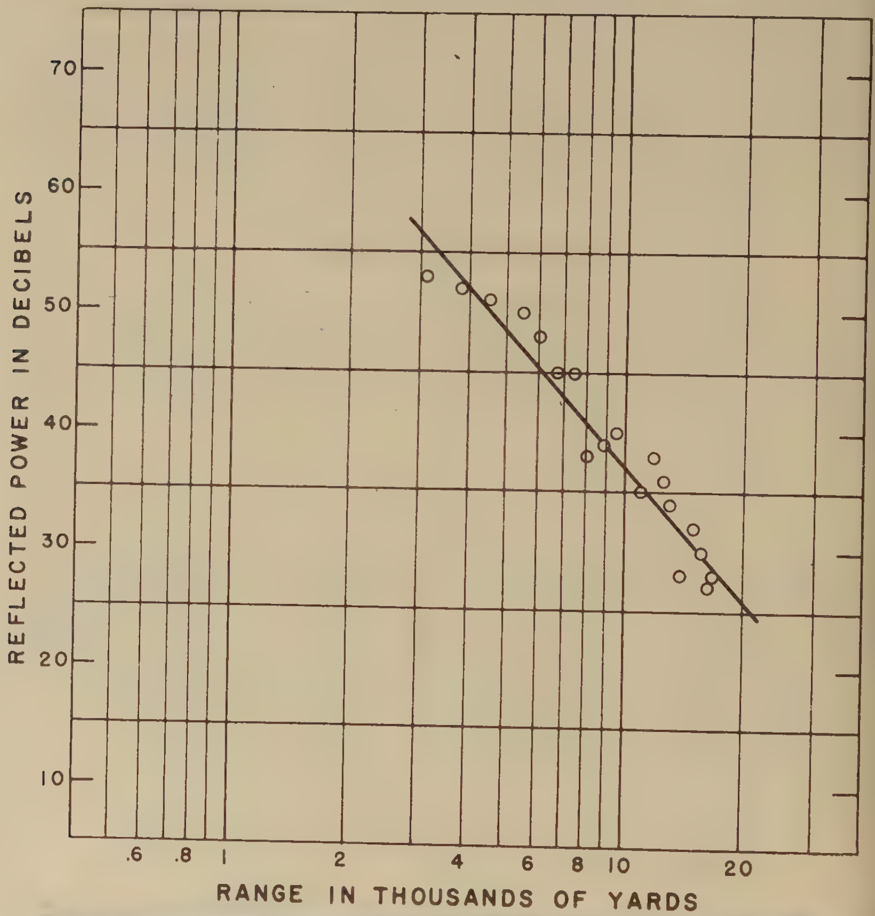

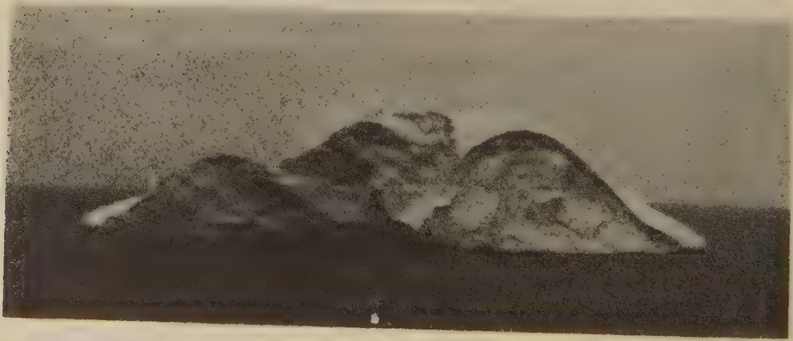

FIGURE 31.—Reflected power expressed in decibels above minimum discernible signal plotted as a function of range for vertical face aspect of the large iceberg (80 by 334 feet; 18,040 sq. feet).

rectivity of the reflected power with a resulting rapid increase in the echo strength with decrease in range. This was, in fact, the case as shown by figure 32. The locus of these observations shows an inverse sixth power attentuation with range. The other shape which is an exception to the idealized model iceberg equations is the wedge- and subdued dome-shaped iceberg or growler. Reduced ranges are to be expected for these shapes, and on five documented occasions, low domes- and/or wedge-shaped growlers were not detected by radars in peak condition operated by the writer or experienced radar operators.

GRAND BANKS RADAR PROPAGATION

Meteorology

In many instances those conditions which give fog and create the most need for radar also cause subnormal propagation of radar waves. When moist warm air from the Gulf Stream, or Atlantic Current continuation thereof, flows over the colder water of the Labrador Current and Grand Banks, advection fog normally results. This is a common occurrence in the Grand Banks area during much of the ice hazard season. In fact, the Grand Banks off Newfoundland and the potential iceberg drift area of the North Atlantic Shipping Lanes are the poorest visibility areas of all the oceans during the entire year with the exception of an area south of the Kamchatka Peninsula, Pacific Ocean, during June, July and August [*16*]. The advection fog is often accompanied by strong southerly winds and concomitant radar sea return. The combination of fog, moderate winds and derelict hazard is the rule rather than the exception; and consideration should be given to atmospheric conditions of an area being transited before the reliance of radar is evaluated. Although the average propagation conditions on the Grand Banks has not been determined yet; a qualitative discussion of this important topic is given below.

Radar Propagation

Under "standard" atmospheric conditions, air temperature and moisture content decrease uniformly with height above the sea surface resulting in a uniform decrease in the index of refraction. This standard rate of variation in refractive index is given by

$$\frac{dn}{dh} = -0.039 \times 10^{-6} \text{ per meter.}$$

Because microwaves bend toward a level of relatively higher index of refraction, radar waves bend downward in the standard atmosphere. This downward curvature of approximately $\frac{1}{4}$ the earth's curvature results in an extension of the radar horizon to about 15 percent more than the geometric horizon or about 8 percent more than the visual horizon. Whenever the rate of variation deviates considerably from the standard rate either by deviation in slope or in linearity, changes occur which might prove either favorable or unfavorable for radar propagation. The relation of temperature, partial pressure of water vapor, and atmospheric

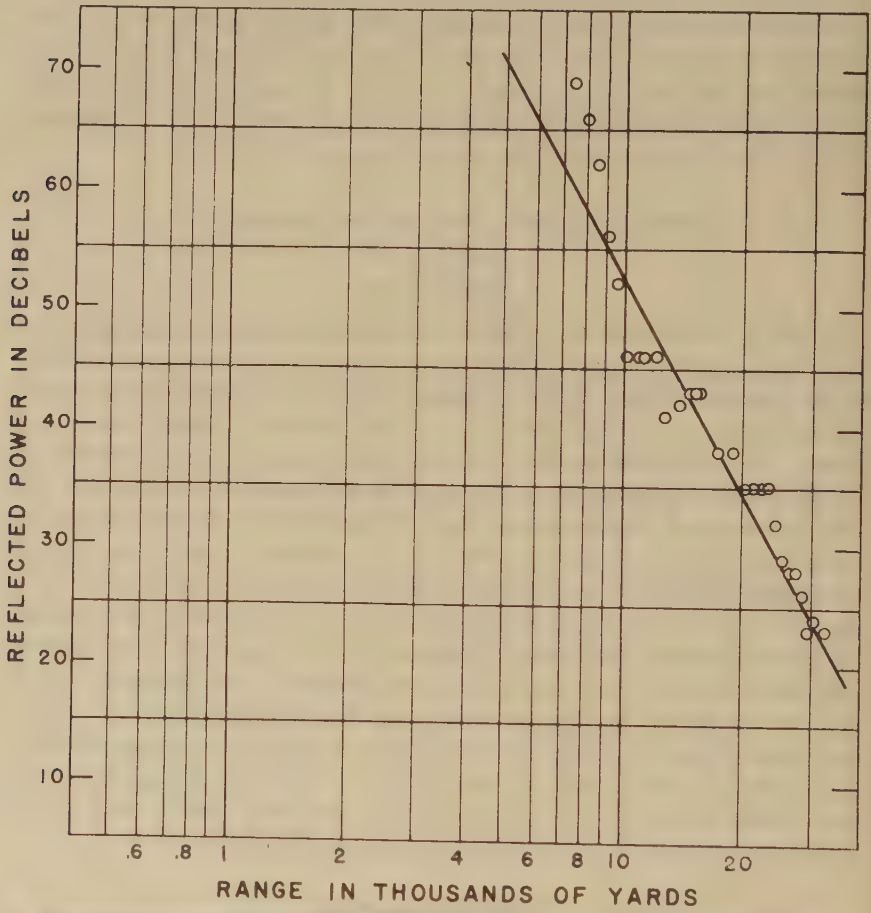

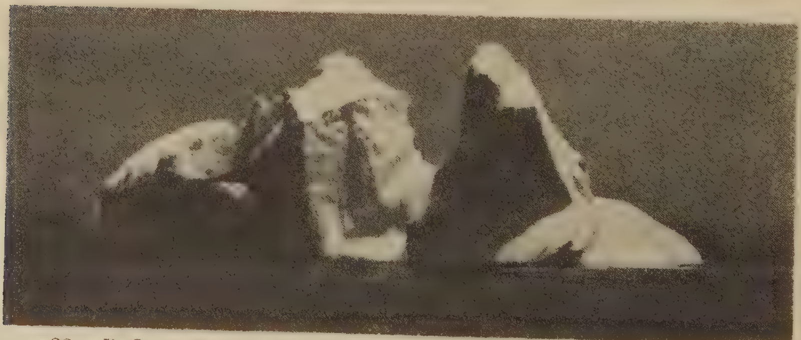

FIGURE 32.—Reflected power expressed in decibels above minimum discernible signal plotted as a function of range for a large iceberg (109 by 300 feet; 19,050 sq. feet) whose observation aspect indicates directivity of reflected radiation.

pressure to the index of refraction is given by the well known expression:

$$(n-1)10^6=\frac{79}{T}\left(p-e+\frac{4{,}800e}{T}\right)$$

The dependence of refractive index on pressure leads to a regular decrease with height, but the change of barometric pressure with weather produces only an insignificant effect on the gradient. The variations in this index in the lower atmosphere owe their existence to stratifications in which the temperature and moisture change rapidly with height. As temperature decreases with height n increases, and as humidity decreases n decreases. The effect of humidity variation is distinctly more pronounced than the effect of temperature, and humidity variations constitute the main cause of nonstandard conditions with temperature variations a contributing factor. The major effects of nonstandard refraction on radar propagation occur only for rays which emerge from the transmitter at angles less than ½ degree. For angles between ½ and 1½ degrees the refractive effects consist merely in minor modifications of the expected radar coverage, while for angles above 1½ degrees the refractive effects are negligible. These considerations are best clarified by figure 33 which

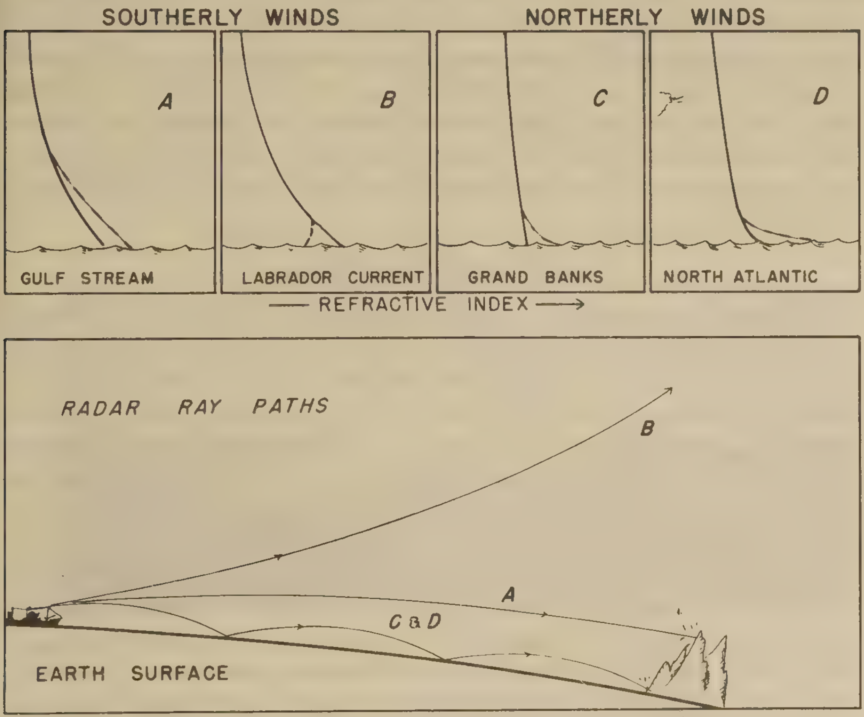

FIGURE 33.—Diagrammatic illustration of refractive index changes: A = moist warm air blowing from the south over warm water; B = moist warm air from the south blowing over cold water; C = cold dry air blowing over cold water; and, D = cold air from the north blowing over warm water.

is a diagrammatic illustration showing the variation in radar propagation conditions with air flow trajectory. Under conditions of moist warm air blowing over warm water (fig. 33A) little change is expected in the air mass and more-or-less standard conditions prevail. However, as this moist warm air moves over cold water surfaces as the Labrador Current or shipping lanes during early spring (fig. 33B), the air loses heat and moisture in the lower levels, and as the moisture loss predominates the index of refraction increases with height for the first few hundreds of feet and radar waves bend upward more rapidly than normal. This results in subnormal microwave propagation and reduced radar ranges as illustrated by the ray path "B". Unfortunately, this condition predominates in the ice areas during the early spring and summer months. Close under the Newfoundland coast, dry cold air blowing over the cold water surface will result in increased moisture in the lower levels and a condition of superrefraction or "ducting" (fig. 33C). Under these circumstances and those resulting from this cold relatively dry air from the north blowing over the warm water surface of the south (fig. 33D), a large portion of the energy of the radar pulse is confined to a narrow region in the lower atmosphere resulting in extended ranges. This phenomena of superrefraction is a common occurrence at sea and ranges are extended 3 to 5 times. Unfortunately, this supernormal condition usually exists during clear days when extended radar ranges are not required. An analysis of the weather observations taken while the iceberg maximum range observations were being made indicates that average and better-than-average ranges might be expected on clear days, and that below-average ranges are to be expected on foggy days which is in conformance with theory.

Quantitative Measurements

To assess the magnitude of decreased ranges due to the subnormal propagation conditions which might be found on the Grand Banks area it would be necessary to make serial measurements of the vertical distribution of temperature and humidity over an extended period of time. From these observations ray diagrams or coverage charts might be constructed and an estimate made of the reduction or increase in the expected range. A more practical approach would be to treat the problem statistically using the routine data of sea temperature, air temperature, humidity, and wind speed as proposed by Anderson and Gossard [*17*] and others. To gain confidence in any of the quantitative radar data it was necessary to make as many weather observations as practical in the Grand Banks area. Where possible a sounding was made with the captive Wiresonde instrument which accurately measures temperature and humidity at any desired altitude interval. Measurements from the surface to above 300 feet were made at frequent intervals depending on the expected gradient. As a result it was possible to obtain excellent information on the propagation conditions during 30 percent of the radar tests.

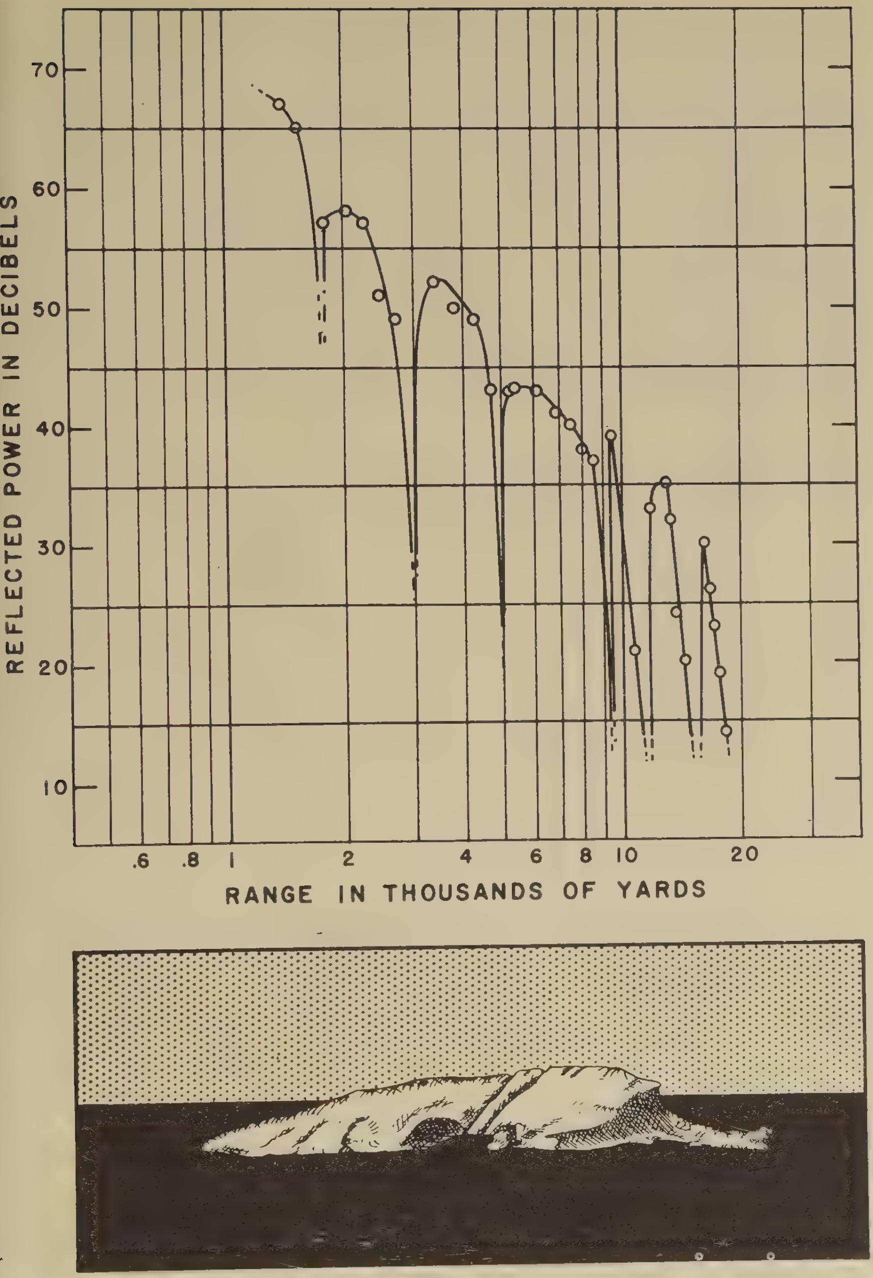

FIGURE 34.—Reflected power expressed in decibels above minimum discernible signal plotted as a function of range for the low lying iceberg (33 by 247 feet; 5,360 sq. feet). The fade areas were well documented on this target whose maximum range of detection was 19,600 yards. Subnormal propagation conditions existed; c.f. figures 35 and 36. The sea was calm.

Of particular interest is the test-run made on a small iceberg (33 by 247 feet) during which six well documented fade areas were passed through. The results of power measurements on this berg are shown in figure 34, and the results of a Wiresonde sounding taken immediately after the power measurements are shown in figure 35. From these observed temperature and relative humidity distributions, and the resultant index of refraction variation compared to that for standard conditions, it is immediately apparent that subnormal conditions existed. To further investigate this phenomena, a ray diagram (fig. 36) was constructed graphically using a method similar to that developed by Anderson and Abbott [*18*]. Accordingly, the maximum detection range to be expected for this target is approximately 17,000 yards; whereas, the maximum range expected for the standard conditions for a target of this height is 36,000 yards. The range of iceberg detection was actually 19,600 yards and this increased range of detection over that expected from the ray diagram is attributed mostly to diffraction. Also shown diagrammatically in figure 36 is the space comparison between the actual fades (fig. 34) and the fades expected from destructive interference phenomena deduced from the ray diagram. The solid wedge areas indicate the approximate range of theoretical fades. The shape of the expected fade curves has not been computed. Smooth sea conditions prevailed during the test-run. There was indication of sharp fades during other test-runs when the sea surface was smooth and this is in accordance with what one would expect by consideration of the surface roughness and its effect on reflection.

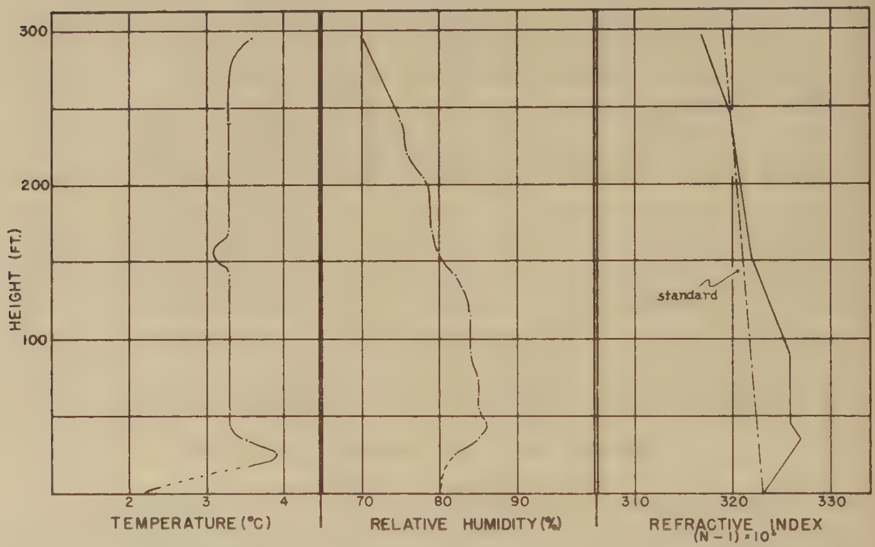

Figure 35.—Vertical distribution of temperature, relative humidity, and refractive index observed by Wiresonde in the vicinity of iceberg of figure 34.

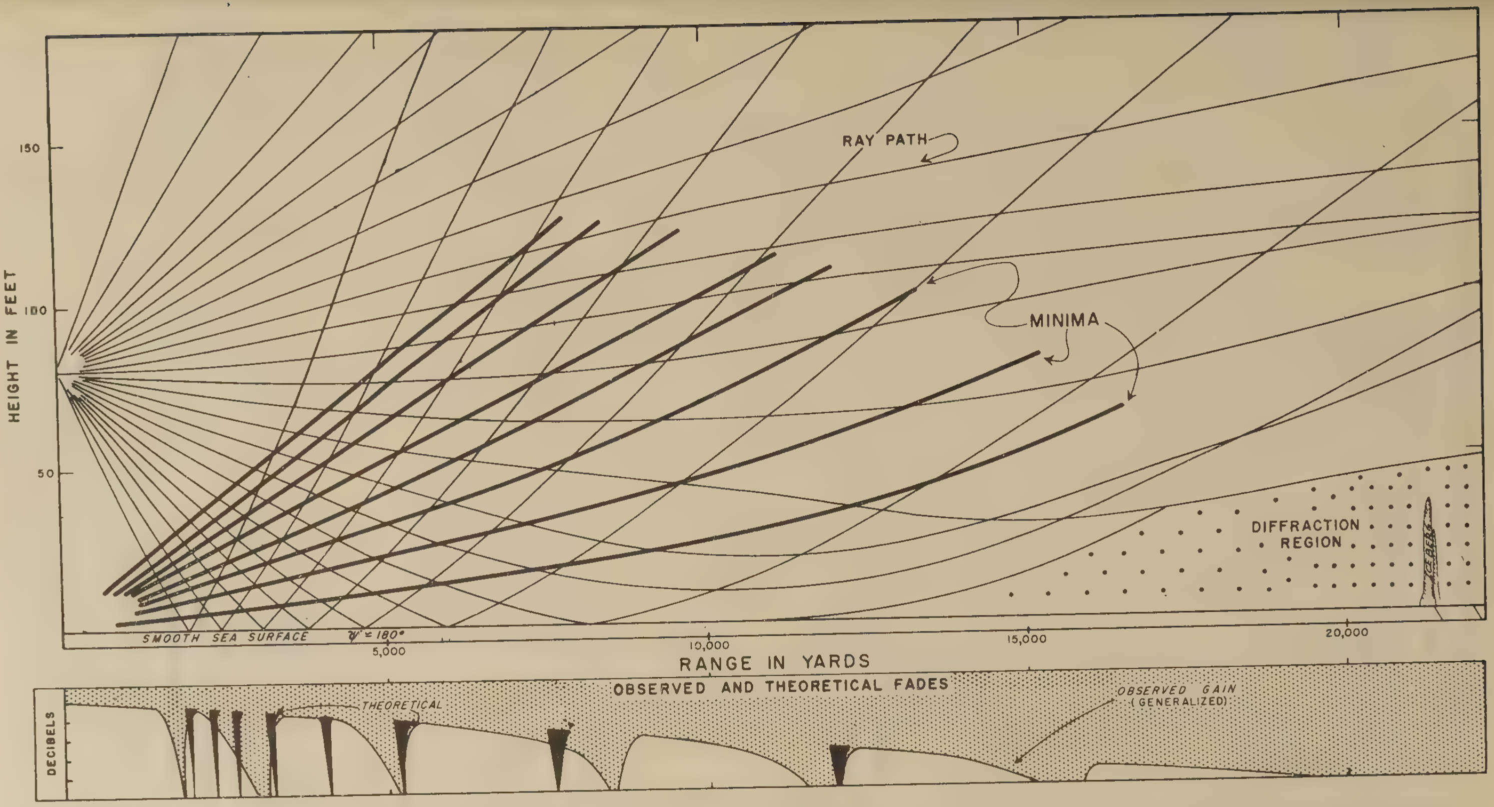
HEIGHT IN FEET
150
100
50
RAY PATH
MINIMA
DIFFRACTION REGION
ICEBERG
SMOOTH SEA SURFACE
ψ = 180°
5,000
10,000
15,000
20,000
RANGE IN YARDS
OBSERVED AND THEORETICAL FADES
DECIBELS
THEORETICAL
OBSERVED GAIN (GENERALIZED)

FIGURE 36.—Ray diagram showing the location of minima and the correlation between observed and expected fade areas for the iceberg of figure 34. Solid wedge areas indicate approximate range of expected diminished signal strength.

Expected Average Propagation Conditions

At this time it cannot be said with certitude to what extent the conditions on the Grand Banks may reduce radar ranges; however, there is little doubt that the subnormal propagation conditions are the rule rather than the exception. It is possible to estimate the magnitude of range reduction which might be expected due to the atmospheric conditions prevalent on the Grand Banks and contiguous areas of the North Atlantic Ocean. A qualitative consideration of the processes involved indicates that the average temperature and humidity distribution from the surface to 150 feet at the Tail of the Grand Banks during spring is characterized by increase in temperature with height and near constant relative humidity approaching 100 percent. An examination of radiosonde observations from coastal stations and the computed average index of refraction conditions presented in the U.S. Climatic Atlas of the Oceans [*16*] indicate that the expected average condition would be one of isorefractive index from the surface to a few hundred feet. Ray diagrams for this condition and the condition of standard propagation (index of refraction gradient of -1.19×10^{-8} units per foot) have been constructed and are shown in figure 37. The top diagram represents the internationally accepted standard conditions and the bottom diagram shows a comparison between the standard conditions and the average subnormal conditions defined here for the Grand Banks. The minima for both *S*- and *X*-band for the standard conditions have been superimposed on those for the "average" conditions. This comparison indicates that the magnitude of decreased detection in the Grand Banks region is insignificant at short ranges and that there is no preference to radar frequency for short range detection during subnormal propagation conditions. The temperature and humidity conditions upon which the lower ray diagram was constructed are considered to be conservative generalizations of subnormal conditions; and it should be remembered that at times a rapid increase in temperature in the first 100 feet accompanied by a constant high relative humidity or humidity increasing with height might lead to slightly reduced ranges on small targets and relatively greatly reduced ranges on large targets.

Fog Attenuation

The prevalence of fog in the potential ice areas has led to a theoretical investigation of the attenuation to be expected due to fog. Observations indicate that fair weather clouds and fog are composed of water droplets whose diameters do not exceed 0.02 centimeters. For this size droplets the attenuation formula becomes independent of the drop size distribution and takes on the remarkably simple form [*5*]:

$$\alpha_{db/km}=\frac{24.55m\epsilon_i}{\lambda\{(\epsilon_r+2)^2+\epsilon_i^2\}}$$

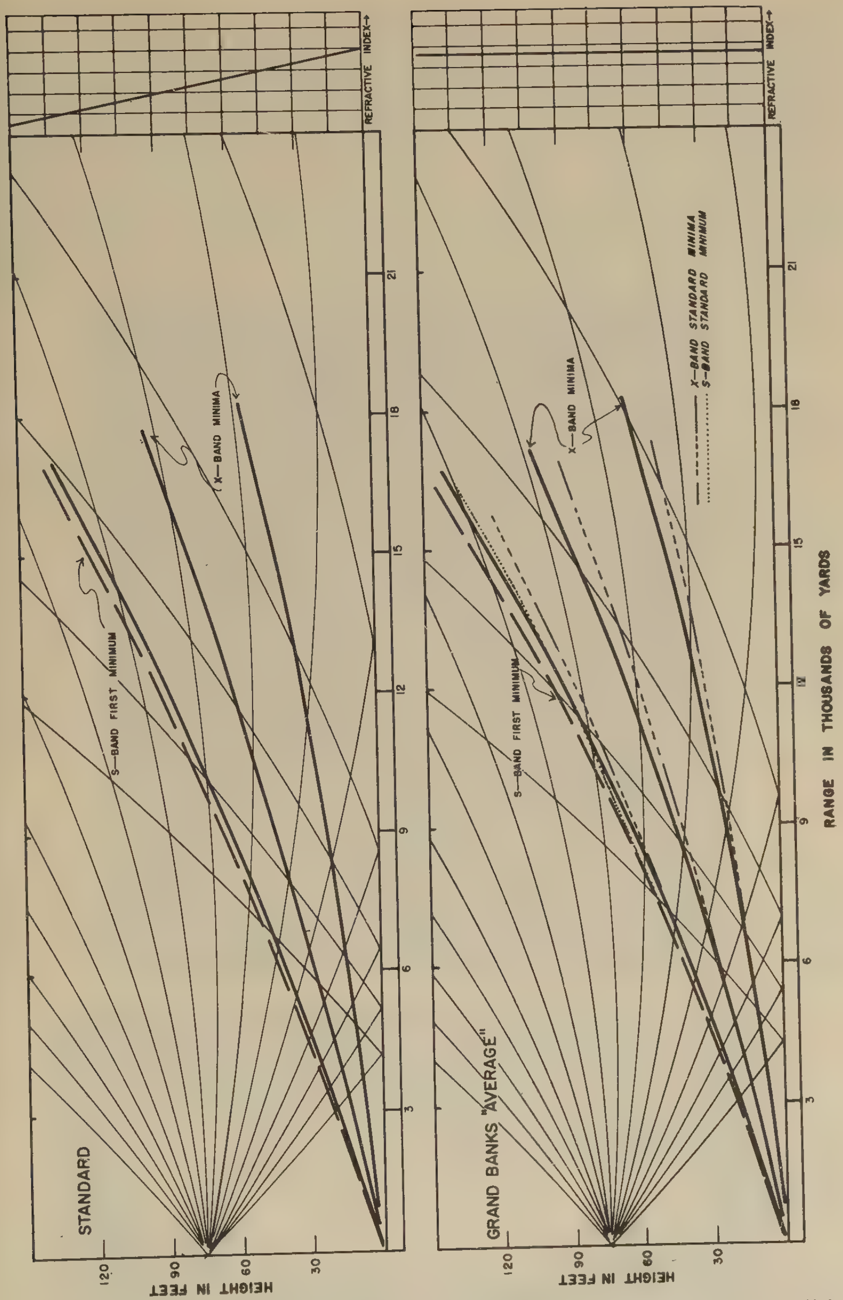
STANDARD
GRAND BANKS "AVERAGE"
REFRACTIVE INDEX→
S—BAND FIRST MINIMUM
X—BAND MINIMA
X—BAND STANDARD MINIMA
S—BAND STANDARD MINIMUM
HEIGHT IN FEET
120
90
60
30
RANGE IN THOUSANDS OF YARDS
3
6
9
12
15
18
21

FIGURE 37.—Ray diagrams illustrate the expected subnormal propagation conditions on the Grand Banks as compared to "standard" conditions for both S- and X-band radar. Top standard diagram is superimposed on bottom diagram to illustrate the difference in lobe pattern between the two conditions. It may be inferred from these diagrams that little change in field strength is to be expected within the first 8,000 yards from the antenna.

where m is the mass of liquid vapor per cubic meter, λ is the wave length in centimeters, and ϵ_r and ϵ_i are the real and imaginary parts of the dielectric constant at the temperature in question for the wave length of radiation. Humphreys [*19*] gives a value of 0.006 gm/m^3 as the liquid water content of fog. As the concentration of 0.6 gm/m^3 is rarely exceeded [*5*] this value is used in the computations below. Based on the 18°C. pure water complex dielectric constants of (63.6—j32.7) for X-band and (79.0—j12.3) for the S-band, the maximum attenuation to be expected on a radar range of 5 miles is 0.55 decibels for the X-band and 0.06 decibels for the S-band. Although there is a ten-fold difference between the two frequencies the values are insignificant when other factors are considered. The attenuation due to water vapor (7.5 gm/m^3) and oxygen over the same range is approximately 0.16 decibels for both frequencies [*20*]. Of interest here is the fact that water suspended in the air in the form of drops contributes less to the refractive index than an equivalent amount of vapor. The formation of fog, therefore, reduces the prefog attenuation by water vapor; however, the importance of diminished visibility far outweighs this slight advantage in fog over prefog conditions.

If there is a temperature inversion in the fog layer, the vapor pressure required for saturation increases with height and substandard conditions usually result. As mentioned above, this is a common occurrence on the Grand Banks during southerly winds. In summary, it is concluded that the attenuation of S- and X-band radar waves due to fog is not significant compared to other factors.

Icebergs Hidden by Weather

Although fog attenuation is not significant, attenuation of radar waves due to rain drops is of considerable importance for frequencies in the X-band and above. The back scattering from rain squalls, as shown in Table I, is often sufficient to obliterate a small target.

Table I

	Rate of fall	Attenuation for 5-mile range (decibels)	
	(in./hr)	X-Band	S-Band
Moderate rain	0.24	3.6	0.03
Heavy rain	.86	12.8	.11
Cloudburst	1.7	31.0	3.2

This tabulation taken from curves presented by Goldstein [*21*] is quite revealing, and would make high frequency radars prohibitive in areas of continuous heavy rain. Fortunately, the passage of frontal systems and their associated rainstorms or sometimes cloudbursts is rather rapid compared to other weather phenomena and if necessary a mariner may stop his vessel until the masking effect has passed. On two occasions during the field experiments growlers were masked by moderate to heavy rain showers. During both occasions the rain squall line was 20 miles wide and moved across the PPI scope at 15–20 kts. During the first occasion a 22-foot growler below Cape Race was hidden intermittently by a storm which lasted one hour. On the second occasion the weather completely masked a 6- by 30-foot blue growler which the *Evergreen* was standing by above the North Atlantic Shipping Track CHARLIE. The growler and weather situation which confronted the writer and radarmen are shown in figure 38. We were unable to detect this target during the passage of the weather

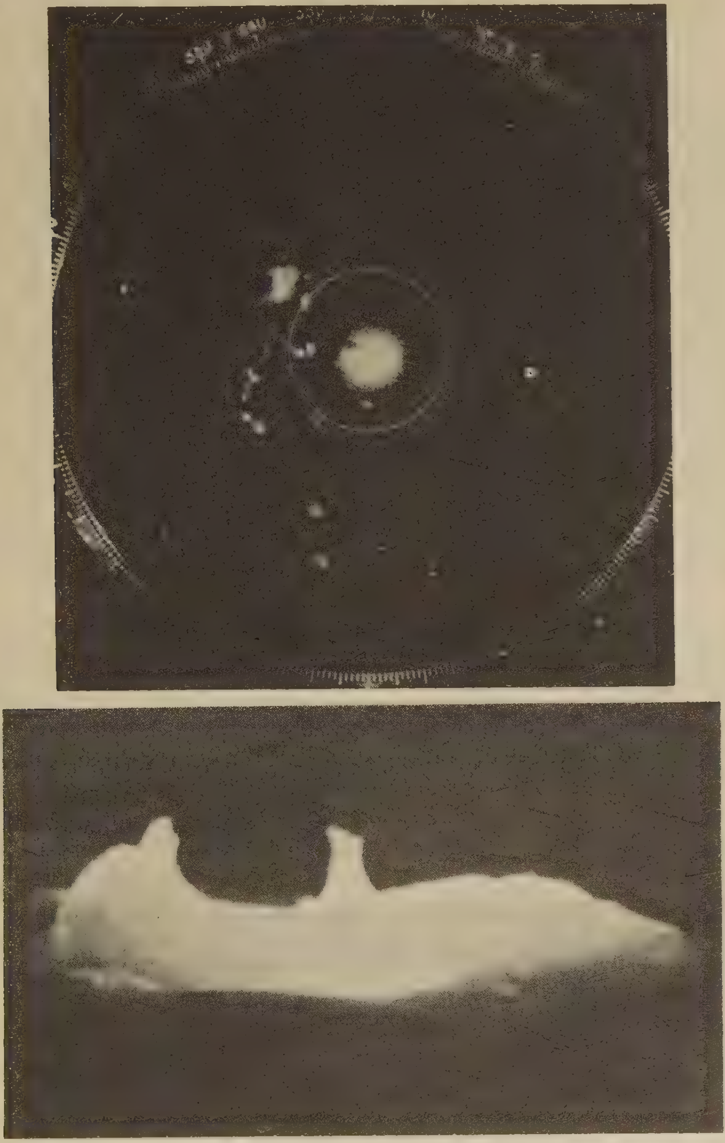

Figure 38.—Illustration of rain squall masking a growler (6 by 30 feet) which should have been discerned at 310° T; 3,000 yds. Situation lasted one hour.

although we knew its position within 200 yds. (approx. 310°T; 3,000 yds). Both FTC and STC anticlutter circuits proved ineffective in this case. Later the growler was sighted just off the bow. This small ice formation was of sufficient size to inflict serious damage to a thin-hull vessel making contact at moderate speed. Of interest here is the fact that the masking effect from snow is less than that from rain as would be expected from considerations of the low reflection coèfficient for snow shown in figure 27.

SEA RETURN

General

Although it has been established that icebergs are very poor reflectors of radar, and that reflection might be further decreased by aspect and subnormal propagation conditions which exist on the Grand Banks during spring, it is well established that most icebergs do provide good targets and during calm sea conditions some reliance can be placed on radar. However, it appears that distinguishing small ice targets in heavy seas might be the limiting factor in the reliability of radar as an instrument for providing safe navigation through ice infested waters. The basic phenomena of sea return or sea clutter have not yet been definitely established; however, it is well known that sea echo from waves acts as a built-in jammer, blanketing and obscuring small target echoes. Other things being equal, the strength of the sea return depends upon the state or roughness of the sea, which in turn depends largely upon the wind force. As demonstrated in 1945 [*3*], the range of sea clutter on the scope is very nearly directly proportional to the state of the sea and the wind force.

The radar cross section and echo strength of sea return are difficult quantities to measure or compute because among other things the reflection surfaces extend from the ship to an indefinite range. The variation of reflected power with range does not necessarily follow the same relation as that for a ship or iceberg target as is apparent from the fact that the reflection from waves is less at longer ranges due to a decrease in the angle of incidence. In general, the decrease in sea return with range is more rapid than that for other targets.

Quantitative Measurements

Of prime importance to this study was the quantitative determination of the masking effect of sea return. Many mariners have reported that ice targets have gone undetected due to masking by sea return but it remained, however, to make quantitative measurements under controlled conditions to definitely assess the importance of sea return. Numerous measurements were made on all states of the sea from the maximum range of sea return to as close as practical on the "A" scan. It was early observed that this measurement required the most objective treatment and close adherence to a standard technique. The data were taken on four bearings and as has been demonstrated before the strongest echo arrived from windward. A good correlation does not exist between wave height estimates and the reflected power curves from the two different ships which made these measurements; however, enough measurements have been made to quantitatively show that sea return for wave heights above 4 feet is sufficient to entirely obscure dangerous growlers. This is is best illustrated by figure 39 in which the reflected power curves for a growler and a 4.5-foot sea are compared. Because this figure illustrates the important results of very carefully controlled measurements under ideal conditions a detailed account of the observations is given: During the day of 28 May 1959 the CGC *Androscoggin* commenced test-runs on a large growler (22 by 76 ft.; 665 sq. feet). From a temperature and humidity sounding (Wiresonde) from the surface to 290 feet, the atmospheric conditions were assessed as being near standard throughout the first 200 feet. The sea at this time was approximately 2 feet high, 500 feet long. Because a small growler (4 by 20 feet) in the vicinity was being partly obscured by sea return, the ship remained near the 22-foot growler throughout the day for anticlutter measurements. That evening the wind increased to 20 kts and the seas to 4.5 feet high, 200 feet long. Considerable difficulty was experienced in detecting the 22-foot growler and the 4-foot growler was completely obscured. Twenty-eight measurements of the reflected power from the sea were made at short range intervals on four bearings. The observations made in the windward direction were 10 decibels greater than those made in the backsides direction and 5 decibels greater than those made parallel to the waves. The curve for the windward measurements is presented in figure 39. The 20-knot winds and intermittent rain preclude subnormal propagation conditions. The optimum detection range for this target was 6,200 yards and although the maximum range observed earlier that day was 11,200 yards, the maximum range during the 4.5-foot sea was 9,000 yards. This formation could not be detected in the sea return using the available anticlutter devices. It should be mentioned that although the aspect shown in figure 39 was the aspect observed during the test-run earlier that day, a slight rotation would present a considerably smaller physical cross section. This formation no doubt was rocking and rotating during the observations, but an indeterminate error throughout these measurements is precluded by the fact that this formation was observed continuously for 11 hours and found to be of the same shape after 18 hours. These measurements caused some concern as although they were supported by other less precise observations the fact that 4.5-foot waves reflected better than a 22-foot growler whose aspect showed some target gain seemed to conflict with reason. The theoretical analysis of this problem presented below has reestablished the validity of these observations.

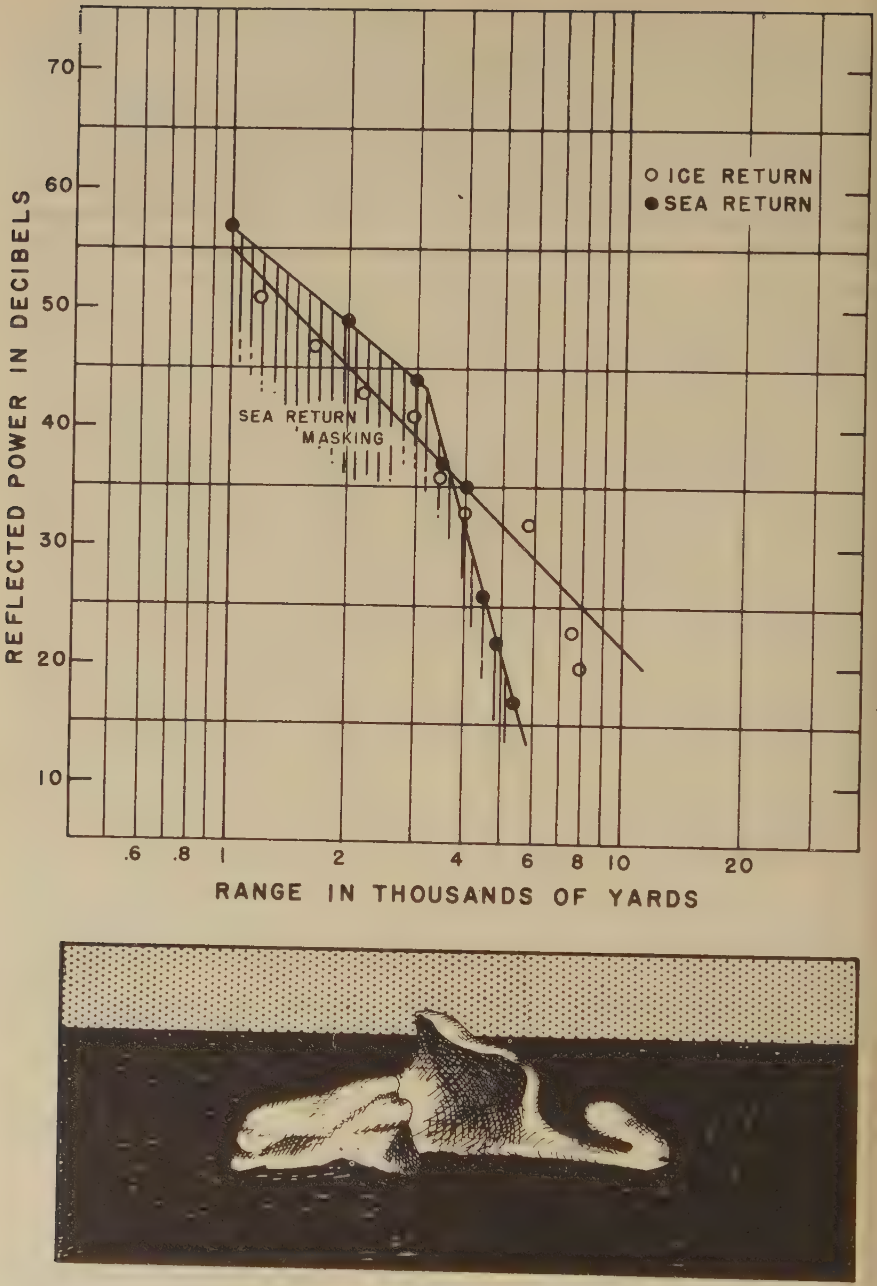

FIGURE 39.—Reflected power expressed in decibels above minimum discernible signal plotted as a function of range for a growler (22 by 76 feet; 665 sq. feet) and sea return (4.5 feet high. 200 feet long). The measurements were made during standard propagation conditions under known overall radar performance.

Behavior of Sea and Ice to Frequency and Polarization

One of the subordinate objectives of this program was to evaluate the various characteristics of radar systems. Below the subjects of optimum frequency and polarization are treated by a theoretical analysis based on Fresnel's original equations in their complex form. The reflection coefficient of a surface exhibiting conductivity is complex and as thoroughly presented by McPetrie [*22*], the coefficient may be conveniently represented by a phase component K and an inquadrature component K' where the reflection coefficient R takes the form $(K+jK')$. Recalling equation (11):

$$\epsilon_c = \epsilon_r - j\epsilon_i = \epsilon_r - 2j\frac{K}{f} = (n - j\zeta)^2 \tag{11}$$

it is apparent that the reflection coefficient, being a function of the complex dielectric, is a function of the conductivity, frequency, and angle of incidence. This parameter is also a function of the polarization and it was therefore necessary to perform the tedious computations in order to accurately determine the relation of frequency and polarization to the optimum ice detecting characteristics. Computations based on the equations given below were made for S- and X-band frequencies, vertical and horizontal polarizations and angles of 0°, 20°, 40°, 50°, 60°, 70°, 80°, 82°, 83.5°, 84°, 86°, 88°, and 90° for both pure ice and sea water, and from the best known values of the complex dielectric constants for the radiation considered. McPetrie [*22*] has derived from the original Fresnel equations the following relations for the reflection coefficient. If the reflection coefficient for horizontally polarized waves is designated $(K_h + jK_h')$, the values for these components are given by:

$$K_h = \frac{\cos^2\theta - (c^2+d^2)}{\cos^2\theta + (c^2+d^2) + 2c(\cos\theta)}$$

$$K_h' = \frac{-2d(\cos\theta)}{\cos^2\theta + (c^2+d^2) + 2c(\cos\theta)}$$

in which θ is the electromagnetic angle of incidence ($\theta = 0$ for normal incidence) and c and d are given by:

$$c = \sqrt{\frac{\{(\epsilon_r - \sin^2\theta)^2 + \epsilon_i^2\}^{\frac{1}{2}} + \epsilon_r - \sin^2\theta}{2}}$$

$$d = -\sqrt{\frac{\{(\epsilon_r - \sin^2\theta)^2 + \epsilon_i^2\}^{\frac{1}{2}} - \epsilon_r + \sin^2\theta}{2}}$$

where ϵ_i and ϵ_r are the imaginary and real parts of the dielectric constant.

For the case of radiation polarized with the electric field in the plane of

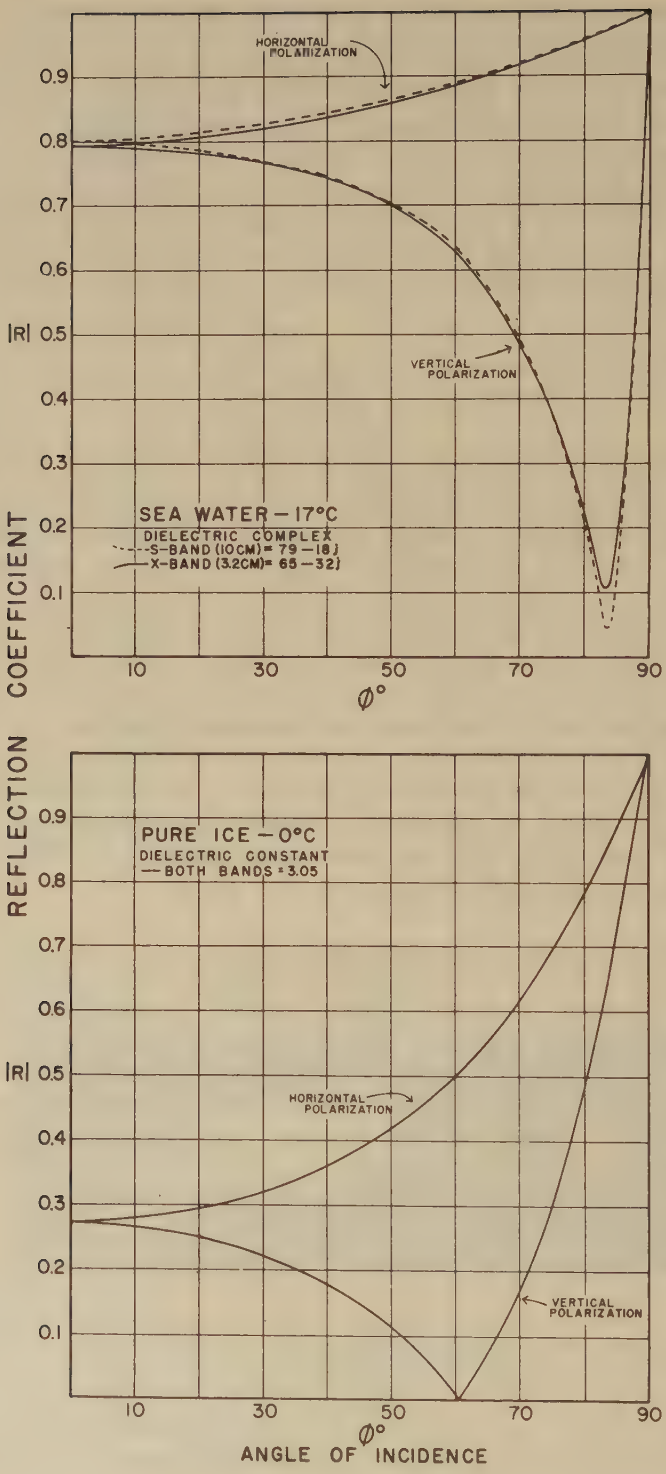

FIGURE 40.—The variation of reflection coefficient with angle of incidence for ice and sea water irradiated by S- and X-band frequencies. Curves for vertical and horizontal polarization were computed from Fresnel's complex equations.

incidence the components K_v and K_v' of the reflection complex $(K_v+jK_v$ are given by:

$$K_v=\frac{(\epsilon_r^2+\epsilon_i^2)\cos^2\theta-(c^2+d^2)}{(\epsilon_r^2+\epsilon_i^2)\cos^2\theta+(c^2+d^2)+2(\epsilon_r c-\epsilon_i d)\cos\theta}$$

$$K_v'=\frac{-2(\epsilon_r d+\epsilon_i c)\cos\theta}{(\epsilon_r^2+\epsilon_i^2)\cos^2\theta+(c^2+d^2)+2(\epsilon_r c-\epsilon_i d)\cos\theta}$$

in which the symbols have the same significance as in the equations above. It can be seen from these equations that the reflection coefficient tends to unity as the angle of incidence approaches 90°, and is zero for all angles of incidence for a body having zero conductivity and unity dielectric constant. The results of these computations are shown in figure 40. A number of conclusions can be drawn from this figure:

1. The reflection coefficient of ice is three times less than that of sea water. This fact helps explain the results of relative power measurements shown in figure 39.
2. In both cases of polarization, the reflection coefficient is less for vertical than for horizontal polarization for all angles of incidence.
3. *S*- and *X*-band behave the same on both ice and sea water for all practical purposes. Field experiments in 1946 [*3*] confirm the fact that ice is not frequency sensitive; however, because the reflection from droplets contributes appreciably to the sea echo, there is some measured [*5*] frequency dependence of the radar cross section per unit area for sea echoes.
4. The Brewster angle for pure ice is 60°13′. An examination of the vertical polarization curves reveals that although, theoretically, less sea return would be observed using vertically polarized radiation, the reduced ice reflection coefficient is the limiting factor. It appears that the mariner using vertically polarized radar is at a disadvantage during calm or slight sea conditions. A limited number of qualitative measurements using vertical polarization for the detection of growlers in sea return during the 1946 studies [*2*] gave negative results.

EVALUATION OF ANTICLUTTER CIRCUITS

General

The masking effect of sea return and weather has long been of concern to radar manufacturers and mariners. The program for the field work of this investigation was designed to place most of the emphasis on an evaluation of the effectiveness of commonly used anticlutter devices in the discrimination of small ice targets from sea clutter. Two types of devices most common to commercial marine radars were evaluated on different sized targets during various stages of the sea. The observations were documented by PPI photographs, cognizance of set performance, and knowledge of the atmospheric propagation conditions. The two devices are:

FTC—Fast time constant is a differentiating circuit which effectively reduces the gain within the clutter area only. It is normally used to limit scope clutter caused by reflections from atmospheric hydrometeors.

STC—Sensitivity time control circuit reduces the gain of the receiver during the reception of short range signals.

The effectiveness of these circuits in some situations is best illustrated by comparison of the PPI scope presentation with and without application of anticlutter devices as shown in figure 41. These photographs are from a series of observations made on the 22-foot growler, subject of figure 39. The top photograph shows the growler at 333°T; 6,000 yards and sea return from a 4-foot sea extending out to 5,000 yards. The gain and video circuits were set for the maximum discernment of the target. Figure 41 (bottom) is a photograph of the PPI scope under the same conditions as above except the STC circuit is used to decrease the near gain and thereby obliterate the sea return. This was the optimum presentation that could be obtained. It was found when working with growlers in sea return that the FTC circuit is valueless and on two occasions when weather obscured the target (c.f. fig. 38) this device was ineffective.

Results

Intensive studies of the effectiveness of FTC and STC in discriminating growlers in sea return have indicated that FTC is valueless and STC is very effective if used with the proper combination of video and receiver gain; however, on three different occasions it was not possible to detect growlers in sea return although the radar was in peak condition and the propagation conditions were near normal or only slightly subnormal. It should be remembered that these anticlutter devices were designed to decrease the gain in a particular area on the scope and thereby reduce the brilliant clutter and allow the strong persistent echo of a target to stand out. The STC and FTC action appears to be useless unless the target echo is stronger than the sea echoes and as has been demonstrated the basic electrical properties of ice leave it as a poor reflector compared to sea water. Of value to ice detection is the new type of logarithmic receiver in which the effective gain is proportional to the logarithm of the signal amplitude. This receiver characteristic provides higher gain for weak signals and relatively lower gain for strong signals. However, the effective use of this device or other controls including video and receiver gain requires a skilled and experienced operator. It was only after many months of constant radar surveillance that the writer was able to master the intricacies of Lin-Log, STC and gain combinations which allowed the full potentials of the system to be utilized Evaluation of operators who have

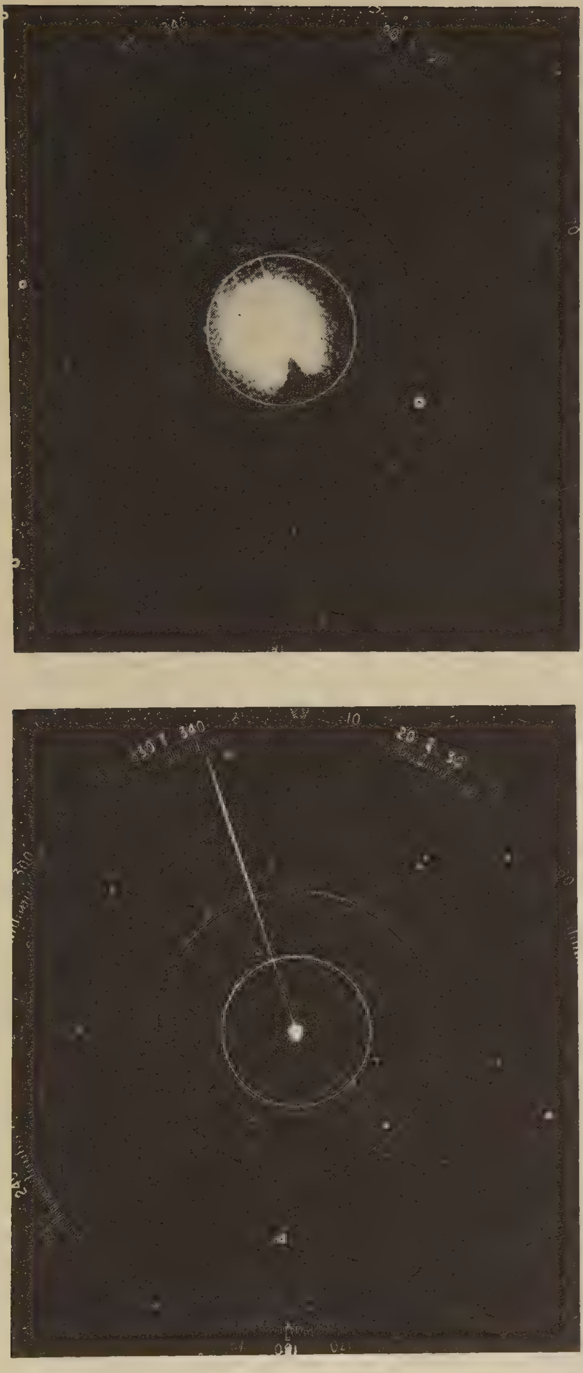

FIGURE 41.—Effect of anticlutter devices as aids to discernment of a growler from sea clutter. Top photograph shows sea return extending to 5,000 yds and a 22-foot growler at 333°T; 6,000 yards. Bottom photograph is the same situation with STC applied.

as their primary duty the radar watch on board ships has revealed that the use of anticlutter devices often times decreases the radar's effectiveness due to lack of training or experience. It is known that vessels are transiting the North Atlantic Ocean with the FTC circuit activated without any knowledge of its function or use. Other vessels reduce sea return by decreasing the video or receiver gain although STC is available on the radar set. It is not too infrequently discovered that radio operators, radar operators, merchant officers, and even naval watch officers do not know the function of the anticlutter devices for their radar sets on which they rely so heavily during reduced visibility. This lack of knowledge and improper use of these devices leads one to the conclusion that in many cases it is best not to have them available at all. In summary, we can safely say that if an ice target is not picked up beyond the sea return it will not be detected at all and a fatal collision might result.

CONCLUSIONS AND DISCUSSION

General

It has been established by both observation and basic theory that an intrinsic property of icebergs is poor electromagnetic reflection and that reliance cannot be placed on radar for safe navigation during moderate sea conditions because if a dangerous ice fragment is not detected beyond the sea return, it will not be detected at all. Below, the conclusions reached for each topic of investigation are viewed and summarized in relation to the following radar system parameters:

Power Output
Receiver Sensitivity
Bandwidth
Frequency
Polarization
Antenna Rotation
Anticlutter Devices

Power Output, Receiver Sensitivity, and Bandwidth

We find that a reasonable approach to the assured detection of ice might be to improve the system parameters to such an extent that all dangerous ice targets can be detected beyond the sea return. This follows from the fact that the rate of attenuation of sea return with range is greater than that for a point target. Examination of the free space radar equation (2) reveals that it is necessary to increase the power output 16 times in order to double the maximum range of detection. This tremendous power increase has been precluded in the past by considerations of cost and space; however, recent developments in power generating devices might allow an improvement in the maximum range of detection without necessitating unreasonable cost and space requirements. The system might be improved by decreasing the wave guide attenuation or the distance between the antenna and the receiver-transmitter unit.

The relation between power output and range may be applied also to the minimum discernible signal and the maximum range of detection. An interesting relation can be derived for the absolute minimum discernible signal obtainable. It has been shown [5] that the maximum range of detection for a target per power output is a function of the receiver bandwidth. The minimum perceptible signal is in part related to the thermal noise; and because the thermal noise of a receiver is independent of the receiver construction, and the internal noise is usually several times the thermal noise, it is possible to derive the absolute minimum as follows. Thermal noise is generated by the random motion of electrons in a conductor and the rms thermal noise voltage which appears across terminals of any circuit element is a function of the frequency interval (receiver bandwidth) only; it is given by

$$V_n = \sqrt{4kT \cdot f \cdot R}$$

where R is the resistance across which the noise voltage is measured, f the bandwidth in cycles per second, T the absolute temperature, and k Boltzmann's constant. If we assume, for the purpose of the limiting case, that the receiver is without any internal noise and all of the noise is generated in the antenna which is at 17°C., the noise power is given by:

$$P = 4 \times 10^{-15} f \text{ watts}$$

where f is now in megacycles. This means that the minimum detectable signal cannot be less than 4×10^{-15} watts times the bandwidth. For the receiver most used in the field work, the minimum discernible signal was 10^{-13} watts for the 20- and 40-mile scales and the bandwidth was 2 Mc/s. Therefore the minimum discernible signal was about 11 decibels above the absolute minimum of 8×10^{-15} watts. To illustrate the importance of maintaining a low minimum discernible signal, a target was examined under two known minimum discernible signal values on the same radar with the same power output within two minutes of time. These controlled conditions were provided by making use of the two minimum discernible signal values for the AN/SPS-23 radar; i.e., -91.9 dbm for the 8-mile range, and -100.1 for the 20-mile range scales. A medium growler was brought to within 2,000 yards of the *Evergreen* and two PPI photographs were taken on either range setting. The growler, shown at the bottom of the figure, was clearly painted on the 20-mile range setting (fig. 42A), but was hardly discernible on the 8-mile setting. This difference in reception for the 20- versus the 8-mile range settings has been observed on many occasions. The propagation conditions at that time were subnormal. The ratio of blips to the number of times the antenna scanned this target was 1.0 for the 20-mile range, but only 0.5 for the 8-mile range at 4,600 yards. As the maximum range of this target on the 8-mile scale was 4,850 yards,

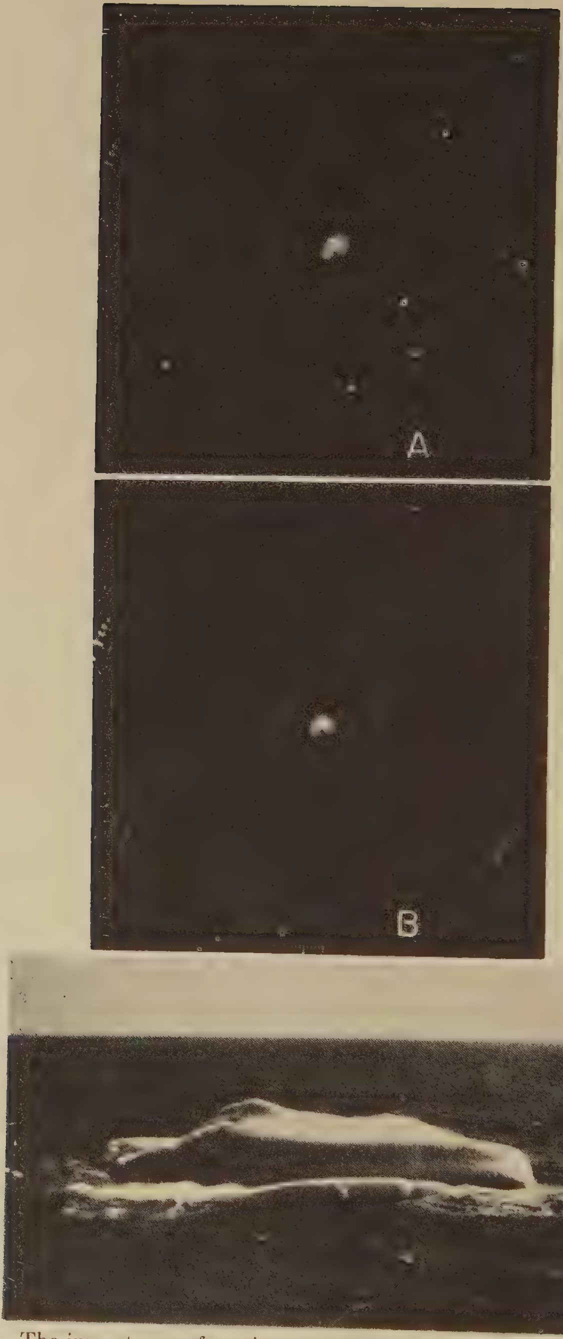

Figure 42.—The importance of receiver parameters is shown by a comparison of the radar reception of an echo from the growler shown using two different values of minimum discernible signal. Photograph A shows a strong blip on the 20-mile scale (min. dis. sig. = 100 decibels below one milliwatt); and B shows no targets on the 8-mile scale (min. dis. sig. = 92 dbm). B was taken immediately after A.

a good probability exists that it would never have been picked up unless continuous surveillance of radar was maintained or the minimum discernible signal was lower than −92 dbm. The necessity of keeping a system in near peak operating condition is strikingly illustrated by this example.

Frequency and Polarization

As shown in figure 40, ice and sea water behave similarly to both *X*- and *S*-band frequencies with the exception that the reflection from droplets in sea spray is frequency sensitive (greater reflection the greater the frequency [*5*]). Less weather attenuation is found in the lower frequencies, but a better display (less conducive to operator fatigue) is found on the higher frequency sets. All things considered, there is no preference to the frequency of radiation for an ice detecting radar.

The rapid decrease in reflection coefficient with angle of incidence for vertical polarization indicates that horizontal is the preferred polarization. Circular polarization was not examined.

Antenna Rotation

An evaluation of antenna rotation was facilitated by the use of continuous rotation and 30° and 60° sector scans. It had been observed on many occasions that sector scan does provide a more definite detection and would probably be of value in detecting a weak ice target. The value of sector scan was qualitatively determined by a series of PPI photographs taken under the same propagation, target, and radar conditions. The favorable results to be expected in defining a weak target by sector scan are shown in figure 43. Figure 43A is a photograph of the PPI scope with the antenna in continuous rotation. This photograph shows, very faintly, two targets indicated by open circles. Immediately after this picture was taken the antenna was placed on sector scan. Although the rotation was only about two times faster on 60° sector scan, the two previously barely discernible targets appear many more times brilliant and a third target, previously undetected, became visible. The exposure for these pictures was exactly the same in all cases; however, photograph 43A suffered in development. There is little doubt that this antenna control device is advantageous, and assuming continuous rotation will be employed periodically, sector scanning ahead of the ship is recommended for iceberg navigation. The difference between 30° and 60° sector scan was negligible; therefore, 60° scan should be used. These observations suggest another device which might prove very effective in the discernment of a persistent weak echo amidst random echoes from the sea. This electronic integrating device, known as a "memory tube," might prove to be a definite asset in commercial radar sets.

Anticlutter Devices

Certainly the quest for a reliable radar should not exclude anticlutter devices; however, the proper use of any device involves the competency of the operator and the use of these devices present on many radar instal-

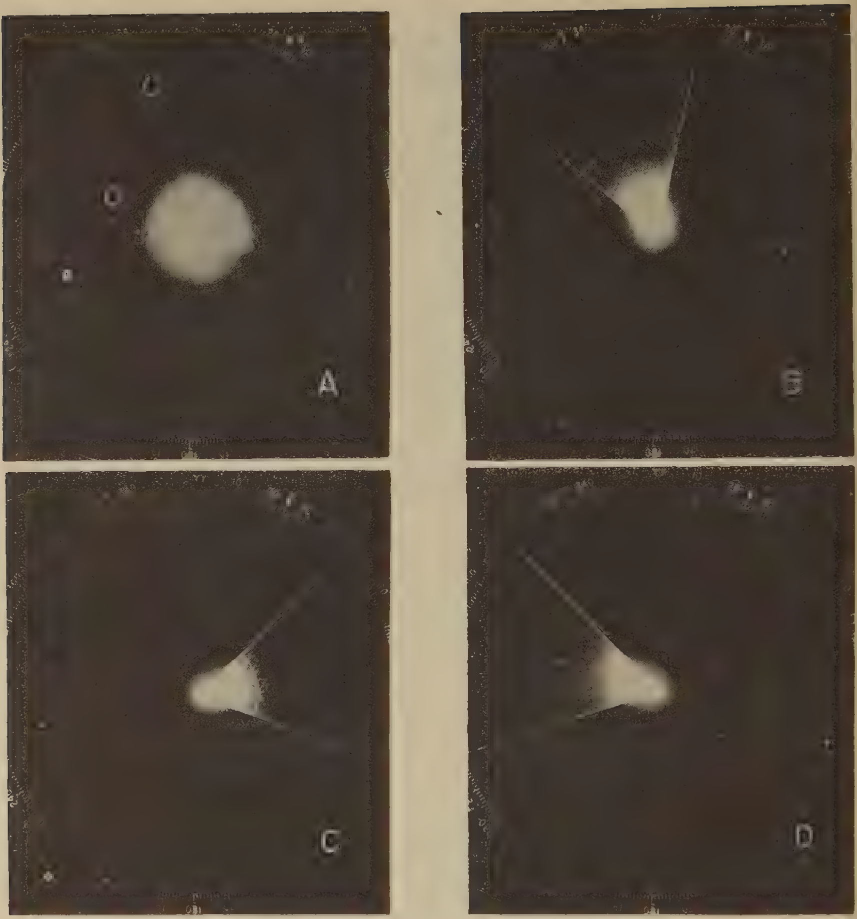

Figure 43.—PPI scope photographs illustrating the effectiveness of sector scan for the detection of icebergs (please see text).

lations today is beyond the training and skill of the majority of operators. It is recommended that rather than perfecting new devices which might more confuse the operator, a method of automatically applying various elements of sensitivity time control, fast time constant, and logarithmic echo amplification be considered. Perhaps a spectrum analyzer can be developed which could activate, automatically, these elements in the proper quantities depending on the spectrum of the sea return. This would certainly improve the potentials of a radar for detecting not only ice, but all targets in sea return.

Finally, based on the unequivocal conclusions of the studies conducted during the past 15 years:

> ***All Ship Masters, Mates, and Owners are Warned That Safe Passage Through Iceberg Areas of The North Atlantic Ocean Cannot be Assured by the Use of Radar.***

21 December 1959

BIBLIOGRAPHY

1. Barnes, C. A., H. M. Chandler, E. R. Challender, and H. H. Whaley. 1945. Radar Detection of Floating Ice. unpublished technical rept., INTICEPAT, 1945.
2. Read, G. H., and R. A. Pasciuti. 1946. Radar Detection of Floating Ice During the 1946 Ice Season. unpublished technical rept., INTICEPAT, 1946.
3. Budinger, T. F. 1959. Ice Detection by Radar, Consolidated and Abridged Report of 1945 and 1946 Studies. Interim technical rept. no. 1, INTICEPAT, 1959.
4. Hood, A. D. 1958. An Analysis of Radar Ice Reports Submitted by Hudson Bay Shipping (1953–1957). National Research Council of Canada rept. no. 4698, 1958.
5. Attwood, S. S. 1949. Radio Wave Propagation, Consolidated Summary Technical Report. Academic Press, New York, 548 pp., 1949.
6. Debye, P. 1929. Polar Molecules. Chemical Catalogue Company, Inc., New York, p. 44, 1929.
7. Lane, J. A., and J. A. Saxton. 1952. Dielectric Dispersion in Pure Polar Liquids at Very High Radio-Frequencies. Proc. Roy. Soc. London, Ser. A, no. 213, p. 400, 1952.
8. Errera, M. J. 1924. La Dispersion des Ondes Hertziennes dans les Solides au Voisinage du Point de Fusion. Journal de Physique, Ser. 6, vol. 5, p. 304, 1924.
9. Saxton, J. A. 1950. Reflection Coefficient of Ice and Snow at V. H. F. Wireless Engineer, vol. 27, p. 17, 1950.
10. Lamb, J. 1946. Measurements of the Dielectric Properties of Ice. Trans. Faraday Soc., vol. 42A, p. 238, 1946.
11. Smyth, C. P., and C. S. Hitchcock. 1932. Dipole Rotation of Crystalline Solids. Journal Amer. Chem. Soc., vol. 54, p. 4631, 1932.
12. Lorentz H. A. 1909. The Theory of Electrons. G. E. Stechert & Co., New York, note 55, p. 306, 1909.
13. Barnes, H. T. 1928. Ice Engineering. Renouf Publishing Co., Montreal, Canada, 364 pp., 1928.
14. Smith, E. H. 1928. The Marion Expedition to Davis Strait and Baffin Bay. U. S. Coast Guard Bull. no. 19, p. 111, 1928.
15. Garlick, J. K. 1953. A Survey of Low Reflection Coefficients for Various Types of Land and Frozen Sea for Normal Incidence at 1600 Mc/s. Royal Aircraft Establishment Technical Note no. RAD.536, London, 1953.
16. Anonoymous. 1955. U. S. Navy Marine Climatic Atlas of the World, North Atlantic Ocean, vol. 1, Navaer 50–1C–528, 1955.
17. Anderson, L. J., and E. E. Gossard. 1955. Prediction of Oceanic Duct Propagation from Climatological Data. IRE Trans. on Antennas and Propagation, vol. AP–3A, no. 4, p. 163, 1955.
18. Anderson, L. J., and R. R. Abbott. 1943. A Report on Radar Wave Propagation. U. S. Navy Radio and Sound Laboratory Report No. WP4, 1943.
19. Humphreys, W. J. 1940. Physics of the Air. McGraw-Hill Book Co., 1940.
20. Van Vleck, J. H. 1945. Further Theoretical Investigations on the Atmospheric Absorption of Microwaves. OEMsr–262, Service project AN–25, Div. 14, Report 664, 1940 (c.f. reference 5).
21. Goldstein, L. 1949. Dielectric Constant, Absorption and Scattering. Radio Wave Propagation, vol. II, p. 269, 1949.
22. McPetrie, J. S. 1938. The Reflection Coefficient of the Earth's Surface for Radio Waves. Inst. of Elec. Eng. Journal, vol. 82, p. 214, 1938.

* U.S. GOVERNMENT PRINTING OFFICE : 1960 O—551808

Contribution No. 1094

Särtryck ur Tellus nr 3, 1960

The Origin of Trade-Wind Orographic Shower Rains

By A. H. WOODCOCK, Woods Hole Oceanographic Institution[1]

(Manuscript received February 6, 1960)

Abstract

The purpose of the work reported here was to learn more about rain formation through a study of the extensive Project Shower and other data on the physics and the chemistry of rains. Most of the observations used have been published. It is demonstrated that the water and chloride content of orographic shower rains in Hawaii can be roughly computed from the observed amounts of sea-salt aerosols and water vapor in the sub-cloud layer over the sea, assuming wet adiabatic ascent of the air. From this and several other relationships among the properties of the air and rains, it is tentatively concluded that the showers originate within especially moist parcels of air which are carried into the orographic cloud by the trade winds, and which were previously formed in the sub-cloud layer over the windward sea. Specific suggestions are made for testing the degree to which potential shower-forming air may be identified over the sea or the windward shore prior to rain formation.

1. Introduction

Since the beginning of the century numerous workers have, for various reasons, been interested in the chemistry of precipitation (see review papers by ERIKSSON 1952 and JUNGE 1958). Among the many results of this world-wide interest has been the discovery that the chloride concentration in rains tends to decrease with increases in rain amount. In the present paper, the numerous data concerning the chlorinity and other properties of the rain and the atmosphere are examined in order to see what deductions can be made, if any, about rain-forming processes. Recently derived information about the individual sea-salt particles in the atmosphere is also utilized.

The presence of chlorides in precipitation waters has long been used as an example of the capacity of rain to "wash" particulate and other matter from the air as the drops fall from cloud base to ground. Recent tests in 1951 and 1952 (WOODCOCK and BLANCHARD 1955) revealed, however, that similar chloride concentrations were also present in rains sampled within the rain-producing clouds, making it necessary to revise the "washout" idea of earlier workers to include washout from the cloudy air as well as sub-cloud air. In the present paper it is demonstrated that, through alterations in the time, duration and position of rainwater sampling, one can reveal useful relationships between the chloride concentrations and other characteristics of the rains and of the atmosphere from which they fall.

The Project Shower data resulting from a cooperative field study of Hawaiian trade-wind orographic showers (SQUIRES 1955), is the primary source of the information used in the present work. These data have been given in a series of reports in Tellus vol. 9, No. 4, 1957.[1]

2. Comparison of observed and computed chloride concentrations in rains

In a previous study of the rains of Hawaii (WOODCOCK and BLANCHARD 1955) is was computed from observational data and with certain assumptions, that about 20 to 40 per cent of the airborne salt could be found in solution in the rains which fall near cloud-base altitude

---

[1] Contribution No. 1094 of the Woods Hole Oceanographic Institution. Work supported by the Office of Naval Research, under Contract Nonr-798(00) (NR-082-124).

[1] Hereafter referred to by the abbreviation PST.

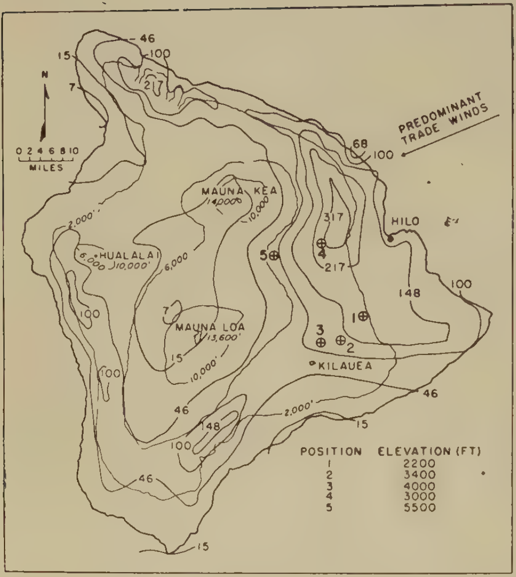
PREDOMINANT TRADE WINDS
N
0 2 4 6 8 10 MILES
MAUNA KEA 14,000'
HUALALAI 10,000'
MAUNA LOA 13,600'
KILAUEA
HILO
POSITION ELEVATION (FT)
1 2200
2 3400
3 4000
4 3000
5 5500

Fig. 1. Isohyetal map of the island of Hawaii, showing the locations of the earlier rainsampling stations. The later more elaborate study required the expanded network shown in Fig. 2.

(stations 1 and 4, Figure 1). These rain showers drift in the wind stream up the mountain slope, the rain being "winnowed" in the general direction of stations 3 and 5 as indicated by BLANCHARD (1957). Rain samples taken at position 5 were found to contain only about five per cent of the salt. It was suggested at the time that the remainder of the salt and water of the rains might be found among the drops which fall over the intervening distance of about 20 km.

During the Project Shower field program, daily rain amounts were sampled at closely spaced stations roughly along the average line of drift of the trade-wind air, with the purpose of examining this idea of winnowed drops. From these samples numerous data are available showing the daily rainfall and saltfall as a function of distance downwind and up the mountain slope from stations 32 and 5 on the Kulani and Saddle Roads (see Figure 2). In this section the properties of the rains from these locations will be shown to be related to the amounts of airborne salt particles and the amounts of water condensed in the clouds.

The purpose here is to present an analysis of a part of the published Project Shower data which indicates that the Hawaii orographic shower rains are produced in certain parcels of air. In simple terms, the actual operation performed here is a comparison of the ratios

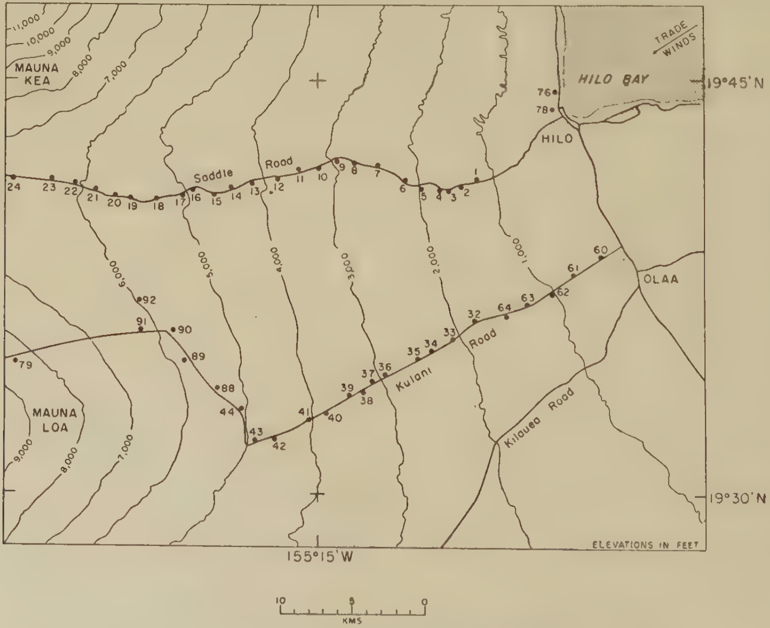
TRADE WINDS
HILO BAY
19°45'N
HILO
MAUNA KEA
Saddle Road
Kulani Road
Kilaueo Road
OLAA
MAUNA LOA
19°30'N
155°15'W
ELEVATIONS IN FEET
10 5 0
KMS

Fig. 2. Map of a section of the windward side of the island of Hawaii. The numbered dots on the Saddle and Kulani roads mark the positions of the Project Shower rain gages used in the present study.

Table 1. Data used in comparing the average chlorinity of the orographic shower rains of Hawaii to the chlorinities derived by the use of the "shower parcel" model

			a	b*	c*	d	e	f	g	h
Date	Rain Sampling		Airborne Chloride particles	Rainfall	Saltfall (in rain)	Cloud base altitude over sea	Cloud top altitude	Water content of rain	Chloride conc. of rain observed (c/b)	Chloride conc. of rain comp. (a/f)
	position	duration hours	μgms kg^{-1}	10^6 liter	10^6 mg Cl	m	m	gms kg^{-1}	mg l^{-1}	mg l^{-1}
Oct. 1954										
19—20	S	24	3.1	0.34	0.36	336	2,410	3.8	1.0	0.7
20—21	S	»	9.2	1.08	3.96	610	2,740	4.0	3.7	2.3
25—26	S	»	6.4	0.80	0.05	»	2,920	4.2	0.1	1.5
»	K	»	»	0.49	0.20	»	»	»	0.4	»
26—27	S	»	»	0.51	0.23	»	2,470	3.5	0.5	1.5
»	K	»	»	0.67	1.02	»	»	»	1.5	»
Nov. 1954										
2—3	S	24	6.5	0.08	0.22	458	1,830	2.5	2.7	2.6
»	K	»	»	0.08	0.39	»	»	»	4.8	»
6—7	S	»	3.9	0.80	0.14	404	3,020	5.0	0.2	0.8
»	K	»	»	0.69	0.45	»	»	»	0.7	»
7	S	3	4.9	0.11	0.07	503	2,710	4.2	0.6	1.2
»	K	»	»	0.12	0.12	»	»	»	1.0	»
9—10	S	24	2.8	0.14	0.19	305	2,010	3.1	1.3	0.9
»	K	»	»	0.16	0.23	»	»	»	1.5	»
25—26	S	»	6.8	0.27	0.37	915	3,110	3.6	1.4	1.9
29—30	S	»	8.5	0.27	0.71	670	2,860	4.0	2.6	2.1
»	K	»	»	0.28	0.95	»	»	»	3.4	»
Dec. 1954										
N30—1	S	22	11.9	0.40	1.34	610	2,840	4.1	3.3	2.9
»	K	»	»	0.49	2.23	»	»	»	4.6	»
1—2	S	24	10.7	1.24	2.38	630	3,260	4.8	1.9	2.2
»	K	»	»	0.88	3.14	»	»	»	3.5	»
2	S	2	11.1	0.17	0.34	640	3,020	4.4	2.0	2.5
»	K	»	»	0.09	0.35	»	»	»	3.9	»
2—3	S	21	9.3	1.10	0.93	610	3,140	4.5	0.8	2.1
»	K	»	»	1.34	0.82	»	»	»	0.6	»
3—4	S	24	5.2	0.11	0.19	900	2,220	2.1	1.8	2.5
»	K	»	»	0.15	0.37	»	»	»	2.4	»
3	S	2.5	—	0.06	0.09	670	3,050	4.5	1.5	—
»	K	2.5	—	0.05	0.03	»	»	»	0.7	—

* Rain and salt falling on a strip one meter wide, which extends from gages 5 and 32 to the upper limits of the rain areas.

of the total saltfall and rainfall on the mountain to the ratio of salt load of the sub-cloud air and the total water condensed as this air ascends in the clouds.

The information used to derive these ratios is listed in Table 1, along with other pertinent facts which will enable the reader to find the original data in PST. The primary observations are contained in columns a through h, Table 1, and are discussed in that order below.

a. The quantities of chloride in the sub-cloud air over the sea are taken from pages 522 and 523 (PST), and are the sums of the products of the median number particle weight in each weight range category and the number of particles in each range.

b. Integrated total amounts of rainfall in rain gages 5 through 25 on the Saddle Road and numbers 32 through 44 on the Kulani Road are given. Uniform steps of about 1,570 meters were used in this integration, in order to smooth out small differences in the spacing of the sampling station. The rainfall amounts given represent the total falling on a strip one meter wide.

Effectively samples are thus obtained at various successive times in the life histories of the showers, which begin on the lower slopes and rain out as they drift up the slope about parallel with the lines of sampling stations (see Figure 2). Only stations within the orographic clouds are included in this analysis, thus avoiding any question of salt collected by the rain in falling from cloud base to ground. (Excluded from this analysis are the Kulani Road data of November 26—27, which included rains of the 25th to 26th, and the Kona Storm rains of the 27th to 29th of November, when flights were cancelled.)

c. Integrated total fall of chloride dissolved in the rains is derived in the same manner as the integrated rainfall discussed above under (b).

d. Cloud base altitudes over the sea as measured by aircraft are given. These were found on occasion to differ by one hundred meters or more in places only a few miles apart. The altitudes given are the minimum values observed during the flights.

e. The average altitude at which the radiosonde record showed drying of the air ≤ 50 % relative humidity. Four ascents were made daily (PST pp. 569 to 580). This drying of the air was often associated with the trade-wind temperature inversion, but is thought to be a better indicator of average cloud top than is the temperature.

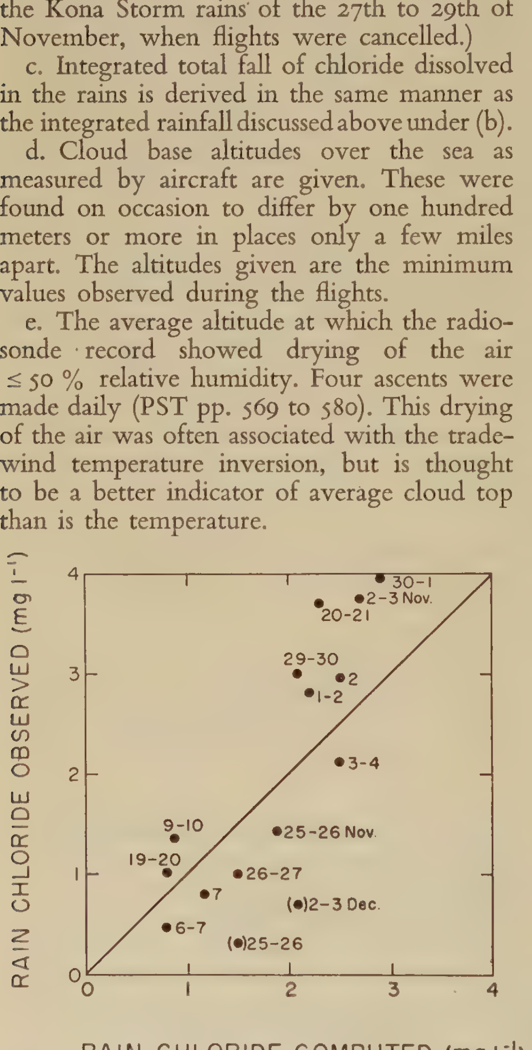

Fig. 3. A comparison of the average observed chlorinity of the integrated total rainfall on the Saddle and Kulan roads and the rainfall chlorinity computed from the "shower parcel" model. The numbers near the points refer to the days of the month, as given in Table 1.

f. The average water content of the rain is derived by assuming that an air parcel, equal in vertical extent to the distance from sea surface to cloud base (i.e., equal to d), flows into the orographic cloud and is lifted wet-adiabatically from cloud base to within one-half of the distance d below the cloud top. Cloud-base mixing ratio is approximated from the Hilo radiosonde records (PST pp. 569—580), a tephigram being used to derive the total condensed water.

g. Column g lists the ratios of the total saltfall to the rainfall (c/b). This chloride concentration is thought to be equal to that which would be found in rains if one could catch all of the water falling from the showers as they move up the mountain slopes.

h. These computed chloride concentrations (a/f) are compared to the average of those observed (g). The reason for making this comparison is the idea that the rains are generated in certain ascending parcels of air. It is thought that the salt content of these parcels is equal to the average in the sub-cloud layer over the sea and that their water content equals that released in the wet adiabatic ascent of the parcel.

Figure 3 shows the relationship between the average of the chloride concentrations observed on the Saddle and Kulani Roads (Table 1, column g) and those estimated through the use of the rain-generating parcel model mentioned in h, above. (On October 19th through 21st, the Kulani Road gages were not yet in operation.)

3. Discussion of Figure 3

At first glance the relationship of the observed and computed chlorinities in this graph may seem poor. The values seem remarkably similar however, when one reviews the variability of many important factors involved.

For instance, if many rains begin upwind of gages 5 and 32 (Figure 2) and near the coast during a 24-hour period, the higher salinity drops which are the first to come from the showers (TURNER 1955, WOODCOCK 1953) will fall before the showers pass over the sampling stations, thus causing these drops to be inadequately represented in the two lines of gages. The low-chloride rains of October 25 to 26 and December 2 to 3 may be due to this factor (see Figure 3 and the isoheytal maps pp. 587 and 589 PST).

Showers moving in directions not parallel to the lines of gages can also alter the assumed average pattern of the first larger drops falling in the lower-level gages and the smaller drops falling in gages successively further up the slope in the direction of shower drift. Such showers might serve to increase or to decrease the observed twenty-four hour average chlorinities such as those given in Figure 3.

On many occasions only one measurement of airborne salt was available for a 24-hour period. The data however show differences of two to three times in airborne salt in a day, thus adding a further potential error in the computed concentrations of Figure 3.

Errors can arise in the estimation of condensed water from uncertainties as to the time of occurrence of the most of the rain[1] and consequently as to which of the four daily radiosonde records to use in estimating cloud thickness and the amounts of condensed water. The average inversion altitude, as reflected in the drying of the air $\leq 50\,\%$, has been used here in estimating condensed water amounts, though if one knew the time of occurrence of most of the rain, it might be much more realistic to use only one of the radiosonde records as specifying the state of the lower atmosphere.

Leopold's suggestion of the possible existence of local convergence over the region of maximum rainfall (Leopold 1949) may also be important here, though occasional observation from aircraft revealed no marked increase in cloud top altitudes in this region of the orographic cloud.

The presently most satisfactory explanation of the results on Figure 3 is one requiring the assumption that the major growth of the raindrops takes place in parcels of ascending air, and that in the drop growth process all of the salt particles in these parcels become dissolved in the rain waters. Alternative assumptions of fallout of all salt and condensed water in the whole cloud, or of washout of total cloud salt by rain formed in the parcels alone, produce computed salinity values which in all cases fall to the right of the forty-five degree line on Figure 3.

We might also suppose that the salt and water does not come from the sub-cloud parcels exclusively, but is fractionally extracted from most of the cloud in some accretion process such as that suggested by Bowen (1950). If this occurs, then the relationship suggested by Figure 3 requires that this accretion process in each shower extract an amount of water and salt from the cloud which is approximately proportional to the cloud-base-to-inversion distance and to the weight of salt in the sub-cloud layer respectively.

Proportionalities such as these seem reasonable, but the sequence of events pictured in Bowen's model seems clearly inapplicable to the Hawaii orographic shower rains. For instance, Wexler (1954) has shown that application of Bowen's model to the growth of marine aerosols in cumuli should result in an early fall out of the giant (10^{-9} gm) sea-salt particles as small raindrops, whereas the more numerous smaller (10^{-10} gm) particles should fall later in the shower as larger drops. Howver, Woodcock and Blanchard (1955) found that the initial drops falling at the beginning of a shower at cloud base were large and few in number and later Turner showed that the salt content of the large drops ranged from about 2×10^{-9} to 10^{-8} grams (see Turner 1955, Figure 4, curves b). Woodcock and Blanchard (1955) also showed that the numbers of these drops per cubic meter of air approximated the numbers of the giant salt particles of the masses given, suggesting a growth mechanism which tended to conserve the number per unit volume of air as the giant nuclei grow to raindrop size. Thus if one assumes that the coalescense of many droplets containing smaller amounts of salt have chanced to become one drop whose salt content is equivalent to the mass of the larger sea-salt particles, he is faced with the problem of explaining the number correspondence mentioned above.

The purpose of emphasizing here the large amounts of salt in the large raindrops, however, is to suggest that the evidence is against the Bowen mechanism as one which is consistent with the results given in Figure 3, since the mechanism fails to account for some of the details of the character of the rains represented. On the other hand, the salt nuclei hypothesis of raindrop formation outlined by the author

---

[1] The rain recorders should have been in continuous operation.

(Woodcock 1952) and tested in collaboration with Blanchard (1955), does not conflict with Turner's observations (Woodcock and Blanchard 1955). It is pertinent to repeat here that this hypothesis led to the suggestion that the fraction of the rain and chloride which was not found near cloud base, should be found among the drops distributed up the mountain slopes by the winnowing action of the wind. The integrated total fall of salt and water on these slopes (columns b and c, Table 1), does indeed appear to be a rough summation of the total amount of these substances in the rain-generating parcel of air.

Entrainment of air from the orographic cloud into the shower-producing parcels has not been considered. An implication of Figure 3 is that entrainment into the parcels, if it occurs, does not greatly alter their relative salt and water contents.

Impactor samples of salt aerosols taken by Junge (PST pp. 535) near ground levels well within the orographic clouds, and during "drizzle", showed an almost complete absence of chloride among the "giant particles" (0.8 to 8 μ radius). This might be mistakenly interpreted as indicating that the rains had washed out all of the particles with which we are concerned here. However, within the cloud most of the giant sea-salt particles would have grown into cloud droplets larger than Junge's upper limiting size of 8 μ (Keith and Arons 1957), and thus would have fallen out in the 50 cm long "precipitation tube", before reaching the sampling surfaces of his impactor (Junge 1958).

The foregoing discussion of Figure 3 is not regarded as proof that the major growth of the raindrops occurs exclusively in parcels of sub-cloud air ascending in the orographic cloud. At this time, however, the author is unable to think of a more plausible notion. Later in this paper a further method for testing this idea in the future is outlined.

The mechanics of rain formation which can lead to the observational results given in Figure 3 and to those upon which the salt-nuclei raindrop hypothesis (Woodcock and Blanchard 1955) is based remain unknown to the author, though Komabayasi (1958) has made an interesting approach to the latter problem. Recent work by C. G. H. Rooth (unpublished) on an additional theoretical model, involving drop growth in air parcels having the form of spherical vortices, is producing some useful results. In the meantime, some of the implications of the present air-parcel idea of shower rain origin seem worth additional investigation here in an effort to mark out promising paths for further exploratory field work.

The author has long entertained the idea that parcels of air in which showers are to form may be identifiable in the tradewind stream over the sea, prior to their passage over the windward shore and into the orographic clouds. The following study supports

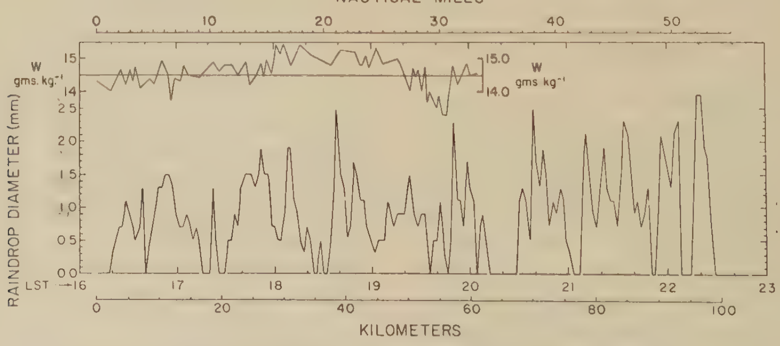

Fig. 4. The lower part of this graph gives the maximum drop diameter (± 0.1 mm) found on the drop-recorder tape, exposed at station 4 on Oct. 21, 1954, as a function of time. The distance scales represent the motion of the lower air (at 8.5 knots) during the time the rain recorder was operating. The upper part of the graph shows horizontal differences in mixing ratio which were taken from Figure 5. (A correspondence of upper and lower traces on Figure 4 is not to be expected.) See text for more explanation.

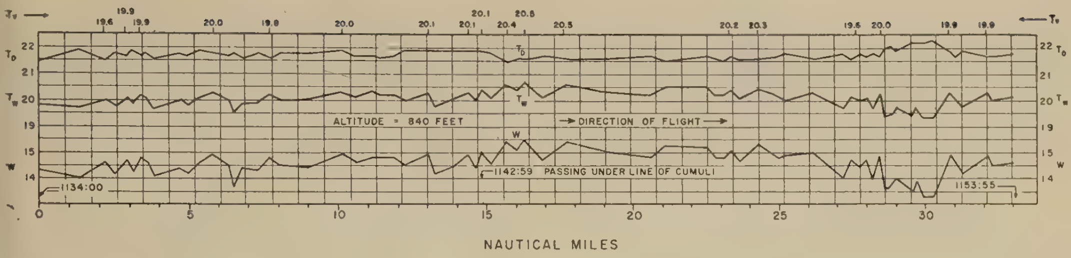

Fig. 5. Reproduction of some of Johnson's data (PST p. 498, Fig. 5) showing differences in the distribution of temperature and water vapor on Oct. 21, 1954, in a horizontal flight made about parallel to the surface wind and windward of Hawaii. The purpose here is to illustrate the effects of the differences in the amounts of vapor upon the virtual temperature when the sub-cloud layer is lifted above the saturation altitude. The numbers at the top of the figure were added to show the range of virtual temperatures which will exist in the moist parcels if the layer is lifted adiabatically to the 911 mb level. Note that the virtual temperature of these parcels exceeds that of the environmental air at the time (see Table 2).

this idea in a way which enables one to form some specific questions upon which to base suggestions for further work.

4. Identifying potential rain-forming air parcels

Concerning the idea of the existence of specific shower-producing parcels in the sub-cloud layer over the sea, it is interesting to ask how many showers fall each twenty-four hours, and what property differences in the layer might show a frequency of recurrence similar to that of the showers.

Unfortunately, there was only one day during the project when a rain recorder was in operation at a time when measurements were also made in the sub-cloud air over the sea and when the flight was made parallel with the surface wind.

On October 21, 1954, between 1610 and 2250 HST, a rain-recorder indicated about thirty-four showers passing station 4 (see map, Figure 1). Each increase in raindrop size, or each peak in recorded maximum size (see lower part of Figure 4) is counted as a separate shower, since there seems to be no clear physical basis for discrimination among them at this time.

Between 1054 and 1217 on the same day, wet- and dry-bulb temperature measurements were made in the lower air over the sea along a flight path parallel with the surface wind and windward of the sampling area on Hawaii (see PST p. 498). A part of the flight data is reproduced here in Figure 5 and at the top of Figure 4. The timing of these aircraft measurements was such that some of the air in which the flight was made would flow over the island sampling area during the rain-sampling period. The Hilo wind for the 300 m to 2,100 m layer, averaged 8.5 knots during the rain-sampling period (PST p. 570). Thus, about 57 nautical miles of air flowed over the Saddle Road during the rain-sampling interval (see distance scale on Figure 4).

Examination of Figures 4 and 5 shows that the factor which might significantly alter the stability of this lower air as it is forced up into the orographic cloud and one which varies spatially at frequent intervals in flight parallel with the wind, is the amount of water vapor.[1] It will be noted that there are 18 marked peaks in the mixing ratio (W) in the 33 nautical mile flight path. The vapor content and temperature of these moist air parcels was such that their virtual temperature, upon adiabatic lifting to 911 mb and higher, would exceed that of the environment at the time by at least 0.5 °C (see Table 2). Figure 6 shows graphically these excess temperatures, using the environmental conditions specified by the Hilo radiosonde and by Johnson's airplane sounding. These more unstable parcels of air from the sub-cloud layer should ascend

---

[1] The results of cross-wind flights by Johnson are not useful here because the rain recorders indicate the showers that occur along the line of flow of the trades, and not those that occur normal to them. It is noteworthy that the frequency of occurrence of horizontal differences in W in the sub-cloud air was not the same during the parallel-with-the wind flight on October 21, and cross-wind flights on other days (see PST, pp. 498, 501, 502 and 503). Measurements should have been made on both headings at about the same time and altitude on each of the days studied.

Table 2. Results of airplane sounding made by Johnson (PST p. 499) at 1218 to 1241 HST, on Oct. 21, 1954, over the sea a few miles southeast of Hilo. The pressures were derived from the altimeter readings, and the virtual temperatures were derived through the use of Table 72 of the 1958 Smithsonian Meteorological Tables. The columns marked "moist parcels" give the virtual temperatures of the dryest and the wettest of the 18 moist parcels indicated on Figure 4, assuming adiabatic ascent above the condensation lifting level. Note that temperature (T_V) excess over that of the environment (columns 6, 9, 10 and 11) becomes large only above about 1,020 m.

Altimeter reading	Johnson's Sounding					"Moist Parcels"		Hilo Radiosonde		
						dryest	wettest	interpolated values		
	P	T_D	T_W	W	T_V	T_V	T_V	1100	1700	2300
m	mb	C	C	gm kg^{-1}				T_V	T_V	T_V
256	983	22.1	20.2	14.6	24.7					
348	972	21.0	19.8	14.7	23.6					
430	963	20.1	18.8	13.9	22.6					
470	958	20.2	17.9	12.8	22.5					
510	953	19.8	17.9	13.0	22.1					
560	948	19.5	17.0	12.0	21.6					
607	942	19.3	16.6	11.7	21.4					
665	936	18.6	17.0	12.5	20.8					
760	926	18.4	15.8	11.2	20.4	20.4	21.1	21.0	19.2	20.2
850	915	17.8	15.5	11.3	19.8	19.9	20.6	20.4	18.9	19.6
890	911	17.1	15.9	12.0	19.1	19.6	20.4	20.2	17.9	19.3
940	905	16.8	14.8	11.0	18.7	19.4	20.1	19.8	17.3	18.8
1,020	897	16.6	14.8	11.1	18.5	19.0	19.8	19.3	16.6	18.2
1,050	894	16.1	14.7	11.3	18.1	18.9	19.6	19.2	16.4	18.0
1,280	868	14.9	12.6	9.7	16.6	17.7	18.4	17.5	15.5	16.0
1,320	864	14.7	12.5	9.7	16.4	17.4	18.3	17.2	15.4	15.7
1,380	858	14.5	12.1	9.5	16.2	17.2	18.0	16.8	15.3	15.2
1,460	849	13.8	11.0	8.6	15.3	16.8	17.5	16.2	15.0	14.5
1,495	846	13.8	11.2	9.0	15.4	16.7	17.3	16.0	15.0	14.3
1,640	831	12.7	10.8	9.1	14.3	15.9	16.7	15.0	14.5	13.2
1,680	827	12.2	10.9	9.5	13.8	15.7	16.4	14.7	14.2	12.8
1,700	825	11.9	10.5	9.2	13.5	15.6	16.4	14.6	14.0	12.7
1,780	817	11.5	10.2	9.1	13.1	15.1	15.9	14.1	13.6	12.1
1,830	812	11.0	10.0	9.2	12.6	15.1	15.7	13.8	13.2	11.7
1,975	797	10.6	8.2	7.7	11.9	14.0	15.0	12.8	12.1	10.5
2,130	782	9.4	8.9	9.0	10.9	13.2	14.1	11.8	11.0	—
2,300	765	8.8	6.2	6.8	10.0	12.4	13.2	10.7	9.8	—
2,440	753	8.3	5.8	6.7	9.4	11.8	12.6	9.8	8.9	—
2,560	744	10.6	0.7	1.5	10.9	11.0	11.9	10.4	8.0	—
2,750	723	10.7	0.5	1.5	11.0	10.0	10.9	11.8	6.6	—
3,040	697	8.5	—0.9	1.4	8.7	8.3	9.3	—	9.0	

more rapidly in the orographic cloud than other parts of this layer. MALKUS (1954) has shown that virtual temperature excesses of 0.5 to 2 °C are commonly associated with the most rapidly ascending air in trade-wind cumulus clouds. It is assumed that it is within these moist parcels that the showers develop after the sub-cloud air passes up the windward slopes of the island and into the orographic cloud.

Thus, in the 57 nautical miles of air flow over station 4 on the Saddle Road, about 31 of these moist parcels should pass. Thirty-four showers were estimated from the rain-recorder tapes. The purpose here is that of simply emphasizing the rough similarity of the spatial distribution of showers and moist parcels (see Figure 4), and to point out that the parcels would have the highest virtual temperature in the clouds. We do not know the structure of the air which actually passed over the rain-recorder station. However, we do know that more than 75 % of the 120 nautical miles of air measured by Johnson on the 21st showed structure similar to that represented at the top of Figure 4.

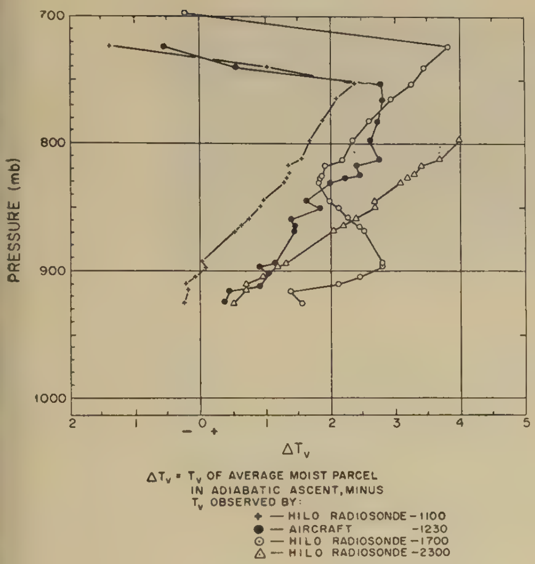

Fig. 6. Virtual temperature differences between the average moist parcel (Fig. 5) in adiabatic ascent and that within the lower atmosphere at various times during the observation period. Aircraft sounding made over sea about ten nautical miles southeast of Hilo.

5. Discussion of Figures 4 and 5, and Table 2

It may be argued that the difference between the virtual temperature of the "moist parcels" and that of the adjacent "dryer parcels" (a few tenths to one degree) seems small. It should be remembered, however, that as the lower air orographically ascends, the moist parcels will be the first to reach the condensation lifting level, and hence will be the first to experience the additional buoyancy as latent heat is released. The recurring showers, and the similarity of their number to that of the moist parcels present a picture of chain-like rain-forming air masses linearly imbedded within the wind stream passing over the island. This perhaps explains the cellular nature of the orographic cloud, particularly towards its seaward edge, as noted by Squires and Warner among the records from their numerous flights made within this cloud to determine the droplet size distribution and liquid water content (see PST, p. 487). Many more measurements of moist parcel number and shower number are needed however. One naturally wonders what the moisture structure of the sub-cloud layer might be in the absence of shower activity on the island and when known influencing factors such as the temperature inversion and wind characteristics seem favorable for showers.

It will be noted that Johnson has indicated a mixing ratio accuracy of ± 0.2 gm kg^{-1} as derived from his psychrometric measurements. This error is due primarily "to the inaccuracy in determining the correction for dynamic heating" (PST p. 496). We are largely concerned here with differences rather than absolute values in mixing ratio. Since air speed was constant, dynamic heating errors would also be constant. The wet- and dry-bulb temperature (and hence mixing ratio) differences encountered in flight are concluded therefore to be real.

Similar spatial differences in water vapor had been previously observed from ships and aircraft in trade-wind regions of the Atlantic and on the windward shore of one of the Hawaiian islands (see Figures. 7 and 8). It is thought that these features are common in the sub-cloud air of these and perhaps other latitudes. In fact the data on Figure 9 show that moist parcels are present in the lower wind stream a short time after continental air passes over the sea, though in this case it is thought that the moist regions are of very limited vertical extent.

Sensitive shielded mercury thermometers were used to make the measurements reported on Figure 9. Response time was 60 % full scale in seven seconds and thermometer error correction was applied to the nearest five-hundredths of a degree. Readings were made each thirty seconds at a fixed location on the

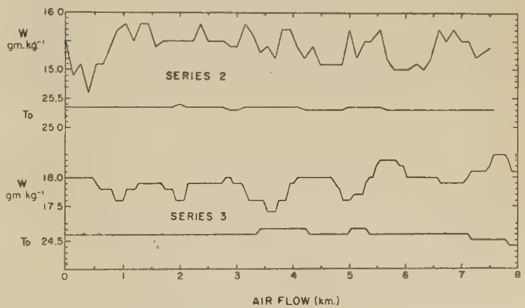

Fig. 7. Horizontal differences in the temperature and mixing ratio in the lower atmosphere of an Atlantic trade-wind area. It can be seen that these differences are very similar in frequency and amplitude to those presented in Fig. 4, 8 and 9. Table 3 and text give more information about these data.

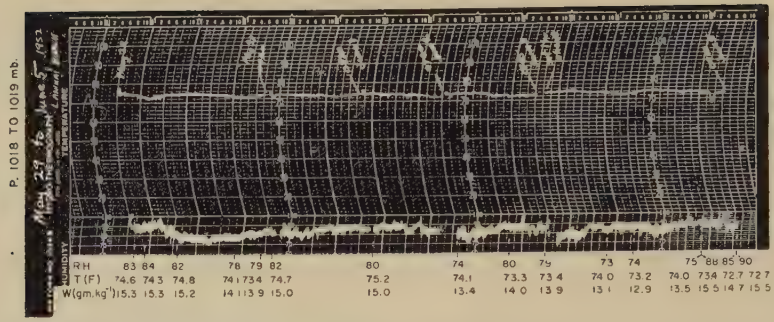

Fig. 8. One of five similar hygro-thermograph records from instrument exposed to trade winds at Lanikai Beach, Oahu, Hawaii. Location about 30 meters from windward shore, at site shielded from direct solar radiation and rain. For comparison, data from sling psychrometer measurements given in table below. Thermometer error corrected to nearest 0.1°, and times adjusted to error of the thermograph clock. Hygrothermograph shows short period RH changes of 4% to 10% with little dry temperature change. Mercury thermometers confirm these differences, when consecutive readings are made a few minutes apart (see results of last four measurements on table).

outer end of a pier near the Woods Hole laboratories, the passing air being metered with a recording anemometer.

The series two temperature measurements (Table 3 and Figure 7) were made at the bow of the research vessel Atlantis while it was in the Atlantic trade-wind area and moving windward. A sling psychrometer was used, and the thermometers were read each fifteen seconds. Radiation shielding was supplied by metal foil, and thermometer error corrected to the nearest one-tenth degree. The series three data were kindly supplied by Mr. A. F. Bunker of the Woods Hole Oceanographic Institution, from his aircraft measurements.

The effects of short-period variations in the thermal structure of the lower 3,000 m of the trade-wind atmosphere in altering the stability of the moist parcels (inadiabatic ascent), is clearly illustrated on Figure 6. A progressive increase in the T_V difference within a short time and distance is apparent, showing the potential importance of almost continuous scanning of this part of the atmosphere in trying to understand events in the clouds which are imbedded therein.

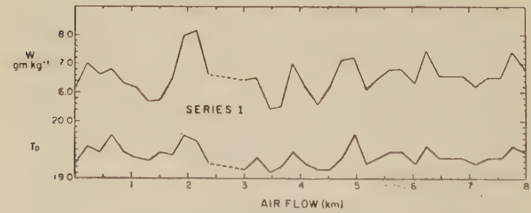

Fig. 9. Temperature and mixing ratio found within the wind stream shortly after air passed from land to water surface. See Table 3 and text for further information.

6. Estimate of shower diameters using parcel method

If most of the water condensing within the ascending shower-producing parcels eventually falls out along the lines of gages on the mountain slopes, one should be able to estimate the average sizes of the showers from the data on Table 1 and from the number of showers indicated by the rain recorders. The apparent average shower diameter (S) is estimated as follows:

$$S = \frac{R\,10^3}{Whn} \tag{1}$$

where R = average total rain; see Figure 2 and Table 1, column b (liters m^{-1})

W = total water condensed; Table 1, column f (gms kg^{-1})

h = vertical distance from sea surface to cloud base; Table 1, column d. (m)

n = shower number (counted as on Figure 4).

Table 3. Additional data concerning observations given on Figures 7, 8 and 9

Series	Date	Time zonal	Lat. N	Long. W	Alt. m	Surface Wind		Atmos. Pressure mb	Sea Surface Temp. C	Place	Fetch km
						Speed m sec^{-1}	Direction				
1	July 11, 1945	1400	41°31′56″	70°40′15″	3	7	320	1015	22.6	dock	19
2	Apr. 24, 1947	0630	20°38′	69°00′	4	3	90	1017	26.2	ship's bow	> 1,000
3	Nov. 14, 1958	1100	18°40′	65°50″	305	7	70	977	—	aircraft	> 4,000

Unfortunately none of the Project Shower data properly fulfill the requirements of equation (1). This is not surprising, since the program of observations was not designed to answer the questions posed. During the best single twenty-four hour observation period (Dec. 1—2, Table 1 and PST pp. 548 and 549), the rain-recorders missed more than eight hours. The two- and three-hour intervals of Nov. 7 and Dec. 2 and 3, are also uncertain because the time required to read the numerous rain gages was about one-half of the total sampling time. Thus, on Dec. 2, the rainfall in the Saddle Road gage number 5 (see Figure 2 and PST p. 514) represents the period 1414 to 1612, while the last gage, number 25, caught rains falling between 1509 and 1715 (see data file Pineapple Research Institute, Honolulu, Hawaii).

Using interpolations and extrapolations of the rain gage and rain-recorder data to cover the unknown time intervals, shower diameters of from 1,700 to 4,100 meters were computed for the above dates, using equation (1).[1] This diameter range is consistent with the few individual showers distinguishable in the liquid water records obtained in the orographic cloud by Squires and Warner (PST, see especially Figure 12 and pp. 487—489). Also, the Hilo rawinsonde data indicate in general a sufficient air flow inland to transport air parcels of the number and size required. Examination of the rain-recorder records shows however that variability in shower activity with time makes the validity of extrapolations or interpolations very uncertain.

Thus the major usefulness of equation (1) at this time is to point out that it constitutes a further means of testing the shower-parcel idea, when applied to data obtained during a properly designed observation program.

7. Conclusions

The idea that the showers originate in specific moist parcels of air enables one to advance tentative explanations for the following characteristics of Hawaiian orographic rains which have been revealed by the Project Shower data.

1. Chloride concentration
2. Shower frequency
3. Total water content
4. Horizontal dimensions

This result suggests that these rains form in units of air within the trade wind stream which may be identifiable prior to their arrival over the land. Despite the limited extent of some of the data supporting this idea, a reasonably consistent shower model has evolved. The importance in meteorological studies of locating shower-forming air before the shower occurs, makes further work seem clearly worthwhile. Prior location would of course be a forecasting aid and would simplify and make more economic studies of the effects upon shower production of artificially altering the nuclei population and other characteristics of potential shower-producing air parcels.

Since the chloride and water contents of Hawaiian rains seem to be explicable through

---

[4] It will be noted that the drop maxima, shown by the peaks on rain records such as Figure 4, are represented by n in equation (1) as if individual showers contributed equal amounts of rain to the lines of gages. It is clear however that these showers are widely different in intensity at any one location (e.g. PST p. 545). The high-rate rains have larger drops and presumably briefer duration, while the low-rate rains have smaller drops and presumably longer duration. Thus an equal value for R, in equation (1), can result from a 30 mm hr^{-1} rain lasting three minutes or a 3 mm hr^{-1} rain of thirty minutes duration.

the use of the moist-parcel idea, the application of this idea to rains in other areas, becomes a question worth consideration.

The parcel idea suggests that orographic shower frequency is related to the frequency of occurrence of certain moist parcels having virtual temperature excesses over those of the environment comparable to or exceeding those shown on Figure 6.

The occurrence of orographic showers in regions such as Hawaii should be predictable from measurements made within the cloud and sub-cloud layers of the lower atmosphere which are soon to pass over the area concerned. Horizontal runs and vertical soundings by aircraft, similar to those made by Johnson, are best; their number and extent depending upon the variability with time, distance and altitude of virtual temperature, mixing ratio, and perhaps other factors such as wind shear.

Figure 8 indicates that the moist air parcels of higher levels probably extend to within a few meters of the sea surface. If so, a simple means of testing them as a source of showers would be to set up a line of observing stations along the coast normal to the dominant winds and windward of a network of recording rain gages. Thus one could continuously scan the surface air two-dimensionally (or perhaps three-dimensionally using towers) for moist parcels and for showers. Frequent local radiosonde and rawinsonde ascents would also be needed as indicated in the present study.

Relatively long term field programs should be initiated at favorable locations, with the purpose of understanding and perhaps exploiting the relationships indicated here between certain properties of the air stream and the precipitation resulting when this air is subsequently lifted.

Acknowledgements

This paper is one of the results of Project Shower, a international cooperative field study to which many persons and organizations contributed (Squires 1955). Without their simultaneous efforts, focused upon the complex of interrelated events often too simply termed "orographic showers", the present work could not have been performed. The author's co-workers, Mr. D. C. Blanchard and Mr. Claes Rooth contributed to this work through generous critical readings and discussions.

REFERENCES

Blanchard, D. C., 1957: Discussion of raindrop distributions found during Project Shower, Hawaii, 1954. Artificial Stimulation of Rain, pp. 213—223, Pergamon Press, New York.

Bowen, E. G., 1950: The formation of rain by coalescence. *Aust. Jour. Sci. Res.*, A, 3, pp. 193—213.

Eriksson, E., 1952: Composition of atmospheric precipitation. *Tellus* **4**, pp. 280—303.

— 1955: Airborne salts and the chemical composition of river waters. *Tellus* **7**, pp. 243—250.

Junge, C. E., 1954: The chemical composition of atmospheric aerosols, I: Measurements at Round Hill field station, June—July 1953. *J. Meteor.* **11**, pp. 323—333.

— 1958: Atmospheric chemistry; Advances in Geophysics, IV, pp. 1—108, Academic Press, Inc., New York, N.Y.

Keith, C. H., and Arons, A. B., 1954: The growth of sea-salt particles by condensation of atmospheric water vapor. *J. Meteor.* **11**, pp. 173—184.

Komabayasi, M., 1958: Some aspects of rain formation in warm cloud (I) Salinity of individual raindrops and other quantities concerning rainfall. *Coll. Met. Papers No.* **108**, pp. 205—220, Geophysical Institute, Tokyo Univ., Tokyo, Japan.

Leopold, L. B., 1949: The interaction of trade wind and sea breeze, Hawaii, *J. Meteor.* **6**, pp. 312—320.

Malkus, J. S., 1954: Some results of a trade-cumulus cloud investigation. *J. Meteor.* **11**, pp. 220—237.

Project Shower Data, 1957: An investigation on warm rainfall in Hawaii. *Tellus* **9**, pp. 471—590.

Squires, P., 1955: Project Shower; An investigation on warm rain in the Hawaiian islands, *Nature* **175**, pp. 748—750.

Turner, J. S., 1955: The salinity of rainfall as a function of drop size. *Quart. J. Roy. Met. Soc.* **81**, pp. 418—429.

Wexler, R., 1954: Growth of rain in warm clouds. Unpublished manuscript. Woods Hole Oceanographic Inst.

Wood, W. E., and Wilsmore, N. T. M., 1929: Salinity of rain in Western Australia. *J. Roy. Soc. W. Austr.* **15**, pp. 22—30.

Woodcock, A. H., 1952: Atmospheric salt particles and raindrops, *J. Meteor.* **9**, pp. 200—212.

— 1953: Salt nuclei in marine air as a function of altitude and wind force. *J. Meteor.* **10**, pp. 362—371.

Woodcock, A. H., and Blanchard, D. C., 1955: Tests of the salt-nuclei hypothesis of rain formation. *Tellus* **4**, pp. 437—448.

Printed in Sweden
ESSELTE, STHLM 60

Contribution No. 1095

(*Reprinted from Nature, Vol.* 186, *No.* 4718, *pp.* 71–72, *April* 2, 1960)

Strontium-90 in the 'Mixed Layer' of the Atlantic Ocean*

OCEANOGRAPHY and marine geochemistry have only relatively recently been able to take advantage of isotopic tracer techniques; unfortunately, the conceptual framework devised for isotope studies in biochemistry and physiology is not readily applicable to systems of very large spatial extension.

In considering the significance of the ocean reservoirs in the geochemistry of carbon dioxide, and in using the distribution of carbon-14 to derive rates of ocean mixing in both vertical and horizontal planes, it has been conventional[1] to divide the oceans into shallow surface reservoirs assumed to be well mixed, and deep reservoirs assumed to be only slowly renewed from the surface. Since, in some applications, the quantitative expression of this picture is extremely sensitive to the assumed depth of the surface reservoir, and to its rate of renewal from below, it seems important to point out that these parameters are measurable by using relatively short-lived radioisotopes, which are added to the system at the surface. In the case of the Atlantic Ocean, North and South, this condition is well met by radioactive strontium-90 from bomb test fall-out. To the Atlantic, strontium-90 has been added, measurably, only as fall-out to the ocean surface. In this form the isotope is wholly soluble in water[2]; and in sea water, the dilution of the radioisotope by both stable strontium and stable calcium in solution is so great that neither biological nor chemical processes produce significant changes in strontium-90 concentration. Thus, its vertical transport depends wholly on vertical movement of the water in which it is dissolved.

As a part of an extended study of the marine geochemistry of long-lived radioisotopes from fall-out, we are obtaining a number of series of measurements of the change in strontium-90 concentration with depth in the ocean. Some of these measurements, together with descriptions of the methods employed, have been published[3]. We now present (Table 1) seven series of strontium-90 analyses, all but one previously unreported. These series agree in showing very significant concentrations of radiostrontium at depth in the open ocean, both north and south of the

---

* Contribution No. 1095 from the Woods Hole Oceanographic Institution.

Table 1. STRONTIUM-90 IN ATLANTIC WATER COLUMNS

Station position	15° 49′ S. 35° 50′ W.	8° 26′ S. 7° 45′ E.	16° 15′ N. 43° 37·5′ W.	36° 23′ N. 70° 33′ W.	31° 15′ N. 68° 10′ W.	34° 30′ N. 65° 42′ W.	34° 39′ N. 67° 24′ W.
Date collected	1/2.4.57	1.3.57	22.11.57	13.7.57	8.12.57	11/12.7.58	15/16.7.58
^{90}Sr disinteg./min. per 100 litres at depth :							
0 m.	4·1 ± 0·5	5·0 ± 1·0	6·3 ± 0·6	10·5 ± 0·6	10·9 ± 0·6	7·6 ± 0·6	9·1 ± 0·6
100			5·4 ± 0·5		7·7 ± 0·6	13·0 ± 0·7	8·2 ± 0·6
300		2·4 ± 1·0				11·8 ± 0·9	5·5 ± 0·5
400			2·2 ± 0·3		3·9 ± 0·6		
500				4·1 ± 0·6		7·3 ± 0·4	6·4 ± 0·5
700		< 0·3			2·3 ± 0·4	3·7 ± 0·5	3·4 ± 0·5
1,000	1·5 ± 0·6			< 1·0		< 0·9	1·7 ± 0·3
1,200			1·6 ± 0·8				

Note.—Deviations reported are those expected from counting statistics only.

equator. The number of analyses is still too few to justify very precise integration of the curves of strontium-90 versus depth, but an average concentration, from 300 to 700 m., of about half the surface value, is indicated. The upper 100 m. appears likely to be well mixed, as generally assumed, with a sharp gradient from 100 to 300–400 m. Appreciable concentrations at 1,000–1,200 m. are frequent, although we have never found measurable radiostrontium in samples from 3,000–5,000 m.

We wish to emphasize here only two features of these distributions: the indicated mass transport, and the time-scale. The water columns so far sampled appear to have from three to four times as much total strontium-90 below 100 m. as remains above that depth; and it is reasonable to assume that this radioisotope has all been added since mid-1954[4]. The possibility of vertical transport by sinking along sigma-T surfaces appears to be strictly ruled out by the short times available, and the enormous horizontal distances which would have to be traversed. A more or less direct vertical movement by wind-driven mixing is indicated. The facts of the close agreement of samples from 400–500 m. from the two 1957 Sargasso Sea stations, and the significantly higher figures for the July 1958 stations, support the postulate of vertical transport during the winter period of surface-water cooling and high wind velocities.

It is unfortunate that present uncertainty about the mechanism and rate of stratospheric fall-out should preclude conversion of our figures for total vertical transport of strontium-90 into annual rates of down-mixing (and hence of up-mixing) of ocean surface-water in mid-latitudes. For this, more observations over a longer time span will be needed, and this will be profitably supplemented by the collections of precipitation which have begun on weather ships. It does now seem reasonable to point out that the same mechanism which has produced in three years at depths of 300–700 m. an approximately 1 : 1 mixture of surface-layer strontium-90, and pre-1954 sub-surface strontium-90, would have produced the same sort of dilution of surface seawater carbon-14. Broecker's weighted average[5] of carbon-14 in North Atlantic water at 200–400 m. very closely approximates this same 1 : 1 ratio. Clearly, to assign the reduction in carbon-14 activity to radioactive decay, and conclude a 'crude age' of 290 years, become untenable, in the light of our demonstration that surface-added radioactivity reaches this same concentration ratio in three years. An attempt must be made to interpret these reductions in specific activity, and that in the surface layer as well, as standing concentrations maintained by mixing processes. Unlike the situation in biochemistry, here the gradient area across the boundary between two reservoirs contains a major fraction of the tracer in the system. A very much larger flux of carbon-14 across the sea surface must then be postulated to maintain the very much greater reservoir indicated. Our strontium-90 measurements, as well as the first of the weather ship fall-out measurements[6], indicate that much more fall-out may have been delivered per unit area to the sea surface than has been reported for the land. It is of course possible simply that the sea surface is a more efficient collector of fall-out than any which have been devised for shore-based study, and that retention in the water column is more reliable than on soil. Without a theory of the processes responsible for this difference, if real, we cannot tell whether this may also help to clarify the problem of the transfer of carbon-14.

A more detailed report of this work is being prepared for early publication elsewhere. Various aspects of the programme have been supported by the United States Atomic Energy Commission (contracts *AT* (30–1)—1918, *AT* (30–1)—2174), the United States Office of Naval Research (contract *NONR*–2196) and the United States National Science Foundation. Most of the stations mentioned have been collected as part of the U.S. International Geophysical Year programme.

VAUGHAN T. BOWEN

Woods Hole Oceanographic Institution,
Woods Hole, Massachusetts.

THOMAS T. SUGIHARA

Department of Chemistry,
Clark University,
Worcester, Massachusetts.

[1] Arnold, J. R., and Anderson, G. C., *Tellus*, **9**, 28 (1957). Craig, H., *ibid.*, **9**, 1 (1957). Eriksson, E., Int. Oceanographic Congress, New York (1959).

[2] Martell, E. A., U.S.A.E.C. Bulletin *AECU*-3262, p. 59 (1956).

[3] Bowen V. T., and Sugihara, T. T., *Proc. U.S. Nat. Acad. Sci.*, **43**, 576 (1957); Proc. Second U.N. Int. Conf. Peaceful Uses Atom. Energy, Geneva, 1958, Paper *UN*-403 (1958). Sugihara, T. T., *et al.*, *Anal. Chem.*, **31**, 44 (1959).

[4] Dunham, C. L., in "Fallout from Nuclear Weapons Tests", 1, 23 (U.S. Gov. Printing Office, 1959).

[5] Broecker, W. S., *et al.*, Int. Oceanographic Congress, New York (1959).

[6] U.S.A.E.C. report *HASL*-77, p. 25 (1950).

Printed in Great Britain by Fisher, Knight & Co., Ltd., St. Albans.

Contribution No. 1096

Journal du Conseil . Vol. 25 . No. 3

Marine Phytoplankton and the Distribution of Nitrite in the Sea[1])

By

Ralph F. Vaccaro and John H. Ryther

Woods Hole Oceanographic Institution, Woods Hole, U.S.A.

High concentrations of nitrite-nitrogen in natural waters mark locations where important biologically induced changes in combined nitrogen are progressing (Rakestraw, 1936). Nitrate-nitrogen on the other hand is the end product of the nitrogen regeneration cycle and tends to accumulate in deep oceanic waters as the most abundant form of inorganic nitrogen. Generally nitrite and nitrate as well as ammonia are suitable sources of nitrogen for photosynthesis and growth of plankton algae; hence increasing concentrations of these substances in the layer of active plant growth represent an excess of nitrogen regeneration over assimilation.

In nitrate culture media autotrophic plankton algae assimilate nitrogen by reducing nitrate-nitrogen to hydroxylamine or ammonia and finally to amide-nitrogen (Virtanen and Rautanen, 1952; Inada, 1958). During this process significant amounts of extracellular nitrite may accumulate in the media especially in dark cultures provided with an excess of nitrate (Zobell, 1935; Orr, 1926; Kessler, 1957). It has been suggested that this type of phytoplankton activity may influence the appearance and disappearance of nitrite in the surface layers of natural waters (Rakestraw, 1936; Hutchinson, 1958).

Usually the nitrifying bacteria (Cooper, 1937; von Brand *et al.*, 1937) and the denitrifying bacteria (Brandt, 1929; Braarud and Klem, 1931) are cited as the biological agents responsible for the regenerative oxidation and reduction of inorganic nitrogen in the sea. However, nitrifying bacteria have not been successfully isolated from offshore waters although their presence has been demonstrated in coastal waters and marine sediments. Likewise, the arguments stressing bacterial denitrification are tenuous because, for optimal effficiency, these organisms require low oxygen tension and large amounts of available organic material. Only in a few anaerobic or microaerobic oceanic locations can it be clearly demonstrated that the denitrifying bacteria decisively control

---

[1]) Contribution No. 1096 from the Woods Hole Oceanographic Institution. This work was supported in part by the National Science Foundation, Grant NSF 10709 and under Contract AT(30–1)–1918 with the U. S. Atomic Energy Commission.

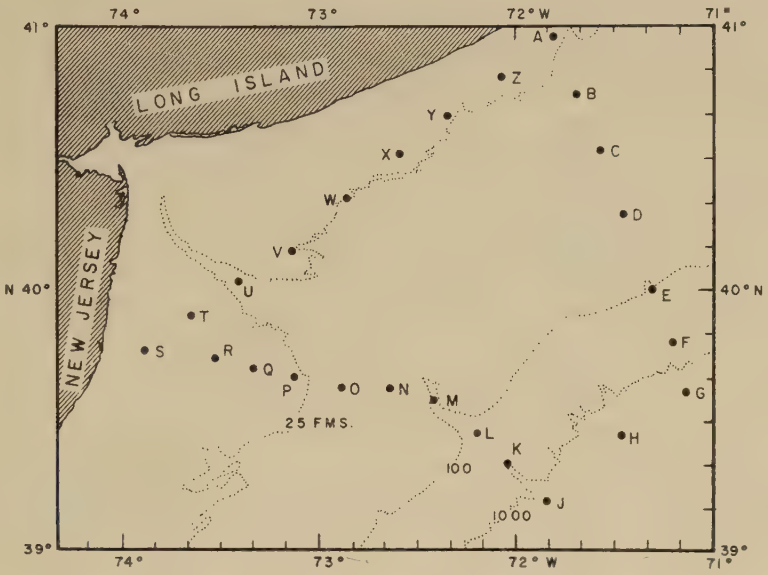

Figure 1. Location of stations occupied during the coastal cruises.

the distribution of inorganic nitrogen (Richards and Vaccaro, 1956; Brandhorst, 1959).

In this paper we report some laboratory experiments designed to provide information on the cultural conditions which lead to the production of extracellular nitrite by some representative marine phytoplankton. These experiments have led us to compare the *in situ* seasonal and geographic distributions of nitrite and nitrate with estimates of the standing crops of phytoplankton in various Atlantic waters. The areas studied include the Atlantic continental shelf off New York, the Sargasso Sea, and the tropical Atlantic Ocean. The shelf observations (Fig. 1) represent a part of our studies of the plankton ecology off the coast of New York. Comparable observations for the Sargasso Sea were kindly provided by Dr. David W. Menzel of the Bermuda Biological Station and the data for the tropical Atlantic were observed by the senior author from the R/V "Atlantis" in 1952.

Extracellular Nitrite Production by Marine Phytoplankton in Laboratory Cultures

Methods

For each experiment the cells were suspended in a complete medium designated as medium E (Table 1) in which nitrate was the principle source of available nitrogen. A preconditioning process preliminary to each experiment insured that the cells were either nitrogen sufficient or nitrogen deficient as desired. To induce nitrogen deficiency illuminated cells (fluorescent lighting, 1300 foot candles) were suspended for several hours prior to the beginning of the experimental observations in a medium free of available nitrogen but otherwise complete. Nitrogen sufficient cells were obtained by providing a

Table 1

Media for isolation and maintenance of marine algae

Recommended by Dr. R. R. L. GUILLARD, Woods Hole Oceanographic Institution.

$NaNO_3$	150 mg (1·765 mg atoms)
$NaH_2PO_4 \cdot H_2O$	10 mg (72·5 μg atoms)
Fe sequestrene*)	10 mg (1·3 mg Fe)
$Na_2SiO_3 \cdot 9H_2O$	30–60 mg (3–6 mg Si)
Vitamins:	
Thiamin · HCl	0·2 mg
Biotin	1·0 μg
B_{12}	1·0 μg
Trace metals:	
$CuSO_4 \cdot 5H_2O$	0·0196 mg (0·005 mg Cu)
$ZnSO_4 \cdot 7H_2O$	0·044 mg (0·01 mg Zn)
$CoCl_2 \cdot 6H_2O$	0·022 mg (0·005 mg Co)
$MnCl_2 \cdot 4H_2O$	0·360 mg (0·1 mg Mn)
$Na_2MoO_4 \cdot 2H_2O$	0·03 mg (0·005 mg Mo)
Sea water	To one litre

*) Sodium iron salt of ethylene dinitrilo tetraacetic acid (EDTA). Ferric chloride and EDTA or the sodium salt of EDTA can be mixed to give the same amounts of iron and the chelator; adjust pH to about 4·5. Ferric sequestrene is made by Geigy Industrial Chemicals, Saw Mill River Road, Ardsley, New York.

normal amount of nitrate-nitrogen during a comparable period of time. The effect of light was studied by incubating the cultures under neutral density filters (Kodak Wratten No. 96 gelatin film) which transmitted 100, 50, 25, 10, 1 or zero % of the incident light intensity. For all experiments the incident illumination provided over the filters was 1300 foot candles and the incubation temperature was controlled at 18° ± 2°C. Aliquot samples were removed at selected intervals for estimation of cell counts and for chemical analyses of nitrite (RIDER and MELLON, 1946) and nitrate (MULLIN and RILEY, 1955) on the cell free filtrates. Sterile techniques were maintained throughout.

Experimental Data

Two experiments were conducted by enriching nitrogen deficient cultures of the flagellate *Isochrysis* sp. and the centric diatom "*Lauderia*"[1]) with nitrate. During the first two days of the experiment the *Isochrysis* population (Figure 2 a) removed about 70 μg A/L of nitrate-nitrogen from solution, presumably to overcome the original nitrogen deficiency. Little or no change in nitrate occurred over the next two days but following the fourth day nitrate disappeared at a rapid rate so that a negligible amount was measured on the seventh day. The nitrite increased gradually during the first three days but more rapidly thereafter, until a maximum concentration of 3 μg A/L was measured on the seventh day. By this time the nitrate was practically exhausted and within an additional 24 hours almost all the nitrite also disappeared so that the combined quantities of nitrate and nitrite-nitrogen amounted to less than 1 μg A/L. The population increased only four-fold during the first three days; however, during the final five days a one hundred fold increase occurred.

---

[1]) Unidentified centric diatom tentatively classified as *Lauderia* by Dr. R. R. L. GUILLARD, Woods Hole Oceanographic Institution.

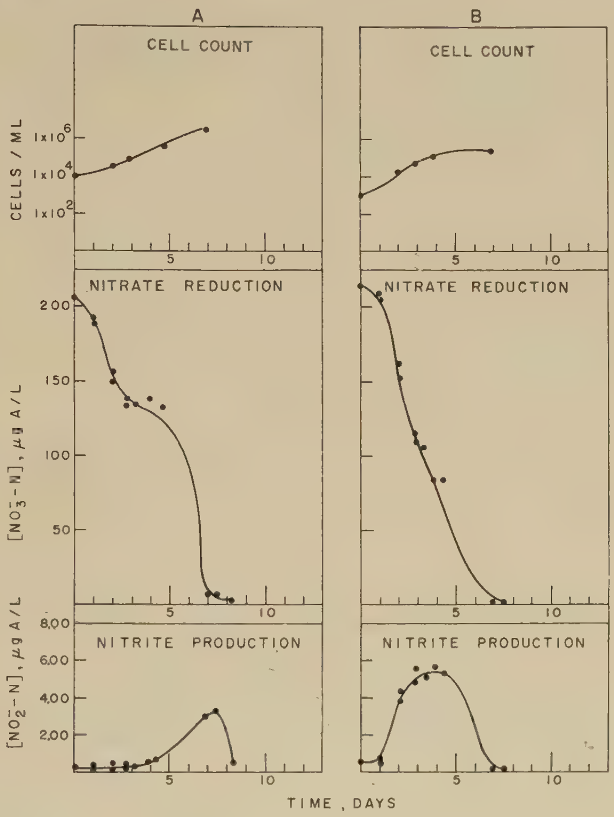

Figure 2 A and B. Cell counts, nitrate reduction and nitrite production, µg A/L, by *Isochrysis* sp. and "*Lauderia*" sp. Incident radiation 1300 foot candles. Both cultures nitrogen deficient at onset of experiment.

In the "*Lauderia*" experiment (Figure 2 b) about 210 µg A/L of nitrate-nitrogen was removed at a constant rate between the second and seventh days. By this time only trace amounts of nitrate remained in solution. Nitrite increased after the first day and by the third day reached a maximum concentration of 4·7 µg A/L. Thereafter the nitrite disappeared rapidly with only trace amounts persisting after the seventh day. The "*Lauderia*" population went through a typical exponential growth curve with the maximum population attained in about five days.

In an experiment conducted with the diatom *Skeletonema costatum*, changes in nitrite and nitrate were observed for a nitrogen deficient population in the light. The results are shown in Figure 3 A. After three days the nitrate was nearly exhausted. The nitrite in the medium, originally 0·3 µg A/L, increased for the first two days, reaching a maximum concentration of 0·9 µg A/L after 2¹/₄ days, and then decreased. The nitrite produced was about 0·34 per cent. of the amount of nitrate assimilated. A normal culture of *Skeletonema costatum* was enriched with 250 µg A of NO_3–N and placed in the dark. After three days, as can be seen from Figure 3 B these cells had assimilated 100 µg A of nitrate-

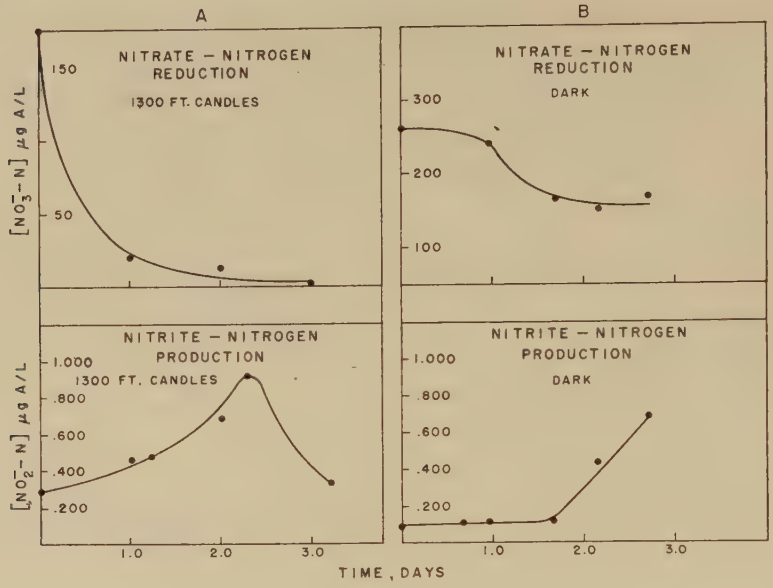

Figure 3 A. Nitrate reduction and nitrite production, μg A/L, by *Skeletonema costatum* preconditioned to nitrogen deficiency. Incident radiation 1300 foot candles.

Figure 3 B. Nitrate reduction and nitrite production, μg A/L, in the dark by *Skeletonema costatum* preconditioned with a normal amount of nitrate.

nitrogen and the nitrite content of the media was increased by 0·58 μg A/L (0·58%).

The effect of different light intensities on the production of nitrite by nitrogen deficient *Skeletonema costatum* is shown in Figure 4. This culture was enriched with 200 μg A NO_3 N/L at the start of the experiments. During the next two days the cell numbers increased at all light intensities but decreased in the dark. In each instance the initial uptake of nitrate was extremely rapid with 88% of the nitrate disappearing within the first few hours. Thereafter the concentration of nitrate in the dark culture remained relatively constant while nitrate was slowly removed in the remaining cultures. Significant increases in nitrite were observed at all light intensities but the highest concentrations of nitrite were produced in the dark and the amount decreased progressively as light intensity increased.

Nitrate, Nitrite, and Chlorophyll *a* in Coastal Waters

In coastal waters, low concentrations of ammonia, nitrite, and nitrate prevail in summer but high concentrations are observed during the late autumn and winter months. The winter accumulation of inorganic nitrogen has been related to vertical diffusion from deeper water masses and/or the sediments, and to reduced photosynthesis accompanying minimal winter light intensities (Braarud and Klem, 1931). However, in the Gulf of Maine the winter nitrite maxi-

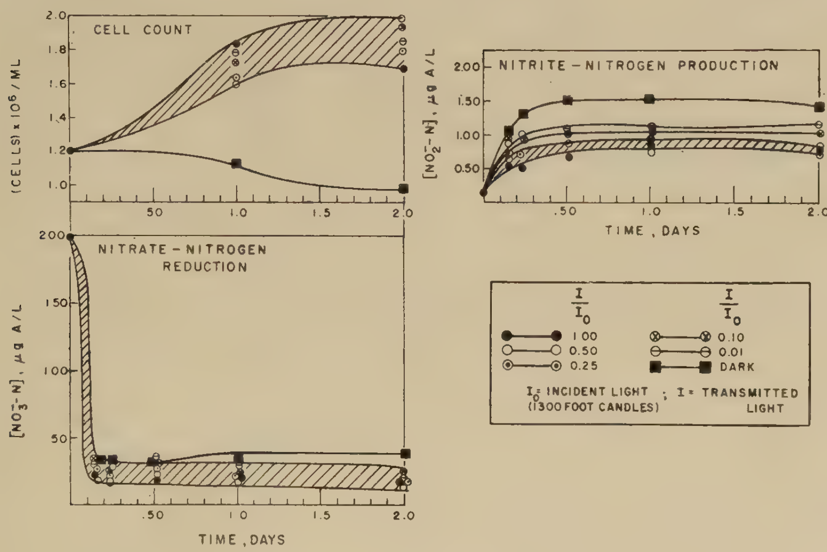

Figure 4. Cell counts, nitrate reduction, and nitrite production, µg A/L, at different light intensities by *Skeletonema costatum* preconditioned to nitrogen deficiency.

mum preceeds that of nitrate suggesting a biological sequence between the appearance of nitrite and nitrate (Rakestraw, 1936). In the same area at locations where the depth of the water column exceeds 200 m the maximum nitrite concentration commonly occurs at an intermediate depth (50 m) and thus differs from the depth of the maximum nitrate concentration (Rakestraw, 1936; Redfield and Keys, 1938).

For the past three winters our studies of the plankton ecology of the continental shelf have included analyses of nitrite, nitrate, and chlorophyll *a*. This information has been summarized by averaging the data from three adjacent station locations (Stations B, C, and D in Figure 1) to give both the 10 and 40 m averages during three consecutive winters (Figure 5). The nitrite and nitrate analyses were completed at Woods Hole on frozen water samples collected at sea. Chlorophyll *a* analyses were made from acetone extractions of the particulate matter removed at sea by AA millipore filtration (Richards with Thompson, 1952; Creitz and Richards, 1955).

Between September and March the concentration of nitrate increases steadily from less than 1 µg A/L to about 6 µg A/L at 10 m and from 3 to about 6 µg A/L at 40 m. Within the same interval of time a 2–6 fold increase in nitrite occurs but as in the Gulf of Maine the maximum nitrite concentration consistently preceeds the nitrate maximum by some 10–12 weeks. The corresponding chlorophyll *a* measurements demonstrate a winter flowering with the maximum standing crop coinciding with the December nitrite maximum. The effect of winter mixing is demonstrated by the relative homogeneity of the water column during the late winter months. During the spring flowering in March 1957, no comparable increase in nitrite was measured at a time when the rate of nitrate assimilation exceeded the rate of nitrate regeneration.

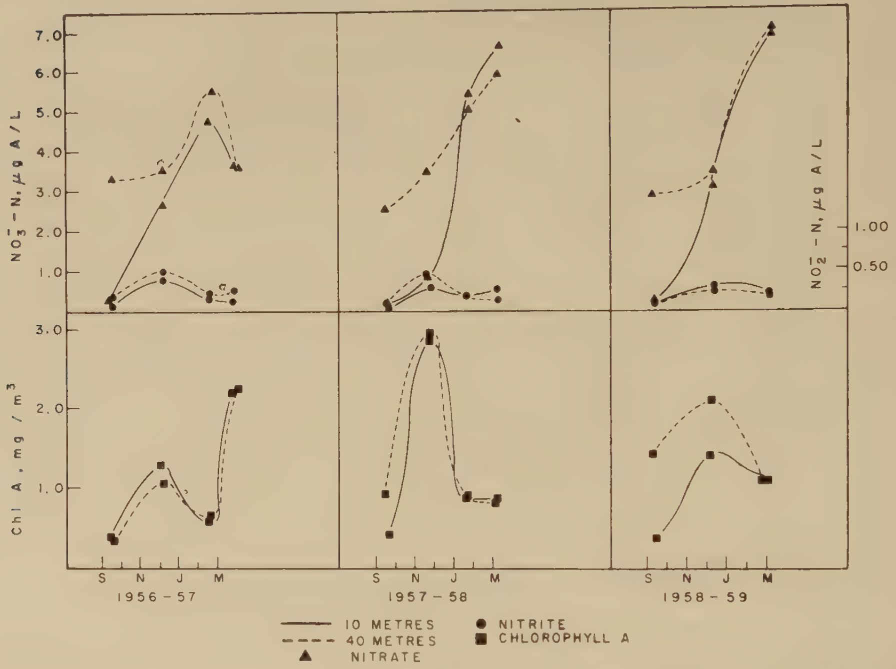

Figure 5. Winter variations in nitrate and nitrite, µg A/L, and chlorophyll *a*, mg/m^3, on the Atlantic continental shelf. Triangles, nitrate-nitrogen; solid circles, nitrite-nitrogen; and solid squares, chlorophyll *a*. Solid lines 10 m and dashed lines 40 m observations.

Nitrate, Nitrite, and Chlorophyll *a* in Deep Oceanic Waters

In deeper oceanic waters small but persistent concentrations of nitrite occur in the upper euphotic zone. Somewhat deeper and nearer the conpensation depth for photosynthesis the nitrite concentration frequently increases rapidly until a maximum concentration is reached between 75–125 m. Usually increasing concentrations of nitrate and phosphate accompany the nitrite maximum. At still greater depths in the Atlantic increasing amounts of both nitrate and phosphate are not associated with high nitrite concentrations and practically all the inorganic nitrogen occurs as nitrate. The distribution of these organic derivatives in the sea supports the existence of a complementary *in situ* relation between the assimilation and regeneration of nitrogen in the water column (Redfield, 1934; Seiwell, 1935; Riley, 1951). A typical example of the changes in nitrite and nitrate with depth was observed by Ketchum and Vaccaro (unpublished) in March 1952 at R/V "Atlantis" Station 4962 (Figure 6).

A more detailed description of the changes in nitrite, nitrate, and chlorophyll *a* with depth has been provided by Dr. Menzel (unpublished) who has observed these changes at 10 m intervals within the upper 150 m of the Sargasso Sea (Figure 7). The station location was 15 miles north of Bermuda where the depth of the water column is some 3000 m. The compensation depth of 80 m for photosynthesis was calculated from a Secchi-disc reading. Within the upper 50 m only minor variations in nitrite, nitrate, and chlorophyll *a* were noted.

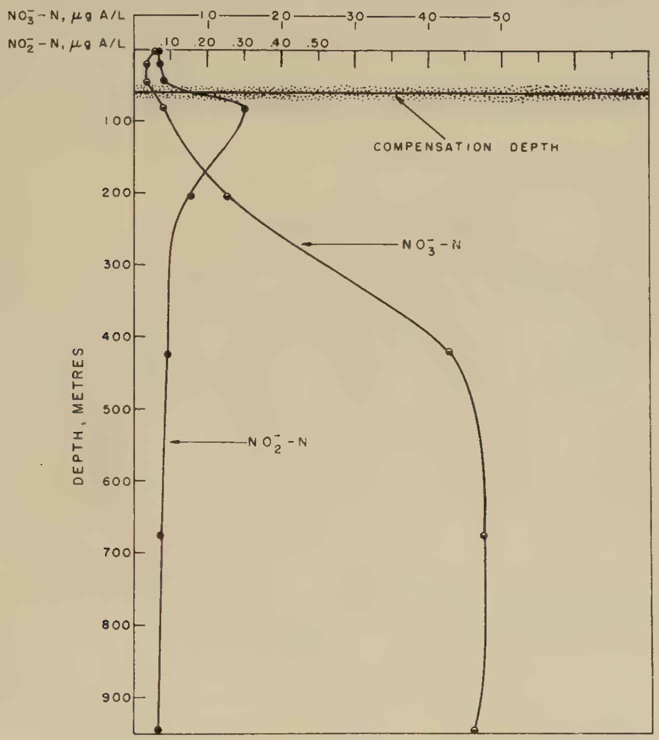

Figure 6. Profiles of nitrite and nitrate, μg A/L, from the tropical Atlantic. R/V "Atlantis", Station 4964 (01°11·5′N, 37°59·5′W), March 1952.

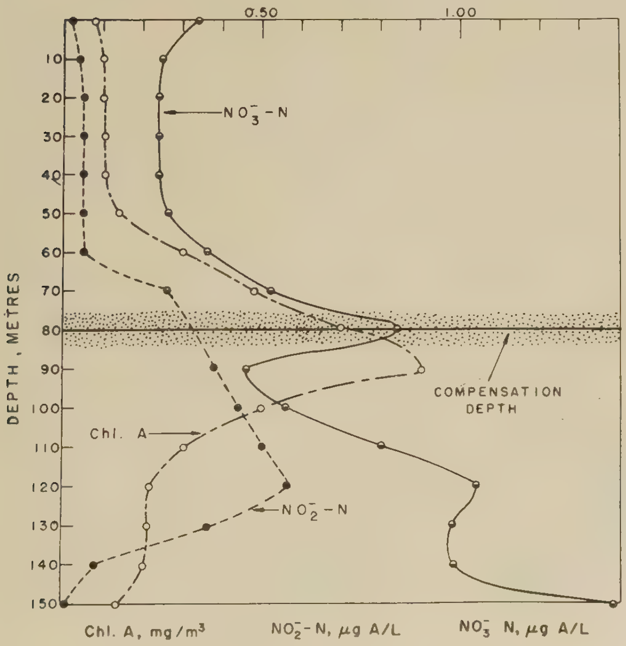

Figure 7. Profiles of nitrite and nitrate, μg A/L, and chlorophyll *a*, mg/m³, in relation to the compensation depth. Location, Sargasso Sea off Bermuda. R/V "Panularis", May 1959.

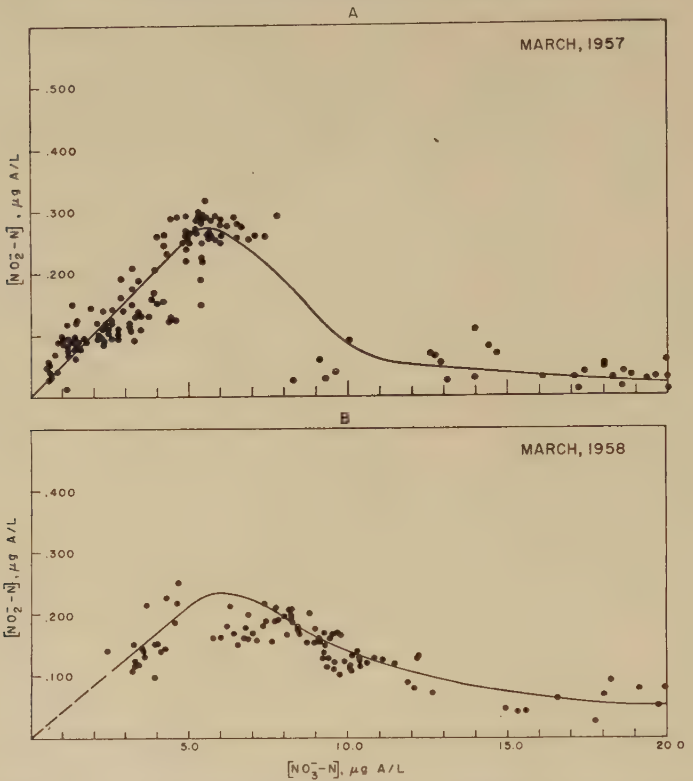

Figure 8 A and B. Relations between nitrite and nitrate, μg A/L, on the Atlantic continental shelf and slope. A, March 1957. B, March 1958.

Between 50 and 80 m, however, the concentrations all increased significantly. The inverse relation between nitrate and chlorophyll *a* just below the compensation depth, especially in the vicinity of the 90 m chlorophyll maximum, suggests that the observed distribution is not fortuitous but results from nitrate-nitrogen assimilation during prolonged phytoplankton residence. The nitrite concentration below 80 m continued to increase until a maximum concentration of 0·56 μg A/L was attained at 120 m. At still greater depths the nitrite concentration decreased until only trace amounts persisted below 150 m.

The recurrent similarity between the changes in nitrite and nitrate on the Atlantic continental shelf, the Sargasso Sea, and the tropical Atlantic suggest a possible uniformity in the ratio of change for the two forms of nitrogen. For this reason lines of regression have been plotted for two complete continental shelf cruises, March 1957 and March 1958 (Figure 8 A and B). The data used include all the available observations between the surface and a maximum depth of 500 m for all the shelf and slope stations shown in Figure 1. March data were selected because the maximum surface variation in the concentration of nitrate occurs at this time when the outbreak of spring flowering is not yet a widespread phenomenon.

For concentrations of nitrate between 0 and 5·5 μg A/L the results demonstrate a linear relation between these changes. At no time did concentrations of nitrite exceeding 0·10 μg A/L occur if the nitrate concentration was depressed below

1·0 μg A/L. The calculated ratio of change for this segment of the two curves indicates an equivalence of about 0·05 μg A/L of nitrite-nitrogen per unit increase in nitrate-nitrogen. For nitrate concentrations exceeding 5·5 μg A/L the corresponding nitrite concentrations show a systematic reduction, with less than 0·10 μg A/L usually associated with nitrate concentrations exceeding 12 μg A/L.

Discussion

According to bacteriological concepts of nitrogen regeneration in the sea, the appearance of nitrite is an intermediate step in the formation of nitrate. Therefore the production of nitrite should preceed that of nitrate and nitrite accumulation depends upon a favourable adjustment of the rates of inorganic nitrogen oxidation and reduction. Both the seasonal distribution of nitrite in coastal waters and nitrite changes with depth in the open sea have been explained on this basis.

However, our phytoplankton experiments demonstrate that in the presence of adequate amounts of nitrate the reduction of nitrate to amide nitrogen is often accompanied by an accumulation of extracellular nitrite in the culture media, the amount of nitrite produced being inversely related to the incident radiation. These observations suggest a mechanism whereby plant cells may also contribute *in situ* nitrite to the sea given the specified environmental conditions. Both the sequence of events in early winter on the continental shelf and the vertical changes associated with the compensation depth in the Sargasso Sea appear to support this concept.

In early winter on the continental shelf nitrate production exceeds nitrate-nitrogen assimilation even though increasingly high concentrations of chlorophyll *a* appear. At no other time of year is a comparable standing crop of phytoplankton accompanied by such high concentrations of nitrate and other plant nutrients. Since nutrients are not critical at this time, the factor most likely limiting phytoplankton growth is a light deficiency. In any event, the occurrence of the maximum annual concentration of nitrite in waters rich in phytoplankton and nitrate, but light limited, appears to mean that the principle requirements for nitrite production outlined in our experiments are satisfied.

Similarly, in the deep ocean, maximum concentrations of phytoplankton occur near the lower limit of the photic zone (RILEY, STOMMEL and BUMPUS, 1949; JERLOV, 1959). Observations taken in May in the Sargasso Sea (Figure 7) show a seven-fold increase in chlorophyll *a* and a three-fold increase in nitrate at the compensation depth (80 m) as compared with the surface. It seems apparent that the sequence of events with time accompanying the winter appearance of nitrite on the continental shelf become depth dependent in the deep ocean. In the Sargasso Sea the maximum concentration of nitrite ultimately appeared considerably below the compensation depth at 120 m where the accompanying amounts of nitrate and chlorophyll *a* were three times the surface concentrations.

A diagrammatic presentation of the supplementary roles of bacteria, plants, and animals in the oxidations and reductions of inorganic nitrogen in the sea is presented (Figure 9). The blocked and circled numerals identify changes brought about by plants and bacteria respectively while the triangle-enclosed numbers are reserved for animal contributions to the cycle.

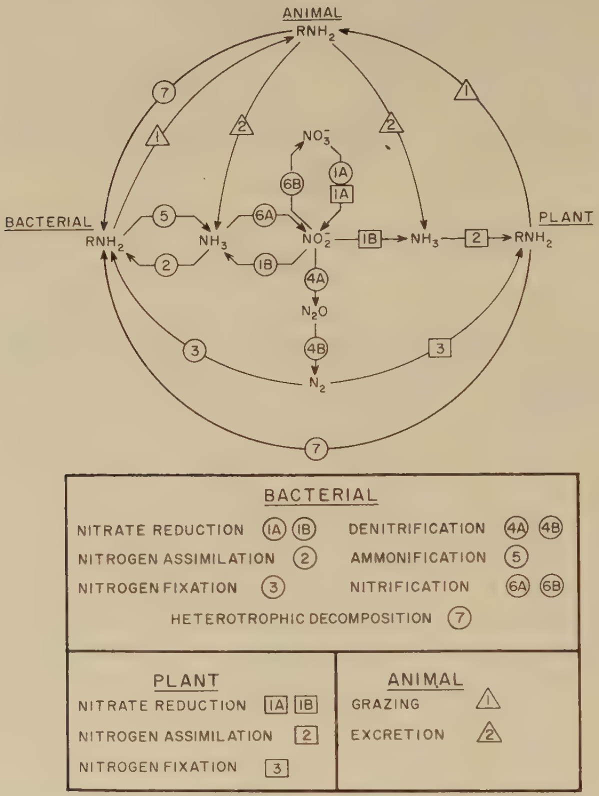
ANIMAL
RNH₂
BACTERIAL
RNH₂
PLANT
RNH₂
NH₃
NO₃⁻
NO₂⁻
NH₃
N₂O
N₂
BACTERIAL
NITRATE REDUCTION (1A) (1B)
DENITRIFICATION (4A) (4B)
NITROGEN ASSIMILATION (2)
AMMONIFICATION (5)
NITROGEN FIXATION (3)
NITRIFICATION (6A) (6B)
HETEROTROPHIC DECOMPOSITION (7)
PLANT
NITRATE REDUCTION 1A 1B
NITROGEN ASSIMILATION 2
NITROGEN FIXATION 3
ANIMAL
GRAZING 1
EXCRETION 2

Figure 9. The physiological origins of nitrite and other forms of inorganic nitrogen in the sea. The letter 'R' designates the non-nitrogenous part of the appropriate organic molecule.

Bacteria are shown to make the most versatile contributions to the inorganic nitrogen cycle, particularly in so far as they dominate its regenerative aspects. On the other hand, phytoplankton, as well as bacteria, can assimilate ammonia, nitrite, and nitrate into proteinaceous substances in what is the primary plant contribution to the nitrogen economy of the sea. Animal additions to the inorganic nitrogen cycle are probably limited to the excretion of ammonia or its organic precrusors. However in a stable water mass, where plant access to inorganic nitrogen is limited, ammonia of animal origin is presumably a very important source of available nitrogen.

Summary

1. The assimilation of nitrate-nitrogen by marine phytoplankton is often accompanied by the production of significant amounts of extracellular nitrite. The highest nitrite concentrations were produced by cultures grown in reduced light containing cells recovering from nitrogen deficiency. Within the range of 0–1300 foot candles, the amount of nitrite produced varied inversely with the intensity of light provided.

2. In the upper layers of the ocean increasing concentrations of nitrite can be expected provided that the following environmental requirements are met:

(i) an adequate standing crop of phytoplankton is present and (ii) an excess of nitrate is available. An intensification of the phenomenon can be expected at reduced light intensities.

3. In temperate coastal waters these requirements are most often approached during the early winter months while in more tropical deep oceanic waters where seasonal variations are less pronounced they typically occur at the lower limits of the photic layer. The evidence connecting the appearance of nitrite in the sea with the activity of marine phytoplankton populations appears equally substantial to that often cited to demonstrate a comparable role for nitrifying and denitrifying bacteria.

References

Braarud, T., & Klem, A., 1931. "Hydrographical and chemical investigations in the coastal waters off Møre and in the Romsdalsfjord". Hvalråd. Skr., **1**: 1–88.

Brandhorst, W., 1958. "Nitrite accumulation in the north-east tropical Pacific". Nature, Lond., **182**: 679.

Brandt, K., 1929. "Phosphate und Stickstoffverbindungen als minimum Stoffe für die Produktion im Meer". Rapp. Cons. Explor. Mer, **53**: 5–35.

Cooper, L. H. N., 1937. "The nitrogen cycle in the sea". J. mar. biol. Ass. U. K., **22**: 183–204.

Creitz, G. I., & Richards, F. A., 1955. "The estimation and characterization of plankton populations by pigment analyses. III. A note on the use of millipore membrane filters for the estimation of plankton pigments". J. Mar. Res., **14**: 211–16.

Hutchinson, G. E., 1957. "A Treatise on Limnology". Vol. I. New York, John Wiley & Sons.

Inada, Y., 1958. "Stimulatory and inhibitory effect of light on the nitrate assimilation by *Chlorella*". J. gen. appl. Microbiol., **4**: 153–62.

Jerlov, N. G., 1959. "Maxima in the vertical distribution of particles in the sea". Deep-Sea Res., **5**: 173–84.

Kessler, E., 1957. "Untersuchungen zum Problem der photochemischen Nitratreduktion in Grünalgen". Planta, **49**: 505–23.

Mullin, J. B., & Riley, J. P., 1955. "The spectrophotometric determination of nitrate in natural waters with particular reference to sea water". Analyt. chim. Acta, **12**: 464–80.

Orr, A. P., 1926. "The nitrite content of sea water". J. mar. biol. Ass. U.K., **14**: 55–61.

Rakestraw, N. W., 1936. "The occurrence and significance of nitrite in the sea". Biol. Bull. Woods Hole, **71**: 133–67.

Redfield, A. C., 1934: "On the proportions of organic derivatives in sea water and their relation to the composition of plankton". In: James Johnstone Memorial Vol., Univ. of Liverpool, 176–92.

Redfield, A. C., & Keys, A. B., 1938. "The distribution of ammonia in the waters of the Gulf of Maine". Biol. Bull. Woods Hole, **79**: 83–92.

Richards, F. A., with Thompson, T. G., 1952. "The estimation and characterization of plankton populations by pigment analysis. II. A spectrophotometric method for the estimation of plankton pigments". J. Mar. Res., **11**: 156–72.

Richards, F. A., & Vaccaro, R. F., 1956. "The Cariaco Trench an anaerobic basin in the Caribbean Sea". Deep-Sea Res., **3**: 214–28.

Rider, B. F., & Mellon, M. G., 1946. "Colorimetric determination of nitrites". Industr. Engng. Chem., (Anal.) **18**: 96–99.

Riley, G. A., 1951. "Oxygen, phosphate and nitrate in the Atlantic Ocean". Bull. Bingham oceanogr. Coll., **9**: 1–125.

Riley, G. A., Stommel, H., & Bumpus, D. F., 1949. "Quantitative ecology of the plankton of the western North Atlantic". Bull. Bingham oceanogr. Coll., **12**: 1–169.

Seiwell, H. R., 1935. "The cycle of phosphorus in the western basin of the North Atlantic". Pap. phys. Oceanogr., **3**(4): 1–56.

Virtanen, A. I., & Rautanen, N., 1952. "Nitrogen assimilation". In: The Enzymes, New York, Academic Press, 1089–1130.

von Brand, T., Rakestraw, N. W., & Renn, C. E., 1937. "Experimental decomposition and regeneration of nitrogenous organic matter". Biol. Bull. Woods Hole, **72**: 165–75.

ZoBell, C. E., 1935. "The assimilation of ammonia nitrogen by *Nitzschia clausterium* and other marine phytoplankton". Proc. Nat. Acad. Sci., Wash., **21**: 517–22.

Contribution No. 1097

THE CULTURE OF DUNALIELLA TERTIOLECTA BUTCHER—A EURYHALINE ORGANISM[1]

JACK McLACHLAN[2]

Abstract

Dunaliella tertiolecta Butcher was found to be a euryhaline organism which grew at salinities ranging from 3.75 to 120°/₀₀. All the conservative elements of sea water, with the exception of chlorine, were found necessary for growth of the alga. The minimum requirement for sodium was much greater than that for any other element, and it was not possible to substitute other monovalent cations for the minimum requirement. Also, the alga could tolerate high concentrations of sodium chloride. The potassium and sulphur concentrations of the medium could be reduced to very low levels. *Dunaliella* could also tolerate high concentrations of these two elements. The addition of lithium to the medium inhibited the growth of the alga. High concentrations of sodium could partially eliminate the inhibition due to lithium. The minimum concentrations of calcium and magnesium necessary for growth approached the concentrations found in fresh waters. Calcium and magnesium were inhibitory at high concentrations, but the inhibition at high concentrations could be prevented if a Mg/Ca ratio of 4 was maintained over a wide range of concentrations in the medium.

Introduction

The genus *Dunaliella* includes both fresh and salt water species (22), a situation which is not uncommon (9). This genus is of world-wide distribution and is generally present in brine lakes (4, 15, 29). *Dunaliella* has been observed to bloom under conditions of high salt concentration (20), and some strains are able to grow in media saturated with sodium chloride (14, 29).

Some species of *Dunaliella*, including *D. tertiolecta*, occur in sea water (cf. ref. 8). As a medium, sea water is a complex solution of salts, and final analysis may reveal the presence of all elements of the periodic table (21). The conservative elements[3] in sea water are present in large concentration and occur at a constant ratio regardless of the salinity of the water. Most of these elements are known to be essential constituents in plant nutrition. Kalle (21) considers sea water as an ideal medium for growth of marine plants, but very little is known of the relationship between the concentration of conservative elements and growth of microorganisms (10, 38). The few studies which have been made (1, 10, 17, 33, 34) have indicated considerable liberty can be taken with the composition of the medium. A number of fresh-water algae have been found to grow well and tolerate conditions of high salt concentration (13, 36). It has been suggested that, as a group, green algae seem to be most adaptable to a wide variety of conditions (32).

Previous work with *Dunaliella tertiolecta* has shown that the alga could be cultured equally well in an artificial medium and in an enriched sea water

---

[1] Manuscript received February 24, 1960.
Contribution No. 1097 from the Woods Hole Oceanographic Institution, Woods Hole, Massachusetts, U.S.A.

[2] Public Health Service Research Fellow of the National Institutes of Health. Present address: Division of Applied Biology, National Research Council, Ottawa, Canada.

[3] Conservative elements as used in this paper refer to Cl^-, $SO_4^=$, Na^+, Mg^{++}, Ca^{++}, and K^+. In sea water the ratio of these ions remains virtually unchanged regardless of the salinity, or through the activity of plants and animals.

medium (24). It was the purpose of this study to investigate the concentration limits of the various conservative elements of sea water which are required for growth or are tolerated by *D. tertiolecta*, and to determine if the alga had any requirements which would clearly distinguish it as a marine organism.

Materials and Methods

An axenic culture of *Dunaliella tertiolecta* Butcher[4] was used throughout this investigation. The alga had been originally isolated from sea water but was cultivated on an artificial medium for approximately a year prior to the experimental work. The basic artificial medium, which contained no organic growth factors, was the same as used in previous work (24). The composition of this medium (designated A medium) and of two modifications which were also used (designated B medium and C medium) are presented in Table I. In B medium only the sodium chloride concentration was reduced; in C medium the concentrations of sodium chloride, magnesium sulphate, magnesium chloride, and calcium chloride were reduced as compared with A medium.

TABLE I

Composition of the basic artificial media*

	A medium		
$NaCl$	410 mM	$FeCl_3$	1.5 μM
$MgSO_4$	24 mM	H_3BO_3	185.0 μM
$MgCl_2$	20 mM	$MnCl_2$	7.0 μM
$CaCl_2$	10 mM	$ZnCl_2$	0.8 μM
KNO_3	1 mM	$CoCl_2$	0.02 μM
K_2HPO_4	100 μM	$CuCl_2$	0.0002 μM
Na_2SiO_3	100 μM	Na_2EDTA	30.0 μM
	B medium		
	$NaCl$	15 mM	
	Other salts as in A medium		
	C medium		
$NaCl$	50.0 mM	$MgCl_2$	2.75 mM
$MgSO_4$	2.0 mM	$CaCl_2$	1.25 mM
	Other salts as in A medium		

*Chlorides standardized by titration.

The alga was cultivated in 125-ml Erlenmeyer flasks containing 50 ml of medium. The flasks were plugged with cotton and were shaken by hand several times daily. Illumination was provided by cool-white 40-w fluorescent lamps with an intensity at the level of the culture shelf of approximately 3500 meter-candles, as measured by a General Electric type DW-68 light meter. The temperature was maintained at 18° C.

Cells were harvested from either two or three flasks for each treatment within an experiment. The cells were killed and stained with $K_2 - I_2 -$ acetic acid. The rate of growth was determined periodically by making four to eight replicate cell counts per treatment using a Levy hemocytometer counting chamber. The most rapid rate of growth in each treatment is reported. The cultures were harvested in the log phase of growth; the concentration of cells at this time was usually between 100×10^4 and 200×10^4 cells per milliliter. The maximum cell concentrations obtained under the experimental conditions were approximately 5×10^6 cells per milliliter. The rate of growth is expressed as the number of divisions per day using the equation: $\log_2 (N_t/N_0)/t$ where N_0 is the concentration of cells at inoculation and N_t the concentration of cells at time t (27).

---

[4] Previously this strain was referred to as *D. euchlora* WHOI-1 (24, 25, 26), but recently was identified correctly by Dr. R. W. Butcher as *D. tertiolecta*. This type was first isolated from Oslo Fjord (8).

Results

1. Salinity

The concentrations of sodium chloride, magnesium chloride, magnesium sulphate, and calcium chloride were varied from 1/16× to 4× the concentration of A medium. Concentrations greater than 4× that of A medium precipitated and were therefore not used. The rates of growth from 1/2× to 2× were approximately the same (Fig. 1). The rates of growth at concentrations of 1/8× and 4× were considerably reduced, but these treatments ultimately achieved the same final cell concentration as the treatments at concentrations from 1/4× to 2×. No growth occurred at 1/16× concentration. Growth occurred over a range of salinities from 3.75 to 120‰. These results suggest that the rate of growth may have been limited by high or low total salt concentration of the medium.

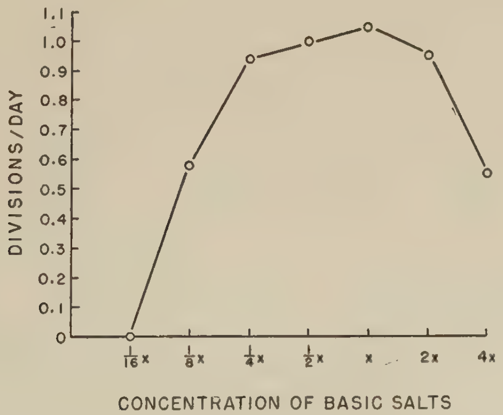

FIG. 1. The rate of growth of the alga at various salinities. × represents the concentration of basic salts (salinity) in A medium.

2. Sodium Chloride

Preliminary results showed that the concentration of sodium chloride in A medium could be varied from 25 to 1000 m*M* without affecting the rate of growth or the final cell concentration.

In A medium containing more than 1000 m*M* sodium chloride, the rate of growth was reduced, and growth was completely suppressed at 2000 m*M* (Fig. 2). However, in all treatments in which growth occurred, the same final cell concentration was obtained. The rate of growth in the 1800 m*M* sodium chloride treatment was approximately the same as the rate of growth of the 4× treatment of the previous experiment (Fig. 1). The total salt concentration of the 1800 m*M* sodium chloride and 4× treatments was approximately the same (ionic concentration ca. 3800 m*M*), which indicates the osmotic pressure between 1000 and 1800 m*M* sodium chloride affected the rates of growth. The sharp break in the response curve between 1800 and 2000 m*M* sodium chloride may suggest that sodium chloride is intrinsically toxic at higher concentrations.

The treatments containing 0 to 25 m*M* sodium chloride were inoculated from a stock culture grown on B medium, so very little sodium chloride was carried over with the inoculum. The rates of growth decreased from 25 to 10 m*M* sodium chloride, and more rapidly from 10 to 0 m*M* sodium chloride (Fig. 2). These results suggest that the decrease in the total salt concentration between 25 and 10 m*M* sodium chloride affected the rate of growth. The rate of growth between 0 and 10 m*M* was also affected by the decreased salt concentration of these treatments. However, the total salt concentration in treatments from 0 to 10 m*M* sodium chloride exceeded the total salt concentration of the 1/8× treatment of the previous experiment. As none of the treatments from 0 to 8 m*M* sodium chloride obtained a maximum cell concentration, these results suggest that sodium chloride per se limited growth.

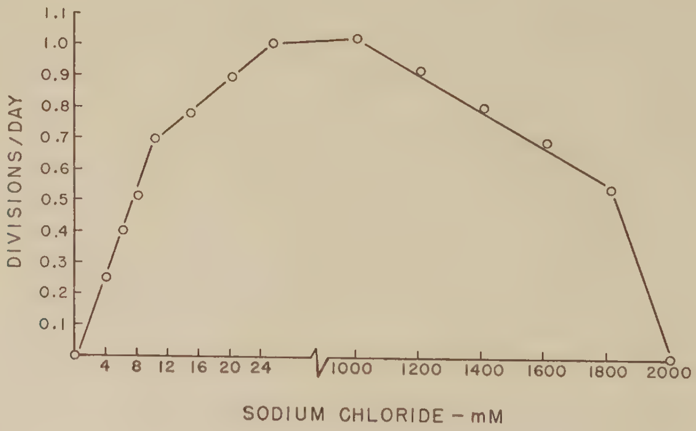

FIG. 2. The rate of growth of the alga in various concentrations of sodium chloride. The concentration of the other salts was maintained at the concentration of A medium.

The rate of growth in C medium was unaffected between 80 and 100 m*M* sodium chloride (Fig. 3). A decrease in the rate of growth occurred in all treatments containing less than 80 m*M* sodium chloride, but the maximum cell concentrations were obtained in all treatments in which growth occurred.

In the lowest sodium chloride concentration in which growth occurred (30 m*M*), the total salt concentration was considerably less than that of the 0 m*M* sodium chloride treatment of the previous experiment. Therefore, growth in this experiment was suppressed by a low total salt concentration before sodium chloride became deficient.

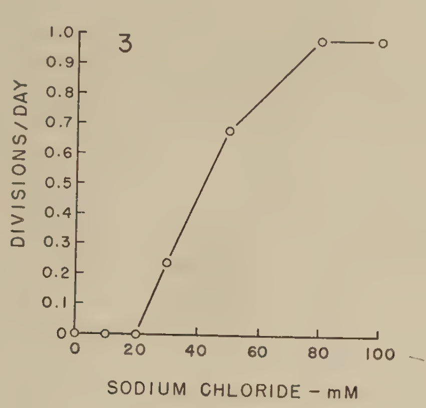

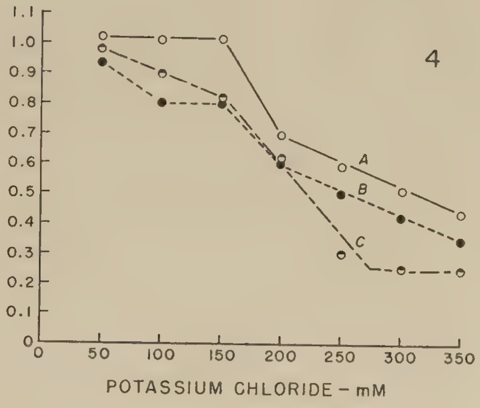

FIG. 3. The rate of growth of the alga in various concentrations of sodium chloride. The concentration of the other salts was maintained at the concentration of C medium.

FIG. 4. The rate of growth of the alga in various concentrations of potassium chloride in A, B, and C media.

3. Potassium Chloride

The addition of 50 m*M* potassium chloride to B and C media increased the rate of growth over that of the controls containing 1.2 m*M* potassium (as potassium nitrate and potassium phosphate). Concentrations exceeding 50 m*M* potassium chloride depressed the rate of growth (Fig. 4). The rate of growth in A medium was unaffected until the potassium chloride concentration exceeded 150 m*M*. These results suggest a slight antagonism between potassium and sodium between 50 and 150 m*M* potassium as B and C media contained considerably less sodium than A medium. The inhibition in all cultures containing more than 150 m*M* potassium chloride was probably due to potassium toxicity per se.

Stock cultures in A medium were grown without the addition of potassium; nitrate and phosphate were added as sodium salts. The stock cultures were allowed to grow for 12 days and then inoculated into media containing micromolar concentrations of potassium chloride. The results (Fig. 5) show that 40 to 50 μM potassium were necessary to permit a normal rate of growth. Essentially the same final cell concentration was obtained in treatments containing 30 μM or more potassium. Cell division could be directly related to the concentration of potassium in the medium (Table II). From these data it was possible to calculate that the alga required approximately 6.0×10^{-8} μg-atoms of potassium per cell. These results also show that sodium could not be substituted for potassium in growth of the alga.

TABLE II

The effect of various concentrations of potassium on the maximum cell concentration

μM potassium added	No. cells/ml × 10^4	Per cent of control	μg-atoms potassium per cell × 10^{-8}
0	No growth	—	—
10	168	32	5.95
20	337	64	5.94
30	495	94	6.04
40	485	93	—
50	510	97	—
1200	525	100	—

4. Sodium Chloride and Potassium Chloride

Preliminary results indicated that it was not possible to substitute potassium chloride for sodium chloride. Two series of cultures were established with the concentration of sodium chloride varied in each series from 0 to 25 mM; magnesium and calcium salts were added at the concentration of B medium. In one series potassium chloride was added at the concentration of B medium (1.2 mM), and in the other series at a concentration of 50 mM.

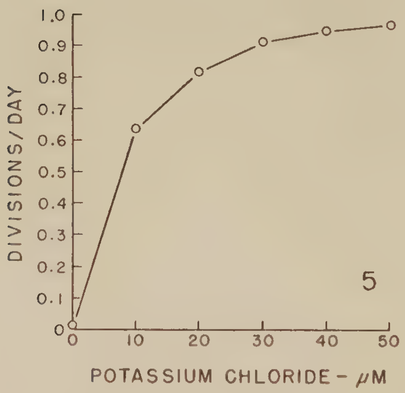

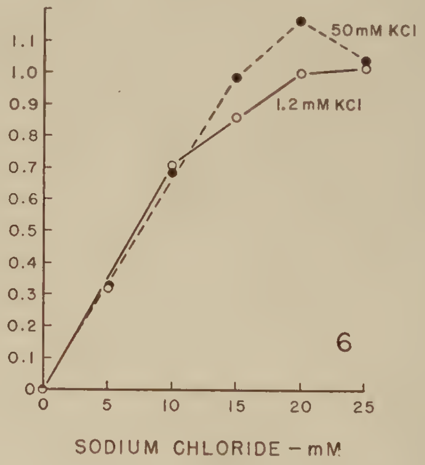

FIG. 5. The rate of growth of the alga in various micromolar concentrations of potassium chloride in A medium.

FIG. 6. The rate of growth of the alga in various concentrations of sodium chloride in B medium to which either 50 mM or 1.2 mM potassium chloride was added.

All cultures were inoculated from B medium stock cultures to reduce the amount of sodium chloride carried over with the inoculum. No increase in the rate of growth was effected by the addition of 50 mM potassium chloride in cultures containing 10 mM or less sodium chloride (Fig. 6), even though the total salt concentration of the medium was sufficient to permit a more rapid rate of growth. The rate of growth was, therefore, limited by the sodium chloride concentration. Fifty millimolar potassium chloride stimulated the rate of growth at sodium chloride concentrations of 15 and 20 mM. The rate of growth in the 20 NaCl – 50 KCl treatment was greater than that of the other treatments, and was the most rapid rate recorded during this study. The rates of growth in the 15 NaCl – 50 KCl and 25 NaCl – 50 KCl treatments were comparable with the highest rates obtained in other experiments in this study.

5. Lithium Chloride

All concentrations of lithium chloride added to A, B, and C media inhibited the rate of growth (Fig. 7). A maximum cell concentration was obtained only in A medium containing 50 mM lithium chloride. These results suggested an antagonism between sodium and lithium as A medium contains considerably more sodium than B and C media. Cells of treatments in which maximum cell concentrations were not obtained became greatly enlarged, and after a short period of growth, chlorotic.

In treatments containing 50 mM lithium chloride and various concentrations of sodium chloride, the rate of growth was dependent upon the sodium chloride concentration (Fig. 8). However, concentrations of sodium chloride greater than 400 mM did very little to enhance the rate of growth. Maximum cell concentrations were obtained only in treatments containing 200 mM or more sodium chloride. As in the previous experiment, cells in the lower sodium chloride concentrations enlarged and soon turned chlorotic.

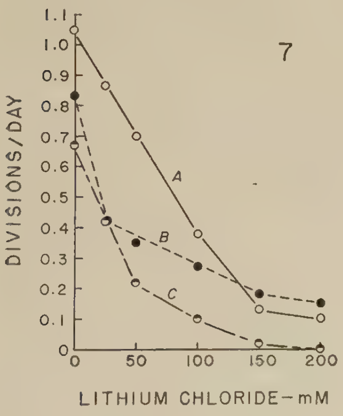

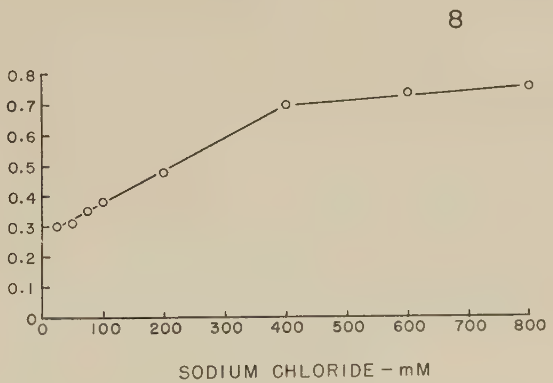

FIG. 7. The rate of growth of the alga in various concentrations of lithium chloride in A, B, and C media.

FIG. 8. The rate of growth of the alga in various concentrations of sodium chloride in B medium with all treatments containing 50 mM lithium chloride.

6. Sulphur

Cultures containing micromolar concentrations of sodium sulphate were inoculated from a stock culture which contained 0.25 mM sodium sulphate. In all treatments, magnesium was added as magnesium chloride at the concentration of A medium. No growth occurred in the treatment in which sulphur had been omitted. A minimum concentration of approximately 150 μM was necessary to effect a normal rate of growth (Fig. 9). All treatments containing 50 μM or more sodium sulphate reached the same final cell concentration.

The final cell concentration of the 25 μM treatment was only 26% of the final cell concentration of the 50 μM treatment. This may suggest that sulphur is not directly involved in cell division. Hase *et al.* (16) found a sulphur deficiency unique in causing a complete cessation of cell division.

It was possible to add sodium sulphate up to a concentration of 300 mM in A medium without affecting the rate of growth or the final cell concentration. Concentrations exceeding this resulted in a precipitation of calcium sulphate. It was also possible to replace sodium chloride in A, B, and C media with sodium sulphate without affecting growth. Some studies (20) have indicated that it is not possible to replace sodium chloride with other sodium salts.

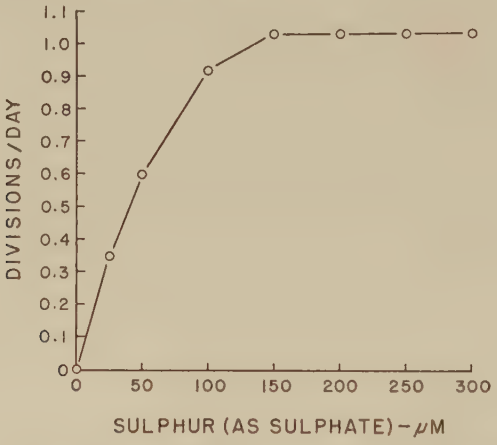

FIG. 9. The rate of growth of the alga in various micromolar concentrations of sodium sulphate in A medium.

7. *Calcium Chloride*

Calcium chloride was added at various concentrations to A, B, and C media. The carry-over of calcium with the inoculum was about 200 μM in treatments based on A and B media, and about 25 μM in treatments based on C medium. The rate of growth was inhibited at 50 mM in A medium, at 40 mM in C medium, and at 30 mM in B medium (Fig. 10). These results suggest that the inhibitory effects of excess calcium were antagonized by sodium since one of the important differences between B medium and C and A media is that the sodium chloride concentration is more than three to almost 30 times higher in the latter two than in the former. All treatments containing added calcium reached the same final cell concentration. The low rate of growth in A medium with low calcium concentration may also indicate an antagonism between calcium and sodium chloride. In B and C media, the reduced rate of growth at the lower calcium concentrations undoubtedly reflects the low total salt concentration of these treatments.

8. *Calcium Chloride and Sodium Chloride*

Treatments were prepared with 60 mM calcium chloride and concentrations of sodium chloride from 25 to 800 mM. At concentrations of 25 and 50 mM sodium chloride, the reduced rate of growth was similar to that of the previous experiment, i.e. in the B and C media (Fig. 10). The rate of growth from 100 to 800 mM sodium chloride was the same and comparable with the 60 mM calcium chloride (A medium) of the previous experiment. Therefore, inhibition due to excess calcium can be somewhat mitigated by increasing the sodium concentration, but the inhibition of the rate of growth could not be entirely overcome by an increased sodium concentration.

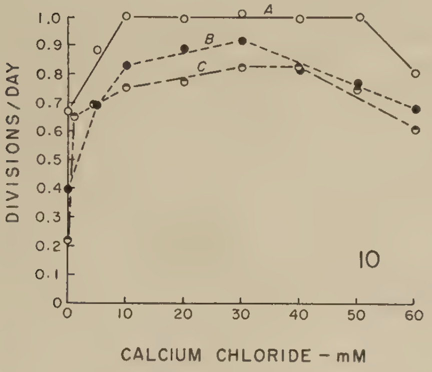

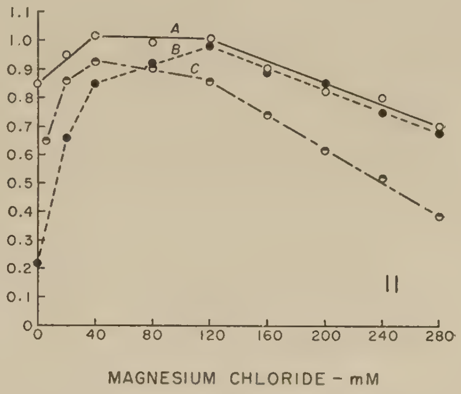

FIG. 10. The rate of growth of the alga in various concentrations of calcium chloride in A, B, and C media.

FIG. 11. The rate of growth of the alga in various concentrations of magnesium chloride in A, B, and C media.

9. Magnesium Chloride

Magnesium chloride inhibited the rate of growth at concentrations exceeding 120 mM in A, B, and C media (Fig. 11). The degree of inhibition of the rate of growth may be related to the Mg/Ca ratio as C medium contains considerably less calcium than A and B media. All treatments based on A medium and all treatments based on B medium, except the one containing no added magnesium, reached the same final cell concentration. A maximum cell concentration was not obtained in treatments containing 240 and 280 mM magnesium chloride in C medium. This again suggests inhibition due to excess magnesium which was less antagonized by calcium.

10. Calcium and Magnesium

Treatments were established in which the Mg/Ca ratio was held constant at 4.0, but the concentration of Mg/Ca was varied from 0.8/0.2 to 240/60 mM. There was no difference in the rate of growth over this range of magnesium and calcium concentrations, and all cultures reached the same final cell concentration. Therefore, inhibitory effects of excess magnesium and calcium could be overcome by maintaining a favorable Mg/Ca ratio.

Discussion

The results of this investigation have shown that *Dunaliella tertiolecta* is definitely an euryhaline organism. Other studies with this genus (14, 22) and with other organisms (cf. refs. 6, 7, 35) have demonstrated tolerances to a wide range of salinities. Most organisms studied, though, do not grow well at salinities much greater than normal sea water (35‰). Some investigators (1, 13) were able to grow their organisms at concentrations varying from those present in fresh waters to full strength sea water. However, *Dunaliella tertiolecta* could not tolerate an osmotic pressure comparable with fresh waters.

Dunaliella tertiolecta has a conspicuous requirement for sodium. Sodium could be provided either as sodium chloride or sodium sulphate. Presumably other sodium salts could also suffice as long as the anion was not toxic. The requirement for sodium was specific, and none of the other monovalent cations examined were able to replace the minimum sodium requirement.

Osterhout (28) reported a sodium requirement in macroscopic marine algae, and several studies have confirmed a requirement in microscopic marine algae (10, 17, 18, 19, 31). In some of these studies it was shown that some organic compounds were able to substitute partially, but not completely, for sodium. Fungi (38) and bacteria (20) have a sodium requirement, and Stiles (37) has indicated a requirement for sodium may be a general phenomenon among marine plants. On the other hand, other studies have shown that not all marine algae have an obvious sodium requirement. Allen (1) and George (13) were ostensibly able to grow several marine species in sodium-free media, and Mayer (23) has found a marine *Chlorella* which grows better when sodium is omitted from the medium.

In blue-green algae, a group virtually unknown from the plankton of the sea (5), some fresh-water species have an absolute sodium requirement (2, 3). Other studies with fresh-water algae have shown a stimulation from the addition of sodium while others have shown that sodium can partially replace potassium (37).

Potassium was found necessary for the growth of *Dunaliella*, but only in quantities which presumably fulfilled the metabolic requirements of the alga. There was no indication that sodium could replace potassium as a metabolite. The quantity of potassium necessary for normal growth was far less than the concentration found in sea water. Pintner and Provasoli (31) and Vishniac (38) also demonstrated that the potassium requirement for several other marine organisms could be greatly reduced from that of sea water. At the other extreme, *D. tertiolecta* was able to tolerate a potassium concentration many times that of sea water.

Osterhout (28) demonstrated that lithium was not able to replace sodium. In the present study, it was also shown that lithium could not replace sodium in the growth of *Dunaliella*. Lithium was found to be toxic at all concentrations used. A beneficial action from the addition of lithium has been observed in the growth of some plants, but more generally the effect is depressing (37). Frerking (12) has claimed that lithium is toxic to plants requiring calcium, but not to algae and fungi supposedly free from calcium.

If chloride is necessary for growth of *Dunaliella*, it is in much less demand than sodium. It was not possible to replace all chloride with sulphates due to difficulties with precipitation. It has not been demonstrated that chloride is necessary for the growth of marine algae, but it has been found essential in the development of some land plants (37). Eyster (11) did find that the growth of a fresh-water alga under autotrophic conditions was stimulated by the addition of chloride.

It was possible to obtain a normal cell concentration of *Dunaliella* at a calcium concentration comparable with that of fresh waters. Droop (10) and Hutner (17) have also reported calcium requirements of the same order of magnitude. Contrariwise, Allen (1) found little flexibility with regard to calcium, and reduced growth resulted when the concentration fell below that of normal sea water.

Growth of *Dunaliella* occurred over a wide range of magnesium concentrations varying in concentration from that characteristic of fresh waters to a concentration greatly exceeding that of normal sea water. Similar results were also obtained by Droop (10) and Hutner (17), but one of the organisms studied by Droop had a magnesium optimum higher than that of North Atlantic waters. Pintner and Provasoli (31) found their organisms were inhibited at a magnesium concentration greater than that of normal sea water.

Vishniac (38) and Vollenweider (39) have reported that magnesium and calcium could replace each other to a certain extent. Several experiments were carried out to determine if either element could substitute for the other in the growth of *D. tertiolecta*. All experiments were negative and indicated substitution did not occur. The alga could tolerate, however, wide variations in the Mg/Ca ratio as long as one or the other was not limiting. This also seems to be true of other organisms (32). Toxic effects of high concentrations of calcium or magnesium could be eliminated by maintaining a proper Mg/Ca ratio. Pintner and Provasoli (30) also indicated that toxic effects of high magnesium concentrations in their medium could be overcome by increasing the calcium concentration.

With the possible exception of chloride, all major elements in sea water were found necessary for the growth of *Dunaliella tertiolecta*. Apart from sodium, the concentrations necessary for the development of this alga were of the same order of magnitude as those necessary for the growth of fresh-water algae. The osmotic and sodium requirements are the principal features which distinguish this alga as a marine organism. The sodium requirement is not merely one of osmoregulation as other salts cannot substitute for sodium. Other salts can substitute for sodium as osmoregulators as long as a minimum concentration of sodium (ca. 10 mM) is maintained in the medium. It can be concluded that, when culturing this organism, the first deficiency to be encountered will be sodium. Droop (10) has reached a similar conclusion with other organisms.

The alga also showed considerable tolerance to increased concentrations of other elements in sea water. In concentrating sea water, the osmotic pressure of the medium limited growth before a single element became toxic. By increasing the concentration of each element singly, magnesium was found to be most toxic. Generally the dominant ion in alkali lakes is magnesium which may explain the absence of this species from these habitats, particularly if the calcium concentration is low. The alga was more tolerant towards high concentrations of potassium than towards the other elements.

It was not possible to increase significantly the rate of growth over that of enriched sea water media (24) under the various conditions used in this study. This would tend to support the conclusion of Kalle (21) that sea water is an ideal medium for plant growth.

Acknowledgments

Grateful appreciation is extended to Dr. Paul R. Gorham and Dr. Bostwick H. Ketchum for reading the manuscript.

References

1. Allen, M. B. The effect of salinity and of mineral nutrition on the metabolism of *Platymonas*. Plant Physiol. **31**, Suppl. xix (1956).
2. Allen, M. B. The cultivation of Myxophyceae. Arch. Mikrobiol. **17**, 34–53 (1952).
3. Allen, M. B. and Arnon, D. I. Studies on the nitrogen-fixing blue-green algae. II. The sodium requirement of *Anabaena cylindrica*. Physiol. Plantarum, **8**, 653–660 (1955).
4. Baas-Becking, L. G. M. Salt effects on swarmers of *Dunaliella viridis* Teod. J. Gen. Physiol. **14**, 765–779 (1931).
5. Bowman, H. H. M. Salinity data on marine and inland waters and plant distribution. Ohio J. Sci. **56**, 101–106 (1956).
6. Braarud, T. Salinity as an ecological factor in marine phytoplankton. Physiol. Plantarum, **4**, 28–34 (1951).
7. Braarud, T. and Rossavik, E. Observations on the marine dinoflagellate *Prorocentrum micans* Ehrenb. in culture. Avhandl. Norske Vindenskaps-Akad. Olso, 1–18 (1951).
8. Butcher, R. W. An introductory account of the smaller algae of British coastal waters. Part I. Introduction and Chlorophyceae. Fisheries Investigations, Ser. IV, 1–74 (1959).
9. Butcher, R. W. Contributions to our knowledge of the smaller marine algae. J. Marine Biol. Assoc. United Kingdom, **31**, 175–191 (1952).
10. Droop, M. R. Optimum, relative and actual ionic concentrations for growth of some euryhaline algae. Verh. Internatl. Ver. Limnol. **13**, 722–730 (1958).
11. Eyster, C. Chloride effect on the growth of *Chlorella pyrenoidosa*. Nature, **181**, 1141–1142 (1958).
12. Frerking, H. Uber die Giftwirkung der Lithiumsalze auf Pflanzen. Flora, **108**, 449–453 (1915).
13. George, E. A. A note on *Stichococcus bacillaris* Naeg. and some species of *Chlorella* as marine algae. J. Marine Biol. Assoc. United Kingdom, **36**, 111–114 (1957).
14. Gibor, A. The cultivation of brine algae. Biol. Bull. **111**, 223–229 (1956).
15. Hamburger, C. Zur Kenntnis der *Dunaliella salina* und einer Amöbe aus Salinenwasser von Carliari. Arch. Protistenk. **6**, 111–130 (1905).
16. Hase, E., Morimura, Y., Mihara, S., and Tamiya, H. The role of sulfur in the cell division of *Chlorella*. Arch. Mikrobiol. **32**, 87–95 (1958).
17. Hutner, S. H. Essentiality of constituents of sea water for growth of a marine diatom. Trans. N.Y. Acad. Sci., Ser. II, **10**, 136–141 (1948).
18. Hutner, S. H. and Provasoli, L. The phytoflagellates. *In* Biochemistry and physiology of protozoa. Vol. 1. *Edited by* A. Lwoff. Academic Press, Inc., New York. 1951. pp. 27–128.
19. Hutner, S. H., Sanders, M., McLaughlin, J., and Scher, S. Electrolyte requirements of protists and archeometabolism. Ann. N.Y. Acad. Sci. **69**, 286–291 (1957).
20. Ingram, H. Micro-organisms resisting high concentrations of sugars and salts. *In* Microbiol ecology. 7th Symposium Soc. Gen. Microbiol. Cambridge University Press, London. 1957. pp. 90–133.
21. Kalle, K. Das Meerwasser als Mineralstoffquelle der Pflanze. *In* Handbuch der Pflanzenphysiologie. Vol. IV. *Edited by* W. Ruhland. Springer-Verlag, Berlin. 1958. pp. 170–178.
22. Lerche, W. Untersuchungen über Entwicklung und Fortpflanzung in der Gattung *Dunaliella*. Arch. Protistenk. **88**, 236–268 (1937).
23. Mayer, A. M. Personal communication. 1959.
24. McLachlan, J. The growth of unicellular algae in artificial and enriched sea water media. Can. J. Microbiol. **5**, 9–15 (1959).

25. McLachlan, J. and Yentsch, C. S. Observations on the growth of *Dunaliella euchlora* in culture. Biol. Bull. **116**, 461–471 (1959).
26. McLeod, G. C. and McLachlan, J. The sensitivity of several algae to ultra-violet radiation of 2537 Å. Physiol. Plantarum, **12**, 306–309 (1959).
27. Monod, J. The growth of bacterial cultures. Ann. Rev. Microbiol. **4**, 371–394 (1949).
28. Osterhout, W. J. V. Plants which require sodium. Botan. Gaz. **54**, 532–536 (1912).
29. Pierce, G. J. The behavior of certain micro-organisms in brine. *In* The Salton Sea. Carnegie Inst. Wash. Publ. No. 193, 1914. pp. 49–69.
30. Pintner, I. J. and Provasoli, L. The nutrition of *Volvox globator* and *V. tertuis*. Proc. Internatl. Botan. Congr. 9th Congr. Montreal, 1959. **2**, 300–301 (1959).
31. Pintner, I. J. and Provasoli, L. Artificial cultivation of a red-pigmented marine blue-green alga, *Phormidium persicinum*. J. Gen. Microbiol. **18**, 190–197 (1958).
32. Provasoli, L. Nutrition and ecology of protozoa and algae. Ann. Rev. Microbiol. **12**, 279–308 (1958).
33. Provasoli, L., McLaughlin, J., and Droop, M. The development of artificial media for marine algae. Arch. Mikrobiol. **25**, 392–428 (1957).
34. Provasoli, L., McLaughlin, J., and Pintner, I. Relative and limiting concentrations of major mineral constituents for the growth of algal flagellates. Trans. N.Y. Acad. Sci., Ser. II, **16**, 412–417 (1954).
35. Ryther, J. H. The ecology of phytoplankton blooms in Moriches Bay and Great South Bay, Long Island, New York. Biol. Bull. **106**, 198–208 (1954).
36. Steiner, M. and Eschrich, W. Die osmotische Bedeutung der Mineralstoffe. *In* Handbuch der Pflanzenphysiologie. Vol. IV. *Edited by* W. Ruhland. Springer-Verlag, Berlin. 1958. pp. 334–354.
37. Stiles, W. Other elements. *In* Handbuch der Pflanzenphysiologie. Vol. IV. *Edited by* W. Ruhland. Springer-Verlag, Berlin. 1958. pp. 599–614.
38. Vishniac, H. S. The nutritional requirements of *Labyrinthula* spp. J. Gen. Microbiol. **12**, 455–463 (1955).
39. Vollenweider, R. A. Ökologische Untersuchungen von planktonic Alger auf experimenteller Grundlage. Schweiz. Z. Hydrol. **12**, 193–262 (1950).

Contribution No. 1099

Reprinted from BIOLOGICAL BULLETIN, Vol. 119, No. 1, pp. 145–152, August, 1960
Printed in U. S. A.

EXPERIMENTAL STIMULATION OF GAMETOGENESIS IN HYDROIDES DIANTHUS AND PECTEN IRRADIANS DURING THE WINTER[1]

HARRY J. TURNER, JR. AND JAMES E. HANKS

Woods Hole Oceanographic Institution, Woods Hole, Massachusetts

There is a long list of benthic marine invertebrates found in the Woods Hole, Mass. region that reproduce during the summer months. The majority of the species of organisms suitable for embryological experiments, listed by Costello *et al.* (1957), fall into this category. In addition, the extensive investigations of Redfield and Deevey (1952) have shown that most members of the fouling community attach during the summer months at Woods Hole and in other localities where there is a considerable difference between the summer and winter temperature extremes.

The question arises as to which of the various environmental variables controls reproduction. Hutchins (1947) studied the world-wide distribution of a variety of benthic marine forms and came to the conclusion that the northward extension of the ranges of a number of organisms is regulated by the minimal summer temperature that permits propagation, thus suggesting that elevated temperatures either stimulate gametogenesis or induce spawning.

Experimentally, Townsend (1940) obtained ripe gametes from the sea urchin *Arbacia* by holding specimens in aquaria at a temperature of 18° to 19° C. for one to two months in the late fall and winter. An ample supply of food was provided. Subsequently, Loosanoff and his co-workers have contributed greatly to the field by demonstrating the stimulating effects of elevated temperatures on the development of the gonads of certain commercial mollusks. Loosanoff and Davis (1950) succeeded in bringing the hard clam, *Venus mercenaria,* into reproducing condition during the winter months by gradually raising the temperature over a period of three weeks from that of the natural environment (5.0 to 7.0° C.) to 20° C. They mentioned that the same could be accomplished by placing the clams directly in water at 20° C. but some mortality occurred. Later (1952) these investigators studied the influence of temperature on the maturation of the gonad of the eastern oyster, *Crassostrea virginica,* and demonstrated a logarithmic increase in the rate of ripening of the gametes as temperatures were elevated from 15° C. to 30° C. They also determined that physiologically ripe gametes were formed earlier in the males than in the females under the same conditions. The importance of nutrition on gonad development was indicated by the failure of oysters in "poor" condition, *i.e.,* containing little glycogen, to respond satisfactorily to the thermal stimulus.

Experimental work on the effect of temperature on gonad development of other benthic marine invertebrates appears to be lacking. The investigations to be described were undertaken to determine if certain organisms occupying approximately the same geographical range as that of the oyster and the hard clam would respond in a similar fashion. The serpulid polychaete, *Hydroides dianthus* (= *H. hexagonus*) (Verrill), ranges from Cape Cod to Florida (Pratt, 1948) and is found from the low tide mark to depths of several fathoms. It reproduces from the middle of June to the end of October (Grave, 1933) and the ripeness of the gametes may be easily determined by removing the worms from their tubes and observing the products issuing from the nephridiopores (Grave, 1933). The bay scallop, *Pecten irradians* Lamarck, ranges from Cape Cod to Texas (Turner, 1953). It is a hermaphroditic species that spawns from mid-June to mid-August in the Woods Hole region (Belding, 1931). The ripening of the reproductive products may be determined on macroscopic examination by the development of a bright orange color in the ovary at the distal extremity of the visceral mass.

---

[1] Contribution No. 1099 from the Woods Hole Oceanographic Institution. This investigation was supported by the National Science Foundation NSF-G8905.

MATERIAL AND METHODS

Specimens of *H. dianthus* were obtained from the supply department of the Marine Biological Laboratory in the middle of December. They had been freshly collected from the adjacent waters where the temperature was approximately 8° C. The specimens were attached to old *Venus* and *Pecten* shells in a community which included *Astrangia,* sulphur sponges and dead barnacle shells. The tubes ranged between 5 and 7 cm. in length, well beyond the size of earliest sexual maturity (Grave, 1933).

Bay scallops were collected from the Eel Pond, Woods Hole, in December and January, in shallow water at low tide. They averaged a little over 3 cm. in the longest dimension and were the young of the year (Belding, 1931). There were no year-and-one-half old specimens in the Eel Pond and those usually found in nearby localities had been almost completely depleted by commercial fishing. Consequently, larger specimens were not available in adequate numbers for experimental work.

At the beginning of the experiments, a number of specimens of *H. dianthus* were removed from their tubes and placed in warm (23° C.) sea water to determine if they would extrude ripe gametes. No gametes were extruded and the worms were preserved in saturated aqueous mercuric chloride with 5% acetic acid for histological study. Similarly a number of scallops were opened and examined for the characteristic orange color of the ripe ovary. None showed this character and a number of appropriate anatomical portions were preserved in the same manner as were the worms.

The worms were subjected to an elevated temperature in aerated still water. Several tube-encrusted shells, containing about two dozen worms, were placed in a non-toxic five-gallon polyethylene container of warmed sea water held at 23° C. by a constant temperature bath. The water was changed every three days and continuously aerated. Suspensions of the planktonic alga, *Phaeodaloctyllum tricornutum* (= *Nitzschia closterium, forma minutissima*), were added daily for food. The amount added was adjusted to the quantity that the worms would just consume in 24 hours. A control was set up and maintained in an identical manner except that the container was placed in a tank supplied by the laboratory sea water system in which the temperature declined slowly from an initial level of 8° C. The illumination of the experimental group and the control group was practically identical. Growth of the tubes was determined in most cases by measuring the new white addition at the mouth beyond the discolored and fouled original tubes. In cases where the tubes were not sufficiently discolored to make new growth clearly distinguishable, a gram of powdered alizarin was added to the sea water and kept in suspension for 24 hours. The worms readily took up the alizarin and combined it with the calcareous material of the new growth, forming a prominent purple ring of alizarin lake. This treatment provided a very satisfactory method of marking the tubes and apparently had no deleterious effect on the worms. Specimens were removed on the third, fifth, seventh, and tenth days, tested for extrusion of gametes and preserved for histological examination. The experiment was repeated four times during December, January and early February.

Preliminary experiments indicated that bay scallops could not be maintained successfully in still water so they were treated in a different manner. In late January a number of specimens were placed in a 3′ × 3′ × 8″ Fiberglas tank supplied with running warmed sea water at a rate of $\frac{1}{2}$ gallon per minute. The apparatus used to warm the water was similar to that described by Loosanoff (1949) but modified to use electric power instead of gas. The temperature was maintained at 23° C. No food was added because the laboratory facilities for rearing phytoplankton were inadequate to supply the vast quantities required in running sea water systems. Consequently the scallops had to subsist on such quantities of food materials as remained in the water after it had passed through the intake line, reserve tank, and lengthy distributing system. A control was set up in a similar manner except that it was supplied with sea water at the ambient temperature which was holding steady at approximately 3° C. The lighting conditions over both groups were identical. Specimens were removed weekly, examined grossly for gonad development and preserved for sectioning.

RESULTS

Hydroides dianthus

None of the worms shed gametes when first obtained, nor did any taken from the control group which was maintained at a temperature approximating that of the natural environment at any subsequent time. In the experimental group which was maintained at 23° C., gametes were first obtained after seven days of warming. Males shed copious quantities of reproductive material consisting largely of spermatocytes and spermatids with a few tailed spermatozoa. By this time, females shed numerous eggs which were very much smaller than normal size and could not be fertilized. On the tenth day all males tested produced normal spermatozoa and the females shed eggs, the majority of which were of normal size. These eggs were successfully fertilized, underwent normal cleavage according to the usual time schedule (Costello *et al.*, 1957), and produced vigorous trochophores. During the ten days of warming all the worms increased the length of their tubes from three to five millimeters, indicating that they were vigorous and healthy. Worms in the control group showed no measurable growth.

The sequence of events during gametogenesis of the tube worm was followed in histological sections. The winter gonad consists of a series of pairs of syncytial masses of germ cells, one pair to each of the abdominal segments. Each segment contains a mass of reproductive material on either side at the ventro-lateral aspect of the wall of the coelom. Figure 1, A is a typical cross-section of a worm pre-

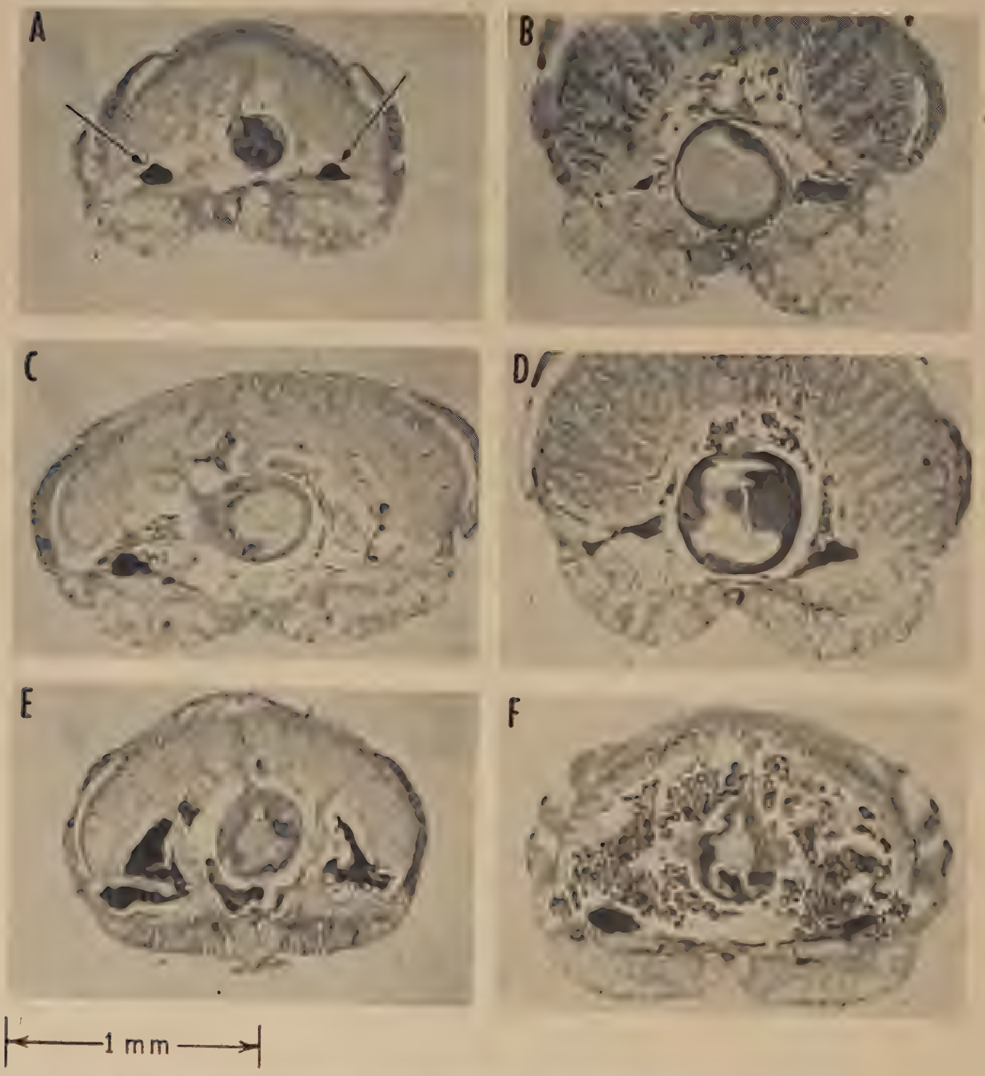

FIGURE 1. Transverse sections of *H. dianthus*. Delafield's haematoxylin and eosin stain. A, Specimen collected in December. Germinal masses indicated by arrows. B, Female held at 23° C. for five days. A few oocytes free in the coelom. C, Male held at 23° C. for three days. Numerous spermatocytes free in the coelom. D, Female held at 23° C. for seven days. Numerous oocytes partially grown free in the coelom. E, Male held at 23° C. for ten days. Mature spermatozoa in the coelom. F, Female held at 23° C. for ten days. Mature ova in the coelom.

served in mid-winter. There was little evidence of sexual differentiation at this time although some specimens contained masses with slightly enlarged nuclei, suggestive of primitive ovocytes. All specimens examined contained a few mitotic figures in the germinal masses, indicating that the germinal material was proliferating slowly.

Sexual differentiation became apparent in males after three days of warming. Cells broke away from the germinal masses into the coelom where the maturation divisions took place (Fig. 1, C). This process continued for the next seven days and by the tenth day the coelom was packed with mature spermatozoa, as shown in Figure 1, E.

No significant changes in the female gonads were observed until the fifth day of warming. At this time the nuclei began to enlarge as typical germinal vesicles and a few ovocytes broke free into the coelom (Fig. 1, B). By the seventh day, there were more free ovocytes in the coelom and some had shown appreciable growth (Fig. 1, D). By the tenth day, the coelom was completely filled with ovocytes, the majority of which were of mature size (Fig. 1, F).

There was remarkable uniformity in the rate of development of the gonads in all specimens examined and this was repeated in each of the four experiments run in sequence. At no time did any of the animals taken from the low temperature controls show any evidence of gametogenesis.

Pecten irradians

The reaction of the bay scallops to the elevated temperature was slower and more erratic than that of the tube worm. Approximately 5% died during the course of the experiment. A few specimens failed to show any development of the gametes, and in many, gametogenesis proceeded for a short time and then ceased. The majority of the specimens examined eventually produced tailed spermatozoa and ova which appeared to be structurally mature on histological examination. However, normal spawning did not occur so that physiological maturity could not be determined.

The bay scallop is hermaphroditic. The gonad consists of cylindrical, branching, tubular follicles ramifying through the visceral mass in the blood space surrounding the digestive tract. The follicle wall consists of a single layer of squamous epithelium with germ cells scattered along the inside. Male and female germ cells develop in separate follicles.

Sections of specimens taken from the natural environment in January showed no significant gametogenesis. The follicles of the male gonad as they appeared in sections are shown in Figure 2, A. The follicle walls of the female gonad (Fig. 2, B) appeared to be thicker because of the larger sizes of the ovogonia but there was no evidence of significant development.

Marked changes occurred after the scallops had been subjected to a temperature of 23° C. for one week. Rapid proliferation of the germinal material in the male resulted in a multi-layered lining of the follicles, consisting of spermatogonia and spermatocytes (Fig. 2, C), while the germ cells of the female gonad (Fig. 2, D) enlarged considerably and develop characteristic germinal vesicles with prominent nucleoli (Fig. 2, D.)

At the end of the third week of warming, the ovarian portion of the gonad acquired the orange pigmentation characteristic of the ripe ovary and the testicular portion took on a light, cream color with a plump appearance. Histological sections showed that the male follicles were lined with many layers of spermatozoa with the tails projecting out into the much reduced lumens (Fig. 2, E). The ovarian follicles were much enlarged and were completely filled with ova of mature size

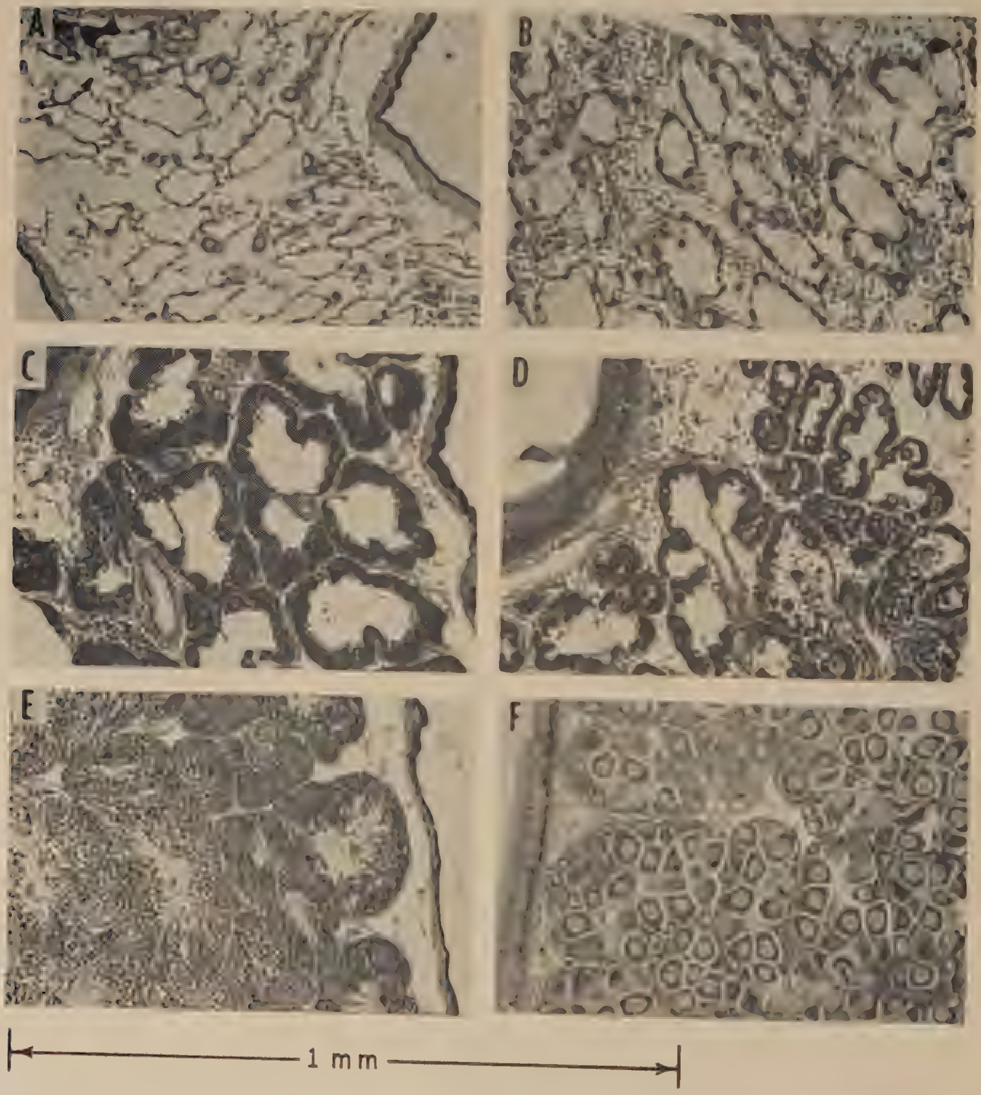

Figure 2. Sections of gonads of *P. irradians*. Delafield's haematoxylin and eosin stain. A, Male gonad of specimen collected in January. B, Female gonad of same specimen. C, Male gonad of specimen held at 23° C. for one week. D, Female gonad of the same specimen. E, Male gonad of specimen held at 23° C. for three weeks. F, Female gonad of same specimen.

(Fig. 2, F). None of the specimens taken from the control group showed any evidence of gametogenesis during January and February.

DISCUSSION

It is clear from the foregoing that the tube worm, *Hydroides dianthus,* and the bay scallop, *Pecten irradians,* respond to artificially elevated temperatures during the winter in a manner similar to that shown by many commercial molluscs, as described by Loosanoff, by developing their gametes out of season. All of the tube worms subjected to a temperature approximating that of the natural environment during the normal reproductive period developed ripe gametes within ten days. These underwent normal fertilization, cleavage, and developed into viable larvae.

The response of the bay scallop was somewhat erratic and the development of the gametes was much slower. It is quite probable that the experimental conditions were not entirely satisfactory, particularly in regard to nutrition. Oysters and clams maintained in the laboratory sea water system grow thin and watery after a time, indicating that suspended nutrient material is sparse. Consequently, the scallops held in running sea water at the elevated temperature undoubtedly had to synthesize the reproductive materials from stored substances which may have varied considerably among individuals at the time they were collected. Individuals in which gametogenesis failed to go on to completion were probably those with inadequate supplies of reserve nutrients, similar to the oysters in "poor" condition described by Loosanoff and Davis (1952). In any event it is clear that temperatures approximating those existing during the normal spawning period will stimulate gametogenesis in both *P. irradians* and *H. dianthus* if imposed experimentally during the winter months when the temperature of the natural environment is approaching the seasonal minimum.

SUMMARY

1. Temperatures approximating those existing during the normal summer reproductive period will stimulate gametogenesis in *Hydroides dianthus* and *Pecten irradians* if artificially imposed during the coldest winter months.

2. *H. dianthus* will produce mature gametes in ten days if held in aerated sea water at 23° C. and fed adequate quantities of *Phaeodactyllum tricornutum.*

3. *P. irradians* may produce gametes that appear to be mature on histological examination in three weeks if held in running sea water warmed to 23° C. but in many cases development fails to go to completion.

4. Failure of gametogenesis to reach completion in some specimens of *P. irradians* may be due to inadequate food supply under the conditions of the experiment.

LITERATURE CITED

BELDING, D. L., 1931. The Scallop Fishery of Massachusetts. Marine Fisheries Series—No. 3. Commonwealth of Mass., Dept. of Cons., Div. of Fish. and Game, Marine Fish. Sec.

COSTELLO, D. P., M. E. DAVIDSON, A. EGGERS, M. H. FOX AND C. HENLEY, 1957. Methods for Obtaining and Handling Marine Eggs and Embryos. Marine Biological Laboratory, Woods Hole, Mass.

GRAVE, B. H., 1933. Rate of growth, age at sexual maturity, and duration of life of certain sessile organisms, at Woods Hole, Massachusetts. *Biol. Bull.,* **65**: 375–386.

HUTCHINS, L. W., 1947. The bases for temperature zonation in geographical distribution. *Ecol. Monogr.,* **17**: 325–335.

LOOSANOFF, V. L., 1949. Method for supplying a laboratory with warm sea water in winter. *Science,* **110**: 192–193.

LOOSANOFF, V. L., AND H. C. DAVIS, 1950. Conditioning *V. mercenaria* for spawning in winter and breeding its larvae in the laboratory. *Biol. Bull.,* **98**: 60–65.

LOOSANOFF, V. L., AND H. C. DAVIS, 1952. Temperature requirements for maturation of gonads of northern oysters. *Biol. Bull.,* **103**: 80–96.

PRATT, H. S., 1948. A Manual of the Common Invertebrate Animals, Revised Edition. The Blakiston Co., Philadelphia.

REDFIELD, A. C., AND E. S. DEEVEY, JR., 1952. Pt. II. The Biology of Fouling. In: Marine Fouling and its Prevention. United States Naval Institute, Annapolis. Chap. 5. The Seasonal Sequence, 48–76.

TOWNSEND, G., 1940. Laboratory ripening of *Arbacia* in winter. *Biol. Bull.,* **79**: 363.

TURNER, H. J., JR., 1953. A review of the biology of some commercial molluscs of the East Coast of North America. *In*: Sixth Report on Investigations of the Shellfisheries of Mass., Dept. of Nat. Res., Div. of Marine Fisheries, 39–74.

Contribution No. 1100

Deep-Sea Research, 1960, Vol. 7, pp. 163 to 182. Pergamon Press Ltd., London. Printed in Great Britain

Some chemical and hydrographic observations along the north coast of South America—I. Cabo Tres Puntas to Curaçao, including the Cariaco Trench and the Gulf of Cariaco

Francis A. Richards*

(*Received* 16 *December* 1959)

Abstract—Chemical and hydrographic observations were made on five north-south sections along the Caribbean coast of Venezuela in October and November, 1958. In addition, 15 stations were occupied in the Gulf of Cariaco. Chemical determinations included dissolved oxygen, total and inorganic phosphorus, nitrate, silicate and, in the anaeric waters of the Gulf of Cariaco and the Cariaco Trench, hydrogen sulphide.

Except for some low-salinity near-surface water, these waters form a single mass, on the basis of the temperature-salinity diagram, in agreement with the findings of Parr (1937). Minimum salinities are found at 700–800 m and can be attributed to Antarctic Intermediate sources. Maximum salinities are in the upper 200 m, at depths which increase to the north.

Near the coast, isopleths of salinity, temperature, density and the nutrient ions generally slope upward toward the south, particularly in the eastern sections. This is interpreted as evidence of upwelling along this coast, a phenomenon which appears to be the only important source of nutrients in the photic zone, and which accounts for the high biological productivity of the region.

The Gulf of Cariaco was filled with nearly isohaline water having the same temperature correlations as the Caribbean water outside at the time of the observations. Upwelling at the eastern end of the Gulf is clearly evident from the temperature, oxygen and nutrient distributions. The water deeper than about 54 m is isolated from, and is colder than, water at equal depths outside. Past observations indicate that this deep water may be renewed some (and possibly all) years, in February. These deep waters are isolated, vertically, by a sharp temperature gradient, are stagnant, and contain sulphides. The upwelling in the east results in high biological productivity in the region, which is evident from the rich flora and fauna.

An estimate of the productivity of the region has been made from the fixation of phosphate-phosphorus which upwells near the coast, north of Puerto La Cruz. The calculation indicates a production of 0·14 gm C/m^2/day, a figure which is consistent with estimates made in the region by other methods. An estimate made in the Gulf of Cariaco, also on the basis of the fixation of inorganic phosphate, indicated a daily production of 2·8 to 5·7 gm C/m^2.

Summario—En octubre y noviembre de 1958 se hicieron algunas observaciónes químicas e hidrográficas a lo largo de la costa Caribe de Venezuela. En el curso del trabajo la temperatura y la constitución química de las aguas de la región fueron estudiadas en forma de cinco secciones a lo largo de la costa en sentido norte-sur y además en 15 estaciónes hidrográficas en el Golfo de Cariaco. Los estudios químicos incluyeron análisis del oxígeno dissuelto, del fósforo inorgánico y totál, nitrato, silicato y, en aguas anaéricas del Golfo de Cariaco como en la Trinchera de Cariaco, sulfito de hidrógeno.

Con la sola excepción de un tanto de agua de baja salinidad cerca de la superficie, el agua formó una sola masa según el diagrama de temperatura-salinidád, de acuerdo con los resultados de Parr (1937). Las salinidades mínimas, encontradas entre 700 y 800 metros de profundidád, pueden atribuirse a las aguas de crigen Antártico Intermedio. Salinidades máximas se encontraron a profundidades de 200 metros o menos, según la distancia de la costa. La salinidád máxima se encuentra cerca de la superficie en las regiones costeras, y a mayores profundidades hacia el norte.

---

*Present address: Department of Oceanography, University of Washington, Seattle, 5 Washington.

Cerca de la costa, las superficies de igual salinidád, temperatura, densidád y sales nutritivas se inclinan hacia la superficie hacia el sur; esta tendencia se nota especialmente en las secciones orientales. Tal inclinación se interpreta como seña de surgencia de aqua de niveles inferiores a lo largo de la costa, lo cuál eleva el aqua de mas alto contenido de sales nutritivas hacia la superficie y la zona fótica. Esto explica la elevada producción biologica que se encuentra en la región.

El Golfo de Cariaco se halló lleno de agua casi isohalina la cual tuvo las mismas characterísticas de temperatura como las aguas del Mar Caribe en la vecinidád. El fenómeno de surgencia de agua de niveles inferiores ocurre en la regiôn oriental del Golfo según la distribución de oxígeno dissuelto, temperatura, y sales nutritivas. El agua a profundidades majores de approximadamente 54 metros está aislada y posée temperaturas menores a las que se observan a profundidades iguales en el mar afuera del Golfo. Observaciones obtenidas en tiempos pasados indican que estas aguas mas profundas del Golfo suelen renovarse en algunos años, y posiblemente cada año, en febrero. Estas aguas de produndidád se encuentran aisladas por medio de un distinto cambio en la distribución verticál de temperatura; por lo tanto, se hallan estancados y contienen sulfido de hidrógeno. La producción biologica de la región del Golfo es elevada gracias a la surgencia de agua de niveles inferiores en la porción oriental; la abundancia faunística y florística son testigos a esto.

Fué possible calculár la producción biologica al norte de Puerto La Cruz por medio de las observaciones de contenido de fosfato cerca de la costa. Los resultados indican que 0·14 gramos de carbón se fijan por metro quadrado por dia. Este presupuesto está de acuerdo con los resultados de otras investigaciones en la región, las cuales se hicieron con otros métodos. En el Golfo de Cariaco, un presupuesto de la producción biológica por medio del fosfato dió como resultado desde 2·8 a 5·7 gramos de carbón fijados por metro cuadrado y por día.

INTRODUCTION

The relationships of the hydrography and the chemistry of the inshore regions of the southeastern Caribbean Sea to biological productivity and to deposition of sediments in the area are the principal foci of interest in the present study. Other discussions of the hydrography and chemistry of the Caribbean (Parr, 1937a, 1937b, 1938; Seiwell, 1938; Rakestraw and Smith, 1937; Worthington 1955, 1956) have dealt with more general offshore phenomena, and have left questions concerning inshore events to inference. However, this region should be of more than ordinary

Table 1. *Hydrographic stations occupied in the Southeastern Caribbean region.*

	Station numbers	*Inclusive dates*	*Publication*
Atlantis	1502–1507	14–22/III/33	Bulletin Hydrographique pour l'année 1933 (1934).
Atlantis	2751–2799	13–25/I/37	Unpublished.
Atlantis	5231–5235	5/XII/54	To be published in Bulletin Hydrographique pour l'année 1954.
Atlantis	5266–5271	8–10/II/55	To be published in Bulletin Hydrographique pour l'année 1955.
Atlantis	5596–5607	1–9/IX/57	To be published in Bulletin Hydrographique pour l'année 1957.
Atlantis	5659–5697	28/X–6/XI/58	To be published in Bulletin Hydrographique pour l'année 1958.
Crawford	332–350	22–25/II/58	Metcalf (1959)

N.B.—*Reduced station data may be had upon application to the Director, Woods Hole Oceanographic Institution.*

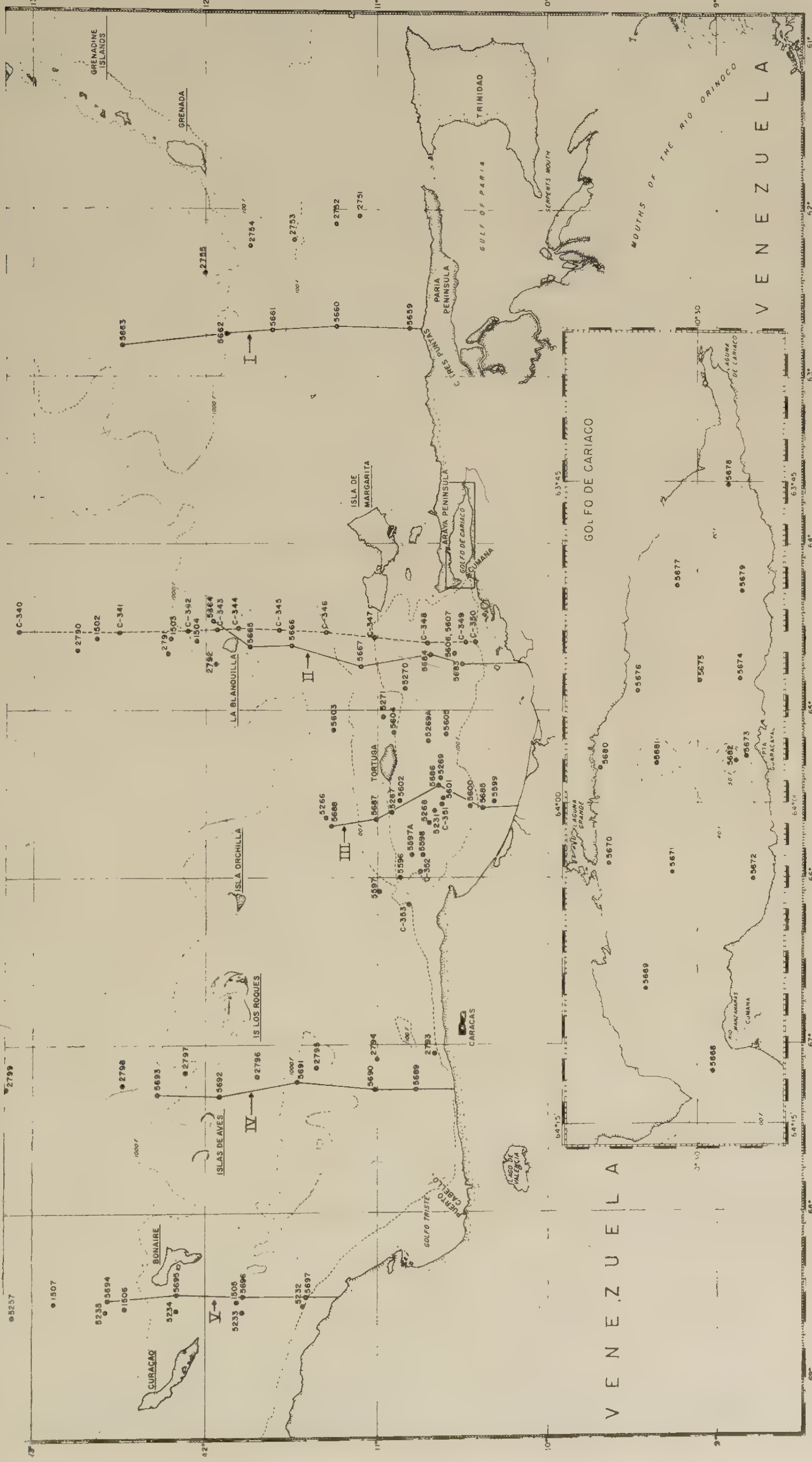
GRENADINE ISLANDS
GRENADA
TRINIDAD
GULF OF PARIA
SERPENTS MOUTH
MOUTHS OF THE RIO ORINOCO
PARIA PENINSULA
TRES PUNTAS
ISLA DE MARGARITA
ARAYA PENINSULA
GOLFO DE CARIACO
CUMANA
LA BLANQUILLA
TORTUGA
ISLA ORCHILLA
IS LOS ROQUES
CARACAS
ISLAS DE AVES
LAGO DE VALENCIA
PUERTO CABELLO
GOLFO TRISTE
BONAIRE
CURAÇAO
VENEZUELA
I
II
III
IV
V

FIG. 1. Stations and hydrographic sections occupied in the region by R. V. *Atlantis* and R. V. *Crawford*. *Crawford* station numbers have the prefix 'C.' Dates of the stations are given in Table 1.

oceanographic interest, characterized as it is by upwelling along the coast; by the anaeric Cariaco Trench (RICHARDS and VACCARO, 1956; RICHARDS and BENSON, 1960); and by the Gulf of Cariaco, which, although it has a fjord-like topography and a remarkably high rate of organic productivity, has no significant fresh-water influx.

The hydrographic and chemical observations in the Gulf of Cariaco are, to the best of our knowledge, the first made there. The Gulf, an embayment between the Araya Peninsula and the main coast of Venezuela, is a little over 35 miles long (east to west) and 9 miles wide (north to south). Its opening to the Caribbean, about 2 miles wide (near the city of Cumana), has a sill depth of about 54 m. The fairly regular bottom is indented by a centrally located basin having a maximum depth of about 80 m a little north of Punta Guaracayal (Fig. 1).

The Araya Peninsula is arid, but the land to the south rises steeply, and enjoys sufficient orographic rainfall to support a tropical vegetation. Small streams with small watersheds enter the head of the Gulf through Laguna de Cariaco, but during the period of observation there was essentially no fresh water in the nearly isohaline Gulf, where salinities varied only between 36·60 and 36·70‰. Thus, the density stratification and stability in the Gulf were largely thermal effects.

The discussion is based, for the main part, on observations of salinity, temperature, dissolved oxygen, inorganic and total phosphorus, nitrates and silicates made on Cruise 246 of R.V. *Atlantis* in October and November, 1958. All sources of the data which are used are given in Table 1 and FIG. 1.

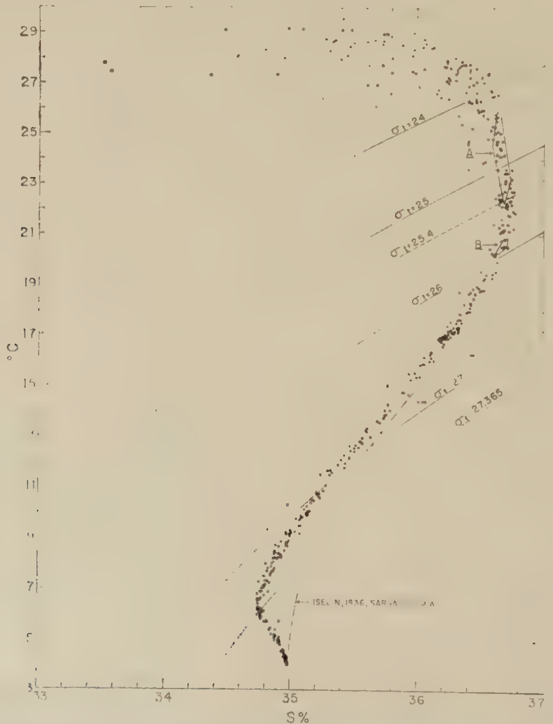

FIG. 2. Temperature-salinity correlations in the regions studied and in coastal waters to the west. The line indicated is the T/S correlation ISELIN (1936) found for the Sargasso Sea. Areas A and B enclose all the points from the Gulf of Cariaco.

WATER MASSES OF THE REGION

Insofar as water masses are characterized by the salinity-temperature diagram (Helland-Hansen, 1916), all of these north coastal waters, with exceptions in the superficial warm layers, are of a single type (Fig. 2) which has been discussed by Parr (1937a). Maximum salinities, greater than 36·5‰, are found in the upper 200 m, and are associated with σ_t values of 25·4. Parr attributes this maximum salinity water to a wedge, of Sargasso Sea origin, which penetrates to the southwestward and through the passages between the Greater Antilles and northern Lesser Antilles and which both overlies and underlies water of North Equatorial origin entering the more southerly of the passages between the Lesser Antilles. Salinity minima occur near $\sigma_t = 27{\cdot}365$, the value found by Parr, at about 6 °C and 700–800 m in depth. This low salinity water stems largely from the Antarctic Intermediate water mass, has large negative salinity anomalies (computed from Iselin's 1936 diagram) and high silicate concentrations (Richards, 1958). This σ_t surface (27·365, Parr's value) represents the core of the Antarctic Intermediate water in the region. The deeper, colder waters of the Caribbean are additionally different from extra-Caribbean waters by virtue of their lower oxygen and higher nutrient-salt concentrations.

LOW-SALINITY SURFACE WATER

In the Caribbean region included in Fig. 1, there is a general trend for surface salinities to decrease and for surface temperatures to increase northward from the coast. This trend is clearly shown in the *Meteor* atlas of surface salinities and temperatures (Böhnecke, 1936) and by Parr (1937a, 1938). This distribution is apparently the result of upwelling, which brings colder, more saline water to the surface along the Venezuelan coast. Imposed upon this general distribution of surface salinity are tongues or streaks of even fresher water of extra-Caribbean origin. As shown by Böhnecke, the latter has two sources : (a) South American rivers and (b) the equatorial North Atlantic. According to van Andel and Postma (1954), low-salinity water flows north-westward along the northeastern South American coast around both sides of the island of Trinidad, to enter the Caribbean between Grenada and the Paria Peninsula. The *Meteor* atlas indicates that the contribution of the Orinoco River to this source is relatively minor in comparison with the Amazon, but according to Postma (private communication) the Orinoco water may be of major importance in the Caribbean. Böhnecke's charts indicate that the influence of the South American rivers on the Caribbean is slight from January until May, and although by May these waters have spread upward along the Brazilian and Guiana coasts to the latitudes of the Windward Islands, surface salinities between the Paria Peninsula and Grenada are not less than 35·5‰. Surface salinities lower than 35·5‰ are found in the Caribbean beginning in June and increasing in their range until July, when values lower than 33·75‰ may be observed west of the Windwards. After July, this fresher water recedes from the Caribbean for the rest of the year. By October, water less saline than 35·0‰ from the equatorial North Atlantic joins with that from the South American rivers, forming a continuum from the Venezuelan Basin to the West coast of Africa, but by December the two sources are again separated by water more saline than 35·0‰, and Böhnecke shows no water fresher than 35·5‰ in the Caribbean region (Fig. 1) in December. Although the available hydrographic sections are inadequate to describe the course of this low-salinity water in detail, they are in general agreement with BÖHNECKE's charts. In January, 1937, water less saline than 35·5‰ was observed at the surface at Stations 2751, 2752 and 2753, and was apparently attributable to South American river discharge. During this 1937 cruise, the low-salinity water was sufficiently dissipated to be no longer evident as a salinity minimum in a section along 67 °W, nor was the low-salinity surface water evident in the February 1958, *Crawford* section (FIG. 3), which, although in good detail along 64° 30′W, was occupied during the dry season. On the other hand, low-salinity water was clearly present at the time of the October-November *Atlantis* observations, centered at Station 5661 (FIG. 3, Sect. I, minimum salinity 33·52‰) and at Station 5665 (Sect. II, minimum salinity 34·94‰). However, the surface salinities in Section IV of this cruise steadily decrease in the northward direction, and none are sufficiently low to distinguish low-salinity water of Atlantic origin from the general trend, a distribution similar to that observed at these latitudes in January 1937.

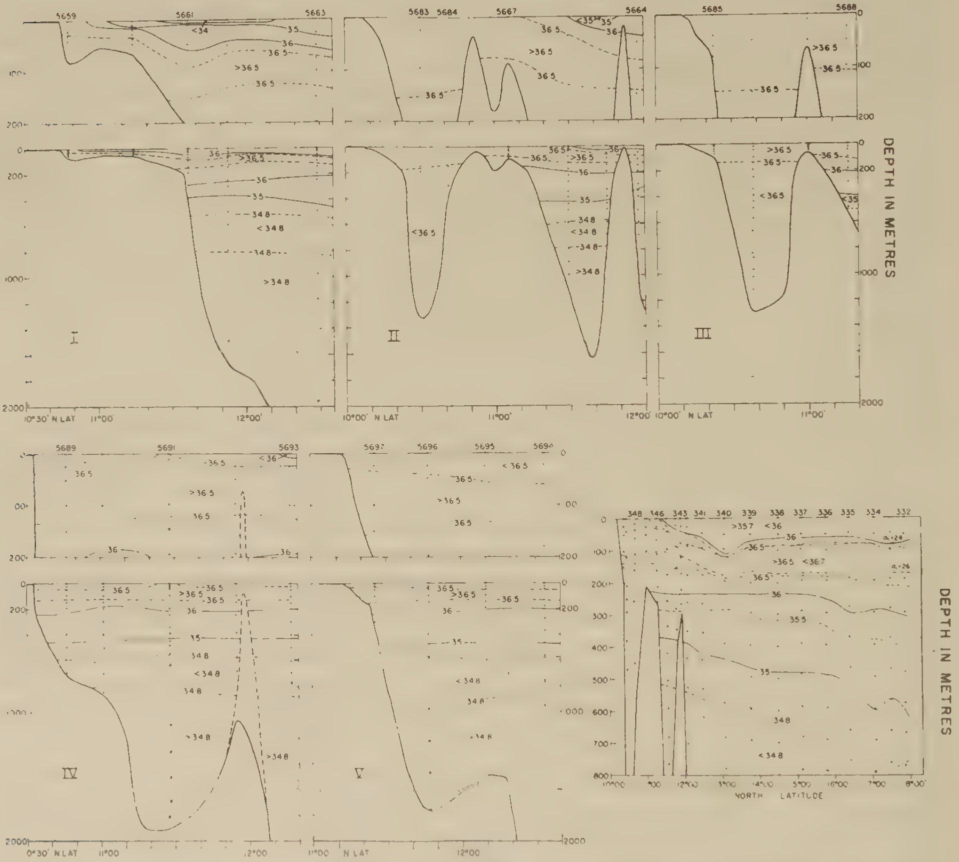

FIG. 3. Salinity sections. Numbers I through V occupied by *Atlantis*, October and November, 1958. The lower right section occupied by *Crawford*, February, 1958.

As has been indicated in the introduction, the water of the Gulf of Cariaco was, at the time of the observations, essentially isohaline. The points from the Gulf fall on the temperature-salinity diagram for the general region without anomalies, but are divided into two groups (Areas A and B, Fig. 2), according to whether the samples were from above or below sill depth. Areas A and B of Fig. 2 are sufficiently separated to emphasize the isolation of the bottom, stagnant water below sill depth.

The Cariaco Trench is a unique locality of stagnation (Richards and Vaccaro, 1956). From 600 m to the bottom at about 1400 m, it is as nearly isohaline as the precision of the salinity determinations permits one to judge. Between its sill depth (*ca.* 150 m) and 600 m, salinities are higher than those at equal depths outside the trench, immediately to the north (Stations 5683, 5684, 5685, 5686, Fig. 3). Somewhat below the sill depth, the density *in situ* in the trench (Fig. 4) is less than at the same depths in the open Caribbean, because of the higher temperatures inside. The distribution of density across the sill is critical to the trench's remaining unflushed, but the observations which have been made do not permit determining the extent, if any, of advective replacement of the anaeric waters in it. The chemical conditions in the trench indicate that at most the flushing is slow, weak, or intermittent.

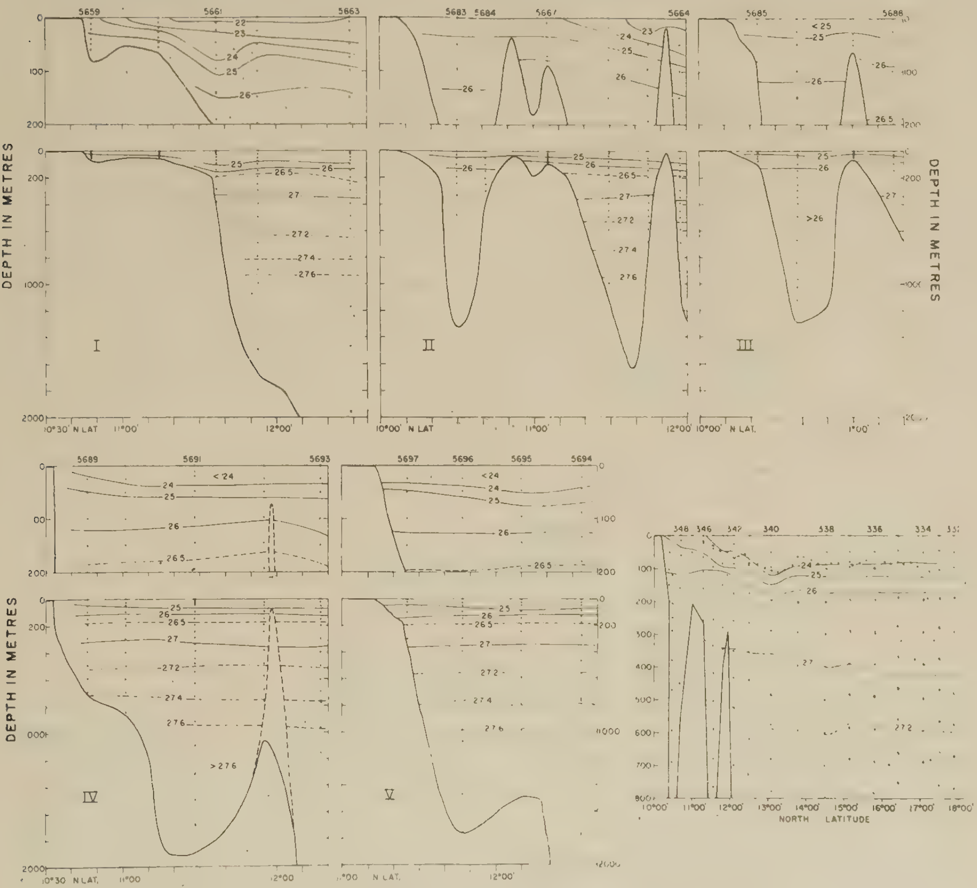

Fig. 4. Density (σ_t) sections. The sections are those shown in Figs. 1 and 3. The line – – – + – – – – – + – – – – shows the bathythermometrically determined depth of the upper isothermal mixed layer.

To recapitulate, the temperature-salinity diagram (FIG. 2) shows the water of this region to be of a single type, with relatively small, surface-borne accretions of fresh water entering the system from the surface of the Atlantic. These accretions fluctuate with the rainy and dry seasons.

MERIDIONAL DISTRIBUTION OF SALINITY AND TEMPERATURE

In general, the surface waters in the southern part of this region are more saline and colder than they are to the north (FIG. 3). Sigma-*t* surfaces (FIG. 4) at depth are nearly level (in the north-south direction), but there is a slight upward tilt, to the south, of the isopycnals in the upper 200–300 m. These observations and the chemical observations indicate upwelling along this coast. This upwelling is apparently the only continuing source of the nutrient-salt supply responsible for the high basic productivity and biological populations of the region, because the nutrient levels in the surface waters entering the region are uniformly low.

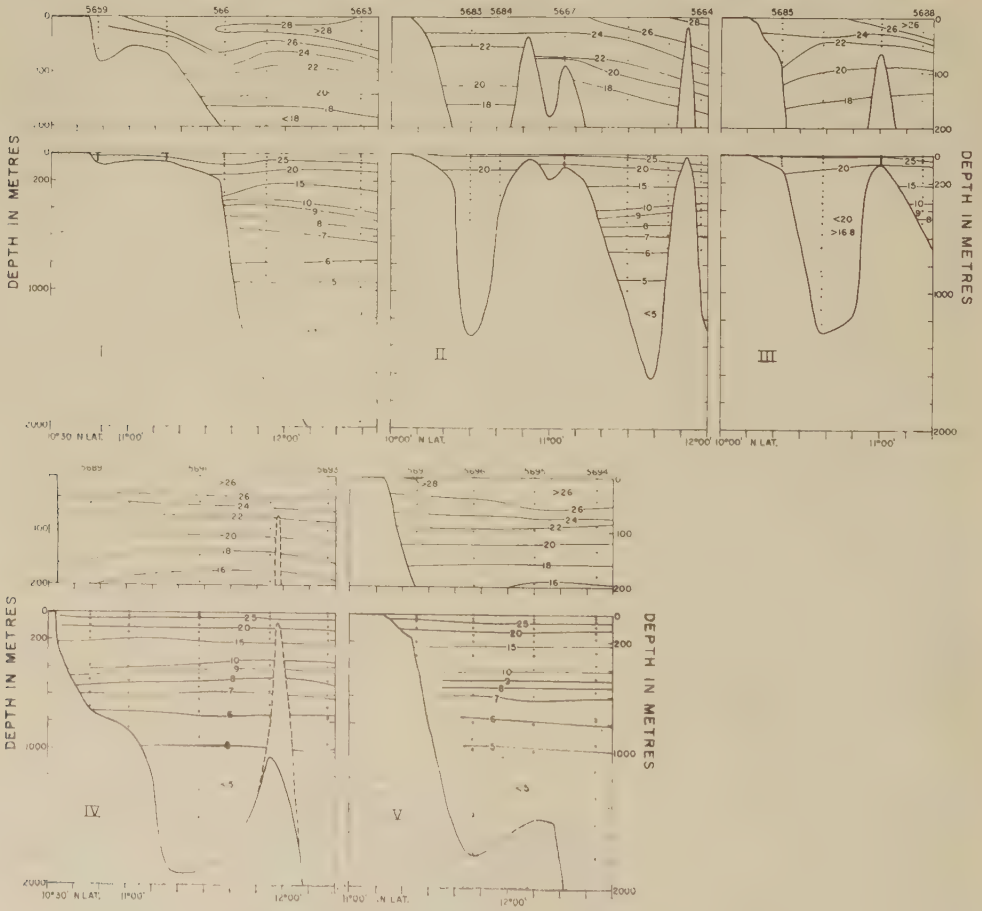

FIG. 5. Temperature sections (*Atlantis*). The locations are shown in FIG. 1.

DISTRIBUTION OF TEMPERATURE

The surface temperatures in the region (FIG. 5) varied from 21·22° to 28·59 °C, and in general the lowest were found nearest the coast. In the upper 100 m, the isotherms slope upward, to the south. This upward slope is more extreme in the eastern three sections, and in Section I the warmest water was found below the surface at Stations 5661, 5662 and 5663 (FIG. 5). At greater depths, the isotherms were nearly level. No water warmer than 5 °C was found at depths greater than 1000 m.

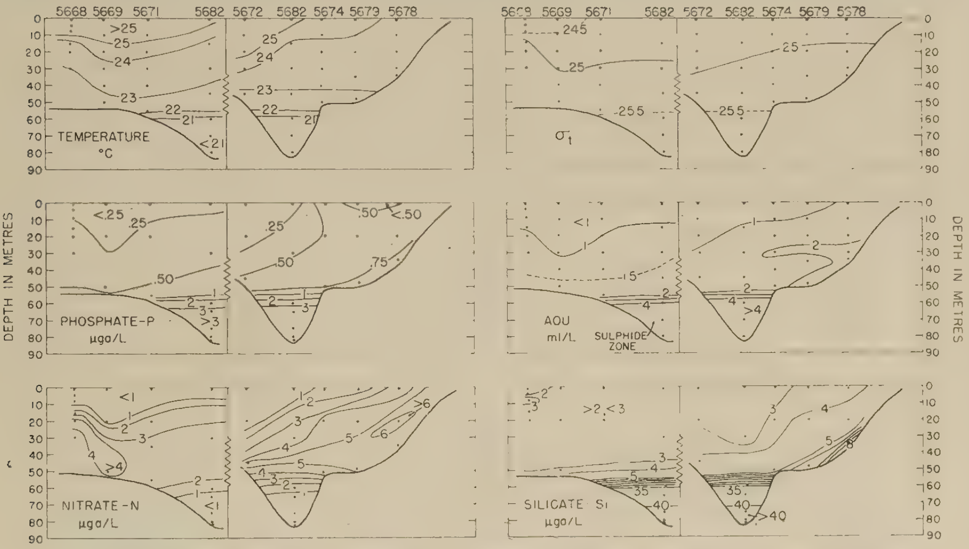

FIG. 6. Physical and chemical variables in a section along the length of the Gulf of Cariaco. Station locations are shown in FIG. 1.

TEMPERATURES IN THE GULF OF CARIACO

The surface temperatures in the Gulf (FIG. 6) gradually decrease to the eastward, dropping from 25·8 °C at the mouth of the Gulf to 23·9 °C at the head. At the time of the observations, water at about 22·5 °C could enter the Gulf over the sill. This cold water appears to flow into the Gulf over the sill and then to rise to the surface layer in the eastern reaches of the Gulf.

The Gulf waters deeper than about 55 m are isolated from the open Caribbean by the shallow sill. In the deeper basin of the Gulf, there is a relatively steep thermal gradient between the sill depth (54 m) and 60 m, the temperature dropping at least 1·5 °C in this vertical distance. This gradient establishes a high order of vertical stability and a considerable barrier to vertical mixing of water from depths greater than 60 m. Water as cold as 20·37 °C was observed in the depths of this basin. This cold water was stagnant, oxygen-free, and contained hydrogen sulphide. During the period of observation, 20·4 °C water was not present at depths less than about 120 m at the nearest station occupied outside the Gulf. However, five hydrographic stations (Table 2) are available from the Cariaco Trench, to the west of the mouth of the Gulf of Cariaco, which show something of the temperature variability in this part of the water column. On only one of these occasions, 9 February 1955, was the outside water at depths between 50 and 80 m sufficiently cold to supply the now anaeric water filling the deepest part of the Gulf. This situation was also approached on 25 February 1958, so there may be either annual or intermittent flushing of the basin.

Table 2. Temperatures in the Cariaco Trench and Gulf of Cariaco.

Depth (m)	*Cariaco Trench*					*Gulf of Cariaco*
	5231 5/XII/55	5269 9/II/55	5606–7 8–9/XI/57	C–349 25/II/58	5683 2/XI/58	1/XI/58
40	25·4	22·7	26·6	22·4	23·3	23·1
50	24·8	21·6	25·2	22·2	22·2	22·2
60	24·2	20·9	24·9	22·0	21·9	20·9
70	23·8	20·6	24·6	21·9	21·6	20·4
80	23·4	20·4	24·4	21·8	21·4	20·4

Table 3. Stability values in the Gulf of Cariaco (Station 5682).

Depth (m)	σ_t, gm l^{-1}	$\Delta\sigma_t$, gm l^{-1}	*Approximate Stability*, m^{-1}
1	24·56		
		0·38	$2{\cdot}5 \times 10^{-5}$
15	24·94		
		0·15	1×10^{-5}
30	25·09		
		0·20	$1{\cdot}3 \times 10^{-5}$
45	25·29		
54 (sill depth)		0·52	$3{\cdot}5 \times 10^{-5}$
60	25·81		
		0·10	$6{\cdot}7 \times 10^{-6}$
70	25·91		
		0·02	$1{\cdot}3 \times 10^{-6}$
80	25·93		

It has been suggested that the stability (estimated as numerically, but not dimensionally, equal to $10^{-3}\,\Delta\sigma_t/\Delta D$ where ΔD is the depth difference in metres) across the sill may determine whether or not a basin can become anaeric (RICHARDS and VACCARO, 1956). The stability requirements are not fully established, but RICHARDS and VACCARO's paper implies that values of the order of $10^{-5}\,m^{-1}$ are sufficient, while those of the order of $10^{-6}\,m^{-1}$ are insufficient for anaeric conditions to develop. In the Gulf of Cariaco, the stability across the sill (Table 3) is sufficiently high to meet the above criterion. Other criteria must also be satisfied for a basin to become anaeric; fundamentally, the rate of supply of organic matter (oxygen consumption) must exceed the rate of ventilation, or supply of oxygenated waters, for some period of time. Thus, in regions where upwelling can insure high rates of organic production, these rates can outstrip circulatory replenishment of oxygen, even in arid regions in low latitudes where evaporation may exceed precipitation, if stability values at sill depth of the order of 10^{-5} are exceeded.

DISSOLVED OXYGEN AND THE APPARENT OXYGEN CONSUMPTION

In Sections I, II and III the surface oxygen concentrations vary but little, between 4·25 and 4·45 ml/l (FIG. 7). All the surface samples were slightly undersaturated, but not greatly so. Values of the apparent oxygen utilization (FIG. 8) in the surface samples were never large enough to indicate the immediate presence of intense *foci* of upwelled water and, although it will be developed later that this coast is a region of extensive upwelling, the surface waters were not observed to be far out of equilibrium with the atmosphere. The isopleths of oxygen consumption do, in the upper 100 m, shoal to the southward, and this is taken as an indication of upwelling in the region.

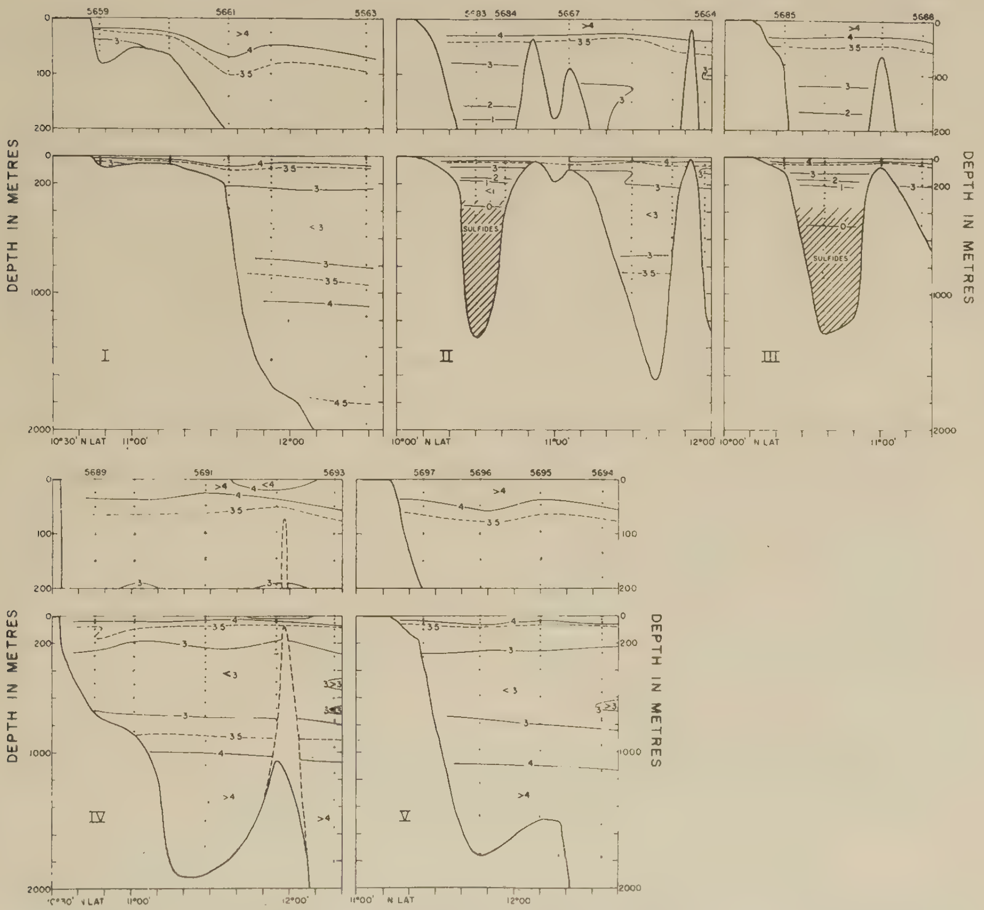

FIG. 7. Dissolved oxygen (ml/l) and the location of sulphide zones in the sections. Station locations are shown in Fig. 1.

The oxygen minimum layer, containing *ca.* 2·7 ml/l, is found near the σ_t value of approximately 27·1—a value appreciably less than that characterizing the core of the Antarctic Intermediate water, and also less than the values associated with the oxygen minima in the North Atlantic, Pacific, and Indian Oceans, $\sigma_t = 27{\cdot}23$ (see RICHARDS, 1957, p. 204). According to SEIWELL (1938), the modal value of σ_t at the minimum oxygen concentration in the Caribbean is 27·171 ± 0·007 (*sic*), which density occurs at about 500 m in the four sections here considered. The density of the water with which the maximum oxygen consumption is associated appears to be somewhat greater than that at which the minimum oxygen concentrations are found, the former more closely approaching the core of the Antarctic Intermediate water at $\sigma_t = 27{\cdot}36$.

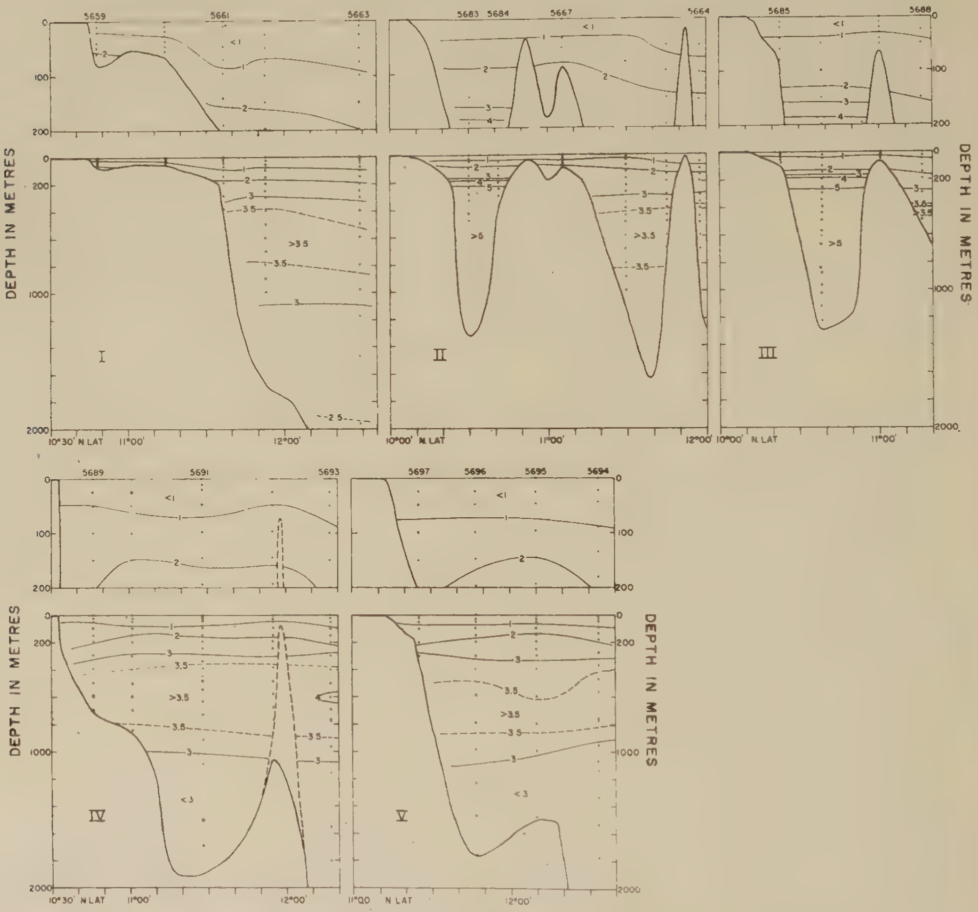

FIG. 8. Apparent oxygen utilization (ml/l) in the sections. Station locations are shown in FIG. 1.

Appreciably unsaturated water reaches the surface at the head of the Gulf of Cariaco, with values of the apparent oxygen utilization as large as 1·18 ml/l at the surface. This appears to be a region of intense, active, rapid upwelling, in which there is an appreciable spatial lag before the water is again oxygenated by contact with the atmosphere, by photosynthesis, or both. However, the observations are more closely spaced here than in the open Caribbean sections, so it is not implicit that the upwelling here is more intense than it may be in correspondingly small areas along the open coast. All the oxygen has been consumed from the water deeper than about 65 m in the Gulf, and sulphide-sulphur concentrations of up to 33 μga/l were observed.

NUTRIENT IONS

Inorganic phosphate, total phosphorus, nitrate and silicate concentrations were observed on Sections I and II (FIG. 9), in the Gulf of Cariaco (FIG. 6), and at Stations 5686 and 5693. The analytical methods were those listed by RICHARDS (1958).

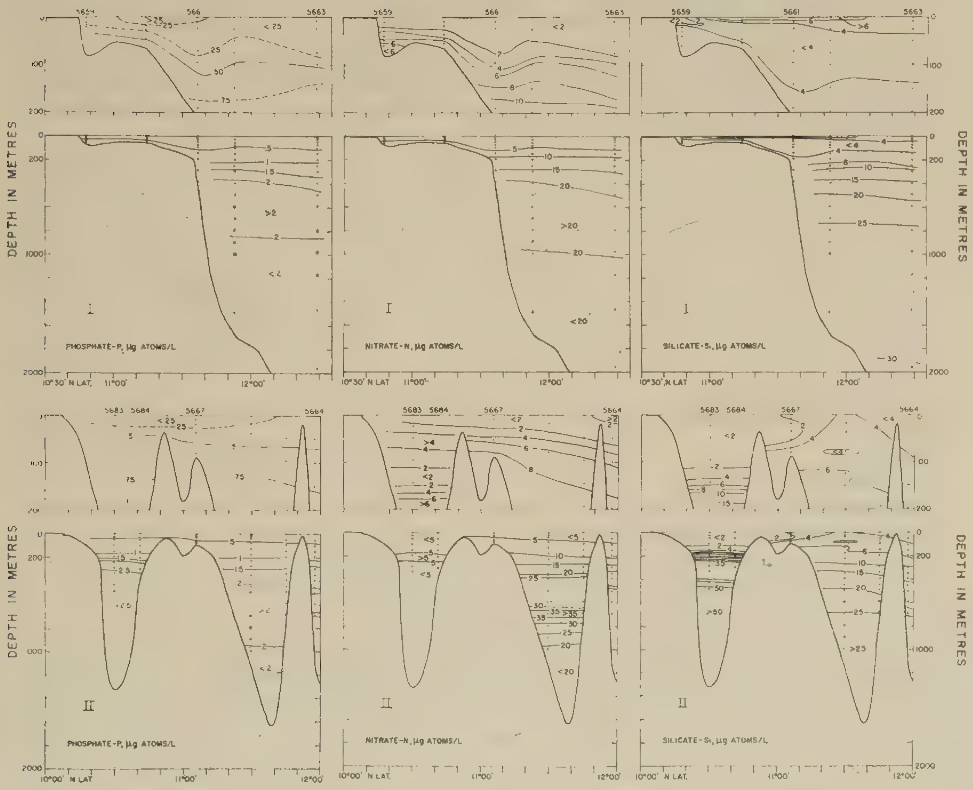

FIG. 9. Distribution of phosphate-phosphorus, nitrate-nitrogen, and silicate-silicon in Sections I and II. Station locations are shown in FIG. 1.

NUTRIENTS IN THE SURFACE, LOW SALINITY WATER

Pursuing the presumption that the surface samples at Stations 5661, 5662 and 5665 have fairly large admixtures of river water, the characteristics of this water can be compared with other, more saline surface water, such as at Stations 5664 and 5667 (Table 4).

The outstanding property of the low-salinity water is its higher silicate content, and, in two of the three cases, high concentrations of organic phosphorus, corresponding to its low phosphate-phosphorus and nitrate-nitrogen contents. The high silicates suggest the presence of silt (or perhaps diatom frustules) in the water, and the low phosphates and nitrates suggest that photosynthetic production of organic matter has stripped the river water of these latter nutrients, prior to or shortly after its entering the Caribbean. The sub-surface distribution of the nutrients in Sections I and II gives no evidence that the low-salinity water is a rich source of nutrients other than silicate.

A major feature of the nutrient distributions in Section I is the upward slope, to the south, of the shallower isopleths between Stations 5660 and 5661. Equal concentrations of nutrients are found at about 50 m at the southernmost of these stations, and at 150 m to the north. This distribution appears to be the consequence of typical upwelling produced by a wind blowing parallel to a coast, with the coast on the left-hand side (SVERDRUP *et al.*, 1946, p. 501, FIG. 124). Similar distributions were observed, somewhat less strikingly, in Section II, but this section is topographically more complicated because here the Cariaco Trench is located within the limits of the continental shelf. Thus the upwelled water reaches shallower layers closer to the shore in Section I than it does in Section II, where the major uplift of water occurs along the continental slope north of the Cariaco Trench. (The rise between Stations 5664 and 5665 shown on the diagrams of Section II is the shallow ground surrounding La Blanquilla Island, and does not prevent communication between the waters at Stations 5664 and 5665 both to the east and to the west of the section. However, this feature does appear to initiate the upward flow of waters to the south and southwest).

Table 4. Comparison of low-salinity and high-salinity surface samples.

	Stations				
	5661	5662	5663	5664	5667
Salinity ‰	33·57	33·52	34·57	35·73	36·62
Phosphate–P, μ ga/l	0·28	0·18	0·16	0·35	0·22
Total P μ ga/l	0·32	0·52	0·76	0·36	0·34
Organic P μ ga/l	0·04	0·34	0·60	0·01	0·12
Nitrate-N μ ga/l	0·20	0·10	0·10	3·52	0·60
Silicate-Si μ ga/l	7·20	7·90	5·30	2·80	3·60
Temperature, °C	27·48	27·80	28·06	28·59	25·66

NUTRIENTS IN THE GULF OF CARIACO

It is apparent from the distribution of nutrients along the length of the Gulf of Cariaco (FIG. 6) that water enters the Gulf at depths between 30 m and the sill depth, about 54 m. The water then rises to the surface layers in the eastern part of the Gulf and enters the photic zone. The westward wind drift carries the surface layer out of the Gulf, but photosynthetic processes rapidly decrease the concentrations of nutrients to low levels. Thus, at the mouth of the Gulf, water flows in at depths greater than about 30 m and simultaneously flows out at shallower depths. This circulation results in marked chemical and physical gradients in the western part of the Gulf, whereas the water column is more homogeneous to the east, where upwelling occurs. The characteristics of the inflowing water, the upwelling water, and the outflowing water are compared in Table 5. It is apparent that the differences between the nutrient concentrations in the deep, incoming water and in the shallow, outflowing water should closely represent net changes brought about by biological activity within the Gulf. However, the rather large difference in the total phosphorus content of the eastern part of the Gulf and of the western shallow water probably represents either conversion into higher forms not captured by the sampling bottles or deposition of phosphorus in sedimentary material, or both. The higher concentrations of total phosphorus in the east (*e.g.*, Stations 5674, 5678, 5679) must come from some source other than the sub-surface inflowing water; the distribution of total phosphorus suggests that some of it is being reissued from the sediments and from the sequestered anaeric water below sill depth.

Table 5. Representative concentrations in water flowing into, upwelling in, and flowing out of the Gulf of Cariaco, and in the anaeric basin.

	Deep, (at mouth)	*East (end)*	*Shallow (at mouth)*	*Anaeric water (of the basin)*
Phosphate–P, μ ga/l	0·5	0·5	0·1–0·2	> 3·3
Total P μ ga/l	0·4–0·5	0·6–0·8	0·3–0·4	> 3·5
Nitrate–N μ ga/l	4	4	0·2	nil
Silicate–Si μ ga/l	2·5–4·0	4	1·2	> 41
Oxygen Consum. ml/l	1·5	1·0–1·5	0·1	Total
Temperature °C	23–24	23–24	25	< 21
Sulphide sulphur, μ ga/l	nil	nil	nil	> 25

The anaeric waters of the deepest part of the Gulf (Table 5) comprise a special case of nutrient entrapment, with concentrations which are extraordinarily high in comparison with freely circulating aerated ocean waters at comparable depths.

MAGNITUDE AND EXTENT OF UPWELLING IN THE REGION

In regions of coastal upwelling, the transport of nutrients into the euphotic zone occurs *across* the geostrophic flow, which is a longshore current in this region (see the distribution of density, Fig. 4). Criteria other than the dynamic topography must, therefore, be used in order to estimate the magnitude of upwelling and its accompanying transport of nutrients. The calculations which follow are an attempt to make such an estimate; they are presented primarily to suggest a method by which such transports might be estimated, even though the present treatment may not be fully borne out by the data from any single cruise. In particular, it will be assumed that our Section II and the *Crawford* section of February 1951 were simultaneous, or rather that similar conditions prevailed at these two times. However, the results are interesting in themselves and are consistent with the other estimates of biological productivity in the region.

The cross-current transport estimate depends on the magnitude of the northward transport of surface waters due to the winds. Estimates of these northward transports have been made by MONTGOMERY (1936) and by BROOKS (1939), using MONTGOMERY'S methods. They calculate, from average pressure distributions, that in this region (10°–15°N, 60°–65°W) there is a nearly northward transport of surface water of 2·97 tons/m/sec in July (MONTGOMERY) and of 2·06 in January (BROOKS). These estimates apply to some offshore region theoretically uninfluenced by the coast. BROOKS further states that the drift current is essentially limited to a surface homogeneous layer usually less than 50 m thick.

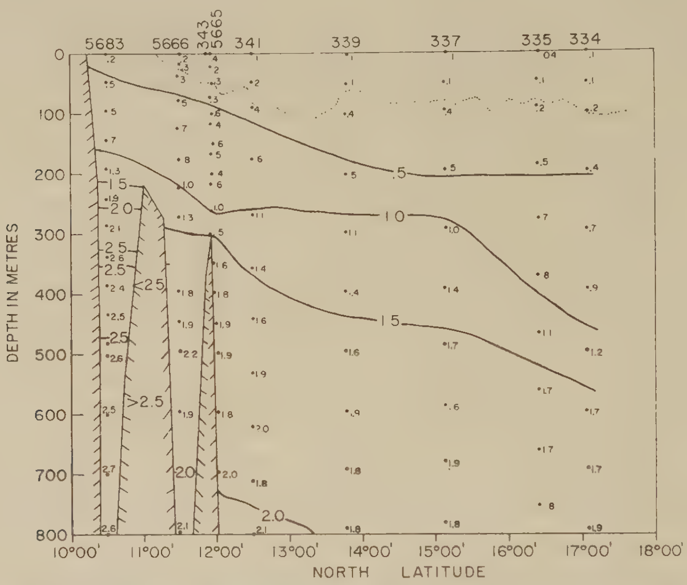

FIG. 10. Distribution of inorganic phosphate (μ ga/l) along a composite section from Section II (see FIG. 1) and the *Crawford* section of February, 1958. The upper dotted line shows the bottom of the upper isothermal layer, determined from the bathythermograph record made on the *Crawford* section.

It will be assumed that BROOKS' estimate for the northward volume transport in January applies and is achieved at *Crawford* Station 341 and northwards. From inspection of Sections I and II, the *Crawford* section, and the distribution of inorganic phosphate along a composite section made up of Section II and the *Crawford* section (FIG. 10) the following conditions will be assumed :

1. The northward transport estimated by BROOKS is confined to the upper mixed layer, which will be assumed to be 90 m thick at and north of *Crawford* Station 341 (the actual thickness of this layer is shown by the bathythermograph record of the thickness of the isothermal surface layer, FIGS. 4 and 10). This water has the average chemical charatceristics

$$S = 35{\cdot}8‰$$

$$PO_4^{-3} - P = 0{\cdot}1\ \mu\ \text{ga/l}$$

$$\textit{Silicate-Si} = 4\ \mu\ \text{ga/l.}$$

2. The northward flowing water in the upper 90 m consists of a mixture of : (a) waters which upwell in the region south of Station 341 from between the

isentropic surfaces where $\sigma_t = 24$ (near the bottom of the mixed surface layer) and $\sigma_t = 26$; and (b) lower salinity surface water from the east. The upwelling water has the volume transport V_u and the average chemical characteristics

$$S = 36{\cdot}5‰$$

$$PO_4^{-3} - P = 0{\cdot}45\ \mu\ \mathrm{ga/l}$$

$$\textit{Silicate-Si} = 1{\cdot}0\ \mu\ \mathrm{ga/l}$$

(It will be noted that the silicate concentrations at the north end of Section II, between $\sigma_t = 24$ and 26, are appreciably higher than 1 μ ga/l. However, they would be reduced by biological activity to about 1 μ ga/l upon rising, south of Station 341, into the euphotic zone so that the upwelling water, rising to mix with surface water, would ultimately have about this concentration).

3. The surface waters from the east which mix with the upwelled water have the volume transport V_e, an unknown salinity S_e, and the average chemical characteristics

$$PO_4^{-3} - P = 0{\cdot}1\ \mu\ \mathrm{ga/l}$$

$$\textit{Silicate-Si} = 7\ \mu\ \mathrm{ga/l}$$

4. The silicate in the surface water from the east is considered to be conservative, because nitrate concentrations appear to be too low to support further photosynthesis in the surface layer.

It is desirable to introduce silicates into the discussion because the surface, low-salinity water is particularly high in silicate, enabling it to be traced. Phosphate, on the other hand, is low both in this water and in the mixed water flowing northward along Section II. Silicate is thus distinctive. In addition, it is difficult to know what average value to assign to the salinity of the upper layer of Section I, with the result that S_e and V_e are unknown.

With the above assumptions, it is possible to estimate both the amount of upwelled water and the biological consumption of phosphorus from that water, and still maintain a balance of salt in the model :

$$V_u + V_e = 2{\cdot}06\ \mathrm{ton/m/sec}\ \text{(volume balance)}$$

$$V_u \times 36{\cdot}5 + V_e S_e = 2{\cdot}06 \times 35{\cdot}8\ \text{(salt balance)}$$

$$V_u \times 1 + V_e \times 7 = 2{\cdot}06 \times 4\ \text{(silicate balance)}$$

Solving,

$$V_u = 1{\cdot}03\ \mathrm{tons/m/sec}$$

$$V_e = 1{\cdot}03\ \mathrm{tons/m/sec}$$

$$S_e = 35{\cdot}09‰$$

The model can be used to compute the biological productivity induced along the coast by the upwelling, from the conversion of the inorganic phosphate into organic matter *via* photosynthesis, as follows :

North of *Crawford* Station 341, the surface layer contains approximately 0·1 μ ga $PO_4^{-3} - P$/l, *i.e.*, 0·35 μ ga/l of the phosphate-phosphorus originally present in the upwelled water has been converted into organic matter by the time the upwelled water is 150 miles ($2{\cdot}78 \times 10^5$ metres) offshore. Therefore, in a strip one metre wide extending 150 miles seaward, the conversion of phosphorus is, for each square metre per day ($8{\cdot}6 \times 10^4$ seconds)

$$\frac{8{\cdot}6 \times 10^4 \times 1{\cdot}03 \times 10^3 \times 0{\cdot}35}{2{\cdot}78 \times 10^5} = 111\ \mu \text{ ga } PO_4^{-3} - \text{P/m}^2\text{/day.}$$

The photosynthetic conversion of this amount of phosphorus is equivalent to the production of 0·14 gm of organic carbon/m²/day (FLEMING, 1940).

The only tests of the model lie in the independent estimates of productivity which have been made in this region, and in the value of $S_e = 35{\cdot}09‰$, which is not unreasonable. The productivity estimate is somewhat less than that of 0·48 gm C/m²/day made by RYTHER (RICHARDS and VACCARO, 1956) from carbon^{14} determinations of photosynthetic rates. Estimates made by CURL (1960) along this section during *Atlantis* Cruise 246, using the method of RYTHER and YENTSCH (1957), were 0·32, 1·40 and 0·78 gm C/m²/day; these estimates represent gross photosynthesis, while the change in phosphate should more nearly represent net productivity.

A similar estimate of an organic production rate can be made from the phosphate and hydrographic data in the Gulf of Cariaco. The estimate of the outward wind drift of the surface water is based on the navigational record of the ship's drift on stations. The distributions of density and phosphate (FIG. 6) indicate that water containing 0·5 μ ga $PO_4^{-3} - P/1$ upwells in the area between Station 5674 and the head of the Gulf, and that between Stations 5674 and 5682 there is a decrease in phosphate-phosphorus of *ca.* 0·35 μ ga/l. The outward drift of water is at a speed of about one knot, and in a distance of 4 to 8 miles (4 to 8 hours), 0·15 μ ga/l of phosphate-phosphorus is photosynthetically converted to organic matter. The euphotic zone here is about 10 m deep, so in it $0{\cdot}15 \times 10^3 \times 10\ \mu$ ga P is fixed in 4 to 8 hours under each square metre, i.e., 1·5 mga or 46·5 mg P/m²/4–8 hours. If the photosynthetic period per day is 12 hours, the daily production of organic carbon would be *ca.* 2·8 to 5·7 gm/m². CURL (1960) made two estimates of productivity in the Gulf: one of 0·52 gm C/m²/day at the head of the Gulf, and one of 3·8 gm C/m²/day near Station 5670.

The distribution of salinity, temperature, and dissolved oxygen along *Atlantis* Sections I to V and along the February 1958 *Crawford* section indicate that the degree of upwelling decreases toward the west, and although there is some suggestion of upwelling in Section IV there is scarcely any trace of it in the observations along Section V.

SUMMARY AND CONCLUSIONS

These Venezuelan coastal waters are of two main sources, as described by PARR (1937a). The first is a contribution from the western Sargasso Sea which intrudes, as a salinity maximum in the upper 200 m, both under and over water from the second source, water of equatorial Atlantic origin which enters the Caribbean through southern Antillean channels. The latter water contains an accretion of lower-salinity Antarctic Intermediate water, which is evident as a salinity minimum at 700 to 800 m. A third superficial low-salinity component, of South American river and/or equatorial Atlantic origin, may be present to a greater or lesser extent, varying with the season and, in turn, with fluctuations in the outfall of the Orinoco and Amazon Rivers.

This coast is a region of high biological productivity which results from the upwelling of water (from depths of some 90 to 160 m, 150 km offshore) into the inshore surface layers, a process which introduces water containing *ca.* 0·45 μ ga/l of inorganic phosphate-phosphorus and *ca.* 6 μ ga/l of inorganic nitrate-nitrogen into the euphotic zone, where these nutrients sustain the photosynthetic production of organic matter. This transport has been estimated to result in an average net production of 0·14 grams of organic carbon per m^2 per day in a region extending 150 km offshore.

A study of the Gulf of Cariaco shows that it, too, is a region of upwelling and relatively high biological productivity. The waters in the Gulf at depths greater than the sill depth are sufficiently colder and denser than the overlying waters that they do not exchange and have become stagnant. They contain no oxygen and have large concentrations of sulphides, phosphates and silicates. A consideration of the distribution of temperature outside the Gulf indicates the possibility that this deep water may be replaced in February, either annually or intermittently.

Acknowledgments—The author wishes to acknowledge the shipboard help of the Captain, ship's company, and scientific party of the R. V. *Atlantis* during her cruise to the Caribbean in the latter months of 1958. Particular thanks are due to Mr. L. A. E. DOE, Drs. JOHN ZIEGLER, HERBERT CURL, Jr., PEDRO ROA MORALES and FRANCISCO MAGO LECCIA. The advice and criticism of his colleagues at Woods Hole Oceanographic Institution was, as usual, invaluable. Part of the work was supported by the Office of Naval Research, Contract Nonr 2196 (00) NR 083-004 with the Woods Hole Oceanographic Institution. Stenographic, editorial, and drafting assistance at the Department of Oceanography of the University of Washington are also gratefully acknowledged.

Woods Hole Oceanographic Institution,
Woods Hole, Mass.

Contribution No. 1100 *from the*
Woods Hole Oceanographic Institution.

REFERENCES

BÖHNECKE, G. (1936) Atlas : Temperatur, Salzegehalt und Dichte an der Oberfläche des Atlantischen Ozeans. *Deutsche Atlantische Exped. Meteor*, 1925–27, *Wiss. Erg.*, **5** Atlas, vii + 76 pp.

BROOKS, E. M. (1939) Transport and convergence of the North Atlantic drift current computed from the average January pressure distribution. *J. Mar. Res.*, **2** (2), 163–167.

CONSEIL Permanent International pour l'Exploration de la mer (1934) *Bulletin Hydrographique* pour l'année 1933, p. 41.

CURL, H. Jr. (1960) Primary production measurements in the north coastal waters of South America. *Deep-Sea Res.* **7**, 183–189.

FLEMING, R. H. (1940) The composition of plankton and units for reporting populations and production. *Sixth Pacific Sci. Congr., Calif.*, 1939, *Proc.*, **3**, 535–540.

HELLAND-HANSEN, BJØRN (1916) Nogen hydrografiske metoder. 16 *Skand. Naturforsker möte*, Kristiania (Oslo) 1916.

ISELIN, C. O'D. (1936) A study of the circulation of the North Atlantic Ocean. *Pap. Phys. Oceanogr. Meteorol.*, **4**, (4) 1–101.

METCALF, W. G. (1959) Oceanographic data from the Caribbean Sea *Crawford* Cruise 17, February–March 1958 for the International Geophysical Year of 1957–1958. Woods Hole Oceanographic Institution, Woods Hole, Mass. Reference No. 59–9. (Unpublished manuscript).

MONTGOMERY, R. B. (1936) On the momentum transfer at the sea surface. III. Transport of surface water due to the wind system over the North Atlantic. *Pap. Phys. Oceanogr. Meteorol.*, **4** (3), 23–30.

PARR, A. E. (1937a) A contribution to the hydrography of the Caribbean and Cayman Seas, based upon the observations made by the Research Ship *Atlantis* 1933–1934. *Bull. Bingham Oceanogr. Coll.*, **5** (4), 1–110.

Parr, A. E. (1937b) On the longitudinal variations in the dynamic elevation of the surface of the Caribbean Current. *Bull. Bingham Oceanogr. Coll.*, **6** (2), 1–20.

Parr, A. E. (1938) Further observations on the hydrography of the eastern Caribbean and adjacent Atlantic waters. *Bull. Bingham Oceanogr. Coll.*, **6** (4), 1–29.

Rakestraw, N. W. and Smith, H. P. (1937) A contribution to the chemistry of the Caribbean and Cayman Seas. *Bull. Bingham Oceanogr. Coll.*, **6** (1), 1–41.

Richards, F. A. (1957) Oxygen in the Ocean. *Geol. Soc. Amer. Mem.* **67**, v. 1, 185–238.

Richards, F. A. (1958) Dissolved silicate and related properties of some western North Atlantic and Caribbean waters. *J. Mar. Res.* (in press).

Richards, F. A. and Benson, Bruce B. (1960) Nitrogen/argon and nitrogen isotope ratios in two anaerobic environments, the Cariaco Trench in the Caribbean Sea and Dramsfjørd, Norway. *Deep-Sea Res.* (in press).

Richards, F. A. and Vaccaro, R. F. (1956) The Cariaco Trench, an anaerobic basin in the Caribbean Sea. *Deep-Sea Res.*, **3**, 214–228.

Ryther, J. H. and Yentsch, C. S. (1957) The estimation of phytoplankton production in the ocean from chlorophyll and light data. *Limnology and Oceanography*, **2** (3), 281–286.

Seiwell, H. R. (1938) Application of the distribution of oxygen to the physical oceanography of the Caribbean Sea region. *Pap. Phys. Oceanogr. Meteorol.*, **6** (1), 1–60.

Sverdrup, H. U., Johnson, M. W. and Fleming, R. H. (1946) *The Oceans.* Prentice-Hall Inc., New York, x + 1087 pp.

Van Andel, Tj. H. and Postma, H. (1954) Recent sediments of the Gulf of Paria. *Verh. der Koninklijke Nederlandse Akad. van Wetensch.*, Afd. Natuurkunde, Eerste Reeks, **20** (5), 244 pp.

Worthington, L. V. (1955) A new theory of Caribbean bottom-water formation. *Deep-Sea Res.*, **3** (1), 82–87.

Worthington, L. V. (1956) The temperature increase in Caribbean deep water since 1933. *Deep-Sea Res.*, **3** (3), 234–235.

Printed in Great Britain by The Salisbury Press Ltd., Publicity House, Wilton Road, Salisbury, Wilts. (25950)

Contribution No. 1101

Deep-Sea Research, 1960, Vol. 7, pp. 190 to 200. Pergamon Press Ltd., London. Printed in Great Britain

A note on water movement in the Greenland–Norwegian Sea

WILLIAM G. METCALF

(*Received* 28 *September* 1959)

Abstract—The oceanography of the Greenland–Norwegian Sea which was described by Norwegian oceanographers in the early part of the present century is reviewed in the light of recent winter data.

The dynamic topography and two-hundred metre temperatures indicate a circulation generally similar to that given in the earlier descriptions except that the cyclonic movement in the Norwegian Sea appears to be further west and the Norwegian Current appears to be much broader than it was previously considered to be.

Deep water identical to that of the Norwegian Sea and appreciably warmer than that of the Greenland gyral core lies on at least three sides of that gyral, and it is suggested that this is the major source of Polar Basin deep-water. It is probably formed within the Norwegian gyral. Deep-water in the Greenland–Norwegian Sea may not be formed each winter but only during particularly cold seasons. Deep-water which is formed within the Greenland gyral eventually loses its cold identity through gradual mixing with the surrounding water from the Norwegian gyral.

A temperature–depth diagram demonstrates two distinct types of intermediate and deep-water as well as two groups of stations showing some of the charateristics of each type within a single water column. Bottom topography is believed to play a significant role in the distribution of this type of station.

Further field studies, especially in the western part of the Greenland Sea, are needed to fill the large gaps in our knowledge of the circulation pattern.

INTRODUCTION

THE oceanography of the area between Norway and Greenland was the object of intensive study during the early part of the present century resulting in very thorough descriptions especially by NANSEN (1906) and HELLAND-HANSEN and NANSEN (1909). A great part of our knowledge today of this region is the result of the work of these investigators. The present paper is based upon winter oceanographic data gathered from 1951 to 1955, inclusive, which may clarify and modify some of the earlier work.

The geographical terminology of the region has undergone numerous changes in the past fifty years, and it is felt that in order to reduce the confusion as much as possible, the terms used in this paper should be defined. The region as a whole (FIG. 1) bounded on the north by the passage between Svalbard and Greenland and on the south by the Greenland–Iceland–Faroe–Shetland Ridge, is referred to as the Greenland–Norwegian Sea.* The portion of the area north of Jan Mayen Island and of the East and West Jan Mayen Ridges, is termed the Greenland Sea; that to the south the Norwegian Sea. The Norwegian Sea is divided by the Iceland–Jan Mayen Ridge into the Norwegian Basin on the east and the Iceland Basin on the west. Similarly, the Greenland Sea is divided by the North Jan Mayen Ridge into the large Greenland Basin occupying most of that sea and the smaller Jan Mayen Basin in the south-west corner. The eastern boundary of the Greenland–Norwegian Sea is Norway, the shallow Barents Sea and Svalbard. Greenland forms the entire western side.

---

* FIG. 1 shows an east–west ridge, the Nansen Ridge, extending between Svalbard and Greenland, and this was formerly considered to be the northern boundary of the region under discussion. However recent evidence reveals a relatively deep passage through this supposed ridge thus forming a connection between the Greenland–Norwegian Sea and the Polar Basin at depths as great as 3000 or 3500 m (BALAKSHIN, 1959).

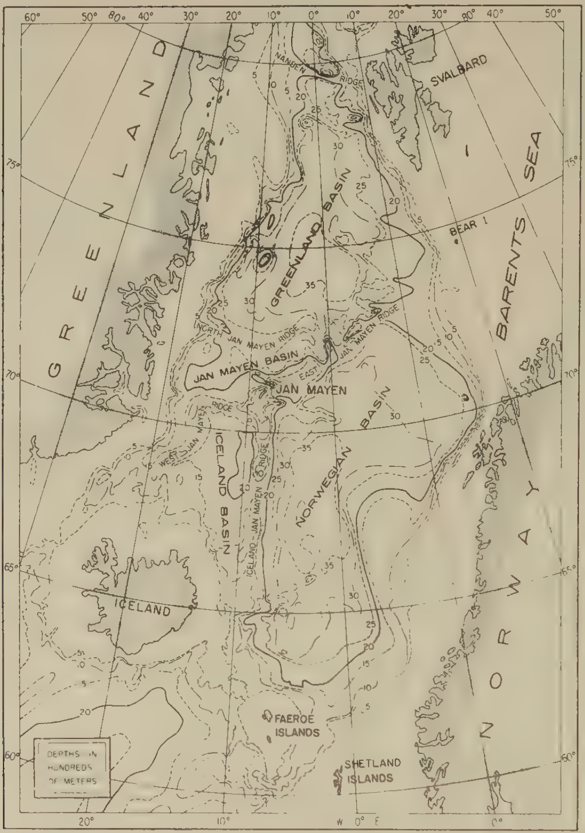
GREENLAND
SVALBARD
BARENTS SEA
BEAR I
NANSEN RIDGE
GREENLAND BASIN
NORTH JAN MAYEN RIDGE
JAN MAYEN BASIN
EAST JAN MAYEN RIDGE
JAN MAYEN
NORWEGIAN BASIN
WEST JAN MAYEN RIDGE
ICELAND BASIN
ICELAND - JAN MAYEN RIDGE
ICELAND
FAEROE ISLANDS
SHETLAND ISLANDS
NORWAY
DEPTHS IN HUNDREDS OF METERS
60°
50°
40°
30°
20°
10°
0°
75°
70°
65°
60°
W 0° E

Fig. 1. Bathymetry of the Greenland–Norwegian Sea (after Stocks 1950).
Note : The existence of a channel with depths of 3000 m or greater extending north–south through the Nansen Ridge has recently been described (Belakshin, 1959 and Laktionov, 1959).

CIRCULATION

Helland-Hansen and Nansen (1909) described the circulation of the Greenland–Norwegian Sea as being composed of two major cyclonic gyrals, one in the Norwegian Sea and one in the Greenland Sea, together with a number of smaller permanent, semi-permanent and transitory vortices. In addition, they described the warm north-flowing Norwegian Current on the east, the cold south-flowing East Greenland Polar Current on the west, and several smaller currents. Their schematic representation of this circulation is well known and has been generally accepted as being reasonably accurate (Fig. 2).

The purpose of the present paper is to discuss some of the recent winter oceanographic observations made in this region between 1951 and 1955 inclusive and to compare the recent results with the earlier work. The recent material substantiates to a considerable degree the earlier conclusions and emphasizes a rather out-standing separation between the two major cyclonic movements. For convenience, the southern cyclonic circulation will be called the Norwegian gyral and the northern one the Greenland gyral.

FIG. 3 represents the dynamic topography of the area as determined by the dynamic height anomalies based on the 1500 decibar surface. This level was chosen simply because of the availability of the data to that depth. Many of the hydrographic stations did not extend deeper. Approximately sixty stations were used in the calculations. These scattered over an area the size of the Greenland–Norwegian Sea can, of course, give little more than a hint of the situation, and undoubtedly the contours could have been drawn in many different ways. The observations were gathered in connection with five different cruises in four different winters, and it is to be expected that certain irregularities would appear due to annual variations in current positions from year to year and unavoidable inaccuracies in navigation. Therefore, in drawing the contours for FIG. 3, a small amount of smoothing of the lines and averaging of

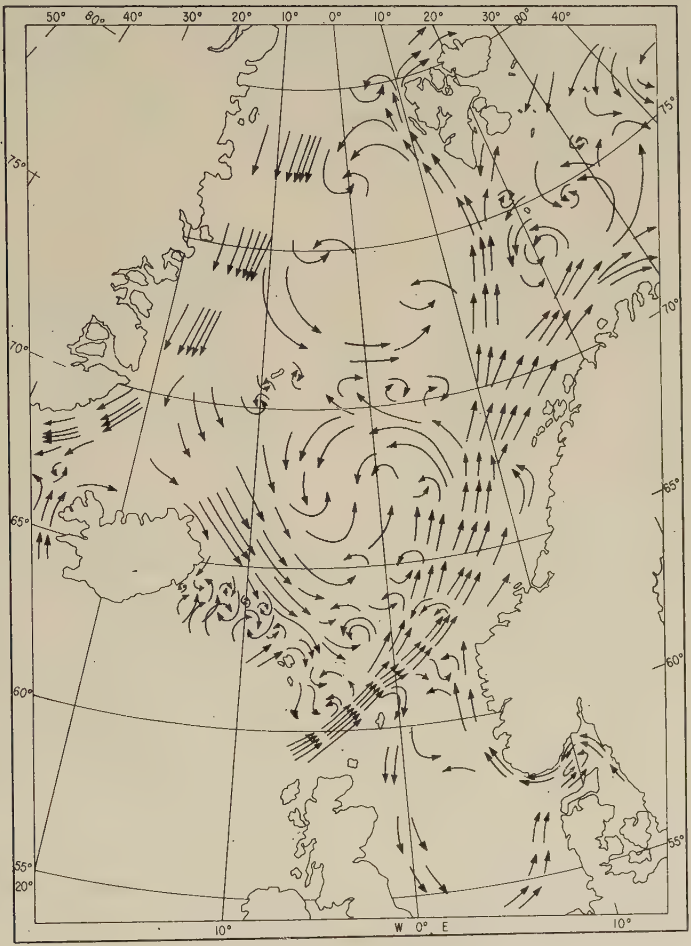

FIG. 2. Surface currents of the Greenland–Norwegian Sea (after HELLAND-HANSEN and NANSEN, 1909).

the data was carried out in order to produce what is felt to be a picture of average conditions.

In a comparison between the HELLAND-HANSEN and NANSEN interpretation and the present one, a difference in the position of the Norwegian gyral is apparent. In the earlier chart, it was shown centred on a line running approximately between the Faroe Islands and southern Svalbard; the more recent data indicate that it lies considerably west of that position, centred on a line extending between Iceland and Jan Mayen Island. The north-flowing Norwegian current is shown to be very much broader than previously described. The Norwegian gyral is thus restricted for the most part to the Iceland Basin, extending only slightly east of the Iceland–Jan Mayen Ridge into the Norwegian Basin. The many small vortices and vagaries of the currents shown throughout the region in the HELLAND–HANSEN and NANSEN chart do not appear in the present one. The averaging of the data for several years smooths out this type of current structure. However it is likely that many such smaller currents and eddies are present at any given time.

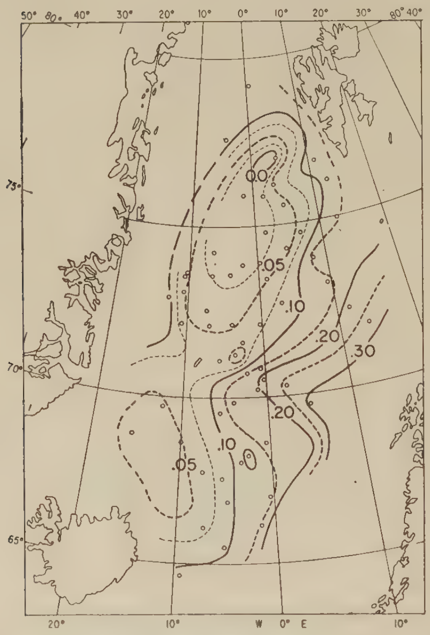

FIG. 3. Geopotential topography of the sea surface relative to the 1500 decibar surface. Composite of data from four winters, 1951–1955 inclusive.

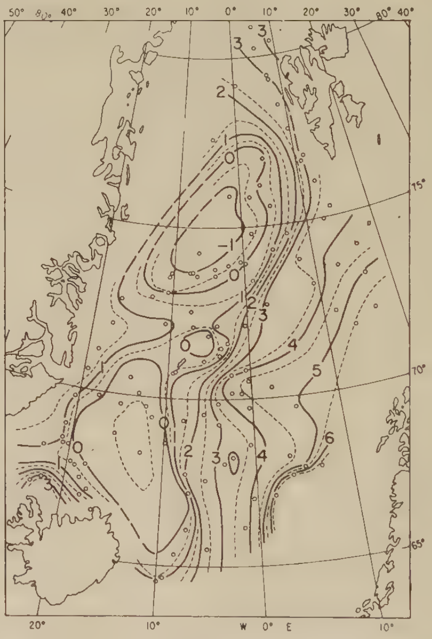

FIG. 4. Two-hundred metre temperatures of the Greenland–Norwegian Sea. Composite of data from four winters, 1951–1955 inclusive.

FUGLISTER (1954) has demonstrated that in the North Atlantic Ocean, gradients in the 200 metre temperature are associated with the average current pattern. A 200 metre temperature chart (FIG. 4) of the Greenland–Norwegian Sea based upon the recent winter data was drawn from the data of over 130 stations occupied during four different winters. As was the case in connection with the previous figure, certain inconsistencies were found due to the non-synoptic character of the data. Again, a small amount of averaging of the data and smoothing of the contours was carried out to produce what is considered to be an average picture. The 200 metre temperature contours as well as the dynamic topography emphasize the position of the Norwegian gyral in the western half of the Norwegian Sea and a very broad Norwegian Current extending over the whole eastern half of that sea.

The East Jan Mayen Ridge is shown by STOCKS (1950) to rise to within about 600 metres of the sea surface in some places. Depths of greater than 2000 metres are shown in a narrow passage between two high peaks, and at the eastern end of the ridge the depths are between 1500 and 2000 metres. As the Norwegian Current approaches this ridge, some of the water it carries is diverted to the west as part of the Norwegian gyral while the rest flows northeast. This latter portion then flows around the eastern side of the Greenland gyral, and some of the water from the upper levels enters the Polar Basin slightly below the sea surface between Greenland and Svalbard. The remaining portion appears to continue in a cyclonic direction as the outer margin of the Greenland gyral.

Table 1. Two stations in the cold core of the Greenland gyral including the coldest one in the present data.

Station No. 38. 18 *March* 1955. 75° 52′ *N.*, 01° 46′ *W. Depth* 3840 *m.*

Depth (m)	*Temp.* (°C)	*Salinity* (‰)	*Oxygen* (ml/L)
1	− 1·61	34·87	8·18
45	− 1·67	34·87	8·15
90	− 1·62	34·87	8·11
181	− 1·18	34·90	7·73
370	− 1·30	34·89	7·72
565	− 1·23	34·89	7·73
878	− 1·20	34·90	7·72
1332	− 1·08	34·91	7·42
1794	− 1·06	34·92	7·47
2265	− 1.06	34·91	7·39
2745	− 1·06	34·91	7·43
3241	− 1·06	34·90	7·39
Station No. 39. 18 *March* 1955. 74° 15′ *N.*, 06° 38′ *W. Depth* 3330 *m.*			
1	− 1·58	34·87	8·17
48	− 1·64	34·86	7·91
96	− 1·59	34·86	7·85
194	− 1·00	34·91	8·00
392	− 1·13	34·90	7·56
596	− 1·24	34·90	7·61
799	− 0·95	34·92	7·63
1269	− 1·09	34·92	7·60
1759	− 1·06	34·92	7·39
2252	− 1·06	34·91	7·56
2747	− 1·07	34·92	7·75
3243	− 1·05	34·95	7·41

THE DEEP-WATER

The term deep-water is used here to indicate water below 1500 metres where the temperature and salinity are relatively constant. In the recent data, the deep-water in the core of the Greenland gyral is shown to be − 1·00° or colder with a single exception (− 0·99°). That of the Norwegian sea is − 0·97° or warmer without exception (Tables 1 and 2). However, this less cold deep-water is also found on the east, north and northwest borders of the Greenland gyral (Table 3). Whether or not it is present along the west side has not been determined due to ice conditions which precluded field work on that side, but conditions along the southwest side of the gyral suggest that it is. It thus appears that deep-water from the Norwegian Sea is carried by the Norwegian Current either through a gap in the East Jan Mayen Ridge or around the end of that ridge, or more likely both, and takes a position around the edges of the cyclonic eddy in the Greenland Sea.

Table 2. Two typical Norwegian Sea stations.

Station No. 25. 10 *February* 1954. 65° 33′ *N*., 05° 18′ *W*. *Depth* 2743 *m*.

Depth (m)	*Temp.* (°C)	*Salinity* (‰)	*Oxygen* (ml/L)
1	2·71	34·90	7·69
10	2·70	34·89	7·72
30	2·69	34·98	7·74
50	2·68	34·88	7·65
100	2·79	34·90	7·69
200	2·37	35·04	7·49
396	0·83	34·96	7·43
792	−0·51	34·92	7·36
1188	−0·78	34·91	7·09
1585	−0·95	34·92	7·16
1980	−0·93	34·92	7·15
2475	−0·93	34·95	7·13
Station No. 5. 5 *March* 1955. 69° 15′ *N*., 13° 00′ *E*. *Depth* 2926 *m*.			
1	5·95	35·03	6·79
40	6·07	35·15	6·70
80	—	35·15	6·74
162	6·12	35·17	6·71
332	4·91	35·09	6·81
509	2·25	34·99	6·96
627	0·66	34·94	7·06
856	−0·37	34·93	6·98
1092	−0·72	34·93	7·09
1504	−0·89	34·92	6·92
1942	−0·90	34·91	6·93
2406	−0·92	34·91	6·94

NANSEN (1906) and HELLAND-HANSEN and NANSEN (1909) have described the formation of deep-water in the Greenland–Norwegian Sea as taking place to a small extent in the Norwegian Sea but primarily in the Greenland Sea. This latter formation was described as being the source of the deep-water of the Polar Basin also. It is within the cold centre of the Greenland gyral that this formation presumably takes place. However, the deep-water of the Polar Basin was shown by NANSEN (1902), SVERDRUP (1933), SHIRSHOV (1944) and others to be − 0·91° or warmer. This temperature is characteristic of the deep layers of the Norwegion Sea and of the Norwegian Current as it comes from that sea. The entire water column within the core of the Greenland gyral is appreciably colder than this figure, and this cold water is completely cut off from the Polar Basin by the presence of warmer deep-water in the northern part of the Greenland Sea. Therefore it is suggested that it is in the Norwegian Sea not in the Greenland Sea, that the greatest amount of the deep-water of the Polar Basin is formed. The very cold deep-water formed in the Greenland Sea apparently is gradually mixed with the much greater volume of warmer deep-water from further south which is found around the periphery of the Greenland gyral thus losing its identifying characteristics of very low temperature. As the result of this mixing, some of it may eventually find its way into the Polar Basin and so make a minor contribution to the deep-water of that basin.

Table 3. *Three stations located on east the, north and northwest sides respectively of the Greenland gyral where water typical of the Norwegian Sea is found.*

Station No. 33. 14–15 *March* 1955. 76° 44′ *N.*, 11° 06′ *E. Depth* 1920 *m.*

Depth (m)	*Temp.* (0°C)	*Salinity* (‰)	*Oxygen* (ml/L)
1	3·22	34·99	7·49
38	3·45	35·06	7·36
77	3·47	35·09	7·14
159	3·22	35·09	6·74
337	3·06	35·09	6·71
534	1·35	34·99	6·34
689	—	34·94	6·68
870	– 0·42	34·93	6·52
1053	– 0·64	34·92	6·59
1242	– 0·79	34·92	6·24
1532	– 0·91	34·92	6·65
1825	– 0·96	34·92	6·75

Station No. 36. 17 *March* 1955. 79° 08′ *N.*, 00° 20′ *E. Depth* 2834 *m.*

1	– 1·59	34·33	8·13
42	– 1·54	34·35	7·95
83	2·42	34·94	7·20
168	2·61	35·02	7·18
344	2·20	35·01	7·18
531	1·51	35·01	7·18
590	—	34·93	—
740	0·08	34·92	7·17
1117	– 0·48	—	7·16
1498	– 0·71	34·93	7·11
1885	– 0·85	34·93	7·11
2119	– 0·87	34·93	7·10

Station No. 37. 17 *March* 1955. 77° 32′ *N.*, 04° 20′ *W. Depth* 1829–2926 *m.* (*deepened rapidly during station*)

1	0·21	34·60	7·16
37	0·20	34·60	7·73
76	0·62	34·66	7·17
154	1·82	34·92	7·16
324	1·67	35·01	6·71
519	0·59	34·97	7·33
581	0·40	34·96	7·37
793	– 0·29	34·93	7·27
1014	– 0·44	34·93	6·90
1402	– 0·67	34·83	7·14
1815	– 0·89	34·92	7·17
2250	– 0·96	34·92	7·16

At one station occupied by the *Nautilus* in the Polar Basin, a single observation of – 0·01° was found at 1648 metres (SVERDRUP, 1933). This observation does not fit in well with the others from the same expedition, but if it is correct, it may represent a surge of Greenland gyral water which was pushed through the warmer water normally lying north of it. Nowhere else in the Polar Basin is deep-water found which is this cold, and it is not likely that much of it actually breaks through into this basin very frequently.

There is evidence that deep-water formation in the North Atlantic Ocean is not taking place under present climatic conditions (WORTHINGTON, 1954). However, its possible formation in the Norwegian Sea as recently as 1951 has been suggested by METCALF (1955). Although the oxygen data available are not considered sufficiently accurate to shed much light on this subject, 90% oxygen saturation and above in the deep-water of the Greenland–Norwegian Sea is not uncommon indicating a certain amount of recent communication between the surface and the deep-water. Generally, the oxygen saturation is higher in the core of the Greenland gyral than elsewhere in the region indicating more activity there. It is suggested that deep-water formation, while probably not taking place each winter, does occur periodically during particularly cold winters and more frequently, though not necessarily in greater amounts, in the Greenland gyral than in the Norwegian gyral.

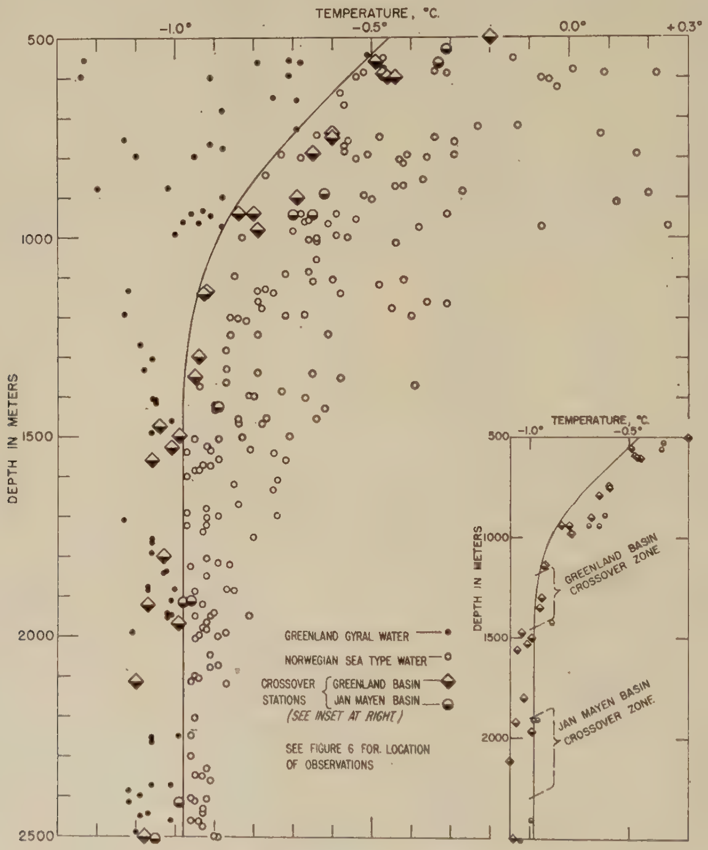

FIG. 5. Temperature vs. depth diagram.

TEMPERATURE–DEPTH RELATIONSHIP

In the intermediate water (600 to 1500 metres) and the deep-water, there is little if any distinct salinity variation geographically in the area studied. A temperature-salinity diagram showed a separation into two groups on the basis of temperature alone, the salinity in the deep-water being 34·92 – 34·93‰ with remarkably little spread throughout the entire Greenland–Norwegian Sea. For this reason, a temperature vs. depth diagram has been drawn using all observations between 500 and 2500 metres from those stations extending deeper than 1500 metres (FIG. 5).

Observations from stations in the centre of the Greenland Sea and from stations in the centre of the Norwegian Sea were plotted, and it was found that a smooth curve could be constructed separating the two groups. Below about 1450 metres, this curve becomes a straight line at — 0·98°. The water of the core of the Greenland gyral lies on the cold side of the curve throughout its length. However, observations falling on the warm side of the curve were found not only throughout the Norwegian Sea but also around the periphery of the Greenland gyral on the east, north and northwest sides, as would be expected from the earlier discussion of the circulation (FIG. 6).

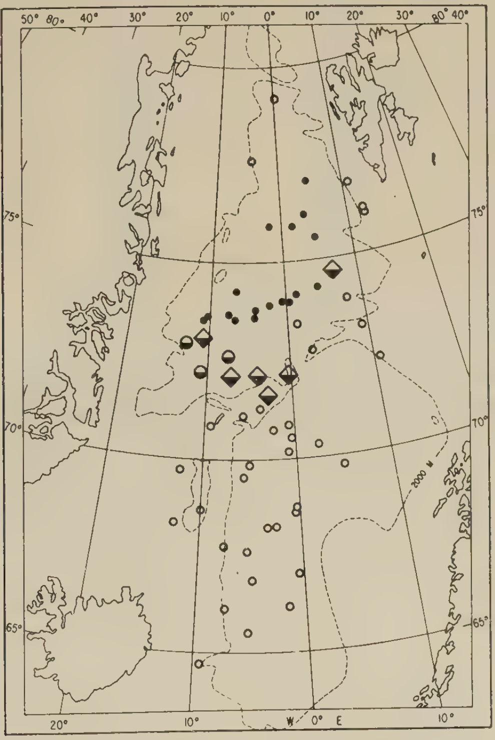

FIG. 6. Location of stations used in construction of FIG. 5.

Not all the stations occupied throughout the region fall readily on one side or the other of the curve throughout its length. Out of the 62 stations represented in FIGS. 5 and 6, nine showed a cross-over from the warmside of the curve in the upper levels to the cold side in the deeper levels, indicating that they represent conditions intermediate between the two main classes. All of these ‘cross-over’ stations, as they have been termed, are found along the southwest, south and southeast margins of the Greenland Sea. They all show water in the upper levels with Norwegian Sea characteristics and water in the deeper levels with Greenland gyral characteristics.

In eight of the nine cases, a well defined submarine ridge lies a short distance upstream of the stations which suggests that the height of the ridge may determine the depth in the water column at which the cross-over takes place by affecting the flow of the deep-water.

Table 4. A station exhibiting Norwegian Sea intermediate water lying over Greenland gyral deep water.

Station No. 43. 19 *February* 1954. 72° 05′ *N.*, 04° 00′ *W. Depth* 2441 *m.*

Depth (m)	*Temp.* (°C)	*Salinity* (‰)	*Oxygen* (ml/L)
1	− 1·70	34·50	8·63
20	− 1·61	34·54	—
40	− 1·66	34·53	8·65
60	− 0·98	34·62	—
80	0·87	—	7·57
100	1·36	34·96	—
123	1·41	34·96	7·01
148	1·37	34·96	—
173	1·22	34·99	7·44
197	1·10	34·98	—
247	0·95	34·97	7·28
296	0·64	34·99	—
323	0·48	—	7·21
371	0·29	34·95	7·27
749	− 0·60	34·97	7·17
1134	− 0·92	34·92	6·37
cross-over 1526	− 1·01	34·98	6·98
(see text) 2114	− 1·10	34·97	6·78

Table 5. A Jan Mayen Basin station exhibiting a cross-over within the deep water from Norwegian Sea type to Greenland gyral type.

Station No. 42. 19 *February*, 1954. 72° 32′*N*, 07° 34′W. *Depth* 2743 *m.*

Depth (m)	*Temp.* (°C)	*Salinity* (‰)	*Oxygen* (ml/L)
1	− 1·73	34·73	8·10
20	− 1·76	34·69	8·33
51	− 1·76	34·70	8·35
101	− 0·17	34·83	8·26
152	0·99	34·98	8·39
202	—	35·01	8·51
372	0·19	34·97	8·14
563	− 0·33	34·96	7·91
941	− 0·70	34·94	7·94
1424	—	34·95	7·91
1912	− 0·96	34·95	7·37
cross-over 2509 (see text)	− 1·05	34·92	7·06

Those five stations (FIG. 6) which lie along the south and southeast margins of the Greenland Sea just downstream from the East Jan Mayen Ridge, show cross-overs in the intermediate water between 1200 and 1450 metres (FIG. 5 inset; Table 4). This is approximately the depth of the East Jan Mayen Ridge as shown by STOCKS (1950).

The three stations (Table 5) in the Jan Meyan Basin exhibit cross-overs in the deep water between 1900 and 2300 metres (Fig. 5 inset). The sill depth of the North Jan Mayen Ridge upstream from these stations is very imperfectly known, but the figures 1900 to 2300 are not unreasonable. The Jan Mayen Basin is open at the east end to the Greenland Basin at great depth and is filled below the depth of the cross-over with typical Greenland gyral deep-water.

The remaining cross-over station, lying north of the Jan Mayen Basin, shows a cross-over at 1450 metres. Paucity of topographical data makes the relationship, if any, between the bottom topography and the cross-over depth impossible to determine. When further survey work is carried out in this area, it will be interesting to discover whether there is a submarine ridge or mount upstream from this position. A better knowledge of the bathymetry and more oceanographic field data than are now available is required before this can be resolved. Accurate navigational data is especially important in this type of oceanographic problem. Unfortunately it is also especially difficult in this region.

Acknowledgment—This work was sponsored by the Office of Naval Research under Contract N6onr–27701 and is based on data taken on board U.S. Navy ships.

Woods Hole Oceanographic Institution
Woods Hole, Mass.

Woods Hole Oceanographic Institution Contribution No. 1101.

REFERENCES

Balakshin, L. L. (1959) The water circulation and bottom contour of the northern part of the Greenland Sea. *Reprints of Papers Int. Oceanogr. Congress.* 31 Aug. – 12 Sept. 1959. *Amer. Assoc. Adv. Sci.*, 430–431.

Fuglister, F. C. (1954) Average temperature and salinity at a depth of 200 metres in the North Atlantic. *Tellus.* **6**, (1) 46–58.

Helland-Hansen, B. and F. Nansen (1909) The Norwegian Sea. *Report Norwegian Fish. Mar. Invest.* **2**, (1) (2), 390 pp.

Laktionov, A. F. (1959) Bottom topography of the Greenland Sea in the region of Nansen's sill. *Piroda*, **10**, 95–97, (In Russian).

Metcalf, William G. (1955) On the formation of bottom water in the Norwegian Basin. *Trans. Amer. Geophys. Union*, **36**, (4), 596–600.

Nansen, Fridtjof (1902) The oceanography of the North Polar Basin. *Norwegian N. Polar Exped.* 1893–96, *Sci. Results*, **3**, (9) 127 pp.

———— (1906) Northern waters. *Vid. Selskabets Skrifter*, **1**. Math.-Naturv. Klasse, (3) 145 pp.

Shirshov, Petr P. (1944) Scientific results of the drift station North Pole. *Akad. Nauk. SSSR. Obshchee sobranie.* Feb. 1944. Trans. by the Amer. Met. Soc.

Stocks, Theodor (1950) Die Tiefenverhältnisse des Europäischen Nordmeers. *Deutsche Hydrograph. Zeits.*, **3**, (1/2), 93–100.

Sverdrup, H. U. (1933) Scientific results of the *Nautilus* expedition, 1931, Part 2. *Pap. Phys. Oceanogr. Meterorol.*, **2**, (1), 63 pp.

Worthington, L. V. (1954) A preliminary note on the time scale in North Atlantic circulation. *Deep-Sea Res.* **1**, 543–551.

Printed in Great Britain by The Salisbury Press Ltd., Publicity House, Wilton Road, Salisbury Wilts. (25952)

Contribution No. 1102

Deep-Sea Research, 1960, Vol. 7, pp. 183 to 189. Pergamon Press Ltd., London. Printed in Great Britain

Primary production measurements in the north coastal waters of South America

HERBERT CURL, JR.

(*Received* 16 *December* 1959)

Abstract—Measurements of surface light intensity, water transparency and concentration of chlorophyll *a* were made in the northern coastal waters of South America during October and November 1958. Phytoplankton collections were made simultaneously. The highest gross production rates were encountered in the Gulf of Cariaco (3·75 g C/m^2/day), over the Cariaco Trench (2·30 g C/m^2/day), in Lake Maracaibo (1·23 g C/m^2/day) and the Gulf of Venezuela (1·20 g C/m^2/day). Upwelling appears to be the source of nutrients for production in the Gulfs of Cariaco and Venezuela. This relationship is less well established over the Cariaco Trench. High silt concentrations limit light for photosynthetic production in the Gulf of Darien, at the mouth of the Magdalena River and to the east of Margarita Island. Phytoplankton reduces materially the light available for photosynthesis in Lake Maracaibo.

INTRODUCTION

THE MEASUREMENT of primary production rates may be used to confirm our understanding of physical, chemical and biological phenomena, to delimit areas where observations on such phenomena should be undertaken and to complement marine deposition studies. Such measurements are interesting in their own right since they indicate the base on which successively higher trophic levels may build.

In the region being considered there has been only one estimation of primary production (RYTHER, *vide infra*), using the C^{14} method. However, many indications of very high productivity (flocks of fish-eating birds, large catches of ' herring ' by hand seining in the Gulf of Cariaco, sightings of schools of scombrids, etc). are present in a number of localities on the northern coast.

The present data were obtained on Cruise 246 of the R. V. *Atlantis* during October through November, 1958 from Trinidad, B. W. I. to the Gulf of Darien, Columbia. This coast line and its geography have been described extremely well by MURPHY (1936).

For our purpose it is sufficient to divide the coastal waters (FIG. 1) into four separate regions :

(1) Trinidad to the Paraguana Peninsula, including the Gulf of Cariaco and the Cariaco Trench, under the influence of the Equatorial Current flowing from east to west and the Northeast Tradewinds.

(2) Lake Maracaibo, which is fed by orographic rainfall to the south and flushes very slowly, and the Gulf of Venezuela with upwelling taking place on its eastern side.

(3) The region from the Goajira Peninsula to the mouth of the Magdalena River, which is poorly known. Water from the Magdalena River appears to flow northeast toward the Goajira Peninsula in accordance with the Coriolis principle and thence northwestward.

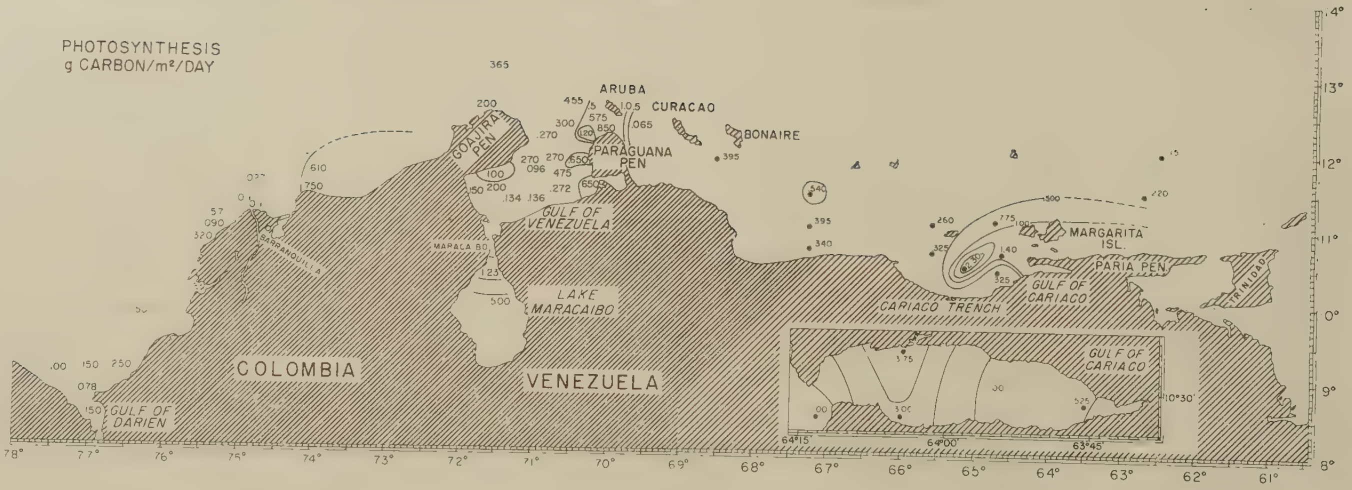
PHOTOSYNTHESIS
g CARBON/m²/DAY
ARUBA
CURACAO
BONAIRE
GOAJIRA PEN
PARAGUANA PEN
GULF OF VENEZUELA
MARACAIBO
LAKE MARACAIBO
BARRANQUILLA
COLOMBIA
VENEZUELA
GULF OF DARIEN
CARIACO TRENCH
GULF OF CARIACO
MARGARITA ISL.
PARIA PEN
TRINIDAD
78°
77°
76°
75°
74°
73°
72°
71°
70°
69°
68°
67°
66°
65°
64°
63°
62°
61°
8°
9°
10°
11°
12°
13°
14°
64°15'
64°00'
63°45'
10°30'
365
200
455
575
850
120
300
.270
270
270
096
650
475
.272
650
100
150
200
.134
.136
1.05
.065
395
540
395
340
260
325
775
100
500
140
325
220
15
123
500
610
750
57
090
320
.00
150
250
078
150
375
300
525
00

Fig. 1. Primary production between Trinidad, B.W.I. and Gulf of Darien, Columbia, expressed as *g* Carbon/m²/day.

(4) The Gulf of Darien region, which is probably the centre of an eddy and is even less well known than the preceding region.

Discussions of the hydrography of one or more of the regions may be found in Parr (1937), Rakestraw and Smith (1937), Dietrich (1939), Redfield and Ketchum (1953), Redfield (1955), Redfield, Ketchum and Bumpus (1955), Worthington (1955, 1956) and Richards (1960).

METHODS

Plankton tows and water samples for chlorophyll *a* analysis were taken in conjunction with hydrographic and geological observations. Tows were made with nets of number 10 nylon and preserved in neutralized ten per cent formalin. Aliquots have been analyzed for chemical composition and will be reported elsewhere. Water samples were taken with samplers coated with a non-toxic, non-dissolving plastic.

One or more litres of water were filtered through HA ' Millipore ' membrane filters and the filters stored in a refrigerated dessicator. Chlorophyll *a* determinations were made on the filtered material ashore according to the method of Creitz and Richards (1955). Light intensity measurements were made with a General Electric exposure meter and light penetration measurements were made with a Secchi disc. Average light values were taken from Kimball's (1928) tables.

Phytoplankton production estimates were made according to the method of Ryther and Yentsch (1957) using chlorophyll and light data. As pointed out by these authors the method measures ' average ' production. Criticism of the method centres about interpreting variation in the coefficient of light saturated photosynthesis to chlorophyll (Verduin, 1959). The interpretations of the present data assume that variations in the chlorophyll-photosynthesis ratio are real and not due to experimental error, and that such variations differ from the mean by a factor of two or less while the measured parameters may vary by more than an order of magnitude.

Table 1. *Total Chlorophyll* a *in the euphotic zone and depth of the euphotic zone by stations. Refer to* Richards (1960, Fig. 1) *for geographic locations of stations. Euphotic depth is the depth to which one per cent of the surface light penetrates as calculated from* Secchi *disc measurements.*

Station	*Euphotic depth* (m)	*Chl.* a mg/m^2	*Station*	*Euphotic depth* (m)	*Chl.* a mg/m^2
5661	43	10·3	5722	9	7·9
5664	43	8·0	5725	12	7·6
5667	31	38·0	5726	25	20·0
5678	25	24·0	5727	25	29·0
5683	54	20·0	5732	10	170·0
5684	50	230·0	5733	85	18·0
5686	56	21·0	5735	15	12·0
5687	43	15·3	5736	85	34·0
5697	37	6·3	5740	3	1·0
5698	36	40·0	5741	3	0·9
5699	36	37·0	5742	10	2.0
5700	62	63·0	5743	54	4·0
5701	50	15·0	5750	35	6·0
5704	52	33·0	5751	22	4·0
5710	34	19·0	5752	10	9·0
5715	27	13·5			

RESULTS

The euphotic depths varied from 30 metres in the Gulf of Cariaco and to the west of Margarita Island to 85 metres in the vicinity of Curaçao (Table 1). The contours of the isopleths suggest a westward movement of the surface water, with decreasing turbidity to the west. The shallow light penetration at the mouth of the Gulf of Cariaco was accompanied by a high standing crop of phytoplankton (200×10^3 cells per litre). The shallow light penetration between Margarita Island and Tortuga Island was obviously due to silt but whether of local origin or from mixing with Orinoco River water is not certain. Vertical mixing was impeded by the large vertical thermal gradient but relatively low salinities indicated some admixture of coastal water (Richards, 1960).

Calculated phostosynthetic rates in this area (Fig. 1) ranged from a low of 0·115 g C/m^2/day to the west of Grenada to 3·75 g C/m^2/day on the north shore of the Gulf of Cariaco. The second highest production rate occurred over the south central portion of the Cariaco Trench (2·30 g C/m^2/day). The configuration of the isopleths form a tongue extending from Margarita southwestward to over the trench.

Light penetrates the least in northern Lake Maracaibo as a result of high standing crops of phytoplankton ($1{\cdot}5 \times 10^6$ cells per litre) and in the southern portion of the Gulf of Venezuela as a result of silt suspension. The deepest light penetration occurs on the eastern side of the Gulf. Relatively high photosynthetic rates were found in the eastern portion of the Gulf of Venezuela and in the vicinity of Aruba. The highest rates were found in the northern end of Lake Maracaibo (1·23 g C/m^2/day) and off the Paraguana Peninsula (1·20 g C/m^2/day) (Fig. 1). In this region the lowest rates of production were associated with the most turbid water.

Both the transparency and the production from the western waters are a reflection of the Magdalena River flow, which was beginning to increase in November. The lowest transparency and production rates along the entire coast were found at the mouth of the Magdalena River. The euphotic depth isopleths are crowded to the west of the river mouth and expanded to the east, suggesting an eastward flow of the surface waters. The production isopleths indicate low rates to the west in clear water, and relatively high rates (0·750 g C/m^2/day) in equally clear water to the east presumably as a result of admixture with nutrient rich river water.

The last region shows no unusual features and appears to be relatively unproductive (*ca.* 0·150 g C/m^2/day).

For comparison with other areas, Steemann Nielsen (1959) gives a typical primary production rate of 0·050 g C/m^2/day in the centre of tropical anticyclonic eddies and a rate of 0·50 g C/m^2/day in other parts of the tropical oceans. On the continental shelf area off New York, Ryther and Yentsch (1958) found between 0·10 and 0·60 g C/m^2/day fixation as monthly averages, with extremes values of zero and 2·8 g C/m^2/day.

DISCUSSION

It has been shown that there are at least four areas of high basic productivity on the northern coast of South America. The high productivity over the Gulf of Cariaco is probably due partly to upwelling (Richards, 1960) and partly to nutrient supply in surface coastal waters. Upwelling is strong to the east of Margarita but the turbidity of the water prevents any substantial photosynthesis until some of the suspended matter has an opportunity to settle out in the still waters over the trench. Unpublished work by D. S. Shonting (Fig. 2) in 1957 shows the magnitude of this phenomenon. Using a white light source and a photomultiplier photometer, Shonting measured the 90 scattering by particles at four stations. His figures show the distribution of light scattering particles in the Cariaco Trench. Apparently one third of the original sediment load settles out in the shallow eastern basin and another third settles out in the central basin.

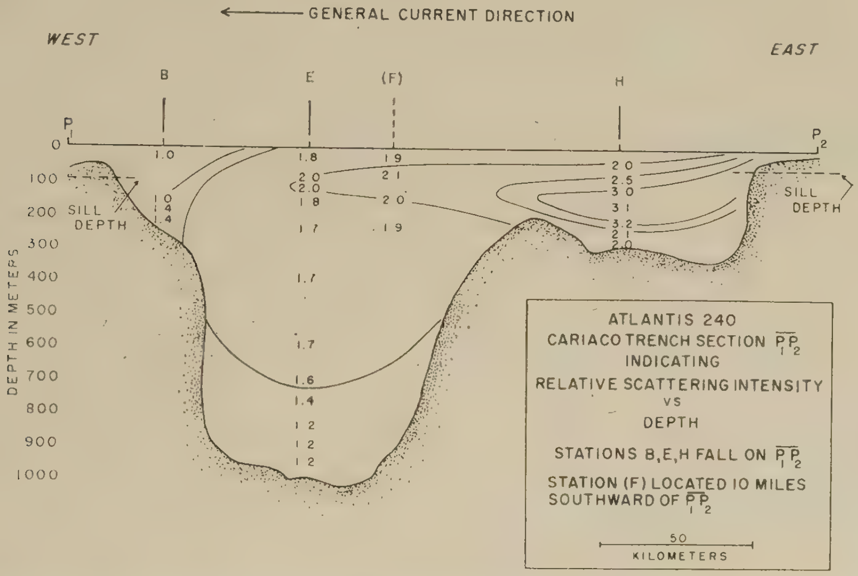

FIG. 2. Intensity of relative scattering (90°) by white light in the Cariaco Trench plotted against depth. (From unpublished data of D. S. SHONTING).

According to data presented by RICHARDS in a comparison of high and low salinity surface water in the Cariaco Trench region, there was virtually no difference in dissolved phosphorus but considerably higher silicate and lower nitrate in the low salinity water. The low salinity water has much higher concentrations of organic phosphorus and total phosphorus indicating that it is a potentially richer source of these nutrients but that they have been used up in producing organic matter. RICHARDS estimated the amount of net production taking place in a north-south section in the eastern Cariaco Trench region from upwelling rates deduced by BROOKS (1939) and the north-south differences in phosphate–phosphorus concentrations. The computed rate of net production was 0·14 g C/m^2/day. In the same area RYTHER (cited in part in RICHARDS and VACCARO (1956) and in part unpublished), using the C^{14} method made productivity measurements in 1955 ranging from 0·27 to 0·48 g C/m^2/day, (Table 2).

The C^{14} measurements, under an assumed nutrient sufficiency, represent net photosynthesis, whereas the chlorophyll-light estimates represent gross photosynthesis. The ratio of net to gross photosynthesis is in the vicinity of 0·9 in a normal population in the logarithmic growth phase. This may reduce to zero if the population is making no net growth whatsoever (RYTHER and YENTSCH, 1958; KETCHUM *et al.*, 1958). A ratio of 0·1 over the central basin of the trench suggests that the observation was made at the end of a plankton bloom, inasmuch as the phytoplankton standing crop was large.

The waters flowing over the Cariaco Trench from east to west become clearer and less productive. The trench itself is thus an ideal location as a trap for organic material formed in its proximity.

In the Gulf of Cariaco RICHARDS (1960) has made a strong case for upwelling at the eastern end. The surface water flows westward half the length of the Gulf before maximum rates of production are achieved.

Table 2. Comparison of primary productivity measurements in the eastern surface waters of the Cariaco Trench by three methods : C^{14} (*net*), *phosphate-phosphorus depletion* (*net*) *and chlorophyll-light* (*gross*).

Location	RYTHER (1955) C^{14} (net)	RICHARDS (1958) PO_4–P *depletion* (*net*) g C/m²/day	CURL (1959) *Chlorophyll a-light* (*gross*)
Caribbean	0·27	—	
Cariaco Shelf	0·35	—	0·78
Cariaco Trench	0·48	0·14	1·40
Southern Edge	—	—	0·32

Lake Maracaibo is relatively rich in phosphorus and presumably in other nutrients (REDFIELD *et al.*, 1955). At the time of our visit there was a very high standing crop of phytoplankton. In October 1952 GESSNER (1956) found an average of 6×10^6 cells per litre, mostly *Microcystis* and *Lyngbya*. In 1958 there was almost no silt in the water but the water transparency was low due to the plankton population itself. Consequently the calculated production was low.

In the Gulf of Venezuela the wind pattern appears to control basic production. The water on the western side is roiled and supports a low standing crop. There is evidence for weak upwelling on the eastern side (REDFIELD, 1955) and production rates are fairly high in a number of non-contiguous localities. In contrast to the Gulf of Cariaco, the Cariaco Trench and Lake Maracaibo, all of which have poorly ventilated basins and the deep water more or less anaerobic, the Gulf of Venezuela is open to the sea and undergoes at least seasonal flushing. Thus, there is virtually no accumulation of organic matter in the sediments along the eastern shore (W. ATHEARN, personal communication). However, the basin of Calabozo Bay (the southwestern portion of the Gulf) has an organic-rich sediment (J. ZEIGLER, personal communication) due in part to trapping material formed in Lake Maracaibo (REDFIELD, 1955) and to *in situ* production on the south coast of the Goajira Peninsula.

During November 1958 the main flow of the Magdalena River could be traced to the northeast. The light and photosynthesis data indicate that as the water cleared production increased. Unfortunately we have no data for the waters just to the west of the Goajira Peninsula. This would appear to be an ideal coast for upwelling as deep water is close inshore and the prevailing winds are unimpeded by physiographic features.

In the Gulf of Darien and surrounding waters, currents and general circulation are not known well enough to permit interpretation of the present data. If the waters remain turbid throughout the year there is little likelihood of much organic production.

Woods Hole Oceanographic Institution,
Woods Hole, Massachusetts.

Contribution No. 1102 *from the Woods Hole Oceanographic Institution. This work was carried out with the assistance of research grants from the National Science Foundation and the Office of Naval Research. Grateful acknowledgement is made to* C. S. YENTSCH, J. H. RYTHER and B. H. KETCHUM *for assistance and criticism.*

REFERENCES

BROOKS, E. M. (1939) Transport and convergence of the North Atlantic drift current computed from the average January pressure distribution. *J. Mar. Res.*, **2** (2), 163–167.
CREITZ, G. I. and RICHARDS, F. A. (1955) The estimation and characterization of plankton populations by pigment analyses. III. A note on the use of "millipore" membrane filters in the estimation of plankton pigments. *J. Mar. Res.*, **14**, 211–216.
DIETRICH, G. (1939) Das Amerikanische Mittelmeer. *Gesellsch f. Erdkunde zu Berlin, Zeitschr.* 1939, **314**, 108–130.
GESSNER, F. (1956) Das plankton des Lago Maracaibo. *Ergeb. Deut. Limnol. Ven. Exped.* 1952, **1**, 67–92.
KETCHUM, B. H., RYTHER, J. H., YENTSCH, C.S. and CORWIN, N. (1958) Productivity in relation to nutrients. *Rapp. Proc. Verb. Cons. Perm. Int. Expl. Mer.*, **144**, 132–140.
KIMBALL, H. H. (1928) Amount of solar radiation that reaches the surface of the earth on the land and on the sea, and the methods by which it is measured. *Mon. Weath. Rev.* **56**, 393–398.
MURPHY, R. C. (1936) Oceanic birds of South America. N.Y., Amer. Mus. Nat. Hist. 2 vol., pp. 609, 644.
PARR, A. E. (1937) A contribution to the hydrography of the Caribbean and Cayman Seas. *Bull. Bingham. Oceanogr. Coll.* **5**, 1–110.
RAKESTRAW, N. W. and SMITH, H. P. (1937) A contribution to the chemistry of the Caribbean and Cayman Seas. *Bull. Bingham. Oceanogr. Coll.* **6**, 1–41.
REDFIELD, A. C. (1955) The hydrography of the Gulf of Venezuela. *Pap. Mar. Biol. & Oceanogr., Suppl. Deep-Sea Res.* **3**, 115–133.
REDFIELD, A. C. and KETCHUM, B. H. (1953) Report to Creole Petroleum Corp. on the distribution of salt in Lake Maracaibo, Venezuela. *Woods Hole Oceanographic Inst. Ref.* 53–73 (unpublished manuscript).
REDFIELD, A. C., KETCHUM, B. H. and BUMPUS, D. F. (1955) Report to Creole Petroleum Corp. on the hydrography of Lake Maracaibo, Venezuela. *Woods Hole Oceanographic Inst. Ref.* 55–9 (unpublished manuscript).
RICHARDS, F. A. (1960) Some hydrographic and chemical observations along the north coast of South America—I. Cabo Tres Puntas to Curacao, including the Cariaco Trench and the Gulf of Cariaco. *Deep-Sea Res.* **7**, 163–182.
RICHARDS, F. A. and VACCARO, R. F. (1956) The Cariaco Trench, an anaerobic basin in the Caribbean Sea. *Deep-Sea Res.* **3**, 214–228.
RYTHER, J. H. and YENTSCH, C. S. (1957) The estimation of phytoplankton production in the ocean from chlorophyll and light data. *Limnol. and Oceanogr.* **2**, 281–286.
RYTHER, J. H. and YENTSCH, C. S. (1958) Primary production of continental shelf waters off New York. *Linmol. and Oceanogr.*, **3**, 327–335.
STEEMANN NIELSEN, E. (1959) Primary production in tropical marine areas. *J. Mar. biol. Ass. India*, **1**, 7–12.
VERDUIN, J. (1959) Photosynthesis by aquatic communities in northwestern Ohio. *Ecology* **40**, 377–383.
WORTHINGTON, L. V. (1955) A new theory of Caribbean bottom-water formation. *Deep-Sea Res.* **3**, 82–87.
WORTHINGTON, L. V. (1956) The temperature increase in Caribbean deep water since 1933. *Deep-Sea Res.* **3**, 234–235.

Printed in Great Britain by The Salisbury Press Ltd., Publicity House Wilton Road, Salisbury, Wilts. (25951)

Contribution No. 1103

Särtryck ur Tellus nr 2, 1960

pCO_2 in Sea Water and its Effect on the Movement of CO_2 in Nature[1, 2]

By JOHN KANWISHER, Woods Hole Oceanographic Institution
Woods Hole, Massachusetts

(Manuscript received August 31, 1959)

Abstract

A method is described for measuring pCO_2 in sea water. A gas phase is analyzed continuously by infrared absorption for CO_2 while it is equilibrated gently with the water in a countercurrent column. It has been used to determine the changes in pCO_2 produced by variations of temperature and total CO_2. Partial pressure shows large changes for small increments in these two independant variables. These properties of sea water are useful in estimating the movement of CO_2 between the atmosphere and oceans. It appears, for instance, that most of the fossil fuel CO_2 released by man has been effective in increasing the percentage of this gas in air.

Such diverse problems as biological produc-
vity, climatic change, and carbon dating are
nked to an understanding of the movement
f carbon dioxide in nature. Pertinent to all of
ıese is a knowledge of the concentration of
ıis gas in air and its exchange between the
ceans and the atmosphere.

Transport within the atmosphere and oceans
chiefly by mixing processes. But the move-
ıent of CO_2 across the sea surface depends
n diffusion. Since tension or partial pressure is
ıe driving force of diffusion, an understanding
f air-ocean exchange of CO_2 must include a
uantitative knowledge of the factors such as
mperature and total CO_2 which effect the
nsion of this gas in the sea.

When CO_2 from the atmosphere dissolves in sea water it enters the following chain of reactions:

$$\begin{array}{l} \downarrow\uparrow \quad CO_2 \\ \quad CO_2 + H_2O \rightleftarrows H_2CO_3 \rightleftarrows HCO_3^- \rightleftarrows CO_3^= \end{array}$$

The sums of these forms will be called total CO_2 in this paper. The partial pressure or tension exerted by the physically dissolved CO_2 is denoted by pCO_2. HARVEY (1955) has reviewed the considerable work of Buch and others that has been done on the chemistry of the CO_2 system in sea water. The amounts present as bicarbonate and carbonate ions can be found from pH, temperature, and salinity with the aid of the apparent dissociation constants for carbonic acid determined by Buch in sea water. Henries law is not valid for the relationship between pCO_2 and total CO_2 since only that component present as a physically dissolved gas is responsible for the tension.

---

[1] Contribution no. 1103 from the Woods Hole
ceanographic Institution, Woods Hole, Mass.

[2] Supported by NSF grant G-4813.

Buch has computed a series of tables in which pCO_2 and total CO_2 can be determined from pH, temperature, and salinity. The agreement between pCO_2 computed from these tables and that measured directly has been rather poor if one considers the limited range of surface sea water (BUCH 1939, DEACON 1940). Part of the cause is due to the inability to measure pH with sufficient precision. An error of .02 pH units will change the estimated partial pressure by 10 percent. Direct tension measurements may be equally inaccurate due to the difficulties of measuring a component that makes up only 1 part in 3000 of a gas mixture. Buch's tables are, in addition, inconvenient for deriving the relationship of pCO_2 and total CO_2 and also the effect of temperature on pCO_2 when total CO_2 remains unchanged. This is due to the pH changes that occur. It was the need for these two relationships that resulted in the present work.

There is an additional reason for directly measuring the CO_2 partial pressure properties. Buch defined apparent dissociation constants, K′1 and K′2 for the carbonic acid system in sea water using concentrations of ions rather than activities. When a comparison is made with the known dissociation constants it is found that the carbonate ions exert an activity equal to only 2 percent of their measured chemical concentration, (The Oceans, page 205). Some recent work of GARRELLS et al (1960) shows that this is due to complexing of CO_3 ions, primarily with Mg and Na. Thus the actual situation in sea water can be considered:

$$CO_2 + H_2O \xrightleftharpoons{K_1'} H_2CO_3 \xrightleftharpoons{K_2'} HCO_3^- \rightleftarrows$$

$$CO_3^= + Mg \xrightleftharpoons{K_3'} MgCO_3 + Na^+ \xrightleftharpoons{K_4'} NaCO_3^-$$

Other cations have only a minor effect. There is a small amount of complexing involving the bicarbonate ion.

In addition, the first dissociation constant, K'_1, is defined using the total unionized CO_2 for the undissociated carbonic acid. Actually only about 1/1000 of this is H_2CO_3, so K'_1 is 1,000 times smaller than the true K_1. It seemed possible that these approximations could have an effect on the dynamics of the CO_2 system in sea water.

Since this work has been finished a paper by Bolin and Eriksson has appeared that treats theoretically much of what I have done experimentally. The agreement with my measured values is rather good which indicates that the possible effects mentioned above are not drastic. Their work will be referred to further.

Method: A method has been developed for the continuous recording of CO_2 partial pressure in sea water. The apparatus is shown in Figure 1. A Fernbach flask containing about 3 liters of sea water is surmounted by a gas equilibrating column. Water is pumped from the flask to the top of the column where i flows down by gravity over a packing of Ber saddles and re-enters the flask. The air stream enters at the bottom of the column and leave at the top. Both countercurrent flow and a large surface facilitate tension equilibration between the air and the gases in solution. The entire apparatus is placed in a temperature bath

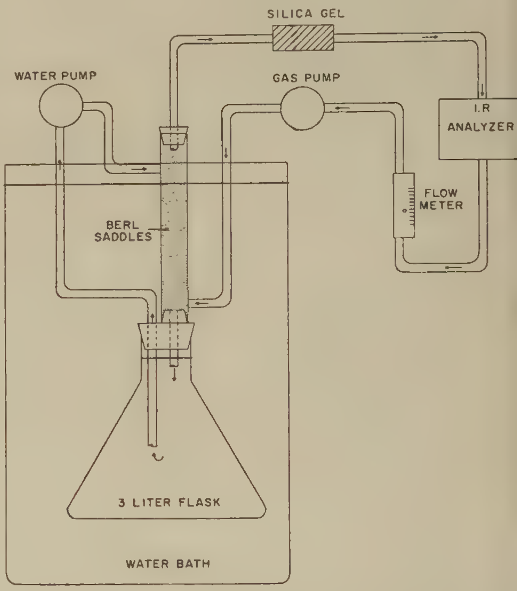

Fig. 1. Diagram of apparatus for pCO_2 determination

A closed 500 ml. volume of air continuously circulates through the column, a drying tube infra red CO_2 analyzer, and pump. Since the ratio of sea water to air volume is 6:1, very little CO_2 must be supplied by the water to bring the air into equilibration at the normally occurring values of pCO_2. The three liters of sea water contain about 135 ml. of total CO_2. The amount in the air at 300 ppm is only 1 percent of this. A correction has been computed at the higher tensions.

The analyzer is a dual path type with a CO_2 filled pneumatic detector, (model 200, Mine Safety Appliances Co.) The beam chopper is quartz which does not absorb appreciably in the infrared until 4u. Thus only the longer wave length absorption bands are effective. This results in a 2,000 to 1 differentiation against water vapor. In spite of this the gas stream must be dried. If it were not, that amount of water vapor in 20° C saturated air would appear as a 20 ppm CO_2 signal. The infrared principle offers a 10 to 100 times increase in sensitivity over previous methods in determining CO_2 in gaseous mixtures.

It is necessary to frequently calibrate the analyzer with gas mixtures of known CO_2 content. These are made by volumetrically diluting 100 percent CO_2 with nitrogen in a 20 liter stainless steel spirometer. The CO_2 is injected from a syringe. If pure gases are used the accuracy depends primarily on measurement of volume, with some errors introduced by temperature differences at which the volumes are determined. Given values could be repeated to within 1 percent.

The amount of total CO_2 in the sea water has been varied in different ways. Distilled water was saturated with 1 atmosphere of CO_2 gas at a known temperature to produce a solution of known concentration. This was checked by measuring its electrical conductivity. Small amounts of the solution were titrated into the 3 liters of sea water from a syringe, while pCO_2 was continuously recorded. Introduction of equivalent amounts of CO_2 free water caused no pCO_2 shift.

Biological material, fish and sea weeds, were also used to introduce known amounts of CO_2. Their CO_2 output rate was initially determined by enclosing them in a container and using gas analysis. The material was then introduced into the sea water for varying lengths of time to provide the desired CO_2 increase. Photosynthesis of sea weeds, measured by oxygen increase, was used to remove known amounts of CO_2.

The increase in CO_2 from biological activity and the normal gas exchange of a stored sample require that the water for pCO_2 determinations be immediately at hand if the value is to represent that which occurred in the ocean. For this reason, I have been able to make measurements only on water from Woods Hole Harbor. This has a salinity of about 31.5 ‰. The buffering capacity of sea water for CO_2 will increase in proportion to salinity so the data given can be extrapolated.

Results

Figure 2 shows the large changes in pCO_2 that result when the temperature of a single water sample is varied. The total CO_2 remains unchanged during a run since the system is sealed and the biological activity in the water sample is negligable. The CO_2 partial pressure at the sea temperature at the time of this run was 285 ppm. The air at this time had a concentration of 315 ppm. The sea was distinctly undersaturated with reference to the atmosphere.

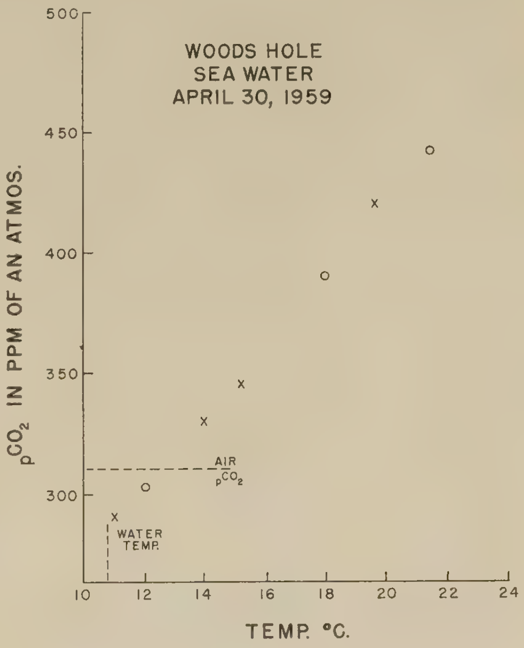

Fig. 2. Effect of temperature on pCO_2 in a local water sample. The cross points were taken with increasing temperature and the circles with decreasing to show that the effect is reversible.

The tension increases about 4 ½ %/° C. Harvey (1955 pg. 6) states that pCO_2, increases 1 %/°C and this is what one finds from Buchs tables at constant pH. However, with constant total CO_2, pH decreases about .01 units for each °C increase. It is this pH change and its resulting effect on the various equilibria of the carbonate system that accounts for the larger observed sensitivity of pCO_2 with temperature. It is unnatural to speak of temperature variation with constant pH since this can only happen if the normal temperature induced pH change is buffered with the addition of acid or base. This latter is in effect a change in alkalinity which has been shown not to occur to any extent in sea water. Revelle and Suess arrived at a 7 percent change per °C in some undescribed manner. Bolin and Ericsson unfortunately did not include the effect of temperature in their theortical analysis of the CO_2 system.

Figure 3 is a plot of the temperature variation of pCO_2 with varying amounts of total CO_2. The parallel straight lines on a logarithmic plot show that the effect of temperature is constant in percent per degree regardless of the initial tension. The meaning of these curves is clear. If one is to measure pCO_2 meaningfully to 1 percent then the temperature must be regulated to .2° C and this must be related with equal accuracy to the sea temperature.

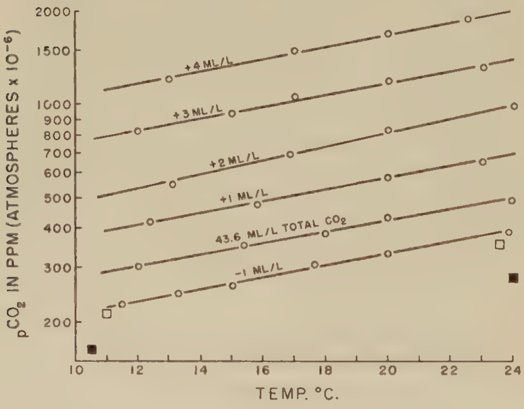

Fig. 3. Temperature variation of pCO_2 with different amounts of total CO_2.

The variation of pCO_2 with changes in total CO_2 is shown in Figure 4. It is readily apparent that sea water undergoes large changes in pCO_2 from the variations in CO_2 that are regularly produced by biological and physical processes. This increase in tension must be due to the increase in the physically dissolved component of the carbonate system. It can be computed (using the solubility of CO_2) that about a $^1/_{13}$ of any CO_2 added to sea water stays as a physically dissolved gas. Fresh waters low in alkalinity should show at least 10 times as great a tension change since most of the CO_2 stays in solution. My determinations on distilled water have confirmed this.

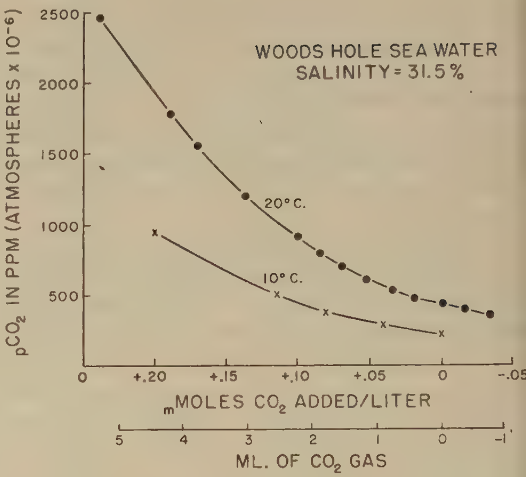

Fig. 4. Variation of pCO_2 with changes in total CO_2. The 10° C values were taken on the same water sample after the 20.

Discussion:

The measured CO_2 partial pressure properties of sea water can be applied to some considerations of the movement of CO_2 in nature. The curves in Figures 3 and 4 can be used in estimating, for example, the amount of CO_2 that must enter or leave a water mass to keep pCO_2 constant when the temperature is varied. The important point to consider is the large sensitivity of tension to changes in both temperature and total CO_2.

Different levels in the oceans show large variations in CO_2 partial pressure. Intermediate ocean depths are typically low in O_2 due to biological activity and are thus high in CO_2. These layers may be nearly anaerobic in the tropical Pacific and Atlantic and the partial pressure will therefore be as high as 2,000 to 3,500 ppm. I measured a pCO$_2$ of 3,000 ppm in the nearly anaerobic bottom layer of a polluted harbor at Woods Hole. The presence of such high values is probably of little significance to the air-ocean mixing of CO$_2$ since waters of this type rarely reach the surface. The high pCO$_2$ layer is separated from the mixed surface layer by a temperature produced density difference which inhibits vertical mixing. As small amounts do mix across this thermocline they are diluted into the mixed layer with relatively little effect. Since the higher CO$_2$ is accompanied by nutrient salts it may be largely fixed by photosynthesis before the elevated tension can be relieved by CO$_2$ diffusing into the air. This general argument may be valid for all cold bottom water formed at high latitudes which moves at depth to the tropics.

The surface water does show more limited variations in pCO$_2$ which are unrelated to mixing or to temperature change. COOPER (1937) found that these changes in the English Channel accompany the seasonal variations in photosynthesis and respiration of marine organisms. I have found such changes in the coastal water at Woods Hole. The partial pressure is below atmospheric during a plankton bloom when photosynthesis is fixing CO$_2$, and is higher than the air when the organic material is decaying. One might expect the largest excursions in Artic waters during the long hours of daylight. Buch has found a pCO$_2$ of 150 ppm in the summer near Spitzbergen.

It appears that biologically produced pCO$_2$ gradients at the sea surface are larger than those due to seasonal temperature changes. From the data presented here a 20° seasonal temperature shift requires about 1.5 ml/l difference in CO$_2$ to keep pCO$_2$ constant. The seasonal photosynthetically fixed CO$_2$ may be several times this. The two effects partly nullify each other since the water has more CO$_2$ made available from spring warming at the very time that photosynthesis is maximum. Unfortunately this reasoning depends largely on scanty data from coastal areas rather than the open sea.

In theory a knowledge of pCO$_2$ in space and time along with pertinent data on the physical state of the sea surface could be used to calculate net CO$_2$ fluxes. In practice this would be very difficult. However, surface pCO$_2$ does give qualitative information about where and in what direction the gas is diffusing. Isotope data provides an independent means of arriving at an average rate over a long period. CRAIG (1957) calculated that a given CO$_2$ molecule has an average residence time of 7 years in the atmosphere before diffusing into the ocean.

There has been considerable discussion of the effects and fate of the CO$_2$ that has been released by man's burning of fossil fuels. This has equaled more than 14 percent of the amount already in the atmosphere, (REVELL and SUESS 1957). BOLIN and ERIKSSON (1959) have presented a comprehensive discussion of the problem and have shown that most of the increase must still be in the atmosphere. The problem is essentially one of estimating how much of the potential increase has been buffered by the seas capacity to absorb CO$_2$. The pCO$_2$ properties presented here provide a basis for estimating this. BOLIN and ERIKSSON used a theoretically derived figure.

Any higher atmospheric pCO$_2$ must approach tension equilibrium with the seas and in the process some net CO$_2$ will pass into the water bringing its partial pressure up and lowering that of the air. Since the oceans contain some 60 times as much CO$_2$ as the air it would not be surprising if they had the ability to buffer out a large part of any atmospheric increase. We need consider here though only that portion of the oceans in touch with the sea surface, the mixed layer above the thermocline. Wooster (CRAIG 1957) has estimated from oceanographic data that the average depth of the thermocline is 75 meters, therefore less than 2 percent of the ocean water is in diffusion equilibrium with the atmosphere at one time. This contains only slightly more total CO$_2$ than is in the atmosphere. Referring to Figure 4, a 10 percent increase in partial pressure is produced by a .6 percent increase in the total CO$_2$. Thus one finds that less than 10 percent of any atmosperic increase would be removed by the amount of water in the mixed layer at one time. Since the same water does not remain in the mixed layer due to continual exchange with bottom water, some estimate of the rate of turnover of the mixed layer is needed. From oceanographic current data it seems unlikely that the mixed layer could have been renewed more than 2 to 5 times in the last 50 years. It is clear even from these rough figures that any CO_2 released from burning fossil fuels has been largely effective in increasing the concentration of this gas in the atmosphere. Over longer periods of time, hundreds to thousands of years, all of the deep water will equilibrate at the surface and something like 90 percent of any atmospheric increase will be absorbed. However, man is burning fuel at an increasing rate so if one considers only the solubility effect described here, the CO_2 should continue to increase.

Bolin and Eriksson have presented a mathematically formalized version of this argument using the same two-layer model of the sea. They show that the amount of CO_2 increase is quite insensitive to a wide range of turnover rates for the deep ocean. This is a consequence of the small amount of water in the mixed layer aided by the poor buffering capacity for CO_2. Even if one assumes a short turnover time, which means the surface layer has been renewed many times, the total amount of water passing through it can absorb only a small part of any atmospheric CO_2 increase. Callendar (1958) concluded from a consideration of actual measurements that there has been a 10 percent atmospheric increase. The above argument support this view.

Revell and Suess (1957) arrived at the much lower estimate of 3 to 6 percent for the atmospheric CO_2 increase due to fossil fuels. This difference is largely due to their using a model of the sea which assumes it is a well mixed reservoir. This is difficult to rationalize with our present oceanographic knowledge.

Fossil fuel CO_2 contains no C^{14} so its introduction decreases the specific activity of the atmospheric CO_2. The effect has been measured and found to be less than a few percent. This might at first seem incompatable with an atmospheric CO_2 increase of several times that. This can be explained by considering both the dynamic exchange and the tension equilibration taking place in the surface layer. It has already been mentioned that the water in the surface layer at one time can absorb less than $^1/_{10}$ of any atmospheric increase. But if diffusion back and forth across the sea surface is rapid enough, the surface layer CO_2 would completely mix with that in the air. The Suess effect decrease would be about 50 percent since these are nearly equal reservoirs. Craig's (1957) estimate of 7 years as the average turnover rate of air CO_2 indicates this is nearly the case. His figure also demonstrates that tension equilibration with the atmosphere is nearly complete for water passing through the mixed surface layer. Isotope data only gives information on the size of the effective reservoir, independant of hydrographic considerations, with which the atmospheric CO_2 has been mixed.

The long term fate of the present or any other CO_2 increase is complicated. The solubility buffering described here will reduce the present increase to less than 3 percent. The slightly greater total CO_2 in the sea water will increase the solubility for $CaCO_3$. Sea water is in contact with this in bottom sediments and in animals such as corals. Bolin and Eriksson show that this increases by 3 times the capacity of sea water for CO_2. Thus the eventual increase left in the atmosphere will be less than $^1/_{10}$ of the original.

Further compensation of the greater amount of CO_2 may result from an increase in photosynthesis both on the land and in the sea. This would result in some of the newly released CO_2 being fixed as organic material. The increased Ca ion might concievably accelerate the formation of animal and plant $CaCO_3$. In the event of no further CO_2 disturbance these interdependant factors would eventually produce what we can consider the long time average value of atmospheric CO_2. The tendency towards equilibrium of carbonates with CO_2 (Urey, 1952) must be only one of many factors determining this value.

The regulatory mechanism just described would have a time constant of at least many centuries so oscillations of such periods might

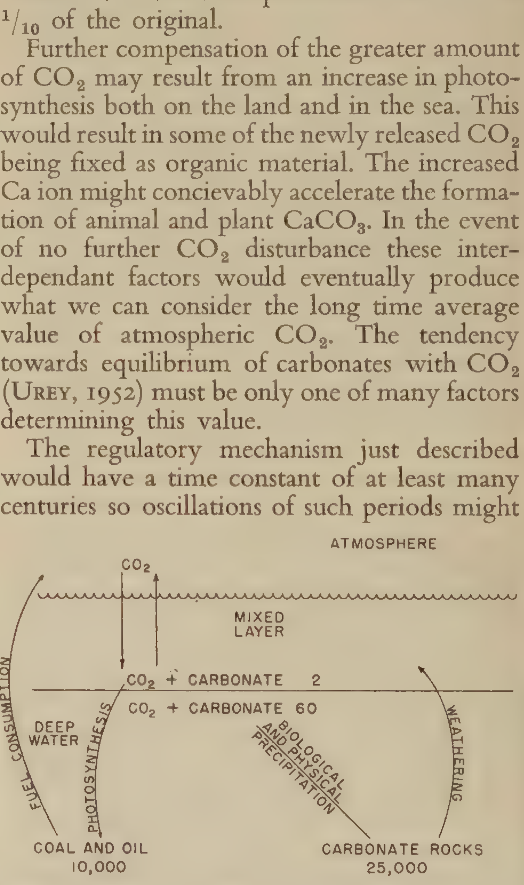

Fig. 5. Diagram abstracted from Redfield to show that large amounts of CO_2 have moved through the ocean-atmosphere system in geological time. The quantities are expressed on the basis of atmospheric CO_2 equals 1.

be expected. Figure 5 shows the amounts of carbon in different forms in nature expressed in units of atmospheric CO_2 (Redfield 1958). It is clear that in geological times large amounts of CO_2 have passed through the atmosphere-ocean pool. Since this flux has involved such cataclismic events as volcanic activity there must have been variations in the amount of CO_2 in transit.

Plass (1959) and others feel that a rise in the earths surface temperature will result from more CO_2 in the air because of the increased absorption of thermal radiation which would otherwise be lost to space. It is tempting to attribute such things as climatic variations in historical and geological times to such a factor. The complicated atmospheric dynamics involved force one to view a cause and effect relationship of CO_2 and climate with caution. Fortunately man is providing his own experiment to test this hypothesis, (Revelle and Suess).

REFERENCES

Bolin, B., and Eriksson, E., 1959: Changes in the carbon dioxide content of the atmosphere and sea due to fossil fuel combustion. *The Rossby Memorial Volume.*

Buch, K., 1939: Beobachtungen über das Kohlensäuregleichgewicht und über den Kohlensäureaustausch zwischen Atmosphäre und Meer im Nordatlantischen Ozean. *Acta Acad. Abo, Math. et Phys.*, **11**, no. 9.

Cooper, L. H. N., 1939: Phosphate in the English channel. *J. Mar. Biol. Ass. U. K.* **23**, p. 181.

Craig, H., 1957: The natural distribution of radio carbon and the exchange time of carbon dioxide between the atmosphere and sea. *Tellus*, **9**, p. 1.

Deacon, G. E. R., 1940: Carbon dioxide in the Artic and Antartic Seas. *Nature*, **145**, p. 250.

Garrels, R. M., Thompson, M. E., and Siever, R., 1960: Control of carbonate solubility by carbonate complexes. (In press.)

Harvey, H. W., 1955: The chemistry and fertility of sea waters. *Cambridge University Press.*

Redfield, A. C. 1958: The biological control of chemical factors in the environment. *American Scientist*, **46**, p. 205.

Revell, R., and Suess, H., 1957: Carbon dioxide exchange between atmosphere and ocean and the question of an increase of atmospheric CO_2 during past decades. *Tellus*, **9**, p. 18.

Sverdrup, H. U., Johnson, M. W., and Fleming, R. H., 1942: The Oceans. New York: Prentice-Hall, Inc.

Urey, H. C., 1952: The Planets. New Haven: Yale Univ. Press.

PRINTED IN SWEDEN
ESSELTE, STHLM 60

Contribution No. 1106

GROWTH RESPONSE OF CHLAMYDOMONAS AND HAEMATOCOCCUS TO THE VOLATILE FATTY ACIDS[1]

RAYMOND G. STROSS[2]

Abstract

The first five straight-chain saturated fatty acids were tested to determine their effect on cell division of phytoflagellates. *Chlamydomonas reinhardti* Danseard and *Haematococcus pluvialis* Flotow were selected for measurement because of information available from similar studies of the long-chain acids. Cultures were grown at five concentrations of the sodium salt within the range of 0.5 to 10.0 mmoles/liter.

Acetate stimulated the rate of cell division, while butyrate, the other acid with an even number of carbons, produced an inconsistent although negligible effect.

The fatty acids with an odd number of carbons inhibited division of cells, with propionate being most and valerate least effective. Inhibition in these tests, in which initial pH was kept constant, was proportional to the initial concentration of the acid salt. Additional tests showed propionate inhibition to be approximately proportional to a calculated amount of undissociated acid in the medium. *H. pluvialis* was 9–12 times more sensitive than was *C. reinhardti.*

The possibility of propionic acid inhibition of algae in acid lakes is discussed.

Introduction

Lipids produced by algae in culture are thought to be autoinhibitory to division of the cells (14, 15, 16). The partially oxidized products of long-chain unsaturated fatty acids are thought to be responsible (20), although the saturated acids are also effective inhibitors of growth (17). Proctor (17) concluded that higher fatty acids may be responsible for previously observed instances of inhibition in algal cultures. One necessary condition, however, appears to be a strongly alkaline medium, which probably is necessary for liberation into the medium of sufficient amounts of fatty acids from cell glycerides. This requirement of high pH may impose a severe restriction on the effectiveness of long-chain fatty acids in most unpolluted lakes.

That volatile fatty acids inhibit growth of algae and protozoa has been known for a long time and is discussed in older reviews of the subject (3, 10). These acids appear to be less toxic than those of longer chain-length, although their toxicity is known to increase at low pH of the medium. The so-called acetate flagellates appear to be especially resistant even in acid media (9). Growth of algae in axenic culture probably is not inhibited by the volatile fatty acids because little if any is produced (1, 12). On the other hand, algae in lakes are exposed to these acids and may be influenced by the presumably small concentrations encountered there. Two species of flagellates, one of known resistance, the other quite sensitive, were employed in this study to demonstrate the differential influence of the volatile fatty acids on the growth of algae and the importance of the acidity of the medium in controlling degree of response.

---

[1] Manuscript received April 22, 1960.

Contribution No. 1106 from the Woods Hole Oceanographic Institution, Woods Hole, Mass. Supported by Postdoctoral Fellowship from National Institutes of Health.

[2] Department of Zoology, University of Maryland, College Park, Md.

Can. J. Microbiol. Vol. 6 (1960)

Methods

Pure cultures of *Chlamydomonas reinhardti* Danseard I. U. strain No. 89 and *Haematococcus pluvialis* Flotow, obtained from R. R. L. Guillard, were used. The normal acids, formic through valeric, added as the sodium salt, were tested in a range of concentration of 0.5 to 10.0 mmoles/liter. The culture medium for tests which compared the effect of the five acids was adjusted to pH 7.25 initially, but it became progressively acid with growth of the culture. To determine effect of the acids, the division rate of treated and control cultures was compared at the end of log growth of the control cultures.

In evaluating the influence of pH of the medium on the degree to which propionate retarded division rate, the cultures were grown for a 30-hour period during which the populations had grown sufficiently for accurate measurement, but the uptake of salts from the medium had not been sufficiently great for a change in pH to occur. Tris buffer was ineffective in a part of the range of pH employed in these experiments, but was added for the sake of uniformity.

Both species were grown in the same inorganic medium (Table I). All cultures were suspended in 50 ml of medium contained in 125-ml cotton-stoppered flasks. They were placed in 250–300 foot-candles of continuous light which was provided by fluorescent lamps of daylight type. In the tests comparing the effect of the various acids, *Chlamydomonas* was grown at 18° C and *Haematococcus*, at 23° C. The latter temperature was used in testing the response of *Chlamydomonas* to the fatty acids at different pH.

TABLE I

Culture medium

NH_4NO_3	300 mg
K_2HPO_4	100
$MgSO_4$	200
$CaCl_2$	100
Fe sequestrene (13% Fe)	4.0
Tris buffer	400
Trace elements	1.0 ml
Double distilled H_2O	1000

NOTE: Cultures were adjusted to pH desired with dilute hydrochloric acid.

Division rates were determined by cell counts at inoculation and at harvest (4.0 days). Four replicate counts of each duplicate (eight samples) were made in a Levy haemocytometer (11). Results are expressed as a percentage of the number of divisions per day in the control cultures.

Results

With the exception of butyrate, the response of *Chlamydomonas* in replicate assays was uniform. Propionate, formate, and valerate retarded growth in proportion to the initial concentration of acid salt, with the degree of inhibition being in the order mentioned (Table II).

TABLE II

Effect of straight-chain volatile fatty acids on division rate of *Chlamydomonas reinhardti* at initial pH 7.25. Values are listed as percentage of division rate of control cultures at the end of log growth (ca. 1.35/day)

	Millimoles/liter of acid salt				
	0.5	1.0	2.0	4.0	10.0
Propionate	96	88	81	67	35
Formate	98	95	92	88	72
Valerate	102	100	99	98	97
Butyrate	100	101	100	100	97
Acetate	109	111	111	112	114

Acetate stimulated growth at all concentrations, the smallest level used resulting in a marked stimulation. Because of an increase in pH of the cultures with growth of the cells, a phenomenon peculiar to acetate, the larger amounts of acetate were not effective in proportion to the initial concentration, probably because of pH inhibition. The results from the tests of butyrate, although unsatisfactory, suggested that this acid present in the range of concentration employed in this study has negligible effect on the division rate of *Chlamydomonas*. In these tests the division rate of *Chlamydomonas* in the controls was 1.35 times per day, being slightly more or less depending on time of harvest. The fact that acetate stimulated the rate of cell division indicated a faster rate is possible at 18° C with the provision of higher intensities of light or an enrichment of CO_2.

Influence of pH

In this, as in other studies (7, 8), pH of the medium controlled the degree of inhibition by the fatty acid. Erickson *et al.* (7) showed the response of *Chlorella* to acetic acid to be nearly proportional to the concentration of undissociated acid when pH was equal or greater than the p*K* of the acid, a response demonstrated for many kinds of weakly dissociating organic acids (18). Because propionate provided the severest inhibition in this study, it was used to test the degree of inhibition at several concentrations of the free acid. These were provided by adjustment of initial pH at three to five levels, depending on the test, within the range of pH 6.60 and 7.25. In calculating the concentration of free acid, the nutrient salts which were present in the medium were assumed not to interfere with the proportion of dissociated and undissociated acid as expressed in the Henderson-Hasselbalch equation. In the 30-hour tests 2.0 mmoles/liter of propionate were added.

The inhibition caused by propionic acid was roughly proportional to its concentration in the medium (Fig. 1). The degree to which cell division of *Chlamydomonas* was inhibited was, however, dependent on the age of the cells used for inoculation. Cells from stationary-phase inocula were less sensitive than were those from log-phase. Moreover, resistance, or lack of depression in division rate, appeared to increase with the length of the period in which inoculum cultures were in stationary phase. Resistance to the free acid may be explained as a result of the cells dividing, owing to a reserve of food stored in the older cells. Because the cultures divided approximately two times, depending on age of inocula, during the 30-hour "incubation" period, a reserve of food may shorten the time required for the initial division.

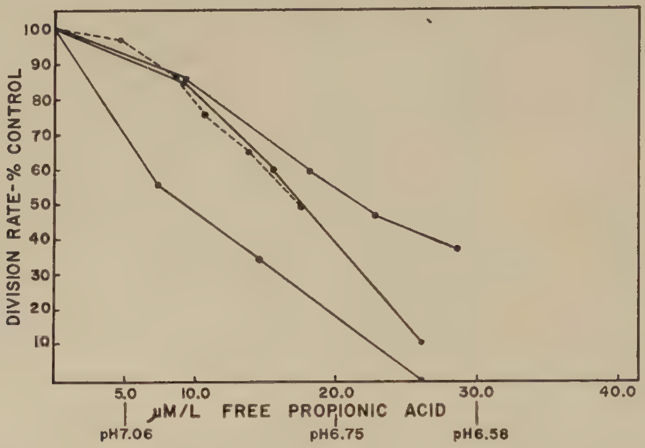

FIG. 1. Inhibition of division rate of *Chlamydomonas* cells grown in the presence of propionic acid expressed as percentage of rate in the control. Solid lines are for cultures containing 2.0 mmoles/liter of the acid salt. The dotted line represents additions of 1.0 mmole/liter. From left to right the lines indicate results of testing 3-, 5-, and 8-day-old inocula (dotted line results from 5-day inoculum). (Note that pH values apply only to solid lines or to an acid-salt concentration of 2.0 mmoles/liter.)

Similar tests run on *Haematococcus* showed it to be more sensitive to propionic acid. Concentrations of 0.05, 0.1, 0.2, and 0.3 mmoles/liter of the acid salt were tested in a range of pH similar to that used for *Chlamydomonas*. The procedure differed in that the cultures were permitted to incubate until the controls reached the end of log-phase growth. The use of initial pH for calculating the amount of undissociated fatty acid in the medium was considered permissible since growth and, therefore, change in pH were small in cultures where the fatty acid was effective. Division rate in the controls was 1.2 times per day.

Growth of *Haematococcus* in the presence of propionic acid is expressed as a function of pH and of the calculated amount of free acid (Fig. 2). The sensitivity of this species may be illustrated by comparison of rate of cell division in 0.1 and 0.2 mmole/liter of the acid salt at pH 6.6. At the former concentration cell division was scarcely affected, whereas at 0.2 mmole/liter inhibition was nearly complete. This species was approximately 10 times more sensitive to free propionic acid than was *Chlamydomonas*. The much greater sensitivity of *Haematococcus* to the volatile fatty acids, which was shown to exist for pelargonic and capric salts (17), was not true in tests of longer-chain fatty acids in which case the sensitivity of the two species to the presence of the salts was rather comparable (17).

In conjunction with the above experiments the medium from senescent cultures of *Chlorella* was examined for total concentration of fatty acids.

C. pyrenoidosa I. U. No. 251 and *C. vulgaris* (a strain isolated by J. McLachlan) were grown in a medium and atmosphere which produce a high content of fats in the cells (12, 19). After the cultures had remained for 1 month in a senescent state, which was indicated by the fading of chlorophyll in *C. pyrenoidosa*, the cultures were harvested by centrifugation, and the fatty acids in the cell-free medium prepared for measurement by titration in a standard manner (2). The density of cells at this time was in the range of 70–90 million cells/ml. At pH 5.0–6.0, the range in which the cells were grown, the average content of fatty acids in the medium of five cultures was 4.5 μeq/liter with a range from 3.0 to 6.9 μeq/liter. Because there seemed to be no difference in the amount existing in the medium of the two species of *Chlorella*, the average may be representative for cultures at similar pH, cell density, and nutrient medium.

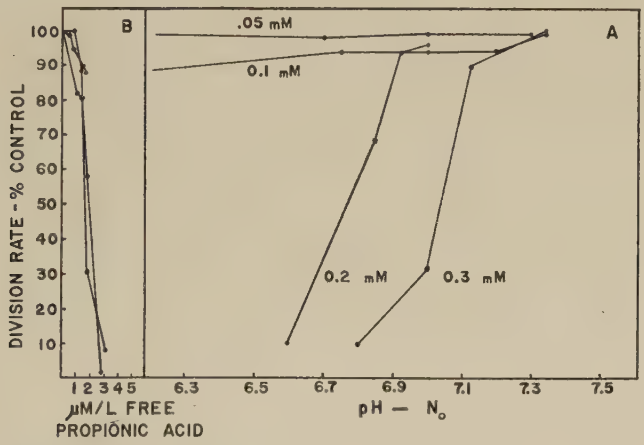

FIG. 2. Inhibition of division rate of *Haematococcus* cells grown in the presence of propionic acid. Portion A of the graph shows inhibition of acid salt as a function of pH at inoculation. Response at the four concentrations of acid salt is expressed as percentage of division rate in control cultures. Portion B shows response as a function of the calculated amount of free propionic acid in the medium. (Note: These tests differ from those in Fig. 1 in that the cultures were incubated until the stationary phase of growth was reached in the controls. Considered at the end of log growth, a division rate of 80% that of the control is roughly equivalent to an LG-50.)

On the basis of Milner's analysis (12) of the fatty acid composition of *C. pyrenoidosa* only a trace of the total acids liberated was volatile. Assuming an average molecular weight of palmitic acid, a value consistent with the findings of Milner, the medium contained approximately 1.2 mg/liter of total fatty acid. This would seem to be an inadequate amount to cause inhibition of cell division of *Haematococcus* even if the entire 1.2 mg were present as propionic acid. Whether the higher fatty acids in the *Chlorella* medium would affect cell division of *Haematococcus* at strongly alkaline pH would depend on the proportion of saturated acids which are considered to be the more toxic (4). It should be pointed out that larger quantities of fatty acids may accumulate in the medium of *Chlorella* cultures grown at alkaline pH (17).

Discussion and Conclusions

The response of *Chlamydomonas* and *Haematococcus* to dilute concentrations of the completely water-soluble fatty acids is correlated with the number of carbon atoms in the molecule, a fact which has been demonstrated on other flagellates (5). Formic and propionic acids, with an uneven number of carbon atoms, inhibit growth, whereas acetate is stimulatory at least under culture conditions used in this study. Because the degree of inhibition is proportional to the amount of free acid in the medium, an assay of formate at the same pH as propionate would not be expected to show an equal response, owing to the difference in pK of the two acids. At the pH of these assays there was supposedly 10 times more propionic acid in the medium. A possibly greater permeability of the cell to formic acid, however, does not permit a rigorous comparison to determine the actual effect of the two fatty acids. Butyrate and valerate, because of their limited solubility in water, are not considered in the discussion.

An active uptake of the acetate ion is suggested in the assays with *Chlamydomonas*. Normally, the cells prefer ammonium to the nitrate ion when the two are present together, as indicated by a decline in pH with growth of the culture. When acetate is added, pH of the medium increases markedly. Since there is no reason to suspect a change in preference, the increase in pH suggests the uptake of acetate is greater than the uptake of ammonium ion. If passage of acetate were by simple diffusion, then the pH in cultures with the other completely water-soluble acids should have behaved in a similar manner. An active uptake of the acetate ion would explain the increasing effect of the dissociated acid at pH 5.0 and above as noted for *Chlorella* elsewhere (6).

Although propionic acid probably is never inhibitory to growth of algae in axenic culture, there is a possibility of it having an adverse effect on natural populations of algae under certain circumstances. Lakes and ponds which receive drainage from the manures of ruminants should contain propionic acid because its production in the rumina of cattle is second only to acetic (21). Although propionic acid is not reported in the older analyses of unpolluted lakes (22), more recent work demonstrates trace amounts in river waters (13). An appreciable production may be expected in lakes in which water near the bottom is devoid of oxygen for considerable periods each year and, thus, favorable for microbial excretion of the volatile acids. The most effective situation may be in bog lakes which combine anaerobiosis with low pH. In any event the effect, because of the presumably small concentration of the acid, is likely to be one of providing the more acid resistant species with a competitive advantage owing to the limited rate at which crucial nutrients are supplied.

Acknowledgments

I am indebted to Drs. G. L. Clarke and B. H. Ketchum for providing me with space and facilities in their laboratories at Woods Hole. Drs. R. W. Krauss and H. W. Schoenborn have read the manuscript and offered many valuable suggestions.

References

1. Allen, M. B. Excretion of organic compounds by *Chlamydomonas*. Arch. Mikrobiol. **24**, 163–168 (1956).
2. Barker, H. A. Separation, identification, and estimation of lower fatty acids. Methods in enzymology. Vol. 3. Academic Press, Inc., New York. 1957. pp. 373–382.
3. Bresslau, E. Die Bedeutung der Wasserstoffionenkonzentration für die Hydrobiologie. Verhandl. intern. Ver. Limnol. **3**, 56–108 (1926).
4. Camien, M. N. and Dunn, M. S. Saturated fatty acids as bacterial antimetabolites. Arch. Biochem. Biophys. **70**, 327–345 (1957).
5. Cosgrove, W. B. and Swanson, B. K. Growth of *Chilomonas paramecium* in simple organic media. Physiol. Zoöl. 287–292 (1952).
6. Davson, H. and Danielli, J. F. The permeability of natural membranes. The Macmillan Co., New York. 1943.
7. Erickson, L. C., Wedding, R. T., and Brannaman, B. L. Influence of pH on 2,4-dichlorophenoxyacetic and acetic acid activity in *Chlorella*. Plant Physiol. **30**, 69–74 (1955).
8. Holz, G. G. The oxidative metabolism of a cryptomonad flagellate *Chilomonas paramecium*. J. Protozool. **1**, 114–120 (1954).
9. Hutner, S. H. and Provasoli, L. The phytoflagellates. *In* The biochemistry and physiology of protozoa. Vol. 1. *Edited by* A. Lwoff. Academic Press Inc., New York. 1951. pp. 27–128.
10. Jahn, T. L. Problems of population growth in the protozoa. Cold Spring Harbor Symposia Quant. Biol. **2**, 167–180 (1934).
11. McLachlan, J. L. The growth of unicellular algae in artificial and enriched sea water media. Can. J. Microbiol. **5**, 9–15 (1959).
12. Milner, H. W. The fatty acids of *Chlorella*. J. Biol. Chem. **176**, 813–817 (1948).
13. Mueller, H. F., Larson, T. E., and Lennarz, W. J. Chromatographic identification and determination of organic acids in water. Anal. Chem. **30**, 41–44 (1958).
14. Pratt, R. Influence of size of the inoculum on the growth of *Chlorella vulgaris* in freshly prepared culture medium. Am. J. Botany, **27**, 52–56 (1940).
15. Pratt, R. Studies on *Chlorella vulgaris*. V. Some properties of the growth-inhibitor formed by *Chlorella* cells. Am. J. Botany, **29**, 142–148 (1942).
16. Pratt, R. and Fong, J. Studies on *Chlorella vulgaris*. II. Further evidence that *Chlorella* cells form a growth inhibiting substance. Am. J. Botany, **27**, 431–436 (1940).
17. Proctor, V. W. Studies of algal antibiosis using *Haematococcus* and *Chlamydomonas*. Limnol. and Oceanog. **2**, 125–138 (1957).
18. Simon, E. W. and Beevers, H. The effect of pH on the biological activities of weak acids and bases. I. The most usual relationship between pH and activity. New Phytologist, **51**, 163–190 (1952).
19. Spoehr, H. A. and Milner, H. W. The chemical composition of *Chlorella*; effect of environmental conditions. Plant Physiol. **24**, 120–149 (1948).
20. Spoehr, H. A., Smith, J., Strain, H., Milner, H., and Hardin, G. Fatty acid antibacterials from plants. Carnegie Inst. Wash. Publ. No. 586 (1949).
21. Stewart, W. E., Stewart, D. G., and Schultz, L. H. Rates of volatile fatty acid production in the bovine rumen. J. Animal Sci. **17**, 723–736 (1958).
22. Vallentyne, J. R. The molecular nature of organic matter in lakes and oceans, with lesser reference to sewage and terrestrial soils. J. Fisheries Research Board Can. **14**, 33–82 (1957).

Contribution No. 1107

Reprinted from JOURNAL OF METEOROLOGY, Vol. 17, No. 6, December, 1960, pp. 670–674
Printed in U. S. A.

SEASONAL HEAT STORAGE IN THE NORTH ATLANTIC OCEAN[1]

Kirk Bryan and Elizabeth Schroeder

Woods Hole Oceanographic Institution

(Manuscript received 2 May 1960)

ABSTRACT

The seasonal range in heat content of the upper two hundred meters of the water column has been calculated for latitude zones between 20N and 65N in the North Atlantic. The calculation was based on 20,000 bathythermograph observations. The average range in heat content from the end of January to the end of August for the entire area is 36 kg-cal per cm². A maximum heat storage occurs in mid-latitude in an area just north of the mean position of the Gulf Stream.

For comparison, the heat storage due to local heating was computed for the same area. Estimates of net radiation, evaporation and turbulent heat flux by Budyko (1955) were used for this purpose. The average change in heat content over the same period according to this calculation is 31 kg-cal per cm². The results indicate that, for the Atlantic as a whole, seasonal changes in the transport of heat by ocean currents and/or seasonal changes in the exchange with deeper layers amplify heat storage near the surface at mid-latitudes but reduce it above 50N.

1. Introduction

An extremely important component of the Earth's heat balance is the storage of heat in the summer hemisphere and its release in the winter hemisphere. Except in certain land areas where a considerable seasonal fluctuation in soil moisture takes place, heat storage is severely limited by the comparatively slow rate of heat conduction in the solid earth. The relatively low heat capacity of air restricts seasonal heat storage by the atmosphere. The hydrosphere, on the other hand, is partly transparent to short-wave radiation, has a great heat capacity, and is in nearly constant turbulent motion. It is able, therefore, to play a dominant role in seasonal heat storage. Within the accuracy of current data, and considering the heat budget of very large areas, seasonal heat storage in the land and in the atmosphere, compared to that in the oceans, may be ignored. By using current estimates of radiation, it is possible to roughly determine the magnitude of this storage. According to London (1957), the Northern Hemisphere receives a net excess of heat by radiation during the height of summer of about 2.9×10^{20} cal per day. During the winter, there is a corresponding deficit. Unfortunately, very little is known about the meteorology and oceanography of the equatorial regions, but apparently no comparable amount of heat transport, changing sign with the seasons, takes place there. Assuming that the entire excess is stored in the oceans during the Northern Hemisphere spring and summer and that the excess measured by London varies sinusoidally with a period of one year, the average amount of heat stored during the six months of excess heating would be 22 kg-cal per cm².

If this seasonal heat storage were evenly distributed throughout the entire volume of the oceans, it would not be detectable with present data. Observations indicate, however, that seasonal heat storage of the general magnitude indicated above takes place in the upper one hundred to one hundred and fifty meters of the ocean. Since the advent of the bathythermograph shortly before World War II, a large number of observations of the temperature structure of the upper few hundred meters has been made. Unfortunately, the greater number of these observations is concentrated near the coasts in Northern Hemisphere middle latitudes. Surface-temperature observations are naturally much more extensive and have been more conveniently summarized. Gabites (1950) used observed seasonal fluctuations of surface temperature in conjunction with a simplified model of the seasonal thermocline to make an estimate of heat storage. In a more-recent study, Fritz (1958) has used empirical formulas based on Pacific hydrographic data to estimate heat storage for the Northern Hemisphere from surface temperatures. The first estimate of heat storage based directly on bathythermograph observations was made by Pattullo (1957). This extremely valuable study was based on a series of sites in the Northern Hemisphere for which a fairly long time record of observations was available. Pattullo also made an estimate for the Southern Hemisphere, but in this case only a small number of bathythermograph observations taken at irregular intervals could be utilized.

The present study is an attempt to use the large

---

[1] Contribution No. 1107 from the Woods Hole Oceanographic Institution.

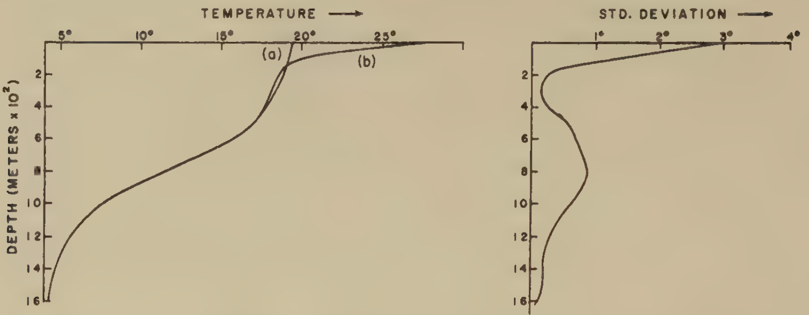

FIG. 1. Data from the *Panulirus* time series of deep stations taken near Bermuda. (a) Average February–March temperature trace. (b) Average August–September temperature trace. (c) Standard deviation of temperature for all seasons of the year.

amounts of bathythermograph data for the North Atlantic that have been collected by research and naval vessels. The advantage of using these data is that it allows a calculation of the range of heat content of the upper part of the water column over large areas where weather-ship data or other long time series of bathythermograph observations are not available. The principal error involved in the computation is due to variations in the annual cycle of heat storage from one year to the next. Although the data have been collected over two decades, observations may only be available for one or two years of this period for any given locality. Weather conditions may have been quite different from normal during the sample years. In areas of the Atlantic affected by the Gulf Stream, advection of heat by meandering currents may also cause large year-to-year variations in the heat-storage cycle. Instrumental error, while by no means negligible, is small in comparison to this sampling error. The data are entirely insufficient to extend the calculations below 20N or above 65N.

In spite of these difficulties, the results obtained by averaging these data should be superior to extrapolating values obtained from a comparatively small number of weather ships and other stations for which continuous time series of bathythermograph observations are available. Thanks to a summary of bathythermograph observations compiled under the direction of F. Fuglister, a great deal of the organization of the data had already been carried out. This summary gives the average temperature by one-degree squares of latitude and longitude and the month of the year for all available data collected in the Atlantic area by United States vessels, as well as for all published foreign data. Some of these data were collected before World War II, but the bulk of them have been received in the last decade.

2. Method

From the standpoint of heat-budget calculations the rate of heat storage,

$$\frac{\partial H}{\partial t} = \int_{-D}^{0} \rho c_p \frac{\partial T}{\partial t} \partial z, \qquad (1)$$

is the important term. In the equation above, H is the total sensible heat of the water column, D is the depth of the water column, ρ is the density, T the temperature, and c_p the specific heat. Unfortunately, the computation of $\partial H/\partial t$ would involve finding small differences, and it is preferable to consider the integral,

$$\Delta H = \int_{t_1}^{t_2} \left[\left[\int_{-200}^{0} \rho c_p T \partial z + \int_{-D}^{-200} \rho c_p T \partial z \right] \partial t, \qquad (2)$$

where z is given in meters. t_1 and t_2 refer to the periods of minimum and maximum heat content of the water column.

Although a small number of bathythermograph observations penetrates down to 300 m and beyond, there are relatively few observations below 200 m. Thus, it is only feasible to obtain a measure of the first term in brackets of (2).

The question arises as to how much of a contribution to ΔH is neglected by not considering the remainder of the water column. Some temperature traces based on several years of *Panulirus* data taken near Bermuda are plotted in fig. 1. This set of deep stations is one of the very few continuous time series of this type. Note that the main difference between the late summer trace and winter trace lies within two hundred meters of the surface. The quantity of heat stored in this change of temperature structure is in order of magnitude agreement with indirect estimates of the seasonal heat storage. The curve on the right in fig. 1 gives the standard deviation of temperature against depth for

TABLE 1. The distribution of bathythermograph data used to calculate seasonal heat storage. The amount of February and March data is indicated above the amount of August and September data.

	West longitude										
°N	80	75	70	65	60	50	40	30	20	10	0
75–79									4		
70–74					11				2	9	7
										6	
65–69					60			16	21	21	12
								16	72	26	15
60–64					13	26	28	124	30	58	141
					45	15	19	90	36	45	98
55–59					12	284	21	45	52	141	44
					150	420	41	36	95	40	261
50–54					9	51	24	22	71	22	
					102	56	53	96	128	38	
45–49				14	34	186	39	54	20	26	
				22	141	351	45	86	33	49	
40–44			1350	338	267	53	250	23	47	158	
			2379	514	409	84	427	55	12	21	
35–39		892	571	44	114	47	99	45	14	105	
		671	1431	235	234	88	179	68	24	131	
30–34	263	136	142	198	73	66	74	65	44	40	
	204	96	62	271	108	91	38	58	15	23	
25–29	223	100	153	40	126	32	16	13	22		
	111	51	34	23	47	25	12	9	29		
20–24	82	238	164	94	56	29	36	32	52		8,706
	63	90	24	28	15	1	7	6	20		11,326

all seasons. The maximum standard deviation near the surface is associated with the formation of the seasonal thermocline. A minimum coincides with the intermediate water which forms a very thick layer in the Sargasso Sea. The second peak is apparently connected with fluctuations of short duration caused possibly by internal waves on the main thermocline. Due to the very high "noise level" connected with these internal waves, it is very difficult to be sure that small seasonal changes do not take place there. Rather slight changes distributed through a deep layer could result in considerable storage of heat below the intermediate water. From such considerations, it is evident that the measurable heat storage associated with the seasonal thermocline must be accepted as only a tentative figure for the total seasonal storage in the ocean.

In studies of heat balance, it would be desirable to use ΔH defined by (2) to obtain some description of dH/dt. A harmonic analysis has been made by Pattullo (1957) of 13 sites in the North Atlantic with a long series of bathythermograph observations. The results indicated that a Fourier expansion of the seasonal variation of dH/dt converged fairly rapidly. For most sites removed from coasts, the amplitude of the second harmonic was only 20 per cent of the first harmonic. The first harmonic changed sign at the end of August and the end of February with a standard deviation for the 13 sites of about one month. By using this information, the gross properties of dH/dt may be inferred from (2).

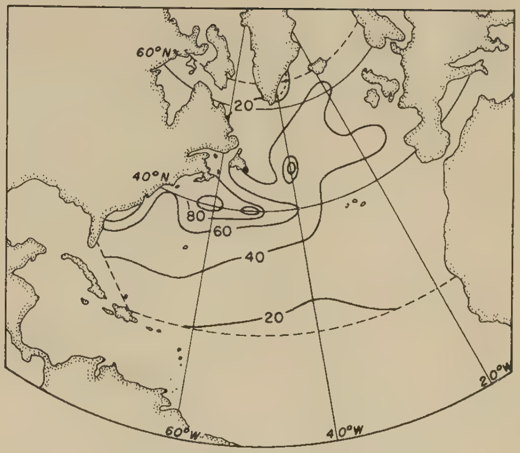

FIG. 2. A smoothed chart of ΔH from 0 to 200 m, given in terms of kg-cal/cm².

The quantity ΔH, omitting the second term in brackets, was calculated for sites spaced 2 deg of latitude and 10 deg of longitude apart for the whole North Atlantic from 20N to 66N. Near the North American coast, the east-west spacing between grid points was decreased to 5 deg of longitude in order to give greater resolving power in an area of strong gradients. First a temperature-*versus*-depth curve was drawn for February, March, August and September for every degree of latitude along each 10-deg meridian. Where no data appeared in the summary for a given degree square, a substitution was made using the monthly average for adjacent degree squares to the east or west. In some cases, it was necessary to use data 3 deg of longitude away from the chosen meridian. The next step was to smooth the readings at each level along the meridian by taking a running average over 3 deg of longitude. The weighting was by the number of original measurements, except in cases where the number at one latitude was very much greater than in adjacent squares to the north and south.

In table 1, the amount of data is indicated. Note the relative scarcity of data at low and high latitudes. The figures refer only to the number of bathythermograph observations used. Of these observations, only 40 per cent penetrated to 100 m and only 15 per cent to 200 m. At sites where no observations existed to define the curve below 100 m properly, the curves were extrapolated linearly down to values to the mean annual temperature at 200 m taken from a chart constructed by Fuglister for the North Atlantic.

3. Results

In table 2, calculated values of ΔH are given for each site. A smoothed chart of these values is shown in fig. 2. This may be compared with a chart in fig. 3 of

Table 2. Calculated $(\Delta H)_{0-200\text{m}}$ in kg-cal/cm².

°N	80	75	70	65	60	50	40	30	20	10	0
	West longitude										
66								9	63	70	39
64							−29	69		30	27
62					−25	8	−26	38	38	26	53
60					−14	60	−12	36	47	31	57
58					−13	46	35	39	39	52	44
56					9	36	33	47	22	49	58
54						35	27	52	31	35	
52						27	80	52	26	12	
50					23	22	48	50	29	40	
48					46	31	106	45	45	37	
46					54	44	138	31	38	38	
44					89	51	23	28	26	24	
42				74	111	59	39	19	29	29	
40			54	125	107	99	60	32	34	28	
38			46	108	89	84	37	26	29	31	
36		72	54	70	59	47	44	15	34	27	
34		53	49	56	49	23	39	42	24	29	
32		62	40	41	52	42	23	37	30	38	
30	87	49	43	36	50	29	26	39	24	31	
28	50	52	47	45	32	30	8	32	40		
26	15	35	36	38	15	9	19	29	56		
24	39	31	13	31	50	20	16	25	26		
22		21	23	5	36	19	7	24	15		
20		9	23	−1	21	18	13	27	39		

Table 3. Zonal averages of $(\Delta H)_{0-200\text{m}}$ in kg-cal/cm².

Latitude	20°	25°	30°	35°	40°	45°	50°	55°	60°
	19	27	36	41	56	48	43	36	26

the double amplitude of the first harmonic of the seasonal cycle of heat content given by Pattullo. As mentioned previously, the first harmonic dominates in the North Atlantic, so that its double amplitude is nearly equivalent to ΔH. Although fig. 3 is based on only 16 sites for this area, the two charts are in general agreement. Over most of the area, ΔH is remarkably uniform, ranging from 20 to 30 kg-cal per cm². The maximum values are near the American coast, where it might be expected that warm or cold air masses coming off the land would have the most influence. The existence of local maxima slightly removed from the coast indicates the importance of the strong surface-temperature gradients just north of the mean position of the Gulf Stream.

In table 3, average values of ΔH are shown for different latitude zones. These values are more reliable than those of table 2, since non-systematic errors due to insufficient sampling tend to cancel if an average is taken over a large number of sites. The average value of ΔH for the entire area between 20N and 60N is 36 kg-cal per cm². This value is larger than, but in the same general range as, the estimate of 22 kg-cal per cm² for the average of all the Northern Hemisphere oceans derived from London's (1957) radiation calculations.

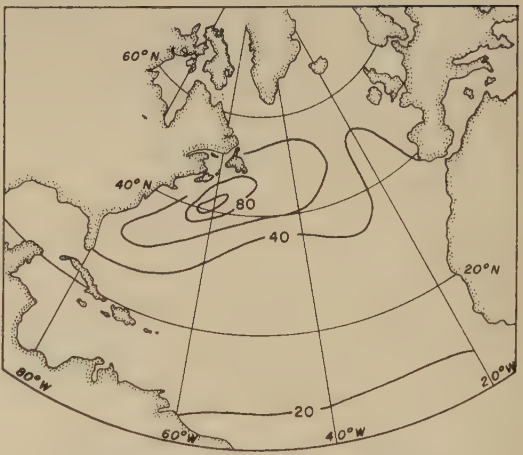

Fig. 3. Double amplitude in kg-cal/cm² of the first order term in a series expansion of $H(t)$ (after Pattullo).

4. Discussion

From the standpoint of atmospheric heat balance, it is very difficult to use a heat-storage estimate for the Atlantic without a corresponding estimate for the Pacific. If one considers oceanic heat balance, however, it is feasible to investigate the seasonal heat budget of each ocean basin separately. The equation of heat balance of a water column extending from the surface of the ocean to the bottom may be written

$$\frac{dH}{dt} = R - LE - T + A \qquad (3)$$

where R is the net radiation received by the water column, E is the rate of evaporation at the surface, T is the turbulent flux of heat away from the surface, and A is the heat added by warm currents. Small terms involving the flow of heat through the ocean floor and the conversion of mechanical energy into heat energy have been neglected. Letting a bar indicate the annual mean and a prime denote the seasonal deviation, eq (3) may be rewritten as

$$0 = \bar{R} - L\bar{E} - \bar{T} + \bar{A}, \qquad (4)$$

$$\frac{dH'}{dt} = R' - LE' - T' + A'. \qquad (5)$$

By taking the integral with respect to time of (5),

$$\int_{t_1}^{t_2} A'dt = \Delta H - \int_{t_1}^{t_2} [R' - LE' - T']dt. \qquad (6)$$

t_1 and t_2 again refer to the periods of minimum and maximum heat content of the water column respectively.

Estimates of R, E and T for the North Atlantic

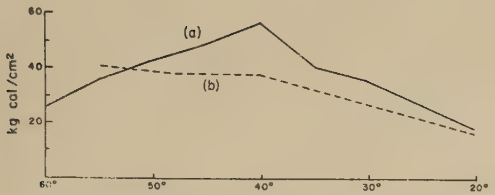

FIG. 4. (a) Difference between the average heat content of the upper 200 m of the water column in February and March and the average for August and September calculated from bathythermograph observations. (b) The integral from the end of February to the end of August of the net flux of heat through the ocean surface due to seasonal component of radiation, evaporation and turbulent heat flux. Estimated from *The Atlas of Heat Balance.*

exist in the literature. Reviews of the methods and some of the results are given by Budyko (1956) and Sverdrup (1957). Essentially, the methods are based on empirical formulas involving weather data reported by shipping. The most comprehensive work in this field is the *Atlas of Heat Balance* by Budyko (1955). This has been used as a convenient, up-to-date source for estimates of R', E' and T' in order to evaluate the integral on the right-hand side of eq (6). This integral, which will be denoted by Q, appears to involve a small difference between large quantities and the consequent loss in accuracy that this would imply. Actually, this is not the case for most of the Atlantic, since R' is negatively correlated with respect to E' and T' in the seasonal cycle; that is, evaporation and turbulent heat flux are lowest in summer when the net radiation reaches its highest value.

Zonally-averaged values of Q are plotted in fig. 4. They may be compared with the zonally-averaged values of ΔH in the same figure. If one assumes that the two curves are correct, the difference, $\Delta H - Q$, is entirely due to seasonal changes in the convergence of heat transport by currents. Near 40N, the difference between the two curves reaches a maximum of 20 kg-cal per cm². By making use of (6), this figure implies that the convergence of heat transport is 6.6 kg-cal per cm² per month higher on the average from the end of February to the end of August than for the remaining six months of the year. According to charts by Budyko (1955) and Sverdrup (1957), the zonally averaged annual value at 40N is only 4.5 and 3.4 kg-cal per cm² per month respectively. Thus, the curves in fig. 4 imply very large changes in the convergence of heat transport, which are in phase with the heating cycle below 50N and out of phase above 50N. Such an effect would reduce the heat exchange between the ocean and the atmosphere in middle latitudes and consequently make the Atlantic less effective in moderating climate than it would be otherwise.

A similar result was obtained by Pattullo (1957), who found that seasonal heat storage exceeded estimated local heating by an average of 40 per cent for a series of stations in the North Atlantic and the North Pacific. Since the temperature field in middle and high latitudes changes radically from winter to summer, it is reasonable that seasonal changes in heat transport should take place. The very high values indicated in the present study and in Pattullo's investigation, however, may be largely due to inaccuracy of the estimates of local heating and the heat storage. For example, the use of bathythermograph data could lead to a systematic over-estimate of heat storage, if warming takes place below the first few hundred meters in opposite phase to the warming near the surface. The *Panulirus* data (see fig. 1) suggest that this phenomenon does take place in the Sargasso Sea near Bermuda.

REFERENCES

Budyko, M. I., 1955: *Atlas Teplovogo Balansa.* Leningrad, 41 pp.

Budyko, M. I., 1956: *Teplovoi Balans Zemnoi Poverkhnosti.* Leningrad, Gidrometeorogicheskoe Izdatel'stvo, 255 pp.

Fritz, S., 1958: Seasonal heat storage in the ocean and heating of the atmosphere. *Arch. Meteor. Geophys. Biokl.*, A, **10**, 291–300.

Gabites, J. F., 1950: *Seasonal variation in the atmospheric heat balance.* Sc.D. Thesis, Mass. Inst. Tech.

London, J., 1957: *A study of the atmospheric heat balance.* Final Rep., Dept. Meteor., New York Univ., 99 pp.

Pattullo, J. G., 1957: *The seasonal heat budget of the oceans.* Sc.D. Thesis, UCLA, 104 pp.

Sverdrup, H. U., 1957: Oceanography in *Handbuch der Physik*, Vol. 48, Geophysik II. Springer-Verlag, Berlin, Gottingen and Heidelburg, 608–670.

Contribution No. 1111

OCEANOGRAPHIC RESEARCH REQUIRED IN SUPPORT OF RADIOACTIVE WASTE DISPOSAL

Abstract

For low-level waste disposal in coastal waters the character of the biota and the eating habits of local human populations will determine the safe limits of contamination. In such a situation the sedimentary bottom populations will be important, since they will be exposed continuously, while planktonic and fish populations will drift through or enter the area of contamination sporadically.

In the open ocean, on the other hand, planktonic populations are of prime importance, both as the food supply of pelagic edible species, and because they may be effective in transporting isotopes.

Similar questions face biologists studying either sedentary or planktonic populations. These include the need to know the distribution and density of populations of various species, the rate of growth of the individuals and of the populations, the seasonal cycle of production and of abundance, the ability of various organisms to accumulate various elements, and the ways in which these elements are transported through the food web, to the bottom through sedimentation or vertically within the water column through migration and exchange.

For each specific waste-disposal problem a survey of the local biota will be required, as will the subsequent monitoring of the operation.

RECHERCHES OCEANOGRAPHIQUES NECESSAIRES POUR L'ELIMINATION DES DECHETS RADIOACTIFS

Résumé

En ce qui concerne l'évacuation des déchets de faible activité dans les eaux côtières, les limites de sécurité pour la contamination seront déterminées par le milieu biologique et le régime alimentaire des habitants de la région. Dans une telle situation, ce sont les populations du fond sédimentaire qui joueront un rôle important puisqu'elles subissent une exposition permanente alors que le plancton et les poissons n'entrent dans les régions contaminées qu'en passant ou dans des cas isolés.

En revanche, dans la haute mer, les populations planctoniques sont d'une importance primordiale à la fois comme source alimentaire pour les espèces pélagiques comestibles et comme transporteurs éventuels d'isotopes.

Des questions semblables se posent aux biologistes qui étudient les populations sédentaires ou planctoniques. Il faut qu'ils connaissant entre autres la distribution et la densité des populations de diverses espèces, la rapidité de croissance des individus et de ces populations, le cycle saisonnier de la reproduction et de l'abondance, la faculté de divers organismes d'accumuler divers éléments, et la façon dont ces éléments atteignent le fond au moyen de la chaîne alimentaire par voie de sédimentation, ou sont transportés verticalement au sein de la colonne d'eau par migration ou échange.

Pour chaque problème concret que soulève l'élimination des déchets, il faudra étudier le milieu biologique local et, par la suite, faire le contrôle radiologique de l'opération.

ОКЕАНОГРАФИЧЕСКОЕ ИССЛЕДОВАНИЕ, НЕОБХОДИМОЕ В ПОДДЕРЖКУ УДАЛЕНИЯ ОТХОДОВ

Резюме

Для удаления отходов с низким уровнем активности в прибрежные воды определяющим фактором уровня заражения будет служить характер животного и растительного мира и средства питания местного населения. При таком положении вещей следует уделить внимание осадочному животному миру, поскольку он будет подвергаться облучению непрерывно, тогда как планктоны и рыба будут лишь проплывать или заходить в зоны спорадичного заражения.

С другой стороны, в открытом океане планктоны играют первостепенное значение, как с точки зрения того, что они являются морской разновидностью пищевого продукта, так и с точки зрения того, что они являются носителями изотопов.

С подобными вопросами сталкиваются биологи, изучающие либо мир непередвигающихся живых организмов, либо мир планктонов. Здесь необходимо знать расселение и плотность различных разновидностей этих организмов; скорость роста отдельных организмов и их семейств в целом; время их размножения и изобилия; способность различных организмов аккумулировать в себе различные элементы, а также пути, по которым эти элементы переносятся пищевой тканью на дно посредством осаждения или вертикально в водяном слое посредством миграции и обмена.

Для каждой специфической проблемы по удалению отходов требуется исследование местного характера животного и растительного мира, а также последующего контроля самой операции по удалению отходов.

INVESTIGACIONES OCEANOGRAFICAS NECESARIAS PARA LA EVACUACION DE DESECHOS RADIACTIVOS

Resumen

Cuando se trata de evacuar desechos de baja actividad en aguas costeras, las condiciones de seguridad de la operación quedan determinadas por el carácter de la fauna y la flora y por la forma de alimentación de la población humana local. En dicho caso habrá que estudiar especialmente los organismos bentónicos sedentarios, que estarán expuestos continuamente a la irradiación, en tanto que los peces y el plancton atravesarán la zona contaminada o sólo entrarán en ella de cuando en cuando.

En cambio, las poblaciones planctónicas son de fundamental importancia en mar abierto, tanto por servir de alimento a las especies pelágicas comestibles como porque pueden transportar isótopos.

Los biólogos que estudian las poblaciones bentónicas o planctónicas deben resolver problemas similares. Por ejemplo: la necesidad de conocer la distribución y la densidad de poblaciones de distintas especies; el índice de crecimiento individual y colectivo; el ciclo estacional de producción y de abundancia; la capacidad de algunos organismos para acumular diversos elementos, y la forma en que esos alimentos son transportados a través de la cadena de alimentación al fondo del mar (por medio de la sedimentación) o verticalmente, dentro de la columna de agua (por migración e intercambio).

Para cada problema concreto de evacuación de desechos será necesario estudiar la fauna y flora local, así como el consiguiente monitoraje de la operación.

OCEANOGRAPHIC RESEARCH REQUIRED IN SUPPORT OF RADIOACTIVE WASTE DISPOSAL

Bostwick H. Ketchum
Woods Hole Oceanographic Institution[1]
Woods Hole, Mass.
United States of America

The new oceanographic research required to evaluate radioactive waste disposal in the sea will include contributions from the disciplines of physical, chemical, geological and biological oceanography. Since the return of radioactivity to man will be principally through the biological cycle, the studies required in marine biology will be emphasized.

Two categories of problems in waste disposal must be recognized. One is concerned with the disposal of low-level wastes in inshore coastal waters or estuaries, and the other with the disposal of higher-level wastes in the open sea. It seems probable that quasi-general solutions to the problems of the open sea are attainable, so that we may at least extrapolate from one area to another. Conditions in coastal regions and estuaries are so variable, in both space and time, that each case will be unique and each must be solved individually.

Two sorts of investigations will be required in order to permit a more rational evaluation of the possibilities and limitations of sea disposal of radioactive wastes. When confronted with this problem the biologist quickly recognizes his lack of basic and fundamental knowledge concerning the distribution and rate of growth of marine organisms and their populations, and of the interrelationships between various organisms and the elements which might be expected as contaminants. Studies of these basic problems are being conducted, but the rate of progress is slow compared with the rate at which the information is required. It should also be pointed out that these basic problems can be studied anywhere in the world and the results will be pertinent and applicable wherever the same species of marine organisms are found.

A second category of investigations which will be required includes studies in direct support of a specific disposal operation. Each proposed or planned disposal operation should include, as an integral part thereof, a survey of the biota and an evaluation of the expected transport of the contaminant through the biota or by water currents so that the possibilities of return to man either directly in the water or indirectly through the food cycle can be evaluated. Monitoring of the operation will always be necessary, and should be planned not only to assure the human population that their health and safety is adequately protected, but also to increase knowledge concerning the basic scientific problems.

The basic studies of the interactions of marine organisms and their populations with radioisotopes, and the more specific evaluation of a waste-disposal operation, will both provide information of mutual value. For example, when we know enough concerning the basic biological problems, a census of the biota in a proposed disposal area will provide biologists with information from which they can evaluate possible accumulation of various radioisotopes

---

[1] Contribution 1111. Supported in part by the USAEC under contract AT (30—1) 1918.

in the biota and the possibility of various organisms serving as food for species important to man. Conversely, if the monitoring of a disposal operation is properly planned, we can learn much about the basic biological problems of accumulation and transport.

Marine biological problems

Among the general biological problems which require immediate attack may be enumerated the interaction between different species of organisms and specific elements which may be presented to them in their environment, the effects of accumulation of radioisotopes on marine organisms and on their populations, the transfer of elements along the food chain, and the effects of the organisms upon the distribution of elements in the sea.

Accumulation.

The metabolic processes of organisms result in tissues with concentrations of elements differing widely from the concentrations supplied in food or in the environment. Some elements, in particular organisms, are more or less greatly concentrated, others are more or less greatly excluded. A reasonable working hypothesis is that, for any given element, sufficient study will reveal a concentrating species. Considerable information is available for those elements most obviously essential for life, such as carbon, nitrogen and phosphorus. Less information is available concerning the elements required in trace amounts for existence, and almost completely unknown are those trace elements which apparently are not essential for life.

Two approaches to the problems of the accumulation of elements within organisms are available, and both should be pursued much more actively than they are today.

A laboratory study of accumulation involves exposing a particular organism or population to an environment containing the element under investigation. With the simpler forms of life, such as the planktonic algae or bacteria, cultures or populations can be exposed to the element and the accumulation studied as a function of concentration of the element and of the size and rate of growth of the population. With higher organisms, however, and particularly with marine species which have pelagic larval forms, the studies must be conducted at various stages of the life cycle and the transport or the retention of the element from one stage to the next evaluated. This is particularly true since many of the sedentary forms have pelagic larvae which can be carried over great distances by the water currents, so that new members of the population may not be derived from parents in the same vicinity. Indeed, radioactive tagging of these larvae might prove a way of following the dispersal of a species from a breeding centre.

The other approach to the study of the accumulation of elements by marine organisms is the determination of the chemical composition of organisms collected in their natural habitat. Any radioisotope added to the water will approach the same specific activity in the organism as in the water, and the degree of accumulation will, of course, be proportional to the concentration of the natural element in the organism. From such data one can predict the ultimate accumulation in the organisms from a knowledge of the specific activity in the water, or conversely can specify a permissible specific activity in the sea from a knowledge of the accumulation within the organism.

Both these approaches have their advantages and disadvantages. The tracer technique has a remarkably high sensitivity and can be used for the elements which are present in living organisms or in the environment in concentrations too low to permit adequate chemical analysis. It is, however, difficult to reproduce the natural environment adequately, and many important marine species cannot be bred in the laboratory, and indeed the adults can be maintained only briefly for the purposes of the experiment. In many of the experiments which have been done in the past using radioisotopes, the difference between a chronic exposure and a single dose has not been clearly recognized. In a chronic exposure the organism would be expected to achieve a steady state with the environment which would approach, if the exposure were sufficiently long, a specific activity equal to that of the medium. In the single-dose experiments, however, there is little chance for the steady state to be achieved unless the dose is unusually large. This type of experiment does give valuable information concerning the rate of excretion and turnover of the element being studied. The advantages of the approach by chemical analysis include the possibility of doing a large number of specimens in a routine way and in being able to determine the accumulation by organisms which we are still unable to culture in the laboratory. The disadvantages lie in the lack of sensitivity for some rare elements, and the impossibility of determining the excretion rate or turnover time for the element within the organism. Since both approaches provide valuable information and supplement each other, they should both be pursued more actively than they are now.

Effects on populations and individuals.

Entirely too little is known concerning the somatic and genetic effects of ionizing radiation upon marine organisms. Marine organisms living beneath the surface are normally exposed to much less ionizing radiation than are terrestrial plants and animals. A given increase in their environment would consequently produce a larger proportional increase in the radiation to which they are exposed.

It is generally presumed that conditions which will produce a negligible return to man will have no effect on the populations in the sea. This assumption may well be correct, but it should be recognized as an assumption and should be subjected to experimental test before it is accepted as a fact.

Many marine organisms live a precarious existence indeed. The larvae produced by a single mating pair in the marine environment may number millions, and only two of these need survive in order to maintain the population. The natural mortality in the sea is thus enormously great, and it is conceivable that a very small effect could be catastrophic. The studies reviewed by DONALDSON and FOSTER (1) indicate that the larval stages of fish are the most sensitive, a result which might be expected from the observations that the growing tissues are more sensitive than mature cells (2). Thus rapidly-growing larval forms, where already the mortality among marine organisms tends to be extraordinarily high, should also be the stage in the life cycle where the sensitivity to ionizing radiation would also be at its maximum.

The genetic effects of ionizing radiation on marine organisms are virtually unknown. In part this is because marine organisms are difficult to grow in the laboratory, and other forms, easier to work upon, have consequently been used in most genetic studies. Since marine organisms live in an environment with a low natural background of radioactivity, it is likely that a given added dose will represent a greater proportional increase of mutation rate than it would in terrestrial organisms. Because of the great fluctuations of population size common for marine species, the likelihood of fixation of semi-lethal mutants in the population may be increased. This could make a high mutation rate more dangerous than in other populations. It seems clear, therefore, that studies of the genetics of marine organisms should be encouraged, not only in relation to the possibilities of waste disposal in the sea, but also because the marine organisms come from an environment low in natural radioactivity.

Transfer along food chains.

The transfer of both energy and elements in the sea from one organism to another is effected by a food chain, or web, which in some cases attains a high degree of complexity. Fundamentally, however, the chain consists of three essential steps: the production of organic matter by the plants, which consist of planktonic algae only in the open sea but include both planktonic and attached algae in shallower coastal waters; the herbivores, which also are planktonic in the open sea but may consist of both planktonic and sedentary forms inshore; and the carnivores. This last step may be a multiple one, with a secondary carnivore eating a primary one and so forth, so that the three simple steps may be multiplied when considering a particular species of higher carnivore. At each step in the cycle only part of the material consumed is converted to new living organisms, most of it being required to satisfy the respiratory needs or excreted undigested and unused. There is consequently a loss of energy at each step. A comparable loss of elements is much less certain, however. Some species of both herbivores and carnivores can retain virtually all the ingested amounts of particular elements for long periods or for their entire life cycle. This is particularly true for elements in the structural tissues. It must also be remembered that some higher organisms can assimilate some elements directly from the water and are not restricted to obtaining them from food.

The rate of accumulation of elements from the sea will depend directly on the rate of growth of the various populations. Many studies of the distribution and growth of populations in the sea have been made, but the influence of environmental factors on these population growths is not yet completely understood. This type of basic information is essential in order to predict how populations and their seasonal and geographic changes in size will interact with the disposal of radioactive materials. Certainly the population size will differ by several orders of magnitude in northern coastal waters at different seasons. Likewise different geographical areas differ by several orders of magnitude in the maximum size of the population they can support. It is probably possible now to produce a gross map of the world distribution of various populations, and in some relatively restricted areas detailed maps of distribution of some species are available. Much more needs to be known, however, before the biological oceanographer can select areas which would be suitable or unsuitable for the disposal of radioactive wates.

As our information concerning the accumulation of elements by various species becomes more complete, we can evaluate the steady-state distribution of an element among various populations in the sea. The rate of accumulation, and consequently the fate of an element added to the sea, will depend upon a better knowledge of the turnover time within populations, which may be quite different from the biological half-life of the element or its turnover time within an individual specimen. This type of information can only be derived by studies of natural populations.

Transport by organisms.

Because of the movement of organisms which are independent of the direct circulation of the water, the plants and animals of the sea can modify the distribution of radioisotopes or other chemicals in the water column. By their vertical migrations, organisms can transport elements either up or down from regions of high to regions of low concentration. Organisms or their excretory products sink out of the surface layers and transport elements downward in the sea. Other organisms can resist sinking and accumulate at the surface. Sedentary organisms living in a current can accumulate elements from a much larger volume than that available to them at any one time. Mass horizontal migrations of organisms can transport elements and lead to high concentrations.

In the open sea, planktonic populations are of prime importance, both as the food supply of pelagic edible species and because they may be effective in transporting isotopes (3, 4). HARLEY *et al* (5) found that the plankton of the central Pacific Ocean contained, on an average, nearly five hundred times the water concentration of fallout activity. Throughout most of the open ocean areas of the world the surface water is separated from the deep water by an intense density gradient. Physical mixing processes across such gradients are necessarily slow, and the length of time for which wastes added to the deep waters would remain isolated from the surface has been variously estimated at between a few hundred and a thousand years. These estimates, reviewed by WOOSTER and KETCHUM (6) and CRAIG (7), take into account only the transport which would be expected from physical processes. In these same areas, however, the zooplankton undergo diurnal migrations which generally penetrate much or all of the thermocline or density gradient. KETCHUM and BOWEN (4) have calculated that the transport of readily-exchangeable materials as a result of this migration can equal or exceed the transport by physical processes. Any exchange by this mechanism would, of course, reduce the time of retention of materials which had been added to the deep waters of the ocean.

To evaluate the importance of this mechanism of vertical exchange of materials will require much more definite information than is now available concerning the nature and biomass of the organisms which undergo the migration, and the accumulation by these organisms of various elements. The rate at which the organism approaches equilibrium with the environment is extremely important in this case, since those elements which are exchanged rapidly will be transported most effectively.

Sedimentary processes constantly carry materials downward in the sea. The effect of these processes is apparent from the distribution of nutrients essential for plant growth, since the concentration of these is always reduced at the surface and is at its maximum at intermediate depths. Teh maximum nutrient concentration is always closely associated with a minimum concentration of oxygen, which indicates that these are related to the decomposition of organic matter. Evaluation of the effects of this process on radioisotopes added to the sea will require a knowledge, not only of the biomass of the organisms, but also of the surface area, since sorption of elements is as effective a mechanism of accumulation as are metabolic processes. This is particularly true of the microplankton, which affords by far the greatest surface area in the open sea where other suspended materials are rare.

Many species of fish migrate horizontally over wide areas of the ocean. A classic example is the Pacific salmon, which returns from the open sea to breed in the stream in which it was spawned. Long migrations of tuna, mackerel and many other species are well known. Bowen (unpublished) has computed that the tuna, which accumulate zinc in the liver, are an important transport mechanism for this element in the Pacific. The information required to evaluate the importance of this process is again the basic biological knowledge of the population size, routes of migration of the species, and the degree of accumulation of various elements within their tissues.

Discussion

Information on all these basic biological problems is required before a final evaluation of the capacity of the sea, or of a given area, for radioactive wastes will be available. It is well to remind ourselves constantly that pollution develops insidiously, and that long periods of time will be required for the recovery of an over-polluted area. It is therefore wise to proceed cautiously with radioactive waste disposal in the oceans, and to ensure continuing monitoring of conditions and re-evaluation of disposal operations.

These precautions are particularly necessary in coastal and estuarine waters. Here the circulation is complex and changeable, since it depends upon variable wind and rainfall conditions. In the shallow, inshore waters the circulation does not provide prolonged isolation from the biological cycle. Planktonic populations, and even some species of fish, may be expected to be transient visitors to an inshore disposal site. Sedentary populations and the sediments on the bottom are stationary in spite of continuous motion of the water, and may be expected to accumulate contaminants from the large column of water flowing past. Thus they will integrate variations in the operation over long periods of time. From the monitoring point of view this may be a great advantage, since the sedentary organisms themselves and the bottom sediments may be expected to give higher concentrations of some elements and to give more meaningful results from a monitoring programme than could be obtained from direct analysis of the water or of the transient plankton populations.

The deep waters of the open sea, on the other hand, offer promise of significantly long periods of isolation or retention of radioisotopes so that their incorporation in the biological system and their subsequent return to man would be minimal. Much work has been done in recent years in an effort to evaluate the age of the deep ocean waters, and it can be expected that the results of some of the oceanographic investigations during the International Geophysical Year will add substantially to our knowledge in this regard. In the open sea the plankton forms by far the greatest part of the biomass, and may be expected to concentrate added radioisotopes many times (5). The plankton may be expected to spend a substantial part of its life-cycle in a contaminated water mass, moving with it in its slow circulation. Plankton studies in the open sea should therefore receive emphasis, since it seems probable that incorporation of radioisotopes in bottom organisms or sediments would in effect remove them from the rest of the biological cycle and increase the time of retention in the depths.

In conclusion, encouragement of biological oceanographic research in support of radioactive waste disposal is imperative for several reasons. In the first place, the biological cycle offers the most direct route for the return of radioactivity to man. For low-level waste disposal in coastal waters the character of the biota and the eating habits of the local human population will always determine the safe limits of contamination. Biological activity will lead to higher concentrations of some elements within the organism than is presented in the environment. Furthermore, through the motions of the organisms, elements can be transported both vertically and horizontally in ways which would not be expected from currents and physical processes alone. Finally, in monitoring operations analysis of organisms promises the most meaningful results. Not only will the organisms concentrate some elements so that these can be more easily detected, but they will also integrate the variations which may occur during the operation.

REFERENCES

(1) DONALDSON, L. R. and FOSTER, R. F., National Academy of Sciences—National Research Council Publication No. 551, 96 (1957).
(2) RUGH, R., *Anatomical Records* **103**, 500 (1949).
(3) KETCHUM, B. H., National Academy of Sciences—National Research Council Publication No. 551, 52 (1957).
(4) KETCHUM, B. H. and BOWEN, V. T., Proc. 2nd UN Int. Conf. Peaceful Uses of Atomic Energy, A/Conf. 15/P/402 (1958).
(5) HARLEY, J. R. (ed.), "Operation Troll", United States Atomic Energy Commission, New York Operations Office (1956).
(6) WOOSTER, W. S. and KETCHUM, B. H., National Academy of Sciences—National Research Council Publication No. 551, 43 (1957).
(7) CRAIG, H., National Academy of Sciences—National Research Council Publication No. 551, 103 (1957).

Contribution No. 1112

(*Reprinted from Nature, Vol.* 188, *No.* 4756, *pp.* 1100–1101,
December 24, 1960)

Pigments of a Fossil Echinoderm*

SEVERAL years ago, I described[1] the discovery of crystallized organic pigments ('fringelite') in a fossil crinoid (*Millericrinus*) of upper Jurassic age. Additional specimens have now been collected at the two original locations (Fringeli and Liesberg, both in north-western Switzerland). The pigments are isolated by solvent extraction and separated by repetitive chromatography and fractional crystallization. Six pigments (fringelite *A–F*) have been isolated : additional pigments remaining in the fossil

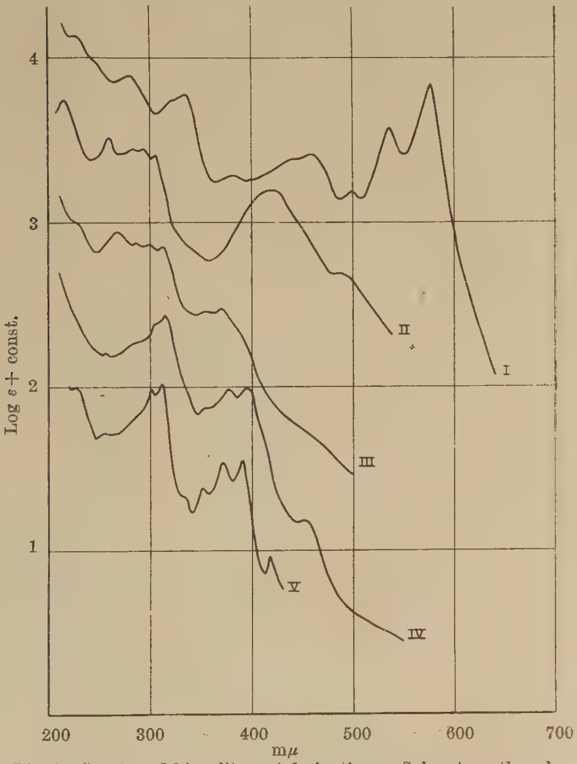

Fig. 1. Spectra of fringelite and derivatives. Solvent, methanol. I, Fringelite *E* ; II, acetyl derivative of fringelite *E* ; III and IV, hydroacetyl derivatives ; V, fossil alkyl-benzperylene

after exhaustive extraction with pyridine can be dissolved in concentrated sulphuric acid in which they exhibit an absorption spectrum similar to that of the more soluble fringelites. All these pigments are similar in respect to their absorption spectra, the colour of their solutions (red in organic solvents, green in sulphuric acid), the formation of green, insoluble sodium salts and the ease with which acetyl- and benzoyl-derivatives are formed. In all these properties the fringelites strongly resemble extended quinones of the type of aphin[2] or hypericin[3]. They even give the characteristic aphin-reaction, a blue(-violet) colour, on treatment with acetic anhydride containing a small amount of sulphuric acid.

---

* Contribution No. 1112 of the Woods Hole Oceanographic Institution.

The visible and ultra-violet absorption spectrum of fringelite *E* in methanol (Fig. 1, curve I) shows a general resemblance to that of erythroaphin *fb* (ref. 4); however, differences in band positions and relative extinctions of the band systems at 450 and 550 mμ indicate the presence of a similar but not identical chromophoric system. The acetyl-derivative of curve II is obtained by exhaustive acetylation with pyridine-acetic anhydride. Hydroacetyl derivatives (curves III and IV) are formed by reduction with zinc dust in the same medium. Curve IV, except for a displacement to longer wave-lengths (amounting to 13·5 mμ for the main band at 298·5 mμ and 8 mμ at 383 mμ, both in methanol), is nearly identical with that of the 6-ring aromatic hydrocarbon 1.12-benzperylene; curve III shows the typical bands of highly substituted phenanthrenes. The same phenanthrene band system is also evident in curve II (the acetyl pigment) in addition to absorption at longer wave-lengths caused by the carbonyl groups of the quinone.

From these spectral data we conclude that the fringelites are polyhydroxyquinones of 1.12-benzperylene. The aromatic hydrocarbon is substituted by the quinone oxygens in such a way that three aromatic rings with phenanthrene configuration remain undisturbed. By hydrogenation this quinone is reduced to the hydroquinone with the benzperylene spectrum IV, which, by more vigorous treatment, is transformed into the phenanthrene-derivative III.

The ultimate reduction products obtained in the laboratory and in Nature provide further proof for this structure. Zinc-dust fusion[5] leads to 1.12-benzperylene-type hydrocarbons of varying degrees of substitution, in addition to small amounts of a pyrene derivative. An alkyl-benzperylene also occurs naturally in the fossil sea lily[1].

The various fringelites seem to differ mainly in the number and position of their hydroxyl groups. The spectral data and the formation of a pyrene-derivative in the zinc-dust fusion suggest that the quinone-oxygens are located in 4 and 9 positions. The presence of alkyl substituents, the position of which is not yet clear, is indicated by a considerable spectral band shift from the synthetic benzperylene to the fossil hydrocarbon and the products of the zinc dust fusion. However, the 6 and 7 positions do not seem to be bridged by an alicyclic ring or substituted by an alkyl-chain since coronene is not formed in the zinc-dust fusion.

It has been suggested[6] that the pigments of recent crinoids are closely related to the hydroxynaphthoquinones of other echinoderms (echinochromes, spinochromes). In my previous paper I had suggested that the fringelites and the fossil benzperylene are the products of successive redox and condensation reactions between two echinochrome molecules, a hypothesis that has been further corroborated by the present findings. Fringelite *F* and the even more polar materials soluble only in concentrated sulphuric acid would be the primary condensation products; they are also the major pigments (several gm./kgm. of the fossil). The small amounts of the less polar pigments (mgm./kgm. for fringelites *D* and *E* and µgm./kgm. for pigments *A*, *B* and *C*) and the hydrocarbon have been formed from the major pigments by reduction and elimination of substituents.

The highest pigment concentration occurs in the massive (2–3 in. diameter) roots and lower parts of the stem; small stems (½ in. diameter) and crowns rarely contain more than traces of pigments. Other fossils of the same locations, including small sea urchins and their spines, are completely devoid of pigments. Apparently, conditions for the preservation of the pigments were sufficiently good only below the sediment-water interface where the roots and heavy stems accumulated during or immediately after the lifetime of the crinoids.

Discovery of the fringelites is geochemically significant, permitting for the first time the reconstruction of a complex reaction sequence, involving reduction, condensation, oxidation and further reduction and elimination of substituents under the final formation of a polynuclear aromatic hydrocarbon. A knowledge of such transformation reactions permits conclusions about the chemical environment and the organic reactivity in the sub-surface.

A more detailed report of this work is being prepared for publication in *Geochimica et Cosmo-*

chimica Acta. This investigation has been supported by a research contract with the United States Office of Naval Research (Contract *NONR*-2196 (00)).

MAX BLUMER

Woods Hole Oceanographic Institution,
Woods Hole, Massachusetts.

[1] Blumer, M., *Mikrochemie*, **36/37**, 1048 (1951).

[2] Brown, R. R., Calderbank, A., Johnson, A. W., Joshi, B. S. Quayle, J. R., and Todd, A. R., *J. Chem. Soc.*, 959 (1955).

[3] Brockman, H., and Muxfeldt, H., *Naturwiss.*, **40**, 411 (1953).

[4] Calderbank, A., Johnson, A. W., and Todd, A. R., *J. Chem. Soc.*, 1285 (1954).

[5] Clar, E., *Ber.*, **72**, 1645 (1939). Brown, R. R., Johnson, A. W., Quayle, J. R., and Todd, A. R., *J. Chem. Soc.*, 107 (1954).

Dimelow, E. J., *Nature*, **182**, 812 (1958).

Printed in Great Britain by Fisher Knight & Co., Ltd., St. Albans.

Contribution No. 1115

Reprinted from Biological Bulletin, Vol. 119, No. 3, pp. 399–415, December, 1960
Printed in U. S. A.

THE FEEDING BEHAVIOR AND RESPIRATION OF SOME MARINE PLANKTONIC CRUSTACEA[1]

ROBERT J. CONOVER

Woods Hole Oceanographic Institution, Woods Hole, Mass.

Interest in the respiratory rate and food requirements of the marine zooplankton probably dates from the studies of Pütter (1907, 1909), but data are presently available for only a dozen or so species of neritic copepods and for *Euphausia pacifica* (Lasker, 1960). *Paraeuchaeta norvegica,* studied by Raymont and Gauld (1951), is the only marine copepod for which respiratory measurements are available, which commonly occurs at depths greater than 100 meters.

In the present work a number of shipboard and laboratory experiments were performed with oceanic species of copepods, amphipods and euphausids, some from deep water, to learn if such organisms were amenable to artificially controlled conditions, and to obtain additional respiratory data for a very important but little-studied group of animals. A few species previously investigated from other localities (*i.e., Calanus finmarchicus*) were also included for comparative purposes.

In addition to the respiratory measurements, representatives of most species investigated were also kept in laboratory culture vessels where observations were made on their behavior and food habits. Some individuals of the copepod, *Calanus hyperboreus,* have been maintained in the laboratory for approximately one year which would seem to be the life span for it. Because of its large size, long life span, and ability to adapt to laboratory conditions, this species is currently the subject of intensive experimental investigation.

The author would like to express his appreciation to Dr. G. L. Clarke, Dr. Herbert Curl, Michael Mullin, William Dawson, Henry Fuller, John Clarke, Thomas Renshaw and Masateru Anraku, all of whom gave field or laboratory assistance during different phases of the work reported here. Dr. Robert Guillard supplied the phytoplankton cultures and Dr. Rudolf Scheltema supplied *Artemia* eggs and certain planktonic larvae used in feeding experiments. Dr. Robert Hessler supplied the *Artemia* used in the respiratory experiments.

MATERIALS AND METHODS

The zooplankton organisms used in the present program included the copepods: *Calanus finmarchicus, C. hyperboreus, Paraeuchaeta norvegica, Pleuromamma robusta, Bathycalanus* sp., *Rhincalanus nasutus, Euchirella rostrata;* the amphipods *Phronima* sp., *Euthemisto compressa,* and *Hyperia galba,* and an unidentified euphausid probably belonging to the genus *Thysanoessa.* All these animals are of large size and easily recognizable with the naked eye, even on shipboard. For the graphic analyses of respiratory rates use was also made of some data, hitherto unpublished in the present form, for the small neritic copepod *Acartia clausi.*

---

[1] Contribution No. 1115 from the Woods Hole Oceanographic Institution. This research was supported by the National Science Foundation under Research Grants 3838, 8913 and 8339.

The animals were captured with a ¾-meter or 1-meter net of mesh size #00 or #000, with a glass jar of one quart capacity secured in the cod-end. Tows were generally 15 to 30 minutes at depth, but in the case of the deeper tows the time required to reach the desired depth and to recover the net again increased the total towing time appreciably. Before the net was brought aboard after fishing, care was

TABLE I

Summary of all experimental data on the respiratory rates of zooplankton

Copepods	Location of experimental tow and estimated depth	Date	No. & stage	Experimental temp. ° C.	Dry weight/animal mg.	Respiration rate:	
						µl./animal & day	µl./mg. dry wt. & day
Calanus finmarchicus	Georges Bank 41°00′ N 67°35′ W 25 m.	Aug. 18, 1958	4 V	7.5	0.188	4.4	23.0
		Aug. 18, 1958	4 V	7.5	0.188	5.4	28.8
		Aug. 18, 1958	15 V	7.5	0.232	5.5	23.3
		Aug. 18, 1958	4 ♀	7.5	0.211	9.5	44.1
		Aug. 18, 1958	15 ♀	7.5	0.214	9.0	42.0
		Aug. 18, 1958	4 V	18.5	0.188	9.0	47.3
		Aug. 18, 1958	4 V	18.5	0.188	8.9	51.9
		Aug. 18, 1958	15 V	18.5	0.199	8.7	42.0
		Aug. 18, 1958	4 ♀*	18.5	0.211	15.7	74.2
Calanus finmarchicus	Gulf of Maine 42°25′ N 69°47′ W 200 m.	Aug. 20, 1958	15 V	8	0.294	4.7	16.2
		Aug. 20, 1958	15 V	8	0.264	3.9	14.8
		Aug. 20, 1958	15 V	8	0.334	3.6	10.9
		Aug. 20, 1958	4 V	8	0.277	5.4	19.5
		Aug. 20, 1958	4 V	8	0.277	4.7	16.9
Calanus hyperboreus	Slope water 41°46′ N 65°28′ W 1000 m.	Aug. 19, 1958	7 V	<10	1.55	18.3	11.8
			5 ♀	<10	3.68	24.8	5.5
			1 ♀	<10	3.62	26.0	7.1
Paraeuchaeta norvegica	Slope water 41°46′ N 65°28′ W 1000 m.	Aug. 19, 1958	5 ♀	<10	3.88	47.6	12.2
			5 ♀	<10	3.80	51.5	13.8
			1 ♀	<10	4.59	48.7	10.5
Pleuromamma robusta	Slope water 38°28′ N 70°59′ W 450 m.	Aug. 15, 1958	3 ♀	8	0.283	19.0	66.5
			3 ♀	8	0.283	15.5	54.3
Bathycalanus sp.	Slope water 41°46′ N 65°28′ W 1000 m.	Aug. 19, 1958	1 ♀	5.1	17.9	163.4	9.1

* 3 animals died.

TABLE I—*Continued*

Copepods	Location of experimental tow and estimated depth	Date	No. & stage	Experimental temp. ° C.	Dry weight/animal mg.	Respiration rate:	
						µl./animal & day	µl./mg. dry wt. & day
Rhincalanus nasutus	Slope water 39°48′ N 71°12′ W 400 m.	April 22, 1959	2 ♀	6.5	0.826	13.0	15.7
			2 ♀	6.5	1.079	15.3	14.2
			2 ♀	6.5	1.019	15.0	14.7
Euchirella rostrata	Slope water 39°48′ N 71°12′ W 400 m.	April 22, 1959	3 ♀	6.5	0.890	22.4	25.2
			3 ♀	6.5	0.947	28.6	34.9
			3 ♀	6.5	0.820	25.6	27.0
Acartia clausi	Long Island Sound 5–10 m.	July 22, 1953	119 ♀	5.0	0.0041	0.30	73.1
		Jan. 6, 1954	47 ♀	5.0	0.0047	0.37	78.7
		Jan. 26, 1954	156 ♀	5.6	0.0073	0.67	91.8
		Feb. 2, 1954	49 ♀	5.0	0.0072	0.69	95.8
		July 3, 1954	100 ♀	5.9	0.0044	0.40	90.9
		July 10, 1954	52 ♀	5.9	0.0049	0.22	42.6
Euphausids (unidentified)	Slope water 41°46′ N 65°28′ W 1000 m.	Aug. 19, 1958	3 **	5.1	2.67	43.1	16.1
			1	5.1	3.39	105.7	31.0
Amphipods							
Phronima sp.	Slope water 38°28′ N 70°59′ W 450 m.	Aug. 15, 1958	1	8	27.3	284.9	10.4
Euthemisto compressa	Gulf of Maine 42°25′ N 69°47′ W 200 m.	Aug. 20, 1958	4	4	4.97	92.7	18.6
			4	4	4.87	87.5	18.0
			4	4	4.35	72.3	16.6
Hyperia galba	Gulf of Maine 42°35′ N 69°35′ W 250 m.	Dec. 4, 1959	1	5.6	3.52	51.2	14.5
			1	5.6	8.24	81.0	9.8
			1	5.6	4.62	70.7	15.3
			1	5.6	10.15	114.2	11.2

** 1 animal in poor condition.

taken to have on hand fresh sea water pre-cooled to a temperature at or near that of the depth fished. The cod-end was immersed in this water and the contents of the glass jar only were retained. It was assumed that animals crushed against the meshes of the net were likely to be damaged, so that the net was never washed down and the entire process of getting the organisms from their natural temperature conditions to conditions simulating them was carried out as rapidly as possible. If the temperature difference between the surface water and the depth fished was great, the mortality among the deep-water forms was high despite the precautions taken. However, the animals were sorted immediately and only the healthy specimens kept for experimental work.

On shipboard, a portable refrigerator which opened from the top was used as an experimental laboratory. In the earlier studies, some difficulty was encountered in regulating the temperature of this box when it was opened frequently. A larger expansion valve, enabling higher refrigerant pressures, eliminated this difficulty, and in its present form the box can be kept open for long periods even in summer without excessive temperature change. On return to land facilities, a constant temperature room and conventional refrigerated water baths provided supplementary, controlled-temperature conditions when required.

Since most of the animals used in this study came from water deeper than 200 meters, 5–6° C. was chosen as the temperature at which the experimental and observational studies would be run, although for reasons mentioned above this was not attained in every case (see Table I). Initially it was hoped to compare the respiration of some of the animals at 5° and at surface temperature, to enable the computation of a rough Q_{10}. However, prolonged exposure to warmer surface waters proved lethal to most of the experimental material so that except for the relatively eurythermal *Calanus finmarchicus,* such a comparative study was not possible.

Respiration was measured using glass-stoppered bottles of appropriate size. Animals were placed in a small quantity of water in a bottle, and then the bottle and contents were flushed several times with water of known oxygen content, using a siphon arrangement with a bolting cloth screen to prevent loss of the experimental material. Control bottles were prepared in precisely the same manner except that the animals were omitted. All bottles were filled completely, taking care to insure that no air bubbles were included. As Marshall *et al.* (1935) demonstrated an increase in respiration for *Calanus finmarchicus* on exposure to light, all bottles were placed in black cloth bags during the run, regardless of the experimental conditions. At the end of a suitable period of time (8 to 48 hours), single samples from the experimental and the control bottles were siphoned into smaller glass-stoppered bottles and the oxygen content determined by the Winkler method. The oxygen utilization was determined from the difference between the bottles containing animals and those without. (For a detailed description of the method, with a discussion of its advantages and disadvantages, see Conover, 1956, 1959.)

The animals themselves were generally dried for weighing while in fresh condition, or in some instances a sample of the same species and stage of animal was dried as representative of the experimental animals. Animals were weighed on a suitable quartz helix microbalance made by the Microchemical Specialties Company, Berkeley, California. In the case of the smaller organisms such as *Calanus finmarchicus* a balance with working sensitivity of 2 mg. ± 1 μg. was used. For larger forms a 20 mg. ± 10 μg. balance was employed. Aside from the accuracy of weighing in this manner, the process is extremely rapid and largely free from errors due to sudden temperature change, varying humidity, etc. In a few instances, the animals were too large for either helix and they were weighed on a conventional analytical balance.

In the respiration experiments, as well as in laboratory culture studies, antibiotics were used to control bacterial growth and respiration. Dihydrostreptomycin sulfate in concentration 50 mg./L. was generally used in respiratory studies, sometimes supplemented with 10 mg./L. of chloromycetin. Chloromycetin was found to have an inhibitory effect on the feeding of *Calanus finmarchicus* when used at 50 mg./L. (Conover, Marshall and Orr, 1959). Since oxygen utilization attributable to bacteria was generally less than 0.1 ml./L., even in 48-hour experiments, with streptomycin alone, chloromycetin was eventually eliminated altogether from the experimental procedure.

For laboratory culture experiments, the organisms were kept in polyethylene "freezer containers" of pint, pint and a half, quart, or gallon size, depending on the size and number of animals to be cultured. These containers proved non-toxic to all animals tested, and, when fitted with their plastic tops, were safe from spillage or breakage in a rough sea. For most organisms, one or two animals in the pint-sized container proved most satisfactory; the containers then could be conveniently stacked four or five high without danger of upsetting, and in this size the sides are low enough to permit easy observation with a dissecting microscope.

Sea water for cultures was passed through a type AA Millipore filter (pore size 0.80 μ), cooled, and aerated before use. In the earlier studies, the culture water was generally taken from the same area that produced the animals, but it was found that local water from Vineyard Sound was also satisfactory. Streptomycin and penicillin "G" potassium 50 mg./L. were used together at first, but later alternated at each change of culture medium to lessen the possibility of "antibiotic resistance" developing among the contaminating bacteria.

The phytoplankton organisms tried as food for the animals included *Skeletonema costatum, Thalassiosira decipiens, T. fluviatilis, Chaetoceros affinis, Rhizosolenia setigera,* and *Coscinodiscus asteromphalus,* all from laboratory cultures. Living *Artemia* nauplii and *Pinnotheres* zoeae, fresh-caught harbor copepods including *Acartia clausi, A. tonsa, Temora longicornis, Centropages hamatus, Eurytemora hirundoides,* and *Labidocera aestiva,* as well as various invertebrate larvae in the plankton were given as animal food. Bits of mussel, clam, and living and dead offshore zooplankton were also given to some of the larger carnivorous forms. The number of fecal pellets produced was used as a criterion for the amount of feeding although in a few instances change in the number of food organisms was also determined.

No attempt was made to determine the food in nature by examination of gut contents. Food passes through the animal's gut very rapidly and particularly in the case of offshore forms the gut is usually empty.

Observations on Feeding and Behavior of Animals in the Laboratory

Copepods

Calanus finmarchicus. Marshall and Orr (1955a, 1955b) have summarized what is known concerning the feeding and behavior of this species, and little can be added by this investigation. *Calanus finmarchicus* is known to eat a wide variety of diatoms, dinoflagellates, and other flagellated forms. Nannoplankton is eaten but the animal showed a decided preference for larger food (Marshall and Orr, 1955b). In addition, radiolarians, tintinnids, and crustacean remains have been found in the gut (Marshall and Orr, 1955a). In the present study, *C. finmarchicus* ate *Skeletonema, Rhizosolenia,* and both species of *Thalassiosira.* Although it may take in animal food inadvertently, it would seem that this species is primarily a herbivore.

Calanus hyperboreus. This species is generally regarded as an arctic form, where it commonly occurs in the surface waters. It is moderately abundant in the Gulf of Maine and has been observed in the slope water at depths greater than 400 meters as far south as about 38° N. Juveniles were captured a mile south of Gay Head on Martha's Vineyard, Massachusetts, in March and April, 1958.

When first returned to the laboratory, *C. hyperboreus* generally did not eat any plant or animal food readily, but after one to two weeks healthy specimens ate all phytoplankton species presented to them, including *Skeletonema costatum, Thalassiosira decipiens, T. fluviatilis, Chaetoceros affinis* and *Coscinodiscus asteromphalus.* Many large fecal pellets were produced, often two or three millimeters long, which on microscopic examination contained some green material and abundant smashed tests of the species of diatom fed.

This species is anatomically very similar to *C. finmarchicus* and is almost certainly herbivorous in northern seas. However, it is difficult to understand how it can obtain plant food in sufficient abundance to sustain it in the slope waters south of Woods Hole, Massachusetts, in summer when the waters of the euphotic zone are too warm for it. Possibly the animal goes into a state of "quiescence" when food is scarce, which may explain why no food is taken when it is first brought into the laboratory. Recent unpublished experiments suggest that the increase in activity after some days in the laboratory is also accompanied by an increase in respiratory rate.

Sømme (1934) observed that breeding animals frequently ate their own eggs. This observation has been confirmed in the present study, but it was found that egg-eating was much greater when animals had no other food available than when abundant phytoplankton was present.

Paraeuchaeta norvegica. Lowndes (1935) examined living and preserved specimens of this large copepod and concluded that it was entirely carnivorous. The animal refused all plant food presented to it in the current work. On the other hand, some of the laboratory specimens fed on small neritic copepods readily as long as they were alive. *Acartia tonsa* and *Centropages hamatus* were taken frequently, although it is questionable whether *Paraeuchaeta* would encounter either in nature commonly. It did not eat *Artemia,* though some decapod larvae were consumed. During feeding, fecal pellets were produced which contained obvious animal fragments. If both plant and animal material were fed simultaneously, the fecal pellets produced contained only animal remains.

The maxillipeds in this animal are large, prehensile and carried far forward in "praying mantis" fashion. The actual capture of the prey was not observed but the animal would seize the end of a needle or micropipette when irritated in a manner which must closely duplicate the process of food getting. The strength of the animal was surprising and a smaller copepod would have little chance of escape once it was grasped by the maxillipeds. Curiously, some of the laboratory specimens hooked their maxillipeds over their first antennae. In this position they seemed quite helpless and unable to get free. When the maxillipeds were released by the investigator, the animal seemed quite healthy, but usually caught the maxillipeds again in a few hours.

Bathycalanus sp. There can be little doubt that these large red copepods from deep water must be carnivorous, although no food, plant or animal, was taken during the three weeks they were kept in the laboratory. The female whose respiration was measured was over 13 mm. long with antennae reaching over 2.5 cm. from tip to tip. In swimming, the movements were generally unhurried, almost deliberate, but when disturbed the animal dashed about the culture vessel in a frantic effort to escape, frequently sustained for some seconds.

Rhincalanus nasutus. This species survived well under laboratory conditions and ate any species of phytoplankton offered (*Skeletonema costatum, Thalassiosira decipiens, Rhizosolenia setigera*). One female lived for three months before being accidentally killed, during which time she matured and laid numerous fertile eggs. Attempts to raise the nauplii were unsuccessful.

Euchirella rostrata. These robust-appearing copepods did not survive particularly well in the laboratory although a few fecal pellets were produced when the animals were fed on *Skeletonema, Thalassiosira decipiens* and *Rhizosolenia.* All were dead within five weeks of capture, but during this period several females matured and laid. The eggs, which were a deep purple, were remarkable for their size relative to the animal which produced them. The lengths of the cephalothorax for the captive animals ranged from about 2.9 to 3.1 mm., while the eggs produced measured over 0.4 mm. in diameter. In contrast, *Rhincalanus nasutus,* size range 4.2–4.7 mm., laid eggs about 230 μ in diameter, and in the still larger *Calanus hyperboreus,* cephalothorax 5.5–6.0 mm., the eggs ranged from 190–210 μ. *Euchirella* laid only a few eggs at a time and they were very buoyant. Unfortunately none of the eggs developed.

The density of this animal in the adult stage was remarkably high in contrast to its eggs. The animals did not swim continuously in the laboratory containers and when swimming ceased, they sank rapidly to the bottom. The carapace seemed unusually sclerosed for so small an animal, being hard and smooth to the point of a dissecting needle. Their movements were exceedingly rapid and they leaped about vigorously when out of water. One individual traveled a measured distance of 20 cm. in a single leap from the shallow dish, containing water several millimeters deep, in which it was being examined. Although it was not demonstrated that *Euchirella rostrata* does prefer animal food, the generally poor feeding on phytoplankton, robust anatomy and prehensile head appendages make it virtually certain that the animal is largely carnivorous.

Other copepods. Only a few specimens of *Pleuromamma robusta* were taken in near-surface tows over the continental slope and no observations on the organisms in captivity were made. The structure of the mouth parts and general morphology would suggest that it is largely herbivorous (George Grice, personal communication).

No attempts were made to culture *Acartia clausi* at this time but earlier studies (Conover, 1956) leave little doubt that it is primarily a herbivore. However, two observations of considerable interest were made on the closely related species *A. tonsa.*

On one occasion, some *A. tonsa* taken from Woods Hole harbor were given as food to a larger carnivorous copepod (*Paraeuchaeta norvegica*) in the company of some *Artemia* nauplii. During the experiment, an *Acartia* male was found which had firmly grasped with its head appendages an *Artemia* nauplius. When both animals were transferred to another dish for observation the male released the nauplius which was seen to have its abdomen almost totally eaten. The *Acartia* was given additional *Artemia* nauplii but died shortly thereafter without any further predation.

On another occasion, *A. tonsa* was observed in the act of feeding on a culture of large *Thalassiosira decipiens* (cells 70–85 μ in diameter). A female (cephalothorax length 0.87 mm.), lying ventral side up on the bottom of the dish, was seen to grasp single *Thalassiosira* cells with rapid movements of the maxillipeds, bringing them to the mouth region. Several times the individual cell could be seen poised on the edge of the labrum for an instant before it passed inside the animal without being broken or apparently damaged in any way. Once inside, the cells could be seen through the transparent carapace like beads on a string lined up along the foregut. The cells were carried posteriorly by a series of peristaltic movements during which they continued to be discrete, undamaged cells until quite suddenly they lost their distinct outline and seemed to fuse into a mass which soon became noticeably darker in color. The material was passed posteriorly and eventually extruded as a fecal pellet. The entire process took about 30–45 minutes, depending on which cell was timed. On examination the pellet was seen to contain only shattered frustules of *T. decipiens* and some unidentified organic matter.

Amphipods

Only two *Phronima* were taken during the program and one was dried after the respiration experiment. Despite their transparent, somewhat delicate appearance, the organisms were quite dense with a tough, sclerosed exoskeleton. The specimens studied here were found free-living in the plankton but the animal is frequently found "living" in an empty test of a salp. Most probably the organism eats the salp in whose test it is found, for it would seem poorly equipped for filter feeding.

Euthemisto compressa was found to produce an occasional fecal pellet when given phytoplankton (*Skeletonema*) but was obviously much more successful with animal food. For instance, between October 3 and October 6, 1958, a single female was observed to eat four harbor copepods and two zoeae, one nearly as large as itself. Gravid females were taken in the plankton on several occasions, and even the newly hatched young seemed carnivorous, swarming all over a piece of dead euphausid given them. *Hyperia galba* likewise is largely carnivorous and was observed to eat bits of mussel (*Mytilus edulis*), smashed snail (*Littorina littorea*) as well as living and dead copepods. This species is frequently associated with *Aurelia aurita* or other large medusae and may share the food captured by its larger host, but it can be a free-living member of the plankton community as well (Bigelow, 1925).

Both *Euthemisto* and *Hyperia* are quite dense, heavily sclerosed, and strong swimmers. Curiously, their carapaces are strongly hydrophobic and despite their density and obvious strength, they are very prone to become caught in the surface film.

Euphausids

Of all the oceanic organisms tried, the euphausids seemed to be the most difficult to keep in the laboratory. Specimens taken on August 19, 1958, were all dead by September 4, before anything could be ascertained about their food habits. On other occasions, *Thysanoessa, Meganyctiphanes,* and *Nematoscelis* have been observed to eat phytoplankton (*Skeletonema costatum, Thalassiosira fluviatilis*), but the rate of consumption would seem to be much too low to meet food requirements. These animals did not survive appreciably better than the first group.

Several workers have noted that euphausids consume a variety of foods. *Nyctiphanes couchii,* a neritic species, eats diatoms and organic detritus predominantly but also catches *Sagitta,* smaller crustaceans, and is cannibalistic in the laboratory (Lebour, 1925). Similarly, *Meganyctiphanes norvegica* consumed plant detritus when it was present in the water, but also fed on *Calanus finmarchicus, Paraeuchaeta norvegica* and smaller copepods (MacDonald, 1927). Very probably most euphausids are omnivorous, but it is difficult to explain their extreme sensitivity to deficiencies of the laboratory environment.

RESPIRATION IN RELATION TO SIZE OF PLANKTONIC ORGANISM

It is generally believed that the respiratory rate of poikilothermal animals is related to some power of body weight by the expression

$$R = kW^{x} \tag{1}$$

where R is the volume of oxygen consumed, W the body weight, k a constant for a given set of conditions, and x is the exponent, generally between 0.66 and 1.00. When oxygen consumption is plotted against weight on log log paper the data should give a straight line with a regression coefficient equivalent to x in equation (1).

Raymont and Gauld (1951) obtained a regression coefficient of 2.19 (or 2.30 with a single aberrant value removed) when log respiration was plotted against log length of the cephalothorax for four species of marine copepods ranging in length over a size range of nearly an order of magnitude. If it is assumed that weight varies as the cube of the length, then the coefficient obtained by Raymont and Gauld becomes 0.73 (or 0.77) in the form of equation (1).

In the case of nine species of small neritic copepods, Conover (1959) computed an overall regression coefficient of 0.86 for log respiration against log dry weight. For these copepods with a total size range considerably less than an order of magnitude, weight was found to vary as the power 3.17 of cephalothorax length.

The range of variation in weight of the organisms included in the current investigation is nearly four orders of magnitude and the variation in respiratory rate per organism is likewise considerable (Table I). A log log plot of respiration against weight would be expected to give a straight line relationship with a positive regression coefficient. However, if the respiration rate is first divided by the weight of the animal, the log log plot of this value R' against weight W should yield a negative regression coefficient. Of the two methods, the second shows more clearly the decrease in metabolic rate with increasing size, and its use should save a step in the calculation of energy flow and production rates.

The least squares regression on double logarithmic coordinates of the respiratory rates as μl. oxygen/mg. dry weight and day plotted against dry weight in μg., excluding only the values for *Calanus finmarchicus* at 18.5° C. and those for *Pleuromamma robusta,* gives the equation

$$\log R' = -0.35 \log W + 2.2888. \qquad (2)$$

In exponential form equation (2) becomes

$$R' = 194\ W^{-0.35}. \qquad (3)$$

For comparative purposes, equation (3) may be converted to the form of equation (1) by replacing R' with its equivalent R/W,

$$R = 194\ W^{0.65}. \qquad (4)$$

It can be readily seen that the exponential constant in (4) is decidedly lower than that observed by Conover (1959), and also is lower than the probable exponent computed from Raymont and Gauld (1951). Weymouth *et al.* (1944) obtained a coefficient of 0.798 for *Pugettia producta* and Vinberg (1950) recorded 0.81 for

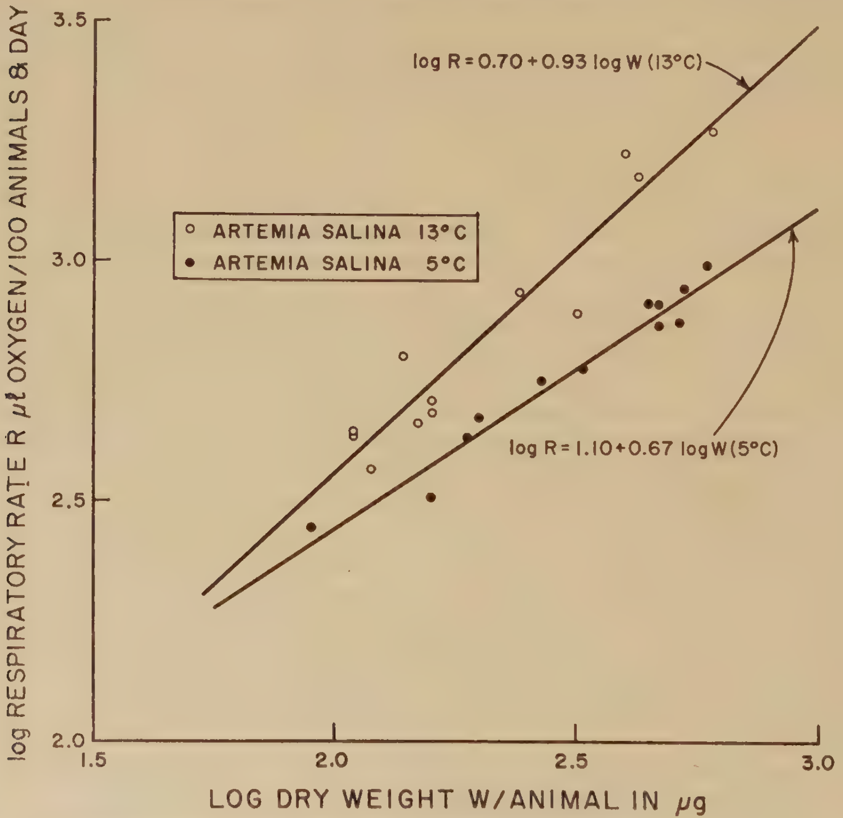

FIGURE 1. Regression lines for *Artemia salina,* showing log respiration in μl. O_2 animal and day plotted against log dry weight at 5° and 13° C.

TABLE II

Analysis of variance for regression of log respiration against log dry weight at two temperatures for Artemia salina

Null hypothesis: That there is no difference in regression coefficients for log respiration against log weight measured at 5° and 13° C.

Sources of variation		Degrees of freedom	Sums of squares	Mean square	Variance ratio
5° C.	Linear relation	1	0.319323	0.319323	173.73
	Error about line	10	0.018383	0.001838	—
13° C.	Linear relation	1	0.625688	0.625688	103.16
	Error about line	10	0.060651	0.006065	—
	Combined slope	1	0.921432	0.921432	233.17
	Between regression coefficients	1	0.023579	0.023579	5.97
	Combined error	20	0.079034	0.003952	

Variance ratio F for difference between regression coefficients = 5.97; $F_{0.975}$ (1, 20) = 5.87. Since F (1, 20) >5.87, reject null hypothesis.

Gammarus lacustris. Assuming that surface area is proportional to the square of length and that weight is proportional to the cube of length, von Bertalanffy (1951) suggested that an exponential constant of 0.667 indicates direct proportionality of metabolism to the relative surface area of the organisms. The exponential constant from equation (4) might, therefore, suggest that the surface rule applied in the case of the zooplankton investigated in the current study but not for the earlier work. However, there is also the possibility that the lower coefficient of proportionality observed here may result from the different temperature at which the experiments were run. In contrast with the temperatures of 4–8° C. used in the present work, Raymont and Gauld (1951) performed their experiments at about 17° C. and Conover (1959) used 20° as the experimental temperature. Vinberg (1950) and Weymouth *et al.* (1944) also used temperatures appreciably higher than those in the present work.

To test the hypothesis that the temperature at which a series of experiments is performed with different sized organisms might affect the proportionality of respiratory rate to size, an initial experiment with three species of calanoid copepods, ranging in weight from 0.017 to 5.45 mg., was set up at two temperatures, 5° and 13° C.; however, the scatter around the least squares regression lines was too great to permit disproof of the null hypothesis that there was no difference in the log log regression coefficient of respiration against weight at the chosen temperatures. A second experiment at the same two temperatures was then performed with a single species, *Artemia salina,* which can be cultured in the laboratory so as to supply a number of different size classes. The least square regression lines for log respiration against log weight for *Artemia* at 5 and 13° C. are shown in Figure 1. The regression coefficients, 0.67 at 5° C. and 0.93 at 13° C., can be demonstrated to be statistically different at $P = 0.025$ (Table II). According to von Bertalanffy (1951) the two regression coefficients obtained here for the same animal would be indicative of two very different metabolic types.

So long as the Q_{10} for any temperature change is the same for an animal over its entire size range, the regression of respiration against weight should give the same coefficient of proportionality regardless of the experimental temperature. In this regard, Rao and Bullock (1954) reviewed data from several sources, and concluded that the Q_{10} of various measures of activity commonly increases with increasing size over the range of ordinary physiological temperatures, although there were several cases in which the trend was reversed. *Artemia* was not one of the animals considered by Rao and Bullock, but the present data would seem to suggest that this animal does have a Q_{10} which varies with size.

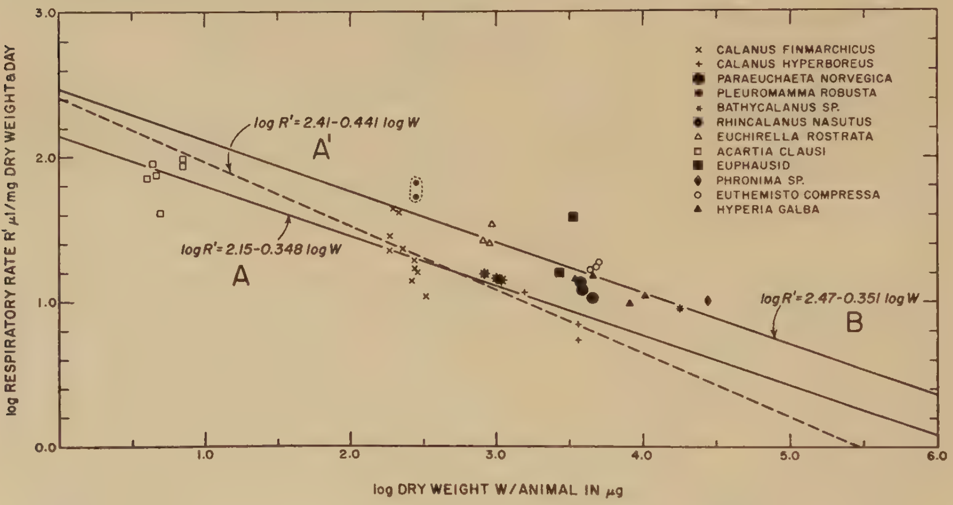

FIGURE 2. Scatter diagram and regression lines showing the relation between log respiration in µl. O_2/mg. dry weight and day and log dry weight in µg. Line A is fitted to data for suspected herbivores. Line A′ is fitted to data for herbivores, omitting values for *Acartia clausi.* Line B is fitted to data for suspected carnivores. See text for further explanation.

In the case of studies involving several different organisms taken from nature, there is the additional complexity of species differences in Q_{10}. Rao and Bullock (1954) also showed that the habitat temperatures of the animal prior to examination could affect Q_{10}. In this regard, Berg and Ockelmann (1959) observed a seasonal shift in the size-respiration relationship for the fresh-water snail *Lymnaea palustris.* Other factors, such as nutritional status, reproductive activity or some endogenous rhythm, might lead to increased variability in the observations. The resultant of one or several factors of the sort described here might be to increase or decrease the spread of values at one end of the temperature scale while having the opposite effect at the other end, regardless of the size of the animals being studied. Both the slope of the regression line and the scatter of points around it would be affected.

RESPIRATION IN RELATION TO FOOD HABITS

It was noted early in the study that *Calanus hyperboreus* and *Paraeuchaeta norvegica* taken in the same tow and studied under the same conditions had different respiratory rates despite their similarity in size and weight (see Table I). Both animals were kept in the laboratory for a lengthy period, and it became obvious that one, *Calanus hyperboreus,* was principally herbivorous while the other was entirely carnivorous. Raymont (1959) found that *Tortanus discaudatus,* also believed to be a carnivore, appeared to have a higher metabolic rate in relation to its body size than other copepods inhabiting the same type of environment.

In Figure 2 the respiratory rate at low temperatures for all the animals studied has been plotted against their weight on double log paper. On examination of the scatter diagram it seemed that the suspected carnivores in general had higher rates than the known herbivores. To test this hypothesis, separate regression lines were fitted to the data for the herbivores, *Calanus finmarchicus, C. hyperboreus, Rhincalanus nasutus,* and *Acartia clausi* (line A), and a second line fitted for the suspected carnivores, *Paraeuchaeta norvegica, Bathycalanus, Euchirella rostrata, Phronima, Euthemisto compressa, Hyperia galba,* and the euphausids (B). For the herbivores an additional regression line was also computed, omitting the data for *Acartia* since it had been acquired originally for different reasons (A′). Obviously the slope of the regression lines for the herbivores (including *Acartia* data) and the non-herbivores is not significantly different (0.348 and 0.350, respectively). With the *Acartia* data omitted the slope of the regression line fitted to the herbivore data becomes 0.441, but it can be shown statistically (Student's t test) that the slopes are still not significantly different.

TABLE III

Analysis of covariance for respiratory rates of herbivores (Acartia clausi *included*) *and non-herbivores*

Null hypothesis: That there is no difference in the respiration rate per mg. of dry body weight for herbivorous and non-herbivorous zooplankton

Sources of variation	Degrees of freedom	Sums of squares for respiration	Sums of products for respiration and weight	Sums of squares for weights	Errors of Estimate		
					Sums of squares	Degrees of freedom	Mean square
Total	38	3.76580	−10.74861	43.19223	1.09095	37	
Between animals having different food habits	1	0.38487	−2.80085	20.38336			
Within each type	37	0.38093	−7.94776	22.80887	0.61153	36	0.01699
For test of significance of mean respiration with effect of weight removed					0.47942	1	0.47942

Variance ratio $F = \frac{0.47942}{0.01699} = 28.2$; $F_{0.999}(1, 40) = 12.61$. Since $F(1, 36) > 12.61$, reject null hypothesis.

To test the null hypothesis that there is no difference between the regression lines for herbivores and non-herbivores, an analysis of covariance was employed as shown in Table III. Since the slope for the herbivorous animals was not affected by removing the *Acartia* data, it was decided to include this in the overall analysis. It is one of the advantages of covariance analysis that differences between groups of measurements can be tested in a single operation without the effect of other measurements that would normally complicate the interpretation. Thus, errors of estimate are calculated from the sums of squares and sums of products in such a way that the variance ratio tests only the respiratory rates after adjustment to remove the effect of the variable weight. Since the F test suggests that the distribution of respiration rates in relation to feeding type observed here would occur by chance much less than one time in a thousand, clearly the reason for the distribution bears some consideration.

Certain of the non-herbivorous zooplankton organisms studied were observed to be quite dense, with a hardened exoskeleton. Thus, organisms such as *Euchirella rostrata, Euthemisto compressa,* and *Hyperia galba* are presumably carrying around a considerable weight of inert organic material. More muscle protein, also quite dense, and more energy would be required to maintain the organism in the water column against its negative buoyancy.

There is little doubt that many herbivorous copepods also carry a high portion of their body weight as inert organic material, but in this case the substance may be oil with a positive buoyancy. In the case of the large *Calanus hyperboreus,* copepods of approximately the same external dimensions may differ in dry weight by several hundred per cent because of differences in the amount of stored oil.

It is also probable that a carnivorous animal is normally more active than an herbivorous one, regardless of their basal metabolic rates. The predator has to move about actively in search of the prey and then must overcome the natural reluctance of the prey to be caught by using its greater physical strength and swiftness. On the other hand, the prey organism in this association is more often than not the herbivorous copepod which can feed while it swims with a more or less continuous expenditure of a smaller amount of energy, since its food has at best extremely feeble power of escape.

Finally the possibility remains that a real difference could exist in the form of the organic matter oxidized by the herbivore and non-herbivore. Thus, an organism which burns carbohydrate exclusively would use decidedly less oxygen per unit of carbon oxidized than one which metabolizes oxygen-poor fats.

Before leaving the subject of respiration, a few remarks should be made concerning *Pleuromamma robusta* and its somewhat enigmatic position metabolically. As remarked earlier, it would appear that this species belongs in the herbivorous group, but so far as its respiration is concerned the organism would seem to be more closely allied to the non-herbivores. Clearly, with only two points on the graph it is not certain that any real difference exists between this and other herbivorous forms so far as respiration is concerned, and yet it remains possible that the very high metabolic rate observed for this form may be in some way related to the fact that it has a powerful bioluminescent organ. The species should certainly be given further attention.

Discussion

There is a persistent tendency for the biologist working with the most complex of organized systems to seek a simple solution or approximation which holds for the majority of cases. Thus certain scientific "laws" as $Q_{10} = 2$, metabolism equals a constant times weight to some power between 0.7 and 0.8, weight equals cube of length, and so on have come into common usage in environmental studies. Most of these "laws" had their origin in laboratory studies on mammals and they need reexamination before being applied to many ecological situations. It would be a great advantage to the biological oceanographer to have a single expression which would predict the metabolism of a population of organisms with a given size distribution under any temperature conditions, but as more data become available the evidence would suggest that such a prediction equation, if it is ever formulated, will give a high-speed computer a good workout.

The relationship between metabolism and size in the warm-blooded organisms on the average has the form

$$M = 70W^{0.74} \text{ cal./day}, \qquad (5)$$

but as Kleiber (1947) admits, the basis for this relationship is not really understood for the best known group of mammals. In the case of warm-blooded organisms metabolism is usually measured at or near the same temperature and the necessity to maintain this temperature against external environmental temperatures often very different would seem to give some importance to the relative surface area across which heat would be lost or gained.

In the sea, among the cold-blooded organisms there is tremendous variety in body form, biochemical mechanism and chemical composition. The surface of the marine organism is important for several reasons. Besides heat, nutrient substances, excretory substances, and gases pass back and forth across body membranes, and the frictional resistance of the surface area with the surrounding medium is critical for all organisms which move from place to place, whether they swim or are carried by their environment. It would seem very coincidental indeed should all the myriad forms of life be governed by a law derived from the warm-blooded organisms.

Among the marine invertebrates these problems have been examined in detail only for the Crustacea, and here it is true that there are relationships between metabolism and size very similar to those derived for homeothermal organisms. However, the effect of environmental temperatures on these relationships has not been given much prior consideration.

That other factors besides size and the direct effect of temperature influence respiratory rates of zooplankton forms has also been demonstrated recently. Conover (1956) observed a possible seasonal adaptation to the changing temperature regime for *Acartia clausi* and *A. tonsa*. Subsequently Conover (1959) and Marshall and Orr (1958) demonstrated seasonal differences in the respiration rate of several neritic species. Conover (1959) also demonstrated a significant difference between the respiratory rate of *Acartia clausi* in Long Island Sound and in Southampton Water. It can be seen from Table I of this study that *Calanus finmarchicus* had a decidedly higher respiratory rate on Georges Bank than in the Gulf of Maine. In this case, the populations are separated by not more than a hundred miles of water. To this list can now be added the difference in metabolism between organisms belonging to the same community but differing in their position within the food chain.

As a final note of complexity to the already confused picture of metabolic relationships for the planktonic organisms, it must be emphasized that even though reliable data were available for respiration per unit mass for a group of organisms, conversion of this information to food requirements or energy flow might introduce an appreciable error, due to insufficient knowledge regarding the nature of the food substance oxidized. It is well known that an animal requires more oxygen to oxidize fat than to oxidize carbohydrate. Although more energy is produced per volume of oxygen used in the case of carbohydrate metabolism, there is also more energy available per gram of fat than per gram of carbohydrate. Raymont and Conover (unpublished data) observed that several zooplankton organisms oxidized carbon in some form at a rate of at least ten times greater than changes in their carbohydrate reserves would predict. For instance, in the case of *Calanus hyperboreus*, the respiration rate was equivalent to an oxidation of 10 to 20 μg. of carbohydrate per day, an amount somewhat greater than the total carbohydrate content of the animals, and yet there was no detectable change in the total sugars.

It is becoming increasingly popular among environmental biologists to think of production as a single dynamic process which can be made to conform to some idealized mathematical model. Such an approach has had useful application, for instance in the North Sea pelagic fishery studies by Cushing (1955, 1959). Yet, as Steele (1960) points out, herring eat *Calanus* but they do not eat salps, even though each has a similar position in the food chain. Perhaps it is fortunate that salps are not particularly abundant in the North Sea! In any event, there would seem to be a good argument in favor of an increased emphasis on certain qualitative aspects of energy dynamics and food relations in the marine environment as a supplement to the purely quantitative approach.

SUMMARY

1. The respiration rate of twelve species of zooplankton, the majority from oceanic waters and from depths greater than 100 meters, has been measured at temperatures close to that of their environment (4–8° C.). In most cases healthy specimens were brought to the laboratory and their food habits and behavior studied.

2. The following species seemed largely herbivorous: *Calanus finmarchicus, C. hyperboreus,* and *Rhincalanus nasutus.*

3. The copepod *Paraeuchaeta norvegica,* and the amphipods *Euthemisto compressa* and *Hyperia galba* all took animal food readily. *Bathycalanus* sp., *Euchirella rostrata* and the euphausids also are believed to be at least partially carnivorous although they demonstrated little or no feeding.

4. The animals studied had a total range in dry weight of nearly four orders of magnitude. When log respiration was correlated with log weight, a positive linear regression coefficient of 0.65 was obtained. This value, which is lower than most previously determined regression coefficients relating size and metabolism in the Crustacea, may result from the lower temperatures used in these experiments compared with those used in the earlier work.

5. As confirmatory evidence, size and metabolism were related by a coefficient of 0.67 at 5° and 0.93 at 13° in the case of *Artemia salina.*

6. Those zooplankton animals which seemed to be largely carnivorous on the basis of the behavioral studies had a significantly higher respiratory rate than those which seemed to be predominantly herbivorous.

7. Some of the possible explanations and ecological implications of the above-mentioned observations are discussed.

LITERATURE CITED

Berg, K., and K. W. Ockelmann, 1959. The respiration of freshwater snails. *J. Exp. Biol.,* **36**: 690–708.

von Bertalanffy, L., 1951. Metabolic types and growth types. *Amer. Nat.,* **85**: 111–117.

Bigelow, H. B., 1925. Plankton of the offshore waters of the Gulf of Maine. *Bull. U. S. Bur. Fish.,* **40**, pt. II, 509 pp.

Conover, R. J., 1956. Oceanography of Long Island Sound, 1952–1954. VI. Biology of *Acartia clausi* and *A. tonsa. Bull. Bingham Oceanogr. Coll.,* **56**: 156–233.

Conover, R. J., 1959. Regional and seasonal variation in the respiratory rate of marine copepods. *Limnol. and Oceanogr.,* **4**: 259–268.

Conover, R. J., S. M. Marshall and A. P. Orr, 1959. (unpublished report) Feeding and excretion of *Calanus finmarchicus* with reference to the possible role of the zooplankton in the mineralization of organic matter. WHOI Ref. no. 59–32.

Cushing, D. H., 1955. Production and a pelagic fishery. *Fish. Invest., Lond., ser. II,* **18**: 104 pp.

Cushing, D. H., 1959. On the nature of production in the sea. *Fish. Invest. Lond., ser. II,* **22**: 40 pp.

Kleiber, Max, 1947. Body size and metabolic rate. *Physiol. Rev.,* **27**: 511–541.

Lasker, R., 1960. Utilization of organic carbon by a marine crustacean: analysis with carbon-14. *Science,* **131**: 1098–1100.

Lebour, M. V., 1925. The Euphausiidae in the neighbourhood of Plymouth and their importance as herring food. *J. Mar. Biol. Assoc.,* **13**: 402–429.

Lowndes, A. G., 1935. The swimming and feeding of certain calanoid copepods. *Proc. Zool. Soc. Lond.,* **1935**: 687–715.

MacDonald, Roderick, 1927. Food and habits of *Meganyctiphanes norvegica. J. Mar. Biol. Assoc.,* **14**: 753–784.

Marshall, S. M., and A. P. Orr, 1955a. The biology of a marine copepod *Calanus finmarchicus* (Gunnerus). Oliver and Boyd, Edinburgh, 187 pp.

Marshall, S. M., and A. P. Orr, 1955b. On the biology of *Calanus finmarchicus.* VIII. Food uptake, assimilation, and excretion in adult and stage V *Calanus. J. Mar. Biol. Assoc.,* **34**: 495–529.

Marshall, S. M., and A. P. Orr, 1958. On the biology of *Calanus finmarchicus.* X. Seasonal changes in oxygen consumption. *J. Mar. Biol. Assoc.,* **37**: 459–472.

Marshall, S. M., A. G. Nichols and A. P. Orr, 1935. On the biology of *Calanus finmarchicus.* VI. Oxygen consumption in relation to environmental conditions. *J. Mar. Biol. Assoc.,* **20**: 1–27.

Pütter, August, 1907. Die Ernährung der Wassertiere. *Zeitschr. allg. Physiol.,* **7**: 283–320.

Pütter, August, 1909. Die Ernährung der Wassertiere und der Stoffhaushalt der Gewasser. U. G. Fischer, Jena. 168 pp.

Rao, K. P., and T. H. Bullock, 1954. Q_{10} as a function of size and habitat temperature in poikilotherms. *Amer. Nat.,* **88**: 33–44.

Raymont, J. E. G., 1959. The respiration of some planktonic copepods. III. The oxygen requirement of some American species. *Limnol. and Oceanogr.,* **4**: 479–491.

Raymont, J. E. G., and D. T. Gauld, 1951. The respiration of some planktonic copepods. *J. Mar. Biol. Assoc.,* **29**: 681–693.

Sømme, J. D., 1934. Animal plankton of the Norwegian coast waters and the open sea. *Rept. Norweg. Fish. Invest.,* **4**(9): 163 pp.

Steele, J. H., 1960. Plant-animal food cycles in the sea. *Nature,* **185**: 218–219.

Vinberg, G. G., 1950. Intensity of metabolism and the size of Crustacea. *Zhur. Obsch. Biol.,* **11**: 367–380. (In Russian)

Weymouth, F. W., J. M. Crisman, V. E. Hall, H. S. Belding and J. Field II, 1944. Total and tissue respiration in relation to body weight: a comparison of the kelp crab with other crustaceans and with mammals. *Physiol. Zoöl.,* **17**: 50–71.

Contribution No. 1116

Reprinted from
BULLETIN OF MARINE SCIENCE
OF THE GULF AND CARIBBEAN
Vol. 10, No. 4, pp. 485-490
DECEMBER, 1960

COPEPODS OF THE GENUS *OITHONA* FROM THE GULF OF MEXICO[1]

GEORGE D. GRICE
Woods Hole Oceanographic Institution

ABSTRACT

Five species of *Oithona (O. plumifera, similis, brevicornis, nana* and *simplex)* are reported from the Gulf of Mexico. Their distribution is indicated and a key is presented for their identification.

INTRODUCTION

The genus *Oithona* (Copepoda: Cyclopoida) is frequently represented in marine zooplankton samples by one or more species and numerous individuals. In a monograph on the genus, Rosendorn (1917) recognized twenty species of *Oithona* and two other species of a related genus, *Paraoithona.* He presented figures of the species and provided taxonomic keys for their identification. Additional descriptions and keys are included by Kiefer (1929) and his treatment of the genus.

COLLECTING AND IDENTIFYING

Although the species of *Oithona* are widely distributed and occur in all types of marine environments (estuarine, neritic and oceanic waters), they may, nevertheless, be easily overlooked. This can result from the use of a coarse collecting net which permits them to escape through the mesh, or, when they are detected in a plankton sample, the confusion of two or more species because of their superficial similarity. As many of the estuarine and inshore-neritic species of *Oithona* are quite small (commonly 0.45 to 0.80 mm), it is necessary to use a fine mesh net in order to collect them. A No. 10 net is recommended for obtaining those species which occur along the Gulf coast. Once collected, the individuals need to be more or less completely dissected in order to make reliable determinations.

PREVIOUS RECORDS FROM THE GULF OF MEXICO

Five species of *Oithona* have been reported from the Gulf of Mexico. Four of these have been recorded from estuarine and neritic waters of the Florida west coast and one species from the Louisiana coast. These five species cannot, however, be considered as the sole representatives of this genus in the Gulf of Mexico. The cyclopoid

---

[1] Contribution No. 1116 from the Woods Hole Oceanographic Institution, Woods Hole, Massachusetts. Manuscript prepared while the author was employed on U.S. Atomic Energy Commission Contract AT(30-1)—1918.

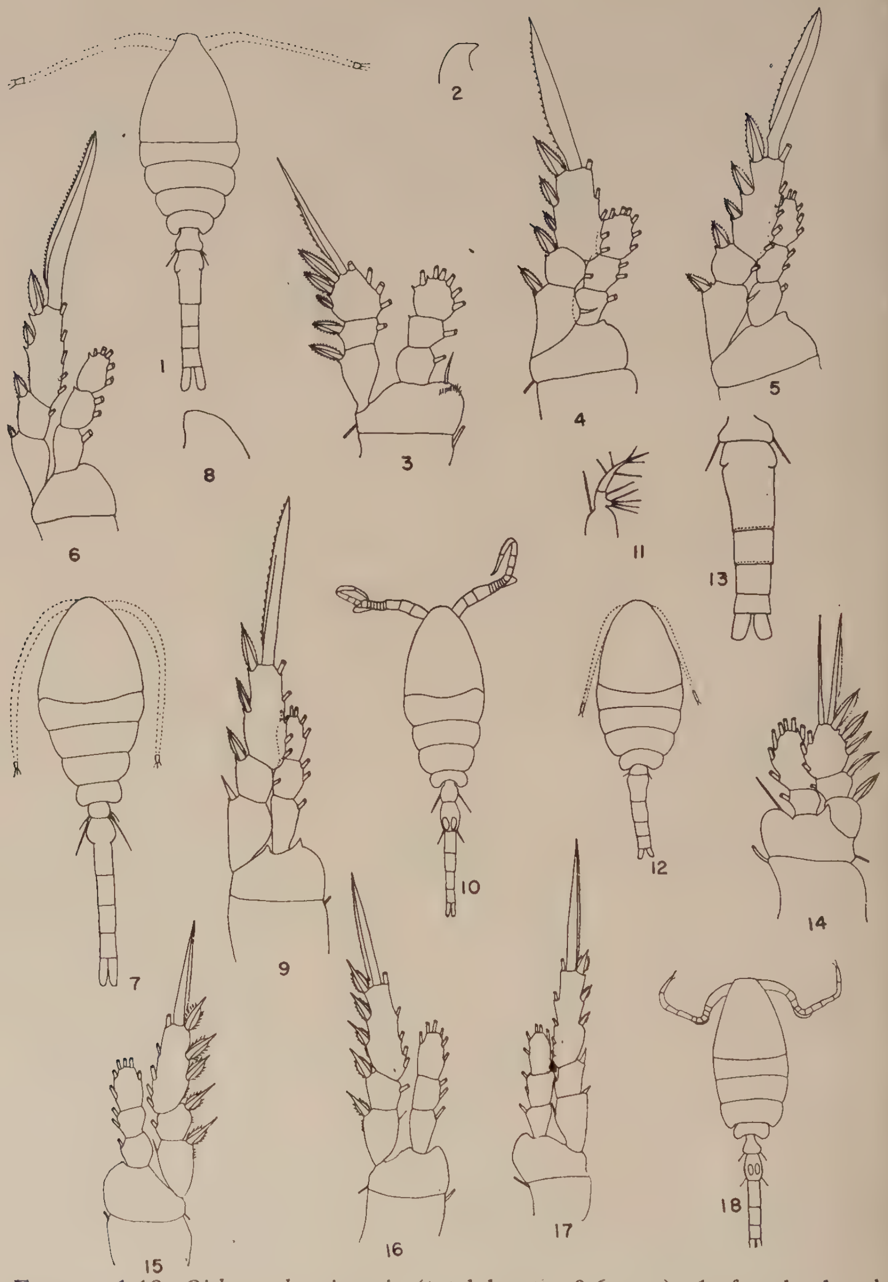

FIGURES 1-18. *Oithona brevicornis* (total length, 0.6 mm). 1, female dorsal view; 2, tip of forehead, lateral view; 3, first foot; 4, second foot; 5, third foot; 6, fourth foot. *Oithona nana* (total length, 0.75 mm). 7, female, dorsal view; 8, tip of forehead, lateral view; 9, fourth foot; 10, male (total length, 0.60 mm) dorsal view; 11, second basipod segment of mandible. *Oithona simplex* (total length, 0.49 mm). 12, female, dorsal view; 13, posterior part of body; 14, first foot; 15, second foot; 16, third foot; 17, fourth foot; 18, male (total length, 0.47 mm) dorsal view. *O. brevicornis, O. nana* and the female *O. simplex* drawn from specimens collected three miles off Alligator Harbor in December, 1954. The male *O. simplex* drawn from a specimen collected three miles off the mouth of the Marco River in October, 1954.

copepods of waters beyond the continental shelf and of most neritic areas of the Gulf exclusive of the Florida coast have not been studied and it is probable that several additional species will be added when the plankton of these areas become better known.

NOTES ON THE SPECIES

Oithona plumifera Baird.—This species is an inhabitant of the offshore waters of the Florida west coast. It is not likely to be taken nearer to shore than about ten miles except in the Panama City and Pensacola areas where several typical offshore species occur (see Grice, 1960). Although not figured here, *O. plumifera* is easily distinguished from the four other species. The female has a prominent rostrum which is visible in dorsal view and the male is distinguished by a combination of specific characters given in the key below. The total length of the female is about 1.3 mm while that of the male is about 0.9 mm.

O. plumifera has been reported from the Florida west coast by Davis (1950)), King (1950) and Grice (1960).

Oithona similis Claus.—This species has been reported by Foster (1903), who stated that he found it in St. John's Bayou and Calcasieu Pass on the Louisiana coast. There are no other records of it from the Gulf of Mexico. Rosendorn (1917) gives the length of female *O. similis* as 0.78 mm and that of male as 0.67 mm.

Oithona brevicornis Giesbrecht (Figs. 1-6).—This is a very abundant and widespread species. It occurs along the entire Florida west coast but chiefly in estuarine and nearshore waters. The female varies in length from .50 to .60 mm. The male of this species is apparently quite rare. Figures of this sex are given by Rosendorn (1917) and later by Wilson (1932a).

This species has been recorded from Alligator Harbor (Grice, 1956) and from the Florida west coast and Florida Keys (Grice, 1960).

Oithona nana Giesbrecht (Figs. 7-11).—I here follow Rosendorn (1917) and Kiefer (1929) in referring this species to the genus *Oithona* rather than to the genus *Oithonina* as first proposed by Sars (1918) and later diagnosed by Wilson (1932b).

O. nana is another widespread species which occurs in estuaries as well as in neritic waters of the Florida west coast. Like the above species, it is an abundant member of the copepod plankton. In length the female varies from 0.58 to 0.76 mm and the male from 0.51 to 0.53 mm.

This species has been reported from Florida by Gunter *et al.* (1948), Davis (1950), Davis and Williams (1950), King (1950) and Grice (1956, 1960).

Oithona simplex Farran (Figs. 12-18).—Gulf of Mexico specimens diverge slightly from those described by Farran (1913) in two respects. The first segment of the endopod of the first pair of feet has one seta and the second segment of the exopod of the fourth pair of feet has one inner seta. These segments as described and figured by Farran have 0 and 2 setae, respectively.

In discussing this species, Rosendorn (1917) stated that the endopod of the first pair of feet consists of three segments and not two as shown by Farran. My specimens agree with Farran's in this respect. There is also some confusion regarding the number of setae on the third endopodal segment of the fourth pair of feet. Rosendorn apparently misinterpreted Farran's method of presenting the number and position of the setae on the various endopodal segments of the swimming feet. Rosendorn stated that there are four setae on Farran's figure of the third endopodal segment of the fourth feet and not three setae as he (Farran) mentioned in the text. Actually, Farran indicated in his seta formula that there were three inner edge and one outer edge seta on this segment. In addition there is one seta on the terminal part of the segment which Farran shows in his figure but does not mention in the seta formula given in the text. There is thus a total of five setae on the third endopodal segment of the fourth feet which is also the number present on Gulf of Mexico specimens.

O. simplex is another widespread and abundant species. It has been found in estuaries and neritic waters of the entire Florida west coast (Grice, 1960). I have also found it in samples collected throughout the year at stations located fifteen miles off the Florida west coast.

According to Rosendorn (1917), this is the smallest species in the genus. In length the female varies from 0.44 to 0.49 mm and the male from 0.44 to 0.48 mm.

O. simplex has been reported from the Florida west coast and Florida Keys by Grice (1960).

KEY TO THE SPECIES

The following key is modified from one presented by Rosendorn (1917). It is applicable only to those species collected from estuarine and inshore-neritic waters of the eastern Gulf of Mexico, and even with these species it is desirable, of course, to check one's determination with the original description.

SEX

Posterior part of body consists of five segments,
 anterior antennae not geniculate ....female
Posterior part of body consists of six segments,
 anterior antennae geniculate ....male

FEMALE

(example of exopod spine formula used in key— 1, 1, 3 = 1 spine on outer margin of first segment, 1 spine on outer margin of second segment and 3 spines on outer margin of the third segment of the exopod)

I. Rostrum present
 A. In dorsal view, forehead extending in a point ....*O. plumifera*
 B. In dorsal view, forehead wide, not pointed
  a. Exopod segments of first pair of feet
   with 1, 1, 2 spines ....*O. similis*
  b. Exopod segments of first pair of feet
   with 1, 1, 3 spines ....*O. brevicornis*
II. Rostrum absent
 A. Exopod segments of fourth pair of feet with
  1, 1, 2 spines ....*O. nana*
 B. Exopod segments of fourth pair of feet with
  1, 1, 3 spines ....*O. simplex*

MALE

I. Exopod segments of first pair of feet with 1, 1, 3 spines
 A. Exopod segments of fourth pair of feet with
  1, 1, 2 spines
  a. Second basipod segment of mandible with
   two blunt projections ....*O. brevicornis*
  b. Second basipod segment of mandible with
   1 strong and 1 fine seta ....*O. nana*
 B. Exopod segments of fourth pair of feet with
  1, 1, 3 spines ....*O. simplex*
II. Exopod segments of first pair of feet with 1, 1, 2 spines
 A. Exopod segments of third pair of feet with
  1, 1, 2 spines ....*O. similis*
 B. Exopod segments of third pair of feet with
  1, 1, 3 spines ....*O. plumifera*

LITERATURE CITED

DAVIS, C. C.
 1950. Observations of plankton taken in marine waters of Florida in 1947 and 1948. Quart. J. Fla. Acad. Sci., 12(2): 67-103.
DAVIS, C. C. AND R. H. WILLIAMS
 1950. Brackish water plankton of mangrove areas in southern Florida. Ecol. 31(4): 519-531.
FARRAN, G. P.
 1913. Plankton from Christmas Island, Indian Ocean. II. On Copepoda of the genera *Oithona* and *Paraoithona*. Proc. Zool. Soc. London, 1913: 181-193.

FOSTER, E.

1903. Notes on the free-swimming copepods of the waters in the vicinity of the Gulf Biological Station, Louisiana. Gulf. Biol. Sta., 2nd Rep., (1903), Bull. 2: 69-79.

GRICE, G. D.

1956. A qualitative and quantitative seasonal study of the Copepoda of Alligator Harbor. Fla. State Univ. Studies, 22. Papers Oceanogr. Inst. Florida, 2: 37-76.

1960. Calanoid and cyclopoid copepods collected from the Florida Gulf Coast and Florida Keys in 1954 and 1955. Bull. Mar. Sci. Gulf & Carib., *10* (2): 217-226.

GUNTER, G., R. H. WILLIAMS, C. C. DAVIS AND F. G. W. SMITH

1948. Catastrophic mass mortality of marine animals and coincident phytoplankton bloom on the west coast of Florida, November 1946 to August 1947. Ecol. Monogr., *18*: 309-324.

KIEFER, F.

1929. Crustacea Copepoda. 2. Cyclopoida gnathostoma. Das Tierreich, pt. 53, 102 pp.

KING, J. E.

1950. A preliminary report on the plankton of the west coast of Florida. Quart. J. Fla. Acad. Sci., 12 (2): 109-137.

ROSENDORN, I.

1917. Copepoda 1: Die gattung *Oithona*. Wiss Ergebn. deutschen Tiefsee-Exped. *Valdivia*. *23*: 1-58.

SARS, G. O.

1918. Copepoda Cyclopoida. An account of the crustacea of Norway. Vol. 6.

WILSON, C. B.

1932a. The copepod crustaceans of Chesapeake Bay, Proc. U.S. nat. Mus., *80*: 1-54.

1932b. The copepods of the Woods Hole region, Massachusetts. Bull. U. S. nat. Mus., 158: iv-xix, 1-635.

Contribution No. 1124

Reprint from

Eclogae geol. Helv. 1958	Vol. 51	No. 3	Page 542	Basel, December 1958

A Study of the Relation between Dynamics and Sediment Pattern in the Zone of Shoaling Wave, Breaker, and Foreshore[1]

12. – ROBERT L. MILLER, (University of Chicago, U.S.A.), and JOHN M. ZEIGLER, (Woods Hole Oceanographic Institute U.S.A.): **A Study of the Relation between Dynamics and Sediment Pattern in the Zone of Shoaling Wave, Breaker, and Foreshore.** With 7 textfigures.

ABSTRACT

A theoretical model is presented, for the expected patterns of sediment size and sorting in the region of shoaling wave, breaker, and beach foreshore. This model is based on theoretical considerations and published experimental results, and is intended to hold for the above mentioned dynamic zones in a state of equilibrium. Comparison with detailed observations in three natural situations and with published sediment size and sorting patterns appear to give good agreement with the model. The implication is that such generalized patterns may serve in the recognition of departures from equilibrium and change in general environment in the study of contemporary sediments; and possibly in the recognition of dynamic environments in ancient rocks.

The interpretation and prediction of contemporary sediment patterns on beach and nearshore areas has attracted the attention of a number of investigations. In the present study we focus attention on that portion which extends from the breaker zone to the top of the foreshore and seaward to a depth not exceeding two fathoms. Our purpose is to combine published theoretical and experimental work in such a way as to formulate or predict sediment patterns, by using variables representing the water movements and the sediment size and degree of sorting1). The predicted patterns are then compared with observed patterns collected by us in various field locations and with published sediment patterns.

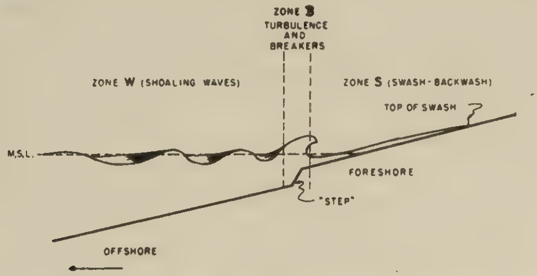

Fig. 1. The dynamic zones which characterize the surf region

---

1) The measure of sorting used in this paper differs from those customarily employed, in that the effect of size is removed from the measure of "spread" of the frequency distribution by deviding by the Median. Thus our sorting is defined as $S = (P_{80}-P_{20})/P_{50}$ e.g. P_{80} is the 80th percentile.

[1] Contribution No. 1124 from the Woods Hole Oceanographic Institution.

We take the point of view that the beach and surf region can be subdivided into several zones which are characterized by dynamics peculiar to that zone with resulting cut and fill leading to typical sorting and size patterns. Figure 1 shows the dynamic zones which we feel characterize the surf region.

The "step" is a topographic feature which appears when conditions are favorable, it is a distinct break in slope just under the average wave crest at the point of plunge. The zones will be discussed in some detail in the main body of the paper. In brief, Zone W is characterized by shoaling wave dynamics, Zone B, just at the breaking wave, and including the step when present, is characterized by extreme turbulence and vortices, and Zone S, the beach foreshore up to the limit of swash, is characterized by sheet flow first up then down the foreshore.

A considerable problem was encountered in reducing the relatively large amount of field data to a usable form. We chose to describe the sediment in terms of median and sorting values contoured over the study areas. However, the median sediment size and degree of sorting values are not contoured directly: rather a surface of best fit is passed thru all the sample points. This gives a pattern free of local irregularities in sediment size and degree of sorting. The technique of fitting surfaces to sedimentary data is described by MILLER (1956) for this context. In the present study the computations involved in fitting surfaces to the data were done by the high speed computor AVIDAC, at Argonne Laboratories in Chicago, and by I.B.M.

Zone of shoaling waves (W)

A hypothesis relating the dimensions of shoaling waves to the movement of sediment was proposed by P. CORNAGLIA and described briefly by MUNCH-PETERSON (1950). He says that sediment particles in shallow water will tend to move shoreward under the greater velocity of the crest of a wave. However as the water deepens (in a seaward direction) the forward movement under the crest is equalled by the backward movement under the trough. Net movement is zero and for a given size, a "null point" or "neutral line" can be established. Seaward of this null point the net movement aided by gravity, is seaward for that size; landward of the null point for the given size, the net movement is landward. Thus for a certain bottom slope and wave characteristic, each particle size has an individual null point.

The existence of these null points in a wave tank have been verified for a fixed slope of 1:15 by IPPEN and EAGLESON (1950). We have combined their equation in rearranged form (eqn. 1 appendix) with an equation for wave celerity due to AIRY (1842) (eqn. 2 appendix) and a nomogram for terminal fall velocity of spheres in water (ROUSE, 1937) to form prediction curves for the position of null points in a given region of shoaling waves, fig. 2. From these curves the position of the neutral lines for several beaches was computed. Before proceeding, careful examination of the Cornaglia proposition is necessary. Two models are examined.

Model I. *No seaward motion under gravity.* Fig. 3a shows a hypothetical situation in which a uniform size distribution is brought to equilibrium in its distribution, under the action of shoaling waves.

Model II. *Seaward movement of particles downslope from their null points.* Fig. 3b shows the expected equilibrium pattern for the initial uniform distribution. It is clear from inspection of the figure that median size tends to increase toward Zone B (the breaker zone) in either case. However, in Model I sorting improves shoreward. In Model II, sorting is uniformly excellent over the zone of shoaling waves.

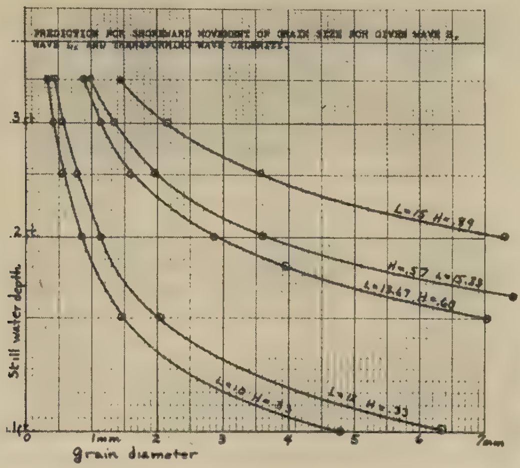

Fig. 2

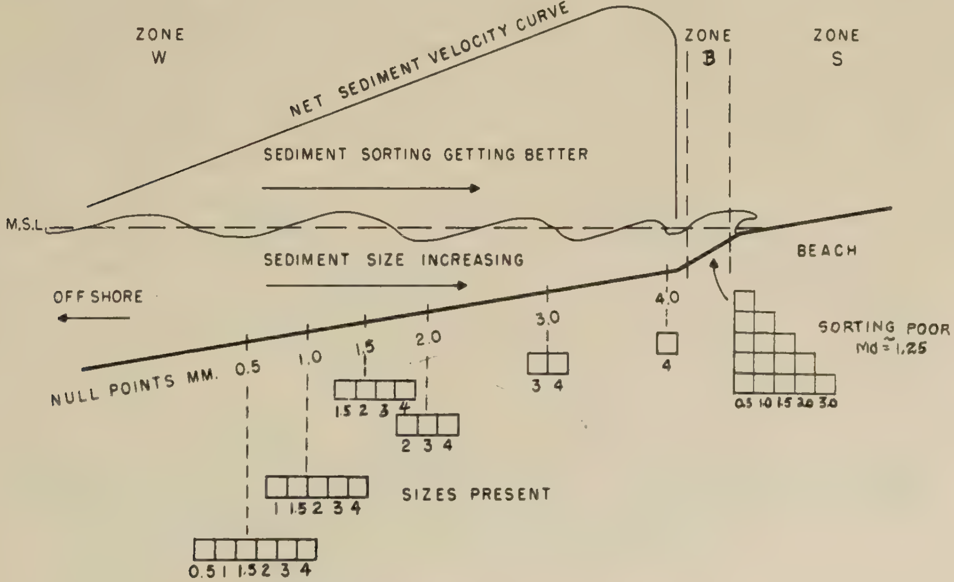
ZONE W
NET SEDIMENT VELOCITY CURVE
ZONE B
ZONE S
SEDIMENT SORTING GETTING BETTER
M.S.L.
SEDIMENT SIZE INCREASING
BEACH
OFF SHORE
NULL POINTS MM.
0.5
1.0
1.5
2.0
3.0
4.0
1.5 2 3 4
2 3 4
3 4
4
SORTING POOR
Md ≅ 1.25
0.5 1.0 1.5 2.0 3.0
SIZES PRESENT
1 1.5 2 3 4
0.5 1 1.5 2 3 4

Fig. 3a. No seaward motion under gravity

We now examine trend maps (polynomial surfaces of best fit to field data), for several places. (Figs. 4, 5, 6). These trend maps were taken at low tide in each instance. It was found by detailed studies of the effect of the tidal cycle, that the pattern established at low tide was reverted to, at the beginning of the next tidal

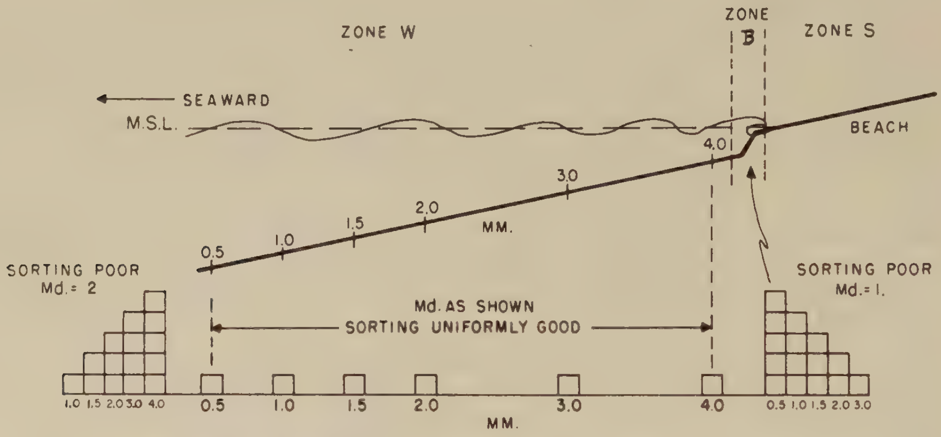
ZONE W
ZONE B
ZONE S
SEAWARD
M.S.L.
BEACH
4.0
3.0
2.0
1.5
1.0
0.5
MM.
SORTING POOR
Md.= 2
SORTING POOR
Md.= 1.
Md. AS SHOWN
SORTING UNIFORMLY GOOD
1.0 1.5 2.0 3.0 4.0
0.5
1.0
1.5
2.0
3.0
4.0
0.5 1.0 1.5 2.0 3.0
MM.

Fig. 3b. Seaward movement of particles downslope from their null points

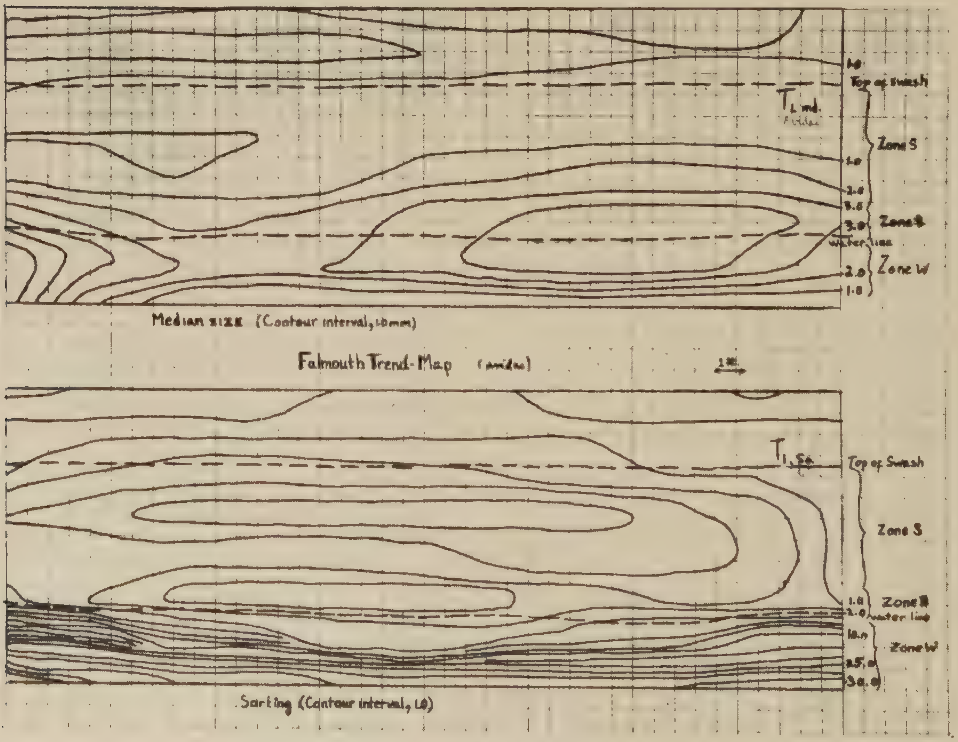
1.0
Top of swash
T_{L} md.
Zone S
1.0
2.0
3.0
3.0
Zone B
water line
2.0
Zone W
1.0
Median size (Contour interval, 1.0 mm)
Falmouth Trend-Map
T_{1} So.
Top of Swash
Zone S
1.0
Zone B
2.0
water line
Zone W
25.0
30.0
Sorting (Contour interval, 1.0)

Fig. 4

cycle. It is clear from examination of these trend maps at least, that our expectation under Model I is verified. We therefore tentatively propose that Zone W (shoaling waves) equilibrium conditions lead to a regular increase of median size contours toward the breaker zone, and a decrease in the sorting contours (improved sorting) toward the breaker zone.

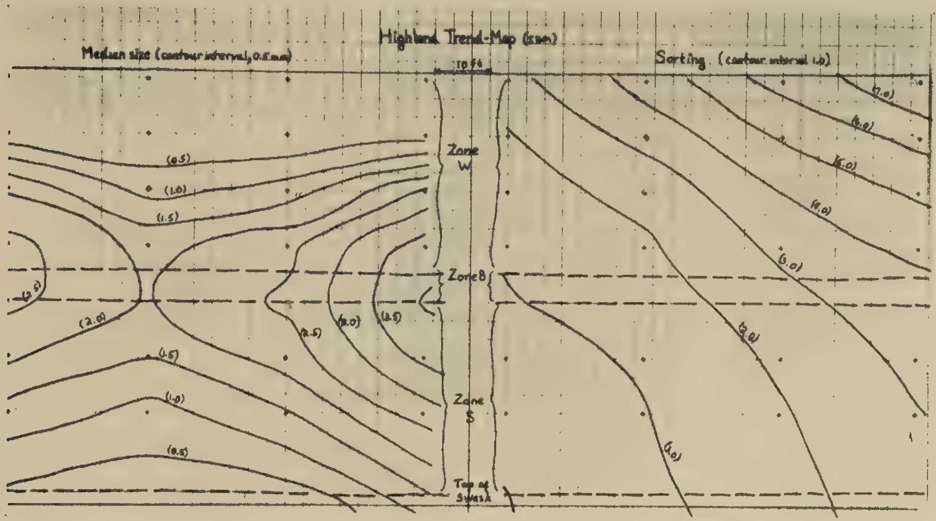

Fig. 5

Zone B, Breaker Zone

This is the region in which the forward net sediment velocity of Zone W drops to zero. It is where the breaking wave is met at its base by the returning backwash of a previous wave. The point of collision of the breaker and the swash, in our opinion is characterized by a turbulent region in which the net movement is vertically upward so that a sorting action occurs. Although the returning swash does not always catch the base of the next wave just at the point of plunging, it does so a majority of the time. The flow characteristics of the backwash are a function of the sope of the foreshore, the size of wave creating the parent swash, and the size of sediment on the foreshore. Just as the incoming breaker deposits its load, it is met by the returning backwash also carrying an accumulation of sediment. If the slope of the foreshore is sufficiently steep, a moderately well-sorted, relatively coarse "step" may be built in this turbulent zone.

The sediment which builds the "step" is derived in part from the load abruptly deposited by the incoming wave at this point. Thus the slope of the bottom in the near offshore is also important (see discussion in the section on Zone W, Shoaling waves). The remainder of the sediment is carried down the foreshore slope by the backwash from the previous wave.

In the way described above, a grading or sorting action occurs in the vertical direction within the breaking wave over Zone B. The finer material does not settle out as rapidly as the coarse material, and the finest is probably carried forward into the foreshore. We should, under these circumstances, expect that the coarsest material be concentrated at the step, whereas finer material should be found on both the seaward and landward sides. Our field observations have supported our hypothesis in part. Limitations in space do not allow presentation of tables and details. However, we found in repeated sampling of the breaker itself just at the point of breaking, a distinct gradation in a vertical direction in size and amount of sediment, from coarse and large volume at the bottom to fine and least volume at the top. Detailed traverses across the breaker zone in a horizontal direction at 14 separate beaches also showed consistent maxima in median size of sediment size at the breaker zone.

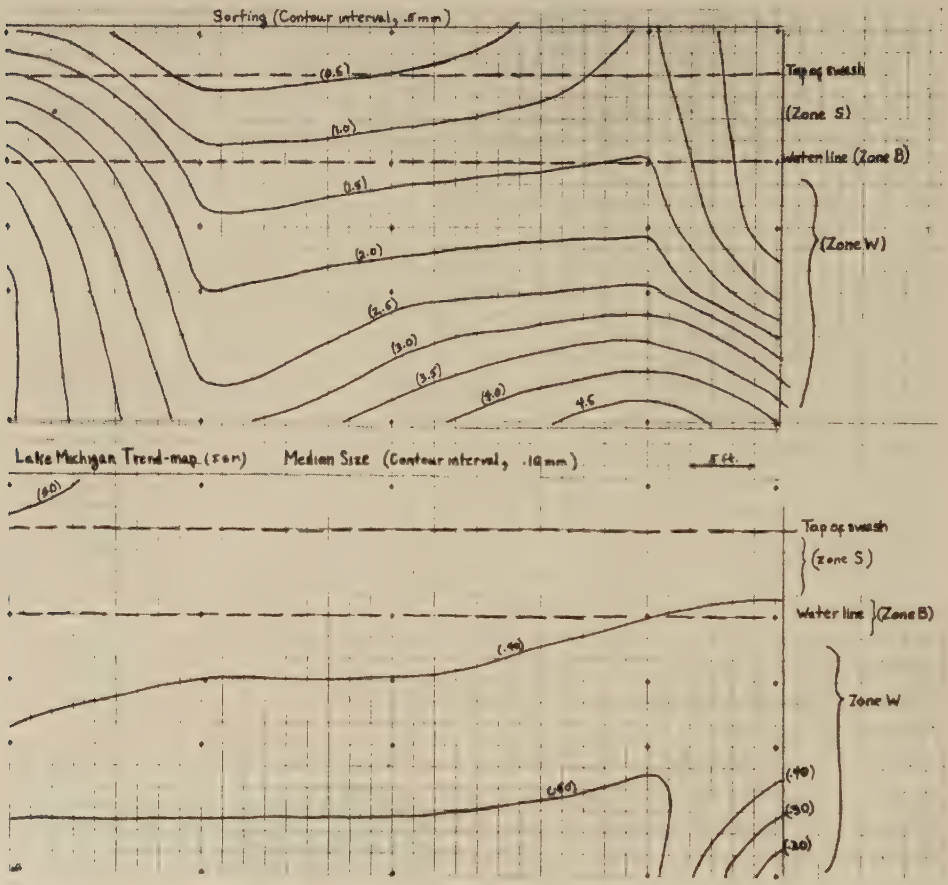
Sorting (Contour interval, .5mm)
(0.5)
(1.0)
(1.5)
(2.0)
(2.5)
(3.0)
(3.5)
(4.0)
4.5
Top of swash
(Zone S)
water line (Zone B)
(Zone W)
Lake Michigan Trend-map (sor)
Median Size (Contour interval, .10mm)
5 ft.
(.60)
Top of swash
(zone S)
Water line
(Zone B)
(.40)
Zone W
(.50)
(.40)
(.30)
(.20)

Fig. 6

In summary this section presents a hypothesis for the mechanism in the breaker zone which results in the sediment pattern consistently observed at this place in nature. The field evidence presented in this section supports the hypothesis of net vertical movement in the base of the turbulent breaker, with a secondary sorting action on the material thrown into suspension. It is clear however that the hypothesis presented is qualitative, and is only one possible explanation.

Foreshore (Zone S)

In this section we put together our field observations and field measurements of flow velocity, and published experimental observations, to form a model for the sediment pattern of the foreshore. The model will express our expectation of sediment size and sorting patterns. We then examine the natural pattern at several places in which the following information is available: slope of foreshore, average depth of backwash, and an estimate of the horizontal velocity gradient from top of swash to lower end of backwash return flow.

The model: The model consists of the following elements:

1. *An assumption as to the size and sorting pattern left just after the upwash has passed over the foreshore.* 2. *Consideration of the velocity required to start a grain of a given size moving downslope under the backwash.* In this instance, a relation between turbulent flow and initiation of sediment transport on a rough sloping bottom has been experimentally determined by IPPEN and VERMA (1953) (eqn. 3 appendix). 3. *Velocity distribution on the foreshore.* Surface velocity of backwash was measured over measured traverse normal to water edge by float and stop-watch. Repeated measurements were taken. For first approximation we assume a linear surface velocity gradient from zero at the initiation of backwash, to a maximum at the edge of Zone B (breaker zone). By using the measured velocity as an average in a horizontal sense, we have two points, and linear extrapolation gives the surface velocity at any point on the foreshore. 4. *Computation of theoretical contours of size and sorting on the foreshore.* By extrapolating in a vertical sense from the surface velocity (using an equation due to KREY (ROUSE 1938) (eqn. 4 appendix) we arrive at near bottom velocities. Now considering the edge velocity just required to move a grain on a rough bottom under turbulent flow, as determined by IPPEN and VERMA (loc. cit.) we may determine the position on a given foreshore where a certain grain size will begin to move down slope, taking into account the flow conditions.

We found that very nearly the complete range of sizes begins to move down slope within the upper 10% of the foreshore under backwash. If we therefore refer back to element 1 of the model, and assume a gradation of size from coarse at the foot to fine at the top of the foreshore *under swash* the following is implied by the model: (A.) a nexpected gradation of sediment sizes to coarsest at the foot of the foreshore, *under the backwash;* (B.) the sorting is more difficult to predict, but we would expect a rapid improvement in sorting in a downslope direction near the top of the foreshore and an irregular sorting pattern over the lower portions of the foreshore.

Examination of figs. 4, 5, 6 appear to support the above proposition, at least at the places investigated. A search of the literature also appears to lend credence to this hypothesis. See for example BASCOM 1951, EVANS 1939, KRUMBEIN 1938.

Summary and Discussion

Essentially this paper represents an effort to establish a pattern of sediment size and sorting, free of local fluctuation and representative of foreshore and nearshore in a state of equilibrium. The region is divided into three dynamic zones, zone W that of shoaling waves landward of nearshore bars, Zone B, the breaker zone, and Zone S, the swash-backwash zone. Each zone is treated separately. Published hypotheses, and experimental investigations which included the properties we could also measure in the field, were combined by us into model form, representing a proposed mechanism and a resulting sediment pattern. The model was then compared with trend-maps of several field locations in which very local fluctuations were removed. By substituting observed values for the parameters of the model a detailed comparison was made in the case of Falmouth Beach and nearshore. Highland Beach and Lake Michigan Beach were compared with the model in a less detailed way. And published lists were compared with the model for the foreshore zone.

In this way three levels of comparisons were made: first, where both wave and current data, and a trend map was available; second, trend map only; and third, published data only. Agreement of model with the natural cases although tempered by the information available, was still sufficiently good to warrant publication.

An immediate extension of the earlier discussion of Zone W is to consider the implications of two initial frequency distributions of sediment size which are closer to reality than that of the uniform distribution.

A. *Initial symmetrical frequency distribution, as an approximation to the normal distribution.*

A simplified frequency distribution using unit percent by weight with a median of 2·0 mm serves as a representative of the large class of approximately normal or moderately skewed distributions found in nature. As in the earlier discussion, assume this initial distribution is distributed over the near-shore region under discussion and that subsequently wave motion begins and continues until a stable pattern is established. We apply dynamic Model I (discounting seaward movement for the sizes under consideration). As in the simpler model using a uniform distribution, the same trends are evident. The median sizes increase in a shoreward direction, and the sorting improves in a shoreward direction. The most notable differences seem to be: 1) the rate at which the sorting and median sizes change in the shoreward direction. This alters the relative position of the individual contour lines, but not the basic pattern, 2) the nature of the accumulation finally dumped at the "Step" in Zone B.

B. *Initial bimodal frequency distribution, representing the general form of certain glacial deposits.*

Interpretation is similar to that of the symmetrical distribution.

The underlying sediment pattern in the nearshore-foreshore region under consideration appears to us to be composed in part of the following factors:

1. The nature of the initial sediment distribution including the range of sizes, as well as the relative amounts in the various size classes.
2. The availability and kind of sediment being brought in both from the seaward side of the shoreline e.g. by littoral drift, and from the landward side e.g. by wind, storm, abnormally high tides, and slope wash. See for example, Inman & Chamberlin (1955).

3. The nature of the local wave and current system is an average sense, discounting the temporary effect of violent storms on one hand, and abnormally quiescent periods on the other.
4. The nature of removal of sediment, e.g. along the shore.

If the last three factors are considered to represent averaged conditions in a stable situation, we may consider this region to be an open system, in equilibrium over a period of time. It should be possible to characterize such a situation in terms of an underlying pattern of median size and sorting of sediment from which extremely local variation has been removed.

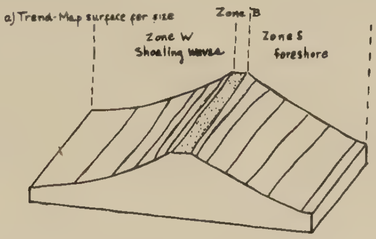
a) Trend-Map surface for size
Zone B
Zone W
Shoaling waves
Zone S
foreshore

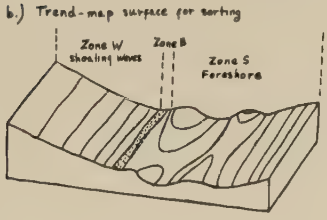
b.) Trend-map surface for sorting
Zone W
Shoaling waves
Zone B
Zone S
Foreshore

Fig. 7

APPENDIX

equation 1) $\frac{H\,L\,C}{d^2}\,(,0865) = w$

equation 2) $C^2 = \frac{g\,L}{2\pi}\tanh\frac{2\pi d}{L}$

equation 3) $\bar{v}_e = 0{\cdot}12w\left[S^{1/2}\,\frac{D}{K_e}\,(S_s - 1)\right]^{-0,3}$

equation 4) $v = v_{\max}\left\{\frac{\log(1+y/a)}{\log(1+t_d/a)}\right\}$

(notation)

H = wave height
L = wave length
C = wave celerity
d = still water depth
w = terminal fall velocity of the sediment particle
D = particle diameter
S_s = specific gravity of grain
K_e = effective hydraulic roughness length
y = variable distance from bottom
t_d = total depth of flow
a = a very small distance between boundry and reference axis
$\bar{v}_e$ = average edge velocity
$v_{\max}$ = maximum velocity in vertical gradient

Our investigations have led us to propose the composite trend map as a model shown in Fig. 7 representing the nearshore-foreshore region in a state of equilibrium as discussed above. Departures from this equilibrium state, e.g. wasting or building beach should be reflected in departures of the trend map from this composite model.

BIBLIOGRAPHY

AIRY, G. B. (1842): *On waves and tides*, Encyclopaedia Metropolitan, London, p. 289.

BASCOM, W. H. (1951): *The relationship between sand size and beach face slope.* Trans. Am. Geophys. union. *32*, no. 6, pp. 866–874.

EVANS, O. F. (1939): *Sorting and transportation of material in the swash and backwash.* J. Sed. Petr. *9*, no. 1, pp. 28–31.

INMAN, D. L., & CHAMBERLIN, T. K. (1955): *Particle size distribution in nearshore sediments*, S.E.P.M. Spec. Bull. no. 3, pp. 106–127.

IPPEN, A. T., & EAGLESON, P. (1955): *A study of sediment sorting by waves shoaling on a plane beach*, M.I.T. Hydrodyn. Lab. Tech. Rept. no. 18.

IPPEN, A. T., & VERMA, R. P. (1953): *The motion of descrete particles along the bed of a turbulent stream*, Proc. Minn. Internat. Hydro. Conv.

KRUMBEIN, W. C. (1938): *Local areal variation of beach sands*, Bull. G. S. A. *49*, pp. 653–658.

MILLER, R. L. (1956): *Trend surfaces: 1. the relation of sediment size parameters to current-wave systems and physiography*, J. Geol. *64*, no. 5, pp. 425–446.

MUNCH-PETERSON (1950): *Munch-Peterson's littoral drift formula*, Bull. Beach Erosion *4*, no. 4, pp. 1–31.

ROUSE, H. (1937): *Nomogram for the settling velocity of spheres*, Rept. Comm. Sed. 1926–37, Nat. Res. Council Div. Geol. Wash. D.C. pp. 57–64.

– (1938): *Fluid mechanics for hydraulic engineers*, McGraw-Hill, N.Y.

Contribution No. 1125

Deep-Sea Research, 1960, Vol. 7, pp. 219 and 220. Pergamon Press Ltd., London. Printed in Great Britain

LETTER TO THE EDITORS

The Line of Zero Set

(*Received* 28 *June* 1960)

WHEN electrodes are towed in tandem from the stern of a ship under way the G.E.K. (geomagnetic electro-kinetograph) senses the transverse component of water motion or set of the ship. When the indicated rate of transverse motion is reduced to zero the ship can be said to be steaming on a course which is parallel to the local surface current direction in either the upstream or downstream sense. If, while tracking the current, the position of the ship is determined at regular intervals by means of some radio-navigational aid, a line is generated on a chart which reflects certain properties of the flow. This line, in an accelerated system, does not fall within any of the existing hydrodynamic classifications : streamline, streak-line, or path-line. But it may be considered that the *line of zero set* has a family resemblance to these more conventional concepts, and could be a useful index in natural situations where the field of surface motion is otherwise undetermined.

The operational principles of sailing a line of zero set were mentioned by the writer in 1951 (VON ARX, 1951) but an actual field trial of the method was not made until there was need, during the April–June 1960, multiple ship survey of the Gulf Stream, to delineate the courses of flow between several parallel lines of oceanographic stations. During this cruise the convolutions of the main current of the Gulf Stream were tracked for a distance approaching 2100 nautical miles between Longitudes 49°–69°W. The results of this experiment will be reported in another place.

It was found that steering a line of zero set was most easily accomplished where the currents were strong. (When the indicated current speed fell below 25 cm/sec it was perhaps the current itself that became sufficiently irregular in direction to make tracking difficult). Where the current speed was in excess of 50 cm/sec, tracking was always practicable provided the zero point of the electrodes could be determined at intervals of about an hour. During both tracking and zero point operations the ship could move through the water at the highest speed suited to existing weather conditions.

During the recent cruise it was possible to observe the depth of certain key isotherms as indicated by thermistor beads towed at the surface and 100 m levels on a thermistor chain. (W. S. RICHARDSON and C. J. HUBBARD, 1960). When the ship was tracking the band of highest surface velocities the 15 °C isotherm tended to remain at or near a depth of 100 metres below the keel. This relationship between the depth of key isotherms and the position of the maximum current gave some assurance that the line of zero set was being followed except where there were pronounced convolutions in the course of the current, or apparent breaks in its continuity. On several occasions the line of zero set led the ship into a region of weak but strongly curved currents. A transverse search in these areas revealed no strong or well defined currents nearby but rather a broad area of degenerate motion which reorganized itself into a strong current downstream and several tens of miles nearer the coast. These features seem to have been associated with shallow (100 to 200 metres deep) floods of Gulf Stream water into the region normally occupied by Slope Water.

Two other effects tended to lead the ship out of mid-stream. One was due to the influence of beam winds and seas which caused the cable to tow at an angle to the keel. This had to be corrected by deliberately crabbing upwind. The other effect was related to the divergent motion of surface water from the current maximum in the Gulf Stream. The band of maximum surface velocity is normally only a few miles wide. On the left of the current maximum the current seemed to often possess a relatively strong transverse component of flow toward Slope Water which with frontal sinking probably accounts for the tendency for organic films and even large forms of flotsam to collect at the surface outcrop of the frontal interface. Airplane observations of the motions of fluorescein dye markers placed in a line at right angles to the frontal outcrop show that Gulf Stream Water to the left of mid-stream flows toward Slope Water at rates as high as 20 cm/sec. A ship steering downstream on a line of zero set may follow this flow and find itself running to the left of the band of maximum current into the region of weaker currents near the frontal outcrop.

Conversely, were the ship to follow a line of zero set against the current it is presumed, but not yet demonstrated, that the course might tend to be led into the band of maximum velocity, provided that the surface motion diverges from the band of maximum current. It is possible, of course, that the surface motion toward the frontal outcrop is not associated with divergence in mid-current but rather with transverse flow across the full width of the Gulf Stream.

Lines of zero set were steered as follows : (1) the zero point of the electrodes was measured hourly by the conventional manoeuver of turning the ship through 90° to its base course and returning to base course through a 180° turn and a final 90° turn so as to present the electrodes to the longitudinal component of flow in the direct and the reverse senses. The average of the two readings at right angles to base course was taken as the zero point of the electrical system. From the signals observed on base course and at right angles to base course the current speed and direction were determined in the usual way. (2) With knowledge of both zero point and local current direction the ship was then steered downstream, which caused the electrical signal to coincide with the zero point. Small corrections of heading were then applied as the signal showed signs of departing from electrical zero.

This procedure can be followed on either upstream or downstream sailings. When the ship is headed downstream in a current of speed C and a transverse set S is noted, it is possible to correct the course by an angle whose tangent is S/C. The sense of this correction depends on the heading :—

Downstream, correct port set by turning to port
Upstream, „ „ „ „ „ „ starboard.

Under ordinary circumstances course changes of a few degrees are required several times each hour to keep the ship on the line of zero set.

Woods Hole Oceanographic Institution,
Woods Hole, Mass.

WILLIAM S. VON ARX

Contribution No. 1125 *from the Woods Hole Oceanographic Institution.*

REFERENCES

VON ARX, W. S. (1951) *J. Inst. Navigation,* **4**, 117–125.

RICHARDSON, W. S. and HUBBARD, C. J. (1960) A contouring temperature recorder. *Deep-Sea Res.* **6**, 239–244.

Printed in Great Britain by The Salisbury Press Ltd., Publicity House, Wilton Road, Salisbury, Wilts. (25957)

Contribution No. 1126

Reprinted from Biological Bulletin, Vol. 119, No. 2, pp. 210–223, October, 1960
Printed in U. S. A.

SWIMMING SOUNDS AND THE SCHOOLING OF FISHES

JAMES M. MOULTON

Bowdoin College, Brunswick, Maine

SWIMMING SOUNDS AND THE SCHOOLING OF FISHES[1, 2, 3]

JAMES M. MOULTON

Bowdoin College, Brunswick, Maine

This paper deals with the swimming sounds of some Bermuda fishes; it describes these sounds and relates them to the behavior of free fishes. E. V. Shishkova (1958a, 1958b) has recently published spectrograms of the sound produced by the movement of schools of scad (*Trachurus trachurus,* Carangidae) in the Black Sea. Such sounds are of interest in their possible significance to the behavior of fishes at sea, and as a reflection of fish behavior. The swimming sounds of fishes offer a possible means of control of fish school movements. The laughter which Hérubel derived (1912, p. 127) from the idea of controlling schools of herring is gradually fading. Sounds engendered by clupeids and the closely related engraulids are hitherto unreported, although a questionable account of herring sounds exists (Murray, 1831), and Maine fishermen describe sound stemming from large herring schools.

"Swimming sound" here conveys that collection of noises created in the water by movements of fish bodies, which characterize the movements of a given species. Such sound may stem from the rubbing together of skeletal parts, from the contraction of swimming muscles, or from water disturbed by various body movements. Shishkova refers to the swimming sound of *T. trachurus* as "hydrodynamic noise," which term she also applies to that noise caused by water flowing along a ship's hull; her data do not permit determining to what extent other events than water flowing over fish bodies contribute to the sound she describes. Since a similar criticism applies to my data, the more general term "swimming sound" seems preferable. Swimming sound is incidental to swimming and includes only those noises characteristically produced during swimming of a given species.

Listening equipment used in the investigation consisted of an AX-58-C Rochelle salt hydrophone and a Woods Hole Suitcase amplifier. Recordings were made during the summer of 1958 on a PT6-BN and a PT6BA2HZ Magnecorder tape recorder at 3¾, 7½ and 15 inches/sec., and analyzed on a Kay Vibralyzer vibration frequency analyzer. Recordings were played back into the water with an Ekotape tape recorder Model 205, a Craftsman C550 amplifier and a QBG transducer. Recordings at sea were made from the motor launch ABUDEFDUF of the Bermuda Biological Station, Mr. Brunell Spurling, Captain.

---

[1] Contribution No. 1126 from the Woods Hole Oceanographic Institution.

[2] Contribution No. 271 from the Bermuda Biological Station.

[3] The work was performed at the Bermuda Biological Station and at Bowdoin College under Grant NSF-G4403 of the National Science Foundation, and through assistance of the Woods Hole Oceanographic Institution and of the Bowdoin College Faculty Research Fund established by the Class of 1928.

Swimming Sounds of Some Bermuda Fishes

Anchoviella choerostoma (Goode)—Hog-mouth fry. This small engraulid occurred in large and small schools on Bermuda shores during the summer of 1958. The schools were most commonly seen in shallow bays along the north shore of St. George's and Hamilton Islands where they are said to be driven by the commonly observed activity of predators (chiefly carangids and lutianids) feeding on the schools (B. Spurling, personal communication). *Menidia* (Atherinidae) is probably similarly driven on Long Island shores (Butner and Brattstrom, 1960). E. L. Mark (1905) described some Bermuda fishes as gathering schools of smaller fishes to lure prey for the former.

Once established in a bay, a school may remain for several days and even for weeks, gradually reducing in size under peripheral predation and the depredations of fishermen obtaining bait for which the fry are highly valued. A large school darkens the water so that it may be seen over a considerable distance, and the experienced Bermuda boatman can readily distinguish between that discoloration caused by a fish school and that due to rock formation and weed patches.

Observations on the behavior of a large school at sea, estimated to contain several million individuals, of *A. choerostoma* were obtained mainly in Bailey's Bay on August 7, 1958. The launch was repeatedly brought over the school which moved in and out relative to shore during recording. Recordings were obtained when the sea surface was calm and the only extraneous noise stemmed from the system and from snapping shrimp.

No predators were seen feeding during recording; activity around the borders of *A. choerostoma* schools on other occasions consisted of feeding by jacks (*Caranx* spp.) and pompano (*Trachinotus palometa*). Small *Caranx latus* (2 to 6 inches) were frequently netted with *A. choerostoma* and individuals were tolerated as members of small schools of the latter (up to 1000) maintained in the laboratory; the jacks fed on the host schools. *Jenkinsia* and *Sardinella* (Clupeidae) were also taken with *Anchoviella* on occasion.

For recording, the launch drifted over the Bailey's Bay school, engine off; although not obviously so, the behavior of the school was probably modified to some extent by the presence of the boat. During recording, the school was either lying at rest with individual fish turning slowly within a narrow circumference, or the

Table I

Characteristics of swimming sounds

Species	Size	Sound	Maximum frequency	Frequency of greatest intensity	Time duration
Anchoviella choerostoma	3 inches	Streaming	1.6 kc.	Below .5 kc.	Variable
		Veering of school	2 kc.	Below .8 kc.	.2–.6 sec.
Caranx latus	2–6 inches	Veering of individual	1.7 kc.	Below 1 kc.	.03 sec.
Caranx ruber	1 foot	Veering of individual	1.6 kc.	Below .7 kc.	.05 sec.
Trachinotus palometa	1 foot	Veering of individual	.7 kc.	Below .25 kc.	.06 sec.

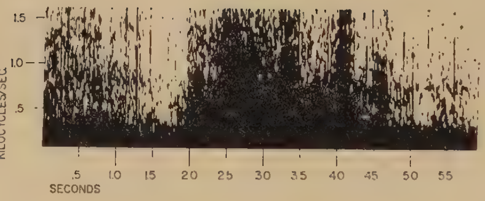

1

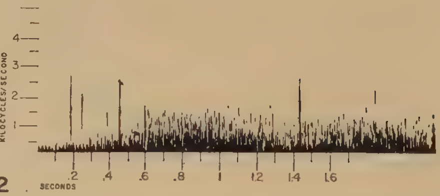

2

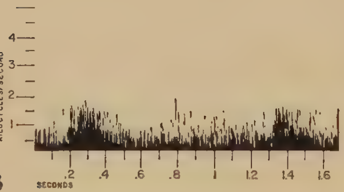

3

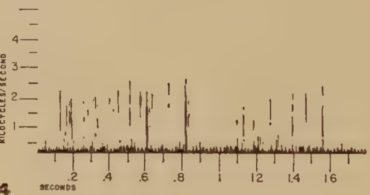

4

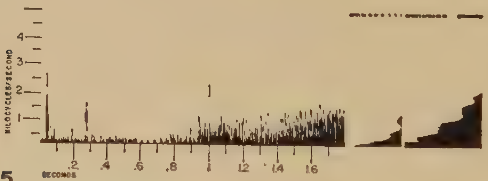

5

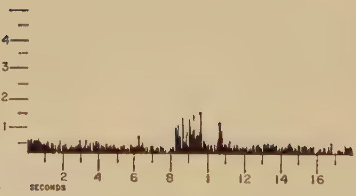

6

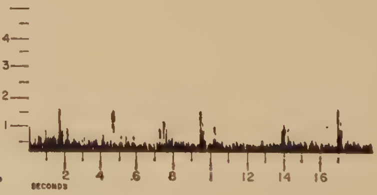

7

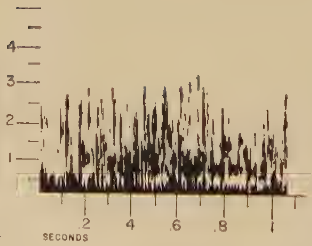

8

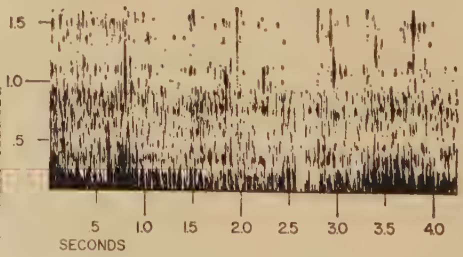

9

FIGURE 1. Streaming, resting and veering of *Anchoviella choerostoma*.
FIGURE 2. Beginning of a streaming movement of *A. choerostoma*.
FIGURE 3. Two veerings during streaming of *A. choerostoma*.
FIGURE 4. Background and system noise during recording at sea in Bailey's Bay, August 7, 1958.

school had assumed a single direction and the fish were streaming around and by the hydrophone, or the school in the process of streaming suddenly veered in direction with a resultant sharp increase in sound intensity.

Sound could not be recorded from the school at rest; streaming and veering both produced considerable sound (Table I). Sounds similar to these are aptly described by Shishkova (1958a) for *T. trachurus* as being like a pouring or a splash and like a rise and fall in system noise. The greater the degree of veering, the greater the intensity of its noise. The school streamed slowly and rapidly past the hydrophone; sound intensity fluctuated with variations in speed of movement of the school.

Suitcase amplifier and Magnecorder settings varied from 0 + 4–10 and 20–3 db, respectively, to 0 + 14–7 and 30–3 db during recording; at all settings, some veerings of the school overloaded the system.

The entire school covered approximately half an acre; during the observation period, the school broke occasionally into two or three smaller groups. The school and its subdivisions tended to disperse somewhat and gather closely again, so that concentration of fish varied. At times, the school appeared layered, a thinner upper stratum moving in a different direction than the lower bulk of the school. All recordings were done over sandy bottom while the school lay in 2 to 4 fathoms of water; the hydrophone was lowered to mid-depth of the school. When streaming, the school moved past the hydrophone leaving a circular area clear of fish, extending about 6 inches from the casing. With a casing of different color, this interval might be expected to vary (Breder, 1951).

When the school was at rest, it could be stimulated to move by the slightest flexing and stiffening of the observer's knees aboard the 21-foot launch when visual clues were excluded. The casting of a shadow over the school by hand and body movements did not cause this behavior. If the school were at rest when pressure was applied to the deck of the boat by the knee-bend method, it would begin to stream; if it were streaming, it would veer and usually alter the speed of swimming to some extent.

The lower portion (up to 1.5 kc.) of a frequency analysis of sounds stemming from a typical sequence of movements of the *Anchoviella* school is shown in Figure 1. During the 6 seconds of recording illustrated, the school came nearly to rest, began moving again at 2 seconds, veered a few times between 2 and 5 seconds, then quieted again. Abbreviated vertical streaks in the background are due to snapping shrimp; some system noise is indicated below .25 kc.

A similar sequence of events is shown in Figure 2 over a broader frequency scale (5 kc.) and briefer time interval (1.7 seconds). Here the beginning of a streaming movement is shown, again with a few snapping shrimp spectra in the background. Figure 3 shows the spectra of two veerings of the school during a streaming movement. In each of these records, there has been sufficient attenua-

---

Figure 5. Sections through spectrum of recording of *A. choerostoma* school while at rest and while streaming.

Figure 6. Veering of *Caranx latus* school.

Figure 7. Feeding and swimming sounds of *Caranx latus*.

Figure 8. Veering of *Caranx ruber*.

Figure 9. Veering of *Trachinotus palometa*.

tion to bring the schooling movements clearly into the foreground. In Figure 4, the ambient underwater sound of the area (mainly snapping shrimp) and system noise is shown after the *Anchoviella* school had moved inshore from the launch on one occasion.

Figure 5 shows sound intensity spectra (sections) during a recording made from the school at rest and after it had begun to stream. The first section was taken at .6 second of the time scale (school at rest), and the other at 1.3 seconds (school streaming). These sections provide a qualitative indication of the amount of sound stemming from a streaming movement at various frequencies at a point in time. Swimming sound of another *Anchoviella* school of considerably smaller dimensions could not be separated from background noise, due mainly to wave action during a moderate sea state with the equipment employed. In summary, *Anchoviella* swimming sound lies mainly below 2 kc. (Table I). Veering of the school introduces sharp intensity increases of between .2 and .6 second duration.

Attempts failed to record the swimming sound of *Anchoviella* in the laboratory from groups of 500 to 1000 individuals; the sound did not rise above extraneous noise. These experiments were performed in a cement tank, the fish being confined by a wood and plastic screen to an area 8 feet × 2 feet × 1 foot deep. The AX-58-C hydrophone was placed across the tank and fish driven around it. This paper presents evidence that the swimming activity of even small groups of *Anchoviella* is probably important in maintaining the coherence of the school; the swimming sound of a large school is one component of this activity.

A school of blue-fry (*Atherina harringtonensis,* Atherinidae) passing slowly under the launch on August 7 near Bay Island in Bailey's Bay did not respond to the knee-bend method successful in stimulating streaming and veering in *Anchoviella.* The blue-fry school was in the form of a compact ball of perhaps 1000 fish, each turning in its own particular pathway within the school as the latter passed beneath the boat. No swimming sound could be detected.

Caranx latus Agassiz and *C. ruber* (Bloch)—Yellow Jack and Skip Jack. These carangids, common in Bermuda, feed voraciously on *Anchoviella* as well as on other fishes. The *C. latus,* from 2 to 6 inches in length, were captured in small numbers with *Anchoviella* and separately off the dock of the Bermuda Biological Station. Observations are based mainly on aquarium experiments. Two large impounded schools of adult *Caranx ruber* were recorded on the west side of Coney Island on June 26 and August 6, 1958, through the kindness of a commercial fisherman (Mr. Spurling, Senior), and a third school was recorded during underwater listening in Castle Roads on July 11.

Since pharyngeal tooth stridulation may accompany the swimming sound of *Caranx* spp., this habit bears comment. Pharyngeal tooth stridulation of *Caranx hippos* has been described (Burkenroad, 1931; Fish, 1948; Moulton, 1958), and Fish (1948, 1954) describes the stridulating sounds of a number of other carangids. The pharyngeal tooth stridulation is produced more readily by young jacks hand-held gently under water (*C. latus, C. hippos*) than by adult jacks so treated (Moulton, 1958, p. 364); it was recorded at Bermuda from adult *C. ruber* held next to the hydroprone in an impounded school, and by *C. crysos* speared off Nonsuch Island on August 17.

Several attempts failed to elicit pharyngeal tooth stridulation from adult pompano (*Trachinotus palometa,* Carangidae) and *Calamus bajanado* (blue-bone porgy, Sparidae), both of which are equipped with formidable pharyngeal teeth. Adult grunts (*Haemulon sciurus,* Pomadasyidae) of some species, on the other hand, stridulate readily when similarly treated.

The present account deals mainly with the thumping sound produced by veering of *Caranx* spp., but pharyngeal tooth stridulation is also produced at times during this maneuver.

Several small groups (from 12 to 20) of young *C. latus* were confined in aquaria 1½ feet × 1¼ feet × 1 foot deep with the hydrophone. Undisturbed, these fish milled about the aquarium equidistant from each other, each on its own pathway. When a hand was flicked at the aquarium or a stick poked into the water, the small group of jacks became at once a tightly coherent school, streaming about the aquarium and veering on repetitive stimuli as had the *Anchoviella* at sea. Streaming did not introduce sound detectable above background; veering did. This movement even of individual fish resulted in distinct thumps similar to those described by Fish (1954) from shocked *C. crysos* (7.75 mm.?). When stemming from a group of *C. latus,* the thumps occurred in volleys (Fig. 6, Table I).

During feeding on bits of meat, the *C. latus* dispersed through the aquarium. The thumps then became scattered as individuals darted for food, and were accompanied by occasional sounds of the stridulation of teeth (Fig. 7).

During the Coney Island recordings, the hydrophone was hung in the midst of schools of *C. ruber* before and during raising of the net. Veering of the fish about the hydrophone caused volleys of thump-like sounds similar to those of *C. latus,* but somewhat deeper in predominant tone (Fig. 8, Table I). Swimming sound engendered by streaming movements was also detected in these recordings and that obtained at Castle Roads.

Trachinotus palometa Regan—Gaff-topsail Pompano. The swimming sound of two pompano approximately 1 foot long was recorded in the cement tank. The animals were not fed during recording. Only thumps coincident with veering occasioned by sudden hand movements in the water were recorded. Sound spectrograms of two flurries of activity are illustrated (Fig. 9, Table I).

Diplodus argenteus (C. and V.)—Bream. Attempts failed to record a swimming sound from 6 of these fish (Sparidae) approximately 8 inches long in a Station aquarium. The only sound detected was made by the fish bumping against the sides and bottom of the tank as a probe was moved gently about the aquarium. These sounds are not clear and sharp like carangid thumps; they are variable and random and are not clearly correlated with describable behavioral phenomena.

Various spear fishermen at Bermuda during 1958, including reliable observers from the Station, reported hearing sounds underwater produced during evasive swimming of grouper (Serranidae) and parrotfish (Scaridae), "any large fish," and hogfish (*Lachnolaimus maximus,* Labridae), as well as grunts of the hamlet or Nassau grouper (*Epinephalus striatus*) and volleys of squirrelfish (*Holocentrus ascensionis*) sound (Moulton, 1958).

The Playback of Underwater Sound to Fish Schools

The playback of underwater sound has been useful in modifying fish behavior (Moulton, 1956a, 1956b; Tavolga, 1956, 1958). The habit of *Caranx* of feeding on *Anchoviella* led to playing back to the *Anchoviella* school recorded on August 7 recordings of the stridulation sound of *C. latus* and of the swimming sound which accompanies its feeding. The transducer was lowered to mid-school level. The *Anchoviella* cleared the area beneath the launch more quickly during this playback than during recording. Further, during sound playback, the school showed a greater tendency to divide than during recording.

A collateral observation is of interest: When playback began of the stridulation sound at sea, an adult barracuda (*Sphyraena barracuda,* Sphyraenidae) came abruptly to a spot about 8 feet from the suspended transducer and lay quietly facing it for about three minutes. This behavior was unique to all observers, including Mr. Spurling, an experienced Bermuda fisherman and boat captain. (Mr. Spurling's comment: "I've never seen a barracuda act like that before.")

Stridulating sounds and thumps of young *C. latus* played back to about 500 *Anchoviella* in the Station cement tank were accompanied by quickened swimming and milling which gradually subsided. Approximately one-fourth of the fry moved to the opposite end of the tank over and under a horizontally suspended hydrophone which they did not pass spontaneously before sound transmission, and during hand movements in the tank.

Playback to the impounded school of *C. ruber* recorded at Coney Island on August 6, as it milled within the net, of a series of pharyngeal tooth stridulations of *C. latus* recorded in Station aquaria, initially was accompanied by an immediate movement of the school to the far end of the net. After some minutes of playback, the school failed to respond to these sounds and to feeding sounds. These sounds were listened to by surface divers and sounded like the amplified sounds heard during recording.

After the swimming sound of the large school of *Anchoviella* had been recorded at sea on August 7, the recording was played back into an aquarium containing young *C. latus.* The latter showed quickened swimming movements of a non-directional type. It has already been mentioned that small *C. latus* may join *Anchoviella* schools, feeding on the members of the school; they may be attracted to the school by its swimming sound.

Pharyngeal tooth rasps played back to the source species (*C. latus*) in a Station aquarium on August 1 appeared to initiate feeding reaction. The fish became exceedingly active, swimming about furiously, and facing the transducer to nibble at its rubber surface. After several minutes the activity subsided and the fish swam about as usual.

Swimming Movements and Schooling Behavior of Caranx and Anchoviella

The normal behavior of schooling fishes. Caranx, Trachinotus, and *Anchoviella* are truly schooling fishes, and whether at sea or in aquaria, groups of these fishes form cohesive schools. Their behavior bears examination as it relates to factors maintaining the school at sea.

When adult pompano attacked *Anchoviella* schools at sea, the former were in compact school formation, and usually swam directly through the school of fry; feeding of *Caranx crysos* at the periphery of a school was characterized by irregular darting movements and swift swimming of individual jacks.

At rest in aquaria and at sea, the *Anchoviella* school is clearly outlined, although individuals take independent pathways within the school in daytime as at night. When the school is streaming, and when a schooling fish (*Menidia menidia*) of the Woods Hole area is subjected to a tidal current in a live car, these fishes line up parallel to each other and veer together upon appropriate stimulus.

The importance of water currents in mediating behavior of fishes is further underlined by the behavior of small amberjack (2-inch *Seriola* sp., Carangidae) lurking under sargassum weed clumps southeast of Bermuda on August 18. The fish abandoned each clump as the 65-foot *Panulirus* drifted down upon it, and swam directly to another clump, often some yards away but always along the same line of weed and thus within the same convergent zone (Woodcock, 1944, 1950). Due to a combination of factors, significantly wind and Coriolis force, sargassum weed in the open sea tends to arrange itself in parallel rows, the rows being spaced at quite regular intervals under a given set of conditions, and parallel to wind direction (Woodcock, 1944, 1950). Water currents, probably even micro-currents, are of great importance in the open sea in determining the distribution of fishes (see Hasler, 1956); persistent sensory orientation to a particular current or moving body of water may be of considerable importance in maintaining not only the position but also the cohesiveness of fish schools, particularly through hours of darkness (Moulton, 1957a).

Members of a single school vary in their behavior. Schools of 500 to 1000 *Anchoviella* in the cement tank tended to divide at rest into two or three smaller groups; one group was usually markedly larger than the other(s). These groups, treated alike from capture, differed in sensitivity to stimuli; some were easily frightened, others held their position in the face of a variety of stimuli (*e.g.,* a prodding stick or hand).

In a study of variation in reactions to stimuli, a plastic screen confined a single school of about 1000 *Anchoviella* to an 8-foot section of the cement tank during attempts to record swimming sound. The hydrophone was placed across the tank, 3½ feet from the end containing the fish. During transmission of jack stridulation recordings in the area containing the fish, approximately one-fourth of the school moved past the hydrophone. Pushing down on a small board floating over the school (in simulation of the knee-bend method) caused approximately one-half the remaining fish to pass the hydrophone. Then a hand was waved vigorously in the water with the balance of the school; a recalcitrant two dozen fish still remained in the smaller portion of the tank, gathered in a cohesive school.

Young *Caranx latus* tend to school with *Anchoviella;* in an aquarium, a school of 12 of the former formed a tight formation immediately above the back of a 10-inch squirrelfish (*Holocentrus ascensionis,* Holocentridae). They turned with the squirrelfish as it moved slowly about the tank; the latter made no move toward the jacks. Another group of 20 *C. latus* was confined for several hours in an aquarium with an adult spiny lobster (*Panulirus argus*). So long as they were contained together, night and day, the *C. latus* remained at the top of the tank in a tight school. The spiny lobster was removed one night under artificial light, and at once the 20 jacks dispersed over the bottom of the aquarium and assumed a striking striped pattern completely unlike their usual drab coloration.

Experiments on blinded fish. In order to examine factors other than vision mediating the schooling of fish, adult *Anchoviella* were blinded by bilateral eye removal under anaesthesia (MS222 1:3000, Sandoz Pharmaceuticals) and allowed to recover, or became blinded through eye loss in a syndrome developing within hours of capture in a school held in the cement tank. On successive trials, a blind individual was placed in an aquarium with 12 normal individuals. When the latter were at rest, individuals milling slowly about, the blinded individuals swam through the group and about the aquarium generally until reaching the side of the tank, then took up new headings; they did not orient to the normal fish.

If the normal fish were startled by a hand movement next to the aquarium, they streamed and veered as did large schools at sea; at such times, the blinded individual immediately joined the normal fish in school formation and behaved as did the latter. Similarly, in the cement tank, blinded *Anchoviella* moved with the larger group of normal fish during streaming movements. When the normal fish came to rest again, blinded individuals returned to random movements, while even at rest the normal fish maintained approximately equal intervals between individuals. Isolated blinded fish did not respond to hand movements adjacent to the aquarium.

Unilaterally blinded *Anchoviella* maintained position with the normal fish when the latter were within the field of vision. This latter observation is in agreement with observations obtained on *Menidia* behavior at Woods Hole in 1957, where the experiments were performed in a live car suspended from a raft in Great Harbor; bilaterally blinded fish swam directly through groups of normal fish at rest and oriented independently of normal fish in currents flowing through the live car, while unilaterally blinded specimens maintained position with schools located at least in part on the side of the unoperated eye (Moulton, 1957a).

While movements of the individual members of the fish school are important in maintaining the remarkable integrity of the school, the members of the school are probably sensitive to pressure waves created by the school and probably orient to these waves; the movements of the school as a whole are probably important in maintaining its own integration.

Anchoviella did not disperse through the cement tank after dark as *Jenkinsia* (Breder, 1951) and chub mackerel—*Scomber colias,* Scombridae (Shlaifer, 1942) —do in aquaria. Schools of 500 to 1000 were in tight formation in the center of the cement tank in resting behavior during several examination periods on dark nights when an electric light was turned on, and behavior did not change notably with the light; the basement-located tank was too dark on moonless nights for me to see the fish in it.

C. latus in small numbers confined alone in darkness for several hours did not noticeably change their distribution when a light was turned on. Neither *C. latus* nor *Anchoviella* seems to depend so markedly on light for schooling formation as apparently do *Jenkinsia* and *Scomber.*

A Ghana Fishery Depending on Swimming Sound

A. P. Brown, in an anthropological account of the fishing industry of the Labadi District of the Gold Coast (Irvine, 1947, p. 25), mentioned the three-pronged paddles found in the sea-going canoes of the Coast, without indication as to their use. Inquiry was made subsequent to a United Nations news release suggesting an application to the fisheries.

The paddle, for possession of one of which I am indebted to Mr. D. A. Hammond of the Fisheries Department, Accra, is in typical form 4 feet 9 inches in length with a handle 1¾ inches in diameter. The foot-long flattened blade terminates in three broad, blunt teeth, comprising 4½ inches of the blade length, each approximately 2 inches in width at the base, the center one tapering slightly more than the other two. Mr. Hammond describes the use of this paddle as follows:

"The use of the paddle as (a) hearing aid in fishing is well-known to our fishermen from Ada to Takoradi. It is particularly used by the herring fishermen. 'Herring' here refers to *Sardinella aurita* and *S. cameroonensis.* It is also used, however, to detect shoals of shad (*Ethmalosa dorsalis*), long-finned herring (*Ilisha melanota*) and cassava fish (*Cynoscion senegalla*). (Identifications from Irvine, 1947).

"Where there are no surface fish visible, the method is to place the broad part of the paddle in the water over the stern of the canoe, place the ear to the top of the handle, and rotate the paddle very slowly. Only skillful and experienced fishermen are appointed to do it. The face of the paddle acts as a sounding board and receives the vibrations which it transmits to the hearer. By rotating the paddle, the fisherman is able to get the direction of movement of the fish and from the intensity of the sound, he can judge how (distant) the fish (are). Those fish which move in large shoals—for example, herring or shad, as well as the large rocks in the sea, make distinct sounds. From the sound, the fisherman can tell whether it is a fish or rock. The sound of the herring is characteristic and never mistaken. This method is particularly successful in waters of 7 to 10 fathoms and between 11 P.M. and 3 A.M. Those paddles which are particularly good are treasured. Some of them are very old." A variety of the Ghana-type paddle is said to be used for a similar purpose in Liberia (Mr. William Watkins, personal communication).

Underwater listening occurs in various parts of the world as an important aspect of commercial fisheries (Cousteau, 1953; Kesteven, 1949; Marshall, 1954; Parry, 1954; Westenberg, 1953). It is likely that in the fishery described by Mr. Hammond, the swimming sound of the clupeids (sciaenids may produce other sounds) is conveyed by the three-pronged paddle to the fisherman's ear.

Discussion

The schooling behavior of teleosts probably depends primarily on vision in the daytime (Shlaifer, 1942; Breder, 1951). Yet schools of *Anchoviella, Clupea harengus* and other schooling fishes maintain their schools at sea through hours of darkness; herring fishermen depend on this fact in "lighting up" herring schools at night (Moulton and Backus, 1955). While it may be that light stemming from luminescent organisms and that of moon and stars on clear nights may afford sufficient stimulus to abet schooling at night, some conditions of darkness at sea undoubtedly preclude vision and require other stimuli as predominant in providing for maintenance of the fish school at night. Certainly other factors than vision enable blinded fish (*Anchoviella, Menidia*) to move with their respective schools.

The possible role of water currents in maintaining fish schools at sea has been briefly discussed.

Significant factors in low frequency sensitivity of teleosts are the lateral line and isolated cutaneous receptors (von Frisch, 1938; Griffin, 1950; Lowenstein, 1957). Tracy (1920a, 1920b) and others have suggested that the connection between air bladder and inner ear of clupeids (engraulids possess a similar connection—Berg, 1947) may be more important as a pressure control device related to gas physiology of the air bladder than to hearing facility. While it is not unlikely that the paired passages may serve in both capacities, the remarkable sensitivity of *Anchoviella,* as well as of some clupeids (Moulton and Backus, 1955; Moulton, 1956a), to pressure waves in the water is suggestive of special adaptations to reception of pressure changes.

Anchoviella are sensitive to very slight pressure waves in the water; the swimming sounds described fall within the frequency range of sensitivity of all fishes studied in this connection. It is now simply conjectural, although some supporting evidence has been presented, to suggest that the swimming sounds of various carangids and of *Anchoviella* furnish a mechanism in addition to water currents and visual sensitivity by which schools of fish at sea are maintained under a variety of circumstances. Either these sounds or the body movements from which they stem must be a primary factor.

The swimming sounds described are to a degree species-specific. Shlaifer (1942) observed that chub mackerel, pairs of which will school together, will not school with abnormally moving fish of the same species. Normal *Menidia* and *Anchoviella* do not arrange themselves in schooling formation with blinded individuals; the latter will school with the former. It is suggested that the fish school at sea is maintained by a number of factors, given the proper amounts of food and minimum predation: sensitivity to particular water currents and masses, vision, and the behavior of the school as a whole which acts an an acoustical core and as a wave pressure source to which individuals of the schooling species orient. It is suggested that the swimming sound is not simply a mechanical or accidental sound, but that it possesses biological significance. It is demonstrated that source species and other species may react to amplified swimming sound.

Another factor influencing the maintenance of the fish school is reflected in differential sensitivity of *Anchoviella* to increasingly dispersive stimuli. After a series of such stimuli, a core of recalcitrant individuals remains in the test area in an experimental tank, and may furnish the nucleus around which more sensitive members of the school fluctuate at sea; streaming and veering may orient around a group of relatively insensitive individuals forming an "anchor" to the school.

It is clear that the swimming sound of different species of schooling fishes (*Anchoviella, Caranx, Trachinotus*) varies in its characteristics with species as well as with size of the fishes concerned. Large schools of fishes as small as *Anchoviella* (about 3 inches) and as large as *Caranx ruber* (about 1 foot) introduce considerable sound into the water. This may in future be utilized in experiments on schooling fishes in waters less clear than those studied, to test influence of various stimuli on schooling fishes and to explore sensitivity to these stimuli. Although Shishkova (1958a) abandoned the hope of stemming acoustically the flow of anchovies from the Russian Sea of Azov into the Black Sea, and of masking ship noise with swimming sound, other possible uses of swimming sound exist; a likelihood is present that fishermen can control acoustically to some extent the movements of clupeid and engraulid schools.

The characteristics of these sounds are more like those of sounds produced under circumstances related to defensive behavior of fishes than of sounds produced under other circumstances (Moulton, 1957b). The sound attendant on veering may have some protective value. If this were true, large schools of herring and anchovies would be more resistant to predation by other fishes than would small schools. The joining of *Anchoviella* schools by young *C. latus* may be primarily protective for the latter; their feeding on the host school would simply indicate poor "guestmanship."

The swimming sounds described, as well as sound stemming from the movement of any large fish in the sea, are probably due to a number of factors; hydrodynamic noise, to which Shishkova relates all of the sound, skeletal movements, and contraction of axial musculature during strong swimming movements against a gas-filled, resonating air bladder. None of the sounds described are continuous even during steady streaming movements, indicating that they stem from the bodies of individual fishes during muscle contraction, rather than from the hydrodynamic effects of continuous water flow around fish bodies.

All of the swimming sounds studied lie below 2 kc., and thus are of lower frequencies than many sounds created by fishes by organs apparently specialized for sound production (Moulton, 1958). These results differ from those of Shishkova (1958b) who found components of *T. trachurus* swimming sound at 16 kc. (It seems likely that her fish were chewing or stridulating during recording.) The frequency span of greatest intensity of swimming sound, as indicated by darkening of vibragrams, is lower for large fish than for small (Table I).

After submission of the manuscript of this paper for publication, the author's attention was called to a recent extensive study of social groupings in fishes by Breder (1959). Of special pertinence to the present work is Breder's caution that the responses of members of a fish school to light and darkness will vary with individuals, and that light exposure which fish have received earlier will be of great importance.

The author is grateful to Dr. Richard H. Backus for constructive criticism of the manuscript of this paper.

SUMMARY

1. The swimming sounds of four schooling species of Bermuda fishes are described. The sounds stem from streaming and veering of schools at sea.

2. Responses of schooling species to playback of sounds stemming from schools are described. Exploitation of these responses in experimental and commercial fishing is suggested.

3. On the basis of observation at sea and of laboratory experiments, mechanisms useful in maintaining formation of schools at sea are discussed. These include vision, water currents and pressure waves initiated by the movements of fish bodies and the sounds they engender.

4. An African acoustical fishery, probably relying on the swimming sounds of fishes, is described.

LITERATURE CITED

Berg, L. S., 1947. Classification of Fishes. J. W. Edwards, Ann Arbor, Michigan.

Breder, C. M., Jr., 1951. Studies on the structure of the fish school. *Bull. Amer. Mus. Nat. Hist.*, **98**, Art. 1: 1–27.

Breder, C. M., Jr., 1959. Studies on social groupings in fishes. *Bull. Amer. Mus. Nat. Hist.*, **117**: 393–482.

Burkenroad, M. D., 1931. Notes on the sound producing marine fishes of Louisiana. *Copeia*, 1931, No. 1: 20–28.

Butner, A., and B. H. Brattstrom, 1960. Local movement in *Menidia* and *Fundulus*. *Copeia*, 1960, No. 2: 139–141.

Cousteau, J.-Y., 1953. The Silent World. Harper and Brothers, New York.

Fish, M. P., 1948. Sonic fishes of the Pacific. ONR Contr. N6 ori-195, T. O. 1, Tech. Report No. 2.

Fish, M. P., 1954. The character and significance of sound production among fishes of the western North Atlantic. *Bull. Bingham Oceanographic Collection*, **14**, Art. 3: 1–109.

von Frisch, K., 1938. The sense of hearing in fish. *Nature*, **141**: 8–11.

Griffin, D. R., 1950. Underwater sounds and the orientation of marine animals, a preliminary survey. Proj. NR 162–429, T. O. 9, between ONR and Cornell University, Tech. Report No. 3.

Hasler, A. D., 1956. Perception of pathways by fishes. *Quart. Rev. Biol.*, **31**: 200–209.

Hérubel, M. A., 1912. Sea Fisheries. T. Fisher Unwin, London.

Irvine, F. R., 1947. The Fish and Fisheries of the Gold Coast. The Crown Agents for the Colonies, London.

Kesteven, G. L., 1949. Malayan Fisheries. Malaya Publishing House, Ltd., Singapore.

Lowenstein, O., 1957. The sense organs: the acousticolateralis system. Chap. 2, Part 2, of The Physiology of Fishes, Vol. 2, ed. by M. E. Brown. Academic Press, New York.

Mark, E. L., 1905. The Bermuda Islands and the Bermuda Biological Station for Research. *Proc. AAAS*, **54**: 471–501.

Marshall, N. B., 1954. Aspects of Deep Sea Biology. Philosophical Library, New York.

Moulton, J. M., 1956a. The movements of menhaden and butterfish in a sound field. *Anat. Rec.*, **125**: 592.

Moulton, J. M., 1956b. Influencing the calling of sea robins (*Prionotus* spp.) with sound. *Biol. Bull.*, **111**: 393–398.

Moulton, J. M., 1957a. Report to the Director of the Woods Hole Oceanographic Institution. Unpublished.

Moulton, J. M., 1957b. Sound production in the spiny lobster *Panulirus argus* (Latreille). *Biol. Bull.*, **113**: 286–295.

Moulton, J. M., 1958. The acoustical behavior of some fishes in the Bimini area. *Biol. Bull.*, **114**: 357–374.

Moulton, J. M., and R. H. Backus, 1955. Annotated references concerning the effects of man-made sounds on the movements of fishes. Maine Dept. of Sea and Shore Fisheries, Fisheries Circular No. 17: 1–7.

Murray, J., 1831. Herring making sounds. *Mag. Nat. Hist.*, **1831**: 148.

Parry, M. L., 1954. The fishing methods of Kelentan and Trengganu. *In:* Malayan Fishing Methods, by T. W. Burden and M. L. Parry, *J. Malayan Br. Roy. Asiatic Soc.*, 27, Part 2.

Shishkova, E. V., 1958a. (Concerning the reactions of fish to sounds and the spectrum of trawler noise.) *Rybnoye Khozyaystvo*, **34**, No. 3: 33–39.

Shishkova, E. V., 1958b. (Recording and analysis of noise made by fish.) *Trudy VNIRO*, **36**: 280–294.

Shlaifer, A., 1942. The schooling behavior of mackerel. *Zoologica*, **27**: 75–80.

Tavolga, W. N., 1956. Visual, chemical and sound stimuli as cues in the sex discriminatory behavior of the gobiid fish *Bathygobius soporator*. *Zoologica,* **41**, Part 2: 49–64.

Tavolga, W. N., 1958. The significance of underwater sounds produced by males of the gobiid fish, *Bathygobius soporator*. *Physiol. Zoöl.,* **31**: 259–271.

Tracy, H. C., 1920a. The clupeoid cranium in its relation to the swimbladder diverticulum and the membranous labyrinth. *J. Morph.,* **33**: 439–483.

Tracy, H. C., 1920b. The membranous labyrinth and its relation to the precoelomic diverticulum in clupeoids. *J. Comp. Neurol.,* **31**: 219–257.

Westenberg, J., 1953. Acoustical aspects of some Indonesian fisheries. *J. du Conseil pour l'Exploration de la Mer,* **18**: 311–325.

Woodcock, A. H., 1944. A theory of surface water motion deduced from the wind-induced motion of the *Physalia*. *J. Mar. Res.,* **5**: 196–205.

Woodcock, A. H., 1950. Subsurface pelagic sargassum. *J. Mar. Res.,* **9**: 77–92.

Contribution No. 1128

Reprinted from SCIENCE, November 11, 1960, Vol. 132, No. 3437, pages 1397-1398

Discovery of Eocene Sediments in Subsurface of Cape Cod

Abstract. Spores, pollen, and charcoal taken from two wells drilled near the tip of Cape Cod have been identified as Eocene. These are the first Eocene rocks to be identified in Massachusetts. Interpretation of seismic records taken in the Gulf of Maine and Cape Cod Bay will be influenced by this discovery.

Two wells drilled near Provincetown, Mass., on the hook of Cape Cod (Fig. 1) penetrated fluvioglacial material and entered lignitic silts and sand identified as Eocene on the basis of spores, pollen, and foraminifera. Well No. 1 entered Eocene at 86 feet and was still in it at 264 feet. Well No. 2 entered Eocene at 193 feet and was drilled to a total of 203 feet.

The spores and pollen processed by W. S. Hoffmeister from the coal samples at 86 feet 3 inches and at 186 feet from Well No. 1 (Holden's Pond) and at 192 feet 10 inches from Well No. 2 (Stark's Well) have a definite Eocene aspect. Although Upper Cretaceous elements are also present, the evidence points to an Eocene age (probably Lower Eocene). There is a marked similarity between the spores and pollen of these coals and those of a Wilcox (Eocene) sample from Tennessee. Encountering the foraminiferal genus *Elphidium* at 230 feet in the No. 1 well helps to confirm the Eocene age for these sediments, for this genus is not found in material older than Eocene.

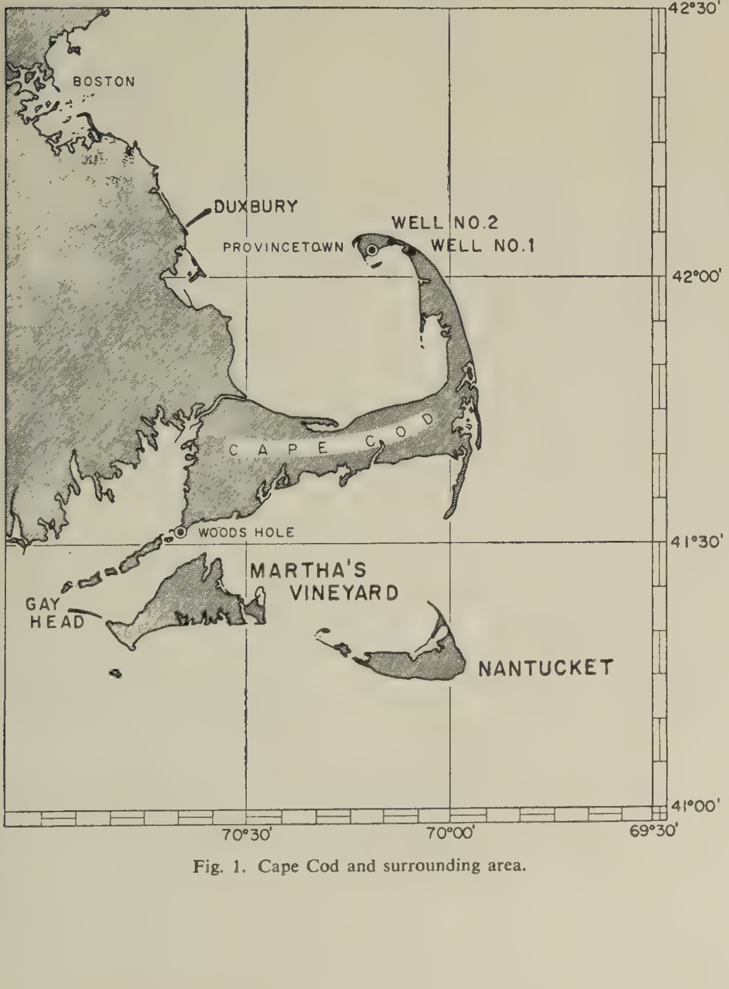

Fig. 1. Cape Cod and surrounding area.

No Eocene, in place, had been previously identified from Massachusetts. Coastal plain sediments of Cretaceous and Miocene age crop out at Gay Head on the island of Martha's Vineyard 45 miles southwest of Provincetown. Miocene material resting on granite is known from the subsurface near Duxbury, Mass. (*1*).

In addition to extending the known range of Eocene deposits, discovery of Tertiary sediments beneath the fluvioglacial deposits of Cape Cod is important to marine geophysicists who wish to identify sub-bottom reflections more precisely as to composition and age. The thickness and extent of Pleistocene deposits overlying reflections interpreted as basement has long been a problem in understanding seismic records from the Cape Cod and Cape Cod Bay area (*2*).

Note added in proof: After this report was submitted for publication, a third well at the westernmost tip of the hook (Race Point) also penetrated Eocene, at 213 feet.

J. M. ZEIGLER, W. S. HOFFMEISTER*
GRAHAM GIESE, HERMAN TASHA
Woods Hole Oceanographic Institution,
Woods Hole, Massachusetts

References and Notes

1. J. B. Woodworth and E. Wigglesworth, "Geography and geology of the region including Cape Cod, the Elizabeth Islands, Nantucket, Martha's Vineyard, No Mans Land, and Block Island," *Museum Comp. Zool., Harvard College* **52**, 15 (1934); B. K. Emerson, "Geology of Massachusetts and Rhode Island," *U.S. Geol. Survey Bull. 597* (1917), 289 pp.
2. The work was sponsored by the geography branch of the Office of Naval Research under contracts Nonr-1245 (00) NR 388-018 and Nonr-2196 (00) NR 083-004. We are particularly grateful to Mr. Frank Stark of Provincetown and Mr. Edmond Dalpe, supervisor of Pilgrim Springs State Park, for permitting us to drill on property under their supervision. We express our thanks to Dr. F. P. Shepard, Dr. Carl Hubbs, and Dr. Hans Seuss, of Scripps Institution of Oceanography, for their cooperation in determining a radiocarbon date (older than 42,000 years) from some of. the lignitic material. Thanks are due to Hoffmeister's colleagues at the Jersey Production Research Center and to Dr. L. R. Wilson of the University of Oklahoma, all of whom confirmed an Eocene age for these coals. This report is contribution No. 1128 from the Woods Hole Oceanographic Institution.

* Jersey Production Research Company, Tulsa, Okla.

21 July 1960

Contribution No. 1130

Deep-Sea Research, 1960, Vol. 7, pp. 142 to 147. Pergamon Press Ltd., London. Printed in Great Britain

INSTRUMENTAL NOTE

A Telemetering Hydrophone

Willard Dow

(*Received* 20 *July* 1960)

Abstract—This report describes a deep, telemetering hydrophone which transmits its information acoustically through the water to a surface vessel. The instrument has the advantage of requiring no electrical cable to the ship and, being self-contained, may be quickly hung on any suitable supporting line or wire. Alternatively, any type of inexpensive single-conductor cable of sufficient strength, such as oil-well logging cable, may be used to replace the acoustic link for some purposes if desired.

(1) INTRODUCTION

A telemetering hydrophone has been developed for listening at great depths in the ocean. This device has the advantage that a multi-wire electrical cable incorporating a low-loss coaxial line is not required to connect the hydrophone to the receiving vessel or other listening post. Electrical cables of this nature having sufficient reinforcement to withstand the considerable strain involved, almost invariably have to be of special design and must be made to order at high cost. They are usually of such diameter and inflexibility as to make handling difficult without large winches and sheaves particularly designed for their use. The weight and bulk of such installations present severe problems particularly aboard small vessels where deck space is at a premium.

This deep hydrophone is capable of telemetering its information acoustically through the water to the receiving point from depths of 12,000 feet or more. The device is completely self-contained and may be quickly clamped to any wire or line capable of supporting 70 pounds.

Alternatively, for quiet operation at greater depths, any cheap single-conductor cable capable of withstanding the strain (such as $\frac{1}{4}$ in. oil well logging cable) may be used effectively to pipe the information to the surface, in spite of the high transmission loss and other undesirable electrical characteristics usually found in cable types which are not designed for wide-band transmission.

Performance

The first model of the Telemetering Hydrophone was constructed in 1954 and tested at sea (Fig. 1) in April, 1955 from R/V *Atlantis*. In spite of the low output power, about 1 watt, the device operated successfully using the acoustic link to a depth of 6,500 ft. However, battery life was short and the dynamic range was only about 10 db at maximum depth.

An improved model incorporating a built-in pulse generator for calibration purposes, a more efficient modulator and a 4-watt power output stage, was constructed in 1956, and battery life was extended to six hours. Signal-to-noise ratio ranged from 20 db at approximately 10,000 ft to 35 db at the surface. Broadband noise referred to the hydrophone preamplifier input (across the crystal) was 4 microvolts (μv) for a 5 kc bandwidth.

Transistorizing the deep unit in 1958 permitted an extension in battery life to 12 hours (before recharging), an increase in power output to 30 watts, a wider dynamic range (55 db) and a decided improvement in stability and reliability of the transmitter and its power supply. Other specifications are similar to those for the 1956 model.

The transistorized gear has already seen considerable sea duty at depths down to 18,000 ft using logging cable. It is expected that the acoustic link will also prove effective over a greater range than has been possible with the low powered units.

(2) PLAN OF OPERATION

The plan of operation is shown in Fig. 2, and Fig. 3 pictures the deep gear assembly. A hydrophone (A) is suspended by a 40 ft electrical cable (B) from the bottom of the transmitting unit (C) which, in turn, is clamped to a trawl wire, nylon cord or other supporting line.

The hydrophone, together with its built-in preamplifier, has a frequency range of 50 cycles to 5 kc. Both omni-directional and line hydrophones having vertical directivity have been used.

The output signal from the hydrophone preamplifier is passed through the short cable to the transmitter where, after further amplification, it is applied as modulation to a 21 kc carrier. The modulated carrier is then amplified and used to drive a high-frequency projector (D) beamed vertically upward toward the ship.

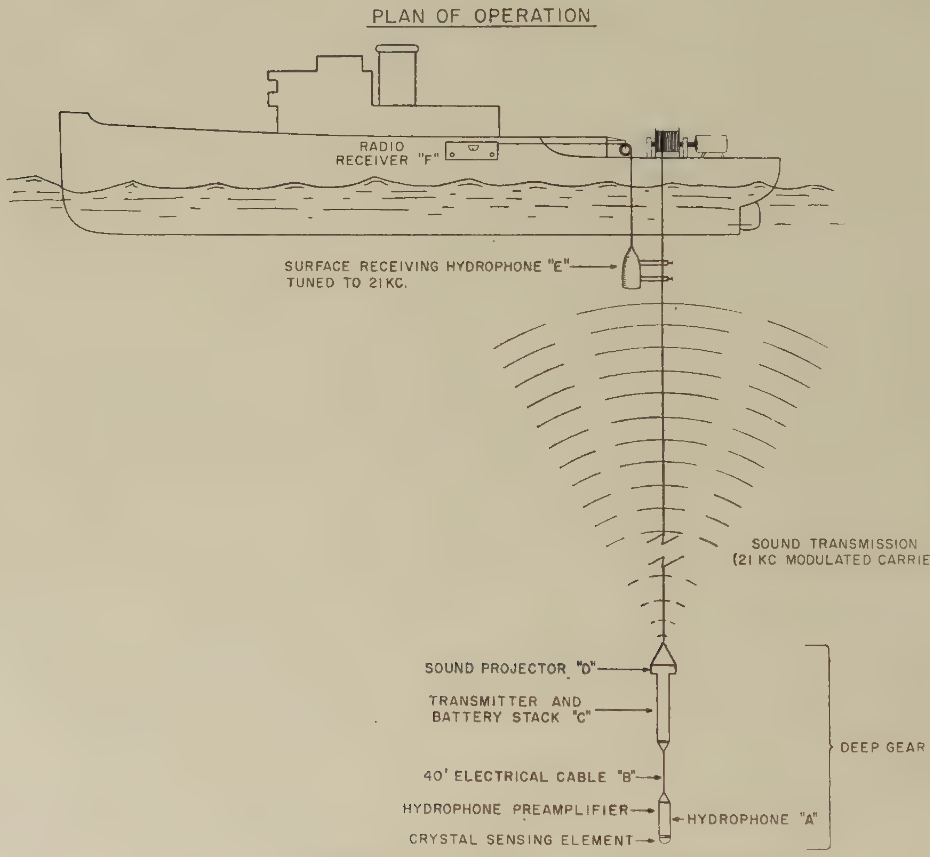
PLAN OF OPERATION
RADIO RECEIVER "F"
SURFACE RECEIVING HYDROPHONE "E" TUNED TO 21 KC.
SOUND TRANSMISSION (21 KC MODULATED CARRIER)
SOUND PROJECTOR "D"
TRANSMITTER AND BATTERY STACK "C"
40' ELECTRICAL CABLE "B"
HYDROPHONE PREAMPLIFIER
CRYSTAL SENSING ELEMENT
HYDROPHONE "A"
DEEP GEAR

FIG. 2. Gear suspended from ship at sea in operating position.

When the transmitter has been lowered to a point about 10 ft above the desired depth, the surface receiving hydrophone (E) is clamped to the line which is then lowered the additional 10 ft or until the surface unit is completely immersed. This receiving hydrophone being beamed toward the deep transmitter is now in a position to receive the acoustic carrier. After passing through the hydrophone preamplifier, this carrier is transmitted through a short cable to a conventional low-frequency radio receiver (F) in the ship's laboratory where it is further amplified and then demodulated to recover the original intelligence. The highly-selectivity tuned radio frequency circuits in the hydrophone preamplifier and radio receiver effectively eliminate low-frequency ship and water noise, 60-cycle pickup and other interference outside the pass-band, which is centered at 21 kc. As a result, the system has remarkably low background noise from these sources, usually 60–80 db below maximum output.

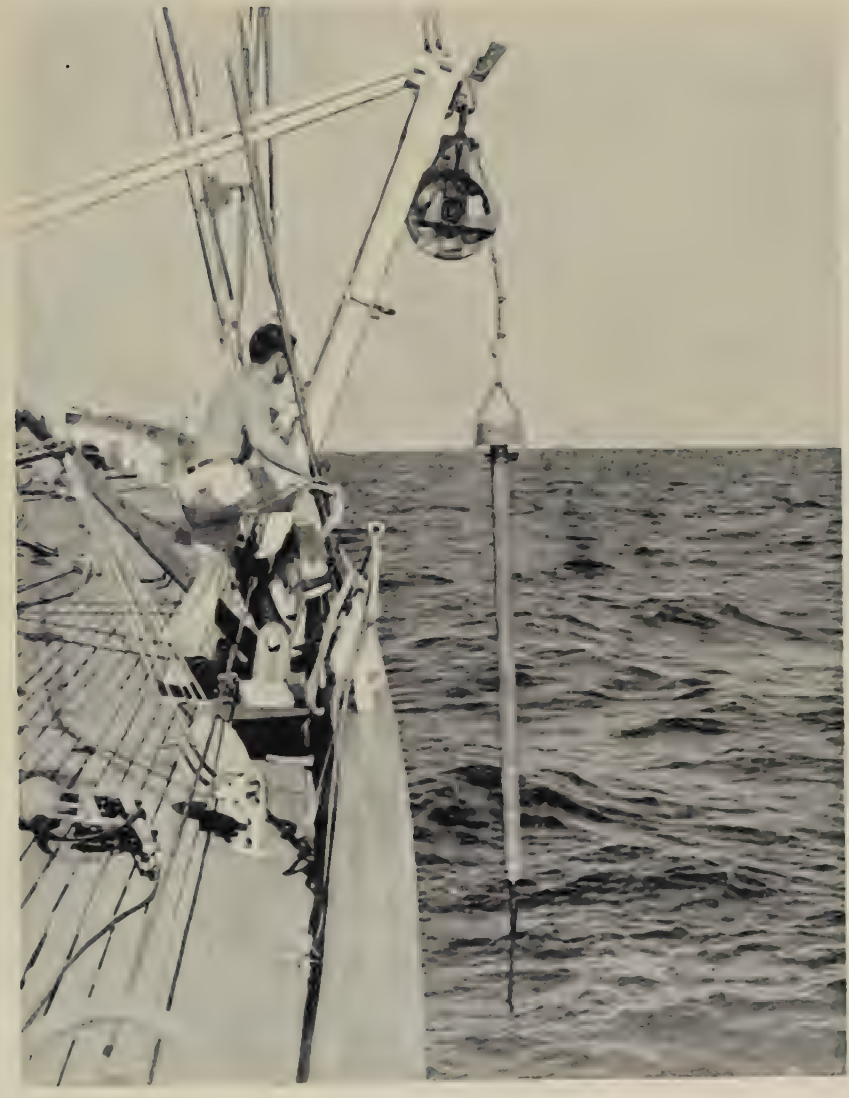

FIG. 1. Deep Transmitter ready for lowering from R/V *Atlantis* in April 1955 (Surface receiving hydrophone lies on deck at lower left of photograph).

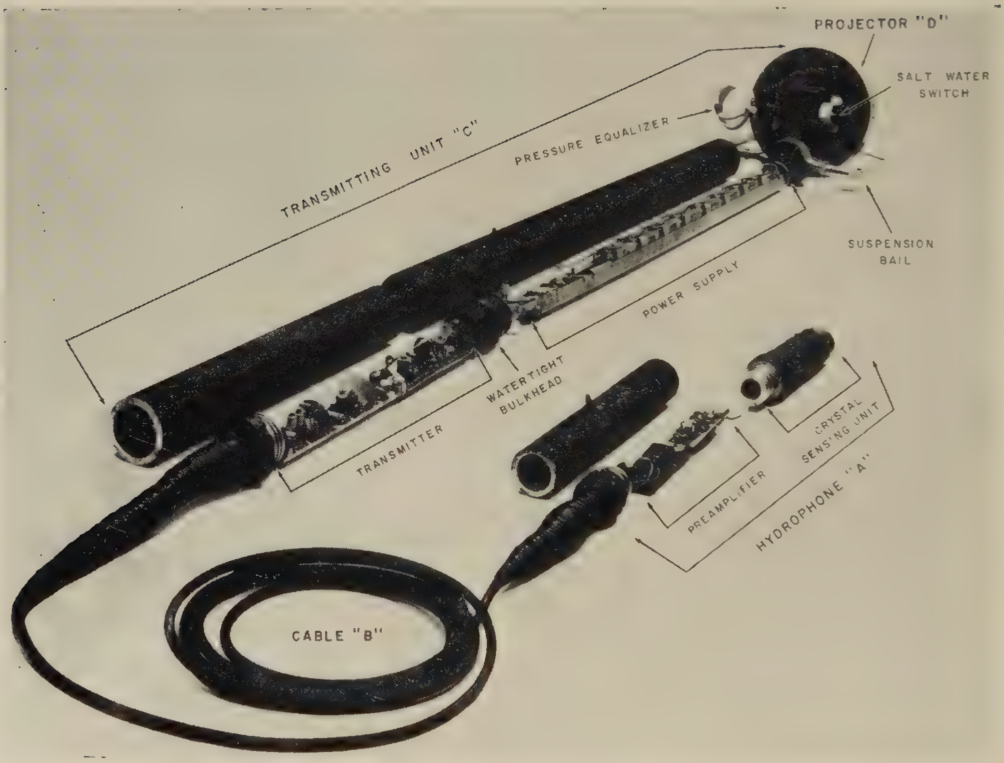
PROJECTOR "D"
SALT WATER SWITCH
TRANSMITTING UNIT "C"
PRESSURE EQUALIZER
SUSPENSION BAIL
POWER SUPPLY
WATERTIGHT BULKHEAD
TRANSMITTER
CRYSTAL SENSING UNIT
PREAMPLIFIER
HYDROPHONE "A"
CABLE "B"

FIG. 3. Component assembly of Deep Gear.

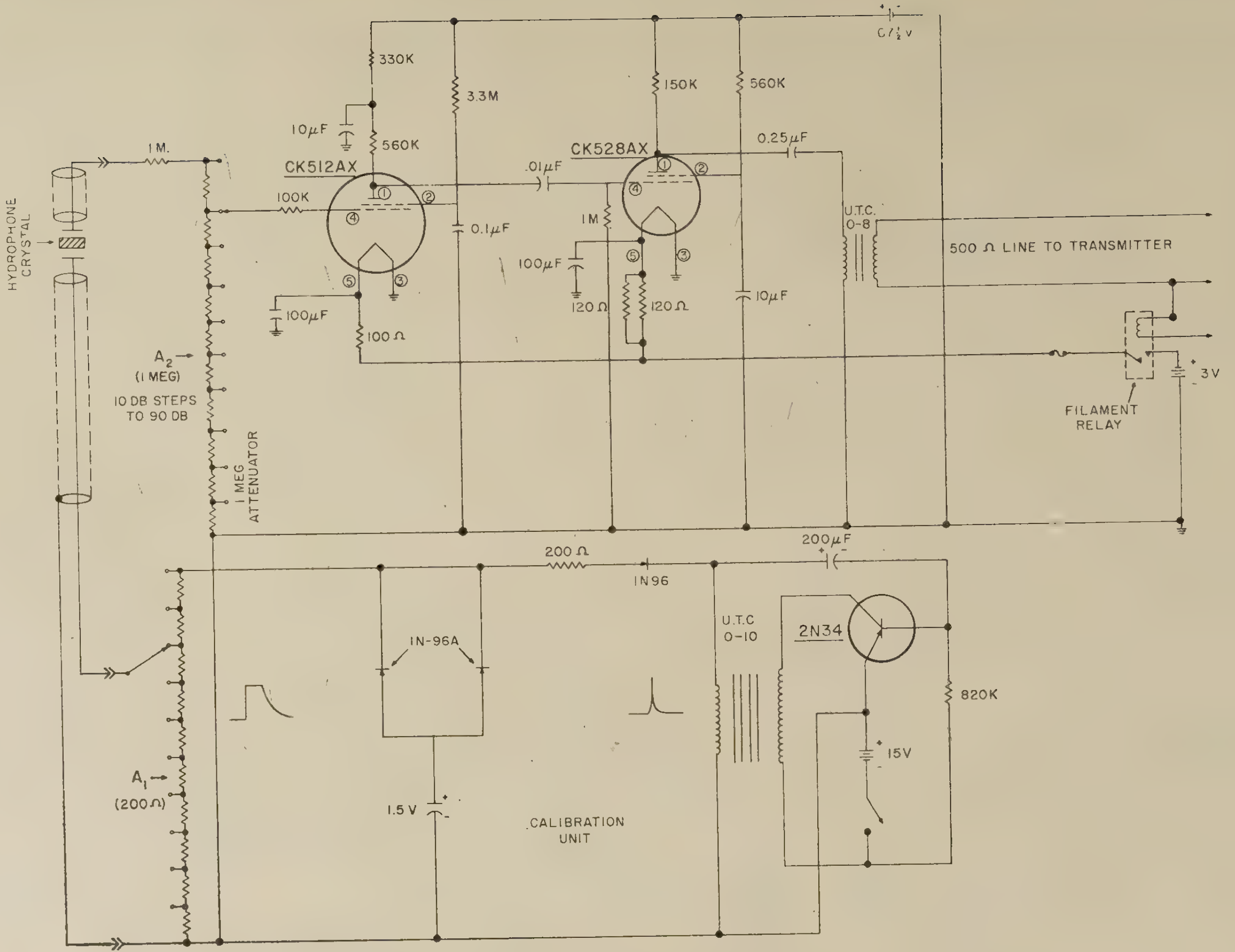
HYDROPHONE CRYSTAL
1 M.
330K
3.3M
10μF
560K
CK512AX
100K
①
②
③
④
⑤
0.1μF
100μF
100Ω
.01μF
CK528AX
150K
560K
0.25μF
1M
100μF
120Ω
120Ω
10μF
C 7½ V
U.T.C. 0-8
500 Ω LINE TO TRANSMITTER
FILAMENT RELAY
3V
A₂
(1 MEG)
10 DB STEPS TO 90 DB
1 MEG ATTENUATOR
200μF
200 Ω
1N96
U.T.C 0-10
2N34
820K
15V
IN-96A
1.5 V
CALIBRATION UNIT
A₁
(200Ω)

FIG. 4. Schematic Diagram of Deep Hydrophone Preamplifier (Vacuum Tube Version).

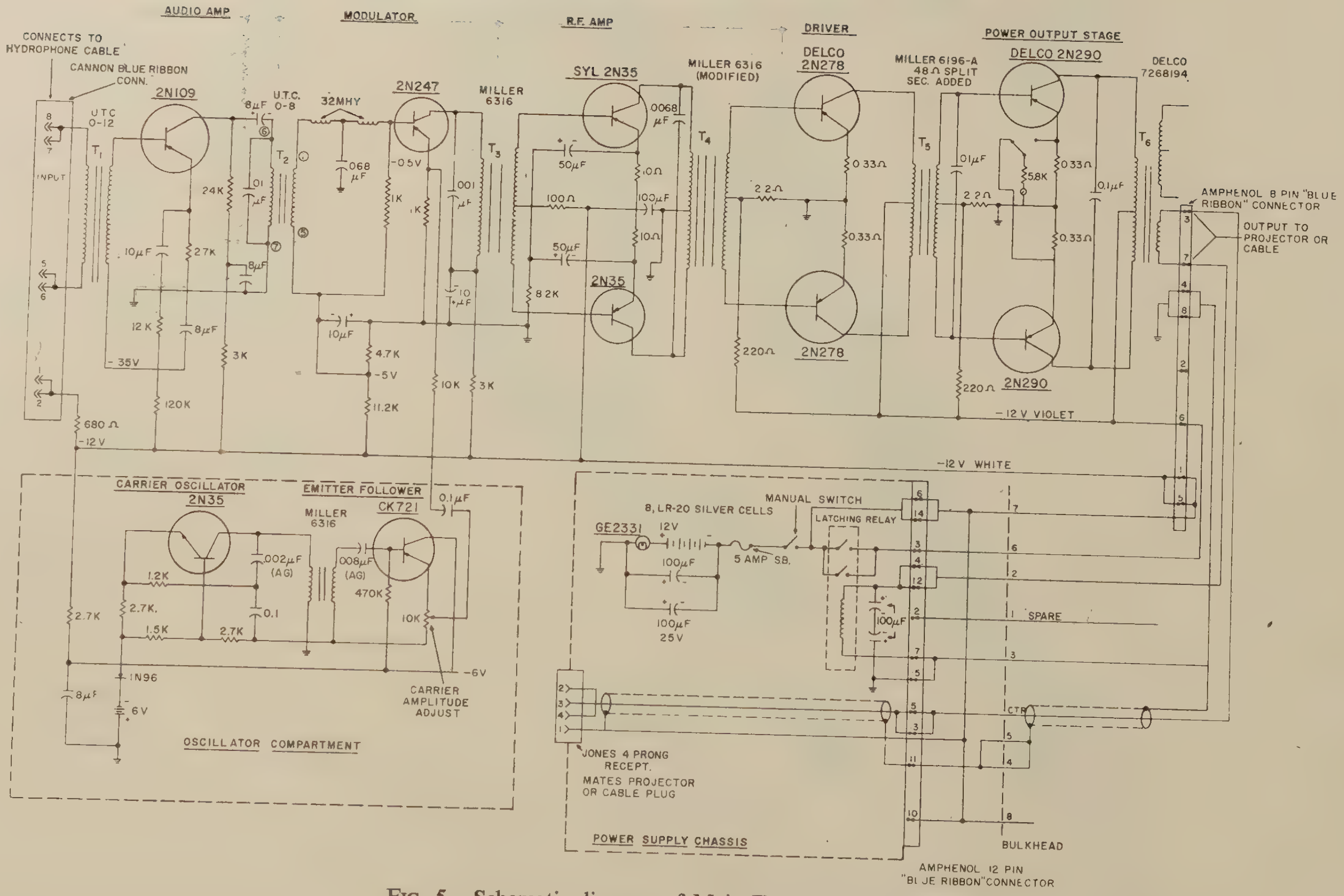
AUDIO AMP
MODULATOR
R.F. AMP
DRIVER
POWER OUTPUT STAGE
CONNECTS TO HYDROPHONE CABLE
CANNON BLUE RIBBON CONN.
INPUT
UTC 0-12
T1
2N109
24K
27K
10μF
12 K
8μF
- 35V
3K
120K
680 Ω
-12 V
8μF
U.T.C. 0-8
T2
01 μF
32MHY
068 μF
2N247
-0.5V
1K
1K
10μF
4.7K
-5V
11.2K
10K
3K
001 μF
10 μF
MILLER 6316
T3
SYL 2N35
50μF
100Ω
10Ω
100μF
82K
2N35
0068 μF
MILLER 6316 (MODIFIED)
T4
DELCO 2N278
2N278
0.33Ω
2.2Ω
220Ω
MILLER 6196-A 48Ω SPLIT SEC. ADDED
T5
DELCO 2N290
2N290
01μF
5.8K
0.1μF
DELCO 7268194
T6
AMPHENOL 8 PIN "BLUE RIBBON" CONNECTOR
OUTPUT TO PROJECTOR OR CABLE
- 12 V VIOLET
-12 V WHITE
CARRIER OSCILLATOR 2N35
EMITTER FOLLOWER CK721
MILLER 6316
0.1μF
.002μF (AG)
008μF (AG)
470K
1.2K
2.7K
1.5K
0.1
10K
-6V
1N96
6V
CARRIER AMPLITUDE ADJUST
OSCILLATOR COMPARTMENT
MANUAL SWITCH
8, LR-20 SILVER CELLS
GE2331
12V
100μF
100μF 25V
5 AMP SB.
LATCHING RELAY
SPARE
CTR
JONES 4 PRONG RECEPT.
MATES PROJECTOR OR CABLE PLUG
POWER SUPPLY CHASSIS
BULKHEAD
AMPHENOL 12 PIN "BLUE RIBBON" CONNECTOR

FIG. 5. Schematic diagram of Main Transmitting Unit.

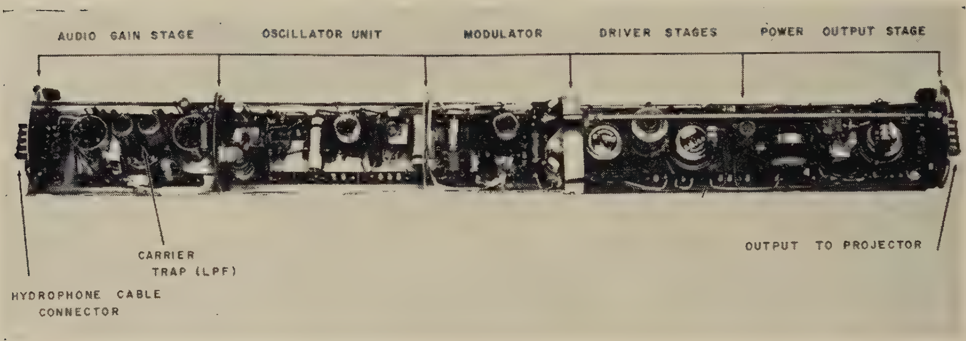
AUDIO GAIN STAGE
OSCILLATOR UNIT
MODULATOR
DRIVER STAGES
POWER OUTPUT STAGE
CARRIER TRAP (LPF)
HYDROPHONE CABLE CONNECTOR
OUTPUT TO PROJECTOR

FIG. 6. Layout of Deep Transmitter Chassis.

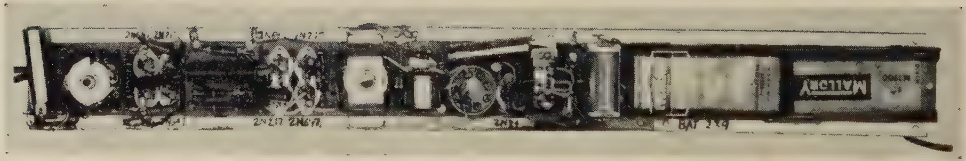
MALLORY
BAT 2×4

FIG. 7. Layout of Deep Hydrophone Preamplifier Chassis (transistor version).

Operation with logging cable is similar except that the carrier is transmitted directly from the deep transmitter to the radio receiver via the insulated centre conductor, sea water being used as the return. However, even this simple, small-diameter electrical cable together with its special slip-ring winch not only requires more careful maintenance at sea but does not offer the convenience and adaptability of the acoustic version as will be seen in the discussion of applications at the conclusion of this paper.

The design of the new equipment (Model 3) will now be discussed in detail.

(3) ELECTRONIC DESIGN

Fig. 4 is a schematic diagram of the hydrophone preamplifier. The Ammonium Dihydrogen Phosphate (ADP) crystal hydrophone responds to sounds in the deep ocean in the frequency range from 50 cycles to 5 kc. In series with the crystal element is a 200 ohm step attenuator (A1) across which is impressed a short calibration pulse every 8 seconds. This pulse, which is developed by a type 2N34 transistor pulse-generator, is rectified and clipped by type 1N96 diodes to maintain constant amplitude regardless of battery and temperature conditions.

The attenuator controls the voltage applied to the calibration resistor. Input attenuator (A2) controls the signal voltages applied to the input of the two-stage preamplifier. These attenuators are at present pre-adjusted for the operation desired by removing a pipe plug in the side of the preamplifier case. (A system for remote control of attentuation by signals from the surface is now under construction).

After passing through the preamplifier* the audio signal is transmitted through a short cable to the main transmitting unit (Figs. 5 and 6) where, after passing through an additional audio gain stage and a carrier trap in the form of a low pass filter, it is applied to the base circuit of the 2N247 type transistor modulator.

A 21 kc oscillator unit comprising a type 2N35 transistor oscillator and CK721 type transistor emitter-follower supplies carrier power to the emitter circuit of the modulator and the 21 kc modulated carrier appears across the primary of transformer T_3.

This carrier, after passing through two class-B, linear, driver-amplifier stages and a final power-stage, is applied through matching transformers (T_6) to the acoustic projector or electrical cable depending on the type of operation desired.

The 12-volt power-supply consists of eight 20 ampere-hour silver cells. The latching-relay circuit shown in the diagram is part of a remote-control system which permits the transmitter to be switched on and off in the ship's laboratory. Its function is primarily to conserve battery power between experiments when the gear is down or being lowered. At present it is operable only when the electrical cable is being used but an acoustically-triggered switch is being developed.

(4) STRUCTURAL DESIGN

The structural layout of the deep gear is shown in Fig. 3. The ADP crystal in the deep receiving hydrophone unit is mounted in an aluminium tube having large sound-windows. A flexible neoprene boot is stretched over this tube and the unit is filled with oil under low pressure and sealed.

The hydrophone preamplifier is contained in a two-inch diameter aluminium tube. The preamplifier compartment is separated from the crystal unit and hydrophone cable by watertight buikheads containing sealed electrical feed-throughs. Similar bulkheads are used to separate the transmitter, power supply and projector compartments in the transmitting unit, so that if any one section should develop a leak others the will not be affected. The compartments are made watertight by double 0-ring sliding seals between the bulkhead units and the inside walls of the aluminium tubes. These tubes are shown lying beside the electronic chassis in Fig. 4. They are secured to the bulkheads with bolts. The internal chassis which contain the electronic assemblies plug into electrical connectors mounted on the bulkhead walls so that they may be easily extracted for service or to recharge batteries by removing either bulkhead.

The projector contains an ADP crystal assembly in an oil-filled aluminium case covered by a rubber sound-window. Since it is a conventional, shallow, sonar unit, its rear terminal seals are not designed to withstand the 10,000 lbs./sq. in. pressures that the telemetering gear is subjected to in the deep ocean. Therefore, these seals are backed up by a small oil-filled compartment mounted on

*The preamplifier shown is a vacuum tube component of the Model 2 equipment adapted for use with Model 3 pending completion of the new transistorized preamplifier shown in Fig. 7.

the back of the projector housing (Fig. 3). The oil in this compartment is subjected to the same sea pressure as is presented to the crystal side of the projector rear wall so there is no pressure differential across the terminal seals. Sea pressure is transferred to the interior of the small compartment by means of a sealed, soft-rubber tube exposed to the ocean and filled with oil which is in communication with the oil in the compartment.

An insulated terminal mounted on the wall of the compartment is connected to a relay circuit in the battery stack. When the gear is immersed, the terminal is connected to ground (case) via the salt water path thereby energizing the relay and turning on the gear. This salt-water switch insures that the gear cannot accidentally be left operating on deck, precaution required not only to prevent battery discharge, but to protect the power transistors from the high, deck-temperatures of the tropics.

(5) APPLICATIONS

As pointed out in the introduction of this paper, the principal advantage of the acoustic-link system is that no electrical conductor is required to connect the receiving hydrophone to the ship or other listening post. It is also quite obvious that the deep instrument, being self-contained, can be made to operate completely free of the ship. This fact permits such developments as bottom-mounted or midwater-moored listening units capable of supplying information over high-frequency, acoustic-carrier links beamed toward ship or shore.

Acoustic-carrier telemetering of information from a towed " fish " has proved successful (Dow, 1954) and such a fish can readily be made to listen to sounds in the sea by building into it a transmitter similar to the one described here. There are numerous other applications. For example, the deep unit has been used to detect sounds reflected from sub-bottom strata. Heretofore bottom reflection studies in deep water have been carried out with hydrophones near the surface, and either shallow or deep sound sources. However, when the receiving hydrophone is close to the bottom the path of the reflected signal through the water becomes very short with the result that transmission losses are greatly reduced and masking from side reflection is eliminated.

The possibilities of using the gear in this way are presently being explored. LUSKIN *et al.* (1960) following a design similar to the one outlined here have recorded seismic refraction arrivals in deep water. At Woods Hole tests are being planned which will combine the instrument described above with a repetitive pulse source (The Edgerton Thumper) both submerged near the bottom in deep water.

Acknowledgements—The author wishes to thank the following for their contributions to the development of the instrument.

Dr. J. B. HERSEY conducted many acoustic tests at sea and provided valuable help and advice. He also assisted in the preparation of this paper. STEPHEN STILLMAN developed the final structural design of the various internal chassis in the deep gear, then fabricated and wired them. He also assisted materially with the acoustic tests at sea and in many other respects. LLOYD HOADLEY, SYDNEY KNOTT and WARREN WITZELL helped to design and build the original watertight cases for the deep gear as well as for the deep and surface hydrophones. ROY L. RATHER of the Commercial Engineering Corporation and several members of the staff at the Woods Hole Oceanographic Institution have provided valuable assistance with the equipment both in the laboratory and at sea.

Woods Hole Oceanographic Institution,
Woods Hole, Massachusetts

Contribution No. 1130 *of the Woods Hole Oceanographic Institution. This work was performed under Contract Nonr*-1367 *with the Office of Naval Research, U.S. Navy Department.*

REFERERENCES

DOW W. (1954) A Telemetering Depth Meter, *Deep-Sea Res.*, **2**, 145–151.

EDGERTON, GERMESHAUSEN and GRIER, Inc. (1960) Instructions for installation and operation of E. G. and G. Sonar Thumper Type ST-8.

LUSKIN *et al.* (1960). Paper given at AGU Forty-first Annual Meeting, April 27-30, 1960.

Printed in Great Britain by The Salisbury Press Ltd., Publicity House, Wilton Road, Salisbury, Wilts. (25136)

Contribution No. 1134

THE DISTRIBUTION OF PHOSPHORUS IN THE DEEP OCEANS OF THE WORLD

By

ALFRED C. REDFIELD

Woods Hole Oceanographic Institution

Reprinted from:
Association d'Oceanographie Physique, Union
Geodesique et Geophysique Internationale,
Proces-Verbaux, No.7 (G.16), pp. 189-193.

G 16

THE DISTRIBUTION OF PHOSPHORUS IN THE DEEP OCEANS OF THE WORLD

By

ALFRED C. REDFIELD

Woods Hole Oceanographic Institution [1]

Measurements made on the cruises of the "*Carnegie*" and "*Dana*" in 1928—1930 demonstrated that the deeper waters of the Pacific and Indian Oceans contained much more phosphate-phosphorus than the North Atlantic. The "*Dana*" data indicated that nitrate-nitrogen varied in much the same way as phosphorus, and more detailed studies in the Sargasso Sea showed a similar relation obtained for the apparent utilization of oxygen and the change in the carbonate content (4). The proportions in which the elements C, O, N, and P change from place to place is such as would be produced by the oxidation (or synthesis) of varying amounts of planktonic material.

The magnitude of these changes is large. Phosphorus varies from more than 3 mg. atoms/m^3 in the deep water of the North Pacific and Indian Oceans to less than 1.25 in the northern Atlantic and to less than 0.5 in the Mediterranean — a total variation of 6: 1. When this is compared to the uniformity of composition of the principal ions of sea water and the small variation in total salinity it is evident that some very effective processes are at work separating the biologically active elements from the more conservative components of the water. As GRAHAM and MOBERG point out in discussing the "*Carnegie*" results (3), and CLOWES shows for the Southern Ocean (1), the phenomena are to be explained by the sinking of organic matter, formed at the surface, to greater depths were it is decomposed, and the redistribution of the deeper water thus modified by the oceanic circulation.

Since the cruises of the "*Carnegie*" and "*Dana*" much more data on

---

[1] Contribution No. 1134 from the Woods Hole Oceanographic Institution.

oceanic phosphorus have become available owing principally to the work of the "*Discovery*" in the Southern Ocean, the "*Meteor*" in the South Atlantic, the circumnavigation by the Swedish Deep-Sea Expedition, and the investigations of the North Atlantic and the North Pacific Oceans by the Woods Hole and Scripps Institutions of oceanography. I have consequently thought it timely to prepare a chart showing the general distribution of phosphorus in the deeper water of the world oceans. My interest is primarily in the nature of the process which produces such a profound geochemical effect on the world oceans. Since the end effect depends in part on the circulation of the deep water, the result has bearing on the subject of this symposium.

The chart was constructed for a depth of 2 000 meters. This depth is below the major influence of the zone of maximum phosphate and of the antarctic intermediate waters. At greater depths the concentration is relatively uniform, varying about ± 10 %. Fifteen hundred measurements were used. When grouped and averaged by 10° squares values were available for more than 75 per cent of the ice-free oceans. In the North Atlantic these values were contoured directly at intervals of 0.25 mg. atoms/m^3. Elsewhere the values for each four contiguous 10° squares were combined, the average of the four values being assigned to the common meeting point. This permitted unambiguous contouring.

The resulting chart is shown in Figure 1. It is believed to give a useful picture of the general quantities of phosphorus in the several regions of the oceans.

An interpretation of the chart in relation to the movement of the water at 2 000 m. (and by presumption at greater depths) may be made on the following assumptions:

1. In the absence of mixing phosphorus concentration will increase with the time the water remains at depth, and in a current will increase downstream. The motion is consequently in the direction of increasing gradient.

2. The mixing at depth of adjacent streams having different phosphorus contents leads to intermediate concentrations.

Assumption (1) is based on the continual sinking of organic matter into the layer. In the ocean as a whole its effect is balanced by the lesser phosphate content of the water sinking from above, relative to the greater content of rising water which is displaced.

The lowest phosphorus concentrations, and presumably the youngest deep water, is found north of 50° N in the Atlantic where surface

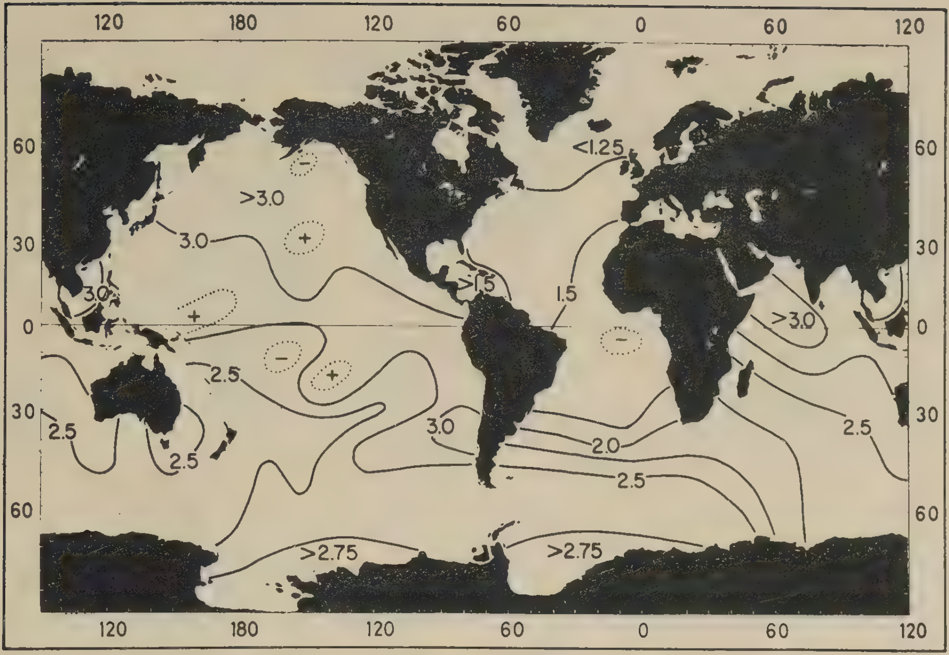

Fig. 1. The general distribution of phosphorus at 2000 m. Figures indicate phosphorus concentration in mg. atoms/m³.

water, denuded of phosphorus in its northward drift, is presumed to sink to form the North Atlantic deep water having a content of 1.25 mg. atoms/m³. Along the Atlantic trough the phosphorus concentrations increase gradually, indicating a southward drift, in accordance with assumption (1). Beyond 35° S the contour spacing shows a steeper gradient. This suggests the mixing of the Atlantic water with water of higher phosphate concentration, emerging from the Pacific sector of the Southern Ocean through Drake's Passage, in accordance with assumption (2).

In the Southern Ocean the lowest phosphorus concentrations (2.0—2.25 mg. atoms/m³) are found in a band extending southeastward from Africa to Antarctica. This appears to be the result of intermixture with deep Atlantic water. Continuing eastward around the Southern Ocean the concentrations increase gradually until the values found in the Atlantic sector are restored in accordance with assumption (1) and perhaps owing to admixture of water of higher phosphorus from the western Pacific involving assumption (2).

Moving northward from the Southern Ocean into the Indian and Pacific Oceans, the phosphorus at 2 000 m. increases progressively

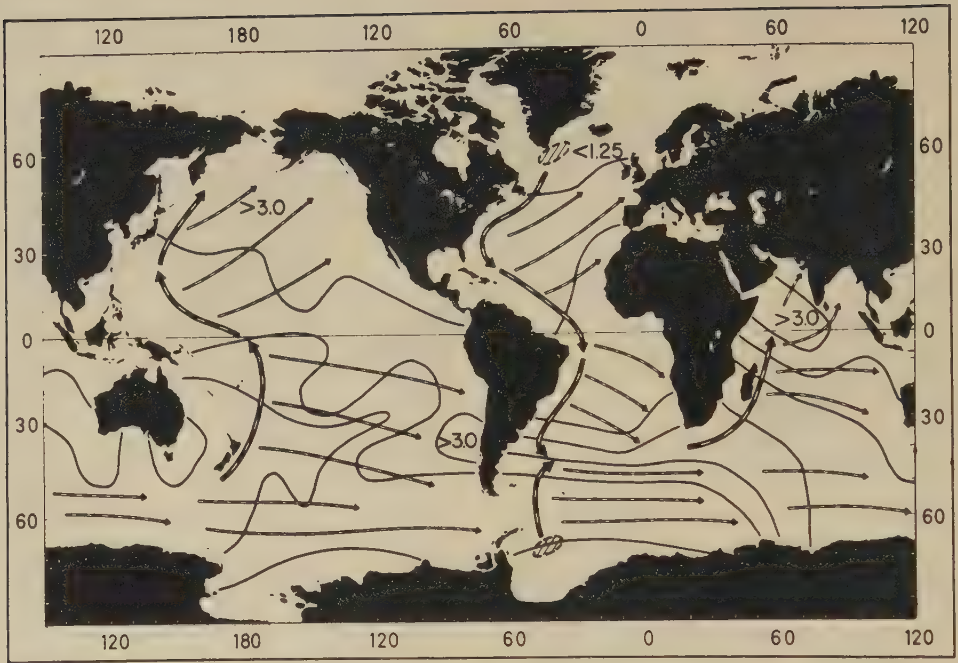

Fig. 2. Deep-water movements and phosphorus distribution at 2 000 m.

to more than 3.0 mg. atoms/m³, suggesting a northward drift (assumption (1)). In both cases, and in the North Atlantic also, the phosphorus contours indicate higher concentrations on the eastern side of the basins, indicating that the most rapid movement into the basins is along their westward side.

The chart does not indicate anything about the formation of deep water in the Antarctic. This is because the surface water is generally quite high in phosphorus. Clowes (1) states that the phosphate content of the Antarctic bottom water is always large, but with some exceptions is less than that of the warm deep water which lies above it. The detailed data on which the chart is based actually show values for the phosphorus at 2 000 meters at stations close to Antarctica between 50° and 100° E which are lower than those farther north. Their presence is masked by the statistical treatment. It is possible that they represent the effect of the formation of bottom water in the Weddell Sea which Deacon describes (2).

This paper is presented as a supplement to Mr. Stommel's deductions regarding the deep circulation of the oceans. It is noteworthy that the map was prepared prior to any knowledge of these deductions. In Figure 2 current arrows have been drawn on the map in accordance with his more generalized diagram, and are found everywhere to follow the pattern deduced from my assumptions.

Radioactive isotope chemistry promises a technique for measuring the time element in the deep circulation. Its procedures add to the difficulty and expense of exploring the ocean. They cannot be adapted easily to the present routine of hydrographic observation. Nor can they be effectively pursued without the aid of all available oceanographic knowledge in planning the points of observation. The examination of such charts as the one I have presented should be of value in planning the geochemical exploration of the sea, which Mr. STOMMEL has proposed in such a timely way.

REFERENCES

1. CLOVES, A. J.: Phosphate and Silicate in the Southern Ocean. Discovery Reports, Vol. XIX, Cambridge, 1940.
2. DEACON, G. E. R.: The hydrology of the Southern Ocean. Discovery Reports, Vol. XV, Cambridge, 1937.
3. GRAHAM, H. W. and E. G. MOBERG: Chemical results of the last cruise of the "Carnegie". Sci. Res. of Cruise VII of the Carnegie during 1928—1929. Chemistry I. Carnegie Inst., Washington, Publ. 562. Washington, D. C., 1944.
4. REDFIELD, A. C.: On the proportions of organic derivatives in sea water and their relation to the composition of plankton. The James Johnstone Memorial Volume, Liverpool, 1934.

Report for the year 1960

THE WOODS HOLE OCEANOGRAPHIC INSTITUTION

annual report 1960

contents

TRUSTEES 4

MEMBERS OF THE CORPORATION 5

RESEARCH STAFF 7

ADMINISTRATIVE STAFF 10

DIRECTOR'S REPORT

oceanography 1930 - 1960 11
physical oceanography 14
mathematics and theoretical oceanography 19
marine meteorology 20
geophysics and submarine geology 24
underwater acoustics 28
chemistry 30
marine biology 32
instrumentation 39
fleet operations 42
personnel 47
visitors 48
employees and staff 50
publications 52

TREASURER'S REPORT 56

BALANCE SHEETS 58

TRUSTEES

AS OF 31 DECEMBER 1960

HONORARY TRUSTEES

Henry B. Bigelow, Museum of Comparative Zoology, Cambridge 38, Massachusetts
L. O. Colbert, 4408 29th Street, N. W., Washington, D. C.
Alexander Forbes, 610 Harland Street, Milton, Massachusetts
Horace S. Ford, 77 Massachusetts Avenue, Cambridge 39, Massachusetts
A. G. Huntsman, 217 Indian Road, Toronto, Canada
Arnaud C. Marts, 521 Fifth Avenue, New York, New York
Lawrason Riggs, Riggs, Ferris and Geer, Room 1201, 74 Trinity Place, New York 6, New York
Harlow Shapley, Sharon Cross Road, Peterborough, New Hampshire
Henry L. Shattuck, 10 Milk Street, Boston, Massachusetts
Selman A. Waksman, Institute of Microbiology, Rutgers University, New Brunswick, New Jersey

TO SERVE UNTIL 1964

Detlev W. Bronk, The Rockefeller Institute for Medical Research, 66th Street and York Avenue, New York 21, New York.
Noel B. McLean, Edo Corporation, College Point 56, Long Island, N. Y.
Daniel Merriman, Bingham Oceanographic Laboratory, Yale University, New Haven, Connecticut.
Emanuel R. Piore, International Business Machines Corporation, 590 Madison Avenue, New York 22, New York.
Alfred C. Redfield, Maury Lane, Woods Hole, Massachusetts
Gerard Swope, Jr., c/o International General Electric Co., 570 Lexington Avenue, New York, New York

TO SERVE UNTIL 1963

James S. Coles, Bowdoin College, Brunswick, Maine
Carl H. Eckart, Scripps Institution of Oceanography, La Jolla, California
Homer H. Ewing, Greenville, Wilmington 7, Delaware
Cecil H. Green, 1000 Exchange Bank Bldg., Airlawn Station, Dallas 35, Texas
Milford R. Lawrence, Siders Pond Road, Falmouth, Massachusetts
Francis C. Welch, 73 Tremont Street, Boston, Massachusetts

TO SERVE UNTIL 1962

Charles Francis Adams, Raytheon Manufacturing Company, 138 River Street, Waltham 54, Massachusetts
Columbus O'D. Iselin, Woods Hole Oceanographic Institution, Woods Hole, Massachusetts
Augustus P. Loring, Loring, Walcott Office, Inc., 35 Congress Street, Boston, Massachusetts
Albert E. Parr, American Museum of Natural History, Central Park West at 79th Street, New York, New York
Athelstan F. Spilhaus, Institute of Technology, University of Minnesota, Minneapolis 14, Minnesota
Alfred M. Wilson, Minneapolis-Honeywell Regulator Co., 2747 4th Avenue, South, Minneapolis 8, Minnesota

TO SERVE UNTIL 1961

Harvey Brooks, Division of Applied Science, Harvard University, Cambridge 38, Massachusetts
Frank A. Howard, 30 Rockefeller Plaza, New York, New York
Robert R. Shrock, Department of Geology and Geophysics, Massachusetts Institute of Technology, Cambridge 39, Massachusetts
Edward H. Smith, 437 Sippewissett Road, Quissett, Massachusetts
Raymond Stevens, c/o Arthur D. Little, Inc., 25 Acorn Park, Cambridge 40, Massachusetts
E. Bright Wilson Jr., Department of Chemistry, Harvard University, Cambridge 38, Massachusetts

EX. OFFICIO

Edwin D. Brooks, Jr., P. O. Box 1135, Boston 3, Massachusetts
Mary Sears, Woods Hole Oceanographic Institution, Woods Hole, Massachusetts
Paul M. Fye, Woods Hole Oceanographic Institution, Woods Hole, Massachusetts

OFFICERS

Raymond Stevens, President of the Corporation, c/o Arthur D. Little, Inc., 25 Acorn Park, Cambridge 40, Massachusetts
Henry B. Bigelow, Chairman of the Board of Trustees, Museum of Comparative Zoology, Cambridge 38, Massachusetts
Edwin D. Brooks, Jr., Treasurer, P. O. Box 1135, Boston 3, Massachusetts
Mary Sears, Clerk of the Corporation, Woods Hole Oceanographic Institution, Woods Hole, Massachusetts

MEMBERS OF THE CORPORATION

Charles Francis Adams, Raytheon Manufacturing Company, 138 River Street, Waltham 54, Massachusetts

Oliver Ames, III, "Edgewater", Beverly Farms, Massachusetts

Philip B. Armstrong, Medical Center of Syracuse, State University of New York, Syracuse, New York

Eric G. Ball, Harvard Medical School, Shattuck Street, Boston, Massachusetts

Henry B. Bigelow, Museum of Comparative Zoology, Cambridge 38, Massachusetts

Detlev W. Bronk, The Rockefeller Institute for Medical Research, 66th Street and York Avenue, New York 21, N. Y.

Edwin D. Brooks, Jr., P. O. Box 1135, Boston 3, Massachusetts

Harvey Brooks, Division of Applied Science, Harvard University, Cambridge 38, Massachusetts

George F. Carrier, Department of Mechanical Engineering, 211 Pierce Hall, Harvard University, Cambridge 38, Massachusetts

John P. Chase, 75 Federal Street, Boston, Massachusetts

C. Lloyd Claff, Single Cell Research Foundation, Inc., 5 Van Beal Road, Randolph, Massachusetts

L. O. Colbert, 4408 29th Street, N. W., Washington, D. C.

Kenneth S. Cole, National Institutes of Health, Bethesda 14, Maryland

James S. Coles, Bowdoin College, Brunswick, Maine

Edward M. Douglas, West Chop, Massachusetts

Henry B. DuPont, Wilmington, Delaware

Ferdinand Eberstadt, 39 Broadway, New York 6, New York

Carl H. Eckart, Scripps Institution of Oceanography, La Jolla, California

Harrison P. Eddy, c/o Metcalf & Eddy, 1300 Statler Building, Boston, Massachusetts

Gifford C. Ewing, P. O. Box 508, Rancho Santa Fe, California

Homer H. Ewing, Greenville, Wilmington 7, Delaware

Alexander Forbes, 610 Harland Street, Milton, Massachusetts

Horace S. Ford, 77 Massachusetts Avenue, Cambridge, Massachusetts

Paul M. Fye, Woods Hole Oceanographic Institution, Woods Hole, Massachusetts

John A. Gifford, 14 Wall Street, New York 5, New York

Cecil H. Green, 1000 Exchange Bank Building, Airlawn Station, Dallas 35, Texas

Paul Hammond, Hammond, Kennedy & Legg Co., 230 Park Avenue, New York, N. Y.

Caryl P. Haskins, Carnegie Institute of Washington, Washington, D. C.

Hudson Hoagland, Worcester Foundation for Experimental Biology, 222 Maple Avenue, Shrewsbury, Massachusetts

Frank A. Howard, 30 Rockefeller Plaza, New York, New York

Columbus O'D. Iselin, Woods Hole Oceanographic Institution, Woods Hole, Massachusetts

Frank B. Jewett, Jr., Vitro Corporation of America, 261 Madison Avenue, New York 16, N. Y.

J. Seward Johnson, Cedar Lane Farm, Oldwick, New Jersey

Augustus B. Kinzel, Union Carbide Corporation, 30 East 42nd Street, New York 17, New York

Milford R. Lawrence, Siders Pond Road, Falmouth, Massachusetts

Alfred L. Loomis, Room 2420, 14 Wall Street, New York, New York

Augustus P. Loring, Loring, Walcott Office, Inc., 35 Congress Street, Boston, Massachusetts

Arnaud C. Marts, 521 Fifth Avenue, New York, New York

Robert E. McConnell, First National Bank, Hobe Sound, Florida

Noel B. McLean, Edo Corporation, College Point 56, Long Island, New York

Daniel Merriman, Bingham Oceanographic Laboratory, Yale University, New Haven, Connecticut

Henry S. Morgan, 2 Wall Street, New York, New York

Frank Pace, General Dynamics Corporation, 445 Park Avenue, New York 22, New York

Albert E. Parr, American Museum of Natural History, Central Park West at 79th Street, New York, New York

John C. Pickard, Box 3684, Greenville, Delaware

Sumner T. Pike, Lubec, Maine

Emanuel R. Piore, International Business Machines Corp., 590 Madison Avenue, New York 22, New York

Alfred C. Redfield, Maury Lane, Woods Hole, Massachusetts

George H. Richards, 68 Williams Street, New York, New York

Lawrence B. Richardson, General Dynamics Corporation, 1710 H. Street N. W., Washington 6, D. C.
Lawrason Riggs, Riggs, Ferris and Geer, Room 1201, 74 Trinity Place, New York 6, New York
William W. Rubey, Institute of Geophysics, University of California, Los Angeles 24, California
Francis C. Ryder, 37 Larchwood Drive, Cambridge 39, Massachusetts
Mary Sears, Woods Hole Oceanographic Institution, Woods Hole, Massachusetts
Frederick Seitz, Department of Physics, University of Illinois, Urbana, Illinois
Harlow Shapley, Sharon Cross Road, Peterborough, New Hampshire
Henry L. Shattuck, 10 Milk Street, Boston, Massachusetts
Robert R. Shrock, Department of Geology and Geophysics, Massachusetts Institute of Technology, Cambridge 39, Massachusetts
Edward H. Smith, 437 Sippewissett Road, Quissett, Massachusetts
Athelstan F. Spilhaus, Institute of Technology, University of Minnesota, Minneapolis 14, Minnesota
H. Burr Steinbach, Department of Zoology, University of Chicago, Chicago 37, Illinois
Raymond Stevens, c/o Arthur D. Little, Inc., 25 Acorn Park, Cambridge 40, Massachusetts
Julius A. Stratton, President, Massachusetts Institute of Technology, Cambridge 39, Massachusetts
Gerard Swope, Jr., c/o International General Electric Co., 570 Lexington Avenue, New York, New York
Selman A. Waksman, Institute of Microbiology, New Brunswick, New Jersey
Thomas J. Watson, Jr., International Business Machines Corporation, 590 Madison Avenue, New York 22, New York
Francis C. Welch, 73 Tremont Street, Boston, Massachusetts
Alfred M. Wilson, Minneapolis-Honeywell Regulator, 2747 4th Avenue, South, Minneapolis 8, Minnesota
E. Bright Wilson, Jr., Department of Chemistry, Harvard University, Cambridge 38, Massachusetts

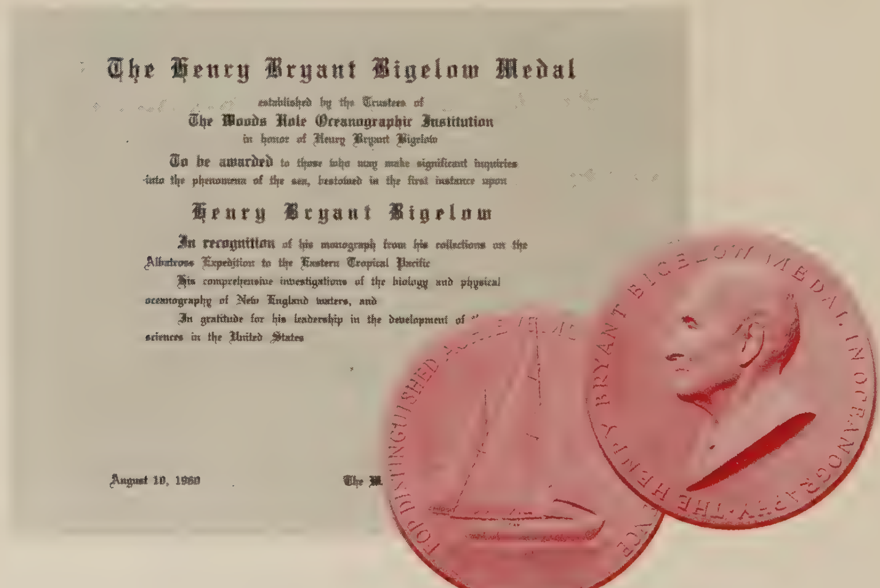

The Henry Bryant Bigelow Medal

established by the Trustees of
The Woods Hole Oceanographic Institution
in honor of Henry Bryant Bigelow

To be awarded to those who may make significant inquiries into the phenomena of the sea, bestowed in the first instance upon

Henry Bryant Bigelow

In recognition of his monograph from his collections on the Albatross Expedition to the Eastern Tropical Pacific

His comprehensive investigations of the biology and physical oceanography of New England waters, and

In gratitude for his leadership in the development of

sciences in the United States

August 10, 1960

"The Henry Bryant Bigelow Medal . . . To be awarded to those who may make significant inquiries into the phenomena of the sea, bestowed in the first instance upon Henry Bryant Bigelow, August 10, 1960."

RESEARCH STAFF

Arnold B. Arons, Associate in Physical Oceanography
Professor of Physics, Amherst College
William D. Athearn, Research Associate in Geology
Richard H. Backus, Marine Biologist
Lincoln Baxter II, Research Associate in Physics
Edward R. Baylor, Research Associate in Physiology
David L. Belding, Associate in Marine Biology
Professor of Bacteriology and Experimental Pathology (Emeritus) Boston University; Consultant, U. S. Fish & Wildlife Service
Bruce Benson, Associate in Physics
Professor of Physics, Amherst College
Henry B. Bigelow, Associate in Oceanography
Professor of Zoology (Emeritus), Harvard University; Research Oceanographer, Museum of Comparative Zoology
Duncan C. Blanchard, Research Associate in Meteorology
Max Blumer, Geochemist
Bert Bolin, Associate in Meteorology
Director, Institute of Meteorology, University of Stockholm;
Director, International Institute of Meteorology, Stockholm
Vaughan T. Bowen, Geochemist
Lecturer in Zoology, Yale University
Alvin L. Bradshaw, Research Associate in Oceanography
Robert R. Brockhurst, Research Associate in Physics
John G. Bruce, Jr., Research Associate in Oceanography
Kirk Bryan, Jr., Research Associate in Meteorology
Dean F. Bumpus, Oceanographer
Elizabeth T. Bunce, Research Associate in Physics
Andrew F. Bunker, Meteorologist
Adjunct Associate Professor in Oceanography, New York University
Cornelia L. Carey, Associate in Marine Bacteriology
Associate Professor of Botany, (Retired), Barnard College
Dayton E. Carritt, Chemist
Professor of Oceanography, Massachusetts Institute of Technology
Joseph Chase, Research Associate in Physical Oceanography
George L. Clarke, Marine Biologist
Associate Professor of Zoology, Harvard University
Nathaniel Corwin, Research Associate in Chemistry
Herbert C. Curl, Jr., Research Associate in Marine Biology
C. Godfrey Day, Research Associate in Physical Oceanography
Willard Dow, Electronics Engineer
Richard S. Edwards, Research Associate in Geophysics
Alan J. Faller, Meteorologist
Harlow G. Farmer, Jr., Research Associate in Hydraulics
Charles J. Fish, Associate in Marine Biology
Professor of Marine Biology, University of Rhode Island; Director, Narragansett Marine Laboratory
David H. Frantz, Jr., Research Associate in Engineering
Frederick C. Fuglister, Physical Oceanographer
Paul M. Fye, Chemist; Director
Michael Garstang, Research Associate in Meteorology
John W. Graham, Research Associate in Geology
George D. Grice, Jr., Research Associate in Marine Zoology
Robert R. L. Guillard, Research Associate in Marine Biology
Earl E. Hays, Physicist

John B. Hersey, Geophysicist
    Associate Professor of Oceanography, Massachusetts Institute of Technology

Louis N. Howard, Associate in Mathematics
    Associate Professor of Mathematics, Massachusetts Institute of Technology

Edward M. Hulburt, Research Associate in Marine Biology

Columbus O'D. Iselin, Henry Bryant Bigelow, Oceanographer
    Associate Professor of Physical Oceanography, Harvard University,
    Research Oceanographer, Museum of Comparative Zoology;
    Professor of Oceanography, Massachusetts Institute of Technology

John W. Kanwisher, Biophysicist

Bostwick H. Ketchum, Senior Oceanographer
    Lecturer in Biological Oceanography, Harvard University

David D. Ketchum, Research Associate in Electronics

Sydney T. Knott, Jr., Research Associate in Engineering

Robert H. Kraichnan, Associate in Theoretical Physics
    Senior Research Scientist, Mathematics, New York University

Edward J. Kuenzler, Research Associate in Marine Biology

Richard G. Leahy, Research Associate in Geology

Joseph Levine, Research Associate in Meteorology

Joanne S. Malkus, Meteorologist

Willem V. R. Malkus, Physical Oceanographer
    Professor of Oceanography, Massachusetts Institute of Technology

Paul C. Mangelsdorf, Jr., Research Associate in Physical Chemistry

Frank J. Mather III, Research Associate in Oceanography

James W. Mavor, Jr., Associate in Applied Physics
    Associate Professor of Mechanical Engineering, Northeastern University

Giles W. Mead, Jr., Associate in Ichthyology
    Curator of Fishes, Harvard University

William G. Metcalf, Physical Oceanographer

Arthur R. Miller, Physical Oceanographer

Robert L. Miller, Associate in Submarine Geology
    Associate Professor, Qualitative Sedimentology, The University of Chicago

Hilary B. Moore, Associate in Marine Biology
    Professor in Marine Biology and Assistant Director, Marine Laboratory, University of Miami

James M. Moulton, Associate in Marine Biology
    Associate Professor of Biology, Bowdoin College

Jerome Namias, Associate in Meteorology
    Chief, Extended Forecast Section, U. S. Weather Bureau

A. Conrad Neumann, Research Associate in Sedimentary Geology

Geoffrey D. Nicholls, Associate in Geochemistry
    Lecturer, Department of Geology, University of Manchester, Manchester, England

Charles B. Officer, Jr., Associate in Geophysics
    Associate Professor of Geology, Rice Institute

David M. Owen, Research Associate in Underwater Photography

Alfred C. Redfield, Senior Oceanographer (Emeritus)
    Professor of Physiology (Emeritus), Harvard University

Charles E. Renn, Associate in Engineering
    Professor of Sanitary Engineering, School of Engineering, The Johns Hopkins University

Francis A. Richards, Associate in Chemical Oceanography
    Associate Professor in Chemistry, Department of Oceanography, University of Washington,
    Seattle, Washington

William S. Richardson, Physical Chemist

Helen M. Roberts, Associate in Mathematics
    Assistant Professor of Mathematics, University of Connecticut

Allan R. Robinson, Associate in Physical Oceanography
    Assistant Professor of Geophysics, Harvard University

F. Claude Ronne, Research Associate in Photography

Claës G. H. Rooth, Research Associate in Meteorology

John H. Ryther, Marine Biologist

Howard L. Sanders, Research Associate in Marine Biology

Harold E. Sawyer, Research Engineer

William E. Schevill, Associate in Oceanography
Research Associate in Zoology, Museum of Comparative Zoology, Harvard University

Karl E. Schleicher, Research Associate in Physics

William C. Schroeder, Ichthyologist
Associate Curator of Fishes, Museum of Comparative Zoology, Harvard University

Mary Sears, Planktonologist

Raymond Siever, Associate in Geology
Associate Professor of Geology, Harvard University

Edward H. Smith, Associate in Oceanography
Sippewissett Road, Quissett, Mass.

Floyd M. Soule, Associate in Physical Oceanography
Oceanographer, U. S. Coast Guard

Allard T. Spencer, Research Associate in Engineering

Edward A. Spiegel, Associate in Astrophysics
Assistant Professor of Astrophysics, University of California

Athelstan F. Spilhaus, Associate in Physical Oceanography
Dean, Institute of Technology, University of Minnesota

Melvin E. Stern, Physicist

Henry M. Stommel, Physical Oceanographer
Professor of Oceanography, Harvard University

Edward D. Stroup, Associate in Physical Oceanography
Research Associate in Oceanography, The Johns Hopkins University

Thomas T. Sugihara, Associate in Geochemistry
Associate Professor of Chemistry, Clark University

William H. Sutcliffe, Jr., Research Associate in Marine Biology
Director, Bermuda Biological Station for Research, Inc.

Parker D. Trask, Associate in Submarine Geology
Professor of Geological Engineering, University of California

Harry J. Turner, Jr., Marine Biologist
Lecturer in Zoology, University of New Hampshire

Ralph F. Vaccaro, Research Associate in Microbiology

George Veronis, Mathematician

Allyn C. Vine, Physical Oceanographer

Gordon H. Volkmann, Research Associate in Physical Oceanography

William S. von Arx, Physical Oceanographer
Professor of Oceanography, Massachusetts Institute of Technology

Arthur D. Voorhis, Research Associate in Physics

Robert G. Walden, Research Associate in Electronics

Stanley W. Watson, Research Associate in Marine Bacteriology

Pierre Welander, Physical Oceanographer
Docent, International Institute of Meteorology, Stockholm, Sweden

Geoffrey G. Whitney, Jr., Research Associate in Physical Oceanography

Alfred H. Woodcock, Oceanographer

George P. Woollard, Associate in Geophysics
Professor of Engineering Geology and Geophysics, University of Wisconsin

L. Valentine Worthington, Physical Oceanographer

Charles S. Yentsch, Research Associate in Marine Biology

John M. Zeigler, Research Associate in Marine Geology
Lecturer in Geology, University of Chicago

ADMINISTRATIVE STAFF

Paul M. Fye	Director
Richard G. Leahy	Technical Assistant to the Director
James R. Mitchell	Administrative Assistant to the Director
Ronald A. Veeder	Development Program Manager
W. Redwood Wright	Public Information Officer
Norman T. Allen	Archivist
Harvey MacKillop	Controller
Richard S. Edwards	Marine Superintendent
John F. Pike	Port Captain

SPOONER

Woods Hole Oceanographic Institution Directors during thirty years of outstanding leadership in oceanographic research are, left to right: Henry B. Bigelow, Paul M. Fye, Columbus O'D. Iselin, and Edward H. Smith.

DIRECTOR'S REPORT

oceanography 1930 - 1960

Anniversaries are a time for reminiscing and a time for evaluating past accomplishments and future hopes. In 1960 the Institution completed three decades of oceanographic research and witnessed thirty years of outstanding scientific achievements. Today, in preparing this prelude for our Annual Report 1960, the first Director and present Director have jointly reviewed the accomplishments, triumphs and frustrations during this period.

We have thought of the past three years as heady times in oceanography but so, too, were the first three years of the Institution. From 1957 to 1960 our operating budget has doubled (from 2.4 million to 5.0 million dollars) but between 1930 and 1933 it increased over 2½ times (from $44,600 to $114,900). In comparing budgets it is customary to use a common dollar value. Here we might suggest as the proper inflationary factor for the oceanographic dollar the six-fold increase in operating cost of the ATLANTIS.

In the early years names famous or to become famous were quickly added to the Institution's roster: Redfield, Rakestraw, Rossby, Parr, Stetson, Waksman, Iselin and Wilkins. In like manner, we hope that those recently added to our staff will bring new kudos to our Institution.

Similarly our fleet has changed over the years and the names of at least eighteen research vessels have been enrolled in the pursuit of science at the Institution. None has served more faithfully or brought more renown than the ATLANTIS, which this year has completed one and one-half million miles of cruising and the five thousandth hydrographic station. Indeed, the pace set during the first year and a half of operation which saw 251 days at sea and 450 hydrographic stations has seldom been matched in later years. In the most recent comparable period, however, she has been at sea 389 days.

Perhaps the most revolutionary change in the thirty years has been in the equipment used by oceanographers. A fathometer was not installed on ATLANTIS until November 1932 and the first radio for transmitting and receiving was not acquired until a year later. The Nansen bottle, bucket thermometer and collecting nets have had few basic changes over the years. A heavy bottom dredge was added in 1934 and coring equipment in 1935. The Rossby "Oceanograph" evolved into the Spilhaus bathythermograph. The impact of modern electronics by way of the vacuum tube and of solid-state physics in the form of the transistor has been effective only in recent years. Now the measurement of bottom profiles, of sub-bottom structure, of surface temperatures, down to 400 feet, all computed and controlled automatically, is completely routine. Instruments free of cumbersome wires, that can be programmed to go to the bottom and back, taking data all the way and techniques for recording specific parameters constantly or telemetering data on demand to the laboratory are today becoming commonplace.

In looking over the 1134 papers carrying a Contribution Number from the Woods Hole Oceanographic Institution we appear to have indeed carried out the mandate of our charter " to prosecute the study of oceanography in *all* its branches." Was it prophetic of events to come and of another NAUTILUS that our first paper written by Harald Sverdrup and Floyd M. Soule was concerned with the Scientific Results of the NAUTILUS under the command of Sir Hubert Wilkins? Impossible as it is to evaluate the scientific contributions of this Institution during its first thirty years, we believe the high scientific standards established in the beginning have been maintained.

One aspect of our work of which we are justly proud has remained unchanged. This is the continued excellent cooperation between scientist and sailor and between master and chief scientist. Sverdrup writes in that first paper

> "The interest which Wilkins himself took in the scientific work is illustrated by the fact that on the day when the loss of the diving rudder was discovered and we actually were lying in the ice with a disabled submarine, he had no thought of returning to safety before we had tested our scientific equipment under conditions which were worse than those to be expected on a journey partly under the ice. I can, I believe, safely state that on August 22 every one on board except Wilkins would have been willing to return, acknowledging a complete defeat, but he did not for one moment consider the possibility of returning before every opportunity for scientific work had been taken."

This spirit has been demonstrated on every cruise. The heroic recovery of a deep bottom cast without benefit of winches by the CRAWFORD crew and the difficult sail without engines by the ATLANTIS last December, missing Christmas at home, are only two recent examples.

So it is to the people who have sojourned for a time in our Institution, over 4300 in all, that we would at the end of three decades pay tribute. Each one – from Pop Schroeder in the attic to Stan Eldridge in the basement, from Chief Backus in the engine rooms to Virginia Walker in the front office, from the beaker washers to the senior scientists – all have our great appreciation of a job well-done. We sincerely hope that in the days ahead the same spontaneous enthusiasm and unbridled curiosity will continue as the flag at our masthead.

Henry B. Bigelow

HENRY B. BIGELOW

Paul M. Fye

PAUL M. FYE

HAHN

physical oceanography

The most concerted research effort that was undertaken at the Institution during 1960 was a multi-ship, three-month investigation of the Gulf Stream in the area, Woods Hole, Bermuda and the Grand Banks. During April, May and June the Institution's Research Vessels ATLANTIS, CRAWFORD and CHAIN were fully occupied with this project. In addition, the R/V ARIES was used during the last phase of the work, and the Coast Guard Ice Patrol Vessel EVERGREEN assisted during the initial survey. A long range Navy patrol plane and the Institution's DC-3 aircraft were used for tracking telemetering drift-buoys and for sea-surface thermal radiation measurements.

This major survey, which has come to be known as GULF STREAM '60, was divided into three parts. During the first phase, eleven lines of hydrographic stations were occupied on north-south sections running from the continental shelf to the latitude of Bermuda. Over two hundred stations were taken in this half million square miles of ocean, giving a unique three-dimensional picture of the Gulf Stream system and its environment from surface to bottom. Bathythermograph observations to 900 ft. were made between station positions for a detailed picture of thermal conditions in the surface layer. Bottom topography was recorded by precision fathometers. The Navy patrol plane was used during this phase of the cruise to track the main course of the Stream visually and with the infrared radiation thermometer. At the end of the three weeks required to complete the preliminary part of the survey, the ATLANTIS, CRAWFORD and CHAIN met in Bermuda where data from the various sources were compared and plans formulated for the second phase of the work.

On the basis of pronounced horizontal temperature gradients, the Gulf Stream was found to have formed a very large meander recalling the picture obtained on Operation CABOT in 1950. However, in this case, the southwesterly loop appeared to be much longer than the southern meander of CABOT. The currents and countercurrents found south of the Grand Banks also seemed to be similar to those obtained during CABOT. The more detailed examination of the area during GULF STREAM '60 showed, however, that the CABOT results were an oversimplification of the situation. Even with the long lines of stations spaced only one hundred miles apart, it is apparent that important convolutions of the current system can be missed. During the ten weeks some very marked changes appeared to take place in some areas; yet other portions of the Stream remained unchanged. Although it would appear that the meanders change their dimensions with time, it is very difficult on the basis of the present data to imagine them as moving waves imposed on the general current system.

The second period of the study was confined to the western half of the area in the vicinity of the large meander. The work was divided into four principal parts. With vertically buoyant floats, the ATLANTIS observed the deep currents in the main body of the Stream and the CRAWFORD the currents in the upper layers. The CHAIN traced the surface currents, using the geomagnetic electrokinetograph (GEK) and towed thermistor array. The aircraft were used to track radio drift-buoys which were set adrift from the ATLANTIS. In addition, hydrographic and bathythermograph data were obtained, and experiments were also carried out from the CHAIN using free-falling instrumented floats to obtain continuous measurements from surface to bottom.

One of the surprising results, which developed early in the second period of GULF STREAM '60 when the CHAIN made a series of stations through the major loop of the Stream, was the remarkable constancy of this significant feature. This persistent pattern in April and May was confirmed by using the GEK to track the line of zero set of the ship along the major meander. The previous concept of the Gulf Stream meanders had been that they changed rapidly with translatory velocities as large as eleven miles per day. Furthermore, the convolutions in the main current are not shallow phenomena but involve the water to great depths. Hence, the situation is not a simple one. The aerial observations, the GEK results and thermal measurements indicate that in many cases the very surface layer seems to depart from the deeper ones. The correct interpretations of the shifting three-dimensional stream with time are most complex.

During the third period the CRAWFORD and ATLANTIS teams again looked for the loop of cold water extending to the south from about 64°W and found it had moved only some 50 miles to the northwest. The tip of this long boot-shaped loop had closed off into an eddy of about 100 miles in diameter. Both ships launched deep floats at the 3000 meter level on the two sides of this eddy and found currents of about 8 cm/sec moving counter-clockwise in the same general direction as the surface current.

At the same time the CHAIN made a series of stations from 35°N to 39°30′N along longitude 63°W. Then she followed the maximum surface current over 1500 miles through a major loop to the north and another to the south. The data indicated that there had been slow but distinct changes in the meanderings of the Gulf Stream. During this phase of the program the ARIES made deep current measurements in the south-central area.

The final interpretation of the data obtained on this survey will depend largely on the results of the deep-current measurements made by the ATLANTIS and CRAWFORD. Deep-pinging floats were used to follow currents

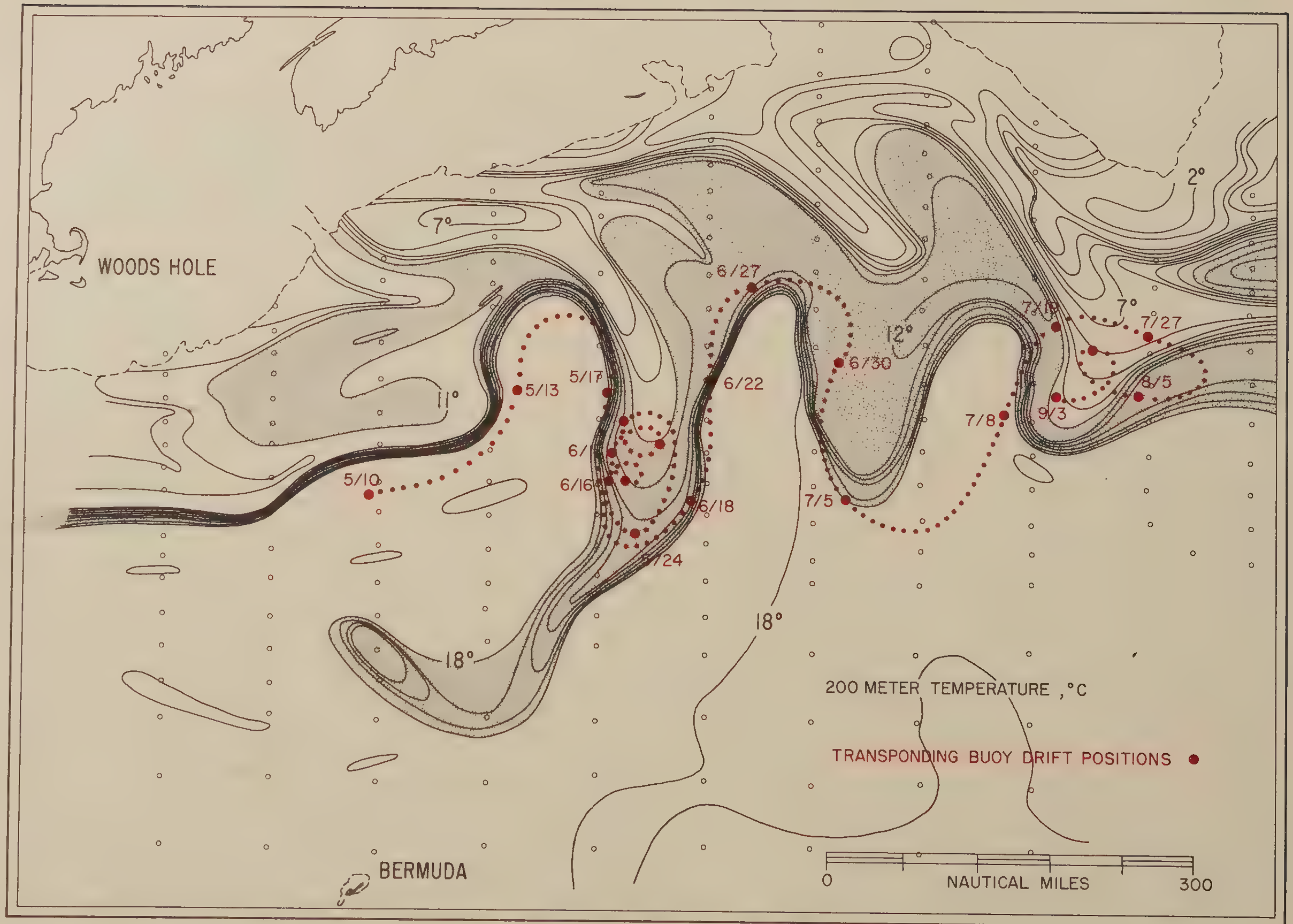
WOODS HOLE
BERMUDA
2°
7°
7°
11°
12°
18°
18°
5/10
5/13
5/17
6/
6/16
6/18
6/24
6/22
6/27
6/30
7/5
7/8
7/19
7/27
8/5
9/3
200 METER TEMPERATURE ,°C
TRANSPONDING BUOY DRIFT POSITIONS ●
0
NAUTICAL MILES
300

An interpretation of GULF STREAM '60 using 200-meter temperatures (°C) and surface GEK observations. Red dots show drift positions and dates of one of the transponding buoys used during the survey.

at the 700 m and 3000 m levels during both the second and third periods of the expedition. The CRAWFORD placed buoys in the main current at the 700 m level and found that they moved with a velocity and in the direction predicted by the temperature structure at this depth. Contrary to expectation, the ATLANTIS, with floats set for 3000 meters, found that the one-third knot current at that depth was still flowing in the same direction as the surface current. This result was surprising in view of the usual dynamic calculation of surface currents which assumes a level of no horizontal motion at a depth of 2000 meters. Recent theoretical work had also predicted the thickness of the Stream to be no greater than 1600 meters. The deep countercurrent found earlier, and taken as a confirmation of this theory, was, however, located off the Blake Plateau where it would not be expected to flow directly beneath the Gulf Stream. These, on the other hand, were the first direct measurements of deep current directly under the western boundary current. As a consequence, some revision of prevailing theory may be required.

Several other projects in physical oceanography undertaken during the year illustrate the increased utilization of novel instrumentation. Using such devices as neutrally buoyant floats, telemetering drift-buoys, parachute drogues and a variety of newly designed current meters, several studies involving the direct measurement of specific current regimes were undertaken. Some of these investigations were carried out from the CRAWFORD in the area of the North Atlantic salinity maximum east of the Bahamas. The CHAIN, in conjunction with the Scottish Fisheries Research Ship EXPLORER, likewise used similar techniques on the Iceland-Faroes Ridge and on several shorter cruises off the edge of the continental shelf to the southeast of Woods Hole.

In addition, measurements of horizontal velocity shear near the sea surface by use of towed pitometers were undertaken from the CHAIN during October and November. First analysis of these measurements indicates that the direction of the observed shears agreed quite well with the direction of ship's drift.

A second instrumented wave tower for telemetering wave height and slope, as well as wind speed and direction, was erected in Buzzards Bay. The data were transmitted by an FM radio link to Woods Hole, recorded and coded for analysis by the Institution computer. The instrumentation system on the buoy functioned as planned, but the project was brought to a halt by the collapse of the tower during a hurricane in the fall.

The oceanographic program on the continental shelf has now been under way for five years and has revealed the need for moored oceanographic stations to measure temperature and current velocity at a network of stations.

Thus, the analysis of the temperature fluctuations on Brown's Ledge over a period of 56 days indicated that abrupt shifts in temperature there are the result of new water masses moving in rather than changes within a given mass. Prevailing winds can contribute to the persistence of one water type in a particular locality for appreciable periods.

As a result of the analysis of the drift bottle returns over the past ten years, the non-tidal surface currents in the Gulf of Maine can now be described. The Maine eddy appears north of 43°N from November to January. It expands southward in February and March to the northern edge of Georges Bank, and it remains there from April through August. Then, in September and October it contracts northward once more. Surface motions on Georges Bank are westward in March, but become a clockwise eddy about the shallower parts of the Bank in April and May. These eddies degenerate in June, and, during the six months, August through January, the currents are generally toward the east and southeast.

South of New England, the surface currents in March and April are closely interwoven with those of Georges Bank, acting as the western extension of the Georges circulation. By May, however, there is a definite indraft at the surface from the outer limits of the continental shelf between South Channel and 71°W. This indraft continues through August after which the circulation turns west and then presumably offshore.

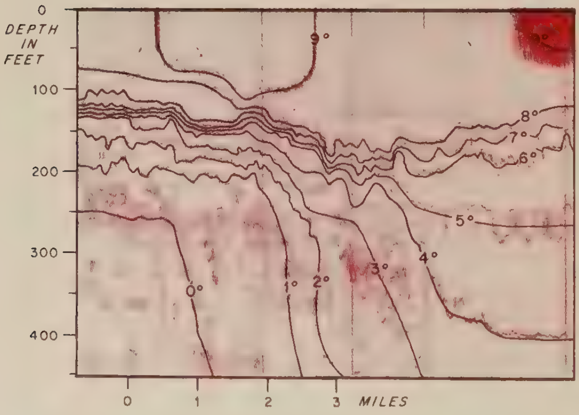

Record from CHAIN cruise 13, August 18, 1960, with identification (°C) overprint, shows Atlantic-Arctic water convergence.

mathematics and theoretical oceanography

The investigations into electrically driven motions in fluids of low conductivity were terminated with a study of the surface motions which are the consequence of the combination of the distortion (caused by surface tension) of the interface between two fluids and a steady applied electric field. It was shown that intense motions could be set up at the interface because of the distribution of charge which results from the distortion of the interface. Values of the electric potential and the scale of motion as functions of the microscopic parameters at the point of onset of instability were derived.

The gravitational instability of a gas mixture was examined for the case when a gradient of component concentration had been set up by the diffusive process. As a consequence of this, it appears that the classical theory of Bénard convection can be applied to this problem provided that the density term in the Rayleigh number is reinterpreted in terms of the actual densities of the concentration gradients. When the diffusion coefficient is much larger than the viscosity, a large stabilizing effect enters. However, there is no evidence that the diffusion coefficient can be much larger than the viscosity coefficient in real gases.

The possible application of information theory to fluid flow was also tested. In particular, an attempt was made to deduce the "preferred" solution in non-linear fluid flow from the principle of maximum uncertainly. This work is being continued.

Studies on turbulence were continued, and it was found possible to deduce the gross qualitative structure of shear flow and thermal turbulence from a new application of similarity theory. It is believed that the simplicity of this formulation will make more complicated fields of motion accessible to analysis. This similarity argument is based on two assumptions, viz., that the mean fields in statistically steady turbulent flows do not exceed the conditions for marginal inviscid stability and that the smallest scale of motion which is unstable on the mean field is the smallest scale which contributes to the transport process. The theoretically deduced mean temperature profile compares favorably with observations. Quantitative agreement is within ten per cent of the observed results.

A laminar jet, in a "shallow layer" of less dense water is in geostrophic equilibrium above an infinitely deep resting layer of denser water. The quasihydrostatic process for releasing energy in this thermoclinic model was compared with other baroclinic and barotropic models. It was shown that a small amplitude disturbance can grow only if there is a transfer of kinetic energy from the horizontal variations in the mean jet, and that conversions of the available mean potential energy can only occur concomitantly with this process. An examination of the characteristic equation, following the arguments of Lord Rayleigh's theory for non-divergent jets, shows that the finite depth of the thermocline inhibits inflectional instability.

A study of the data collected on a detailed survey of the Gulf Stream off Onslow Bay has revealed several interesting features. The largest lateral amplitudes were found to be about 50 kilometers where the meanders exhibited an asymmetric structure at the surface. This may be an indication of the lateral transfer of heat and energy. The pattern of asymmetry is similar, on a much smaller scale, to that for multiple currents found downstream from Cape Hatteras. Because of their periods, the Florida Current meanders are not incipient forms of the larger ones downstream, nor are they induced by a tidal pumping action in the Gulf of Mexico. Furthermore, their surface transfer of momentum is against the mean velocity gradient. Hence, the Florida Current meanders, instead of being a mechanism for the dissipation of the mean current, as had been expected, are actually adding energy to it.

Using additional observations collected by the Marine Laboratory at the University of Miami over an eight-year period, the surface transfer of momentum across the current between Miami and the Bahamas was computed. The results are similar to those found for the current off Onslow Bay; namely, that there is a transfer of momentum by the perturbations against the mean velocity gradient.

marine meteorology

Attacks on the main problem of marine meteorology, the interactions of the atmosphere and ocean, have been pressed from many different angles during the year. Convection and cloud physics have been studied by means of theoretical and experimental models and measurements from airplanes in the clouds themselves. Large-scale studies of the cloud patterns across the Pacific Ocean have been made, as well as studies of the small-scale variations of the water vapor pattern in the trade winds off the Bahamas. Much needed direction and insight into the problems of marine meteorology is contained in a new survey book covering the field of air-sea interaction.

The importance of cumulus clouds in marine and global meteorology is twofold. First, they are the most effective process for transporting water vapor from the thin sub-cloud layer to a thick layer which carries the vapor to the equatorial regions. Second, once arriving in low latitudes, cumulus clouds tower to the stratosphere releasing the latent heat of condensation of the vapor which provides energy for the global wind system of the atmosphere.

Because of the key role of cumulus clouds in the transfer of energy, much attention has been focussed on the physics of cloud drops and cloud formation. Aircraft observations of clouds in the Bahamas and in the neighborhood of Woods Hole have been made. These consisted of nose-camera photographs, wet- and dry-bulb temperatures, measurement of liquid water content and turbulent vertical velocity records in and around cumulus and stratiform clouds. The observations are being reduced for interpretation in terms of a theoretical "bubble" model of buoyant elements in cumulus clouds. A crucial aspect of the work is the empirical evaluation of arbitrary parameters introduced into the "bubble" model with the help of the above observations.

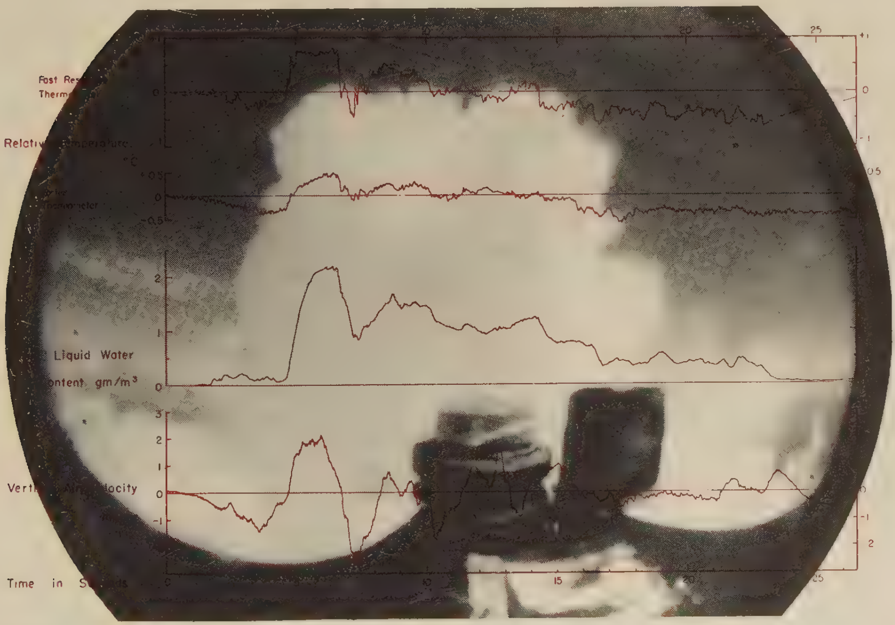

LEVINE

Meteorological measurements while flying through cumulus clouds.

Laboratory experiments complement the direct observations of the atmosphere. For convenience liquids are used rather than gases. A small mass of dyed salt water released into a large mass of fresh water acquires the character of a turbulent vortex ring (and resembles a miniature nuclear bomb explosion). By adding salt to the fresh water in different concentrations at different depths, we change the behavior of this vortex ring. For example, at a level where there is an abrupt change in the salinity (density), the ring can be observed to spread suddenly. Such experiments yield information and concepts for describing the spread of giant cumulonimbi at the tropopause and the penetration of trade-wind cumuli into the trade inversion.

Work on the relation of cumulus to hurricanes has continued, and papers have been published describing the energy transformations and the relations of the diameter of the clouds to vertical velocities.

Before the water vapor and heat can be transported by cumulus clouds, they must first be diffused by turbulence from the ocean to the base of the clouds. This process has been observed from the DC-3 airplane for several years from Newfoundland to Trinidad. A recent paper presents the turbulent heat and water vapor transport through the sub-cloud layer. The variation of these quantities with latitude, the ratio of heat to water vapor flow and the downward flow of heat from the upper air are described. The airborne radiometer was developed and used to determine the net radiational flux in the atmosphere so that the heat budget of the ocean-air system could be established. Observations made in the trade-wind air have been reduced and heat budgets for a few days have been constructed.

The introduction of the Recomp II computer this year allowed an ambitious project to be carried out that otherwise would have been impractical. In order to determine how the water vapor of the trade wind air varies at different heights below the clouds, a three-airplane study of the air off Eleuthera was carried out in August. Values of dry- and wet-bulb temperatures were recorded every three seconds in three airplanes during 10 to 20-minute flights with the airplanes stacked at different levels. An hour of computer time is sufficient to handle the staggering amount of data accumulated on each run.

For a better understanding of the shearing stress of the wind on the water surface, a small spherical anemometer is being developed to measure the three components of the turbulent wind.

An empirical study in forecasting the temperature of southern New England winters by means of November pressure distributions has been continued. Of the various features of pressure distribution which have been tested as indicators of our winter temperatures, the most reliable is a well-defined trans-Arctic ridge as indicated by the isobars along the Atlantic side of the ridge. Strong flow from Siberia to the United States, together with the development of a trough off the east coast, are found to be indications of colder-than-normal winters. On the other hand, an ill-defined trans-Arctic ridge with little indicated flow of air from Siberia to the United States and a well-developed east coast high cell often precede a warmer-than-normal winter.

Earlier ideas about the retention of particles immersed in cell-like or vortical circulations in fluids and about the growth of raindrops on a basic nucleus of sea salt led to a much discussed theoretical study of raindrop growth in cloud parcels. This work progressed to some experimentally testable conclusions about the time variability of the numbers, sizes and salinities of raindrops falling from the base of warm shower clouds in maritime air. It also underlines the importance of filling the gaps in our knowledge of the dynamics of cumulus growth if further progress in understanding of the microphysical processes is to be made.

A more detailed study of Project SHOWER data led to the conclusion that tradewind shower rains may be generated in distinct parcels of unusually moist cloud air which are identifiable near sea level prior to the

WRIGHT

Re-comp II has been used to broaden our consideration of many heretofore "impossible" problems.

lifting of the air and the formation of clouds. The total rainfall from showers formed in marine air appears to be related to the amount of salt spray in this sub-cloud.

To further such studies, semi-continuous rain recorders capable of effectively counting all showers and giving their drop sizes are being built. A modified flame photometer for the measurement of sodium concentration in individual raindrops has been designed and tested.

Steam clouds from the flow of lava into the sea during the 1960 volcanic eruption at Kilauea in Hawaii offered a unique opportunity to learn about the potential importance of coastal volcanoes as sources of salt-nuclei in the atmosphere. Particle sampling flights by aircraft through these clouds revealed high concentrations of minute droplets containing sea salt. The salt particle production rate by the action of hot lava in contact with sea water was many millions of times greater than that of an equal area of the sea surface. The size range of these salt particles was from about 0.1 to 10 microns radius. These results are meteorologically important during periods of intensive volcanism.

An extensive and important study of bursting bubbles at the sea surface as a source of electrically charged saline particles in the atmosphere was completed during 1960. Climatic atlases and the extensive data assembled over the years on the distribution of sea salt in marine atmospheres permitted a careful evaluation of the flux of salt from the world oceans as a function of wind force and altitude. The flux of positive charge from the world oceans, carried into the air by the droplets ejected by bursting bubbles, has been found to lie between 100 and 200 amperes. The annual flux of sea salt is about 10^{10} metric tons.

geophysics and submarine geology

The study of the sea floor by means of echo sounding, dredging, underwater photography, coring, geothermal gradient methods and seismic reflection and refraction has continued to be a principal activity. Although, during the year, these have been carried out from the Equator to north of the Arctic Circle, some of the most interesting investigations have been completed in waters adjacent to the Institution. Using the seismic profiler, reflection surveys carried out by the BEAR extended and confirmed earlier work, indicating that two passages in Narragansett Bay are underlaid by sediment-filled gorges and bed rock. These gorges have exceedingly irregular profiles and in places are over 400 ft below sea level.

A fascinating correlation of sub-bottom structures in Cape Cod Bay was also completed during the summer. Glacial deposits, preglacial topography and underlying late Mesozoic structures were successfully charted in the bay. As an interesting adjunct to this work, coring operations on the Cape proper and a test well put down in the Provincetown area demonstrated the presence of Eocene sediments at a depth of about 100 ft. These cores have also proven useful in the identification of seismic horizons which were initially discovered with the continuous seismic profiler in Cape Cod Bay.

On the two long cruises during 1960, one to the Caribbean and Bahama area and the other to the Norwegian Sea, a variety of interesting geophysical observations were made. Unlike many of the other geophysical investigations, photography permits a study of results relatively quickly. During the year about 500 stereoscopic pairs of photographs of the ocean bottom were taken from the CHAIN. These pictures, partly in black and white and partly in color, revealed many scenes of rugged rocks, of mud and of sand, often with ripplemarks. Nearly everywhere there was abundant evidence of animals living on the sea floor. The color and structure of rock beds have proven useful in studying submarine canyons and rift valleys. One group of photographs taken at a depth of seven kilometers on the north wall of the Puerto Rico Trench show freshly fractured rock surfaces. In the same vicinity companion photographs show large boulders of native rock. This group of photographs has become especially exciting since the recently completed analysis of seismic profiles taken at the same time strongly suggests that the top of the basaltic layer (the "third-layer" of seismologists) outcrops on the north wall at this depth. This, in fact, may be an area, where due to great tectonic activity, the base of the earth's crust may actually be exposed.

Using a variety of high intersity sound sources, seismic reflection techniques have been used to determine the sub-bottom structure in the Baltic, across the Norwegian Channel, across the continental shelf and slope west of Norway, in the North Sea and in the English Channel. The seismic reflection studies in the English Channel were made in collaboration with British geologists who had previously carried out an extensive coring program there. The series of reflection profiles at the edge of the Norwegian shelf showed nearly horizontal beds outcropping on the continental slope at depths of 700 meters. These were supplemented by dredgings which recovered freshly broken calcareous rock from depths greater than 500 meters. Reflection surveys were also carried out in several Norwegian fjords and outlined the form of the rocky channel in which sediments were deposited. Sedimentary material for biochemical analysis was also collected from the bottom of fjords where little oxygen is present in the water.

On the CHAIN's passage across the Atlantic in mid-summer, vertical temperature gradients were measured in ocean sediments at several locations. Heat conductivity was also measured in core samples taken at the same places to provide data for computing heat flow from the earth's interior. The majority of these measurements resulted in nearly normal heat flow (close to 1.3×10^{-6} cal/cm^2 per sec) but one in the Mid-Atlantic Ridge resulted in a value greater than 6×10^{-6} cal/cm^2 per sec.

The sound velocity of bottom sediments has been measured directly on deep sea cores and compared with high resolution echo soundings which showed multiple echoes. The latter suggest reflections from flat beds only a few feet below the bottom surface. It has been especially interesting to carry out detailed sound-velocity measurements on the cores on shipboard. These velocities are well correlated with other characteristics of the cores and the positions of abrupt changes in velocity correspond well with echo-sequences where the latter persist horizontally over large areas. Less persistent echo-sequences do not correspond with the characteristics identified in the core material.

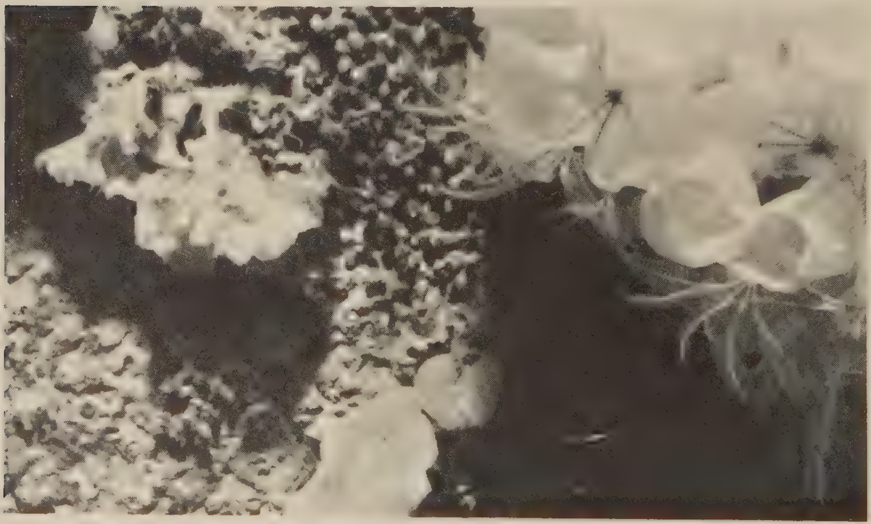

PRATT

In addition, cores were collected in several areas for special geological and geochemical investigations. Two series were collected in the Caribbean during the winter as part of a general program to determine the circulation and sediment patterns there. One set, taken along the downwind side of the Windward Islands, will be used to examine the alteration of volcanic minerals by sea water. Another from a large area of the Yucatan Basin and nearby plateau will afford an opportunity to study the distribution of the biologically derived components of sediments in relation to the physical properties of the environment. Again, special emphasis has been given the low oxygen content in the basins.

In the late summer, the ATLANTIS made a short cruise to a clay area on the continental shelf east of Cape Cod where several new analytical techniques were attempted on freshly collected material. Thus, a higher salinity content was demonstrated in the interstitial water of the sediment in the upper part of the core than occurs in the bottom water iself. In contrast to this, lower interstitial salinities were found deeper down in the core and suggest a transition across a Pleistocene interface. The acidity of the interstitial water was greater than that of the bottom water. This is considered to be due to high CO_2 pressures developed by the bacterial decomposition of organic material.

Outstanding examples of high speed photography of the deep ocean floor, near Bermuda, showing various animals. Photo below: Owen stereo camera. Photo opposite: Edgerton camera.

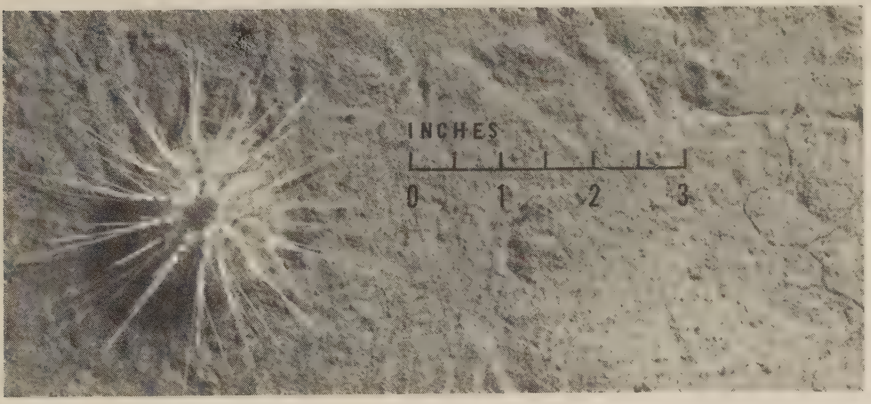

OWEN

underwater acoustics

Interest has continued in the animals which through their diurnal vertical migrations form layers in the ocean. These can be detected by the scattering of sound. Using explosives as sound sources, broad-band sound scattering observations were made at about forty-stations from the northern Norwegian Sea to the Bahamas on two ocean crossings. A new sound spectrum analyzer permits better and more rapid analyses while still at sea. The frequency-dependent characteristics of scattering layers at three widely separated localities in the western Atlantic and the changes in the scattering spectrum during vertical migrations will be published shortly. The frequency-depth relationship continues to be compatible with our concepts of the behavior of the swim-bladder in bathypelagic fishes with changes in pressure. These fish are presumed to be the sound-scattering agents.

During 1960 considerable attention was paid to an unusual sound-scattering feature restricted to the slope water off the coasts of the northeastern United States and Canada. This peculiar phenomenon, nicknamed "Alexander's Acres," is located northeast of Cape Hatteras in an area bounded to the north and west by the 200-fathom curve and to the south and east by the Gulf Stream. "Alexander's Acres" is detected at a mid-day depth of about 200 fathoms and migrates up to the surface at night. Unlike the ordinary deep-scattering layer whose reverberation is diffuse and relatively weak, this layer consists of groups of strong scattering agents. Their reverberations cause crescentic patterns on the echo-sounder record much like those found in shallow water over the fishing banks. In 1959 this scatterer had been continuously distributed over thousands of square miles between Cape Hatteras and the latitude of New York. In 1960 it had a rather spotty distribution and was even missing over much of this area. In other words, here is an oceanic population which fluctuates from year to year as do many coastal animals. The identification of this animal, thought to be a fish, would be of great interest. However, attempts to photograph it with the echo-sounder camera apparatus on various cruises of the BEAR have been unsuccessful as were preliminary attempts to catch it with deep-set gill nets and longlines. In the successful fishing trip of the CRAWFORD in November, reported below, there was a good correlation between the appearance of "Alexander's Acres" on the fathometer record and a successful catch of large fish.

An analysis of echo-sounder records made by YAMACRAW and CHAIN in the Strait of Gibraltar and its approaches at times when dynamic studies were also being made there has demonstrated the value of such records in studying circulation problems. It was shown that sound scatterers in the Strait of Gibraltar are useful in determining the boundary between the surface layer of east-flowing Atlantic water and the deep layer of west-flowing Mediterranean water. Moreover, in the Strait, a scatterer was observed whose daily pattern of vertical migration is reversed. It moved upward in the daytime and downward at night. Such a scatterer was not detected on records made in either the easterly or westerly approaches to the Strait. These observations were presented at the meetings of the International Union of Geodesy and Geophysics in Helsinki during the summer of 1960.

Acoustic analyses of whale sounds has continued, as opportunity offered, and so far twelve species of whales and porpoises have been definitely associated with their corresponding sound records. It is extremely difficult to identify the source of sounds heard at sea, and so this apparently small score is in reality a considerable achievement.

A thorough understanding of sound transmission can only be achieved with a knowledge of its relationship to the properties of sea water and the earth beneath. This has required the development of instruments for measuring the environment in greater detail, particularly high-energy sound sources. Sounds received from these sources in the ocean consist of a train of pulses having characteristics of their transmission paths through the ocean. Techniques developed over many years for identifying the transmission paths and measuring the energy flux in these pulse trains have been applied in experi-

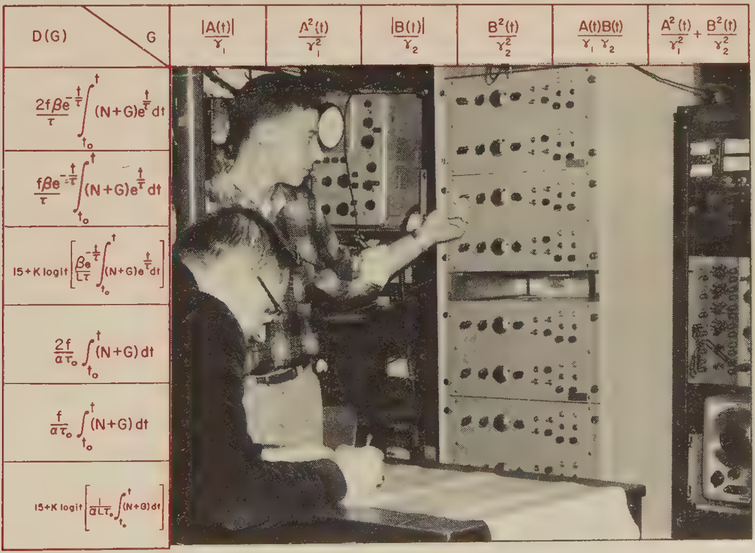
D(G)
G
$\frac{|A(t)|}{\gamma_1}$
$\frac{A^2(t)}{\gamma_1^2}$
$\frac{|B(t)|}{\gamma_2}$
$\frac{B^2(t)}{\gamma_2^2}$
$\frac{A(t)B(t)}{\gamma_1 \gamma_2}$
$\frac{A^2(t)}{\gamma_1^2} + \frac{B^2(t)}{\gamma_2^2}$
$\frac{2f\beta e^{-\frac{t}{\tau}}}{\tau}\int_{t_0}^{t}(N+G)e^{\frac{t}{\tau}}dt$
$\frac{f\beta e^{-\frac{t}{\tau}}}{\tau}\int_{t_0}^{t}(N+G)e^{\frac{t}{\tau}}dt$
$15+K\,\mathrm{logit}\left[\frac{\beta e^{-\frac{t}{\tau}}}{L\tau}\int_{t_0}^{t}(N+G)e^{\frac{t}{\tau}}dt\right]$
$\frac{2f}{a\tau_0}\int_{t_0}^{t}(N+G)\,dt$
$\frac{f}{a\tau_0}\int_{t_0}^{t}(N+G)\,dt$
$15+K\,\mathrm{logit}\left[\frac{1}{aL\tau_0}\int_{t_0}^{t}(N+G)\,dt\right]$

New sea-going analog computer, developed at Woods Hole, provides a variety of computations for the scientist.

ments in the North Atlantic Ocean over long, nearly horizontal sound paths. Other observations using short inclined sound paths were made to measure the reflection from the ocean floor. Large quantities of such data collected continuously while under way necessitate the development of automatic data processing aids, now in progress.

Continuous records in over ten thousand miles of towing, made with the thermistor array have delineated the time-space variations in the shallow temperature structure over deep water. In addition, similar studies were made of the "cold wall" of the Gulf Stream south of the Grand Banks, in the Strait of Gibraltar, and in the boundary between Arctic and Atlantic waters in the Norwegian Sea. These investigations were concerned with the effect of tides, of other short-period disturbances acting within the water, and of the local weather on the thermal structure near the sea surface.

"Sound-scattering by Marine Organisms" and three other related chapters have been prepared for the forthcoming book, "The Sea: Ideas and Observations." These are concerned with the physics of underwater sound-scattering, biological sounds and a collection of observational underwater sound data which have been accumulated from the deep ocean.

chemistry

Throughout the year, continued emphasis has been placed upon the use of various radioactive fission products in the general study of ocean circulation. So far, strontium-90 has proven to be the most useful isotope, and its distribution in the ocean has several interesting features.

A North Atlantic station made by the CRAWFORD in March illustrated strikingly the effectiveness of heavy winter winds in vertical mixing of surface waters. For two days an unusually severe storm made hydrographic work impossible in this area, and it appeared to have significantly raised the salinity and temperature in the 500-800 meter water level. Fission product samples taken after the storm from the surface to 500 meters showed uniform strontium-90 values. This evidence of mixing is particularly striking since we have not previously postulated massive storm mixing to depths below about 300 meters.

A Gulf Stream station made late in 1959 showed a very sharp strontium-90 gradient in which a zone of high concentration was found to be between 300 and 500 meters while a year and a half earlier, this zone was between 80 and 250 meters. The 300 meter level is somewhat higher than the surface value and may be a consequence of reduced atomic testing in 1959. The sharp gradient in lanthanide radioactivity remained between 100 meters and 300 meters, confirming earlier evidence that the processes controlling vertical movements are different for strontium and for the lanthanides.

A study of our total strontium-90 data based on the integration of the curves for strontium-90 at various depths indicated both a very considerable mass transport of water to the 300-500 meter depths in periods of only 2-3 years and that the total strontium-90 in the water column in Atlantic mid-latitudes is much higher per unit area than that estimated for comparable latitudes on land. This surprising result is strengthened by the finding that the strontium-90 content is higher in coastal and island samples. This suggests that the simple explanation that the sea-surface is the optimal fall-out collector is unlikely and that instead there is involved a specific phenomenon of marine or near-marine meteorology.

An increasing emphasis has been placed on electrochemical problems, especially those involved in the operation of the GEK (geomagnetic electrokinetograph). An experimental investigation of this, by replacing the long cables and towed electrodes with salt bridges and deck-mounted electrodes, appears to have real promise and is being pursued actively. Using this means, it should be possible to eliminate or compensate for the sensitivity of electrodes to salinity, temperature, pressure and oxygen tension without introducing any new sources of error.

Other electrochemical problems being studied are the determination of the activity coefficient of electrolytes in sea water, the contributions of the various components of sea water to its conductivity, theoretical analyses of diffusion and molecular motion in liquids, the question of instrinsic thermal electromotive force in the ocean and potentiometric frontal analysis in ion exchange chromatography.

Studies of the composition of sea water by use of ion exchange resins in the analysis have been initiated. These resins permit simple separation procedures that should give more accurate results for the major dissolved constituents. These experiments are aimed at testing the validity of the notion of the constancy of relative proportions for the major dissolved constituents in sea water. Earlier work has shown that both calcium and magnesium can each be separated from all other dissolved constituents with an increase in the accuracy of several orders of magnitude. Measurements of the calcium chloride ratio in samples obtained in the Bahamas have been shown to be different than the ratio obtained in open ocean water. At present attempts are being made to measure the total anion or cation equivalents in sea water by determining the acid or base produced by passage through either a cation or anion exchange resin bed. The ratio of these quantities to chlorinity should provide a direct measure of the theory of constancy of relative proportions.

Various techniques have been considered for the isolation of the very dilute organic components of sea water. The most promising is a modified chromatographic method in which the extractant, an organic solvent, is stabilized in a column on an inert carrier, such as a swollen polymer. The concentrating efficiency is much higher than in conventional batch extractions, and organic extracts of approximately 1 milligram per gallon of sea water have been obtained. These extracts were separated by acid-base fractionation, and their absorption spectra and interfacial properties have been examined.

marine biology

Our interests in life in the sea range from the floating microscopic phytoplankton and zooplankton to the largest fish, porpoises and whales and are primarily focused upon the ecology and distribution of species within various populations. These problems invariably require a combination of experimental studies in the laboratory and observations of the populations as they occur in nature at sea.

The ecology, physiology and distribution of phytoplankton populations in both coastal and oceanic waters have been the principal areas of interest. A study of the seasonal and spatial distribution of various species occurring between Montauk Point and Bermuda has been completed. The frequency at which each species was observed at various salinities shows that those species commonly classified as oceanic, often the flagellates, were indeed more frequent in the high salinity waters seaward from the shelf, and those considered as coastal, predominantly diatoms, were more frequent in the lower salinities of the shelf water. It appears, however, that salinity alone is not sufficient explanation for the comparative rarity of the diatoms in the open sea since in the spring bloom observed near Bermuda many so-called coastal diatoms were present in large numbers in waters of relatively high salinity.

Fortunately our ability to culture these organisms from the open sea has kept pace with our requirements for physiological experimentation. During the last year a number of truly oceanic species of the plankton algae have been isolated and cultured. These include representatives of the green algae, the diatoms and the coccolithophorids. With these organisms in pure culture a number of controlled physiological experiments designed to explain their occurrence and abundance may now be attacked. For example, our controlled studies have shown that coccolithophorids have a lower requirement for iron than diatoms. Thus, the low iron content of the open ocean waters may be one of the reasons why coccolithophores are most successful there than diatoms.

An intensive study of the phosphorus metabolism of unicellular algae has been carried on using the radioactive tracer, phosphorus-32. Algal cells can assimilate phosphorus rapidly from the environment in order to satisfy their needs, and when a cell has assimilated all that it requires, the exchange rate between the phosphorus in the cell and that in the medium decreases ten to a hundred fold. Radioactive tracer techniques have also shown that cells in pure culture are able to reduce the concentration of phosphorus in their environment to 1/10 to 1/100 that which it is possible to detect by ordinary analytical methods. This suggests that a bioassay technique using radiophosphorus may be the only way now available to obtain accurate analyses of the amount of phosphorus left in the ocean at the end of intense phytoplankton blooms. Comparisons of the rates of uptake of phosphorus by different species of planktonic algae may further aid in explaining the distribution of these species in nature.

Studies of the ocean-wide distribution of phosphorus have been continued, particularly on the data obtained during the cruises of the International Geophysical Year. From evaluation of the total water transport in the cross sections of the north Atlantic Ocean combined with the distribution of inorganic and total phosphorus, it is possible to derive a regional estimate of the mean productivity potential of different areas of the ocean. This analysis has now been completed on sections at 40°N, 8°N and 24°S and illustrates the interrelationship between the mass circulation of the oceans and the biological processes which can be carried on in various parts.

Two exciting advances have been made in our studies of the nitrogen cycle of the oceans. Available nitrogen is almost completely exhausted in the surface waters of the Sargasso Sea by the end of summer or early fall, and at this time of year we have repeatedly observed large blooms of the blue-green filamentous alga *Trichodesmium thiebautii* in these waters. The ability of this alga to fix atmospheric nitrogen for use in its metabolism has been studied in natural sea populations and there is only a small nitrogen fixation by this species. This may well explain its success in the impoverished Sargasso Sea waters at this time of year.

The second achievement relating to the nitrogen cycle has been the successful culturing of nitrifying bacteria from the water column in the open sea. For decades unsuccessful attempts to isolate these have led many to assume that all of the nitrifying process must go on in the bottom sediments where the bacteria had been found. The fact that maximum concentrations of nitrite and nitrate are found at intermediate depths is a convincing argument that the nitrifying process must indeed go on in the water column. The successful culture depended upon obtaining large samples of water, which are enriched with ammonia and the cultures started immediately on shipboard. During the last year the presence of these nitrifying bacteria and the process of nitrification has been demonstrated in samples of oceanic water collected from the continental shelf, from the slope water beyond the edge of the continental shelf, from the Gulf Stream and from the Sargasso Sea. This suggests that they are widely distributed in the ocean. The laboratory studies on the physiology of these nitrifying bacteria also demonstrated that they are true chemoautotrophs which use ammonia as their sole source of energy for the fixation of carbon and for growth. The

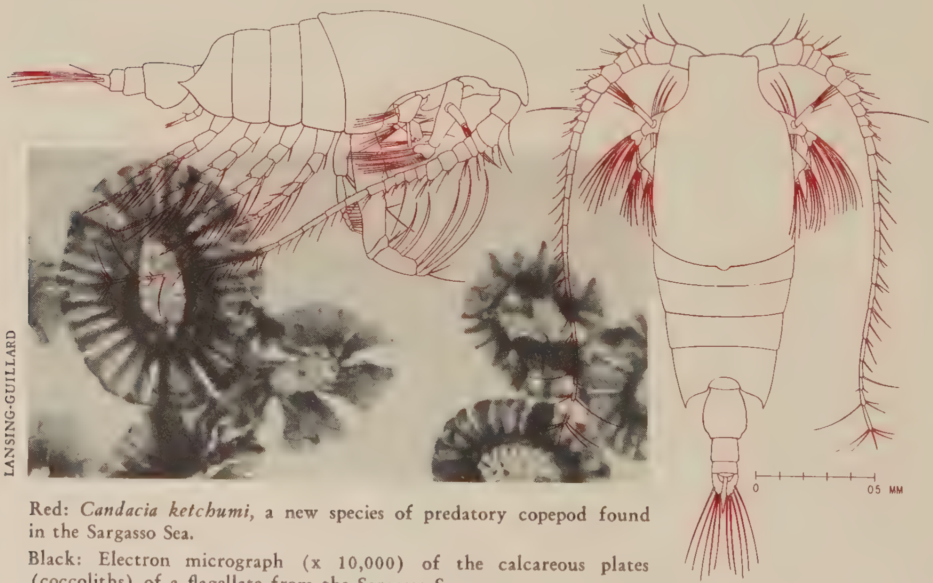

LANSING-GUILLARD

Red: *Candacia ketchumi*, a new species of predatory copepod found in the Sargasso Sea.

Black: Electron micrograph (x 10,000) of the calcareous plates (coccoliths) of a flagellate from the Sargasso Sea.

marine nitrifiers are euryhaline and can grow over a wide range of salinity whereas terrestrial nitrifying bacteria are unable to survive in full-strength sea water. This, and other differences between the physiology of the marine nitrifying bacteria and the terrestrial ones, suggest that the marine population is indeed different and probably consists of different species.

A study of the zooplankton collections made on cruises taken at four periods during the year between Montauk Point and Bermuda have been completed. Nearly 400 species have been identified, including two which were previously undescribed. Sixty had not previously been recorded in this area of the northwest Atlantic Ocean. The identification of many of these four hundred animals has been confirmed by cooperating taxonomic specialists. A reference collection of these has been established at Woods Hole. The copepods were the most abundant group of organisms in both neritic and oceanic waters. The next most abundant groups were the chaetognaths and euphausiids. In addition to being numerically the most abundant, the copepods, in spite of their generally small size, frequently formed more than half of the total weight of zooplankton. There was considerable seasonal variation in the size of the collections from the continental shelf, somewhat less in the samples obtained from slope waters, and very little in those obtained in the Gulf Stream and Sargasso Sea. The largest concentrations of zooplankton were generally found at or near the edge of the continental shelf with considerably smaller quantities of plankton as the distance seaward from the edge of the shelf increased.

In the Woods Hole region itself, the distribution of various species of zooplankton in the waters of Buzzards Bay, the Cape Cod Canal, and Cape Cod Bay are being intensively studied. This is an interesting area because Cape Cod is one of the temperature barriers to the distribution of northern and southern species of animals, and the presence of many species appears to be related to the temperature changes. The sharp horizontal temperature gradient, often as much as 12°C, between the two bays, permits distribution studies to be correlated with laboratory experiments on the effect of temperature and salinity changes, on respiration and feeding rates.

A knowledge of the structure and taxonomy of each species is fundamental to our distribution studies. Two intensive taxonomic studies have been carried on. First, the study of the functional morphology and musculature of the bottom-dwelling crustacean, *Hutchinsoniella*, and its relationship to the evolution of other major groups of Crustacea has been continued. Second, evidence is also accumulating that two or perhaps three supposed species of the genus *Euphausia* may really be different stages of a single species. At least one of these appears to be a juvenile form and, consequently, not a valid species.

Laboratory studies of the metabolism and nutrition of *Calanus hyperboreus* have suggested that this copepod may have three mechanisms which permit it to survive long periods of starvation. This ability would be particularly important for this species since it is most abuntant in Arctic regions where adequate food material is present in the water only during the brief Arctic summer. These survival mechanisms include the ability to decrease the respiratory rate in the absence of food, the adjustment of the density of the organism so that it is neutrally buoyant with its environment, and the storage of fat in quantities which may exceed 50% of its dry weight. The result of the low food requirements, the elimination of necessary motion and the food storage is that *Calanus* can survive for many months in a dormant state.

Studies of the optical properties of crustacean eyes have been continued. With microphotometric measurement of polarized light transmission, it has been possible to develop a model which confirms a previous explanation of the ability of one species to detect and orient to polarized light in water. Electrophysiological studies of another species make it appear that dark adaptation is a property of the central nervous system rather than of the optical system involving regeneration of the visual pigments.

Measurements of light penetration into the sea carried out in the Brownson Deep 50 miles north of Puerto Rico revealed the presence of the clearest ocean water ever measured. Daylight was detectable to a depth of 950 meters. Comparison with measurements of the visual sensitivity of certain deep-sea fishes indicated that these animals can distinguish between day and night at that depth or even slightly deeper. Bioluminescence was recorded to depths of 3750 m in the Brownson Deep. The brightest luminescent flashes were more than a million times brighter than the probably visual threshold for the deep-sea fishes. Thus, the flashes can be seen for a considerable distance in this very clear water and may be useful in recognition of one animal by another.

Laboratory experiments on the physiology and possible function of bioluminescence were carried out on the marine copepod *Metridia lucens*. This copepod produces a very bright flash which has its peak intensity in the blue-green range of visible light which has maximum penetration in clear sea water. Under normal conditions, *Metridia* does not luminesce spontaneously but can be stimulated electrically or do so when the animal is attacked by a predator. Placing a group of *Metridia* in a flask with an active predator, *Meganycpthanes*, produced a brilliant display characteristic of this copepod. The number of flashes was always greater than the number of *Metridia* eaten. This suggests that bioluminescence in this species may be used in nature to startle or distract an enemy.

Further evidence has been obtained that the breeding cycle of bottom-dwelling invertebrates is closely associated with changes in temperature. Additional species have been stimulated to breed in the laboratory during the winter (when the natural populations are not breeding) by providing elevated temperatures, artificial light to increase the length of day and abundant food. In a species of mud snail, *Nassarius obsoletus*, the growth rate of the larvae is decreased as the salinity decreases below 23‰ or as the tem-

WRIGHT

Tuna specimens brought ashore from R/V CRAWFORD after the successful November long-line fishing investigations. Over two hundred tuna were tagged and released.

perature is decreased below 22°C. The duration of the larval period is also lengthened at the lower temperature. These experiments pose interesting questions concerning the breeding cycle of the deep-sea invertebrates where the environment is always cold and dark. It is hoped to extend these observations by making studies of the development of the gonads of deep-sea organisms at various times of the year to determine whether they have a seasonal cycle of breeding, and if so, whether this is stimulated by environmental conditions or by an internal clock mechanism.

The location of the bluefin tuna in the late fall has long been a mystery. They disappear from our coastal waters in September or October and appear in the spring in the Caribbean area. Little is known about this migration. A most successful cruise on the CRAWFORD in November provides new information about the distribution and migration of tuna by discovering a very large concentration along the 1000-fathom curve off southern New England and Long Island. The catches were made by long-line fishing in which as much as eight or ten miles of multiple-hook lines were set and recovered three or four hours later. Our program of tagging the migratory pelagic fish to determine the extent of their migrations has been continued. Likewise, the study of the maturity and breeding cycle of bluefin tuna has progressed by histological study of the gonads and by tow-net collections and identification of juvenile specimens.

Studies of the schooling behavior of fishes were initiated at the Institution last summer by a visiting investigator and one of our summer Fellows. Why fishes "school," whether this is a learned or an instinctive characteristic of the species, and at what stage in the development of the individual the schooling habit is initiated, have long been vexing and interesting problems. These questions have been attacked by rearing juvenile fishes in isolation from their siblings so that they can be placed with a schooling population at various stages in their development. Such juveniles school very quickly when placed in schools of their own species, but they do not school with a lone member of their own species or with other species. The onset of the schooling tendency in the juveniles appears to be more related to the size of the individual than it is to the age.

The stranding of a live fin whale on a local beach not only caused considerable excitement but made it possible to conduct some physiological studies on a cetacean a hundred times larger than those which had been previously available to our staff. Both studies of thermoregulation by this whale and a hurried electrocardiogram were made before the whale was finally towed out to sea for the last time.

instrumentation

Two major related areas in instrumentation have been emphasized at the Institution during the year. These are the utilization of buoy-supported systems for collecting data and the development of increasingly refined techniques for handling the large amounts of data that are now being obtained.

Although work aboard ship has become more efficient in terms of the amount of research that can be done each day at sea, it is apparent that anchored buoys can provide an economic platform for the collection of oceanographic data. The results of last year's experiments in measuring deep currents in the Bermuda area indicated that observations over a longer period are required. This only appears feasible by using buoy stations. The scientific and engineering problems associated with such a large scale experiment will be studied by establishing a line of twenty-four moored buoys between Woods Hole and Bermuda; three in shallow water, the remainder in deep water. Each station will have a surface float with wind recording equipment and six to eight current meters attached at intervals down the mooring line. This equipment has been designed and built during the last six months. Each of the instruments, some two hundred in all, is self-recording and has a life in excess of 120 days. The stations will be visited every three to four months to recover the records, to refurbish the instruments and to replace the mooring lines.

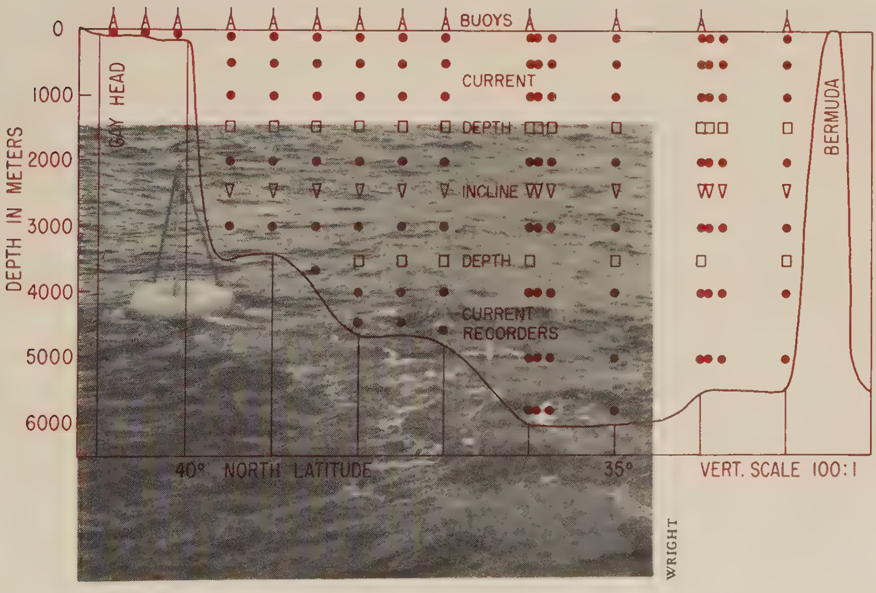

WRIGHT

Anchored buoy station and proposed line of stations for long-term oceanographic measurements.

Transducers, transmitters and receiving equipment for telemetering buoys developed at the Institution over the past few years have been modified in several ways. With a telemetering thermometer, water temperature can be measured on demand to an accuracy of approximately 0.15°C. Not only is this device economical to manufacture, but it has also been designed for direct digital output. The thermistor scanning system is triggered by an interrogating tone. As each of twenty-three thermistor outputs on a buoy is scanned, a servo amplifier is balanced against a reference potentiometer coupled to a shaft encoder. This encoder activates a relay matrix to convert the decimal output of the shaft into a modified binary code. This is then telemetered as one tone or a combination of two tones. The signal at the receiver is reconverted to a decimal code which is automatically typed out as the resistance of the thermistor.

In an attempt to develop a method for tracking drifting buoys from a shore installation, a preliminary investigation into the feasibility of retransmitting doppler shift information from transit satellites was made. As the power output of the satellites is increased, it is anticipated that the doppler shift signal could be recorded in the laboratory upon interrogation of the buoy and thus the buoy's position at the time of the satellite's passage computed.

The early TIROS I pictures made as part of the weather satellite program were difficult to interpret because of the unfamiliar appearance of cloud structures when seen from above. The Institution has cooperated throughout the year with the Air Force Geophysical Directorate by taking time-lapse photographs of the whole sky during those times when the satellite passed overhead in daylight.

The development of a gyro-erected optical navigation system (GEON) shows great promise. With a Mark 19 Sperry Gyro compass, stabilization for optical tracking is provided and a meridional reference maintained. With this equipment, it is possible for a ship to track its position to an accuracy of one nautical mile by celestial navigation continuously day or night whenever the skies are clear. Moreover, with the gyro indication of the local meridian plane, it is possible to obtain a fix by sighting only one celestial object.

The acquisition of acoustical data has tremendously increased during the last few years so that improved data-handling and processing equipment is now essential. During the year the first 8-channel analogue computers, developed at the Institution over a period of several years, were delivered. These can provide output functions such as the deviation from the arithmetic mean, the square of the inputs and any time integral of these qualities. Accurate computations can also be made for input wave forms containing Fourier components from 10 cps to 70,000 cps. The unit has already been tested at sea and has proven very effective in reducing the time required to analyze large quantities of acoustical data. Several of these units are being evaluated by us prior to delivery to other laboratories.

A spectrum analyzer has also been designed and successfully used at sea during the year. With an appropriate frequency, a signal can be graphically shown over an 8-kilocycle band between 120 and 32,000 cycles as a function of time. With this instrument the hundred channels are fed to a hundred-and-forty stylus recorder. The time variation of the output from each filter is recorded in order as a brown hue, the darkness of which varies with the intensity of the signal. The original sound is separately recorded on magnetic tape which can be replayed to permit the rapid analysis of additional bands.

Work has continued on the development and use of the National Bureau of Standards sound velocity meter. A very necessary adjunct to this instrument has been some method of satisfactorily measuring its depth as it is lowered in the water. This has been accomplished with an upside-down echo sounder attached to the sound velocity meter which provides the necessary depth information by measuring the acoustical travel time from the instrument to the surface regardless of the shape of the suspending wire. The bottom echo can also be measured so that the instruments can be lowered as close to the ocean bottom as required.

Two devices to produce higher power sound sources have been developed and utilized extensively for the continuous recording of sub-bottom reflections while the ship is under way. One, known as the Sparker, employs a high voltage underwater electric spark; the other, known as the Thumper, produces acoustic power by the eddy current deflection of an aluminum disc held in a plastic core. Since these sound sources produce low frequencies capable of penetrating the bottom, reflections from bodies of rock and layers of sediment below the bottom can be studied. The comparatively weak early models now in routine use have penetrated over a thousand feet of sediments in water of the same depth.

An attempt was made to improve the measurement of bottom slopes at right angles to the ship's path by placing a second transducer at some distance from the hull. To do this, a P5M seaplane wing was hinged to the side of the ship as a 45-ft. outrigger. Tests were carried out in the harbor on the ASTERIAS, in Vineyard Sound on the CRAWFORD, and on the high seas on a destroyer. An initial evaluation of this unusual arrangement indicates that it may provide a technique to determine the slope of the bottom topography on a single traverse of an area.

fleet operations

Although there were no major changes in the Institution's fleet during the year, considerable attention was devoted to the design of the new research vessel which will serve as a replacement for the ATLANTIS. As mentioned in the 1959 Annual Report, this vessel was made possible by a grant from the National Science Foundation. It is expected that the design and construction specifications will be completed in early 1961 and that the ship will be under construction before the end of that year.

In the belief that acoustical tools for general oceanographic studies will become increasingly important in the future, considerable emphasis has been placed on making certain that this vessel will be as acoustically quiet as possible. Low noise, slow speed control and economic maintenance and operation have dictated the use of reciprocating steam power plants. The change from diesel to steam power required an increase in the overall length of the vessel from 175 ft. to 210 ft. This increase will allow us to keep an 8,000-mile range at sea, as well as provide increased deck area and laboratory space for scientific purposes. The other general specifications of the vessel call for a beam of 44 ft, a displacement of 1800 tons, and a cruising speed of 12 knots.

To increase the effectiveness of the Helio-Courier light aircraft which the Institution purchased during 1959, a hangar to protect the aircraft was built on Dyer's dock, adjacent to the Institution. The end of this pier was modified in such a way that the aircraft can be run up out of the water on a ramp. Thus, an aircraft on floats can easily be used from the Institution property on the waterfront at almost all periods of the year. The hangar also facilitates the maintenance work on the aircraft.

The major activity at sea during the year was a 2½-month cruise during the spring, when ATLANTIS, CHAIN, and CRAWFORD were employed in a multi-ship survey of the Gulf Stream in the area northeast of the line between Woods Hole and Bermuda. In addition, the ARIES was also used during the third phase of the work, and the U. S. Coast Guard's Ice Patrol Vessel EVERGREEN participated in the first part of the program. With the exception of a month's cruise to the western Caribbean in the winter, the ATLANTIS served during the remainder of the year in the Bermuda area or in the offing of Woods Hole. In late December, she again proved the usefulness of her sailing rig, as she sailed home from a point west of Bermuda when her shaft was broken and she was unable to use her main engine.

The CHAIN operated in the Caribbean during the winter of 1960 and in the Gulf Stream and vicinity in the spring. She then embarked on a five-month cruise to the Baltic Sea, to the Norwegian Sea above the Arctic Circle between Iceland and the Norwegian Coast, and to the Irish and North Seas, as well as along the northerly track across the North Atlantic en route to Woods Hole. During this cruise to western Europe, a considerable number of foreign scientists participated in the research activities which were carried out on board. As a result of all this, her ability to support a varied and increasing by complex program at sea continues to impress all who participate in the work. The CHAIN visited Helsinki at the time of the meetings of the International Union of Geodesy and Geophysics, and many foreign oceanographers also had the opportunity to visit her there during the meetings.

Although the longest period at sea during the year was the Gulf Stream survey, already mentioned, the CRAWFORD took a long cruise to the east of the Bahamas during the winter. In addition to a number of trips out of Woods Hole, several were made to the continental shelf for various biological investigations.

As during the previous year, the ARIES operated almost entirely in the Bermudas area on the deep-current tracking problem except for her participation in the Gulf Stream survey and a short period in the Bahamas area. This work was completed by the end of the year, and the ARIES was readied for sale. She was sold early in 1961.

The BEAR operated principally in local waters with one long cruise in mid-summer to the Blake Plateau. In the late fall and early winter, however, the BEAR was used in the Tongue of the Ocean for a detailed survey of the bottom topography and sediment characteristics there. Since precise navigation was required for this, a special network of Decca stations was set up. The calibration and utilization of this navigational system posed many unusual operating conditions which had not previously been experienced.

The Institution's fleet put in 963 research days at sea during 1960. This is almost 100 days more than the record in 1959 and is an index of the increased research activity.

The DC-3-type aircraft supplied by Office of Naval Research and the Helio-Courier light plane have both been used extensively for a variety of meteorological and oceanographic problems. The Helio-Courier's slow-speed flight characteristics make it particularly useful for photographic and visual observations, made in connection with some of the biological and geological problems. The DC-3 has acquired more instruments to increase its usefulness as a research tool. In mid-summer both of the aircraft were used in collaboration with chartered light plane in a multi-plane meteorological sampling program to the east of Eleuthera in the Bahamas. Despite the great diversity in the flying characteristics of the aircraft involved, this operation proceeded very successfully and has encouraged plans for similar programs in the future.

ATLANTIS

Cruise No.	Dates	Areas of Operation	Days	Chief Scientist
253	18 Jan. – 18 Jan.	Local	1	Athearn
254	20 Jan. – 12 Mar.	Blake Plateau, Western Caribbean	24	Stetson, Athearn
255	8 Apr. – 15 June	Gulf Stream	69	Miller, Worthington
256	17 June – 30 June	Boston-Yard	14	
257	7 July – 20 Aug.	Bermuda Area	45	Bruce
258	30 Aug. – 2 Sept.	Local	4	Kanwisher
259	4 Oct. – 6 Oct.	Local	3	Stetson
260	11 Oct. – 7 Nov.	Bermuda Area	28	Pratt
261	16 Nov. – 25 Dec.	30°N 50°W	40	Worthington

ARIES

Cruise No.	Dates	Areas of Operation	Days	Chief Scientist
21–32	2 Feb. – 20 May	Bermuda Area	59	Swallow, Crease
33	25 May – 6 June	S. Gulf Stream	13	Swallow
34–36	17 June – 8 Sept.	Bermuda Area	66	Swallow, Crease
37	3 Nov. – 14 Dec.	Bermuda Area	42	Bruce

BEAR

Cruise No.	Dates	Areas of Operation	Days	Chief Scientist
232–249	1 Apr. – 22 June	Local	38	Hersey, Conover, Stetson, Hays, Zeigler
250	8 July – 27 July	Blake Plateau	20	Stetson
251	19 Aug. — 20 Aug.	Boston-Yard	2	
252–253	22 Aug. – 9 Sept.	Local	9	Backus, Knott
254	12 Sept. – 13 Sept.	Boston-Yard	2	
255–257	19 Sept. – 26 Oct.	Local	8	Backus, Knott, Amberseno
258	9 Nov. 1960 – 6 Jan. 1961	Nassau Area	60	Athearn

CHAIN

Cruise No.	Dates	Areas of Operation	Days	Chief Scientist
11	26 Jan. – 22 Mar.	Eastern Caribbean, Bahamas Area	28	Metcalf, Hays
12	5 Apr. – 15 June	Gulf Stream	72	Worthington, Fuglister
13	30 June – 12 Nov.	North Sea, Baltic Sea, Norwegian Sea, North Atlantic	136	Dow, Hays, Hersey, Worthington, Backus
14	21 Nov.	Boston-Yard		

CRAWFORD

Cruise No.	Dates	Areas of Operation	Days	Chief Scientist
37	16 Jan. – 9 Mar.	30°N 50°W	25	Worthington
38	14 Mar. – 19 Mar.	Bermuda-Woods	6	Corwin
39	26 Mar. – 26 Mar.	Local	1	Day Cruise for Science Students
40	7 Apr. – 15 June	Gulf Stream	70	Metcalf
41	13 July – 27 July	Local	15	Volkmann
42	2 Aug. – 7 Aug.	Local	6	Corwin
43	11 Aug. – 17 Aug.	Continental Shelf	7	Ketchum
45	22 Aug. – 23 Aug.	Continental Shelf	2	Watson
46	2 Sept. – 2 Sept.	Local	1	Mass. Science Fair Winners
47	6 Sept. – 9 Sept.	Local	4	Conover
48	12 Sept. – 13 Sept.	Boston-Yard	2	
49	19 Sept. – 23 Sept.	Local	5	Ketchum
50	28 Sept. – 30 Sept.	Local	3	Curl
51	3 Oct. – 5 Oct.	Boston-Yard		
52	12 Oct. – –12 Oct.	Local	1	Day Cruise for Science Students
53	13 Oct. – 17 Oct.	Gulf of Maine	5	Conover
54	19 Oct. – 21 Oct.	Local	3	Curl
55	25 Oct. – 30 Oct.	30°N 70°W	6	Metcalf
56	11 Nov. – 28 Nov.	Continental Shelf	18	Mather
57	29 Nov. –	Boston-Yard		

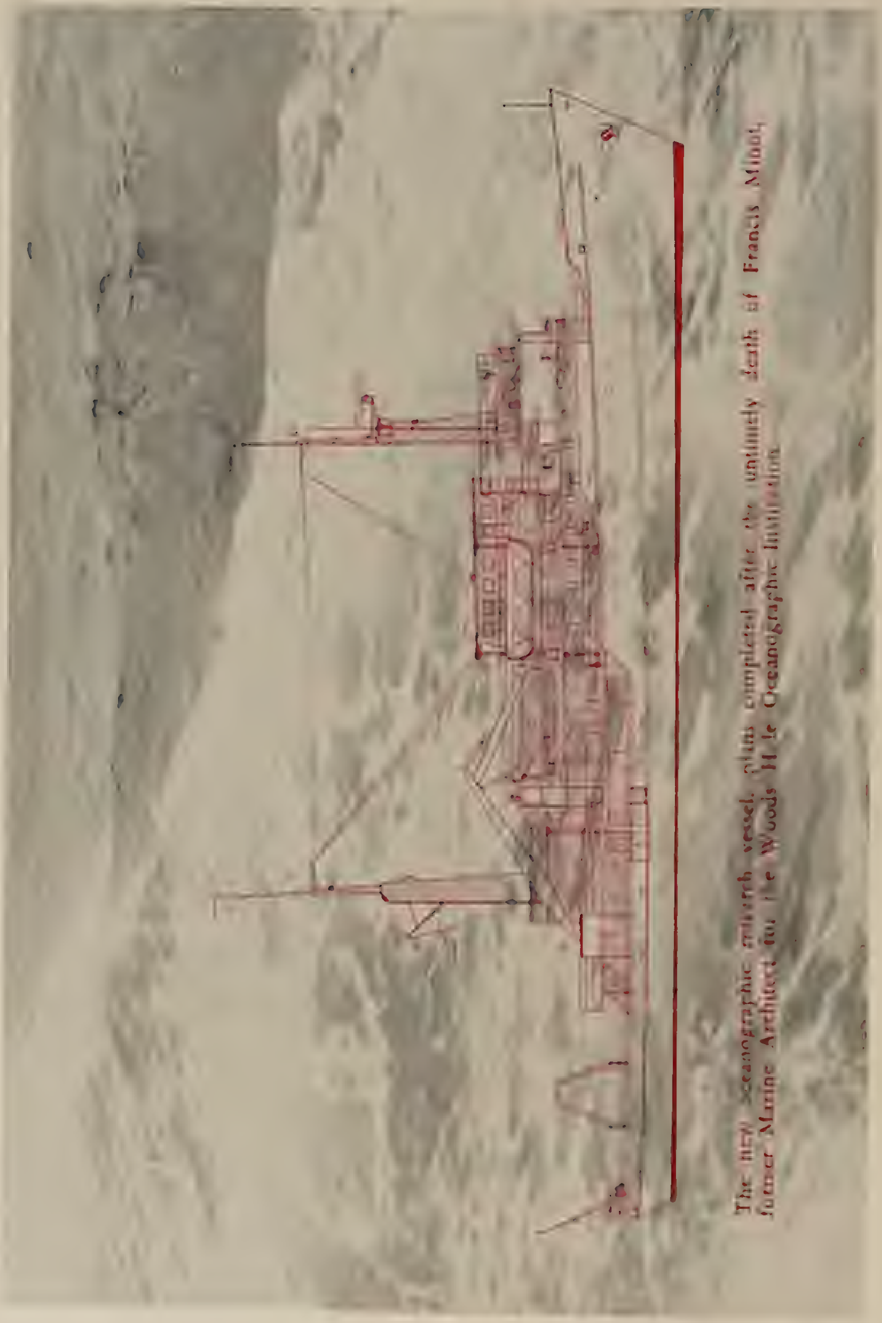

The new oceanographic research vessel, plans completed after the untimely death of Francis Minot, former Marine Architect for the Woods Hole Oceanographic Institution.

CAULFIELD

personnel

The following persons were awarded grants, honoraria or fellowships during 1960:

Walter H. Adey	University of Michigan
Michael Bayard	Carl Schurz High School, Chicago, Illinois
Robert A. Berner	Harvard University
Fred Bisshop	Brown University
Duncan C. Blanchard	Massachusetts Institute of Technology
Robert Roy Blandford	California Institution of Technology
William Blumen	Massachusetts Institute of Technology
David B. Clarke	University of Wisconsin
Richard A. Cone	University of Chicago
Richard A. Craig	Florida State University
Robert C. Crowdes	Harvard University
L. A. Earlston Doe	New York University
Ronald L. Duty	Brown University
Walter Eckhart	Yale University
Robert Ellis	Miami University
Michael Emptage	Middlebury College
John S. Farlow III	Johns Hopkins University
Frederick C. Fuglister	Massachusetts Institute of Technology
Augustine S. Furumoto	St. Louis University
Michael Garstang	Florida State University
Kenneth I. Gross	Brandeis University
William R. Holland	University of California at Los Angeles
Louis N. Howard	Massachusetts Institute of Technology
John Polk Kerr	University of Michigan
Robert H. Kraichnan	New York University
Eric B. Kraus	Snowy Mountain Hydro-electric Authority, Cooma, Australia
Joseph Levine	Massachusetts Institute of Technology
David T. Mason	University of California
David A. McGill	Yale University
Dennis Wilson Moore	Harvard University
Norman S. Neidell	Brown University
Gilbert S. Omenn	Princeton University
Bernard L. Oostdam	McGill University, Canada
Joseph Pedlosky	Massachusetts Institute of Technology
Mary Alys Plunkett	Vassar College
John Reitzel	Harvard University
Judith Sandberg	Hahnemann Medical College, Philadelphia Pennsylvania
Peter M. Saunders	Imperial College, London, England
Vincent J. Schaefer	Munitalp Foundation, Schenectady, New York
Alan B. Steinbach	University of Rochester
Bruce A. Taft	Johns Hopkins University
David G. Towell	Massachusetts Institute of Technology
Andrew J. Umen	Williams College
Bruce A. Warren	Massachusetts Institute of Technology

visitors

Distinguished scientists from this and many other countries honored the Institution visits during 1960. These included:

Masateru Anraku	Faculty of Fisheries, Hokkaido University, Japan
Richard G. Bader	Agricultural and Mechanical College of Texas
John P. Barlow	Cornell University, Ithaca, New York
Otis Barton	Palm Desert, California
Neil L. Brown	Commonwealth Scientific and Industrial Research Organization, Cronulla, Australia
William M. Cameron	Bedford Oceanographic Laboratory, Canada
Angelo Campanella	HRB-Singer, State College, Pennsylvania
R. Morrison Cassie	New Zealand Oceanographic Institute, Wellington, New Zealand
Vivienne Cassie	New Zealand Oceanographic Institute, Wellington, New Zealand
Sydney Chapman	High Altitude Observatory, Boulder, Colorado
Keith E. Chave	Department of Geology, Lehigh University, Bethlehem, Pennsylvania
Roland A. Cox	National Institute of Oceanography, England
James Crease	National Institute of Oceanography, England
Ronald I. Currie	National Institute of Oceanography, England
Odd Dahl	Norwegian Defense Research Department, Norway
L. Draper	National Institute of Oceanography, England
I. Engelsen	Norwegian Defense Research Establishment, Norway
Nestor C. L. Granelli	Servicio de Hidrografia Naval, Argentina
David Grant	Department of Biology, Yale University, New Haven, Connecticut
E. M. Hassan	University of Alexandria, United Arab Republic
William E. Hazen	Department of Zoology, University of Chicago, Chicago, Illinois
Koji Hidaka	Geophysical Institute, Tokyo University, Japan
M. S. Longuet-Higgins	National Institute of Oceanography, England
Jacob Hoffman	U. S. Navy Hydrographic Office, Washington, D. C.
Louis M. Lauzier	Fisheries Research Board of Canada
Douglas K. Lilly	U. S. Weather Bureau, Washington, D. C.
Richard S. Lindzen	Harvard University, Cambridge, Massachusetts
Eugenie Lisitzin	Havforskningsinstitutet, Finland
Jacob Magnússon	University Research Institute, Iceland

Ramón Margalef	Instituto Investigaciones Pesqueras, Barcelona, Spain
William E. Mead	Hudson Laboratories, Dobbs Ferry, New York
C. H. Mortimer	Scottish Marine Biological Association, Millport, Scotland
Michael M. Mullin	Harvard University, Cambridge, Massachusetts
H. Nodtvedt	Norwegian Defense Research Establishment, Norway
Necip Olcaj	Seyirve Hidrografi, Istanbul, Turkey
B. R. Pelletier	Department of Mines, Ottawa, Canada
Arthur K. Saz	National Institutes of Health, Bethesda, Maryland
Evelyn Shaw	American Museum of Natural History, New York
William B. Snow	Ramo-Wooldridge Company, Canoga Park, California
John C. Swallow	National Institute of Oceanography, England
Bernard Tobin	International Business Machine Corporation, Owego, New York
David J. Tranter	Division of Fisheries & Oceanography, CSIRO, New South Wales, Australia
Tj. H. Van Andel	Scripps Institution of Oceanography
Roman Vishniac	Yeshiva Medical School, New York
Harold P. Weixtraub	Thayer Academy Summer Science Program, Braintree, Massachusetts
Kuchiro Yamamoto	Hokkaido University, Hakodate, Japan

employees and staff

The following personnel were in the employ of the Institution for the twelve-month period ending December 31, 1960.

Allen, Ethel B.
Allen, Norman T.
Allen, Robert W.
Anderson, Nellie E.
Ashmore, Herbert A.
Athearn, William D.
Backus, Cyril
Backus, Harold
Backus, Jeanne M.
Backus, Richard H.
Barbour, Rose L.
Barrett, Joseph R., Jr.
Barstow, Elmer M.
Bartlett, Martin R.
Baxter, Lincoln II
Baylor, Edward R.
Becker, Edward B.
Behrens, Henry G.
Bergstrom, Stanley W.
Betterley, Robert
Blanchard, Duncan C.
Blumer, Max
Bodman, Ralph H.
Bowen, Vaughan T.
Bowman, Warren O.
Bradley, Mabel D.
Bradshaw, Alvin L.
Bray, Winfield S.
Brockhurst, Robert R.
Broughton, Jane F.
Brown, Joseph C.
Bruce, John G., Jr.
Bryan, Kirk, Jr.
Bryant, Edwin T.
Bumer, John Q.
Bumpus, Dean F.
Bunce, Elizabeth T.
Bunker, Andrew F.
Burnham, Charles A.
Cabral, John P.
Cabral, John V.
Cain, Henry A.
Cangiamila, Angelo
Carlson, Alfred G.
Carlson, Ruth H. E.
Carter, Alwyn L.
Carter, Richard J.
Casiles, David F.
Cavanaugh, James J.
Chadwick, Constance W.
Chaffee, Margaret A.
Chalmers, Agnes C.
Chase, Joseph
Christian, John A.
Chute, Edward H.
Clarke, George L.
Clarkin, William H.
Colburn, Arthur D., Jr.
Condon, John W.
Conley, William J.
Conover, Robert J.
Cook, Alden H.
Cook, Hans
Corwin, Nathaniel
Cotter, Jerome M.
Coughlin, Brooks W.
Crocker, Marion W.
Crouse, Porter A.
Curl, Elizabeth L.
Curl, Herbert C., Jr.
Davis, Charles A.
Day, C. Godfrey
Day, Joseph V.
Densmore, Charles D.
Devitt, Howard B.
Dimmock, Richard H.
Dimock, Alan D.
Dow, Willard
Dufur, Dana H.
Dunkle, William M., Jr.
Edwards, Richard S.
Eldridge, Stanley N.
Fahlquist, Davis A.
Faller, Alan J.
Ferguson, Sandra K.
Ferris, Alice H.
Ferris, George A.
Fielden, Frederick E.
Fisher, Stanley O.
Flaherty, John J., Jr.
Frantz, David H.
Fraser, John G.
Fuglister, Frederick C.
Fye, Paul M.
Gallagher, Gloria S.
Gallagher, Rosemary
Gallagher, William F.
Gaskell, Fred
Giese, Graham S.
Gifford, James E.
Gill, Barbara L.
Gingrass, Norman
Graham, John W.
Grant, Carlton W.
Grant, Carlton W., Jr.
Grice, George D., Jr.
Guillard, Robert R. L.
Hahn, Jan
Halpin, William T.
Halverson, Leonard G.
Hannah, Mary Ann
Hart, Arch D.
Hatzikon, Kaleroy L.
Hayes, Carlyle R.
Hays, Earl E.
Hays, Helen C.
Hellwig, Jessica D.
Hersey, John B.
Hessler, Robert R.
Hiller, Emerson H.
Hoadley, Lloyd D.
Hodgkins, Harry L.
Hodgson, Sloat F.
Houston, Leo C.
Howe, Paul M.
Howland, Myron P., Jr.
Howland, Paul C.
Hulburt, Edward M.
Hunt, Otis E.
Innis, Charles S., Jr.
Iselin, Columbus O'D.
Jenkins, Delmar R.
John, Alfred C.
Johnston, Alexander T.
Kahler, Yolande A.

Caron, Henri L.
Karram, Calvin D.
Ketchum, Bostwick H.
Ketchum, David D.
Knott, Sydney T., Jr.
Kostrzewa, John A.
Kuenzler, Edward J.
Lambert, Joseph L.
Langenheim, Anne E.
Leahy, Richard G.
Leiby, Jonathan
Levine, Joseph
Lyon, Thomas
Macaulay, Franklin A.
Mackey, Malcolm R.
MacKillop, Harvey
Maddux, Duane E.
Malkus, Joanne S.
Malkus, Willem V. R.
Martin, George E.
Mather, Frank J., III
Matthews, Francis S.
McCloskey, Margaret E.
McCormack, Eileen M.
McElliott, Joseph M.
McHardie, James
Mellor, Florence K.
Merchant, Floyd L.
Metcalf, William G.
Miller, Arthur R.
Minot, Mary K.
Mitchell, James R.
Mogardo, Juanita A.
Morehouse, Clayton B.
Morrison, Kenneth
Motta, Joseph C.
Munns, Robert G.
Mysona, Eugene J.
Nalwalk, Andrew J.
Oliver, Isabel
Orr, Joseph A., Jr.
Ortolani, Mary
Ostiguy, Betty P.
Owen, David M.
Palmieri, Michael, Jr.
Parker, Charles E.
Pasley, Gale G., Jr.
Foster, Donald B.
Pedersen, Miner, A.
Pennypacker, Thomas R.
Perkins, Calvin F.
Phillips, Helen F.
Pierce, Samuel F.
Pike, John F.
Pimental, John M.
Poole, Stanley E.
Pratt, Richard M.
Richardson, William S.
Rockwell, Robert E.
Rogers, Henry A., Jr.
Rogers, Mary D.
Ronne, F. Claude
Roth, Claës G. H.
Rose, Lawrence
Rossby, Harriet A.
Ryther, John H.
Salthouse, James E.
Sandblom, John D.
Sanders, Howard L.
Sawyer, Harold E.
Schevill, William E.
Schilling, John L.
Schleicher, Karl E.
Schroeder, Elizabeth H.
Schroeder, William C.
Sears, Mary
Seibert, Harry H.
Shaleski, Eleanor M.
Sharp, Arnold G.
Shields, William J.
Shultz, William S.
Siever, Raymond
Slabaugh, Luther V.
Snyder, Robert M.
Soderland, Eloise M.
Solberg, Otto
Souza, Thomas A.
Spencer, Allard T.
Spooner, Charles E.
Stansfield, Richard
Stern, Melvin E.
Stetson, Thomas R.
Stevens, Raymond G.
Stewart, Glenda R.
Kanwisher, John W.
Stillman, Stephen L.
Stimpson, John W.
Stimson, Paul B.
Stommel, Henry M.
Sugihara, Thomas T.
Sutcliffe, Thomas O. L.
Swinhart, Orrin L.
Tasha, Herman
Terry, William A.
Thunberg, Jon C.
Thurston, Theodore G.
Tometich, Louis J.
Turner, Harry J., Jr.
Vaccaro, Ralph F.
Vefder, Ronald A.
Veronis, George
Vine, Allyn C.
Volkmann, Gordon H.
von Arx, William S.
von Dannenberg, Carl R.
Voorhis, Arthur D.
Walden, Robert G.
Walker, Jean D.
Watkins, William A.
Watson, Margaret E.
Watson, Stanley W.
Watt, Helen M.
Webster, Jacqueline
Webster, Thomas F.
Weeks, Robert G.
Whitney, Geoffrey G., Jr.
Wilde, Phillips B.
Wilkins, Charles H.
Williams, George A.
Wilson, Edward
Wilson, Esther N.
Wing, Asa S.
Wing, Carleton R.
Winslow, Elisha F.
Witzell, Warren E.
Woodcock, Alfred H.
Woodward, Fred C., Jr.
Worthington, L. Valentine
Yentsch, Charles S.
Zeigler, John M.

publications

During 1960, seventy-seven papers bearing contribution numbers were published. See Author, Subject-Locality, Taxonomic Index published in 1957 for a complete list through 1956 and subsequent annual reports for the list of publications appearing since 1956.

No. 803. E. M. Hulburt, J. J. A. McLaughlin and P. A. Zahl. *Katodinium dorsalisulcum,* a New Species of Unarmored Dinophyceae. *J. Protozool.*, Vol. 7, No. 4, pp. 323-326. 1960.

No. 836. Frank J. Mather, III and Howard A. Schuck. Growth of Bluefin Tuna of the Western North Atlantic. *Fish. Bull.* 179, *Fish. Bull., U. S. Fish and Wildlife Service,* Vol. 61., pp. 39-52. 1960.

No. 990. Francis A. Richards. Dissolved Silicate and Related Properties of Some Western North Atlantic and Caribbean Waters. *Sears Found., Jour. Mar. Res.*, Vol. 17, pp. 449-465. 1958. (In *Collected Reprints* for 1960).

No. 991. Sherwood D. Tuttle. Evolution of the New Hampshire Shore Line. *Bull. Geol. Soc., Amer.*, Vol. 71, pp. 1211-1222. 1960.

No. 1000. Alfred C. Redfield. The Influence of the Continental Shelf on the Tides of the Atlantic Coast of the United States. *Sears Found., Jour. Mar. Res.*, Vol. 17, pp. 432-448. 1958. (In *Collected Reprints* for 1960).

No. 1005. Sheina M. Marshall and A. P. Orr. Some Uses of Antibiotics in Physiological Experiments in Sea Water. *Sears Found., Jour. Mar. Res.*, Vol. 17, pp. 341-346. 1958. (In *Collected Reprints* for 1960).

No. 1007. Bostwick, H. Ketchum, Ralph F. Vaccaro and Nathaniel Corwin. The Annual Cycle of Phosphorus and Nitrogen in New England Coastal Waters. *Sears Found., Jour. Mar. Res.*, Vol. 17, pp. 282-301. 1958. (In *Collected Reprints* for 1960).

No. 1009. James B. Lackey. *Calkinsia aureus* gen. et sp. nov.; a New Marine Euglenid. *Trans. Amer. Micr. Soc.*, Vol. 79, No. 1, pp. 105-107. 1960.

No. 1018. Floyd M. Soule and R. M. Morse. Physical Oceanography of the Grand Banks Region and the Labrador Sea in 1958. U. S. Coast Guard Bull., No. 44, pp. 22-99. 1960.

No. 1023. Henry Stommel and A. B. Arons. On the Abyssal Circulation of the World Ocean. I. Stationary Planetary Flow Patterns on a Sphere. *Deep-Sea Research,* Vol. 6, No. 2, pp. 140-154. 1960.

No. 1031. Andrew F. Bunker. Heat and Water-Vapor Fluxes in Air Flowing Southward over the Western North Atlantic Ocean. *Jour. Meteorol.*, Vol. 17, No. 1, pp. 52-63. 1960.

No. 1033. Howard L. Sanders. Benthic Studies in Buzzards Bay. III. The Structure of the Soft-Bottom Community. *Limnol. and Oceanogr.*, Vol. 5, No. 2, pp. 138-153. 1960.

No. 1034. J. S. Malkus and H. Riehl. On the Dynamics and Energy Transformations in Steady-State Hurricanes. *Tellus*, Vol. 12, No. 1, pp. 1-20. 1960.

No. 1035. Bostwick H. Ketchum. Marine Pollution Problems in the North Atlantic Area. In: Biological Problems in Water Pollution, Trans. Second Seminar, April 20-24, 1959, Cincinnati, Ohio, Sponsorship, Water Supply and Water Pollution Research Program, *Robert A. Taft Sanitary Engineering Center, U. S. Dept. Health, Education and Welfare, Publ. Health Service, Technical Rept.*, No. W-60-3, pp. 212-217. 1960. (Not in *Collected Reprints*).

No. 1040. William E. Schevill and Richard H. Backus. Daily Patrol of a *Megaptera. Jour. Mammalogy,* Vol. 41, No. 2, pp. 279-281. 1960.

No. 1042. D. W. Menzel and J. H. Ryther. The Annual Cycle of Primary Production in the Sargasso Sea off Bermuda. *Deep-Sea Research,* Vol. 6, No. 4, pp. 351-367. 1960.

No. 1044. Joanne S. Malkus. Recent Developments in Studies of Penetrative Convection and an Application to Hurricane Cumulonimbus Towers. In: *Cumulus Dynamics*, Pergamon Press, London and New York, pp. 65-84. 1960.

No. 1046. William S. Richardson and Charles J. Hubbard. The Contouring Temperature Recorder. *Deep-Sea Research*, Vol. 6, No. 3; pp. 239-244. 1960.

No. 1049. John H. Ryther. Organic Production by Plankton Algae and its Environmental Control. In: Ecology of Algae, the Pymatuning Symposia in Ecology, 18-19 June 1959, *Spec. Publ., Univ., Pittsburg Press*, No. 2, pp. 72-83. 1960.

No. 1051. Joanne S. Malkus and Claude Ronne. Cloud Distributions over the Tropical Oceans in Relation to Large-Scale Flow Patterns. In: Physics of Precipitation, *Amer. Geophys. Union, Monogr.*, No. 5, pp. 45-60. 1960.

No. 1052. J. B. Hersey. Acoustically Monitored Bottom Coring. *Deep-Sea Research*, Vol. 6, No. 2, pp. 170-172. 1960.

No. 1053. Wolfgang Wieser and John Kanwisher. Vorschlag zum Anlegen einer "Stoffwechselkartei" für marine Tiergemeinschaften. *Zool Anz.*, Vol. 165, Nos. 9/10, pp. 370-375. 1960.

No. 1054. Wolfgang Wieser. Benthic studies in Buzzards Bay. II. The Meiofauna. *Limnol. and Oceanogr.*, Vol. 5, No. 2, pp. 121-137. 1960.

No. 1055. Henry Stommel and A. B. Arons. On the Abyssal Circulation of the World Ocean. II. An Idealized Model of the Circulation Pattern and Amplitude in Oceanic Basins. *Deep-Sea Research*, Vol. 6, No. 3, pp. 217-233. 1960.

No. 1056. George C. Matthiessen. Observations on the Ecology of the Soft Clam, *Mya arenaria*, in a Salt Pond. *Limnol and Oceanogr.*, Vol. 5, No. 3, pp. 291-300. 1960.

No. 1058. Charles S. Yentsch. The Influence of Phytoplankton Pigments on the Colour of Sea Water. *Deep-Sea Research*, Vol. 7, No. 1, pp. 1-9. 1960.

No. 1059. Wolfgang Wieser and John Kanwisher. Growth and Metabolism in a Marine Nematode, *Enoplus communis* Bastian. *Zeits. Vergl. Physiol.*, Vol. 43, pp. 29-36. 1960.

No. 1062. Joyce C. Lewin and Ralph A. Lewin. Auxotrophy and Heterotrophy in Marine Littoral Diatoms. *Canadian Jour. Microbiol.*, Vol. 6, pp. 127-134. 1960.

No. 1064. G. G. Whitney, Jr. Procedure for and Comments on Ice Point Tests of Deep Sea Reversing Thermometers. *Limnol. and Oceanogr.*, Vol. 5, No. 2, pp. 232-235. 1960.

No. 1065. Allan R. Robinson. The General Thermal Circulation in Equatorial Regions. *Deep-Sea Research*, Vol. 6, No. 4, pp. 311-317. 1960. (Reprints erroneously marked as Contribution No. 1081).

No. 1067. John H. Ryther and David W. Menzel. The Seasonal and Geographical Range of Primary Production in the Western Sargasso Sea. *Deep-Sea Research*, Vol. 6, No. 3, pp. 235-238. 1960.

No. 1068. E. M. Hulburt, J. H. Ryther and R. R. L. Guillard. The Phytoplankton of the Sargasso Sea off Bermuda. *Jour. du Conseil*, Vol. 25, No. 2, pp. 115-118. 1960.

No. 1069. Alan J. Faller. Further Examples of Stationary Planetary Flow Patterns in Bounded Basins. *Tellus*, Vol. 12, No. 2, pp. 159-171. 1960.

No. 1070. Andrew A. Fejer and Richard H. Backus. Porpoises and the Bow-Riding of Ships Under way. *Nature*, Vol. 188, No. 4752, pp. 700-703. 1960.

No. 1073. John M. Zeigler, G. G. Whitney, Jr. and Carlyle R. Hayes. The Woods Hole Rapid Sediment Analyzer. *J. Sed. Petr.*, Vol. 30, No. 3, pp. 490-495. 1960.

No. 1074. Richard Barakat and Robert Barakat. Optical Studies of the Diffraction of Water Waves by Circular and Thin Elliptic Cylinders. *Jour. Appl. Physics*, Vol. 31, No. 3, pp. 474-478. 1960.

No. 1075. H. Barnes and Margaret Barnes. The Effect of Temperature on the Oxygen Uptake and Rate of Development of the Egg-Masses of Two Common Cirripedes, *Balanns balanoides* (L.) and *Pollicipes polymerus* J. B. Sowerby. *Kieler Meeresforschungen*, Vol. 15, No. 2, pp. 242-251. 1959. (In *Collected Reprints* for 1960).

No. 1076. Richard H. Backus. Notes on Western North Atlantic Sharks, No. 2. *Copeia,* 1960, No. 3, pp. 243-245. 1960.

No. 1077. Kirk Bryan. The Instability of a Two-Layered System Enclosed between Horizontal, Coaxially Rotating Plates. *Jour. Meteorol.,* Vol. 17, No. 4, pp. 446-455. 1960.

No. 1078. J. H. Steele and C. S. Yentsch. The Vertical Distribution of Chlorophyll. *Jour. Mar. Biol. Assoc.,* U. K., Vol. 39, pp. 217-226. 1960.

No. 1079. W. A. Mordy. Differences in Coalescence Tendencies in Computed Condensation Cloud Droplet Spectra. In: Physics of Precipitation, *Amer. Geophys. Union, Monogr.,* No. 5, pp. 184-190. 1960.

No. 1080. James E. Hanks. A Method for Preparing the Marine Polychaet, *Pectinaria gouldi* (Verrill) for Histological Study. *Trans. Amer. Micr. Soc.,* Vol. 79, No. 4, pp. 470-471. 1960.

No. 1081. E. A. Spiegel and G. Veronis. On the Boussinesq Approximation for a Compressible Fluid. *The Astrophysical Jour.,* Vol. 131, No. 2, pp. 442-447. 1960.

No. 1082. G. Veronis. An Approximate Theoretical Analysis of the Equatorial Undercurrent. *Deep-Sea Research,* Vol. 6, No. 4, pp. 318-327. 1960.

No. 1083. Raymond Wexler and Ruth Wexler. Cold Clouds over Tropical Oceans. In: *Cumulus Dynamics,* Pergamon Press, London and New York, pp. 129-134. 1960.

No. 1084. Henry Stommel. Wind-Drift near the Equator. *Deep-Sea Research,* Vol. 6, No. 4, pp. 298-302. 1960.

No. 1086. Dean F. Bumpus. Sources of Water Contributed to the Bay of Fundy by Surface Circulation. *Jour. Fish. Res. Bd., Canada,* Vol. 17, No. 2, pp. 181-197. 1960.

No. 1087. G. Fraenkel. Lethal High Temperatures for Three Marine Invertebrates, *Limulus polyphemus, Littorina littorea and Pagurus longicapus. Oikos,* Vol. 11, No. 2, pp. 171-182. 1960.

No. 1088. J. H. Ryther and E. M. Hulburt. On Winter Mixing and the Vertical Distribution of Phytoplankton. *Limnol. and Oceanogr.,* Vol. 5, No. 3, pp. 337-338. 1960.

No. 1089. C. Godfrey Day. Bottom Water Temperature on Browns Ledge off Southern Massachusetts. *Jour du Conseil,* Vol. 25, No. 3, pp. 235-239. 1960.

No. 1090. George L. Clarke and Lloyd R. Breslau. Studies of Luminescent Flashing in Phosphorescent Bay, Puerto Rico, and in the Gulf of Naples Using a Portable Bathyphotometer. *Bull. Inst. Océanogr., Monaco,* No. 1171, pp. 1-32. 1960.

No. 1091. Floyd M. Soule and P. A. Morrill. Physical Oceanography of the Grand Banks Region and the Labrador Sea in 1959. *U. S. Coast Guard Bull.,* No. 45, pp. 98-154. 1960.

No. 1092. Frank J. Mather, III. Recaptures of Tuna, Marlin and Sailfish Tagged in the Western North Atlantic. *Copeia,* 1960, No. 2, pp. 149-151, 1960.

No. 1093. Thomas F. Budinger. Iceberg Detection by Radar. *U. S. Coast Guard Bull.,* No. 45, pp. 49-97. 1960.

No. 1094. A. H. Woodcock. The Origin of Trade Wind Orographic Shower Rains. *Tellus,* Vol. 12, No. 3, pp. 315-326. 1960.

No. 1095. Vaughan T. Bowen and Thomas T. Sugihara. Strontium-90 in the 'Mixed Layer' of the Atlantic Ocean. *Nature,* Vol. 186. No. 4718, pp. 71-72. 1960.

No. 1096. Ralph F. Vaccaro and John H. Ryther. Marine Phytoplankton and the Distribution of Nitrite in the Sea. *Jour. du Conseil.,* Vol. 25, No. 3, pp. 260-271. 1960.

No. 1097. Jack McLachlan. The Culture of *Dunaliella tertiolecta* Butcher, a Euryhaline Organism. *Canadian Jour. Microbiol.,* Vol. 6, pp. 367-379. 1960.

No. 1099. Harry J. Turner, Jr. and James E. Hanks. Experimental Stimulation of Gametogenesis in *Hydroides dianthus* and *Pecten irradians* during the Winter. *Biol. Bull.*, Vol. 119, No. 1, pp. 145-152. 1960.

No. 1100. Francis A. Richards. Some Chemical and Hydrographic Observations along the North Coast of South America — 1. Cabo Tres Puntas to Curaçao, Including the Cariaco Trench and the Gulf of Cariaco. *Deep-Sea Research*, Vol. 7, No. 3, pp. 163-182. 1960.

No. 1101. William G. Metcalf. A Note on Water Movement in the Greenland-Norwegian Sea. *Deep-Sea Research*, Vol. 7 No. 3, pp. 190-200. 1960.

No. 1102. Herbert Curl, Jr. Primary Production Measurements in the North Coastal Waters of South America. *Deep-Sea Research*, Vol. 7, No. 3, pp. 183-189. 1960.

No. 1103. John Kanwisher. pCO_2 in Sea Water and its Effect on the Movement of CO_2 in Nature. *Tellus*, Vol. 12, No. 2, pp. 209-215. 1960.

No. 1104. C. Godfrey Day. Oceanographic Observations, 1959, East Coast of the United States. *U. S. Fish and Wildlife Service, Spec. Sci. Rept.-Fish.*, No. 359, 114 pp. 1960. (Not included in *Collected Reprints*).

No. 1106. Raymond G. Stross. Growth Response of *Chlamydomonas* and *Haematococcus* to the Volatile Fatty Acids. *Canadian Jour. Microbiol.*, Vol. 6, pp. 611-617. 1960.

No. 1107. Kirk Bryan and Elizabeth Schroeder. Seasonal Heat Storage in the North Atlantic Ocean. *Jour. Meteorol.*, Vol. 17, No. 6, pp. 670-674. 1960.

No. 1108. F. C. Fuglister. Atlantic Ocean Atlas of Temperature and Salinity Profiles and Data from the International Geophysical Year of 1957-1958. *Woods Hole Oceanogr. Inst., Atlas Series*, Vol. 1, 209 pp. 1960. (Not included in *Collected Reprints*).

No. 1111. Bostwick H. Ketchum. Oceanographic Research Required in Support of Radioactive Waste Disposal. In: Disposal of Radioactive Wastes, International Atomic Energy Agency, Vienna, pp. 283-291. 1960. (Not in *Collected Reprints*).

No. 1112. Max Blumer. Pigments of a Fossil Echinoderm. *Nature*, Vol. 188, No. 4756, pp. 1100-1101. 1960.

No. 1115. Robert J. Conover. The Feeding Behavior and Respiration of Some Marine Planktonic Crustacea. *Biol. Bull.*, Vol. 119, No. 3, pp. 399-415. 1960.

No. 1116. George D. Grice. Copepods of the Genus *Oithona* from the Gulf of Mexico. *Bull. Mar. Sci., Gulf and Carib.*, Vol. 10, No. 4, pp. 485-490. 1960.

No. 1124. Robert L. Miller and John M. Zeigler. A Study of the Relation between Dynamics and Sediment Pattern in the Zone of Shoaling Wave Breaker and Foreshore. *Eclogae Geol. Helv.*, Vol. 51, No. 3, pp. 542-551. 1958. (In *Collected Reprints* for 1960).

No. 1125. William S. von Arx. The Line of Zero Set. *Deep-Sea Research*, Vol. 7, No. 3, pp. 219-220. 1960.

No. 1126. James M. Moulton. Swimming Sounds and the Schooling of Fishes. *Biol. Bull.*, Vol. 119, No. 2, pp. 210-223. 1960.

No. 1128. J. M. Zeigler, W. S. Hoffmeister, Graham Giese and Herman Tasha. Discovery of Eocene Sediments in Subsurface of Cape Cod, Massachusetts. *Science*, Vol. 132, No. 3437, pp. 1397-1398.

No. 1130. Willard Dow. A Telemetering Hydrophone. *Deep-Sea Research*. Vol. 7, No. 2, pp. 142-147. 1960.

No. 1134. Alfred C. Redfield. The Distribution of Phosphorus in the Deep Oceans of the World. *Assoc. Océanogr., Phys., Union Géodes. et Géophys. Int., Proc. Verb.*, No. 7 (G16), pp. 189-193. 1960.

SPOONER

TREASURER'S REPORT

The financial statements for the year 1960 have been audited by Lybrand, Ross Bros. & Montgomery.

The book value of endowment funds at December 31, 1960 was $3,483,053 of which $1,028,349 represented accumulated net gains from sales of investments. The market value of endowment assets on the same date, including real estate at book amount, was $5,288,653. Endowment fund investments and income received therefrom are summarized in Schedule C.

Income received on endowment assets was $192,354 for the year ended December 31, 1960, compared with $188,639 the previous year. Included in endowment income was $6,024 of real estate income representing a 5% return on this investment. The balance of real estate income, $6,177 was transferred to endowment assets to amortize cost of property. Endowment income represented a return on endowment fund assets of 3.6% at year-end market quotation, 5.5% on the book amount and 7.8% on the contributed amount of the endowment fund.

Endowment income was allocated for 1960 operating expenses at the rate of 6% of the book amount of original endowment funds, or $146,079. Of the balance of endowment income, $46,275, there was transferred to the income and salary stabilization reserve $45,375 and to unexpended balance of gifts from Oceanographic Associates as income from investment of life memberships $900.

The Institution's 1960 contribution to the Woods Hole Oceanographic Institution's Employees Retirement Trust amounted to $98,574. The trust is administered by three trustees. The balance of the old Retirement Fund, administered by the Treasurer, amounted to $73,060 as of December 31, 1960. This balance consisted of amounts on deposit in sixteen savings bank accounts held in trust for ten members of the plan. No contributions to the Old plan were made in 1960. Interest totaling $2,622 was credited to the savings accounts during the year.

In the financial statements that follow it is interesting to note that for each dollar spent 80 cents was spent for direct costs of research activity, 15 cents for general and administration expenses and 5 cents for plant operation and miscellaneous. Administrative salaries amounted to only 5 cents of each dollar of total expense. Included in the 15 cents of general and administration expenses was 3 cents for staff benefits (group insurance, social security taxes, and contributions to retirement plan).

BALANCE SHEET

AS AT DECEMBER 31, 1960

ASSETS

Endowment Fund Assets:		
Investments (Schedule C):		
Bonds (market quotations $1,858,977)		$1,933,381
Stocks (market quotations $3,288,768)		1,408,764
Real estate		114,293
		3,456,438
Cash		26,615
		3,483,053
Plant Fund Assets (note):		
Laboratory plant and equipment		879,032
Vessels and equipment		812,998
Other property		161,541
Vessels under construction		151,816
Total plant		2,005,387
Expenditures in anticipation of funds		49,685
Advance to current funds		303,688
		2,358,760
Current Fund Assets:		
Cash		753,818
Time deposit		50,000
Marketable security		246
Accounts receivable:		
U. S. Government	$193,552	
Other	32,356	225,908
Unbilled costs on research contracts:		
U. S. Government	476,954	
Other	3,254	480,208
Supplies inventories		40,258
Deferred charges		25,094
		1,575,532
Less advance from plant funds		303,688
		1,271,844
		$7,113,657

Note — Since 1945 the Institution has provided for depreciation of plant assets other than vessels at annual rates of 2% on buildings and 5% to 33-1/3% on equipment, carrying the amounts to general plant and equipment reserve.

LIABILITIES

Endowment Funds:		
Unrestricted		$2,033,284
For upkeep of plant		419,420
Henry Bryant Bigelow Chair of Oceanography		2,000
Accumulated net gain on sales of investments		1,028,349
		3,483,053
Plant Funds:		
Invested in plant		2,005,387
Unexpended:		
Fund for acquisition of capital assets		300,000
Fund for construction of a small vessel		49,868
General plant and equipment reserve		3,505
		2,358,760
Current Liabilities and Funds:		
Accounts payable and accrued expenses		384,599
Contribution payable to employees' retirement plan and trust		98,574
Unexpended balances of gifts and grants for research:		
Government	$448,107	
Other	25,442	473,549
General fund:		
Income and salary stabilization reserve	311,457	
Unappropriated	3,665	315,122
		1,271,844
		$7,113,657

STATEMENT OF INCOME, OPERATING EXPENSES AND UNAPPROPRIATED GENERAL FUND

FOR THE YEAR ENDED DECEMBER 31, 1960

INCOME:		
Receipts for sponsored research:		
For direct costs		$3,733,013
For indirect costs		807,235
Fees for use of facilities		138,613
		4,678,861
Endowment income (Schedule C)	$192,354	
Less amounts added to income and salary stabilization reserve ($45,375) and to unexpended balance of gifts from Oceanographic Associates ($900)	46,275	146,079
Miscellaneous		18,266
Total income availed of		4,843,206
OPERATING EXPENSES:		
Direct costs of research activity (Schedule A):		
Salaries and wages		1,198,870
Vessel operations		1,115,952
Materials and services		1,398,766
Travel		107,730
		3,821,318
Indirect costs:		
General and administration (Schedule B)	697,962	
Plant operation (Schedule B)	209,531	
Miscellaneous	16,597	924,090
Total operating expenses		4,745,408
Excess of income		97,798
Additions to plant from current funds — books and equipment purchased		37,789
		60,009
Unappropriated general fund, January 1, 1960		43,656
		103,665
Appropriated for acquisition of capital assets		100,000
Unappropriated general fund, December 31, 1960		$ 3,665

SCHEDULE A
DIRECT COSTS OF RESEARCH ACTIVITY

FOR THE YEAR ENDED DECEMBER 31, 1960

	Salaries and Wages	Vessel Operations	Materials and Services	Travel	Total
U. S. GOVERNMENT CONTRACTS.	$1,158,950	$1,110,942	$1,326,125	$95,560	$3,691,577
OTHER SPONSORED RESEARCH....	5,816		33,732	1,888	41,436
Total direct costs of sponsored research	1,164,766	1,110,942	1,359,857	97,448	3,733,013
INSTITUTIONAL RESEARCH:	34,104	5,010	38,909	10,282	88,305
Total direct costs of research	$1,198,870	$1,115,952	$1,398,766*	$107,730	$3,821,318

*Includes grants and fellowships: $64,226.

SCHEDULE B
GENERAL AND ADMINISTRATION EXPENSES AND EXPENSES FOR PLANT OPERATION

FOR THE YEAR ENDED DECEMBER 31, 1960

GENERAL ADMINISTRATION:		
GENERAL EXPENSES:		
Staff benefits:		
Contributions to retirement plan		$98,574
Social security taxes		49,100
Group Insurance		6,056
		153,730
Shop services		134,467
Housing, net		7,731
ADMINISTRATION EXPENSES:		
Salaries and wages	$259,391	
Insurance, travel, supplies and other	142,643	402,034
		$697,962
PLANT OPERATION:		
Salaries and wages		58,169
Provision for depreciation (credited to general plant and equipment reserve)..		55,510
Other repair costs	26,859	
Heat, light and power	24,952	
Other..	44,041	95,852
		$209,531

SCHEDULE C

SUMMARY OF INVESTMENTS

AS AT DECEMBER 31, 1960

	Book Amount	% of Total	Market Quotation	% of Total	Endowment Income
Bonds:					
Government	$587,768	17.01	$588,399	11.18	$18,701
Railroad	451,147	13.05	423,428	8.05	18,710
Public utility	341,050	9.87	321,695	6.11	17,994
Industrial	408,519	11.82	381,855	7.26	13,485
Financial and investment	144,897	4.19	143,600	2.73	7,075
Total bonds	1,933,381	55.94	1,858,977	35.33	75,965
Stocks:					
Preferred	259,746	7.52	235,551	4.48	12,242
Common:					
Public utility	356,869	10.32	992,306	18.86	28,305
Industrial	556,061	16.09	1,610,667	30.61	52,962
Miscellaneous	236,088	6.83	450,244	8.55	16,856
Total common stocks	1,149,018	33.24	3,053,217	58.02	98,123
Total stocks	1,408,764	40.76	3,288,768	62.50	110,365
Real Estate	114,293	3.30	114,293*	2.17	6,024
Total investments	$3,456,438	100.00	$5,262,038	100.00	$192,354

*At book amount.

LYBRAND, ROSS BROS. & MONTGOMERY

ACCOUNTANTS AND AUDITORS

Woods Hole Oceanographic Institution
Woods Hole, Massachusetts

We have examined the balance sheet of Woods Hole Oceanographic Institution as at December 31, 1960 and the related statement of income, operating expenses and unappropriated general fund for the year then ended. Our examination was made in accordance with generally accepted auditing standards, and accordingly included such tests of the accounting records and such other auditing procedures as we considered necessary in the circumstances; however, it was not practicable to confirm receivables from United States Government departments, as to which we have satisfied ourselves by means of other auditing procedures.

In our opinion, the accompanying financial statements present fairly the position of Woods Hole Oceanographic Institution at December 31, 1960 and the results of its operations for the year then ended, on a basis consistent with that of the preceding year.

Boston, Massachusetts
May 16, 1961

Lybrand, Ross Bros. & Montgomery

List of Contributions

LIST OF CONTRIBUTIONS
FROM THE WOODS HOLE OCEANOGRAPHIC INSTITUTION

See Author, Subject-Locality, Taxonomic Indexes, published in 1957, for a complete list through 1956.

No. 800. M. S. Gordon and Richard H. Backus. New Records of Labrador Fishes with Special Reference to Those of Hebron Fjord. *Copeia*, No. 1, pp. 17–20. 1957.

No. 801. Floyd M. Soule and J. E. Murray. Physical Oceanography of the Grand Banks and the Labrador Sea in 1955. *U. S. Coast Guard Bull.*, No. 41, pp. 59–114. 1956.

No. 802. James M. Moulton and Richard H. Backus. Annotated References Concerning the Effects of Man-Made Sounds on the Movements of Fishes. *Dept. Sea and Shore Fish.*, *Fish. Circ.*, Augusta, Maine, No. 17, 8 pp. 1955.

No. 803. E. M. Hulburt, J. J. A. McLaughlin and P. A. Zahl. *Katodinium dorsalisulcum*, a New Species of Unarmored Dinophyceae. *Jour. Protozool.*, Vol. 7, No. 4, pp. 323–326. 1960.

No. 804. W. V. R. Malkus. Outline of a Theory of Turbulent Shear Flow. *Jour. Fluid Mech.*, Vol. 1, Pt. 5, pp. 521–539. 1956.

No. 805. John Mackiewicz and Richard H. Backus. Oceanic Records of *Lasionycteris noctivagans* and *Lasiurus borealis*. *Jour. Mammalogy*, Vol. 37, No. 3, pp. 442–443. 1956.

No. 806. Allyn C. Vine. Oceanographic Instrumentation. *Science*, Vol. 122, No. 3173, pp. 748–751. 1955.

No. 807. P. F. Scholander and William E. Schevill. Counter-Current Vascular Heat Exchange in the Fins of Whales. *Jour. Appl. Physiol.*, Vol. 8, No. 3, pp. 279–282. 1955.

No. 808. E. Steemann Nielsen. The Interaction of Photosynthesis and Respiration and Its Importance for the Determination of ^{14}C-Discrimination in Photosynthesis. *Physiologia Plantarum*, Vol. 8, pp. 945–953. 1955.

No. 809. Duncan C. Blanchard. The Supercooling, Freezing and Melting of Giant Waterdrops at Terminal Velocity in Air. Proceedings of the First Conference on the Physics of Cloud Precipitation Particles, Woods Hole, September 7–10, 1955. In: Artificial Stimulation of Rain, pp. 233–249. Pergamon Press Ltd., New York, London, Paris. 1957.

No. 810. Karl E. Schleicher and Alvin Bradshaw. A Conductivity Bridge for Measurement of the Salinity of Sea Water. *Jour. du Conseil*, Vol. 22, No. 1, pp. 9–20. 1956.

No. 811. G. W. Morgan. On the Wind-Driven Ocean Circulation. *Tellus*, Vol. 8, No. 3, pp. 301–320. 1956.

No. 812. Duncan C. Blanchard. Discussion of Raindrop Distributions Made during Project Shower, Hawaii, 1954. Proceedings of the First Conference on the Physics of Cloud Precipitation Particles, Woods Hole, September 7–10, 1955. In: Artificial Stimulation of Rain, pp. 213–223. Pergamon Press Ltd., New York, London, Paris. 1957.

No. 813. R. W. HOLMES. The Annual Cycle of Phytoplankton in the Labrador Sea, 1950–51. *Bull. Bingham Oceanogr. Coll.*, Vol. 16, Art. 1, 74 pp. 1956. (Not included in *Collected Reprints*).

No. 814. RICHARD H. BACKUS, STEWART SPRINGER and EDGAR L. ARNOLD, JR. A Contribution to the Natural History of the White-Tip Shark, *Pterolamiops longimanus* (Poey). *Deep-Sea Research*, Vol. 3, pp. 178–188. 1956.

No. 815. WILLIAM E. SCHEVILL. *Lagenorhynchus acutus* off Cape Cod. *Jour. Mammalogy*, Vol. 37, No. 1, pp. 128–129. 1956.

No. 816. P. F. SCHOLANDER, L. VAN DAM and THEODORE ENNS. Nitrogen Secretion in the Swimbladder of Whitefish. *Science*, Vol. 123, No. 3185, pp. 59–60. 1956.

No. 817. HAROLD E. EDGERTON and LLOYD D. HOADLEY. Cameras and Lights for Underwater Use. *Jour. Soc. Motion Pict. and Television Eng.*, Vol. 64, pp. 345–350. 1955.

No. 818. P. F. SCHOLANDER, JOHN W. KANWISHER and D. C. NUTT. Gases in Icebergs. *Science*, Vol. 123, No. 3186, pp. 104–105. 1956.

No. 819. JOHN H. RYTHER. Photosynthesis in the Ocean as a Function of Light Intensity. *Limnol. and Oceanogr.*, Vol. 1, No. 1, pp. 61–70. 1956.

No. 820. WILLIAM S. VON ARX. An Experimental Approach to Problems in Physical Oceanography. In: Progress in Physics and Chemistry of the Earth, Vol. 2, pp. 1–29. Pergamon Press Ltd., London, New York, Paris. 1957.

No. 821. GEORGE L. CLARKE and GUNTHER K. WERTHEIM. Measurements of Illumination at Great Depths and at Night in the Atlantic Ocean by Means of a New Bathyphotometer. *Deep-Sea Research*, Vol. 3, pp. 189–205. 1956.

No. 822. P. F. SCHOLANDER. Hydrostatic Pressure in Coconuts. *Plant Physiol.*, Vol. 30, No. 6, pp. 560–561. 1955.

No. 823. JOHN C. AYERS. A Dynamic Height Method for the Determination of Currents in Deep Lakes. *Limnol. and Oceanogr.*, Vol. 1, No. 3, pp. 150–161. 1956.

No. 824. PARKER D. TRASK. The *Atlantis* Marine Geological Expedition to Peru and Chile. *Nature*, Vol. 177, pp. 454–455. 1956.

No. 825. JOHN H. RYTHER. The Measurement of Primary Production. *Limnol. and Oceanogr.*, Vol. 1, No. 2, pp. 72–84. 1956.

No. 826. ROBERT L. MILLER. Trend Surfaces: Their Application to Analysis and Description of Environments of Sedimentation. 1. The Relation of Sediment-Size Parameters to Current-Wave Systems and Physiography. *Jour. Geology*, Vol. 64, No. 5, pp. 425–446. 1956.

No. 827. JOANNE STARR MALKUS. On the Maintenance of the Trade Winds. *Tellus*, Vol. 8, No. 3, pp. 335–350. 1956.

No. 828. ALFRED C. REDFIELD and ARTHUR R. MILLER. Water Levels Accompanying Atlantic Coast Hurricanes. In: Interaction of Sea and Atmosphere. *Meteorol. Monogr.*, Vol. 2, No. 10, pp. 1–23. 1957.

No. 829. ARTHUR R. MILLER. The Effect of Steady Winds on Sea Level at Atlantic City. In: Interaction of Sea and Atmosphere. *Meteorol. Monogr.*, Vol. 2, No. 10, pp. 24–31. 1957.

No. 830. FRANCIS A. RICHARDS and RALPH F. VACCARO. The Cariaco Trench, an Anaerobic Basin in the Caribbean Sea. *Deep-Sea Research*, Vol. 3, pp. 214–228. 1956.

No. 831. David C. Nutt and Lawrence K. Coachman. The Oceanography of Hebron Fjord, Labrador. *Jour. Fish. Res. Bd., Canada*, Vol. 13, No. 5, pp. 709–758. 1956.

No. 832. William E. Schevill and Barbara Lawrence. Food-Finding by a Captive Porpoise (*Tursiops truncatus*). *Breviora, Mus. Comp. Zool.*, No. 53, 15 pp. 1956.

No. 833. A. F. Bunker. Turbulence Measurements in a Young Cyclone over the Ocean. *Bull. Amer. Meteorol. Soc.*, Vol. 38, No. 1, pp. 13–16. 1957.

No. 834. Richard H. Backus and J. B. Hersey. Echo-Sounder Observations of Midwater Nets and Their Towing Cables. *Deep-Sea Research*, Vol. 3, pp. 237–241. 1956.

No. 835. Joseph Chase. The Bermuda-Azores High Pressure Cell. Its Surface Wind Circulation. *Miscelânea Geofísica*, Luanda, Angola, pp. 29–54. 1956. (In *Collected Reprints* for 1957).

No. 836. Frank J. Mather, III and Howard A. Schuck. Growth of Bluefin Tuna of the Western North Atlantic. *Fish. Bull.* 179, *Fish Bull., U. S. Fish and Wildlife Service*, Vol. 61, pp. 39–52. 1960.

No. 837. A. H. Woodcock. Dimorphism in the Portuguese Man-of-War. *Nature*, Vol. 178, No. 4527, pp. 253–255. 1956.

No. 838. E. M. Hulburt. The Taxonomy of Unarmored Dinophyceae of Shallow Embayments on Cape Cod, Massachusetts. *Biol. Bull.*, Vol. 112, No. 2, pp. 196–219. 1957.

No. 839. C. B. Officer, J. I. Ewing, R. S. Edwards and H. R. Johnson. Geophysical Investigations in the Eastern Caribbean: Venezuelan Basin, Antilles Island Arc, and Puerto Rico Trench. *Bull. Geol. Soc. Amer.*, Vol. 68, pp. 359–378. 1957.

No. 840. Francis A. Richards. On the State of our Knowledge of Trace Elements in the Ocean. *Geochimica et Cosmochimica Acta*, Vol. 10, No. 4, pp. 241–243. 1956.

No. 841. Henry R. Johnson, Richard H. Backus, J. B. Hersey and D. M. Owen. Suspended Echo-Sounder and Camera Studies of Midwater Sound Scatterers. *Deep-Sea Research*, Vol. 3, pp. 266–272. 1956.

No. 842. John H. Ryther. Interrelation between Photosynthesis and Respiration in the Marine Flagellate, *Dunaliella euchlora*. *Nature*, Vol. 178, pp. 861–862. 1956.

No. 843. Joanne Starr Malkus. Trade Cumulus Cloud Groups: Some Observations Suggesting a Mechanism of Their Origin. *Tellus*, Vol. 9, No. 1, pp. 33–44. 1957.

No. 844. Francis A. Richards. Some Current Aspects of Chemical Oceanography. In: Progress in Physics and Chemistry of the Earth, Vol. 2, pp. 77–128. Pergamon Press Ltd., London, New York, Paris. 1957.

No. 845. Henry Stommel. Florida Straits Transports, 1952–1956. *Bull. Mar. Sci., Gulf and Caribbean*, Vol. 7, No. 3, pp. 252–254. 1957.

No. 846. Henry Stommel. On the Determination of the Depth of No Meridional Motion. *Deep-Sea Research*, Vol. 3, pp. 273–278. 1956.

No. 847. Athelstan Spilhaus. Control of the World Environment. *Geogr. Rev.*, Vol. 46, No. 4, pp. 451–459. 1956.

No. 848. Henry B. Bigelow and William C. Schroeder. A Study of the Sharks of the Suborder Squaloidea. *Bull. Mus. Comp. Zool.*, Vol. 117, No. 1, pp. 1–150. 1957. (Not included in *Collected Reprints*).

No. 849. Duncan C. Blanchard. Electrically Charged Drops from Bubbles in Sea Water and Their Meteorological Significance. *Jour. Meteorol.*, Vol. 15, No. 4, pp. 383–396. 1958.

No. 850. H. Walden and H. G. Farmer. Auswertung von Seegangsregistrierungen des Forschungsschiffes "Atlantis" mit dem "Ship-Borne Wave Recorder" sowie Vergleich mit entsprechenden Seegangsberechnungen aus den Windverhaltnissen (Hindcasting). *Deutsche Hydrogr. Zeitschrift*, Bd. 10, Heft 4, pp. 121–134. 1957.

No. 851. Allyn C. Vine, Some Trends in Oceanographic Instrumentation. *Proc. UNESCO Symp. Phys. Oceanogr.*, Tokyo, 1955: 49–52. 1957. (Not included in *Collected Reprints*).

No. 852. Francis A. Richards and Nathaniel Corwin. Some Oceanographic Applications of Recent Determinations of the Solubility of Oxygen in Sea Water. *Limnol. and Oceanogr.*, Vol. 1, No. 4, pp. 263–267. 1956.

No. 853. Irving I. Schell. On the Nature and Origin of the Southern Oscillation. *Jour. Meteorol.*, Vol. 13, No. 6, pp. 592–598. 1956.

No. 854. Richard H. Backus. Northern Record of the Snake Eel *Ophichthus gomesi* (Castelnau). *Copeia*, No. 1, p. 61. 1957.

No. 855. A. B. Arons and Henry Stommel. A β-Plane Analysis of Free Periods of the Second Class in Meridional and Zonal Oceans. *Deep-Sea Research*, Vol. 4, pp. 23–31. 1956.

No. 856. Gordon Volkmann, John Knauss and Allyn Vine. The Use of Parachute Drogues in the Measurement of Subsurface Ocean Currents. *Trans. Amer. Geophys. Union*, Vol. 37, No. 5, pp. 573–577. 1956.

No. 857. Richard H. Backus. Notes on Western North Atlantic Sharks. *Copeia*, No. 3, pp. 246–248. 1957.

No. 858. George L. Clarke and Richard H. Backus. Measurements of Light Penetration in Relation to Vertical Migration and Records of Luminescence of Deep-Sea Animals. *Deep-Sea Research*, Vol. 4, pp. 1–14. 1956.

No. 859. G. Veronis and Henry Stommel. The Action of Variable Wind Stresses on a Stratified Ocean. *Sears Found., Jour. Mar. Res.*, Vol. 15, No. 1, pp. 43–75. 1956.

No. 860. I. Friedman and A. H. Woodcock. Determination of Deuterium-Hydrogen Ratios in Hawaiian Waters. *Tellus*, Vol. 9, No. 4, pp. 553–556. 1957.

No. 861. J. I. Ewing, C. B. Officer, H. R. Johnson, and R. S. Edwards. Geophysical Investigations in the Eastern Caribbean: Trinidad Shelf, Tobago Trough, Barbados Ridge, Atlantic Ocean. *Bull. Geol. Soc. Amer.*, Vol. 68, pp. 897–912. 1957.

No. 862. James M. Moulton. Influencing the Calling of Sea Robins (*Prionotus* spp.) with Sound. *Biol. Bull.*, Vol. 111, No. 3, pp. 393–398. 1956.

No. 863. S. T. Knott and J. B. Hersey. Interpretation of High-Resolution Echo-Sounding Techniques and Their Use in Bathymetry, Marine Geophysics, and Biology. *Deep-Sea Research*, Vol. 4, pp. 36–44. 1956.

No. 864. H. B. Moore and E. G. Corwin. The Effects of Temperature, Illumination, and Pressure on the Vertical Distribution of Zooplankton. *Bull. Mar. Sci., Gulf and Caribbean*, Vol. 6, No. 4, pp. 273–287. 1956.

No. 865. Richard S. Edwards and Francis A. Richards. A Bottom-Water Sampler. *Deep-Sea Research*, Vol. 4, pp. 65–66. 1956.

No. 866. M. S. Rutstein. Flooded Quarries for Experimental Work. *Trans. Amer. Geophys. Union*, Vol. 35, No. 5, pp. 688-690. 1957.

No. 867. Irving Friedman, Daniel R. Norton, Douglas B. Carter and Alfred C. Redfield. The Deuterium Balance of Lake Maracaibo. *Limnol. and Oceanogr.*, Vol. 1, No. 4, pp. 239–246. 1956.

No. 868. M. S. Gordon. Observations on Osmoregulation in the Arctic Char (*Salvelinus alpinus* L.). *Biol. Bull.*, Vol. 112, No. 1, pp. 28–33. 1957.

No. 869. Helen S. Vishniac. On the Ecology of the Lower Marine Fungi. *Biol. Bull.*, Vol. 111, No. 3, pp. 410–414. 1956.

No. 870. W. S. Wooster and Bostwick H. Ketchum. Transport and Dispersal of Radioactive Elements in the Sea. In: The Effects of Atomic Radiation on Oceanography and Fisheries. *Nat. Acad. Sci.-Nat. Res. Council, Publ.* No. 551, Chap. 4, pp. 43–51. 1957.

No. 871. Bostwick H. Ketchum. The Effects of the Ecological System on the Transport of Elements in the Sea. In: The Effects of Atomic Radiation on Oceanography and Fisheries. *Nat. Acad. Sci.-Nat. Res. Council, Publ.* No. 551, Chap. 5, pp. 52–59. 1957.

No. 872. P. F. Scholander and John Krog. Countercurrent Heat Exchange and Vascular Bundles in Sloths. *Jour. Applied Physiol.*, Vol. 10, No. 3, pp. 405–411. 1957. (Not included in *Collected Reprints*).

No. 873. Lawrence K. Coachman, E. Hemmingsen and P. F. Scholander. Gas Enclosures in a Temperate Glacier. *Tellus*, Vol. 8, No. 4, pp. 415–423. 1956. (Not included in *Collected Reprints*).

No. 874. J. B. Hersey. Electronics in Oceanography. In: Advances in Electronics and Electron Physics, Vol. 9, pp. 239–295. Academic Press, Inc., New York. 1957. (Not included in *Collected Reprints*.)

No. 875. Duncan C. Blanchard and A. H. Woodcock. Bubble Formation and Modification in the Sea and Its Meteorological Significance. *Tellus*; Vol. 9, No. 2, pp. 145–158. 1957.

No. 876. Harry J. Turner, Carl J. George and Joseph H. Connell. Eighth Report on Investigations of the Shellfisheries of Massachusetts. *Com. Mass., Dept. Nat. Res., Div. Mar. Fish.*, 25 pp. 1955.

No. 877. Floyd M. Soule and J. E. Murray. Physical Oceanography of the Grand Banks Region and the Labrador Sea in 1956. *U. S. Coast Guard Bull.*, No. 42, pp. 35–100. 1957. (In *Collected Reprints* for 1958).

No. 878. J. W. Kanwisher and H. Leivestad. Thermal Regulation in Whales. *Norwegian Whaling Gazette*, No. 1, pp.1–5. 1957.

No. 879. P. F. Scholander and L. van Dam. Micro Gasometric Determination of Oxygen in Fish Blood. *Jour. Cell. and Comp. Physiol.*, Vol. 48, No. 3, pp. 529–532. 1956. No. 3, pp. 517–522. 1956.

No. 880. P. F. Scholander. Observations on the Gas Gland in Living Fish. *Jour. Cell. and Comp. Physiol.*, Vol. 48, No. 3, pp. 523–528. 1956.

No. 881. P. F. Scholander, L. van Dam and Theodore Enns. The Source of Oxygen Secreted into the Swimbladder of Cod. *Jour. Cell. and Comp. Physiol.*, Vol. 48, No. 3, pp. 517–522. 1956.

No. 882. H. L. Sanders. The Chepalocarida and Crustacean Phylogeny. *Syst. Zool.*, Vol. 6 No. 3, pp. 112–129. 1957.

No. 883. John C. Ayers and Roger Bachmann. Simplified Computations for the Dynamic Height Method of Current Determination in Lakes. *Limnol and Oceanogr.*, Vol. 2, No. 2, pp. 155–157. 1957.

No. 884. JOHN M. ZEIGLER and F. C. RONNE. Time-Lapse Photography - - an Aid to Studies of the Shoreline. *Research Reviews*, Office of Naval Research, Washington, April, pp. 1–6. 1957.

No. 885. SHANNON R. TORPHY and JOHN M. ZEIGLER. Submarine Topography of Eastern Channel, Gulf of Maine. *Jour. Geology*, Vol. 65, No. 4, pp. 433–441. 1957.

No. 886. HARRY J. TURNER and DAVID L. BELDING. The Tidal Migrations of *Donax variabilis* Say. *Limnol and Oceanogr.*, Vol. 2, No. 2, pp. 120–124. 1957.

No. 887. J. W. KANWISHER. Freezing and Drying in Intertidal Algae. *Biol. Bull.*, Vol. 113, No. 2, pp. 275–285. 1957.

No. 888. J. W. KANWISHER and ALFRED EBELING. Composition of the Swim-Bladder Gas in Bathypelagic Fishes. *Deep-Sea Research*, Vol. 4, pp. 211–217. 1957.

No. 889. A. H. WOODCOCK and A. T. SPENCER, An Airborne Flame Photometer and its Use in the Scanning of Marine Atmospheres for Sea-Salt Particles. *Jour. Meteorol.*, Vol. 14, No. 5, pp. 437-447. 1957.

No. 890. WILLEM A. VAN BERGEIJK and EMIL WITSCHI. The Basila Papilla of the Anuran Ear. *Acta Anatomica*, Vol. 30, pp. 81–91. 1957. (Not included in *Collected Reprints*).

No. 891. P. F. SCHOLANDER, L. VAN DAM, J. W. KANWISHER, H. T. HAMMEL and M. S. GORDON. Supercooling and Osmoregulation in Arctic Fish. *Jour. Cell. and Comp. Physiol.*, Vol. 49, No. 1, pp. 5–24. 1957.

No. 892. P. F. SCHOLANDER and L. VAN DAM. The Concentration of Hemoglobin in Some Cold Water Arctic Fishes. *Jour. Cell. and Comp. Physiol.*, Vol. 49, No. 1, pp. 1–4. 1957.

No. 893. CHARLES S. YENTSCH and JOHN R. RYTHER. Short-Term Variations in Phytoplankton Chlorophyll and Their Significance. *Limnol. and Oceanogr.*, Vol. 2, No. 2, pp. 140–142. 1957.

No. 894. RICHARD H. BACKUS and HAROLD BARNES. Television-Echo-Sounder Observations by Midwater Sound Scatterers. *Deep-Sea Research*, Vol. 4, pp. 116-119. 1957.

No. 895. ROBERT G. WALDEN, DAVID D. KETCHUM and DAVID H. FRANTZ, JR. Buoy Telemeters Ocean Temperature Data. *Electronics*, McGraw-Hill Co., New York, Vol. 30, No. 6, pp. 164–167. 1957.

No. 896. RICHARD H. BACKUS. The Fishes of Labrador. *Bull. Amer. Mus. Nat. Hist.*, Vol. 113, Art. 4, pp. 273-337. 1957. (Not included in *Collected Reprints*).

No. 897. HAROLD BARNES. The Northern Limit of *Balanus balanoides* (L). *Oikos*, Vol. 8, No. 1, pp. 1–15. 1957.

No. 898. CHARLES S. YENTSCH. A Non-Extractive Method for the Quantitative Estimation of Chlorophyll in Algal Cultures. *Nature*, Vol. 179, pp. 1302-1304. 1957.

No. 899. HENRY STOMMEL and GEORGE VERONIS. Steady Convective Motion in a Horizontal Layer of Fluid Heated Uniformly from Above and Cooled Non-Uniformly from Below. *Tellus*, Vol. 9, No. 3, pp. 401–407. 1957.

No. 900. ARTHUR R. MILLER. The Effects of Winds on Water Levels on the New England Coast. *Limnol. and Oceanogr.*, Vol. 3, No. 1, pp. 1–14. 1958.

No. 901. FRANK J. MATHER III and ROBERT H. GIBBS. Distributional Records of Fishes from Waters off New England and the Middle Atlantic States. *Copeia*, No. 3, pp. 242–244. 1957.

No. 902. John H. Ryther and Charles S. Yentsch. The Estimation of Phytoplankton Production in the Ocean from Chlorophyll and Light Data. *Limnol. and Oceanogr.*, Vol. 2, No. 3, pp. 281-286. 1957.

No. 903. W. H. Sutcliffe, Jr. An Improved Method for the Determination of Preserved Plankton Volumes. *Limnol. and Oceanogr.*, Vol. 2, No. 3, pp. 295–296. 1957.

No. 904. Dean F. Bumpus. Surface Water Temperature along Atlantic and Gulf Coasts of the United States. *U. S. Fish and Wildlife Service, Spec. Sci. Rept. — Fisheries*, No. 214, 153 pp. 1957. (Not included in *Collected Reprints*).

No. 905. William D. Athearn. Comparisons of Clay from the Continental Shelf off Long Island with the Gardiners Clay. *Jour. Geology*, Vol. 65, No. 4, pp. 448–449. 1957.

No. 906. John H. Ryther and Charles S. Yentsch. Primary Production of Continental Shelf Waters off New York. *Limnol. and Oceanogr.*, Vol. 3, No. 3, pp. 327–335. 1958.

No. 907. Vaughan T. Bowen and T. T. Sugihara. Strontium 90 in North Atlantic Surface Water. *Proc. Nat. Acad. Sci.*, Vol. 43, No. 7, pp. 576–580. 1957.

No. 908. L. V. Worthington and William E. Schevill. Underwater Sounds Heard from Sperm Whales. *Nature*, Vol. 180, p. 291. 1957

No. 909. Jan Hahn. Oceanus Goes to the Bottom of the Sea. *Oceanus*, Vol. 5, Nos. 1 and 2, pp. 20–31. 1957.

No. 910. J. C. Swallow and L. V. Worthington. Measurements of Deep Currents in the Western North Atlantic. *Nature*, Vol. 179, pp. 1183–1184. 1957.

No. 911. G. C. McLeod. The Effect of Circularly Polarized Light on the Photosynthesis and Chlorophyll *a* Synthesis of Certain Marine Algae. *Limnol. and Oceanogr.*, Vol. 2, No. 4, pp. 360–362. 1957.

No. 912. Robert H. Gibbs, Jr. A Taxonomic Analysis of *Myctophum affine* and *M. nitidulum*, Two Lantern-Fishes Previously Synonymized, in the Western North Atlantic. *Deep-Sea Research*, Vol. 4, pp. 230–237. 1957.

No. 913. E-an Zen. Preliminary Report on the Mineralogy and Petrology of Some Marine Bottom Samples off the Coast of Peru and Chile. *Amer. Mineralogist*, Vol. 42, pp. 889–903. 1957.

No. 914. James M. Moulton. Sound Production in the Spiny Lobster *Panulirus argus* (Latreille). *Biol. Bull.*, Vol. 113, No. 2, pp. 286–295. 1957.

No. 915. Joanne S. Malkus. On the Structure and Maintenance of the Mature Hurricane Eye. *Jour. Meteorol.*, Vol. 15, No. 4, pp. 337-349. 1958.

No. 916. G. G. Whitney, Jr. Factors Affecting the Accuracy of Thermometric Depth Determinations. *Jour. du Conseil*, Vol. 22, No. 2, pp. 167–173. 1957.

No. 917. Henry Stommel. A Survey of Ocean Current Theory. *Deep-Sea Research*, Vol. 4, pp. 149–184. 1957.

No. 918. Dean F. Bumpus. Oceanographic Observations 1956, East Coast of the United States. *U. S. Fish and Wildlife Service, Spec. Sci. Rept. — Fisheries*, No. 233, 132 pp. 1957. (Not included in *Collected Reprints*).

No. 919. John M. Zeigler, W. D. Athearn and H. Small. Profiles across the Peru-Chile Trench. *Deep-Sea Research*, Vol. 4, pp. 238–249. 1957.

No. 920. A. H. Woodcock. The Release of Latent Heat in Tropical Storms due to the Fall-Out of Sea-Salt Particles. *Tellus*, Vol. 10, No. 3, pp. 355-371. 1958.

No. 921. P. F. Scholander. Oxygen Dissociation Curves in Fish Blood. *Acta Physiol. Scand.*, Vol. 41, No. 4, pp. 340–344. 1957.

No. 922. Robert H. Gibbs, Jr. Preliminary Analysis of the Distribution of White Marlin, *Makaira albida* (Poey), in the Gulf of Mexico. *Bull. Mar. Sci., Gulf and Caribbean*, Vol 7, No. 4, pp. 360–369. 1957.

No. 923. Alfred C. Redfield. The Inadequacy of Experiment in Marine Biology. In: Perspectives in Marine Biology, Symposium held at Scripps Inst. of Oceanogr., Univ. Cal., March 24-April 2, 1956, pp. 17–23. Univ. California Press. 1958.

No. 924. Mary A. Plunkett. The Qualitative Determination of Some Organic Compounds in Marine Sediments. *Deep-Sea Research*, Vol. 4, pp. 259-262. 1957.

No. 926. Dean F. Bumpus, Joseph Chase, C. Godfrey Day, David H. Frantz, Jr., David D. Ketchum and Robert G. Walden. A New Technique for Studying Non-Tidal Drift with Results of Experiments off Gay Head, Mass., and in the Bay of Fundy. *Jour. Fish Bd., Canada*, Vol. 14, No. 6, pp. 931–944. 1957.

No. 927. Malcolm S. Gordon. Osmotic and Ionic Regulation in Scottish Brown Trout and Sea Trout (*Salmo trutta L.*). *Jour. Exper. Biol.*, Vol. 36, No. 2, pp. 253–260. 1959.

No. 928. H. Barnes and Margaret Barnes. The Rate of Development of *Balanus balanoides* (L.) Larvae. *Limnol. and Oceanogr.*, Vol. 3, No. 1, pp. 29–32. 1958.

No. 929. Theodore R. Folsom and Allyn C. Vine. On the Tagging of Water Masses for the Study of Physical Processes in the Oceans. In: The Effects of Atomic Radiation on Oceanography and Fisheries. *Nat. Acad. Sci.-Nat. Res. Council, Publ.* No. 551, Chap. 12, pp. 121–132. 1957.

No. 930. William S. von Arx. "Dister": A Displacement Sequence Stereoscope. *Jour. Meteorol*, Vol. 15, No. 2, pp. 230–231. 1958.

No. 931. William S. von Arx. Synoptic Photography. *Weather, Roy. Meteorol. Soc.*, London, pp. 179–197. 1958.

No. 932. Henry B. Bigelow and William C. Schroeder. Four New Rajids from the Gulf of Mexico. *Bull. Mus. Comp. Zool.*, Vol. 119, No. 2, pp. 201–233. 1958.

No. 933. G. Veronis. On the Transient Response of a β-plane Ocean. *Jour. Oceanogr. Soc., Japan*, Vol. 14, No. 1, pp. 1–5. 1958.

No. 934. William S. Richardson and Charles H. Wilkins. An Airborne Radiation Thermometer. *Deep-Sea Research*, Vol. 5, pp. 62–71. 1958.

No. 935. Joyce C. Lewin, R. A. Lewin and D. E. Philpott. Observations on *Phaeodactylum tricornutum*. *Jour. Gen. Microbiology*, Vol. 18, No. 2, pp. 420–426. 1958.

No. 936. Joyce C. Lewin. The Taxonomic Position of *Phaeodactylum tricornutum*. *Jour. Gen. Microbiology*, Vol. 18, No. 2, pp. 427–432. 1958.

No. 937. H. Barnes. Temperature and the Life Cycle of *Balanus balanoides* (L.). In: Marine Boring and Fouling Organisms, pp. 234–245. Univ. Washington Press, Seattle. 1959. (Not included in *Collected Reprints*).

No. 938. Harry J. Turner. The Effect of Nutrition on the Color of the Callus of *Polinices duplicatus*. *The Nautilus*, Vol. 72, No. 1, pp. 1–3. 1958.

No. 939. Henry Stommel, A. B. Arons and A. J. Faller. Some Examples of Stationary Planetary Flow Patterns in Bounded Basins. *Tellus*, Vol. 10, No. 2, pp. 179–187. 1958.

No. 940. Howard L. Sanders. Benthic Studies in Buzzards Bay. I. Animal-Sediment Relationships. *Limnol. and Oceanogr.* Vol. 3, No. 3, pp. 245–258. 1958.

No. 941. Dean F. Bumpus and C. Godfrey Day. Drift Bottle Records for the Gulf of Maine and Georges Bank, 1931–56. *U. S. Fish and Wildlife Service, Spec. Sci. Rept. — Fisheries*, No. 242, 61 pp. 1957.

No. 942. Frank J. Mather, III and Robert H. Gibbs, Jr. Distribution of the Atlantic Bigeye Tuna, *Thunnus obesus*, in the Western North Atlantic and the Caribbean Sea. *Copeia*, 1958, No. 3, pp. 237–239. 1958.

No. 943. W. V. R. Malkus and G. Veronis. Finite Amplitude Cellular Convection. *Jour. Fluid Mech.*, Vol. 4, Pt. 3, pp. 225–260. 1958.

No. 944. J. B. Hersey and M. S. Rutstein. Reconnaissance Survey of Oriente Deep (Caribbean Sea) with a Precision Echo Sounder. *Bull. Geol. Soc. Amer.*, Vol. 69, pp. 1297–1304. 1958.

No. 945. Alan J. Faller. An Optical Method for the Measurement of Surface Waves in the Laboratory. *Trans. Amer. Geophys. Union*, Vol. 39, No. 4, pp. 716–720. 1958.

No. 946. Bostwick H. Ketchum, John H. Ryther, Charles S. Yentsch and Nathaniel Corwin. Productivity in Relation to Nutrients. *Rapp. et Proc.-Verb., Cons. Perm. Internat. Explor. de la Mer*, Vol. 144, pp. 132–140. 1958.

No. 947. William C. Schroeder. The Lobster, *Homarus americanus*, and the Red Crab, *Geryon quinquedens*, in the Offshore Waters of the Western North Atlantic. *Deep-Sea Research*, Vol. 5, pp. 266–282. 1959.

No. 948. Susan I. Scholander and Joan T. Kanwisher. Latitudinal Effect on Respiration in Some Northern Plants. *Plant Physiol.*, Vol. 34, No. 5, pp. 574-576. 1958. (Not included in *Collected Reprints*).

No. 949. H. Barnes and Margaret Barnes. Further Observations on Self-Fertilization in *Chthamalus* sp. *Ecology*, Vol. 39, No. 3, p. 550. 1958.

No. 950. H. Barnes and Margaret Barnes. A Comparison of the Annual Growth Patterns of *Balanus balanoides* (L.) with Particular Reference to the Effect of Food and Temperature. *Oikos*, Vol. 10, No. 1, pp. 1–18. 1959.

No. 951. Takashi Ichiye. A Theory of Vertical Structure of Density in the Ocean. *Jour. Oceanogr. Soc., Japan*, Vol. 14, No. 2, pp. 35–40. 1958.

No. 952. Takashi Ichiye. Tsunami Waves—What are known about them—How we have studied them. *The Port Engineer*, Calcutta, India, Vol. 7, No. 1, pp. 5–19 [1–14]. 1958.

No. 953. Henry Stommel. Letter to the Editors: The Abyssal Circulation. *Deep-Sea Research*, Vol. 5, pp. 80–82. 1958.

No. 954. Bernhard Haurwitz, Henry Stommel and Walter H. Munk. On the Thermal Unrest in the Ocean. In: The Atmosphere and the Sea in Motion (The Rossby Memorial Volume), pp. 74-94. Rockefeller Institute Press, New York. 1959.

No. 955. G. C. McLeod. Delayed Light Action Spectra of Several Algae in Visible and Ultraviolet Light. *Jour. Gen. Physiol.*, Vol. 42, No. 2, pp. 243–250. 1958.

No. 956. John M. Zeigler, Carlyle R. Hayes and Sherwood D. Tuttle. Beach Changes during Storms on Outer Cape Cod, Massachusetts. *Jour. Geology*, Vol. 67, No. 3, pp. 318–336. 1959.

No. 957. James M. Moulton. The Acoustical Behavior of Some Fishes in the Bimini Area. *Biol. Bull.*, Vol. 114, No. 3, pp. 357–374. 1958.

No. 958. Robert L. Miller and John M. Zeigler. A Model Relating Dynamics and Sediment Pattern in Equilibrium in the Region of Shoaling Waves, Breaker Zone, and Foreshore. *Jour. Geology*, Vol. 66, No. 4, pp. 417-441. 1958.

No. 959. Floyd M. Soule and R. M. Morse. Physical Oceanography of the Grand Banks Region and the Labrador Sea in 1957. *U. S. Coast Guard Bull.*, No. 43, pp. 81–131. 1958.

No. 960. James M. Moulton. A Summer Silence of Sea Robins, *Prionotus* spp. *Copeia* 1958, No. 3, pp. 234–235. 1958.

No. 961. Robert H. Gibbs, Jr., and Bruce B. Collette. On the Identification, Distribution, and Biology of the Dolphins, *Coryphaena hippurus*, and *C. equiselis*. *Bull. Mar. Sci. Gulf and Carib.*, Vol. 9, No. 2, pp. 117–152. 1959.

No. 962. E-an Zen. Clay Mineral—Carbonate Relations in Sedimentary Rocks. *Amer. Jour. Sci.*, Vol. 257, pp. 29-43. 1959.

No. 963. Takashi Ichiye. The Response of a Stratified Bounded Ocean to Variable Wind Stresses. *Oceanogr. Mag.*, Tokyo, Japan, Vol. 10, No. 1, pp. 19–63. 1958.

No. 964. Theodore J. Smayda. The Seasonal Incoming Radiation in Norwegian and Arctic Waters, and Indirect Methods of Measurement. *Jour. du Conseil*, Vol. 24, No. 2, pp. 215–220. 1959.

No. 965. Theodore J. Smayda. Biogeographical Studies of Marine Phytoplankton. *Oikos*, Vol. 9, No. 2, pp. 158–191. 1958.

No. 967. Joanne S. Malkus and Georg Witt. The Evolution of a Convective Element: A Numerical Calculation. In: The Atmosphere and the Sea in Motion (The Rossby Memorial Volume), pp. 425–439. Rockefeller Institute Press, New York. 1958.

No. 968. Bostwick H. Ketchum and Vaughan T. Bowen. Biological Factors Determining the Distribution of Radio-Isotopes in the Sea. *Proc. 2nd Internat. Conference on the Peaceful Uses of Atomic Energy*, Geneva, Sept. 1–15, 1958, Vol. 18, pp. 429–433. 1958.

No. 969. Joanne Starr Malkus. On the Structure of the Trade Wind Moist Layer. *Papers in Physical Oceanography and Meteorology*, Vol. 13, No. 2, pp. 1–47. 1958. (Not included in *Collected Reprints*).

No. 970. Vaughan T. Bowen amd T. T. Sugihara. Marine Geochemical Studies with Fall-out Radioisotopes. *Proc. 2nd Internat. Conference on the Peaceful Uses of Atomic Engery*, Geneva, Sept. 1–15, 1958, Vol. 18, pp. 434–438. 1958.

No. 971. Francis L. Parker and William D. Athearn. Ecology of Marsh Foraminifera in Poponesset Bay, Massachusetts. *Journ. Paleont.*, Vol. 33, No. 2, pp. 333– 343. 1959.

No. 972. Charles S. Yentsch and Ralph F. Vaccaro. Phytoplankton Nitrogen in the Oceans. *Limnol. and Oceanogr.*, Vol. 3. No. 4, pp. 443–448. 1958.

No. 973. J. B. Hersey, Elizabeth T. Bunce, R. F. Wyrick, and F. T. Dietz. Geophysical Investigation of the Continental Margin between Cape Henry, Virginia, and Jacksonville, Florida. *Bull. Geol. Soc. Amer.*, Vol. 70, pp. 437–466. 1959.

No. 974. Melvin E. Stern. The Moving Flame Experiment. *Tellus*, Vol. 11, No. 2, pp. 175 179. 1959.

No. 975. Jack McLachlan and Guy C. McLeod. The Use of Conversion Factors for the Determination of the Concentration of Nutrients in Culture Media. *Limnol. and Oceanogr.*, Vol. 4, No. 2, pp. 218–219. 1959.

No. 976. Alfred C. Redfield. The Biological Control of Chemical Factors in the Environment. *Amer. Scientist*, Vol. 46, No. 3, pp. 205–222. 1958.

No. 977. C. Godfrey Day. Surface Circulation in the Gulf of Maine Deduced from Drift Bottles. *Fish. Bull.* 141, *U. S. Fish and Wildlife Service, Fish. Bull.*, Vol. 58, pp. 443–472. 1958.

No. 978. John H. Ryther, Charles S. Yentsch and Ralph F. Vaccaro. The Dynamics of a Diatom Bloom. *Biol. Bull.*, Vol. 115, No. 2, pp. 257–268. 1958.

No. 979. A. T. Spencer and D. C. Blanchard. A Portable Raindrop Recorder for Semi-Continuous Determination of Size Distributions. *Trans. Amer. Geophys. Union.* Vol. 39, No. 5, pp. 853–857. 1958.

No. 980. G. D. Nicholls, Herbert Curl, Jr., and V. T. Bowen. Spectrographic Analyses of Marine Plankton. *Limnol. and Oceanogr.*, Vol. 4, No. 4, pp. 472–478. 1959.

No. 981. Takashi Ichiye. On Convective Circulation and Density Distribution in a Zonally Uniform Ocean. *Oceanogr. Mag.*, Tokyo, Japan, Vol. 10, No. 1, pp. 97–135. 1958.

No. 982. T. T. Sugihara, H. I. James, E. J. Troianello and V. T. Bowen. Radiochemical Separation of Fission Products from Large Volumes of Sea Water. Strontium, Cesium, Cerium, and Promethium. *Analyt. Chem.*, Vol. 31, No. 1, pp. 44–49. 1959.

No. 983. P. F. Scholander. Counter Current Exchange: A Principle in Biology. *Hvaldrådets Skrifter*, No. 44, 24 pp. 1958.

No. 984. Charles S. Yentsch and John H. Ryther. Relative Significance of the Net Phytoplankton and Nanoplankton in the Waters of Vineyard Sound. *Jour. du Conseil*, Vol. 24, No. 2, pp. 231–238. 1959.

No. 985. G. Veronis. Cellular Convection with Finite Amplitude in a Rotating Fluid. *Jour. Fluid Mech.*, Vol. 5, Pt. 3, pp. 401-435. 1959.

No. 986. C. Godfrey Day. Oceanographic Observations, 1957, East Coast of the United States. *U. S. Fish and Wildlife Service, Spec. Sci. Rept. — Fisheries*, No. 282, 123 pp. 1959. (Not included in *Collected Reprints*).

No. 987. Alan J. Faller and William S. von Arx. The Modeling of Fluid Flow on a Planetary Scale. *Proceedings of the Seventh Hydraulics Conference*, Iowa Institute of Hydraulic Research, pp. 53–72. 1959.

No. 988. John M. Zeigler. Origin of the Sea Islands of the Southeastern United States. *Geogr. Rev.*, Vol. 49, No. 2., pp. 221–237. 1959.

No. 989. Malcolm S. Gordon. Ionic Regulation in the Brown Trout (*Salmo trutta L.*). *Jour. Exper. Biol.*, Vol. 36, No. 2, pp. 227–252. 1959.

No. 990. Francis A. Richards. Dissolved Silicate and Related Properties of Some Western North Atlantic and Caribbean Waters. *Sears Found., Jour. Mar. Res.*, Vol. 17, pp. 449–465. 1958. (In *Collected Reprints* for 1960).

No. 991. Sherwood D. Tuttle. Evolution of the New Hampshire Shore Line. *Bull. Geol. Soc., Amer.*, Vol. 71, pp. 1211–1222. 1960.

No. 992. Elizabeth Schroeder, Henry Stommel, David Menzel and William Sutcliffe, Jr. Climatic Stability of Eighteen Degree Water at Bermuda. *Jour. Geophys. Res.*, Vol. 64, No. 3, pp. 363-366. 1959.

No. 993. Jack McLachlan. The Growth of Unicellular Algae in Artificial and Enriched Sea Water Media. *Canad. Jour. Microbiol.*, Vol. 5, pp. 9–15. 1959.

No. 994. Gilbert L. Voss. The Cephalopods Collected by the R/V Atlantis during the West Indian Cruise of 1954. *Bull. Mar. Sci., Gulf and Caribbean*, Vol. 8, No. 4, pp. 369–389. 1958.

No. 995. John C. Ayers. The Hydrography of Barnstable Harbor, Massachusetts. *Limnol. and Oceanogr.*, Vol. 4, No. 4, pp. 448–462. 1959.

No. 996. Edward R. Baylor. The Responses of Snails to Polarized Light. *Jour. Exper. Biol.*, Vol. 36, No. 2, pp. 369–376. 1959.

No. 997. Guy C. McLeod and Jack McLachlan. The Sensitivity of Several Algae to Ultraviolet Radiation of 2537 Å. *Physiol. Plant.*, Vol. 12, pp. 306–309. 1959.

No. 998. H. Barnes. Regarding the Southern Limits of *Balanus balanoides* (L.). *Oikos*, Vol. 9, No. 2, pp. 139–157. 1958.

No. 999. C. B. Officer, J. I. Ewing, J. F. Hennion, D. G. Harkrider and D. E. Miller. Geophysical Investigations in the Eastern Caribbean: Summary of 1955 and 1956 Cruises. In: Physics and Chemistry of the Earth, Vol. 3, pp. 17-109. Pergamon Press Ltd., New York. 1959.

No. 1000. Alfred C. Redfield. The Influence of the Continental Shelf on the Tides of the Atlantic Coast of the United States. *Sears Found., Jour. Mar. Res.*, Vol. 17, pp. 432–448. 1958. (In *Collected Reprints* for 1960).

No. 1001. L. R. Breslau and H. E. Edgerton. The Luminescence Camera. *Jour. Biol. Photogr. Assoc.*, Vol. 26, No. 2, pp. 49–58, 1958.

No. 1002. Harry J. Turner, Jr. and James E. Hanks. Infestation of *Pecten irradians* by *Polydora*. *The Nautilus*, Vol. 72, No. 4, pp. 109–111. 1959.

No. 1003. Allan Robinson and Henry Stommel. The Oceanic Thermocline and the Associated Thermohaline Circulation. *Tellus*, Vol. 11, No. 3, pp. 295–308. 1959.

No. 1004. Allan Robinson and Henry Stommel. Amplification of Transient Response of the Ocean to Storms by the Effect of Bottom Topography. *Deep-Sea Research*, Vol. 5, pp. 312–314. 1959.

No. 1005. Sheina M. Marshall and A. P. Orr. Some Uses of Antibiotics in Physiological Experiments in Sea Water. *Sears Found., Jour. Mar. Res.*, Vol. 17, pp. 341–346. 1958. (In *Collected Reprints* for 1960).

No. 1006. Bert Bolin. On the Use of Tritium as a Tracer for Water in Nature. *Proc. 2nd Internat. Conference on the Peaceful Uses of Atomic Energy*, Geneva, Sept. 1–15, 1958, Vol. 18, pp. 336–338. 1958. (In *Collected Reprints* for 1959).

No. 1007. Bostwick H. Ketchum, Ralph F. Vaccaro and Nathaniel Corwin. The Annual Cycle of Phosphorus and Nitrogen in New England Coastal Waters. *Sears Found., Jour. Mar. Res.*, Vol. 17, pp. 282–301. 1958. (In *Collected Reprints* for 1960).

No. 1008. Henry Stommel. Florida Straits Transports: June 1956–July 1958. *Bull. Mar. Sci., Gulf and Caribbean*, Vol. 9, No. 2, pp. 222–223. 1959.

No. 1009. James B. Lackey. *Calkinsia aureus* gen. et sp. nov.; a New Marine Euglenid. *Trans. Amer. Micr. Soc.*, Vol. 79, No. 1, pp. 105–107. 1960.

No. 1010. Jack McLachlan and Charles S. Yentsch. Observations on the Growth of *Dunaliella euchlora* in Culture. *Biol. Bull.*, Vol. 116, No. 3, pp. 461–471. 1959.

No. 1011. John W. Graham. Metabolically Induced Precipitation of Trace Elements from Sea Water. *Science*, Vol. 129, No. 3360, pp. 1428–1429. 1959.

No. 1012. Joseph Levine. Spherical Vortex Theory of Bubble-Like Motion in Cumulus Clouds. *Jour. Meteorol.*, Vol. 16, No. 6, pp. 653–662. 1959.

No. 1013. John Kanwisher. Histology and Metabolism of Frozen Intertidal Animals. *Biol. Bull.*, Vol. 116, No. 2, pp. 258–264. 1959.

No. 1014. John Kanwisher. Polarographic Oxygen Electrode. *Limnol. and Oceanogr.*, Vol. 4, No. 2, pp. 210–217. 1959.

No. 1015. L. V. Worthington. The 18° Water in the Sargasso Sea. *Deep-Sea Research*, Vol. 5, pp. 297–305. 1959.

No. 1016. John H. Ryther. Potential Productivity of the Sea. *Science*, Vol. 130, No. 3376, pp. 602–608. 1959.

No. 1017. John W. Graham and Susan C. Cooper. Biological Origin of Manganese-Rich Deposits of the Sea Floor. *Nature*, Vol. 183, pp. 1050–1051. 1959.

No. 1018. Floyd M. Soule and R. M. Morse. Physical Oceanography of the Grand Banks Region and the Labrador Sea in 1958. *U. S. Coast Guard Bull.*, No. 44, pp. 29–99. 1960.

No. 1019. George L. Clarke and Charles J. Hubbard. Quantitative Records of the Luminescent Flashing of Oceanic Animals at Great Depths. *Limnol. and Oceanogr.*, Vol. 4, No. 2, pp. 163–180. 1959.

No. 1020. Richard Barakat. A Note on the Transient Stage of the Random Dispersal of Logistic Populations. *Bull. Math. Biophysics*, Vol. 21, pp. 142–151. 1959.

No. 1021. W. V. R. Malkus. Magnetoconvection in a Viscous Fluid of Infinite Electrical Conductivity. *Astrophys. Jour.*, Vol. 130, No. 1, pp. 259–275. 1959.

No. 1022. Carl E. Tschiegg and Earl E. Hays. Transistorized Velocimeter for Measuring the Speed of Sound in the Sea. *Jour. Acoust. Soc. Amer.*, Vol. 31, No. 7, pp. 1038–1039. 1959.

No. 1023. Henry Stommel and A. B. Arons. On the Abyssal Circulation of the World Ocean. I. Stationary Planetary Flow Patterns on a Sphere. *Deep-Sea Research*, Vol. 6, No. 2, pp. 140–154. 1960.

No. 1024. Patrick Butler. Palynological Studies of the Barnstable Marsh, Cape Cod, Massachusetts. *Ecology*, Vol. 40, No. 4, pp. 735-737. 1959. (Published posthumously).

No. 1025. Bert Bolin and Erik Eriksson. Changes in the Carbon Dioxide Content of the Atmosphere and Sea due to Fossil Fuel Combustion. In: The Atmosphere and the Sea in Motion (The Rossby Memorial Volume), pp. 130–142. Rockefeller Institute Press, New York. 1959.

No. 1026. John H. Ryther and R. R. L. Guillard. Enrichment Experiments as a Means of Studying Nutrients Limiting to Phytoplankton Production. *Deep-Sea Research*, Vol. 6, pp. 65–69. 1959.

No. 1027. Charles S. Yentsch and John H. Ryther. Absorption Curves of Acetone Extracts of Deep Water Particulate Matter. *Deep-Sea Research*, Vol. 6, pp. 72–74. 1959.

No. 1028. W. A. Mordy. Computations of the Growth by Condensation of a Population of Cloud Droplets. *Tellus*, Vol. 11, No. 1, pp. 16–44. 1959.

No. 1029. Irving I. Schell. On a Criterion of Representativeness of Sea Surface Temperature Date. *Bull. Amer. Meteorol. Soc.*, Vol. 40, No. 11, pp. 571–574. 1959.

No. 1030. J. S. Hart and Laurence Irving. The Energetics of Harbor Seals in Air and in Water with Special Consideration of Seasonal Changes. *Canad. Jour. Zool.*, Vol. 37, pp. 447–457. 1959.

No. 1031. Andrew F. Bunker. Heat and Water-Vapor Fluxes in Air Flowing Southward over the Western North Atlantic Ocean. *Jour. Meteorol.*, Vol. 17, No. 1, pp. 52–63. 1960.

No. 1032. Joseph Chase. Wind-Induced Changes in the Water Column along the East Coast of the United States. *Jour. Geophys. Res.*, Vol. 64, No. 8, pp. 1013–1022. 1959.

No. 1033. Howard L. Sanders. Benthic Studies in Buzzards Bay. III. The Structure of the Soft-Bottom Community. *Limnol. and Oceanogr.*, Vol. 5, No. 2, pp. 138–153. 1960.

No. 1034. J. S. Malkus and H. Riehl. On the Dynamics and Energy Transformations in Steady-State Hurricanes. *Tellus*, Vol. 12, No. 1, pp. 1–20. 1960.

No. 1035. Bostwick H. Ketchum. Marine Pollution Problems in the North Atlantic Area. In: Biological Problems in Water Pollution, Trans. Second Seminar, April 20–24, 1959, Cincinnati, Ohio, Sponsorship, Water Supply and Water Pollution Research Program. *Robert A. Taft Sanitary Engineering Center, U.S. Dept. Health, Education and Welfare, Publ. Health Service, Technical Rept.*, No. W60–3, pp. 212–217. 1960 (Not included in *Collected Reprints*).

No. 1036. E-an Zen. Mineralogy and Petrography of Marine Bottom Sediment Samples Off the Coast of Peru and Chile. *Jour. Sed. Petrol.*, Vol. 29, No. 4, pp. 513–539. 1959.

No. 1037. H. Barnes and Margaret Barnes. Note on Stimulation of Cirripede Nauplii. *Oikos*, Vol. 10, No. 1, pp. 19–23. 1959.

No. 1038. John T. Conover. Seasonal Growth of Benthic Marine Plants as Related to Environmental Factors in an Estuary. *Publ., Inst. Mar. Sci., Univ. Texas*, Vol. 5, pp. 97–147. 1959.

No. 1039. John H. Ryther. Light Adaptation by Marine Phytoplankton. *Limnol. and Oceanogr.*, Vol. 4, No. 4, pp. 492–497. 1959.

No. 1040. William E. Schevill and Richard H. Backus. Daily Patrol of a *Megaptera*. *Jour. Mammalogy*, Vol. 41, No. 2, pp. 279–281. 1960.

No. 1041. A. C. Redfield. Biological Considerations — The Fourth Phase. Conference on Physical and Chemical Properties of Sea Water, Easton, Maryland, Sept. 4–5, 1958. *Nat. Acad. Sci. — Nat. Res. Council, Publ.* 600, pp. 101–112. 1959. (Not included in *Collected Reprints*).

No. 1042. D. W. Menzel and J. H. Ryther. The Annual Cycle of Primary Production in the Sargasso Sea off Bermuda. *Deep-Sea Research*, Vol. 6, No. 4, pp. 351–367. 1960.

No. 1043. George L. Clarke and Lloyd R. Breslau. Measurements of Bioluminescence off Monaco and Northern Corsica. *Bull. Inst. Océanogr., Monaco*, No. 1147, pp. 1–31. 1959.

No. 1044. Joanne S. Malkus. Recent Developments in Studies of Penetrative Convection and an Application to Hurricane Cumulonimbus Towers. In: Cumulus Dynamics, Pergamon Press, London and New York, pp. 65–84. 1960.

No. 1046. William S. Richardson and Charles J. Hubbard. The Contouring Temperature Recorder. *Deep-Sea Research*, Vol. 6, No. 3, pp. 239–244. 1960.

No. 1047. David A. McGill, Nathaniel Corwin and Bostwick H. Ketchum. The Temperature Correction of Oceanic Inorganic Phosphorus Analyses. *Deep-Sea Research*, Vol. 6, pp. 60–64. 1959.

No. 1048. C. Godfrey Day. Oceanographic Observations, 1958, East Coast of the United States. *U. S. Fish and Wildlife Service, Spec. Sci. Rept. — Fisheries*, No. 318, 119 pp. 1959. (Not included in *Collected Reprints*).

No. 1049. John H. Ryther. Organic Production by Plankton Algae and its Environmental Control. In: Ecology of Algae, the Pymatuning Symposium in Ecology, 18–19 June 1959, *Spec. Publ., Univ. Pittsburg Press*, No. 2, pp. 72–83. 1960.

No. 1051. Joanne S. Malkus and Claude Ronne. Cloud Distributions over the Tropical Oceans in Relation to Large-Scale Flow Patterns. In: Physics of Precipitation, *Amer. Geophys. Union, Monogr.*, No. 5, pp. 45–60. 1960.

No. 1052. J. B. Hersey. Acoustically Monitored Bottom Coring. *Deep-Sea Research*, Vol. 6, No. 2, pp. 170–172. 1960.

No. 1053. Wolfgang Wieser and John Kanwisher. Vorschlag zum Anlegen einer "Stoffwechselkartei" für marine Tiergemeinschaften. *Zool. Anz.*, Vol. 165, Nos. 9/10, pp. 370–375. 1960.

No. 1054. Wolfgang Wieser. Benthic studies in Buzzards Bay. II. The Meiofauna. *Limnol. and Oceanogr.*, Vol. 5, No. 2, pp. 121–137. 1960.

No. 1055. Henry Stommel and A. B. Arons. On the Abyssal Circulation of the World Ocean. II. An Idealized Model of the Circulation Pattern and Amplitude in Oceanic Basins. *Deep-Sea Research*, Vol. 6, No. 3, pp. 217–233. 1960.

No. 1056. George C. Matthiessen. Observations on the Ecology of the Soft Clam, *Mya arenaria*, in a Salt Pond. *Limnol. and Oceanogr.*, Vol. 5, No. 3, pp. 291–300. 1960.

No. 1058. Charles S. Yentsch. The Influence of Phytoplankton Pigments on the Colour of Sea Water. *Deep-Sea Research*, Vol. 7, No. 1, pp. 1–9. 1960.

No. 1059. Wolfgang Wieser and John Kanwisher. Growth and Metabolism in a Marine Nematode, *Enoplus communis* Bastian. *Zeits. Vergl. Physiol.*, Vol. 43, pp. 29–36. 1960.

No. 1060. Karl E. Schleicher. A Note on the Constancy of the T/S Relationship in a Water Mass. Die Expeditionen von F. F. S. "Anton Dohrn" und V. F. S. "Gauss" im Internationalen Geophysikalischen Jahr 1957/1958. *Deutsche Hydrogr. Zeitschr.*, Ergänzungsheft, Reihe B (4°), No. 3, pp. 46–48. 1959.

No. 1061. Wolfgang Wieser and John Kanwisher. Respiration and Anaerobic Survival in some Sea Weed-Inhabiting Invertebrates. *Biol. Bull.*, Vol. 117, No. 3, pp. 594–600. 1959.

No. 1062. Joyce C. Lewin and Ralph A. Lewin. Auxotrophy and Heterotrophy in Marine Littoral Diatoms. *Canadian Jour. Microbiol.*, Vol. 6, pp. 127–134. 1960.

No. 1064. G. G. Whitney, Jr. Procedure for and Comments on Ice Point Tests of Deep Sea Reversing Thermometers. *Limnol. and Oceanogr.*, Vol. 5, No. 2, pp. 232–235. 1960.

No. 1065. Allan R. Robinson. The General Thermal Circulation in Equatorial Regions. *Deep-Sea Research*, Vol. 6, No. 4, pp. 311–317. 1960. (Reprints erroneously marked as Contribution No. 1081).

No. 1067. John H. Ryther and David W. Menzel. The Seasonal and Geographical Range of Primary Production in the Western Sargasso Sea. *Deep-Sea Research*, Vol. 6, No. 3, pp. 235–238. 1960.

No. 1068. E. M. Hulburt, J. H. Ryther and R. R. L. Guillard. The Phytoplankton of the Sargasso Sea off Bermuda. *Jour. du Conseil*, Vol. 25, No. 2, pp. 115–128. 1960.

No. 1069. Alan J. Faller. Further Examples of Stationary Planetary Flow Patterns in Bounded Basins. *Tellus*, Vol. 12, No. 2, pp. 159–171. 1960.

No. 1070. ANDREW A. FEJER and RICHARD H. BACKUS. Porpoises and the Bow-Riding of Ships Under Way. *Nature*, Vol. 188, No. 4752, pp. 700–703. 1960.

No. 1073. JOHN M. ZEIGLER, G. G. WHITNEY, JR. and CARLYLE R. HAYES. Woods Hole Rapid Sediment Analyzer. *J. Sed. Petr.*, Vol. 30, No. 3, pp. 490–495. 1960.

No. 1074. RICHARD BARAKAT and ROBERT BARAKAT. Optical Studies of the Diffraction of Water Waves by Circular and Thin Elliptic Cylinders. *Jour. Appl. Physics*, Vol. 31, No. 3, pp. 474–478. 1960.

No. 1075. H. BARNES and MARGARET BARNES. The Effect of Temperature on the Oxygen Uptake and Rate of Development of the Egg-Masses of Two Common Cirripedes, *Balanus balanoides* (L.) and *Pollicipes polymerus* J. B. Sowerby. *Kieler Meeresforschungen*, Vol. 15, No. 2, pp. 242–251. 1959. (In *Collected Reprints* for 1960).

No. 1076. RICHARD H. BACKUS. Notes on Western North Atlantic Sharks, No. 2. *Copeia*, 1960, No. 3, pp. 243–245. 1960.

No. 1077. KIRK BRYAN. The Instability of a Two-Layered System Enclosed between Horizontal, Coaxially Rotating Plates. *Jour. Meteorol.*, Vol. 17, No. 4, pp. 446–455. 1960.

No. 1078. J. H. STEELE and C. S. YENTSCH. The Vertical Distribution of Chlorophyll. *Jour. Mar. Biol. Assoc., U.K.*, Vol. 39, pp. 217–226. 1960.

No. 1079. W. A. MORDY. Differences in Coalescence Tendencies in Computed Condensation Cloud Droplet Spectra. In: Physics of Precipitation, *Amer. Geophys. Union, Monogr.*, No. 5, pp. 184–190. 1960.

No. 1080. JAMES E. HANKS. A Method for Preparing the Marine Polychaete, *Pectinaria gouldi* (Verrill), for Histological Study. *Trans. Amer. Micr. Soc.*, Vol. 79, No. 4, pp. 470–471. 1960.

No. 1081. E. A. SPIEGEL and G. VERONIS. On the Boussinesq Approximation for a Compressible Fluid. *The Astrophysical Jour.*, Vol. 131, No. 2, pp. 442–447. 1960.

No. 1082. G. VERONIS. An Approximate Theoretical Analysis of the Equatorial Undercurrent. *Deep-Sea Research*, Vol. 6, No. 4, pp. 318–327. 1960.

No. 1083. RAYMOND WEXLER and RUTH WEXLER. Cold Clouds over Tropical Oceans. In: Cumulus Dynamics, Pergamon Press, London and New York, pp. 129–134. 1960.

No. 1084. HENRY STOMMEL. Wind-Drift near the Equator. *Deep-Sea Research*, Vol. 6, No. 4, pp. 298–302. 1960.

No. 1086. DEAN F. BUMPUS. Sources of Water Contributed to the Bay of Fundy by Surface Circulation. *Jour. Fish. Res. Bd., Canada*, Vol. 17, No. 2, pp. 181–197. 1960.

No. 1087. G. FRAENKEL. Lethal High Temperatures for Three Marine Invertebrates: *Limulus polyphemus*, *Littorina littorea* and *Pagurus longicarpus*. *Oikos*, Vol. 11, No. 2, pp. 171–182. 1960.

No. 1088. J. H. RYTHER and E. M. HULBURT. On Winter Mixing and the Vertical Distribution of Phytoplankton. *Limnol. and Oceanogr.*, Vol. 5, No. 3, pp. 337–338. 1960.

No. 1089. C. GODFREY DAY. Bottom Water Temperature on Browns Ledge off Southern Massachusetts. *Jour. du Conseil*, Vol. 25, No. 3, pp. 235–239. 1960.

No. 1090. GEORGE L. CLARKE and LLOYD R. BRESLAU. Studies of Luminescent Flashing in Phosphorescent Bay, Puerto Rico, and in the Gulf of Naples Using a Portable Bathyphotometer. *Bull. Inst. Océanogr., Monaco*, No. 1171, pp. 1–32. 1960.

No. 1091. Floyd M. Soule and P. A. Morrill. Physical Oceanography of the Grand Banks Region and the Labrador Sea in 1959. *U. S. Coast Guard Bull.*, No. 45, pp. 98–154. 1960.

No. 1092. Frank J. Mather, III. Recaptures of Tuna, Marlin and Sailfish Tagged in the Western North Atlantic. *Copeia*, 1960, No. 2, pp. 149–151. 1960.

No. 1093. Thomas F. Budinger. Iceberg Detection by Radar. *U. S. Coast Guard Bull.*, No. 45, pp. 49–97. 1960.

No. 1094. A. H. Woodcock. The Origin of Trade-Wind Orographic Shower Rains. *Tellus*, Vol. 12, No. 3, pp. 315–326. 1960.

No. 1095. Vaughan T. Bowen and Thomas T. Sugihara. Strontium-90 in the 'Mixed Layer' of the Atlantic Ocean. *Nature*, Vol. 186, No. 4718, pp. 71–72. 1960.

No. 1096. Ralph F. Vaccaro and John H. Ryther. Marine Phytoplankton and the Distribution of Nitrite in the Sea. *Jour. du Conseil*, Vol. 25, No. 3, pp. 260–271. 1960.

No. 1097. Jack McLachlan. The Culture of *Dunaliella tertiolecta* Butcher — a Euryhaline Organism. *Canadian Jour. Microbiol.*, Vol. 6, pp. 367–379. 1960.

No. 1099. Harry J. Turner, Jr. and James E. Hanks. Experimental Stimulation of Gametogenesis in *Hydroides dianthus* and *Pecten irradians* during the Winter. *Biol. Bull.*, Vol. 119, No. 1, pp. 145–152. 1960.

No. 1100. Francis A. Richards. Some Chemical and Hydrographic Observations along the North Coast of South America — 1. Cabo Tres Puntas to Curaçao, Including the Cariaco Trench and the Gulf of Cariaco. *Deep-Sea Research*, Vol. 7, No. 3, pp. 163–182. 1960.

No. 1101. William G. Metcalf. A Note on Water Movement in the Greenland-Norwegian Sea. *Deep-Sea Research*, Vol. 7, No. 3, pp. 190–200. 1960.

No. 1102. Herbert Curl, Jr. Primary Production Measurements in the North Coastal Waters of South America. *Deep-Sea Research*, Vol. 7, No. 3, pp. 183–189. 1960.

No. 1103. John Kanwisher. pCO_2 in Sea Water and its Effect on the Movement of CO_2 in Nature. *Tellus*, Vol. 12, No. 2, pp. 209–215. 1960.

No. 1104. C. Godfrey Day. Oceanographic Observations, 1959, East Coast of the United States. *U. S. Fish and Wildlife Service, Spec. Sci. Rept.-Fisheries*, No. 359, 114 pp. 1960. (Not included in *Collected Reprints*).

No. 1106. Raymond G. Stross. Growth Response of *Chlamydomonas* and *Haematococcus* to the Volatile Fatty Acids. *Canadian Jour. Microbiol.*, Vol. 6, pp. 611–617. 1960.

No. 1107. Kirk Bryan and Elizabeth Schroeder. Seasonal Heat Storage in the North Atlantic Ocean. *Jour. Meteorol.*, Vol. 17, No. 6, pp. 670–674. 1960.

No. 1108. F. C. Fuglister. Atlantic Ocean Atlas of Temperature and Salinity Profiles and Data from the International Geophysical Year of 1957–1958. *Woods Hole Oceanogr. Inst. Atlas Series*, Vol. 1, 209 pp. 1960. (Not included in *Collected Reprints*).

No. 1111. Bostwick H. Ketchum. Oceanographic Research Required in Support of Radioactive Waste Disposal. In: Disposal of Radioactive Wastes, International Atomic Energy Agency, Vienna, pp. 283–291. 1960.

No. 1112. Max Blumer. Pigments of a Fossil Echinoderm. *Nature*, Vol. 188, No. 4756, pp. 1100–1101. 1960.

No. 1115. Robert J. Conover. The Feeding Behavior and Respiration of Some Marine Planktonic Crustacea. *Biol. Bull.*, Vol. 119, No. 3, pp. 399–415. 1960.

No. 1116. George D. Grice. Copepods of the Genus *Oithona* from the Gulf of Mexico. *Bull. Mar. Sci., Gulf and Carib.*, Vol. 10, No. 4, pp. 485–490. 1960.

No. 1124. Robert L. Miller and John M. Zeigler. A Study of the Relation between Dynamics and Sediment Pattern in the Zone of Shoaling Wave, Breaker, and Foreshore. *Eclogae Geol. Helv.*, Vol. 51, No. 3, pp. 542–551. 1958. (In *Collected Reprints* for 1960).

No. 1125. William S. Von Arx. The Line of Zero Set. *Deep-Sea Research*, Vol. 7, No. 3, pp. 219–220. 1960.

No. 1126. James M. Moulton. Swimming Sounds and the Schooling of Fishes. *Biol. Bull.*, Vol. 119, No. 2, pp. 210–223. 1960.

No. 1128. J. M. Zeigler, W. S. Hoffmeister, Graham Giese and Herman Tasha. Discovery of Eocene Sediments in Subsurface of Cape Cod, Massachusetts. *Science*, Vol. 132, No. 3437, pp. 1397–1398.

No. 1130. Willard Dow. A Telemetering Hydrophone. *Deep-Sea Research*, Vol. 7, No. 2, pp. 142–147. 1960.

No. 1134. Alfred C. Redfield. The Distribution of Phosphorus in the Deep Oceans of the World. *Assoc. Océanogr. Phys., Union Géodés. et Géophys. Int., Proc. Verb.*, No. 7 (G 16), pp. 189–193. 1960.